Volume 186 Number 1

THE BIOLOGICAL BULLETIN

FEBRUARY, 1994

Published by the Marine Biological Laboratory

THE BIOLOGICAL BULLETIN

PUBLISHED BY
THE MARINE BIOLOGICAL LABORATORY

FEBRUARY, 1994

Printed and Issued by
LANCASTER PRESS, Inc.
3575 HEMPLAND ROAD
LANCASTER, PA

THE BIOLOGICAL BULLETIN

THE BIOLOGICAL BULLETIN is published six times a year by the Marine Biological Laboratory, MBL Street, Woods Hole, Massachusetts 02543.

Subscriptions and similar matter should be addressed to Subscription Manager, THE BIOLOGICAL BULLETIN, Marine Biological Laboratory, Woods Hole, Massachusetts 02543. Single numbers, $37.50. Subscription per volume (three issues), $90.00 ($180.00 per year for six issues).

Communications relative to manuscripts should be sent to Michael J. Greenberg, Editor-in-Chief, or Pamela L. Clapp, Managing Editor, at the Marine Biological Laboratory, Woods Hole, Massachusetts 02543. Telephone: (508) 548-3705, ext. 428. FAX: 508-540-6902. E-mail: pclapp@hoh.mbl.edu.

POSTMASTER: Send address changes to THE BIOLOGICAL BULLETIN, Marine Biological Laboratory, Woods Hole, MA 02543.

Second-class postage paid at Woods Hole, MA, and additional mailing offices.
ISSN 0006-3185

INSTRUCTIONS TO AUTHORS

The Biological Bulletin accepts outstanding original research reports of general interest to biologists throughout the world. Papers are usually of intermediate length (10–40 manuscript pages). A limited number of solicited review papers may be accepted after formal review. A paper will usually appear within four months after its acceptance.

Very short, especially topical papers (less than 9 manuscript pages including tables, figures, and bibliography) will be published in a separate section entitled "Research Notes." A Research Note in *The Biological Bulletin* follows the format of similar notes in *Nature*. It should open with a summary paragraph of 150 to 200 words comprising the introduction and the conclusions. The rest of the text should continue on without subheadings, and there should be no more than 30 references. References should be referred to in the text by number, and listed in the Literature Cited section in the order that they appear in the text. Unlike references in *Nature*, references in the Research Notes section should conform in punctuation and arrangement to the style of recent issues of *The Biological Bulletin*. Materials and Methods should be incorporated into appropriate figure legends. See the article by Lohmann *et al.* (October 1990, Vol. **179**: 214–218) for sample style. A Research Note will usually appear within two months after its acceptance.

The Editorial Board requests that regular manuscripts conform to the requirements set below; those manuscripts that do not conform will be returned to authors for correction before review.

1. ***Manuscripts.*** Manuscripts, including figures, should be submitted in triplicate. (Xerox copies of photographs are not acceptable for review purposes.) The submission letter accompanying the manuscript should include a telephone number, a FAX number, and (if possible) an E-mail address for the corresponding author. The original manuscript must be typed in no smaller than 12 pitch, using double spacing (*including* figure legends, footnotes, bibliography, etc.) on one side of 16- or 20-lb. bond paper, 8½ by 11 inches. Please, no right justification. Manuscripts should be proofread carefully and errors corrected legibly in black ink. Pages should be numbered consecutively. Margins on all sides should be at least 1 inch (2.5 cm). Manuscripts should conform to the *Council of Biology Editors Style Manual*, 5th Edition (Council of Biology Editors, 1983) and to American spelling. Unusual abbreviations should be kept to a minimum and should be spelled out on first reference as well as defined in a footnote on the title page. Manuscripts should be divided into the following components: Title page, Abstract (of no more than 200 words), Introduction, Materials and Methods, Results, Discussion, Acknowledgments, Literature Cited, Tables, and Figure Legends. In addition, authors should supply a list of words and phrases under which the article should be indexed.

2. ***Title page.*** The title page consists of a condensed title or running head of no more than 35 letters and spaces, the manuscript title, authors' names and appropriate addresses, and footnotes listing present addresses, acknowledgments or contribution numbers, and explanation of unusual abbreviations.

3. ***Figures.*** The dimensions of the printed page, 7 by 9 inches, should be kept in mind in preparing figures for publication. We recommend that figures be about 1½ times the linear dimensions of the final printing desired, and that the ratio of the largest to the smallest letter or number and of the thickest to the thinnest line not exceed 1:1.5. Explanatory matter generally should be included in legends, although axes should always be identified on the illustration itself. Figures should be prepared for reproduction as either line cuts or halftones. Figures to be reproduced as line cuts should be unmounted glossy photographic reproductions or drawn in black ink on white paper, good-quality tracing cloth or plastic, or blue-lined coordinate paper. Those to be reproduced as halftones should be mounted on board, with both designating numbers or letters and scale bars affixed directly to the figures. All figures should be numbered in consecutive order, with no distinction between text and plate figures. The author's name and an arrow indicating orientation should appear on the reverse side of all figures.

4. ***Tables, footnotes, figure legends, etc.*** Authors should follow the style in a recent issue of *The Biological Bulletin* in preparing table headings, figure legends, and the like. Because of the high cost of setting tabular material in type, authors are asked to limit such material as much as possible. Tables, with their headings and footnotes, should be typed on separate sheets,

numbered with consecutive Roman numerals, and placed after the Literature Cited. Figure legends should contain enough information to make the figure intelligible separate from the text. Legends should be typed double spaced, with consecutive Arabic numbers, on a separate sheet at the end of the paper. Footnotes should be limited to authors' current addresses, acknowledgments or contribution numbers, and explanation of unusual abbreviations. All such footnotes should appear on the title page. Footnotes are not normally permitted in the body of the text.

5. ***Literature cited.*** In the text, literature should be cited by the Harvard system, with papers by more than two authors cited as Jones *et al.*, 1980. Personal communications and material in preparation or in press should be cited in the text only, with author's initials and institutions, unless the material has been formally accepted and a volume number can be supplied. The list of references following the text should be headed Literature Cited, and must be typed double spaced on separate pages, conforming in punctuation and arrangement to the style of recent issues of *The Biological Bulletin*. Citations should include complete titles and inclusive pagination. Journal abbreviations should normally follow those of the U. S. A. Standards Institute (USASI), as adopted by BIOLOGICAL ABSTRACTS and CHEMICAL ABSTRACTS, with the minor differences set out below. The most generally useful list of biological journal titles is that published each year by BIOLOGICAL ABSTRACTS (BIOSIS List of Serials; the most recent issue). Foreign authors, and others who are accustomed to using THE WORLD LIST OF SCIENTIFIC PERIODICALS, may find a booklet published by the Biological Council of the U.K. (obtainable from the Institute of Biology, 41 Queen's Gate, London, S.W.7, England, U.K.) useful, since it sets out the WORLD LIST abbreviations for most biological journals with notes of the USASI abbreviations where these differ. CHEMICAL ABSTRACTS publishes quarterly supplements of additional abbreviations. The following points of reference style for THE BIOLOGICAL BULLETIN differ from USASI (or modified WORLD LIST) usage:

A. Journal abbreviations, and book titles, all underlined (for *italics*)

B. All components of abbreviations with initial capitals (not as European usage in WORLD LIST *e.g., J. Cell. Comp. Physiol.* NOT *J. cell. comp. Physiol.*)

C. *All* abbreviated components must be followed by a period, whole word components *must not* (*i.e., J. Cancer Res.*)

D. Space between all components (*e.g., J. Cell. Comp. Physiol.*, not *J.Cell.Comp.Physiol.*)

E. Unusual words in journal titles should be spelled out in full, rather than employing new abbreviations invented by the author. For example, use *Rit Visindafjélags Islendinga* without abbreviation.

F. All single word journal titles in full (*e.g., Veliger, Ecology, Brain*).

G. The order of abbreviated components should be the same as the word order of the complete title (*i.e., Proc.* and *Trans.* placed where they appear, not transposed as in some BIOLOGICAL ABSTRACTS listings).

H. A few well-known international journals in their preferred forms rather than WORLD LIST or USASI usage (*e.g., Nature, Science, Evolution* NOT *Nature, Lond., Science, N.Y.; Evolution, Lancaster, Pa.*)

6. ***Reprints, page proofs, and charges.*** Authors receive their first 100 reprints (without covers) free of charge. Additional reprints may be ordered at time of publication and normally will be delivered about two to three months after the issue date. Authors (or delegates for foreign authors) will receive page proofs of articles shortly before publication. They will be charged the current cost of printers' time for corrections to these (other than corrections of printers' or editors' errors). Other than these charges for authors' alterations, *The Biological Bulletin* does not have page charges.

Editor's Note

In the December issue, we promised to provide additional information about submitting reports to the Biological Bulletin's Marine Models Electronic Record (BB-MER). The editors and computer technicians are continuing to refine the details, and we are thus unable to publish them in this issue. Stay tuned; we hope to have them for you next time.

Reference: *Biol. Bull.* **186:** 1–8. (February, 1994)

Misguided Cells: The Genesis of Human Cancer

J. MICHAEL BISHOP

The George Williams Hooper Foundation, University of California, San Francisco, California 94143-0552

Science is the transcendant human achievement of our age. We have not yet learned how to keep peace, to restore the poor, or to arrest the decline of our planet. But in building science, we have found a way to understand ourselves and the world around us in ever increasing depth and detail. Scientists could not have done this without lavish support from their fellow citizens. So it is only natural—indeed, it is obligatory—that we of science should share the joy of our discoveries and the grandeur of the puzzles that remain.

Can this be done? Is it possible for those of us schooled and practiced for decades in the ways and means of science to explain the world to our friends in other spheres? Great figures in the history of science have had no doubt about this:

Joseph Lagrange: "A mathematician has not fully understood his own work until he can go out and explain it to the first [person] he meets on the street." (If that be true, then in my experience, there are a lot of confused mathematicians in the world.)

Lord Rutherford: "A physicist's theories are worthless unless he can explain them to the barmaid at the local pub." (Thus did Lord Rutherford make life miserable for the barmaids in the Britain of his time—they were badgered to distraction by aspirant physicists.)

Enrico Fermi: "If you truly understand something, you can explain it to anyone."

My challenge here is to demonstrate the truth of those aphorisms for cells and cancer. It is a less daunting challenge than you might think: cancer was once one of the most complex of biological problems, seemingly beyond our comprehension; but now, as understanding burgeons, cancer can be readily explained.

This paper is based on a Friday Evening Lecture delivered at the Marine Biological Laboratory on 6 August 1993.

The ability of cells to multiply lies at the root of life; it also prefigures the baleful threat of cancer. One person in every four among us here will develop cancer; one in every five will die of the disease. These are tragic dimensions, but they are no larger than the intellectual challenge cancer presents. Every second, twenty-five million cells divide in our bodies. The divisions usually occur in the right place, at the right time, governed by mechanisms we have yet to understand. When the governance fails, cancer may arise. Why does the governance fail? How does it fail? What hope do we have of penetrating the complexities of cancer cells?

These questions have been before the human mind for a very long time, and until recently, the answers had seemed distant indeed. But over the past decade, a great change has occurred in how we think about cancer. Where once we viewed the cancer cell as an unfathomed black box, now we have pried open the box and cast in the first dim light. Where once we viewed cancer as a bewildering variety of diseases with causes too numerous to count, now we are on the track of a single unifying explanation of how most or all cancers might arise. The track is paved with cells.

The nature of cells

Robert Hooke first brought cells to public view. Hooke was a seventeenth century English physicist, meteorologist, engineer, architect, and biologist who also found time to fabricate some of the earliest microscopes.

Some time between 1660 and 1665, Hooke placed a thin slice of cork under the lens of his home-made magnifier. Three centuries of technological development have improved very little on Hooke's first image. Hooke described what he saw as "little boxes or cells distinct from one another." The term "cell" caught on, and we still use it to describe the elementary building blocks of living tissues. No single word now better embodies the sum of life:

the image of a cell is more portentous than even that of DNA.

But there is an irony here. Hooke chose the word cell for its connotation of a rigid and static enclosure, which is what he saw in his microscope. Never has a connotation been less apt. Hooke was indeed looking at rigid enclosures. But the living units that had been within, the units we now call cells, were gone.

We do not know the exact day on which Hooke first saw his "little boxes," and we have no reason to believe that he ever appreciated the magnitude of his discovery. Indeed, it would be close to three centuries before anyone else did. Then, in the space of little more than 50 years, in the period between 1835 and 1900, scientists at last perceived the nature of the cell and the central place of the cell in life on our planet. The perception came in several steps.

Mathias Schleiden, a student of plants, was perhaps the first to propose that cells represent the unit from which living organisms are built, an irreducible unit with a life all of its own. Three years later, Theodor Schwann adapted this proposal to animals.

Still, the origin of cells remained a mystery. The popular view was that each cell formed *de novo*—as if by magic—from the juices of the body, from a mystical substance known as the blastema in embryos, the cytoblastema in adults. But that view would not last. Its downfall was foreshadowed by the work of the great German embryologist, Karl Ernst von Baer, who discovered the mammalian oocyte (egg) from which we all have grown (with a modest assist from sperm).

Von Baer surmised that the growth and development of the embryo from a fertilized egg was dependent upon continuous cleavage of some elemental component, whose nature he never grasped. But von Baer did realize that the search for those imagined cleavages would lead to what he called "the innermost tabernacle of embryology."

Another German embryologist, Robert Remak, followed von Baer into the tabernacle and eventually reached the conviction that all cells in the embryo arise from the division of preexisting cells. The pathologist Rudolf Virchow then generalized the scheme and gained lasting credit for it, perhaps because he publicized it in the form of a Latin phrase that many a student has committed to memory: "omnis cellula a cellula": all cells come from cells.

This "theory of the cell," as it was called, immediately illuminated several great problems in biology. Now it could be seen that all of life had a structural continuity: every new individual arises from the union of two cells. Cells are the vehicles for inheritance, whatever its chemical nature might be—a mystery that was to go unsolved for almost another century.

And if all the cells of an organism arise from the single product of fertilization, then cells must possess an inherent ability to individualize themselves, to assume different functions, to differentiate (as we say in the shop talk of biologists); and they do this even though they have a common origin in fertilization and share a common genetic dowry.

When I lecture high school students, I find no aspect of biology more absorbing for them than the image of the sperm and the egg, uniting to engender a new individual. Skeptics among you might conclude that the student interest in fertilization is salacious. Granted: the mere mention of sperm brings the gleam of lust to many an adolescent eye (the egg seems less provocative, perhaps because of a mistaken association with cholesterol).

But I prefer to believe that students are moved by the wonder of embryogenesis: the fertilized egg, a single cell, multiplying myriad times over to produce the human organism. Our form and our function, our consciousness, passions, intellect, and creativity—all are rooted in the properties of individual cells. The great cell biologist E. B. Wilson put it well: ". . . the secrets of the mind are slumbering in the ganglion cell." [The cognescenti among us will recognize an anatomical error here, forgivable since the aphorism dates from 1898. But the poetry remains unblemished and evocative.]

Here too is the stuff and manner of evolution: cells must change if species are to evolve. But the play of evolution introduced a subtlety into the biological continuity of cells. August Weissman made this subtlety clear when he embellished the theory of the cell with two lineages. One lineage assembles the body of each living creature and is a biological dead-end—the somatic lineage (from "soma," for body); another lineage perpetuates the germ cells, sperm and egg, from one generation to the next—the germinal lineage, or germ line, the carrier of our genetic dowry.

Weissman argued correctly that the separation between these two lineages will last for all time: changes in a somatic cell cannot be retrofitted to the inheritance of a germ cell. In this one point, he challenged Charles Darwin, because Darwin had imagined that germ cells collect information from somatic cells throughout the course of life, and that the received information is part of the variation on which evolution relies. So far as we can tell, Weissman was correct; Darwin wrong.

The formulation by Weissman gave new form to an astonishing continuity that reaches from every cell now alive, back into the ultimate depths of biological time, back to the first coacervate of primitive living matter from which we all arose. We have laid bare a kinship between ourselves and all the other creatures that inhabit the earth—animals and plants alike; a kinship that was formed by the sculpting hand of evolution; a kinship that some would like to banish from our teaching because it embarrasses their religious convictions. Deny evolution and

you also deny the theory of the cell, which is by now no longer a theory, of course. Deny evolution and you profane a deep truth of human existence.

The theory of the cell and the conclusions to which it led were based on inference, not experiment. The images that Schleiden, Schwann, Remak, Virchow, and Weissman saw through their microscopes were static, frozen in time and space. Thus, the dynamic features of the cell theory as conceived in the nineteenth century were triumphs of the human imagination.

The image that is bestowed upon us by the theory of the cell is brick-like. Cells are the bricks with which all creatures are built—300 trillion of these bricks in each of our own bodies. But these are not ordinary bricks: they have an elaborate internal structure that allows them to live and breathe; they move from one place to another with purpose; they have distinctive personalities and assignments; they converse by means of chemical and molecular languages; and they multiply—ten thousand trillion times over during the course of each human lifetime.

Cells and cancer

The greatest wonder of cells, though, is that each knows what it is to do, and when, and where. Cancer is a failure of this wonder: the cancer cell violates its social contract with other cells, proliferating and spreading in an unfettered way.

The theory of the cell owes much to the study of cancer. Virchow himself was motivated primarily by interest in the origin of cancer cells rather than normal cells. But he knew a good thing when he saw it. If all cells come from other cells, then surely cancer cells must come from normal cells rather than from bad juices, as was formerly imagined. Virchow envisioned many cells turning malign to form a single cancer. Here he was wrong. We now know that most cancers begin as single cells that then grow into colonies of innumerable cells, all derived from the original founder.

The early steps in the genesis of cancer probably occur in many of our cells during a lifetime, only to be aborted before matters get out of hand. But occasionally, the course of events continues to a lethal end—a homogeneous colony of cancer cells with the potential to expand its size without surcease. Reasonable calculations suggest that billions of cells may take the first step towards cancer in each of us during the course of our lives. Why then do any of us survive to tell the tale? There are at least two answers to that question.

First, one step is not enough: several insults are required to produce a fully malignant cell, and the likelihood that these will combine in a single cell is very low. We will speak more of these combined insults later.

Second, our bodies can mount potent defenses against both foreign intruders (such as microbes and transplanted tissues) and errant natives (such as cancer cells). We know all too little of these defenses, but they are real.

Thus, most of us will develop no more than one cancer in our lifetimes; and the cancer usually will have originated from a single wayward cell, whose progeny have negotiated the several steps necessary to reach malignancy and have successfully eluded the defense mechanisms of the body.

What changes the personality of the first cell in this scheme; what fuels its progression to a lethal tumor? Humankind has spent the last century trying to answer these questions. We are now tantalizingly close to an answer. Our progress has come from attention to genes, so let's pause for a brief lesson on genes and DNA.

Genes and DNA

The command center for our cells is located within a compartment known as the nucleus, on structures known as chromosomes. When individual chromosomes are stained and magnified many hundreds of times, each displays a distinctive pattern of bands—a sort of microscopic fingerprint. We of *Homo sapiens* possess 24 different chromosomes, including the X and Y sex chromosomes, and each has a different fingerprint.

Chromosomes carry the instructions that dictate the structure and activities of our cells. These instructions are inscribed on that remarkable molecule known as DNA. Several yards of DNA are crammed into each human cell: how the cramming is accomplished remains a great mystery.

The instructions carried by DNA are composed of a chemical vocabulary that we call genes. Genes are interpreted by a universal molecular pathway that first copies DNA into smaller molecules known as RNA, and then RNA into even smaller molecules known as proteins. Proteins are the handmaidens of genes: the molecules that get most of the jobs done; the pieces from which much of the cell is built; the engines that drive the chemical reactions of life.

It now appears that cancer results from mistakes in this chain of command; mistakes that originate from damage to DNA. Usually, these are not mistakes that are inherited; instead, they occur at various times during our lives, gradually accumulating to a catastrophic threshold, beyond which lies the cancer cell. To recall the language of August Weissman, most cancers arise from genetic mistakes in our somatic cells rather than in our germ line.

The mistakes take two forms. Some cause a gain of function: the damaged gene acts when it should not and thus disturbs the control of cellular proliferation. Others eliminate a gene or its function, with the same consequences. We call these mistakes dominant and recessive, respectively. We will explore the significance of this nomenclature later.

Understanding cancer: essential beginnings

How have these genetic mistakes been found? Like so much else in science, the initial progress came not from a deliberate search but from unexpected quarters, and the essential beginnings were taken by resorting to simplifications. The first of these simplifications was to view cancer as a disease of individual cells and to study this disease not in the body of an animal but in a petri dish. The second was to exploit agents that will rapidly and reproducibly convert cells to cancerous growth under experimental circumstances; preeminent among these agents are viruses that cause tumors in animals. By examining these two simplifications in greater detail, we will learn much about how science is done and why it succeeds.

Whole tumors are not easy objects for experimental study. So we resort to the belief that the properties of individual cancer cells probably explain the behavior of tumors. We can define these properties by growing the cancer cells outside of the animal, using an artificial mixture of nutrients to feed the cells and glass or plastic vessels to contain the cells.

Under these circumstances, cancer cells misbehave exactly as we might have expected from the properties of whole tumors: they continue to grow when they should not—when they have become crowded by their neighboring cells; and they develop a very different appearance from their normal counterparts. The normal cells are flat, extended, and grow in orderly arrays; the cancer cells are rounded, disordered, literally crawling all over one another—a convincing caricature of the cells in an invasive cancer.

The fact that we can describe a cancer cell does not mean that we understand it. To understand how cancer arises, we need to track the events that occur from the moment a cell is first set on the path to cancerous growth to the final lethal outcome. We cannot do this with human cancer: usually, the disease is well advanced before it catches our eye. But we *can* do it by using viruses that cause tumors in animals and convert cells to cancerous growth in the test tube.

The utility of viruses for the experimentalist rests on a genetic simplification. The DNA of human cells is large enough to accommodate one million genes. For reasons that are not yet entirely clear, we do not have one million genes; but we do have tens of thousands, most of them not yet even identified. Each gene has its own specific chore, and among these chores, there must be many that are important in the genesis of cancer. By contrast, viruses generally have less than a dozen genes, and often only one of these genes is required to produce cancer. So simply put, viruses can simplify the study of cancer by more than a thousandfold.

Over the recent decades, scientists have exploited the simplifications offered by viruses to help find a set of human genes whose activities may lie at the heart of many cancers, no matter what their causes. We view these genes as a keyboard on which many different carcinogens might play. An enemy has been found, and we have begun to understand its lines of attack.

Viruses

The story began with Peyton Rous, who in 1910, while working at the Rockefeller Institute, discovered a virus that could transmit cancer from one chicken to another—the first cancer virus brought to full view. For this remarkable discovery, Rous was for many years criticised and disparaged: his finding was beyond the ken of most scientists of his time.

Others proved more perceptive, Henry James among them. The expatriate American author toured the Rockefeller Institute and was introduced to Peyton Rous in 1910, when the youthful Rous was in the midst of his work on the chicken cancer virus that he had discovered. (James was deep into the miseries of age and but two years from his death.) When James was told that Rous was in charge of cancer research at the Rockefeller, he responded fervently: "How magnificent! To be young and to have divine power."

The opinion of Henry James not withstanding, Peyton Rous also failed to achieve divine power; indeed, he eventually despaired of convincing anyone that he was right, gave up the pursuit of his historic discovery, and entered another field of research. Fortunately, Rous had good genes: he lived long enough to receive the Nobel Prize after he had passed the age of 80; the rest of the scientific world had finally caught up with him.

Rous has been memorialized in a way that I find more notable than the Nobel Prize: he has been enshrined in literature, portrayed as the character Rippleton Holabird in *Arrowsmith*, Sinclair Lewis' romantic novel about life in science. (Rippleton Holabird: consciously or subconsciously, that *nom de querre* must have been inspired by the fact that Rous did his seminal work with chickens.)

Paul de Kruiff was the microbiologist who coached Sinclair Lewis during the writing of *Arrowsmith*. They put virtually the entire staff of the Rockefeller Institute into the novel—not always in a good light. For good measure, de Kruiff left us his own analysis of why Rous gave up research on cancer viruses: "Dr. Rous was so amazed at his own discovery that it was rumored he couldn't stand the mental strain of going on with it and you couldn't blame him."

That analysis is not as outlandish as it might sound to you. Scientists admit to what one of our colleagues (Mark Ptashne) has called "psychic risks" in doing an unorthodox experiment. Our egos suffer brutally from failure.

We now know that the virus discovered by Rous exemplifies a distinctive sort of virus known as retroviruses

(among which is HIV, the cause of AIDS); that it does indeed cause cancer; and that it contains but four genes, arrayed along a single molecule. Three of these genes are used to reproduce the virus, but the fourth causes cancer—it is an "oncogene." We call this oncogene *src* because the cancers it induces are *sarcomas.*

Proto-oncogenes

The discovery that the virus of Peyton Rous and many other viruses use genes to elicit cancer brought clarity to what had been a muddled business. There had been hints before that the elemental secrets of cancer might lay hidden in the genetic dowry of cells. But in cancer viruses we found the first explicit examples of genes that can switch a cell from normal to cancerous growth.

Might the cell itself have such genes? Can the complexities of human cancer be reduced to the chemical vocabulary of DNA? The answer came from asking yet another question, based on the logic of evolution. The *src* gene serves no obvious purpose for Peyton Rous' virus—it contributes nothing to the growth or survival of the virus. Why then is it there?

When that question was asked, it led to a penetrating discovery. *Src* is present in the virus of Peyton Rous because of an accident of nature. The gene was acquired from the cells in which the virus grows, in an elaborate molecular ballet. The virus is a pirate; the booty is a cellular gene with the potential to become a cancer gene.

That discovery opened a floodgate of revelation. The DNA of vertebrates contains many genes that can be pirated into viruses like that of Peyton Rous, there to become oncogenes. We call these cellular genes proto-oncogenes because each has the potential to become an oncogene in a virus. Each proto-oncogene can be found in many different species—from *Homo sapiens* to birds, insects, even sea urchins—arrayed across one thousand million years of evolution. This conservation tells us that each of these genes serves a vital purpose for the organisms in which it is found.

It seems most unlikely that evolution installed proto-oncogenes in our cells to cause cancer. These genes must normally have more noble purposes. Why then does their transfer into retroviruses give rise to oncogenes? The answer lies in the elaborate molecular gymnastics by which proto-oncogenes are pirated into the genomes of retroviruses. During the pirating, proto-oncogenes suffer damage—mutations—that can convert them to oncogenes: from Dr. Jekyll to Mr. Hyde.

We also imagine that any other influence that can damage a proto-oncogene might give rise to an oncogene, even if the damage occurred without the gene ever leaving the cell; without the gene ever confronting a virus. In this view, proto-oncogenes become the precursors to cancer genes within our cells, and damage to genes becomes the underpinning of all cancers, even those that are not caused by viruses.

Consider, then, what retroviruses have done for us. Piracy of proto-oncogenes by retroviruses is an accident of nature, serving no purpose for the virus. But the event has profound implications for cancer research. In an extraordinary act of benevolence, retroviruses have brought to view cellular genes whose activities may be vital to many forms of carcinogenesis. It might have required many decades more to find these genes by other means among the morass of the human DNA. Instead, we have the genes made manifest in retroviruses, excerpted from amid the morass and made available for our closest scrutiny.

In time, scientists learned to go beyond retroviruses: we found other ways to uncover proto-oncogenes. The tally has now reached 100 or more. And we have learned that many of these can have a role in the genesis of human cancer. Having learned where to look from retroviruses, we could now examine the status of proto-oncogenes in human cancer cells. What we found was nothing short of astonishing. We can point to a variety of human malignancies in which damage to one or another proto-oncogene has been found with some consistency. In each instance, the damage causes a gain of function—unwanted activity of the gene. A list of such malignancies impresses because of the diversity of tumors involved, because of their identities (several can be counted among the principal nemeses of humankind) and because the list has been assembled after only a few years of pursuit, with imperfect tools: there is doubtless more to come.

Tumor suppressor genes

The discovery and exploration of proto-oncogenes provided a new view of the cancer cell, rich in detail and prospect. But there is another set of genes that are equally important in the genesis of cancer, and whose time has now come. Their story goes as follows.

We are called diploid organisms by geneticists, because our cells possess two copies of most of our genes. The oncogenes we have discussed until now are genetically dominant; their abnormalities are expressed even when a normal copy of the same gene is also present in the cell—evil overrides good, to use an image I find useful for medical students and physicists. But it now appears that most or all human tumors also bear genetic lesions that make their presence known only when both copies of a gene have been lost or inactivated. We call these lesions recessive. The possibility that recessive mutations, that the loss or inactivation of genes, might contribute to cancer emerged in two ways.

First, it is possible to induce the fusion of two different cells and thus to cause the intermingling of their genetic endowments in a single progeny. Experimental fusion of normal and cancer cells often suppresses the abnormalities of the cancer cell: the hybrid cells grow normally rather than as cancer cells. The cancer cells therefore appear to be defective in functions that are required for the regulation of cellular proliferation and other behavior. Fusion with a normal cell restores the necessary function and, thus, suppresses cancerous growth. The responsible genes are now known as "tumor suppressor genes," and their defectiveness in cancer cells represents an example of recessive genetic damage.

Second, the cells of some human cancers contain chromosomes that have lost part of their DNA—a lesion that we call deletion and that is sometimes visible through a microscope. Consider an example that involves a deletion within chromosome number 13 in human retinoblastoma, a malignant tumor of the retina that occurs only in young children. The loss of genes is a recessive lesion, of the sort imagined from the experiments with cell fusion. If you have understood the concept of recessiveness, you also realize that nothing ill will happen until the counterpart of the deleted gene on the other copy of chromosome 13 has also been damaged. That is exactly what happens in the genesis of retinoblastoma: both copies of a tumor suppressor gene on chromosome 13 are lost or otherwise inactivated.

It has required several decades for these findings to have an impact, but now that impact is being felt in spades. From several lines of enquiry, evidence has been obtained for recessive genetic lesions in most if not all forms of human cancer. At least ten of the affected genes have been identified directly by the use of recombinant DNA, including genes involved in retinoblastoma; carcinomas of the breast, bowel, bladder, lungs, and kidney; tumors of the nervous system; and leukemias.

Any present effort to enumerate recessive lesions in human cancer is freighted with uncertainty. Taking the literature at face value, I count on the order of a dozen. There are probably many more. It is worth noting that even the first fruits of the often maligned human genome project would make these genes easier to find.

Moreover, the identification of lesions in tumor suppressor genes has added an additional dimension to the molecular genetics of cancer, because some of these lesions account for inherited predispositions to specific cancers. Recalling August Weissman again: the damage has affected DNA in the germinal lineage and, thus, is passed from generation to generation. But I emphasize that this seems to be the exception, not the rule. Most cancer genes arise from damage in the somatic lineage and, thus, affect only a single individual.

In summary, two sorts of genetic damage figure in the genesis of human cancer: dominant—with targets known as proto-oncogenes; and recessive—with targets known variously as tumor suppressor genes, recessive oncogenes, or anti-oncogenes. The proto-oncogene causes trouble only if it continues to produce an active protein, whereas the recessive oncocogene is pathogenic only when it is defective or lost. These are diametrically opposite maladies, yet they both play on the cell to give an identical outcome: cancer. How does this happen? The proliferation of cells is driven by an internal engine that is governed in at least three ways.

First, multiple accelerators activate the engine when it has been idling and keep it running as long as cell division is required. Proto-oncogenes exemplify these accelerators. Damage to a proto-oncogene jams the accelerator and drives the cell to relentless division.

Second, multiple governors retard or arrest the engine when the cell should cease division. Tumor suppressor genes exemplify the governors. Remove a governor, and the cell is unleashed to relentless division.

Third, the engine runs according to a strict schedule: each step in division occurs in a predictable sequence and at a predictable time; and the sequence repeats itself in a cyclical manner—hence, "cell division cycle."

The cellular clock

In other words, cells possess an internal clock that sets the schedule for cell division. The existence and nature of this clock emerged in fascinating ways. One of these ways can be illustrated by removing the nucleus from a fertilized frog egg. Such an egg has no chromosomes and does not divide. Still, it heaves rhythmically, on the same schedule as cell division, frustrated in its drive to multiply, but still responding to the clock. In other words, once up and running, the clock has no need of genes: it is entirely self-sufficient.

The works of the cellular clock have just come into view, mainly from research on the cells of yeast and frogs. One notable feature of the clock is the fidelity with which it has been conserved throughout the course of evolution. It was invented more than a billion years ago and has remained virtually unchanged until the present. At least some of its components can be moved from a human cell to a yeast and function there just as well.

One of the great remaining mysteries about the clock is how the accelerators and governors of the cell cycle adjust its rhythm. Once in hand, the solution to that mystery should cast new light on the inner workings of both normal and cancerous cells.

In his novel, *Tough Guys Don't Dance*, Norman Mailer reminded us that the development of cancer is not a simple matter: more than one event is likely to be involved.

"None of these doctors has a feel for cancer . . . The way I see the matter, it's a circuit of illness with two switches . . . Two terrible things have to happen before the crud can get its start. The first cocks the trigger. The other fires it. I've been walking around with the trigger cocked for forty-five years." (The speaker was a smoker who, in Mailer's plot, died of lung cancer four pages later.)

Mailer got things right—in this instance, at least. Malignant tumors arise from a protracted sequence of events whose components have never been decisively counted or named. The common view is that each step in the sequence creates an additional aberration. For example, an emerging cancer cell might independently acquire the capabilities for extended proliferation, invasion of adjacent tissue, and spread through the body. We do not know the details of why or how this happens. For the moment, we cannot assign distinct steps in tumorigenesis to individual genes. But everywhere we look, we find evidence that damage to multiple genes, both proto-oncogenes and tumor suppressor genes, figures in the genesis of virtually every cancer.

Prominent examples include (1) carcinoma of the colon, which may harbor recessive lesions on chromosomes 5, 17, and 18, and a point mutation in the proto-oncogene KRAS; (2) carcinoma of the lung, in which amplification of myc genes, and recessive mutations affecting chromosome 3 and the retinoblastoma gene (Rb) have been found with some regularity; (3) neuroblastoma, which may feature recessive mutations on both chromosome 1 and 11, as well as amplification of the proto-oncogene NMYC; and (4) carcinoma of the breast, in which relatively consistent lesions may include amplification of the proto-oncogenes NEU and MYC, and recessive lesions affecting Rb, chromosome 3, and chromosome 11.

Each additional lesion adds insult to injury, the eventual sum being a malignant tumor. The catalog of genetic lesions is nothing short of extraordinary. Less than 20 years ago, we knew nothing of these lesions and had no means by which to find them. No other field of modern biomedical science can boast of more rapid progress.

Why should it require so many separate steps to make a cancer cell? We know that the machinery to regulate the proliferation of cells is elaborate, with numerous components working in concert, sometimes redundantly. The machinery seems to have become deliberately complex. Perhaps this complexity represents an evolutionary failsafe, designed to ward off the anomalies that lead to cancer.

If you think about it, we are nigh onto perfect in this regard: our bodies reduce a billion risks of cancer to less than one per lifetime. We calculate that every gene in our DNA is damaged some ten billion times in a lifetime, yet somehow, the machinery of our cells voids virtually all of this damage.

What then fuels tumor progression? If our cells are so good at rectifying genetic damage, why do they ever accumulate the catastrophic combination of mutations required to generate a full-blown cancer cell? The answer to this question is now in hand and represents one of the most remarkable insights from contemporary biomedical research.

As cells progress through the division cycle, they monitor themselves for the completion of crucial events, such as the replication of DNA, repair of mutations, and construction of the apparatus required for mitosis. If all is not well, a feedback device slows the engine of the cell cycle, buying time for defects to be remedied. That failing, the cell may destroy itself in order to avoid becoming an outlaw.

Some of the mutations in cancer cells cripple this self-inspection or the feedback it generates, allowing cells to be more sloppy and, thus, to produce more mutations that survive to cause trouble. In other words, one mutation may beget many more, and that can fuel the progression to frank malignancy. It takes little imagination to recognize how important all of this is likely to be for future efforts to prevent the occurrence of cancer and to deal with it once it has appeared.

The future

Which brings us to a look into the future. How might all this research progress that I have reviewed for you eventually aid in the management of cancer? It is too early to give a decisive answer to this question, but there are ways in which genetic dissection can already be used in the diagnosis and prognosis of cancer. I will illustrate two.

Neuroblastoma is the most common cancer of children under the age of two. The tumors are assigned to four stages, according to severity: I and II, relatively localized and usually curable; and III and IV, more widespread and inevitably fatal. A proto-oncogene called N-myc is often damaged and malfunctioning in neuroblastomas, a dominant disorder. But the genetic malady occurs only in those tumors of stages III and IV, where it signifies a particularly poor prognosis. As a result, damage to NMYC is now regarded as the single best parameter for staging neuroblastomas, a dire prognostic sign that is used in the counseling of patients and their families, and in the choice of therapy.

The gene affected by recessive damage in human retinoblastomas has been identified and isolated by molecular cloning. Therefore, it is now possible to chart the inheritance of damaged copies of this gene in families afflicted with congenital retinoblastoma and, thus, to identify children at risk for the disease either before or after birth.

Beyond these two limited examples lie much broader prospects. For example, we can reasonably envision a not-

too-distant day when we will perform molecular cytology on human sputum, urine, and feces, screening for the early genetic lesions that signal the precursors to lung, bladder, and colon cancer. With current technologies, we can detect one mutant cell, one precursor to cancer among 10,000 normal cells. It should be only a few years before such detection becomes a matter of routine.

What of treatment? Are we likely to acquire new antidotes for cancer from our study of oncogenes? There is little like'ihood that we will be able to repair or replace the damaged genes of cancer cells in the foreseeable future: we have not yet learned how to operate on the DNA of living human cells with the necessary surgical precision and efficiency. There is talk of restoring functional copies of tumor suppressor genes to cancers in which they are defective. The strategy has been tested with some success in cell culture, but deployment in human subjects presently seems many years distant.

If we focus on the protein handmaidens of genes, however, we can see more cause for hope. Given sufficient information about how these proteins act, we may be able to invent ways to interdict their action, even to exploit the specificity of genetic damage and thus to reverse the effects of oncogenes.

I am eager not to appear naive. No single therapy against an oncogene product is likely to become a panacea. We must deal with a large variety of damaged genes, whose actions present great chemical and enzymological diversity; and we must be prepared to cope with evolving genetic damage within cancer cells that can bring a variety of oncogenes into play sequentially. In 1983, a prominent figure in American cancer research told the *New York Times* that "scientists should learn how to manipulate oncogenes to protect or treat patients within the next five years." The prediction has not come to pass. The words ring hollow, now, except as a cautionary tale.

In summary: many things cause cancer, but all may act through the same malady—damage to DNA. From an accident of nature, piracy by retroviruses, we gained our first glimpse of a genetic keyboard on which many different causes of cancer can play, a final common pathway to the disease we know as cancer.

Over the past decade, that glimpse has broadened into a view of intricate detail and great potential. We have learned that cancer cells harbor both dominant and recessive genetic damage; we have identified dozens of genes that are affected by this damage; we have begun to chart the course by which the damaged genes collaborate to propel a cell to cancerous growth; and we have glimpsed how this knowledge will eventually serve at the bedside of the cancer patient.

The story of cancer research in our time embodies a great truth about scientific discovery that I want now to emphasize. We cannot prejudge the utility of scholarship; we can only ask that it be sound.

Peyton Rous isolated his virus from chickens—beasts not renowned for glamour—witness this quote from the German film director, Werner Herzog: "Stupidity is the devil. Look in the eye of a chicken and you will know. It's the most horrifying, cannabalistic and nightmarish creature in this world."

The chicken virus discovered by Peyton Rous 70 years ago was the first cancer virus to be isolated. Decades later, the oncogene *src* of this virus became the first retroviral oncogene to be identified; the action of the *src* protein, the first biochemical mechanism implicated in cancer growth; and the discovery of *src* in normal cells, the first sighting of proto-oncogenes—of potential cancer genes in our cells.

Similarly, the engine that drives the division of cells and the clock that governs its rhythm have been uncovered mainly through the study of two other humble creatures: baker's yeast and its relatives, and the frog. Here is a familiar but oft-neglected lesson: the proper conduct of science lies in the pursuit of nature's puzzles, wherever they may lead. We cannot prejudge the utility of any scholarship, we can only ask that it be sound. We cannot always assault the great problems of biology at will; we must remain alert to nature's clues and seize on them whenever and wherever they may appear—even if it be in a chicken, a frog, or baker's yeast.

Bit by bit, the inner workings of the cancer cell are coming under our sway. With this knowledge, we seek devices for diagnosis, for prognosis, and for rational designs of therapy and prevention of cancer. But a greater intellectual adventure overshadows even these: the quest to understand the cell in all of its particulars, to know what keeps us whole and what renders us asunder. The great French mathematician and physicist Henri Poincare phrased the point well (I will take liberties with the gender in his text):

"The scientist does not study nature because it is useful; she studies it because she delights in it, and she delights in it because it is beautiful. If nature were not beautiful, it would not be worth knowing, and if nature were not worth knowing, life would not be worth living."

Or H. G. Wells: "The motive that will conquer cancer will not be pity nor horror; it will be curiosity to know how and why . . . Pity never made a good doctor, love never made a good poet. Desire for service never made a discovery."

Reference: *Biol. Bull.* **186**: 9–16. (February, 1994)

Regional Differences in Methyl Farnesoate Production by the Lobster Mandibular Organ

DAVID W. BORST[1], BRIAN TSUKIMURA[1], HANS LAUFER[2], AND ERNEST F. COUCH[3]*

[1]*Department of Biology, Illinois State University, Normal, Illinois 61790-4120;* [2]*Department of Cellular Biology, University of Connecticut, Storrs, Connecticut 06268; and* [3]*Department of Biology, Texas Christian University, Fort Worth, Texas 76129*

Abstract. Visual examination of the mandibular organ (MO) from the lobster, *Homarus americanus*, disclosed two distinct morphological regions: a fan-folded region along one edge of the gland, and a smooth, unfolded region comprising the rest of the gland. Because MOs produce methyl farnesoate (MF), the MF content of both regions was measured. In freshly dissected glands, more than 95% of the MF was found in the fan-folded region of the gland. In MO sections incubated with [^{3}H-*methyl*]methionine (a radiolabeled precursor of MF), more than 90% of MF synthesis was found in the fan-folded region. Eyestalk ablation, a procedure that increases MO activity, caused the MF content of MOs to increase more than 130-fold, but had little effect on the regional distribution of MF. Histological observations indicated that these two regions had different cellular compositions. The fan-folded region contained two cell types (A and B). The A cells were mitotically active and appeared to be undifferentiated. The B cells contained a large number of small vacuoles. The unfolded region was largely composed of a third cell type (C). The C cells were large and morphologically complex, containing many mitochondria and large vacuolar-like structures. They contained relatively few small vacuoles. On the basis of appearance and location, B cells appear to be the likely site of MF synthesis. The physiological importance of C cells is unknown.

Introduction

Mandibular organs (MOs) from several crustacean decapods have been shown to produce methyl farnesoate, a sesquiterpene structurally related to the insect juvenile hormones (JH) (Borst *et al.*, 1987; Laufer *et al.*, 1987; Tobe *et al.*, 1989; Borst and Laufer, 1990). This synthetic activity is consistent with MO ultrastructure, which has features typical of endocrine cells producing lipid and steroid hormones (Aoto *et al.*, 1974; Byard *et al.*, 1975; Demeusy, 1975; Hinsch and al Hajj, 1975; Hinsch, 1977; Buchholz and Adelung, 1980). Similar ultrastructural features are observed in the insect corpus allatum (CA) (Cassier, 1979; Tobe and Stay, 1985), the site of JH synthesis. These similarities of ultrastructure and of biochemical product suggest that the crustacean MO is the homologue of the insect CA.

Although MF is a major MO product, several reports have suggested that this tissue produces other endocrine products. For example, significant amounts of progesterone have been detected in lobster MOs by radioimmunoassay (Couch *et al.*, 1987). Moreover, lobster MOs convert pregnenolone to progesterone *in vitro* (Tsukimura, 1988). MOs from other species, such as the mud crab *Scylla serrata* and the crayfish *Procambarus clarkii*, produce and release farnesoic acid *in vitro* (Tobe *et al.*, 1989; Ding and Tobe, 1991). However, the importance of either compound as a secretory product *in vivo* is still uncertain.

Because of its large size, the lobster MO is an ideal tissue for investigating MO function (Byard *et al.*, 1975). In this paper we describe studies on the structure and function of this tissue.

Materials and Methods

Animals

Male lobsters (200–300 g) were obtained from the Marine Resources Department at the Marine Biological Laboratory, Woods Hole, Massachusetts. Animals were kept

Received 20 July 1992; accepted 22 November 1993.

Abbreviations: MO = mandibular organ; MF = methyl farnesoate; EF = ethyl farnesoate.

in running seawater at ambient temperature (15 to 20°C) until used. The eyestalks of some animals were severed at their base; bleeding was limited by cauterization. Animals were eyestalk-ablated 2 weeks before use.

Materials

Acetonitrile and diethyl ether (both HPLC grade), and hexane (Optima grade) were purchased from Fisher Scientific (Pittsburgh, PA). [^{3}H-*methyl*]methionine (specific activity = 200 mCi/mmol) was obtained from Dupont/NEN (Boston, Massachusetts). JB-4 glycol methacrylate was purchased from Polysciences, Inc. (Warrington, Pennsylvania). MF was obtained from Dr. D. A. Schooley (Zoecon Research Institute, Palo Alto, California) as a mixture of two isomers (approximately 70% 2*E*,6*E* and 30% 2*Z*,6*E*). The 2*E*,6*E* isomer was purified by normal phase high performance liquid chromatography (np-HPLC; see below). Ethyl farnesoate was prepared from 2*E*,6*E* methyl farnesoate as previously described (Borst *et al.*, 1987).

Mandibular organ dissection

MOs were removed from the area adjacent to the apodeme of the mandibular abductor. Some MOs were cut transversely with a razor blade into four strips or sections (I–IV) of approximately equal width (see Fig. 1). In a few cases, each section was further divided into three or more pieces of equal size by cutting perpendicular to the first cut.

MF quantification

Whole MOs or MO sections were homogenized in distilled water with a Dounce homogenizer; the homogenizer was then rinsed with 1% NaCl and the rinse combined with the homogenate. The homogenate (or the culture medium, see next section) was added to acetonitrile and sufficient saline to give a final acetonitrile:water ratio of 5:4. Ethyl farnesoate (5 or 10 ng) was added as an internal standard, and the samples were extracted twice with hexane. MF present in these pooled hexane extracts was determined by npHPLC. Briefly, this method involves separating the hexane extract on a silica column (5 μm, 4.6 mm × 25 cm) with 1.0% diethyl ether in hexane. Material appearing in the same elution volume as 2*E*,6*E* methyl farnesoate was quantified by absorption at 220 nm. This value was adjusted for recovery by comparison to the internal standard. This method has been validated by gas chromatography/mass spectroscopy and has a detection limit of 0.1 ng/injection (Borst and Tsukimura, 1991).

Measurement of MF synthesis

The synthesis of MF *in vitro* was measured in sections or pieces of MOs incubated at room temperature with gentle shaking in *Homarus* saline (Welsh and Smith, 1960) supplemented with glucose (0.1%) and 200 μ*M* [^{3}H-*methyl*]methionine. After two hours, MF was extracted from the tissue and the incubation medium.

These extracts were then used to determine MF synthesis by two different methods. In one approach, np-HPLC was used to calculate the amount of MF synthesized during the incubation of MOs. This method is facilitated by the observation that freshly dissected MO pairs from the same animal contain similar amounts of MF (see Results, Fig. 2). The MF contained in incubated gland sections and their culture media was quantified by npHPLC. The sum of these values was then compared to the MF found in sections of the unincubated contralateral pair. The difference between these values is the amount of MF synthesized by the MO during the incubation.

In a second method, the relative level of MF synthesis was determined by calculating the transfer of radiolabeled methyl groups from [^{3}H-*methyl*]methionine to MF during incubation (Borst *et al.*, 1987; Laufer *et al.*, 1987). Because lobster MOs synthesize and release more than one radiolabeled organosoluble compound (Borst *et al.*, 1987), the hexane extracts of MO sections and their culture media were fractionated using the npHPLC conditions described above. The radioactive material eluting at the retention time of MF was quantified with a liquid scintillation counter. The sum of the radiolabeled MF in the tissue sections plus that released into their culture medium is a measure of MF synthesis by the MO. While this *in vitro* labeling procedure is more sensitive than the npHPLC procedure used above, it can be affected by factors other than the absolute synthetic rate of the MO. Therefore, the results are relative indicators of the level of MF synthesis and are best presented as DPM incorporated into MF (Tobe *et al.*, 1989).

Histology

Whole MOs were fixed in modified Karnovsky's (1965) fixative, which consists of 2.7% glutaraldehyde and 2% formaldehyde buffered with 0.1 *M* sodium cacodylate (pH 7.3) and adjusted to an osmolality of 835 milliosmoles with 10% sucrose. After fixation, the tissue was washed with cacodylate buffer, dehydrated in ethanol, and embedded at 5°C in glycol methacrylate by the method of Butler (1984). Sections were cut dry at 2 μm thickness with machine-made Ralph-Bennett knives (Butler, 1979) and stained with either Heidenhain's iron hematoxylin or Lee's stain (Bennett *et al.*, 1976).

Results

Morphology

The MO has a fan-shaped appearance with a broad fan-folded edge at one end and a narrow smooth (un-

folded) edge at the other end (see Fig. 1). *In situ*, MOs are oriented with the fan-folded edge posterior and dorsal; this edge is the major site of attachment of the gland to the apodeme of the mandibular abductor. The narrow edge of the MO is anterior and ventral. Macroscopic examination of several MOs suggested that they have two morphological regions. The fan-folded edge of the gland (approximately 25% of the glandular area) is thinner and has a light yellow color. The rest of the MO is thicker and dark beige or tan. MOs from animals that had been eyestalk-ablated 14 days earlier had a larger and thicker fan-folded region.

MF content and distribution

MF content was measured in freshly dissected whole glands. MF content varied markedly (from 3.2 to 196.8 ng/MO) between animals, with an average content of 55.5 (±12.7, SEM) ng/MO (n = 16). In individual animals, the MF contents of the left and right MOs were strongly correlated (r = 0.977; Fig. 2).

MOs from eyestalk-intact and eyestalk-ablated male lobsters were analyzed to determine regional content and synthesis of MF. MOs from these animals were divided into four sections of approximately equal width (Fig. 1). For MOs from eyestalk-intact animals, division of the gland into four sections placed the fan-folded region entirely in section I. For MOs from eyestalk-ablated animals, enlargement of the fan-folded region resulted in some of this region being included in section II.

In every lobster studied (n = 16), MF content was localized in the fan-folded region of the MO (section I). Figures 3 and 4 show the distribution of MF in MOs taken from two groups of animals (eyestalk-intact and eyestalk-ablated, respectively) that were analyzed at the same time and under similar conditions. Figure 3A shows the distribution of MF in MOs from the eyestalk-intact animals (n = 4). One MO from each animal was analyzed for MF immediately after dissection. The total MF content (the sum of the MF found in sections I–IV) of the freshly dissected glands was 43.1 (±7.7, SEM) ng/MO. Most (95.3% ± 3.3, SEM) of the MF in each gland was found in section I, with the remainder (4.7% ± 3.3, SEM) in section II. No MF was detected in sections III and IV.

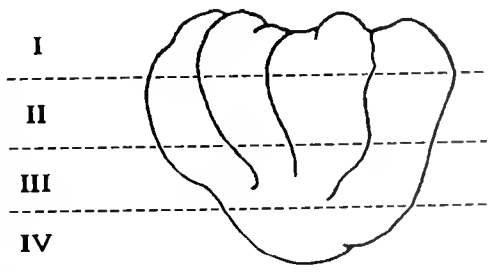

Figure 1. Drawing of the lobster mandibular organ (MO). In some experiments, glands were divided into the four sections (I–IV) indicated by the horizontal dashed lines. Each section was then extracted or incubated *in vitro*. The fan-folded edge of the gland is in section I.

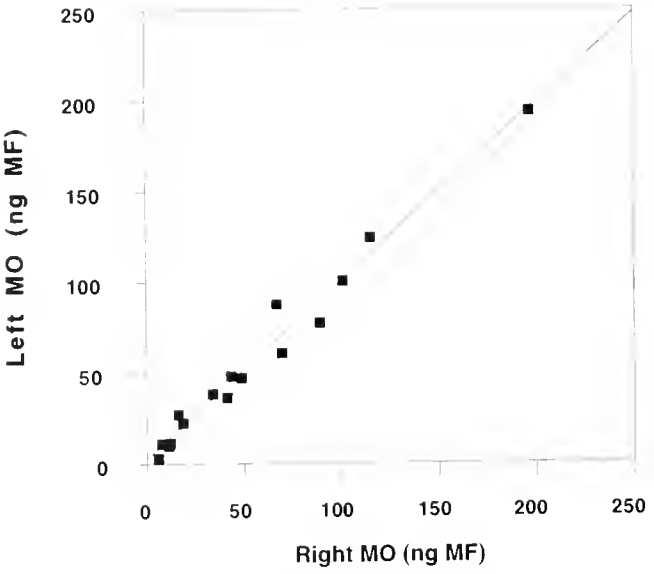

Figure 2. Symmetry of methyl farnesoate (MF) content in right and left MOs. Whole MOs were extracted and their MF content determined by normal phase high performance liquid chromatography (npHPLC). Each point indicates the MF content of the left and right MOs of a single animal (n = 16). The line represents the linear regression; r = 0.977 and the slope = .978.

Although the distribution of MF in freshly dissected MO suggested that MF was produced in the fan-folded region in eyestalk-intact animals, MF might have been produced elsewhere in the MO and then sequestered in the fan-folded region. Therefore, the contralateral MOs from the animals shown in Figure 3A were divided into sections and incubated separately in medium containing [^{3}H-*methyl*]methionine. After incubation, the MF content of each section and the MF released into the incubation medium were determined by npHPLC. The incorporation of radiolabeled methionine into MF was also determined in these samples.

The total MF content of these incubated MO sections was 170.7 (±36.7 SEM) ng/MO. Of this amount, 7.8% (±0.9, SEM) was released into the medium. Because the MF content of paired MOs from eyestalk-intact animals is similar (Fig. 1), the amount of MF produced during incubation was determined by subtracting the MF content of the unincubated contralateral glands (43.1 ng/MO). Thus, MF production during the 2-h incubation was approximately 128 ng/gland. Most (90.8% ± 4.7, SEM) of the MF contained in each incubated MO was found in section I, though small amounts were present in the other three sections (Fig. 3A). Thus, MF production during the incubation was largely restricted to the fan-folded region.

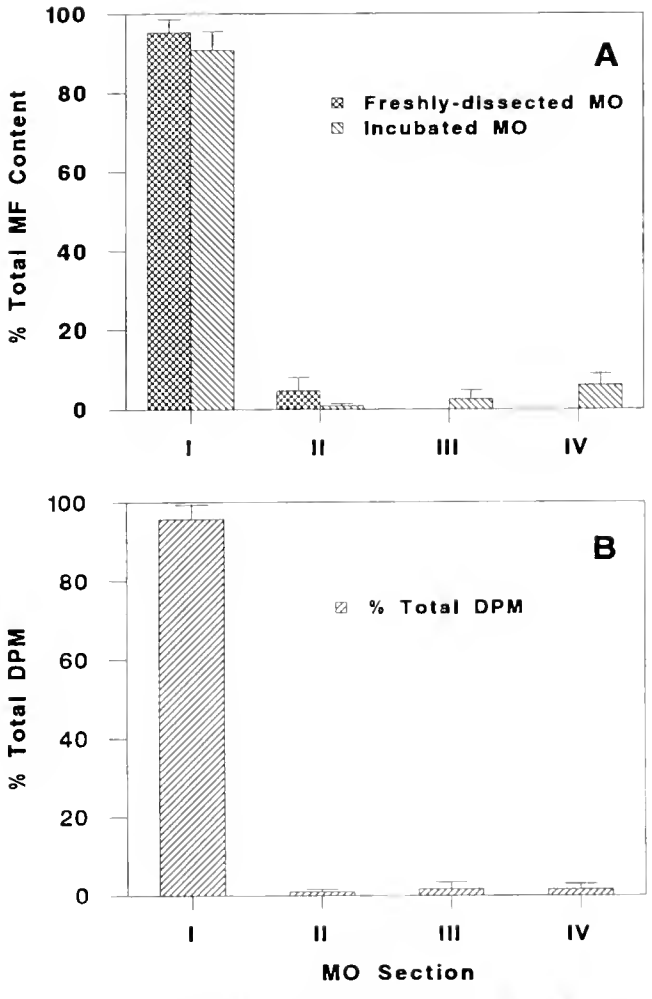

Figure 3. Regional distribution and synthesis of MF in MOs from eyestalk-intact lobsters. Both MOs from each animal (n = 4) were divided into four sections as in Figure 1. (A) MF content: Sections of the left MO were analyzed for MF content by npHPLC. The MF content of each section is expressed as a percentage of the total MF content of the MO (% Total MF Content). No MF was detectable in sections III and IV. Sections of the right gland were incubated individually for 2 hours in *Homarus* saline supplemented with [^{3}H-*methyl*]methionine. The MF content of each incubated section and its culture medium was also quantified by npHPLC and is displayed as a percentage of the total MF content of the incubated MO. (B) Radiolabel incorporation: The radiolabeled MF in the MO sections incubated above was calculated from the amount of radioactivity present in the fractions eluting with MF during npHPLC. Results are expressed as a percentage of the total radioactive MF produced by the gland (% Total DPM).

This conclusion was confirmed by analyzing the incorporation of [^{3}H-*methyl*]methionine into MF by the incubated MO sections (Fig. 3B). The total synthesis of radiolabeled MF by the MO sections was 66,600 (±17,760, SEM) DPM/gland. Of this amount, 14.3% (±3.1, SEM) was released into the medium. Most (95.7% ± 3.6, SEM) of the radiolabeled MF found in each MO was in section I, though small amounts were found in the other sections.

The production of radiolabeled MF was studied further by dividing the four MO sections from two animals into several (3 or 6) pieces. Each piece was then incubated with [^{3}H-*methyl*]methionine and MF synthesis determined. More than 99% of the radiolabeled MF was produced by pieces obtained from section I. Every piece produced MF, and those from the middle of this section produced the largest amounts (data not shown).

The distribution of MF was also determined in freshly dissected MOs from eyestalk-ablated animals (n = 4). The total MF content of these glands was 5,627 (±730, SEM) ng/gland, about 130-fold greater that the MF content of MOs from the group of eyestalk-intact animals ($P < .0001$; *t*-test). As in the intact animals, the MF content of MOs from the eyestalk-ablated animals was localized to the fan-folded region of the MO (Fig. 4). Most (74.3% ± 9.2, SEM) of the MF in each gland was found in section I; but a substantial amount (20.3% ± 9.0, SEM) was found in section II due to the enlargement of the fan-folded region. The other two sections contained only small amounts of MF (<4% each).

Histology

Light microscopy showed that the two regions of the MO contain different cell types. Two cell types (A and B) are found in the fan-folded region of the gland. A single cell type (C) predominates in the rest of the gland. The A cells are a minor cellular constituent of the fan-folded region and were not always seen. When present, they were found along the outer edge of the fan-folded region and

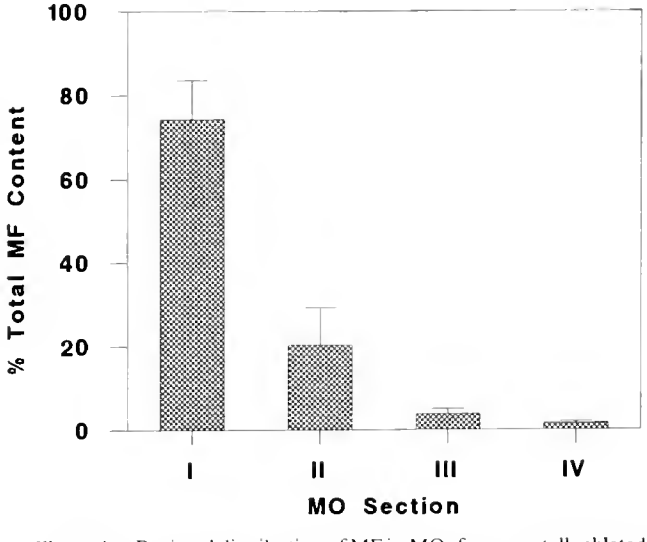

Figure 4. Regional distribution of MF in MOs from eyestalk-ablated lobsters. The left MOs from each animal (n = 4) were divided into four sections. Each section was analyzed for MF content by npHPLC. The MF content of each section is expressed as a percentage of the total MF content of the MO (% Total MF Content).

were arranged into cords. Of the three cell types, the A cells are the smallest and have the highest ratio of nuclear to cytoplasmic material (see Fig. 5). These cells frequently contain mitotic figures. Their nuclei are oval or irregularly shaped. The A cells have no distinguishing cytoplasmic features and may be relatively undifferentiated.

The B cells are the predominant cell type in the fan-folded region, extending from the interior of the gland to the A cells, when the latter are present. The B cells are larger than the A cells and have smaller nuclear-to-cytoplasmic ratios, reflecting an increase in cytoplasmic mass. Their nuclei are round or oval, and their cytoplasm contains many small vacuoles (Fig. 6). Situated between the A cells and the B cells are cells with characteristics intermediate to those of the A and B cells; they may be immature B cells.

The C cells are very large and have the smallest nuclear-to-cytoplasmic ratio (Fig. 7). Their nuclei are spherical, and their cytoplasm contains several distinct cytological features, including large vacuolar-like structures. In preliminary electron micrographs (not shown) these structures contain large masses of smooth endoplasmic reticulum. The cytoplasm of the C cells also contains many mitochondria, but relatively few small vacuoles.

Discussion

The gross morphology of the lobster MO suggests that the fan-folded edge is distinct from the rest of the gland. This was confirmed by the studies reported in this paper, which demonstrated that these two regions differ in both their biochemical and histological characteristics.

Biochemical studies showed that MF in unincubated MOs was localized in the fan-folded region of the MO. The possibility that this region is the site of MF synthesis was tested by determining the production of MF by individual MO sections *in vitro*. The MF measured in these sections was found largely in the fan-fold region, indicating that MF synthesis was occurring primarily in this region. The production of radiolabeled MF was also highest in this region. Taken together, these studies demonstrate that MF production is an important function of the fan-folded region of the MO.

The total MF content of the incubated MO sections was fourfold greater than that of the unincubated contralateral MO. Thus, the production of MF by the MO during incubation was substantial [63 ng (256 pmole) per hour]. This level falls within the range of synthetic rates observed previously for other species (Sagi *et al.*, 1991). About 8% of the MF present in the MO was released during the 2-h incubation, confirming reports by others (Tobe *et al.*, 1989; Ding and Tobe, 1991) that MF release by incubated MO is low. This low level of MF release *in vitro* stands in contrast to the apparent rapid release of MF by the MO *in vivo* (Tsukimura and Borst, 1992). Overall, these observations suggest that the mechanisms responsible for releasing MF are impaired during the *in vitro* incubation. We have previously shown that the percentage of MF released *in vitro* increases when MOs from *Libinia emarginata* were incubated in culture medium supplemented with hemolymph. Thus, the hemolymph of this crab appears to contain a factor that facilitates MF release (Borst *et al.*, 1990). Lobster MOs may require a similar factor for MF release.

Regional production of MF was also observed in MOs from eyestalk-ablated animals. Eyestalk ablation causes hypertrophy of the MO in several crustaceans (Byard, *et al.*, 1975; Hinsch, 1977; Le Roux, 1983) as well as an increase in MF synthesis by MOs (Laufer *et al.*, 1987). We have previously shown that eyestalk ablation has an acute effect on the MF content of lobster MOs, causing a 13-fold increase in MF content 2 days after eyestalk ablation (Tsukimura and Borst, 1992). This effect is confirmed and extended in this study, in which the MF content of the MO increased 130-fold in animals that were eyestalk ablated for 2 weeks. Nevertheless, the increase in MF content did not affect the distribution of MF in MOs. Thus, the rest of the gland does not represent reserve MF production capacity that can be activated when the gland is stimulated. These observations do not rule out the possible involvement of other glandular regions in the synthesis of MF precursors such as farnesoic acid.

Analysis of paired MOs from individual lobsters showed that the glands contain similar amounts of MF. This confirms and extends a previous study, in which the mean MF contents of right MOs and left MOs were statistically similar (Tsukimura and Borst, 1992). The symmetrical MF content of paired MOs was a critical prerequisite for measuring MF production during incubation.

The similar MF content of paired lobster MOs suggests that these glands produce MF at similar rates *in vivo*. In contrast, the *in vitro* biosynthesis of MF by paired MOs from the mud crab *Scylla serrata* and the crayfish *Procambarus clarkii* is asymmetric (Tobe *et al.*, 1989; Ding and Tobe, 1991). In addition, asymmetric biosynthesis of JH *in vitro* has also been observed in the corpora allata from several insect species (Tobe and Stay, 1985). However, such comparisons are difficult to interpret. The relationship of *in vitro* MF synthesis to the activity of the MO *in vivo* is not clear, because tissues incubated *in vitro* are no longer controlled by endogenous regulatory systems. For the lobster, this is particularly significant, because eyestalk factors can rapidly affect MF production by the MO (Tsukimura and Borst, 1992).

Our histological studies also show two distinct regions in the lobster MO. The fan-folded region contains two cell types. The physical relationship of these cells, as well as the presence of morphologically graded transitional

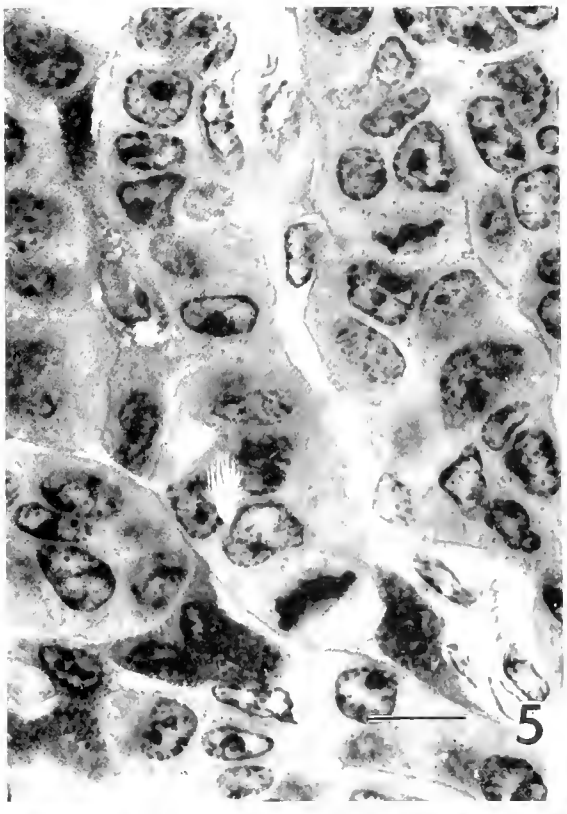

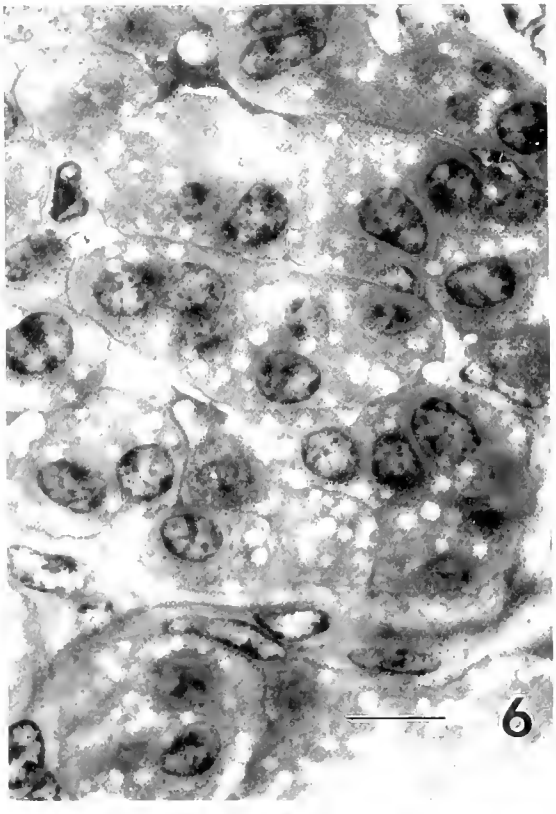

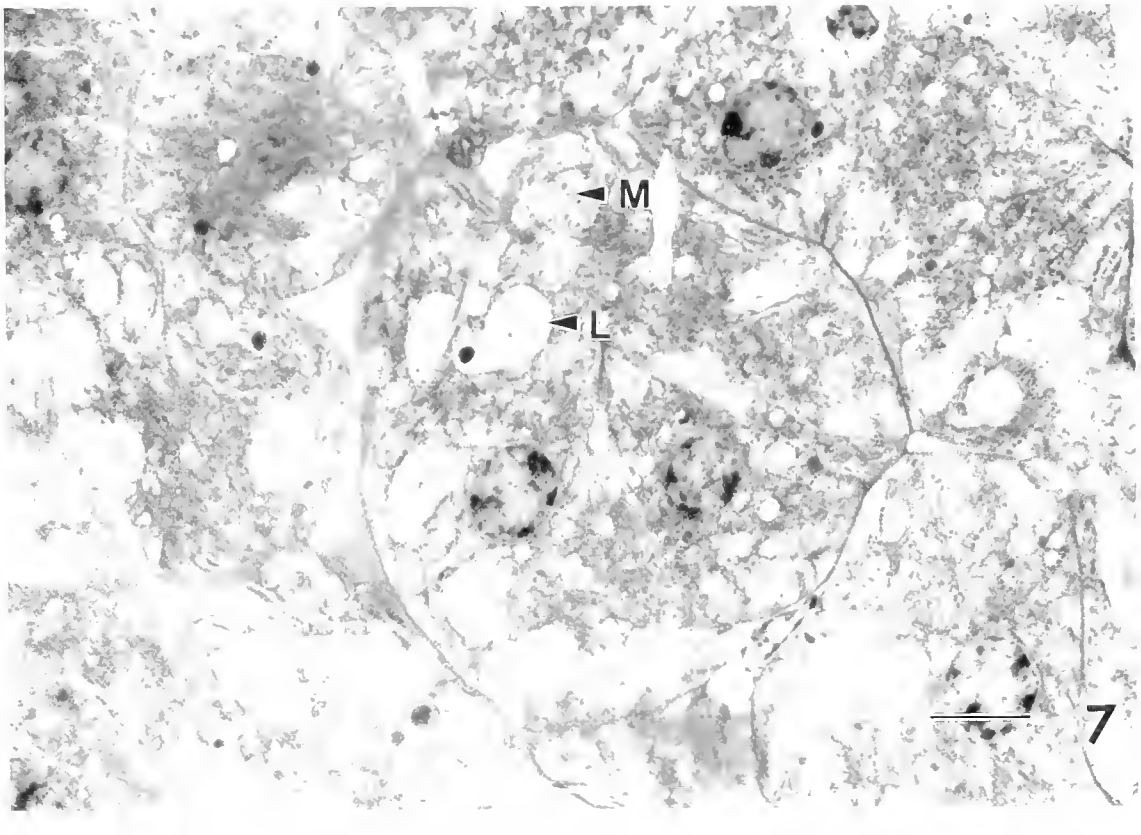

Figure 5. Light micrograph of A cells found in fan-folded region of the MO. Note arrangement of these cells into cords. The cells have irregularly shaped, small nuclei and a homogeneous cytoplasm. Mitotic figures are present. Scale = 5 μm.

forms, suggests that A cells provide the precursor cells that differentiate into B cells. Based on their morphological characteristics and location within the fan-folded region, the B cells are the most likely site of MF synthesis.

The rest of the gland contains predominantly C cells, whose function and relationship to the other two cell types are unknown. Preliminary ultrastructural studies suggest that these cells are active metabolically and may be involved in the synthesis of lipids or steroids. We speculate that they may be the sites of the progesterone metabolism previously reported in MOs from female lobsters (Couch *et al.*, 1987; Tsukimura, 1988). However, to the best of our knowledge MOs from male lobsters have never been investigated for the presence of this steroid. In any case, the lobster MO may have several products, so the physiological importance of this tissue may be complex.

The histological and biochemical complexity of the lobster MO was unexpected, partly because of the similarity between the MOs of other crustaceans and the CA of insects. In insects, the CA contains only one type of glandular cell (Tobe and Stay, 1985). Likewise, cytological observations of MOs from other crustaceans (Aoto *et al.*, 1974; Byard *et al.*, 1975; Demeusy, 1975; Hinsch and al Hajj, 1975; Hinsch, 1977; Buchholz and Adelung, 1980) also suggest that the glands are relatively homogeneous. MOs from adult female spider crabs, *L. emarginata*, have two cell types that differ in their staining properties, but have similar ultrastructural characteristics. In addition, there is no indication that these cells were regionally distributed in the MO of this species (Hinsch, 1981). Likewise, we found no evidence for regional distribution of MF synthesis in MOs from *L. emarginata* (Tsukimura, Martin, and Borst, unpub. data).

Our studies show that the lobster MO is more complex than the MOs of other species, containing at least three cell types localized in two areas of the gland. Thus, the lobster MO appears to be unique, and may represent the fusion of two tissues, one of which synthesizes MF and the other of which produces one or more other products.

Acknowledgments

This research was supported by grants to D.W.B. from the National Science Foundation (DCB-8919833) and the Illinois-Indiana Sea Grant (project #R/A-2) under the National Sea Grant College Program (COMM NA89AA-D-SG058) and to E.C. from the TCU Research Fund of Texas Christian University. This study is a publication of the Intensive Commercial Aquaculture Facility of Illinois State University. We thank Dr. J. K. Butler for his help in these studies, and express our appreciation for the helpful comments from two anonymous reviewers and the editors of this journal.

Literature Cited

Aoto, T., Y. Kamiguchi, and S. Hisano. 1974. Histological and ultrastructural studies on the Y organ and the mandibular organ of the freshwater prawn, *Palaemon paucidens*, with special reference to their relations with the molting cycle. *J. Fac. Sci. Hokkaido Univ.* **19:** 295–308.

Bennett, H. S., A. D. Wyrick, S. W. Lee, and H. J. McNeil, Jr. 1976. Science and art in preparing tissues embedded in plastic for light microscopy with special reference to glycol methacrylate, glass knives and simple stains. *Stain Technol.* **51:** 71–97.

Borst, D. W., and H. Laufer. 1990. Methyl farnesoate, a JH-like compound in crustaceans. Pp. 35–60 in *Recent Advances in Comparative Arthropod Morphology, Physiology, and Development*, A. F. Gupta, ed. Rutgers University Press, New Brunswick, NJ.

Borst, D. W., and B. Tsukimura. 1991. Quantification of methyl farnesoate levels in hemolymph by high-performance liquid chromatography. *J. Chromatogr.* **545:** 71–78.

Borst, D. W., H. Laufer, M. Landau, F. S. Chang, W. A. Hertz, F. C. Baker, and D. A. Schooley. 1987. Methyl farnesoate and its role in crustacean reproduction and development. *Insect Biochem.* **17:** 1123–1128.

Borst, D. W., C. G. Buerkett, and B. Tsukimura. 1990. Factors affecting methyl farnesoate release from mandibular organs (MOs) *in vitro*. *Am. Zool.* **30:** 29a.

Buchholz, C., and D. Adelung. 1980. The ultrastructural basis of steroid production in the y-organ and the mandibular organ of the crabs *Hemigrapsus nudus* (Dana) and *Carcinus maenas L. Cell Tiss. Res.* **206:** 83–94.

Butler, J. K. 1979. Methods for improved light microscope microtomy. *Stain Technol.* **54:** 53–69.

Butler, J. K. 1984. Improved methods for molding, facing, and sectioning of glycol methacrylate embedded tissue blocks. *Stain Technol.* **59:** 315–321.

Byard, E. H., R. R. Shivers, and D. E. Aiken. 1975. The mandibular organ of the lobster, *Homarus americanus*. *Cell Tiss. Res.* **162:** 13–22.

Cassier, P. 1979. The corpora allata of insects. *Int. Rev. Cytol.* **57:** 1–73.

Couch, E. F., N. Hagino, and J. W. Lee. 1987. Changes in estradiol and progesterone immunoreactivity in tissues of the lobster *Homarus americanus*, with developing and immature ovaries. *Comp. Biochem. Physiol.* **87A:** 765–770.

Demeusy, N. 1975. Observations sur le fonctionnement des glandes mandibulaires du Décapode brachyoure *Carcinus maenas L.*: animaux témoins et animaux sans pédoncules oculaires. *C. R. Acad. Sci. Paris* **281D:** 1887–1889.

Figure 6. Light micrograph of B cells in the fan-folded region. The nuclei of these cells are oval or round and larger than those of A cells. The B cells have a more abundant ground cytoplasm than A cells and contain many clear vacuoles. Scale = 5 μm.

Figure 7. Light micrograph of C cells in the unfolded region. Note the large spherical nuclei and large cytoplasmic volume of these cells. The cytoplasm is morphologically complex, containing many mitochondria (M), large vacuolar-like structures (L), and some clear vacuoles. Scale = 5 μm.

Ding, Q., and S. S. Tobe. 1991. Production of farnesoic acid and methyl farnesoate by mandibular organs of the crayfish, *Procambarus clarkii*. *Insect Biochem.* **21:** 285–291.

Hinsch, G. W. 1977. Fine structural changes in the mandibular gland of the male spider crab, *Libinia emarginata* following eyestalk ablation. *J. Morphol.* **154:** 307–316.

Hinsch, G. W. 1981. The mandibular organ of the female spider crab, *Libinia emarginata*, in immature, mature, and ovigerous crabs. *J. Morphol.* **168:** 181–187.

Hinsch, G. W., and H. al Hajj. 1975. The ecdysial gland of the spider crab, *Libinia emarginata L.* I. Ultrastructure of the gland in the male. *J. Morphol.* **145:** 179–188.

Karnovsky, M. J. 1965. A formaldehyde-glutaraldehyde fixative of high osmolarity for use in electron microscopy. *J. Cell Biol.* **27:** 137A.

Laufer, H., D. Borst, F. C. Carrasco, M. Sinkus, C. C. Renter, L. W. Tsai, and D. A. Schooley. 1987. Identification of a juvenile hormone-like compound in a crustacean. *Science* **235:** 202–205.

Le Roux, A. 1983. Réactions de l'organe mandibulaire à l'ablation des pédoncules oculaires chez les larves et les juvéniles de *Palaemonetes varians* (Leach) (Decapoda, Natantia). *C. R. Acad. Sci. Paris* **296D:** 697–700.

Sagi, A., E. Homola, and H. Laufer. 1991. Methyl farnesoate in the prawn *Macrobrachium rosenbergii*: synthesis by the mandibular organ *in vitro*, and titers in the hemolymph. *Comp. Biochem. Physiol.* **99B:** 879–882.

Tobe, S. S., and B. Stay. 1985. Structure and regulation of the corpus allatum. *Adv. Insect Physiol.* **18:** 305–432.

Tobe, S. S., D. A. Young, and H. W. Khoo. 1989. Production of methyl farnesoate by the mandibular organs of the mud crab, *Scylla serrata*: validation of a radiochemical assay. *Gen. Comp. Endocrinol.* **73:** 342–353.

Tsukimura, B. 1988. The role of presumptive mandibular organ secretions in ovarian growth of the shrimp, *Penaeus vannamei*. Ph.D. dissertation, University of Hawaii.

Tsukimura, B., and D. W. Borst. 1992. Regulation of methyl farnesoate levels in the lobster, *Homarus americanus*. *Gen. Comp. Endocrinol.* **86:** 297–303.

Welsh, J. H., and R. I. Smith. 1960. Pp. 159–160 in *Invertebrate Physiology*. Burgess Publishing Co., Minneapolis, MN.

Reference: *Biol. Bull.* **186:** 17–28. (February, 1994)

Sperm Diffusion Models and *In Situ* Confirmation of Long-Distance Fertilization in the Free-Spawning Asteroid *Acanthaster planci*

R. C. BABCOCK[1,*], C. N. MUNDY[1], AND D. WHITEHEAD[2]

[1]*Australian Institute of Marine Science, PMB No. 3, Townsville MC, 4810, Australia, and*
[2]*2483 East 26th Ave., Vancouver, British Columbia, Canada V5R 1K6*

Abstract. This study was undertaken to compare fertilization rates of the sea star *Acanthaster planci* that were predicted using sperm diffusion models with those that were determined under natural conditions in the field. During experimentally induced spawnings, measured fertilization rates for broadcast eggs were high. More than 70% of the eggs were fertilized at distances as great as 8 m downstream from a single spawning male starfish, and more than 20% were fertilized at separations of more than 60 m. Fertilization was still measurable, at 5.8%, 100 m downstream. Lateral diffusion of sperm away from the axis of flow produced fertilization rates of 13.8% at 8 m normal to the flow and 32 m downstream. The large volumes of sperm released by male *A. planci* are the primary cause of high rates of fertilization for eggs derived from widely spaced individuals. Models of sperm diffusion using high sperm release rates such as those found in this starfish accurately confirmed the fertilization rates measured *in situ* for two populations of *A. planci* with widely differing rates of sperm release.

We observed some changes in starfish density and degree of aggregation in the study population for spawning periods during two spawning seasons, though these were not striking. High levels of aggregation may not be necessary for fertilization success in this starfish, due to the potential for long-distance fertilization and the probability that, for any spawning starfish, the total number of zygotes formed will be greater at some distance from the point of spawning. Although fertilization rates in areas distant from the sperm source were relatively low, the total area for potential gamete encounters is much greater and may make a large contribution to net fertilization. We predict that other behaviors, such as migration to shallow water, commonly associated with spawning in *A. planci* and other marine invertebrates will have measurable impacts on fertilization success.

The potential for high levels of fertilization in *A. planci* was realized during natural spawnings. Fertilization rates as high as 99% were recorded when levels of spawning synchrony were high.

Received 10 December 1992; accepted 30 August 1993.

* Current address: University of Auckland Leigh Marine Laboratory, P.O. Box 349, Warkworth, New Zealand.

AIMS Contribution 658.

Introduction

Do free-spawning marine invertebrates ever achieve high rates of fertilization? Attempts to answer this question have increased in frequency and taken a variety of forms, most of which use echinoderms as conceptual and empirical models. The question arises for two main reasons. First, many—perhaps even most—observations of natural spawning have involved isolated or lone individuals (usually males) or only a small proportion of the population present. This is true for echinoids (*Diadema:* Randall *et al.*, 1964; Levitan, 1988; *Strongylocentrotus:* Pennington, 1985, Pearse *et al.*, 1988), holothuroids (Mosher, 1982; McEuen, 1988; Pearse *et al.*, 1988), and asteroids (Minchin, 1987; Pearse *et al.*, 1988; Babcock and Mundy, 1992; Gladstone, 1992). Similar behaviors have also been noted for other groups such as tridacnid clams (Braley, 1984) and sponges (Reiswig, 1970). Second, experimental studies of *in situ* fertilization rates for free-spawning species show that fertilization can be very low or even fail completely unless animals spawn with a high degree of synchrony and are in extremely close proximity (<1 m) during spawning (Pennington, 1985; Levitan, 1991, Levitan *et*

al., 1992). Numerical modeling studies of sperm diffusion support these empirical results by predicting that concentrations of sperm will be too low to effect high levels of fertilization except when animals are close together (Denny and Shibata, 1989).

Nevertheless, the continued existence of thousands of such species in the seas today suggests that high levels of fertilization can, and do, occur in free-spawning marine invertebrates. It seems unlikely that so much effort would be devoted to gamete production instead of other functions if all the gametes were to be wasted. The strongest evidence that high rates of fertilization can be commonplace is indirect, coming from the evolution of a wide variety of mechanisms to prevent polyspermy (*e.g.*, echinoids: Scheul, 1984). Although most observations have been of asynchronous or isolated spawnings, virtually all of the taxa listed above have been observed in the act of large-scale synchronous spawnings (Hoppe and Reichert, 1987; Reiswig, 1970; Pennington, 1985; Babcock and Mundy, 1992; McEuen, 1988; Minchin, 1987). Such large-scale synchronous spawnings are likely to be much more important to the reproductive output of the population than indicated by their low frequency.

For free-spawning marine organisms to attain high levels of fertilization, the numbers or concentration of viable sperm adjacent to eggs must be above a certain level. Two types of adult behavior, synchronization of spawning and aggregation of reproductive adults, can increase the concentration of sperm in space and time. A third strategy is to increase sperm output. Levitan (1991) postulated that, in terms of zygote production, "small organisms living at high population density may be just as fecund as large organisms living at low population density." That study was unable to demonstrate any effect of adult size on fertilization rate, though adult density was shown to have a major influence, with success ranging from 7.3% (with 1 male per square meter), to 45% (with 16 males per square meter).

Our study of *in situ* fertilization rates concentrated on the crown-of-thorns starfish, *Acanthaster planci*. This large (25–40 cm diameter), highly fecund asteroid is characterized by population outbreaks that have impacted large areas of coral reef throughout the Indo-Pacific region over the last 30 years (Moran, 1986). Several hypotheses have been formulated to explain these outbreaks. One set of theories proposes that they are a natural result of enhanced reproductive success of starfish in aggregations (Dana, 1970; Vine, 1970; Moore, 1978). Such aggregations can form naturally as a result of feeding behavior (Ormond *et al.*, 1973) or environmental disturbances such as cyclones (Dana, 1970). Recent measurements of fertilization rates for *A. planci* suggest that the reproductive biology of *Acanthaster* populations may have unusual aspects that contribute to periodic huge increases in abundance. Fertilization rates greater than 20% have been reported for eggs released 64 m downstream from a single spawning male *Acanthaster* (Babcock and Mundy, 1992). This level of fertilization is approximately equivalent to that found for spawning sea urchins at distances of less than 1 m (Pennington, 1985; Levitan, 1991). The scale at which *A. planci* is able to maintain reproductive contact is two orders of magnitude greater than that reported for urchins or any other marine invertebrates (*e.g.*, hydroids: Yund, 1990; ascidians: Grosberg, 1991). The source of this difference could lie either in the greater size of *Acanthaster* and the large mass of gametes it releases (Babcock and Mundy, 1992) or in the physiology of the gametes.

We observed individuals in a population of starfish over two spawning seasons in an effort to determine whether, over the course of the spawning season, there were any differences in vertical distribution, degree of aggregation, or other factors that might enhance fertilization rates. Natural spawning events gave us an opportunity to measure fertilization rates *in situ* and assess the importance of spawning synchrony to fertilization success.

Combining empirical and modeling approaches, we attempted to determine whether number of gametes alone could adequately explain the ability of *Acanthaster* to fertilize at great distances. We also observed a natural population to assess how the results of modeling studies could be related to natural spawning behavior. In a series of field trials, we examined the effects of population density on fertilization success, and compared these directly with the results of modeling studies.

Materials and Methods

Behavioral observations

The population of starfish at Davies Reef (Lat. 18°50′ S, Long. 147°39′ E) in the central Great Barrier Reef was regularly sampled and observed visually over two spawning seasons (December–January) of 1990–91 and 1991–92. The observation site was in the lagoon of the reef, adjacent to the site of the fertilization experiments. Depths varied between 1 and 10 m, and many coral heads and patch reefs with abundant live coral were present. A belt transect 200 m long, 10 m wide and divided into 10 quadrats of equal size (20 m × 10 m) was established in the area. The number and behavior (spawning/not spawning) of starfish in each quadrat on the transect were recorded on 60 occasions (20 at night). A total of 214 dives (55 at night) were made on this population in the course of collecting these data and while making general observations or conducting fertilization experiments. All natural spawnings of *Acanthaster* were noted and, when females were observed spawning, eggs were collected to enable us to measure natural fertilization rates.

Induced spawning experiments

Rather than manipulating the density of populations (Levitan *et al.*, 1991), we varied the distance between spawning pairs of male and female starfish *in situ*, both along the direction of the current and normal to it. The low density of the starfish in the field and the large scale over which the experiment had to be conducted were logistic reasons for using pairs of animals rather than arrays of spawning animals. Currents prevailing during the experiments were of a sufficient velocity (0.07–0.25 $m \cdot s^{-1}$) that the major effects were likely to be observed downstream (Babcock and Mundy, 1992). The sex of animals to be used in the trials was determined in advance with a syringe and 14-gauge needle. Each animal was injected with 20–30 ml 10^{-4} *M* 1-methyl adenine to induce spawning. Because they reacted more slowly, females were treated approximately 10–15 min before males. Most of the fertilization trials took place at Davies Reef in 1991–92; however an additional set of trials was run in June 1991 at Sesoko Island, Okinawa, and a few trials using increased numbers of spawning male starfish were also conducted at Davies Reef late in the 1991–92 spawning season.

Immediately after the starfish were injected with methyl adenine, current direction was determined by release of fluorescein dye. The male starfish was placed at the point of dye release and the female was moved a predetermined distance directly downstream. Divers monitored the male starfish, and released extra dye when sperm release was fully under way. Sampling of eggs commenced when the dye cloud reached the female, or as soon thereafter as the female began releasing eggs. The spawning female was incrementally moved upstream from the most distant sampling point, and eggs were sampled at progressively smaller distances downstream from the spawning male. Sampling points in the trials were 100 m, 64 m, 32 m, 16 m, 8 m, 4 m, 2 m, 0 m (adjacent downstream), as well as −4 m and −8 m (upstream). The exact sampling routine in each trial varied because it was not possible to sample every position each time. This sampling strategy allowed us to measure the effect of sperm transport and diffusion in a direct downstream direction. Starfish were also deployed on a grid of coordinates at various distances perpendicular to the flow to allow measurement of the effects of lateral sperm diffusion. At distances of 32, 16, 8, 4, 0, and −4 m, an additional series of samples was taken from females at varying distances normal to the flow (16, 8, 4, 2, and 0 m). Samples at Sesoko Island were taken only along the direct downstream vector, up to a distance of 32 m. In all cases, sampling was begun at the most distant point downstream and proceeded upstream past the spawning male animal, the last point acting as a sperm-free control. Immediately before and after each spawning trial, current speed was measured using a tape, neutrally buoyant markers, and a stopwatch. The trials were planned so that the current would flow in a consistent direction for the duration of the trial.

Samples of eggs were collected using a submersible plankton pump equipped with 64-μm-mesh filter cartridges (Babcock and Mundy, 1992) that allowed the collection of 12 individually metered samples (1–21) during each trial. Once collected, these samples were completely isolated from water outside by means of one-way valves. Trials of this device demonstrated that neither the volume of water pumped through the filter cartridges (48 trials ranging from 0.5 to 3 l, $R^2 = 0.02$) nor the period of time eggs remained in contact with the water sample (2 min to about 1 h, $p = 0.95$), affected the eventual level of fertilization (Mundy *et al.*, unpublished data). Two samples were taken at each sampling point and preserved at the termination of the experiment. Fertilization of a subsample of the eggs was then scored in the laboratory.

Individual *A. planci* from both Davies Reef and Sesoko Island were sampled to determine the mean size and mean gonad weight of the two populations. To estimate the average mass of gametes spawned by Davies Reef starfish, we used mean gonad weights for the population immediately before and after natural spawning events observed on Davies Reef in 1990 and 1991.

Sperm diffusion modeling

The shedding of sperm into a flow was modeled as a plume diffusion problem in which the concentration of particles downstream from a point source was described under a set of simplifying assumptions (Csanady, 1973; Denny and Shibata, 1989). In this model the water column is assumed to be moving at a mean velocity $\bar{U}$ parallel to the x-axis within a turbulent benthic boundary layer. A point source shedding sperm at a constant rate Q_S located at the x, y origin, at a distance h, above the substratum gives a function for the concentration of *A. planci* sperm S,

$$S(x, y, z) = \frac{Q_s}{2\pi \bar{U} \sigma_y \sigma_z} \exp \frac{-(y^2)}{2\sigma_y^2} \times \left\{ \exp \frac{-(z+h)}{2\sigma_z^2} + \exp \frac{-(z-h)}{2\sigma_z^2} \right\} \quad \text{Eq. 1.}$$

where the spatial standard deviations for diffusion are modeled by the functions

$$\sigma_y = \alpha_y \left(\frac{u^*}{\bar{U}} \right) x^\beta \quad \text{Eq. 2.}$$

$$\sigma_z = \alpha_z \left(\frac{u^*}{\bar{U}} \right) x^\beta \quad \text{Eq. 3.}$$

The values for the empirically determined diffusion parameters α_y, α_z describe the shape of the plume, and β describes the rate of growth of the eddies acting to disperse the plume as it spreads out. Without separate data from which to determine the α_z, α_y and β parameters, it was necessary to estimate their values by fitting the model to the fertilization success data. Ranges for suitable values of the plume shape parameters were suggested by Denny (1988). He suggested ranges of 0.5 to 3 for α_z, 1 to 3 for the ratio α_y/α_z, and 0.9 to 1.33 for β. The shear velocity u^* is a function of the Reynold's shear stress and is taken to be a measure of the turbulence intensity. It is used to describe the mean distance a particle is moved by the turbulent eddies over a small interval of time. The calculation of real values for the shear velocity is beyond the scope of this simple model, and we have adopted the values cited by Denny (1988) where the shear velocity is a constant fraction (10%) of the mean velocity.

At shallow depths the upper surface boundary is likely to play a significant role by restricting the dispersion of gametes. The original model (Csanady, 1973) was designed to work for atmospheric dispersion, recognising only a lower boundary to the flow. Given the depth of water at the field site (7 m) and the scale at which the effects of sperm diffusion were observed (100 m), it was necessary to include a term describing surface reflection. By adding a mirror source located above the sea-surface boundary, we reflect any sperm that diffuses as far as the surface back into the flow. In water of depth D, the resultant sperm concentration is

$$S = \frac{Q_s}{2\pi \bar{U}\sigma_y\sigma_z} \exp\frac{-(y^2)}{2\sigma_y^2}\left\{\exp\frac{-(z+h)^2}{2\sigma_z^2} + \exp\frac{-(z-h)^2}{2\sigma_z^2} + \exp\frac{-[(2D-z-h)]^2}{2\sigma_z^2}\right\} \quad \text{Eq. 4.}$$

By calculating the probability of sperm colliding with ova (Vogel *et al.*, 1982; Denny and Shibata, 1989), the percent fertilization success at a point is determined from the sperm concentrations.

$$F(x, y, z) = 1 - \exp(-\phi t u^* S) \quad \text{Eq. 5.}$$

The shear velocity is used as a measure of the distance a sperm travels in unit time. Time t is the time spent observing collisions at a point. The area ϕ is ~3% of the cross-sectional area (*cf.* Levitan *et al.*, 1992) of an unfertilized *A. planci* egg 0.2 mm in diameter or approximately 9.42×10^{-10} m^2. Because shear velocity is assumed to be a constant fraction of the mean velocity, all the velocity terms in the calculation of fertility success reduce to a constant. Although the calculated sperm concentrations vary with flow velocity, this variation is canceled by the u^* term in the calculation of fertilization success. This shortcoming could be remedied through models that better relate shear velocity to flow velocity and by empirically relating fertilization success to sperm concentration.

Denny and Shibata (1989) followed a cohort of sperm and ova as it advected downstream. By iterating simultaneous differential equations for the concentrations of sperm and ova and calculating the predicted fertilization rate in a closed vessel (Vogel *et al.*, 1982), they were able to estimate fertilization rates and compare the results of their model with those of Pennington (1985) for *Strongylocentrotus*. Fertilization success for *A. planci* was measured by sampling eggs over a period of about 30 s (the time taken to sample 1–2 l water). In terms of our model, concentration and fertilization are calculated at discrete positions, with each point experiencing relatively constant sperm concentrations over the time taken to sample the eggs. We have not modeled the dispersion of ova, since sampling was in the free flow immediately downstream from spawning females. It is assumed that the ratio of sperm to ova is sufficient to ensure that the concentration of eggs has a negligible effect on the results. Because most fertilization is likely to take place in open water over the female starfish, very soon after the eggs and sperm mix (90% in the first 20 s; Denny and Shibata, 1988), we used the equation appropriate for estimating sperm-egg collisions in a turbulent flow, rather than that for an enclosed vessel (*i.e.*, Denny and Shibata 1988, p. 880).

Data collected from our *A. planci* population at Davies Reef before and after natural spawnings during the 1990–91 and 1991–92 spawning season (Babcock and Mundy, 1992; and unpublished data) gave an average gamete release for males of 60–106 g, shed over about 45 min. These values are about one-third of the prespawning gonad mass. We estimated the amount of gonad spawned by male starfish at Sesoko Island as 14 g, based on shedding of one-third of the gonad and measurements of total gonad weight. Male starfish from Davies Reef were 2.8 times larger than those at Sesoko Island (mean whole wet-weights; Davies Reef 2220 g, Sesoko Island 780 g). Assuming that the concentration of undiluted *A. planci* sperm is equal to that of urchin sperm (2×10^{16} sperm · m^{-3}; Tyler *et al.*, 1956) and that the sperm are essentially neutrally buoyant, the release rate, Qs, of sperm is 4.44–7.84 $\times 10^8$ sperm · s^{-1}. We used a mean sperm release rate per animal of 6.14×10^8 sperm · s^{-1} for Davies Reef starfish, and 1.5×10^8 sperm · s^{-1} for Sesoko Island starfish.

The model assumes a constant flow velocity throughout the water column. Flow velocities recorded at the field site during experiments ranged from 0.07 to 0.25 m · s^{-1} with a mean velocity $\bar{U}$ of 0.12 m · s^{-1}. The high degree of mixing in a turbulent boundary layer allows us to make this assumption except near the substratum, where the assumption fails because the flow velocity must reduce to zero. It is assumed that sampling takes place far enough

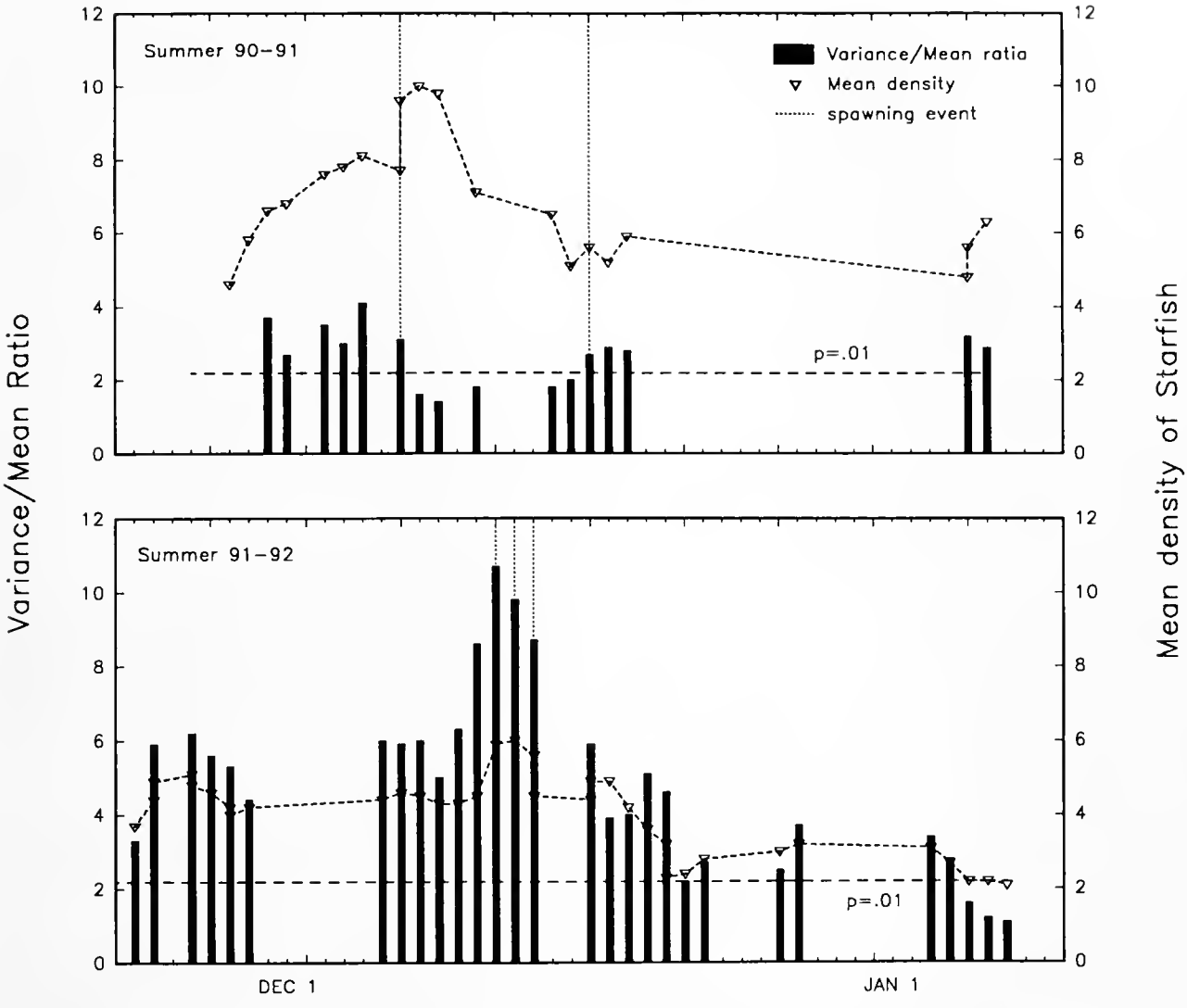

Figure 1. Starfish number and degree of aggregation for *Acanthaster planci* at Davies Reef. Variance/mean ratios (aggregation index) are calculated from counts of starfish along a 200 × 10 m belt transect during December and January of 1990–91 and 1991–92. Data for both counts and aggregation index are presented as three-point running means. Dates of spawning are indicated by vertical dotted lines. The 0.01 significance level for the aggregation index is taken from the table of Chi-square values; df = 9. Dates of observed natural spawnings: 1991; Dec 7 (38 females, 50 males), Dec 17 (three males). 1992; Dec 11 (1 female, 2 males), Dec 12 (2 females, 6 males), Dec 13 (1 male). 1992; Jan 23 (2 males [not included in figure]).

above the substratum to avoid any significant velocity gradient. The model assumes a smooth bottom and is unable to deal with the complex flow around corals that intrude into the flow. Such corals tend to slow and redirect the flow passing around them, generating turbulence. The turbulence would have the beneficial effect, in terms of the model, of smoothing the flow velocity variation within the water column. For the purposes of the model, it is assumed that the "bottom" is situated at a theoretical level just above the region where most of the coralline disturbance to the flow takes place. We also assume that both the male and female are positioned 0.5 m above this bottom. In terms of the experiment, this assumption is reasonable because the spawning starfish were placed on top of outcroppings, at heights between 0.5 and 1.5 m above the substratum.

The field site for the fertilization experiments was a 100 m channel, about 7 m deep and 35 m wide, between two large patch reefs within the lagoon at Davies Reef. The bottom was sandy, with many coral outcroppings between 0.5 m and 2 m in height. The bottom of the site at Sesoko Island was similar; however the site was at the

Table I

Field fertilization rates for A. planci: *Percent fertilization, plus or minus standard error, and sample size (n) for experimentally induced spawnings in which eggs were collected at varying distances from spawning male starfish*

	Davies Reef						Sesoko Island
	Single male					5 males	Single male
	Distance offset from directly downstream (m)						
Distance male to female (m)	0	2	4	8	16	0	0
−8	$0.7^{\pm 3.3}$ (6)	—	—	—	—	$2.5^{\pm 1.5}$ (8)	—
−4	$16.1^{\pm 3.0}$ (50)	—	—	—	—	—	—
0	$90.1^{\pm 2.1}$ (60)	—	$0.5^{\pm 0.9}$ (4)	0	0	$98.7^{\pm 0.4}$ (9)	$75.6^{\pm 1.9}$ (27)
2	$86.5^{\pm 2.6}$ (12)	—	—	—	—	—	$47.2^{\pm 10.3}$ (9)
4	$71.8^{\pm 8.4}$ (10)	$10.7^{\pm 5.7}$ (2)	0	0	—	—	$48.6^{\pm 5.0}$ (21)
8	$71.9^{\pm 9.5}$ (15)	$80.3^{\pm 7.6}$ (10)	$29.5^{\pm 8.1}$ (19)	—	—	—	$38.9^{\pm 4.3}$ (24)
16	$41.5^{\pm 5.2}$ (32)	—	$39.1^{\pm 11.7}$ (10)	$4.1^{\pm 2.1}$ (18)	—	$33.7^{\pm 4.7}$ (10)	$25.9^{\pm 3.8}$ (21)
32	$26.8^{\pm 3.9}$ (37)	—	$31.9^{\pm 10.3}$ (10)	$13.8^{\pm 7.6}$ (10)	$2.6^{\pm 1.4}$ (10)	$30.2^{\pm 5.0}$ (10)	$16.7^{\pm 3.9}$ (12)
64	$20.5^{\pm 5.8}$ (16)	—	—	—	—	$23.8^{\pm 5.0}$ (9)	—
100	$5.8^{\pm 1.4}$ (11)	—	—	—	—	$19.6^{\pm 4.8}$ (11)	—

Positive values indicate downstream positions; negative values indicate female starfish upstream of spawning male.

bottom of the outer reef slope (5 m), with currents traveling parallel to the reef front and thus bounded only on one side.

Results

Behavioral observations

We observed natural spawnings of *Acanthaster* on six occasions during the summers of 1990–91 and 1991–92 (Fig. 1). Of the four spawnings seen in 1991–92, females released eggs on only one occasion, 12 December 1991, when eight starfish (six male and two female) were observed, probably at the end of a spawning event involving many more animals. Fertilization rates in the eggs sampled directly downstream from a spawning female averaged 99%. We obtained egg samples from an additional two spawnings seen in 1990. Fertilizations ranged from 83%, during the peak of a large spawning, to 23%, at the end of spawning or during a minor spawning (details in Babcock and Mundy, 1992). Density of starfish on the study site and the degree of aggregation varied during each spawning season (Fig. 1). In both seasons the highest densities of starfish were counted on and around times when major spawnings were seen. It was not possible to determine where the additional animals came from, but it is likely that the changes in abundance were a result of animals being less cryptic around the time of spawning, rather than any more specific movement of the population. Variance/mean ratios were higher in the weeks prior to or during the first major spawnings, indicating a greater tendency to aggregate, than they were later in the season when most of the spawning had already taken place. Although the population showed a significant level of aggregation during most of the surveys, the frequency of such observations was lower after spawning.

Induced spawning experiments

Fertilization rates for single female starfish at Davies Reef were still at detectable levels (5.8%) 100 m directly downstream from spawning male starfish, and were higher than 20% at 32 m and 64 m. For adjacent starfish, mean fertilization rates were 90.3%, but dropped to 16% at 4 m up-

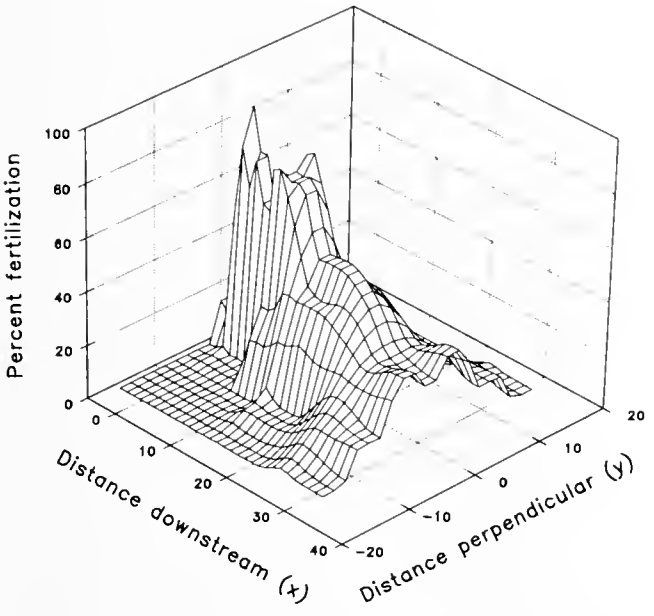

Figure 2. Three-dimensional representation of observed mean fertilization rates for *Acanthaster planci* at Davies Reef. Values used were means obtained from Table I for variations in fertilization at a range of coordinates surrounding a spawning male starfish. Current flows from left to right along the downstream (x) axis. (Missing data points interpolated using graphics features of SigmaPlot 5.)

stream, and to 0.7% at 8 m upstream (Table I). Fertilization rates dropped more rapidly as female starfish were moved away from the direct downstream (x) axis (Fig. 2). For example, no fertilization was recorded at 4 m downstream and 4 m normal, but at 8 m downstream, the sperm plume had diffused outward to the extent that mean fertilization was 29.5% at 4 m normal to the downstream axis. At 32 m downstream, fertilization was still measurable (2.6%) at 16 m perpendicular to the direct downstream axis, rising to 13.8% at 8 m and 31.9% at 4 m perpendicular.

For trials with more than one starfish, fertilization rates were expected to be higher than for single starfish at corresponding distances (Table I). This was not always the case, however, partly because these trials were conducted later in the season when the starfish had smaller gonads and partly because of the variability related to smaller sample sizes. Nevertheless, the average fertilization rate at 100 m downstream was 21.8% when five male starfish were induced to spawn. The maximum fertilization rate recorded at 100 m in trials with five males was 42%. Fertilization rates from starfish at Sesoko Island were lower than those from starfish at Davies Reef at equivalent distances downstream (Table I).

Effects of current speed on observed fertilization rates were slight and not significant over the range of current speeds experienced (Stepwise regression. Distance downstream: partial $r^2 = 0.521$, $F = 129.5$, $p = .0001$. Current velocity: partial $r^2 = .014$, $F = 3.5$, $p = .063$). Trials in which currents reversed during the course of the experiment were not included in this analysis.

Sperm diffusion modeling

Diffusion coefficients. In order to determine the plume coefficients α_z, α_y and β, we concentrated on matching the model prediction to the results recorded along the axis 4 m ($y = 4$) to the side of the flow axis (Table I). By fitting the model to this more complex data set, which contained rising then falling values, we were able to obtain a more satisfactory set of coefficients to describe the diffusion of the plume than if we had used $y = 0$.

The model's predictions were found to be most sensitive to the β value. In general, the lower the β value the flatter the curve and the closer the sets of parameters matched. Because the range of values suggested by Denny and Shibata was for a model without a sea-surface boundary, we decided that a small deviation from these values would be acceptable. Values of $\beta = 0.5$, $\alpha_z = 0.65$, and $\alpha_y = 1.15$ were selected as the set of parameters that best matched the model to the data while remaining within an acceptable range for the values. Levels of turbulence and diffusion experienced in the lagoon of Davies Reef are likely to be lower than those used by Denny and Shibata (1989), whose model described extremely turbulent surf zones.

Separation distance (x, y). Comparing the model to the measured data (Fig. 3) reveals a fit that we believe is a reasonable enough representation of actual sperm diffusion to permit discussion of the model's behavior in more general terms. At short distances from the origin, predicted values were slightly higher than those we observed in our samples. This discrepancy could be an artifact of the use of induced spawnings if some of the eggs that were shed

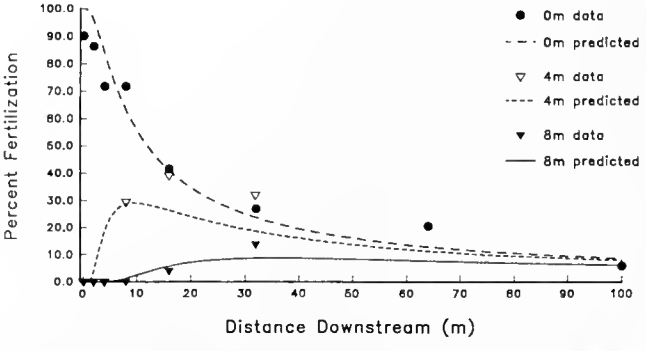

Figure 3. Observed and predicted mean fertilization rates for starfish at Davies Reef. Data points are from Table I, 0, 4, and 8 m offset from direct downstream axis. Predicted values are those derived using values that provided the best fit to data 4 m offset from x axis ($y = 4$). $\alpha_y = 1.15$; $\alpha_z = 0.65$; $\beta = 0.5$; $Qs = 6.14 \times 10^8$; $\phi = 9.42 \times 10^{-10}$; $U = 0.12\ \mathrm{m \cdot s^{-1}}$; $u^* = 0.1$; Depth = 7 m; release height $h = 0.5$ m; vertical separation $z = 0.5$ m.

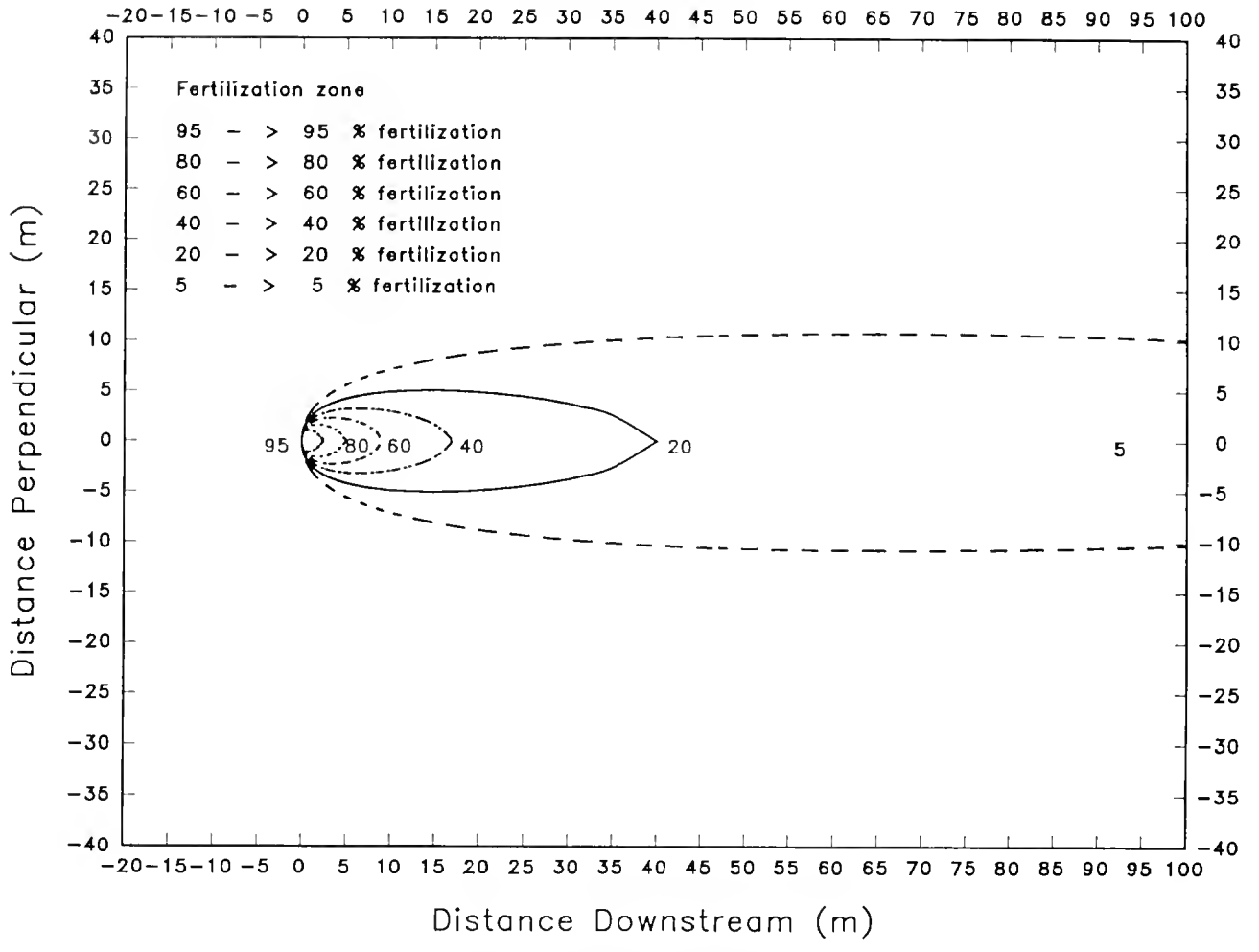

Figure 4. Fertilization contours for eggs released in a field downstream from a spawning male starfish. Parameters for model as for Figure 3. *Y*-coordinates for different fertilization rates were determined by substituting the relevant levels of fertilization in Eq. 5, and solving for *y*. Current flow is along the *x* axis from left to right. Fertilization zone contours correspond to 5 > 5%, 20 > 20%, 40 > 40%, 60 > 60%, 80 > 80%, and 95 > 95%.

were not mature and lacked the potential to be fertilized; inhibition of fertilization by high concentrations of fluorescein is also a possibility (Finkel *et al.*, 1981). Further from the origin the predicted values are generally lower than observed values. We also predicted fertilization success in two dimensions over the floor of the reef, producing contour maps of predicted fertilization success (Fig. 4). According to the model, fertilization will be greater than 5% within a long narrow plume region reaching out past 100 m downstream of the source, but the plume will only spread to a distance of about 15 m each side of the source. At 30 m downstream, 20–40% of the eggs of a spawning female would be fertilized, and at downstream separations less than 5 m, more than 80% of the ova would be fertilized, indicating that the success of spawning exhibits relatively low sensitivity to downstream separation when the starfish are aligned along the flow axis. These predictions agree well with our observations (Table 1), providing an excellent correlation between observed means for field data and median values for predicted data points (Spearman rank correlation $r_s = .82$, $p < .0005$, $n = 23$).

Water depth (z). In water shallower than 20 m, where *A. planci* are likely to be found, the plume is confined between the surface and the sea floor. As the depth of water increases, the plume is able to disperse through a greater volume, and reflection of sperm from the surface takes longer to occur. Because of this, vertical separation of spawning animals will have an increasingly detrimental effect on fertilization success as depth increases (Fig. 5). In an animal such as *Acanthaster* that has the capacity to effect fertilization at distances that are large relative to total water depth, the presence of a term describing reflection from the surface is essential to an understanding of the effect of water depth on fertilization rate.

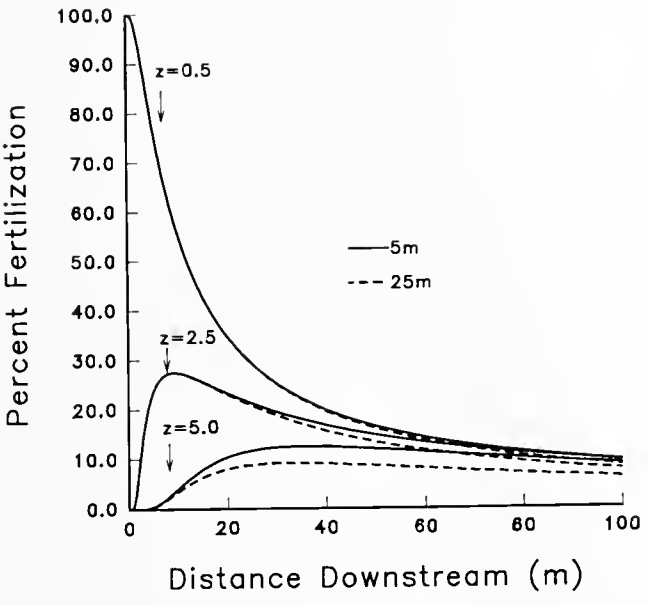

Figure 5. Predicted effects of depth and vertical separation on predicted fertilization rates. Diffusion parameters as for Figure 3.

Sperm release rate (Q_s). The phenomenal fertilization success of *A. planci* can be directly attributed to the animal's high sperm output. By examining the effect of differing sperm outputs, we examined how the spawning of more than one animal, or reduced levels of sperm production, could determine the success of external fertilization. The importance of sperm output level to fertilization success is clearly visible in the comparison of animals from Sesoko Island with those from Davies Reef. When sperm release values in the model were reduced so that they would correspond to those observed for starfish at Sesoko Island, there was a high level of agreement between the predictions and observed fertilization rates (Fig. 6). A group of five spawning male starfish is predicted, using the same model, to be capable of generating fertilization rates in excess of 40% at distances of 100 m or more downstream. Indeed the highest mean fertilization rate we observed for a group of five spawning males was 42% at 100 m (although the mean was much lower, 19.6%). If we compare these observations to the predictions of the model based on the gamete release rate of urchins such as *Strongylocentrotus* (1–3 g, Denny and Shibata, 1989), it becomes apparent why *A. planci* are capable of fertilization at distances much greater than those that are possible for urchins. Sperm release rate can clearly be a major factor determining the outcome of reproductive behavior in a free-spawning marine organism such as *Acanthaster*.

Discussion

Free-spawning marine invertebrates can and do achieve high levels of fertilization during normal spawning events, as confirmed by results presented here as well as by those of other studies (Babcock and Mundy, 1992). In some spawnings of *A. planci*, success can be low, but the majority of gametes are shed during events in which the probability of fertilization is high (Babcock and Mundy, 1992). Levels of synchrony in the spawnings we observed were variable, and most spawnings involved only male starfish; such behavior may be wasteful of sperm. The release of eggs appeared to be more critically controlled, occurring only when many males were spawning. On the only such occasion observed in 1991–92, more than 99% fertilization was recorded for eggs released at the peak of spawning. Similar measurements made by Babcock and Mundy (1992) during 1990–91 indicate that spawning at the peak of a reproductive event involving a large proportion of the population will produce measurably higher fertilization rates (83%) than spawning at the end of the same event, or on occasions when only a small proportion of the population is spawning (~23%). Variations in spawning synchrony have been shown to produce corresponding changes in fertilization rate for holothurians (Babcock *et al.*, 1992) as well as for some mass-spawning corals (Oliver and Babcock, 1992).

Although members of the population may spawn several times, the relative contribution of each spawning event to the seasonal reproductive output probably varies considerably. Not only is the number of gametes released dependent on the numbers of animals participating and the intensity of spawning, but the probability of fertilization also varies in direct proportion to these factors. Thus variations in sperm release rate that would result from changes in synchrony are analogous to the critical impact of sperm release rate on sperm concentration and ultimately on fertilization (Fig. 6). In *Acanthaster*, for example, even though the reproductive season may be as long as two months and animals may spawn several times, the bulk of larvae may be produced in just one large reproductive event. The likelihood that particular events contribute disproportionately to reproductive output is increased by the presence of seasonal changes in the fertility and viability of gametes during the course of the season (Babcock and Mundy, 1994).

Adult aggregative behaviors in free-spawning invertebrates can also act to increase sperm concentrations at the time of spawning (Levitan, 1991). It is more likely that males in aggregations will shed sperm close to females where the sperm will have a better chance of fertilizing eggs. Aggregative spawning behavior has been clearly observed in other asteroids (*e.g.*, Minchin, 1987), but if *Acanthaster* has some means of aggregating at the time of spawning (Beach *et al.*, 1975), the intensity of this aggregation is not great (Fig. 1). Increases in the density of the population at Davies Reef indicated a change of starfish behavior and may represent an increase in aggregation

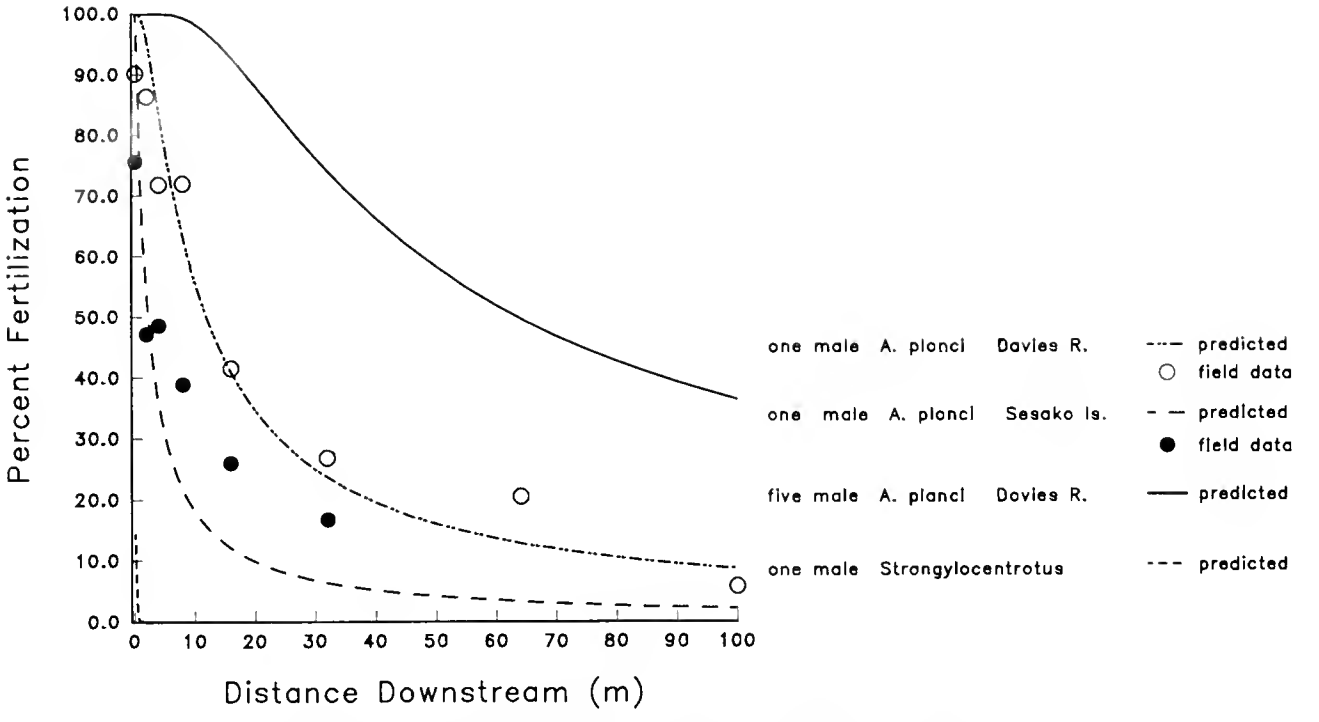

Figure 6. Effects of varying sperm release rate on predicted fertilization rate. Predictions and data for values on the direct downstream axis ($y = 0$). Model parameters for *Acanthaster planci* as for Figure 3. Sperm release rates: 1 male, Davies R. = 6.14×10^8; 5 males, Davies R. = 3.07×10^9; 1 male, Sesoko Is. = 1.5×10^8; 1 *Strongylocentrotus* = 1×10^7; all other parameters for estimates of *Strongylocentrotus* fertilization as in Denny and Shibata (1989), except $\alpha_y = 1.24$ and $\alpha_z = 1.98$.

on a scale too large for our sampling to detect. The fact that *Acanthaster* routinely aggregates in response to both the physical structure of the habitat (*e.g.*, cryptic resting places [personal obs.]) and the feeding of other starfish (Ormond *et al.*, 1973) does not preclude the usefulness of such behavior in terms of reproductive success.

The number of zygotes formed at relatively large distances from a sperm source may be high, as has been noted by Grosberg (1991), due to an increase in the total area under consideration, even though the proportion of eggs fertilized is lower than that in the small area immediately surrounding the source. This is an important factor in reproductive success not only at the population level but also in terms of the pattern of gene flow of individual organisms. For individual starfish, a high level of aggregation may not be necessary to optimize the transfer of genes to the next generation; despite the high level of fertilization for animals in close proximity, the total numbers of eggs fertilized by the sperm of a single spawning male may actually be greater at considerable distances from the site of sperm release (Fig. 7). As long as other members of the population are spawning in the vicinity and the release of gametes is essentially simultaneous or epidemic, intense aggregation is not essential to ensure significant fertilization success for this animal. It is interesting to note that outbreaking populations of starfish may be better able to synchronise their spawning behavior (Okaji, 1991), probably through spawning pheromones such as those demonstrated by Miller (1989).

Other behaviors associated with spawning may act to increase the probability of spawning. *Acanthaster* populations have been observed to move into shallow water at the time of spawning (*e.g.*, Owens, 1971), as have populations of other asteroids (Minchin, 1987). In animals that live along coastlines or other steeply sloping substrata, this movement will have the effect of aggregating the population, reducing the distance separating the population in the horizontal as well as the vertical dimension. In addition, the dilution of gametes will be reduced in shallow water, due to reflection and constrainment by the surface (Fig. 5). An extreme example of this phenomenon may be the reproductive behavior of polychaetes whose epitokes aggregate at the surface (*e.g.*, Palolo worms; Caspers, 1984), or hermaphroditic corals that shed buoyant gamete bundles that break apart at the surface (Oliver and Babcock, 1992).

Large-scale movements of populations may be true migrations of a sort, but they may also be the consequence of simple climbing behaviors. On a smaller scale, starfish commonly arch themselves up off the bottom when

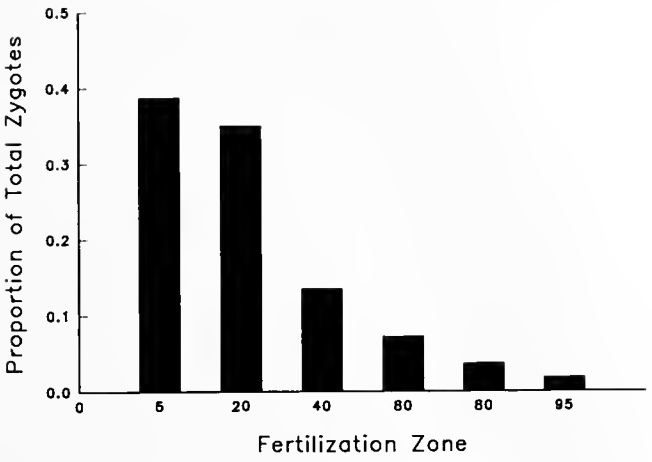

Figure 7. Number of zygotes formed at varying distances from sperm source. Values are those predicted for the case of a single male *Acanthaster planci* spawning in a field of uniformly distributed female starfish. Density of female starfish is taken to be half the mean density of starfish on our study transect at Davies Reef during 1990–92, or 0.0124 female starfish · m^2. Based on our gonad index data (Babcock and Mundy, 1992; and unpublished data) each of these females could spawn an average of 220 g of eggs during a natural spawning event. At approximately 9 $\times 10^4$ eggs · g^{-1} (Conand, 1985), this gives an egg release of 1.98×10^7 per female or 2.46×10^5 eggs · m^2. The area defined by each fertilization zone (*cf.* Fig. 4) was then multiplied by this value to provide a total egg production value in each zone. The number of zygotes produced in each zone was calculated as the product of the total egg production and the median value for fertilization rate in each zone. Zygote production was not calculated for the area in which fertilization rates were predicted to be less than 5%.

spawning, and similar behaviors (*i.e.*, rearing) are seen in holothurians (McEuen, 1988). We frequently observed such behaviors in spawning *Acanthaster*, as have many other authors (Pearson and Endean, 1969). This activity is commonly associated with spawning in various benthic marine animals (McEuen, 1988). In some situations, gametes can actually pile up on the substratum adjacent to spawning animals (Minchin, 1987). Such situations are unlikely to result in high levels of fertilization, and their consequences would be reduced by arching behavior that would raise the gonopores further into the flow field.

The results of field experiments on the fertilization success of *A. planci* spawnings indicate a high level of success at separations as great as 100 m. At first glance these results appear to contradict the results of empirical field studies (*e.g.*, Pennington, 1985), as well as existing models of sperm diffusion for sea urchins (Denny and Shibata, 1989), which predicted low success even at small separations. Here we examine the model under spawning conditions similar to those of *A. planci*. Given the fertilization success of *A. planci* recorded during field experiments, the question is whether turbulent diffusion alone can bring sperm and ova together over large source separations. Given the large volumes of sperm released by *Acanthaster*, we conclude that turbulent diffusion is a sufficient mechanism to enable this animal to achieve the observed levels of fertilization success. The level of fertilization recorded in our trials generally varied according to the mass of gonads available to be spawned. Fertilization was thus appreciably lower for the smaller Sesoko Island starfish than for Davies Reef starfish, and the levels observed were consistent with the predictions of our sperm diffusion model. This result contrasts with the conclusions of Levitan (1991) that body size and the amount of gametes released were not significant factors in fertilization success. This difference may have several sources. Firstly, the numbers of sperm released may not have been sufficiently large to produce a consistent difference with size, despite the relative difference in gonad volume between large and small urchins. Secondly, low current speeds and the short lifespan of urchin sperm relative to that of *Acanthaster* (J. Benzie, unpublished data) may also have contributed. We demonstrated that the same model that has been used to describe the rapid dilution of gametes and decline in fertilization success in echinoids is also consistent with our results, and that it is the exceptionally high rate of gamete release that, so far, sets this animal apart. Smaller organisms may be more reliant on phenomena such as aggregation, or even pseudo-copulation (*e.g., Archaster typicus;* Run *et al.*, 1988), to ensure fertilization.

Acknowledgments

We would like to thank the crews of the vessels *Lady Basten, Harry Messel* and *Sirius*, and numerous volunteer field assistants, particularly those who returned for more than one trip; their experience helped greatly in making this work possible. RCB extends thanks to K. Yamazato, M. Yamguchi, and the staff and students of the Sesoko Marine Science Centre for their assistance and warm hospitality. Thanks are also due to Peter Moran and John Keesing, both of whom provided a great deal of valuable advice and practical assistance. Miles Furnas, Brian King, Richard Miller, and two anonymous reviewers made constructive comments on the manuscript. The research was supported by the Great Barrier Reef Marine Park Authority and funds from the Australia/Japan Bi-lateral Science and Technology Program.

Literature Cited

Babcock, R. C., and C. N. Mundy. 1992. Reproductive biology, spawning and field fertilization rates of *Acanthaster planci*. *Aust. J. Mar. Freshwater Res.* **43:** 525–534.

Babcock, R. C., and C. N. Mundy. 1994. Seasonal changes in fertility and fecundity in *Acanthaster planci*. *Seventh International Coral Reef Symposium*, Guam. In press.

Babcock, R., C. Mundy, J. Keesing, and J. Oliver. 1992. Predictable and unpredictable spawning events: *in situ* behavioral data from free-spawning coral reef invertebrates. *Invert. Reprod. Devel.* **22:** 213–228.

Beach, D. H., N. J. Hanscomb, and R. F. G. Ormond. 1975. Spawning pheromone in crown-of-thorns starfish. *Nature* **254:** 135–136.

Braley, R. D. 1984. Reproduction in the giant clams *Tridacna gigas* and *T. derasa in situ* on the North-Central Great Barrier Reef, Australia, and Papua New Guinea. *Coral Reefs* **3:** 221–227.

Caspers, H. 1984. Spawning periodicity and habitat of the Palolo worm *Eunice viridis* (Polychaeta: Eunicidae) in the Samoan Islands. *Mar. Biol.* **79:** 229–236.

Conand, C. 1985. Distribution, reproductive cycle and morphometric relationships of *Acanthaster planci* (Echinodermata, Asteroidea) in New Caledonia, western tropical Pacific. Pp. 499–506 in *Echinodermata: Proceedings of the Fifth International Echinoderm Conference,* Galway. B. F. Keegan and B. D. S. O'Connor, eds. Balkema, Rotterdam.

Csanady, G. T. 1973. *Turbulent Diffusion in the Environment.* Reidel, Boston.

Dana, T. F. 1970. *Acanthaster*: a rarity in the past? *Science* **169:** 894.

Denny, M. W. 1988. *Biology and the Mechanics of the Wave Swept Environment.* Princeton University Press, Princeton, N.J.

Denny, M. W., and M. F. Shibata. 1989. Consequences of surf-zone turbulence for settlement and external fertilization. *Am. Nat.* **134:** 859–889.

Finkel, T., H. Levitan, and E. J. Carroll, Jr. 1981. Fertilization in the sea urchin *Arbacia punctulata* inhibited by fluorescein dyes: Evidence for a membrane mechanism. *Gamete Res.* **4:** 219–229.

Gladstone, W. 1992. Observations of crown-of-thorns starfish spawning. *Aust. J. Mar. Freshwater Res.* **43:** 535–537.

Grosberg, R. K. 1991. Sperm-mediated gene flow and the genetic structure of a population of the colonial ascidian *Botryllus schlosseri*. *Evolution* **45:** 130–142.

Hoppe, W. F., and M. J. M. Reichert. 1987. Predictable annual mass release of gametes by the coral reef sponge *Neofibularia nolitangere* (Porifera: Demospongiae). *Mar. Biol.* **94:** 277–285.

Levitan, D. R. 1988. Asynchronous spawning and aggregative behavior in the sea urchin *Diadema antillarum* Phillipi. Pp. 181–186 in *Echinoderm Biology: Proceedings of the Sixth International Echinoderm Conference,* R. Burke, ed. Balkema, Rotterdam.

Levitan, D. R. 1991. Influence of body size and population density on fertilization success and reproductive output in a free-spawning invertebrate. *Biol. Bull.* **181:** 261–268.

Levitan, D. R., M. A. Sewell, and Fu-Shiang Chia. 1991. Kinetics of fertilization in the sea urchin *Strongylocentrotus franciscanus* interaction of gamete dilution, age and contact time. *Biol. Bull.* **181:** 371–378.

Levitan, D. R., M. A. Sewell, and Fu-Shiang Chia. 1992. How distribution and abundance influence fertilization success in the sea urchin *Strongylocentrotus franciscanus*. *Ecology* **73:** 248–254.

McEuen, F. S. 1988. Spawning behaviors of northeast Pacific sea cucumbers (Holothuroidea: Echinodermata). *Mar. Biol.* **98:** 565–585.

Miller, R. L. 1989. Evidence for the presence of sexual pheromones in free-spawning starfish. *J. Exp. Mar. Biol. Ecol.* **130:** 205–221.

Minchin, D. 1987. Sea-water temperature and spawning behavior in the seastar *Marthasterias glacialis*. *Mar. Biol.* **95:** 139–143.

Moore, R. J. 1978. Is *Acanthaster planci* an r-strategist? *Nature* **271:** 56–57.

Moran, P. J. 1986. The *Acanthaster* phenomenon. *Oceanogr. Mar. Biol. Annu. Rev.* **24:** 379–480.

Mosher, C. 1982. Spawning behavior of the aspidochirote holothurian *Holothuria mexicana* Ludwig. Pp. 467–468. in *Echinoderms: Proceedings of the International Conference,* Tampa Bay. J. M. Lawrence, ed. Balkema, Rotterdam.

Okaji, K. 1991. Delayed spawning activity in dispersed individuals of *Acanthaster planci* in Okinawa. Pp. 291–295 in *Biology of Echinodermata,* T. Yanagisawa, I. Yasumasu, C. Oguro, N. Suzuki, and T. Motokawa, eds. Balkema, Rotterdam.

Oliver, J. K., and R. C. Babcock. 1992. Aspects of the fertilization ecology of broadcast spawning corals: sperm dilution effects and *in situ* measurements of fertilization. *Biol. Bull.* **183:** 409–417.

Ormond, R. F. G., A. C. Campbell, S. H. Head, R. J. Moore, P. R. Rainbow, and A. P. Saunders. 1973. Formation and breakdown of aggregations of the crown-of-thorns starfish, *Acanthaster planci* (L.). *Nature* **246:** 167–169.

Owens, D. 1971. *Acanthaster planci* starfish in Fiji. Survey of incidence and biological study. *Fiji Agric. J.* **33:** 15–23.

Pearse, J. S., D. J. McClary, M. A. Sewell, W. C. Austin, A. Perez-Ruzafa, and M. Byrne. 1988. Simultaneous spawning of six species of echinoderm in Barkely Sound, British Columbia. *Int. J. Invertebr. Reprod. Dev.* **14:** 279–288.

Pearson, R. G., and R. Endean. 1969. A preliminary study of the coral predator *Acanthaster planci* (L.) (Asteroidea) on the Great Barrier Reef. *Queensland Dept. of Harbours and Marine, Fisheries Notes* **3:** 27–55.

Pennington, J. T. 1985. The ecology of fertilization of echinoid eggs: the consequences of sperm dilution, adult aggregation, and synchronous spawning. *Biol. Bull.* **169:** 417–430.

Randall, J. E., R. E. Schroeder, and W. A. Stark, Jr. 1964. Notes on the biology of the echinoid *Diadema antillarum*. *Carib. J. Sci.* **4:** 421–433.

Reiswig, H. M. 1970. Porifera: sudden sperm release by tropical Demospongiae. *Science* **170:** 538–539.

Run, J.-Q., C.-P. Chen, K.-H. Chang, and F.-S. Chia. 1988. Mating behavior and reproductive cycle of *Archaster typicus* (Echinodermata: Asteroidea). *Mar. Biol.* **99:** 247–253.

Schuel, H. 1984. The prevention of polyspermic fertilization in sea urchins. *Biol. Bull.* **167:** 271–309.

Tyler, A. A., A. Monroy, and C. B. Metz. 1956. Fertilization of fertilized sea urchin eggs. *Biol. Bull.* **110:** 184–195.

Vine, P. J. 1970. Densities of *Acanthaster planci* in the Pacific Ocean. *Nature* **228:** 341–342.

Vogel, H. G., P. Czihak, P. Chang, and W. Wolf. 1982. Fertilization kinetics of sea urchin eggs. *Math. Biosci.* **58:** 189–216.

Yund, P. O. 1990. An *in situ* measurement of sperm dispersal in a colonial marine hydroid. *J. Exp. Zool.* **253:** 102–106.

Reference: *Biol. Bull.* **186:** 29–40. (February, 1994)

Ontogeny of Osmoregulatory Structures in the Shrimp *Penaeus japonicus* (Crustacea, Decapoda)

N. BOUARICHA[1], M. CHARMANTIER-DAURES[2,*], P. THUET[2], J.-P. TRILLES[2], AND G. CHARMANTIER[2]

[1]*Institut de Biologie, B.P. 358 RP Imama, Tlemcen 13000, Algeria, and* [2]*Laboratoire d'Ecophysiologie des Invertébrés, Université des Sciences, Montpellier 2, 34095 Montpellier cedex 05, France*

Abstract. The ontogeny of differentiated osmoregulatory epithelia in the branchial chamber (gills, branchiostegite, pleura, epipodite) was studied by transmission electron microscopy throughout the postembryonic development of *Penaeus japonicus*. These epithelia are characterized by typical cytological features, including apical microvilli and numerous basal infoldings associated with mitochondria.

Differentiated osmoregulatory structures are not observed in the early larval stages: nauplii and zoea 1. In the next larval stages, zoeas and mysis, gills and epipodites are developed as buds only, but osmoregulatory epithelia are observed in the branchiostegites and pleurae. The differentiated structures of the branchiostegites and pleurae are still present in postlarvae but disappear in juveniles and adults. Gills and epipodites develop progressively in the postlarval stages, with early differentiation of osmoregulatory epithelia in the epipodites. In juveniles and adults, the gill epithelium is poorly differentiated; in contrast, abundant differentiated osmoregulatory structures are observed in the epipodites.

Ontogenetical comparisons of these observations with previous studies in the same species reveal strong correlations between the development of osmoregulatory epithelia, the ability to osmoregulate, the activity of Na^+-K^+ ATPase, and salinity tolerance during the postembryonic development of *Penaeus japonicus*.

Introduction

Among the few comprehensive histological studies of osmoregulatory structures in decapod crustaceans, most have concerned the gills of crabs (Drach, 1930; Chen, 1933; Smyth, 1942) and of shrimps such as *Palaemonetes varians* (Allen, 1892), *Crangon vulgaris* (Debaisieux, 1970), and *Penaeus aztecus* (Foster and Howse, 1978).

Ultrastructural studies of the gills of adult crustaceans are numerous (review in Bouaricha, 1990), but to our knowledge, comparable information about larvae and postlarvae is lacking. In penaeid shrimp, a description of the ontogeny of gills in *Penaeus japonicus* was given by Hudinaga (1942), but without histological data.

Gills are among the most permeable external surfaces of crustaceans, and they are considered the primary site for ionic and osmotic regulation (Robertson, 1960; Lockwood, 1962, 1968; Gilles, 1975; Croghan, 1976; Kirschner, 1979; Pequeux and Gilles, 1981, 1988; Towle, 1984a). In some earlier studies, patches of salt-transporting tissue were also described on the branchial chamber epithelium in larvae of *Penaeus aztecus* (Talbot *et al.*, 1972) and *Callianassa jamaicense* (Felder *et al.*, 1986).

This study presents a general and histological description of the gills in juvenile and adult *P. japonicus* and their ontogeny during larval and postlarval development, with particular attention directed at the localization of epithelia involved in osmoregulation. We also looked for similar tissues in the branchiostegite, pleura, and epipodite. Our ultimate goal was to evaluate the validity of a hypothetical relationship between the ontogeny of osmoregulatory structures in gills and other epithelia and the ontogeny of osmoregulation demonstrated by the changes in osmoregulatory capacity (Charmantier, 1986; Charmantier *et al.*, 1987, 1988; Charmantier-Daures *et al.*, 1988) and in the activity of Na^+-K^+ ATPase (Bouaricha, 1990; Bouaricha *et al.*, 1991) during the postembryonic development of *P. japonicus*.

Received 5 November 1992; accepted 16 September 1993.

* To whom correspondence should be addressed.

Material and Methods

Animals

Penaeus japonicus larvae, postlarvae, and adults were obtained from the Ifremer center (Deva-Sud, Palavas, Hérault, France) and from a local shrimp-farm (Poissons du soleil, Balarue les Bains, Hérault). The different developmental stages were identified according to morphological criteria (Hudinaga, 1942). Larval development consists of six naupliar, three zoea, and three mysis stages. A metamorphic molt transforms the late mysis 3 larva into the first postlarval stage. Postlarvae progressively acquire the adult morphology through about 20 molts. Postlarval stages are designated by an abbreviation of stage; *e.g.*, PL4 for fourth stage postlarva. Molt stages were controlled by microscopical observation of pleopods according to the technique widely used with adult crustaceans (Drach and Tchernigovtzeff, 1967); only animals in stage C were used.

Microscopy

All stages were fixed in Halmi's fluid, sectioned in the transverse plane, stained with Masson's trichrome (variant Goldner; Martoja and Martoja, 1967), and examined with a light microscope. For electron microscopy, animals were fixed in 2.5% glutaraldehyde in 0.1 *M* saline cacodylate buffer adjusted to the osmotic pressure of seawater with sodium chloride. Samples were post-fixed in 1% OsO_4 in the same buffer and embedded in Spurr's medium. Ultrathin sections, stained sequentially with uranyl acetate and lead citrate, were examined with a JEOL 200CX electron microscope at 100 kV.

Results

Structure of gills in juvenile and adult

Eighteen gills are present in each branchial chamber: one podobranchial gill, eleven arthrobranchial gills, and six pleurobranchial gills. In *P. japonicus*, as in other species of penaeid shrimps, all gills are dendrobranchiate, and this consists of an axis that supports a series of paired branches set at right angles along its length (Fig. 1). Each branch then gives rise to perpendicularly oriented filaments that bifurcate at least once (Figs. 2 and 3). Mucus pores are located on both sides of the axis.

The internal structure of the gills includes a longitudinal septum dividing the lumen of each axis, branch, and filament into afferent (external) and efferent (internal) vessels (Figs. 3 and 4).

The histology of the gill is as follows. The surface of each branch or filament is covered by a thin cuticle that overlies a simple epithelium. A central lacunar system expands in the tip of each filament into a hemolymphatic lacuna. Connective tissues are present in the septa of filaments and axis of the gill (Fig. 4).

Changes in gill structure during development

In mysis stages 2 and 3, the branchial chamber is widely open. The gills, appearing as small buds on the coxopodite of the thoracic appendages, are limited by a simple epithelium enclosing a hemolymph lacuna (Fig. 5).

In postlarvae PL1, the curved larger branchiostegite partly encloses the branchial chamber. The gill bud is longer, and the hemolymph lacuna is wider (Fig. 6).

In PL4, the septum that divides the axis of the gill is present. The gill epithelium gives rise to branches (Fig. 7) that are present along the whole length of the gill in PL5. At this stage, afferent and efferent vessels are differentiated in the largest gills, and the branchial chamber is completely enclosed by a lateral-ventral infolding of the branchiostegite. In PL10, the gills are about 1 mm long. The epithelium on the surface of the branches is only 0.1–0.7 μm thick, except near the nuclei; few organelles are visible in the cytoplasm (Fig. 8). Only this type of slightly differentiated epithelium was observed on transverse and longitudinal serial sections of the gills.

In 3-month-old juveniles, the epithelium of the branches and filaments (Figs. 9 and 10) is about 0.8 μm thick; it is thicker near nuclei (1.4–2.2 μm) and at the tip of the filaments (1.5 μm) that are widened to form a distal lacuna. The cytoplasm contains but few organelles (Fig. 10), and these include spherical (0.4 μm) or elongated (1 μm) mitochondria. Microvilli occur infrequently on the apical cytoplasmic membrane. Infoldings of the basal lamina are limited (Fig. 9).

In 5-month-old juveniles, the apical cytoplasmic membrane of the gill epithelium is differentiated, giving rise to microvilli, 0.3–0.8 μm high, that delimit important subcuticular spaces (Fig. 11). The cytoplasm contains many large mitochondria, but other organelles are still scarce.

No difference in structure was noted between the different filaments along the length of the gill axis, or between the anterior and posterior gills.

Pleurae

The pleural epithelium covers the lateral internal surface of the branchial chamber (Figs. 5 and 24).

In zoea 2 larvae, this epithelium presents two aspects: thin (1.4–4 μm) and only slightly differentiated, or thicker (4–7 μm) and with typical differentiations, *i.e.*, large invaginations of the basal membrane enfolding mitochondria (Fig. 13). The apical cytoplasm contains the nucleus, numerous vesicles of reticulum, free ribosomes, and mitochondria (Fig. 12).

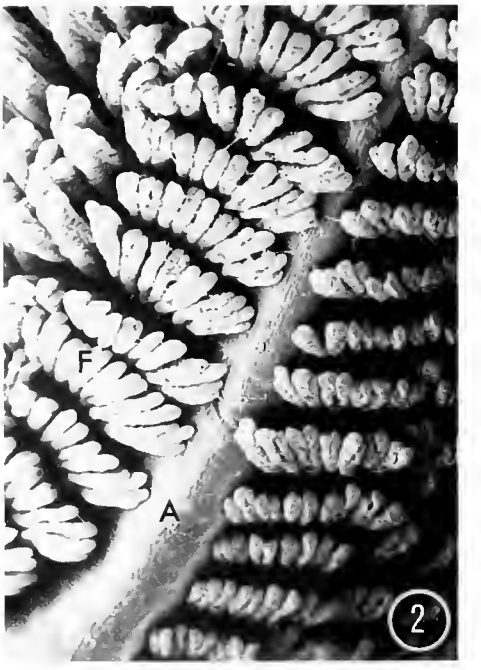

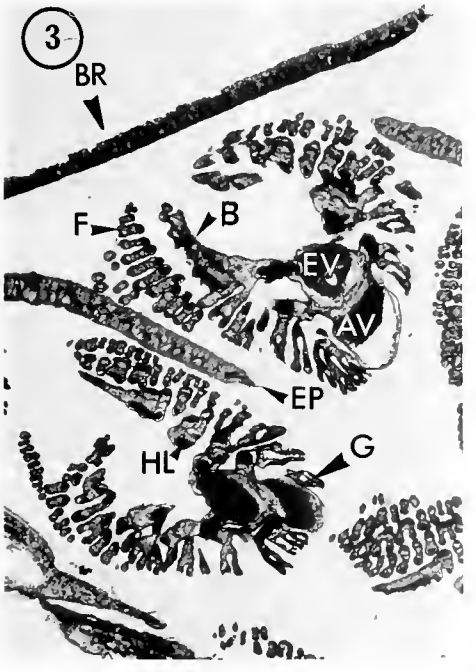

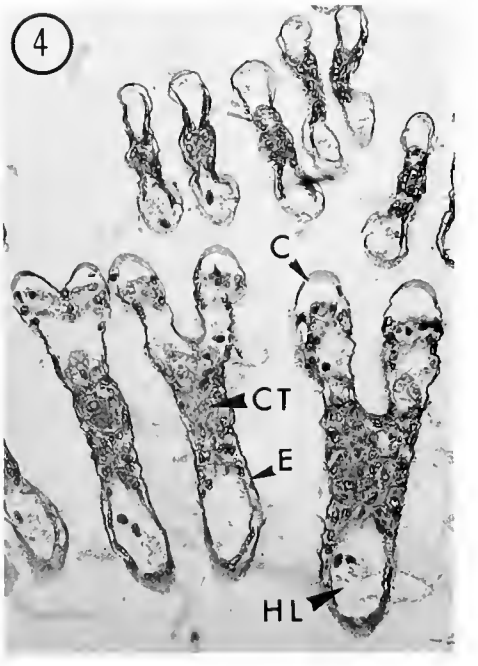

Figures 1–4. Gills of juvenile *Penaeus japonicus*. A: axis, AV: afferent vessel, B: branches, BR: branchiostegite, C: cuticle, CT: connective tissue, E: epithelium, EP: epipodite, EV: efferent vessel, F: filament, G: gills, HL: hemolymphatic lacuna.

Figures 1–2. Dorsal face of a dendrobranchiate gill showing the axis and the filaments (×25 and ×90, respectively).

Figure 3. General organization of the branchial chamber of a juvenile (×250). The outside of the branchial chamber is closed by the branchiostegite. Subtransverse sections of gills show the axis divided into afferent and efferent vessels and branches and filaments. Epipodites are intercalated between the gills.

Figure 4. Transverse section of gill filaments in an old juvenile. The monolayer epithelium is covered by a thin cuticle. Each tip of the filament is occupied by a hemolymphatic lacuna.

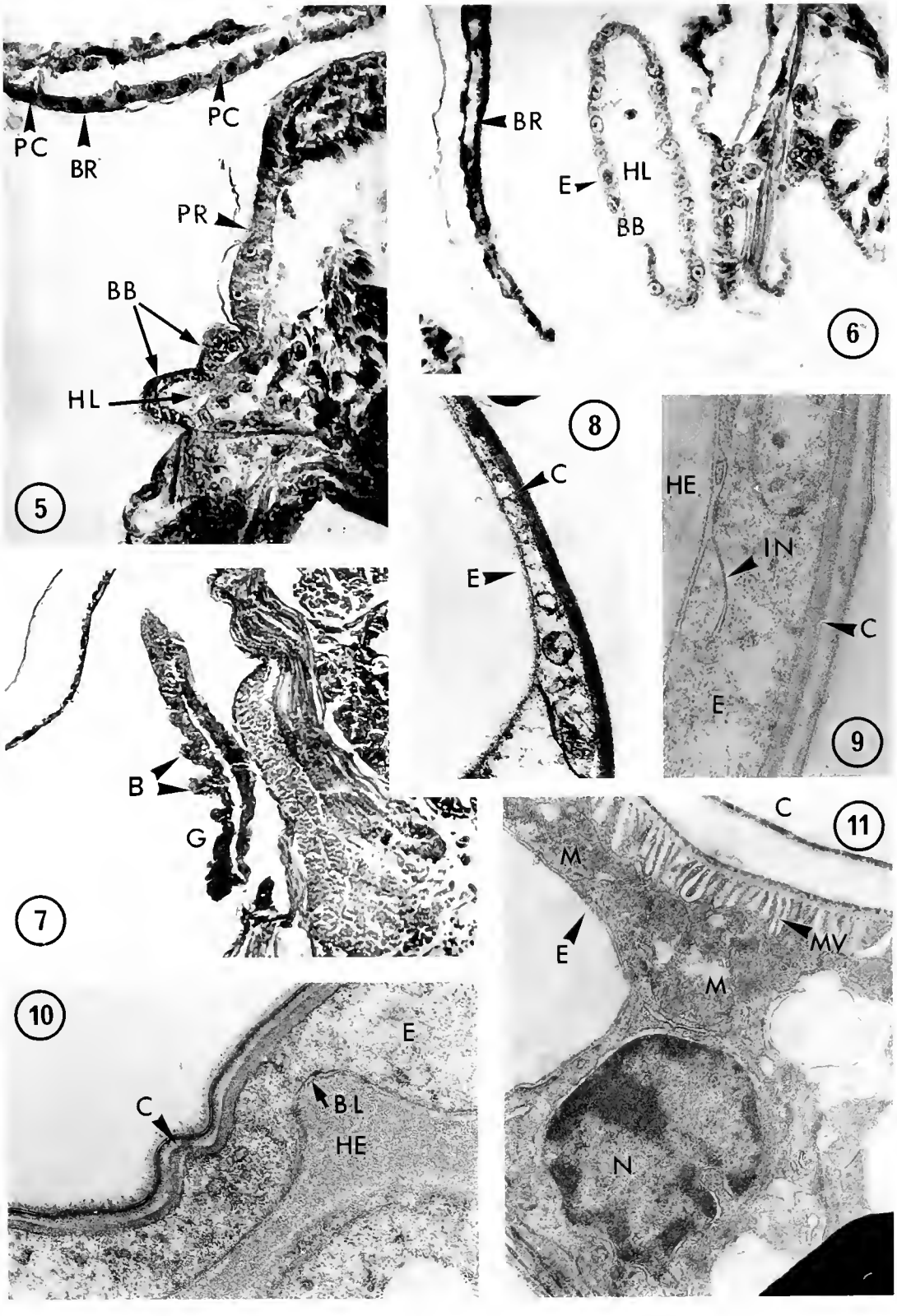

Figures 5–11. Ontogeny and structure of gills in *Penaeus japonicus*. B: branches, BB: branchial bud, BL: basal lamina, BR: branchiostegite, C: cuticule, E: epithelium, G: gill, HE: hemolymph, HL: hemolymphatic lacuna, IN: infolding, M: mitochondria, MV: microvilli, N: nucleus, PC: pillar cell, PR: pleura.

Figure 5. Mysis 3 larva (× 400). Early gill buds on a thoracic appendage.

In mysis 3 larvae, the two forms of pleural epithelium are also present. The differentiated epithelium is located in the central region of the pleural dorsoventral axis. Differentiations are more pronounced than in zoeas (Fig. 14). Although the total thickness of the epithelium is similar (4–8 μm) to the previous stage, basal infoldings have expanded (1.2–3 μm); mitochondria are very abundant; and the apical membrane bears thin microvilli, 0.8 μm long, either scarce or close-ranked.

In postlarvae, although observations were available from light microscopy only, the differentiations present in mysis seem to have been retained. Longitudinal streaks that characterize basal infoldings can be observed on epithelial cells of the pleura.

In adults, no differentiated epithelial structure was observed on any of several serial transverse sections of the pleura.

Branchiostegites

The branchiostegite is almost horizontally oriented in the larval stages, resulting in an open branchial chamber. In later stages, the chamber is progressively closed by the folding down of the branchiostegite (Figs. 5 and 18). At all the developmental stages, the branchiostegite comprises two simple epithelia, external and internal, separated by a hemolymph lacuna. The epithelia are linked by pillar cells (Fig. 5). The external epithelium, under the cuticle, is thin and slightly differentiated. The internal epithelium is thicker, and its structure varies with the developmental stage.

In stage mysis 3, the internal epithelium is 8 μm thick and shows differentiated zones similar to those described for the pleura (Fig. 15); the apical cytoplasmic membrane presents patches of microvilli, 0.1–1 μm long. The basal cytoplasmic membrane forms many deep infoldings separating cytoplasmic areas that contain abundant round or elongated mitochondria. Nuclei are located in the narrow median zone, above the basal infoldings. They are large and oval (2.6 × 4 μm), with spots of chromatin; the external layer of the nuclear membrane carries numerous ribosomes. Rough endoplasmic reticulum and irregularly shaped mitochondria can be observed around the nuclei.

In PL 10 postlarvae, the internal epithelium is thicker (12–14 μm) and presents the same differentiations as in the mysis (Figs. 16 and 17), with long (1–2 μm) and abundant microvilli at the apical pole (Fig. 16) and with numerous elongated basal infoldings, sometimes nearly as high as the cell. Many elongated mitochondria are located between the infoldings and under the microvilli.

In adults, this type of differentiated epithelium was not observed in any of the serial sections of the branchiostegite. The internal epithelium is composed of high cells. The nucleus is centrally located. The cytoplasmic membrane shows ample, sinuous interdigitations. Different organelles can be observed in the cytoplasm: abundant rough endoplasmic reticulum forming a tubular network connected to small vesicles, elongated mitochondria, large golgi profiles with numerous vesicles, and oriented fibril bundles. Apical microvilli or basal infoldings were not observed.

Epipodite

The epipodites, or mastigobranchs, are elongated, thin, biramous structures, attached to coxopodites of some thoracic appendages. Six of them are present in each branchial chamber of adult shrimp.

In mysis 2 and 3 larvae, the first epipodites appear as small buds. This aspect is retained until the early postlarval stages. They lengthen and become biramous and covered with setae in PL5. According to Hudinaga (1942), their full complement is reached by PL11.

In PL5 postlarvae, epipodites are formed of a simple epithelium enclosing a vascular network locally enlarged in lacunae (Figs. 18 and 19); the tip is widened around a hemolymph lacuna. In light microscopy, the basal part of the cells presents a striated appearance, similar to the differentiated zones observed in the branchiostegite and the pleurae.

In 5-month-old juveniles and in adults, epipodites present two simple epithelia separated by a central connective tissue. The epithelium is made of high columnar cells (30 μm in adults), with the nuclei located in the apical part of the cell under a thin cuticle (Fig. 20). The ultrastructure of the epithelial cells features both apical and basal infoldings (Figs. 21, 22, and 23). The apical infoldings are oriented at right angles to the cuticle. Mitochondria, tubules of rough endoplasmic reticulum, and numerous small round vesicles are located between them (Fig. 21). The basal infoldings are organized as a compact network, penetrating deeply, up to 20 μm, into the cytoplasm. Abundant elongated mitochondria (0.4 × 2.5 μm) are inserted between the infoldings.

Figure 6. Postlarva PL 1 (×400). Gill bud structure: a thin epithelium delineating a central hemolymphatic lacuna.

Figure 7. Postlarvae PL 4 (×400). First branchial branches on a gill.

Figure 8. Postlarvae PL 10 (×13000). Epithelium of a branchial branch.

Figures 9–10. Juvenile (×17500). Branchial epithelium. Thin epithelium and few intracellular organelles.

Figure 11. Juvenile (×8000). Branchial epithelium with apical microvilli and some mitochondria.

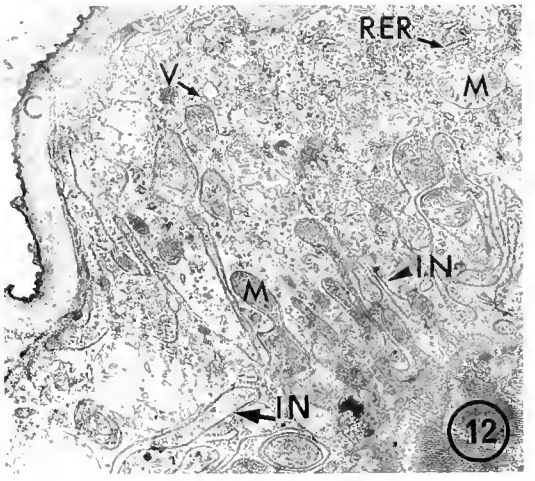

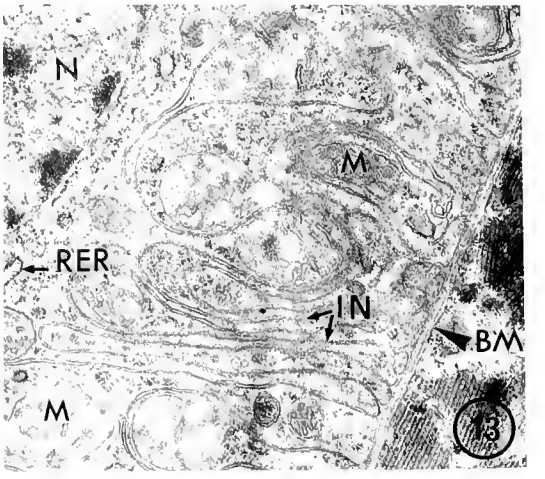

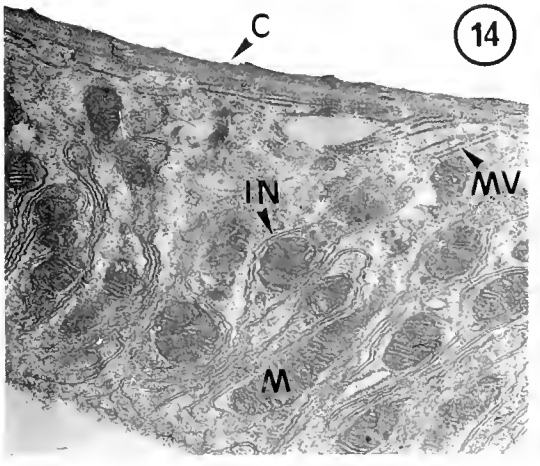

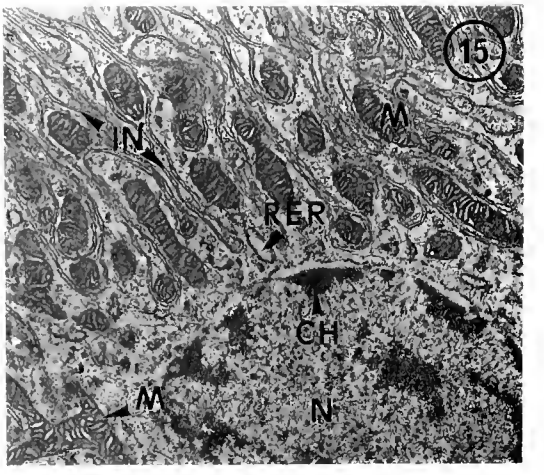

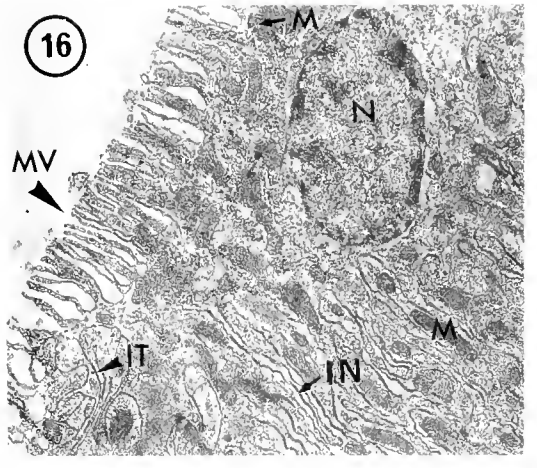

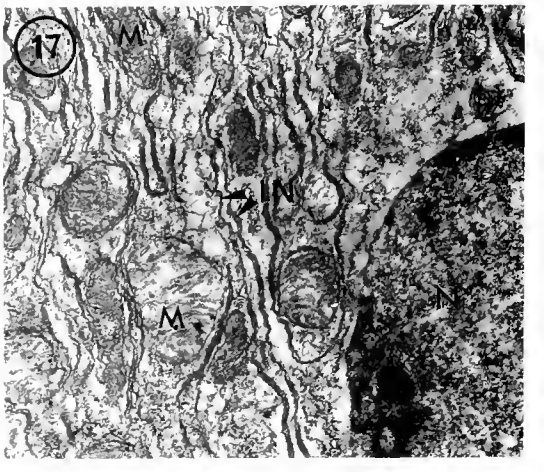

Figures 12–17. Pleura and branchiostegite of larvae and postlarvae of *Penaeus japonicus*. BM: basal membrane, C: cuticle, CH: chromatin, IN: infoldings, IT: interdigitation, M: mitochondria, MV: microvilli, N: nucleus, RER: rough endoplasmic reticulum, V: vesicle.

Figures 12–13. Pleura, zoea 2 (×9200 and ×15000, respectively). Pleural epithelium with numerous basal infoldings associated with mitochondria.

Figure 14. Pleura, mysis 3 (×9100). The pleural epithelium contains two types of differentiations: apical microvilli and basal infoldings with mitochondria.

Figure 15. Internal layer of the branchiostegite, mysis 3 (×8300). Numerous basolateral infoldings associated with mitochondria.

Discussion and Conclusions

Gills

Gill buds appear at the end of the larval phase, and their development progresses during the postlarval period. The branchial formula is complete at stage PL 11 (Hudinaga, 1942).

Only one type of gill epithelium was observed in the postlarvae. This thin epithelium containing few nuclei and very few organelles was not differentiated. A similar type of epithelium was described in adult *Callinectes sapidus* (Copeland and Fitzjarrell, 1968) and *Ocypode ceratophthalma* (Storch and Welsch, 1975). These observations, and our own, suggest that this epithelium is probably involved in gas exchange.

The epithelium begins to differentiate in juveniles with the formation of microvilli on the apical cytoplasmic membrane of the cell, under the cuticle. The differentiation progresses in juveniles that are more than 5 months old, resulting in a higher density of mitochondria under the microvilli.

In juveniles and adults, we found that the epithelium of the gills is formed of thin cells having, as their only apical differentiated structures, microvilli and mitochondria. These cells were also described in *Penaeus aztecus* (Foster and Howse, 1978) and in *Palaemontes pugio* (Doughtie and Rao, 1978). They are the principal cells of the gills of palaemonid and penaeid shrimps (Taylor and Taylor, 1992). Similar epithelia have been reported in the posterior gills of *Eriocheir sinensis* (*Barra et al.*, 1983) and *Gecarcinus cruentata* (Martelo and Zanders, 1986). This type of epithelium could be involved in osmoregulation, a hypothesis supported by the increase in the size of the microvilli in *P. aztecus* that were transferred to low or high salinities (0.9 and 59‰; Foster and Howse, 1978).

The comparison with other species demonstrates that the gill epithelium is only slightly differentiated in *P. japonicus*. In *Gecarcinus lateralis* (Copeland, 1968), *Callinectes sapidus* (Copeland and Fitzjarrell, 1968), *Astacus leptodactylus* (Bielawski, 1971), *Astacus pallipes* (Fisher, 1972), *Gecarcinus oceanicus* (Milne and Ellis, 1973), *Procambarus clarkii* (Burggren *et al.*, 1974), *Jaera nordmanni* (Bubel, 1976; Bubel and Jones, 1974), *Asellus aquaticus* (Babula, 1979), *Holthuisana transversa* (Taylor and Greenaway, 1979), *Eriocheir sinensis* (Barra *et al.*, 1983), *Uca mordax* (Finol and Croghan, 1983), and *Crangon crangon* (Papathanassiou, 1985), the gill epithelium is characterized by apical microvilli and basolateral infoldings associated with mitochondria. These ultrastructural features are typical of tissues involved in active ionic transport (Pease, 1956; Berridge and Oschman, 1972). In some of these species—*Gecarcinus lateralis* (Copeland and Fitzjarrel, 1968), *Carcinus maenas* (Goodman and Cavey, 1988, 1990; Compere *et al.*, 1989), *Procambarus clarkii* (Burggren *et al.*, 1974)—two types of epithelia coexist in the gill, a thin one supposedly implicated in gas exchange, and a differentiated epithelium involved in hydromineral exchanges. In adult *P. japonicus*, we observed only one type of epithelium with apical microvilli but without basal infoldings.

In addition, we saw no morphological or ultrastructural differences between the anterior, median, and posterior gills of *P. japonicus*. We thus conclude that a single type of epithelium exists in *P. japonicus*, as in *P. aztecus* (Foster and Howse, 1978) and in the crab *Holthuisana transversa* (Taylor and Greenaway, 1979). In other species, anterior and posterior gills are histologically different. In *Eriocheir sinensis* (Barra *et al.*, 1983), the anterior gills have a thin, little-differentiated epithelium, probably involved in respiration; the epithelium of the posterior gills is differentiated and certainly implicated in osmoregulation. This hypothesis is confirmed by physiological data, since only the posterior gills are involved in osmotic and ionic regulation (Schoffeniels and Gilles, 1970; Pequeux and Gilles, 1981, 1988). This topographic difference has also been observed in *Astacus pallipes* and *A. leptodactylus* (Dunel-Erb *et al.*, 1982) and in *Asellus aquaticus* (Babula, 1979).

In summary, the gills of *P. japonicus* appear as buds during the last larval stages and grow progressively during the first postlarval stages. The gill epithelium differentiates slightly and progressively in juveniles and adults, with apical microvilli and mitochondria beneath it. The differentiated gills are implicated mainly in respiration and, less than in other species, probably in osmoregulation. This last function is also shared by other structures of the branchial chamber. The structure of the gill epithelium in *P. japonicus* (and probably other penaeids) is simpler than that in most other crustacean groups.

Branchiostegite and pleura

The branchiostegite and pleural epithelia are not differentiated in nauplii and zoea 1. Differentiation appears in zoea 2 and persists in the postlarvae; the most typical features are apical microvilli, deep basal and lateral infoldings, and abundant mitochondria. These elements were called "mitochondrial pumps" by Copeland (1964).

Figure 16. Internal layer of the branchiostegite, postlarvae PL 10 (×6500). Numerous apical microvilli and basal infoldings with mitochondria.

Figure 17. Internal layer of the branchiostegite, postlarvae PL 10 (×13000). Detail of the interrelations between infoldings and mitochondria.

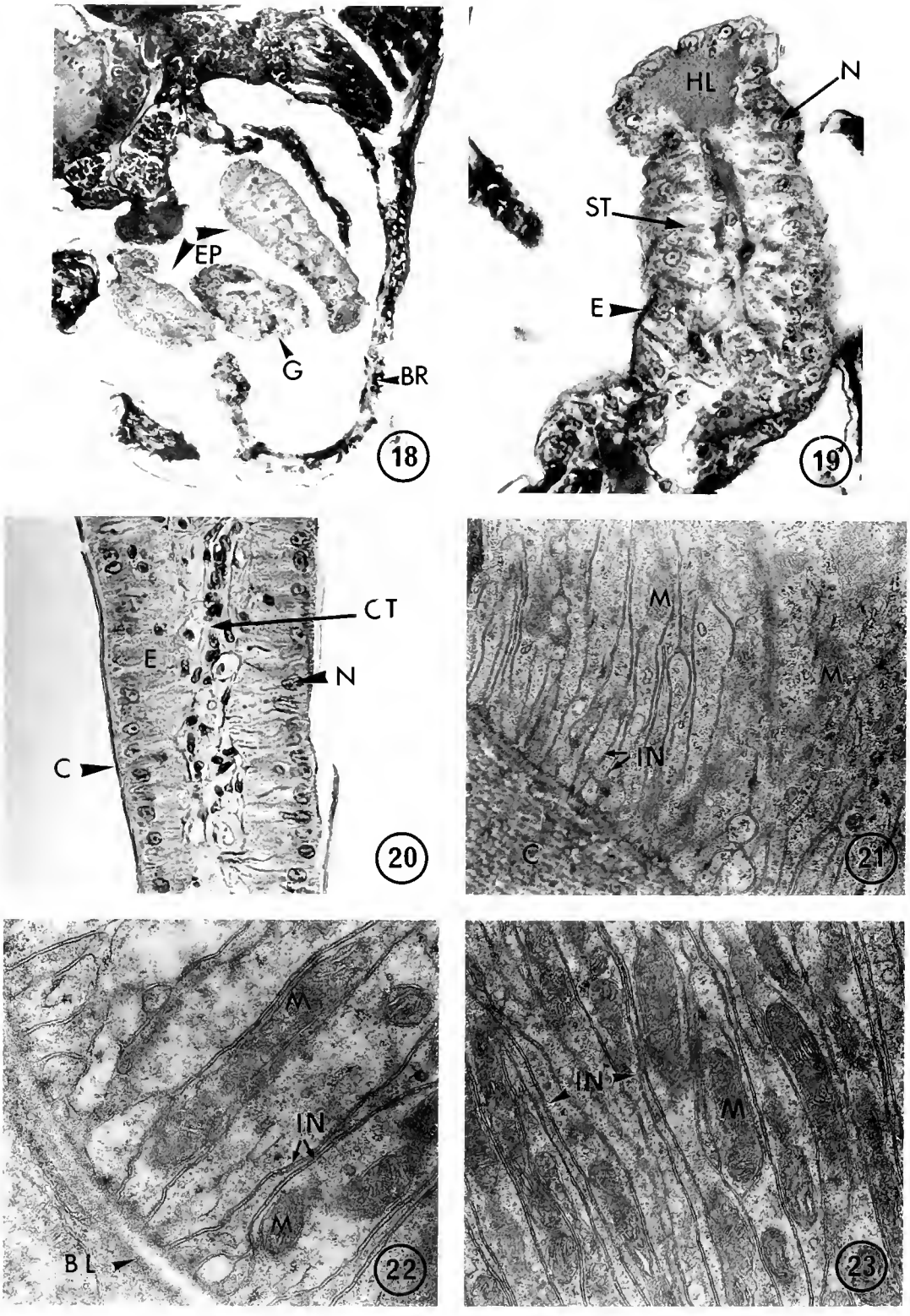

Figures 18–23. Epipodites in postlarvae and adult of *Penaeus japonicus*. BL: basal lamina, BR: branchiostegite, C: cuticle, CT: central connective tissue, E: epithelium, EP: epipodite, G: gill, HL: hemolymphatic lacuna, IN: infoldings, M: mitochondria, N: nucleus, ST: striation.

Figure 18. Transverse section of the branchial chamber, postlarvae PL 5 (× 200). The branchial chamber is almost completely enclosed by the folded branchiostegite. Epipodites are intercalated between the gills.

A similar type of epithelium, localized on the internal surface of the branchial chamber, has been found in larvae and postlarvae of *P. aztecus* (Talbot *et al.*, 1972) and in the two zoeal stages of *Callianassa jamaicense* (Felder *et al.*, 1986).

Our observations demonstrate that the differentiation of the branchiostegite and pleural epithelia has disappeared in adults. We hypothesize that branchiostegite and pleural epithelia have an osmoregulatory function in the young stages of *P. japonicus* before the adult structures (*i.e.*, gills and epipodites; see next paragraph) differentiate and take up this function. This hypothesis is supported by the very low level of Na^+-K^+ ATPase activity in the branchiostegite of adult *P. japonicus* (Bouaricha, 1990; Bouaricha *et al.*, 1991). Similar results have been described in *Artemia salina:* the nauplii, which are strong regulators, possess a dorsal gland with the typical differentiations of a tissue implicated in osmoregulation (Conte *et al.*, 1972; Hootman and Conte, 1975). This gland degenerates when "gills" develop (Dejdar, 1930).

Rough endoplasmic reticulum, ribosomes, and golgi profiles are very abundant in the branchiostegite of adult *P. japonicus*, after the regression of its microvilli; this tissue could thus shift from osmoregulation to other functions.

Epipodite

Epipodites and gills appear concurrently during postlarval development. Epipodite cells appear striated (light microscopy) in postlarvae, and electron microscopical observations demonstrate that this epithelium is thicker and more differentiated than that in the other adult tissues studied (*i.e.*, gills, branchiostegites, pleurae). The cells of the epithelium are very similar to the thick cells, or ionocytes, described on the posterior pair of gills in crabs (review in Taylor and Taylor, 1992). Copeland's "mitochondrial pumps" are present in all cells and along the whole length of the epipodites. Very few comparable studies are available in other species. Buchanan (1889) proposed a gill-cleaning function for *Penaeus* epipodites. According to Hudinaga (1942), who described them and included them in the gill formula under the name of mastigobranchia, epipodites are gill structures. In *Crangon vulgaris* (Debaisieux, 1970), the epipodite, as studied by light microscopy, has a thick epithelium. In *Astacus pallipes* and *A. leptodactylus,* Bock (1925) described the epipodites as wide vascular structures offering a large exchange surface; an electron microscopical study of these structures revealed important differentiations similar to those described in *P. japonicus* (Dunel-Erb *et al.*, 1982).

Epipodites and gills have a common phylogenetic origin (Mill, 1972). In decapods, podobranchiate gills originate from epipodites. In *P. japonicus,* podobranchiate gills and epipodites are attached at the same location on the coxopodite of maxillipeds. Their common origin, their topographical and histological similarities, and their features typical of ion-transporting tissues suggest that epipodites are probably involved in osmoregulatory mechanisms. This is further supported by the high level of Na^+-K^+ ATPase activity measured in epipodites of adult *P. japonicus* (Bouaricha, 1990; Bouaricha *et al.*, 1991).

In summary, osmoregulatory structures are progressively established during the postembryonic development of *P. japonicus* (Fig. 24). In larval stages, before gills and epipodites are present, the features typical of osmoregulatory epithelia were observed in pleurae and branchiostegites. During the postlarval stages, the osmoregulatory structures are still present in the branchiostegites and pleurae, but these disappear in the juveniles and adults. Gills and epipodites continue developing during the postlarval stages. In juveniles and adults, the gill epithelium is thin, slightly differentiated, and certainly most involved in respiration. From our observations in adults, both the gills and epipodites could be involved in osmoregulation. But the robust and dense osmoregulatory structures in the epipodites of adult *P. japonicus* point to a major osmoregulatory function of the epipodites, a new finding in penaeid shrimps and in decapod crustaceans.

Relation between the ontogeny of osmoregulatory structures and the ontogeny of osmoregulation

Previous studies conducted in *P. japonicus* on ATPase activity (Bouaricha, 1990; Bouaricha *et al.*, 1991), osmoregulation (Charmantier, 1986; Charmantier *et al.*, 1988), and salinity tolerance (Charmantier *et al.*, 1987; Charmantier-Daures *et al.*, 1988) during the postembryonic development, as well as the results of this study, support the existence of correlations between the establishment of osmoregulatory structures and the ontogeny of osmoregulatory physiological processes.

Figure 19. Epipodite, postlarvae PL 5 (×500). The simple epithelium encloses a vascular network enlarged in a lacuna at the tip.

Figure 20. Epipodite, adult structure. Two simple columnar epithelia, separated by a central connective tissue.

Figures 21–22. Epipodite, adult (×13000 and ×23000). Apical (Fig. 21) and basal (Fig. 22) part of the epithelium with numerous infoldings associated with mitochondria.

Figure 23. Epipodite, adult (×14000). Detail of association between mitochondriae and infoldings.

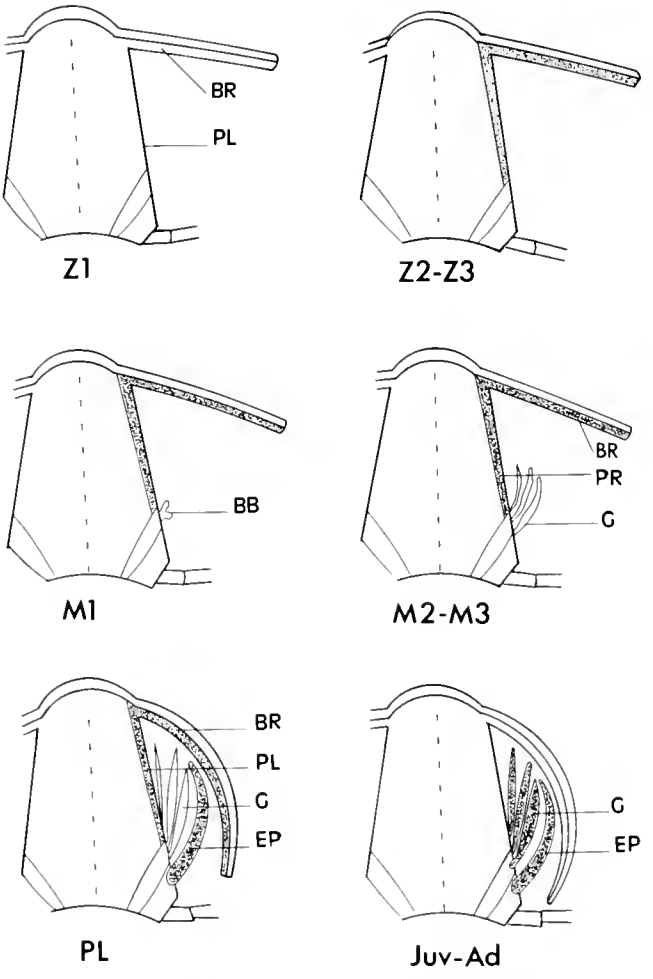

Figure 24. Ontogeny of osmoregulatory epithelia (dotted areas) throughout the postembryonic development of *Penaeus japonicus*; schematic transverse sections through the cephalothorax. Z: zoeae, M: mysis, PL: postlarva, Juv-Ad: juvenile and adult, BR: branchiostegite, EP: epipodite, G: gills, PR: pleura.

In young larvae (nauplii and zoea 1), osmoregulatory structures that can be related to the nonexistent ATPase activity are absent (Bouaricha *et al.*, 1991), because Na^+-K^+ ATPase is located in basolateral membranes of ion-transporting tissues (Towle, 1981; Towle, 1984a, b; Towle and Kays, 1986). These stages are probably osmoconformers and are not tolerant to low salinities (Charmantier *et al.*, 1988).

In later larval stages (mysis 2–3), osmoregulatory tissues are present in the branchial chambers, on the inner side of the branchiostegites, and on the pleurae. The gills and the first epipodites appear as buds at these stages (Hudinaga, 1942; Bouaricha, 1990). The activity of Na^+-K^+ ATPase increases slightly, but these stages retain an osmoconforming type of regulation and a low tolerance to variations in salinity.

After metamorphosis, *i.e.*, in postlarvae, osmoregulatory tissues disappear from the branchiostegites and pleurae while appearing during the postlarval phase in the gills and mainly in the epipodites. ATPase activity increases correlatively and reaches a maximum in PL5 and, to a lesser extent, in PL 6 (Bouaricha *et al.*, 1991). Osmotic regulation becomes hyper- and hypoosmotic starting in PL 1, and hyper- and hypoosmoregulatory capacities reach a maximum in PL 5–6 and later stages (Charmantier *et al.*, 1988). Salinity tolerance also increases in PL 5–6 and later stages; under natural conditions, these stages will have migrated from the open sea to coastal, lagunal, and estuarine habitats that are subject to ample fluctuations in salinity.

In conclusion, the ontogeny of osmoregulatory structures described in this study is strongly correlated with the ontogeny of the physiological processes of osmoregulation, and both are correlated with the ecology of *P. japonicus*.

Acknowledgments

The authors wish to thank Mrs. Mary-Alice Garcia and Mrs. Evelyse Grousset for their technical assistance. Two

anonymous reviewers and Dr. Michael J. Greenberg made helpful comments on the manuscript.

Literature Cited

Allen, E. 1892. On the minute structure of the gills of *Palaemonetes varians*. *Q. J. Microsc. Sci.* **34:** 75–84.

Babula, A. 1979. Structure of the respiratory organs of the fresh water isopod *Asellus aquaticus* L. (Crustacea). *Bull. Soc. Amis Sci. Let. Poznan* **19:** 75–82.

Barra, J. A., A. Pequeux, and W. Humbert. 1983. A morphological study on gills of a crab acclimated to fresh-water. *Tissue & Cell* **15:** 583–596.

Berridge, M. J., and J. O. Oschman. 1972. *Transporting Epithelia.* Academic Press, New York. 91 pp.

Bielawski, J. 1971. Ultrastructure and ion transport in gill epithelium of the crayfish *Astacus leptodactylus* Esch. *Protoplasma* **73:** 177–190.

Bock, F. 1925. Die respirations Organe von *Potamobius astacus* Leach. (*Astacus fluviatilis* Fabr.). Ein Beitrag zur Morphologie der Decapoden. *Z. Wiss Zöol.* **124:** 51–117.

Bouaricha, N. 1990. Ontogenèse de l'osmorégulation chez la crevette *Penaeus japonicus*. Doctoral Thesis, Université de Montpellier, France. 176 pp.

Bouaricha, N., P. Thuet, G. Charmantier, M. Charmantier-Daures, and J.-P. Trilles. 1991. Na^+-K^+ ATPase and carbonic anhydrase activities in larvae, postlarvae and adults of the shrimp *Penaeus japonicus* (Decapoda, Penaeidea). *Comp. Biochem. Physiol.* **100A:** 433–437.

Bubel, A. 1976. Histological and electron microscopical observations on the effects of different salinities and heavy metal ions, on the gills of *Jaera nordmanni* (Rathke) (Crustacea, Isopoda). *Cell Tissue Res.* **167:** 65–95.

Bubel, A., and M. B. Jones. 1974. Fine structure of the gills of *Jaera nordmanni* (Rathke) (Crustacea, Isopoda). *J. Mar. Biol. Ass. U.K.* **54:** 737–743.

Buchanan, F. 1889. On the ancestral development of the respiratory organs in the Decapoda Crustacea. *Q. J. Microsc. Sci.* **28:** 457–467.

Burggren, W. W., B. R. McMahon, and J. W. Costeron. 1974. Branchial water- and blood-flow patterns and the structure of the gills of the crayfish *Procambarus clarkii*. *Can J. Zool.* **52:** 1511–1518.

Charmantier, G. 1986. Variation des capacités osmorégulatrices au cours du développement post-embryonnaire de *Penaeus japonicus* Bate, 1888 (Crustacea, Decapoda). *C. R. Acad. Sci. Paris* **303:** 217–222.

Charmantier, G., N. Bouaricha, M. Charmantier-Daures, P. Thuet, J.-P. Trilles and Equipe Merea de Palavas. 1987. Tolérance à la salinité au cours du développement larvaire et post-larvaire de *Penaeus japonicus*. *Equinoxe* **17:** 20–22.

Charmantier, G., M. Charmantier-Daures, N. Bouaricha, P. Thuet, D. E. Aiken, and J.-P. Trilles. 1988. Ontogeny of osmoregulation and salinity tolerance in two decapods crustaceans: *Homarus americanus* and *Penaeus japonicus*. *Biol. Bull.* **175:** 102–110.

Charmantier-Daures, M., P. Thuet, G. Charmantier, and J.-P. Trilles. 1988. Tolérance à la salinité et osmorégulation chez les post-larves de *Penaeus japonicus* et *P. chinensis*. Effet de la température. *Aquat. Liv. Res.* **1:** 267–276.

Chen, P. S. 1933. Zur Morphologie und Histologie der respirations Organe von *Grapsus grapsus* L. Jena. *Z. Naturw. N.F.* **61:** 31–88.

Compere, P., S. Wansoo, A. Pequeux, R. Gilles, and G. Goffinet. 1989. Ultrastructural changes in the gill epithelium of the green crab *Carcinus maenas* in relation to the external salinity. *Tissue & Cell* **21:** 299–318.

Conte, F. P., S. R. Hootman, and P. J. Harris. 1972. Neck organ of *Artemia salina* nauplii. A larval salt gland. *J. Comp. Physiol.* **80:** 239–246.

Copeland, D. E. 1964. Salt absorbing cells in gills of crabs, *Callinectes* and *Carcinus*. *Biol. Bull.* **127:** 367–368.

Copeland, D. E. 1968. Fine structure of salt water uptake in the land crab, *Gecarcinus lateralis*. *Am. Zool.* **8:** 417–432.

Copeland, D. E., and A. T. Fitzjarrell. 1968. The salt absorbing cells in the gills of the blue crab (*Callinectes sapidus* Rathbun) with notes on modified mitochondria. *J. Zellforsch.* **92:** 1–22.

Croghan, P. C. 1976. Ionic and osmotic regulation of aquatic animals. Pp. 59–94 in *Environmental Physiology of Animals*, J. Bligh, J. L. Cloudsley-Thomson, and A. G. McDonald, eds. Blackwell, Oxford.

Debaisieux, P. 1970. Appareil branchial de *Crangon vulgaris* (Décapode nageur). Anatomie et histologie. *La Cellule* **69:** 64–82.

Dejdar, E. 1930. Die Korrelationen zwischen Kiemensacken und Nackenschild bei Phyllopoden (versuch einer Analyse mit Hilfe elektiver Vitalfärbung). *Z. Wiss. Zool.* **136:** 422–452.

Doughtie, D. G., and K. R. Rao. 1978. Ultrastructural changes induced by sodium pentachlorophenate in the grass shrimps, *Palaemonetes pugio*, in relation to the molt cycle. Pp. 213–250 in *Pentachlorophenol: Chemistry, Pharmacology and Environmental Toxicology*, K. R. Rao, ed. Plenum Press, New York.

Drach, P. 1930. Etude sur le système branchial des Crustacés Décapodes. *Arch. Anat. Microsc.* **26:** 83–133.

Drach, P., and C. Tchernigovtzeff. 1967. Sur la méthode de détermination des stades d'intermue et son application générale aux Crustacés. *Vie Milieu* **18:** 596–609.

Dunel-Erb, S., J. C. Massabuau, and P. Laurent. 1982. Organisation fonctionnelle de la branchie d'écrevisse. *C. R. Soc. Biol.* **176:** 248–258.

Felder, J. M., D. L. Felder, and S. C. Haod. 1986. Ontogeny of osmoregulation in the estuarine ghost shrimp *Callianassa jamaicense* var. *louisianensis* Schmitt. *J. Exp. Mar. Biol. Ecol.* **99:** 91–106.

Finol, H. J., and P. C. Croghan. 1983. Ultrastructure of the branchial epithelium of an amphibious brackish-water crab. *Tissue & Cell* **15:** 63–75.

Fisher, J. M. 1972. Fine structural observations on the gill filaments of the fresh water crayfish *Astacus pallipes* Lereboullet. *Tissue & Cell* **4:** 287–299.

Foster, C. A., and H. D. Howse. 1978. A morphological study on gills of the brown shrimp, *Penaeus aztecus*. *Tissue & Cell* **10:** 77–92.

Gilles, R. 1975. Mechanisms of ion and osmoregulation. Pp. 259–347 in *Marine Ecology*, O. Kinne, ed. Wiley-Interscience, New York **2:** 259–347.

Goodman, S. H., and M. J. Cavey. 1988. Epithelial cells in the phyllobranchiate gills of the shore crab. *Am. Zool.* **28:** 142.

Goodman, S. H., and M. J. Cavey. 1990. Organization of a phyllobranchiate gill from the green crab *Carcinus maenas* (Crustacea, Decapoda). *Cell Tissue Res.* **260:** 495–505.

Hootman, S. R., and F. P. Conte. 1975. Functional morphology of the neck organ in *Artemia salina* nauplii. *J. Morph.* **145:** 371–386.

Hudinaga, M. 1942. Reproduction, development and rearing of *Penaeus japonicus* Bate. *Japn. J. Zool.* **10:** 305–353.

Kirschner, L. B. 1979. Control mechanisms in crustaceans and fishs. Pp. 157–222 in *Mechanisms of Osmoregulation in Animals*, R. Gilles, ed. Wiley, New York.

Lockwood, A. P. M. 1962. The osmoregulation of Crustacea. *J. Exp. Biol.* **37:** 257–305.

Lockwood, A. P. M. 1968. *Aspects of the Physiology of Crustacea* Oliver and Boyd, Edinburgh 328 pp.

Martelo, M. J., and P. I. Zanders. 1986. Modifications of gill ultrastructure and ionic composition in the crab *Gecarcinus cruentata* acclimated to various salinities. *Comp. Biochem. Physiol.* **84A:** 383–389.

Martoja, R., and M. Martoja. 1967. *Initiation aux Techniques de L'histologie Animale*. Masson et Cie, Paris. 345 pp.

Mill, P. J. 1972. Gills, podia and papulae. Pp. 14–63 in *Respiration in the Invertebrates*, P. J. Mills, ed, MacMillan Press, London.

Milne, D. J., and R. A. Ellis. 1973. The effects of salinity acclimation on the ultrastructure of the gills of *Gammarus oceanicus* (Segerstrale, 1947), (Crustacea, Amphipoda). *Z. Zellforsch.* **139:** 311–318.

Papathanassiou, E. 1985. Effects of calcium ions on the ultrastructure of the gill cells of the brown shirmp *Crangon crangon* (L.), (Decapoda, Caridea). *Crustaceana* **48:** 6–17.

Pease, D. C. 1956. Infolded basal plasma membranes found in epithelia noted for their water transport. *J. Biophys. Biochem. Cytol. Suppl* **2:** 203–208.

Pequeux, A., and R. Gilles. 1981. Na^+ fluxes across isolated perfused gills of the chinese crab, *Eriocheir sinensis*. *J. Exp. Biol.* **92:** 173–186.

Pequeux, A., and R. Gilles. 1988. NaCl transport in gills and related structures. Pp. 2–47 in *Comparative and Environmental Physiology NaCl Transport in Epithelia*, R. Greger, ed. Springer Verlag, New York.

Robertson, J. D. 1960. Osmotic and ionic regulation. In *Physiology of Crustacea* Vol. I, T. H. Waterman, ed. Academic Press, New York.

Scholfeniels, E., and R. Gilles. 1970. Osmoregulation in aquatic arthropods. Pp. 255–286 in *Chemical Zoology* Vol. 5, *Arthropoda*, Part A. M. Florkin and B. T. Scheer, eds. Academic Press, New York.

Smyth, J. D. 1942. A note on the morphology and cytology of the branchiae of *Carcinus maenas*. *Proc. Roy. Ir. Acad.* **B48:** 105–118.

Storch, V., and V. Welsch. 1975. Über Ban und Funktion der Kiemen und Lungen von *Ocypode ceratophthalma* (Decapoda, Crustacea). *Mar. Biol.* **29:** 363–371.

Talbot, P., C. Wallish, and A. L. Lawrence. 1972. Light and electron microscopic studies on osmoregulatory tissue in the developing brown shrimp *Penaeus aztecus*. *Tissue & Cell* **4:** 271–286.

Taylor, H. H., and P. Greenaway. 1979. The structure of the gills and lungs of the arid-zone crab, *Holthuisana (Austrothelphusa) transversa* (Brachyura: Sundathelphasidae) including observations on arterial vessels within the gills. *J. Zool. Lond.* **189:** 359–384.

Taylor, H. H., and E. W. Taylor. 1992. Gills and lungs: the exchange of gases and ions. Pp. 203–293 in *Microscopic Anatomy of Invertebrates*. Vol. 10: *Decapod Crustacea*. F. W. Harrison and A. G. Humes. Wiley-Liss Inc., New York.

Towle, D. W. 1981. Role of Na^+-K^+ ATPase in ionic regulation by marine and estuarine animals. *Mar. Biol. Lett.* **2:** 107–122.

Towle, D. W. 1984a. Regulatory functions of Na^+-K^+ ATPase in marine and estuarine animals. Pp. 57–170 in *Osmoregulation in Estuarine and Marine Animals*. A. Pequeux and L. Bolis, eds.

Towle, D. W. 1984b. Membrane bound ATPases in arthropod ion transporting tissues. *Am. Zool.* **24:** 177–185.

Towle, D. W., and W. T. Kays. 1986. Basolateral localisation of Na^+-K^+ ATPase in gill epithelium of two osmoregulatory crabs: *Callinectes sapidus* and *Carcinus maenas*. *J. Exp. Zool.* **239:** 311–318.

Reference: *Biol. Bull.* **186**: 41–61. (February, 1994)

Instantaneous Reproductive Effort in Female American Oysters, *Crassostrea virginica,* Measured by a New Immunoprecipitation Assay

KWANG-SIK CHOI[1,*], ERIC N. POWELL[1,†], DONALD H. LEWIS[2], AND SAMMY M. RAY[3]

[1] *Department of Oceanography and* [2] *Department of Veterinary Pathobiology, Texas A&M University, College Station, Texas 77843, and* [3] *Department of Marine Biology, Texas A&M University at Galveston, Galveston, Texas 77550*

Abstract. An immunoprecipitation assay was developed for measuring instantaneous reproductive effort in female American oysters, *Crassostrea virginica.* Oysters were injected with ^{14}C-leucine and incubated *in situ* for 1 to 30 h periodically throughout the annual gametogenic cycle. Gonadal protein labeled with ^{14}C-leucine was precipitated from an oyster homogenate with rabbit anti-oyster egg IgG as the primary antibody. Antibody-oyster egg protein complex was further purified by immunoadsorption with staphylococcal protein A cell suspension. The quantity of oyster eggs was determined by single-ring immunodiffusion. A mathematical model was developed to calculate the instantaneous reproductive rate of oysters and to estimate the number of days required from the initiation of gonadal development to spawning. The oyster population was lightly to moderately infected with a protozoan parasite, *Perkinsus marinus.* A negative correlation between the intensity of infection and the rate of gonadal production suggests that *P. marinus* retards the rate of gamete development. The seasonal cycle of gamete production determined by direct measurements of egg protein production was not equivalent to that determined by standard gonadal-somatic index (GSI), except at the most basic level. GSI was highest during the spring spawning peak, but the rate of gamete production was highest in the fall. Accordingly, the two measurements, rate *versus* standing crop (volume of gonad), reveal a substantially different picture about the details of the spawning season. Estimates of the time required to reach spawning condition ranged from several weeks to 1 or 2 months; these values agree with published estimates derived from less direct methods. Direct rate measurements thus seem to accurately reflect the true rate at which gametic tissue is produced in the field. A positive correlation between oyster size and the estimated days to spawn suggests that larger oysters require longer to prepare to spawn. Furthermore, the range in observed somatic and gametic growth emphasizes the conservatism of somatic growth and the volatility of gonadal growth that is borne out by the results of population dynamics models of oysters.

Received 26 April 1993; accepted 24 November 1993.

* Current address: Environmental Radiological Assessment Dept., Korea Institute of Nuclear Safety, P.O. Box 16, Daeduk-Danji, Taejeon, 305-606, Korea.

† Person to whom correspondence should be addressed.

Introduction

Like other bivalves, the American oyster (*Crassostrea virginica*) goes through three stages during the gametogenic cycle: (1) proliferation of germ cells, (2) vitellogenesis, or the growth and enrichment of gametes, and (3) spawning (Sastry, 1979). Egg constituents such as lipids and proteins accumulate during vitellogenesis (Kennedy and Battle, 1964). These constituents are either mobilized and synthesized from nutrient reserves in other organs or synthesized directly from compounds assimilated during feeding (Soniat and Ray, 1985; Shafee, 1989; Thompson and MacDonald, 1990; Suzuki *et al.*, 1992). Spawning occurs when the cumulative reproductive biomass reaches a certain proportion of the standing stock (Hofmann *et al.*, 1992; Choi *et al.*, 1993). Reproduction is an energetically costly process because much of the net production allocated to reproduction is lost as gametes during

spawning. The fraction of net production diverted to gamete production is called the reproductive effort. Reproductive effort in bivalves is often expressed as the total number or weight of eggs or sperm released per individual or biomass (Sprung, 1983; Deslous-Paoli and Héral, 1988; Hofmann *et al.*, 1992; Choi *et al.*, 1993).

Environmental conditions such as food availability, water temperature, salinity, and parasitism can influence growth and reproduction of oysters in various ways. For example, an increase in water temperature increases the filtration rate of oysters and also results in the diversion of more of the net energy to reproduction, resulting in increased fecundity or spawning frequency (Hofmann *et al.*, 1992). *Perkinsus marinus*, a protozoan parasite, exerts a significant impact on oyster growth and reproduction. Higher infection intensities may retard growth, delay reproductive development, or reduce spawning intensity and frequency (White *et al.*, 1988a, b; Wilson *et al.*, 1988). Infection intensity and prevalence is in part governed by salinity and water temperature. Powell *et al.* (1992) reported that regional and temporal shifts in the infection intensity of *P. marinus* in oysters in the Gulf may be controlled by long-term climatic cycles.

The reproductive effort of oysters can be examined using two approaches. Firstly, the number and developmental stage of the gametes can be assessed. This is essentially a standing crop measurement. Histology is one of the most common methods used for this assessment (Ford and Figueras, 1988; Barber *et al.*, 1988; Gauthier and Soniat, 1989; Wilson *et al.*, 1990). However, the analysis, at best, is only semiquantitative. Recently Choi *et al.* (1993) introduced an immunological technique that allows a quantitative evaluation of reproductive effort of oysters. They reported that the weight of gametes produced per spawn by oysters in Galveston Bay, Texas, amounted to as much as 40% (eggs) or 44% (sperm) of the total weight. Secondly, the rate of gamete production can be measured—for example, by measuring the rate of synthesis of gonadal protein. We will term this the instantaneous rate of gamete production. The two approaches are complementary because environmental factors may affect fecundity by varying either the number of gametes per spawn (measured by standing crop) or the spawning frequency (controlled by the rate of gamete development).

No studies have reported the instantaneous rate of gamete production in oysters because an adequate method was lacking. Accordingly, we developed a technique to measure the rate of gonadal synthesis of gametic protein in oysters based upon a radiolabeled amino acid tracer and an immunological probe. Rabbit anti-oyster egg IgG (Choi *et al.*, 1993) and staphylococcal protein A, an immunoadsorbent, were employed in a radio-immunoprecipitation assay to measure the rate of production of gonadal protein. The present study focuses on the seasonal variation in the rate of gonadal synthesis in female oysters and the effect of environmental conditions such as water temperature and *Perkinsus marinus* parasitism on that process.

Materials and Methods

Field procedures

Adult oysters (7 to 12 cm in length) were collected from Confederate Reef, Galveston Bay (Fig. 1) from August 1990 to July 1991. Collections were made monthly during the reproductive season and less frequently during the remainder of the year. Water temperature and salinity were recorded during each sampling. To administer the ^{14}C-labeled leucine, a rock saw was used to make a v-shaped notch at the posterior end of each oyster shell, and 1.5 to 2 μCi of ^{14}C-labeled L-leucine was injected into the adductor muscle. The oysters were then placed in a

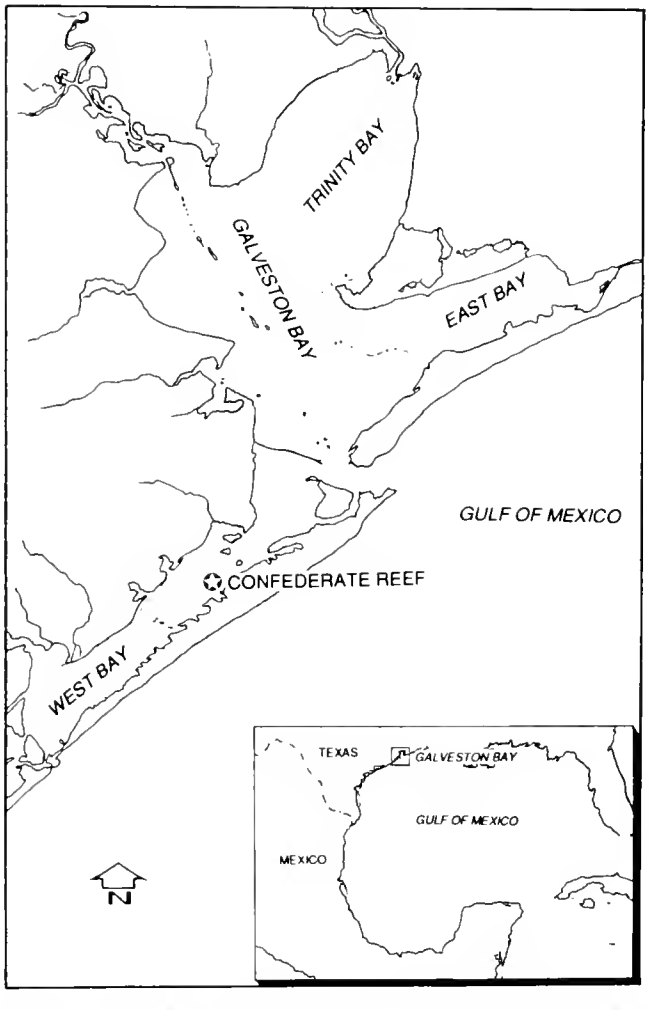

Figure 1. Location of study area, Confederate Reef in West Bay, Texas.

nylon-mesh bag and incubated *in situ* according to the experimental design. Table I summarizes the data collection efforts. After incubation, oysters were opened and the maximum length of the upper shell was recorded. A piece of mantle tissue was taken from each oyster and placed into a 10-ml culture tube containing fluid thioglycollate medium fortified with antibiotics according to Ray (1966) to assess the intensity of infection by *P. marinus*. A narrow cross-sectional slice was taken from the central part of the body and fixed in a 25-ml Bouin's solution for the examination of gametogenic stage. The remaining oyster flesh was frozen on dry ice, transported to the laboratory, and stored at −40°C until used.

Table I

Data collection efforts during the study

Sampling Date	^{14}C-leucine injected (μCi/oyster)	Incubation time (h)	Number assayed
08/16/90	2	10, 20, 30	15
09/26/90	1.5	1, 2, 5, 10	16
10/29/90	1.5	1, 2, 5, 10, 30	50
02/01/91	1.5	1, 2, 5, 10, 30	25
03/19/91	1.5	1, 2, 5, 10, 30	25
04/16/91	1.5	1, 2, 5, 10, 30	25
05/23/91	1.5	1, 2, 5, 10, 30	25
07/15/91	1.5	1, 2, 5, 10, 30	25

Laboratory procedures

The samples of mantle tissue were incubated in thioglycollate medium for 2 weeks (Ray, 1966), at which time the infection intensity of *P. marinus* was scored from 0 (uninfected) to 5 (heavily infected) according to Mackin (1962) as modified by Craig *et al.* (1989).

The frozen oyster samples were thawed and excess water was removed. First the total wet weight of each oyster was measured, then the body mass containing gonadal material was separated from the other somatic tissues and weighed. Wet weight was converted to dry weight using the empirical relation: dry weight = wet weight × 0.196 (Choi *et al.*, 1993). After a known volume of phosphate buffered saline (PBS; 0.15 *M* NaCl, 0.003 *M* KCl, 0.01 *M* phosphate, pH 7.3) was added, the body tissue was homogenized first in a glass syringe tissue grinder and then in an ultrasonicator. The homogenate was centrifuged at 1200 × *g* for 10 min, and the volume of supernatant recorded. The quantity of total protein in the supernatant was determined using the BCA Protein Assay (Pierce, Illinois) with bovine serum albumin as the protein standard.

The quantity of oyster eggs was measured using rabbit anti-oyster egg serum (Choi *et al.*, 1993) and a single-ring immunodiffusion assay according to Mancini *et al.* (1965) and Gallagher *et al.* (1988). A 1.5% (w/v) agarose gel was prepared in barbitone buffer (0.01 *M* sodium barbital, 0.02 *M* barbital, and 0.05% sodium azide as preservative, pH 8.6). A 2-ml aliquot of oyster egg-specific rabbit antiserum was mixed with 18 ml agarose gel and poured onto a 10 × 10 cm glass plate. The gel was solidified in a refrigerator for 10 min and 4-mm-diameter wells were made using a gel puncher. On each plate, 20-μl aliquots of various concentrations of oyster egg protein (positive controls), reproductively inactive female oyster homogenate (negative control), and the oyster homogenate to be analyzed were added to the wells and incubated for 72 h in a humid container at 4°C. After incubation, the plate was pressed, dried, stained with 1% Coomassie brilliant blue (w/v) (Bio-Rad, California) dissolved in 50% ethanol and 10% glacial acetic acid for 2 h, and destained in 50% ethanol and 10% glacial acetic acid for 2 h. After the plate was stained and destained, the diameter of the ring-shaped antigen-antibody precipitates was measured to 0.1 mm and converted to square millimeters. A nonlinear regression curve was constructed from the positive controls to quantify the amount of egg protein. Biomass of the eggs was then estimated from the single-ring immunodiffusion assay results and the following empirical relationship: total dry weight of egg = oyster egg protein (mg ml^{-1})/0.370 (percent weight of protein in oyster egg) × total homogenate volume (ml). A gonadal-somatic index (GSI) was calculated as the ratio of dry weight of oyster eggs to dry weight of total oyster.

^{14}C-labeled leucine used in the synthesis of gonadal protein and other somatic protein was analyzed using protein A immunoprecipitation and trichloroacetic acid (TCA) protein precipitation. For measuring the amount of ^{14}C-leucine incorporated into somatic protein, 1 ml of oyster homogenate was brought up to 10% TCA with 50% TCA to precipitate all proteins in the homogenate. The TCA-oyster homogenate mixture was placed in an ice-filled bucket, incubated for 30 min, and centrifuged. After centrifugation, the supernatant was saved for further analysis of free leucine. TCA-precipitated protein was then rinsed twice with 100% ethanol, dissolved using Solusol (National Diagnostics, New Jersey), and measured using a liquid scintillation counter. The counter readings were corrected for quench by internal standards (Gordon, 1980).

The amount of free leucine in oysters at the time of sacrifice was analyzed from the TCA supernatant by use of an amino acid analyzer with a lithium citrate buffer system and *o*-phthalaldehyde as the detecting agent. Norleucine was added as the internal standard. The eluent fraction containing leucine was collected from the amino acid analyzer with a fraction collector, mixed with Soluscint A (National Diagnostics, New Jersey) and counted

using a liquid scintillation counter. Quench was corrected for as previously described.

The incorporation of ^{14}C-leucine into oyster eggs was estimated using immunoprecipitation with staphylococcal protein A (*Staphylococcus aureus* Cowan I strain cell suspension, Sigma) as an immunoadsorbent (Kessler, 1975). Rabbit anti-oyster egg IgG (2 mg ml^{-1}) was reacted with 1 ml of oyster homogenate (containing up to 2 mg egg protein ml^{-1} as determined from the single-ring immunodiffusion assay) in a test tube and incubated for 1 h at room temperature. After incubation, 100 mg ml^{-1} protein A cell suspension was added according to the manufacturer's directions, incubated for 1 h, and centrifuged at 4000 × *g* for 10 min. The antibody-antigen-protein A complex was rinsed twice with 10 ml PBS and then dissolved in a liquid scintillation solution (Solusol—National Diagnostics, New Jersey). The amount of ^{14}C-leucine in the eggs was determined by liquid scintillation counting as previously described for the TCA precipitate.

Model

Perspective

Three important, but conservative, assumptions are required to use radiolabeled leucine as a tracer in this study. First, oysters do not distinguish ^{14}C-leucine from unlabeled leucine present in oysters, so both isotopes are used indiscriminately during protein synthesis and degradation. Second, the amount of ^{14}C-leucine injected into the oysters is small enough not to disturb the amino acid balance. Third, the labeled leucine does not exchange with somatic or gonadal components by any process other than protein synthesis and degradation.

In order to calculate the instantaneous rate of gonadal production (the amount of gonadal material produced per unit time), the measured rate of incorporation of labeled leucine must be corrected by the specific activity of the free leucine pool (Samarel, 1991). Stated mathematically,

$$dg/dt = [dg^*/dt]\,[f(t)/f^*(t)] \qquad (1)$$

where g is the amount of leucine incorporated (moles g dry wt^{-1}), g^* is the amount of labeled leucine incorporated (dpm g dry wt^{-1}), t is time, f is the amount of free leucine (moles g dry wt^{-1}), and f^* is the amount of labeled free leucine (dpm g dry wt^{-1}).

The experimental protocol requires that f^*, the amount of labeled free leucine, be a function of time because a constant perfusion technique was not used. Because most animals undergo a stress response to experimental manipulation which results in changes in the free amino acid pool, f, the amount of free leucine present, is also likely to be a function of time. As a result, evaluation of equation (1) first requires an evaluation of $f(t)$ and $f^*(t)$.

Most pulse-labeling experiments utilize a number of replicates to permit calculation of the mean effect and the variation about the mean. Such experiments are based on the assumption that all individuals are initially equivalent, to the extent permitted by the normal stochastic variation about the mean. Experiments on reproduction, however, frequently do not meet this assumption, particularly those run in the field where temperature cannot be manipulated to control the reproductive cycle. The individuals used in the experiments we describe could be expected to be in different stages of their reproductive cycle, as indeed they were. Accordingly, no true replicates exist in this set of experiments, and the mean value is not necessarily meaningful for all interpretations. Consequently, equation (1) ideally would be solved separately for each individual.

The problem posed as equation (1) cannot be solved separately for every individual, however. Nevertheless, components of it can be solved for single individuals, provided that the specific rates of some components can be assumed to be common to all individuals. The specific rates that are important in the solution of equation (1) are those controlling the loss of labeled leucine from the free leucine pool, the changes in concentration of the free leucine pool, the rate of uptake of free leucine into the gonadal protein pool, and the rate of loss of leucine from the gonadal protein pool. Because the rates of uptake and loss from the gonadal pool are unlikely to be equivalent in all individuals, we must assume that the rates of processes controlling the specific activity of labeled leucine $[f(t)/f^*(t)]$ are equivalent. This assumption is reasonable because the loss of labeled leucine probably involves diffusional and metabolic processes common to most individuals, and the change in the free leucine pool involves a stress response to a manipulation common to all individuals. In particular, the amount of labeled leucine used in the formation of gonadal tissue is small relative to the amount injected. Accordingly, variations in the metabolic processes involved in reproduction had little effect on the total available pool of labeled leucine.

Calculation of specific activity—the labeled free leucine pool

We assume that the loss of labeled leucine from the free leucine pool is a first-order process. Accordingly,

$$df^*/dt = -kf^* \qquad (2)$$

where k is the first-order rate constant (time^{-1}). Comparison of the results obtained by evaluating equation (2) with the measured values shows that equation (2) does not adequately describe the change in labeled free leucine in the free leucine pool over the experimental time course. Assuming that the labeled leucine exists in two separate pools is, however, much more satisfactory. Hence,

$$df_1^*/dt = -k_1 f_1^* \quad (3)$$

and

$$df_2^*/dt = -k_2 f_2^* \quad (4)$$

where $f_1^* + f_2^* = f_{\text{total}}^*$, the measured value.

The two-pool model does not necessarily imply that only two pools exist or that the pools are continuously discrete. Failure of equation (2) to predict the measured results requires a multipool model if the processes are first-order. Experience indicates that equations (3) and (4) are good curve-fitting routines and often adequately fit data from multiple pools. Accordingly, in using equations (3) and (4), we do not necessarily conclude anything about the processes determining the time course of labeled leucine except that a multiple pool model is required.

We solved equations (3) and (4) using the boundary conditions $t = t_\circ$ at $f^*(t) = f_\circ^*(t)$. We cannot generally set $t_\circ$ equal to zero, the time of injection, because the time course before the first sampling is unknown. Initially, the specific activity would be controlled by processes affecting the distribution of the label throughout the animal as well as by tissue-specific metabolism. Accordingly, the experimental protocol necessitates that $t_\circ$ be the time of the first sampling (usually 1 h). As a consequence, data from the first sampling cannot be used to evaluate any subsequent process rate. That sampling only defines the metabolic milieu at the beginning of the measured time course.

Solving equations (3) and (4) yields

$$f^*(t) = f_1^*(t) + f_2^*(t) = f_{\circ 1}^* e^{k_1(t_\circ - t)} + f_{\circ 2}^* e^{k_2(t_\circ - t)}. \quad (5)$$

We define $f_\circ^* = f_{\circ 1}^* + f_{\circ 2}^*$ as the mean amount of labeled leucine observed in the first sampling period. The two first-order rate constants, k_1 and k_2, and the fraction of the labeled free leucine in each pool, $f_{\circ 1}^*/f_\circ^*$, were obtained iteratively by computer by searching for the values yielding the best fit to the observations using a chi-square-type error term to evaluate the goodness-of-fit.

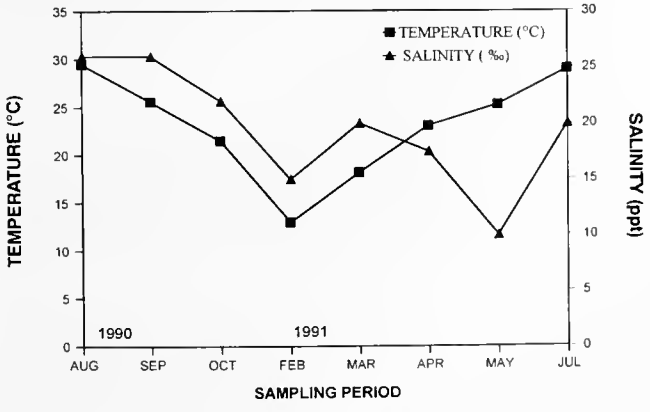

Figure 2. Water temperature (°C) and salinity (‰) at each sampling period.

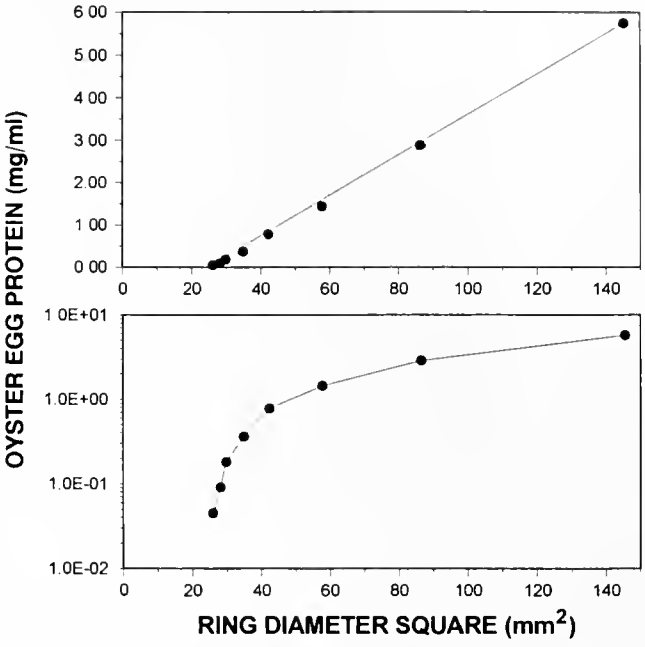

Figure 3. A typical standard curve for the single-ring immunodiffusion assay for rabbit anti-oyster egg serum.

As stated earlier, if the specific rates are assumed equal among all individuals (that is, the specific rates describe a process common to all individuals), then the value for $f^*(t)$ for any individual can be obtained by solving equation (5) using the value of $f_\circ^*$ for that individual. In essence, this assumes that the variation between individuals is produced by the efficiency of injection—some animals received more label than others—rather than the processes controlling loss after injection. Comparing the data obtained during January, where metabolic processes were slowed by low temperatures, with all other observations, suggests that this assumption is valid. The success of injection is the primary determinant controlling the variation in the amount of labeled free leucine available for use in metabolism during the experiment.

Calculation of specific activity—the free leucine pool

The free leucine pool was also not stable during the experimental time course. Typically, free leucine rose in concentration during the first few hours and then declined. This transient rise in concentration was found in most months and probably represents a response to the stress of injection. The invertebrate stress response to experimental manipulation typically includes protein breakdown and a rise in the concentration of free amino acids.

The free amino acid pool is governed by a balance between the addition of amino acid from protein breakdown

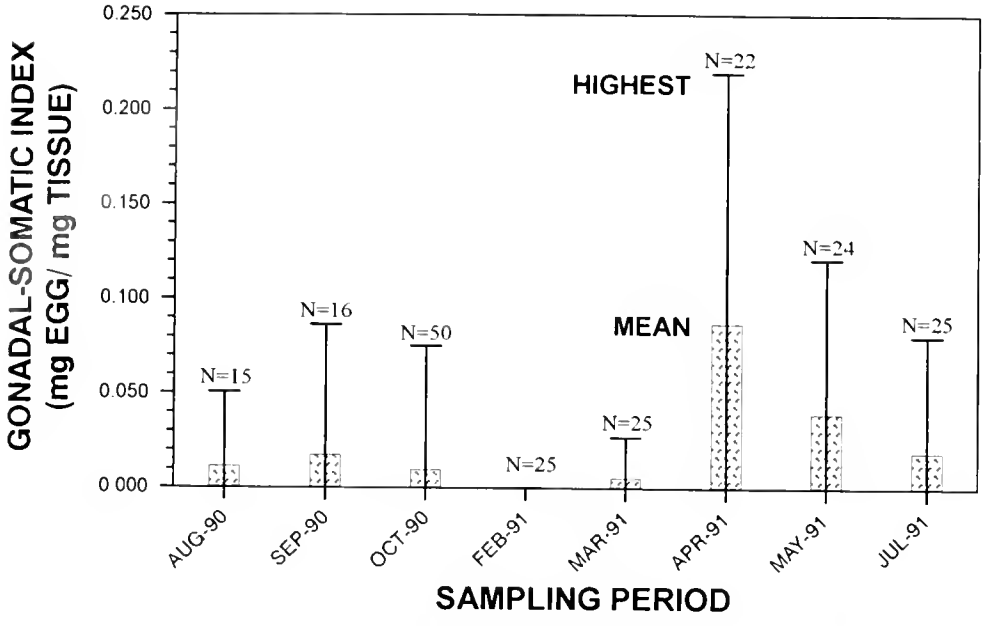

Figure 4. Seasonal variation in the gonadal-somatic index (GSI) of oysters. The mean (bar) and the range (highest and lowest values) are plotted.

or digestive processes and the loss of amino acid by anabolic and catabolic processes. Accordingly, and assuming that all processes are again of first-order,

$$df/dt = \text{production terms} - \text{loss terms} = k_3P(t) - k_4f \quad (6)$$

where $P(t)$ is the precursor pool and k_3 and k_4 are specific rates. $P(t)$ can be described as the result of a first-order reaction analogous to equation (2), where

$$dP/dt = -kP \quad (7)$$

Once again, evaluation of equation (6) generally showed that a one-pool model was inaccurate. A two-pool model generally provided an accurate description of the measured values:

$$df_1/dt = k_3P_1(t) - k_4f_1 \quad (8)$$

and

$$df_2/dt = k_5P_2(t) - k_6f_2 \quad (9)$$

where $f_1 + f_2 = f_{\text{total}}$, the measured value. We assume $f_1/f_2 = P_1/P_2$. Once again, the same caveats and assumptions apply as were discussed in the evaluation of f^*, and the equations for P_1 and P_2 are of the form of equations (3) and (4). Once again, we solved the equations using the boundary conditions $t = t_\circ$ at $f(t) = f_\circ(t)$ and set $t_\circ$ to be the time of the first sampling (usually 1 h). Equation (8) yields

$$f_1(t) = f_{\circ 1}e^{k_4(t_\circ - t)} + [k_3P_{\circ 1}/(k_4 - k_3)][e^{k_3(t_\circ - t)} - e^{k_4(t_\circ - t)}]. \quad (10)$$

Equation (9) yields a similar solution. The four first-order rate constants (k_3, k_4, k_5, k_6) and the fraction of free leucine in each pool, $f_{\circ 1}/f_\circ$ and $f_{\circ 2}/f_\circ$, were obtained iteratively by computer by searching for the values yielding the best fit to the observations using a chi-square-type error term to evaluate the goodness-of-fit.

The values of P_1 and P_2 are unknown. We assume that $P_1 + P_2 = P_{\text{total}}$ is equivalent to the highest value of free leucine measured (f_{total}). To the extent that this is inaccurate, the specific rates calculated (k_3, k_4, k_5, k_6) will not reflect those rates actually present. These values, then, are relative to the estimated protein pool size. However, because these rates are obtained from observations of the free leucine pool and equations (8) and (9) are used solely to estimate f, the use of specific rates scaled to an unknown protein pool size still provides an accurate estimate of the concentration of free leucine at any particular time.

The specific rates of leucine uptake and loss from gonadal protein

The amount of labeled leucine measured in gonadal protein is the net of two processes: free amino acid incorporation during protein synthesis and free amino acid release during protein degradation. Stated mathematically

$$dg^*/dt = \text{growth terms} - \text{loss terms} = k_{gg}f^*(t) - k_{lg}g^* \quad (11)$$

where g^* is the amount of labeled leucine in gonadal tissue and k_{gg} and k_{lg} are the specific rates governing the rates of protein synthesis and degradation, respectively. We use

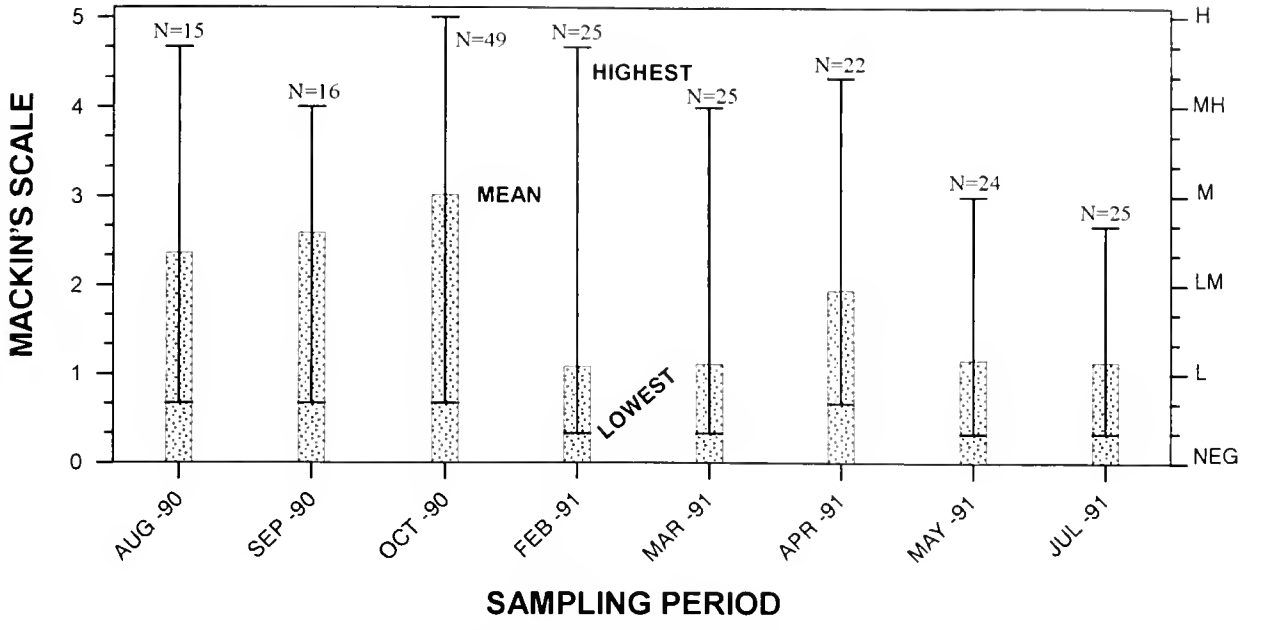

Figure 5. Seasonal fluctuation in infection intensity of *Perkinsus marinus*. The plot includes the mean (bar) and range (highest and lowest values) for each sampling month.

a first-order process for synthesis, rather than zero-order as modeled by Koehn (1991), assuming that the rate of synthesis depends upon substrate supply. Although these rates of reaction can be expected to vary with temperature, we assume that temperature was relatively constant within each experimental time course and so do not include temperature in the equations. Solving (11) yields

$$g^*(t) = g^*_\circ e^{k_{lg}(t_\circ - t)} + k_{gg}[[f^*_1/(k_{lg} - k_1)][e^{k_1(t_\circ - t)} - e^{k_{lg}(t_\circ - t)}] + [f^*_2/(k_{lg} - k_2)][e^{k_2(t_\circ - t)} - e^{k_{lg}(t_\circ - t)}]]. \quad (12)$$

Equation (12) was used to calculate the specific rates (k_{gg}, k_{lg}) for each individual. We obtained f^*_1 and f^*_2 for each individual using equation (5), and the specific f^* measured for each individual. The specific rates, k_1 and k_2, and the fractional division of the protein pool in equation (5) were all estimated from the mean values of f^*. Once again, we assume that the specific rates, k_1 and k_2, are common properties of all individuals. To solve equation (12) for k_{gg} and k_{lg}, g^* must be known; however, g^* cannot be known for most individuals, except those sampled at $t = t_\circ$, because an individual can be measured only once during the time course. Accordingly, we estimated the value of g^* for any individual using the ratio of the mean value of g^* at the first sampling ($\bar{g}^*$ by definition) to that at any other sampling and assumed that this ratio was common among all individuals.

$$g^*_i = [\bar{g}^*(t = t_\circ)/\bar{g}^*(t = t_1)]\, g^*_1(t = t_1) \quad (13)$$

We further assumed that $g^*e^{k_{lg}(t_\circ - t)} \approx g^*$. We then obtained k_1 and k_2 using equation (11) by iterative search by computer using the measured value of $g^*(t)$.

The amount of gonadal protein production (g)

Following the arguments for equation (11),

$$dg/dt = k_{gg} f(t) - k_{lg} g \quad (14)$$

Solving equation (14), and recalling that $f(t)$ is the product of two pools, yields

$$g(t) = g_\circ e^{k_{lg}(t_\circ - t)} + k_{gg}[f_{\circ 1}/(k_{lg} - k_4)[e^{k_4(t_\circ - t)} - e^{k_{lg}(t_\circ - t)}] + f_{\circ 2}/(k_{lg} - k_6)[e^{k_6(t_\circ - t)} - e^{k_{lg}(t_\circ - t)}] + k_3 P_{\circ 1}/(k_4 - k_3)]\{[1/(k_{lg} - k_3)(e^{k_3(t_\circ - t)} - e^{k_{lg}(t_\circ - t)})] + [1/(k_{lg} - k_4)(e^{k_4(t_\circ - t)} - e^{k_{lg}(t_\circ - t)})]\} + [k_5 P_{\circ 2}/(k_6 - k_5)]\{[1/(k_{lg} - k_5)(e^{k_5(t_\circ - t)} - e^{k_{lg}(t_\circ - t)})] + [1/(k_{lg} - k_6)(e^{k_6(t_\circ - t)} - e^{k_{lg}(t_\circ - t)})]\}]. \quad (15)$$

Because we are interested in the amount of gonadal material made since the first sampling ($t_\circ$), the first term in equation (15) ($g_\circ e^{k_{lg}(t_\circ - t)}$) can be discarded. The remaining terms include the specific rates previously calculated and the values for the pool sizes $f_\circ$ and $P_\circ$. The latter are determined for individuals as described previously for f^*.

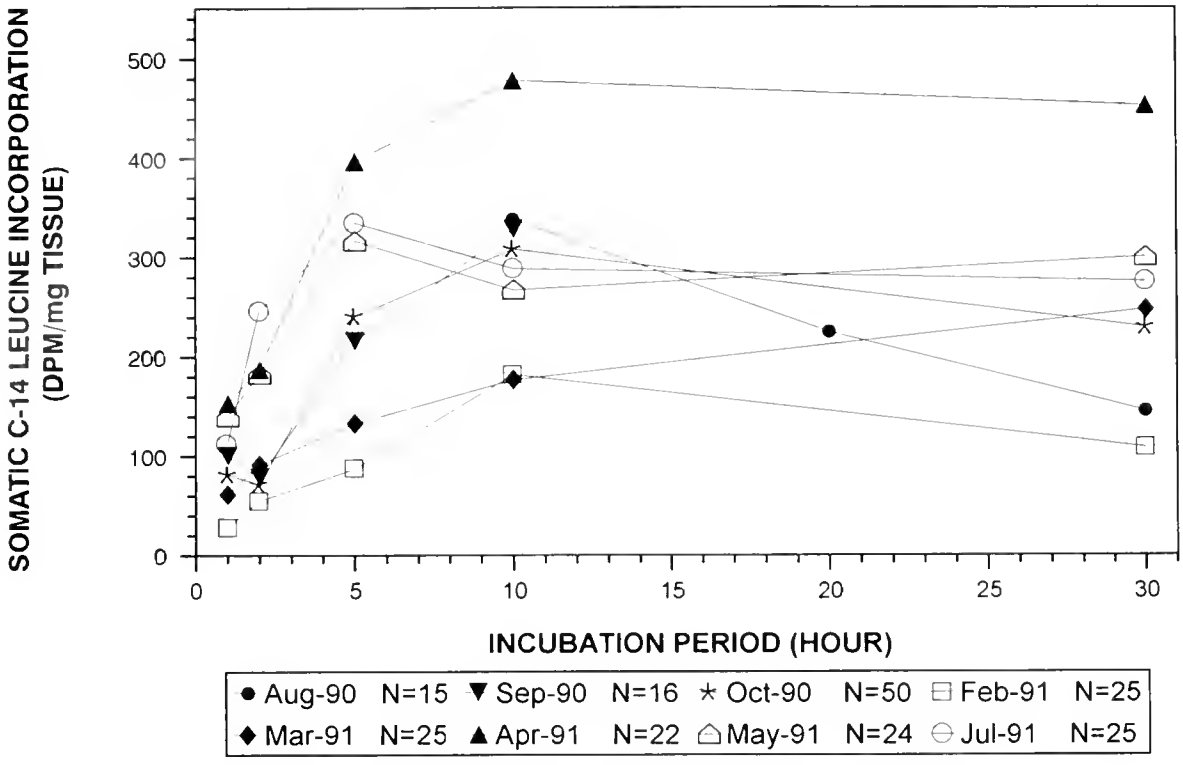

Figure 6. Incorporation of ^{14}C-leucine into somatic protein (dpm mg dry wt $^{-1}$).

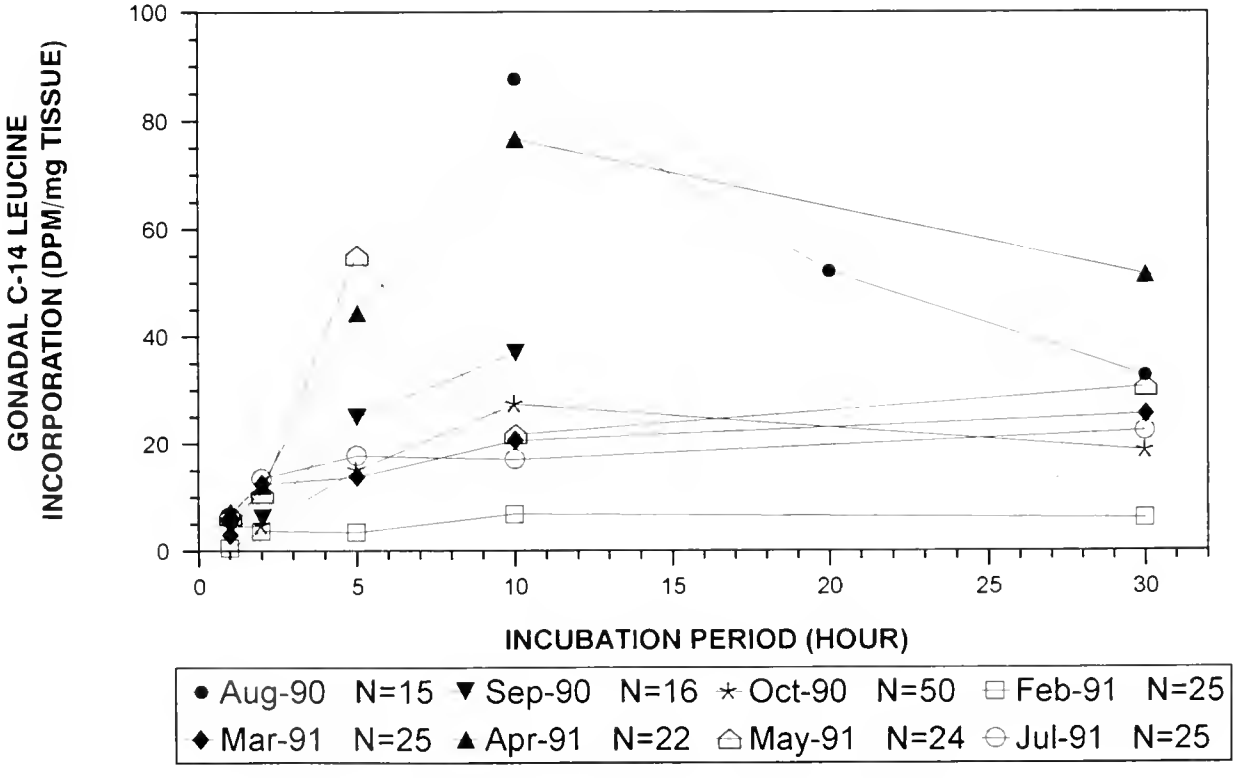

Figure 7. Incorporation of ^{14}C-leucine into egg protein (dpm mg dry wt $^{-1}$).

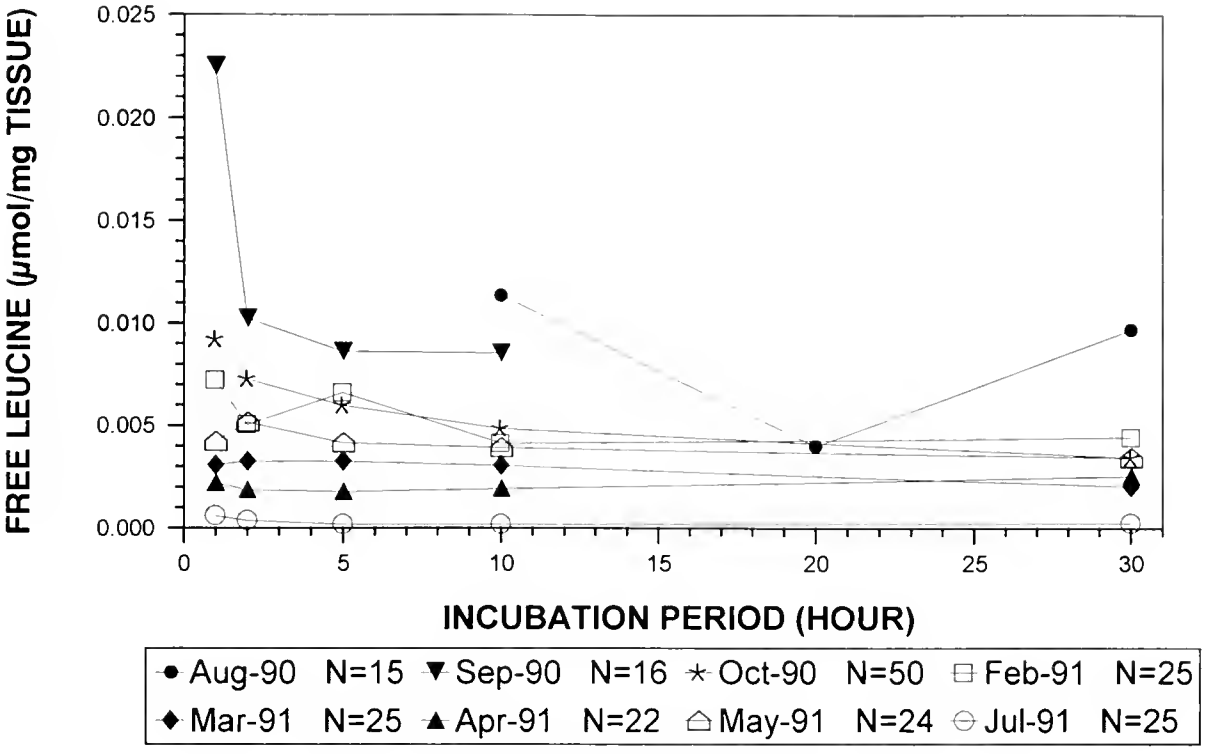

Figure 8. Concentration of free leucine in oysters at the time of sacrifice (μmol mg dry wt $^{-1}$).

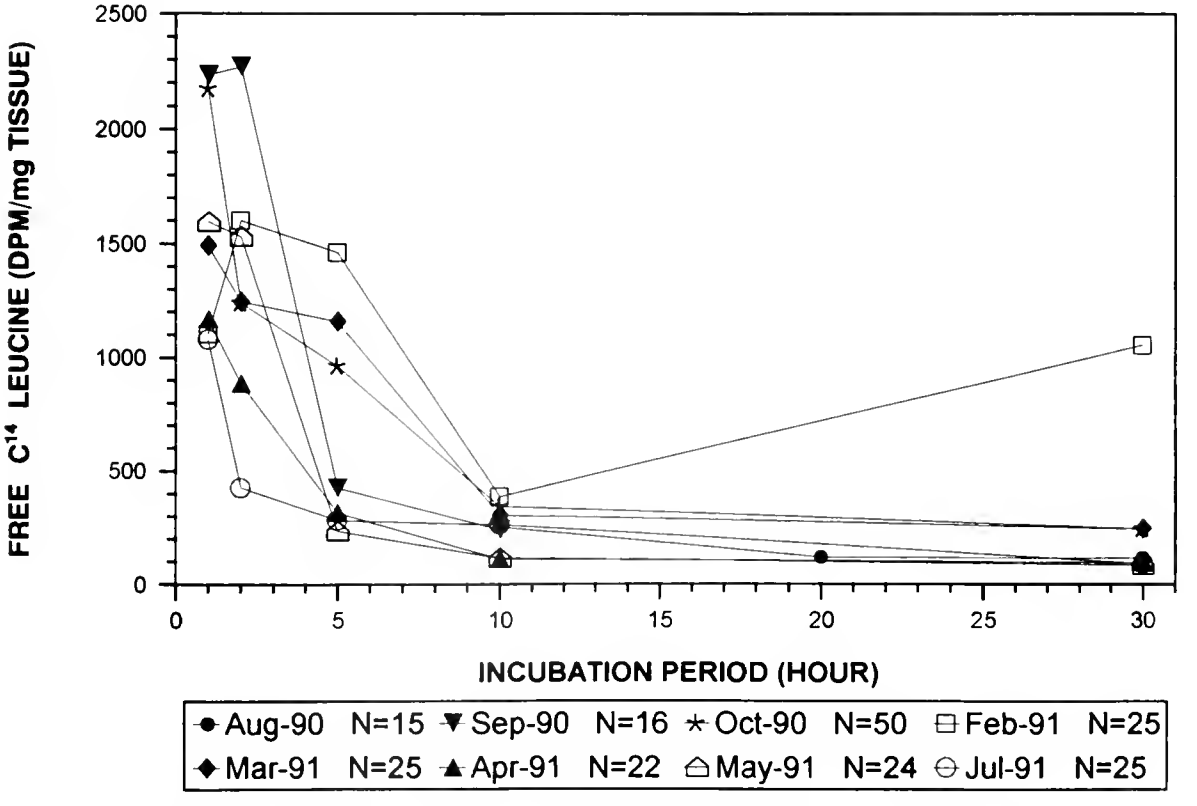

Figure 9. Concentration of free ^{14}C-leucine in oysters at the time of sacrifice (dpm mg dry wt $^{-1}$).

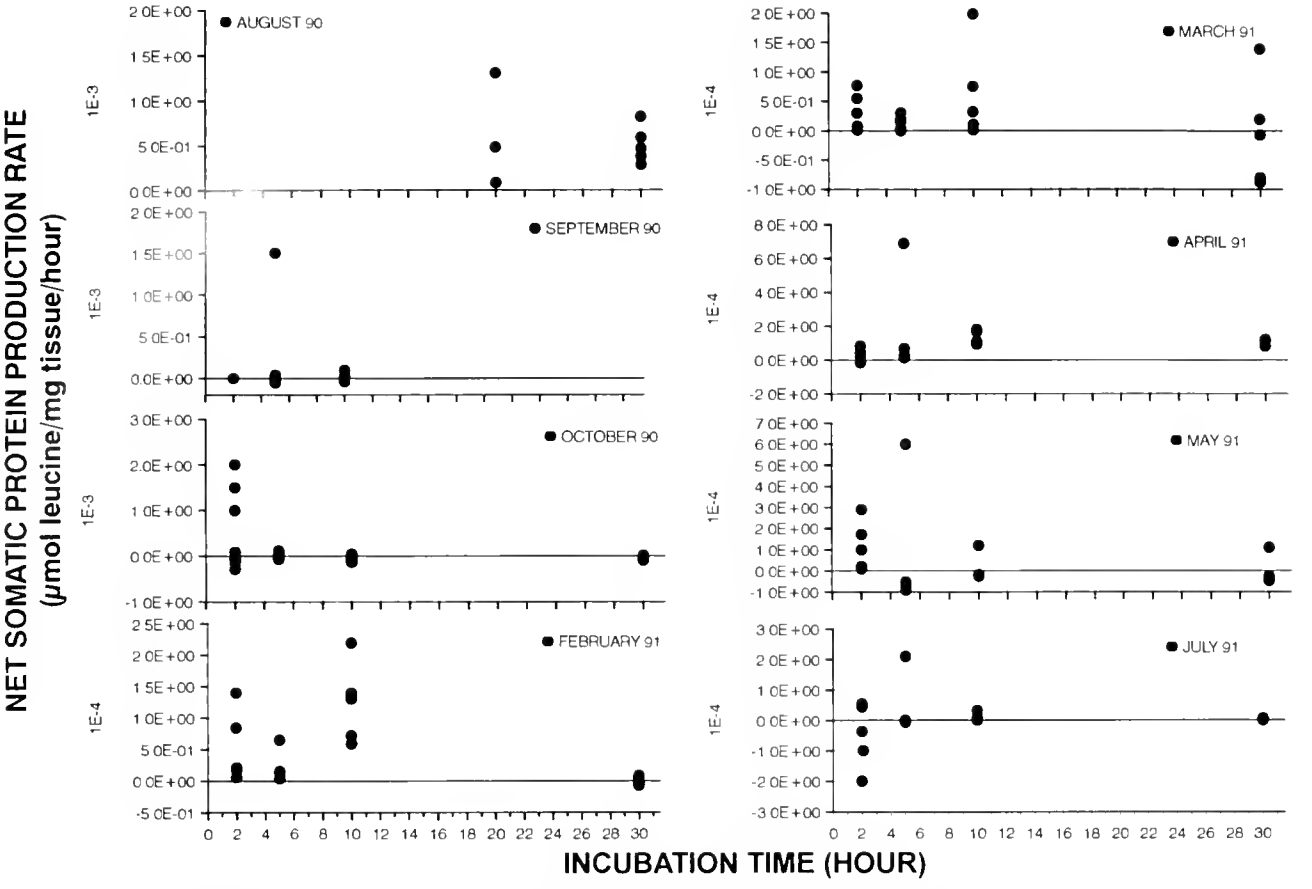

Figure 10. Net rate of somatic protein production (ds/dt) calculated using equation (16) (μmol leucine mg dry wt^{-1} h^{-1}).

Estimated days to spawn

To compare data obtained from different monthly observations, we calculated the estimated number of days required to reach spawning, assuming that the synthesis of egg protein continued uninterrupted at the measured rate. We converted the estimate of the amount of gonadal protein made, obtained from equation (15), to egg weight by multiplying by 2.7 mg egg per mg egg protein (Choi *et al.*, 1993). We assumed that the average oyster at spawning had gonadal material equivalent to about 20% of its dry weight. Choi *et al.* (1993) observed values as high as 40%; however, the mean approximated a value of 20%.

Calculation of oyster somatic production

The amount of leucine measured in oyster somatic tissue is the net of two processes: free leucine incorporation during tissue synthesis and free leucine release during degradation of proteins. The equation is

$$dS/dt = \text{growth terms} - \text{loss terms} = k_{gs}f(t) - k_{ls}S \quad (16)$$

where S is the amount of leucine in the oyster tissue and k_{gs} and k_{ls} are the specific rates controlling the rates of molecular synthesis and degradation, respectively. The calculation of production of oyster somatic tissue was derived in the same manner as the calculation of gonadal production using equations analogous to equations (11) through (15).

Results

Annual gametogenic cycle and reproductive output of oysters

Water temperature and salinity for each sampling period are given in Figure 2. A single-ring immunodiffusion assay was used to measure the quantity of eggs in each female oyster. A typical titration curve (Fig 3) indicated that the single-ring immunodiffusion assay can measure as little as 50 μg oyster egg protein ml^{-1} present in oyster homogenates, with a useful range of 50 μg to 5.5 mg oyster egg protein ml^{-1}. Gonadal-somatic index (GSI), the ratio of the dry weight of oyster eggs to the dry weight of total tissue computed from single-ring immunodiffusion assays,

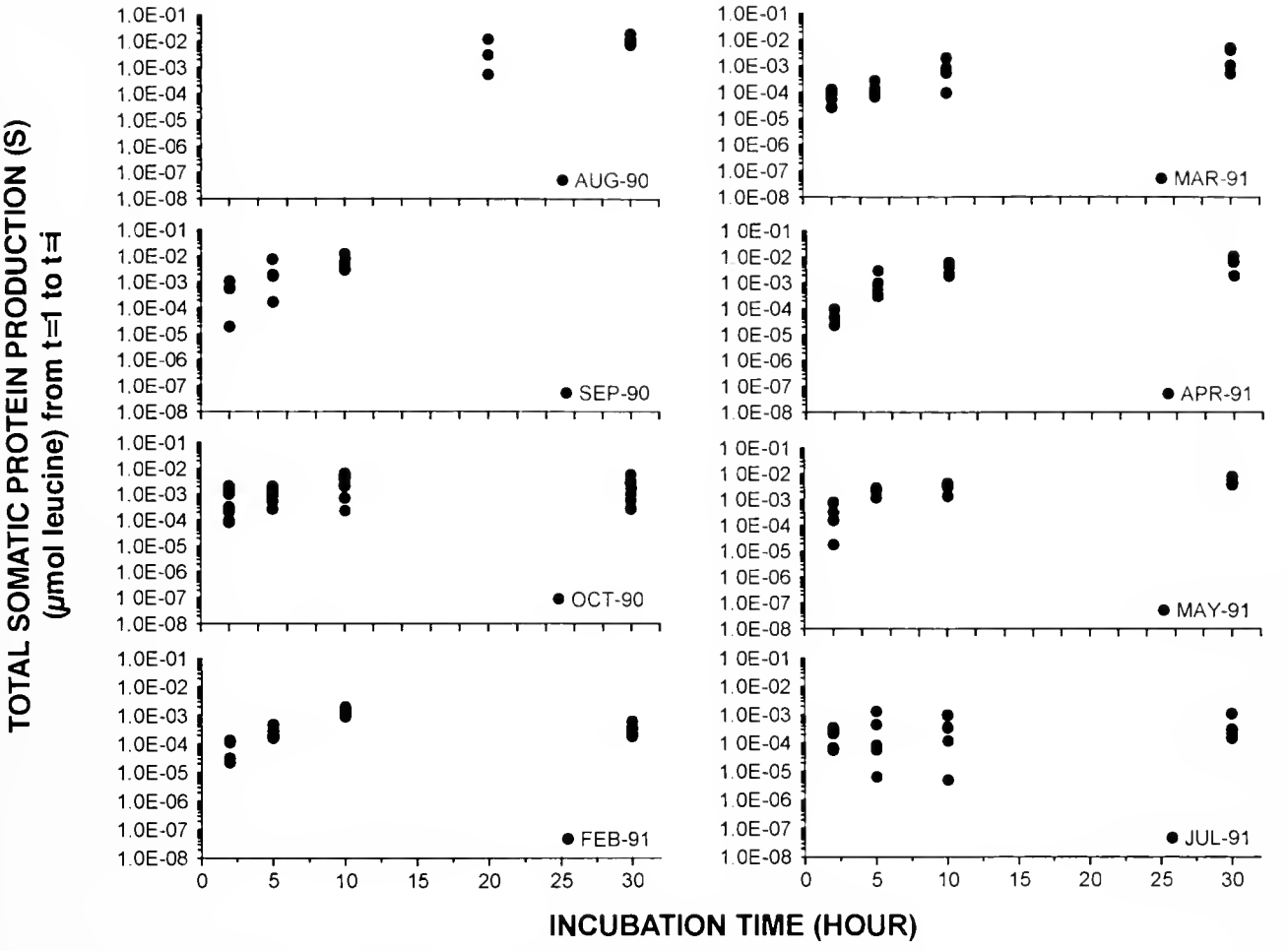

Figure 11. Total somatic protein production (s) (μmol leucine mg dry wt^{-1}) from $t = 1$ to $t = i$.

was used to examine seasonal trends in reproductive effort (Fig. 4). The total quantity of oyster eggs estimated was biased by removing a body section for histological analysis; thus the reported measures of gonadal quantity are not true measures of completely intact oysters.

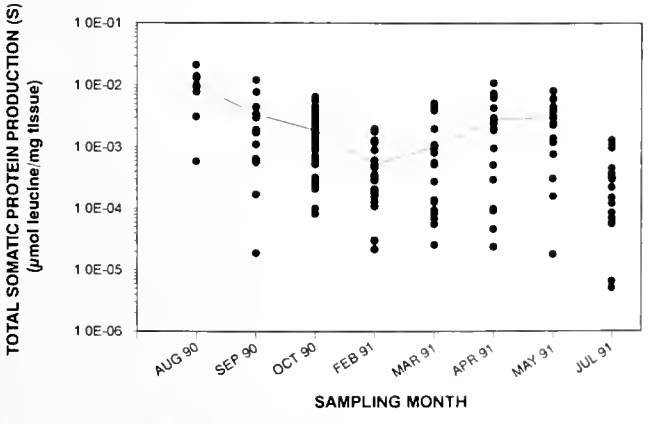

Figure 12. Seasonal fluctuation of somatic protein production (s) (μmol leucine mg dry wt^{-1}). All oysters analyzed are plotted.

Monthly mean GSI increased from mid-August to mid-September, then decreased in late October, indicating that a fall spawning pulse occurred during the intervening period. None of the oysters collected in February 1991 contained a detectable quantity of egg proteins. The GSI increased from mid-March to mid-April, then declined in May, suggesting a spring spawning pulse during those months. GSI dropped from late May to mid-July. Overall, monthly mean GSI was higher during the spring spawning peak than during the fall spawning peak.

Perkinsus marinus *infection*

All oysters collected during the course of study were infected with *Perkinsus marinus*. Monthly median infection intensity varied from 1.1 (a light infection) in February and March to 3.0 (a moderate infection) in October (Fig. 5). A statistically significant correlation was observed between salinity and *P. marinus* infection intensity; oysters

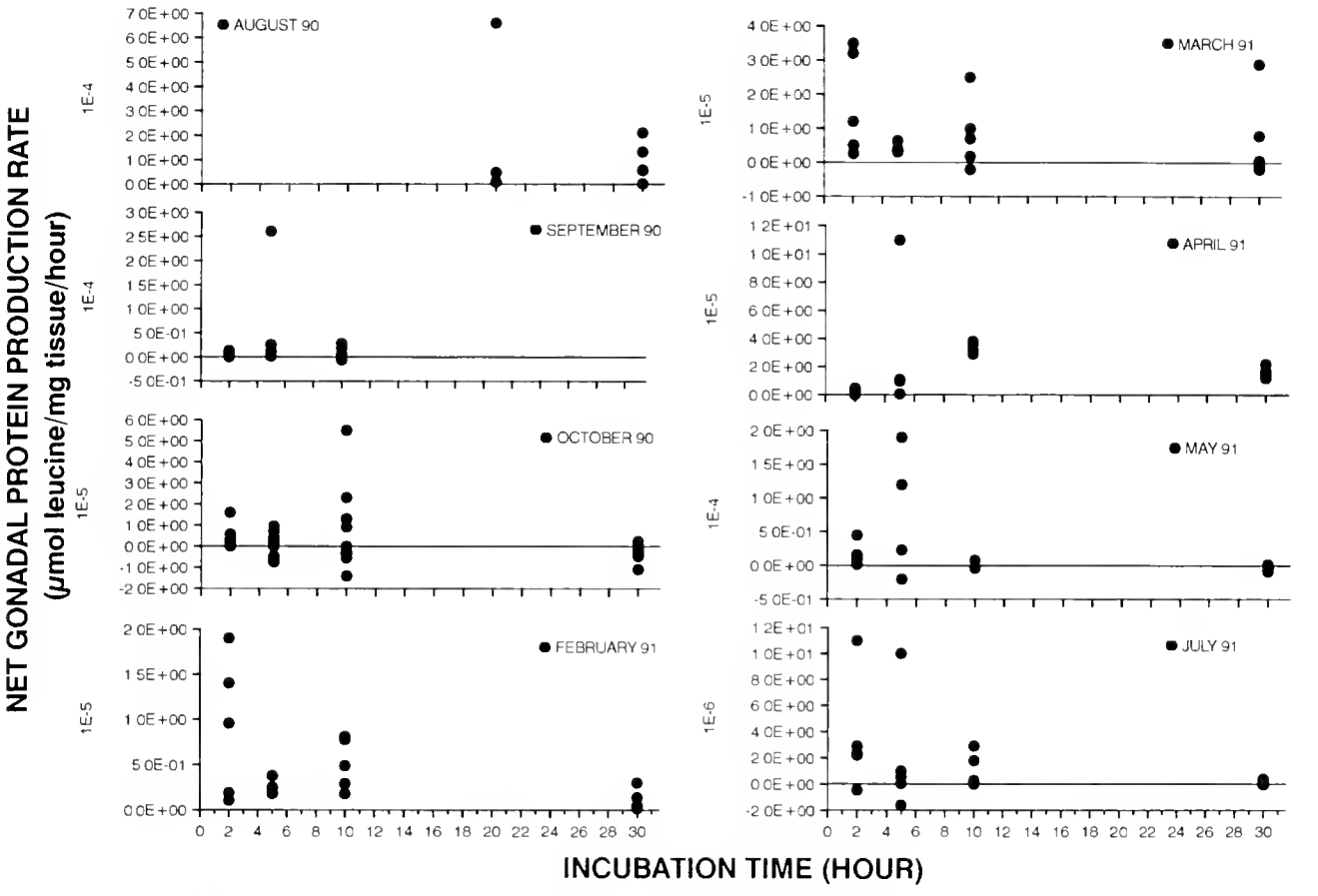

Figure 13. Net rate of egg protein production (dg/dt) calculated using equation (13) (μmol leucine mg dry wt^{-1} h^{-1}).

collected during higher salinity months (August to October 1990, 22 to 26‰) exhibited higher infection intensities than oysters collected during lower salinity months (February to July 1991, 10 to 20‰) (ANOVA, $P < 0.0001$). Multivariate analysis of variance (MANOVA) failed to detect a statistically significant effect of *P. marinus* parasitism on oyster GSI.

Time course of ^{14}C-leucine incorporation

^{14}C-leucine incorporation into somatic protein rose over the first 10 h after injection (Fig. 6) and remained stable or slightly decreased thereafter. The amount of ^{14}C-leucine incorporated into somatic protein was highest in April, moderately high during most of the spring and fall months when tissue growth occurs, and lowest in the winter when oysters typically have a net negative energy balance (Powell *et al.*, 1992).

^{14}C-leucine incorporation into gonadal protein was measured using the rabbit anti-oyster egg IgG and protein A immunoprecipitation technique. A maximum incorporation of ^{14}C-leucine into gonadal protein occurred between 5 and 10 h after injection (Fig. 7). Between 10 and 30 h after injection, ^{14}C-leucine content tended to plateau or decrease. The extent of ^{14}C-leucine incorporation into gonadal protein paralleled the gonadal/somatic index; values were highest in April when gonadal content was highest and lowest in February when gonadal content was also low.

The free leucine pool

After the first 2 h, the free leucine pool was relatively stable during the course of each experiment (Fig. 8). Free leucine was highest in concentration 1 h after injection, declined rapidly over the next 5 to 10 h, and then slowly thereafter. The transient rise in free leucine at the beginning of the experiment may represent a stress caused by experimental manipulation. Aspartic acid produced the same result (Saunders *et al.*, 1994). The transient rise was not due to the amount of amino acid injected, which was small compared to the amino acid pool. Yearly variation

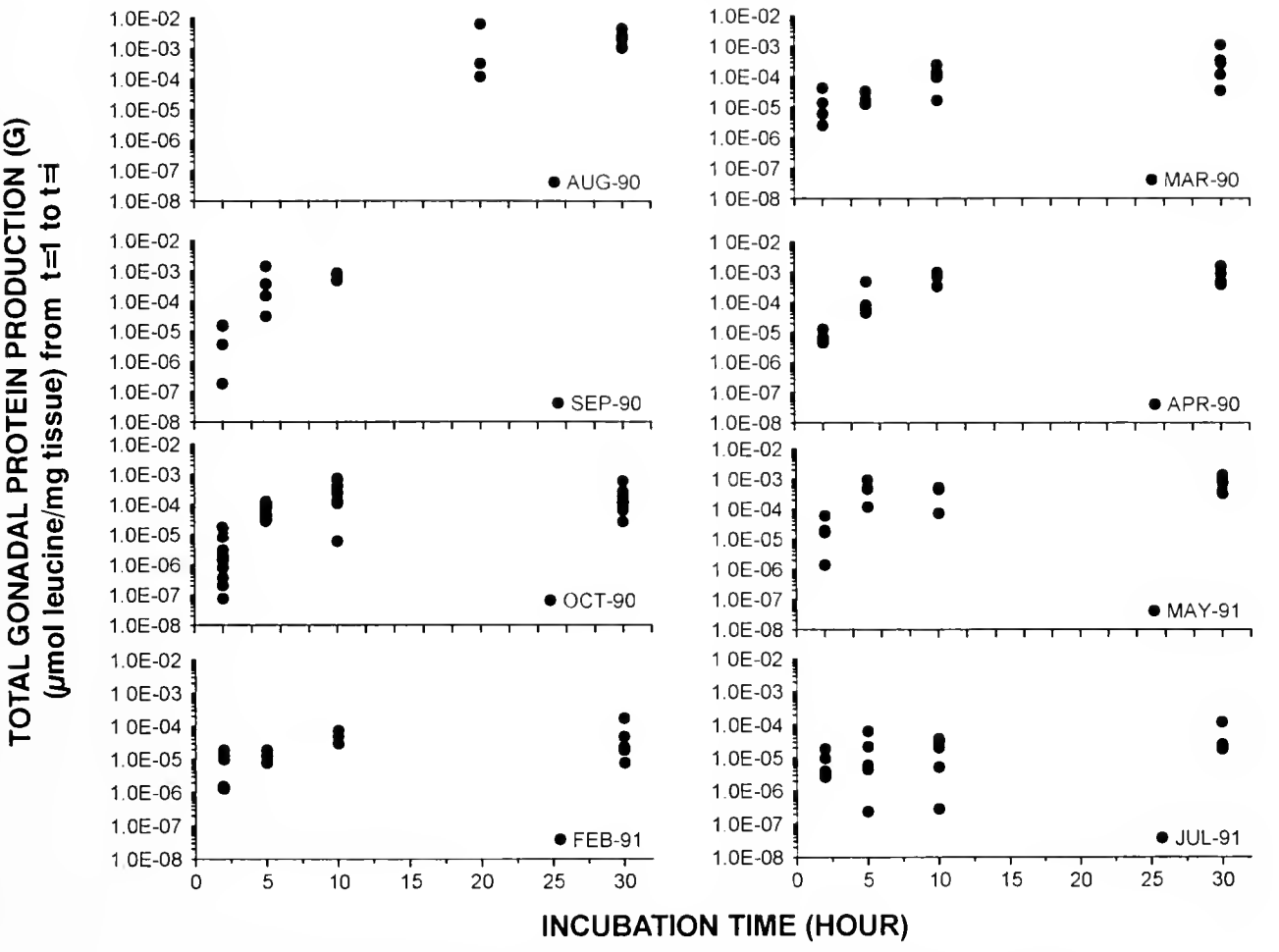

Figure 14. Total egg protein production [g from equation (15)] (μmol leucine mg dry wt^{-1}) from $t = 1$ to $t = i$.

in free leucine did not follow salinity, nor did it follow the reproductive cycle. Values were lowest in July and highest in August and September. Lynch and Wood (1966) also found leucine to be stable over a broad salinity range.

The concentration of free ^{14}C-leucine declined rapidly between 1 and 5 h after injection in most sampling months, probably due to the rapid incorporation of free ^{14}C-leucine into gonadal and somatic protein (Fig. 9). Between 10 and 30 h, the concentration of free ^{14}C-leucine plateaued or slowly declined, except in February, suggesting that protein recycling was buffering the pool. Rates of protein turnover are on the order of 1 to 20 days for many tissue components (Koehn, 1991) and were estimated at 16% of the basal metabolic rate in *Mytilus edulis* (Sibly and Calow, 1989). The amount of incorporation into somatic protein would have provided a source adequate to maintain the free amino acid pool at the measured specific activity at these turnover rates. The higher specific activity in February suggests lower somatic tissue incorporation, which was observed.

Somatic tissue production

The rate of somatic tissue production, the net of the production and degradation terms, was relatively stable over the time course in each sampling month. Most oysters exhibited positive somatic tissue growth during most months and throughout the experimental time course (Fig. 10). The amount of somatic tissue produced increased over the time course, but at a slower and slower rate, in all months (Fig. 11). Either growth rate dropped, the accuracy of our calculations declined as specific activity decreased, or ^{14}C-leucine was lost from the rapidly overturning component of the somatic tissue pool. The latter is the more likely case.

Somatic production varied seasonally. Rates were low during midwinter and midsummer (Fig. 12). These seasonal fluctuations were significant (ANOVA, $P < 0.0001$).

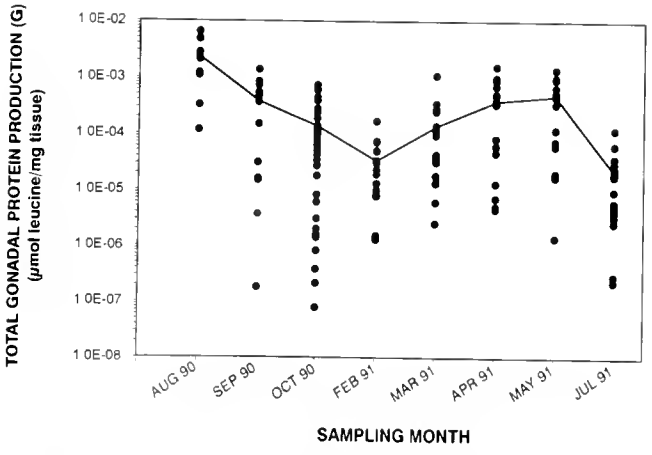

Figure 15. Seasonal fluctuation of egg protein production (g) (μmol leucine mg dry wt $^{-1}$). All oysters analyzed are plotted.

Gonadal protein production

The calculated values for the net rate of gonadal protein production, the sum of the production and loss terms, are shown in Figure 13. As observed in the calculation of somatic production, except in October, most oysters used in the experiment exhibited a greater rate of egg protein production ($k_{gg}f(t)$) than of gonadal protein degradation ($k_{lg}{}^{g}$), resulting in a net gain of egg protein (g) over the time course (Fig. 14). In some oysters sampled in August 1990 and April 1991, the specific rate of gonadal production was up to 20 times greater than the specific rate of gonadal protein degradation. Once again, the amount of protein produced slowed to a plateau at the longest incubation times in some months. Either the rate of production slowed, the calculation of specific activity became more inaccurate, or protein recycling resulted in a net loss of ^{14}C-leucine from the more rapidly overturning portion of the tissue pool.

Overall, the observed seasonal pattern in gonadal synthesis (Fig. 15) coincides with the annual cycle of reproductive effort in oysters shown in Figure 4. Two discrete peaks occur, one in August/September and the other in April/May. The values for gonadal synthesis obtained during the spawning peaks are significantly higher than the values obtained during the intervening periods ($P < 0.0001$). However, gonadal production and gonadal/somatic index (*i.e.*, rate versus quantity) did not correspond exactly. April and May were similar in synthesis rate, but oysters sampled in April had higher GSI (more eggs). The rate of egg synthesis was higher in August/September than in April/May; the opposite was true for the number of eggs present.

Estimated days to spawn

We estimated the number of days required for an animal to become ready to spawn if egg synthesis continued at the measured rate for a sufficiently long period. The estimated days to spawn varied over a wide range; however, most oysters collected during the spawning peaks of August/September and April/May required less than 100 days to come into spawning condition (Fig. 16). In contrast, almost all oysters collected in February and July would have required more than 1000 days at the measured rate to come into spawning condition. Overall, the monthly median value for the estimated days to spawn follows the seasonal changes in oyster reproductive output as shown in Figure 4.

Discussion

Methodology

Use of polyclonal rabbit anti-oyster egg serum (Choi *et al.*, 1993) permitted us to measure the amount of gametic tissue present in oysters. The single-ring immunodiffusion assay could detect as little as 50 μg egg protein ml $^{-1}$. Although the single-ring immunodiffusion assay is less sensitive than ELISA, which detects as little as 200 ng ml $^{-1}$ (Choi *et al.*, 1993), it is simpler than ELISA and can still detect as little as 100 μg of egg protein present in 1 g of oyster tissue.

Immunoprecipitation using rabbit anti-oyster egg IgG as primary antibody and protein A cell suspension as an immunoadsorbent permitted us to measure the rate of incorporation of ^{14}C-leucine into gametic tissue. The instantaneous rate of egg production (dg/dt) at the time of sacrifice can then be calculated from the amount of ^{14}C-leucine incorporated and the specific activity of leucine measured by amino acid analysis. From the cumulative amount of leucine incorporated, we could calculate the instantaneous rate of gamete synthesis and the days re-

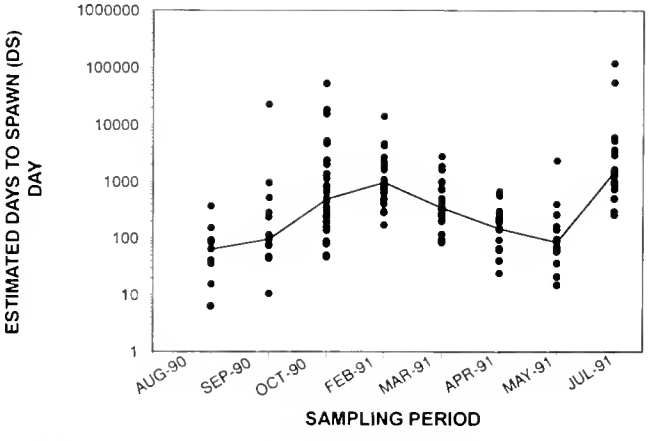

Figure 16. Seasonal fluctuation in the estimated number of days required for an individual to become ready to spawn if the measured rate of egg synthesis were to continue unaltered. All oysters analyzed are plotted.

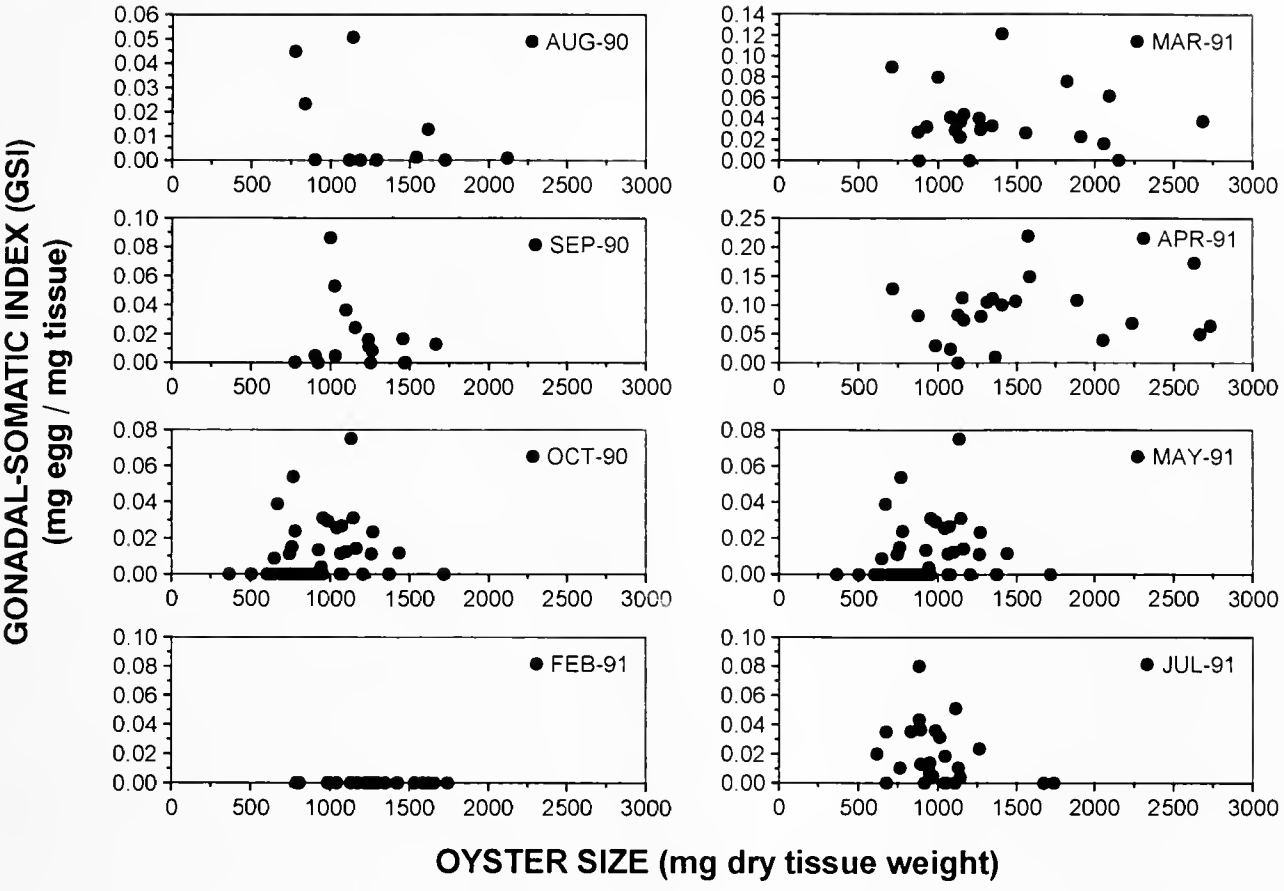

Figure 17. Gonadal-somatic index (mg dry wt egg mg dry wt oyster^{-1}) *versus* oyster size (mg dry wt) for oysters used in this study.

quired to reach spawning condition should that rate be maintained.

Spawning season and GSI

The gonadal-somatic index (Fig. 4) indicates that at least two spawning peaks occurred during the study, one in spring and the other in fall. Choi *et al.* (1993) observed a similar bimodal spawning pulse in an annual gametogenic cycle of female oysters on Confederate Reef. The higher reproductive effort observed in both studies in the spring might be associated with higher food supplies in the spring, as reported by Hopkins (1935) and Soniat and Ray (1985), or with a greater degree of synchrony in gonadal development in the spring population, as suggested by Hofmann *et al.* (1992). In the fall, fewer oysters would be ready to spawn at any one time, reducing the overall mean and the likelihood of collecting an egg-heavy individual (Cox and Mann, 1992; Hofmann *et al.*, 1992). The absence of a statistically significant relationship between size, GSI, and season and the presence of apparently recently spawned individuals in every month of the spawning season (Fig. 17) indicate that portions of the population are spawning during most months, as suggested by the Hofmann *et al.* (1992) model and numerous references to continuous or dribble spawning (Hopkins, 1935; MacKenzie, 1977; Cox and Mann, 1992).

Parasitism by Perkinsus marinus

Perkinsus marinus, like other parasites (*e.g.*, Kabat, 1986), can significantly affect oyster reproduction and growth; however, unlike many parasites, the effect of *P. marinus* on oyster reproduction has been difficult to quantify predictably (Wilson *et al.*, 1988; White *et al.*, 1989; Cox and Mann, 1992; Ellis *et al.*, 1993). Theoretically, *P. marinus* could exert an effect in one of two ways: by reducing the number of eggs per spawn or by reducing the number of spawns per year by slowing the rate of egg protein production. White *et al.* (1988b) and Wilson *et al.* (1988) reported circumstantial evidence that higher infection intensity increases the time required for an individual to attain spawning condition. Choi *et al.* (1993) were unable to observe a relationship between the number

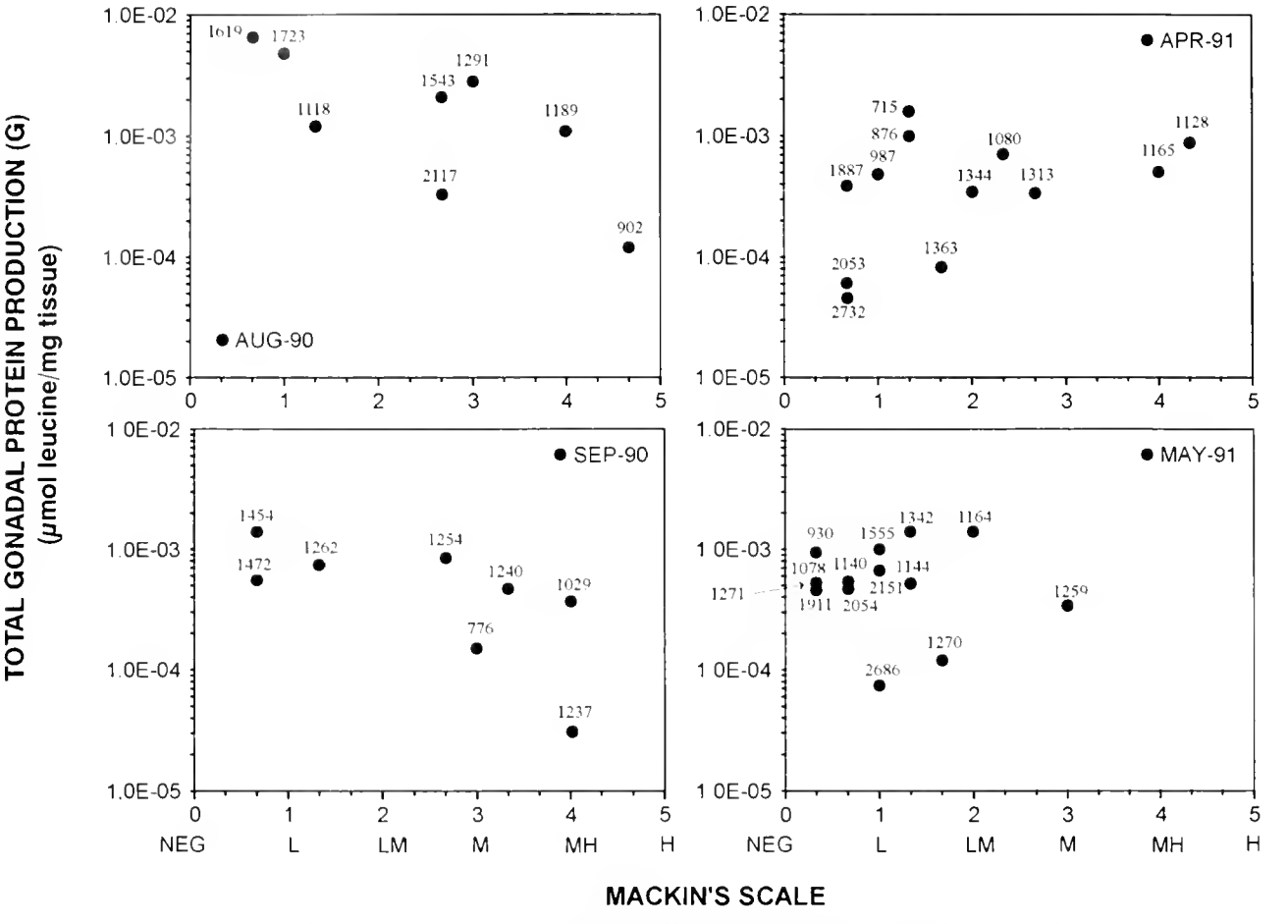

Figure 18. Infection intensity of *Perkinsus marinus* versus the amount of egg protein produced during the time course (*g*) (μmol leucine mg dry wt $^{-1}$). The analysis uses oysters collected during the fall and spring spawning season and only oysters sacrificed beyond 2 h after injection. Numbers indicate specimen tissue dry weight in milligrams.

of eggs and *P. marinus* infection intensity and suggested that *P. marinus* probably slows the rate of reproductive development rather than varying the size of an individual spawn. The asynchrony in spawning under Galveston Bay conditions suggests that such an effect will be difficult to demonstrate unequivocally. However, the effect, if present, might be most noticeable during periods of restricted food supply and at high infection intensities, which typically occur during the summer and fall. In addition, the cumulative impact over the spawning season might be noticeable at that time.

Figure 18 relates gonadal production with the infection intensity of *P. marinus* during the spring and fall peaks in spawning activity. A negative correlation between infection intensity and the rate of egg production is noticeable during the fall spawning season, but not during the spring spawning season. Figure 19 relates infection intensity with the number of days required to come into spawning condition. Again, more heavily infected oysters require more days to prepare for spawning in August and September. During the spring, when no significant trend exists, most infection intensities are too low to exert an impact and the cumulative effect of *P. marinus* parasitism is less.

The gametogenic cycle and the rate of egg protein production

One of the important observations of this study is that the seasonal cycle of gamete production as observed by direct measurements of egg protein production is not equivalent to that observed by standard GSI examination, except in a very general way. Gonadal production is lower in the winter and in midsummer when GSI is also low. Low winter rates are certainly a product of lower filtration rates, which restrict food supply in the winter (Powell *et al.*, 1992). The lower rates in July suggest a pause between the two major spawning events or, equally likely, a reduced

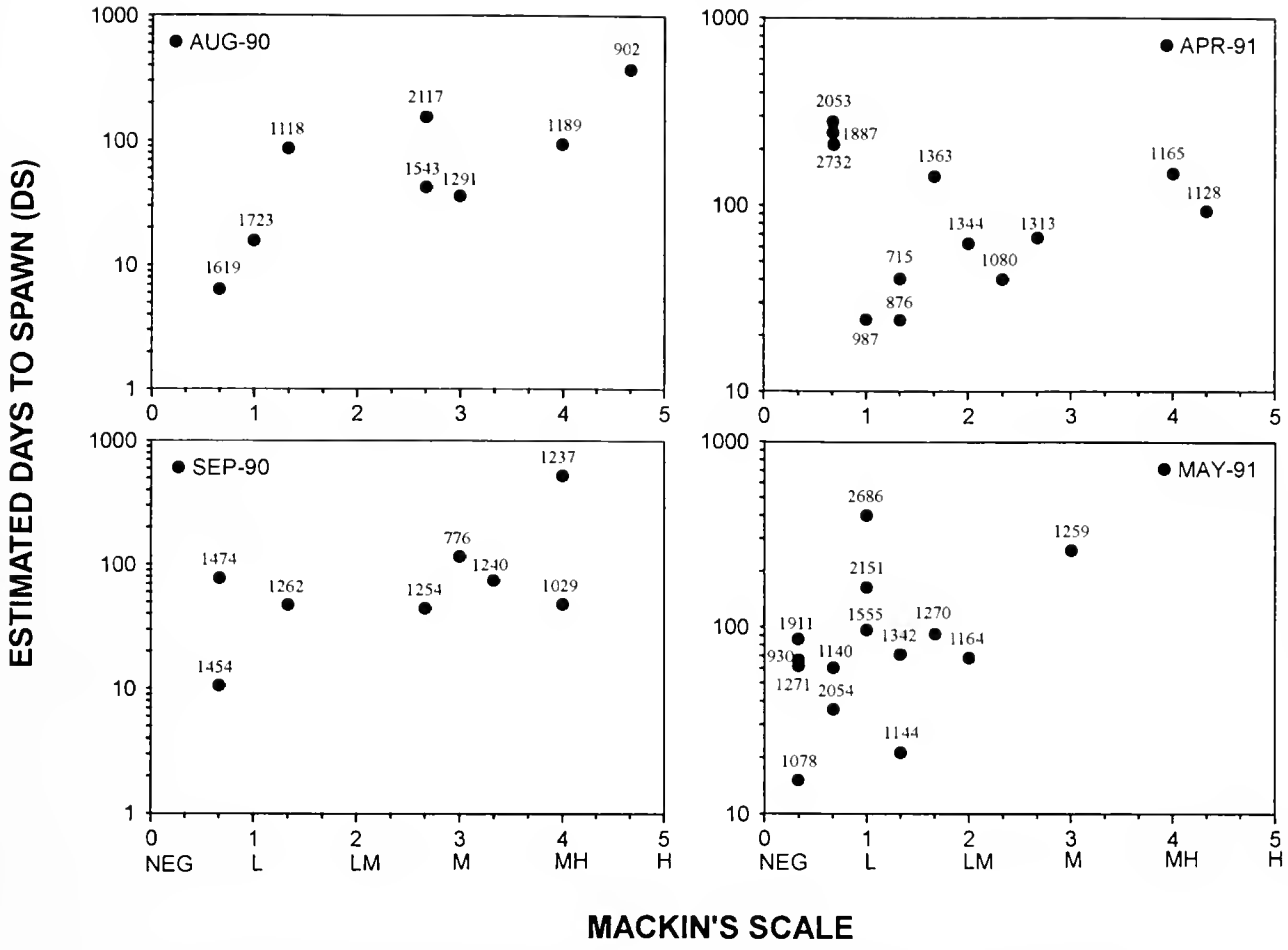

Figure 19. Infection intensity of *Perkinsus marinus* and the estimated days required to become ready to spawn at the egg production rate measured. The analysis uses oysters collected during the fall and spring spawning season and only oysters sacrificed beyond 2 h after injection. Numbers indicate specimen tissue dry weight in milligrams.

food supply during the summer months (our unpublished data show that food supply can drop to low levels during midsummer). Thus, at the most basic level, agreement exists between rate measurements and standing crop measurements (GSI).

Nevertheless, a closer examination shows that the lowest rates of gamete production were observed in July and October rather than in midwinter. Midsummer and fall are typically times of gonadal resorption following spawning, and a higher fraction of oysters was collected in this condition during this time. A perusal of Figures 10 and 12 shows that a smaller fraction of the population was growing in July and October than in other months, suggesting a restricted energy supply at both times as well. Restricted food supply and the temperature-dependent allocation of assimilated energy to reproduction would slow growth in these months. Figures 13 and 15 show that individuals displaying no net growth or gonadal resorption were also found in most months, but a much larger fraction of the population was in this condition in October, as the fall spawning season ceased and gonad was resorbed, rather than in midwinter. Furthermore, highest egg production rates were obtained in August, whereas GSI was highest in April, and a comparison of April and May reveals that egg production rates were essentially equal, whereas April's mean GSI was nearly double the May value. Accordingly, the two types of measurements, rates *versus* standing crop, reveal a substantially different picture about the details of the spawning season.

Days to reach spawning condition

The time required to reach spawning condition is a function of the daily rate of production of gametic tissue. Our estimates of the time required to reach spawning condition of as little as several weeks to 1 or 2 months agree well with estimates reported in the literature (Loosanoff and Davis, 1953; Kaufman, 1979). Accordingly, the

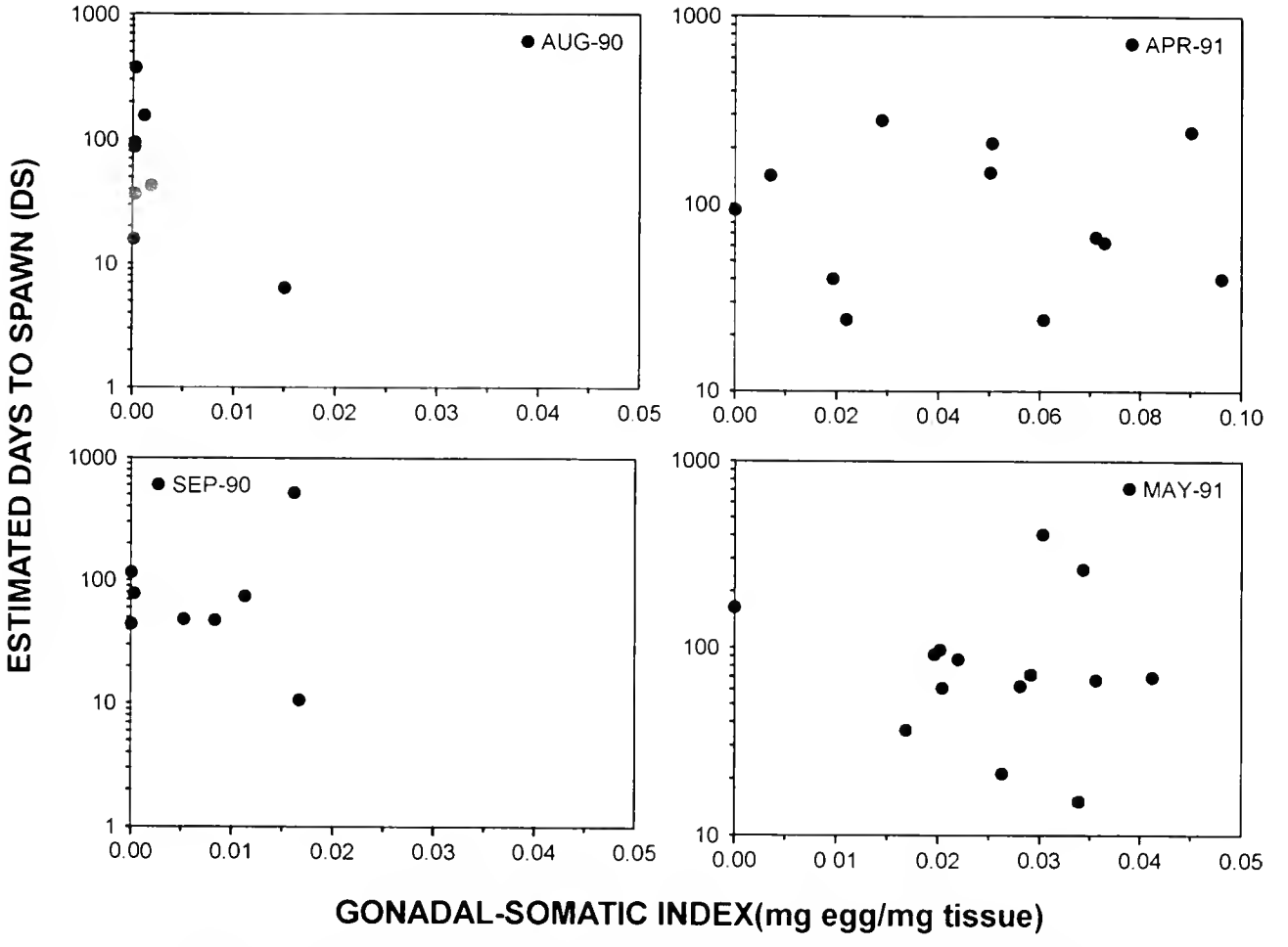

Figure 20. The relationship between estimated days to spawn and gonadal-somatic index (mg dry wt egg mg dry wt oyster^{-1}) during the two primary spawning periods, August/September and April/May. Oysters collected 2 h after injection were not included.

direct rate measurements we have made would seem to accurately reflect the true rate at which gametic tissue is produced in the field. One might expect that oysters with higher GSI would exhibit higher values for the estimated time required to reach spawning condition as we have calculated it, because the rate of gametic tissue production might decline as spawning condition was reached. We found no significant relationship between GSI and the number of days required to reach spawning condition (Fig. 20). Thus the rate of production of gametic tissue apparently does not intrinsically increase or decrease during gonadal maturation, even as spawning nears.

Oyster size is positively correlated with the estimated days to spawn only during the spring spawning peak in April/May, when larger oysters require more days to prepare to spawn (Fig. 21). By the fall, this relationship no longer exists. The significant relationship in the spring probably stems from the spring temperature signal (Loosanoff, 1942; Barber and Mann, 1991), which initiates gonadal development in all adults regardless of size, and from the fact that the spawning trigger would appear to include the requirement that gonadal tissue make up at least 20% of the oyster's biomass. As suggested by Hofmann *et al.* (in press, 1992), smaller oysters have higher food acquisition rates than larger ones and allocate more of the net energy gained to reproduction; thus smaller individuals should reach the 20% level sooner and spawn earlier. The longer time to spawn in larger oysters indicates the importance of the relative capabilities of different oyster size classes to obtain energy and allocate it to reproduction. The absence of a correlation between oyster size and days to spawn in the fall may be due to the gradual decay in the synchrony of reproductive development that accompanied the spring temperature signal. Synchrony declines for two reasons. (1) As the various size classes spawn during the spring and summer, the synchrony of reproduction in the population gradually degrades. The smaller size classes will almost certainly spawn more fre-

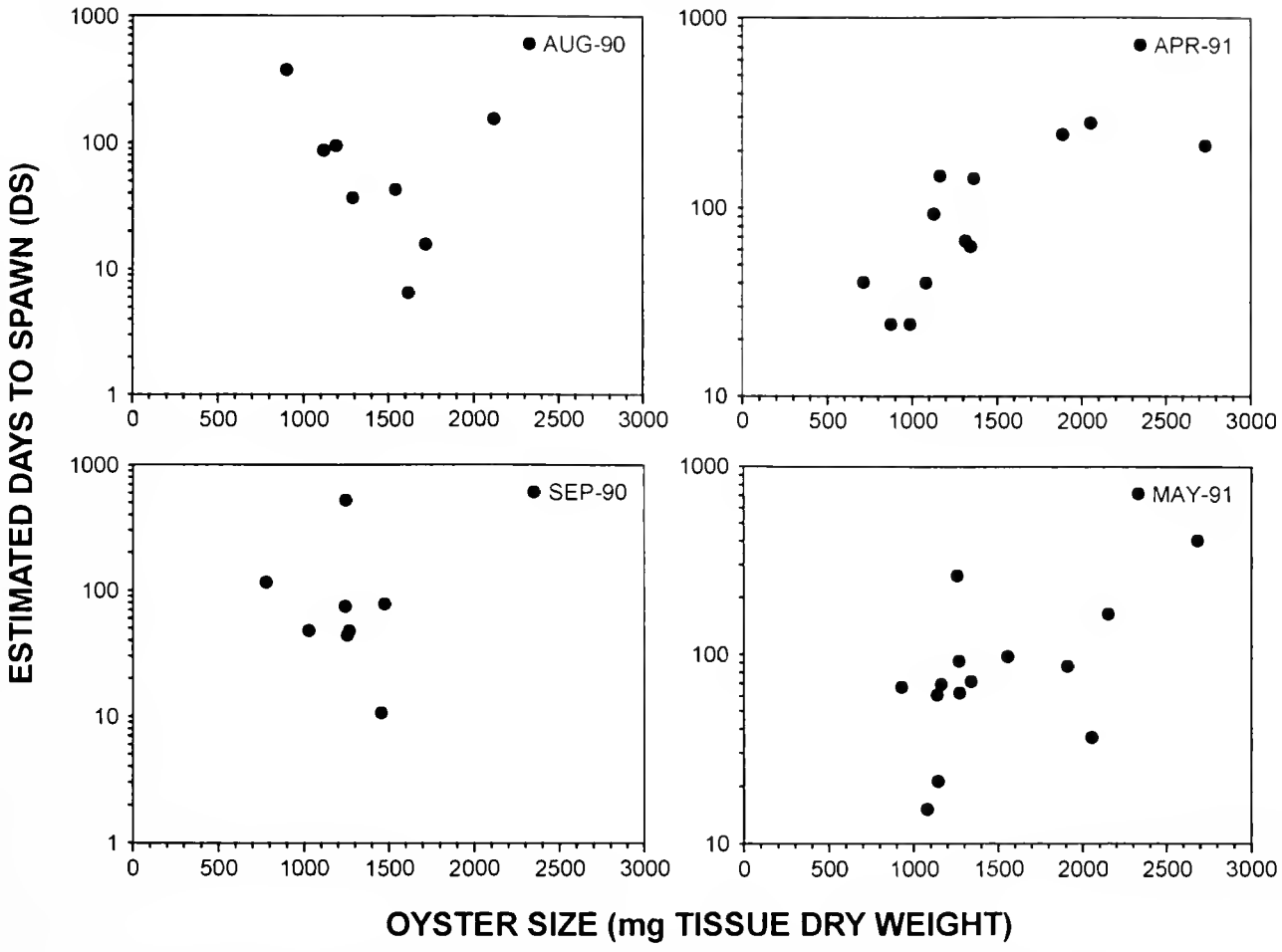

Figure 21. The relationship between oyster dry weight (mg) and the estimated number of days to reach spawning condition. Only oysters collected during the spring and fall spawning peaks are included. Oysters collected 2 h after injection not included.

quently than large oysters over the year. (2) The increase in *P. marinus* infection intensity gradually retards spawning in highly infected individuals. Less heavily infected individuals will spawn sooner (Fig. 19). By the fall, these two factors should result in asynchronously spawning individuals within and between size classes. Probably, the increased infection intensity of *P. marinus* is primarily responsible for the lack of a correlation between days to spawn and size in the fall.

Conclusion

This study represents the first examination of the *in situ* instantaneous rate of reproduction in oysters. Although a general relationship exists between a standard GSI measurement and the rate of production of gametic tissue, upon closer examination, the two differ markedly in detail. The suggestion is that oysters can rapidly produce gametic tissue and can maintain it for extended periods of time without loss or growth, particularly when food supply is low. A high GSI does not necessarily mean a simultaneously high rate of production of gametic tissue.

The data support the overriding importance of food supply and the important role of disease in controlling gametic production. Some of the lowest rates (in July) probably resulted from low food supply. Furthermore, the range in observed somatic and gametic growth emphasizes the conservatism of somatic growth and the volatility of gonadal growth that is borne out by the results of population dynamics models of oysters (Hofmann *et al.*, 1992, in press). Somatic production rates varied by a factor of 10 over the year; for gonadal production, this range was 100. Thus somatic growth was more conservative, and the data support the suggestion that the added assimilation that occurs in the spring with increased filtration rate and higher temperature is largely diverted into the production of gonadal tissue.

Standard GSI measurements, whether histological or by quantitative measure (*e.g.*, Green, 1978; Dolah *et al.*, 1992; Choi *et al.*, 1989), fail to describe the complexity of oyster reproduction. As the season progresses and the synchrony in gonadal development imposed by the initial temperature signal fades, the importance of a measurement of egg production rate increases. Many factors, including food supply and *P. marinus* infection intensity, probably exert their primary influence on the time required to reach spawning condition rather than on the number of eggs per spawn. A rate measurement is required to identify these trends. The apparently weaker fall spawn identified in standard GSI measurements in this study probably reflects this asynchrony rather than a smaller fall output. In fact, rates of egg production were as high or higher in the fall than in the spring, so that the population as a whole retained a significant spawning potential throughout this time. We suggest that measurements of the rate of production of gametic tissue will be required to adequately interpret the seasonal cycle of reproduction in oysters and to identify the real influence of food supply and disease in controlling oyster reproduction.

Acknowledgments

We thank the staff at the Aquatic Research Laboratory at Texas A&M University (TAMU) for help in the development of the immunological probes. E. Wilson-Ormand, G. Saunders, and J. Song helped with field data collection. This work was supported by grant #NA89AA-D-SG139 from the National Oceanic and Atmospheric Administration through the National Sea Grant College Program. The views expressed herein are those of the authors and do not necessarily reflect the views of NOAA or any of its subagencies. Computer funds were provided by the Texas A&M University College of Geosciences and Maritime Studies. The TAMU Office of University Research supported aspects of the field work through the purchase of the R/V *Eddy*. We appreciate this support.

Literature Cited

Barber, B. J., and R. Mann. 1991. Sterile triploid *Crassostrea virginica* (Gmelin, 1791) grow faster than diploids but are equally susceptible to *Perkinsus marinus*. *J. Shellfish Res.* **10:** 445–450.

Barber, B. J., S. E. Ford, and H. H. Haskin. 1988. Effects of the parasite MSX (*Haplosporidium nelsoni*) on oyster (*Crassostrea virginica*) energy metabolism. II. Tissue biochemical composition. *Comp. Biochem. Physiol. A Comp. Physiol.* **91:** 603–608.

Choi, K-S., E. A. Wilson, D. H. Lewis, E. N. Powell, and S. M. Ray. 1989. The energetic cost of *Perkinsus marinus* parasitism in oysters: quantification of the thioglycollate method. *J. Shellfish Res.* **8:** 125–131.

Choi, K-S., D. H. Lewis, E. N. Powell, and S. M. Ray. 1993. Quantitative measurement of reproductive output in the American oyster, *Crassostrea virginica*, using an enzyme-linked immunosorbent assay (ELISA). *Aquacult. Fish. Manage.* **24:** 299–322.

Cox, C., and R. Mann. 1992. Temporal and spatial changes in fecundity of Eastern oysters, *Crassostrea virginica* (Gmelin, 1791) in the James River, Virginia. *J. Shellfish Res.* **11:** 49–54.

Craig, A., E. N. Powell, R. R. Fay, and J. M. Brooks. 1989. Distribution of *Perkinsus marinus* in Gulf Coast oyster populations. *Estuaries* **12:** 82–91.

Deslous-Paoli, J-M., and M. Héral. 1988. Biochemical composition and energy value of *Crassostrea gigas* (Thunberg) cultured in the bay of Marennes-Oléron. *Aquat. Living Resour.* **1:** 239–249.

Ellis, M. S., K-S. Choi, T. L. Wade, E. N. Powell, T. J. Jackson, and D. H. Lewis. 1993. Sources of local variation in polynuclear aromatic hydrocarbon and pesticide body burden in oysters (*Crassostrea virginica*) from Galveston Bay, Texas. *Comp. Biochem. Physiol. C*

Ford, S. E., and A. J. Figueras. 1988. Effects of sublethal infection by the parasite *Haplosporidium nelsoni* (MSX) on gametogenesis, spawning, and sex ratios of oysters in Delaware Bay, U.S.A. *Dis. Aquat. Org.* **4:** 121–133.

Gallagher, E. D., P. A. Jumars, and G. L. Taghon. 1988. The production of monospecific antisera to soft-bottom benthic taxa. *Lect. Notes Coastal Estuarine Stud.* **25:** 74–98.

Gauthier, J. D., and T. M. Soniat. 1989. Changes in the gonadal state of Louisiana oysters during their autumn spawning season. *J. Shellfish Res.* **8:** 83–86.

Gordon, B. E. 1980. A critical examination of some newly available standards for liquid scintillation counting. *Anal. Biochem.* **102:** 163–166.

Green, J. D. 1978. The annual reproductive cycle of an apodous holothurian, *Leptosynapta tenuis*: a bimodal breeding season. *Biol. Bull.* **154:** 68–78.

Hofmann, E. E., E. N. Powell, J. M. Klinck, and E. A. Wilson. 1992. Modeling oyster populations III. Critical feeding periods, growth and reproduction. *J. Shellfish Res.* **11:** 399–416.

Hofmann, E. E., J. M. Klinck, E. N. Powell, S. Boyles, and M. Ellis. In press. Modeling oyster populations II. Adult size and reproductive effort. *J. Shellfish Res.*

Hopkins, A. E. 1935. Factors influencing the spawning and setting of oysters in Galveston Bay, Texas. *Bull. U.S. Bur. Fish.* **47:** 57–83.

Kabat, A. R. 1986. Effects of trematode parasitism on reproductive output of the bivalve *Transennella tantilla*. *Can. J. Zool.* **64:** 267–270.

Kaulman, Z. F. 1979. Dependence of the time of gamete maturation and spawning on environmental temperature in the Virginia oyster *Crassostrea virginica*. *Hydrobiol. J. (Engl. Transl. Gidrobiol. Zh.)* **14:** 29–30.

Kennedy, A. V., and H. I. Battle. 1964. Cyclic changes in the gonad of the American oyster, *Crassostrea virginica* (Gmelin). *Can. J. Zool.* **42:** 305–321.

Kessler, S. W. 1975. Rapid isolation of antigens from cells with a staphylococcal protein a-antibody adsorbent: parameters of the interaction of antibody-antigen complexes with protein A. *J. Immunol.* **115:** 1617–1624.

Koehn, R. K. 1991. The cost of enzyme synthesis in the genetics of energy balance and physiological performance. *Biol. J. Linn. Soc.* **44:** 231–247.

Loosanoff, V. L. 1942. Seasonal gonadal changes in the adult oysters, *Ostrea virginica*, of Long Island Sound. *Biol. Bull.* **82:** 195–214.

Loosanoff, V. L., and H. C. Davis. 1953. Temperature requirements for maturation of gonads of northern oysters. *Biol. Bull.* **103:** 80–96.

Lynch, M. P., and L. Wood. 1966. Effects of environmental salinity on free amino acids of *Crassostrea virginica* Gmelin. *Comp. Biochem. Physiol.* **19:** 783–790.

MacKenzie, C. L., Jr. 1977. Development of an aquacultural program for rehabilitation of damaged oyster reefs in Mississippi. *U.S. Nat. Mar. Fish. Serv. Mar. Fish. Rev.* **39**(8): 1–13.

Mackin, J. G. 1962. Oyster disease caused by *Dermocystidium marinum* and other microorganisms in Louisiana. *Publ Inst Mar Sci Univ Tex* **7:** 132–229.

Mancini, G., A. O. Carbonara, and J. F. Heremans. 1965. Immunochemical quantitation of antigens by single radial immunodiffusion. *Immunochemistry* **2:** 235–254.

Powell, E. N., J. D. Gauthier, E. A. Wilson, A. Nelson, R. R. Fay, and J. M. Brooks. 1992. Oyster disease and climate change. Are yearly changes in *Perkinsus marinus* parasitism in oysters (*Crassostrea virginica*) controlled by climatic cycles in the Gulf of Mexico? *Mar Ecol (Pubbl Stn. Zool Napoli)* **13:** 243–270.

Powell, E. N., E. E. Hofmann, J. M. Klinck, and S. M. Ray. 1992. Modeling oyster populations I. A commentary on filtration rate. Is faster always better? *J Shellfish Res* **11:** 387–398.

Ray, S. M. 1966. A review of the culture method for detection of *Dermocystidium marinum*, with suggested modification and precautions. *Proc. Natl Shellfish Assoc* **54:** 55–69.

Samarel, A. M. 1991. *In vivo* measurements of protein turnover during muscle growth and atrophy. *FASEB (Fed. Am Soc Exp Biol.) J* **5:** 2020–2029.

Sastry, A. N. 1979. Pelecypoda (excluding Ostreidae). Pp 113–292 in *Reproduction of Marine Invertebrates*, Vol. V *Molluscs: Pelecypods and Lesser Classes*, A. C. Giese and J. S. Pearse, eds. Academic Press, New York.

Saunders, G. L., E. N. Powell, and D. H. Lewis. 1994. A determination of *in vivo* growth rates for *Perkinsus marinus*, a parasite of *Crassostrea virginica*. *J Shellfish Res.*

Shafee, M. S. 1989. Reproduction of *Perna picta* (Mollusca: Bivalvia) from the Atlantic coast of Morocco. *Mar Ecol Prog Ser* **53:** 235–245.

Sibly, R. M., and P. Calow. 1989. A life-cycle theory of responses to stress. *Biol J Linn Soc* **37:** 101–116.

Soniat, T. M., and S. M. Ray. 1985. Relationships between possible available food and the composition, condition and reproductive state of oysters from Galveston Bay, Texas. *Contrib Mar Sci* **28:** 109–121.

Sprung, M. 1983. Reproduction and fecundity of the mussel *Mytilus edulis* at Helgoland (North Sea). *Helgol. Meeresunters* **36:** 243–255.

Suzuki, T., A. Hara, K. Yamaguchi, and K. Mori. 1992. Purification and immunolocalization of a vitellin-like protein from the Pacific oyster *Crassostrea gigas*. *Mar Biol (Berl.)* **113:** 239–245.

Thompson, R. J., and B. A. MacDonald. 1990. The role of environmental conditions in the seasonal synthesis and utilization of biochemical energy reserves in the giant scallop, *Placopecten magellanicus*. *Can. J Zool* **68:** 750–756.

van Dolah, R. F., M. Y. Bobo, M. V. Levisen, P. H. Wendt, and J. J. Manzi. 1992. Effects of marina proximity on the physiological condition, reproduction, and settlement of oyster populations. *J Shellfish Res.* **11:** 41–48.

White, M. E., E. N. Powell, and S. M. Ray. 1988a. Effect of parasitism by the pyramidellid gastropod *Boonea impressa* on the net productivity of oysters (*Crassostrea virginica*). *Estuarine Coastal Shelf Sci.* **26:** 359–377.

White, M. E., E. N. Powell, S. M. Ray, E. A. Wilson, and C. E. Zastrow. 1988b. Metabolic changes induced in oysters (*Crassostrea virginica*) by the parasitism of *Boonea impressa* (Gastropoda: Pyramidellidae). *Comp. Biochem. Physiol A Comp Physiol* **90:** 279–290.

White, M. E., E. N. Powell, E. A. Wilson, and S. M. Ray. 1989. The spatial distribution of *Perkinsus marinus*, a protozoan parasite, in relation to its oyster host (*Crassostrea virginica*) and an ectoparasitic gastropod (*Boonea impressa*). *J Mar Biol Assoc UK* **69:** 703–717.

Wilson, E. A., E. N. Powell, M. A. Craig, T. L. Wade, and J. M. Brooks. 1990. The distribution of *Perkinsus marinus* in Gulf coast oysters: its relationship with temperature, reproduction, and pollutant body burden. *Int Rev. Gesamten Hydrobiol.* **75:** 533–550.

Wilson, E. A., E. N. Powell, and S. M. Ray. 1988. The effect of the ectoparasitic pyramidellid snail, *Boonea impressa*, on the growth and health of oysters, *Crassostrea virginica*, under field conditions. *U.S. Fish Wildl Serv Fish Bull* **86:** 553–566.

Reference: *Biol. Bull* **186:** 62–71. (February, 1994)

Multiple Modes of Asexual Reproduction by Tropical and Subtropical Sea Star Larvae: an Unusual Adaptation for Genet Dispersal and Survival

WILLIAM B. JAECKLE

Smithsonian Marine Station at Link Port, 5612 Old Dixie Highway, Fort Pierce, Florida 34946,[†] *Harbor Branch Oceanographic Institution, 5600 Old Dixie Highway, Fort Pierce, Florida 34946, and Smithsonian Environmental Research Center, P.O. Box 28, Edgewater, Maryland 21037-0028*

Abstract. Sea star larvae (Echinodermata: Asteroidea), collected from the subtropical Northwest Atlantic Ocean, exhibited three distinct modes of asexual reproduction. A number of different bipinnariae and brachiolariae reproduced by paratomous cloning of the posterolateral arms. This morphogenesis was identical to that of larvae assignable to the genus *Luidia*. A second mode of asexual reproduction involves the autotomization of an anterior portion of the preoral lobe. Primary larvae with preoral lobes of varying sizes and free-swimming preoral lobes of various stages of morphological development were simultaneously collected. The free-swimming preoral lobes developed complete digestive systems and ultimately assumed the form of typical bipinnaria larvae. Asexual reproduction by larvae may also take the form of budding. The released individual is either a blastula- or gastrula-stage embryo. Subsequent development to a bipinnaria-stage secondary larva, with the possible exception of coelom formation, appears to occur through the events associated with normal larval development. These diverse methods of asexual propagation provide a common mechanism to increase the length of larval life and amplify the number of individuals. Thus asexual reproduction by larvae should increase the likelihood of genet representation in the next generation.

Introduction

The primary ecological role of planktonic invertebrate larvae is to disperse away from parent populations and recruit into habitats suitable for postlarval growth, development, and survival. Dispersal and successful recruitment of planktonic larvae regulates, in part, the geographical distribution of many benthic marine invertebrates (Thorson, 1950; Mileikovsky, 1971; Strathmann, 1974; Jackson and Strathmann, 1981; Roughgarden *et al.*, 1988). The arrival of competent larvae at suitable habitats is influenced by both abiotic and biotic features of the overlying water column (Pechenik, 1987; Strathmann, 1987; Young and Chia, 1987). Potential recruits can be lost to predation (Rumrill, 1990), starvation, and food limitation (Olson and Olson, 1989, and references within), and to dispersal away from appropriate settlement sites (Crisp, 1974; Jackson and Strathmann, 1981; Palmer and Strathmann, 1981; Roughgarden *et al.*, 1988). The greater the time that is required to complete the larval life, the more likely, in theory, that a given larva will be lost from recruitment.

Despite the theoretical disadvantages of a lengthy planktonic existence, larvae of many marine invertebrates are long-lived and potentially able to disperse over large geographic distances (*e.g.*, Thorson, 1961; Scheltema, 1964, 1966, 1971a, b; Scheltema and Williams, 1983). For example, planktotrophic larvae of many phyla (*e.g.*, Mollusca, Sipuncula, Echinodermata, and Brachiopoda) have been collected from surface plankton tows in all major currents of the North Atlantic gyre (Scheltema, 1964, 1966, 1971a, b, 1975; Laursen, 1981; Rice, 1981). Scheltema (1971a) labeled these larvae *teleplanic* ("far wandering") in reference to their potential for long-distance dispersal. Presumably, teleplanic larvae possess morphological, behavioral, and chemical characters and character states that decrease the likelihood of mortality during a

Received 16 August 1993, accepted 22 November 1993.

[†] Current address.

Contribution #347 to the Smithsonian Marine Station at Link Port and #998 to the Harbor Branch Oceanographic Institution.

long dispersal phase. These larvae often possess expansive locomotory and feeding appendages, long elaborations of the body, and poorly calcified structural elements (*i.e.*, shell) (Scheltema, 1971a, b; Wilson, 1978; Domanski, 1984). These features are thought to decrease the rate of sinking and increase the volume of water cleared during feeding. In addition to structural alterations, changes in the physiological state of the larvae may also allow for an extended planktonic existence. Teleplanic larvae are thought to enter a metabolic steady-state (*i.e.*, growth stasis), where the energy demands of metabolism covary with the amount of ingested foods (Scheltema, 1966; Pechenik *et al.*, 1984). If the total energy cost of larval development is fixed for a species (Hoegh-Guldberg and Manahan, 1991), then the flexibility to vary development and metabolic rates with nutrient availability may be a prerequisite for a long larval life.

Yet adaptations that increase the likelihood that the genet (*i.e.*, a genetically discrete individual) will persist can take a different and novel form. Bosch (1988) and Bosch *et al.* (1989) reported that oceanic bipinnaria larvae of *Luidia* sp. (Ph. Asteroidea: Or. Paxillosida) reproduced asexually by paratomous cloning of the posterolateral larval arms. Upon release, the secondary embryos morphologically resemble late-stage gastrulae and rapidly assume the form of young bipinnaria larvae. Bosch *et al.* (1989) recognized that the ability of a larva to replicate itself may serve to lengthen the lifespan and size of each genet. These consequences of asexual reproduction by larvae may enhance the likelihood of successful recruitment into benthic habitats by (1) increasing the duration of the larval life (facilitating long-distance dispersal) and multiplying the number of larvae that may survive to metamorphic competence.

Further sampling has revealed that asexual reproduction by oceanic asteroid larvae in the tropical and subtropical Western Atlantic Ocean is restricted neither to a member of the genus *Luidia* nor to modifications of the posterolateral larval arms. Plankton samples taken in the Florida Current of the Gulf Stream and from the territorial waters of the Commonwealth of the Bahamas contained a number of different bipinnaria (with and without developing juveniles) and brachiolaria larvae that were reproducing asexually by one of three distinct modes. The potential for asexual reproduction has now been found in representatives of at least two different asteroid orders (Bosch, 1988; Bosch *et al.*, 1989; present study) and represents an unusual developmental adaptation to further the existence and lifetime of the genet.

Materials and Methods

Larvae were collected from surface waters (≤60 m in depth) of the Florida Current of the Gulf Stream (*ca.* 27.3° N and 79.6° W to *ca.* 27.3° N and 78.8° W) and at various locations in the territorial waters of the Commonwealth of the Bahamas, chiefly in the area between the Berry Islands (*ca.* 25.5° N, 77.5° W), Eleuthera Island (*ca.* 25.5° N, 76.8° W), and Andros Island (*ca.* 25° N, 77.5° W) and off Grand Bahama Island (*ca.* 26.5° N; 78.8° W). All plankton samples were taken using a 3/4-m diameter net with a 202-μm (pore size) netting that was towed either horizontally or vertically. Sea star larvae were sorted from the total catch as soon as possible after collection and placed in seawater that had been filtered through a bag or string filter (*ca.* 5-μm pore size). Larvae that were maintained in the laboratory were held in finger bowls at 21–25°C and fed a mixture of *Dunaliella tertiolecta* and *Isochrysis galbana* (Tahitian strain). Each day the dishes were inspected for newly released secondary larvae and embryos. All asexually produced individuals were pooled and maintained in the same manner as the primary larvae. With the sole exception of the larva of a species assignable to the genus *Luidia* (Bosch *et al.*, 1989, see below), the taxonomic classification of the examined larvae remains unknown.

Bipinnaria larvae, brachiolaria larvae, and asexually produced individuals were processed in two ways for morphological inspection. For examination of larval gross anatomy, larvae were examined live or fixed in Hollande's fluid (Galigher and Kozloff, 1971) for 24 h, dehydrated with an ascending ethanol series, and examined using both a compound and a dissecting microscope. For studies of external and internal surfaces, larvae and embryos were fixed in 1% OsO_4 in either seawater or distilled water for 1 h, serially dehydrated with ethanol, and critical-point-dried using CO_2 as the transition fluid. The specimens were mounted on stubs, coated with a gold-palladium mixture, and then examined using a Novascan 30 scanning electron microscope.

Results

Field-collected bipinnaria and brachiolaria larvae exhibited three forms of asexual reproduction. Asexually produced individuals were either (1) released as late gastrula-stage embryos or early bipinnaria larvae from either or both posterolateral arms of primary larvae (Figs. 1, 4, 6), (2) developed from an autotomized anterior region of the preoral lobe (Figs. 8–9), or (3) released from the apical tips of the arms of primary larvae in a blastula- or gastrula-like condition (Figs. 2, 3, 14, 15). Based on the morphology and coloration patterns of the examined larvae, it is assumed that each of the three modes of asexual reproduction is exhibited by different species.

The most common method of asexual reproduction observed was the differentiation of either a single or both posterolateral arms to become modified into secondary

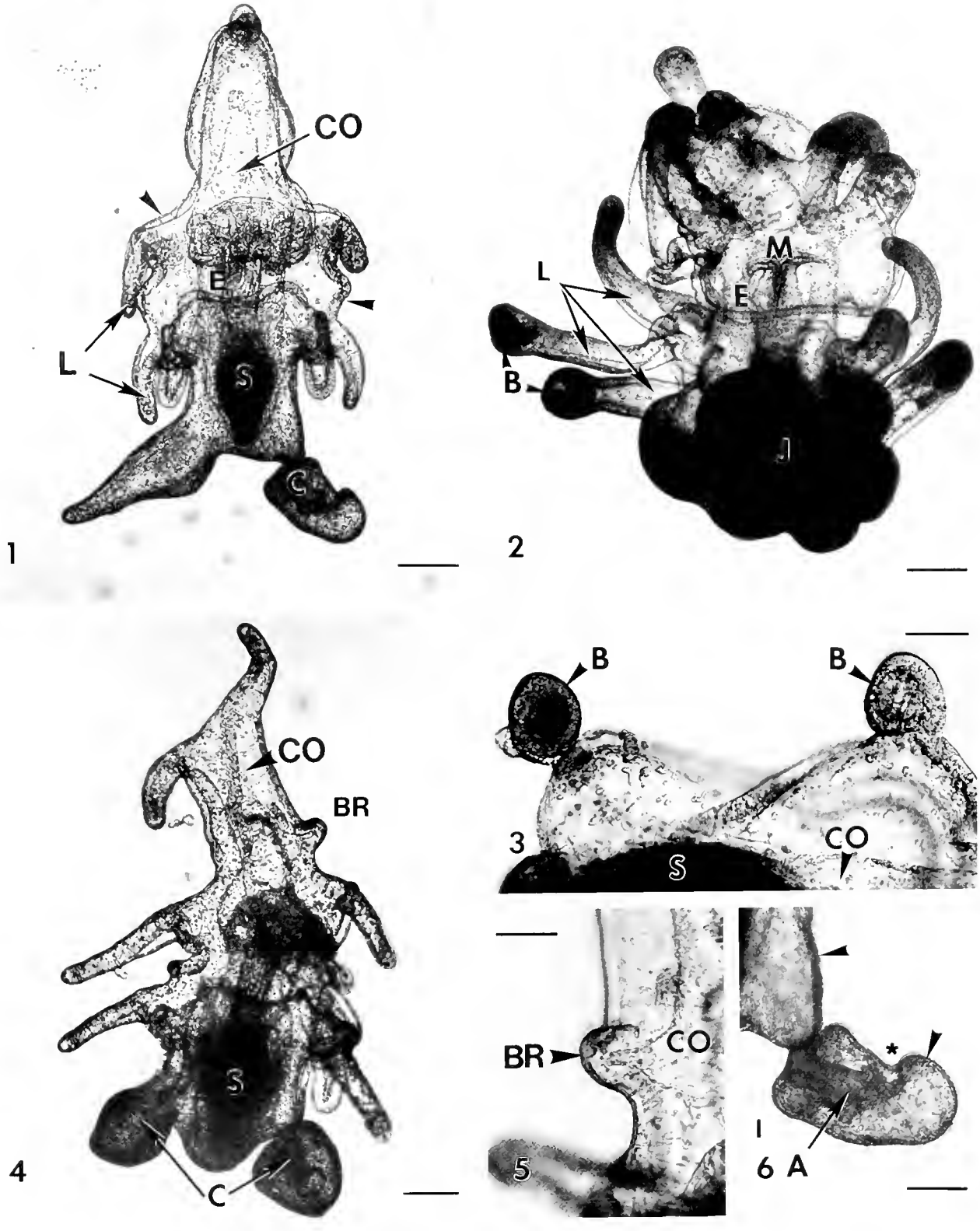

Figures 1–6. Light micrographs of asexual reproduction via paratomous cloning and budding by field-collected bipinnaria and brachiolaria larvae.

larvae (Figs. 1, 4). This mode of asexual propagation was originally described by Bosch *et al.* (1989) for larvae assignable to the genus *Luidia*. In addition to bipinnariae of *Luidia* sp., a number of field-collected brachiolaria larvae also underwent asexual reproduction by modification of the posterolateral larval arms (Fig. 4; note that members of the order Paxillosida do not develop a brachiolaria-stage larva). Although the brachiolar complex was not well formed in any asexually reproducing larva, each possessed a pair of arms on the ventral face of the preoral lobe that contained an extension of the anterior larval coelom; hence these are here considered to be brachiolar arms (Fig. 5). Secondary larvae from both bipinnariae and brachiolariae are generally released as late gastrulae or early bipinnariae. Many attached secondary larvae developed a ciliary band, and the primordium of the circumoral field is evident (Fig. 6). In some exceptional individuals, primary larvae were collected with fully formed secondary bipinnaria larvae still attached.

Asexual reproduction exhibited by oceanic asteroid larvae may also involve the apparent autotomization of the anterior portion of the preoral lobe. A number of morphologically identical bipinnaria larvae of similar body size (here defined as the distance between the posterior margin of the larval body and the posterior margin of the preoral lobe) were obtained from a single plankton tow taken in the Florida Current of the Gulf Stream. Although the body size was similar among individuals, the size of the preoral lobe ranged from complete (Fig. 7) to absent (Fig. 10), with individuals intermediate between the two extremes also present (Fig. 11). The loss of the anteriormost portion of the larval body is probably not an artifact of the collection method because intermediate forms are present (Fig. 11) and close examination of the site of autotomization does not reveal any evidence of mechanically induced tissue damage (Fig. 12). Collected alongside larvae exhibiting preoral lobes of various sizes were a number of free-swimming preoral lobes that developed a complete digestive system (apparently from larval ectoderm) 1–2 days after collection (Figs. 8, 9). The newly released individuals retain a portion of the coelomic system of the primary larva from which the remainder of the secondary larva's coelomic system is presumed to be derived (the assumed site of autotomization is depicted in Fig. 7). Secondary larvae retain the normal anterior-posterior polarity of the primary larvae. Although secondary larvae are initially asymmetrical about the anterior-posterior axis (with the preoral lobe being disproportionately large; Fig. 8), their posterior region presumably grows at an accelerated rate and these larvae assume the proportions of typical bipinnariae (Fig. 9).

A third method of asexual reproduction was infrequently observed and involved the release and subsequent development of a small apical portion of a larval arm. The initiation of larval budding (Figs. 2, 3) coincides with an accumulation of mesenchyme-like cells in the distal tip of the arm (Figs. 3, 13). The tip of each budding arm becomes swollen and rounded (Figs. 4, 13). The tissue linking primary larvae to their secondary embryos (Figs. 3, 14) regresses and the connection is lost. The newly released secondary individual is in a developmental state that is morphologically similar to either a blastula-stage (Fig. 15) or an early gastrula-stage embryo (Fig. 16). The apical surface of these cells is lined with microvilli, and each cell possesses a cilium (not shown). Secondary embryos have a blastocoelic space of variable size (Figs. 14–

Figure 1. Light micrograph of a bipinnaria larva of *Luidia* sp. (ventral view) reproducing asexually through paratomous cloning of the posterolateral arms. Note the difference in appearance between the posterolateral arms and other larval arms (L). The secondary larva (C) of the larval left side is near the point of release from the primary larva. The anterior extension of the anterior coelom (CO) has extended well into the preoral lobe. E—esophagus; S—stomach; arrowhead—ciliary band; scale bar = 65 μm.

Figure 2. Light micrograph of a bipinnaria larva (ventral view) in the early stages of asexual reproduction via budding. Those larval arms that appear to be developing buds (B) differ in appearance from nonbudding larval arms (L). E—esophagus; J—developing juvenile; M—mouth; scale bar = 316 μm.

Figure 3. Light micrograph of the right ventral side of a larva reproducing asexually by developing buds (B). CO—right somatocoel; S—stomach; scale bar = 48 μm.

Figure 4. Light micrograph of a brachiolaria larva reproducing asexually via paratomous cloning of both posterolateral arms. The developing secondary larvae (C) differ in appearance from other unmodified larval arms. Examination of the preoral lobe reveals an extension of the anterior coelom (CO) into an evagination of the epithelium, producing a brachiolar arm (BR). S—stomach; arrowhead—ciliary band; scale bar = 65 μm.

Figure 5. Light micrograph of the brachiolar arm depicted in Figure 4 clearly showing the extension of the anterior coelom (CO) into the brachiolar arm (BR). Scale bar = 29 μm.

Figure 6. Light micrograph of a secondary individual produced by paratomous cloning of the posterolateral arms. The developing archenteron (A) and the beginning of the oral vestibule (*) are visible in this specimen. Arrowheads—ciliary band of both the primary and the secondary larva; scale bar = 39 μm.

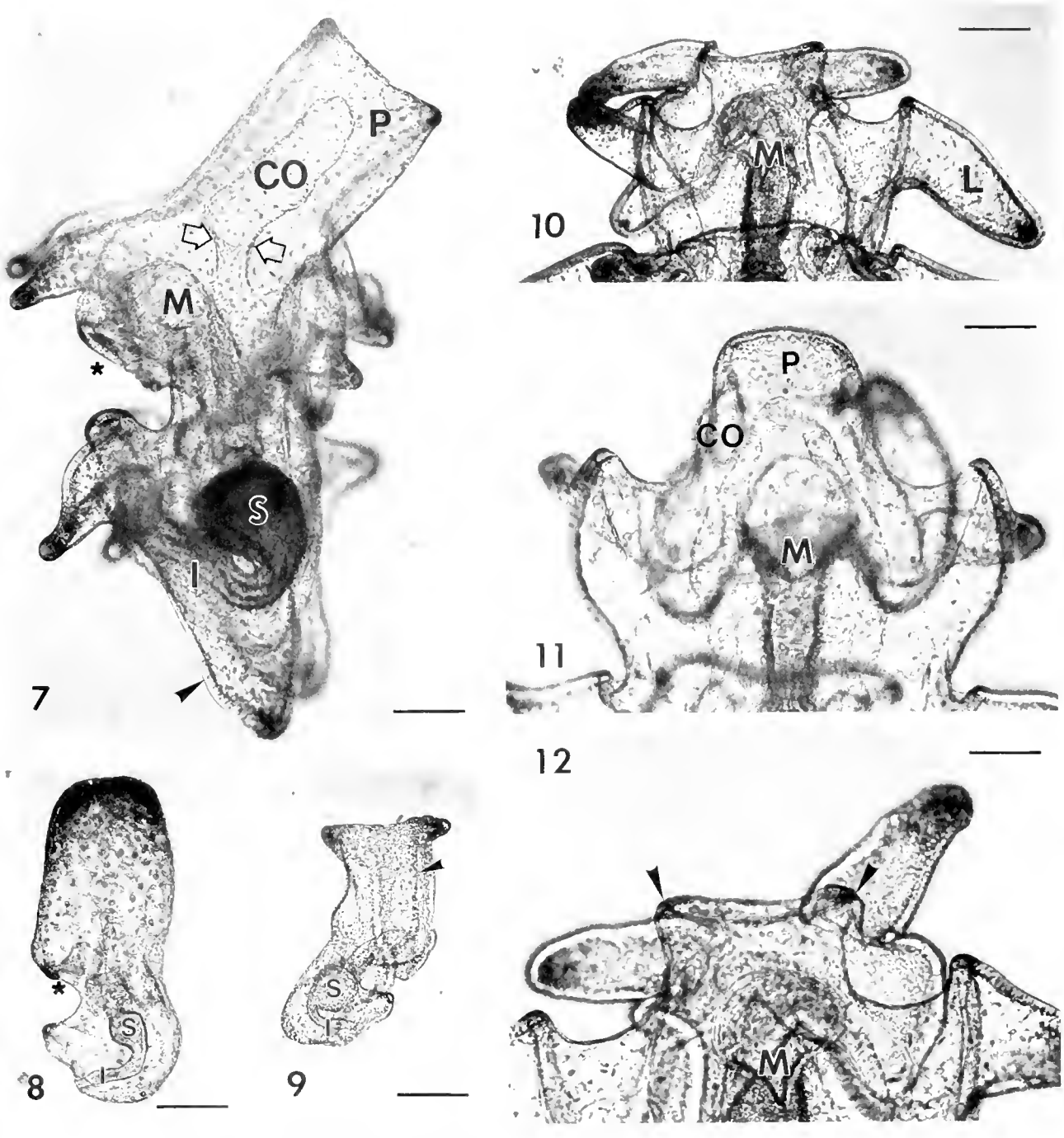

Figures 7–12. Light micrographs of primary and secondary larvae that are involved in or the result of autotomization of the preoral lobe of bipinnaria larvae.

Figure 7. Light micrograph of a left lateral view of a fully formed bipinnaria larva showing the vestibule (*), mouth (M), stomach (S), and intestine (I). Within the preoral lobe (P), the anterior extension of the coelom (CO) is clearly evident. The assumed plane of autotomization is the area suggested by the space between the open arrows. Arrowheads—ciliated band; scale bar = 88 μm.

Figure 8. Light micrograph of a left side view of a developing secondary larva released through the autotomization of a preoral lobe. The digestive system is nearly fully formed. I—intestine; S—stomach; mouth vestibule—(*). scale bar = 70 μm.

Figure 9. A light micrograph of a right side view of a secondary larva that is more developed than the individual depicted in Figure 8. The ciliated band (arrowhead) is clearly differentiated from the other cells of the larval epithelium. I—intestine; S—stomach; scale bar = 100 μm.

Figure 10. Light micrograph showing a ventral view of a bipinnaria larva that has autotomized its preoral lobe. L—larval arm; M—mouth; scale bar = 158 μm.

16, 20) and within the blastocoel there can be a variable number of mesenchyme-like cells (Figs. 14–16, 20–21). If the secondary embryo is released in a blastula-like condition, the cells of one side of the secondary embryo begin to invaginate into the blastocoelic cavity (Fig. 16), ultimately resulting in the formation of a gastrula-like secondary embryo (Fig. 17). Development of the mesoderm of the secondary larva has not been directly observed. Thus coelomic development could occur either from outpocketings of the developing archenteron or from the pool of mesenchyme-like cells that preexist within the blastocoel and accumulate at the distal tip of the archenteron (Figs. 15–18, 20–21). As development proceeds, the cells of the outer epithelium become thinner in profile and the embryo elongates (Figs. 16–18). The developing archenteron comes in contact with the outer epithelium and a secondary opening, the mouth, is formed. The entire process (from release to a feeding individual) requires 24–36 h. In addition to elongation, the developing individual develops the ciliated bands and overall morphology of a bipinnaria larva (Figs. 18, 19).

Discussion

A majority of marine invertebrates produce planktonic larvae that remain in the water column for variable periods of time. This obligate dispersal period allows for (1) recruitment into sympatric populations, (2) maintenance of genetic communication between allopatric populations, and (3) colonization of new or recently opened habitats (*e.g.*, Thorson, 1946, 1950; Scheltema, 1971a, b; Mileikovsky, 1971; Crisp, 1974, 1976; Chia, 1974). Dispersal increases the probability that a species will persist in both ecological and geologic time scales (Jablonski and Lutz, 1983). However, these positive benefits of a planktonic larval stage are countered by the increased likelihood of larval mortality with extended time in the plankton (Vance, 1973, 1974; Strathmann, 1974, 1985; Jackson and Strathmann, 1981; Young and Chia, 1987; Roughgarden *et al.*, 1988). Much recent work on the ecology of invertebrate larvae has been centered on coastal larval forms (*e.g.*, see Young, 1990). Dispersal away from neritic waters by local circulation patterns significantly decreases the likelihood of successful recruitment for coastal larval forms (Roughgarden *et al.*, 1988). In contrast, teleplanic larvae, which possess structural, physiological, and reproductive characteristics to prolong larval life, can disperse great distances and recruit into habitats far from the source population (Scheltema, 1971a, b).

Discussions of the ecology of teleplanic larvae largely center on the velocity of the prevailing ocean currents and the adaptations (*e.g.*, increased size of the feeding structures, decreased weight of inorganic structural elements, and growth stasis) that increase the probability of survival (*e.g.*, Scheltema, 1966; Pechenik *et al.*, 1984). Thorson (1961) believed that "long-distance larvae seem only to occur in special groups of prosobranchs and crustaceans" and doubted that echinoderm larvae were capable of transoceanic dispersal. Thorson did, however, note the observations of Mortensen (1921; p. 147–149) on an ophiopluteus larva (*Ophiopluteus opulentus*) that apparently released a benthic juvenile and then returned to the water column. This larva subsequently regenerated both the ciliary bands and the posterior digestive system and ultimately assumed the morphology of a normal larva. Thorson suggests that "some tropical ophiurans and perhaps some tropical asteroids may have chances to cross even the widest ocean basins, provided that Mortensen's observations on the 'budding larval polyps' holds true." The results of previous studies (Bosch, 1988; Bosch *et al.*, 1989) and the present study reveal that asexual reproduction by echinoderm larvae exists and is not restricted solely to the ophiurans.

All modes of asexual reproduction described in this report involve a serial dedifferentiation and redifferentiation of larval tissue. In all three modes the primary developmental cycle (egg → embryo → larva) is overlapped by a new developmental series (primary larval tissue → secondary embryonic tissue → secondary larval tissue). In secondary larvae produced by all observed modes of asexual reproduction, it appears that the "endodermal" regions are derived from the primary larva's differentiated ectoderm. Further, the concordance between the position of the putative mesenchyme-like cells and the coelomic cavities in secondary larvae, produced either by paratomy or budding, suggests that these cells are responsible for or assist in the production of these mesodermal structures.

The process of asexual reproduction differs among the three modes described in this report. These developmental differences, coupled with the fact that larvae from at least

Figure 11. Light micrograph of a bipinnaria larva with a preoral lobe (P) of intermediate height (dorsal view, plane of focus is midfrontal). The connection between the left and right anterior coeloms (CO) is visible immediately anterior to the mouth (M). Scale bar = 62 μm.

Figure 12. Light micrograph of a higher magnification view of the larva shown in Figure 10. The smooth surface of the site of apparent autotomization is denoted by the arrowheads. M—mouth; scale bar = 91 μm.

13

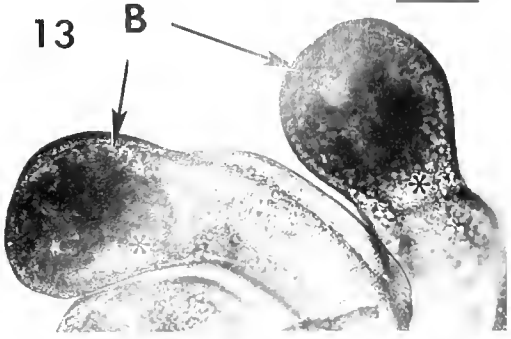

14

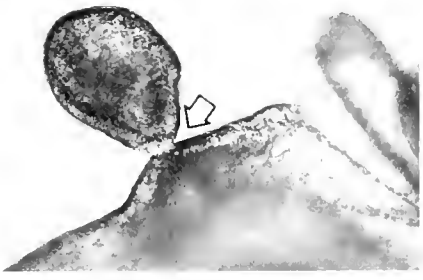

15

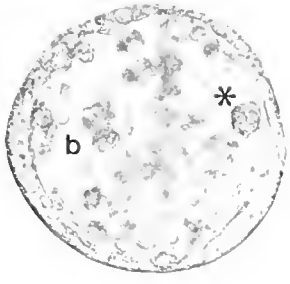

16

17

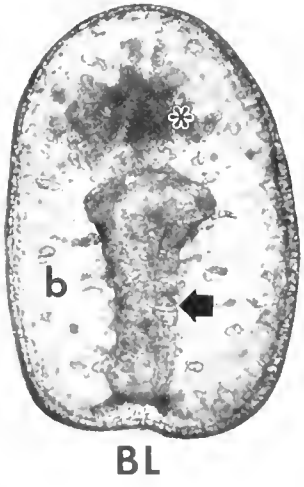

18

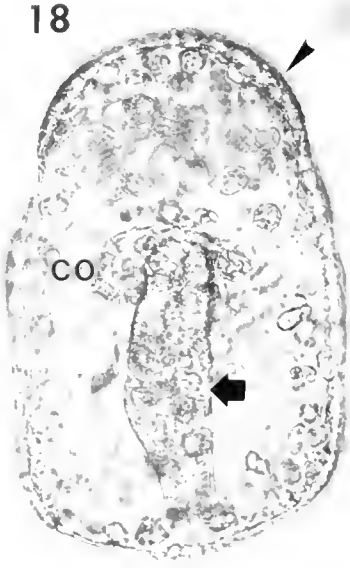

19

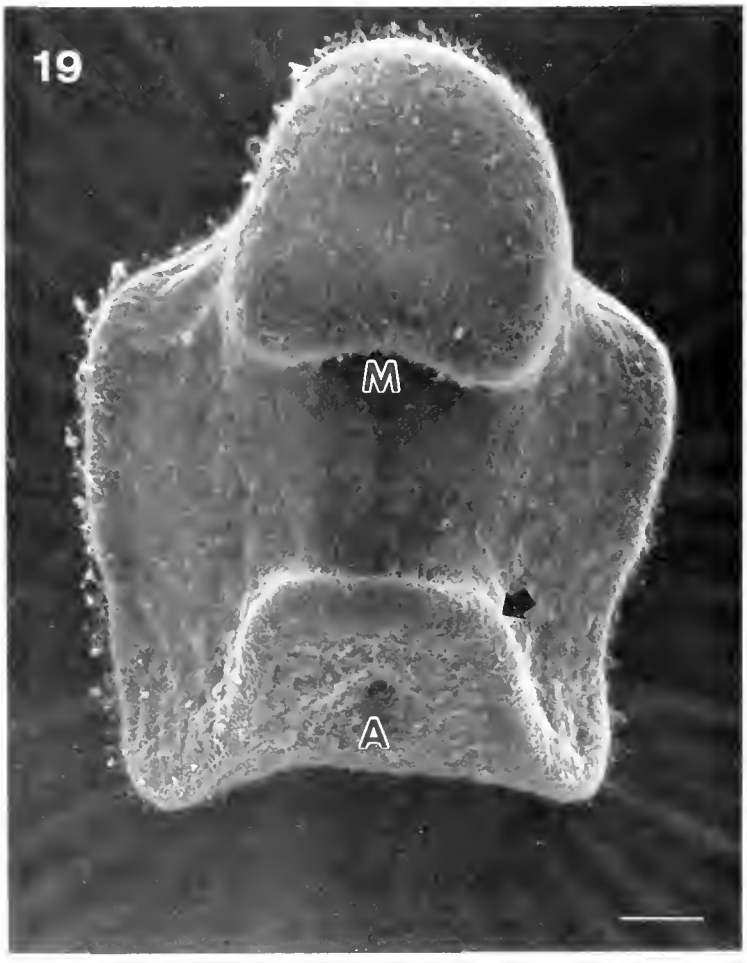

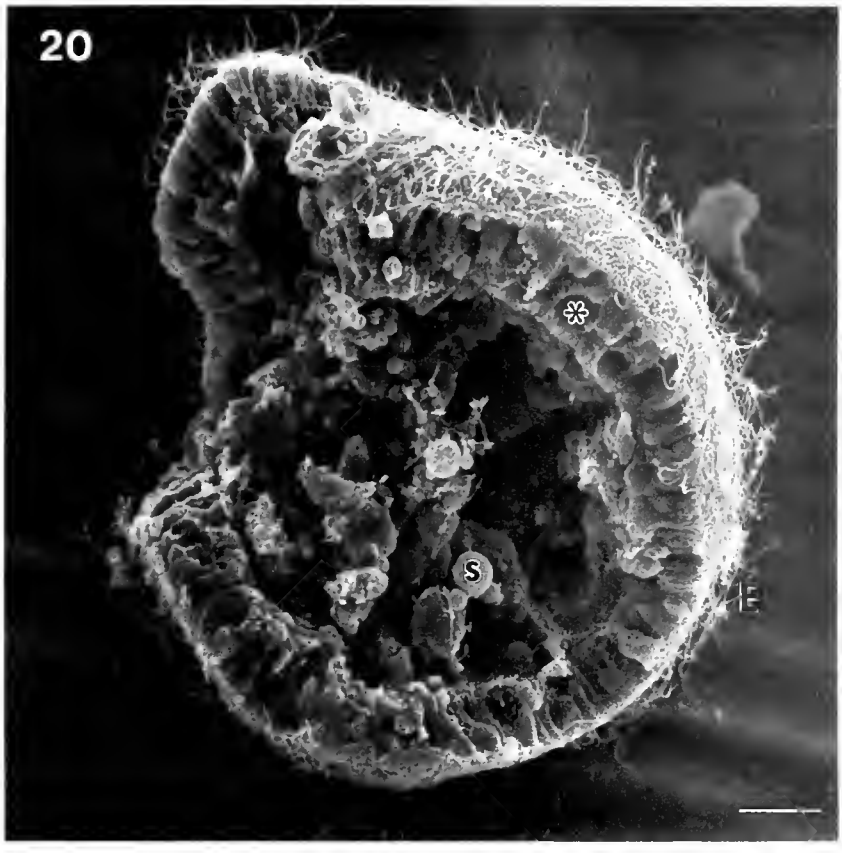

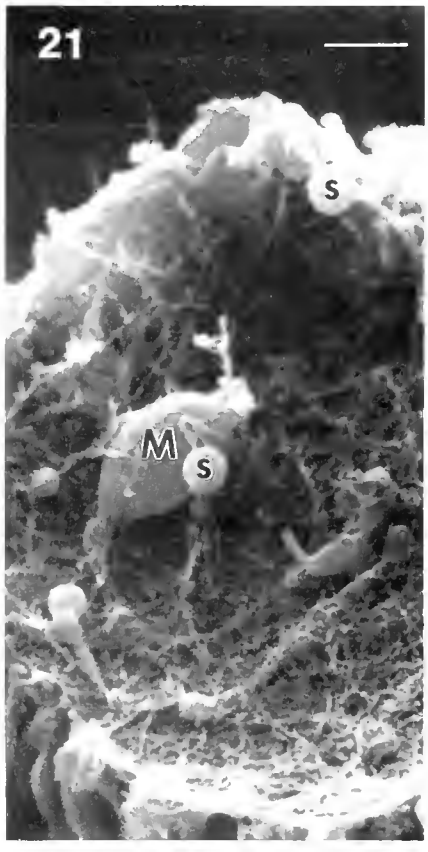

Figures 20–21. Scanning electron micrographs of the exterior and interior surfaces of newly released secondary embryos.

Figure 20. Scanning electron micrograph of a blastula-stage individual that has been broken open. The epithelium (E) is composed primarily of ciliated columnar cells, but circular holes suggest that at least one other cell type is present. The blastocoelic space is filled with cells; in this micrograph small spherical cells (S) are notable. Scale bar = 28 μm.

Figure 21. Scanning electron micrograph of the basal face of the outer epithelium of a blastula-stage embryo. Present are mesenchyme-like cells (M) and smaller spherical cells (S). The inner surface of the epithelium is lined with a fibrous meshwork. Scale bar = 9 μm.

Figures 13–19. Light and scanning electron micrographs that depict the sequence of events during the process of asexual reproduction by budding.

Figure 13. Light micrograph showing the rounded appearance of the arm apices (B) and the associated accumulation of cells (*). Scale bar = 58 μm.

Figure 14. Light micrograph of a bud near the time of release from the primary larva. The site of bud/larva junction is designated by the arrow. Scale bar = 38 μm.

Figure 15. Light micrograph of a released bud in a blastula-like condition. In this individual, the cell-free blastocoel (b) is small and the blastocoelic space contains a large number of cells (*). Scale bar = 33 μm.

Figure 16. Light micrograph of a free-swimming secondary embryo undergoing gastrulation. The developing archenteron (closed arrow) is formed by the invagination of the epithelium into the blastocoel (b). Blastopore—BL; scale bar = 25 μm.

Figure 17. A light micrograph showing a fully formed gastrula-stage secondary embryo produced by asexual reproduction by budding. The well-developed archenteron (filled arrow) leads from the blastopore (BL) into the blastocoel (b). The accumulation of cells at the apex of the archenteron (*) is seen in many individuals and may be involved in the formation of the coeloms of the secondary larva. Scale bar = 27 μm.

Figure 18. A light micrograph of a dorsal view of a newly formed secondary bipinnaria larva. The ciliated band (arrowhead) has formed and the primordium of the coelomic system of the secondary larva (CO) is clearly evident at the anterior extent of the developing larval gut (filled arrow). Scale bar = 23 μm.

Figure 19. Scanning electron micrograph of a fully formed secondary bipinnaria larva that developed from a bud released from a primary larva. Anus—A; mouth—M; ciliated band—(filled arrow); scale bar = 28 μm.

two orders are reproducing asexually (members of the order Paxillosida (*e.g., Luidia*) do not develop a brachiolar complex), suggest that asexual reproduction represents an adaptation to a prolonged planktonic existence. However, the factor or factors that regulate the production of secondary larvae remain obscure.

Despite the theoretical advantages of persistence and amplification of the genet, asexual reproduction may have a negative impact on the primary larvae. All forms of asexual reproduction require a relatively small percentage of the total larval soma, but may significantly reduce the effectiveness of larval feeding. In paratomous cloning (mode 1), each posterolateral arm is completely modified to produce a secondary larva. Although this arm pair is at the posterior margin of the larval body, it may contribute a significant percentage of the total number of food particles captured. Hart (1991) reported that the posterior region of the body of bipinnaria larvae of *Dermasterias imbricata* accounted for nearly a quarter of the observed particle captures. The small portion of an arm lost through budding (mode 3) is less likely to interfere with the particle capture mechanism to the same degree. In contrast, asexual reproduction by autotomization of the preoral lobe (mode 2) is predicted to have a significant impact on the feeding performance of the primary larva. Hart (1991) observed that 50% of the particle captures by larvae of *Dermasterias imbricata* were attributable to the ciliary bands anterior to the mouth.

The obvious benefit afforded a species by larval asexual reproduction is persistence of the genet through an increase in the number of propagules without a concomitant increase in the reproductive effort of the parent generation. The lengthening of the larval lifespan and the amplification of the number of larvae in the plankton should increase the probability of successful representation in the following generation. Persistence of three different modes of asexual reproduction, spanning at least two taxonomic orders, indicates that this adaptation to a prolonged planktonic existence is both ecologically and evolutionarily important.

Acknowledgments

This project would not have been completed without the generosity of Drs. Craig Young, Edie Widder, and Tammy Frank (Harbor Branch Oceanographic Institution), Mary Rice (Smithsonian Marine Station at Link Port), and Kevin Eckelbarger (University of Maine), who allowed the author to participate in their research cruises. The plankton samples would not have been collected without the assistance and patience of vessel captains Sumner Gerard (R/V *Morning Watch*), Daniel Schwarz (R/V *Seward Johnson*), Chris Vogel (R/V *Edwin Link*), Ralph van Hoek (R/V *Sea Diver*), and Edmond Warren (R/V *Sea Diver*). Special thanks are extended to Dr. Mary Rice and her staff (Woody Lee, Sherry Reed, and Hugh Reichardt) for collecting and allowing the author to examine plankton samples taken for her research program. Dr. Sid Bosch (SUNY, Geneseo) and Ms. Elizabeth Balser (Clemson University) are acknowledged for their stimulating discussions about the development of asteroid echinoderms. Ms. Julianne Piraino (Smithsonian Marine Station at Link Port) helped prepare the scanning electron micrographs. The work was support by a Smithsonian Postdoctoral fellowship to W. Jaeckle and by NSF grants OCE-8916264 (to C.M. Young and K.J. Eckelbarger) and OCE-9116560 (to C.M. Young).

Literature Cited

Bosch, I. 1988. Replication by budding in natural populations of bipinnaria larvae of the sea star genus *Luidia*. Pp. 789 in *Echinoderm Biology: Proceedings of the Sixth International Echinoderm Conference*, R. D. Burke, P. V. Mladenov, P. Lambert, and R. L. Parsley, eds. A. A. Balkema, Rotterdam.

Bosch, I., R. B. Rivkin, and S. P. Alexander. 1989. Asexual reproduction by oceanic planktotrophic echinoderm larvae. *Nature* **337:** 169–170.

Chia, F. S. 1974. Classification and adaptive significance of developmental patterns in marine invertebrates. *Thalassia Jugosl.* **10:** 121–130.

Crisp, D. J. 1974. Energy relations of marine invertebrate larvae. *Thalassia Jugosl.* **10:** 103–120.

Crisp, D. J. 1976. The role of pelagic larvae. Pp. 145–155 in *Perspectives in Experimental Biology*, Vol. 1, P. Spencer-Davies, ed. Pergamon Press, Oxford and New York.

Domanski, P. A. 1984. Giant larvae: prolonged planktonic larval phase in the asteroid *Luidia sarsi*. *Mar. Biol.* **80:** 189–195.

Galigher, A. E., and E. N. Kozloff. 1971. *Essentials of Practical Microtechnique*, 2nd ed. Lea and Febiger, Philadelphia. 531 pp.

Hart, M. W. 1991. Particle captures and method of suspension feeding by echinoderm larvae. *Biol. Bull.* **180:** 12–27.

Hoegh-Guldberg, O., and D. T. Manahan. 1991. Metabolic requirements during growth and development of echinoderm larvae. *Am. Zool.* **31:** 4A.

Jablonski, D., and R. A. Lutz. 1983. Larval ecology of marine benthic invertebrates: paleobiological implications. *Biol. Rev.* **58:** 21–88.

Jackson, G. A., and R. R. Strathmann. 1981. Larval mortality from offshore mixing as a link between precompetent and competent periods of development. *Am. Nat.* **118:** 16–26.

Laursen, D. 1981. Taxonomy and distribution of teleplanic prosobranch larvae in the North Atlantic. *Dana-Report* **89:** 1–47.

Mileikovsky, S. A. 1971. Types of larval development in marine bottom invertebrates, their distribution and ecological significance: a re-evaluation. *Mar. Biol.* **10:** 193–213.

Mortensen, T. 1921. *Studies of the Development and Larval Forms of Echinoderms*. G. E. C. Gad. Copenhagen. 266 pp.

Olson, R. R., and M. H. Olson. 1989. Food limitation of planktotrophic marine invertebrate larvae: Does it control recruitment success? *Ann. Rev. Ecol. Syst.* **20:** 225–247.

Palmer, A. R., and R. R. Strathmann. 1981. Scale of dispersal in varying environments and its implications for life histories of marine invertebrates. *Oecologia* **48:** 308–318.

Pechenik, J. A. 1987. Environmental influences on larval survival and development. Pp. 551–608 in *Reproduction of Marine Invertebrates*, Vol. 9, A. C. Giese and J. S. Pearse, eds. Academic Press, New York.

Pechenik, J. A., R. S. Scheltema, and L. S. Eyster. 1984. Growth stasis and limited shell calcification in larvae of *Cymatium parthenopeum* during trans-Atlantic transport. *Science* **224**: 1097–1099.

Rice, M. E. 1981. Larvae adrift: patterns and problems in life histories of sipunculans. *Am. Zool.* **21**: 605–619.

Roughgarden, J., S. Gaines, and H. Possingham. 1988. Recruitment dynamics in complex life cycles. *Science* **241**: 1460–1466.

Rumrill, S. S. 1990. Natural mortality of marine invertebrate larvae. *Ophelia* **32**: 163–198.

Scheltema, R. S. 1964. Origin and dispersal of invertebrate larvae in the north Atlantic. *Am. Zool.* **4**: 299–300.

Scheltema, R. S. 1966. Evidence for trans-Atlantic transport of gastropod larvae belonging to the genus *Cymatium*. *Deep-Sea Res.* **13**: 83–95.

Scheltema, R. S. 1971a. The dispersal of the larvae of shoal-water benthic invertebrate species over long distances by ocean currents. Pp. 7–28 in *Fourth European Marine Biology Symposium*, D. J. Crisp, ed. Cambridge University Press, Cambridge.

Scheltema, R. S. 1971b. Larval dispersal as a means of genetic exchange between geographically separated populations of shallow-water benthic invertebrates. *Biol. Bull.* **140**: 284–322.

Scheltema, R. S. 1975. The frequency of long-distance larval dispersal and the rate of gene-flow between widely separated populations of sipunculans. Pp. 199–210 in *Proceedings of the International Symposium on the Biology of the Sipunculida and the Echiura*, M. E. Rice and M. Todorovic, eds. Naucno Del Press, Belgrade.

Scheltema, R. S., and I. P. Williams. 1983. Long-distance dispersal of planktonic larvae and the biogeography and evolution of some polynesian and western Pacific mollusks. *Bull. Mar. Sci.* **33**: 545–565.

Strathmann, R. R. 1974. The spread of sibling larvae of sedentary marine invertebrates. *Am. Nat.* **108**: 29–44.

Strathmann, R. R. 1985. Feeding and nonfeeding larval development and life-history evolution in marine invertebrates. *Ann. Rev. Ecol. Syst.* **16**: 339–361.

Strathmann, R. R. 1987. Larval feeding. Pp. 465–550 in *Reproduction of Marine Invertebrates*, Vol. 9. A. C. Giese and J. S. Pearse, eds. Academic Press, New York.

Thorson, G. 1946. Reproduction and larval development of Danish marine bottom invertebrates. *Meddr. Komm. Danm. Fisk.-og. Havunders. ser. Plankton* **4**: 1–523.

Thorson, G. 1950. Reproduction and larval ecology of marine bottom invertebrates. *Biol. Rev.* **25**: 1–45.

Thorson, G. 1961. Length of pelagic larval life in marine bottom invertebrates as related to larval transport by ocean currents. Pp. 455–474 in *Oceanography*. Pub 67, AAAS, Washington, DC.

Vance, R. R. 1973. On reproductive strategies in marine benthic invertebrates. *Am. Nat.* **107**: 339–352.

Vance, R. 1974. Reply to Underwood. *Am. Nat.* **108**: 874–878.

Wilson, D. P. 1978. Some observations on bipinnariae and juveniles of the starfish genus *Ludia*. J. Mar. Biol. Assoc. U.K. **58**: 467–478.

Young, C. M. (ed.). 1990. *Ophelia* **32**(1–2).

Young, C. M., and F. S. Chia. 1987. Abundance and distribution of pelagic larvae as influenced by predation, behavior, and hydrographic factors. Pp. 385–463 in *Reproduction of Marine Invertebrates*, Vol. 9. A. C. Giese and J. S. Pearse, eds. Academic Press, New York.

Reference: *Biol. Bull.* **186**: 72–80. (February, 1994)

Aspects of Histocompatibility and Regeneration in the Solitary Reef Coral *Fungia scutaria*

PAUL L. JOKIEL AND CHARLES H. BIGGER

Hawaii Institute of Marine Biology, P.O. Box 1346, Kaneohe, Hawaii 96744, and Department of Biological Sciences, Florida International University, Miami, Florida 33199

Abstract. Discoid coralla of the solitary free-living reef coral *Fungia scutaria* were cut with a rock saw and rejoined in various paired combinations and orientations of autogeneic sections (self to self), isogeneic sections (clone-mate to clone-mate), and allogeneic sections (two different genotypes). Results of these experiments provide the first evidence of histocompatibility in a solitary coral. Autogeneic or isogeneic sections of coralla with one section containing a mouth were joined along cut edges. In all cases, fusion of tissues occurred within weeks, followed by skeletal fusion within months. However, autogeneic or isogeneic sections rejoined along the uncut edges did not fuse. Isogeneic pairings between two sections with mouths produced neither tissue/skeletal fusion nor cytotoxicity at the interface. Individual cut sections were allowed to regenerate. Sections containing the parent mouth did not develop new mouths. However, cut sections lacking a mouth always regenerated multiple mouths along the cut edge, but not along the uncut edge. Sections without mouths cut along a second line parallel to the first cut always regenerated mouths along the cut edge located closest to what had been the mouth area of the original corallum. The new mouths eventually developed into individual polyps.

Introduction

Studies over the last two decades have shown generalized self/not-self recognition in coelenterates (Hildemann *et al.*, 1975a, 1975b, 1977; Grosberg, 1988; Bigger, 1988). Aside from sea anemones, most studies of anthozoan histoincompatibility have involved colonial species (Grosberg, 1988). Among the scleractinia, colonial corals have been used as experimental subjects. Previous attempts to demonstrate allogeneic and isogeneic reactions in solitary reef corals failed to produce a response. For example, the solitary coral *Fungia scutaria* kills other coral species held in direct contact, but no reaction (neither aggressive killing nor immunological cytotoxic response) occurs when two *F. scutaria* coralla are held in contact (Hildemann *et al.*, 1975a, b, 1977; Chadwick, 1988). In preliminary experiments, we discovered that we could elicit a histocompatibility response by cutting the discoid skeletons with a rock saw and rejoining the resulting sections in various pairings and orientations of autogeneic, isogeneic, and allogeneic material. This technique allowed us to design experiments to explore three questions that are basic to our understanding of histocompatibility and regenerative processes in these corals.

Question 1: Do solitary corals display self/not-self histocompatibility responses similar to those observed in colonial scleractinians? Also, will grafts along cut surfaces react differently than grafts along uncut edges? Previous attempts involving intraspecific parabioses of *F. scutaria* failed to produce a histocompatibility or aggressive killing response at uncut edges (Hildemann *et al.*, 1975a, b, 1977; Chadwick, 1988).

Question 2: Does the presence or absence of a mouth influence regeneration or graft reactions? Presence of a mouth is known to influence survival and regeneration in other species of fungiids (Boschma, 1923; Chadwick and Loya, 1990), but nothing is known of the possible influence of the mouth on grafting response.

Question 3: Do naturally occurring aggregations of identical color-morphs of this species truly represent isogeneic clone-mates? These aggregations are believed to be derived asexually from the same anthocauli or ancestral corallum (Wells, 1954; Krupp *et al.*, 1993).

Fungiid corals are common throughout the Indo-Pacific (Hoeksema, 1989). Their free-living mode of existence

Received 22 March 1993; accepted 13 October 1993.

enables them to colonize unstable rubble substrata (Hoeksema, 1988; Chadwick-Furman and Loya, 1992). *F. scutaria* is widely distributed from South Africa and the Red Sea in the west to Hawaii and the Tuamotu Archipelago in the east (Veron, 1986). The dense, discoid skeleton of this species has been shown to be an adaptation for hydrodynamic stability and abrasion resistance in turbulent, shallow water (Jokiel and Cowdin, 1976).

F. scutaria is a gonochoristic broadcast-spawner that releases gametes at dusk (Krupp, 1983). Spawning generally occurs between the second and fourth days following the full moon in the warmest months of the year (Krupp, 1983). The fertilized eggs develop into a typical planula larva within 12 h. The life cycle of fungiid corals has been summarized by Wells (1966) and Hoeksema (1989). After settlement, the planula begins to deposit skeleton and grows into a broadly attached cylindrical corallum called the anthocaulus. The oral end of the anthocaulus then expands radially, forming a disk-shaped structure called the anthocyathus. The resulting structure resembles a mushroom, hence the root word "fungi" was applied to these animals. The anthocyathus disk eventually breaks away from the anthocaulus stalk and begins life as a free-living, solitary corallum. The remaining anthocaulus tissues continue to produce additional anthocyathi, which break free and form additional coralla. Aggregations of identical color-morphs found on reefs are assumed to be clone-mates derived from a single anthocaulus (Wells, 1954, 1966).

Asexual reproduction occurs through budding from residual tissues of a damaged corallum (Bourne, 1887). Anthocaulus-like structures have also been observed arising from "dead" coralla of *Fungia* (Boschma, 1923; Krupp, 1983). Wells (1966) and Veron (1986) suggested that such buds are formed asexually from residual live tissue in damaged or dying parent coralla. Wells (1966) referred to these buds as "asexual anthocauli." The proliferation of new coralla from "dead" adult *F. scutaria* has recently been supported by direct evidence (Krupp *et al.*, 1993).

Materials and Methods

Fungia scutaria coralla were collected from shallow water (depth < 1 m) on patch reefs in the vicinity of Coconut Island, Kaneohe Bay, Hawaii, and held in continuous-flow aquaria supplied with nonrecirculating seawater from Kaneohe Bay. The aquaria were located outdoors in full natural sunlight, so the experimental environment was similar to that encountered in the shallow reef-flat habitat of this species.

The corals were cut with a circular rock saw. A continuous flow of seawater was directed at the diamond blade and the cutting area to prevent heating and drying of the tissues. After cutting, the corals were immediately returned to the continuous-flow aquaria. Regeneration in *Fungia* has long been known to be rapid (Kawaguti, 1937); the tissues grew and covered the exposed cut skeleton within 1 to 2 weeks. This species contains symbiotic zooxanthellae that produce enough photosynthetic product to allow the coral to grow in filtered seawater without heterotrophic feeding (Franzisket, 1969), so even cut sections without mouths will regenerate new tissues and deposit new skeletal material. There was no mortality of cut sections (either with or without mouths) or grafts in the months following the cutting process.

Sections cut for regeneration experiments were placed on plastic mesh racks and observed at regular intervals. The coral sections used in the various grafted combinations were held firmly together on notched acrylic plastic plates measuring 23 cm × 12 cm × 1 cm. The grafts were held securely in contact with monofilament nylon fishing leader (50-pound test). Monofilament strands were looped over the coral fragments and around the notched plastic plate, stretched by pulling the ends with hemostat clamps, and fastened on the back side of the plate with fishing leader crimps. Each graft pairing was labeled with a plastic tag. The plates were held off the bottom of the aquarium in a plastic rack at an angle of 60° to prevent accumulation of detritus or sediment.

Graft interactions were examined daily for the first month and subsequently at monthly intervals. Grafts were examined with the aid of a jeweler's magnifier during routine scoring. When needed, detailed examination was conducted with a platform stereomicroscope at 45× magnification. The term "tissue fusion" was applied to cases where tissues healed completely and became confluent between the two sections as observed under 45× magnification. In cases of "nonfusion," a boundary or gap persisted between the tissues of the two joined sections. Scoring tissues as fused or unfused was unambiguous, and we did not have to resort to histological techniques. At the conclusion of the experiments, the grafted skeletons were cleaned of all tissues by soaking in hypochlorite solution. After drying, the interfaces were examined for skeletal fusion. Sections that fell apart from each other when the monofilament ties were removed were scored as "unfused." Sections that had calcified heavily along the interface into a solid skeleton were termed "fused." Again, there was no ambiguity in the scoring of skeletal fusion.

Initially, we made six grafts of each type described below. Some types of graft pairings were increased in number to answer specific questions that arose during the initial experiments. For example, the first set of allografts showed a lack of cytotoxicity as well as a lack of fusion. Different genotypes of some colonial species show a wide range of rapid to slow and strong to weak reactions (Johnston *et al.*, 1981). Therefore we increased the numbers of pairings to rule out the possibility that we had selected only slow-

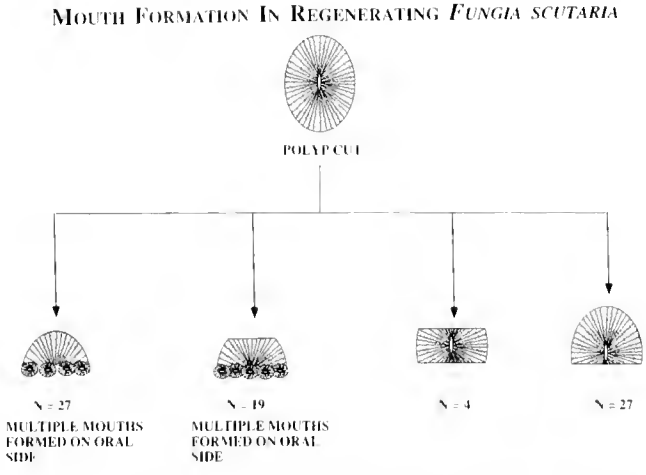

Figure 1. Mouth formation and regeneration in *Fungia scutaria* for cut sections with mouths, cut sections without mouths, and sections with two cut edges.

reactors in the first six grafts. The number was further increased to test the possible effects of different color-morph pairings. The original six grafts were sufficient to show a clear-cut response in many of the graft combinations.

The graft and regeneration experiments were designed to provide several types of information. The autograft experiments tested rates of tissue and skeletal fusion and the importance of cut versus uncut surfaces. Further, these experiments compared reactions between sections with mouths and sections without mouths. The allograft/isograft experiments were designed to provide information on histocompatibility reactions. They also allowed us to test the hypothesis that all identical color-morphs from the same aggregation are clone-mates, whereas corals taken from different reefs are allogeneic, even if they are of the same color-morph.

Regeneration experiments

Coralla were cut into sections with mouths and without mouths and with multiple cuts as shown in Figure 1. Sections were maintained in the continuous-flow microcosm aquaria on plastic mesh racks. During the 7-month regeneration period, we examined the fragments and noted the number and location of new mouths.

Autografts

Given a single corallum, four grafting orientations were of interest to us (Fig. 2, top). The first was a cut directly across the mouth region with subsequent regrafting in the same orientation. The second was a cut across the corallum outside of the mouth region with grafting in the original orientation. The third type of autograft was similar to the second, but we made an additional cut on the uncut outer edge, rotated the cut section 180°, and placed the two cut edges in contact. In the fourth case, the uncut

GRAFTING RESPONSE IN *FUNGIA SCUTARIA*

TISSUE SOURCE	AUTOGRAFT				ISOGRAFT					ALLOGRAFT			XENOGRAFT	
ORIENTATION	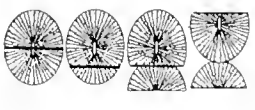												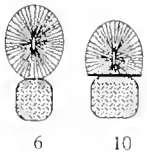	
SAMPLE SIZE	10	20	11	14	6	6	8	6	6	24	6	6	6	10
RESPONSE (% OF GRAFTS)														
FUSION														
TISSUE	100%	100%	91%	22%*	100%	100%	25%*	0	0	0	0	0	0	0
SKELETON	100%	100%	91%	0	100%	100%	0	0	0	0	0	0	0	0
NO RESPONSE	0	0	9%	78%	0	0	75%	100%	100%	100%	100%	0	0	0
ABNORMAL TISSUE	0	0	0	0	0	0	0	0	0	0	0	100%	0	0
KILLING	0	0	0	0	0	0	0	0	0	0	0	0	100%	100%

*OCCASIONAL TISSUE CONNECTIONS—NOT COMPLETE FUSION.

Figure 2. Summary of grafting results for autografts, isografts, allografts, and xenografts of *Fungia scutaria* in various orientations.

edge of the cut piece was rotated 180° and placed in contact with the opposite uncut free edge of the parent corallum.

Isografts

Aggregations of single color-morphs found on the reef have long been assumed to be clone-mates derived from a single ancestral anthocaulus through asexual formation of multiple anthocyathi. *F. scutaria* in Kaneohe Bay display different combinations of tentacle color (green or brown), mouth color (white, purple, brown, or green), and disk color (brown, mottled white-brown, or violet). Pairs of the same color-morphs taken from within such natural aggregations were used in all isografts. The corals were cut on the rock saw and grafted in the five configurations shown at the top of Figure 2. In the first configuration, a section with a mouth was joined to a section that lacked a mouth and had been cut from a putative clone-mate. The second type of isograft was made by grafting two sections that lacked mouths and had been cut from two presumed clone-mate coralla. A third type joined two mouth-bearing sections along their cut edges. The fourth was the same as the third, but joined along the free uncut edges. The fifth type of isograft joined two sections without mouths at the uncut free margins.

Allografts

Allografts were made between corals taken from different reefs and presumably derived from different planulae settlements. Three types of allografts were made (Fig. 2, top). The first type consisted of grafting sections from two different corals, but with both sections having mouths ($n = 24$). Allografts were made between sections containing mouths for identical color-morphs taken from different reefs ($n = 12$) and from pairings of different color-morphs taken from the same reef ($n = 12$). In the second type, only one of the pair had a mouth ($n = 6$); in the third type, neither had a mouth ($n = 6$).

Xenografts

As a control, 16 xenograft pairings were made between *F. scutaria* and the colonial reef coral *Montipora verrucosa* at cut and uncut edges. (Fig. 2). A number of previous studies show rapid killing of *M. verrucosa* by *F. scutaria*. These xenografts served to demonstrate whether the killing response was active during our experiments.

Results

Regeneration experiments

The freshly cut skeletons (Fig. 3a) healed within 1 to 2 weeks. Each section with a mouth began to regenerate septae on the cut surface within 60 days (Fig. 3c). After 7 months, no additional mouths had formed on the 31 sections that initially had a mouth (Fig. 1). Multiple mouths formed within 45 days on all 46 sections that initially lacked a mouth (Fig. 1). At 90 days, many of the mouth areas started to form into anthoblasts and began to separate (Fig. 3b) in a manner reminiscent of polyp formation from an anthocaulus (Fig. 3d). In all 46 cases, the new multiple mouths formed along the cut margin proximal to what had been the mouth area of the original corallum. Areas distal from the original mouth area (on sections with and without a second cut) did not develop new mouths (Fig. 1).

Autografts

All autografts joined along cut surfaces in their original orientation showed complete tissue and skeletal fusion (Figs. 2, 4a, 4c). Fusion of tissue was rapid, with confluences observed within 48 h. Within 60 days, the skeletons were fused to the point that the sections would hold together without support. One of the autografts made at cut surfaces in the rotated orientation did not fuse. Autografts made with contact along the uncut outer free margin did not show skeletal or tissue fusion (Figs. 2, 4b, 4d). In some cases we noted occasional stringlike tissue connections across the graft interface, but these did not persist for more than a few days.

Isografts

All isografts between a section with a mouth and a section without a mouth fused completely if joined along the cut edge, but did not fuse if joined at the uncut free outer edge (Fig. 2). Isografts along cut edges between two mouth-containing sections did not show any skeletal fusion. As in the case of autografts joined at the free edge zone, we noted occasional stringlike tissue connections at the interface. Apparently, recognition was occurring, as evidenced by the limited and nonpersistent connections. However, these connections dissipated, and fusion did not occur between two sections containing mouths. In contrast, grafts between two fragments without a mouth that were joined along the cut surface fused completely and formed a new mouth at the interface (Figs. 2, 5b).

Allografts

Allografts showed no signs of tissue fusion or skeleton fusion, regardless of combination or orientation of the graft (Figs. 2, 5a). Also, there was no sign of cytotoxic killing between the two tissue types. Polyps attempted to push away from each other by "inflating" the coelenteron with water. Mesenteries were extruded, but no tissue damage was observed on live material viewed with a ster-

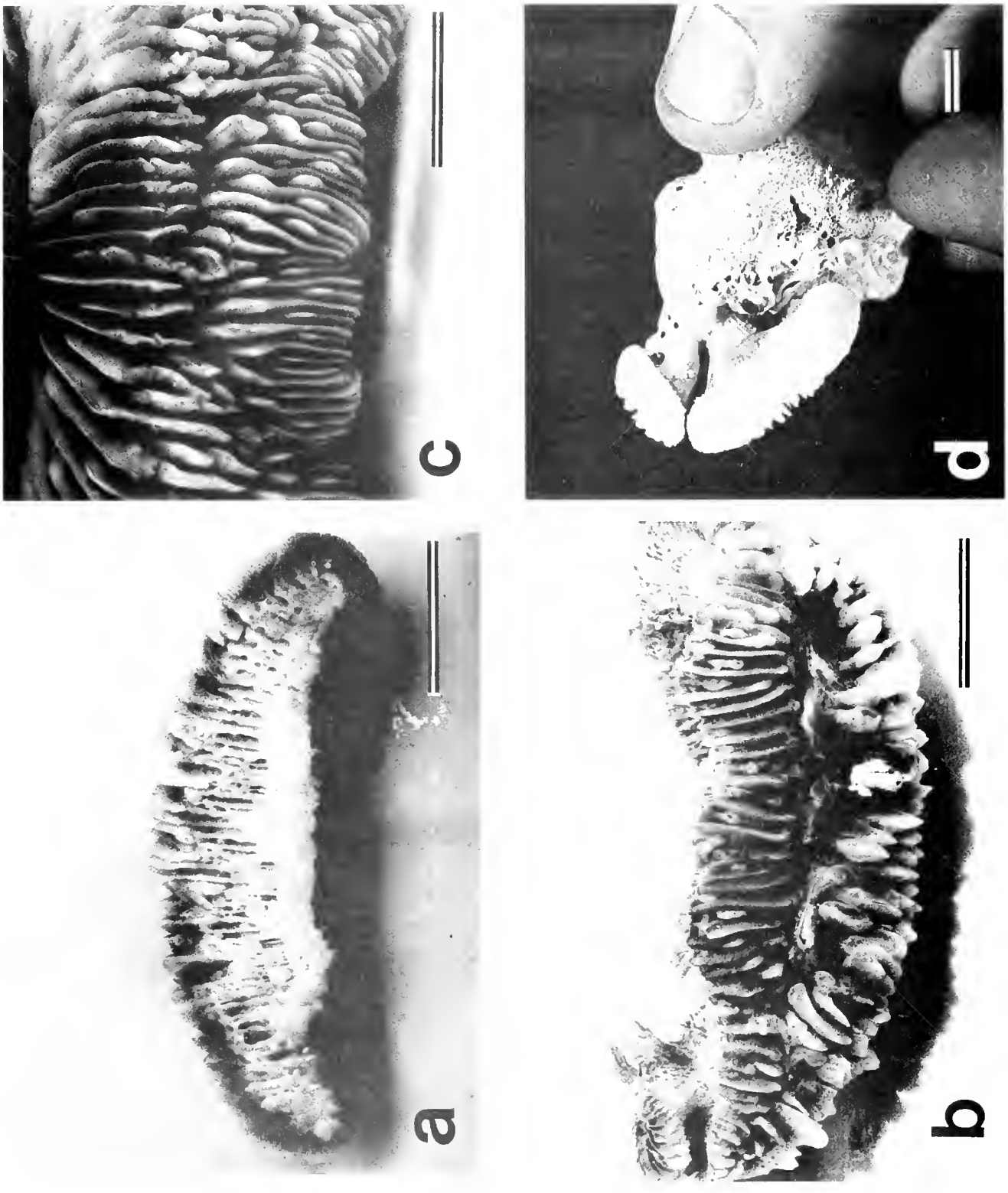
a
b
c
d

eomicroscope at 45×. Pairings between identical color-morphs taken from different reefs did not fuse. Graft combinations using pairings of different color-morphs did not show heightened reactions compared to pairings with the same color pattern from different reefs. Abnormal hyperplasia (not necrosis) and mouths appeared in the fragments paired cut edge to cut edge (*e.g.*, Fig. 5a), but tissue and skeletal fusion did not take place.

Xenografts

Concurrent control xenografts of *F. scutaria* paired with the colonial coral *M. verrucosa* resulted in killing of the *M. verrucosa* along the interface within 3 days. The *F. scutaria* maintained a 1-cm-wide tissue-free zone throughout the 7-month experiment. This control demonstrated the presence of the killing response in our experimental material. The observed lack of cytotoxicity or aggressive killing in autografts, isografts, and allografts of *F. scutaria* was not due to lethargy among the experimental corals.

Discussion

Results of these grafting experiments provide the first evidence of a self/not-self histocompatibility recognition system in a solitary reef coral. The response of *Fungia scutaria* is analogous to that observed in colonial corals (*e.g.*, Hildemann *et al.*, 1975a, b, 1977) in that allografts and presumed isografts fused, but allografts did not fuse. No cytotoxic killing was noted in allografts. Unique and previously unreported observations for *F. scutaria* include the observation that isogeneic mouth-containing individuals do not fuse at cut edges, but isogeneic sections without mouths will fuse. Also, isogeneic grafts do not fuse along the intact free edge of the solitary corallum, as shown by isograft and allograft pairings involving cut *versus* uncut edges.

Grafts between sections from different coralla taken from the same aggregation of *F. scutaria* fused at the same rate and in the same manner as autografts. Scientists have previously suspected that such "families" of *Fungia* probably represent clone-mate aggregations derived from multiple asexual budding from a single ancestral anthocaulus (*e.g.*, Wells, 1954). An alternate hypothesis is that such aggregations are the result of a mass settlement of sibling planulae that each gave rise to an anthocaulus and anthocyathi.

Recently, it has been shown that successful recruitment of sexually derived planulae of *F. scutaria* on the reefs of Kaneohe Bay is rare (Fitzhardinge, 1993; Krupp *et al.*, 1993). More than a decade has passed since spawning of gametes and sexual production of planulae were first observed and described for this species (Krupp, 1983). During the initial study and in many subsequent attempts, D. Krupp (pers. comm.) and other researchers have been unable to induce settlement in planulae of *F. scutaria*. A variety of substrata and environmental regimes have been presented to the planulae, but they have not settled and formed anthocauli. Larvae of the other common Hawaiian coral species readily settle under laboratory conditions, but it seems that the conditions required for settlement of *F. scutaria* are highly specific. We have not found new *F. scutaria* anthocauli developing on fouling plates or on blocks, reef rock, or other substrata placed in the bay to measure recruitment over the years. A long-term study designed to measure coral recruitment in Kaneohe Bay has recently been completed (Fitzhardinge, 1993). About 170 concrete blocks were set in various shallow-water reef environments and monitored for coral recruitment over a period of 3 years. Thousands of settlements of all other common Kaneohe Bay coral species were recorded, but only a single *F. scutaria* anthocaulus was noted. Even the anthocaulus-like structures found attached to natural reef substrates (other than dead parent coralla) often are asexually derived. Close examination of these structures reveals that many arise from highly eroded and encrusted *F. scutaria* coralla that have been incorporated and cemented into the reef matrix. Apparently, asexual reproduction is the dominant means of proliferation of *F. scutaria* in Kaneohe Bay (Krupp *et al.*, 1993).

Given the well-documented importance of asexual reproduction in this species and the rarity of successful sexual reproduction, we conclude that the most parsimonious explanation for the occurrence of aggregations of identical color-morphs is asexual proliferation of coralla. It is hard to imagine how aggregations of isogeneic color-morphs could be achieved by multiple planulae settlements at one site.

Results of the isograft experiments are consistent with the asexually derived clonal hypothesis. Identical color-morphs taken from different reefs, however, were allogeneic and did not fuse. The usefulness and interpretation of histocompatibility responses as a measure of genetic structure of populations is debated (*e.g.*, Curtis *et al.*, 1982;

Figure 3. All scale bars = 1 cm. (a) Freshly cut section of *Fungia scutaria*. (b) Regeneration of mouths from a section cut without a mouth after 7 months. Note formation of a new anthocyathus from the former aboral surface. (c) Regenerated septae on a section with a mouth after 7 months. (d) Two anthocyathi sprouting from isogeneic tissue (anthocauli). Note that isogeneic tissues of the two anthocyathi do not fuse at the edges.

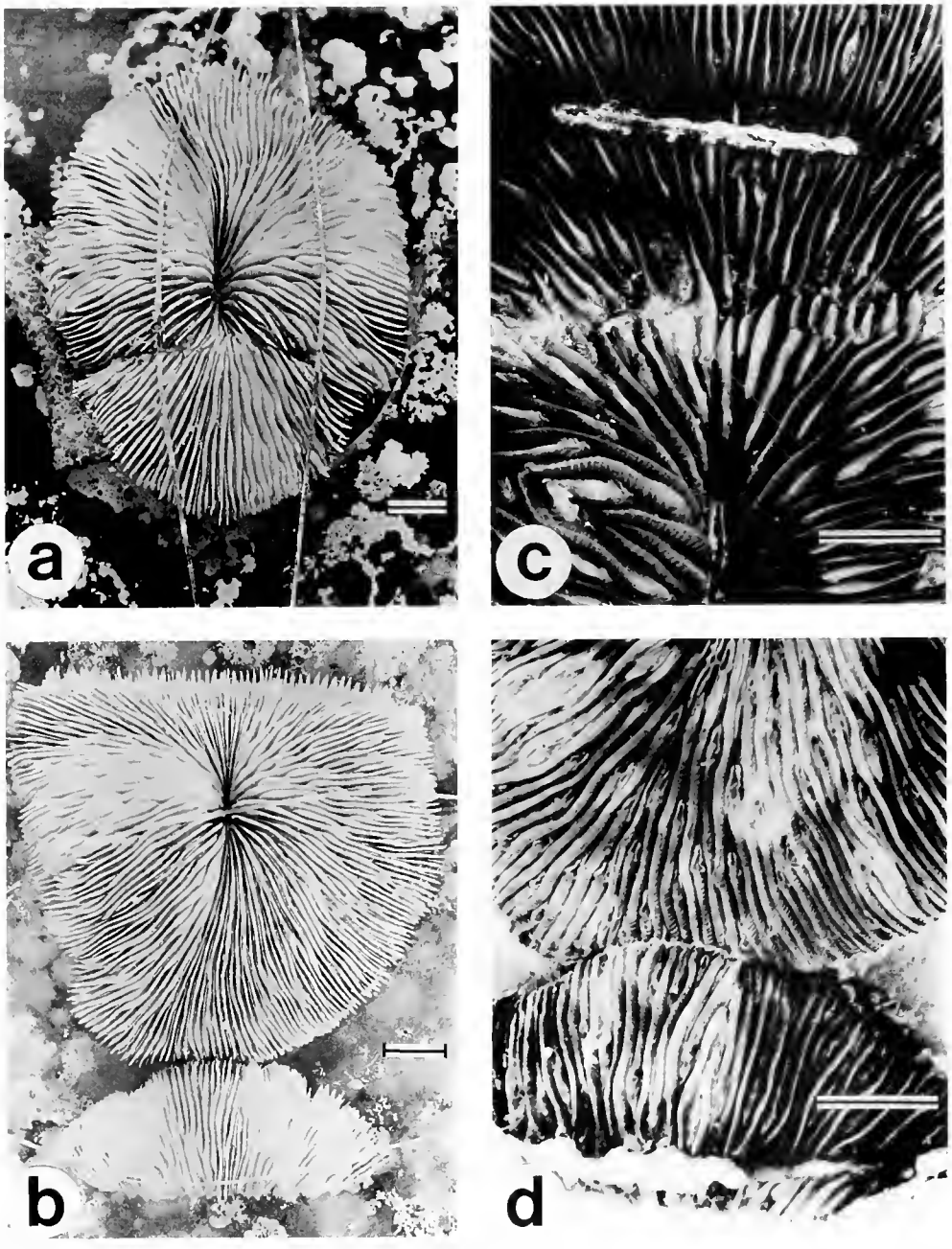

Figure 4. All scale bars = 1 cm. (a) Cleaned skeleton of cut edge to cut edge autograft of *Fungia scutaria* showing fusion of skeleton after 7 months. (b) Cleaned skeleton of uncut edge to uncut edge autograft showing no fusion after 7 months. (c) Autograft fusion of tissues at 7 months along rejoined cut edge. (d) Autograft nonfusion of tissues in uncut edge to uncut edge at 7 months.

Rinkevich and Loya, 1983; Willis and Ayre, 1985; Heyward and Stoddart, 1985; Hunter, 1985; Grosberg, 1988). Nevertheless, in the case of *F. scutaria*, our results are consistent with the notion that aggregations of identical color-morphs are isogeneic.

Organization of tissues in *F. scutaria* into an anthocyathi begins with the formation of a mouth. This is true for development of anthocyathi from anthocauli, formation from fragments without mouths (Fig. 3d), and proliferation of coralla from damaged or dying coralla. Each new mouth becomes a center of polyp development. An edge zone forms around each mouth area, leading to the eventual separation of polyps from each other and from the parent anthocaulus if they are to become solitary

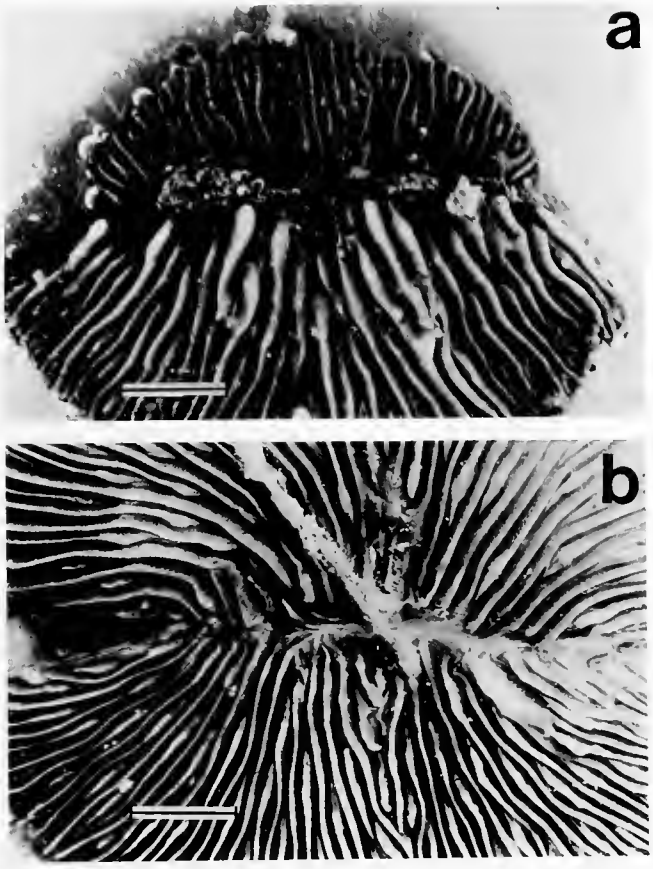

Figure 5. All scale bars = 1 cm. (a) Allograft between two mouthless fragments of *Fungia scutaria* one year after grafting. Note lack of fusion and formation of abnormal hyperplasia along interface. (b) Isograft between mouthless sections one year after grafting. Note fusion of tissues and formation of new mouth along the interface.

polyps. Polyps of *F. scutaria* must possess a mechanism that initially causes separation of the corallum from parent tissue. Juvenile clone-mate anthocyathi on the same anthocaulus will separate even though connected at the base by continuous tissues and touching along the edge zone (Fig. 3d). Once the mouth has formed, there must be further development leading to the separation of a solitary coral from the parent tissue.

Formation of buds from tissues lacking a mouth leads to rapid proliferation of new coralla from parent anthocauli as well as from damaged or senescent coralla. Each bud in turns leads to formation of an anthocyathi. Perhaps the same process that causes polyp separation is responsible for the prevention of refusion of clone-mates once they have separated. "Families" of *F. scutaria* derived from a common anthocaulus do not fuse into a single isogeneic mass (Chadwick, 1988), as would occur with colonial clone-mates on a reef (*e.g.*, Jokiel *et al.*, 1983).

Theories on the mechanisms controlling development have been proposed and tested among hydrozoan coelenterates (*e.g.*, Babloyantz and Hiernaux, 1974), but such studies are generally lacking among the anthozoans. Architectural methods used to describe growth in tropical trees have been used to describe coral growth, including *Fungia* (Dauget, 1991). Fungiid corals provide an attractive experimental model because members of this family show considerable diversity in structure and developmental pattern. For example, the free-living solitary coral *Diaseris fragilis* reproduces asexually by breaking into wedge-shaped fragments, each of which later forms a mouth and develops into a discoid corallum (Yamashiro *et al.*, 1989). The fungiid *Sandalolitha robusta* has multiple mouths, but its early development is similar to that of *Fungia* (Yamashiro and Yamazato, 1987). The anthocyathus detaches from the anthocauli at an early stage and follows a free-living existence thereafter. The number of mouths and tentacles on the disk continues to increase, however, leading to the polystomatous condition. The anthocyathus continues to regenerate additional polyps, which also detach. Unlike *F. scutaria*, *S. robusta* does not show the influence of the mouth in preventing formation of additional mouths.

Results of the regeneration experiments are consistent with the classic observation that extensive budding in *F. fungites* can be induced by selectively killing the mouth region with putty (Boschma, 1923). In our experiments, all sections cut without a mouth formed new mouths, and all sections cut containing a mouth did not form mouths. Location on cut fragment is important in mouth formation. Sections without mouths cut along a second line parallel to the first cut always regenerated multiple mouths along the cut edge proximal to the former mouth area. During the first stage of polyp formation, multiple mouths proliferate from cut sections in a manner analogous to that observed in anthocauli and damaged coralla.

Acknowledgments

This research was inspired by the late Professor W. H. Hildemann, a pioneer in the early development of comparative immunogenetics. Partial support was provided by NIH Grant AI/CA 19470 to W.H.H., NIH Grant RR08205 to C.H.B., and by the Hawaii Institute of Marine Biology. We thank D. Krupp for his comments on the original manuscript and D. Gulko for his assistance in the graphical presentations.

Literature Cited

Babloyantz, A., and J. Hiernaux. 1974. Models for positional information and positional differentiation. *Proc. Natl. Acad. Sci. U.S.A.* **71:** 1530–1533.

Bigger, C. H. 1988. Historecognition and immunocompetence in selected marine invertebrates. Pp. 55–65 in *Invertebrate Historecognition*, R. Grosberg, D. Hedgecock, and K. Nelson, eds. Plenum Press, New York.

Boschma, H. 1923. Experimental budding in *Fungia fungites*. *Proc. K. Akad. Wet., Amsterdam* **26:** 88–96.

Bourne, G. C. 1887. The anatomy of the madreporarian coral *Fungia*. *Q. J. Microsc. Sci.* **27:** 293–324.

Chadwick, N. E. 1988. Competition and locomotion in a free-living fungid coral. *J. Exp. Mar. Biol. Ecol.* **123:** 189–200.

Chadwick, N. E., and Y. Loya. 1990. Regeneration after experimental breakage in the solitary reef coral *Fungia granulosa* Klunzinger, 1879. *J. Exp. Mar. Biol. Ecol.* **142:** 221–234.

Chadwick-Furman, N., and Y. Loya. 1992. Migration, habitat use, and competition among mobile corals (Scleractinia: Fungiidae) in the Gulf of Eilat, Red Sea. *Mar. Biol.* **114:** 617–623.

Curtis, A. S. G., J. Kerr, and N. Knowlton. 1982. Graft rejection in sponges. *Transplantation* **33:** 127–133.

Dauget, J.-M. 1991. Application of tree architectural models to reef-coral growth forms. *Mar. Biol.* **111:** 157–165.

Fitzhardinge, R. 1993. *The Ecology of Juvenile Hawaiian Corals*. Ph.D. Thesis, University of Hawaii, Honolulu, Hawaii. 252 pp.

Franzisket, L. 1969. Riffkorallen können autotroph leben. *Die Naturwissenschaften* **56:** 144–145.

Grosberg, R. K. 1988. The evolution of allorecognition specificity in clonal invertebrates. *Q. Rev. Biol.* **63:** 377–412.

Heyward, A. J., and J. A. Stoddart. 1985. Genetic structure of two species of *Montipora* on a patch reef: conflicting results from electrophoresis and histocompatibility. *Mar. Biol.* **85:** 117–121.

Hildemann, W. H., D. S. Linthicum, and D. C. Vann. 1975a. Transplantation and immunoincompatibility reactions among reef-building corals. *Immunogenetics* **2:** 269–284.

Hildemann, W. H., D. S. Linthicum, and D. C. Vann. 1975b. Immunoincompatibility reactions in corals. Pp. 105–114 in *Immunologic Phylogeny*, W. H. Hildemann and A. A. Benedict, eds., Plenum Publishing Corp., New York.

Hildemann, W. H., R. L. Raison, C. J. Hull, L. Akaka, J. Okumoto, and G. Cheung. 1977. Tissue transplantation immunity in corals. *Proc. Third Int. Coral Reef Symp.* **1:** 537–543.

Hoeksema, B. W. 1988. Mobility of free-living fungid corals (Scleractinia), a dispersion mechanism and survival strategy in dynamic reef habitats. *Proc. Sixth Int. Coral Reef Symp.* **2:** 715–720.

Hoeksema, B. W. 1989. Taxonomy, phylogeny and biogeography of mushroom corals (Scleractinia: Fungiidae). *Zool. Verh.* **254:** 1–295.

Hunter, C. L. 1985. Assessment of clonal diversity and population structure of *Porites compressa* (Cnideria, Scleractinia). *Proc. Fifth Int. Symp. Coral Reefs* **6:** 69–74.

Johnston, I. S., P. L. Jokiel, C. H. Bigger, and W. H. Hildemann. 1981. The influence of temperature on the kinetics of allograft reactions in a tropical sponge and a reef coral. *Biol. Bull.* **160:** 280–291.

Jokiel, P. L., and H. P. Cowdin. 1976. Hydromechanical adaptation in the solitary free-living coral, *Fungia scutaria*. *Nature* **262:** 212–213.

Jokiel, P. L., W. H. Hildemann, and C. H. Bigger. 1983. Clonal population structure of two sympatric species of the reef coral *Montipora*. *Bull. Mar. Sci.* **33:** 181–187.

Kawaguti, S. 1937. On the physiology of reef corals. III. Regeneration and phototropism in reef corals. *Palao Trop. Biol. Stud.* **2:** 209–216.

Krupp, D. A. 1983. Sexual reproduction and early development of the solitary coral *Fungia scutaria* (Anthozoa: Scleractinia). *Coral Reefs* **2:** 159–164.

Krupp, D. A., P. L. Jokiel, and T. S. Chartrand. 1993. Asexual reproduction by the solitary scleractinian coral *Fungia scutaria* on dead parent coralla in Kaneohe Bay, Oahu, Hawaiian Islands. *Proc. Seventh Int. Coral Reef Symp.* 527–534.

Rinkevich, B., and Y. Loya. 1983. Intraspecific competitive networks in the Red Sea coral *Stylophora pistillata*. *Coral Reefs* **1:** 161–172.

Veron, J. E. N. 1986. *Corals of Australia and the Indo-Pacific*. Angus & Robertson Publishers, North Ryde, Australia. 644 pp.

Wells, J. W. 1954. Recent corals of the Marshall Islands. *Prof. Pap. U. S. Geol. Surv.* **260-I:** 385–446.

Wells, J. W. 1966. Evolutionary development in the scleractinian family Fungiidae. *Symp. Zool. Soc. Lond.* **16:** 223–246.

Willis, B. L., and D. J. Ayre. 1985. Asexual reproduction and genetic determination of growth form in the coral *Pavona cactus*: biochemical genetic and immunogenic evidence. *Oecologia (Berlin)* **65:** 516–525.

Yamashiro, H., and K. Yamazato. 1987. Note on the detachment and post-detachment development of the polystomatous coral *Sandalolitha robusta* (Scleractinia, Cnidaria). *Galaxea* **6:** 323–329.

Yamashiro, H., M. Hidaka, M. Nishihira, and S. Poung-In. 1989. Morphological studies on skeletons of *Diaseris fragilis*, a free-living coral which reproduces asexually by natural autotomy. *Galaxea* **8:** 283–294.

Reference: *Biol. Bull.* **186**: 81–89. (February, 1994)

A Substance Inducing the Loss of Premature Embryos From Ovigerous Crabs

MASAYUKI SAIGUSA

Okayama University, College of Liberal Arts & Sciences, Tsushima 2-1-1, Okayama 700, Japan

Abstract. The embryos of an estuarine terrestrial crab (akate-gani; *Sesarma haematocheir*) are attached by a funiculus to ovigerous hairs on the maternal pleopods, and are ventilated by the female until hatching occurs. When females were kept in a small quantity of diluted seawater (about 10‰), hatching and larval release occurred in all cases. In contrast, when the medium was *hatch water* (*i.e.*, the filtered medium into which larvae had been released), most ovigerous females liberated their embryos prematurely, but hatching did not occur. The egg masses (cluster of embryos) carried by these females were not released as usual, but were gradually extruded from the brooding chamber, and within a few days all had dropped to the bottom of the beaker. No morphological changes were found on the outer egg membrane, the funiculus, or the coat investing the ovigerous hairs of females kept in hatch water. But the ovigerous hairs did slip easily out of the *coat*, and this caused the extrusion of the egg masses. The active factor—called *incubation disrupting substance*—was stable with freezing, but heat-labile. In normal females (*i.e.*, those not treated with hatch water), broken egg cases and funiculi remain for a time after hatching with the coat on the ovigerous hairs, but they are gone by the morning after hatching. So the secretion of this incubation-disrupting substance may participate in cleaning the ovigerous hairs of old investing coats and funiculi after larval release, thus preparing for the attachment of the next clutch of embryos. In addition, this substance may play a role in hatching.

Introduction

The newly oviposited eggs of decapod crustaceans, except nonbrooding peneid shrimps, are wrapped in a thick transparent outer membrane and clustered on pleopod setae beneath the folded abdomen of the female (Herrick, 1895; Yonge, 1937, 1946, 1955; Cheung, 1966; Fisher and Clark, 1983; Goudeau and Lachaise, 1983). The embryos are attached to the pleopod setae by a stalk: the funiculus. While attached to the ovigerous hairs by this stalk, the embryos are ventilated by the movement of pleopods of the female until the thick outer membrane breaks, indicating the beginning of hatching. The present study is concerned, in general, with hatching in an estuarine terrestrial crab; it is focused on an active substance that is released *outside* of the egg membrane at the time of hatching.

Hatching enzyme is among the important substances that are discharged upon hatching in many groups of animals. In the teleost *Oryzias latipes*, the enzyme, which is secreted by the embryo, digests the egg membrane, allowing the embryo to emerge (*e.g.*, Ishida, 1944; Yamagami, 1972). This teleost enzyme is actually a mixture of two kinds of proteases that act cooperatively on the inner layer of the egg case (Yasumasu *et al.*, 1989a, b). Embryos of the toad *Xenopus laevis* also secrete a proteolytic enzyme (from the frontal region of the embryos) that digests the fertilization membrane (Carroll and Hedrick, 1974). Katagiri (1975) also demonstrated a hatching enzyme of 55–60 kDa that digests the whole egg case in the frog *Rana chensinensis*. Similarly, sea urchin embryos at the blastula stage (about 10 h after fertilization) secrete a proteolytic enzyme that dissolves the fertilization membrane. Recently, Lapage and Gache (1989) purified the enzyme, a glycoprotein of 51, 52, or 57 kDa that autolyzes to an inactive form of 30 kDa.

Among crustaceans, *adult* barnacles (*Balanus*) release a substance that stimulates the hatching of nauplius larvae (Crisp and Spencer, 1958). If the barnacles were fed, the factor was secreted within 1 or 2 days and the embryos

Received 4 January 1992; accepted 22 November 1993.

hatched; if the barnacles were starved, hatching did not occur. Because the factor could be extracted from the tissues of starved animals in the laboratory, as well as those fed under natural conditions, it may be produced by the barnacle's own metabolism, and not related to a particular food source (Crisp and Spencer, 1958). An active factor extracted and purified from adult barnacle tissues contains a prostaglandin-like compound that stimulates embryonic muscle (Clare *et al.*, 1982).

In the brine shrimp *Artemia salina*, glycerol is highly concentrated in dormant cysts, and then rapidly disappears (Clegg, 1962). When the embryos emerge from their egg cases, glycerol is released into the medium (Clegg, 1964).

Embryos of the terrestrial crab *Sesarma haematocheir* hatch on land around the time of nocturnal high water. Hatching occurs in a very short time, and the timing is highly synchronized among embryos (Saigusa, 1992, 1993). As soon as hatching is complete, the crabs enter the water and release the hatched larvae by making vigorous fanning movements of the abdomen (Saigusa, 1982). The embryos of ovigerous females that were collected from the field and kept in the laboratory did hatch simultaneously. This paper first demonstrates that the filtered water into which zoea-larvae had hatched (*i.e., hatch water*) contains a substance that disrupts the incubation of *other* females. Next, microscopic studies are described that indicate the cause of the liberation of premature embryos from the brooding chamber.

Materials and Methods

Animal handling

Experimental animals were ovigerous females of the terrestrial red-handed crab (akate-gani), *Sesarma haematocheir*, collected from the thicket along a small estuary at Kasaoka, Okayama Prefecture, Japan. (For details of the habitat and the chronology of larval release, see Saigusa, 1982.) Collections were made on 19 August and 2, 4, 9, 14, 15, and 16 September 1991. The crabs were quickly brought into the experimental rooms, where they were kept in plastic containers (70 cm long, 40 cm wide, and 25 cm high) containing shallow water (*ca.* 1 cm deep) and hiding spaces. The water was renewed whenever one or more females released their larvae in the container, and otherwise at intervals of 3–5 days. The crabs were fed every few days.

Light and temperature were controlled in the experimental rooms. A 15-h light and 9-h dark photoperiod, a phase that is much the same as that in the field (light-on at 0500 and light-off at 2000), was employed. Temperature was held constant at 23 ± 1°C. Under this light condition, larval release by females occurs about the time of nocturnal high tides in the field.

Preparation of hatch water

Eggs of *S. haematocheir* are dark brown at the early stages of embryonic development, but become a brownish green (possibly because of yolk consumption) as hatching approaches. Females carrying brownish-green eggs (*i.e.*, embryos that should hatch within a few days) were selected, removed from the plastic containers, and placed individually in glass or plastic beakers (8.5 cm in diameter, 12 cm in height) containing 30 ml of 10‰ seawater. This medium is prepared from natural seawater, which is boiled for 5–10 min, cooled, and then diluted with distilled water; the solution is aerated for at least one day before use. The medium was renewed at intervals of 1–2 days. Under these conditions, all of the females continued to carry eggs until hatching (Table I, top).

Hatching of *S. haematocheir* is highly synchronized; all of the embryos may hatch within about 5–30 min in the laboratory (*e.g.*, see Saigusa, 1993). When hatching was completed, and the female had released all of her larvae into the medium by vigorous abdominal fanning, she was removed, and the medium was filtered through nylon mesh or filter paper (*filtrate 1* in Fig. 1) which removed the zoeas. As shown in Table I, 23 samples of *filtrate 1* were prepared immediately after the larval release

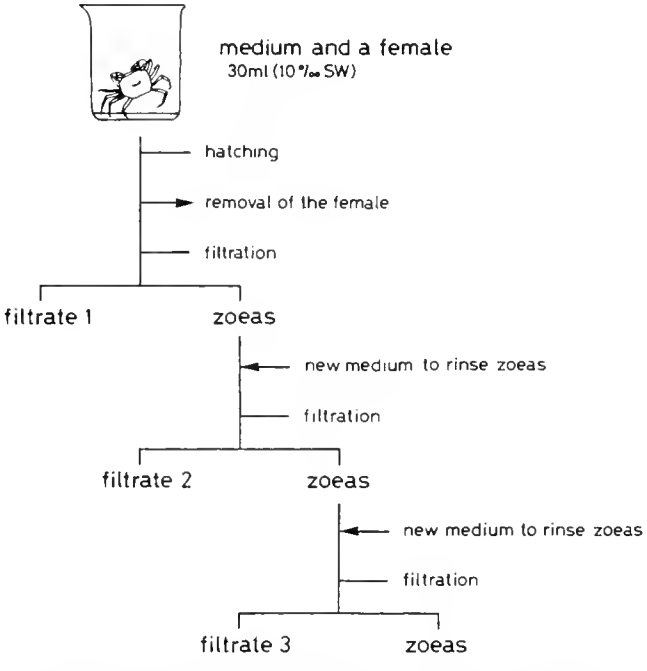

Figure 1. Collection of hatch water. Each medium contained 30 ml of 10‰ seawater. See the text for details.

(*i.e.*, within 30 min); the rest (22 samples) were prepared after a while (*i.e.*, more than 30 min after the release, but before 10:00 on the next morning following release).

The filtered zoeas were immediately immersed in new medium, and this medium was also filtered (*filtrate 2*). Among *filtrate 2*, nine samples were generated immediately after the preparation of *filtrate 1*, and then the zoeas were rinsed and filtered once more (*filtrate 3*) (Fig. 1). The rest of *filtrate 2* (32 samples) was generated within a few hours after the preparation of *filtrate 1*. Because larval release occurs at night, these procedures were usually carried out under illumination provided by a small hand-held light.

Assay of the activity of incubation-disrupting substance

Ovigerous females, that had not been used to collect the hatch water, were selected randomly from the stock containers and placed individually in beakers containing hatch water (*filtrates 1, 2,* or *3*). The activity of incubation-disrupting substance in each filtrate was evaluated in terms of the following three grades: (+), a portion of the egg mass protrudes from the brooding space; (++), the egg-mass protrusion progresses further, and some embryos are scattered at the bottom of the beaker; (+++), all, or almost all, of the egg mass has slipped out of the brooding space. Observations were finished 4 or 5 days after the female had been placed in each beaker. To prevent contamination of the medium by feces and foods, the females were not fed during the experiment. With time, however, they often ate their own embryos, either those released in the beaker or those squeezed out of the brooding chamber. But females never eat their embryos in normal brooding. For these reasons, the effect of test solutions was judged within 4–5 days.

Observations with a scanning electron microscope

Embryos attached to the pleopod setae, as well as those released in the hatch water, were collected and fixed with 5% formalin in distilled water for 2 or 3 days. They were then washed a few times in 50% ethanol, then dehydrated through a graded series of ethanol concentrations and dried in a critical point apparatus (Hitachi HCP-1). The samples were mounted on metallic stubs with a piece of double-sided stick tape, plated with gold, and observed with a scanning electron microscope (JEOL JSM-T300).

Boiling and freezing of the test samples

A sample of *filtrate 1*, obtained from 15 females that had just released their larvae, was boiled for 5 min. After it had cooled, the solution was divided among 15 beakers (30 ml each), and an incubating female was put into each.

Another sample of hatch water (*filtrate 1*), obtained similarly from seven specimens, was frozen at −80°C for 8 days, and then thawed at room temperature. This sample was divided among seven beakers, and an ovigerous female was again placed in each.

Results

Egg attachment to pleopod setae

A female of *Sesarma haematocheir* has four pairs of abdominal appendages, each of which bears one plumose and one non-plumose seta (Fig. 2A). Many fine hairs (*ovigerous hairs*) are arranged in whorls along the non-plumose seta (Fig. 2B). Fertilized eggs are attached to these hairs by a *funiculus* (Fig. 2C, D). When the ovigerous hair was removed with fine forceps, the *coat* that had been wrapped around the hair was broken but remained attached to several funiculi (Fig. 2E). This observation suggests that the investment coat is formed of the same material as the funiculus (Fig. 2E, F). The morphological features shown in Figure 2D, E, and F suggest that this material also constitutes the outer egg membrane, or at least covers the surface of this membrane.

Protrusion and dropping of egg masses from an incubating female

As shown in Figure 3A, an incubating female carries her clutch in the brooding space between the thorax and the flexed abdomen. Premature embryos never slipped out of the brooding space when the females were in 10‰ seawater, and hatching occurred in all cases (Table I). At the completion of hatching, these females released the hatched larvae into the medium with vigorous fanning movements of the abdomen.

Soon after ovigerous females were placed in hatch water, a mass of premature embryos protruded from the brooding chamber, and then dropped into the beaker. This process is shown in Figure 3B–E′. Figure 3B shows a portion of the incubating egg mass starting to protrude from the brooding space (+). In Figure 3C and D, the embryo-protrusion has proceeded further (++). These premature embryos were often released by the females in association with abdominal fanning behavior and were scattered at the bottom of the beaker. In Figures 3E and 3E′, the embryos have all (or almost all) dropped from the brooding chamber (+++). A remarkable feature of this phenomenon is that, from the beginning of embryo-protrusion to the time that all of the egg masses have slipped out of the female takes only a few days. As shown in Table I, 37 of 45 females (82%) treated with hatch water (*filtrate 1*) released their egg masses into the beaker. Clearly, the active substance that disrupts incubation is contained in hatch water.

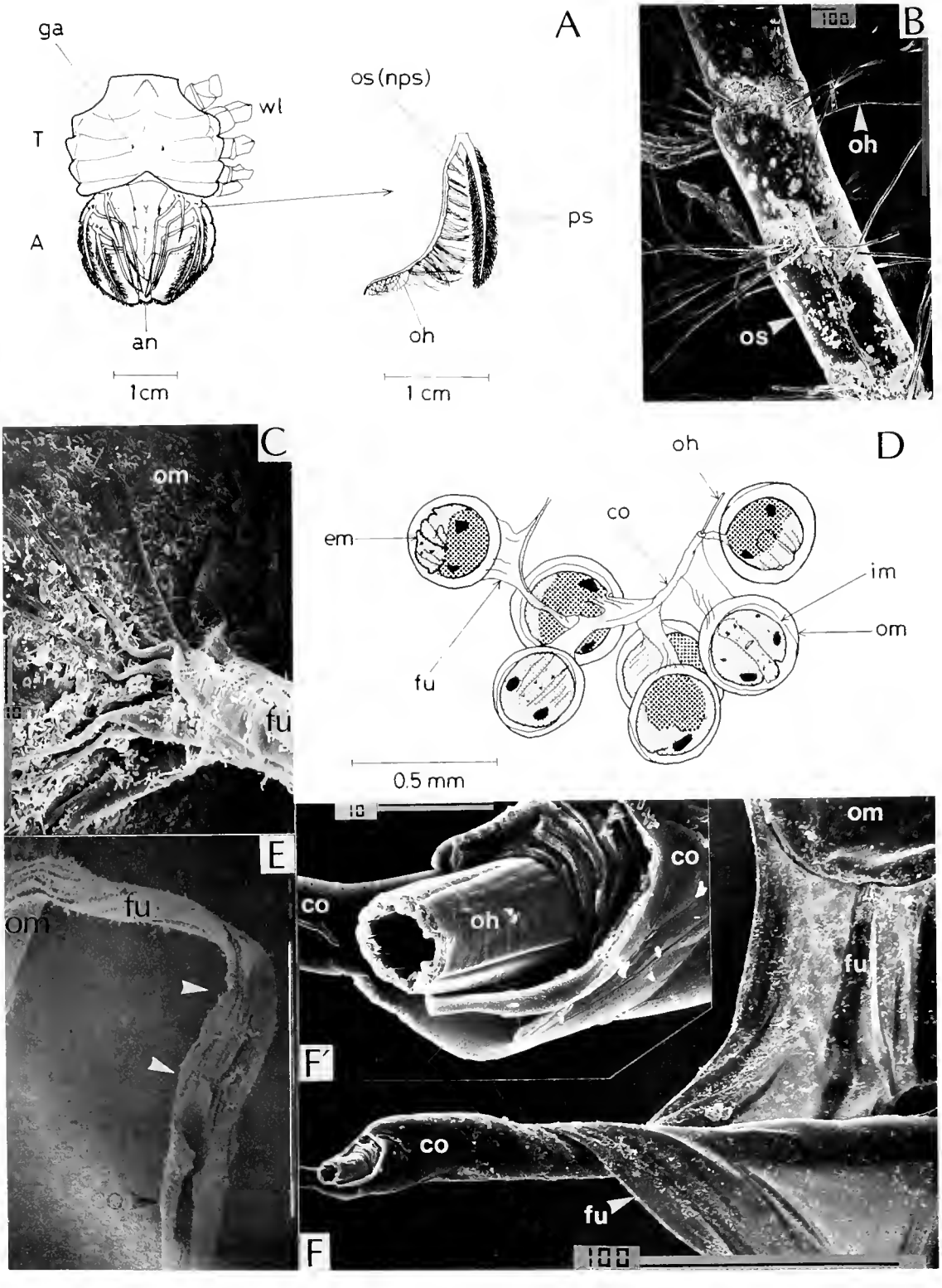

Figure 2. The pleopod setae and attachment of eggs. (A—left) Thorax (T) and abdomen (A) of a *Sesarma haematocheir* female. wl: walking leg; an: anus; ga: genital aperture. (A—right) The second abdominal appendage showing plumose and non-plumose setae. ps: plumose seta; os(nps): non-plumose seta; oh: ovigerous hair. (B) Ovigerous hairs on the non-plumose seta. Scale = 100 μm. (C) The outer egg membrane (om) and funiculus (fu). Scale = 10 μm. (D) Embryos attached to an ovigerous hair by funiculus. This specimen was fixed with 5% formalin and observed in 50% ethanol. em: embryo; fu: funiculus; co: the coat investing an ovigerous hair; oh: ovigerous hair; im: inner (or lining) membrane; om: outer thick membrane. In living

The activity of any sample of hatch water (*filtrate 1*) seems to vary with the number of zoea-larvae released into the medium. When the hatch water was derived from medium into which a large number of zoea had been released, almost all of the females dropped their embryos within 1 day after contact. But hatch water prepared from a medium containing only a small number of larvae, induced this phenomenon 1–3 days later.

Four females, though treated with hatch water (*filtrate 1*), showed no sign of egg mass protrusion (Table I). This negative result, however, could have been due to an insufficient concentration of active substance. When the unresponsive females were isolated after the experiment in a new, unoccupied container, they finally dropped their egg masses some days later (unpub. obs.). In four other females (Table I), normal hatching and larval release occurred before egg mass protrusion could begin. Presumably, these ovigerous females had been collected just prior to hatching, which simply occurred on schedule, uninfluenced by the incubation-disrupting substance reported here.

The 15 samples of boiled hatch water had no effect on incubation: no egg masses protruded from the abdomen (Table I), so the incubation of the test females was clearly maintained. In contrast, the egg masses protruded and dropped as usual when seven females were exposed to hatch water that had been frozen and thawed (Table I). Incubation-disrupting substance is thus stable to freezing, but is heat-labile.

To determine whether the active substance is released in association with larval hatching or is generated by the larvae after the release, the effects of *filtrates 2* and *3* were compared with that of *filtrate 1* (Table I). The activity was markedly decreased in *filtrate 2*, and no effect was detected in *filtrate 3*. Because *filtrate 1* contains most of the incubation-disrupting activity, I speculate that the responsible factor is all released to the medium when the egg membrane opens at the time of hatching.

Microscopic observations of the egg masses liberated prematurely from the female

Clusters of embryos shed into the incubation medium were observed under a stereomicroscope (Fig. 4A). The surface of the embryos (*i.e.*, outer egg membrane) and the funiculus were not different morphologically from the eggs attached to intact females. The embryos were obviously alive (Fig. 4A), and the funiculus remained attached to the coat investing each ovigerous hair. But a clear difference was observed *in the coat* investing ovigerous hairs. Egg masses incubated by untreated females were attached tightly to the ovigerous hairs (Fig. 2F and F′), whereas those dropped in hatch water always lacked an ovigerous hair in the twig of the investment coat (Fig. 4B). Premature embryo release is thus due to the investment coat separating from the ovigerous hairs, and not the funiculus detaching from the coat.

When hatch-water-induced protrusion of egg masses was in progress (+ or ++; Fig. 5A), groups of embryos would easily slip off the ovigerous hairs when gently pulled with a fine forceps (Fig. 5B). These embryos were always accompanied by the funiculus and coat. In contrast, when the egg mass of a control female was pulled, the ovigerous hairs were broken away from the seta (not shown).

Discussion

The embryos of most decapod crustaceans are incubated by the females until hatching occurs. So it may be natural that a portion of the egg cluster is lost from the female during embryonic development. For example, some embryos may be dropped when the female cleans the clutch using her chelae. Laboratory-maintained females of the lobsters *Homarus americanus* and *H. gammarus* often lose a large percentage of embryos because the funiculus has been improperly formed (Talbot and Harper, 1984). In *Sesarma haematocheir*, predation on egg masses by the maggots of a parasitic fly can be the main extrinsic factor for the loss of embryos in the field (unpub. obs.). But the phenomenon reported in the present study is quite different from such types of egg loss.

Disruption of incubation is certainly an unusual phenomenon for ovigerous females; but this phenomenon is obviously adaptive for females that have released their larvae. Observations of the female abdomen just after larval release (Saigusa, 1992, 1993) demonstrated that the broken egg case (outer egg membrane), funiculus, and the coat still remain attached to the ovigerous hairs (see also Fig. 6A). A similar event occurs in the lobsters *H. americanus* and *H. gammarus;* egg cases and stalks remain attached on the ovigerous hairs, and they seem to be cast

Figure 2. (*Continued*) specimens, the embryo completely fills, and is pressed against the egg case, but in the fixed samples, the outer membrane swells, revealing an inner membrane or a membrane lining the egg case (for egg membranes, see Saigusa, 1992). (E) The coat from which an ovigerous hair was removed with a fine forceps. White arrow heads show the region where the funiculus (fu) branches out of the investment coat. Scale = 100 μm. (F) The coat wrapping an ovigerous hair. Scale = 100 μm. Upper left (F′): Magnification of the portion where this hair penetrates the coat. Scale = 10 μm.

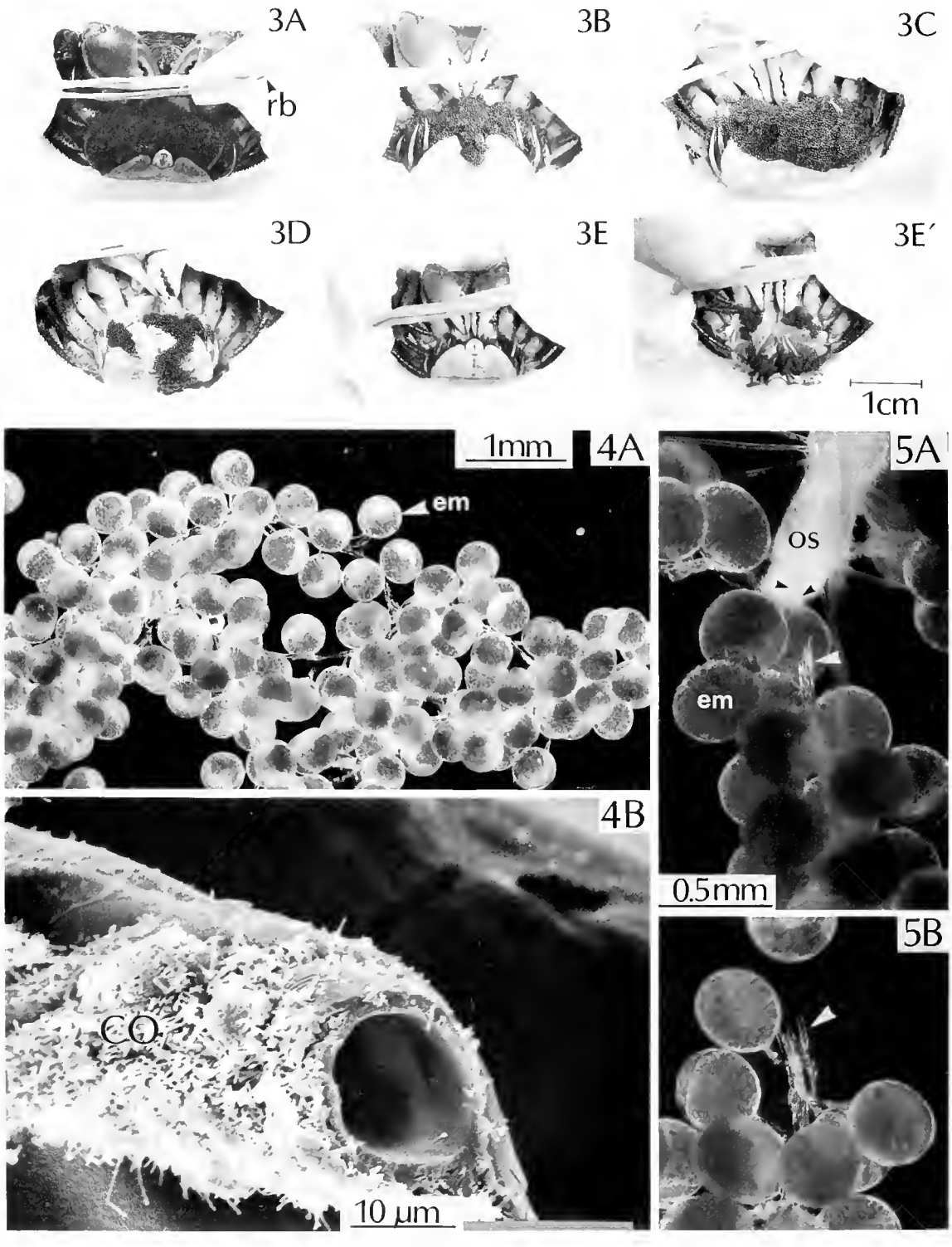

Figure 3. Premature egg-release from a female. (A) A normal clutch incubated by a female. rb: a rubber band to fix the female's body and legs. (B) A female in which egg-release from the brooding chamber is beginning (+). (C and D) Females in which protrusion of egg mass has proceeded further (++). (E) A female from which almost all eggs were released (+++). (E′) The inside of the brooding chamber in this female. Although some eggs still remained in the chamber, they have already been detached from the ovigerous hairs.

Figure 4. Morphology of premature eggs liberated from the female. (A) Embryos (em) extruded from the brooding chamber and dropped to the bottom of the beaker. These embryos (at early developmental stage) are all alive. The coats that invested the ovigerous hairs are seen to be in place. (B) An ovigerous hair is absent from its investment coat (co). An ovigerous hair itself is also hollow, but its appearance is clearly different from that of the coat (compare with Fig. 2F′).

Table I

Liberation of premature embryos induced by the hatch water

Medium	Number	Activity of filtrate (+)	(++)	(+++)	Maintenance of incubation	Hatching and larval release
Fresh medium (10‰ SW)	82	0	0	0	(0)	82
Filtrate 1						
Generated within 30 min after hatching	23	0	0	21	1	1
Generated more than 30 min after hatching	22	0	0	16	3	3
Boiling	15	0	0	0	14	1
Freezing and thawing	7	1	0	6	0	0
Filtrate 2						
Generated within 1 h after hatching	9	0	0	0	8	1
Generated for 3–10 h after hatching	32	1	0	2	23	6
Filtrate 3						
Generated within 1 h after hatching	9	0	0	0	9	0

off from the ovigerous hairs at the next molt (Goudeau *et al.*, 1987).

In contrast to the lobster, the remnants on the ovigerous hairs of *S. haematocheir* completely disappear during the night of the larval release, and the next clutch is produced within a few days. After larval release is complete, females unfold their abdomen and pluck the empty egg cases and funiculi to eat; indeed, some of the remnants are probably disposed of in this way. But it is not conceivable that a purely mechanical plucking behavior can completely clear ovigerous hairs and setae. I conclude that the incubation-disrupting substance, as reported in this paper, causes the investment coat to slip off the ovigerous hair, facilitating post-release remnant-eating of the female, and releasing the remnants that are not eaten. Because the ovigerous hairs completely clean off by the morning following larval release (compare Fig. 6A and B), incubation-disrupting substance may also make it easier for the female crab to get the debris off her ovigerous hairs *without damaging or breaking the hairs* which, after all, must be in good condition to receive the new clutch of eggs. In brief, the incubation-disrupting substance clears the ovigerous hairs for the next clutch of eggs.

What mechanisms cause the investment coat to slip from ovigerous hairs? The exact mechanisms of egg attachment to the ovigerous hairs and the source of the attachment stalk have been controversial for a number of years (Yonge, 1937, 1946, 1955; Cheung, 1966; Fisher and Clark, 1983). Goudeau and Lachaise (1983) showed that the funiculus of the American lobster *Homarus* folds around an ovigerous hair, forming several turns, and that for the innermost coiling turn, the stalk wall adheres tightly to the hair surface, although no adhesive substance is detectable. In *S. haematocheir,* the funiculus extends to the coat wrapping an ovigerous hair, which suggests that the same material forms both the stalk and the coat (Fig. 2E, F). Furthermore, this material might make up the outer egg membrane (at least the surface of the membrane), as well (Fig. 2C). Because the coat dropped from the female shows no obvious morphological changes (Figs. 4A, B), then the egg masses must be liberated, either by a deformation of the ovigerous hairs or by a separation of the coat in some unknown way from the hairs. But the deformation of the ovigerous hairs must be detrimental to the hairs because a new clutch has to be attached to them.

Embryos of the estuarine crab *Rhithropanopeus harrisii* can be detached by bovine or porcine trypsin, and are released into the medium by the pumping movements of the females. Some of them prematurely hatched as im-

Figure 5. Detachment of the egg masses from the ovigerous hairs (living specimen). (A) Two ovigerous hairs (see the black arrow heads) and the investing coat that begins to slip out of these hairs. A white arrow head indicates the edge of the investment coat. em: embryo; os: ovigerous seta. (B) The end (a white arrow head) of a section of coat that had slipped off its enclosed ovigerous hairs.

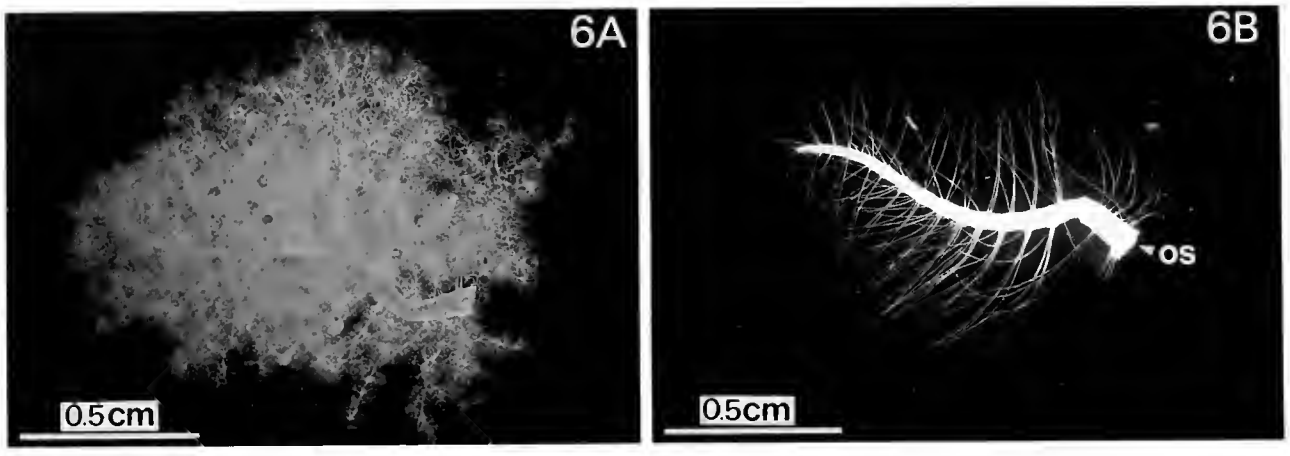

Figure 6. Ovigerous hairs are completely cleaned off by the morning after larval release. (A) An ovigerous seta just after larval release. The empty egg cases, funiculi, and investing coats are still attached to the ovigerous hairs. (B) An ovigerous seta (os) on the next morning (about 10 h) after the larval release.

mobile larvae (Rittschof *et al.*, 1990). In *S. haematocheir*, ovigerous females treated with hatch water certainly liberated premature embryos (Fig. 3B–E'); but in no case was the funiculus dissolved and detached from the investment coat (see Fig. 4A). As shown in Figures 4B, 5A, and 5B, the *coat* did slip off the ovigerous hairs. So what is liberated from *S. haematocheir* females is *masses* of premature embryos, and no individual free embryos.

The next question concerns the other functions of the incubation-disrupting substance. Because this factor is released from the egg case at the time of hatching, the factor must also be more directly involved in hatching. Recently, De Vries and Forward (1991) indicated that a proteolytic activity is released outside of the egg membrane in association with the hatching of estuarine crabs; the assay was based on the proteolysis of casein. But how, exactly, such an enzyme contributes to hatching remains obscure. As shown in Figures 4A, 5A, and 5B, the incubation-disrupting substance dissolved neither the outer egg membrane nor the funiculi. Neither was the investment coat itself dissolved (Fig. 4B). But these negative results might have been due to the relatively coarse scanning microscopy of the egg membrane. In any event, the possibility that the incubation-disrupting substance also functions as a hatching enzyme remains to be explored.

Acknowledgments

This study followed from stimulative discussions with Drs. Masamichi Yamamoto and Hiroko Shirai at Ushimado Marine Biological Laboratory, Okayama University. Dr. Yamamoto kindly helped me with the SEM. The early manuscript was read and edited by Dr. Hiroko Shirai and by Dr. Katsuhiko Endo, Faculty of Science, Yamaguchi University.

Literature Cited

Carroll, E. J., Jr., and J. L. Hedrick. 1974. Hatching in the toad *Xenopus laevis* morphological events and evidence for a hatching enzyme. *Dev. Biol.* **38:** 1–13.

Cheung, T. S. 1966. The development of egg-membranes and egg attachment in the shore crab, *Carcinus maenas*, and some related decapods. *J. Mar. Biol. Assoc. U.K.* **46:** 373–400.

Clare, A. S., G. Walker, D. L. Holland, and D. J. Crisp. 1982. Barnacle egg hatching: a novel role for a prostaglandin-like compound. *Mar. Biol. Lett.* **3:** 113–120.

Clegg, J. S. 1962. Free glycerol in dormant cysts of the brine shrimp *Artemia salina*, and its disappearance during development. *Biol. Bull.* **123:** 295–301.

Clegg, J. S. 1964. The control of emergence and metabolism by external osmotic pressure and the role of free glycerol in developing cysts of *Artemia salina*. *J. Exp. Biol.* **41:** 879–892.

Crisp, D. J., and C. P. Spencer. 1958. The control of the hatching process in barnacles. *Proc. Roy. Soc. Lond. B* **148:** 278–299.

De Vries, M. C., and R. B. Forward, Jr. 1991. Mechanisms of crustacean egg hatching: evidence for enzyme release by crab embryos. *Mar. Biol.* **110:** 281–291.

Fisher, W. S., and W. H. Clark, Jr. 1983. Eggs of *Palaemon macrodactylus* I. Attachment to the pleopods and formation of the outer investment coat. *Biol. Bull.* **164:** 189–200.

Goudeau, M., and F. Lachaise. 1983. Structure of the egg funiculus and deposition of embryonic envelopes in a crab. *Tissue & Cell* **15:** 47–62.

Goudeau, M., P. Talbot, and R. Harper. 1987. Mechanism of egg attachment stalk formation in the lobster, *Homarus*. *Gamete Res.* **18:** 279–289.

Herrick, F. H. 1895. The American lobster—a study of its habits and development. *Bulletin of the United States Fish Commission* **1895:** 1–252 plus 54 plate pages.

Ishida, J. 1944. Hatching enzyme in the fresh-water fish, *Oryzias latipes*. *Annot. Zool. Jpn.* **22:** 137–154.

Katagiri, C. 1975. Properties of the hatching enzyme from frog embryos. *J. Exp. Zool.* **193:** 109–118.

Lapage, T., and C. Gache. 1989. Purification and characterization of the sea urchin embryo hatching enzyme. *J. Biol. Chem.* **264:** 4787–4793.

Rittschof, D., R. B. Forward, Jr., and B. W. Erickson. 1990. Larval release in brachyuran crustaceans—functional similarity of peptide pheromone receptor and catalytic site of trypsin. *J. Chem. Ecol.* **16:** 1359–1370.

Saigusa, M. 1982. Larval release rhythm coinciding with solar day and tidal cycles in the terrestrial crab *Sesarma*. *Biol. Bull.* **162:** 371–386.

Saigusa, M. 1992. Observations on egg hatching in the estuarine crab *Sesarma haematocheir*. *Pac. Sci.* **46:** 484–494.

Saigusa, M. 1993. Control of hatching in an estuarine terrestrial crab. II. Exchange of a cluster of embryos between two females. *Biol. Bull.* **184:** 186–202.

Talbot, P., and R. Harper. 1984. Abnormal egg stalk morphology is correlated with clutch attrition in laboratory-maintained lobsters (*Homarus*). *Biol. Bull.* **166:** 349–356.

Yamagami, K. 1972. Isolation of a choriolytic enzyme (hatching enzyme) of the teleost, *Oryzias latipes*. *Dev. Biol.* **29:** 343–348.

Yasumasu, S., I. Iuchi, and K. Yamagami. 1989a. Purification and partial characterization of high choriolytic enzyme (HCE), a component of the hatching enzyme of the teleost, *Oryzias latipes*. *J. Biochem.* **105:** 204–211.

Yasumasu, S., I. Iuchi, and K. Yamagami. 1989b. Isolation and some properties of low choriolytic enzyme (LCE), a component of the hatching enzyme of the teleost, *Oryzias latipes*. *J. Biochem.* **105:** 212–218.

Yonge, C. M. 1937. The nature and significance of the membranes surrounding the developing eggs of *Homarus vulgaris* and other Decapoda. *Proc. Zool. Soc. Lond. A* **107:** 499–517 plus 1 plate page.

Yonge, C. M. 1946. Permeability and properties of the membranes surrounding the developing egg of *Homarus vulgaris*. *J. Mar. Biol. Assoc. U.K.* **26:** 432–438.

Yonge, C. M. 1955. Egg attachment in *Crangon vulgaris* and other Caridea. *Proc. Roy. Soc. Edin. B* **65:** 369–400.

Reference: *Biol. Bull.* **186:** 90–100. (February, 1994)

Ingestion of Ultraplankton by the Planktonic Larvae of the Crown-of-Thorns Starfish, *Acanthaster planci*

TENSHI AYUKAI

Australian Institute of Marine Science, PMB No. 3., Townsville M.C., Queensland 4810, Australia

Abstract. There has been a debate over whether the growth and development of the larvae of the crown-of-thorns starfish *Acanthaster planci* are severely food-limited. This debate has raised a range of questions, including the one relating to the role of heterotrophic bacteria in the nutrition of larvae. In this study, the feeding rate of larvae on bacteria as well as on other ultraplankton (<5 μm) was determined by counting the number of the fluorescence-labeled cells (FLC) in the gut after short incubation. Preliminary experiments showed no detrimental effect of the fluorescence dye (5-(4,6-dichlorotriazin-2-yl) aminofluorescein) on the development of larvae and demonstrated the usefulness of FLC in feeding experiments as food particles analogous to living cells of ultraplankton. There was no evidence that larvae ingested bacteria. Larvae did ingest two strains of photosynthetic cyanobacteria, which had equivalent spherical diameters (ESD) of 1 and 1.8 μm, but these tiny cells were cleared more than 10 times slower than the larger algae *Phaeodactylum tricornutum* (4.7 μm ESD) and *Dunaliella tertiolecta* (5.1 μm ESD). Regardless of the size of FLC used, the clearance rate (volume of water cleared per animal per unit time) increased by 50–120%, as larvae developed from the late bipinnaria stage to the late brachiolaria stage. These results show that larvae may derive a sizable proportion of their nutrition from ultraplankton, but not from bacteria.

Introduction

Heterotrophic bacteria make up a large, metabolically active component of plankton assemblages in the sea (*e.g.*, Pomeroy, 1974; Azam *et al.*, 1983). Bacterial biomass is usually equal to 10–40% of phytoplankton biomass (*cf.* Ducklow, 1983), but can be greater than phytoplankton biomass in oligotrophic waters (Fuhrman *et al.*, 1989; Cho and Azam, 1990). Furthermore, the proportion of ultraplankton (<5 μm, Murphy and Haugen, 1985) in phytoplankton assemblages reaches more than 50% in a wide range of environments (*cf.* Stockner, 1988). Use of these predominant, small particles as a food source is thought to be enormously advantageous for planktonic larvae surviving under nutrient-impoverished conditions, but their actual use by asteroid larvae has been a matter of controversy over the past decade. Specifically, bacteria were ingested by antarctic asteroid larvae (Rivkin *et al.*, 1986; Pearse *et al.*, 1991), but not by temperate ones (Pearse *et al.*, 1991).

The crown-of-thorns starfish (COTS) *Acanthaster planci* is unique in tropical and subtropical waters. Gut content analysis with a scanning electron microscope (SEM) has shown that the natural diet of COTS larvae almost exclusively comprises relatively rare, large phytoplankton, such as dinoflagellates and pennate diatoms of up to 200 μm in length (P. Dixon, unpub.). Dixon's results have supported the idea that, except during occasional phytoplankton blooms, the availability of the preferred phytoplankton to COTS larvae is very low and therefore the growth and development of COTS larvae are food-limited (Lucas, 1982). In contrast, experiments in which COTS larvae were reared in *in situ* chambers showed no evidence of food limitation under the low phytoplankton conditions common in tropical waters (Olson, 1985, 1987). Results from the rearing studies have been interpreted as indirect evidence that COTS larvae can exploit non-phytoplankton food, including bacteria and dissolved organic matter (Olson and Olson, 1989; Birkeland and Lucas, 1990).

Bacteria were not positively identified in the gut contents of COTS larvae (Dixon, unpub.). However, this may be due to the difficulty in finding bacteria in various food

Received 28 December 1992; accepted 3 September 1993.

remains or the loss of bacteria during a number of processes involved in the SEM sample preparation. Sherr *et al.* (1987) determined the feeding rate of heterotrophic nanoflagellates on bacteria by directly counting the number of heat-killed, DTAF (5-(4,6-dichlorotriazin-2-yl) aminofluorescein)-labeled cells in food vacuoles. The yellow-green fluorescence of DTAF-labeled cells is distinctive and intense, so that this technique has also been used to study the feeding of larger protozoans and rotifers (Rublee and Gallegos, 1989).

The first objective of this study was to test the feasibility of the fluorescence-labeled cell (FLC) technique for determining the feeding rate of COTS larvae on ultraplankton. The possibility of differences in chemical properties between living and heat-killed cells (Paffenhofer and Van Sant, 1985) made it particularly important to examine whether COTS larvae ingest FLC at similar rates to living cells. The second objective was to use the FLC technique to determine the feeding rate of COTS larvae on bacteria and other ultraplankton.

Materials and Methods

COTS larvae were grown in the mass rearing facility at the Australian Institute of Marine Science, using mixtures of three cultured phytoplankton, *Dunaliella primolecta, D. tertiolecta,* and *Phaeodactylum tricornutum.* Because larvae in the tanks were at different developmental stages (the distinction criteria described by Lucas, 1982), about 600–800 larvae were individually sorted from the mass-reared populations, placed in 250-ml bottles (<150 larvae per bottle) filled to the top with filtered seawater, and held without food. After 24 h, only actively swimming larvae in the top quarter of each bottle were removed and used for experiments. This procedure was designed to reduce the chance of using physiologically retarded larvae. Seawater used in experiments was obtained at the rearing facility and filtered through 0.45-μm Millipore filters just before use. Experiments were run at 28°C under dim light.

FLC preparation

Six types of FLC were prepared: three cultured algal species (*P. tricornutum, D. tertiolecta,* and *Tetraselmis* sp); two cultured cyanobacteria species (Strain ACMM326, the culture collection of the Sir George Fisher Centre, James Cook University of North Queensland, and an unidentified strain); and natural bacteria. These cells were heat-killed and stained with the fluorochrome DTAF (Sigma #D2281). Methods were as described by Sherr *et al.* (1987), except for minor modifications to the speed and duration of centrifugation of algal suspensions (1500 rpm for 10 min for *P. tricornutum* and *D. tertiolecta,* 800 rpm for 10 min for *Tetraselmis* sp., 6000 rpm for 15 min for cyanobacteria) and addition of a pre-wash with a 1.5% NaCl solution before incubation in a DTAF solution.

Toxicity of FLC

To test the toxicity of FLC, larvae were allowed to feed on fluorescence-labeled *P. tricornutum* for 2 days and their survival and development were examined. At the beginning, 50 larvae at the early brachiolaria stage were introduced into each of ten 100-ml bottles (five bottles per treatment) filled to the top with a labeled or a living (as control) cell suspension at about 1000 cells ml^{-1}. These bottles were placed on a cell shaker (30 shakes min^{-1}) to keep cells in suspension and incubated at 28°C under an 8 h light-16 h dark cycle.

Gut filling rate

Two conditions must be fulfilled for the FLC method to provide reliable feeding rate estimates: the feeding rate must be constant and the incubation must be short enough that no defecation occurs. Then, providing that the change in FLC concentration during incubations is negligible, the clearance rate (volume of water cleared per animal per unit time) can be calculated by dividing the gut filling rate (cells per animal per unit time) by the FLC concentration.

To ensure these conditions were met, the gut filling rate was determined by measuring the number of FLC in the gut over time. After 24 h starvation, 15 larvae at the early brachiolaria stage were introduced into each of 21 scintillation vials (3 vials per treatment) with 20 ml of filtered seawater, and 200 μl of a labeled *P. tricornutum* suspension was added (the final concentration was 806 cells ml^{-1}). After 2- to 30-min incubations, 1 ml of a 10% buffered glutaraldehyde solution was added to the vials. Preserved samples were then refrigerated for later FLC counting. DTAF fluorescence did not fade out during several weeks of cool storage.

Preserved larvae were examined under a Zeiss epifluorescence microscope equipped with a blue excitation filter set (#487909). Before counting, preserved larvae were poured into plastic tubing with a 80-μm-mesh screen at one end and gently washed with filtered seawater. A small amount of water with larvae was then filtered onto 0.45-μm Millipore filters stained with Irgalan black. After excess seawater was removed, filters with larvae were mounted on glass slides, using a Zeiss immersion oil (#58884). The number of FLC in the gut was counted for 10 larvae in each vial.

Discrimination between FLC and living cells

In this experiment, larvae at the late bipinnaria and early and late brachiolaria stages were allowed to feed on

Table I

Size of algal and bacterial cells used for feeding experiments

Type	L (μm)	ESD (μm)
Phaeodactylum tricornutum	23.9	4.7
Dunaliella tertiolecta	5.6	5.1
Tetraselmis sp.	27.5	17.2
Cyanobacteria, ACMM326	2.2	1.8
Cyanobacteria—small strain	1.0	1.0
Natural bacteria	0.2–0.8	—

L: Length of long axis, ESD: equivalent spherical diameter.

mixtures of FLC and living cells of the algae *P. tricornutum*, *D. tertiolecta*, and *Tetraselmis* sp. and two species of cultured cyanobacteria at various proportions for 5–10 min. FLC and living cells in the gut were counted immediately after experiments, because the autofluorescence of living cells faded rapidly when stored.

Feeding rate

FLC uptake was determined for larvae at the late bipinnaria and early and late brachiolaria stages. Fifteen larvae were introduced into each experimental vial with 20 ml of filtered seawater. After about 2 h, 80–2000 μl of FLC suspension was added to each vial. As described below, larvae ingested FLC selectively over living cells of *Tetraselmis* sp. Therefore, *Tetraselmis* sp. was no longer used in this series of experiments. The concentration range of FLC was 0.55–5.37 $\times 10^3$ cells ml^{-1} for *P. tricornutum*, 0.12–7.46 $\times 10^3$ cells ml^{-1} for *D. tertiolecta*, 0.31–1.27 $\times 10^4$ cells ml^{-1} for cyanobacteria ACMM326, 0.43–10.90 $\times 10^4$ cells ml^{-1} for unidentified cyanobacteria, and 0.78–3.92 $\times 10^5$ cells ml^{-1} for natural bacteria. As shown in Table I, the equivalent spherical diameter (ESD) ranged between 1 and about 5 μm. The duration of incubation was chosen between 3 and 10 min., depending on the type and concentration of FLC. Samples obtained were preserved and processed as described in the measurements of gut filling rates.

Results

Toxicity of FLC

No larvae died during 2-day incubations in either FLC or control treatment, although a few deformed larvae were observed. All larvae observed under an epifluorescence microscope had living cells or FLC of *P. tricornutum* in the gut. In the FLC treatment, the gut walls of larvae were stained with DTAF, indicating that larvae had assimilated DTAF-labeled cell protein.

Gut filling rate

The number of labeled *P. tricornutum* cells in the gut increased linearly with time and did not level off within 20 min (=0.33 h) (Fig. 1). The clearance rate calculated for this time interval was 0.38 ml ind^{-1} h^{-1} (=[302 cells ind^{-1} h^{-1}]/[806 cells ml^{-1}]). The results of 25- and 30-min incubations are not shown because the number of cells in the gut exceeded 100 cells and FLC counting became difficult. Incubation time, although dependent on the type and concentration of FLC, should not exceed 20 min. Generally, 5-min incubations were long enough to determine the feeding rate of COTS larvae.

Discrimination between FLC and living cells

The proportion of FLC to living cells in the gut was plotted against that in experimental medium and a line representing the 1:1 ratio was drawn (Fig. 2). The points for *P. tricornutum*, *D. tertiolecta*, and two strains of cyanobacteria were around the 1:1 line, suggesting that larvae nonselectively ingested living and DTAF-labeled cells of these small algae. On the other hand, the points for *Tetraselmis* sp. deviated upward from the 1:1 line, suggesting selective ingestion of FLC over living cells. The difference between clearance rates of larvae on living cells and FLC was consistently highly significant for *Tetraselmis* sp. (Student's *t*-test, $P < 0.001$ or $P < 0.0001$), but not for other algae (Table II).

Feeding rate

Labeled bacteria were ingested very occasionally by larvae of all three developmental stages examined. Bacteria observed in the gut were usually clumped together and often seen attached to flocculent material. A small

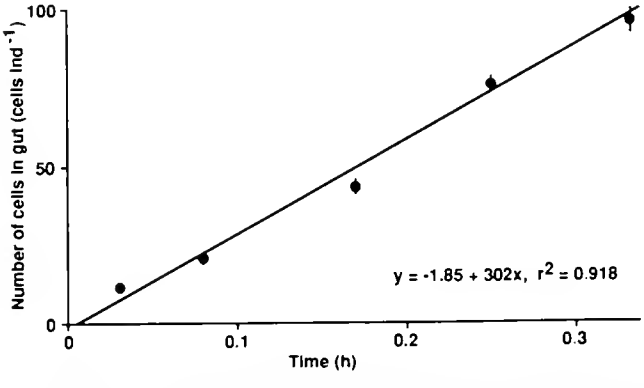

Figure 1. Time-course of the increase in the cell number in the gut of early brachiolaria larvae of *Acanthaster planci* feeding on heat-killed, fluorescence-labeled cells of *Phaeodactylum tricornutum* at a concentration of 806 cells ml^{-1}.

amount of such clumped material was also seen in original FLC solutions. Thus larvae were probably ingesting clumped material rather than individual cells.

The rates of ingestion and clearance of all FLC except *Tetraselmis* sp. by larvae at the late bipinnaria and early and late brachiolaria stages are shown in Figures 3–5. In all experiments, the ingestion rate increased linearly with FLC concentration and there was no evidence of saturation of ingestion rates. The 95% confidence bands of the regression line, although not shown, covered the origin. Thus the clearance rate remained constant over the range of FLC concentrations tested.

The clearance rate of larvae increased by almost two orders of magnitude as the ESD of FLC increased from 1 to 5 μm (Fig. 6). The clearance rate also increased with larval age: from the late bipinnaria to the late brachiolaria stage, the rate increased by 120% for *P. tricornutum*, 80% for *D. tertiolecta*, 50% for the small cyanobacteria strain, and 70% for cyanobacteria ACMM326.

Discussion

Feasibility of the FLC technique

The FLC technique demonstrates both strengths and weaknesses when applied to the feeding of asteroid larvae. With larger food particles, the usefulness of the method is limited, as suggested by the selective ingestion of FLC over living cells of *Tetraselmis* sp. by COTS larvae. For ultraplankton-sized algae, however, this technique has an obvious advantage over the conventional cell counting method. Generally, the feeding rate of zooplankton is determined by measuring the change in cell concentration during incubations (Frost, 1972). This method, because of the low precision and accuracy of cell counting, is inadequate to detect small changes in cell concentration and thus cannot be used for determining the feeding rate of individuals. This problem is particularly serious for small-sized algae, making it impossible to determine the lower size limit of food particles with the cell counting method. DTAF fluorescence, on the other hand, is very intense and clearly visible even through the gut wall of COTS larvae (Fig. 7), leaving little chance for counting errors.

Although some conditions can interfere with the accuracy of FLC counts, these usually can be overcome or avoided. For example, FLC in the gut can densely overlay each other, depending on the orientation of body on filters. This problem can be solved simply by excluding such individuals from counting. Another potential problem, accumulation of FLC in the posterior part of the esophagus, did not become serious within the range of FLC concentrations in the present feeding rate measurements.

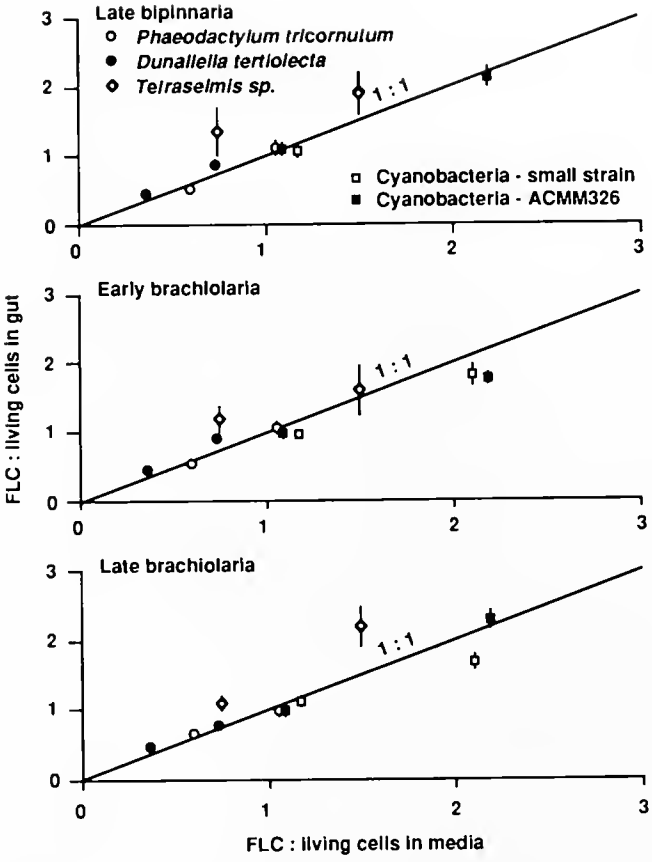

Figure 2. Comparison of the proportion of heat-killed, fluorescence-labeled cells to living cells between experimental media and the gut content of the larvae of *Acanthaster planci*.

Direct count of algal cells in the gut of echinoderm larvae is not new (Strathmann, 1971), but has been limited by the resolution of light microscopy. The use of an epifluorescence microscope in feeding studies promises more reliable data with less effort and time. The autofluorescence of algal cells, if samples are examined immediately after fixation, can be seen in the gut. DTAF-labeled cells produce bright yellow-green fluorescence at the broad blue excitation band (450–490 nm) of the Zeiss filter set used. The autofluorescence of two strains of phycoerythrin-rich cyanobacteria is orange-yellow and more or less similar to DTAF fluorescence. Nevertheless, the DTAF fluorescence can be distinguished easily from the autofluorescence of cyanobacteria, unless the gut becomes congested with cells.

Selective ingestion of FLC over living cells of *Tetraselmis* sp. by COTS larvae may be ascribed to the inefficient capturing of the motile cells of *Tetraselmis* sp. Alternatively, living cells of *Tetraselmis* sp. may release chemical compounds that COTS larvae do not favor. The possibility of such chemosensory feeding has been sug-

Table II

Two-sample t test for the difference between mean clearance rates of the larvae of Acanthaster planci *on living (C_{live}) and heat-killed, fluorescence-labeled cells (C_{FLC}) of five algae*

	C_{live} (ml ind^{-1} h^{-1})	C_{FLC} (ml ind^{-1} h^{-1})	C_{live} *vs.* C_{FLC}
Phaeodactylum tricornutum			
Late bipinnaria	2.64×10^{1} (0.09×10^{1})	2.30×10^{1} (0.11×10^{1})	>*
Early brachiolaria	2.91×10^{1} (0.08×10^{1})	2.52×10^{1} (0.11×10^{1})	>*
Late brachiolaria	3.23×10^{1} (0.11×10^{1})	3.28×10^{1} (0.16×10^{1})	<
Dunaliella tertiolecta			
Late bipinnaria	2.39×10^{1} (0.12×10^{1})	2.62×10^{1} (0.12×10^{1})	<
Early brachiolaria	2.45×10^{1} (0.11×10^{1})	3.03×10^{1} (0.13×10^{1})	<*
Late brachiolaria	2.90×10^{1} (0.08×10^{1})	3.11×10^{1} (0.13×10^{1})	<
Tetraselmis sp.			
Late bipinnaria	1.68×10^{1} (0.11×10^{1})	2.56×10^{1} (0.13×10^{1})	<***
Early brachiolaria	3.01×10^{1} (0.15×10^{1})	3.94×10^{1} (0.25×10^{1})	<**
Late brachiolaria	4.50×10^{1} (0.19×10^{1})	6.45×10^{1} (0.21×10^{1})	<***
Cyanobacteria—small strain			
Late bipinnaria†	5.87×10^{3} (0.51×10^{3})	5.76×10^{3} (0.27×10^{3})	>
Early brachiolaria	6.89×10^{3} (0.34×10^{3})	6.00×10^{3} (0.21×10^{3})	>
Late brachiolaria	7.26×10^{3} (0.29×10^{3})	5.92×10^{3} (0.24×10^{3})	>*
Cyanobacteria—ACMM326			
Late bipinnaria	1.35×10^{2} (0.05×10^{2})	1.31×10^{2} (0.06×10^{2})	>
Early brachiolaria	1.68×10^{2} (0.07×10^{2})	1.40×10^{2} (0.05×10^{2})	>*
Late brachiolaria	1.85×10^{2} (0.08×10^{2})	1.93×10^{2} (0.09×10^{2})	<

Numbers in parentheses are standard errors. The number of larvae for each mean value is 20, except for one case (†) where $n = 10$.
* $P < 0.01$, ** $P < 0.001$, *** $P < 0.0001$.

gested for other asteroid larvae, despite their simple feeding mechanism with a single band of cilia (Strathmann, 1971; Strathmann *et al.*, 1972). It is also known that asteroid larvae show very sophisticated feeding behaviors; *i.e.*, selective ingestion of the most abundant particles from time to time (Rassoulzadegan and Fenaux, 1979). Even if COTS larvae possess chemosensory organs, however, the chemical stimuli from ultraplankton-sized algae are seemingly too weak to elicit the selective feeding response of COTS larvae. Otherwise, COTS larvae would ingest living and heat-killed cells of *P. tricornutum*, *D. tertiolecta*, and two strains of cyanobacteria at different rates. Overall, the FLC technique seems very useful in determining the feeding rate of asteroid larvae on ultraplankton-sized food particles.

Ingestion of bacteria by COTS larvae

Fluorescence-labeled bacteria were not found in the gut of COTS larvae. One of the aspects that were not fully covered in this study is ingestion of bacteria attached on detritus. In reef waters, a large amount of detritus, such as coral mucus, benthic algal fragments, and fecal matter, is released into the water column. Dense colonies of bacteria are often observed on this detritus, particularly on coral mucus (*e.g.*, Ducklow and Mitchell, 1979; Rublee *et al.*, 1980). Up to 50% of bacteria are reported to be associated with detritus in reef waters (Sorokin, 1974; Moriarty, 1979). Attached bacteria are thought to account for 20–30% of the total bacterial biomass in other environments (Sorokin, 1981), although separation of free-living bacteria from attached bacteria by filters or mesh screens is problematic.

Strathmann *et al.* (1972) used high-speed cinematography to show that marine invertebrate larvae with a single band of cilia (including asteroid larvae) capture particles by reversing the beat of several cilia. Gilmour (1988) also reported that asteroid larvae capture particles by direct interception on their cilia. Results of both cinematographic studies indicate that the mechanical disturbance caused by very small particles like bacteria is not strong enough to trigger such ciliary action effectively.

The present observation that COTS larvae are not able to ingest bacteria agrees with results reported for the larvae of the temperate starfish *Asterina miniata* (Pearse *et al.*, 1991), but not for those of the antarctic starfish *Porania antarctica* (Rivkin *et al.*, 1986) and *Odontaster validus* (Pearse *et al.*, 1991). Rivkin *et al.* (1986) reported that the larvae of *P. antarctica* selectively ingested bacteria in bacteria-phytoplankton mixtures. Pearse *et al.* (1991) not only substantiated the results of Rivkin *et al.*, using the larvae of *O. validus*, but also reported that the larvae of

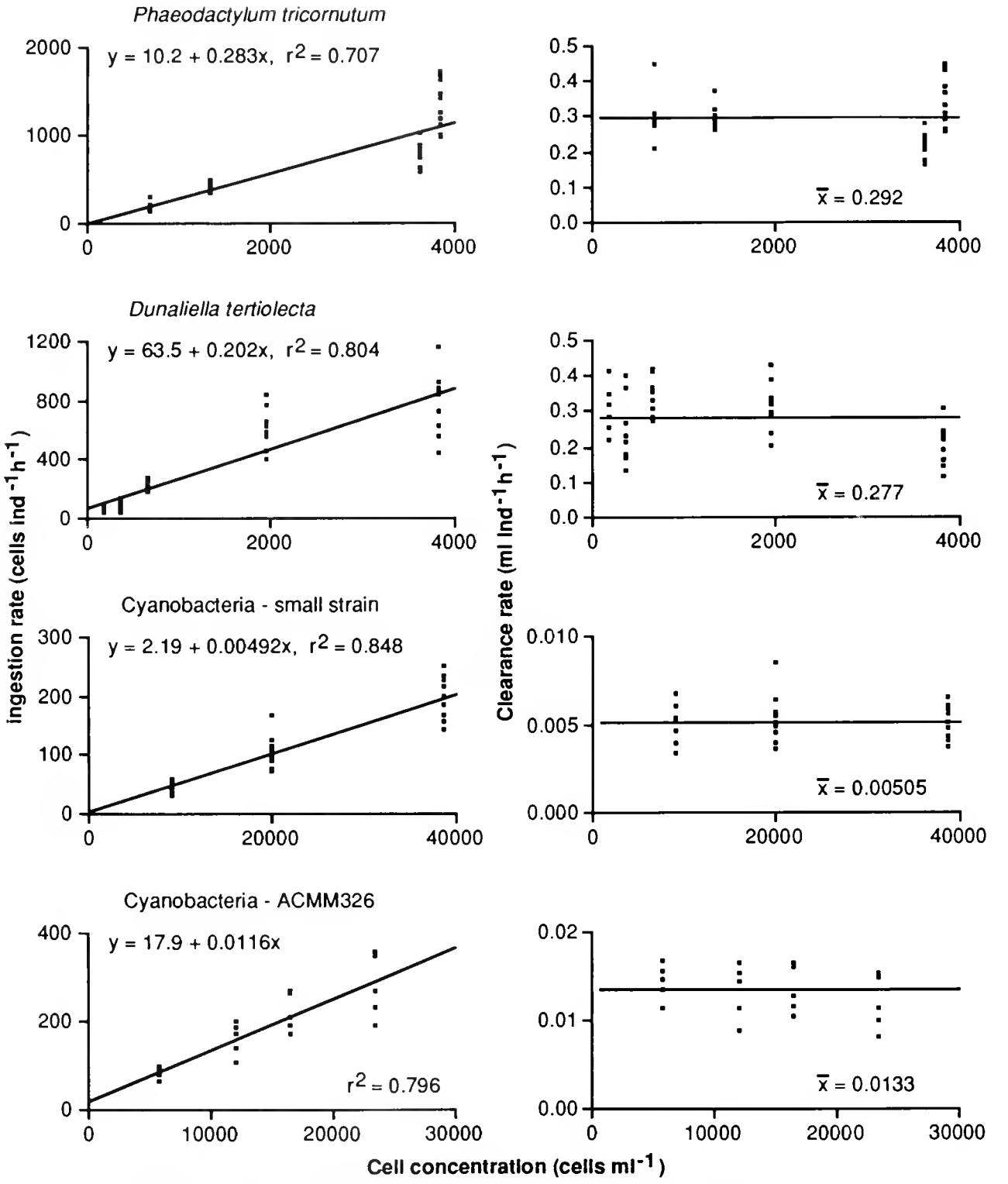

Figure 3. Ingestion and clearance rates of late bipinnaria larvae of *Acanthaster planci* feeding on four types of fluorescence-labeled cells.

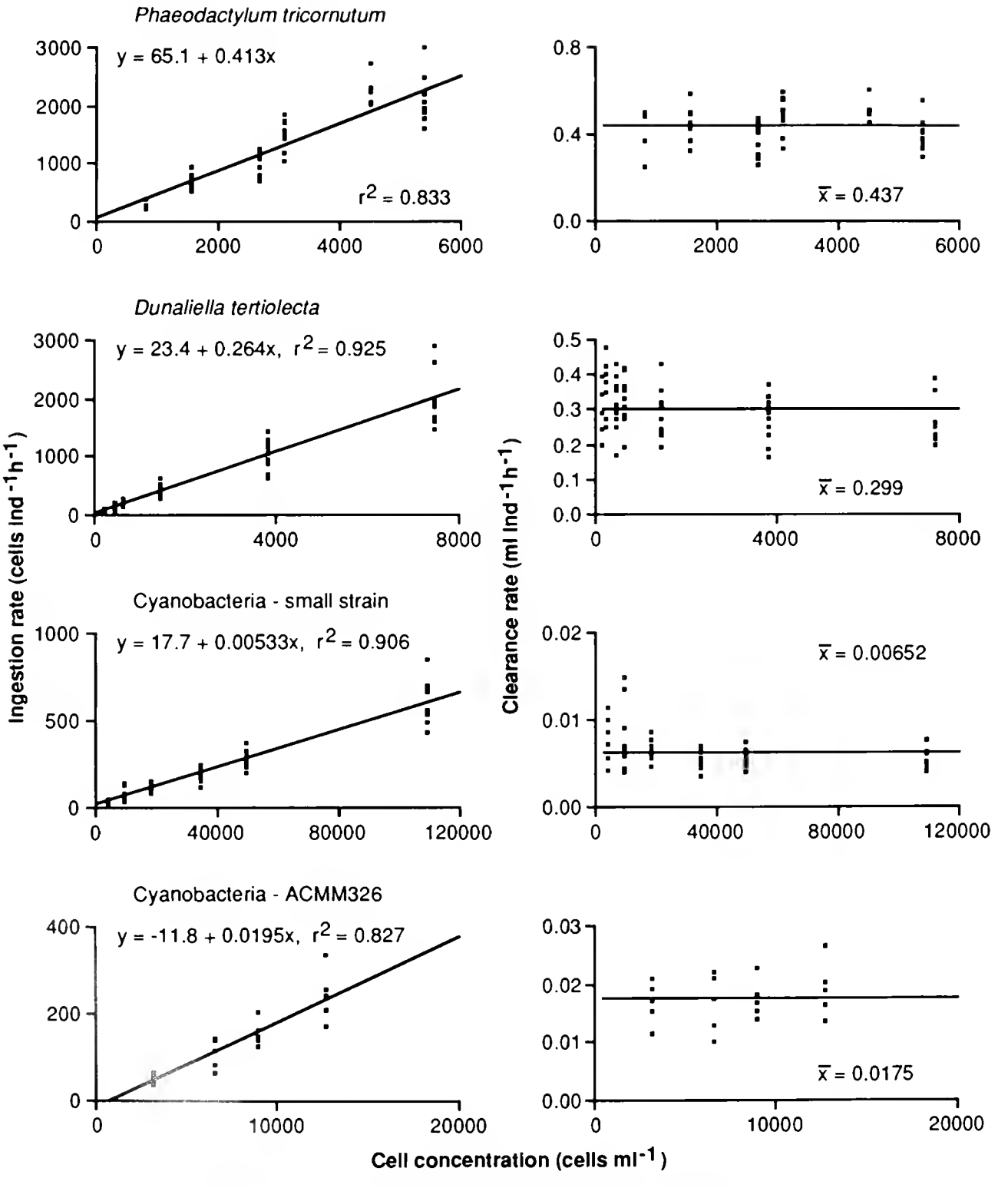

Figure 4. Same as Figure 3, but for early brachiolaria larvae of *Acanthaster planci*.

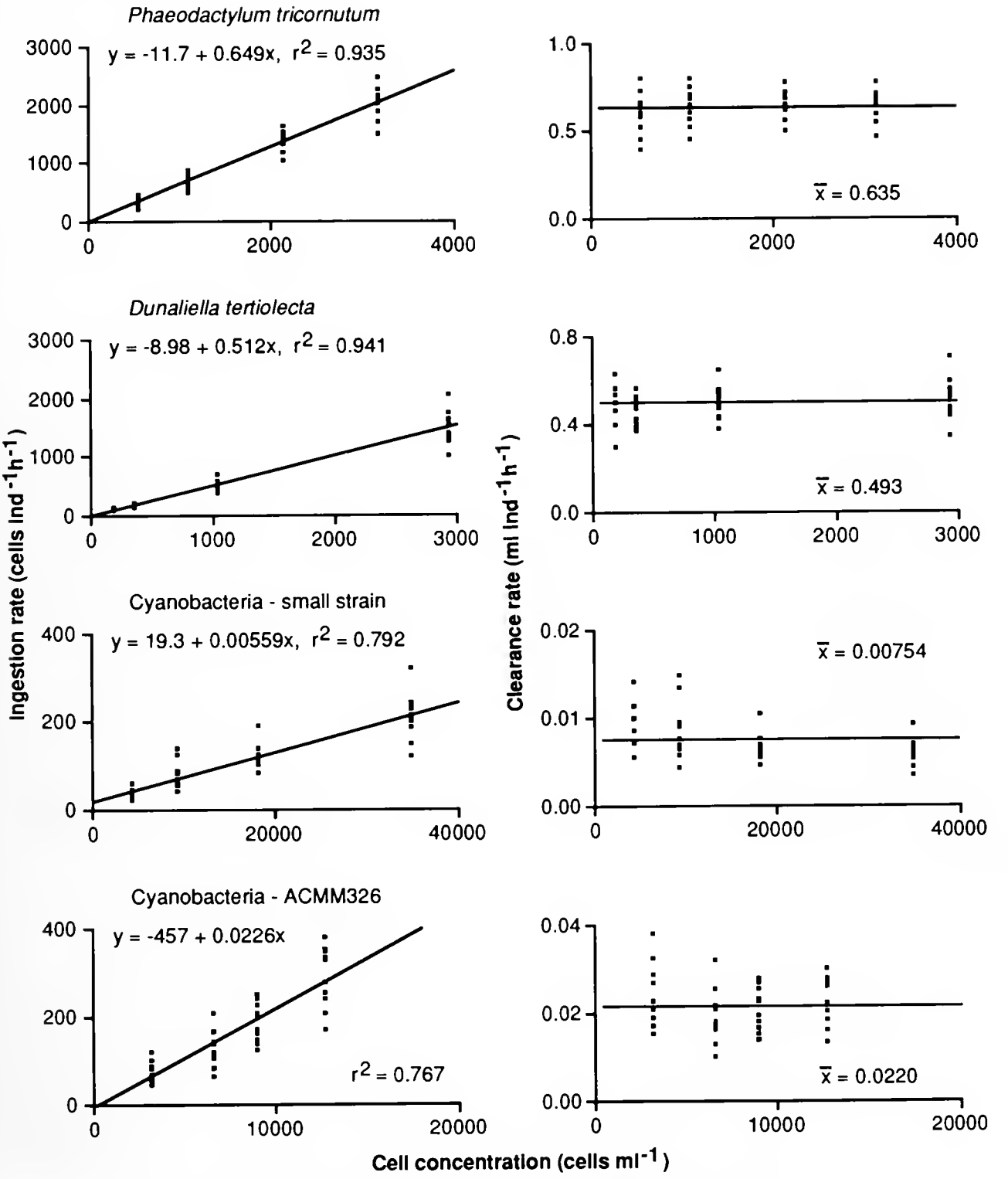

Figure 5. Same as Figure 3, but for late brachiolaria larvae of *Acanthaster planci*.

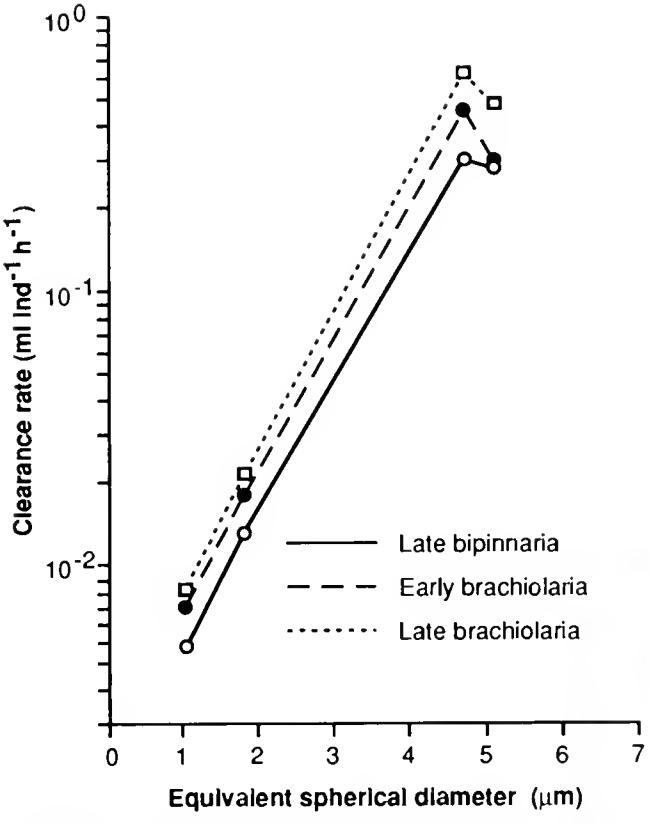

Figure 6. Effect of algal cell size on the clearance rate of the larvae of *Acanthaster planci* at three developmental stages.

O. validus grew equally well when reared on bacteria alone or on bacteria-phytoplankton mixtures. In contrast, the same authors, using the same methods, found no significant ingestion of bacteria by the larvae of *A. miniata*. One explanation for these contradictory results is that antarctic asteroid larvae are adapted to their rather unique environments and have a particle-capturing mechanism different from those of temperate and tropical species, despite their resemblance in morphology. It is also necessary to consider the possible difference in the proportion of attached to free-living bacteria between experiments. As mentioned above, this study does not deny the likelihood of ingestion of attached bacteria by asteroid larvae.

Ingestion of ultraplankton by COTS larvae

In the present experiments, COTS larvae were able to ingest two strains of cyanobacteria, but not bacteria, indicating that about 1 μm represents the minimum size of food particles for COTS larvae. Another important finding is the rather phenomenal increase in clearance rate between particles of 1 and 5 μm ESD: COTS larvae ingested *P. tricornutum* and *D. tertiolecta* more than ten times faster than they did two strains of cyanobacteria.

The majority of ultraplankton bigger than cyanobacteria consist of different forms of flagellates. Cyanobacteria are usually the dominant component of ultraplankton in shelf waters of the Great Barrier Reef (Furnas and Mitchell, 1986). In coral reef lagoons, however, flagellates make a significant contribution to ultraplankton biomass (Ayukai, 1992) and are a potentially important food source for COTS larvae. Although the results of the gut content analysis (Dixon, unpub.) do not support this possibility, flagellates in this size class are extremely fragile and could have been lost during sample fixation and preparation for SEM.

An increase in cell size beyond the ultraplankton size range appears to have relatively little effect on the clearance rate of COTS larvae. For instance, the clearance rates on FLC of *Tetraselmis* sp. (17.2 μm ESD) were similar

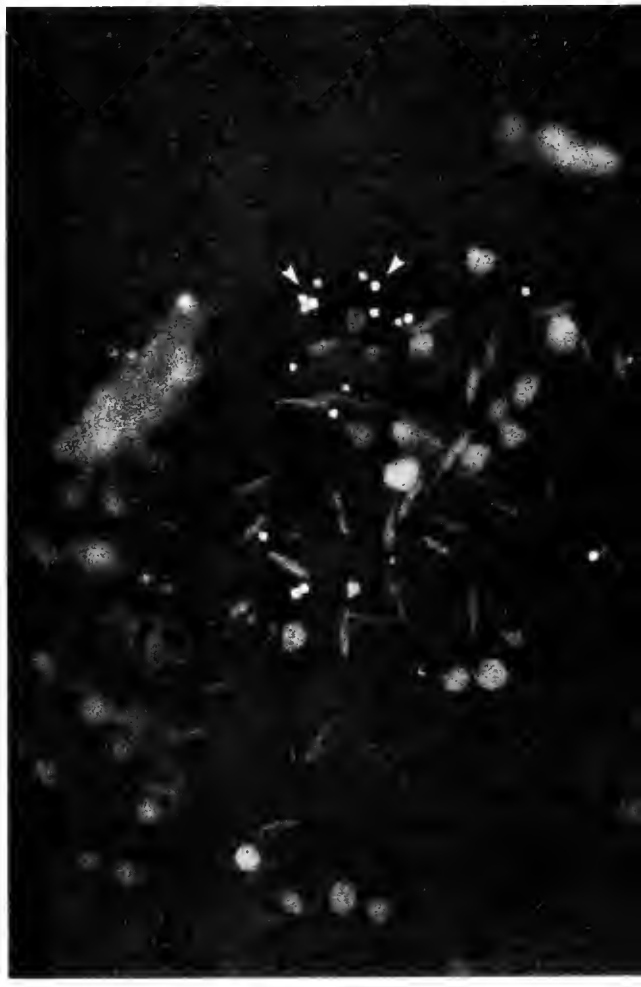

Figure 7. Heat-killed, fluorescence-labeled cyanobacteria (arrows, *ca* 1 μm in diameter) in the gut of brachiolaria larva of *Acanthaster planci*. The autofluorescence of live cells of *Phaeodactylum tricornutum* (pennate) and *Dunaliella tertiolecta* (oval) is also seen in the background.

to those on FLC of *P. tricornutum* and *D. tertiolecta* at bipinnaria and early brachiolaria stages and only two times higher than those on FLC of *P. tricornutum* and *D. tertiolecta* at late brachiolaria stage. The selective feeding of larvae on FLC over living cells of *Tetraselmis* sp. suggests that factors other than cell size (*e.g.*, cell shape, motility, chemical properties) may become more important to COTS larvae capturing larger particles.

The ingestion rate of COTS larvae in this study increased linearly with increasing FLC concentration and the clearance rate remained constant, independent of FLC concentration. This result contradicts the previous study by Lucas (1982), who reported a decrease in clearance rate with increasing cell concentrations. For instance, the clearance rate for *D. tertiolecta* in this study is comparable to his values for *D. primolecta* at low cell concentration (<1000 cells ml^{-1}), but is clearly different at higher concentrations (1000–4000 cells ml^{-1}). This is probably because feeding rates determined using the FLC method better reflect the efficiency of food particle capture by the band of cilia than do rates based on the conventional method, which can be affected by physiological and behavioral factors. As observed under an epifluorescence microscope, the turnover of cells in the gut of COTS larvae is relatively slow. Although the gut is soon congested at high cell concentrations, COTS larvae continue to capture cells, rejecting excess cells in the esophagus by the dorsal flexion of the body (Lucas, 1982). In long incubations at high cell concentrations, it is quite likely that COTS larvae capture many more cells than they actually ingest.

Body length approximately doubles, from about 0.7 to 1.4 mm, as COTS larvae progress from the late bipinnaria stage to the late brachiolaria stage. In this study, the clearance rates of larvae on four types of FLC also increased by 50–120% during this period. This result agrees with a general trend that the clearance rate of planktonic larvae with a single band of cilia is largely proportional to the length of the ciliated band (Strathmann *et al.*, 1972; Strathmann, 1975), which in turn depends on body length.

At present, little is known about the nutritional value of ultraplankton for the growth, development, and survival of asteroid larvae. The variability of the size frequency distribution and biomass of ultraplankton in putative habitats of different asteroid larvae is also unknown. The results presented here should not be extrapolated directly to other asteroid larvae, but do suggest that a significant proportion of ultraplankton is a potential food source for asteroid larvae.

Acknowledgments

This study was funded by the Great Barrier Reef Marine Park Authority. A. Halford, K. Hall, K. Okaji, and Dr. J. Keesing raised the COTS larvae used in this study. I thank Drs. J. Keesing, P. Moran, and two anonymous reviewers for their helpful comments on the manuscript. AIMS contribution no. 656.

Literature Cited

Ayukai, T. 1992. Picoplankton dynamics in Davies Reef lagoon, the Great Barrier Reef, Australia. *J. Plankton Res.* **14:** 1593–1606.

Azam, F., T. Fenchel, J. G. Field, J. S. Gray, L. A. Meyer-Reil, and F. Thingstad. 1983. The ecological role of water-column microbes in the sea. *Mar. Ecol. Prog. Ser.* **10:** 257–263.

Birkeland, C., and J. S. Lucas. 1990. Acanthaster planci: *Major Management Problem of Coral Reefs.* CRC Press, Boca Raton. P. 257.

Cho, B. C., and F. Azam. 1990. Biogeochemical significance of bacterial biomass in the ocean's euphotic zone. *Mar. Ecol. Prog. Ser.* **63:** 253–259.

Ducklow, H. W. 1983. Production and fate of bacteria in the ocean. *BioScience* **33:** 494–501.

Ducklow, H. W., and R. Mitchell. 1979. Bacterial populations and adaptations in the mucus layers on living corals. *Limnol. Oceanogr.* **24:** 715–725.

Frost, B. W. 1972. Effects of size and concentration of food particles on the feeding behavior of the marine planktonic copepod *Calanus pacificus*. *Limnol. Oceanogr.* **17:** 805–815.

Fuhrman, J. A., T. D. Sleeter, C. A. Carlson, and L. M. Proctor. 1989. Dominance of bacterial biomass in the Sargasso Sea and its ecological implications. *Mar. Ecol. Prog. Ser.* **57:** 207–217.

Furnas, M. J., and A. W. Mitchell. 1986. Phytoplankton dynamics in the central Great Barrier Reef—I. Seasonal changes in biomass and community structure and their relation to intrusive activity. *Cont. Shelf Res.* **6:** 363–384.

Gilmour, T. H. J. 1988. Particle paths and streamlines in the feeding behaviour of echinoderm larvae. Pp. 253–258 in *Echinoderm Biology*, R. D. Burke *et al.*, eds. A. A. Balkema, Rotterdam.

Lucas, J. S. 1982. Quantitative studies of feeding and nutrition during larval development of the coral reef asteroid *Acanthaster planci* (L). *J. Exp. Mar. Biol. Ecol.* **65:** 173–193.

Moriarty, D. J. W. 1979. Biomass of suspended bacteria over coral reefs. *Mar. Biol.* **53:** 193–200.

Murphy, L. S., and E. M. Haugen. 1985. The distribution and abundance of phototrophic ultraplankton in the North Atlantic. *Limnol. Oceanogr.* **30:** 47–58.

Olson, R. R. 1985. *In situ* culturing of larvae of the crown-of-thorns starfish, *Acanthaster planci*. *Mar. Ecol. Prog. Ser.* **25:** 207–210.

Olson, R. R. 1987. *In situ* culturing as a test of the larval starvation hypothesis for the crown-of-thorns starfish, *Acanthaster planci*. *Limnol. Oceanogr.* **32:** 895–904.

Olson, R. R., and M. H. Olson. 1989. Food limitation of planktotrophic marine invertebrate larvae: Does it control recruitment success? *Annu. Rev. Ecol. Syst.* **20:** 225–247.

Paffenhofer, G.-A., and K. B. Van Sant. 1985. The feeding response of a marine planktonic copepod to quantity and quality of particles. *Mar. Ecol. Prog. Ser.* **27:** 55–65.

Pearse, J. S., I. Bosch, V. B. Pearse, and L. V. Bosch. 1991. Bacterivory by bipinnarias in the Antarctic but not in California. *Am. Zool.* **31:** 6A.

Pomeroy, L. R. 1974. The ocean's food web: a changing paradigm. *BioScience* **24:** 499–504.

Rassoulzadegan, F., and L. Fenaux. 1979. Grazing of echinoderm larvae (*Paracentrotus lividus* and *Arbacia lixula*) on naturally occurring particulate matter. *J. Plankton Res.* **1:** 215–223.

Rivkin, R. B., I. Bosch, J. S. Pearse, and E. J. Lessard. 1986. Bacterivory: A novel feeding mode for asteroid larvae. *Science* **233:** 1311–1313.

Rublee, P. A., H. Lasker, M. I. Gottfried, and M. R. Roman. 1980. Production and bacterial colonization of mucus from the soft coral *Briarium asbestinum*. *Bull. Mar. Sci.* **30:** 888–893.

Rublee, P. A., and C. L. Gallegos. 1989. Use of fluorescently labelled algae (FLA) to estimate microzooplankton grazing. *Mar. Ecol. Prog. Ser.* **51:** 221–227.

Sherr, B. F., E. B. Sherr, and R. D. Fallon. 1987. Use of monodispersed, fluorescently labelled bacteria to estimate *in situ* protozoan bacterivory. *Appl. Environ. Microbiol.* **53:** 958–965.

Sorokin, Yu. I. 1974. Bacteria as a component of the coral reef community. *Proc. 2nd. Int. Symp. Coral Reef* **1:** 3–10.

Sorokin, Yu. I. 1981. Microheterotrophic organisms in marine ecosystems. Pp. 293–342 in *Analysis of Marine Ecosystems*. Academic Press, New York.

Stockner, J. G. 1988. Phototrophic picoplankton: an overview from marine and freshwater ecosystems. *Limnol. Oceanogr.* **33:** 765–775.

Strathmann, R. R. 1971. The feeding behavior of planktotrophic echinoderm larvae: mechanisms, regulation, and rates of suspension-feeding. *J. Exp. Mar. Biol. Ecol.* **6:** 109–160.

Strathmann, R. R. 1975. Larval feeding in echinoderms. *Am. Zool.* **15:** 717–730.

Strathmann, R. R., T. L. Jahn, and J. R. C. Fonseca. 1972. Suspension feeding by marine invertebrate larvae: clearance of particles by ciliated bands of a rotifer, pluteus, and trochophore. *Biol. Bull.* **142:** 505–519.

Reference: *Biol. Bull.* **186:** 101–114. (February, 1994)

Chromosomal Proteins of the Sperm of a Cephalochordate (*Branchiostoma floridae*) and an Agnathan (*Petromyzon marinus*): Compositional Variability of the Nuclear Sperm Proteins of Deuterostomes

NÚRIA SAPERAS[1,2], MANEL CHIVA[1], ENRIC RIBES[3], HAROLD E. KASINSKY[4], ELLEN ROSENBERG[4], JOHN H. YOUSON[5], AND JUAN AUSIO[6,*]

[1]*Departament d'Enginyeria Química, Universitat Politècnica de Catalunya, Diagonal 647, Barcelona E-08028, Spain;* [2]*Institut de Ciències del Mar, Passeig Nacional s/n, Barcelona E-08039, Spain;* [3]*Unitat de Biologia Cel·lular, Departament de Bioquímica i Fisiologia, Universitat de Barcelona, Diagonal 645, Barcelona E08028, Spain;* [4]*Department of Zoology, University of British Columbia, Vancouver, British Columbia, Canada V6T 1Z4;* [5]*Department of Zoology at Scarborough Campus, University of Toronto, West Hill, Ontario, Canada M1C 1A4; and* [6]*Department of Biochemistry and Microbiology, University of Victoria, Victoria, British Columbia, Canada V8W 3P6*

Abstract. We have isolated and characterized for the first time the chromosomal proteins from the nucleus of the sperm of a lancelet (amphioxus) *Branchiostoma floridae* (Hubbs, 1922) (Phylum Chordata: Subphylum Cephalochordata) and of a lamprey *Petromyzon marinus* (Linnaeus, 1758) (Phylum Chordata: Subphylum Vertebrata: Class Agnatha). In the first case, the major protein component of the sperm-chromatin of a lancelet is a highly specialized protamine-like (PL) protein that has structural and compositional features similar to those of PL-III from bivalve mollusks. In contrast, the chromatin of the sperm of the lamprey has a structural arrangement and protein composition (histones) very similar to that found in the somatic cells of all eukaryotic organisms.

Among the deuterostomes, chromosomal protein variability is considerably greater in representatives of the Phylum Chordata than in echinoderms. The possible evolutionary significance of these findings is discussed.

Introduction

The first nuclear sperm-specific proteins were isolated from vertebrates. They were obtained from the sperm of a salmonid fish *Salmo salar* (Rhine Salmon) and were given the name of protamines (Miescher, 1874; Kossel, 1928). It was clear from the very beginning that these proteins were different "chemically" from the proteins found in the nucleus of somatic cells (Kossel, 1928). Protamines are small (30–40 amino acid) arginine rich (≥50% arginine) proteins that displace the somatic-like spermatogenic histones during spermiogenesis. Besides the early salmonid protamines, other homologous proteins have also been identified in other groups of vertebrates including amphibians (Bols and Kasinsky, 1972, 1973; Kasinsky *et al.*, 1978, 1985; Mann *et al.*, 1982; Takamune *et al.*, 1991), reptiles (Kasinsky *et al.*, 1978; Mann, 1981; Kasinsky *et al.*, 1987; Chiva *et al.*, 1989), birds (Dixon *et al.*, 1985; Chiva *et al.*, 1987, 1988) and mammals (this group has been recently reviewed by Oliva and Dixon, 1991). See also Kasinsky (1989) for an overall review.

Despite their wide distribution and the historical discovery of protamines in vertebrates, the protein composition of the sperm chromatin of this taxonomic group is extremely heterogeneous (Bloch, 1969, 1976; Kasinsky, 1989). Such protein heterogeneity is also shared by other taxonomic groups (Bloch, 1969, 1976). The protein composition of the sperm may thus vary from somatic-type histones (H) to compositionally intermediate protamine-

Received 2 June 1993; accepted 8 November 1993.

* To whom all correspondence should be addressed.

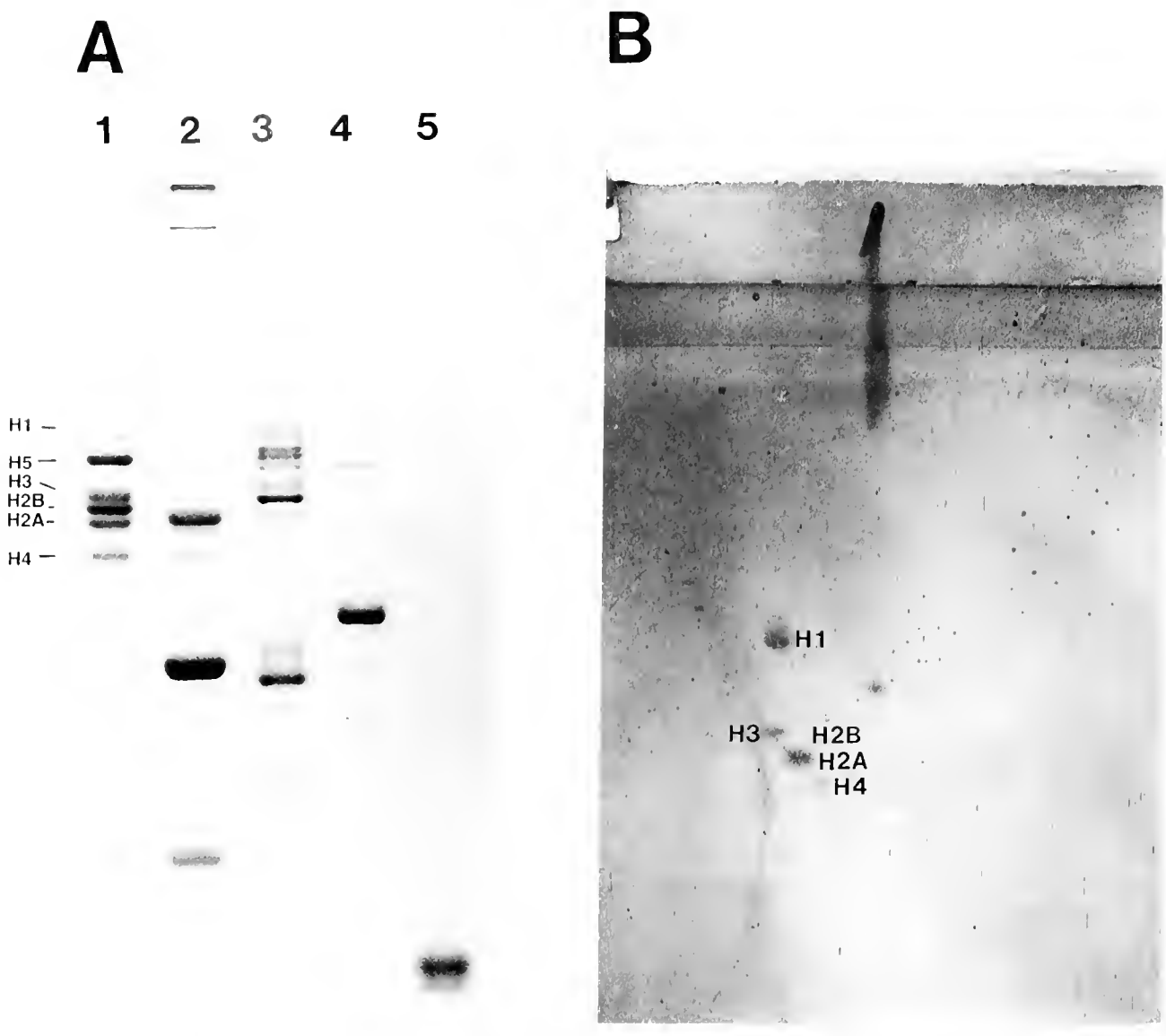

Figure 1. (A) Acetic acid (5%)—urea (2.5 *M*)—PAGE analysis of (1) chicken erythrocyte histones, (2) nuclear sperm proteins from the mussel *Mytilus californianus*, (3) nuclear sperm proteins from the ascidian tunicate *Styela plicata*, (4) nuclear sperm proteins from the lancelet *Branchiostoma floridae*, and (5) salmine (protamine). Direction of electrophoresis is from top (+) to bottom (−). (B) Acetic acid (5%)—urea (6 *M*) (first dimension)—SDS (second dimension) two-dimensional gel electrophoresis of the proteins shown in (A) lane 4.

like proteins (PL) to protamines (P), depending on the organism (Bloch, 1969, 1976). Those organisms that retain the somatic-histone type of proteins often contain sperm-specific histones (H1 and/or H2B) and will be referred to as (H1 type) in this paper.

Although the nature of the compositional protein heterogeneity of the sperm is unclear, from an evolutionary point of view protamines are more specialized proteins and therefore might be expected to have appeared in more evolved organisms, whereas the less specialized histones would be present in more primitive species. From this perspective, the data available on the taxonomic distribution of protamines within and among different taxonomical groups still remains a puzzle. A clear example of this situation has been recently exemplified in the bony fish (Saperas *et al.*, 1993a, b). The organisms within this group have sperm cells with nuclear protein compositions including all the protein types (H, H1, PL, P) described earlier.

The problem of nuclear protein heterogeneity within bony fish has been linked to the controversial evolutionary origin of protamines in fish (see Oliva and Dixon, 1991,

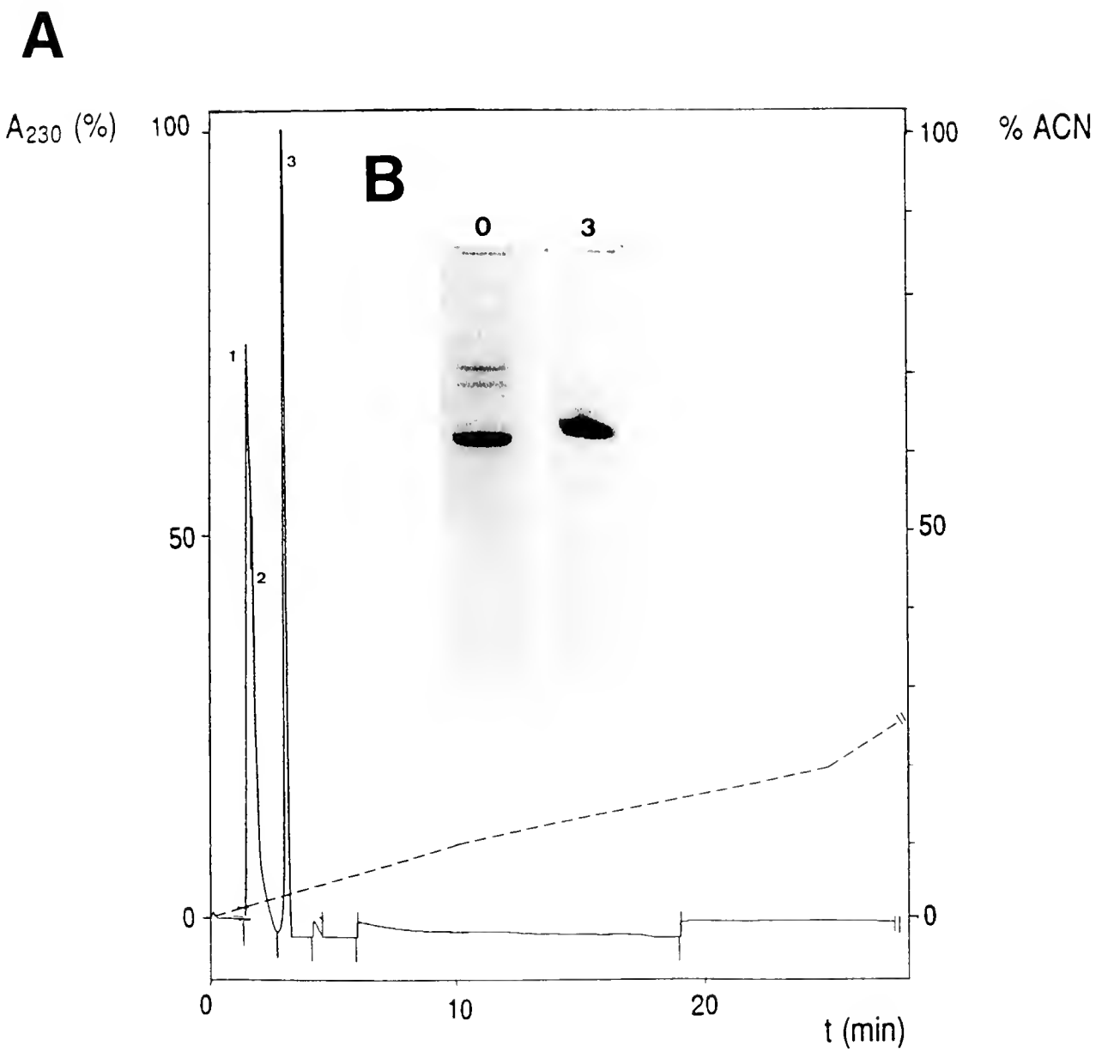

Figure 2. (A) Reverse phase HPLC fractionation of the whole nuclear protein extract (0.4 *N* HCl) from the sperm of *Branchiostoma floridae* on a 5 μm, Spherisorb C_{18}, ODS2 (4.6 × 150 mm) column. A_{230} = absorbance at 230 nm. ACN = acetonitrile. No proteins could be detected in peaks 1 and 2. (B) Acetic acid (5%)—urea (6 *M*) PAGE of 0: starting nuclear protein extract; 3: protein fraction eluted in peak 3 of Figure 2(A). (C) Amino acid sequence of the N-terminal region of the protein shown in (B) lane 3.

Table I

Amino acid analysis (mol %) of the nuclear sperm-specific protein of Branchiostoma floridae *PL(BF) in comparison to the PL-III proteins of* Mytilus trossulus *PL-III (MT) (Mogensen et al., 1991) and* Macoma nasuta *PL-III (MN) (Ausió, 1988)*

	PL(BF)	PL III (MT)	PL III (MN)
Lys	24.7	24.0	25.2
His	—	—	0.2
Arg	25.3	27.5	27.9
Asx	—	—	3.5
Thr	—	3.7	—
Ser	16.5	17.7	28.7
Glx	—	—	0.9
Pro	5.6	5.1	0.6
Gly	6.1	6.9	1.8
Ala	21.7	14.1	9.5
Cys	—	—	—
Val	—	0.9	0.4
Met	—	—	0.1
Ile	—	—	0.5
Leu	—	—	0.5
Tyr	—	—	0.1
Phe	—	—	0.2

for a discussion). Thus it seemed timely to analyze the nuclear sperm-specific proteins of more primitive organisms related to early vertebrate evolution. We have characterized the sperm-specific proteins of an agnathan (*Petromyzon marinus*) and a cephalochordate (*Branchiostoma floridae*) and compared them to the nuclear sperm-specific proteins of different groups of deuterostomes. The possible evolutionary significance of these data is discussed.

Materials and Methods

Living organisms

Adult males of *Branchiostoma floridae* (Hubbs, 1922) were collected as described elsewhere (Holland and Holland, 1989).

Male lampreys, *Petromyzon marinus* (Linnaeus, 1758), were collected during their upstream (prespawning) migration in the watersheds of Lake Ontario, Canada in November 1990, 1991, 1992. The animals were held in the laboratory at Scarborough Campus until sexually mature and then the milt was released by abdominal massage into test tubes for immediate freezing at −70°C or for fixation for electron microscopy. *Lampretra richardsoni* were collected in Southwestern British Columbia.

Nuclei preparation

Nuclei were isolated from ripe sperm cells as described elsewhere (Saperas *et al.*, 1993a).

Protein extraction

Crude protein extracts were obtained by homogenization of the nuclei in 0.4 *N* HCl followed by precipitation of the soluble fraction in 6 volumes of acetone overnight at 4°C.

Reduction of disulfide linkages

S-S linkages were reduced under denaturing conditions as described by Kuehl (1979). In brief, the proteins, at a concentration of 1 mg/ml in 6 *M* urea, 20 m*M* Tris-HCl pH 7.6, were reduced in the presence of 8% β-mercaptoethanol for 3 h at room temperature.

Protein fractionation and purification

Ionic exchange chromatography using carboxymethyl cellulose (Whatman CM52) and reverse phase HPLC [on either C_4 or C_{18} (Vydac)] were carried out as described elsewhere (Saperas *et al.*, 1992).

Amino acid analysis and protein sequence determination

Amino acid analyses were carried out on an Applied Biosystems (ABI) model 420 A derivatizer-analyzer system. The hydrolysis of the protein was carried out in a gas-phase 6 *N* HCl and 1% phenol under an argon atmosphere at 165°C. The N-terminal sequence of the proteins was determined by automated Edman degradation on an Applied Biosystems (ABI) model 470A protein sequencer using the standard program 03 rpth. The phenylthiohydantoins were analyzed on an Applied Biosystems (ABI) model 120A on line HPLC system using a C_{18} Brownlee column (2.1 × 220 mm).

Gel electrophoresis

Acetic acid (2.5 or 6 *M*) urea polyacrylamide gel electrophoresis (PAGE) was performed as described elsewhere (Saperas *et al.*, 1992). Two-dimension gel electrophoresis using acetic acid-urea or acetic acid-urea-triton X-100 for the first dimension and sodium dodecyl sulfate for the second, was carried out as described elsewhere (Saperas *et al.*, 1992).

Electron microscopy

Transmission electron microscopy of the *Petromyzon* sperm was carried out at the Service of Electron Microscopy of the University of Barcelona. The samples were prepared as described elsewhere (Saperas *et al.*, 1993a). Electron microscopy analysis of *Branchiostoma* was carried out by Dr. N. Holland of the Marine Biology Research Division at Scripps Institution of Oceanography (La Jolla, California) as described in Holland and Holland (1989).

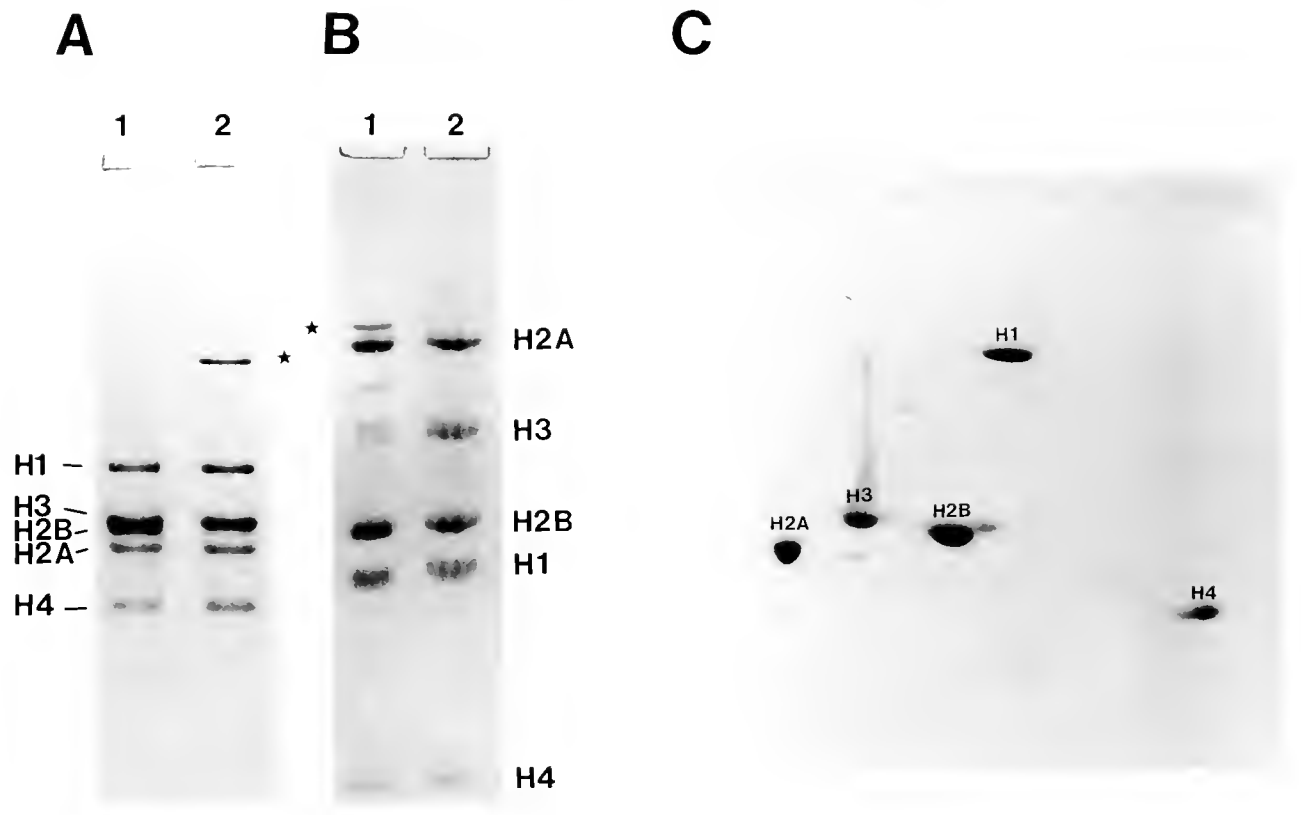

Figure 3. (A) Analysis of a whole nuclear protein extract from the sperm of *Petromyzon marinus* in acetic acid (5%)—urea (2.5 *M*) (1) after and (2) before reduction with β-mercaptoethanol. (B) Acetic acid (5%)—urea (6 *M*)—triton X-100 (6 m*M*) PAGE of a whole nuclear protein extract from the sperm of *Petromyzon marinus* (1) before and (2) after treatment with β-mercaptoethanol. (C) Two-dimensional PAGE in acetic acid-urea-triton X-100 as in (B) (first dimension), SDS (second dimension). The asterisks indicate the position of the histone H3 dimers.

Results

The nuclear sperm-specific proteins of the cephalochordate Branchiostoma floridae

The electrophoretic analysis of a whole protein extract from the nuclei of the sperm of *B. floridae* is shown in Figure 1. The analysis is shown in comparison to somatic histones from chicken erythrocyte (lane 1) and to proteins of the PL-type from a mussel (*Mytilus edulis*, lane 2) and from an ascidian tunicate (*Styela plicata*, lane 3). Several minor bands with electrophoretic mobility similar to that of histones (both in urea-acetic acid, Fig. 1A, or in SDS gels, Fig. 1B) coexist with a major band of higher electrophoretic mobility. The protein corresponding to this major band was purified by reverse phase HPLC (see Fig. 2). The compositional amino acid analysis of this protein is given in Table I. Such composition is clearly indicative of the highly specialized nature of this protein. Only six amino acids are present, four of which (Lys, Arg, Ser, and Ala), account for 88% of the overall amino acid composition. The basic amino acids alone represent 50% of this composition. The number of constitutive amino acids estimated from the electrophoretic mobility of this protein in polyacrylamide urea acetic acid gels (Colom and Subirana, 1979; Ausio and Subirana, 1982a; Daban *et al.*, 1991) was 85 ± 5. Despite the small amount of purified protein available, it was still possible to establish the amino acid sequence of the first nine amino acids of the N-terminal region of this protein. The results are shown in Figure 2C. G/P at the N-terminus of this sequence indicates an almost identical recovery of these two amino acids in the first cycle of Edman degradation. This is most likely due to the existence of some protein microheterogeneity.

The nuclear sperm-specific proteins of the Agnathan Petromyzon marinus

A whole nuclear protein (0.4 *N* HCl extract) from the sperm of *Petromyzon marinus* is shown in Figure 3. Based on their relative electrophoretic mobility in polyacrylamide gels containing either urea-acetic acid, urea-acetic acid-triton X-100 or SDS (Fig. 3A, B, C), the proteins

Table II

Amino acid composition (mol %) of the sperm histones of the lamprey Petromyzon marinus *(PM) in comparison to the somatic histones from calf thymus (CT) (Mayes and Johns, 1982)*

	H1		H2A		H2B		H3		H4	
	PM	CT	PM	CT	PM	CT	PM	CT	PM	CT
Lys	27.6	26.8	9.7	10.2	14.1	14.1	8.3	10.0	10.4	11.4
His	—	—	1.6	3.1	3.3	2.3	1.7	1.7	1.8	2.2
Arg	2.2	1.8	9.8	9.4	8.2	6.9	13.8	13.0	13.4	12.8
Asx	3.9	2.5	6.3	6.2	4.8	5.0	4.2	4.2	4.8	5.2
Thr	3.6	5.6	3.2	3.9	6.6	6.4	7.5	6.8	6.7	6.3
Ser	7.3	5.6	5.2	3.4	10.3	10.4	4.5	3.6	2.0	2.2
Glx	4.7	3.7	9.4	9.8	6.4	8.7	12.0	11.6	6.5	6.9
Pro	9.7	9.2	4.1	4.1	6.2	4.9	4.5	4.6	1.4	1.5
Gly	4.0	7.2	11.4	10.8	5.9	5.4	5.6	5.4	16.8	14.9
Ala	21.8	24.3	13.1	12.9	11.6	10.8	13.3	13.3	7.9	7.7
Cys	—	—	—	—	—	—	0.6	1.0	—	—
Val	6.8	5.4	7.2	6.3	6.0	7.5	4.2	4.4	8.1	8.2
Met	—	—	0.5	—	2.1	1.5	0.8	1.1	0.2	1.0
Ile	1.1	1.5	3.7	3.9	5.8	5.1	4.7	5.3	5.5	5.7
Leu	5.3	4.5	11.9	12.4	4.5	4.9	8.9	9.1	8.6	8.2
Tyr	0.8	0.9	2.3	2.2	2.8	4.0	2.2	2.2	3.6	3.8
Phe	1.1	0.9	0.9	0.9	1.6	1.6	3.3	3.1	2.1	2.1

solubilized by 0.4 *N* HCl behave as the typical somatic nucleosomal histones of most eukaryotes. Under the acidic conditions of this method of extraction, about 70% of histone H3 is present in a dimer conformation (see Fig. 3A, lane 2, 3B, lane 1). This dimer form can be easily converted to the monomer form by treatment with β-mercaptoethanol (Fig. 3A, lane 1, 3B, lane 2). The absence of aggregates larger than dimers, together with the amino acid composition of this histone fraction (Table II) indicate that H3 from *P. marinus* contains only one cysteine residue per molecule as it occurs with most somatic histone H3 proteins (Klyszejko-Stefanowicz *et al.*, 1989). To date, somatic type histones (type H) have been found in the sperm of organisms as diverse as the horseshoe crab (*Limulus polyphemus*) (Muñoz-Guerra *et al.*, 1982a), the frog (*Rana catesbiana*) (Kasinsky *et al.*, 1985), and in some fish such as the goldfish (*Carassius auratus*) (Muñoz-Guerra *et al.*, 1982b), just to mention a few examples (see also Kasinsky, 1989, for a more extensive review).

Figure 4 shows a reverse phase HPLC fractionation of the 0.4 *N* HCl nuclear extract. The individual fractions purified in this way were subjected to amino acid analysis and the compositions are shown in Table II. These results corroborate the true histone nature of the basic proteins from the nucleus of the sperm of *Petromyzon marinus*.

Light and electron microscopy studies

Figure 5A, B, C shows a light microscopy comparison of the sperm of a lancelet (*Branchiostoma floridae*) and two lampreys (*Petromyzon marinus* and *Lampetra richardsoni*). The head of the sperm in the lancelet and in the lamprey *Petromyzon* is rounded, whereas in contrast the sperm of *Lampetra* has an elongated shape as previously reported (Stanley, 1967). The relevance of this observation will be discussed later. The micrographs can also be used to assess the extent of purity of the sperm samples used in the protein preparations.

Figure 6(1) shows an electron micrograph of a partial view of the sperm head of *Petromyzon marinus*. Although for the purposes of this work we are primarily interested in the fine structure of the chromatin complexes within the nucleus, several distinctive regions of the sperm head can still be distinguished clearly in this micrograph. These characteristic structures—acrosomal vesicles (AC), endonuclear canal (EC), and the central fiber (CF)—have also been described in other lampreys (Stanley, 1967; Jamieson, 1984), and they are very similar in all of them except for the elongated shape of the nucleus of *Lampetra* (Stanley, 1967).

At the chromatin level, the fine structure of the nucleus reveals a closely packed granular organization [Fig. 6(2)] which most likely corresponds to the same granular organization observed by Stanley (1967) in *Lampetra*. In the latter case the superficial granular appearance is due to a filamentous fiber structure that is most likely also present in *Petromyzon*. In fact the diameter of the granules observed [Fig. 6(2)] is 3.0 ± 0.5 nm. This diameter is very close to the 2.37 nm observed by low angle X-ray diffraction for the nucleoprotamine fibers of the sperm of

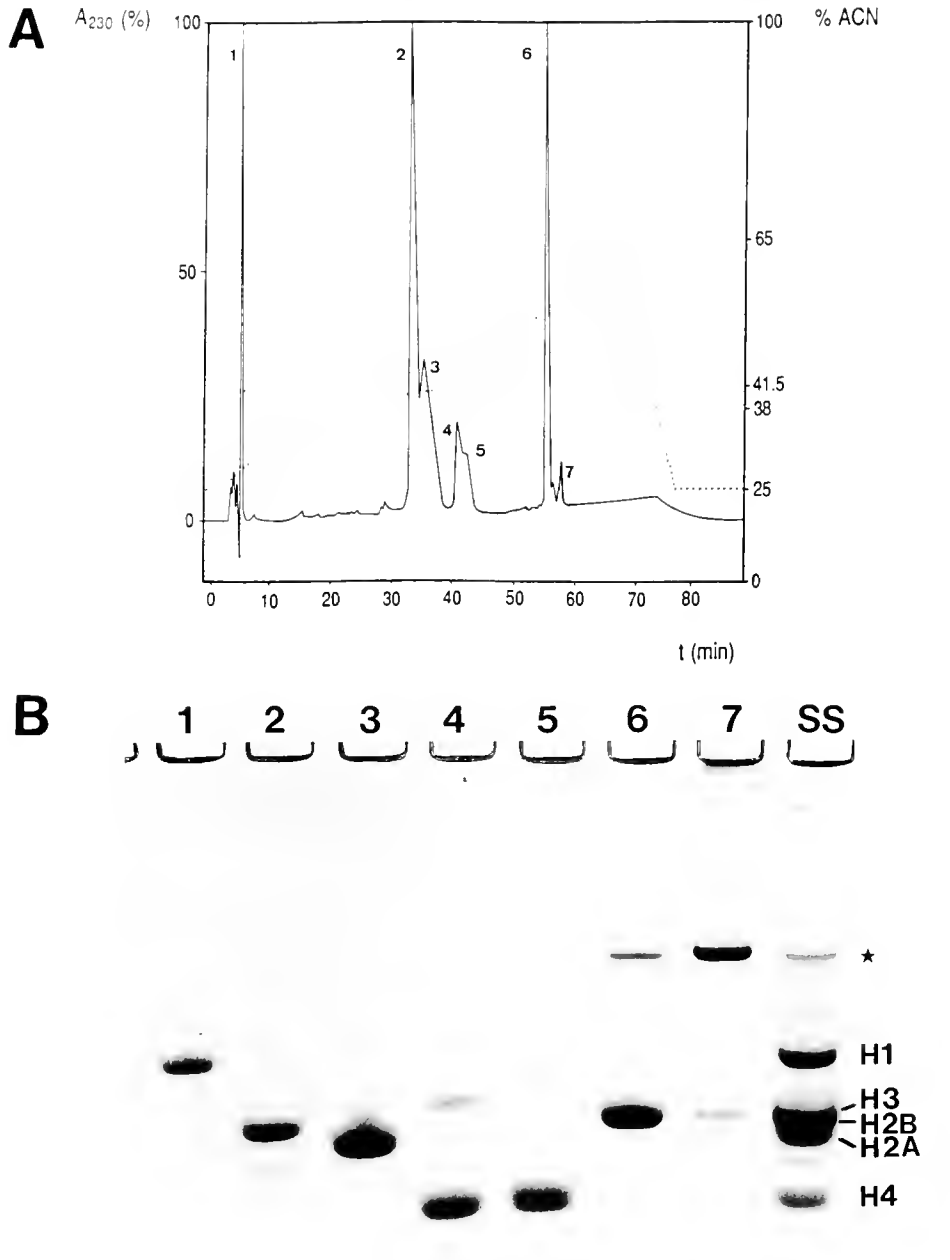

Figure 4. (A) Reverse phase HPLC fractionation of a whole nuclear protein extract from the sperm of *Petromyzon marinus* on a 5-μm, Vydac C_{18} (4.6 × 250 mm) column. (B) Electrophoretic analysis on acetic acid (5%)—urea (2.5 *M*) PAGE of the corresponding elution peaks of Figure 4(A). SS: starting sample. The asterisk indicates the position of the H3 dimers.

Mytilus (Ausió and Subirana, 1982b). This kind of chromatin organization is quite different from that observed in the lancelet [Fig. 6(4)] (Holland and Holland, 1989). In this case as spermiogenesis proceeds, particles 30 nm in diameter (fibers?) coalesce into granules of about 60 nm in diameter in the mature spermatozoa [Fig. 6(3) and 6(4), Holland and Holland, 1989]. These granules have an enormous resemblance to the 40–70 nm granules observed by electron microscopy in the sperm of *Mytilus* (Longo and Dornfeld, 1967).

Discussion

Compositional heterogeneity of the sperm-specific nuclear proteins in deuterostomes

To ascertain the possible significance and evolutionary implications of the protein composition from the nucleus

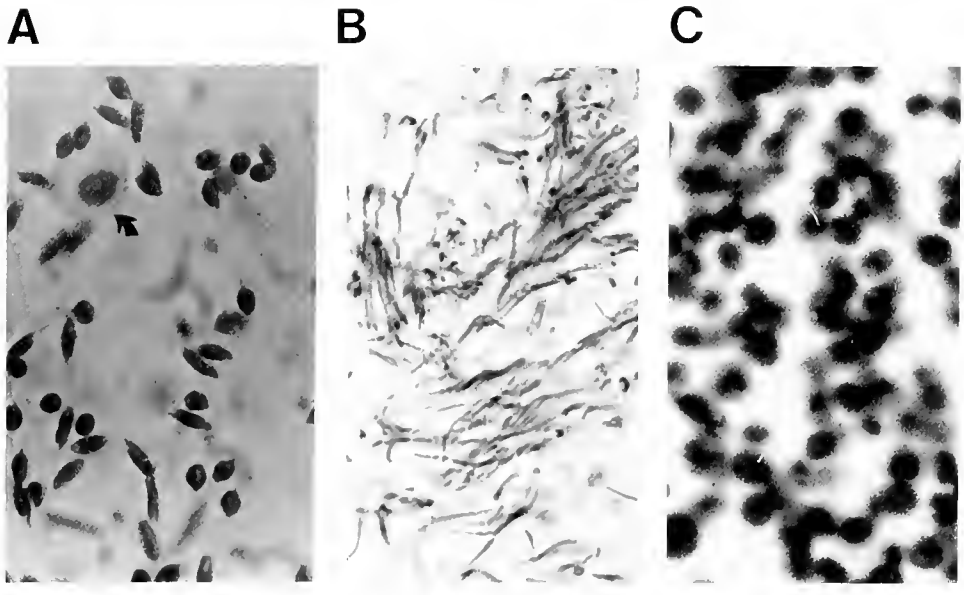

Figure 5. (A) Light microscope phase contrast micrograph of the sperm suspension of *Petromyzon marinus* used to prepare the sperm-specific nuclear proteins shown in Figure 3 and Figure 4. About 2–3% of the sample consisted of erythrocyte contamination (arrow). (B) Light microscope Feulgen stain of a section of an embedded sperm sample from *Lampetra richardsoni testis*. (C) Light microscope Feulgen stain of a sperm suspension from *Branchiotoma floridae*. The magnification was ×1000 in every case.

of the sperm of *Branchiostoma floridae* (Cephalochordata) and *Petromyzon marinus* (Agnatha), the analyses must be carried out in comparison to the different groups of deuterostomes for which the sperm-specific protein composition is already well established. At present some information is available about the chromosomal proteins of the sperm of echinoderms, ascidian tunicates, and fish (see also Fig. 7 and Table III).

The sperm-specific proteins of the echinoderms have been extensively characterized. They consist basically of histone variants (type H of the classification outlined in the Introduction), although in most cases highly specialized sperm-specific histone H1 or H2B fractions have been described (type H1) (see Fig. 7, lanes 1, 2, 3). Thus, within the Subphylum Asterozoa, several representative organisms of the Class Stelleroidea have been analyzed (see also Fig. 7, lane 1) (Subirana and Palau, 1968; Strickland *et al.*, 1980; Zalenskaya *et al.*, 1980). In the sperm of these organisms the histone H1 fraction is different from its somatic counterpart, whereas the core histones (H2A, H2B, H3, H4) exhibit an electrophoretic mobility in PAGE that is indistinguishable from that of the somatic core histones (Zalenskaya *et al.*, 1980). Within the Subphylum Echinozoa, several organisms within each of the classes Echinoidea and Holothuroidea have been characterized (see Fig. 7, lane 2). In the Echinoidea, most of its representative organisms have highly specialized histone H1 and H2B variants (Strickland, W. N. *et al.*, 1980a, b, 1982a, b; Brandt *et al.*, 1979; Giancotti *et al.*, 1980; Zalenskaya and Zalensky, 1980; Imschenetzky *et al.*, 1984). These variants exhibit modified N- or C-terminal regions, which are often characterized by the presence of very characteristic repetitive (tetra or penta)-peptides (Strickland, W. N. *et al.*, 1977; Strickland, M. *et al.*, 1977, 1978; Strickland, W. N. *et al.*, 1980a, b) (see also von Holt *et al.*, 1984, and Poccia, 1991, for more detailed reviews). Within the organisms of the Class Holothuroidea, *Holothuria tubulosa* contains a highly specific heterogeneous histone H1 in addition to the somatic counterpart (Phelan *et al.*, 1972). In addition to the histone complement, all the organisms characterized so far within this class also contain an additional protein with higher electrophoretic mobility (~80 amino acids) (see Fig. 7, lane 3) (Subirana, 1970; Zalenskaya *et al.*, 1980). The sequence of one of these proteins was determined recently (Prats *et al.*, 1989).

In most of the ascidian tunicates, the basic proteins from the nucleus of the sperm consist of a major protamine-like component (PL) that replaces the nucleosomal histones (Chiva *et al.*, 1990, 1992; Saperas *et al.*, 1992) (Fig. 7, lane 4). This protein consists of approximately 145 amino acids and has an amino acid composition and a trypsin-resistant peptide (Saperas *et al.*, 1992) that resembles those of PL-I proteins of mollusks (Ausió *et al.*, 1987; Jutglar *et al.*, 1991). In at least one genus of ascidian tunicates (genus = *Styela*) an additional PL with fewer amino acids (80–85) is also present (see Fig. 7, lane 5, and Fig. 1, lane 3). The amino acid composition of this latter protein resembles that of

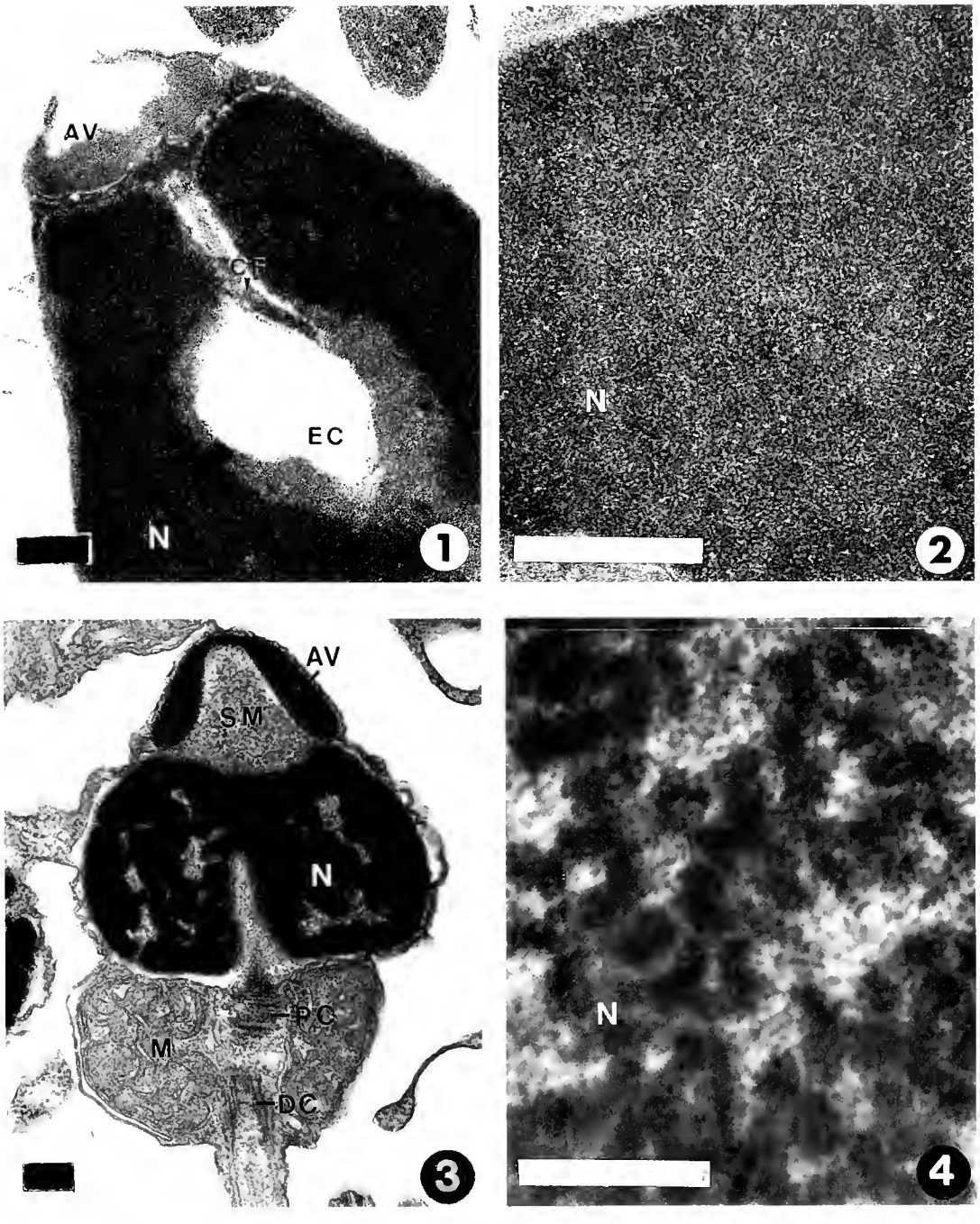

Figure 6. (1) Electron micrograph of the apical region of the sperm of *Petromyzon marinus*, showing the acrosomal vesicle (AV), the endonuclear canal (EC) and the central fiber (CF) and the nucleus (N) (×53,000); (2) Detail of the nucleus of the sperm of *P. marinus* to show the fine structure of chromatin (×140,000). (3) Electron micrograph of a mature sperm cell from *Branchiostoma floridae* acrosomal vesicle (AV); distal centriole (DC); mitochondria (M); nucleus (N); proximal centriole (PC); and subacrosomal material (SM) (×37,000). (4) Detail of the nucleus of the sperm of *Branchiostoma floridae* (× 140,000). All scale bars are 200 nm.

protamines from teleost fish (Saperas *et al.*, 1992). However, it is not clear whether there is an evolutionary relation between these proteins or whether the presence of the additional PL protein only represents a particular solution to the process of chromatin compaction during spermatogenesis for the members of this genus.

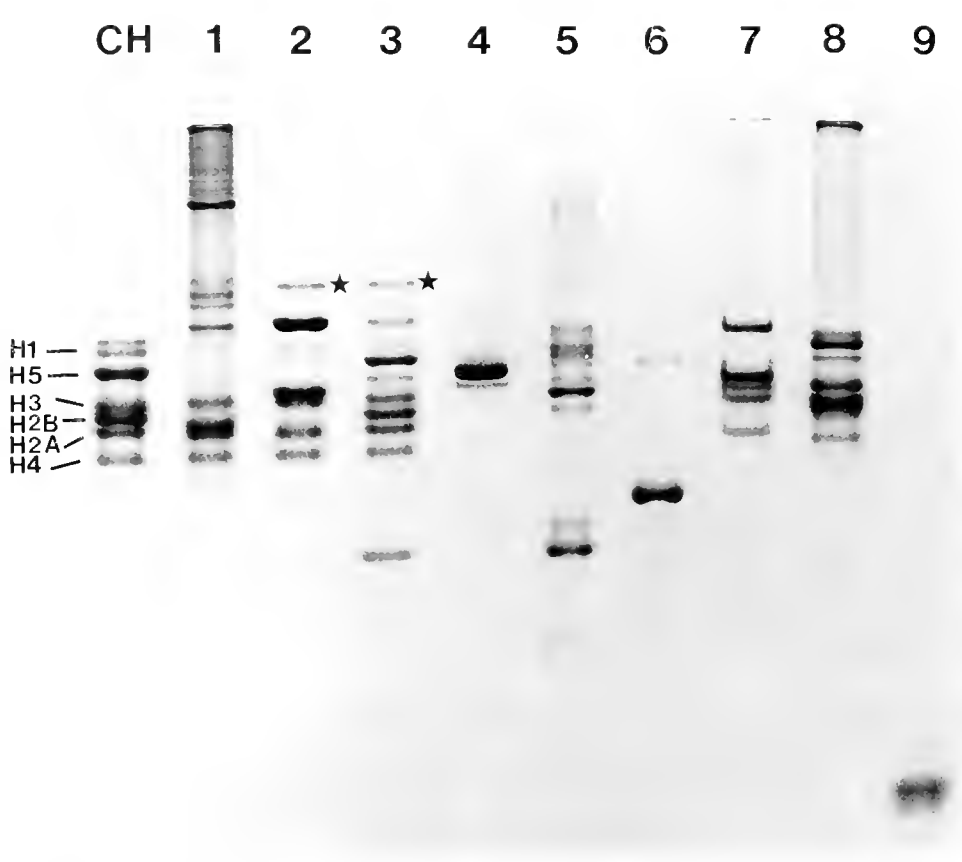

Figure 7. Acetic acid (5%)—urea (2.5 *M*) PAGE of whole nuclear protein extracts from the sperm of several groups of deuterostomes: CH. Chicken erythrocyte histones used as standard; (1) starfish *Psaster ochraceus*, (2) sea urchin *Strongylocentrotus purpuratus*, (3) sea cucumber *Thyone briareus*, (4) ascidian tunicate *Phallusia mammillata*. The proteins shown in this lane are a 0.4 *N* HCl protein extract from nuclei that had been previously treated with 35% acetic acid in order to remove the residual histones. (5) ascidian tunicate *Styela plicata*, (6) lancelet *Branchiostoma floridae*, (7) lamprey *Petromyzon marinus*, (8) fish *Trigla lucerna*; (9) commercial salmon fish protamine (salmine) *Onchorhyncus* sp. The asterisks (*) point to the histone H3-H3 dimers resulting from oxidation of the cysteine residues.

The only cephalochordate that has been characterized thus far from the point of view of its nuclear sperm proteins is that described in the present work. As has already been mentioned in the preceding section, the major nuclear protein of the sperm of *Branchiostoma floridae* is a protamine-like (PL) protein (Fig. 2, Fig. 7, lane 6). The amino acid composition of this protein (Table I) is different from that of fish protamines and from that of the smaller PL present in *Stylelidae*. [P2c (SP) in Table III.] It is very similar, however, to PL-III proteins (Ausió, 1986) from mollusks (Table I). In addition, the amino acid sequence of the first nine N-terminal amino acids (Fig. 2C) with its repetitive "RS" motif largely resembles the primary structure of the N-terminal regions of PL in mollusks (Daban, 1991; Carlos *et al.*, 1993), which also exhibit this kind of repetitive structure. An "RS" repetitive motif is also present in the N-terminal region of the bird protamines (Oliva and Dixon, 1989) and to a different extent is also present in other vertebrate protamines (Kasinsky, 1989; Oliva and Dixon, 1991).

From an evolutionary perspective (Fig. 8), the finding that somatic-like histones are present in the sperm of the agnathan *Petromyzon marinus* is quite unexpected. It is surprising, considering that substitution of histones by more specialized proteins (PL) has already been known to occur in tunicates and in cephalochordates as discussed above. Nevertheless, a similar situation is also found in teleost fish (see Fig. 8), where an apparently random distribution of histones, protamine-like, and protamine proteins is observed among different orders, families, and genera (Saperas *et al.*, 1993a, b).

We envisage two alternative possibilities to explain these observations. The first is that during the evolution of the sperm-specific proteins within the Subphylum Vertebrata (see Fig. 8A), histones represent the early proteins present in the nucleus of the sperm that, during the evolution of

Table III

Amino acid composition (mol %) of different nuclear sperm proteins: histone H1 from starfish Aphelasterias japonica *H1 (AJ) (Zalenskaya* et al., *1980), histone H1 from sea urchin* Parechinus angulosus *H1 (PA) (Brandt et al., 1979), PL(fo) protein from sea cucumber* Holothuria tubulosa *PL(fo) (HT) (Subirana, 1983), proteins P1, P2 from ascidian tunicate* Styela plicata *P1, $P2_c$ (SP) (Saperas* et al., *1992), protein PL from lancelet* Branchiostoma floridae *PL(BF) (this work), and the protamine salmine SL (SI) from* Salmo irideus *(Ando and Watanabe, 1969)*

	H1 (AJ)	H1 (PA)	$PL^{(fo)}$ (HT)	P1 (SP)	$P2_c$ (SP)	PL (BF)	SL (SI)
Lys	24.5	25.1	17.0	14.3	17.4	24.7	—
His	0.8	0.9	—	1.1	—	—	—
Arg	14.5	9.1	25.9	32.5	50.4	25.3	65.6
Asx	1.6	1.8	—	4.6	1.2	—	—
Thr	2.4	2.0	2.1	1.2	3.1	—	—
Ser	9.5	7.2	9.4	4.6	1.1	16.5	12.5
Glx	3.0	2.3	2.9	2.2	—	—	—
Pro	4.6	8.5	6.5	1.4	—	5.6	9.4
Gly	4.6	4.4	—	13.2	18.7	6.1	6.2
Ala	31.4	29.4	29.5	7.1	3.3	21.7	—
Cys	—	—	—	0.7	—	—	—
Val	1.7	4.0	5.0	4.6	—	—	6.2
Met	tr.	1.7	—	1.4	0.7	—	—
Ile	0.8	0.8	1.3	2.4	—	—	—
Leu	0.7	2.1	—	4.5	3.3	—	—
Tyr	tr.	0.8	—	2.2	0.7	—	—
Phe	tr.	0.4	—	2.2	—	—	—
Trp	—	—	—	—	—	—	—

tr: trace amounts.

this group, have been progressively replaced by more specialized proteins (protamine-like and protamines). Other subphyla such as Cephalochordata (lancelet) and Urochordata (tunicates) might have had different (although related) evolutionary pathways, and the histones in these later two groups might have been lost during the diversification of the Phyla Chordata and Echinodermata.

A second evolutionary alternative for the evolution of the chromosomal sperm proteins of deuterostomes is shown in Figure 8B. Accordingly, histones would have been replaced early by a protamine-like (PL) ancestor in chordates. This protein would have given origin to the PL proteins found in urochordates and in cephalochordates and maybe, to the fish protamines. In the lamprey the gene (or its expression) for such highly specialized chromosomal sperm proteins might have been lost. Obviously these are idealized models that represent two extreme alternatives that might be useful for the understanding of the evolutionary complexity of these proteins in deuterostomes. These hypotheses are difficult to test, especially if one considers the quickly changing ideas about evolution of deuterostomes (Stock and Whitt, 1992; Forey and Janvier, 1993; Conway Morris, 1993).

Despite all this, a quick inspection of Figure 8 reveals that the evolutionary trend in deuterostomes (thick arrow in Fig. 8) is to acquire highly specialized protamines (P) that replace the somatic-like histones. As discussed below, this might be closely related to the evolution of fertilization mechanisms in the deuterostomes (Kasinsky, 1989).

Shape of the sperm-nucleus and chromatin organization in Branchiostoma *and* Petromyzon: *further evolutionary considerations*

Figure 5 shows the morphology of the spermatozoa of two lampreys, *Petromyzon marinus* and *Lampetra planeri*. As mentioned previously, the morphology of the sperm of these closely related species is quite different despite the fact that both seem to have a very similar chromatin composition and organization. Furthermore, both organisms are anadromous and have external fertilization, although, as Jamieson (1991, p. 63) points out, in *P. marinus* "the cloacal tube (penis) of the male is fitted closely to the female pore and eggs are fertilized as they leave the body in what appears to be neither truly external nor internal fertilization (Breder and Rosen, 1966)." These observations seem to contradict (at least in this particular instance), the hypothesis that tries to correlate sperm shape with fertilization (internal *versus* external) (Baccetti and Afzelius, 1976; Jamieson, 1991). It also contradicts the hypothesis put forward by Nandi *et al.* (1979) that suggested that the protein composition of chromatin in the sperm (histones *versus* protamines) might depend on the physiochemical conditions (such as salinity) of the medium in which fertilization occurs. Considering that histones are the major protein constituents of the sperm chromatin in *Petromyzon marinus*, the structural organization of the 3-nm chromatin fibers in the mature sperm (as visualized in the electron microscope, Fig. 6, lane 2)

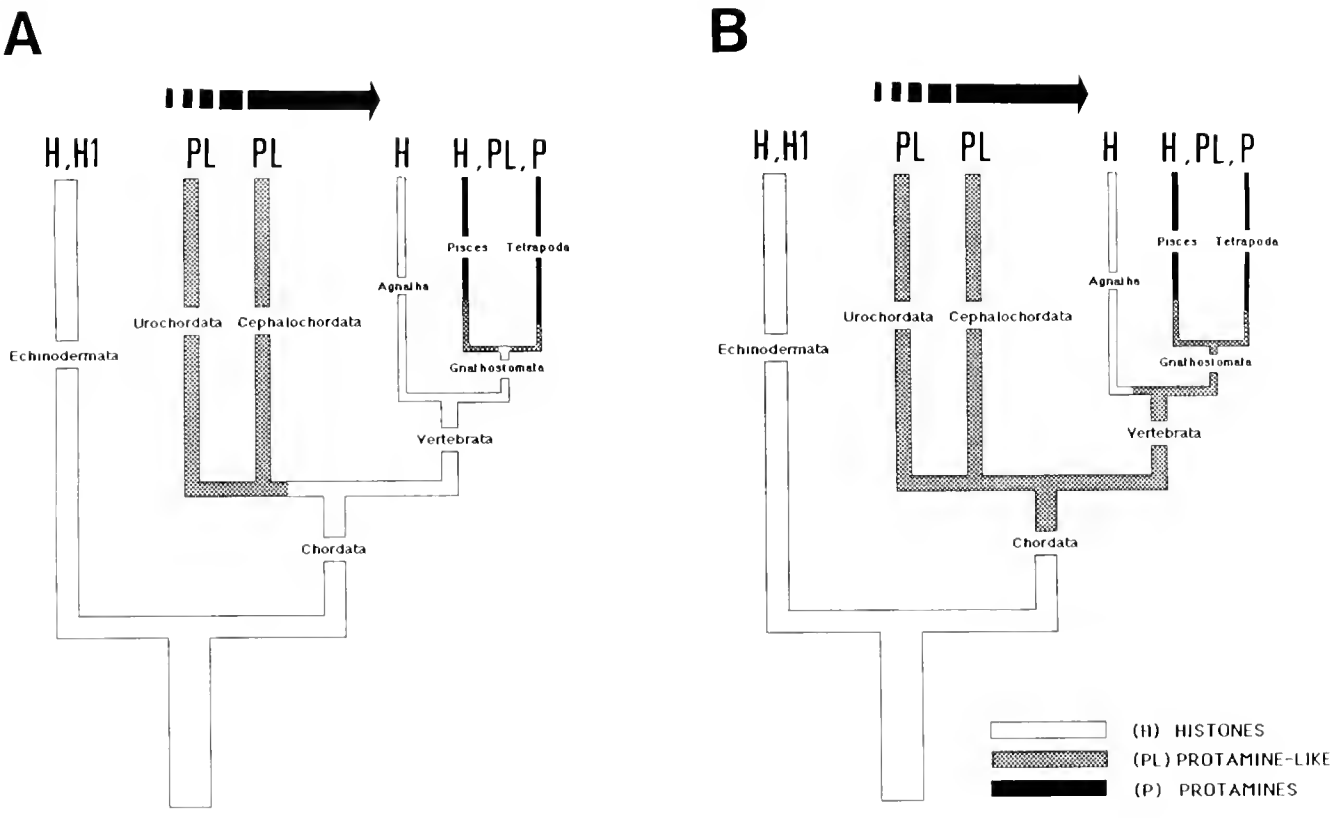

Figure 8. Schematic representation of the phylogenetic relationships of the main groups of deuterostomes, adapted from Stock and Whitt (1992) and from Brusca and Brusca (1990). H: mature sperm containing only histones; H1: mature sperm containing histones with a highly specialized histone H1; PL: mature sperm containing mainly intermediate protamine-like (PL) proteins. P: mature sperm containing protamines. The arrow indicates the progressive transition from the histone type (H) to the protamine type (P) as a result of evolution.

appears to be unique. Association of core histones (H2A, H2B, H3, and H4) with the DNA usually leads to chromatin fibers consisting of randomly spaced nucleosome particles of about 10 nm in diameter. In the presence of histones of the H1 family (that bind to the internucleosomal linker DNA), the fiber compacts into a higher order structure giving rise to fibers of about 30 nm in diameter (see Van Holde, 1988, for a review). Fibers of a similar diameter have also been observed in the chromatin of the sperm nucleus of different organisms containing histones or other sperm-specific proteins (Casas *et al.*, 1993).

The chromatin arrangement observed in *Petromyzon* is very similar to that recently described in the sperm of the fish *Mullus surmuletus* (Saperas *et al.*, 1993b). In the latter case, however, the protein composition of chromatin consists of only two PL proteins and no histones. Therefore, the finding of a 3-nm fiber in *Petromyzon* raises the very challenging possibility that histones could organize chromatin in alternative structures to nucleosomes. In the case of *Branchiostoma floridae*, the sperm shape (Fig. 5C) (Holland and Holland, 1989) is in good agreement with that of a primitive sperm (Baccetti and Afzelius, 1976). The organization of chromatin, as visualized by electron microscopy [Fig. 6(4)] (Holland and Holland, 1989), is similar to that observed in other invertebrate organisms with a similar protein composition (Longo and Dornfeld, 1967; Casas *et al.*, 1993).

Acknowledgments

We are very indebted to Dr. Linda Z. Holland from the Marine Biology Research Division at the Scripps Institution of Oceanography in La Jolla (CA) for providing us with the lancelet specimens and to Dr. Nicholas D. Holland for providing us with the electron micrographs shown in Figure 6(3, 4). We also would like to thank Dr. Mark Elliott and Mr. Richard Cheung for their assistance in obtaining lamprey material and Mr. David Kulak for skillful technical assistance. Finally, we would like to thank Ms. Corinne Rocchini for carefully reading the manuscript and Ms. Terrell Les Strange for typing the manuscript. This work was supported by grant PB 90-

0605 from the CICYT (Spain), by NSERC grant 585854 to Harold Kasinsky, by NSERC grant OGP5945 to John Youson, and by NSERC grant OGP 0046399 to Juan Ausió.

Literature Cited

Ando, T., and S. Watanabe. 1969. A new method for fractionation of protamines and the amino acid sequence of one component of salmine and three components of iridine. *Int. J. Protein Res.* **1:** 221–224.

Ausió, J. 1986. Structural variability and compositional homology of the protamine-like components of the sperm from bivalve mollusks. *Comp. Biochem. Physiol.* [*B*], **85:** 439–449.

Ausió, J. 1988. An unusual cysteine-containing histone H1-like protein and two protamine-like proteins are the major nuclear proteins of the sperm of the bivalve mollusc: *Macoma nasuta*. *J. Biol. Chem.* **263:** 10141–10150.

Ausió, J., and J. A. Subirana. 1982a. Conformational study and determination of the molecular weight of highly charged basic proteins by sedimentation equilibrium and gel electrophoresis. *Biochemistry* **21:** 5910–5918.

Ausió, J., and J. A. Subirana. 1982b. Nuclear proteins and the organization of chromatin in spermatozoa of *Mytilus edulis*. *Exp. Cell. Res.* **141:** 39–45.

Ausió, J., A. Toumadje, R. McParland, R. Becker, W. C. Johnson, Jr., and K. E. van Holde. 1987. Structural characterization of the trypsin-resistant core in the nuclear sperm-specific protein from *Spisula solidissima*. *Biochemistry* **26:** 975–982.

Baccetti, B., and B. A. Afzelius. 1976. The biology of the sperm cell. In: *Monographs in Developmental Biology*, Vol. 10, A. Wolsky, ed. S. Karger A. G., Basel, New York.

Bloch, D. P. 1969. A catalog of sperm histones. *Genetics (Suppl.)* **61:** 93–111.

Bloch, D. P. 1976. Histones of sperm. Pp. 139–149 in *Handbook of Genetics*, Vol 5, R. C. King, ed., Plenum Press, New York.

Bols, N. C., and H. E. Kasinsky. 1972. Basic protein composition of anuran sperm. A cytochemical study. *Can. J. Zool.* **50:** 171–177.

Bols, N. C., and H. E. Kasinsky. 1973. An electrophoretic comparison of histones in anuran testes. *Can. J. Zool.* **51:** 203–208.

Brandt, W. F., W. N. Strickland, M. Strickland, L. Carlisle, D. Woods, and C. von Holt. 1979. A histone programme during the life cycle of the sea urchin. *Eur. J. Biochem.* **94:** 1–7.

Breder, C. M., and D. E. Rosen. 1966. *Modes of Reproduction in Fishes.* The American Museum of Natural History. Natural History Press, New York.

Brusca, R. C., and G. J. Brusca. 1990. *Invertebrates.* Pp. 841–877. Sinauer Associates Inc., Sunderland, Massachusetts.

Carlos, S., L. Jutglar, J. L. Borrell, D. F. Hunt, and J. Ausio. 1993. Sequence and characterization of a sperm-specific histone H1-like protein of *Mytilus californianus*. *J. Biol. Chem.* **268:** 185–194.

Casas, M. T., J. Ausio, and J. A. Subirana. 1993. Chromatin fibers with different protamine and histone compositions. *Exp. Cell. Res.* **204:** 192–197.

Chiva, M., H. E. Kasinsky, and J. A. Subirana. 1987. Characterization of protamines from four avian species. *FEBS Lett.* **215:** 237–240.

Chiva, M., H. E. Kasinsky, M. Mann, and J. A. Subirana. 1988. On the diversity of sperm basic proteins in the vertebrates: VI. Cytochemical and biochemical analysis in birds. *J. Exp. Zool.* **245:** 304–317.

Chiva, M., D. Kolak, and H. E. Kasinsky. 1989. Sperm basic proteins in the turtle *Chrysemis picta*: Characterization and evolutionary implications. *J. Exp. Zool.* **249:** 329–333.

Chiva, M., F. Lafargoe, E. Rosenberg, and H. E. Kasinsky. 1992. Protamines, not histones, are the predominant basic proteins in sperm nuclei of solitary ascidian tunicates. *J. Exp. Zool.* **263:** 338–349.

Chiva, M., E. Rosenberg, and H. E. Kasinsky. 1990. Nuclear basic proteins in mature testis of the ascidian tunicate *Styela montereyensis*. *J. Exp. Zool* **253:** 7–19.

Colom, J., and J. A. Subirana. 1979. Protamines and related proteins from spermatozoa of molluscs: characterization and molecular weight determination by gel electrophoresis. *Biochim. Biophys. Acta* **581:** 217–227.

Conway Morris, S. 1993. The fossil record and the early evolution of the Metazoa. *Nature* **361:** 219–225.

Daban, M. 1991. Protamines de mol·luscs gastròpodes i poliplacòfors. Caracterització i implicacions evolutives. Ph. D. Thesis. E.T.S.E.I.B.—U.P.C., Barcelona.

Daban, M., M. Chiva, E. Rosenberg, H. E. Kasinsky, and J. A. Subirana. 1991. Protamines in prosobranchian gastropods (Mollusca) vary with different modes of reproduction. *J. Exp. Zool.* **257:** 265–283.

Dixon, G. H., J. M. Aiken, J. M. Jankowski, D. I. McKenzie, R. Moir, R., and J. C. States. 1985. Organization and evolution of the protamine genes of salmonid fishes. In *Chromosomal Proteins and Gene Expression*, G. R. Reeck, G. A. Goodwin, and P. Puigdomènech, eds. Plenum Press, New York, NATO ASI Series, Series A: *Life Sciences* **101:** 287–314.

Forey, P., and P. Janvier. 1993. Agnathans and the origin of jawed vertebrates. *Nature* **361:** 129–134.

Giancotti, V., F. Quadrifoglio, M. Lancieri, and G. Geraci. 1980. Separation and properties of an H2B histone variant from the sperm chromatin of the sea urchin *Sphaerechinus granularis*. *Int. J. Biol. Macromol.* **2:** 309–312.

Holland, N. D., and L. Z. Holland. 1989. The fine structure of the testis of a lancelet (=Amphioxus), *Branchiostoma floridae* (Phylum Chordata: Subphylum Cephalochordata = Acrania). *Acta Zool.* **70:** 211–219.

Imschenetzky, M., M. Puchi, A. M. Oyarre, R. Massone, and D. Inostroza. 1984. A comparative study of the histones isolated from sperm of the sea urchin, *Tetrapygus niger*. *Comp. Biochem. Physiol.* **78B:** 393–399.

Jamieson, B. G. M. 1991. *Fish Evolution and Systematics: Evidence from Spermatozoa. With a Survey of Lophophorate, Echinoderm and Protochordate Sperm and an Account of Gamete Cryopreservation.* Cambridge University Press, Cambridge.

Jamieson, B. G. M. 1984. Spermatozoal ultrastructure in *Branchiostoma moretonensis* Kelly, a comparison with *B. lanceolatum* (Cephalochordata) and with other deuterostomes. *Zool. Scr.* **13:** 223–229.

Jotglar, L., J. I. Borrell, and J. Ausió. 1991. Primary, secondary and tertiary structure of the core of a histone H1-like protein from the sperm of *Mytilus*. *J. Biol. Chem.* **266:** 8184–8191.

Kasinsky, H. E. 1989. Specificity and distribution of sperm basic proteins. Pp. 73–163 in *Histones and Other Basic Nuclear Proteins*, L. S. Hnilica, G. S. Stein, and J. L. Stein, eds. CRC Press, Boca Raton, Florida.

Kasinsky, H. E., S. Y. Huang, S. Kwauk, M. Mann, M. J. Sweeney, and B. Yee. 1978. On the diversity of sperm histones in the vertebrates. III. Electrophoretic variability of the testis-specific histones patterns in Anura contrasts with relative constancy in Squamata. *J. Exp. Zool* **203:** 109–126.

Kasinsky, H. E., S. Y. Huang, M. Mann, J. Roca, and J. A. Subirana. 1985. On the diversity of sperm histones in the vertebrates. IV. Cytochemical and amino acid analysis in Anura. *J. Exp. Zool.* **234:** 33–46.

Kasinsky, H. E., M. Mann, S. Y. Huang, L. Fabre, B. Coyle, and E. W. Byrd, Jr. 1987. On the diversity of sperm basic proteins in the

vertebrates. V. Cytochemical and amino acid analysis in Squamata, Testudines and Crocodylia. *J. Exp. Zool.* **247:** 137–151.

Klyszejko-Stefanowicz, L., W. M. Krajewska, and A. Lipinska. 1989. Histone occurrence, isolation, characterization and biosynthesis. Pp. 17–71 in *Histones and Other Basic Nuclear Proteins,* L. S. Hnilica, G. S. Stein, and J. L. Stein, eds. CRC Press, Boca Raton, Florida.

Kossel, A. 1928. *The Protamines and Histones* Longmans Green and Co., London.

Kuehl, J. 1979. Synthesis of high mobility group proteins in regenerating rat liver. *J. Biol. Chem* **254:** 7276–7281.

Longo, F. J., and E. J. Dornfeld. 1967. The fine structure of spermatid differentiation in the mussel, *Mytilus edulis. J. Ultrastr. Res.* **20:** 462–480.

Mann, M. 1981. Variability of sperm histones in Anura contrasts with relative constancy in Urodela, Squamata and Aves. M.Sc. Thesis, University of British Columbia, Vancouver.

Mann, M., M. S. Risley, R. A. Eckhardt, and H. E. Kasinsky. 1982. Characterization of spermatid/sperm basic chromosomal proteins in the genus *Xenopus* (Anura, Pipidae). *J. Exp. Zool.* **222:** 173–186.

Mayes, E. L. V., and E. W. Johns. 1982. Accumulated data. Pp. 223–247 in *The HMG Chromosomal Proteins,* E. W. Johns, ed. Academic Press, New York.

Miescher, F. 1874. Das Protamin, eine neue organische Base aus den Samenfädes des Rheinlachses. *Berichte* **7:** 376–379.

Mogensen, C., S. Carlos, and J. Ausio. 1991. Microheterogeneity and interspecific variability of the nuclear sperm proteins from *Mytilus. FEBS Lett.* **282:** 273–276.

Muñoz-Guerra, S., J. Colom, J. Ausió, and J. A. Subirana. 1982a. Histones from spermatozoa of the horseshoe crab. *Biochem. Biophys. Acta* **697:** 305–312.

Muñoz-Guerra, S., F. Azorin, M. T. Casas, X. Marcet, M. A. Maristany, J. Roca, and J. A. Subirana. 1982b. Structural organization of sperm chromatin from the fish *Carassius auratus. Exp. Cell Res.* **137:** 47–53.

Nandi, A. K., A. Chaudhuri, and R. K. Mandal. 1979. Nature and evolutionary significance of basic proteins in fish spermatozoa. *Indian J. Biochem. Biophys* **16:** 6–10.

Oliva, R., and G. H. Dixon. 1989. Chicken protamine genes are intronless. The complete genomic sequence and organization of the two loci. *J. Biol. Chem.* **264:** 12472–12481.

Oliva, R., and G. H. Dixon. 1991. Vertebrate protamine genes and the histone-to-protamine replacement reaction. *Prog. Nucl. Acid Res. Mol. Biol.* **40:** 25–94.

Phelan, J. J., J. A. Subirana, and R. D. Cole. 1972. An unusual group of lysine-rich histones from gonads of a sea cucumber, *Holothuria tubulosa. Eur. J. Biochem.* **31:** 63–68.

Poccia, D. L. 1991. Sp histones and chromatin structure in male germ line nuclei and male pronuclei of the sea urchin. Pp. 61–65 in *Comparative Spermatology 20 Years After, Vol 75,* B. Baccetti, ed. Serono Symposia Publications from Raven Press, New York.

Prats, E., L. Cornudella, and A. Ruiz-Carrillo. 1989. Nucleotide sequence of a c-DNA for ϕ_0, a histone to protamine transition protein from sea cucumber spermatozoa. *Nucl. Acids Res.* **17:** 10097.

Saperas, N., M. Chiva, and J. Ausio. 1992. Purification and characterization of the protamines and related proteins from the sperm of a tunicate, *Styela plicata. Comp. Biochem. Physiol* **103-B:** 969–974.

Saperas, N., D. Lloris, and M. Chiva. 1993a. Sporadic appearance of histones, H1-related proteins and protamines in sperm chromatin of bony fish. *J. Exp. Zool.* **265:** 575–586.

Saperas, N., E. Ribes, C. Buesa, F. Garcia-Hegardt, and M. Chiva. 1993b. Differences in chromatin condensation during spermiogenesis in two species of fish with distinct protamines. *J. Exp. Zool.* **265:** 185–194.

Stanley, H. P. 1967. The fine structure of spermatozoa in the lamprey *Lampetra planeri. J. Ultrastr. Res.* **19:** 84–99.

Stock, D. W., and G. S. Whitt. 1992. Evidence from 18S ribosomal RNA sequences that lampreys and hagfishes form a natural group. *Science* **257:** 787–789.

Strickland, M., W. N. Strickland, W. Brandt, and C. von Holt. 1977. The complete amino-acid sequence of histone H2B(1) from sperm of the sea urchin *Parechinus angulosus. Eur. J. Biochem* **77:** 263–275.

Strickland, M., W. N. Strickland, W. Brandt, C. von Holt, B. Wittmann-Liebold, and A. Lehmann. 1978. The complete amino-acid sequence of histone H2B(3) from sperm of the sea urchin *Parechinus angulosus. Eur. J. Biochem* **89:** 443–452.

Strickland, M., W. N. Strickland, and C. von Holt. 1980. The histone H2B from the sperm cell of the starfish *Marthasterias glacialis. Eur J. Biochem* **106:** 541–548.

Strickland, W. N., M. Strickland, W. Brandt, and C. von Holt. 1977. The complete amino-acid sequence of histone H2B(2) from sperm of the sea urchin *Parechinus angulosus. Eur. J. Biochem* **77:** 277–286.

Strickland, W. N., M. Strickland, W. F. Brandt, C. von Holt, A. Lehmann, and B. Wittmann-Liebold. 1980a. The primary structure of histone H1 from sperm of the sea urchin *Parechinus angulosus.* 2. Sequence of the C-terminal CNBr peptide and the entire primary structure. *Eur. J. Biochem* **104:** 567–578.

Strickland, W. N., M. Strickland, P. DeGroot, C. von Holt, and B. Wittmann-Liebold. 1980b. The primary structure of histone H1 from sperm of the sea urchin *Parechinus angulosus. Eur. J. Biochem.* **104:** 559–566.

Strickland, W. N., M. Strickland, and C. von Holt. 1982a. A comparison of the amino acid sequences of histones H1 from the sperm of *Echinolampas crassa* and *Parechinus angulosus. Biochim. Biophys. Acta* **700:** 127–129.

Strickland, W. N., M. Strickland, C. von Holt, and V. Giancotti. 1982b. A partial structure of histone H1 from sperm of the sea urchin *Sphaerechinus granulosus. Biochim. Biophys. Acta* **703:** 95–100.

Subirana, J. A. 1970. Nuclear protein from a somatic and germinal tissue of the echinoderm *Holothuria tubulosa. Exp. Cell Res.* **63:** 253–260.

Subirana, J. A. 1983. Nuclear proteins in spermatozoa and their interactions with DNA. Pp. 197–214 in *The Sperm Cell,* J. André, ed., Martinus Nijhoff., The Hague.

Subirana, J. A., and J. Palau. 1968. Histone-like proteins from the sperm of echinoderms. *Exp. Cell Res.* **53:** 471–477.

Takamune, K., H. Nishida, M. Takai, and C. Katagiri. 1991. Primary structure of toad sperm protamines and nucleotide sequence of their cDNAs. *Eur. J. Biochem.* **196:** 401–406.

Van Holde, K. E. 1988. *Chromatin.* Springer-Verlag, Berlin, New York.

von Holt, C., P. de Groot, S. Schwager, and W. F. Brandt. 1984. The structure of sea urchin histones and consideration of their function. Pp. 65–105 in *Histone Genes. Structure, Organization and Regulation,* G. S. Stein, J. L. Stein, and W. F. Marzluff, eds. John Wiley, New York.

Zalenskaya, I. A., and A. O. Zalensky. 1980. Basic chromosomal proteins of marine invertebrates—I. Sperm histones of nine sea urchin species. *Comp. Biochem. Physiol.* **65B:** 369–373.

Zalenskaya, I. A., E. O. Zalenskaya, and A. O. Zalensky. 1980. Basic chromosomal proteins of marine invertebrates II. Starfish and holothuria. *Comp. Biochem. Physiol* **65B:** 375–378.

Reference: *Biol. Bull.* **186**: 115–123. (February, 1994)

Occurrence and Distribution of RFamide-Positive Neurons Within the Polyps of *Coryne* sp. (Hydrozoa, Corynidae)

RAINER GOLZ

Institut für Neuro- und Verhaltensbiologie, Universität Münster, Germany

Abstract. The neuronal network of the hydrozoan polyp *Coryne* sp. contains RFamide-positive neurons. Within the body column, these neurons are centralized in a basal ring and a distal field of ganglionic cells surrounding the peristome. The capitate tentacles are traversed by thick RFamide-positive neurites. Their pericarya are centralized in the knobby heads of the tentacles, forming a brightly fluorescing plaque after immunolabeling with an antibody against the RFamide sequence. Numerous dendrite-like extensions project from these cells towards the cell bodies of the nematocytes. The possible role of these dendrites in communication between adjacent nematocytes is discussed.

Introduction

Cnidarian nematocytes are both sensory and effector cells that respond to adequate external stimulation with the discharge of their nematocysts. This extremely rapid, specialized exocytotic process is triggered by a combination of mechanical and chemical stimuli: a deflection or shift of the cnidocil within its stereovillar support has to be preceded or at least accompanied by the chemical stimulus (Pantin, 1942; Thurm and Lawonn, 1990; Brinkmann and Thurm, 1993).

Physiological experiments and *in vivo* observations of hydrozoan polyps—in most instances made on *Hydra*—revealed that the nematocytes of two individual polyps and even different nematocytes of the same polyp may respond to identical external stimulation with great statistical divergence, indicating the influence of additional external or intrinsic factors. Nematocyst discharge, for example, is affected by the duration of starvation, the contraction/relaxation state of the animal, or environmental conditions (Jones, 1947; Kass-Simon, 1988). Although some of these stimuli may be received by the nematocytes themselves or by adjacent epitheliomuscular cells (Watson and Hessinger, 1989), others are obviously acting on specialized sensory cells (Tardent and Schmid, 1972; Westfall and Kinnamon, 1978; Kinnamon and Westfall, 1982; Westfall and Rogers, 1990; Westfall *et al.*, 1991; Golz and Thurm, 1991, 1993).

Summation and integration of some of these sensory inputs are managed by a net of neurons (Josephson, 1974). The phylogenetically primitive nervous system consists of at least three types of neuronal cells: sensory cells, ganglionic cells, and morphologically distinguishable interneurons (Tardent and Weber, 1976). However, this strict classification has to be used carefully since one and the same neuronal cell may simultaneously be used for all three tasks (Westfall, 1973). The loosely organized neurons are interconnected to a functional network by mono- or bidirectional synapses (Westfall, 1970; Westfall *et al.*, 1971; Westfall and Kinnamon, 1984).

All neurons are located in the interstitial spaces of the epithelial cell layers. Although the sensory cells are usually arranged perpendicular to the mesoglea, most of the other neuronal cell types are situated parallel to it (*e.g.*, Westfall, 1988; Hobmayer *et al.*, 1990). Neurons and non-neuronal cells are in close spatial contact. They are functionally coupled by chemical synapses (Westfall and Kinnamon, 1984; Westfall, 1988). Thus, the occurrence of synapses between neurons and nematocytes (Westfall and Kinnamon, 1984) may indicate an efferent control of the nematocytes. To prove this assumption directly by electrophysiological measurements, our group established a new

Received 27 July 1993; accepted 29 November 1993.

Address for correspondence: Institut für Neuro- und Verhaltensbiologie, Westfälische Wilhelms-Universität, Badestr. 9, 48149 Münster, Germany.

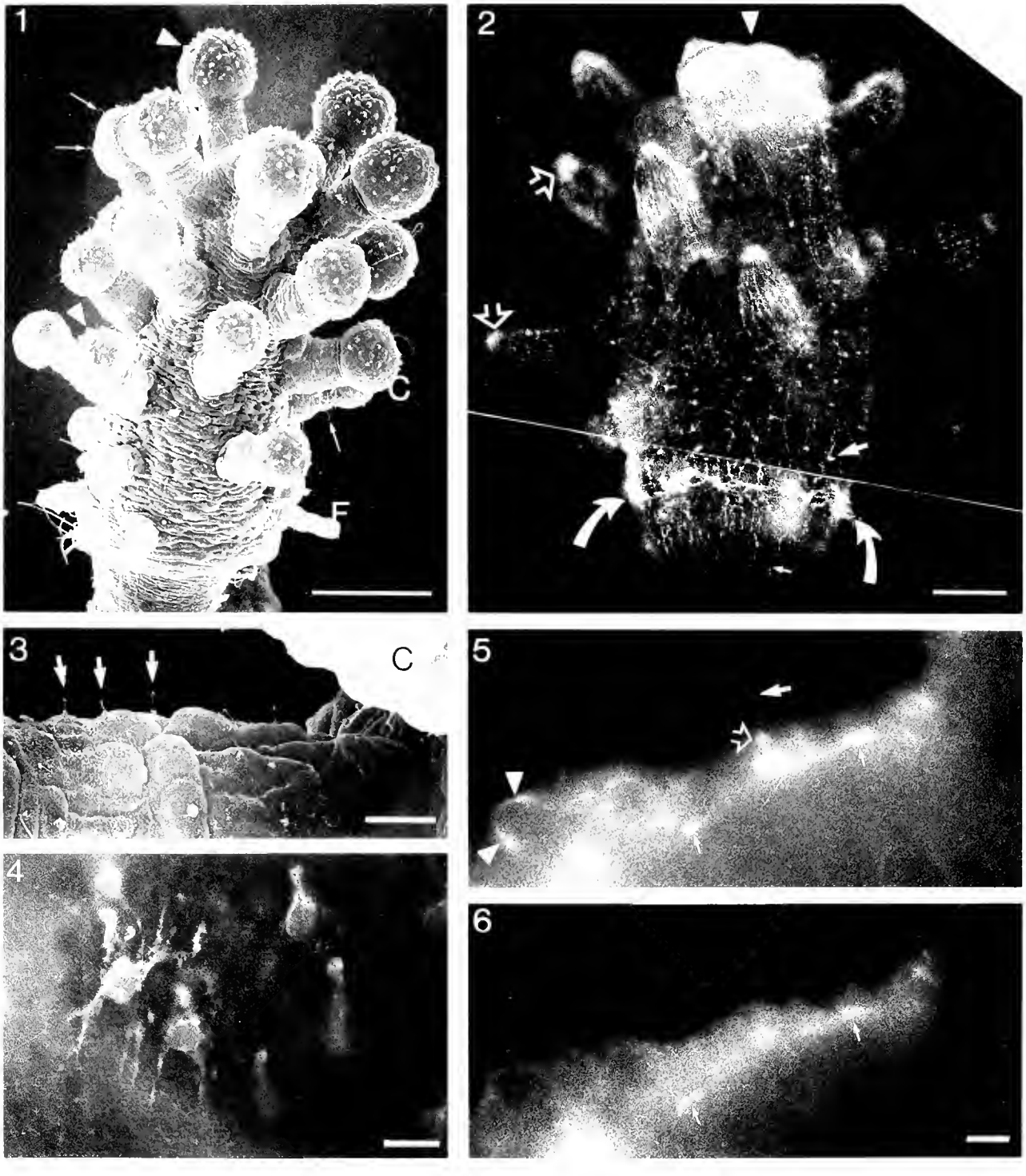

Figure 1. Scanning electron micrograph of *Corymc* sp. The body column of the polyp bears a whorl of filiform tentacles (F) and numerous capitate tentacles (C). Cnidocil complexes of nematocytes are marked by arrowheads; cilia of mechanosensory cells are labeled by arrows. Bar = 100 μm.

Figure 2. Fluorescence microscopical survey of *Corymc* labeled with anti-RFamide. A basal nerve ring (bent arrows), the heads of the capitate tentacles (open arrows), and a field of ganglionic cells around the peristome (arrowhead, cf. Fig. 4) are labeled. From the nerve ring some neurites (small arrow) branch off towards the stolon. Bright spots indicate the cell body of the neurons (arrow). Bar = 100 μm.

Figure 3. Scanning electron micrograph of a filiform tentacle. The cilia of the mechanosensory cells are marked by arrows. C = capitate tentacle of the next whorl. Bar = 10 μm.

model system: the marine hydrozoon *Coryne* sp. (Brinkmann and Thurm, 1991, 1993).

Like its close relative *Coryne pintneri* (*cf.* Stoessel and Tardent, 1971) *Coryne* sp. has hydranths that are characterized by a whorl of filiform tentacles and several rings of capitate tentacles. The latter are structurally differentiated into a short, contractile stalk and a knobby head containing many stenotele nematocytes.

The nematocytes of *Coryne* are amenable to intracellular electrophysiological recordings (Brinkmann and Thurm, 1993). To facilitate the interpretation of electrophysiological data, we started a parallel investigation of the neuronal organization of *Coryne* sp. by means of electron and fluorescence microscopy. To visualize the distribution of neurons, we used an antibody against neuropeptides of the RFamide type. Antibodies against the amidated carboxyterminus of these transmitter substances were produced by Grimmelikhuijzen and coworkers and have been successfully used for the study of cnidarian nervous systems by immunofluorescence and immunocytochemistry (for review see Grimmelikhuijzen *et al.*, 1991).

Materials and Methods

Coryne sp. was cultivated at the Zoological Institute of Münster in artificial seawater at about 14°C. The polyps were fed once a week with freshly hatched brine shrimps. All specimens are descendents of a single colony obtained from the Biological Station of Helgoland.

For electron microscopy, polyps were cut off from their stolons and transferred into artificial, calcium-free seawater supplemented up to 90 m*M* with $MgCl_2$ to prevent fixation-induced contractions. The polyps were fixed with 5% glutaraldehyde, 2% formaldehyde, 10% DMSO, 5 m*M* EGTA, 0.5% tannic acid in 0.1 *M* Na-cacodylate buffer (pH 7.4) for 30 min. The specimens were rinsed with 50 m*M* Na-cacodylate buffer (pH 7.4) and subsequently washed with the same buffer at pH 6.0. After postfixation with 5% tannic acid, 0.5% glutaraldehyde in 50 m*M* Na-cacodylate buffer (pH 6.0) for 15 min, the specimens were rinsed and stained with 1% OsO_4, 0.025% ruthenium red in 50 m*M* Na-cacodylate buffer (pH 6.0) for 5 min. During dehydration in a graded series of ethanol, the specimens were stained for 15 min by exposure to 1% uranyl acetate in 70% ethanol. The specimens were embedded in Spurr's resin following standard procedures. Ultrathin sections were made with a diamond knife on a MT 7000 microtome (Microm), poststained with lead citrate, and examined in a Philips EM 201.

Specimens used for scanning electron microscopy were fixed and dehydrated as described above. Then, the specimens were critical-point dried with carbon dioxide, sputtered with gold, and examined in a Hitachi EM S-530 at 25 kV.

For indirect immunofluorescence, the specimens were prepared using a procedure modified from Grimmelikhuijzen (1985). Polyps were fixed with 4% freshly prepared formaldehyde in phosphate buffered saline (PBS) for at least 12 h at 4°C. Then, the specimens were washed with PBS, incubated with 0.25% Triton X-100 in PBS for about 1 h, briefly washed with PBS, and rinsed with 0.4 *M* glycine, 1% goat normal serum in PBS for at least 4 h. The specimens were incubated at 4°C for about 12 h with the anti-RFamide antiserum 146III (kindly provided by Dr. Grimmelikhuijzen, Hamburg) diluted 1:100 with PBS. In double-labeling experiments, this solution was supplemented with a monoclonal antibody against β-tubulin (Sigma Chem.). After a short rinse with PBS, the specimens were washed with 0.4 *M* glycine, 1% goat normal serum in PBS for about 1 h. The binding of the RFamide-antibody was detected by labeling with FITC-conjugated anti-rabbit-IgG. The distribution of β-tubulin was viewed by labeling with TRITC-conjugated anti-mouse-IgG.

The specimens were examined in an Olympus IMT-microscope using 40×/0.5 or 60×/1.4-optics. Photographs of fluorescing specimens were made on TMAX-100 film exposed and developed as a 400-ASA film.

Results

In *Coryne* sp., the four filiform tentacles within the proximal whorl lack any nematocytes but contain numerous ciliated sensory cells (Figs. 1, 3). The number of whorls formed by capitate tentacles depends on the age of the polyps and reaches from one in newly outgrown animals to up to seven in older polyps. The knobby heads of these tentacles measure about 50 μm in diameter and contain numerous stenotele nematocytes (Figs. 1, 9) which are predominantly located within the upper two-thirds of the heads. Ciliated sensory cells of the same type as those of the filiform tentacles are not only integrated in the

Figure 4. Ganglionic cells stained by anti-RFamide. A group of these cells surround the peristom in a broad belt-like arrangement. Bar = 10 μm.

Figures 5–6. Double-labeled sensory cell in the stalk of a capitate tentacle. The antibody against β-tubulin stains the axoneme of the modified, immotile cilium (arrow in Fig. 5) and the microtubular cytoskeleton (open arrow) of the cell. The fluorescing microtubular basket of a nematocyte is marked by arrowheads. Some neurites (small arrows) are clearly visible. Only these are additionally stained by the anti-RFamide serum (small arrows in Fig. 6). Bar = 10 μm.

ectoderm of the stalks but also located between the nematocytes.

By incubation with the antibody against the RFamide, the polyps of *Coryne* sp. become intensely labeled, indicating the occurrence of RFamide-positive cells within their neuronal networks. Fluorescence microscopical surveys reveal the organization of this network (Fig. 2). The main part of the body column is covered by thin, brightly fluorescing strands that are only loosely interconnected by anastomosing fibers. Intensely fluorescing spots mark the pericarya of the neurons (arrows in Fig. 2). Two regions of the neuronal network are characteristically modified: a ring-like concentration of neurons surrounds the body column at the same level as the filiform tentacles; and groups of RFamide-positive cells are concentrated within the heads of the capitate tentacles. A brightly fluorescing patch around the peristome is formed by ganglionic cells (Figs. 2, 4). As indicated by double-labeling experiments with anti-tubulin and anti-RFamide, the sensory cells within the filiform tentacles do not contain RFamide-like peptides (Figs. 5, 6).

A great number of neurites within the body column originate from the basal nerve ring. From these nerve cells, thin neurites branch off towards the stolon and the peristome. Most of the basally directed neurites seem to terminate at the transition zone between body column and stolon, but a few neurones penetrate into the stolon (Fig. 2). However, the occurrence and distribution of RFamide-positive neurons within the stolons is difficult to determine by immunofluorescence, because the peridermal sheet not only hinders the penetration of antibodies into the tissue, but additionally complicates observations due to its autofluorescence. The distally oriented neurites participate in the formation of the neuronal network interconnecting its distal parts with the basal neuronal ring.

Numerous RFamide-positive cells elongate into the capitate tentacles. Immunofluorescence in the tentacles appears as arrays of thick (2–3 μm) fluorescent strands interspersed with occasional thinner ones (Fig. 7). Focus series revealed that the neurons are restricted to the ectodermal cell layer. The neuronal strands are situated immediately adjacent to the mesoglea. From these neurons only a few dendrite-like extensions project towards the surface of the stalks. However, these projections never correspond with the cytoplasm of the ectodermal ciliated sensory cells that are not stained by the antibody.

The pericarya of the nerve cells are concentrated within the center of the knobby heads (Fig. 8). Their intense fluorescence complicates the detection of subcellular details, but many thin dendrite-like extensions that grow out from the centralized cell bodies are clearly distinguishable from this background. A comparison of micrographs obtained by Nomarski interference contrast optics and fluorescence optics (Figs. 9, 10), reveals that the dendritic extensions project through the voluminous intercellular lumina towards the periphery of the ectodermal cell layer. Most of the dendrite-like extensions terminate near or at the cell bodies of the nematocytes, which themselves are not stained by the anti-RFamide. The second mechanosensitive cell type within the capitate tentacles, the sensory cells, are also not stained by this antibody, thus resembling their counterparts in the filiform tentacles.

Electron microscopical investigations confirmed that the capitate tentacles of *Coryne* sp. contain parallel bundles of neurons (Figs. 11, 12). These bundles are often composed of a central, thick neurite that is accompanied by a few thinner neurites. In cross-sections the thick neurites frequently appear to be encircled by thin protrusions of non-neuronal cells (Fig. 12). The protrusions contain myofilaments, an indication that they are formed by epitheliomuscular cells. Only the neurites are characterized by bundles of microtubules and contain aggregates of dense-cored vesicles with diameters of about 120 nm (Fig. 13). Besides the neurites, no other cellular compartments of the ectodermal cell layer contain similar amounts of microtubules. Thus, the fluorescence microscopical presentation of polymerized tubulin should reflect the distribution of neuronal cells within the tentacles of *Coryne*. By comparing this fluorescence pattern with the pattern obtained by the RFamide-antibody, the occurrence of neurons lacking RFamide-like peptides was investigated.

Double immunofluorescence experiments with anti-β-tubulin and anti-RFamide revealed that both antibodies produce identical staining patterns within the stalk of the tentacles (*cf.* Figs. 14, 15; 18, 19; and 20, 21) and within the filiform tentacles (*cf.* Figs. 16, 17). In the knob-like heads of the capitate tentacles, anti-β-tubulin additionally labels the microtubular cytoskeleton of the nematocytes. However, all neuron-shaped cells that are stained by the antibody against β-tubulin are simultaneously labeled by the anti-RFamide immunoglobulins. The only neuronal cells that contain a prominent microtubular cytoskeleton but lack RFamide-like immunoreactivity are the sensory cells of the filiform and capitate tentacles. Thus, the double-labeling experiments indicate that most of the neurons within the tentacles of *Coryne* sp. use RFamide-like peptides as neurotransmitters.

Discussion

RFamide-positive neurons have been identified in both polyps and medusae of numerous cnidarian organisms. Fluorescence microscopy has been used to examine the staining produced by specific antibodies against the carboxyterminus of RFamide-like neuropeptides and to demonstrate, thereby, the organization and development of the neuronal network in anthozoans (Grimmelikhuijzen *et al.*, 1989), scyphozoans (Anderson *et al.*, 1992)

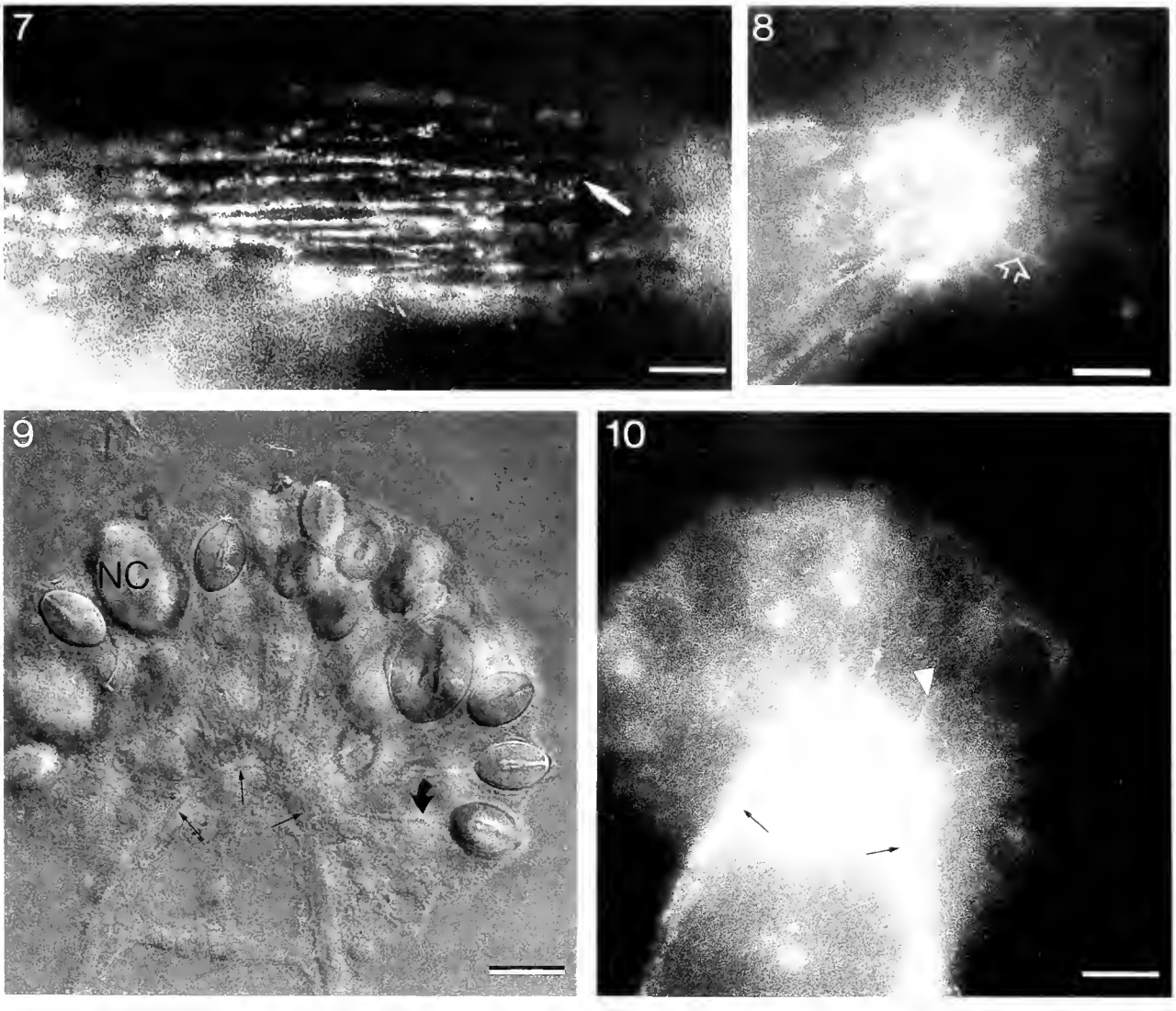

Figure 7. Stalk of a capitate tentacle. Thick parallel RFamide-positive neurites are linked by thin neurites (arrow). Bar = 20 μm.

Figure 8. Head of a capitate tentacle focused on the mesoglea. The pericaryons of the neurites are centralized in the center of the heads. Thin dendritic protrusions (arrowhead) project towards the surface of the tentacle. Bar = 20 μm.

Figures 9–10. Nomarski interference contrast (Fig. 9) and fluorescence image (Fig. 10) of a capitate tentacle. The nematocytes (NC) are anchored at the mesoglea (small arrows) by thin, noncontractile stalks (bent arrow). Nematocytes and sensory cells are not labeled by the antibody against RFamides. RFamide-positive dendrites (arrowhead) terminate at the nematocytes. Bars = 20 μm.

and hydrozoans (Grimmelikhuijzen, 1985; for review see Grimmelikhuijzen *et al.*, 1991).

Although the occurrence of RFamide-like neuropeptides within the cnidarian nervous system is so far widely accepted, the use of nonpeptidic transmitters by cnidarians is still controversially discussed. Morphological, biochemical, and physiological data indicate that at least catecholamines may be additional candidates for neurotransmission (Wood and Lentz, 1964; Martin and Spencer, 1983; Kolberg and Martin, 1988; Takeda and Svendsen, 1991; Carlberg, 1992), but the cellular localization and distribution of these substances within the epithelial tissues and the neuronal network must be clarified more precisely.

In the present work, the antiserum 146III against RFamides, which was produced by Grimmelikhuijzen and coworkers (for details see Grimmelikhuijzen, 1985), was shown to label the neuronal network of the hydrozoan polyp *Coryne* sp. Because the double-labeling experiments with anti-β-tubulin revealed that most of the

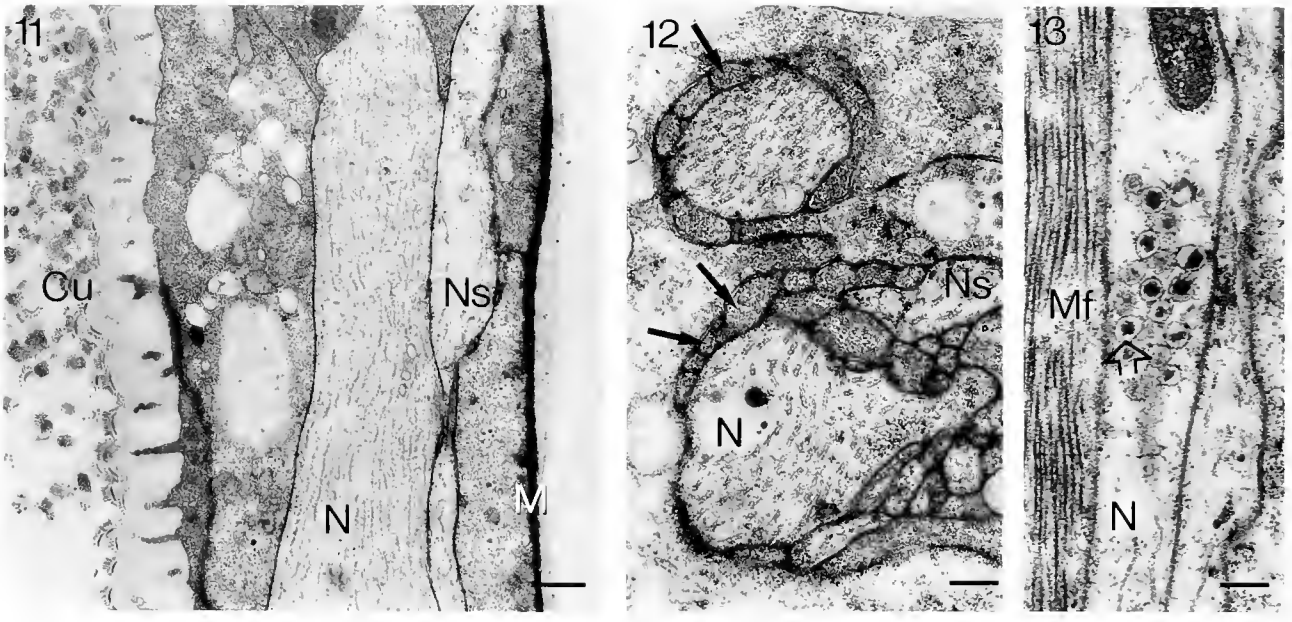

Figures 11–13. Ultrathin sections of neurites within the stalk. Thick neurites (N) are frequently accompanied by thinner neurites (Ns). All neurites are filled with densely packed microtubules. The thick nerve cells are often enclosed by thin non-neuronal protrusions (arrows in Fig. 12). Myofibrils of the epitheliomuscular cells are marked by Mf. The neurites contain dense-cored vesicles with diameters of approximately 120 nm (open arrow in Fig. 13). M = mesoglea, Cu = cuticula-like sheet around the tentacle. Bar in Figure 11 = 500 nm; in Figures 12 and 13 = 200 nm.

light microscopically detectable neurites are RFamide-positive cells, the obtained fluorescence patterns are thought to reflect the main portion of the neuronal system in *Coryne*.

The neuronal organization of *Coryne* closely resembles the neuronal networks of other hydrozoan polyps but also shows some specific structural adaptations. Prominent nerve rings like, for example, the basal one observed in *Coryne*, have been described for *Hydra oligactis*. In this organism, a prominent RFamide-positive nerve ring is located at the transition zone between body column and peristome (Grimmelikhuijzen, 1985; Koizumi *et al.*, 1992). Those regions of the body column from which whorls of tentacles emerge appear to be favored in the formation of nervous rings not only in hydrozoans but also in other cnidarians. Thus, the body column of the eubopolyp *Tripedalia*, for example, was also shown to be surrounded by a massive nervous ring at the level of the tentacular bases (Werner *et al.*, 1976).

Both organisms, *Coryne* sp. and its close relative *Coryne pintneri*, contain many mechanosensitive cells within their filiform tentacles (Tardent and Schmid, 1972). These cells are stimulated by water movements caused by prey organisms or experimental manipulations. After such an adequate stimulation, the polyp responds with a directed bending of its whole hydranth towards the stimulatory source (*cf.* Stoessel and Tardent, 1971). Thereby, the capitate tentacles are brought into the vicinity of a potential prey organism. Since, in *Coryne*, the ring-like centralization of neurons is only associated with the whorl of filiform tentacles, it may probably function as a first site of neuronal integration for incoming signals produced by the sensory cells within this type of tentacles. The coordination or activation of all muscles involved in the directed movements may be achieved by these neurons.

The ultrastructural investigations revealed that the neurons of *Coryne* contain numerous dense-cored vesicles. Koizumi *et al.* (1989) were able to demonstrate by immunocytochemistry that similar vesicles located within the epidermal ganglion cells in the peduncle of *Hydra* contain RFamide-like neuropeptides. Large numbers of these vesicles have been localized within the nerve terminals adjacent to the muscular base of the epitheliomuscular cells, indicating that this neuropeptide may be directly involved in neuromuscular transmission. That RFamides indeed have an excitatory effect on muscle and neuronal systems was demonstrated at least for sea anemones by McFarlane *et al.* (1987).

Although in other hydrozoan polyps, as for example *Hydra oligactis* and *Hydractinia echinata*, the pericarya of RFamide-positive neurons are homogeneously distributed over the entire length of their tentacles (Grimmelikhuijzen, 1985), the capitate tentacles of *Coryne* are characterized by a strong centralization of their RFamide-

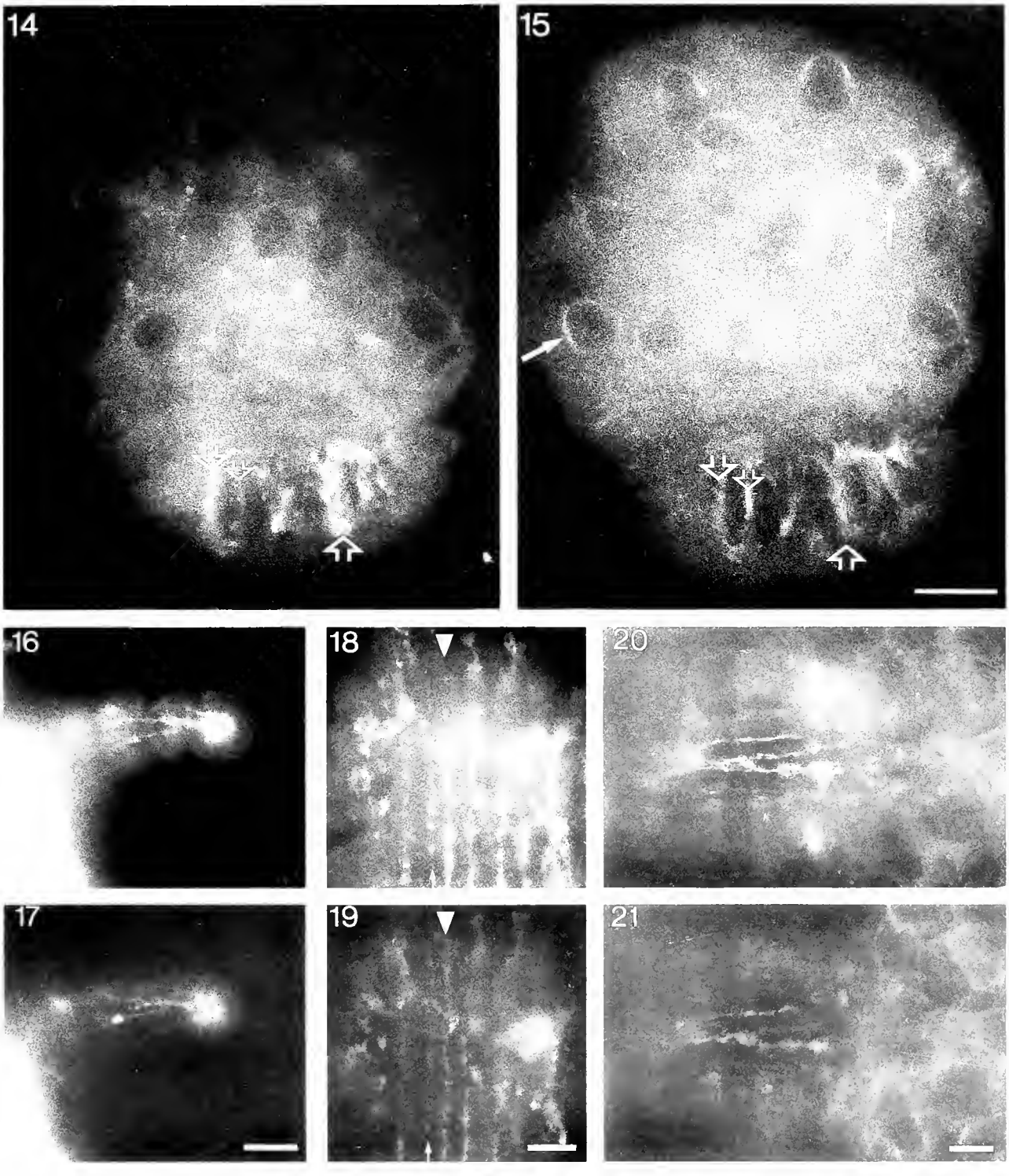

Figures 14–15. Double-labeled capitate tentacle. Both figures have the same focal plane. The antibodies against RFamide (Fig. 14) and β-tubulin (Fig. 15) produce identical staining patterns within the stalks (indicated by open arrows). In the heads of the tentacles, only the microtubular baskets of the nematocytes (arrows) are labeled but no RFamide-based fluorescence occurs. Bar = 20 μm.

Figures 16–21. Pairs of double-labeled tentacle. Figures 16, 18, and 20 represent staining patterns produced by anti-β-tubulin. Figures 17, 19, and 21 show the corresponding patterns obtained by the antibody against RFamides. All tubulin-positive neurites within the filiform tentacles are also stained by anti-RFamide (Figs. 16, 17). Within the stalks of the capitate tentacles, both antibodies produce identical staining patterns in thinner (small arrows) and thicker neurites (arrowheads). Bar in Figure 17 = 20 μm; in Figures 19 and 21 = 10 μm.

positive pericarya. Intracellular electrophysiological recordings revealed that the nematocytes in the knobby heads of *Coryne* become postsynaptically depolarized by the mechanical stimulation of a second nematocyte located within the same tentacle (Brinkmann and Thurm, 1993). Although the discharge of nematocysts does not depend on the presence of nerve cells (Aerne *et al.*, 1991), its probability is affected by such neuronal interactions. The observed concentration of RFamide-positive cells within the center of the knobby heads may be a consequence of the accumulation of all nematocytes in a restricted domain on the tentacular surface. By this arrangement, an effective neuronal interaction between adjacent nematocytes may be achieved. Neuronal interactions between adjacent nematocytes are also discussed to occur in scyphomedusae via RFamide-positive neurons (Anderson *et al.*, 1992).

The sensory cells spaced between the nematocytes within the knobby heads are thought to act on adjacent nematocytes by neuronal interactions similar to those observed between adjacent nematocytes. However, both mechanosensitive cells obviously do not transmit their signals via RFamides.

In each head of the knobby tentacles, neurons and nematocytes seem to be structurally and functionally interconnected in the same way as the corresponding cells within the tentacles of *Hydra:* a distinct number of nematocytes is integrated within an epitheliomuscular cell, thus forming an individual battery complex (Hufnagel *et al.*, 1985). Each battery is usually accompanied by a sensory and a ganglionic cell. The latter cell is not only synaptically linked to the nematocytes of its own battery, but is additionally responsible for the excitation of adjacent epitheliomuscular cells and their batteries of nematocytes (Westfall, 1988; Hobmayer *et al.*, 1990). In analogy to this system, the nematocytes of each capitate tentacle are thought to represent a battery complex. The communication between adjacent batteries, *i.e.*, neighboring capitate tentacles, has then to be mediated by the parallel bundles of neurites within the tentacular stalks.

Acknowledgments

I would like to thank Mrs. M. Otterbein for technical assistance and Prof. U. Thurm for helpful suggestions on the manuscript. I greatly appreciate the kind gift of the RFamide antibody by Dr. C. J. P. Grimmelikhuijzen, Zentrum für Molekulare Neurobiologie, Hamburg. This work was supported by Deutsche Forschungsgemeinschaft (SFB 310).

Literature Cited

Aerne, B. L., R. P. Stidwill, and P. Tardent. 1991. Nematocyst discharge in *Hydra* does not require the presence of nerve cells. *J. Exp. Zool.* **258:** 137–141.

Anderson, P. A. V., A. Moosler, and C. J. P. Grimmelikhuijzen. 1992. The presence and distribution of Antho-RFamide-like material in scyphomedusae. *Cell Tissue Res.* **267:** 67–74.

Brinkmann, M., and U. Thurm. 1991. Electrical responses of hydrozoan nematocytes caused by mechanical stimulation of the cnidocil apparatus. P. 38 in *Proceedings of the 19th Göttingen Neurobiology Conference,* N. Elsner and M. Heisenberg, eds. Thieme Verlag, Stuttgart.

Brinkmann, M., and U. Thurm. 1993. Mechanoreceptive properties of hydrozoan nematocytes *in situ.* P. 155 in *Proceedings of the 21st Göttingen Neurobiology Conference,* N. Elsner and M. Heisenberg, eds. Thieme Verlag, Stuttgart.

Carlberg, M. 1992. Localization of dopamine in the freshwater hydrozoan *Hydra attenuata. Cell Tissue Res.* **270:** 601–607.

Golz, R., and U. Thurm. 1991. Cytoskeletal modifications of the sensorimotor-interneurons of *Hydra vulgaris* (Cnidaria, Hydrozoa), indicating a sensory function similar to chordotonal receptors of insects. *Zoomorphology* **111:** 113–118.

Golz, R., and U. Thurm. 1993. Ultrastructural evidence for the occurrence of three types of mechanosensitive cells in the tentacles of the cubozoan polyp *Carybdea marsupialis. Protoplasma* **173:** 13–22.

Grimmelikhuijzen, C. J. P. 1985. Antisera to the sequence Arg-Phe-amide visualize neuronal centralization in hydroid polyps. *Cell Tissue Res.* **241:** 171–182.

Grimmelikhuijzen, C. J. P., D. Graff, and I. D. McFarlane. 1989. Neurones and neuropeptides in coelenterates. *Arch. Histol. Cytol.* **52 Suppl:** 265–278.

Grimmelikhuijzen, C. J. P., D. Graff, O. Koizumi, J. A. Westfall, and I. D. McFarlane. 1991. Neuropeptides in coelenterates: a review. *Hydrobiologia* **216/217:** 555–563.

Hobmayer, E., T. W. Holstein, and C. N. David. 1990. Tentacle morphogenesis in *Hydra.* II. Formation of a complex between a sensory nerve cell and a battery cell. *Development* **109:** 897–904.

Hufnagel, L. A., G. Kass-Simon, and M. K. Lyon. 1985. Functional organization of battery cell complexes in tentacles of *Hydra attenuata. J. Morphol.* **184:** 323–341.

Jones, C. S. 1947. The control and discharge of nematocysts in *Hydra. J. Exp. Zool.* **105:** 25–60.

Josephson, R. K. 1974. Cnidarian neurobiology. Pp. 245–280 in *Coelenterate Biology,* L. Muscatine and H. M. Lenhoff, eds. Academic Press, New York.

Kass-Simon, G. 1988. Towards a neuroethology of nematocyst discharge in the tentacles of *Hydra.* Pp. 531–541 in *The Biology of Nematocysts,* D. A. Hessinger and H. M. Lenhoff, eds. Academic Press, New York.

Kinnamon, J. C., and J. A. Westfall. 1982. Types of neurons and synaptic connections at hypostome-tentacle junctions in *Hydra. J. Morphol.* **173:** 119–128.

Koizumi, O., J. D. Wilson, C. J. P. Grimmelikhuijzen, and J. A. Westfall. 1989. Ultrastructural localization of RFamide-like peptides in neuronal dense-cored vesicles in the peduncle of *Hydra. J. Exp. Zool.* **249:** 17–22.

Koizumi, O., M. Hazawa, H. Mizumoto, S. Minobe, L. C. Javois, C. J. P. Grimmelikhuijzen, and H. R. Bode. 1992. Nerve ring of the hypostome in *Hydra.* I. Its structure, development, and maintenance. *J. Comp. Neurol.* **326:** 7–21.

Kolberg, K. J. S., and V. J. Martin. 1988. Morphological, cytochemical and neuropharmalogical evidence for the presence of catecholamines in hydrozoan planulae. *Development* **103:** 249–258.

Martin, S. M., and A. N. Spencer. 1983. Neurotransmitters in coelenterates. *Comp. Biochem. Physiol.* **74C:** 1–14.

McFarlane, I. D., D. Graff, and C. J. P. Grimmelikhuijzen. 1987. Excitatory actions of Antho-RFamide, an anthozoan neu-

ropeptide, on muscle and conducting systems in the sea anemone *Calliactis parasitica*. *J. Exp. Biol.* **133:** 157–168.

Pantin, C. F. A. 1942. The excitation of nematocysts. *J. Exp. Biol.* **19:** 294–310.

Stoessel, F., and P. Tardent. 1971. Die Reaktionsmuster von *Coryne pintneri* und *Sarsia reesi* (Athecata: Capitata) auf Berührungsreize. *Rev. Suisse Zool.* **78:** 689–697.

Takeda, N., and C. N. Svendsen. 1991. Monoamine concentrations in *Hydra magnipapillata*. *Hydrobiologia* **216/217:** 549–554.

Tardent, P., and V. Schmid, 1972. Ultrastructure of mechanoreceptors of the polyp *Coryne pintneri* (Hydrozoa, Athecata). *Exp. Cell Res.* **72:** 265–275.

Tardent, P., and C. Weber. 1976. A qualitative and quantitative inventory of nervous cells in *Hydra attenuata* Pall. Pp. 501–512 in *Coelenterate Ecology and Behavior*, G. O. Mackie, ed. Plenum Press, New York.

Thurm, U., and P. Lawonn. 1990. The sensory properties of the cnidocil-apparatus as a basis for prey capture in *Hydra attenuata*. *Verh. Deutsch. Zool. Ges.* **83:** 431–432.

Watson, G. M., and D. A. Hessinger. 1989. Cnidocytes and adjacent supporting cells form receptor-effector complexes in anemone tentacles. *Tissue Cell* **21:** 17–24.

Werner, B., D. M. Chapman, and Ch. E. Cutress. 1976. Muscular and nervous systems of the cubopolyp (Cnidaria). *Experientia* **32:** 1047–1049.

Westfall, J. A. 1970. Ultrastructure of synapses in a primitive coelenterate. *J. Ultrastruct. Res.* **32:** 237–246.

Westfall, J. A. 1973. Ultrastructural evidence for a granule-containing sensory-motor-interneuron in *Hydra littoralis*. *J. Ultrastruct. Res.* **42:** 268–282.

Westfall, J. A. 1988. Presumed neuronematocyte synapses and possible pathways controlling discharge of a battery of nematocysts in *Hydra*. Pp. 41–51 in *The Biology of Nematocysts*, D. A. Hessinger and H. M. Lenhoff, eds. Academic Press, New York.

Westfall, J. A., and J. C. Kinnamon. 1978. A second sensory-motor-interneuron with neurosecretory granules in *Hydra*. *J. Neurocytol.* **7:** 365–379.

Westfall, J. A., and J. C. Kinnamon. 1984. Perioral synaptic connections and their possible role in the feeding behavior of *Hydra*. *Tissue Cell* **16:** 355–365.

Westfall, J. A., and R. A. Rogers. 1990. A combined high-voltage and scanning electron microscopic study of 2 types of sensory cells dissociated from the gastrodermis of *Hydra*. *J. Submicrosc. Cytol. Pathol.* **22:** 185–190.

Westfall, J. A., S. Yamataka, and P. D. Enos. 1971. Ultrastructural evidence of polarized synapses in the nerve net of *Hydra*. *J. Cell Biol.* **51:** 318–323.

Westfall, J. A., J. D. Wilson, R. A. Rogers, and J. C. Kinnamon. 1991. Multifunctional features of a gastrodermal sensory cell in *Hydra*: three-dimensional study. *J. Neurocytol.* **20:** 251–261.

Wood, J. G., and T. L. Lentz. 1964. Histochemical localization of amines in *Hydra* and in the sea anemones. *Nature* **201:** 88–90.

Reference: *Biol. Bull.* **186:** 124–133. (February, 1994)

Quantitative Branching Geometry of the Vascular System of the Blue Crab, *Callinectes sapidus* (Arthropoda, Crustacea): A Test of Murray's Law in an Open Circulatory System

DAVID MARCINEK[1] AND MICHAEL LaBARBERA[2]

[1]*Biology Department, Kalamazoo College, Kalamazoo, Michigan 49006, and* [2]*Department of Organismal Biology and Anatomy, The University of Chicago, 1025 East 57th St., Chicago, Illinois 60637*

Abstract. Murray's law predicts that there will be a radius-cubed relationship between the parent and daughter vessels of a branching system of vessels that carry the flow of a fluid, a relationship that theoretically minimizes the costs of building, maintaining, and operating the system. The vascular system of the blue crab, *Callinectes sapidus*, was replicated by corrosion casting at physiological pressures; vessel diameters were measured off the casts and used to calculate a junction exponent for each branch point. This study is the first quantitative description of the vascular branching geometry in an open circulatory system. The mean value derived from the arctan-transformed junction exponent distribution, 3.020, was not significantly different from the value of 3 predicted by Murray's law. The phylogenetic distance of arthropods from the animals previously studied in this context, sponges and mammals, is evidence for three independent evolutions of this branching relationship in biological fluid transport systems.

Introduction

Organisms and their component cells depend on exchange with their surroundings for nutrient procurement, excretion, respiration, and temperature regulation. Animals commonly meet the demands of exchange with a system of branching pipes, within which there is convective flow of a fluid. Two major types of fluid transport systems are seen in animals (LaBarbera, 1990). In one, used by many suspension feeders, fluid is pumped from an external source past the animal's filtering structures. The second, an internal transport system, is familiar as the circulatory system of most "higher" animals. Circulatory systems can be further divided (LaBarbera and Vogel, 1982) into those in which the circulating fluid is completely contained in a network of vessels (closed circulatory systems) and those in which the circulating fluid leaves well-defined vessels and flows through sinuses to bathe the tissues (open circulatory systems). For a fluid transport system to function effectively, there must be continuous flow of the fluid, which results in large volumes of fluid being pumped at substantial cost to the animals (LaBarbera, 1994).

Is there a design principle for transport of a fluid that both minimizes the cost of volumetric flow and is general enough to apply across the diversity of fluid transport systems observed in biology? This question was first treated over a century ago by Thomas Young in his 1808 Croonian lecture (Sherman, 1981). Since then, several physiologists have addressed the question of an ideal branching pattern, but the "clearest and most general approach" (Sherman, 1981) is that of Murray (1926).

The derivation of "Murray's law" [see Sherman (1981) and LaBarbera (1993) for details] assumes that there is laminar flow of a fluid through circular pipes, an assumption that is not grossly violated in biological fluid transport systems. If the velocity profile is fully developed ("Poiseuille flow," a stable parabolic velocity profile; see

Received 10 August 1993; accepted 22 November 1993.

[1] Present address: Dept. of Biological Sciences, Stanford University, Stanford, CA 94305.

[2] To whom all correspondence should be addressed.

Vogel, 1981), and the fluid is Newtonian (*i.e.*, the viscosity of the fluid is independent of the characteristics of the flow), then the Hagen-Poiseuille equation (Vogel, 1981) states that, for a given volumetric flow rate, the resistance to flow is inversely proportional to the radius of the vessel to the fourth power. This relationship would imply that the cost of moving the fluid can be minimized by maximizing the radius of the vessels. However, Murray's derivation also assumes that there is some cost proportional to the volume of the system; this cost might be the cost to build and maintain the vessel walls (Sherman, 1981), the formed elements in the blood (Murray, 1926), or any other volume-related cost (LaBarbera and Boyajian, 1991). Minimizing these volume-related costs by decreasing vessel radius necessarily increases the costs associated with moving the fluid. The total cost can be minimized only if the volumetric flow rate through a vessel in the system is maintained proportional to the cube of the vessel radius (Murray, 1926), a relationship known as Murray's law. This form of Murray's law is supported by a number of empirical studies on the relationship between volumetric flow rate and vessel radius in the vascular systems of birds and mammals [see LaBarbera (1994) for a review].

Murray's functional relationship makes a clear morphological prediction. At a branch point in a fluid transport system, where a single parent vessel gives rise to two or more daughter vessels, the volumetric flow rate in the parent vessel must be equal to the sum of the volumetric flows in the daughter vessels (the "principle of continuity"; Vogel, 1981). In the equation

$$r_0^x = r_1^x + r_2^x + \cdots r_n^x$$

where r_0 is the radius of the parent vessel and $r_1 \cdots r_n$ are the radii of the daughter vessels, Murray's law thus predicts that x, the junction exponent, will have a value of 3. (Note that other values for the junction exponent are possible. A system in which flow velocity was maintained constant in all vessels would have a junction exponent of 2; a system in which resistance to flow was maintained constant would have a junction exponent of 4.) A radius-cubed relationship of daughter to parent vessels is supported by empirical evidence for multiple species of mammals (Sherman, 1981; LaBarbera, 1990, 1994) and sponges, including Devonian stromatoporoids (LaBarbera, 1990, 1993; LaBarbera and Boyajiian, 1991), an extinct group of sponges. Given the extreme phylogenetic distance between sponges and mammals, the agreement with Murray's law observed in these animals is probably not due to chance occurrence or a single evolution of this system (LaBarbera, 1990).

While previous work provides data on two functionally highly divergent systems (the trophic fluid transport system of sponges and the closed circulatory system of vertebrates), to date there are no available data on the applicability of Murray's law to open circulatory systems. The present study on the vasculature of the decapod crustacean, *Callinectes sapidus*, represents the first quantitative analysis of vessel branching in an open circulatory system.

Materials and Methods

Maryland blue crabs, *Callinectes sapidus* Rathbun (98–185 g wet weight), were purchased from a local fish market on the same day they were received. Because the crabs were shipped on ice, they were placed in plastic containers containing aerated 4–5°C artificial seawater (salinity 32–34‰) and allowed to warm gradually (2 h minimum) to room temperature to minimize temperature shock. After thermal acclimation, the crabs were transferred to 300-l aquaria at room temperature. Because of their aggressive nature, the blue crabs were generally isolated in plastic mesh cages submerged in the aquaria; when isolation was not possible, their chelipeds were bound.

The mortality rate during acclimation was 20–40%, and it reached 50% after two days; animals still alive after two days generally survived until used (1–14 days). The heart and major blood vessels were located, during dissection, with the help of McMahon and Burnett's (1990) description of the brachyuran circulatory system.

Surviving animals were anesthetized by injection of 0.2 ml of 3–5% procaine in distilled water into the coxal joint of a rear periopod or swimming leg; procaine is reported to minimally influence cardiac parameters in crabs (Oswald, 1977). After being injected, the animal exhibited a short period (20–30 s) of excitation followed by retraction of its appendages and subsequent insensitivity to stimuli. We manually drilled a hole through the dorsal carapace, about one-third of the distance from its posterior edge, to access the heart. A 20-gauge hypodermic needle attached by 20 cm of PE-90 catheter tubing to a Gould P32 pressure transducer was inserted into the heart; cardiac pressures were recorded on a Gould 2200 strip chart recorder. Normal heartbeat patterns and systolic pressures were successfully recorded from three anesthetized blue crabs; a typical pressure recording is shown in Figure 1. Measured systolic pressures were 11–14 cm H_2O (mean

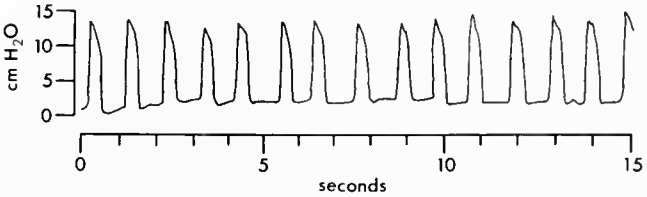

Figure 1. A typical pressure recording from the heart of a blue crab. The vertical scale is pressure (in cm H_2O; 1 cm H_2O = 0.098 kPa); the horizontal scale is time (in seconds).

= 13.1 ± 0.3 cm H_2O), and these pressures (=1.08–1.37 kPa) were maintained throughout circulatory system perfusion and vascular filling. Measured systolic pressures were virtually identical to those reported for other crabs of comparable size (*Cancer productus*—14.1 cm H_2O, *C. maenas*—14.0 cm H_2O; McMahon and Burnett, 1990). During cardiac pressure measurements and throughout the vascular casting procedure, the crab was submerged in seawater.

After pressure measurements were completed, the 20-gauge needle was removed and replaced with an 18-gauge needle connected, via PE-160 tubing, to a 50-ml syringe body (the perfusion reservoir). Hemolymph was rinsed from the vascular system using cold (4–5°C) artificial seawater to inhibit clotting (J. L. Wilkins, Univ. of Calgary, pers. comm.); the air-water interface in the perfusion reservoir was maintained 10–14 cm above the level of the water covering the crab to ensure a proper pressure gradient. One of the posterior periopods was excised at the coxal joint to allow the hemolymph to drain. In some cases, uranine dye was added to the rinse solution to help identify when the rinse emerged from the animal. Rinsing times and volumes ranged from 16 to 36 min and 32 to 53 ml, respectively. When exsanguination appeared to be complete, the vascular system was perfused for 20–30 min with cold (4–5°C) 10% buffered formalin in seawater; the fluid level in the perfusion reservoir was maintained to ensure fixation at physiological pressures.

During exsanguination, the crabs occasionally displayed spontaneous, random movement of their appendages. We attempted to maintain complete anesthesia in some specimens by adding 2–3 ml of procaine solution to the rinse solution; spontaneous appendage movement was reduced, but the vascular casts from these specimens were less complete or without well-defined vessels. The results reported here, therefore, were obtained exclusively from specimens without supplementary anesthesia.

Bateson's #17 (Polysciences, Inc.), diluted with methylmethacrylate to reduce the viscosity of the casting medium (Levesque *et al.*, 1979; Lametschwandtner *et al.*, 1990), was used to fill the vascular system for corrosion casting. Components were mixed according to the manufacturer's protocol in the following proportions: 50 parts Bateson's monomer, 10 parts catalyst B, 1 part promoter C, 50 parts methylmethacrylate (Levesque *et al.*, 1979). Immediately after being mixed, casting compound was poured into a 10-ml syringe attached to an 18-gauge needle via a short segment of catheter tubing; the tubing and needle were bled of air before being inserted into the heart. Because the density of the casting compound (1.079 g/ml) was about that of water, the meniscus of the uncured Bateson's was maintained 10–14 cm above the water covering the crab, ensuring normal systolic pressures in the heart. The casting compound continued to flow into the crabs' hearts for 25–32 min before polymerization stopped the flow; the volumes infused ranged from 5.2 to 9.4 ml.

Shrinkage of the modified Bateson's upon polymerization was measured by filling microcapillary tubes (1.4, 1.0, 0.6, and 0.4 mm internal diameter) with casting compound. After polymerization, the tube was broken and diameters for both the unbroken sections of the tube and casts were measured. The mean diameter shrinkage was 3.8% ± 0.5% (mean ± SE); there was no significant difference in shrinkage between tubes of different sizes (ANOVA: $F_{3,32} = 0.263$, $P = 0.85$).

The specimen was left in seawater overnight to allow the cast to fully polymerize. The exoskeleton was decalcified by immersing the specimen for 24 h in 20–25% acetic acid:H_2O solution; after sections of the decalcified cuticle were cut away and the body thoroughly rinsed of acid, the specimen was transferred to 30% KOH for soft tissue digestion (Lametschwandtner *et al.*, 1990). Maceration continued for up to three days; specimens were rinsed and the KOH solution was changed daily. After treatment in KOH, the remaining chitinous matrix was dissected away and the cast washed; casts were stored in distilled water.

The vascular casts were photographed on Kodak Technical Pan film using a Nikon FM 35-mm camera and MicroNikkor 55-mm macro lens. The cast was fixed to a universal stage and the stage adjusted to ensure that the parent and daughter vessels of the junction being photographed were coplanar and oriented perpendicular to the optic axis of the lens. A stage micrometer was photographed for scale. The negatives were projected at a total magnification of 330× and traced; linear dimensions were measured with a Summa Sketch II digitizing pad connected to an Apple Macintosh IIci. Because vessel diameter varies slightly along the length of the vessels, several diameters were measured along the length of each vessel segment; mean values were used to calculate junction exponents and predicted parent vessel diameters. Where possible, the total vessel segment length between junctions was also measured.

In many instances a junction had vessels projecting or curving into more than one plane; these junctions were excluded from the sample. A number of vessels in the casts appeared flattened, which we interpreted as indicating incomplete filling by the casting compound; these vessels were also excluded from the analysis.

Best fit values for junction exponents were determined to four decimal places with an iterative search program. Where the diameter of one of the daughter vessels was equal to or larger than that of the parent vessel, the junction exponent was considered undefined. Statistical tests of junction exponents, by definition, exclude consideration of junctions where the junction exponent is undefined. To test the full data set for consistency with Mur-

Figure 2. Corrosion casts of the blue crab vasculature. (A) The anterior dorsal region of the thorax and a cheliped before dissection of the cast from the exoskeleton. (B) A vasculature cast removed from the exoskeleton. The heart is the large mass at the bottom center of the photograph; the sternal artery, the major vessel in the midline of the cast, supplies the mandibular region and periopods in blue crabs (see Fig. 3). The arteries serving the tips of one of the chelae can be seen in the upper left.

ray's law, we also compared measured values for parent vessel diameters with parent vessel diameters predicted from the measured daughter vessel diameters, assuming a junction exponent of 3 (LaBarbera and Boyajian, 1991; LaBarbera, 1994). This test allowed inclusion of branch points where the junction exponent was undefined.

All numerical calculations and most statistical tests were performed with StatView II (ver. 1.04; Abacus Concepts, Berkeley, California). One sample and paired sign tests were run on StatView 4 (ver. 4.01; Abacus Concepts); confidence intervals for medians of untransformed junction exponent distributions were determined by bootstrap resampling with replacement (1000 runs) of the distributions using the program Resampling Stats (ver. 1.00; Resampling Stats, Arlington, Virginia). All analyses were run on a Macintosh IIci.

Results

Examples of blue crab vascular casts are given in Figure 2; a schematic diagram of a typical vascular tree is given in Figure 3. Vessel diameters were measured from 106 junctions, pooled from vascular casts of three crabs; 98 of these junctions exhibited dichotomous branching, and 8 possessed three daughter vessels. Vessel diameters ranged from 52 to 785 μm, with parent vessel diameters spanning nearly this full range (71–785 μm; Fig. 4). Segment lengths (the distance between branch points) could be accurately determined on only 159 segments (Fig. 5). Segment length/diameter ratios were extremely variable, ranging from 0.50 to 17.8; the mean value was 3.98 ± 0.62 (median = 3.21).

The frequency distribution of junction exponents was sharply peaked and right skewed (Fig. 6). The mode of this distribution appeared to be between 2 and 3, although both the mean and median gave higher values (Table I). Because the distribution was obviously skewed and significantly different from a normal distribution (Lillifors test; Table II), we used an arctan transformation (LaBarbera, 1994; Suwa *et al.*, 1963) to normalize the data (Fig. 7). The arctan-transformed frequency distribution was not significantly different from a normal distribution (Table II). Neither the median of the untransformed dis-

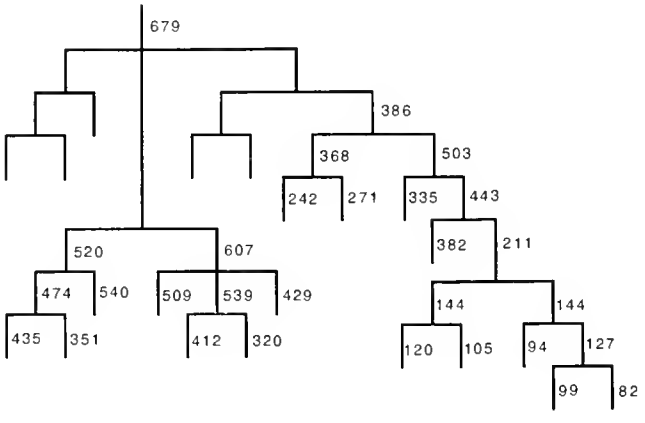

Figure 3. Branching topology and diameters (in μm) of the vessels supplying the mandibular region from a segment of the sternal artery (the parent vessel in this network) in blue crabs. Branches that lack diameter values could not be reliably measured. Note that dichotomous branching is most common, but junctions with more than two daughter vessels do occur.

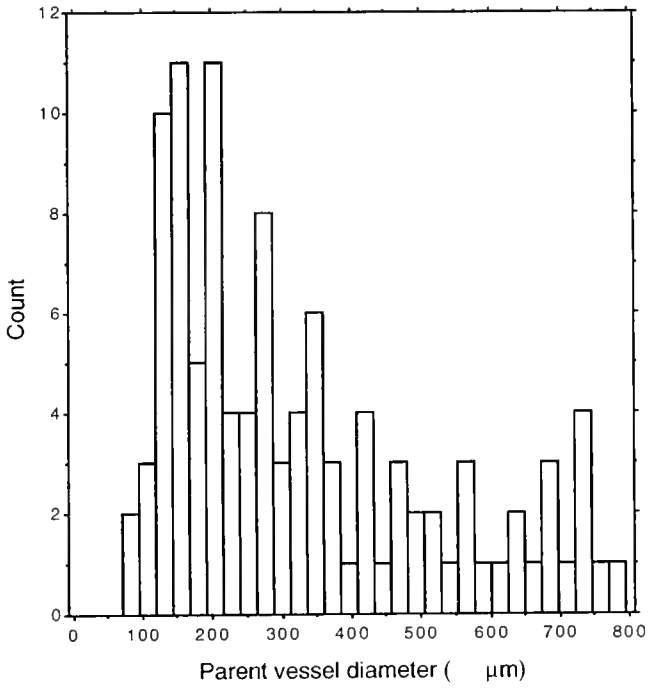

Figure 4. Frequency distribution of the parent vessel diameters (in μm) of the 106 junctions measured from vascular casts of three blue crabs.

tribution nor the (backtransformed) mean of the transformed distribution was significantly different from a value of 3 (Table I); based on confidence intervals, the mean of the untransformed distribution was significantly different from 3.

The pooled exponents were divided into quasi-arbitrary groups on the basis of anatomical location and diameter of the parent vessel (Table I); the particular groupings in Table I were chosen to maintain sample sizes approximately constant. Three groups were established on the basis of anatomical location of the junction—vessels of the anterior-ventral region, the vessels supplying the ventral regions of the thorax and the periopods, and the dorsolateral arteries (which supply the digestive gland and the peripheral thoracic arteries). All three of the groups showed frequency distributions of junction exponents that were significantly non-normal; the aretan-transformed junction exponent distributions were not significantly different from normal distributions (Table II). ANOVA of the transformed distributions ($F_{2,83} = 0.312$; $P = 0.73$) and Kruskal-Wallis rank tests of the untransformed distributions ($P = 0.64$) showed no significant differences between anatomical groups. Neither the medians of the untransformed distributions nor the backtransformed means of the transformed distributions were significantly different from a value of 3 (Table I); based on confidence intervals, one of the three means of the untransformed distributions was significantly different from 3.

Grouping the junction exponents on the basis of diameter of the parent vessel produced a similar pattern. Two of the four groups showed frequency distributions of junction exponents that were significantly non-normal, as was one of the size groups of aretan-transformed junction exponents (Table II); thus, ANOVA could not be used to test for differences between groups. However, Kruskal-Wallis rank tests of the untransformed ($P = 0.20$) and transformed distributions ($P = 0.27$) showed no significant differences between size groups. Neither the medians of the untransformed distributions nor the backtransformed means of the transformed distributions were significantly different from a value of 3 (Table I); among the means of the untransformed distributions, only the mean for the largest size group (431–785 μm) was significantly different from 3.

To include all measured junctions in the analysis (not just junctions where the exponent was defined), we used the measured diameters of the daughter vessels at each junction to predict a diameter for the parent vessel (Table III; a junction exponent of 3 was assumed in these calculations). Again, the data were grouped by anatomical location of the junction and parent vessel diameter. In every case, the mean ratio of the predicted diameter to the observed diameter was greater than 1, implying a tendency for the parent vessel to be slightly smaller than would be predicted by a junction exponent of 3 (or, equivalently, for the daughter vessels to be slightly larger

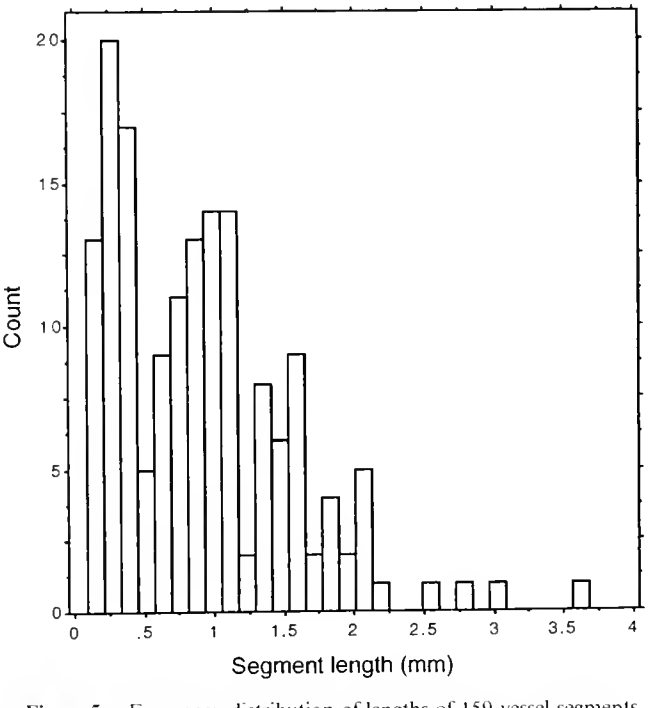

Figure 5. Frequency distribution of lengths of 159 vessel segments in the blue crab arterial system.

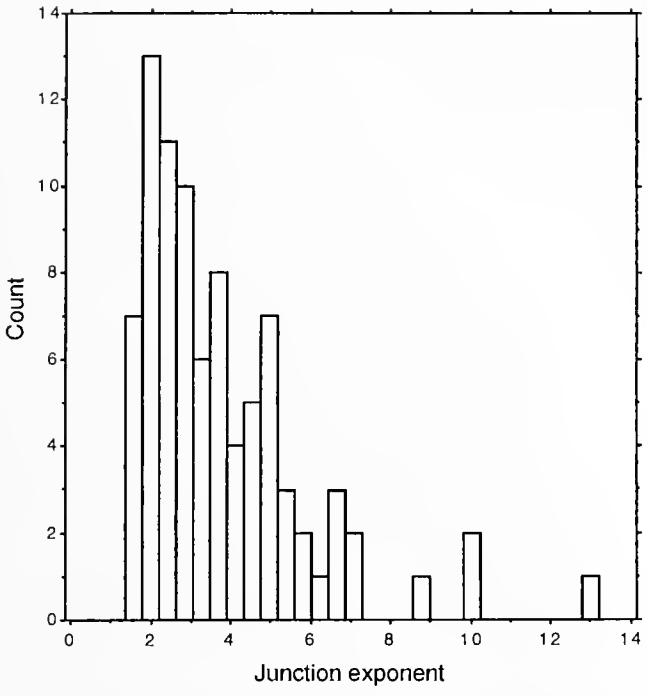

Figure 6. Frequency distribution of the junction exponents calculated from measured parent and daughter vessel diameters at 86 branch points in the arterial systems of three blue crabs. Note that the distribution is strongly right-skewed and non-normal (see Table II) but exhibits a mode at an exponent between 2 and 3.

than would be predicted by a radius-cubed relationship with the parent vessel). Although all ratios were consistently greater than 1, nonparametric two sample sign tests revealed significant differences between observed and predicted diameters only for three groupings: the full data set, the dorso-lateral vessels, and the largest parent vessels (Table III).

Discussion

Tests of Murray's law

The objective of this study was to provide a quantitative description of vessel branching in an open circulatory system and test the results against the idealized geometry of an "optimally designed" fluid transport system as predicted by Murray's law. Given the highly skewed frequency distribution of junction exponents (a feature also seen in the fluid transport systems of sponges and mammals; see LaBarbera, 1994), a simple mean is clearly a poor measure of central tendency of the junction exponent distribution. The large discrepancy between the mean and median of the distribution is a clear indicator of its non-normality, a conclusion confirmed by statistical analysis (Table II). We have provided two alternative measures, the median and the mean of arctan-transformed junction exponents, both of which are more robust indicators of central tendency than a simple mean. Both measures clearly indicate that the junction exponents of vessels in the arterial system of blue crabs are not significantly different from the value of 3 predicted by Murray's law. This conclusion is robust to divisions of the data by either anatomical location or vessel size (Table I). Although both mammals and fossil stromatoporoid sponges have been previously shown to exhibit a fluid transport system in quantitative agreement with Murray's law (data summarized in LaBarbera, 1994), this is the first demonstration that an animal with an open circulatory system exhibits such a vascular architecture.

Most previous quantitative tests of the anatomical predictions of Murray's law (*e.g.*, Suwa *et al.*, 1963; Hutchins *et al.*, 1976; Arts *et al.*, 1979; Wieringa *et al.*, 1988; Griffith and Edwards, 1990) have focused on branch points where junction exponents were (by our definition) defined. The discordance between Table I, where no statistically significant differences were found between the blue crab vasculature and Murray's law, and Table III, where significant differences were apparent, can clearly be attributed to the inclusion of junctions where the junction exponent was undefined, effectively changing the data set being tested. Although inclusion of all junctions yields statistically significant differences between the idealized and real system, the actual error is small; Murray's law predicts parent vessel diameters averaging only 5% larger than the measured vessels.

Proximate mechanisms for generating Murray's law systems

Our conclusion that the blue crab circulatory system approaches Murray's model is significant, not only because it is the first test of Murray's law in an open circulatory system, but also because of the evolutionary position of arthropods in relation to the groups previously examined in this context—sponges (including 375-million-year-old stromatoporoids) and vertebrates (LaBarbera, 1990, 1994; LaBarbera and Boyajian, 1991). The Arthropoda are a distinct evolutionary lineage, separate from both sponges and vertebrates, which are in turn distinct from one another (Turbeville *et al.*, 1991, 1992; Ballard *et al.*, 1992; Wainwright *et al.*, 1993), all three groups diverged before the development of their fluid transport systems (LaBarbera, 1994). Thus, approximations of Murray's law systems must have evolved independently at least three times and were in place at least 375 million years ago (LaBarbera and Boyajian, 1991). The convergent evolution of Murray's law fluid transport systems is probably driven by the substantial costs incurred in moving the large relative volumes these systems transport (see LaBarbera, 1994). Because even small changes in effi-

Table I

Measures of central tendency in the distributions of junction exponents in the blue crab arterial system

		Untransformed				Arctan transformed	
	n	Mean	*P*	Median	*P*	Mean	*P*
All vessels	86 (20)	3.758* (3.300–4.215)	—	3.129* (2.779–3.700)	0.75	3.020 (2.758–3.341)	0.89
Anatomical regions							
Anterio-ventral	29 (6)	4.014* (3.166–4.861)	—	3.079* (2.770–4.581)	>0.99	3.235 (2.767–3.887)	0.35
Ventral thorax, periopods	33 (4)	3.551* (2.901–4.202)	—	3.257* (2.230–3.888)	0.73	2.884 (2.484–3.429)	0.64
Anterio-lateral	24 (10)	3.732* (2.700–4.764)	—	2.999* (2.287–3.847)	>0.99	2.970 (2.500–3.630)	0.92
Parent vessel diameter							
<167 μm	23 (3)	3.785* (2.849–4.721)	—	3.113* (2.358–3.765)	>0.99	3.000 (2.469–3.762)	0.99
168–268 μm	22 (4)	3.529 (2.754–4.304)	0.17	3.036 (2.326–3.888)	>0.99	3.020 (2.587–3.602)	0.95
269–430 μm	19 (7)	3.518* (2.200–4.385)	—	2.144* (2.028–4.550)	0.36	2.634* (2.153–3.329)	—
431–785 μm	22 (6)	4.165 (3.302–5.029)	0.01	3.890 (3.033–4.923)	0.13	3.429 (2.829–4.294)	0.17

Data are presented for both the full data set and arbitrary subdivisions of the vessels according to anatomical location or parent vessel size. Three independent measures of central tendency are given: the mean and median of the original distributions and the mean of the distribution of the arctan transformed values (backtransformed to arithmetic units). In each cell of the table, the 95% confidence interval of the relevant metric is given in parentheses. Distributions that were significantly different from a normal distribution are indicated with an asterisk (see Table II). The numbers in parentheses in the second column represent the number of undefined junctions (see text) for each group. 95% confidence intervals for the medians were calculated by bootstrap resampling of the original data (see text). Where the distributions were not significantly different from a normal distribution, the means were tested against a hypothesized value of 3 using a one-sample *t*-test; medians were tested with a (nonparametric) one-sample sign test.

Table II

Lilliefors (Kolmogorov-Smirnov) tests of normality of the distributions of junction exponents in blue crabs

	n	Untransformed	Arctan transformed
All vessels	86 (20)	<0.0001	0.062
Anatomical regions			
Anterio-ventral	29 (6)	0.017	0.701
Ventral thorax, periopods	33 (4)	0.049	0.129
Anterio-lateral	24 (10)	0.012	>0.999
Parent vessel diameter			
<167 μm	23 (3)	0.018	0.908
168–268 μm	22 (4)	0.084	0.445
269–430 μm	19 (7)	0.001	0.005
431–785 μm	22 (6)	0.427	0.334

The values given are the probabilities that each distribution tested (see Table I) is statistically different from a normal distribution in shape. All untransformed distributions except two of the size categories (168–268 and 431–785 μm) are significantly different from a normal distribution; for the arctan transformed data, only the distribution of exponents from junctions whose parent vessels were between 269–430 μm in diameter was significantly different from a normal distribution.

ciency in these systems are amortized over the lifetime of the animal, selective pressures to decrease these costs are probably large.

LaBarbera (1990) suggested that convergent evolution of Murray's law systems has occurred because of the relative ease with which natural selection can exploit a local, cellular-level signal—hydrodynamic shear stress on the walls of the vessels—to generate an organism-spanning, near-optimal system. In a fluid transport system that follows Murray's radius-cubed relationship, the velocity profiles are geometrically similar everywhere in the system (Sherman, 1981); because velocity gradients at the wall of the vessel are identical, the hydrodynamic shear stresses on the walls of the vessels are identical everywhere in the system if fluid viscosity is constant. A number of workers (Zamir, 1977; Kamiya and Togawa, 1980; Kamiya *et al.*, 1988; LaBarbera, 1990) have suggested that, in the mammalian vascular system, the endothelial cells act as mechanosensors, controlling elements that adjust the diameter of the vessel to maintain shear stress at the walls near some shear set point. Experiments involving both acute and chronic changes in flow through mammalian

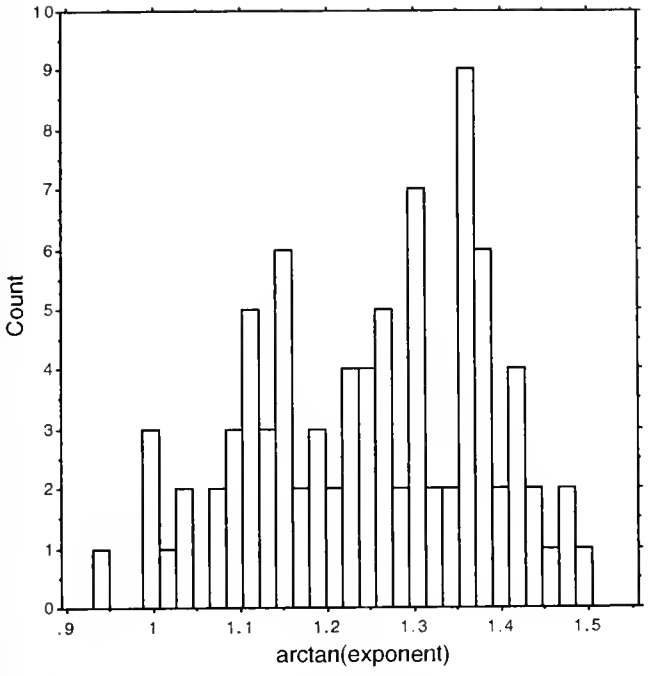

Figure 7. Frequency distribution of the arctan transformed junction exponents for 86 branch points in the arterial system of the blue crab. Note that the transformed distribution is approximately symmetrical and normal (see Table II).

blood vessels have shown that vessel diameter is altered so as to restore the shear stress to pre-experimental levels (reviewed in LaBarbera, 1993, 1994). Two distinct endothelium-mediated mechanisms (LaBarbera, 1993) apparently exist in mammals: (1) In response to *acute* changes in flow rate (= shear stress), smooth muscle tonus and thus vessel caliber is controlled by the release of prostaglandins, nitric oxide, and endothelium-derived relaxing factor (EDRF) (*e.g.,* Koller and Kaley, 1990a,b; 1991), maintaining the vasculature in a Murray's law configuration (Griffith and Edwards, 1990). (2) In response to *chronic* perturbations of flow, proliferation of both cellular and extracellular components or the breakdown of already existing elements remodel vessels, thus changing vessel caliber (*e.g.,* Kamiya and Togawa, 1980; Langille and O'Donnell, 1986; Zarins *et al.,* 1987).

Other mechanisms have been proposed to underlie endothelial responses to changes in flow rate, including changes in local ATP concentrations via flow-induced changes in diffusion boundary thickness (Mo *et al.,* 1991; Nollert and McIntre, 1992), or shear-stress-induced changes in configuration of extracellular membrane-bound proteins (Bevan and Siegal, 1991). Like the mechanosensor hypothesis, both of these hypotheses posit a response of endothelial cells to a signal dependent on the local velocity gradient; all three could result in similar responses of the system to changes in flow rate. Streaming potentials, voltages generated by the interaction of fixed surface charges with the ions carried in the fluid, are also correlated with local velocity gradients (Eriksson, 1974) and have been suggested to underlie responses of some cells to flow (Reich *et al.,* 1990; Berthiaume and Frangos, 1993).

In crustacean circulatory systems, the cells lining the vessels are separated from the vascular fluid by a continuous extracellular intima (Maynard, 1960; Johnson, 1980; Ruppert and Carle, 1983; Factor and Naar, 1990; McMahon and Burnett, 1990). Given the lack of direct contact between living cells and the fluid in the blue crab vasculature, a feedback mechanism that relies on mechanical sensing of shear stress seems unlikely. However, either changes in the local gradient of a molecule (*i.e.,* changes in diffusion boundary layer thickness) or changes in the streaming potential could be detected through the extracellular matrix lining crustacean blood vessels; both, like hydrodynamic shear stress, are dependent on the velocity gradient at the wall of the vessel and thus are attractive candidates for local signals that might control vessel remodeling in blue crabs.

The derivation of Murray's law assumes that a fully developed velocity profile is present everywhere in the system of vessels. But the parabolic velocity profile is disturbed at each branch point (LaBarbera, 1990), and the fluid must typically travel 10–80 vessel diameters downstream before complete re-establishment of Poiseuille flow (Vogel, 1981; LaBarbera, 1994). In biological systems, there are rarely 10 vessel diameters between branch points

Table III

Comparison of measured parent vessel diameters to parent vessel diameters predicted from measured daughter vessel diameters assuming a junction exponent of 3

Vessel diameter	n	*P* (sign test)	Pred/obs (mean ± SE)
All vessels	106	0.003	1.045 ± 0.013
Anatomical regions			
Anterio-ventral	35	0.18	1.056 ± 0.022
Ventral thorax, periopods	37	0.19	1.035 ± 0.027
Anterio-lateral	34	0.02	1.043 ± 0.018
Parent vessel diameter			
<167 μm	26	0.33	1.022 ± 0.022
168–268 μm	26	0.33	1.060 ± 0.035
269–430 μm	26	0.56	1.025 ± 0.027
431–785 μm	28	0.004	1.070 ± 0.020

Mean values for the ratio of the predicted diameters to the observed diameters are given for both the full data set and grouped by anatomical region and by measured size of the parent vessel. All junctions were included in the analysis. A nonparametric two-sample sign test was used to compare the ratio of observed to predicted diameters to a hypothesized value of 1.

(Zamir and Phipps, 1988; LaBarbera, 1994); hence, a static parabolic velocity profile is seldom fully re-established before the next branch point. If vessel diameter is determined by the magnitude of the local velocity gradient, downstream vessel diameters will be larger than predicted by Murray's law. In the case of the blue crab, downstream vessels are invariably daughter vessels, because the hemolymph returns to the heart through sinuses rather than veins. Given the small value of length/diameter ratio in the vessels we measured (mean 3.98), our hypothesis of the exploitation by blue crabs of the magnitude of the velocity gradient at the wall (or some variable dependent on the velocity gradient) as a signal to control vessel remodeling is consistent with the discrepancy we observed between measured parent vessel diameters and diameters predicted assuming a junction exponent of 3 (Table III).

There is no muscular tissue associated with the arterial vessels in crustaceans, with the exception of the valves at the major vascular junctions (Johnson, 1980; McMahon and Burnett, 1990; McMahon, 1992). The lack of smooth muscle in the vessel walls of crustaceans precludes an acute response similar to that observed in vertebrates. The highly elastic nature of crustacean arteries (Shadwick *et al.*, 1990) might play a role in acute control of vessel diameter to maintain a branching geometry that approximates a Murray's law system, but no experimental data are available.

The influence of fluid rheology on fluid transport system design

The branching geometry of vessels in the blue crab circulatory system is better predicted by Murray's law than is the branching geometry of mammalian vessels, where mean junction exponents vary from 1.72 to 3.09 (LaBarbera, 1994). This observation is not surprising given the rheology of the blood in these two groups. The respiratory pigment in crustaceans, hemocyanin, is transported in solution through the vascular system (Taylor, 1982), and the hemolymph contains fewer cellular components than mammalian blood. Unlike mammalian blood, where the high concentrations of erythrocytes cause the blood as a whole to act as a shear-sensitive, non-Newtonian fluid (Kiani and Hudetz, 1991), the maintenance of the respiratory pigment in simple solution in crustaceans should produce a fluid with strictly Newtonian behavior (Wells and Dales, 1976). The classic formulation of Murray's law implicitly assumes constant viscosity of the fluid (LaBarbera, 1993), an assumption violated in the smaller blood vessels of mammals. The junction exponents (mean exponents 2.47–2.93) for stromatoporoids are also closer to 3 than are those for mammals (LaBarbera, 1994); the fluid carried in the trophic fluid transport system of stromatoporoids was seawater, another strictly Newtonian fluid.

Although there have been a number of studies examining Murray's law and the maintenance of the diameter relationships between vessel branches in mammalian circulatory systems, there are virtually none for any other group of animals. More extensive work on the architecture of the fluid transport systems of animals other than mammals may yield important information on the generality of a Murray's law architecture and the variety of mechanisms involved in the production and maintenance of branching geometries that approach Murray's cost-optimized model.

Acknowledgments

This work was partially supported by a Senior Individualized Project Fellowship from the Diebold Foundation to D.M. We thank T. Williams, P. Olexia, D. Evans, and E. Dzialowski for helpful comments on the manuscript.

Literature Cited

Arts, T., R. T. I. Kruger, W. van Gerven, J. A. C. Lambregts, and R. S. Reneman. 1979. Propagation velocity and reflection of pressure waves in the canine coronary artery. *Am. J. Physiol.* **237:** H469–H474.

Ballard, J. W. O., G. J. Olsen, D. P. Faith, W. A. Odgers, D. M. Rowell, and P. W. Atkinson. 1992. Evidence from 12S ribosomal RNA sequences that onychophorans are modified arthropods. *Science* **258:** 1345–1348.

Berthiaume, F., and J. A. Frangos. 1993. Effects of flow on anchorage-dependent mammalian cells—secreted products. Pp. 139–192 in *Physical Forces and the Mammalian Cell*, J. A. Frangos, ed. Academic Press, Inc., New York.

Bevan, J. A., and G. Siegal. 1991. Blood vessel wall matrix flow sensor: evidence and speculation. *Blood Vessels* **28:** 552–556.

Eriksson, C. 1974. Streaming potentials and other water-dependent effects in mineralized tissues. *Ann. N Y. Acad. Sci.* **283:** 321–338.

Factor, J. R., and M. Naar. 1990. The digestive system of the lobster, *Homarus americanus* II. terminal hepatic arterioles of the digestive gland. *J. Morphol* **206:** 283–291.

Griffith, T. M., and D. H. Edwards. 1990. Basal EDRF activity helps to keep the geometrical configuration of arterial bifurcations close to the Murray optimum. *J. Theor. Biol* **146:** 545–573.

Hutchins, G. M., M. M. Miner, and J. K. Boitnott. 1976. Vessel caliber and branch-angle of human coronary artery branch-points. *Circ. Res.* **38:** 572–576.

Johnson, P. T. 1980. *Histology of the Blue Crab, Callinectes sapidus* Praeger Publishers, New York.

Kamiya, A., and T. Togawa. 1980. Adaptive regulation of wall shear stress to flow change in the canine carotid artery. *Am. J. Physiol.* **239:** H14–H21.

Kamiya, A., J. Ando, M. Shibato, and H. Masuda. 1988. Roles of fluid shear stress in physiological regulation of vascular structure and function. *Biorheology* **25:** 271–278.

Kiani, M. F., and A. G. Hudetz. 1991. A semi-empirical model of apparent blood viscosity as a function of vessel diameter and discharge hematocrit. *Biorheology* **28:** 65–73.

Koller, A., and G. Kaley. 1990. Prostaglandins mediate arteriolar dilation to increased blood flow velocity in skeletal muscle microcirculation. *Circ. Res.* **67:** 529–534.

Koller, A., and G. Kaley. 1991a. Endothelial regulation of wall shear stress and blood flow in skeletal muscle microcirculation. *Am. J. Physiol.* **260:** H862–H868.

Koller, A., and G. Kaley. 1991b. Endothelium regulates skeletal muscle microcirculation by a blood flow velocity-sensing mechanism. *Am. J. Physiol.* **258:** H916–H920.

LaBarbera, M. 1990. Principles of design of fluid transport systems in zoology. *Science* **249:** 992–1000.

LaBarbera, M. 1993. Optimality in biological fluid transport systems. Pp. 565–586 in *Fluid Dynamics in Biology,* A. Y. Cheer and C. P. van Dam, eds. American Mathematical Society, Providence, RI.

LaBarbera, M. 1994. The design of fluid transport systems: a comparative perspective. In *Flow Dependent Regulation of Vascular Function,* J. A. Bevan, G. Kaley, and G. M. Rubanyi, eds. Oxford University Press, Oxford. (In Press)

LaBarbera, M., and G. E. Boyajian. 1991. The function of astrorhizae in stromatoporoids: quantitative tests. *Paleobiology* **17:** 121–132.

LaBarbera, M., and S. Vogel. 1982. The design of fluid transport systems in organisms. *Am. Sci.* **70:** 54–70.

Lametschwandtner, A., U. Lametschwandtner, and T. Weiger. 1990. Scanning electron microscopy of vascular corrosion casts—technique and applications: updated review. *Scanning Microsc.* **4:** 889–941.

Langille, B. L., and F. O'Donnell. 1986. Reductions in arterial diameter produces by chronic decreases in blood flow are endothelium-dependent. *Science* **231:** 405–407.

Levesque, M. J., J. F. Cornhill, and R. M. Nerem. 1979. Vascular casting: a new method for the study of the arterial endothelium. *Atherosclerosis* **34:** 457–467.

Maynard, D. 1960. Circulation and heart function. Pp. 161–226 in *The Physiology of Crustacea Vol. I,* T. H. Waterman, ed. Academic Press, New York.

McMahon, B. R. 1992. Factors controlling the distribution of cardiac output in decapod crustaceans. Pp. 51–61 in *Phylogenetic Models in Functional Coupling of the CNS and the Cardiovascular System,* R. B. Hill, K. Kuwasaka, B. R. McMahon and T. Kuramoto, eds. Karger, Basel.

McMahon, B. R., and L. E. Burnett. 1990. The crustacean open circulatory system: a reexamination. *Physiol. Zool.* **63:** 35–71.

Mo, M., S. Eskin, and W. P. Shilling. 1991. Flow-induced changes in Ca^{2+} signaling of endothelial cells: effect of shear stress and ATP. *Am J. Physiol.* **260:** H1698–H1707.

Murray, C. D. 1926. The physiological principle of minimum work. I. The vascular system and the cost of blood volume. *Proc. Natl. Acad. Sci. USA* **12:** 207–214.

Nollert, M. U., and L. V. McIntre. 1992. Convective mass transfer effects on the intracellular calcium response of endothelial cells. *J. Biomech. Engr.* **114:** 321–326.

Oswald, R. L. 1977. Immobilization of decapod Crustacea for experimental procedures. *J. Mar. Biol. Assoc. U K* **57:** 715–721.

Reich, K. M., C. V. Gay, and J. A. Frangos. 1990. Fluid shear stress as a mediator of osteoblast cyclic adenosine monophosphate production. *J. Cell. Physiol.* **143:** 100–104.

Ruppert, E. E., and K. L. Carle. 1983. Morphology of metazoan circulatory systems. *Zoomorphology* **103:** 193–208.

Shadwick, R. E., C. M. Pollock, and S. A. Stricker. 1990. Structure and biomechanical properties of crustacean blood vessels. *Physiol. Zool.* **63:** 90–101.

Sherman, T. F. 1981. On connecting large vessels to small. *J. Gen. Physiol.* **78:** 431–453.

Suwa, N., T. Niwa, H. Fukasawa, and Y. Sasaki. 1963. Estimation of intravascular blood pressure gradient by mathematical analysis of arterial casts. *Tohoku J. Exp. Med.* **79:** 168–198.

Taylor, E. W. 1982. Control and co-ordination of ventilation and circulation in crustaceans: responses to hypoxia and exercise. *J. Exp. Biol.* **100:** 289–319.

Turbeville, J. M., K. G. Field, and R. A. Raff. 1992. Phylogenetic position of Phylum Nemertini, inferred from 18S rRNA sequences: molecular data as a test of morphological character homology. *Mol. Biol. Evol.* **9:** 235–249.

Turbeville, J. M., D. M. Pfeifer, K. G. Field, and R. A. Raff. 1991. The phylogenetic status of arthropods, as inferred from 18S RNA sequences. *Mol. Biol. Evol.* **8:** 669–686.

Vogel, Steven. 1981. *Life in Moving Fluids: The Physical Biology of Flow.* Princeton University Press, Princeton, NJ.

Wainwright, P. O., G. Hinkle, M. L. Sogin, and S. K. Stickel. 1993. Monophyletic origins of the Metazoa: an evolutionary link with the fungi. *Science* **260:** 340–342.

Wells, R. M. G., and R. P. Dales. 1976. Subunit organization in the respiratory proteins of the Polychaeta. *Comp. Biochem. Physiol.* **54A:** 387–394.

Wieringa, P. A., H. G. Stassen, J. D. Laird, and J. A. E. Spaan. 1988. Quantification of arteriolar density and embolization by microspheres in rat myocardium. *Am. J. Physiol.* **254:** H636–H650.

Zamir, M. 1977. Shear forces and blood vessel radii in the cardiovascular system. *J Gen Physiol.* **69:** 449–461.

Zamir, M., and S. Phipps. 1988. Network analysis of an arterial tree. *J Biomech.* **21:** 25–34.

Zarins, C. K., M. A. Zatina, D. P. Giddens, D. N. Ku, and S. Glagov. 1987. Shear stress regulation of artery lumen diameter in experimental atherogenesis. *J. Vasc. Surg.* **5:** 413–420.

Reference: *Biol. Bull* **186:** 134–135. (February, 1994)

In Situ Spawning of Hydrothermal Vent Tubeworms (*Riftia pachyptila*)

CINDY LEE VAN DOVER

Department of Marine Chemistry and Geochemistry, Woods Hole Oceanographic Institution, Woods Hole, Massachusetts 02543

Riftia pachyptila, *the giant vestimentiferan tubeworm, dominates the biomass of many hydrothermal vent sites in the Gulf of California (Guaymas Basin) and on the East Pacific Rise and Galapagos Spreading Center (1). The worms typically occur in large clumps or thickets as mixed populations of males and females. On a dive series made by the submersible* Alvin *in the vicinity of 9°50′ N on the East Pacific Rise, I observed spawning tubeworms while I was sampling associated fauna. This note presents a brief account of the spawning activity.*

A population of adult vestimentiferans (length greater than 1 m) colonizes a 10 m high basalt pillar at 9°49.59′ N, 104°17.37′ W (2511 m depth) within the Venture Hydrothermal Fields (2). Tubeworms cover most of the surface of the pillar and are relatively uniform in size and so densely packed that they present a cylindrical face of red plumes around the pillar. The site, known as Dudley's Pillar, is marked by a round white lid labeled "2" placed during the Haymon and Fornari expedition in May 1991.

On *Alvin* dive #2474 (6 December 1991), several *R. pachyptila* were observed to spawn during an hour of intermittent observations. Each release of gametes consisted of a small, 10–15 cm cloud of eggs or sperm; the gametes were propelled upward by a rapid, partial withdrawal of the worm into its tube. It was not possible to determine if the same individuals were spawning repeatedly. Fewer than 10 individuals comprising a small portion of the tubeworm population (covering about ⅓ to ½ m^2) were observed engaged in spawning activity. The frequency of spawning contractions of individual worms was not determined; the interval between observed spawns was about 2–3 min. Both males and females were observed spawning. After release, the cloud of eggs separated and the eggs, which were slightly negatively buoyant, were observed to sink in amongst the tubeworms. Sperm formed an apparently neutrally buoyant, milky cloud that dispersed in the current within 10 s. Mixing of egg and sperm clouds was not observed. No spawning activity was noted on a visit to the same site 3 days earlier nor on a subsequent dive to the site 4 days later (L. Mullineaux and L. Garland, pers. comm.).

Although the above observations are limited, we can infer several features of the reproductive ecology of hydrothermal vent tubeworms:

1. Spawning in *R. pachyptila* populations is not necessarily *en masse*. Only a few individuals out of a colony of hundreds were involved in the release of gametes. This observation does not preclude mass spawning by a large proportion of the population under appropriate conditions. Concurrent spawning by several individuals, both male and female, suggests synchronization of gamete release among sexually mature animals, presumably mediated by a chemical cue.

2. Spawning behavior within tubeworm populations, as described above, is intermittent, not continuous. Although this might seem patent from the lack of spawning observations during the accumulated tens of hours of observation time over the 15 years since tubeworm populations were first discovered, the possibility of continuous but inconspicuous release of gametes exists. Observations here suggest that individual spawning is best described as an acute rather than a chronic event, with the spawning period lasting on the order of hours.

3. The negative buoyancy of female gametes generates a dispersal shadow that initially lies close to the adult.

Some features of these observations must be reconciled with other studies. Cary *et al.* (3) describe spawning of female *R. pachyptila* in a shipboard pressure chamber.

Received 20 July 1992; accepted 22 November 1993.

Females released streams of eggs, bound by mucus, from the gonopores over a period of 30 min. The eggs were retained in the vestimental cavity for a few minutes before the mucous binding dissolved and the eggs, positively buoyant, floated upward. In unpressurized aquaria, the same authors (3) observed male tubeworms spawning, with semen continuously flowing from the male gonopores. Though it is conceivable that release of a stream of gametes, rather than punctuated and forceful expulsion of gametes as observed *in situ*, is an alternative reproductive strategy, the observations of Cary *et al.* (3) may represent anomalous behavior as a result of trauma during collection, ascent, and depressurization. If this is the case, the positive buoyancy of the eggs may be an artifact of premature gamete release. Southward and Coates (4) suggest, based on characteristics of the acrosome, that Cary *et al.* witnessed expulsion of immature sperm.

Based on morphological criteria of modified sperm in *R. pachyptila*, Gardiner and Jones (5) suggest that this species has some form of direct sperm transfer or internal fertilization. Likewise, the presence of sperm together with eggs in the female genital tracts of *R. pachyptila* suggests the possibility of internal fertilization (6). Cary *et al.* (3) demonstrate that *R. pachyptila* sperm bundles are effective swimmers and suggest that the bundles may become anchored in the vicinity of the female gonopores or within the anterior regions of the oviducts. Southward and Coates (4) suggest that active sperm transfer is likely in a group of related vestimentiferans (*Ridgeia* spp.), and that this transfer takes place when the plumes of closely juxtaposed animals may brush against each other.

In situ observations reconciled with the literature cited above suggest the following spawning scenario in *R. pachyptila:* (1) Neutrally buoyant sperm bundles are expelled forcefully enough to be dispersed over a field of tubeworms; (2) the sperm bundles swim and attach to females, somehow mediating a spawning response in the female; (3) fertilization occurs internally immediately before spawning or externally (within the vestimental chamber?) just after release of the eggs; (4) accumulated eggs are forcefully ejected into the water column where, negatively buoyant, they spend a short period near the site of release; (5) advective conditions of the turbulent, warm-water vent environment disperse gametes and developing larvae away from the adult population.

Acknowledgments

This note benefited from discussion and review by Steve Gardiner, Robert Hessler, and Stein Kaartvedt. I am grateful to Paul McCaffrey, *Alvin* Pilot-in-Training on Dive 2474, who first observed "something unusual" about the tubeworms. This work was supported in part by a grant from the National Science Foundation.

Literature Cited

1. **Van Dover, C. L., and R. R. Hessler. 1990.** Spatial variation in faunal composition of hydrothermal vent communities on the East Pacific Rise and Galapagos Spreading Center. Pp. 253–264 in *Gorda Ridge: A Seafloor Spreading Center in the United States Economic Zone*, G. R. McMurray, ed. Springer Verlag, New York.
2. **Haymon, R. M., D. J. Fornari, M. H. Edwards, S. Carbotte, D. Wright, and K. C. Macdonald. 1991.** Hydrothermal vent distribution along the East Pacific Rise crest (9°09′–54′ N) and its relationship to magmatic and tectonic processes on fast-spreading mid-ocean ridges. *Earth Planetary Sci. Let.* **104:** 513–534.
3. **Cary, S. C., H. Felbeck, and N. D. Holland. 1989.** Observations on the reproductive biology of the hydrothermal vent tube worm *Riftia pachyptila*. *Mar. Ecol. Prog. Ser.* **52:** 89–94.
4. **Southward, E. C., and K. A. Coates. 1989.** Sperm masses and sperm transfer in a vestimentiferan, *Ridgeia piscesae* Jones, 1985 (Pogonophora: Obturata). Can. J. Zool. **67:** 2776–2781.
5. **Gardiner, S. L., and M. L. Jones. 1985.** Ultrastructure of spermiogenesis in the vestimentiferan tubeworm *Riftia pachyptila* (Pogonophora: Obturata). *Trans. Am. Microsc. Soc.* **104:** 19–44.
6. **Jones, M. L. 1981.** *Riftia pachyptila*, new genus, new species, the vestimentiferan worm from the Galapagos Rift geothermal vents (Pogonophora). *Proc. Biol. Soc. Wash.* **93:** 1295–1313.

CONTENTS

Volume 186 Number 2

THE BIOLOGICAL BULLETIN

APRIL, 1994

Published by the Marine Biological Laboratory

THE
BIOLOGICAL BULLETIN

PUBLISHED BY
THE MARINE BIOLOGICAL LABORATORY

APRIL, 1994

Printed and Issued by
LANCASTER PRESS, Inc.
3575 HEMPLAND ROAD
LANCASTER, PA

THE BIOLOGICAL BULLETIN

THE BIOLOGICAL BULLETIN is published six times a year by the Marine Biological Laboratory, MBL Street, Woods Hole, Massachusetts 02543.

Subscriptions and similar matter should be addressed to Subscription Manager, THE BIOLOGICAL BULLETIN, Marine Biological Laboratory, Woods Hole, Massachusetts 02543. Single numbers, $37.50. Subscription per volume (three issues), $90.00 ($180.00 per year for six issues).

Communications relative to manuscripts should be sent to Michael J. Greenberg, Editor-in-Chief, or Pamela L. Clapp, Managing Editor, at the Marine Biological Laboratory, Woods Hole, Massachusetts 02543. Telephone: (508) 548-3705, ext. 428. FAX: 508-540-6902. E-mail: pclapp@hoh.mbl.edu.

POSTMASTER: Send address changes to THE BIOLOGICAL BULLETIN, Marine Biological Laboratory, Woods Hole, MA 02543.

Second-class postage paid at Woods Hole, MA, and additional mailing offices.
ISSN 0006-3185

INSTRUCTIONS TO AUTHORS

The Biological Bulletin accepts outstanding original research reports of general interest to biologists throughout the world. Papers are usually of intermediate length (10–40 manuscript pages). A limited number of solicited review papers may be accepted after formal review. A paper will usually appear within four months after its acceptance.

Very short, especially topical papers (less than 9 manuscript pages including tables, figures, and bibliography) will be published in a separate section entitled "Research Notes." A Research Note in *The Biological Bulletin* follows the format of similar notes in *Nature*. It should open with a summary paragraph of 150 to 200 words comprising the introduction and the conclusions. The rest of the text should continue on without subheadings, and there should be no more than 30 references. References should be referred to in the text by number, and listed in the Literature Cited section in the order that they appear in the text. Unlike references in *Nature*, references in the Research Notes section should conform in punctuation and arrangement to the style of recent issues of *The Biological Bulletin*. Materials and Methods should be incorporated into appropriate figure legends. See the article by Lohmann *et al.* (October 1990, Vol. **179**: 214–218) for sample style. A Research Note will usually appear within two months after its acceptance.

The Editorial Board requests that regular manuscripts conform to the requirements set below; those manuscripts that do not conform will be returned to authors for correction before review.

1. ***Manuscripts.*** Manuscripts, including figures, should be submitted in triplicate. (Xerox copies of photographs are not acceptable for review purposes.) The submission letter accompanying the manuscript should include a telephone number, a FAX number, and (if possible) an E-mail address for the corresponding author. The original manuscript must be typed in no smaller than 12 pitch or 10 point, using double spacing (*including* figure legends, footnotes, bibliography, etc.) on one side of 16- or 20-lb. bond paper, 8½ by 11 inches. Please, no right justification. Manuscripts should be proofread carefully and errors corrected legibly in black ink. Pages should be numbered consecutively. Margins on all sides should be at least 1 inch (2.5 cm). Manuscripts should conform to the *Council of Biology Editors Style Manual*, 5th Edition (Council of Biology Editors, 1983) and to American spelling. Unusual abbreviations should be kept to a minimum and should be spelled out on first reference as well as defined in a footnote on the title page. Manuscripts should be divided into the following components: Title page, Abstract (of no more than 200 words), Introduction, Materials and Methods, Results, Discussion, Acknowledgments, Literature Cited, Tables, and Figure Legends. In addition, authors should supply a list of words and phrases under which the article should be indexed.

2. ***Title page.*** The title page consists of a condensed title or running head of no more than 35 letters and spaces, the manuscript title, authors' names and appropriate addresses, and footnotes listing present addresses, acknowledgments or contribution numbers, and explanation of unusual abbreviations.

3. ***Figures.*** The dimensions of the printed page, 7 by 9 inches, should be kept in mind in preparing figures for publication. We recommend that figures be about 1½ times the linear dimensions of the final printing desired, and that the ratio of the largest to the smallest letter or number and of the thickest to the thinnest line not exceed 1:1.5. Explanatory matter generally should be included in legends, although axes should always be identified on the illustration itself. Figures should be prepared for reproduction as either line cuts or halftones. Figures to be reproduced as line cuts should be unmounted glossy photographic reproductions or drawn in black ink on white paper, good-quality tracing cloth or plastic, or blue-lined coordinate paper. Those to be reproduced as halftones should be mounted on board, with both designating numbers or letters and scale bars affixed directly to the figures. All figures should be numbered in consecutive order, with no distinction between text and plate figures. The author's name and an arrow indicating orientation should appear on the reverse side of all figures.

4. ***Tables, footnotes, figure legends, etc.*** Authors should follow the style in a recent issue of *The Biological Bulletin* in preparing table headings, figure legends, and the like. Because of the high cost of setting tabular material in type, authors are asked to limit such material as much as possible. Tables, with their headings and footnotes, should be typed on separate sheets,

numbered with consecutive Roman numerals, and placed after the Literature Cited. Figure legends should contain enough information to make the figure intelligible separate from the text. Legends should be typed double spaced, with consecutive Arabic numbers, on a separate sheet at the end of the paper. Footnotes should be limited to authors' current addresses, acknowledgments or contribution numbers, and explanation of unusual abbreviations. All such footnotes should appear on the title page. Footnotes are not normally permitted in the body of the text.

5. ***Literature cited.*** In the text, literature should be cited by the Harvard system, with papers by more than two authors cited as Jones *et al.*, 1980. Personal communications and material in preparation or in press should be cited in the text only, with author's initials and institutions, unless the material has been formally accepted and a volume number can be supplied. The list of references following the text should be headed Literature Cited, and must be typed double spaced on separate pages, conforming in punctuation and arrangement to the style of recent issues of *The Biological Bulletin*. Citations should include complete titles and inclusive pagination. Journal abbreviations should normally follow those of the U. S. A. Standards Institute (USASI), as adopted by BIOLOGICAL ABSTRACTS and CHEMICAL ABSTRACTS, with the minor differences set out below. The most generally useful list of biological journal titles is that published each year by BIOLOGICAL ABSTRACTS (BIOSIS List of Serials; the most recent issue). Foreign authors, and others who are accustomed to using THE WORLD LIST OF SCIENTIFIC PERIODICALS, may find a booklet published by the Biological Council of the U.K. (obtainable from the Institute of Biology, 41 Queen's Gate, London, S.W.7, England, U.K.) useful, since it sets out the WORLD LIST abbreviations for most biological journals with notes of the USASI abbreviations where these differ. CHEMICAL ABSTRACTS publishes quarterly supplements of additional abbreviations. The following points of reference style for THE BIOLOGICAL BULLETIN differ from USASI (or modified WORLD LIST) usage:

A. Journal abbreviations, and book titles, all underlined (for *italics*)

B. All components of abbreviations with initial capitals (not as European usage in WORLD LIST *e.g., J. Cell. Comp. Physiol.* NOT *J. cell. comp. Physiol.*)

C. *All* abbreviated components must be followed by a period, whole word components *must not* (*i.e., J. Cancer Res.*)

D. Space between all components (*e.g., J. Cell. Comp. Physiol.*, not *J.Cell.Comp.Physiol.*)

E. Unusual words in journal titles should be spelled out in full, rather than employing new abbreviations invented by the author. For example, use *Rit Vísindafjélags Islendinga* without abbreviation.

F. All single word journal titles in full (*e.g., Veliger, Ecology, Brain*).

G. The order of abbreviated components should be the same as the word order of the complete title (*i.e., Proc.* and *Trans.* placed where they appear, not transposed as in some BIOLOGICAL ABSTRACTS listings).

H. A few well-known international journals in their preferred forms rather than WORLD LIST or USASI usage (*e.g., Nature, Science, Evolution* NOT *Nature, Lond., Science, N.Y.; Evolution, Lancaster, Pa.*)

6. ***Reprints, page proofs, and charges.*** Authors receive their first 100 reprints (without covers) free of charge. Additional reprints may be ordered at time of publication and normally will be delivered about two to three months after the issue date. Authors (or delegates for foreign authors) will receive page proofs of articles shortly before publication. They will be charged the current cost of printers' time for corrections to these (other than corrections of printers' or editors' errors). Other than these charges for authors' alterations, *The Biological Bulletin* does not have page charges.

ERRATUM

The Biological Bulletin, Volume **185**, Number 2, page 232

The following correction should be made in the article by R. R. Strathmann *et al.* titled "Abundance of food affects relative size of larval and postlarval structures of a molluscan veliger" (*Biol. Bull.* **185**: 232–239).

The fourth sentence of the abstract, which reads "Veligers at the measured shell lengths (>200 μm) had significantly larger velar lobes and longer prototrochal cilia than veligers reared in low concentrations of food," should read "Veligers at the measured shell lengths (>200 μm) had significantly larger velar lobes and longer prototrochal cilia *when* reared in low concentrations of food." The word "when" replaces the words "than veligers."

Reference: *Biol. Bull.* **186**: 137–138. (April, 1994)

The Biological Bulletin–Marine Models Electronic Record (BB-MMER): An Electronic Companion to *The Biological Bulletin*

As you read this, *The Biological Bulletin–Marine Models Electronic Record* (BB-MMER; pronounced "bee'-mer") has begun publication. The primary mission and goals of this electronic record were explained in the December 1993 issue of *The Biological Bulletin*; the *BB-MMER* will publish papers on the collection and husbandry of marine model organisms, the preparation of their cells or tissues, and research techniques and experimental protocols specifically applicable to these systems. The *BB-MMER* will also take on special publishing projects for the scientific community, and one of these is described at the end of this editorial.

The *BB-MMER* will have the same editorial board and stable of reviewers as *The Biological Bulletin*, but it will have its own International Standard Serial Number (ISSN) and copyright. All of the records published in the *BB-MMER* will be stored on-line on a server at the Marine Biological Laboratory in Woods Hole. This server—and thus the *BB-MMER*'s archives—will be available 24 hours a day through the Marine Biological Laboratory's World Wide Web Server (see below). The electronic publication and 24-hour availability *via* the Internet will make every article accessible to a global audience. Indeed, over 55% of *Bulletin* subscriptions are foreign, and for those people, this mode of publication is especially useful.

The address of the *BB-MMER* World Wide Web Server is as follows:

http://www.mbl.edu/BBMER.html

If you do not currently have access to the World Wide Web Server, contact your local network manager to have Mosaic software installed on your computer.

Submission

Articles should be submitted as manuscripts in triplicate, as described in the current Instructions to Authors (see the front pages of each issue of the journal). After review, the final accepted version of the paper should be sent on a 3.5″ disk to the editorial office in Woods Hole. We prefer Microsoft Word 5.0 or WordPerfect 5.1 (specify whether Macintosh or PC format), but we will cope in any event.

Publication

Manuscripts that have been reviewed and accepted will be published as follows:

- Most accepted reports will be published immediately in the appropriate section of the *BB-MMER* and will be citable at once (see Citation below). Because the articles in this electronic journal are published as they are accepted, they will, of course, appear irregularly. They will also be listed and summarized briefly, in print, in the next issue of *The Biological Bulletin.*
- Some manuscripts may be considered by the editors to be of general interest, and thus likely to capture a substantial fraction of the broad and diverse readership of *The Biological Bulletin.* These articles may be published in print, and the abstract added, perhaps with additional technical material, to the appropriate electronic section of the *BB-MMER.*

Updating

A major advantage of electronic publishing is that articles can readily be revised and updated. We envision that the process will involve interaction with readers, as follows. All readers will be encouraged to send signed, constructive suggestions directly to the author, with a copy to the editors of the *BB-MMER.* After 6–12 months, the author will collect these comments (together with his or her own second thoughts) and will produce a revision which will be reviewed. Of course, the revision will not suit everyone; unsatisfied correspondents will be encouraged to contribute a note to the *BB-MMER* which will be reviewed and published separately. In summary, the *BB-MMER* will have some characteristics of an electronic

bulletin board, but all material appearing in it will be reviewed.

Citation

Because electronic articles can be revised and updated, they will change with time, and citations of these articles must do the same. Consider, for example, the following article, which has been submitted for electronic publication in the *BB-MMER*. Let us say that it finally appears in June, 1994, that it is updated in March, 1996, and that someone wants to refer to it in September, 1997. The citation would be as follows:

Kuzirian, A. *Hermissenda crassicornis:* a monographic record of a biomedical research model. *BB-MMER* [serial online] 1994 June: [updated 1996 March 25; cited 1997 Sept. 2]. Available from: http://www.mbl.edu/BBMER.html. Directory: MBL Databases, File BBMMER.

Note that the pertinent history is defined by the dates of original publication, of updating, and of last perusal of the article. The citation format shown above is modified from the recommendation of Karen Patrias of the National Library of Medicine. Further information is available from the National Technical Information Service. (Report Number: NLM-LO-9101.)

•••

KEYS TO MARINE INVERTEBRATES OF THE WOODS HOLE REGION

This useful manual was a project of the Marine Biological Laboratory's Systematics-Ecology Program. The Keys were compiled by Prof. Ralph I. Smith with the help of many contributors and were finally published in 1964. There have been a few revisions and additions in the last 30 years, but, while we weren't paying attention (at least not to systematics), the manual, and especially the reference lists, went badly out of date. We believe that the revision of these Keys is a task that can be accomplished quite efficiently in our electronic journal.

In the next few weeks, the manual will be retyped and published in the *BB-MMER*, complete with figures. When it appears, readers who would like to help in the revision should get in touch with us by e-mail at pclapp@mbl.edu; specifying their specialty. We will find people to take charge of the larger taxa and will coordinate the process.

—Michael J. Greenberg
Editor-in-Chief

Reference: *Biol. Bull.* **186:** 139–152. (April, 1994)

The Effects of Sperm Concentration, Sperm:Egg Ratio, and Gamete Age on Fertilization Success in Crown-of-Thorns Starfish (*Acanthaster planci*) in the Laboratory

J. A. H. BENZIE* AND P. DIXON

Australian Institute of Marine Science, PMB No. 3, Townsville MC, Queensland 4810, Australia

Abstract. Laboratory experiments varying gamete concentrations and gamete age demonstrated significant reductions in fertilization success of the starfish *Acanthaster planci* (L.) with decreasing sperm concentration and increasing age of both eggs and sperm. The effect of aging in sperm was faster than that of eggs, and the speed of sperm aging increased with increasing dilution of sperm. Fertilization success was high over a wide range of sperm: egg ratios but declined rapidly at ratios less than 50, particularly at low sperm concentrations. *A. planci* gametes aged more slowly, and the loss of fertilizing capacity of sperm with dilution (the respiratory dilution effect) was far less, than in sea urchins. These characteristics provide a mechanism for enhanced fertilization success at given sperm concentrations and at greater distances and times from the point of gamete release, and may explain the higher fertilization rates achieved over longer distances in the wild by *A. planci* relative to sea urchins. Gametes would remain competent for longer periods at more dilute concentrations and so better achieve long-distance fertilization. Gametes obtained at the end of the breeding season were qualitatively different from those obtained early in the breeding season and showed reduced fertilization success for a given combination of variables, and different fertilization dynamics.

Introduction

Most work on sea urchins and starfish has concentrated on the biochemical and cellular mechanisms underlying gamete maturation and fertilization and early larval development, using a few model species (Ishikawa, 1975; Chia and Bickell, 1983; Kanatani and Nagahama, 1983; Meijer and Guerrier, 1984). Reports on the effects of gamete age and concentration on fertilization success are mostly limited to laboratory studies and rarely address the process in an ecological context (Tyler and Tyler, 1966; Pennington, 1985; Levitan *et al.*, 1991).

Fertilization is affected by the age of the gametes (the time since they were first released into the seawater), the concentration of sperm, and the number of sperm relative to the number of eggs (Lillie, 1915, 1919; Cohn, 1918; Gray, 1928). Additional information on the effect of gamete concentrations on fertilization success has been obtained incidentally from studies using sea urchin sperm as a toxicological assay (Greenwood and Bennett, 1981; Kobayashi, 1984; Dinnel *et al.*, 1987). Pennington (1985) was the first to study fertilization success in the field. He confirmed the loss of fertilizing capacity of sperm of sea urchins with dilution and with increasing gamete age in the laboratory and inferred that the effects of sperm dilution were largely responsible for the marked reductions in fertilization success he observed in field experiments as distance between eggs and spawning males increased. Pennington's theory has been supported by further studies on sea urchins (Levitan, 1991; Levitan *et al.*, 1992), and similar explanations have been advanced to explain rapid reductions in fertilization success with distance in hydroids (Yund, 1990) and ascidians (Grosberg, 1991).

Despite the importance of gamete age and sperm concentration in determining fertilization success between individuals spatially separated to different extents, only one study has attempted to quantify experimentally the conjoint effects of several variables on fertilization success

Received 6 January 1993; accepted 28 December 1993.

* Author to whom correspondence should be addressed.

(Levitan *et al.*, 1991). These authors demonstrated that the theoretical model developed by Vogel *et al.* (1982) accounted for 91% of the variation they observed in fertilization success.

The aim of the present work was to obtain conjoint information on the effects of sperm concentration, sperm: egg ratio, and gamete age on fertilization success in the crown-of-thorns starfish, *Acanthaster planci* (L.). Fertilization dynamics in this species is of particular interest because its large increases in population size (outbreaks), which have caused considerable damage to coral reefs throughout the world (Moran, 1986), could result from fluctuations in fertilization success. Despite intensive research in recent times, many aspects of *A. planci* biology—including fertilization dynamics—are still unknown (Lassig and Kelleher, 1991).

Although *A. planci* has been spawned and reared in captivity, fertilization success was not reported (Yamaguchi, 1974; Lucas, 1982). Information on spawning and fertilization rates in the field has been reported (Babcock and Mundy, 1992), but no studies have examined the influence of gamete characteristics or gamete concentrations on fertilization success. Comprehensive information on the conjoint effects of gamete concentrations and gamete age on fertilization success in *A. planci* is not only specifically relevant to the occurrence of outbreaks in the crown-of-thorns starfish but also adds to the limited information available on the effect of these variables on external fertilization in marine organisms.

Materials and Methods

Starfish were collected from Davies Reef (18 °50′ S, 147 °39′ E) in the Great Barrier Reef on the east coast of Australia from November to February in 1987, 1988, and 1989, in each of the breeding seasons for *A. planci*. Animals were sexed, and their breeding condition assessed, by making a small cut in the proximal part of one arm of the starfish and examining the gonad. Individuals with well-developed gonads were then kept separately in clear acrylic tanks with fresh-flowing seawater until they were used in the experiments. The seawater used in this treatment and in all experiments was approximately 28°C and pH 8.3. The usual range in summer values for the Great Barrier Reef inshore waters is 28–33°C and pH 8.2–8.6.

Gametes were obtained from portions of gonad approximately 5 cm^3 in volume that were removed from individual starfish through a 2-cm cut in the dorsal margin of one side of the proximal part of an arm. The tissue was placed in 100 ml of filtered (0.4 μm) seawater (FSW) containing 10^{-6} *M* 1-methyladenine to induce gamete release. Gonad tissue from female starfish was collected 1 h before gonad tissue from males because females responded more slowly than males to hormonal induction (approximately 45 min for females compared with less than 30 min for males) and eggs had to be counted into beakers before sperm were added. Only gametes extruded during the first 10–15 min in response to the hormonal treatment were used in the experiments.

Eggs were pipetted into a shallow crystallizing dish with clean FSW. After eggs had matured (as evidenced by germinal vesicle breakdown), they were counted into separate beakers for the various experimental treatments. For treatments requiring small numbers of eggs (80 or fewer), eggs were counted out individually from pasteur pipettes. For treatments requiring 100 eggs or more, a monolayer of eggs was settled on the base of the dish over a grid in which each square contained 100 eggs. With the aid of a dissecting microscope, eggs from the appropriate number of squares were sucked into a pasteur pipette and added to the test container.

The sperm solution was separated from male gonad tissue by decanting the solution into another beaker. This original 100 ml of concentrated solution usually contained 12–40 $\times$ 10^6 sperm ml^{-1}. Because 2.5 ml of tissue remained after sperm release, these figures suggest that sperm were stored and extruded at densities of 2 $\times$ 10^8–10^9 sperm ml^{-1}. Given that the extrusion occurred over 20 min, the average rate of sperm release from excised gonad was approximately 10^5–10^6 sperm s^{-1} One milliliter of well-mixed solution was removed and diluted 500 times in FSW to which formalin had been added to fix the sperm before counting. Two drops of solution were placed on a hemacytometer and the number of sperm counted. These data were used to calculate the appropriate aliquot of the original concentrated sperm solution to be diluted with FSW to provide 500 ml of a stock solution containing 2 $\times$ 10^6 sperm ml^{-1}. This stock solution was used as the base for serial dilutions to provide sperm of varying concentrations.

Preliminary tests had shown that sperm maintained at a concentration of 2 $\times$ 10^6 sperm ml^{-1} retained full fertilizing capacity for at least 24 h, but the longest period over which the solution was used in any experiment was less than 8 h. Rates of fertilization at a variety of dilutions from such stock solutions held for 8 h were the same as those from the same dilutions made immediately after the stock solution was created. In other words, stock solutions of 2 $\times$ 10^6 sperm ml^{-1} did not appear to "age" over 24 h. Timing was therefore carried out from the time of dilution from the stock solution held at 2 $\times$ 10^6 sperm ml^{-1}. This approach provided a clear and reproducible start to experiments with "non-aged" sperm.

There was no correlation between initial concentrations at which sperm had been spawned and the relative speed of aging of the sperm in subsequent experiments; the existence of a correlation might suggest that the initial spawning into seawater had irreversibly aged the sperm.

It should be noted that when sperm were released, they accumulated in a thick sludge at the base of the beaker and were therefore accumulating in very high concentrations. The values of 12–40 $\times$ 10^6 sperm ml^{-1} were observed after thorough mixing of the seawater in the beaker at the end of the spawning period.

Serial dilutions were used to obtain stock solutions of each sperm concentration immediately prior to first adding sperm to the eggs. To obtain the desired final concentration of sperm, 1 ml of sperm stock solution was added to every 19 ml of FSW containing the eggs. Stock sperm concentrations derived from 1, 1:10, 1:100, 1:1000, and 1:2000 dilutions of the 2 $\times$ 10^6 sperm ml^{-1} solution provided respective final concentrations of sperm of 10^5, 10^4, 10^3, 10^2, and 50 sperm ml^{-1} in the FSW containing the eggs. Most of the treatments were carried out in 50-ml glass beakers with 19 ml of FSW. However, where a specified sperm:egg ratio would have resulted in less than 10 eggs in 19 ml of FSW, volumes up to 1 liter were used to provide treatments having at least 10 eggs.

Preliminary experiments had demonstrated that no fertilization occurred if sperm concentrations were 10 sperm ml^{-1} or less, and that the proportion of eggs fertilized in any treatment did not increase after 45 min. In all experiments, therefore, only sperm concentrations greater than 10 sperm ml^{-1} were used, and the fertilized eggs were counted 45 min after sperm was first added to the eggs. In treatments using small containers, all eggs were counted and the number of fertilized eggs (those with a raised fertilization membrane) was noted, with the aid of a dissecting microscope. In treatments with large volumes of seawater, the eggs were collected using a pasteur pipette and placed in a small volume of seawater where those with a raised fertilization membrane were counted.

Preliminary experiments also demonstrated marked differences in performance by different individuals of one sex when mated with a given individual of the opposite sex and showed that the ranking of performance varied with the individual of the opposite sex used. Because experimental results could be strongly influenced by using one individual in several matings, subsequent experiments used an individual only once.

Variation in fertilization success at different times and in different years

The logistic difficulties in undertaking the large-scale combinations of sperm concentration, sperm:egg ratio, and differently aged gametes meant that data were collected from experiments conducted at different times in the breeding season and from more than one breeding season. To assess the effects of these variations on fertilization success, data from each time period were obtained on fertilization success at 0, 1, and 2 h after gamete release at sperm:egg ratios of 5000 and sperm concentrations of 10^4 sperm ml^{-1}.

Sperm concentration and sperm:egg ratio experiments

Experiments testing the effects of sperm concentration and sperm:egg ratio used final sperm concentrations of 50, 10^2, 10^3, 10^4, and 10^5 sperm ml^{-1} and sperm:egg ratios of 100, 500, 1000, 2500, and 5000 in every combination, giving a total of 25 treatments. Testing a number of the low sperm:egg ratios at sperm concentrations less than 50 sperm ml^{-1} was impracticable: it would have required several replicates of 10 l or more with only 10 eggs that would have been difficult to relocate and score.

Eggs were collected, and sperm solutions were diluted, immediately before the experiment and were used throughout the experiment, so that both gametes were aging over the course of the experiment. Sperm from the diluted stock concentrations was added to sets of eggs at 0 min, 15 min, 45 min, 1 h 45 min, and every succeeding hour until 6 h 45 min from the first insemination. Two replicates of each test combination were performed per mating, and a total of 10 different matings were used.

Gamete aging experiments

The number of sperm dilutions and sperm:egg ratios was reduced in experiments testing the independent effects of aging in either eggs or sperm because four combinations of "aging" and "fresh" gametes had to be tested. At each time interval, aging sperm was added to aging eggs as in the sperm concentration and sperm:egg ratio experiment. Aging sperm was also used to fertilize a newly collected set of fresh eggs from ovary tissue induced to spawn 45 min prior to that insemination. Freshly diluted stock solutions of fresh sperm were prepared from the 2 $\times$ 10^6 sperm ml^{-1} stock and added to both aging and fresh eggs. The sperm concentrations used were 10^2 and 10^4 sperm ml^{-1} and the sperm:egg ratios were 100, 1000, and 5000; with four combinations of gametes, this gave a total of 24 treatments. Sperm was added to sets of eggs at 0 min, 45 min, 1 h 45 min, and every succeeding hour until 6 h 45 min from the first insemination. Two replicates of each test combination were performed per mating, and a total of six different matings were used.

Statistical analysis

All results were expressed as percent fertilization and were arcsin transformed prior to analysis of variance and stepwise multiple regression using BMDP (Dixon *et al.*, 1983) and SAS (SAS Inc., 1985). Multidimensional plots were produced using graphic programs in SAS.

Table I

Analysis of variance testing for differences between early and late breeding season (time in breeding season), breeding seasons (year), and time since gamete release (gamete age), on fertilization success of Acanthaster planci

Source of variance	Degrees of freedom	Mean square	$F_{0,10}$
Time in breeding season	1	4.61	44.9***
Gamete age	2	0.86	8.4***
Year	1	0.12	1.2^{NS}
Time in breeding season × gamete age	2	0.17	1.7^{NS}
Time in breeding season × year	1	0.67	6.5*
Gamete age × year	2	0.17	1.7^{NS}
Time in breeding season × gamete age × year	2	0.08	0.8^{NS}
Error	49	0.10	

Data were from breeding seasons 2 and 3, fertilization at 0, 1, and 2 h from gamete release, at sperm: egg concentration of 5000 and final sperm concentration of 10^4 sperm ml^{-1} (see Table II for means).

* $P < 0.05$; *** $P < 0.001$; ^{NS} not significant.

Results

Variation in fertilization success at different times in the breeding season and in different years

Analysis of variance demonstrated that time after the gametes were released (gamete age) and period in the breeding season when the mating was made (time in breeding season) had highly significant effects on fertilization success, but that year had no independent effect (Table I). These results reflected the consistent drop in fertilization success with gamete age, whether early or late in the breeding season, and in every year (Table II). Similarly, fertilization rates were consistently lower at the end of the breeding season than early in the breeding season in every year. The significant interaction of time in breeding season with year reflected the fact that the difference in fertilization rates early and late in the breeding season was not the same from year to year.

Sperm concentration and sperm:egg ratio experiments

Data from two breeding seasons were pooled to increase the number of matings included in these tests but, because time at which mating took place within the breeding season had been shown to have a significant influence on fertilization rates, time in breeding season was included as a factor in the analysis. Sperm concentration, sperm: egg ratio, time after gamete release (gamete age), and time in breeding season had highly significant independent effects on percent fertilization (Table III). The large number of significant interaction terms demanded that care be taken in the interpretation of the main effects and indicated that, although the direction of change was the same for various combinations of factors, the degree of change was not. The principal pattern observed in the interaction terms for the analysis of the total data set was the lack of significance, or the lower significance, of interactions including sperm:egg ratio.

Stepwise multiple regression showed that gamete age, sperm concentration, and time in the breeding season all had significant effects, but that sperm:egg ratio had only a slight effect. R^2 values indicated that these variables cumulatively explained 45.2, 56.3, 63.7, and 64.2% of the variation, respectively.

Interpretation of the analysis of variance was assisted by reference to additional analyses in which the data set was first restricted to times less than 3.75 h and then to times less than 3.75 h and sperm concentrations greater than 10^3 sperm ml^{-1}. The restricted analyses were carried out because a large number of the treatments had zero

Table II

Mean percent fertilization rates (± standard errors) early and late in the Acanthaster planci *breeding season for gametes fertilized at 0, 1, and 2 h after gamete release*

Time after gamete release (hours)	Breeding season 1		Breeding season 2		Breeding season 3	
	Early (Nov–Dec 1986)	Late (Jan 1987)	Early (Nov–Dec 1987)	Late (Jan 1988)	Early (Nov–Dec 1988)	Late (Jan 1989)
0	–	94 ± 2 (3)	99 ± 1 (7)	79 ± 11 (5)	97 ± 2 (8)	67 ± 23 (2)
1	—	79 ± 16 (3)	92 ± 3 (7)	86 ± 8 (5)	94 ± 3 (8)	42 ± 39 (2)
2	—	54 ± 19 (3)	74 ± 24 (2)	31 ± 3 (5)	92 ± 7 (8)	19 ± 9 (2)

The sperm:egg ratio was 5000 and the final sperm concentration 10^4 sperm ml^{-1} in all tests. The sample size of independent matings is given in parentheses.

Table III

Analysis of variance testing the effects of time since initial gamete release (gamete age), sperm:egg ratio, sperm concentration, and time within breeding season (time in breeding season) on fertilization success in Acanthaster planci

	Total data set			Time < 3.75 h			Time < 3.75 h, sperm concentration > 1000		
Source of variance	Degrees of freedom (DF)	Mean square (MS)	$F_{0.07}$	DF	MS	$F_{0.11}$	DF	MS	$F_{0.14}$
Gamete age (G)	8	48.98	723.6***	4	27.97	260.8***	4	7.15	52.7***
Sperm:egg ratio (R)	4	1.61	23.7***	4	2.48	23.1***	4	0.24	1.8^{NS}
Sperm concentration (C)	4	22.00	325.0***	4	25.13	254.3***	1	1.58	11.7***
Time in breeding season (T)	1	60.43	892.7***	1	77.84	725.8***	1	17.37	128.2***
G × R	32	0.19	2.9***	16	0.16	1.5^{NS}	16	0.03	0.2^{NS}
G × C	32	1.16	17.1***	16	0.77	7.2***	4	0.31	2.3^{NS}
R × C	16	0.13	1.9*	16	0.27	2.5***	4	0.05	0.4^{NS}
G × T	8	3.46	51.1***	4	1.58	14.7***	4	0.26	1.9^{NS}
R × T	4	0.16	2.3^{NS}	4	0.22	2.0^{NS}	4	0.02	0.1^{NS}
C × T	4	0.43	6.3***	4	1.46	13.6***	1	1.61	11.9***
G × R × C	128	0.06	0.8^{NS}	64	0.07	0.6^{NS}	16	0.04	0.3^{NS}
G × R × T	32	0.06	0.9^{NS}	16	0.10	1.0^{NS}	16	0.04	0.3^{NS}
G × C × T	32	0.63	9.3***	16	0.78	7.3***	4	0.65	4.8***
R × C × T	16	0.09	1.4^{NS}	16	0.16	1.5^{NS}	4	0.04	0.3^{NS}
G × R × C × T	128	0.04	0.6^{NS}	64	0.06	0.5^{NS}	16	0.03	0.2^{NS}
Error	1800	0.07		1000	0.11		400	0.14	

* $P < 0.05$; *** $P < 0.001$; ^{NS} not significant.

fertilization values for many of the longer times after gamete release. It was thought that these values might depress the value of the error term and result in many significant interaction terms. Similarly, many of the lower sperm concentrations provided many zero fertilization records.

Analysis of variance for time restricted to less than 3.75 h showed the same pattern of effects as the complete analysis except for the loss of a significant interaction of gamete age and sperm:egg ratio. In the analysis additionally restricted to higher sperm concentrations, the significance of the main effects of sperm:egg ratio was lost.

Significant interaction terms were observed only for a two-way interaction of sperm concentration and time in breeding season and a three-way interaction of gamete age, sperm concentration, and time in breeding season.

Graphs illustrating fertilization at different times after gamete release for matings made early and late in the breeding season showed a consistent reduction in fertilization rates at all combinations of sperm concentration and sperm:egg ratios in the late breeding season (Fig. 1). Similarly, the higher the sperm concentration, the higher the degree and the greater the persistence of fertilization success. Fertilization rate decreased as gamete age increased, in every combination of factors. The pattern in each graph was similar for every sperm:egg ratio at sperm concentrations greater than 10^3 sperm ml^{-1}, indicating the reason for the lack of significant effects of sperm:egg ratio in the analysis restricted to high sperm concentrations and short times since gamete release. Fertilization rates were lower at lower sperm:egg ratios for given sperm concentrations, particularly for lower sperm concentrations and older gametes. This identified the source of the main effect of sperm:egg ratio in the analysis of the complete data set, the significant sperm:egg ratio × sperm concentration interactions in the analysis restricted to shorter times since gamete release, and an additional sperm:egg ratio × gamete age interaction in the full analysis. Similarly, the strong two- and three-way interactions of gamete age, sperm concentration, and time in breeding season reflected the progressively lower fertilization rates with increased gamete age and decreased sperm concentrations, as well as the exacerbating effect that mating late in the breeding season had on the depressing influence of these factors on fertilization.

The graphs in Figure 1 represent sections taken parallel to the time axis through the fertilization rate response surfaces plotted in Figure 2 as a function of sperm concentration and time since gamete release for different sperm:egg ratios. The surfaces for sperm:egg ratios of 5000 and 500 in the early breeding season were similar, whereas those from the late breeding season showed a reduction in fertilization rates at sperm:egg ratios of 500 relative to those at sperm:egg ratios of 5000 at short time intervals from gamete release. The surfaces from the late breeding season also showed a marked reduction in fertilization relative to those from the early breeding season, as well as the absence of a plateau of high fertilization at short

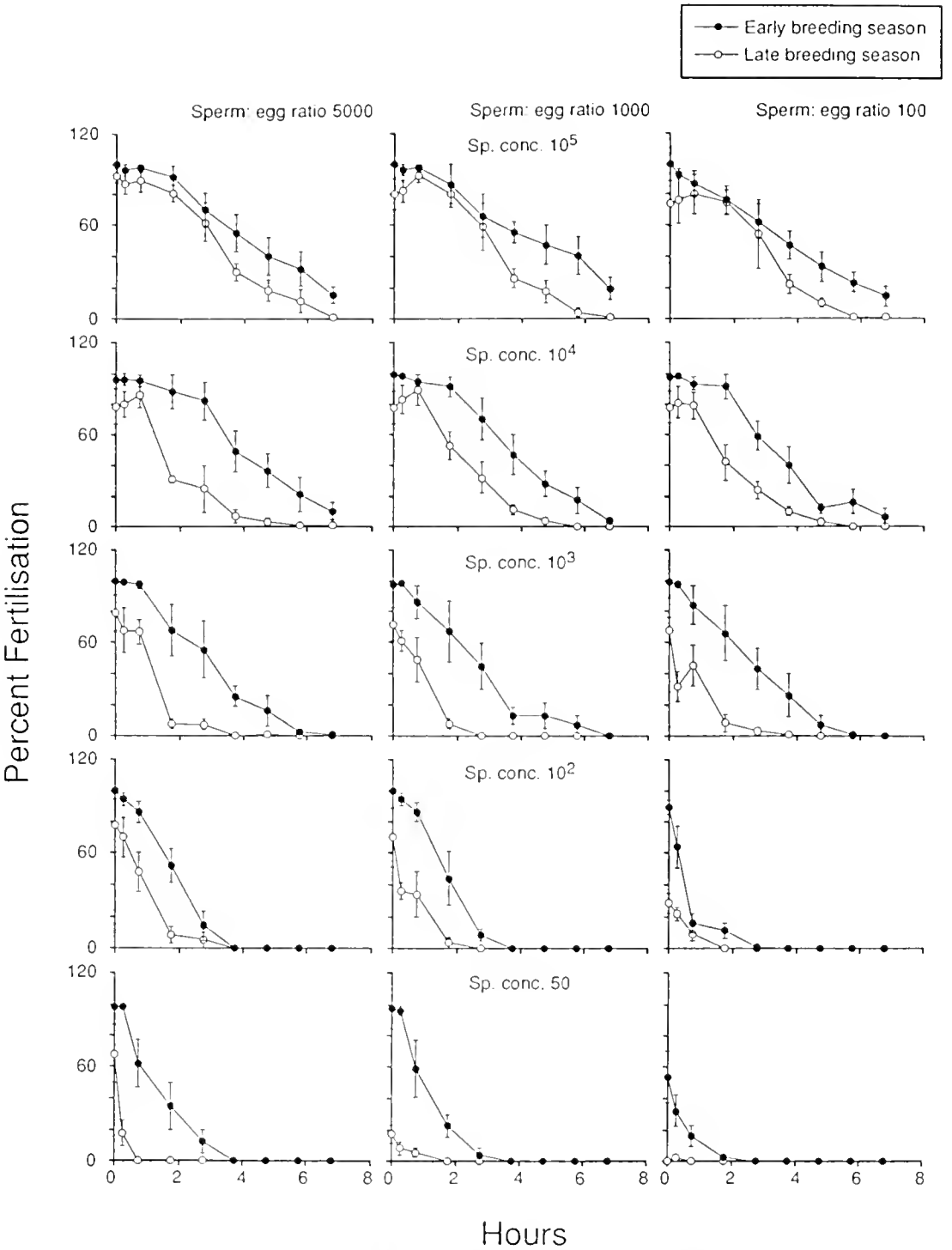

Figure 1. Mean percent fertilization, with standard error, of eggs from *Acanthaster planci* when mixed with sperm at different sperm concentrations (rows) and sperm:egg ratios (columns) over a period of 6 h 45 min. Sperm concentration varied from 50 to 10^5 sperm ml^{-1}, and sperm:egg ratio varied from 100 to 5000. Data from matings early (November–December) and late (January) in the breeding season are plotted separately.

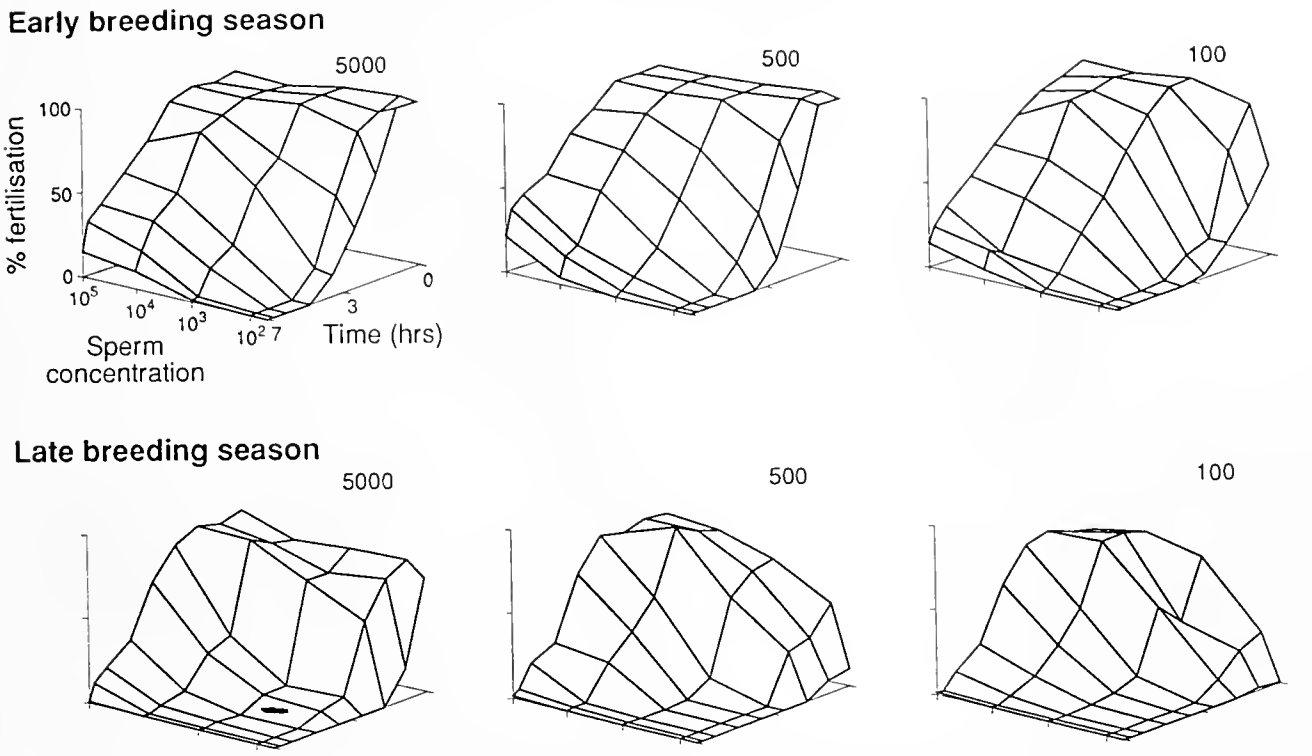

Figure 2. Fertilization response surfaces over a series of sperm concentrations and times since gamete release, plotted for three different sperm:egg ratios for the early and late breeding season.

times from gamete release. The overall geometry of the surface for the sperm:egg ratio of 500 from the late breeding season was depressed relative even to the sperm:egg ratio of 100 from the early breeding season, although its general form was similar. The two-dimensional surface of fertilization in these illustrations appears to be the result of the orthogonal interaction of two sets of sigmoid curves.

The temporal dynamics of fertilization have been summarized in a series of fertilization rate response surfaces plotted at different times from gamete release as a function of sperm:egg ratio and sperm concentration (Fig. 3). Data for the early breeding season show a plateau of high fertilization in the first 45 min, with a drop in fertilization observed only for the lowest sperm:egg ratios and sperm concentrations. The general decline in fertilization with time was more rapid for low sperm concentrations and varied little with sperm:egg ratio. When data from early and late breeding season were compared, the consistently lower fertilization rates and the more rapid decline in fertilization rate with time and at lower sperm concentrations in the late breeding season were clear (Fig. 4). The response surface for the late breeding season also tilted downwards more strongly at the apex of the sperm:egg ratio and sperm concentration axes than that from the early breeding season and folded downwards at relatively higher sperm:egg ratios (compare the 15-min and 45-min graphs in Figs. 3 and 4).

Gamete aging experiments

The gamete aging experiments included data only from the early breeding season and therefore did not require inclusion of time in breeding season as a factor in the analysis. Time since the aging gametes were first released (time), egg type (fresh or aged), sperm type (fresh or aged), sperm:egg ratio, and sperm concentration all had highly significant main effects (Table IV). Fertilization rates decreased with time since gamete release, with aged as opposed to fresh eggs or sperm, with decreasing sperm:egg ratio, and with decreasing sperm concentration (Fig. 5). There were highly significant two-way interactions of sperm concentration with all other factors, reflecting the greater reduction in fertilization rate at lower sperm concentrations with increasing time from gamete release, aged relative to fresh gametes, and decreasing sperm:egg ratio. Fertilization rates were also increasingly depressed the older the aged eggs or aged sperm used, leading to the significant two-way interactions between time since gamete release, egg type, and sperm type.

When the treatments using different sperm concentrations were analyzed separately, both showed significant

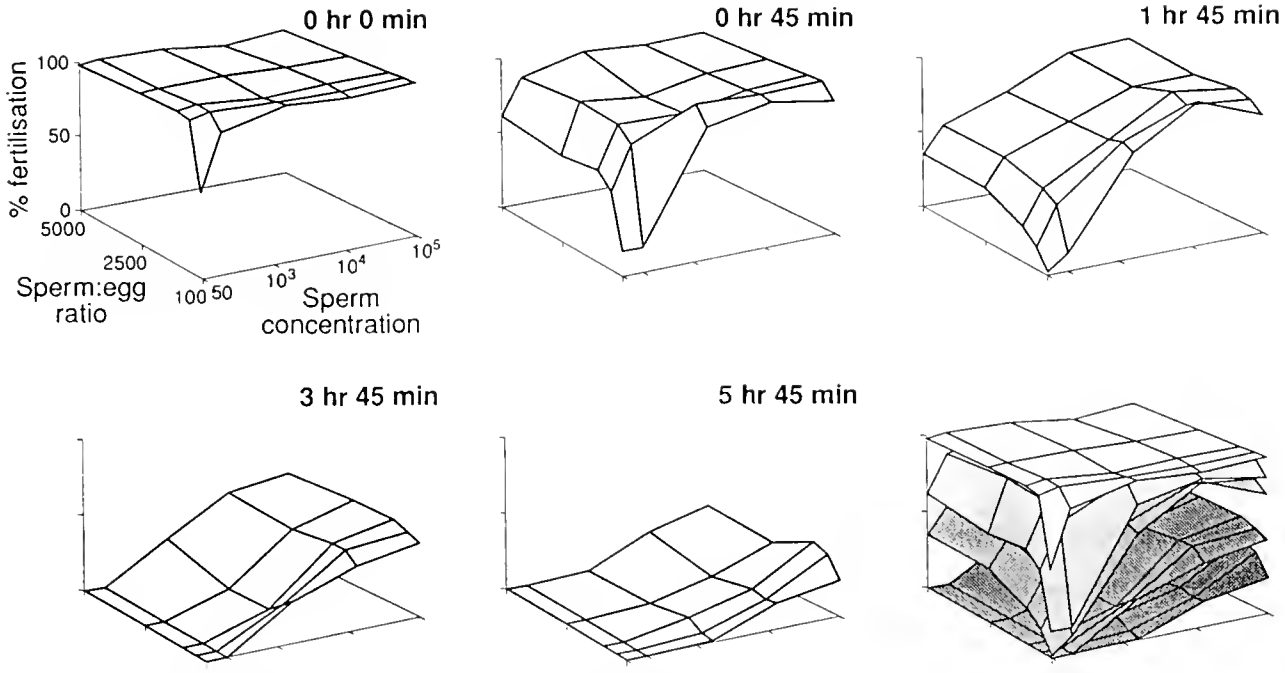

Figure 3. Fertilization response surfaces over a series of sperm concentrations and sperm:egg ratios, plotted at different times from gamete release. The set of six graphs depict the decline in fertilization early in the breeding season, with the sixth graph providing a key to the relative positions of the surfaces shown in the preceding five graphs.

main effects of time since gamete release, egg type, sperm type, sperm:egg ratio, and sperm concentration; both also showed the same suite of significant two-way interactions. However, the two-way interaction of egg type and sperm: egg ratio was nonsignificant in the 10^2 sperm ml^{-1} analysis, and that of sperm type and sperm:egg ratio was nonsignificant in the 10^4 sperm ml^{-1} analysis (Table IV). Far fewer higher order interactions were significant in each case.

The results clearly demonstrated an aging of both gametes, with aging eggs fertilized using fresh sperm showing a decline in fertilization rate after 3 h, dropping to 20% by 7 h (Fig. 5). The aging rate of sperm was much faster and dependent upon sperm concentration. At sperm concentrations of 10^2 sperm ml^{-1}, the fertilization rates of fresh eggs fertilized by aging sperm declined after 1 h, dropping to 0% after 3 to 4 h. At sperm concentrations of 10^4 sperm ml^{-1}, fresh eggs fertilized by aging sperm showed a decline in fertilization rate after 3 h, dropping to 20% by 7 h. Thus at 10^4 sperm ml^{-1}, aging eggs fertilized by aging sperm showed a fertilization rate similar to that of aging eggs and fresh sperm. At high sperm concentrations, fertilization rates were therefore largely determined by egg aging. In contrast, at 10^2 sperm ml^{-1}, aging eggs fertilized by aging sperm showed a pattern similar to that of fresh eggs fertilized by aging sperm. At low sperm concentrations, fertilization rates were therefore determined to a large extent by sperm aging.

Discussion

In this investigation, the first detailed analysis of fertilization dynamics of a starfish, *A. planci* showed general similarities to sea urchins—but there were also marked differences. The relative effects of sperm concentration, gamete age, and sperm:egg ratios on fertilization success in *A. planci* were similar to those reported for several species of sea urchin. Egg density or sperm:egg ratio had little influence on fertilization success, but gamete age and sperm concentration had marked effects, as in sea urchins (Lillie, 1915; Dinnel *et al.*, 1987; Levitan *et al.*, 1991). However, fertilization dynamics in *A. planci* appeared to be more sensitive to sperm:egg ratio than are the sea urchins studied to date. Although Levitan *et al.* (1991) found no significant effect of egg concentration over the range they examined, they used a model developed by Vogel *et al.* (1982) to predict reduced fertilization success for *Strongylocentrotus franciscanus* at low sperm concentrations of 10^2 sperm ml^{-1} (10 sperm μl^{-1}) and high egg concentrations of 10^4 eggs ml^{-1} (10^3 eggs μl^{-1}), equaling sperm:egg ratios of 0.01 or less (see Fig. 8 of Levitan *et al.*, 1991). Effects on fertilization success of *A. planci* were observed at far higher sperm:egg ratios (up to 100 early in the breeding season and up to 500 late in the breeding season) for sperm concentrations of 10^2 sperm ml^{-1} (Fig. 3).

The fertilization response surfaces for the sea urchin *S. franciscanus* (Levitan *et al.*, 1991) and the starfish *A. planci*

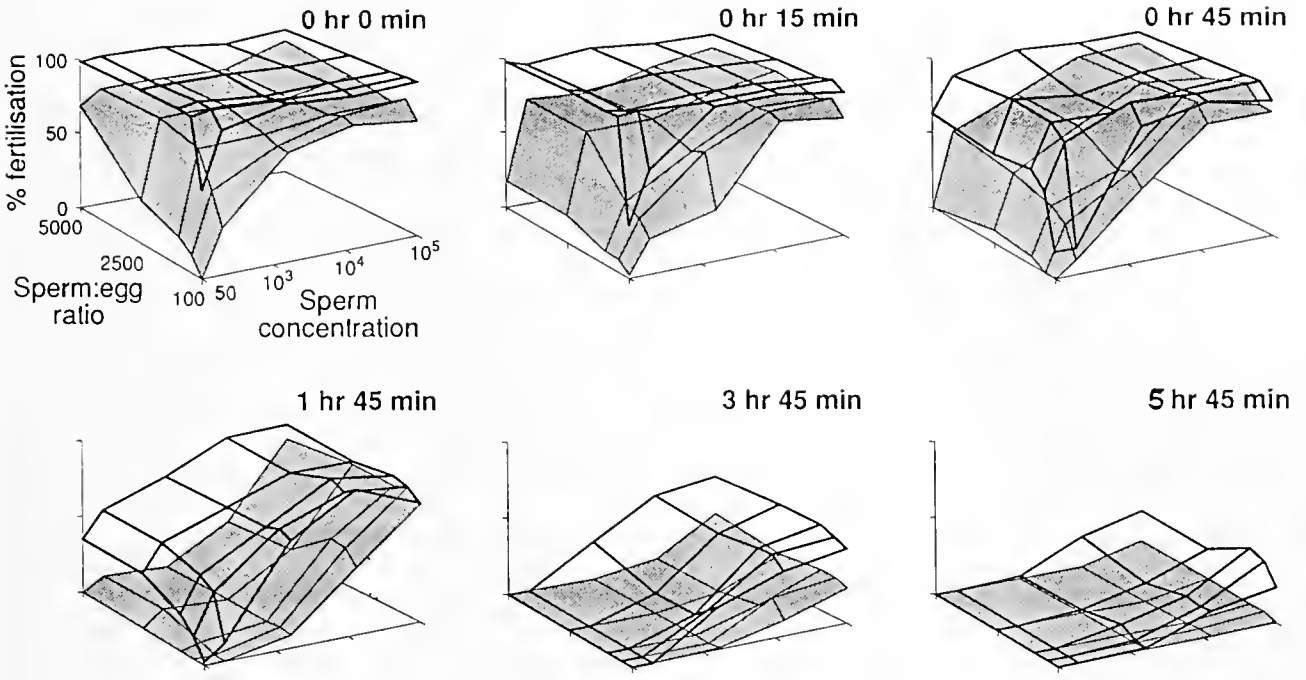

Figure 4. Fertilization response surfaces over a series of sperm concentrations and sperm:egg ratios, plotted at different times from gamete release and comparing the fertilization response surface early (transparent surface) and late (stippled surface) in the breeding season.

were similar in that fertilization success declined with declining sperm concentrations and increasing time from gamete release. The loss of fertilizing capacity of sperm with dilution is called the respiratory dilution effect (Chia and Bickell, 1983) and results from the fact that although the total amount of oxygen consumed by a spermatozoan over its lifespan is independent of dilution, the rate of consumption is far greater at low sperm concentrations, leading to a shorter lifespan at low concentrations. A dilution effect was clearly demonstrated for *A. planci.*

However, the dynamics of fertilization of *A. planci* were very different from those of *S. franciscanus.* Fertilizing capacity was lost more rapidly by *S. franciscanus* at given sperm concentrations and declined more rapidly with increasing dilution of sperm. At sperm concentrations of 10^5 sperm ml^{-1}, fertilization rates for *A. planci* early in the breeding seasons were above 90% for up to 105 min from the time of gamete release, but rates for *S. franciscanus* had declined from over 90% at 10 min to approximately 40% by 80 min (compare Fig. 1 from the present paper with Fig. 2 of Levitan *et al.,* 1991). Similarly, at sperm concentrations of 10^3 sperm ml^{-1}, fertilization rates for *A. planci* were above 90% for up to 45 min, declining to 50% by 105 min; but rates for *S. franciscanus* were less than 40% at time zero, declining to less than 10% by 80 min. Fertilization success in *A. planci* at time zero showed no decline at sperm concentrations from 10^5 to 10^3 sperm ml^{-1}, but fertilization in *S. franciscanus* fell from almost 100% to approximately 30% over the same range. The fertilization dynamics inferred from more restricted data reported for a range of sea urchin species (Lillie, 1915; Gray, 1928; Pennington, 1985) were comparable to that reported for *S. franciscanus* by Levitan *et al.* (1991). Fertilization dynamics cannot be further compared using parameters, such as β, from the Vogel *et al.* (1982) model because these parameters require data on the fertilization success achieved at different gamete contact times, and these data are not available for *A. planci.*

A. planci sperm aged more rapidly than eggs, at least at concentrations likely to be encountered in the field; similar results have been described for the sea urchin *S. droebachiensis* (Pennington, 1985). Detailed data on the independent aging of sea urchin sperm and eggs are lacking, making it impossible to establish whether the extent to which egg aging determines fertilization dynamics at high sperm concentrations and sperm aging determines fertilization dynamics at low sperm concentrations is similar in sea urchins and starfish. It is clear that eggs of the crown-of-thorns starfish are capable of being fertilized for up to several hours after they are first released. *A. planci* sperm also retain their fertilizing capacity for 1 to 2 h even at reasonably dilute concentrations: this is because the sperm of *A. planci* are less affected by the reduced respiratory dilution effect than are sea urchin sperm.

A greater sensitivity of fertilization to sperm:egg ratio and a relatively slow rate of gamete aging appear to char-

Table IV

Analysis of variance testing the effects of time since initial gamete release (time), egg type (whether fresh or aged), sperm type (whether fresh or aged), sperm egg ratio, and sperm concentration, on fertilization success of Acanthaster planci

	Total data set			Sperm concentration = 10^2			Sperm concentration = 10^4		
Source of variance	Degrees of freedom (DF)	Mean square (MS)	$F_{0.07}$	DF	MS	$F_{0.08}$	DF	MS	$F_{0.06}$
Time (T)	6	11.17	161.1***	6	5.08	60.7***	6	6.93	126.2***
Egg type (E)	1	25.71	370.9***	1	4.83	57.8***	1	24.71	449.9***
Sperm type (S)	1	45.12	650.9***	1	66.51	794.6***	1	1.81	32.9***
Sperm:egg ratio (R)	2	8.63	124.5***	2	10.24	122.4***	2	0.91	16.8***
Sperm concentration (C)	1	44.95	648.4***	–	–	–	–	–	–
T × E	6	2.38	34.4***	6	0.50	5.9***	6	2.33	42.5***
T × S	6	2.04	29.4***	6	2.60	31.3***	6	0.38	6.8***
E × S	1	2.24	32.3***	1	2.50	30.1***	1	0.28	5.1***
T × R	12	0.22	3.1***	12	0.61	7.3***	12	0.18	3.2***
E × R	2	0.39	5.6***	2	0.03	0.4^{NS}	2	0.66	12.1***
S × R	2	0.55	7.8***	2	0.87	10.4***	2	0.14	2.5^{NS}
T × C	6	0.85	12.3***	–	–	–	–	–	–
E × C	1	3.84	55.4***	–	–	–	–	–	–
S × C	1	23.20	334.7***	–	–	–	–	–	–
R × C	2	2.53	36.5***	–	–	–	–	–	–
T × E × S	6	0.59	8.6***	6	0.54	6.5***	6	0.17	3.2**
T × E × C	6	0.45	6.5***	–	–	–	–	–	–
T × E × R	12	0.06	0.8^{NS}	12	0.06	0.7^{NS}	12	0.06	1.1^{NS}
T × S × R	12	0.23	3.3***	12	0.51	6.1***	12	0.05	1.0^{NS}
T × S × C	6	0.93	13.5***	–	–	–	–	–	–
E × S × R	2	0.15	2.1^{NS}	2	0.14	1.7^{NS}	2	0.06	1.1^{NS}
E × S × C	1	0.56	8.1**	–	–	–	–	–	–
T × R × C	12	0.57	8.2***	–	–	–	–	–	–
E × R × C	2	0.31	4.4*	–	–	–	–	–	–
S × R × C	2	0.45	6.5**	–	–	–	–	–	–
T × E × S × R	12	0.04	0.6^{NS}	12	0.11	1.3^{NS}	12	0.03	0.5^{NS}
T × E × S × C	6	0.13	1.8^{NS}	–	–	–	–	–	–
T × E × R × C	12	0.07	0.9^{NS}	–	–	–	–	–	–
T × S × R × C	12	0.34	4.9***	–	–	–	–	–	–
E × S × R × C	2	0.06	0.8^{NS}	–	–	–	–	–	–
T × E × S × R × C	12	0.09	1.3^{NS}	–	–	–	–	–	–
Error	792	0.07		396	0.08		396	0.06	

* $P < 0.05$; ** $P < 0.01$; *** $P < 0.001$; ^{NS} not significant.

acterize *A. planci* gametes. However, the extent to which these factors influence fertilization success in the wild depends upon the range of values encountered in the field and their interaction with other variables. For example, Levitan *et al.* (1991) concluded that egg concentration was unlikely to be an important determinant of fertilization success in the sea urchin *S. franciscanus*, except within the first few seconds of gamete release, because of the concentration at which eggs were extruded and the rapidity with which the eggs were diluted by seawater. Assuming that *A. planci* eggs are extruded in a column from each gonopore to give a concentration of 2500 ml^{-1}, the packing density for eggs of 200-μm diameter is at a maximum, and sperm are extruded at a concentration of 500×10^6 sperm ml^{-1}, the sperm:egg ratio would be 200,000—well above the value at which sperm:egg ratio affects fertilization success. Thus, as in *S. franciscanus*, sperm:egg ratio in *A. planci* is unlikely to play a major role in determining fertilization success in the field.

Similarly, the dilution at which sperm are unable to fertilize eggs is likely to be reached well before eggs lose the ability to be fertilized. The dilution of sperm has been shown to be rapid within only a few meters (Denny, 1988; Denny and Shibata, 1989) and to have a major influence on observed fertilization success in a number of marine invertebrates (Pennington, 1985; Yund, 1990; Grosberg, 1991; Levitan, 1991; Levitan *et al.*, 1992). Indeed, even in slow currents, such dilution is likely to occur well within the lifespan of *A. planci* sperm at concentrations as low as 50 sperm ml^{-1}. Gamete lifespan is therefore unlikely to be a major factor in limiting fertilization success over

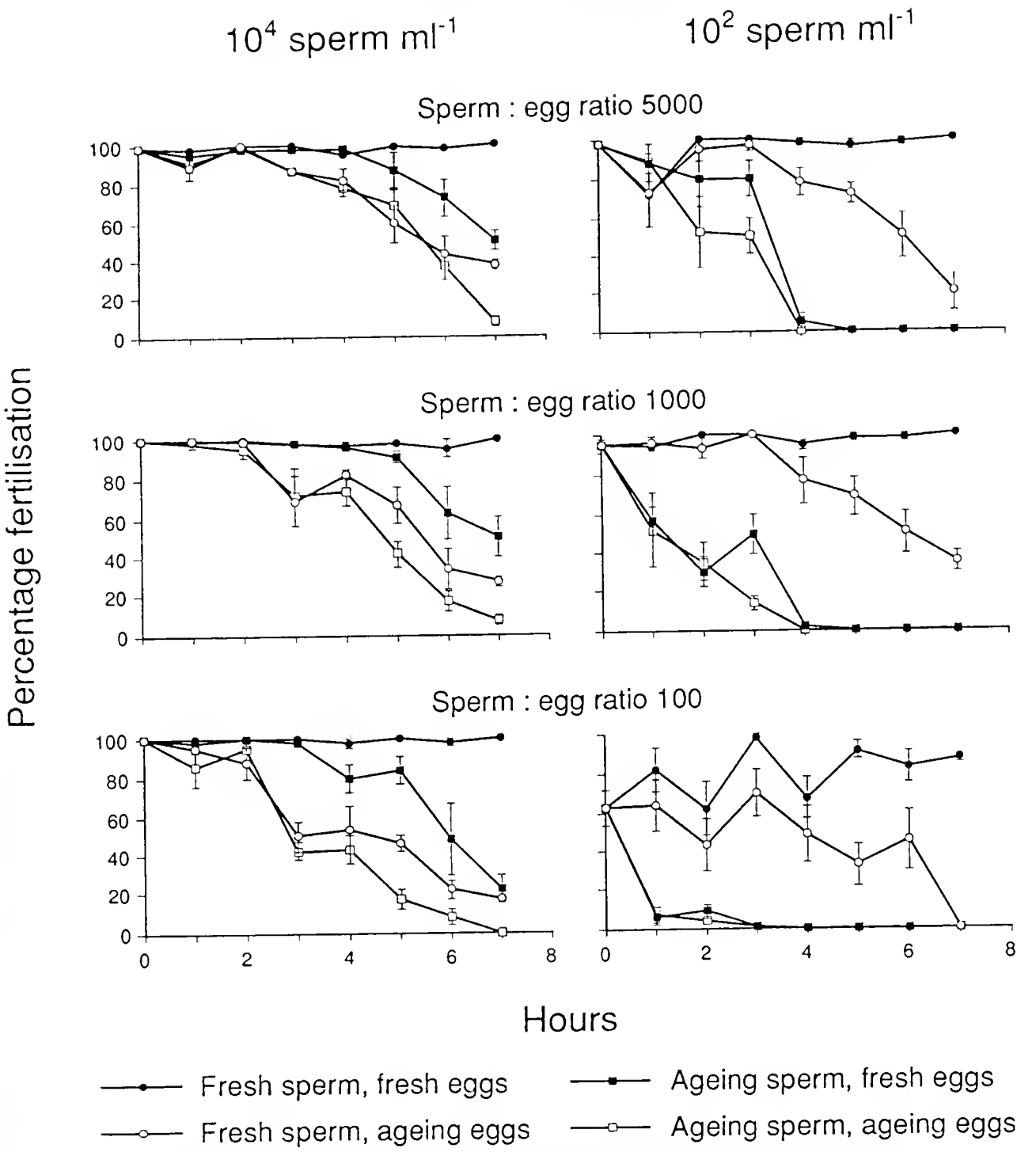

Figure 5. Mean percent fertilization, with standard error, of fresh eggs and aged eggs from *Acanthaster planci* when mixed with fresh and aged sperm at different sperm concentrations (rows) and sperm:egg ratios (columns) over a period of 6 h and 45 min. Sperm concentration was either 10^2 or 10^4 sperm ml^{-1}, and sperm:egg ratio was either 100, 1000, or 5000.

small spatial scales, but the respiratory dilution effect may be critical.

Detailed biochemical work with *Strongylocentrotus purpuratus* has demonstrated that various treatments used to activate sperm all give rise to an increased intracellular pH (Christen *et al.*, 1983a, 1986; Johnson *et al.*, 1983). Sea urchin sperm can be maintained for a long time in a quiescent, "non-aging" state at the pH of seminal fluid, that is, an extracellular pH of approximately 7.5 and an intracellular pH of approximately 7.0 (Christen *et al.*, 1983b). These findings explain the effect of a number of artificial means of inducing sperm motility as well as the extended fertilizing capacity observed for sperm in buffered solutions (Timourian and Watchmaker, 1970; Christen *et al.*, 1983a; Johnson *et al.*, 1983). Sperm are activated in nature when an intracellular pH higher than their activation threshold (approximately pH 7.5) develops after they are released into seawater where the external pH is 8.0 or more. Christen *et al.* (1983a, 1986) have demonstrated that the effects of short exposure to circumstances that activate the sperm are reversible as long as high energy compounds used in respiration are not sufficiently depleted to damage cell function. High pH activates both microtubule movement that depletes ATP and mitochondrial reactions that produce ATP. The former (consumption) is usually more rapid than the latter (production), and the relative rate of these processes determines the time for which sperm are viable at a given environmental pH, and whether the situation is reversible.

Variations in external pH may therefore influence the fertilization success in experiments. However, no major variations in seawater pH were observed in our experiments, and in any case we wished to determine how varying gamete age and concentration would affect fertilization in environments likely to occur in the wild. The biochemical literature is pertinent to the work we report in that it helps explain the mechanisms of sperm aging and allows us to speculate on specific reasons for the difference in sperm aging observed in *A. planci*.

We did not measure the pH of the sperm solution immediately after spawning (when sperm concentrations were $12–40 \times 10^8$ sperm ml^{-1}) or in the stock solution (with 2×10^6 sperm ml^{-1}). However, our observations are consistent with the view that any aging effects of dilution of sperm during the early stages of spawning were reversed when sperm concentrations increased (and possibly external pH decreased) with continuing addition of sperm to the 100 ml of seawater in the beaker. When sperm were released, they accumulated in a thick sludge at the base of the beaker and were therefore very concentrated. The values of $12–40 \times 10^6$ sperm ml^{-1} were observed after the seawater in the beaker was mixed very well at the end of the spawning period. Our observations are also consistent with the view that respiration was at least balanced by ATP production at 2×10^6 sperm ml^{-1}. There was no correlation between initial concentrations at which sperm had been spawned and the relative speed of aging of the sperm in subsequent experiments that might suggest the initial spawning into seawater had irreversibly aged sperm. The fact that *A. planci* sperm held at concentrations of 2×10^6 sperm ml^{-1} do not appear to age over several hours, whatever the reason, is in itself evidence that their fertilization capacity is enhanced relative to that of sea urchin sperm, whose viability extended over several hours only at concentrations of 10^8 sperm ml^{-1} (Levitan *et al.*, 1991).

Our conclusions depend on the use of "non-aged" sperm at the start of our experiments, and our empirical protocols allowed us to do this. The experiments were carried out with natural seawater pumped fresh from the Great Barrier Reef lagoon, replicating the conditions in which natural fertilization would occur and allowing us to estimate fertilization rates in the wild between gametes of given age and concentration. The results do not allow us to identify the mechanisms that give rise to the different rates of aging of sea urchin and crown-of-thorns starfish sperm.

However, one may speculate that, compared to sea urchins, the crown-of-thorns starfish might have (1) more acid seminal fluid, resulting in lower seawater pH at given sperm concentrations; (2) higher pH thresholds for activation of sperm; (3) different rates of reaction for respiration and ATP production with rise in pH, resulting in longer viability; or (4) combinations of the above.

The conclusions are also conservative in that gamete age was calculated from the time of dilution from the stock solution. This was shown to be an appropriate empirical starting point because *A. planci* sperm do not age at this concentration over the time scales of the experiment. If age had been timed from the beginning of sperm release, the sperm would have been considered some 30 min older on average, thus increasing the observed difference in fertilization rates of *A. planci* and sea urchin sperm.

In the field, fertilization rates as high as about 60% at 10 m downstream of a spawning male, dropping to 20% at 60 m distance, have been observed for *A. planci* (Babcock and Mundy, 1992). These values are much greater than those of sea urchins, which show 5% fertilization at 5 m, dropping to zero at distances greater than 10 m (Pennington, 1985). The reduced respiratory dilution effect, and consequent relatively slow aging of sperm, are features of *A. planci* that may well enhance fertilization success by allowing gametes to remain competent for a longer time at more dilute concentrations. Environmental factors such as salinity, temperature, and pH are also likely to affect fertilization success (Rupp, 1973; Greenwood and Bennett, 1981; Dinnel *et*

al., 1987; Christen *et al.*, 1983a, 1986), and hydrodynamics and rates of gamete release will control the degree of dilution of the gametes. However, the characteristics of *A. planci* gametes described here are very different from those of sea urchins and would lead to higher fertilization success at greater distances from spawning adults. The range of gamete concentrations tested was similar to the average values of 2×10^5 sperm ml^{-1} or less, and sperm:egg ratios of 2×10^4 or less, measured in the field (Benzie *et al.*, 1994). The nature of gamete dispersion in the wild and estimates of fertilization success in the wild, using field measurements of gamete concentrations and the laboratory data presented here, are fully discussed in Benzie *et al.* (1994).

A. planci larvae developed from fertilization at the highest laboratory concentration of 10^5 sperm ml^{-1} were often malformed and had not completed gastrulation the following day, in contrast to larvae from treatments using lower sperm concentrations. No extensive rearing of larvae was attempted, but these observations from several tests suggest that polyspermy might have occurred at high sperm concentrations. Individuals of *A. planci* in close proximity in the field are likely to produce concentrations of gametes that will result in some degree of polyspermy. The high fertilization rates achieved may not reflect the number of viable larvae produced in such circumstances, and there may be an upper limit to sperm concentrations with respect to the number of viable larvae produced in a given mating. Similarly, although eggs were fertilized up to 8 h after their release, after only 4 to 5 h many showed abnormal divisions, and eggs were often misshapen. When samples were maintained for 36 h, many of the eggs with raised fertilization membranes had not developed into larvae or had not successfully completed gastrulation.

The viability of eggs fertilized at the end of the breeding season must also be assessed. Fertilization dynamics early and late in the breeding season have never been comprehensively compared for any echinoderm species. Differences observed in the fertilization rate response surfaces early and late in the breeding season suggested that a reduction in the quality of gametes at the end of the breeding season gave rise to different fertilization dynamics in *A. planci* at that time. It is not known whether eggs, sperm, or both were responsible for these differences.

Acknowledgments

We thank D. Bass and T. Parison for technical assistance, P. Moran and J. Keesing for the collection of crown-of-thorns starfish, G. De'ath for statistical advice, and S. Clark for art work. This work was supported by a grant from the Crown of Thorns Starfish Advisory Committee. This is Contribution Number 678 from the Australian Institute of Marine Science.

Literature Cited

Babcock, R., and C. Mundy. 1992. Reproductive biology, spawning and field fertilization rates of *Acanthaster planci*. *Aust. J. Mar. Freshwater Res.* **43:** 525–534.

Benzie, J. A. H., K. P. Black, P. J. Moran, and P. Dixon. 1994. Small-scale dispersion of eggs and sperm of the crown-of-thorns starfish (*Acanthaster planci*) in a shallow coral reef habitat. *Biol. Bull.* **186:** 153–167.

Chia, F.-S., and L. R. Bickell. 1983. Echinodermata. Pp. 545–620 in *Reproductive Biology of Invertebrates, Vol II: Spermatogenesis and Sperm Function*, K. G. Adiyondi and R. G. Adiyondi, eds. John Wiley and Sons, New York.

Christen, R., R. W. Schackmann, and B. M. Shapiro. 1983a. Metabolism of sea urchin sperm, interrelationships between intracellular pH, ATPase activity, and mitochondrial respiration. *J. Biol. Chem.* **258:** 5392–5399.

Christen, R., R. W. Schackmann, F. W. Dahlquist, and B. M. Shapiro. 1983b. ^{31}P-NMR analysis of sea urchin sperm activation, reversible formation of high energy phosphate compounds by changes in intracellular pH. *Exp. Cell. Res.* **149:** 289–294.

Christen, R., R. W. Schackmann, and B. M. Shapiro. 1986. Ionic regulation of sea urchin sperm motility, metabolism and fertilizing capacity. *J. Physiol.* **379:** 347–365.

Cohn, E. 1918. Studies on the physiology of spermatozoa. *Biol. Bull.* **34:** 167–218.

Denny, M. W. 1988. *Biology and the Mechanics of the Wave-swept Environment.* Princeton University Press, New Jersey, 329 pp.

Denny, M. W., and M. F. Shibata. 1989. Consequences of surf zone turbulence for settlement and external fertilization. *Am. Nat.* **134:** 859–889.

Dinnel, P. A., J. M. Link, and Q. J. Stober. 1987. Improved methodology for a sea urchin sperm cell bioassay for marine waters. *Arch. Environ. Contam. Toxicol.* **16:** 23–32.

Dixon, W. J. (ed.). 1983. *BMDP Statistical Software.* University of California Press, Berkeley, 734 pp.

Gray, J. 1928. The effect of dilution on the activity of spermatozoa. *J. Exp. Biol.* **5:** 337–344.

Greenwood, P. J., and T. Bennett. 1981. Some effects of temperature-salinity combinations on the early development of the sea urchin *Parechinus angulosus* (Leske) fertilization. *J. Exp. Mar. Biol. Ecol.* **51:** 119–131.

Grosberg, R. K. 1991. Sperm-mediated gene flow and the genetic structure of a population of a colonial ascidian *Botryllus schlosseri*. *Evolution* **45:** 130–142.

Ishikawa, M. 1975. Fertilization. Pp. 99–147 in *The Sea Urchin Embryo: Biochemistry and Morphogenesis.* G. Czihak, ed. Springer-Verlag, Heidelberg.

Johnson, C. H., D. L. Clapper, M. W. Winkler, H. C. Lee, and D. Epel. 1983. A volatile inhibitor immobilizes sea urchin sperm in semen by depressing intracellular pH. *Develop. Biol.* **98:** 493–501.

Kanatani, H., and Y. Nagahama. 1983. Echinodermata. Pp. 611–654 in *Reproductive Biology of Invertebrates. Vol I: Oogenesis. Oviposition and Oosorption.* K. G. Adiyondi and R. G. Adiyondi, eds. John Wiley and Sons, New York.

Kobayashi, N. 1984. Marine ecotoxicological testing with echinoderms. Pp. 341–405 in *Ecotoxicological Testing for the Marine Environment, Vol. I.* G. Persoone, E. Jaspers, and C. Claus, eds. State University of Ghent and Institute of Marine Scientific Research, Bredene, Belgium.

Lassig, B. R., and G. Kellcher. 1991. Crown-of-thorns starfish on the Great Barrier Reef. Pp. 39–62 in *Environmental Research in Aus-*

tralia Case Studies. Australian Science and Technology Council. Australian Government Publishing Service. Canberra.

Levitan, D. R. 1991. Influence of body size and population density on fertilization success and reproductive output in a free-spawning invertebrate. *Biol. Bull.* **181:** 261–268.

Levitan, D. R., M. A. Sewell, and F.-S. Chia. 1991. Kinetics of fertilization in the sea urchin *Strongylocentrotus franciscanus:* interaction of gamete dilution, age and contact time. *Biol. Bull.* **181:** 371–378.

Levitan, D. R., M. A. Sewell, and F.-S. Chia. 1992. How distribution and abundance influence fertilization success in the sea urchin *Strongylocentrotus franciscanus. Ecology* 73: 248–254.

Lillie, F. R. 1915. Studies of fertilization. VII. Analysis of variations in the fertilizing power of sperm suspensions of *Arbacia. Biol. Bull.* **28:** 229–251.

Lillie, F. R. 1919. *Problems of Fertilization.* University of Chicago Press, Chicago. 278 pp.

Lucas, J. S. 1982. Quantitative studies on the feeding and nutrition during larval development of the coral reef asteroid *Acanthaster planci* (L.). *J. Exp. Mar. Biol. Ecol.* **65:** 173–193.

Meijer, L., and P. Guerrier. 1984. Maturation and fertilization in starfish oocytes. *Int. Rev. Cytology* **86:** 129–196.

Moran, P. J. 1986. The *Acanthaster* phenomenon. *Oceanogr. Mar. Biol. A. Rev.* **24:** 379–480.

Pennington, J. T. 1985. The ecology of fertilization of echinoid eggs: the consequences of sperm dilution, adult aggregation, and synchronous spawning. *Biol. Bull.* **169:** 417–430.

Rupp, J. H. 1973. Effects of temperature on fertilization and early cleavage of some tropical echinoderms, with emphasis on *Echinometra mathaei. Mar. Biol.* **23:** 183–189.

SAS Institute Inc. 1985. *SAS User's Guide: Statistics.* Version 5 edition. SAS Institute Inc., Cary, NC. 1028 pp.

Timourian, H., and G. Watchmaker. 1970. Determination of spermatozoan motility. *Develop. Biol.* **21:** 62–72.

Tyler, A., and B. S. Tyler. 1966. The gametes: some procedures and properties. Pp. 639–682 in *Physiology of Echinodermata.* R. A. Boolootian, ed., Interscience Publishers, New York.

Vogel, H., G. Czihak, P. Chang, and W. Wolf. 1982. Fertilization kinetics of sea urchin eggs. *Math. Biosci.* **58:** 189–216.

Yamaguchi, M. 1974. Growth of juvenile *Acanthaster planci* (L.) in the laboratory. *Pac. Sci.* **28:** 123–138.

Yund, P. O. 1990. An *in situ* measurement of sperm dispersal in a colonial marine hydroid. *J. Exp. Zool.* **253:** 102–106.

Reference: *Biol. Bull* **186:** 153–167. (April, 1994)

Small-Scale Dispersion of Eggs and Sperm of the Crown-of-Thorns Starfish (*Acanthaster planci*) in a Shallow Coral Reef Habitat

J. A. H. BENZIE[1], K. P. BLACK[2], P. J. MORAN[1], AND P. DIXON[1]

[1]*Australian Institute of Marine Science, PMB No. 3, Townsville MC, Queensland, Australia 4810, and* [2]*Victorian Institute of Marine Sciences, 23 St Andrews Place, Melbourne, Victoria, Australia 3002*

Abstract. The dispersal of eggs and sperm of crown-of-thorns starfish, *Acanthaster planci* (L.), was measured in the field using an array of collectors up to 10 m downstream of a spawning starfish. Hydrodynamic measurements, gamete dispersal numerical models, and the gamete cloud dispersal measurements for the first time quantified the relationship between hydrodynamic conditions and the dispersion of eggs and sperm in the field. In general, gamete concentrations fell rapidly and logarithmically with distance from the spawning starfish; egg concentrations at 3 m were 1% of those near the starfish. Simplified dispersal models showed a good correspondence with these field data, and confirmed the observation that eggs rose higher in the water column and spread more laterally at low current speeds over the short spatial scales being considered.

Fertilization rates, predicted from laboratory measurements of fertilization success and the gamete concentrations measured in the field, were estimated to be 90–100% within 1 m and 70–100% at 10 m. These results are explained by high success rates of fertilization (fertilizing capacity) at the measured dilutions, and were similar to fertilization rates previously measured by others for crown-of-thorns starfish in the field.

Although the eggs were observed to spread upwards into the water column due to turbulence, laboratory measurements of sinking rates showed eggs to be very slightly negatively buoyant (median fall velocity of 0.072 mm $\cdot$ s^{-1}), whereas sperm were neutrally buoyant. A significant fraction of eggs also entered the seabed near the starfish; the proportion decreased with increasing current strength. This process may provide a mechanism for enhanced fertilization of these gametes and/or a mechanism for self-recruitment to a given reef population.

Received 3 February 1993; accepted 28 December 1993.

Introduction

Many marine organisms release their gametes into the seawater where fertilization takes place. Theoretical (Vogel *et al.*, 1982) and laboratory (Lillie, 1915, 1919; Cohn, 1918; Gray, 1928; Levitan *et al.*, 1991) studies have demonstrated that gamete concentration plays a key role in the fertilization success of such organisms. This results not only from changes in the probability that gametes will encounter each other, but also from the marked decrease in fertilizing capacity of sperm with increasing dilution (Gray, 1928; Chia and Bickell, 1983).

Illustrative models of the effects of turbulent flow have demonstrated the dominant effect fluid dynamics are likely to have on gamete dispersion and on the likelihood of successful fertilization (Denny, 1988; Denny and Shibata, 1989). Dispersal of gametes at reef scales has been examined (*e.g.*, Black *et al.*, 1991). However, despite the importance of the interaction of gametes and the fluid environment, no experiments have been undertaken at small spatial scales to link the physics of the water body to the measured dispersal of gametes in the natural environment. Such information is of vital importance to understanding the dynamics of external fertilization.

The few field studies of fertilization that have been carried out in sea urchins (Pennington, 1985), hydroids (Yund, 1990), and ascidians (Grosberg, 1991) have all confirmed theoretical predictions (Denny and Shibata,

1989) that fertilization rates drop rapidly with distance from the spawning adult. Pennington (1985) found the proportion of sea urchin eggs fertilized by sperm in seawater sampled at different distances downcurrent of a spawning male was above 60% over 0.1 m, falling to 15% over 0.2 m and to less than 5% over 1 m. Sperm dispersal estimated in ascidians from the spread of genetic markers showed that 20–40% of embryos within 0.05 m of a male source had been fertilized by that male, but that less than 5% had been fertilized over 0.5 m away (Grosberg, 1991). In marine hydroids, fertilization rates were more than 80% within 3 m of the male source, but dropped to zero at distances greater than 7 m (Yund, 1990). The reproductive success of female octocorals, *Briareum asbestinum,* was also greater the closer they were to males and in hydrodynamic conditions where dilution of sperm was likely to be less (Brazeau and Lasker, 1992). This implies that the magnitude of the spatial separation of spawning individuals is crucial to the fertilization success achieved. These data suggest that the aggregation of many species during spawning is a mechanism to enhance fertilization success (Pennington, 1985).

In marked contrast, high fertilization rates have been measured over tens of meters from spawning male crown-of-thorns starfish (Babcock and Mundy, 1992). This result might reflect the large number of gametes released by this starfish (diameter up to 0.5 m) and the fact that individuals are widely dispersed in their natural habitat. Up to 10^8 eggs are produced per female (Birkeland and Lucas, 1990), and up to 140 ml of sperm (Babcock and Mundy, 1992)—at densities of up to 8×10^8 sperm ml^{-1} (Benzie and Dixon, 1994)—are produced per male, although densities may be much lower once the sperm is released into a moving water column. Although there are reports of aggregations of starfish during spawning, these have been observed only in high-density outbreaking populations (Birkeland and Lucas, 1990). The species normally occurs in much lower densities (Moran and De'ath, 1992), which suggests that gamete dispersal needs to be effective.

The influence of water flow has been recognized in all the field studies of fertilization. Differences in the dispersal of sperm inferred from population genetic structuring of ascidian populations at sites in the United States and Italy were thought to be the result of the different flow regimes at the two locations (Grosberg, 1991). The site with slow currents had limited sperm transfer, whereas the site with fast, highly turbulent flows had population structures consistent with sperm dispersal over greater distances. Research by Pennington (1985) showed that the fertilization of eggs was greatest, over distances of 1 m, when current speeds were low (*i.e.*, $< 0.2 \text{ m} \cdot \text{s}^{-1}$). The potential effects of hydrodynamic conditions on fertilization success have also been noted in reef fish (Peterson, 1991), octocorals (Brazeau and Lasker, 1992), and scleractinian corals (Oliver and Babcock, 1992). However, no previous studies have measured the dispersal of the gametes themselves or obtained simultaneous information on current flows, turbulence, and boundary conditions that might have better described the conditions in which the measured fertilization rates were achieved.

The aim of the present work was to establish the dispersion patterns of eggs and sperm of the crown-of-thorns starfish in the field, and to determine the link between gamete dispersion patterns and the physics of the natural environment.

Materials and Methods

Field experiments

Experiments were conducted at Little Broadhurst Reef in the Central Section of the Great Barrier Reef (Fig. 1) along a 40 m × 10 m transect established on a large patch reef within the lagoon. Natural concentrations of eggs and sperm downstream of a spawning starfish were determined using a vertical array of nineteen 12-V bilge pumps (Fig. 2) set into a mobile frame that could be moved up to 10 m downstream of the starfish. Sixteen pumps were arranged at the nodes (450–500 mm apart) in a rectangular

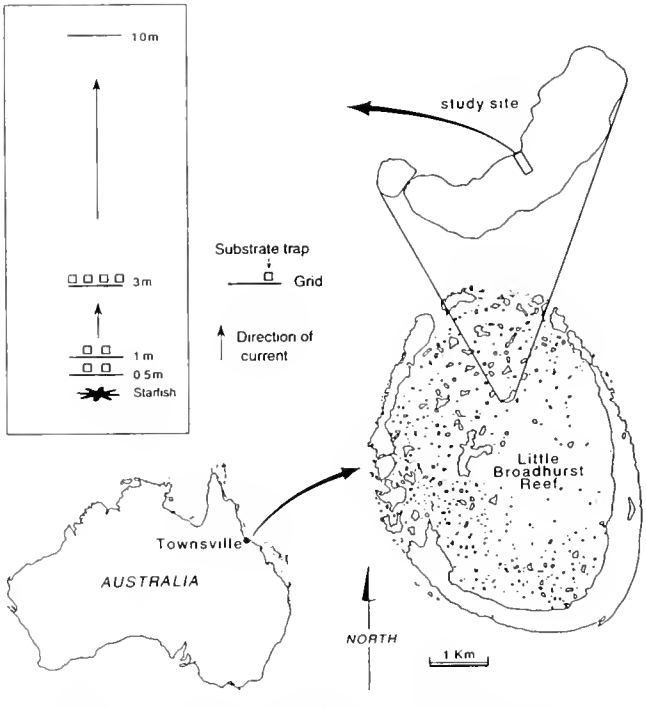

Figure 1. Map showing the location of the experimental site on Little Broadhurst Reef in the Great Barrier Reef, and the setup of the pump array and substrate traps within the study transect relative to the spawning starfish.

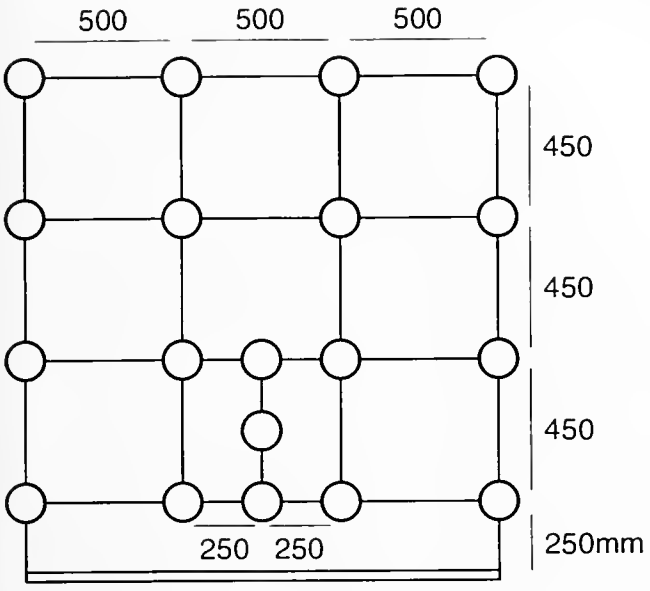

Figure 2. Plan of the pump array.

grid. To improve resolution over the shorter distances, three additional pumps were set about 250 mm apart in the lower middle section of the frame (Fig. 2). Another pump positioned next to the starfish measured the concentration of gametes being released. All pumps were connected by 30-m-long, 12-mm-diameter plastic hoses to filters located on a moored barge. Pumping rates were approximately 2 $l \cdot min^{-1}$.

Up to six "substrate" traps were deployed downstream of the starfish to measure the number of eggs lost to the seabed (Fig. 1). Each trap consisted of a small plastic tray ($0.13 \times 0.13 \times 0.05$ m) filled with moderate-sized pieces of clean, angular pieces of rock, 20–30 mm in diameter. The rock was added to provide substrate with a porosity similar to that of the natural seabed and to provide a similar hydrodynamic environment. Normally two traps were deployed at 0.5 m and 1 m from the starfish, and a further four traps were deployed at 3 m. During Experiment 6 when the current speed was very slow, the four traps from 3 m were positioned adjacent to the spawning starfish. Unlike the pump array, the substrate traps were left open for the full duration of spawning. Each tray had a plastic lid to close the tray during retrieval.

Current speeds were measured using a Neil Brown acoustic vector-averaging current meter, suitable for combined wave and current environments. The current meter was supported on a bottom-mounted metal frame and manually raised and lowered to measure the vertical velocity profile. The meter failed after 3 days of experiments (up to and including Experiment No. 7) and currents on 2 subsequent days were estimated by timing the passage of a dye cloud traveling between the starfish and the pump array. A surface-piercing capacitance probe (Black and Rosenberg, 1991) was deployed to record wave conditions at the sea surface.

To check instrument accuracy, wave probe gain and offset and current meter zero offset were calibrated in still water each day. Instrument output was logged on a portable computer at a sampling rate of 2 Hz. The current meter outputs were later averaged over 17 min (2048 data points) to find mean currents.

Collection. Prior to each experiment, searches were made to remove any crown-of-thorns starfish within the transect. A starfish of known sex was then collected and injected with 1-methyladenine to induce spawning. The females normally began spawning after 20 min, while the males usually took half that time.

Eggs or sperm were collected downstream of the starfish. The pump array used for the collections was moved to 0.5, 1.0, 3.0, and 10.0 m downstream (Fig. 1). Immediately prior to sampling, all lines were disconnected from the downstream filters and the pumps were run for 1 min to flush the hoses. The hoses were reconnected rapidly (in less than 30 s) and filtering was carried out for 2 min. Flow rates for a given pump were consistent, so the volume that passed in 2 min through each pump (about 4 l) was measured several times and averaged. While the pumps were active, dye was released next to the starfish to ensure that the array was correctly positioned downstream. All experiments were undertaken in reasonably clear and calm conditions with wind speeds of less than 10 knots, waves less than 0.5 m, and mostly slow current speeds of less than 0.1 $m \cdot s^{-1}$ (Table 1).

Filtering and counting. Eggs collected from the water column were filtered into a plastic bottle through 80-μm plankton mesh placed in a bucket of seawater. A large volume of seawater in the bottle prevented eggs being crushed or forced through the mesh as would have occurred by filtering in air. On completion of pumping, the filter was removed from the bucket, the external surface of the meshes was washed, and the eggs were trapped in the water draining into a small sample tube at the base of the plastic bottle. The small sample tube was then removed and 1 ml of formalin added to preserve the eggs. Because sperm could pass through the filters, a 20-ml subsample was collected without filtering from the 2-min pumped sample and preserved with formalin.

The contents of each substrate trap were placed in a funnel over a filter and washed with seawater to dislodge any eggs. The surface of each filter was then washed, and the eggs were collected and preserved as described above.

Eggs in each sample were counted at 25× with the aid of a binocular microscope; sperm counts were made at 400× using a phase contrast microscope. Subsamples of

Table I

Information on the sex, duration of spawning, pump and trap positions, and environmental conditions pertaining to each experiment

Exp. No.	Sex	Spawning duration (min)	Pump array position (m)	Substrate trap position (m)	Currents	
					Direction	Speed ($m \cdot s^{-1}$)
1	F	25	0.5, 1, 3	0.5, 1, 3	N	0.02
2	F	20	0.5, 1	0.5, 1, 3	N	0.08
3	F	60	0.5, 1, 3, 10	0.5, 1, 3	N	0.04
4	F	45	0.5, 1	0.5, 1, 3	E	0.05
5	F	65	0.5, 1, 3, 3	0.5, 1, 3	N	0.02
6	F	50	0.5, 0.5	0.1, 0.5, 1	S	0.02
7	F	65	0.5, 1, 3, 10	0.5, 1, 3	S	0.10
8	F	35	10, 10	0.5, 1, 3	S	0.23
9	F	55	0.5, 1, 3	0.5, 1, 3	S	0.07
10	M	20	0.5, 1	—	S	0.03
11	M	20	0.5, 1	—	S	0.03
12	M	20	0.5, 1	—	S	0.03
13	F	25	10, 10	0.5, 1, 3	S	0.25
14	F	50	0.5, 1, 3	0.5, 1, 3	S	0.20
15	M	30	0.5, 1	—	S	0.03
16	M	20	0.5, 1	—	S	0.02
17	M	25	0.5, 1	—	S	0.02

water were extracted, using a pipette, from well-shaken sperm samples and drops applied to a hemacytometer. Counts were obtained from a total of five of the large squares.

Fall velocities. One of the most important factors determining the distribution of eggs or sperm in the water column is the fall velocity (or buoyancy). Because no measurements of the distribution of fall velocity for starfish eggs were available, we applied analysis techniques normally used to measure fall velocity and grain size of fine sediments.

Eggs or sperm were thoroughly mixed in a 1-l measuring cylinder. The room and water temperatures were the same to reduce convection in the cylinder. After the turbulence had ceased, 10-ml subsamples were taken at 0.05 m and at 0.1 m from the surface every 15 min for eggs and every 45 min for sperm. Eggs were sampled over a period of 2.25 h and sperm over 7.5 h. Live eggs were used in two replicate experiments. For sperm, one set was killed by exposure to formalin to test whether the motility of live sperm affected their sinking rates. Data for each gamete type were then fitted separately to a logarithmic decay curve, and estimates of the 10th percentiles were used to determine fall velocities. The temperature of the oceanic water used for these measurements was 23.8°C and the salinity was 35 ppt.

Lagrangian advection/diffusion numerical model of larval dispersal

As gametes progress downstream, they advect with the main current and diffuse due to turbulence. In this paper, we investigate whether the movement of the eggs and sperm can be described by advection/diffusion principles more commonly applied to pollutants or sediment. To this end we adapted a Lagrangian particle model of sediment suspension under waves; this model was previously described by Black and Rosenberg (1991). The particle technique provides a number of numerical advantages; is intuitively a more direct reproduction of the natural processes; and eliminates numerical diffusion, particularly near the starfish where concentration gradients may be large.

In the Lagrangian model, several thousand particles are released with position $X(x, y, z)$ to represent the gametes. The model tracks the vertical and horizontal movement of gametes by sequentially treating the entrainment, diffusion, and then advection each time step. The unknown physical variables that had to be estimated from field data were the vertical dependence of the current $U(z)$, the eddy diffusivities (e_x, e_y and e_z), and the fall velocities.

Entrainment. Starfish eggs are generally released from openings (gonopores) that radiate from the central disk along the tops of the arms. It was estimated that starfish eggs were released from a circle approximately 0.15–0.20 m in diameter (consistent with a starfish diameter of 0.35–0.40 m). Our measurements of the initial concentrations were made 0.05–0.10 m above the starfish. In the model, entrainment was simulated by releasing particles at random initial positions within a cuboid with dimensions representative of the natural case. The length and

width of the cuboid were taken as 0.175 m and the height was 0.075 m.

The model maintained a constant concentration within the cuboid equal to the measured values. At each time step, the number of particles within the cuboid was determined and the appropriate number added to compensate for those that moved downstream.

Diffusion, advection, and concentration. In the Monte Carlo diffusion stage, all particles in the water column "jumped" horizontally or vertically with the step size ΔX_1 governed by the eddy diffusivity, where

$$\Delta X_1 = R_n(6E_s\Delta t)^{0.5} \tag{1}$$

and R_n is a random number in the uniform range $(-1, 1)$; E_s is the lateral, longitudinal, or vertical eddy diffusivity; and Δt is the time step. The factor 6 in eqn (1), rather than 2, results when a uniform random number range is chosen instead of $R_n = \pm 1$.

In the linear advection stage, each particle's vertical position was adjusted according to its fall velocity as

$$\Delta z = W\Delta t \tag{2}$$

The downstream position was adjusted according to the current speed $U(z)$ at the level of the particle (z) above the bottom

$$\Delta x = U(z)\Delta t \tag{3}$$

The concentration at any elevation was the sum of the particles lying in a vertical cell, divided by the cell volume

$$C_z = \sum_{i=1}^{n} N_i/(dxdydz) \tag{4}$$

where n is the number of particles, and dx, dy, and dz are the cell dimensions.

A short time step of $\Delta t = 0.05$ s was chosen to refine the model resolution. In a Lagrangian model, the vertical grid size does not influence the solution, but is selected according to the resolution required. More particles and shorter time steps are needed to properly resolve sharp concentration gradients on fine grids.

To determine concentrations as recorded in the field, particles were tracked until they passed the downstream location of the pump array. The cumulative number of particles per liter of fluid passing though model grid cells of size $dy = dz = 0.2$ m over a 2-min interval was determined. The water volume passing through each cell was

$$V = U(z)dydzt \tag{5}$$

where t is the elapsed time (120 s). To allow an equilibrium to develop in the model (as in the field condition), the simulation ran for 80–600 s (depending on the current strength) before the summation of particle numbers was commenced. The model then ran for a further 120 s.

The velocity profile and roughness length. The vertical velocity profile was assumed to be logarithmic. Thus

$$U(z) = 5.75u_* \log_{10}(z/z_0) \tag{6}$$

where u_* is the friction velocity and z_0 is the roughness length, the height at which the velocity goes to zero. The speed at any elevation was

$$U(z) = U_m \log_{10}(z/z_0)/\log_{10}(z_m/z_0) \tag{7}$$

where U_m is the velocity measured by the current meter at elevation z_m.

Measurements of the measured velocity profile indicated z_0 was in the range 0.08–0.15 (previously reported by Black and Gay, 1990). This value is in accordance with a number of other estimates. Summarized by Black and Hatton (1990), z_0 values of approximately 0.08 m (or friction coefficients equivalent to $z_0 = 0.08$) have been independently obtained using wave height attenuation data and numerical model calibrations (Black and Gay, 1990; Hardy and Young, 1991). Thus, we have taken $z_0 = 0.08$ m in this study.

Eddy diffusivities. The current and wave measurements showed a mean circulation superimposed on an oscillating wave orbital motion. Spectra of the sea-surface time series indicated two wave trains with periods of about 8 and 3 s. The dominant 8-s peak was probably associated with swell, whereas the 3-s waves were generated by local wind.

In wave/current environments, the most common assumption is a parabolic vertical distribution of eddy diffusivity above the wave boundary layer (*e.g.*, Fredsoe *et al.*, 1985), although more than 30 different techniques have been proposed to predict bottom shear stresses and bed roughness scales under the combined action of waves and currents (Simons *et al.*, 1989). Despite this wide choice of models, very few have been fully calibrated against the few suitable field data available.

The complexity of the available relationships varies, but Nielsen (1986) has found that the simplest case of a vertically invariant eddy diffusivity is effective for predicting suspended sediment concentrations, and this was confirmed by Black and Rosenberg (1991) after examining a series of suspended-sediment load measurements under natural waves.

In this paper, we applied a vertically invariant eddy diffusivity for $z > z_0$, and allowed the eddy diffusivity to decrease linearly to zero for $z < z_0$. The linear decrease near the bed was found to have very little effect on the model results. We used the field measurements of egg and sperm concentrations to determine the adequacy of this formulation. Although local wind creates a second boundary layer at the surface, this layer could be neglected in the model because eggs and sperm did not spread to

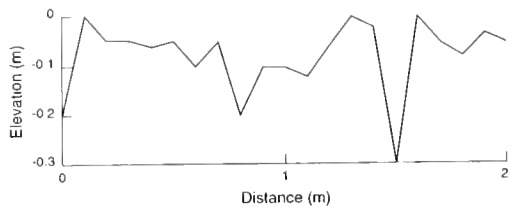

Figure 3. Seabed bathymetry over a 2-m distance at the study site, showing variations of up to 0.3 m.

the surface in significant numbers over the spatial scales considered.

Defined bed level. The velocity of all particles was set to zero in the region below "mean bed level," *i.e.*, within one roughness length (z_0 = 0.08 m) of the bed where the velocity profile is undefined. Zero net current in this zone is probably a reasonable approximation because of the sheltering induced by the coral. However, because the coral is porous, some water movement may still occur, particularly when waves are present. Consequently, random movement was retained below $z = z_0$.

The lowest pumps were estimated to be about 0.3–0.4 m above the minimum bed level ($z = 0$) in the model. The pumps were 0.2 m above the base of the pump array frame while the bed profile at the study site exhibited variations of up to 0.3 m (Fig. 3), and the pump frame base was generally located on the crests of the undulations. Mean bed level is expected to be at an elevation dependent on the magnitude of the roughness length. However, the frame was moved often and there remains some uncertainty, of the order of 0.2 m, in the defined position of the bed in the field data relative to the model.

Boundary conditions. At the surface, a zero flux boundary condition was imposed by reflecting any particles that attempted to move through the surface by diffusion.

The bottom boundary condition is best described as a "settling or trapping" condition, established to investigate the entry of particles into the bed matrix. In this paper, "settlement" is used in the sediment transport sense to denote contact with the seabed. A square grid covering the seabed was established in the model with 0.13-m sides, so that the surface area of each cell was equal to the area of the substrate traps (0.0169 m^2). Particles were said to have settled if their vertical position was within $0.1z_0$ of the defined bottom. Physically, this means that the particles would be well within the hollows in the bed undulations. Model tests showed that the defined level at which settlement was said to occur only marginally influenced the absolute numbers trapped when the defined level was less than z_0. Moreover, changes to the defined settlement level had no obvious influence on the predicted pattern of settlement. Once settled, particles were eliminated from the active pool. To record the event, a particle counter for the cell in which they settled was incremented by 1.

Results

Fall velocities of eggs and sperm

The laboratory measurements of fall velocity indicated a range of small negative buoyancies for the eggs (Fig. 4), with a median fall velocity of 0.072 mm · s^{-1} (0.26 m · h^{-1}). The sperm were essentially neutral whether alive or dead (Fig. 4). Measured sperm concentrations, even after 7 h, remained scattered about the neutrally buoyant curve.

A best fit curve for eggs was determined of the form

$$C/C_0 = e^{-t/\tau} \tag{8}$$

where C is the concentration, C_0 is the concentration at time $t = 0$ (hours), and τ is the decay coefficient (hours). The data exhibited a correlation coefficient of $r = -0.97$ to the curve

$$C/C_0 = e^{-t/0.556} \tag{9}$$

From eqn (7), the time taken for the concentration to halve is 0.384 h, which corresponds with a fall velocity over 0.1 m depth of 0.072 mm · s^{-1}, as given above.

Although the eggs are slightly negatively buoyant, a neutral condition for both the eggs and sperm is a reasonable approximation over the spatial scales being considered. This was subsequently confirmed with the numerical model by comparing results using the measured mean fall velocity and the neutrally buoyant condition.

Dynamics of gamete release

Although there was considerable individual variation, the rate at which female crown-of-thorns starfish released eggs was generally greatest at the beginning of the spawning event and declined logarithmically with time (Fig. 5).

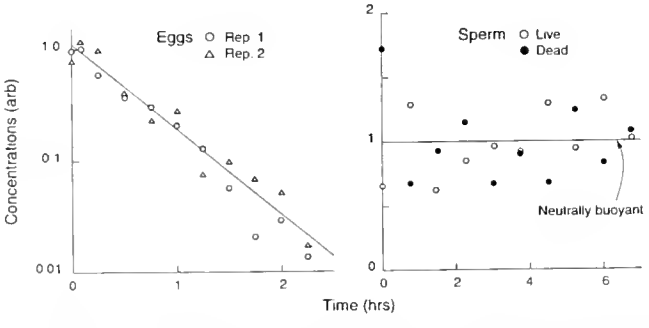

Figure 4. Egg and sperm concentrations at 0.1 m below the surface of the settling tube as a function of time. Note the close correspondence of the two replicate logarithmic plots for live eggs, and the close similarity of the plots for live and dead sperm.

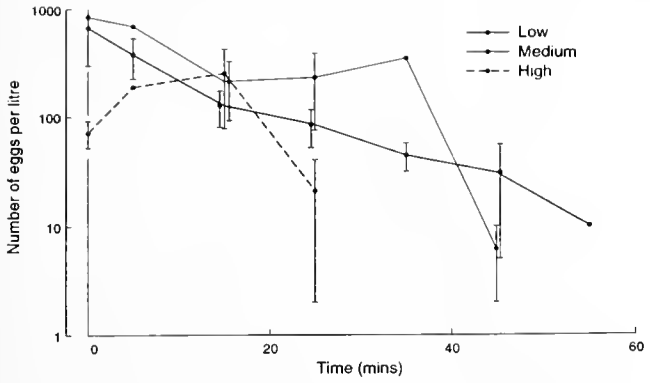

Figure 5. Temporal dynamics of egg release. Number of eggs per liter next to the spawning starfish is plotted on a logarithmic scale as a function of time since the start of spawning, for low, medium, and high current speeds.

This trend was consistent for two of the current flow regimes (low 0.02–0.05 $m \cdot s^{-1}$, medium 0.07–0.10 $m \cdot s^{-1}$). In high flows (0.2–0.3 $m \cdot s^{-1}$), the results were more erratic. Overall, a mean of 10^3 eggs l^{-1} was recorded close to the starfish at the start of spawning, and total production over the mean spawning period of 45 min averaged 2.0×10^4 eggs l^{-1}.

Measurements of egg concentrations adjacent to the starfish are more prone to experimental error in fast currents, particularly with respect to accurate placement of the pump near the starfish, which may explain the smaller observed number of eggs at $t = 0$ during high flows (Fig. 5). In addition, as noted above, the number of eggs released by individual starfish varies considerably.

The rate at which individual male starfish released sperm varied considerably, but no decline in the rate of

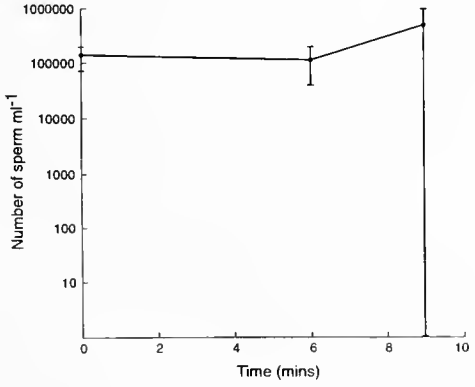

Figure 6. Temporal dynamics of sperm release. Number of sperm per milliliter next to the spawning starfish is plotted on a logarithmic scale as a function of time since the start of spawning. Data were available only for slow currents and for up to 10 min from the start of spawning.

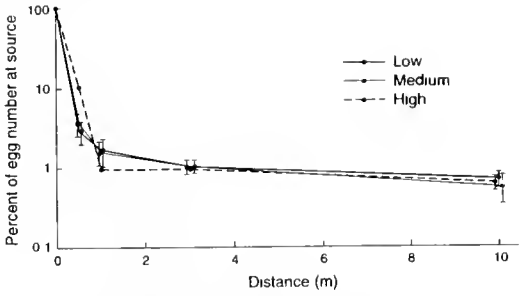

Figure 7. Egg dispersion. Logarithmic plot of eggs per liter as a function of distance from the spawning starfish, for low, medium, and high currents, expressed as a percentage of the number of eggs per liter at the spawning starfish.

release was observed during the first 10 min after the start of spawning at low current flows, the period and conditions for which data were available (Fig. 6). A mean of 10^5 sperm ml^{-1} was recorded close to the starfish at the start of spawning, and total production over the mean spawning period of 10 min averaged 2×10^9. The concentration near the starfish of 10^5 is much less than the concentrations of 8×10^8 sperm ml^{-1} recorded by Benzie and Dixon (1994) in the laboratory. The reduction is indicative of the initial dilutions occurring immediately adjacent to the starfish.

The total of 10^9 sperm is equivalent to a volume of concentrated sperm in the testes of approximately 50 ml (calculated from data in Benzie and Dixon, 1994), and suggests a rate of sperm release of 3×10^6 sperm s^{-1}.

Downstream gamete concentrations

Average egg concentrations, calculated as the mean number of eggs per liter over all pumps with non-zero values, fell rapidly with increasing distance from the spawning adult (Fig. 7). By a distance of 1 m, egg concentrations fell to one hundredth of that near the starfish, taking until 10 m before approximately halving in value again (Table II). Current strength does not strongly affect

Table II

Average concentrations of eggs measured on the frame (as a percentage of the concentration at the starfish) for slow, medium, and fast currents

	Distance downstream (m)			
	0.5	1.0	3.0	10.0
Slow	3.3	2.4	1.5	0.8
Medium	2.2	0.7	0.2	0.3
Fast	10.0	1.0	1.0	0.7

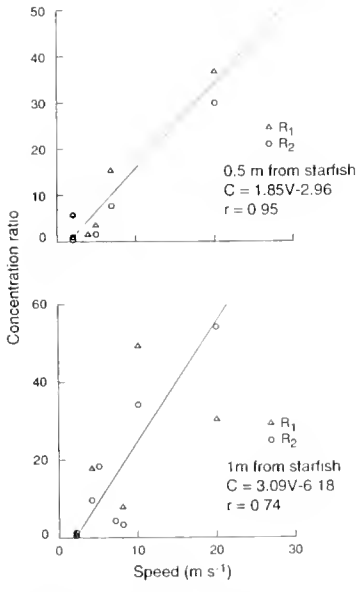

Figure 8. Vertical spread of eggs and sperm. The ratio of egg concentrations for the five pumps on the lowest level and the five pumps on the next highest level (Fig. 2) are plotted against the current speed. R_1 is the ratio of average concentrations, and R_2 is the ratio of maximum concentrations in each level.

the downstream concentration after normalizing by the concentration recorded near the starfish (Fig. 7).

To examine the spread of the gametes as a function of the current strengths, the following two ratios were determined:

$$R_1 = C_{av0}/C_{av1}; \quad R_2 = C_{max0}/C_{max1} \qquad (10)$$

C_{av0} and C_{av1} are the averages of the concentrations measured across the lowest level and the next lowest level of the frame respectively (450 mm apart; Fig. 2). C_{max0} and C_{max1} are the maximum concentrations measured in the same two rows. These ratios indicate whether the gametes spread evenly through the water column or favor the lower or upper level. R_1 and R_2 are both correlated with current strength at 0.5, 1.0, and 3.0 m from the starfish (Fig. 8). This means that the eggs are found closer to the bottom as the current strength increases over these space scales (see also Figure 11, low and medium current case).

At 10 m, egg concentrations were lower near the bed than at the higher levels (Fig. 11). This may be caused by substrate trapping of the near-bed particles (see below) or velocity shear. By acting as a sink, substrate trapping reduces the number of eggs near the bed. The effect of current shear was depicted by dye released near a starfish in slow currents. The dye was observed to spread between the bed and the surface after about 3 min, but the dye in the upper levels reached the downstream location fastest. This can result in higher concentrations in the upper levels in the period before the arrival of the slower moving dye near the bed.

Due to variations in gamete release rates in different starfish, the data do not permit further analysis of the absolute concentrations (without normalizing) as a function of current strength. However, modeling of the spatial distribution of eggs in the pump array described in a later section demonstrated clear differences in the dispersion of the gamete cloud at different current speeds and was in accordance with the field measurements (Fig. 11).

Data for sperm were limited to within 1 m of the spawning male because of the practical difficulties of adequately sampling sperm at greater dilutions. The percentages of sperm at 0.5 and 1.0 m are very similar to those for eggs (Fig. 9). This important result indicates that both are influenced by the hydrodynamics in the same way, and are not showing any major differences in their response as a result of factors such as their size or buoyancy. Sperm concentrations near the starfish (10^5 sperm ml^{-1}) fell to approximately 10^3 sperm ml^{-1} by 1 m.

Bed settlement

An average of 0.007% of the total number of eggs produced over a spawning entered the substrate (Fig. 10). Most did so near the spawning female, at densities up to 6000 eggs m^{-2}. Patterns of settlement into the seabed differed between current speeds (Fig. 10). The proportion of eggs entering the substrate was greater, and the majority settled closer to the starfish, for the slowest currents. At high current speeds few eggs entered the substrate traps, and did so only at some distance from the female.

Model simulations

Three field cases were modeled to encompass a range of current speeds and to provide a complete calibration, verification, and validation sequence over a wide range

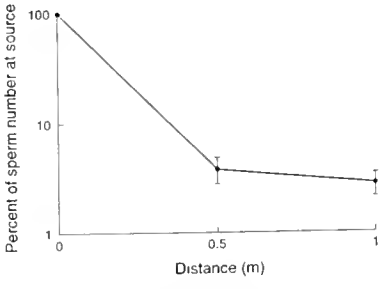

Figure 9. Sperm dispersion. Logarithmic plot of sperm per milliliter as a function of distance from the spawning starfish, expressed as a percentage of the number of sperm per milliliter at the spawning starfish. Data were available only for slow currents and for up to 1 m from the spawning starfish.

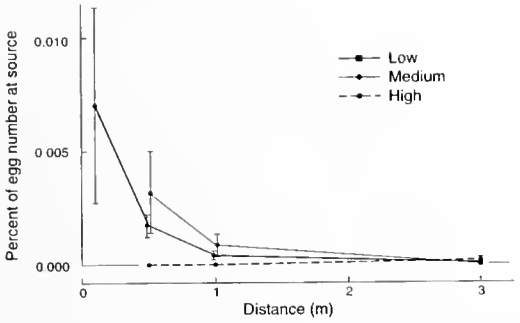

Figure 10. The proportion of the total number of eggs per liter that were produced near the spawning starfish over the course of an experiment and entered the substrate traps at different distances up to 3 m from the starfish, for low, medium, and high current speeds.

of current conditions. The first, Case 1, examined a very slow current (0.02 $m \cdot s^{-1}$) with the pumps 1 m from the starfish; it was compared with data from Experiment No. 1 (Table 1). The second, Case 2, was a simulation over 1 m when the current was faster (0.07 $m \cdot s^{-1}$); it was compared with data from Experiment No. 9 (Table 1). The third simulation, Case 3, examined dispersal at larger spatial scales and fast current speeds (*ca.* 0.25 $m \cdot s^{-1}$); it was compared with two sets of field measurements (made sequentially for replication) during Experiment Nos. 13 and 14 (Table 1).

We applied eddy diffusivity values in the range 0.0005–0.0015 $m^2 \cdot s^{-1}$. Although the tests were not exhaustive, we chose 0.0015 $m^2 \cdot s^{-1}$ for all three directions. This compares favorably with the value of $e_z = 0.0012$ $m^2 \cdot s^{-1}$ found by Black and Rosenberg (1991) in a wave-driven environment, although the horizontal values were smaller than expected (Elder, 1959). The results proved to be sensitive to the choice of eddy diffusivity, but we were unable to distinguish any need for an eddy diffusivity that depended on current strength.

Comparison of model with data. The measurements and model show a clear correspondence in all three cases (Fig. 11). In particular, the spread of the cloud, the spacing of the contours, their absolute magnitude, and their vertical position in the water column are in good agreement. The tendency for the gametes to stay near the seabed is evident in both the model and the measurements. Indeed, the magnitude of deviations between the measurements and the model is less than the variability in the concentrations measured at the starfish, which is a determining input to the model, and is within the variation between replicates. For example, in Case 1, when the current (U) was only 0.02 $m \cdot s^{-1}$, the larvae spread over a greater depth and spread more horizontally than in Case 2 (U = 0.07 $m \cdot s^{-1}$). This is depicted by the measurements and the model. In Case 3, when the currents were very fast (U = 0.25 $m \cdot s^{-1}$), the tendency for the gametes to be found only at the lower levels is exhibited in the model. Also, the magnitude of the predicted concentrations lies within the variability exhibited by the two sequential sets of field measurements (Fig. 11, Case 3). Notably, the horizontal offset between the two sets of field measurements and the model relates only to the positioning of the frame relative to the gamete cloud in the field.

The values of the horizontal eddy diffusivities are supported by the model calibration. In a series of sensitivity simulations, it was found that larger values tended to overly spread the gamete cloud laterally in the model.

Less well predicted is the measured tendency for egg concentrations to be very small near the seabed at distances greater than 10 m (Fig. 11). However, simulations carried out over 60 m and 100 m did exhibit lower concentrations near the bed. In addition, egg numbers decreased near the bed at 10 m in the model due to the losses associated with substrate trapping (Fig. 12). The egg concentrations (rather than egg numbers) in the model remained high because the water volumes predicted to pass through the frame at the low levels were small, in accordance with the small currents in the logarithmic boundary layer. Thus, some refinement of the behavior at near-bed levels may be required.

In general, although the model is far simpler than nature, it appears to contain the essential physics needed to address questions about the dispersal of eggs and sperm. The reduction in concentration with distance from the starfish is evidently being effectively predicted. Moreover, the assumptions made about the shape of the velocity profile and the eddy diffusivity appear to be adequate. The results indicate that the starfish eggs and the much smaller sperm can be treated as passive particles at these temporal and spatial scales.

Models of egg dispersal. The pattern of gamete dispersal in each of the current classes is clearly demonstrated in the diagrams showing egg clouds in both plan (top) view and in cross-section (side view) at the end of the simulation of Cases 1, 2, and 3 (Fig. 13). This is 3.5 min after the first release of eggs. In Case 1, the particles spread throughout the depth. This concurs with field observations in which dye spread between the bed and the surface after about 3 min.

In Case 2, when the current was 0.07 $m \cdot s^{-1}$, the eggs spread through about one third of the depth only. Indeed, in Case 3, when the current was 0.25 $m \cdot s^{-1}$, the eggs remained in the lower half of the water column after 10 m.

Two opposed factors determine the downstream concentrations of eggs and sperm. First, for a given release rate, the concentration of eggs near the starfish will be a function of the current speed, which determines the initial dilution. That is, if eggs are transported away quickly, the

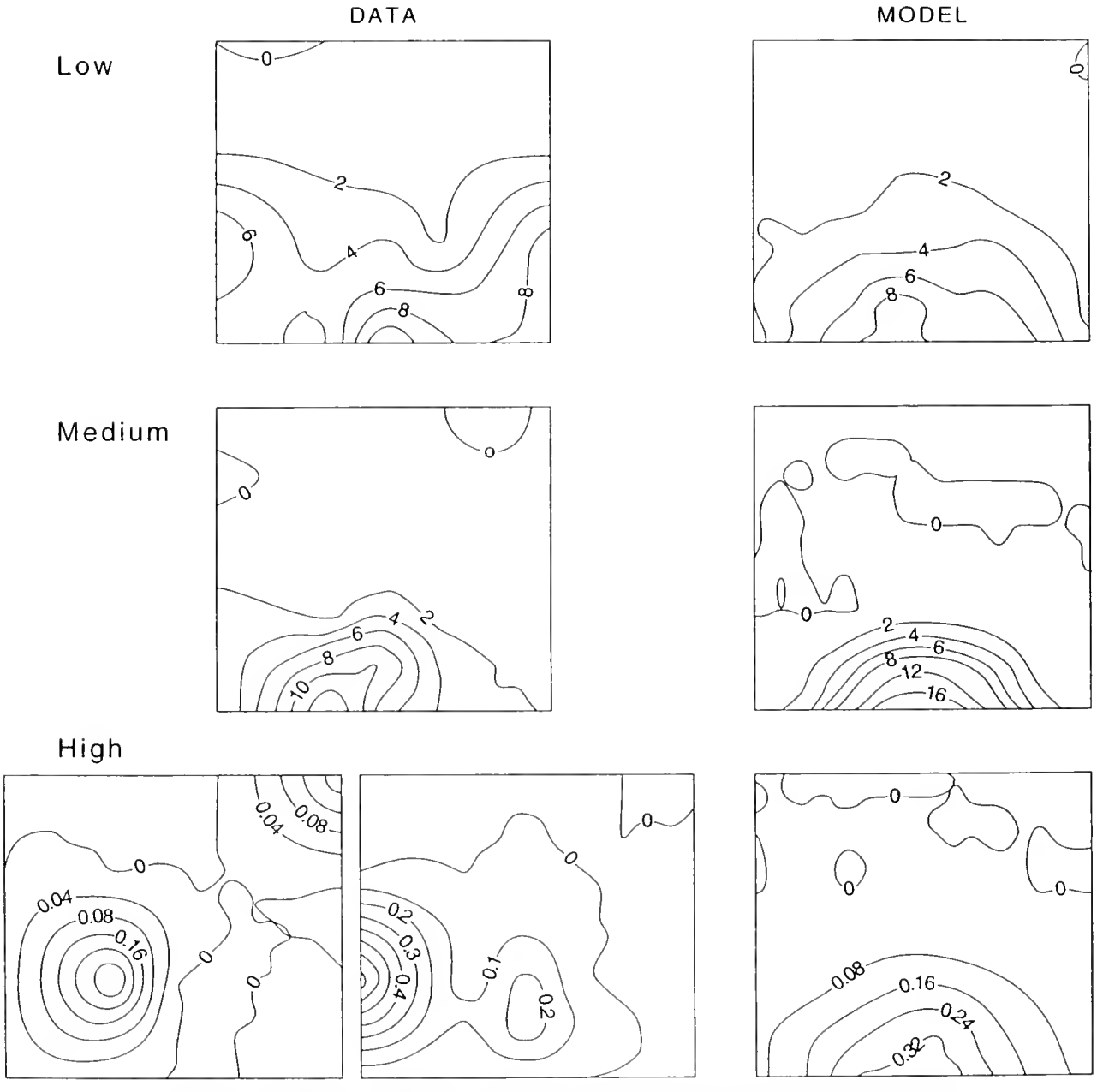

Figure 11. Comparison of measured egg concentrations (eggs per liter) with those predicted from the model for three different cases, representing an example from one each of low (0.02 $m \cdot s^{-1}$ at 1 m distance from the spawning starfish), medium (0.07 $m \cdot s^{-1}$ at 1 m distance), and high (0.25 $m \cdot s^{-1}$ at 10 m distance) speed currents. The horizontal offset between measurements and data relates only to the position of the pump array relative to the egg cloud, and does not indicate any fundamental difference between the model and measurements. In fact, not only is the general fit in dispersion pattern good, the concentrations generated in the model are very close to those measured.

concentration in a region near the starfish will be reduced. The measurements and model also show that the vertical spread of the gametes is less over a given downstream distance in fast currents, which compensates in part for the higher initial dilution. Indeed, Figure 7 indicates that the downstream concentrations normalized by the concentration at the starfish are not a strong function of current strength, even though the ratio of downstream concentrations at different depths indicated that gametes remained closer to the bed in fast flows. The measurements

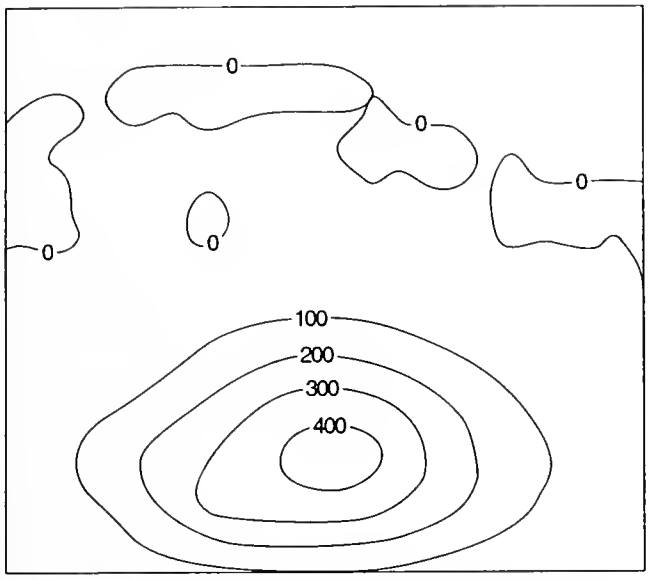

Figure 12. Egg numbers predicted by the numerical model, showing a reduction near the seabed due to substrate trapping at 10 m from the starfish in currents of 0.20 $m \cdot s^{-1}$.

did not indicate a need for an adjustment to the eddy diffusivity as a function of current speed over the range of speed and space scales considered.

The predicted contours of the number of eggs trapped in the seabed for the simulation of Cases 1–3 indicate that, if the starfish spawned in the hollows of the undulations, many of the eggs would be trapped nearby (Fig. 14). The model predicts that hundreds of eggs per 0.0169 m^2 (the size of our settlement dishes) enter the seabed. This is higher than the field measurements, but similar numbers were recorded in one case (Experiment No. 4) when up to 118 eggs were trapped at 0.5 m downstream of the starfish. The traps were very shallow (about 0.05 m) and may not have retained all of the settling eggs. Moreover, the entrances of some bed settlement traps were above mean bed level. At this level, the influence of local hydrodynamics, including wave orbital motion creating currents within the dish, was not known.

Discussion

Inferred fertilization success

A rapid reduction in concentration was measured with increasing distance from spawning crown-of-thorns starfish. These concentrations do not, however, necessarily indicate the levels of fertilization to be expected for the species, even though their rate of decline was similar to the decline in fertilization success reported for sea urchins (Pennington, 1985; Levitan *et al.*, 1991) and ascidians (Grosberg, 1991). In those studies, fertilization success dropped dramatically—from 80 to 100% near the spawning male to about 10% or less over 1 m—and the authors inferred gamete dilution to be the significant factor contributing to the observed decline. Unlike the present study, none of these previous studies measured the field concentrations of the gametes.

To infer fertilization rates from gamete concentrations, we used data obtained from mixing gametes of crown-of-thorns starfish at different concentrations in the laboratory (Benzie and Dixon, 1994). These calculations were based on the mean concentration of sperm observed in the field and on fertilization data from both early and late in the breeding season. Benzie and Dixon (1994) showed that gamete quality, and hence fertilization success, varied according to the time of the breeding season.

If we assume that the diluted sperm pass across a downstream spawning female, the calculations suggested the following rates of fertilization if spawning occurred early in the breeding season: 100% with the female adjacent to the male, 90–100% at 1 m, 90–100% at 3 m, and 70–100% at 10 m. Towards the end of the season the rates of fertilization were estimated as 90% near the male, 80–90% at 1 m, 75–80% at 3 m, and 60–70% at 10 m. These results are consistent with the published fertilization rates of 80–90% at 1 m and 60–70% at 10 m for crown-

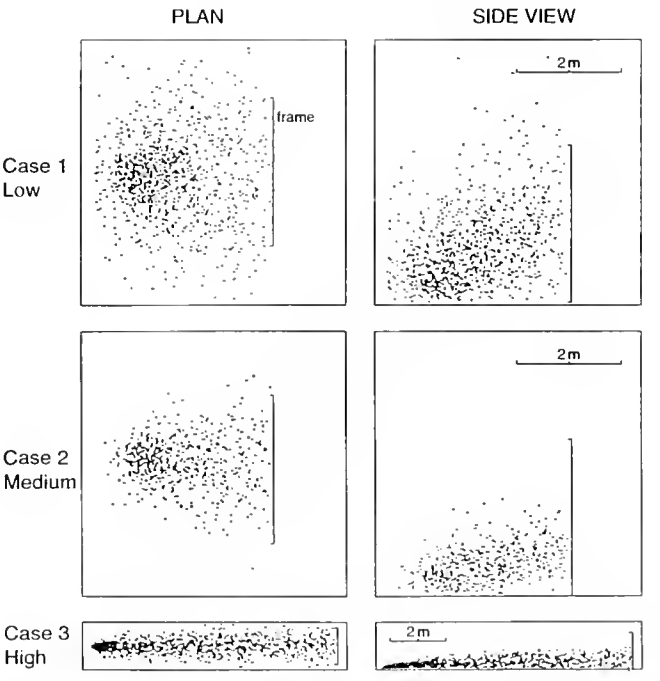

Figure 13. Position of the egg cloud in plan (top) view and cross-section (side view) after 3.5 min of simulation in Cases 1–3, representing one example from each of low, medium, and high speed currents.

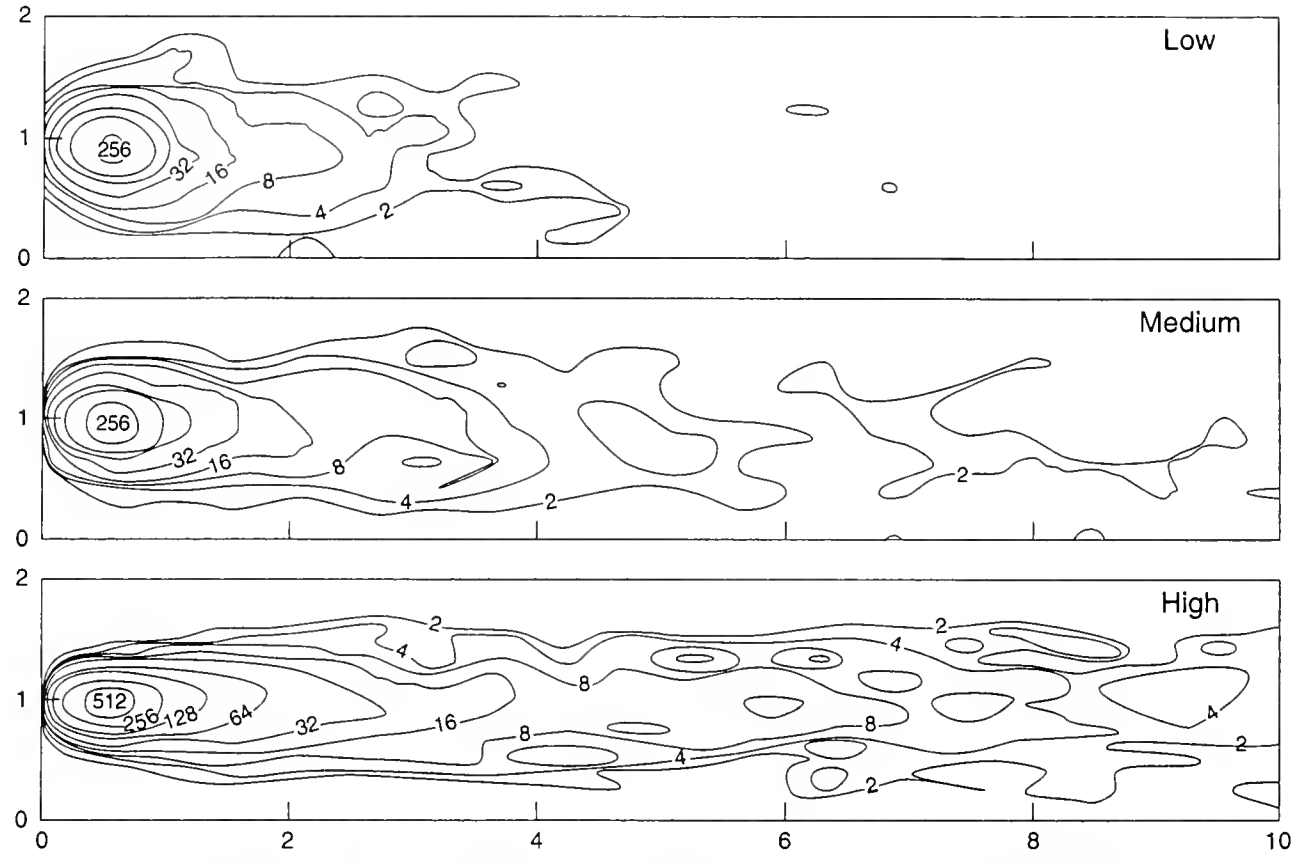

Figure 14. Number of eggs predicted to enter the seabed for each of the Cases 1–3. These cases provide one example from each of low, medium, and high current speeds. The model was run until the eggs had reached the 10-m mark, and then egg numbers were allowed to accumulate for 2 min.

of-thorns starfish in the field (Babcock and Mundy, 1992, 1993).

These fertilization rates are far higher than those observed for sea urchins, and it has been suggested that this is because the crown-of-thorns starfish is far more fecund than other echinoderms (Babcock and Mundy, 1992; Babcock *et al.*, 1993). The measured concentration of the starfish sperm, of approximately 10^5 sperm ml^{-1} near the spawning male in the field, suggested rates of sperm release of 3×10^6 sperm s^{-1}. These data compare well with the rates of sperm release of 10^5–10^6 s^{-1} calculated by Benzie and Dixon (1994) from laboratory measurements, and are similar to the rates of release for sea urchins of 1–3 $\times 10^6$ sperm s^{-1} calculated by Denny and Shibata (1989). Therefore, assuming similar rates of sperm release and similar dispersion patterns in given flow regimes, sperm concentrations for sea urchins at 1 m downstream from the spawning male would be equivalent to those measured for crown-of-thorns starfish (10^3 sperm ml^{-1}).

Fertilization rates expected from such sperm densities, using Figures 1 and 2 from Levitan *et al.* (1991), range from 5 to 30%. This is within the range of field measurements (for fast current speeds and slow currents speeds) made by Pennington (1985). Such measurements have used either samples of large numbers of eggs in syringes (Pennington, 1985) or samples of eggs taken from spawning females set downstream of a male (Babcock and Mundy, 1992; Babcock *et al.*, 1993).

The higher field fertilization rates of crown-of-thorns starfish, relative to sea urchins, therefore reflects the higher fertilizing capacity of starfish sperm at a given dilution, as observed in the laboratory by Benzie and Dixon (1994). The fertilization is evidently not due to a higher production of gametes as suggested by Babcock and Mundy (1992), who used sperm release rates of 4–8 $\times 10^8$ sperm s^{-1} to explain the high fertilization rates in the field. The production of far higher numbers of eggs by crown-of-thorns starfish may still increase the overall numbers of fertilized zygotes produced, but the fecundity of the starfish does not appear to influence rates of fertilization (through increasing gamete concentrations) in the field.

The basic advection models used in this study adequately predicted the distribution of eggs and sperm of crown-of-thorns starfish in the field. Given this, they can be used to predict with some confidence the dispersion patterns of crown-of-thorns gametes over greater spatial scales and for a greater variety of hydrodynamic conditions. Using laboratory data on fertilization rates, average fertilization expected in the gamete cloud at 100 m downstream from a spawning male at currents of 0.25 $m \cdot s^{-1}$ was 25% (range 0–50%). These are very similar to the rates published by Babcock and Mundy (1992) and Babcock *et al.* (1993).

Local substrate settlement

Although small in proportion (0.007%), a significant number of eggs were entrained in the substrate. Most of these entered the substrate near the spawning female at low-medium currents. At high currents, eggs were detected only in the substrate traps at 3 m. These results may explain why the starfish often mount high coral heads to spawn. The elevated position puts the eggs into the water column away from the seabed, maximizing the chance of long-range dispersal. Coral reefs have a high roughness value, and Eckman (1990) found that the rates of settlement should increase monotonically with aerial density of roughness features.

The small-scale hydrodynamics around the substrate traps could not be assessed, but flow patterns in the vicinity of similar collection devices (Gardner, 1980; Butman, 1989; Yund 1991) can vary widely and may reduce capture efficiency under certain conditions. The capture efficiency of the traps used in the present study may also have been reduced by their relatively low sides (0.05 m). Consequently, it is possible that the number of eggs entering the seabed was underestimated, thereby explaining the difference between the measured and model results. In addition, the assumptions made in the model for conditions very near the bed may need further refinement.

The biological significance of egg entrainment to the seabed is not clear. If fertilized, the eggs could complete their larval development within such an environment. Their survivorship, however, is open to question because they may suffer greater mortality due to the effects of benthic predators and physical disturbance (*e.g.*, wave action). The effects of these factors may in turn be offset by the increased availability of nutritional sources. Recent research (Hoegh-Guldberg, pers. comm.) has shown that concentrations of dissolved free amino acids (DFAA), which are an important source of nutrition for larvae of crown-of-thorns starfish, are much higher in the vicinity of the coral substrate. Entrapment of significant numbers of larvae amongst such substrates may provide a mechanism for self-recruitment to the adult population.

Indirect evidence to support the occurrence of this type of phenomenon has been recorded in the field. Moran *et al.* (1985) found many small starfish 1–2 years after large numbers of adult starfish were observed in the same area. Similar events were reported almost 2 years later along the leeward side of the reef (Bell, pers. comm.) and in the north bay of Pelorus Island (Kettle, pers. comm.). Self-recruitment has been reported for other organisms. For example, McShane *et al.* (1988) found that successful recruits of the abalone *Haliotis rubra* were those that remained near the parent in the crannies of reefs on exposed coasts. Comparisons with the larvae of crown-of-thorns starfish are questionable, however, because the larval life of *H. rubra* is 7 days instead of the average 10–16 days for the starfish.

Buoyancy and natural turbulence

Results from the present study also confirmed, contrary to the assumptions of Wolanski and Hamner (1988), that the gametes of the starfish can be treated as passive, weightless particles at the temporal and spatial scales over which our measurements were taken. The fall velocities were much less than the turbulent vertical and horizontal velocities indicated by the eddy diffusivities applied in the model. Although 10% of the eggs remained in suspension after an hour in still water, the percentage would be much higher under more turbulent field conditions if some gametes were resuspended after contacting the bed. Indeed, the most important factor determining gamete numbers remaining in the water column at longer time scales may be the tendency for trapping near the seabed.

The model results, at 10 m from a spawning starfish, indicated a reduction in the number of eggs near the bed, as also measured in the field. We think this is due to the entrapment of gametes in the substrate. In a turbulent environment that mixes the gametes through the vertical, this reduction in concentration would be expected to continue with time. As such, although the eggs and sperm are neutrally buoyant, turbulence brings the gametes into the sphere of influence of the seabed and the potential exists for these to enter into cavities within the substrate. This mechanism could considerably shorten the time that larvae of crown-of-thorns starfish spend in the water column and hence their average excursions during the pelagic phase.

Numerically, for neutrally buoyant material, this trapping process is equivalent to a bottom boundary condition that allows random turbulence to carry particles into the seabed. In sediment-transport models such as the one presented by Black and Rosenberg (1991), the bottom boundary condition (described as a pick-up function) precludes this loss of particles to the bed by random dif-

fusion. The sediment particles "settle" to the seabed only when the fall velocity carries them there. Thus, the data presented in this paper provide some new insight into the dynamics very near the bed. The results suggest that random turbulence over these very rough beds may "inject" eggs and sperm into the seabed, where they remain. In fact, for neutrally buoyant material, seabed trapping (or any form of "settlement") cannot occur if random turbulent movement into the bed is forbidden in the model. The bottom boundary in this case may be described as a "trapping condition." Physically, the gametes may be trapped by snagging or attaching to the substrate.

Summary

In summary, hydrodynamics plays an important role in determining the fertilization success and recruitment of the crown-of-thorns starfish. Denny and Shibata (1989) emphasized the relationship between hydrodynamics and fertilization success, although they did not have accurate measurements of the physical environment. The present study has demonstrated the close relationship that exists between the physical characteristics of the fluid medium into which the gametes are released and their patterns of dispersal in the field.

The high fertilization rates previously reported for the crown-of-thorns starfish have been confirmed from calculations based on the gamete concentrations found in the field and the fertilization rates seen in the laboratory at those concentrations. These high rates of fertilization probably reflect the higher fertilizing capacity of the starfish sperm rather than an increase in the rate of gamete release leading to a higher number of sperm per unit volume of seawater.

The present study has also demonstrated the importanee of hydrodynamics in the recruitment process. This was stressed previously by Butman (1989), who showed that invertebrate larvae can be passively deposited over large spatial scales. Our results indicate that hydrodynamics may also influence recruitment over much smaller scales—through the entrapment of gametes in the substrate. This mechanism for self-recruitment may be important in the onset of primary outbreaks of the crown-of-thorns starfish.

Acknowledgments

This research was partly supported by funds from the Great Barrier Reef Marine Park Authority under the auspices of the Crown of Thorns Starfish Advisory Review Committee, and by the Victorian Institute of Marine Sciences; we thank staff at both institutes for supporting this work. We are particularly grateful to the crew of RV *Harry Messel* and to V. Baker for her assistance in the gamete fall velocity experiments. This is AIMS Contribution Number 679.

Literature Cited

Babcock, R., and C. Mundy. 1992. Reproductive biology, spawning and field fertilization rates of *Acanthaster planci*. *Aust. J. Mar. Freshwater Res.* **43:** 525–534.

Babcock, R., and C. Mundy. 1993. Seasonal changes in fertility and fecundity in *Acanthaster planci*. *Proc. 7th Inter. Coral Reef Symp., Guam.* In press.

Babcock, R., C. N. Mundy, and D. Whitehead. 1994. Sperm diffusion models and *in situ* confirmation of long distance fertilization in the free-spawning asteroid *Acanthaster planci*. *Biol. Bull.* **186:** 17–28.

Benzie, J. A. H., and P. A. Dixon. 1994. The effects of sperm concentration, sperm:egg ratio, and gamete age on fertilization success in the crown-of-thorns starfish (*Acanthaster planci*) in the laboratory. *Biol. Bull.* **186:** 139–152.

Birkeland, C., and J. S. Lucas. 1990. *Acanthaster planci: Major Management Problem of Coral Reefs*. CRC Press, Boca Raton, FL. 257 pp.

Black, K. P., and S. L. Gay. 1990. Reef-scale numerical hydrodynamic modelling developed to investigate crown-of-thorns starfish outbreaks. Pp. 120–150 in *Acanthaster in the Coral Reef: A Theoretical Perspective*, R. Bradbury, ed. Lecture Notes in Biomathematics. Springer-Verlag, Berlin.

Black, K. P., and D. N. Hatton. 1990. *Dispersal of Larvae, Pollutants and Nutrients on the Great Barrier Reef, at Scales of Individual Reefs and Reef Groups, in 2 and 3 Dimensions*. Report to the Great Barrier Reef Marine Park Authority. 77 pp.

Black, K. P., and M. A. Rosenberg. 1991. Suspended sediment load at three time scales. Pp. 313–327 in *Coastal Sediments '91 (ASCE) Seattle Washington Proceedings*. American Society of Civil Engineers, Seattle, WA.

Black, K. P., P. J. Moran, and L. S. Hammond. 1991. Numerical models show coral reefs can be self-seeding. *Mar. Ecol. Prog. Ser.* **74:** 1–11.

Brazeau, D. A., and H. R. Lasker. 1992. Reproductive success in the Caribbean octocoral *Briareum asbestinum*. *Mar. Biol.* **114:** 157–163.

Butman, C. A. 1989. Sediment-trap experiments on the importance of hydrodynamical processes in distributing settling invertebrate larvae in near-bottom waters. *J. Exp. Mar. Biol. Ecol.* **134:** 37–88.

Chia, F.-S., and L. R. Bickell. 1983. Echinodermata. Pp. 545–620 in *Reproductive Biology of Invertebrates, Vol II: Spermatogenesis and Sperm Function*, K. G. Adiyondi and R. G. Adiyondi, eds. John Wiley and Sons, New York.

Cohn, E. 1918. Studies on the physiology of spermatozoa. *Biol. Bull.* **34:** 167–218.

Denny, M. W. 1988. *Biology and the Mechanics of the Wave-Swept Environment*. Princeton University Press, New Jersey. 329 pp.

Denny, M. W., and M. F. Shibata. 1989. Consequences of surf-zone turbulence for settlement and external fertilization. *Am. Nat.* **134:** 859–889.

Eckman, J. E. 1990. A model of passive settlement by planktonic larvae onto bottoms of differing roughness. *Limnol. Oceanogr.* **35:** 887–901.

Elder, J. W. 1959. The dispersion of marked fluid in turbulent shear flow. *J. Fluid Mechanics* **5:** 544–550.

Fredsoe, J., O. H. Anderson, and S. Silberg. 1985. Distribution of suspended sediment in large waves. *J. Waterway, Port, Coastal and Ocean Eng. (ASCE)* **11:** 1041–1059.

Gardner, W. D. 1980. Sediment trap dynamics and calibration: a laboratory evaluation. *J. Mar. Res.* **38:** 17–39.

Gray, J. 1928. The effect of dilution on the activity of spermatozoa. *J. Exp. Biol.* **5**: 337–344.

Grosberg, R. K. 1991. Sperm-mediated gene flow and the genetic structure of a population of the colonial ascidian *Botryllus schlosseri*. *Evolution* **45**: 130–142.

Hardy, T. A., and I. R. Young. 1991. Modelling spectral wave transformation on a coral reef flat. Pp 345–350 in *Proc. 10th Australasian Coastal and Ocean Engineering Conference Auckland, New Zealand Water Quality Centre Publication No 21.* Hamilton, New Zealand.

Levitan, D. R., M. A. Sewell, and F.-S. Chia. 1991. Kinetics of fertilization in the sea urchin *Strongylocentrotus franciscanus*: interaction of gamete dilution, age and contact time. *Biol. Bull.* **181**: 371–378.

Lillie, F. R. 1915. Studies of fertilization. VII. Analysis of variations in the fertilizing power of sperm suspensions of *Arbacia*. *Biol. Bull.* **28**: 229–251.

Lillie, F. R. 1919. *Problems of Fertilization.* University of Chicago Press, Chicago, 278 pp.

McShane, P. E., K. P. Black, and M. G. Smith. 1988. Recruitment processes in *Haliotis rubra* (Mollusca: Gastropoda) and regional hydrodynamics in southeastern Australia imply localised dispersal of larvae. *J. Exp. Mar. Biol. Ecol.* **124**: 175–203.

Moran, P. J., R. H. Bradbury, and R. E. Reichelt. 1985. Mesoscale studies of the crown-of-thorns/coral interaction: a case history from the Great Barrier Reef. *Proc. Fifth Internat. Coral Reef Congress, Tahiti* **5**: 321–326.

Moran, P. J., and G. De'ath. 1992. Estimates of the abundance of the crown-of-thorns starfish *Acanthaster planci* in outbreaking and non-outbreaking populations on reefs within the Great Barrier Reef. *Mar. Biol.* **113**: 509–515.

Nielsen, P. 1986. Suspended sediment concentrations under waves. *Coastal Engineering* **10**: 23–31.

Oliver, J., and R. Babcock. 1992. Aspects of the fertilization ecology of broadcast spawning corals: sperm dilution effects and *in situ* measurements of fertilization. *Biol. Bull.* **183**: 409–417.

Pennington, J. T. 1985. The ecology of fertilization of echinoid eggs: the consequences of sperm dilution, adult aggregation, and synchronous spawning. *Biol. Bull.* **169**: 417–430.

Petersen, C. W. 1991. Variation in fertilization rate in the tropical reef fish, *Halichoeres bivattatus*: correlates and implications. *Biol. Bull.* **181**: 232–237.

Simons, R. R., A. G. Kyriacou, and K. P. Black. 1989. Predicting wave-current interactions at Mallacoota Bay. Pp 297–301 in *Proc. 9th Australasian Coastal and Ocean Engineering Conference, Adelaide, Australia.* Institution of Engineers, Canberra, Australia.

Vogel, H., G. Czihak, P. Chang, and W. Wolf. 1982. Fertilization kinetics of sea urchin eggs. *Math. Biosci.* **58**: 189–216.

Wolanski, E., and W. M. Hamner. 1988. Topographically controlled fronts in the ocean and their biological significance. *Science* **241**: 177–181.

Yund, P. O. 1990. An *in situ* measurement of sperm dispersal in a colonial marine hydroid. *J. Exp. Zool.* **253**: 102–106.

Reference: *Biol. Bull.* **186:** 168–171. (April, 1994)

A Portable, Discrete-Sampling Submersible Plankton Pump and Its Use in Sampling Starfish Eggs

CRAIG MUNDY, RUSS BABCOCK[1], IAN ASHWORTH, AND JOHN SMALL

Australian Institute of Marine Science, PMB No 3, Townsville MC, Queensland 4810, Australia

Abstract. The apparatus was designed to enable divers to obtain discrete replicate samples from known volumes of water. Relatively large volumes of water can be filtered without the need to maintain contact with or return to the surface. These attributes confer a high degree of flexibility in subsurface sampling situations. Although we used the equipment to sample the eggs of invertebrates, it could equally easily be used to sample other small, patchily distributed plankton.

Introduction

In the marine environment, just as in the terrestrial environment, many phenomena of interest to ecologists vary unpredictably in time and space. However, the nature of aquatic environments greatly complicates our attempts to understand these ecosystems. The advent of scuba diving has transformed our understanding of life in marine and fresh waters, through the freedom it has given scientists to explore them directly. Many aspects of marine ecological research continue to present difficulties, particularly when sampling programs must be conducted at fine spatial or temporal scales in a patchy environment.

In a study of *in situ* fertilization rates of the crown-of-thorns starfish, *Acanthaster planci*, we needed to sample eggs repeatedly from positions that were fixed relative to spawning starfish but that were unpredictable in time and space. Sampling had to be conducted both during experimentally induced spawning situations and during spontaneous natural spawning events. The sampling method had to enable us to sample and filter measured quantities of water without damaging starfish eggs, and the equipment had to be easily operated and transported by a scuba diver. We designed and constructed an apparatus that enabled us to fulfill these requirements and obtain data on fertilization rates of *A. planci* and other echinoderms in both natural and experimental situations.

In applying this apparatus to the study of *in situ* fertilization rates, it was important to determine that estimates of fertilization rates were not biased by the sampling procedure or the apparatus. This paper describes the apparatus, the sampling procedure, and the experiments investigating potential sources of bias.

Materials and Methods

Apparatus

Conceptually, the apparatus was a metered plankton pump with 12 replicate filter cartridges (Fig. 1a). Its dimensions were 500 × 400 mm and 550 mm high. Water to be sampled was taken in through a suction hose (13-mm Tygon tubing) and passed through a digital flow meter (GPI electronic digital meter) after filtration. Suction was applied using a pump (Flojet, 12 l/min) attached to the filter cartridge by a second hose. Each numbered filter cartridge consisted of an inner filter tube constructed of clear acrylic and plankton mesh (60 μm), approximately 350 ml in volume, surrounded by a second outer tube of 500-ml volume that screwed into a flange at the top of the inner tube (Fig. 1b). The entire cartridge was then screwed onto the pump by another set of threads on the flange. Water was drawn into the cartridge through a one-way fitting mounted in the pump assembly at the top of the inner tube, and out of the cartridge through a second one-way fitting at the bottom of the outer tube. Thus once the sample was drawn into the tube, it was effectively isolated from the surrounding water mass. As successive samples were taken, the suction hose and the second hose to the pump were removed and reattached to the appropriate cartridge. The flow meter was activated automati-

Received 12 November 1993; accepted 27 January 1994.

[1] Current address: University of Auckland Leigh Marine Laboratory, P.O. Box 349, Warkworth, New Zealand.

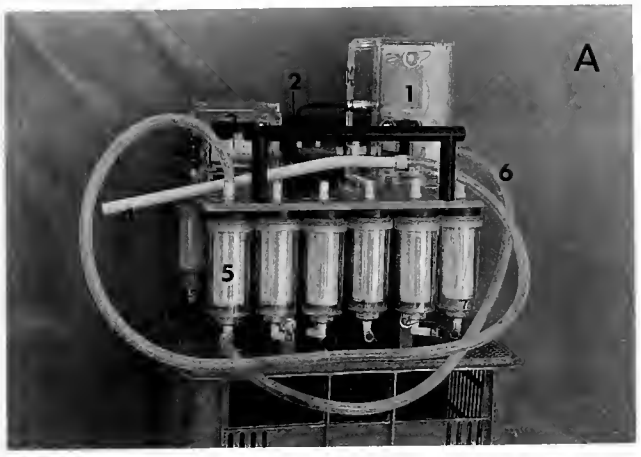

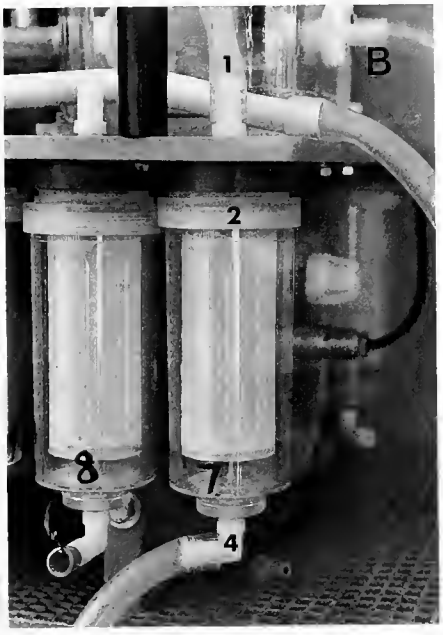

Figure 1. (A) Photograph of apparatus. 1—pump; 2—switch; 3—flow meter; 4—intake hose; 5—filter cartridge assembly; 6—suction hose. (B) Detail of filter cartridge assembly. 1—intake (sample); 2—filter cartridge flange; 3—outer cartridge casing; 4—outlet(suction).

cally, allowing the volume of each sample to be recorded. Power was supplied by two parallel 12-V gel-cell batteries. Batteries, pump, flow meter, and switch were each housed in separate clear acrylic O-ring-sealed housings, giving a maximum safe operating depth of 20 m.

The sampling procedure

The apparatus was used in experiments investigating fertilization rates of eggs from female starfish separated downstream from males at varying distances, and fertilization rates of eggs from female starfish and other echinoderms during natural spawning events. The sampling procedure given here is for experiments involving artificially spawned crown-of-thorns starfish.

The direction and path of the current were determined with fluorescein dye and marked with a plastic-fiber measuring tape. A single male starfish was placed upstream, and the female starfish was placed at a set distance downstream. The sex of starfish was determined by extracting a small amount of gonad with a large-bore syringe. The female starfish was then injected with 20–30 ml of 1×10^{-4} *M* 1-methyl adenine to induce spawning, and the male was injected 10 to 15 min later. A large cloud of fluorescein was released next to the male starfish once spawning was well under way, to mark the passage of the sperm plume. Sampling was started when the female starfish had begun to spawn, but not before the dye cloud had reached the female. Two replicate samples were taken with the female at each prescribed distance, starting from the most distant and proceeding towards the spawning male. Only the female starfish was moved in each trial. Two replicates were always taken with the male and female starfish adjacent to one another (0 m), as a control to establish maximum potential fertilization rates for each experimental pairing. The last pair of samples were taken with the female starfish 8 m upstream from the male, as a sperm-free control. The sperm-free control samples provided a means to ensure that fertilization rates observed in the trial were not due to extraneous sperm from naturally spawning starfish in the area. New animals were obtained for each trial. On completion of the experiment, the apparatus was brought to the surface and transported back to the research vessel, where the eggs were decanted from each filter cartridge and fixed immediately in 10% seawater formalin.

Samples were taken holding the intake of the suction hose approximately 15 cm above the spawning female starfish. Although eggs did accumulate on the surface of the starfish, currents during the experiments (0.07–0.25 $m \cdot s^{-1}$) were sufficient to advect the eggs into the water column. Before sampling at a prescribed distance, the pump, flow meter, and sampling hoses were flushed with water to remove eggs and water from the previous sampling point. The eggs on the surface of the female starfish were shaken free, and sampling was not commenced until a new series of eggs had begun to leave the body surface of the starfish. Current speed was recorded at the site immediately before and after each trial by releasing neutrally buoyant markers and timing their travel along the tape.

Sources of bias

The primary sources of possible bias in the sampling procedure were that (a) variability in the quantity of water sampled through the filter cartridge might influence the fertilization rate and (b) the fertilization rate might in-

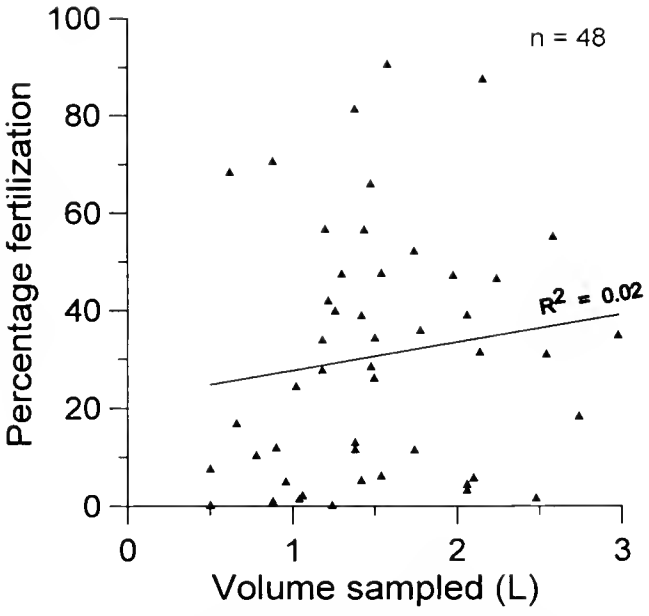

Figure 2. Percentage fertilization at 32 m plotted against volume, *V*, of water sampled. Regression equation: fertilization = 5.741*V* + 21.94 (R^2 = 0.02, n = 48).

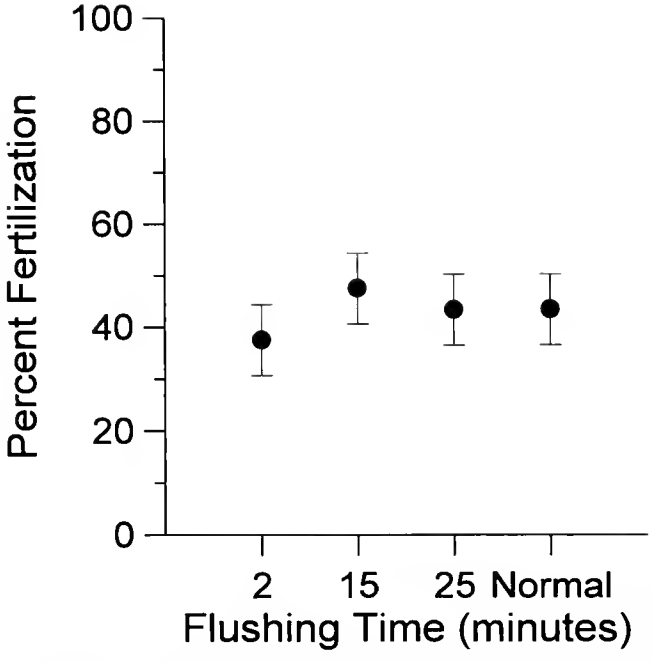

Figure 3. Mean percentage fertilization at 32 m for four flushing treatments (normal and 2, 15, and 25 min), with 95% confidence limits.

crease as a result of the eggs remaining in the filter cartridges at constant sperm concentrations for varying periods of time (under natural conditions it is assumed that sperm continue to decrease in concentration). Both of these sources of bias relate to the possibility of greater sperm exposure for eggs held within filter cartridges than for eggs during the normal dispersal process.

To assess the influence of variable quantities of water passing through the filter cartridges, data from male/female pairs separated by a distance of 32 m were analyzed by linear regression. In this analysis the quantity of water sampled was the independent variable and fertilization rate was the dependent. A second series of experimental trials was carried out to determine the effect of retention time of eggs within the filter cartridge on fertilization rate. In each trial, eight samples of eggs were taken from a single female starfish that was held 32 m downstream from a single spawning male starfish. Two samples were flushed with 4 l of sperm-free water at each of three time intervals (2, 15, and 25 min), and the remaining two samples were processed in the normal manner, remaining in the filter cartridges for about 1 to 2 h before decanting and fixation. The sperm-free water was held in a large double-layered plastic bag beside the apparatus. A further two samples were taken with the female adjacent to the male as an indication of maximum fertilization, and two samples were taken 8 m upstream from the spawning male as a sperm-free control. The eggs were decanted in the normal way. A simple nested ANOVA was used to test for the effect of time prior to flushing on the fertilization rate. The main effect was TIME with four treatments (normal and 2, 15, and 25 min). The nested term was the experimental trial, included to account for variability among experimental trials and differences in fertilization rates among animal pairs.

Results

No relationship was found between the fertilization rate and the quantity of water passed through the filter cartridges during sampling (R^2 = 0.02, Fig. 2). The quantity of water sampled through the cartridges varied between 0.5 and 3.0 l, with an average of 1.5 l.

No significant differences in fertilization rate were found between the four flushing treatments (normal and 2, 15, and 25 min); Fig. 3, Table I, ANOVA df = 3, 20; $p > 0.95$). The mean fertilization rate for the 2-min flush treatment

Table I

ANOVA table for the experiment to determine whether the time eggs were held in the filter cartridge affected fertilization rate

Source	Degrees of freedom	Mean square	*F*	$p > f$
TIME	3	168.18	0.12	0.95
TRIALS	16	1384.33	12.79	0.0001
ERROR	20	108.28		

Four treatments within TIME (normal and 2, 15, and 25 min), and 10 TRIALS nested within the main effect TIME.

(37%) was slightly lower than the fertilization rate observed for the 15 min, 25 min, and normal treatments (48, 44, and 45%), although not significantly so (Fig. 3). The results indicate that most of the fertilization takes place within the first 2 min, and that further periods of confinement with sperm prior to flushing do not increase measured levels of fertilization appreciably. The "normal" procedure of decanting eggs from the filter cartridge upon return to the research vessel does not result in a significant increase in fertilization rate. Levels of fertilization recorded at 8 m upstream from the spawning male were zero; those for adjacent animals ranged from 70 to 90%.

Discussion

The results of fertilization rate experiments presented here agree broadly with those presented elsewhere (Babcock and Mundy, 1992; Babcock *et al.* 1994), with high rates of fertilization for *Acanthaster planci* eggs being recorded at large distances downstream from spawning males. The technique of pumping water samples through filter cartridges worked as expected, with no detectable fertilization upstream from spawning males and high levels of fertilization for adjacent animals. This demonstrates that there is little inhibition of fertilization—if any—as a result of the sampling technique, and no contamination of samples by sperm that might have leaked in from other sampling areas (the samples upstream had no measurable fertilization). The absence of fertilized eggs in the upstream samples also indicates that fertilization membranes were not formed as a mechanical artifact of shear in the tubes.

This apparatus represents a significant improvement on techniques used previously to obtain similar measurements in that it does not rely on passive dispersal of sperm through a porous container (*e.g.*, Levitan *et al.*, 1992). Such containers do allow sperm to penetrate, but they may well reduce flow and exchange of water with the surrounding sea. This reduction would have an effect on fertilization rates. Furthermore, our technique does not rely on preloading of containers with eggs and so can be used in natural spawning situations. Unlike syringe sampling (*e.g.*, Pennington, 1985), it can handle large volumes and is therefore able to sample much more dilute concentrations of eggs.

Neither variable amounts of water pumped through the cartridges (representing varying numbers of sperm pumped past eggs) nor varying periods of retention of sperm with samples in the cartridges introduced significant levels of bias into the results of the sampling. Our method can be used to obtain results with a higher level of accuracy and a greater degree of flexibility than have been previously available for measurements of *in situ* fertilization rates.

Many of the features of the apparatus would lend themselves to applications in other fields, such as the study of micro-scale distribution patterns of planktonic organisms, especially demersal forms. With minor modifications to buoyancy, the equipment could also be adapted to open-water situations—for example, sampling of visible plankton patches over small spatial scales (*e.g.*, Wolanski and Hamner, 1988).

Acknowledgments

We thank Karen Miller and Annabel Miles for assistance with the field experiments. This work was supported by the Great Barrier Reef Marine Park Authority's crown-of-thorns research program. This is Contribution No. 675 from the Australian Institute of Marine Science.

Literature Cited

Babcock, R. C., and C. N. Mundy. 1992. Reproductive biology, spawning and field fertilization rates of *Acanthaster planci*. *Aust. J. Mar. Freshwater Res.* **43:** 525–534.

Babcock, R. C., C. N. Mundy, and D. Whitehead. 1994. Sperm diffusion models and *in situ* confirmation of long-distance fertilization in the free-spawning asteroid *Acanthaster planci*. *Biol. Bull.* **186:** 17–28.

Levitan, D. R., M. A. Sewell, and Fu-Shiang Chia. 1992. How distribution and abundance influence fertilization success in the sea urchin *Strongylocentrotus franciscanus*. *Ecology* **73:** 248–254.

Pennington, J. T. 1985. The ecology of fertilization of echinoid eggs: the consequences of sperm dilution, adult aggregation, and synchronous spawning. *Biol. Bull.* **169:** 417–430.

Wolanski, E., and W. M. Hamner. 1988. Topographically controlled fronts in the ocean and their biological influence. *Science* **241:** 177–181.

Reference: *Biol. Bull.* **186**: 172–181. (April, 1994)

Morphogen-Based Chemical Flypaper for *Agaricia humilis* Coral Larvae

DANIEL E. MORSE[1], AILEEN N. C. MORSE, PETER T. RAIMONDI, AND NEAL HOOKER

Department of Biological Sciences and the Marine Biotechnology Center, Marine Science Institute, University of California, Santa Barbara, California 93106

Abstract. Larvae of the scleractinian coral *Agaricia humilis* settle and metamorphose in response to chemosensory recognition of a morphogen on the surfaces of *Hydrolithon boergesenii* and certain other crustose coralline red algae. The requirement of the larva for this inducer apparently helps to determine the spatial pattern of recruitment in the natural environment. Previous research showed that the inducer is associated with the insoluble cell wall fraction of the recruiting algae or their microbial epibionts, and that a soluble but unstable fragment of the inducing molecule can be liberated by limited hydrolysis, either with alkali or with enzymes specific for cell wall polysaccharides. We now show that the parent morphogen can be solubilized by gentle decalcification of the algal cell walls with the chelators EGTA or EDTA, suggesting that the morphogen may be a component of the calcified recruiting alga itself, rather than a product of any non-calcified microbial epibionts. The solubilized inducer is subsequently purified by hydrophobic-interaction and DEAE chromatography. The purified, amphipathic morphogen retains activity when tightly bound to beads of a hydrophobic-interaction chromatography resin, and this activity (tested with laboratory-reared larvae) is identical in the ocean and the laboratory. We have attached the purified, resin-bound inducer to surfaces coated with a silicone adhesive and thus produced a potent artificial recruiting substratum—*i.e.*, a morphogen-based chemical "flypaper" for *A. humilis* larvae. This material should prove useful in resolving the role of chemosensory recognition of morphogens in the control of substratum-specific settlement, metamorphosis, and recruitment and in the maintenance of species isolation mechanisms in the natural environment.

Received 29 September 1993; accepted 19 January 1994.

Abbreviations: DEAE, diethylaminoethyl; EDTA, ethylenediaminetetraacetic acid; EGTA, ethylene glycol-bis(β-amino ethyl ether) N,N,N¹,N¹-tetraacetic acid; HIC, hydrophobic-interaction chromatography; Tris, tris-hydroxymethylaminomethane.

[1] Author to whom correspondence should be addressed.

Introduction

Chemosensory recognition of unique substrata (algae, microbial films, conspecifics, *etc.*) has been found sufficient, in the laboratory, to induce settlement and metamorphosis of the larvae of a wide variety of marine invertebrate taxa (for reviews see Crisp, 1974, 1984; Scheltema, 1974; Hadfield, 1978, 1986; Chia, 1978; Burke, 1983, 1986; Morse, 1985, 1990; Rittschof and Bonaventura, 1986; Hadfield and Pennington, 1990; Pawlik, 1990; Morse, 1992). In a number of cases, the specificity of this response demonstrated in the laboratory parallels the substratum-specificity of settlement, metamorphosis, and recruitment in the natural environment, and the complex inducer (or a partially purified fraction or presumptive chemical analog) induces substratum-specific settlement and metamorphosis of the target species in the ocean (Crisp, 1974; Morse *et al.*, 1980, 1988; Highsmith, 1982; Sebens, 1983; Hadfield and Scheuer, 1985; Connell, 1985; Raimondi, 1988, 1990a, b; Jensen and Morse, 1984, 1990; Morse and Morse, 1984; Shepherd and Turner, 1985; Raimondi and Schmitt, 1992). Using artificial substrata with or without a sticky coating, Walters (1992) showed that rugophilic barnacle and bryozoan larvae actively select microhabitats for metamorphosis that differ from the sites of their first contact with the substrate. Not yet clear, however, is the extent to which larval recognition

of any *individual, natural morphogenic molecule* may contribute to the control of recruitment and to species isolation in the natural environment, and how this recognition interacts with other determining factors (such as surface rugosity, hydrodynamic regime, other biological interactions, *etc.*) that also are usually present with the chemical cue in the complex natural substratum (*cf.* Butman, 1987; Pawlik *et al.*, 1991). These effects must be resolved if we are to understand the role of larval chemosensory receptors in the control of recruitment and their possible contribution to the evolution of species isolation. What is needed for such experimental resolution (in those cases in which the natural cue is normally nondiffusible) is a kind of morphogen-based chemical "flypaper," an inert substratum to which the highly purified natural morphogen is bound, permitting dissection of the contributions and interactions of the presence of the individual chemical cue and other features of the recruiting substratum and the environment.

As we show here, properties of the alga-associated morphogen of the common Caribbean scleractinian coral *Agaricia humilis* facilitate both its purification and the development of an immobilized, morphogen-based recruiting substratum. Larvae of *A. humilis* are induced to settle and metamorphose by contact-dependent chemosensory recognition of molecules on the surfaces of *Hydrolithon boergesenii* and other specific crustose coralline red algae (Morse *et al.*, 1988; Morse and Morse, 1991). In the absence of this cue, larvae persist without settlement or metamorphosis for ≥30 days in the laboratory (Morse and Morse, 1991). This larval requirement for a substratum-specific morphogen parallels, and thus presumably helps shape, the pattern of recruitment of this species on coralline red algae in the natural environment (Morse *et al.*, 1988).

We previously found that the nondiffusible inducer of settlement and metamorphosis is associated with the insoluble cell wall fraction of the recruiting alga or its microbial epibionts (Morse *et al.*, 1988; Morse and Morse, 1991). We also found that a small (<2000 Da), soluble fragment of the inducing molecule could be liberated by decalcification of the algal cell walls with dilute acetic acid, followed by limited hydrolysis with alkali or with purified enzymes that hydrolyze specific bonds found in cell wall polymers (Morse and Morse, 1991). This biochemical result was consistent with either an algal or a bacterial origin of the inducer, as similar polymers can be found in the cell walls of both groups. Furthermore, the solubilized morphogen fragment was obtained in low yield and proved to be extremely unstable, hindering both its further purification and use.

We now show that the morphogen can be solubilized without hydrolysis, simply by gentle decalcification of the algal cell walls (or other divalent metal-cross-linked insoluble phycocolloids) with the calcium chelator EGTA, or with the divalent metal chelator EDTA, used at the pH of seawater. The fact that the release of the inducer in soluble form is dependent on decalcification strongly suggests that it may be a component of the calcified alga itself, rather than a molecule produced by any associated (non-calcified) microbial epibionts. Significant purification and concentration of the solubilized, amphipathic molecule are achieved by adsorption to a hydrophobic chromatographic support that strongly binds the inducer from high salt, and subsequently releases the molecule at low salt concentration. Further purification then is obtained by anion-exchange chromatography on DEAE. Our data suggest that the morphogen extracted and purified by these procedures has an apparent (or micellar) molecular weight of 6000–8000 Da, and is the parent molecule from which the smaller, unstable hydrolysis fragment originally had been obtained.

The properties of this molecule make it suitable for tests of the role of chemical induction of larval settlement and metamorphosis, both in the laboratory and the ocean environment. The purified morphogen retains activity when adsorbed to beads of the hydrophobic interaction chromatography resin, and it remains bound to the resin in seawater. Activity of the resin-bound inducer is identical in the ocean and the laboratory when tested with *A. humilis* larvae produced in the laboratory. Attachment of the resin-bound inducer to surfaces coated with a silicone adhesive produces a potent artificial recruiting substratum corresponding to a morphogen-based chemical flypaper for *A. humilis* larvae.

Materials and Methods

Larvae

Coral larvae were produced and maintained in culture as described previously (Morse *et al.*, 1988; Morse and Morse, 1991). Adult colonies of *Agaricia humilis*, identified by the taxonomic criteria of Wells (1973) and van Moorsel (1983, 1989), were collected from depths of 1–5 m in Bonaire, Netherlands Antilles, and incubated in the dark in 20–60 l of seawater at 28°C. Planula larvae were released copiously between 1800 and 2300 h, collected from the surface with a Pasteur pipet, and maintained at densities of ≤0.5 larva/ml in 600-ml polyethylene containers of 0.2-μm-filtered seawater containing 2 μg/ml of the antibacterial antibiotic rifampicin at 28°C, under continuous indirect illumination from a 40-W incandescent bulb at 3 m.

Purification of the morphogen

All operations were at 24–28°C unless otherwise noted. *Hydrolithon boergesenii* was cleaned of macroscopic epi-

bionts, scraped from its substratum, blotted dry, and extracted fresh or stored frozen until use. The fresh or frozen coralline alga was ground (in 1-g portions) with a mortar and pestle until a smooth paste was obtained; it was then ground further after the addition of 10 ml of 0.2-μm-filtered seawater containing 2 μg/ml rifampicin (RFSW)/g alga. The algal homogenate was diluted to 40 ml with RFSW, centrifuged 5 min at 10,000 $\times$ *g*, and the aqueous supernatant discarded. The water-insoluble pellet was resuspended in RFSW and washed by centrifugation two more times, as above, and then (except as specified in Table I) added to a solution (1 l/g alga) of 50 m*M* EDTA $(Na)_3$ that had first been adjusted to pH 8.2. Alternatively, EGTA adjusted to pH 8.2 with NaOH was used. Decalcification was allowed to proceed by magnetic stirring of the resulting suspension for 22–24 h, after which the decalcified soluble extract was readjusted to pH 8.2 if necessary, and clarified by vacuum filtration through glass fiber filters (Millipore GFC filters, 47 mm diam., using 1 filter/250 ml).

The resulting clarified demineralized crude extract was adjusted to 2 *M* NaCl to facilitate adsorption of the morphogen to beads of a t-butyl hydrophobic interaction chromatography (HIC) resin (Biorad, Richmond, CA). After adding 2 g (wet weight) of the water-washed and blotted HIC resin/liter, the resin was stirred with the crude inducer for 3 h, and the resin then collected by vacuum filtration on a GFC (47 mm) filter. The filtrate was refiltered through the resin filter-cake two more times, and the resin rinsed on the filter with two 10-ml portions of 2 *M* NaCl to remove traces of the chelator. The resin then was blotted with paper towels to remove excess salt, resuspended in a minimal volume of pre-chilled Tris Cl buffer (1 m*M*, pH 8.2, at 2°C; 3 ml/l of original clarified, demineralized crude extract), and poured into a chromatography column (0.9 cm diam.). The column was eluted with the same chilled buffer and the aid of a low-pressure chromatography pump; fractions (3 ml/l of original clarified, demineralized crude extract) were collected and assayed for morphogenic activity, absorbance, and protein. Fractions containing the peak of activity were pooled. In a typical preparation, 4 $\times$ 1 g portions of *Hydrolithon boergesenii* were individually homogenized, pooled, and decalcified with 4 l of chelator; the resulting solubilized inducer was then adsorbed to 8 g of HIC resin, eluted in 6–10 fractions of 12-ml each, and 3–4 fractions containing the peak of activity were pooled.

Further purification of the morphogen was achieved by anion-exchange chromatography over Trisacryl-DEAE (from LKB) or DEAE-Sephadex (from Pharmacia). A sample of the pooled, most active fractions of the HIC eluate was diluted with an equal volume of Tris Cl buffer (1 m*M*, pH 8.2), and adsorbed to DEAE-resin in a chromatography column (2-ml bed volume/10-ml applied sample; 0.9-cm column diam.). The active morphogen then was eluted with a gradient of increasing NaCl concentration (from 0 to 0.6 *M*) in Tris Cl buffer (1 m*M*, pH 8.2).

Assays of the morphogen in the laboratory

Assays for the induction of larval attachment and metamorphosis (unless otherwise noted) were performed in duplicate samples of 5 larvae/sample, in 10 ml of seawater (0.22-μm-filtered) contained in 20-ml polystyrene disposable breakers incubated at 28°C with indirect illumination (as described above) for 18–24 h; results shown are the average percent metamorphosis $\pm$ deviation from the mean. Metamorphosis, defined as the differentiation and calcification of the septa following permanent attachment and cellular differentiation, was quantified by examination with a binocular microscope. This transition is an unequivocally recognized (and in this species, irreversible) developmental event, and not simply a behavioral change (Morse *et al.*, 1988).

The extracted morphogen was assayed either by direct addition in solution or after adsorption to a hydrophobic support. Following elution from the HIC or DEAE chromatographic resins, samples of the concentrated inducer were assayed directly in solution; up to 1.5 ml of concentrated inducer in 1 m*M* Tris Cl buffer (with 0–0.6 *M* NaCl) could be assayed by direct addition to the larvae in 10 ml filtered seawater. Dilute samples of the inducer in the clarified, demineralized crude extract were assayed by prior adsorption from 2 *M* NaCl to the HIC resin (as described above) or to hydrophobic nitrocellulose filters; the resin beads or the minced filters then were added directly to the small beakers of seawater, and the larvae added for assay. Samples of the chromatographically purified inducer also were assayed after readsorption to the HIC resin. Modifications of the standard assay procedure are described below.

Characterization of the morphogen

The molecular weight of the HIC-purified morphogen was estimated by gel-filtration chromatography (Bio-Gel P6 acrylamide resin; from Biorad), and by dialysis and ultrafiltration (Amicon) using calibrated porosity membranes. Methods were standard, as described previously (Morse and Morse, 1991). Treatment of the HIC-purified morphogen with trypsin was performed with the enzyme covalently linked to insoluble beads (from Sigma, St Louis, MO) to facilitate removal of the protease prior to assays of the remaining morphogenic activity. Aliquots of the purified morphogen (2 ml) were incubated with 0.2 g immobilized trypsin (187 units/g polyacrylamide beads) with

gentle magnetic stirring for 5 h at 28°C, and then separated from the immobilized enzyme by passage (with air pressure) through a small chromatography column that retained the insoluble beads. Parallel incubations were conducted with samples of buffer stirred with equal amounts of the enzyme-linked beads; the treated buffer was separated from the enzyme and subsequently combined with the stirred but untreated morphogen prior to assay. These controls demonstrated that any leaching of the trypsin from its solid support was minimal, as were direct effects on the larvae. Protein concentrations were estimated by the method of Bradford (1976). Adsorbance was measured with a Beckman DU-7 scanning spectrophotometer.

Assays of the morphogen in the field

Because previous laboratory-based studies of settlement have in many cases yielded results not directly reproducible in the natural environment, they have been of little value in predicting the behavior and understanding the ecology of the species under investigation. To overcome this obstacle it was necessary to develop a method for redeploying the purified natural morphogen for tests in the ocean, to determine whether the molecule we had purified retained its activity in the natural environment. The experiment described below allowed us to compare the activity of the chromatographically purified morphogen under laboratory and ocean conditions, the first essential step toward the development of a morphogen-based larval flypaper.

We took advantage of the hydrophobic property of the morphogen to develop a material useful for testing its activity in the ocean environment. After chromatographic purification, the molecule was readsorbed to fresh beads of HIC resin from 2 *M* NaCl, as described above. This resin-bound morphogen retained full activity after washing with several liters of seawater, making it possible to test the efficacy of the HIC-resin-bound morphogen directly in the ocean. To compare the activities of the HIC-resin-bound morphogen in the ocean and the laboratory, minor modifications in the standard assay procedure were employed. Assays were conducted in clear plastic vials (25 × 50 mm, i.d. × h) with the caps replaced by tightly secured mesh (Nitex; 100 μm) sufficient to retain *A. humilis* larvae but permit exchange with environmental seawater (*cf.* Raimondi and Schmitt, 1992, for similar technique). HIC resin (with or without adsorbed morphogen) and 10 laboratory-reared larvae were added to each vial containing fresh seawater, and identical sets were incubated simultaneously in the laboratory and in the ocean. Incubations in the ocean were accomplished by securing the vials with cable-ties to an anchored line maintained in a vertical orientation with a subsurface buoy. The ocean tests were conducted at a depth of 7 m, in the habitat from which the parental *A. humilis* colonies had been obtained. The vials were recovered and examined microscopically for metamorphosis after 22 h.

Incorporation of the purified morphogen on synthetic surfaces

A sample of HIC-purified morphogen (22 ml) was adjusted to 2 *M* NaCl and readsorbed to 0.5 g fresh t-butyl HIC resin as described above; 30 mg of the resulting morphogenically active resin cemented to the bottoms of three polystyrene beakers (3.2-cm diam.; 50-ml capacity) with Dow-Corning silicone adhesive. The beakers were immediately filled with 0.22-μm-filtered seawater, and the unadhered resin and byproducts of adhesive curing were removed by four successive replacements of this seawater over 1 h. After this curing, the silicone resin was no longer sticky. An estimated 50% of the added resin (*ca.* 15 ± 5 mg/beaker = *ca.* 2 mg resin/cm^2) was estimated to remain firmly cemented to the polystyrene surfaces. Water-washed HIC resin without adsorbed morphogen was used to prepare the control surfaces.

Results

Purification of the morphogen

We found that gentle decalcification with either of the chelators, EGTA or EDTA, is sufficient to solubilize significant morphogenic activity from the water-insoluble fraction of the coralline alga *Hydrolithon boergesenii*. The treatment employed completely decalcified the algal cell walls. The properties and subsequent purification behavior of the morphogen solubilized with the two different chelators are thus far indistinguishable; because EDTA is less expensive than EGTA, and because it exhibits superior buffering capacity, we chose to use EDTA routinely. The fact that the inducer is solubilized by the chelators at pH 8.2 (the ambient pH of seawater at the shallow collection sites in Bonaire) suggests that solubilization is achieved without appreciable hydrolysis. The chelator-solubilized morphogen is markedly amphipathic—*i.e.*, it exhibits both hydrophobic and hydrophilic properties. It is this property that has been exploited to concentrate and purify the morphogen and to couple it to an inert support, in which form it can act as a kind of morphogenic flypaper for *A. humilis* larvae.

Because of the amphipathic behavior of the solubilized morphogen, it can be adsorbed from the dilute, decalcified, and clarified crude extract (see Materials and Methods) and concentrated on hydrophobic supports. The addition of NaCl to the clarified crude extract greatly enhances this binding to nitrocellulose filters and to beads of the t-butyl

hydrophobic interaction chromatographic resin. The morphogenic inducer retains its activity after adsorption to these hydrophobic supports and is not eluted by seawater (although penetrance into the pores of the nitrocellulose filters apparently reduces detectability by the larvae, requiring that the filters be minced before assay). The adsorbed inducer can be subsequently released from the HIC support by elution with low ionic strength buffer (Fig. 1). This chromatographic adsorption and subsequent elution concentrated the active morphogen by about 100-fold from the dilute demineralized crude extract (permitting direct assays of the morphogen in solution), resulting in significant purification. As seen in Figure 1, the peak of morphogenic activity is eluted in fractions 2–5, whereas the majority of the light-absorbing contaminants are eluted in the first fraction. At the lower concentrations assayed, activity of the purified inducer is approximately proportional to the amount added (Fig. 2). Induction of metamorphosis is both time- and dose-dependent, with metamorphosis observed as quickly as 2–3 h following addition of high concentrations of the HIC-purified inducer.

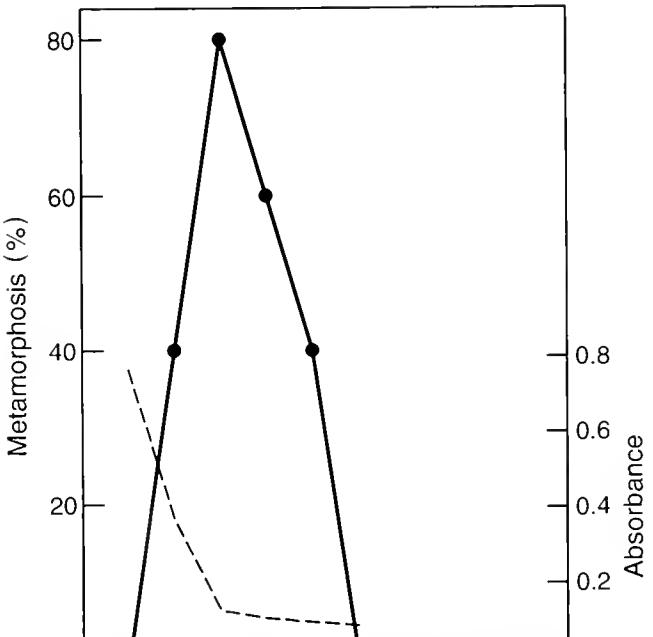

Figure 1. Hydrophobic-interaction chromatography. The clarified demineralized filtrate (4 l) was adjusted to 2 *M* NaCl, adsorbed to 8 g of the t-butyl HIC resin, poured into a column, and eluted with Tris Cl buffer as described in Materials and Methods. Fractions of 12 ml were collected; 0.4 ml of each fraction was assayed for morphogenic activity (solid line). Absorbance at 212 nm is shown (dashed line).

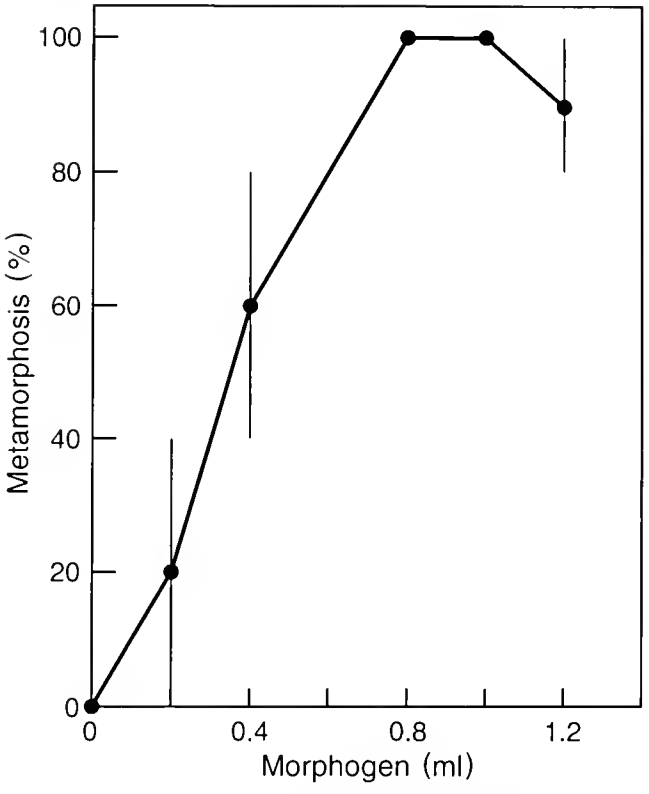

Figure 2. Activity of the HIC-purified and concentrated morphogen. Samples (0.2–1.2 ml) of the pooled morphogen eluted in the peak fractions from the HIC resin (fractions 2–5 from Fig. 1) were assayed in duplicate for morphogenic activity. Controls = 0.5 ml Tris Cl buffer with no morphogen. Error bars indicate deviation from the mean.

The yield of morphogen that can be solubilized (and subsequently purified by HIC) is strongly dependent on the concentration of chelator in the initial extract (Table 1). The results shown in Table IA demonstrate that relatively little inducer is solubilized by prolonged (20 h) stirring of the water-washed crude cell wall fraction in aqueous buffer in the absence of chelator, and that solubilization increases markedly when chelator (0.05 *M* EDTA) is present. The absolute *concentration* of the chelator also is critical to obtain high yields of the soluble morphogen. Thus (Table IB), in three parallel extractions using the same total *amount* of chelator (50 mmole EDTA/g alga), sufficient to completely decalcify the cell walls in all three samples, progressively lower yields of soluble inducer are obtained with progressively higher *concentrations* of EDTA. This behavior is consistent with the hydrophobic property of the amphipathic morphogen; at progressively higher concentrations of the highly charged EDTA salt [nominally, $(Na^+)_4$ $EDTA^{-4}$], the hydrophobic behavior of the morphogen becomes increasingly dominant, apparently causing its retention by adsorption to other hydrophobic molecules (possibly, for

example, the chlorophyll and phaeopigments known to be present) in the water-insoluble algal residue.

The morphogen eluted from the HIC resin can be further purified by anion-exchange chromatography (Fig. 3). It binds ionically to DEAE at low salt concentration and is eluted by a gradient of increasing NaCl molarity. The activity elutes from a Trisacryl-DEAE column with a symmetrical peak in the range of 0.3–0.5 *M* NaCl, indicating moderately strong anionic binding. Similar results (not shown) were obtained using a DEAE-Sephadex chromatographic resin, although the resolution obtained with the Trisacryl (acrylamide-based) ion-exchanger was superior to that obtained with the polysaccharide-based Sephadex resin. From the ratios of morphogenic activity to absorbances, we estimate that the inducer has been purified ≥1000-fold (total purification, relative to the starting crude algal homogenate) after the hydrophobic-interaction chromatography, and ≥4000-fold after the anion-exchange chromatography.

Characterization of the morphogen

The apparent molecular weight of the morphogen eluted from the HIC resin was estimated by analyzing the distribution of morphogenic activity after gel-filtration over Bio-Gel P6, and after dialysis and ultrafiltration through a series of calibrated-porosity membranes. These results yielded estimates consistent with a weight-average apparent molecular weight in the range of 6000–8000 Da; however, this value may be influenced by the ability of the purified amphipathic morphogen to form micellar aggregates. The DEAE-purified morphogen is negative in tests for protein by the Bradford (1976) procedure, although it displays an absorption maximum in the ultraviolet at *ca.* 210–212 nm. The apparent insensitivity of morphogenic activity to trypsin (Table II) indicates that if any peptide is present, it does not contain lysine or arginine in a region essential for activity. The chelator-solubilized and chromatographically purified morphogen retains activity for ≥24 h at 28°C, and for several weeks when frozen.

The properties of this molecule thus far characterized suggest that the chelator-solubilized and chromatographically purified morphogen may be the parent molecule from which the smaller fragment had previously been obtained by enzymatic or alkaline hydrolysis, following demineralization with acetic acid (Table III). The chelator-solubilized morphogen is apparently larger and is more stable than the hydrolytic fragment. The chelator-solubilized inducer contains both hydrophobic and anionic domains, whereas the fragment apparently lacks the hydrophobic domain.

Table I

Solubilization of the morphogen depends on chelator concentration

Experiment	EDTA (mmoles/g alga)	[EDTA] (*M*)	Metamorphosis (%)
A	0	0	10 ± 10
	50	.05	90 ± 10
B	50	.05	90 ± 10
	50	.20	30 ± 30
	50	.50	0 ± 0

Experiment A: Equal portions (2 g each) of a washed, water-insoluble algal homogenate were extracted with 2 l (Na) EDTA (0.05 *M*) or Tris Cl buffer (5 m*M*) by prolonged stirring (20 h; 28°C; pH 8.2). The extracts were clarified, and morphogenic activity in the soluble phase was determined after HIC adsorption and elution as described in Materials and Methods (0.8 ml/assay).

Experiment B: Equal portions (0.3 g each) of a washed, water-insoluble algal homogenate were extracted (20 h; 20°C; pH 8.2) with (Na) EDTA solutions, all containing 15 mmoles of EDTA at the indicated concentrations (*i.e.*, in 30, 75, or 300 ml). The extracts were clarified, and the morphogenic activity in the soluble phase from each was determined by the nitrocellulose-binding assay, as described in Materials and Methods.

Activity of the morphogen in the field

We found that the hydrophobic property of the morphogen can be exploited not only for its purification, but also to develop a material useful for testing its activity in the ocean. Adsorption of the chelator-solubilized morphogen to the HIC resin is reversibly controlled by the ambient salt concentration. After chromatographic purification, the molecule was re-adsorbed to fresh beads of HIC resin from high salt (as described in Materials and Methods). The activity and other properties of the HIC-resin-bound morphogen prepared in this manner proved indistinguishable from those of the resin-bound morphogen prepared directly from the clarified chelator extract. Furthermore, the resin-bound morphogen retained full activity after extensive washing with seawater (*ca.* 0.4 *M* in NaCl), indicating that it would be possible to compare the activities of the HIC resin-bound morphogen in the ocean and the laboratory.

The results of this comparison (Fig. 4) demonstrate that the activity of the HIC-resin-bound morphogen is identical in the ocean and the laboratory—and that relatively small quantities of the morphogen-containing resin are sufficient to induce attachment and metamorphosis of the larvae. The results were similar whether the resin-bound morphogen was prepared from chromatographically purified morphogen or from the clarified chelator solution. In contrast, the control HIC resin, treated in parallel but with no adsorbed morphogen, was inactive. The HIC-resin-bound morphogen loses activity after 1–2 days at 28°C, but remains stable for several weeks at 2°C; this

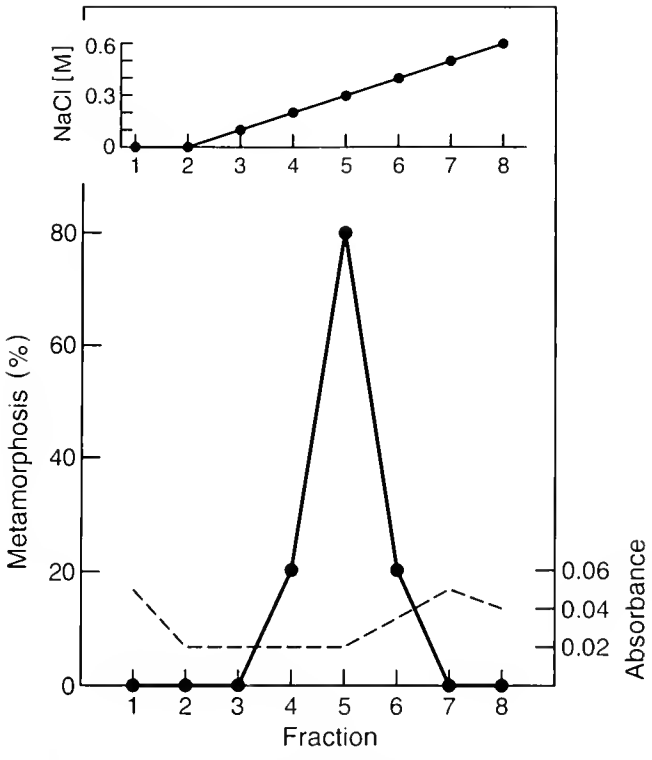

Figure 3. Anion-exchange chromatography. Five ml of the pooled morphogen eluted in the peak fractions from the HIC resin (fractions 2–5 from Fig. 1) was diluted and chromatographed on Trisacryl-DEAE. Elution from the DEAE was performed with a gradient of increasing NaCl concentration (inset) as described in Materials and Methods. Fractions of 5 ml were collected; 1.5 ml of each fraction was assayed for morphogenic activity (solid line). Absorbance at 212 nm is shown (dashed line); the bulk of the applied absorbance remained bound on the column.

behavior is comparable to that of the purified inducer in solution.

Morphogen-based larval flypaper

To produce a practical experimental tool that could be deployed in the natural ocean environment, we incorporated the resin-bound morphogen on a simple, stable platform. We found that the HIC-resin-bound morphogen (prepared from the chromatographically purified morphogen) can be attached to surfaces with a waterproof silicone adhesive, without significant loss of activity. The

Table II

The purified morphogen is insensitive to trypsin

Trypsin treatment	Metamorphosis (%)
Control	90 ± 10
Treated	80 ± 10

HIC-purified morphogen was incubated with immobilized trypsin, separated from the enzyme, and assayed for remaining activity as described in Materials and Methods. Control was a sample of the untreated morphogen, incubated in parallel, and then combined with a sample of buffer that had been incubated in parallel with the immobilized enzyme.

Table III

Chelator solubilizes the parent morphogen

Property	Morphogen Solubilized By: Chelator[1]	Morphogen Solubilized By: Enzymes or alkali[2]
M (Da)[3]	6000–8000	≤2000
Stability	Higher	Low
Binding		
Hydrophobic	Yes	No
Anionic	Yes	Yes

[1] This study.
[2] Data from Morse and Morse, 1991.
[3] Apparent molecular weight.

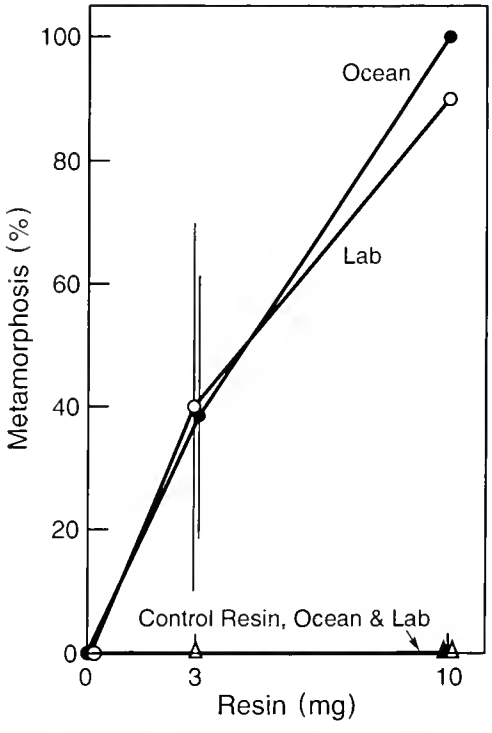

Figure 4. Activity of the HIC resin-bound morphogen in the ocean and the laboratory. Samples of the t-butyl HIC resin, either with adsorbed morphogen (circles) or without morphogen (triangles), were prepared and assayed in mesh-capped vials, in the ocean (filled symbols) and the laboratory (open symbols), as described in the text. Samples were assayed with 10 larvae/vial; results shown are the means ± S.E. (where no error bars are shown, S.E. = 0). Values for 3 mg are displaced horizontally for clarity.

result is a potent morphogen-based larval flypaper that is recognized efficiently by *A. humilis* larvae when tested in the laboratory (Table IV). Larvae exposed to this morphogen-bearing surface rapidly began attachment and metamorphosis, and all of the metamorphosed individuals were found attached to the morphogen-containing surfaces. In contrast, exposures to the comparable surfaces of attached resin that lacked the purified morphogen resulted in no settlement or metamorphosis; the larvae in these treatments continued to swim normally. In a parallel experiment, when the morphogen-based flypaper was prepared either with or without grooves (*ca.* 1-mm deep and 1-mm wide), all of the larvae that settled and metamorphosed in the presence of the grooved substratum did so within the grooves (in contact with the resin-bound morphogen), although the numbers of larvae that settled and metamorphosed were identical on the grooved and smooth substrata. Post-metamorphic growth through development of the feeding polyps occurred normally on the artificial substrata, with no inhibition relative to that seen on the natural host coralline alga. This material should thus make it possible to assess the relative contributions of chemosensory recognition and other factors (texture, hydrodynamics, light, biological interactions, *etc.*) to the control of substratum specificity, settlement, metamorphosis, and recruitment both in the laboratory and, with natural propagules, in the ocean.

Table IV

Morphogen-based chemical flypaper for Agaricia humilis *larvae*

Morphogen on surface	Metamorphosed/total
	9/10
+	9/10
	10/10
	0/10
−	0/10
	0/10

t-Butyl HIC resin, either with adsorbed chromatographically purified morphogen, or without, was cemented to polystyrene surfaces which were then extensively washed with seawater as described in Methods. The prepared surfaces contained *ca.* 2 mg resin/cm^2 and 8 cm^2/trial; each was assayed for morphogenic activity with 10 larvae in 40 ml filtered seawater. Attachment and metamorphosis were observed as early as 2 h, and scored after 21 h; all metamorphoses occurred on the resin-coated surfaces.

Discussion

The natural morphogen recognized by *Agaricia humilis* larvae has been purified ≥4000-fold in three successive steps: differential solubilization (in which the water-soluble molecules are first extracted and discarded, and then the chelator-solubilized molecules are subsequently released); hydrophobic-interaction chromatography; and anion-exchange chromatography. The first step separates the morphogen from the bulk of the algal phycocolloids, proteins, and small molecules. HIC removes the majority of hydrophilic contaminants, and the final DEAE chromatography resolves the inducer both from species more weakly and more strongly anionic than the morphogen. Structural studies of the purified morphogen are now in progress.

The properties of the amphipathic morphogen solubilized from the source alga by gentle demineralization (at the pH of seawater) with the calcium-specific chelator EGTA or its analog, the divalent metal chelator EDTA, suggest that this may be the parent molecule from which the smaller and less stable fragment originally had been obtained by limited enzymatic or alkaline hydrolysis following cell wall decalcification with acetic acid. The fact that solubilization is strongly dependent on demineralization suggests that the inducer of *A. humilis* settlement and metamorphosis may be a component of the recruiting coralline alga itself, rather than of any microbial epibionts that are uncalcified. Ultrastructural immunohistochemical analyses, using antibodies against the purified morphogen, can now resolve this question unequivocally.

The hydrophobic behavior of the amphipathic morphogen can be exploited to test the role of larval chemosensory recognition in the control of substratum-specific settlement, metamorphosis, and recruitment in the natural environment. In steps toward that goal, our results demonstrate that the morphogen remains active after adsorption to beads of the t-butyl HIC resin; the HIC-resin-bound morphogen is not eluted from the beads by seawater and is equally active in the natural ocean environment and the laboratory. Attachment of the resin-bound inducer to surfaces coated with a silicone adhesive produces a potent artificial recruiting substratum corresponding to a morphogen-based chemical flypaper for *A. humilis* larvae. This substratum should prove useful for testing the relative contributions of chemosensory recognition of the algal morphogen and other factors to the control of settlement and metamorphosis under defined conditions in the laboratory, and to the control of recruitment and the maintenance of species isolation mechanisms in the natural environment. This is, to our knowledge, the first highly purified natural inducer of larval settlement and metamorphosis to be incorporated into an artificial substratum suitable for testing in the ocean. Advantages of this uniform, non-sticky, morphogen-based recruiting surface include avoidance of the complexity and variability of the natural algal substrata that usually confound the effects of chemical morphogen, textural complexity, cryptic animal predators, allelopathic competitors, and other chemical and biological interactions.

Use of such synthetic surfaces containing the natural morphogen should permit experimental resolution of the contributions of each of these factors.

Previous results demonstrated that the morphogen solubilized from *Hydrolithon boergesenii* is biologically specific, with respect to both the source of the molecule and the larvae capable of detecting or responding to it (Morse and Morse, 1991). Thus, two sympatric species of coralline algae that do not induce *A. humilis* larvae to metamorphose were shown not to contain the morphogen, and larvae of a sympatric coral that is not induced to settle or metamorphose by *H. boergesenii* also are not induced by the morphogen. However, larvae of the congeneric *A. tenuifolia* are induced to metamorphose by the intact alga and by the morphogen, suggesting that this cue may be group-specific (Morse and Morse, 1991). The morphogen-based chemical flypaper containing the purified inducer should be a useful tool for investigating the specificity of morphogen recognition by the cognate larval receptors and of the possibility that changes in this specificity serve as an axis for the evolution of niche-diversification and speciation.

Acknowledgments

This research has been supported by a grant (OCE92-01242) from the National Science Foundation, Biological Oceanography Program. We thank F. Smart and J. Hydanus for their assistance. We also thank our colleagues in Bonaire, R. Hensen and K. de Meyer of the Marine Park Authority, E. Newton of the Department of Natural Resources, and J. Brandon, R. Haakenberg, H. Geraerts, and T. Randon for their generous hospitality and assistance.

Literature Cited

Bradford, M. A. 1976. A rapid sensitive method for the quantitation of microgram quantities of protein utilizing the principle of protein-dye binding. *Anal Biochem* **72:** 248–254

Burke, R. D. 1983. The induction of metamorphosis of marine invertebrate larvae. Stimulus and response. *Can J Zool.* **61:** 1701–1719.

Burke, R. D. 1986. Pheromones and the gregarious settlement of marine invertebrate larvae. *Bull. Mar Sci.* **39:** 323–331.

Butman, C. A. 1987. Larval settlement of soft-bodied invertebrates: spatial scales of patterns explained by active habitat choice and the emerging role of hydrodynamical processes. *Mar Biol Ann Rev.* **25:** 113–165.

Chia, F.-S. 1978. Perspectives: settlement and metamorphosis of marine invertebrate larvae. Pp. 283–285 in *Settlement and Metamorphosis of Marine Invertebrate Larvae,* F.-S. Chia and M. E. Rice, eds. Elsevier, New York.

Connell, J. H. 1985. The consequences of variation in initial settlement *vs.* post-settlement mortality in rocky intertidal communities. *J Exp Mar Biol Ecol* **93:** 11–45.

Crisp, D. J. 1974. Factors influencing settlement of marine invertebrate larvae. Pp. 177–265 in *Chemoreception in Marine Organisms,* P. T. Grant and A. M. Mackie, eds. Academic Press, New York.

Crisp, D. J. 1984. Overview of research on marine invertebrate larvae, 1940–1980. Pp. 103–126 in *Marine Biodeterioration,* J. D. Costlow and R. C. Tripper, eds. Naval Institute Press, Annapolis.

Hadfield, M. G. 1978. Metamorphosis in marine molluscan larvae: an analysis of stimulus and response. Pp. 165–175 in *Settlement and Metamorphosis of Marine Invertebrate Larvae,* F.-S. Chia and M. E. Rice, eds. Elsevier, New York.

Hadfield, M. G. 1986. Settlement and recruitment of marine invertebrates: a perspective and some proposals. *Bull. Mar Sci.* **39:** 418–425.

Hadfield, M. G., and D. Scheuer. 1985. Evidence for a soluble metamorphic inducer in *Phestilla:* ecological, chemical and biological data. *Bull. Mar Sci.* **37:** 556–566.

Hadfield, M. G., and J. T. Pennington. 1990. Nature of the metamorphic signal and its internal transduction in larvae of the nudibranch *Phestilla sibogae. Bull. Mar Sci.* **46:** 455–464.

Highsmith, R. C. 1982. Induced settlement and metamorphosis of sand dollar (*Dendraster excentricus*) larvae in predator-free sites: adult sand dollar beds. *Ecology* **63:** 329–337.

Jensen, R., and D. E. Morse. 1984. Intraspecific facilitation of larval recruitment: gregarious settlement of the polychaete *Phragmatopoma californica J Exp Mar Biol Ecol.* **83:** 107–126.

Jensen, R. A., and D. E. Morse. 1990. Chemically induced metamorphosis of polychaete larvae in both the laboratory and the ocean environment. *J Chem Ecol.* **16:** 911–930.

van Moorsel, G. W. N. M. 1983. Reproductive strategies in two closely related stony corals (*Agaricia,* Scleractinia). *Mar Ecol. Prog. Ser.* **13:** 273–283.

van Moorsel, G. W. N. M. 1989. Juvenile ecology and reproductive strategies of reef corals. Doctoral Dissertation, Rijksuniversiteit, Groningen. 103 pp.

Morse, A. N. C. 1992. Role of algae in the recruitment of marine invertebrate larvae. Pp. 385–403 in *Plant-Animal Interactions in the Marine Benthos,* D. M. John, S. J. Hawkins and J. H. Price, eds. Systematics Assoc. Special Vol. 46. Clarendon Press, Oxford.

Morse, A. N. C., and D. E. Morse. 1984. Recruitment and metamorphosis of *Haliotis* larvae are induced by molecules uniquely available at the surfaces of crustose red algae. *J Exp. Mar Biol Ecol.* **75:** 191–215.

Morse, D. E. 1985. Neurotransmitter-mimetic inducers of settlement and metamorphosis of marine planktonic larvae. *Bull. Mar. Sci.* **37:** 697–706.

Morse, D. E. 1990. Recent progress in larval settlement and metamorphosis: closing the gaps between molecular biology and ecology. *Bull Mar Sci* **46:** 465–483.

Morse, D. E., and A. N. C. Morse. 1991. Enzymatic characterization of the morphogen recognized by *Agaricia humilis* (scleractinian coral) larvae. *Biol Bull.* **181:** 104–122.

Morse, D. E., M. Tegner, H. Duncan, N. Hooker, G. Trevelyan, and A. Cameron. 1980. Induction of settling and metamorphosis of planktonic molluscan (*Haliotis*) larvae: III. Signaling by metabolites of intact algae is dependent on contact. Pp. 67–86 in *Chemical Signals in Vertebrate and Aquatic Animals,* D. Muller-Schwarze and R. M. Silverstein, eds. Plenum Press, New York.

Morse, D. E., N. Hooker, A. N. C. Morse, and R. Jensen. 1988. Control of larval metamorphosis and recruitment in sympatric agariciid corals. *J Exp Mar Biol Ecol* **116:** 193–217.

Pawlik, J. R. 1990. Natural and artificial induction of metamorphosis of *Phragmatopoma lapidosa californica* (Polychaeta: Sabellariidae), with a critical look at the effects of bioactive compounds on marine invertebrate larvae. *Bull. Mar. Sci* **46:** 512–536.

Pawlik, J. R., C. A. Butman, and V. R. Starczak. 1991. Hydrodynamic facilitation of gregarious settlement in a reef-building worm. *Science* **251:** 421–424.

Raimondi, P. T. 1988. Settlement cues and determination of the vertical limit of an intertidal barnacle. *Ecology* **69:** 400–407.

Raimondi, P. T. 1990a. Patterns, mechanisms, and consequences of variability in settlement and recruitment in an intertidal barnacle. *Ecol. Monogr.* **60:** 283–309.

Raimondi, P. T. 1990b. The settlement behavior of *Chthamalus anisopoma* largely determines its adult distribution. *Oecologia* **85:**349–360.

Raimondi, P. T., and R. J. Schmitt. 1992. Effects of produced water on settlement of larvae: field tests using red abalone. Pp. 415–430 in *Produced Water*, J. P. Ray and F. R. Engelhardt, eds. Plenum Press, New York.

Rittschof, D., and J. Bonaventura. 1986. Macromolecular cues in marine systems. *J. Chem. Ecol.* **12:** 1013–1023.

Scheltema, R. S. 1974. Biological interactions determining larval settlement of marine invertebrates. *Thalass. Jugoslav.* **10:** 263–296.

Sebens, K. P. 1983. Settlement and metamorphosis of a temperate soft-coral larva (*Alcyonium siderium* Verill): induction by crustose algae. *Biol. Bull.* **165:** 286–304.

Shepherd, S. A., and J. A. Turner. 1985. Studies on Southern Australian abalone (genus *Haliotis*). VI. Habitat preference, abundance and predators of juveniles. *J. Exp. Mar. Biol. Ecol.* **93:** 285–298.

Walters, L. 1992. Field settlement locations on subtidal marine hard substrata: Is active larval exploration involved? *Limnol. Oceanogr.* **37:** 1101–1107.

Wells, J. W. 1973. New and old scleractinian corals from Jamaica. *Bull. Mar. Sci.* **23:** 16–58.

Reference: *Biol. Bull.* **186:** 182–194. (April, 1994)

Algal Symbiosis in *Bunodeopsis:* Sea Anemones with "Auxiliary" Structures

REBECCA J. DAY

Department of Zoology, University of the West Indies, Mona, Kingston 7, Jamaica, West Indies

Abstract. This study describes the photobiology of two tropical species of the symbiotic sea anemone genus *Bunodeopsis* from Discovery Bay, Jamaica. *B. antilliensis* was found in shallow water (0.3 m) and experienced higher irradiance levels than *B. globulifera* from deeper water (3 m). Both species contained symbiotic dinoflagellates of the genus *Symbiodinium* within the endodermal cells. The external morphology and expansion-contraction behavior of the two anemone species were closely linked to symbiont distribution. *B. antilliensis* had large vesicles (2.6 mm^3), with 88.5% of the symbiont population in the lower column and basal disk and 11.5% in the tentacles and upper column, and was contracted under normal daylight illumination. In contrast, *B. globulifera* had small vesicles (0.2 mm^3), with 55.5% of the symbionts in the lower column and basal disk and 44.5% in the tentacles and upper column, and was expanded under illumination.

The photosynthetic physiology of the symbionts indicated that those from *B. globulifera* were adapted to lower host habitat irradiances than were those from *B. antilliensis*. The symbionts from *B. globulifera* had a significantly higher chlorophyll *a* content (7.34 ± 0.77 pg · cell $^{-1}$) and photosynthetic efficiency (0.24 $\mu gO_2 \cdot 10^6$ cells · h^{-1}/μmol photons · $m^{-2} \cdot s^{-1}$) and lower saturation irradiance (277 ± 18 μmol photons · $m^{-2} \cdot s^{-1}$) than those from *B. antilliensis*, 4.51 ± 0.29 pg · $cell^{-1}$, 0.17 $\mu gO_2 \cdot 10^6$ cells · h^{-1}/μmol photons · $m^{-2} \cdot s^{-1}$ and 436 ± 78 μmol photons · $m^{-2} \cdot s^{-1}$, respectively. The calculated rate of carbon translocation in both species of *Bunodeopsis* (97%) was high and reflected the low algal protein biomass ratios (2%) and population growth rates (<0.1 · day^{-1}). The CZAR values in *B. antilliensis* (109%) and *B. globulifera* (92%) suggest that both species are potentially autotrophic with respect to carbon available for animal respiration.

Received 16 April 1993; accepted 27 January 1994.

Present address: Department of Palaeontology, The Natural History Museum, Cromwell Road, London SW7 5BD.

Contribution No. 556 of the Discovery Bay Marine Laboratory, Jamaica, West Indies.

Introduction

Most tropical marine Cnidaria, including sea anemones and corals, contain symbiotic dinoflagellate algae of the genus *Symbiodinium* (Trench and Blank, 1987), also known as "zooxanthellae." These algal symbionts are generally located within endodermal cells and are nutritionally important to the associations because they are photosynthetic and much of the fixed carbon is translocated to the cnidarian host (Muscatine and Cernichiari, 1969; Muscatine *et al.*, 1983). The photosynthetic capacity of the symbionts is flexible and varies with host irradiance regime; therefore, animal and algal responses that enhance symbiont exposure to light and photosynthesis will be beneficial to the whole association.

Tropical marine Cnidaria display a diverse array of responses related to the possession of symbionts. Morphological adaptations to symbiosis are illustrated by the "auxiliary" structures of symbiotic sea anemones, which contain high densities of symbiotic algae relative to other body regions (Sebens and deReimer, 1977). Expansion of these structures under illumination maximizes exposure of the symbiont populations to light, thereby enhancing their photosynthesis. Examples of auxiliary structures include the "pseudotentacles" of *Lebrunia coralligens, L. danae* (Gladfelter, 1975), and *Phyllodiscus semoni* (Shick *et al.*, 1991); the diskal tentacles of *Discosoma sanctithomae* (Elliott and Cook, 1989); and the collar of *Phyllactis flosculifera* (Steele and Goreau, 1977).

The algal symbionts experience variations in irradiance regime due to host habitat, morphology, and behavior. Algal symbionts display compensatory responses to maximize photosynthesis; these include variations in photo-

synthetic pigment content and physiology, which may be assessed by parameters of photosynthesis-irradiance (P-I) curves (Chalker, 1981). The nutritional contribution made by the symbiont population to the host may be estimated by the index CZAR, or "the contribution of translocated zooxanthellal carbon to the daily animal respiratory carbon requirements" (Muscatine *et al.*, 1981). A high proportion of photosynthetically fixed carbon is translocated to the host, as shown in the symbiotic sea anemones *Aiptasia pallida* (Clayton and Lasker, 1984) and *Anemonia sulcata* (Stambler and Dubinsky, 1987), and this represents a large contribution to the host's respiratory needs (reviewed in Shick, 1991). The nutritional contribution made by algal symbionts to these sea anemones also varies with the extent of host heterotrophy, zooplankton feeding, or uptake of dissolved nutrients (Zamer, 1986). Investigations of algal and animal responses in symbiotic sea anemones include those for the tropical species *Aiptasia pulchella* (Muller-Parker, 1984, 1985, and 1987; Steen, 1986), *Aiptasia pallida* (Cook *et al.*, 1988; Lesser and Shick, 1989), and *Phyllodiscus semoni* (Shick *et al.*, 1991), and for the temperate species *Anthopleura elegantissima* (Fitt *et al.*, 1982; Shick and Dykens, 1984; Zamer and Shick, 1987) and *Anemonia sulcata* (= *viridis*) (Taylor, 1969; Tytler and Davies, 1984).

This study presents the first detailed description of animal and algal responses that enhance the photosynthesis and the nutritional contribution of the symbionts in the sea anemone *Bunodeopsis* (Boloceroididae; Carlgren, 1924). This genus is of particular interest because these sea anemones have auxiliary structures (Sebens and deReimer, 1977) that contain high densities of symbiotic algae (Hyman, 1940). *B. antilliensis* (Duerden, 1897) and *B. globulifera* (Verrill, 1900) occupy different habitats in terms of depth and irradiance regime. These two species also have distinctly different morphologies and light-related patterns of expansion and contraction behavior. The relationship between these environmental factors and symbiont distribution, photosynthetic pigment content, and physiology of the two species of *Bunodeopsis* is examined in relation to CZAR. Lastly, the extent of zooplankton feeding by these two species of *Bunodeopsis* is investigated in a 24-h *in situ* study.

Materials and Methods

Collection and maintenance

Specimens of *Bunodeopsis* were observed *in situ* and collected from *Thalassia testudinum* beds in Discovery Bay, Jamaica (Lat. 77°25′ W; Long. 18°30′ N) during studies conducted between January 1989 and 1991. Whole *Thalassia testudinum* blades, with the anemones adhering, were placed into self-sealing plastic bags with seawater, and then transferred to glass aquaria (61 × 31 × 30 cm). The aquaria were covered with fine mesh (2-mm mesh size) to contain the sea anemones and placed on tables of flowing seawater. Every second night, anemones were fed to repletion with freshly hatched *Artemia salina* nauplii, applied by pipette directly to the tentacles. Anemones maintained in otherwise constant darkness were exposed to light for less than 5 min during each feeding. Aquaria were cleaned several times each week to prevent fouling.

Morphology and histology

Morphological measurements were made on contracted anemones attached by their basal disks to petri dishes at 50 × under a dissecting microscope with a calibrated ocular micrometer. Basal disk diameter, width, and total number of vesicles were measured for individual anemones. For histological preparations, anemones were narcotized in 7.5% (w/v) $MgCl_2 \cdot 6H_2O$ solution and fixed in Bouin's solution in seawater. Preparation of anemones for transmission electron microscopy was conducted as described by Parke and Manton (1967). Silver-to-gold sections were stained with a saturated solution of uranyl acetate in 50% ethanol and Reynold's lead citrate, and viewed in a Phillips EM 400 transmission electron microscope.

Biomass parameters

Animal and algal biomass parameters were determined for whole anemones and separate body regions for specimens collected in November 1989. Anemones were relaxed in darkness for 10–15 min. at 4°C and narcotized in 7.5% $MgCl_2 \cdot 6H_2O$ (w/v) solution prior to dissection into four body regions (tentacles, capitulum, scapus, and basal disk) at 50 × under a dissecting microscope. Whole anemones or separate body regions were homogenized in Millipore-filtered (0.22-μm pore size) seawater, and the animal and algal fractions were separated by centrifugation as described by Muller-Parker (1984). The algal pellet was resuspended in filtered seawater, and cell numbers were determined in a hemacytometer at 400 ×. Protein content of the animal fraction was assayed by the method of Lowry *et al.* (1951) with bovine serum albumin as standard.

Algal cell size was determined from the diameter of dividing cells, measured parallel to the plane of division at 500 × with a calibrated ocular micrometer, for 10 cells per anemone from eight anemones of each species. Cell volumes were calculated from cell diameters, and the mean cell carbon content was estimated from the equations of Strathmann (1967) determined for phytoplankton (including dinoflagellates and excluding diatoms). From the mean algal density and the weight of carbon per cell, the standing stock of algal carbon was calculated. Total algal protein was estimated as (6.25 × C)/C:N, and the

ratio of algal to "total" (animal plus algal) protein was calculated using a C:N ratio of 9.4:1 (Cook *et al.*, 1988).

To determine whether the algal symbionts had a phased cell division cycle, the mitotic index (number of cells dividing per 100) was recorded for algae isolated from anemones at intervals during a 24-h period. Anemones were freshly collected from study sites every 2 h between 0800 and 1800 h. For nighttime studies, anemones were sampled every 3 h between 2000 and 0600 h from anemones that had been collected from study sites at 1800 and placed into aquaria of flowing seawater (Wilkerson *et al.*, 1983; Fitt and Trench, 1983). The algae were immediately separated from the animal fraction, resuspended in 5 ml of 5% formalin in seawater (v/v), and refrigerated at 4°C until cell counts were made. Three replicate counts were made for three anemones of each species during each sampling time. Chlorophylls *a* and c_2 of the algal symbionts were assayed following the method outlined by Muller-Parker (1984).

Expansion and contraction behavior

Anemones were observed *in situ* at collection sites between January and March 1990, and in aquaria under laboratory conditions. Anemones were considered to be in an "expanded" posture if the oral disk was expanded and the tentacles extended. In "contracted" anemones, the oral disk was contracted, with the tentacles retracted into the gastrovascular cavity, the basal disk extended, and the vesicles inflated. Anemones in intermediate postures were rarely observed. At the study sites, percentage transmission of surface irradiance to depth was recorded as photosynthetically active radiation (PAR: 400–700 nm) with a cosine-corrected Li-Cor quantum sensor (Model 192) and Li-Cor photometer (Model LI 185A). Underwater measurements were made with the meter contained in a clear acrylic housing sealed with an o-ring. *In situ*, the postures of a minimum of 50 anemones and irradiance were noted three times daily at about 0700, 1200, and 1900 h, twice weekly for a period of 8 weeks.

Under laboratory conditions, irradiance was provided by lighting from nearby windows with artificial illumination from overhead cool-white fluorescent lamps (12 h d^{-1}, approx. 100 μmol photons $\cdot m^{-2} \cdot s^{-1}$). Anemones having low symbiont densities were obtained by the method of "cold-stripping" (Steen and Muscatine, 1987). Anemones in seawater were placed into a refrigerator at 4°C for 30 min until the seawater temperature was reduced to about 16°C (when cooled below 16°C, all the anemones died), then transferred to aquaria of flowing seawater (28°C) and maintained in darkness for 2 weeks. Expansion and contraction behavior was observed for two groups of untreated and cold-stripped anemones, which were placed under laboratory irradiance and in constant darkness. The postures of the anemones were noted at 0700, 1200, and 1900 h daily for 2 weeks. At the termination of these studies, biomass parameters were determined for individual anemones from each treatment.

Zooplankton feeding

The extent of zooplankton feeding was assessed by examining coelenteron contents from 10 anemones of each species collected from study sites every 3 h for 24 h. This time interval was chosen because zooplankton prey can be completely digested within 4 to 6 h of capture (Sebens and Koehl, 1984). Nocturnal collections were essential because peak zooplankton activity occurs within 2 h of sunset in Discovery Bay (Ohlhorst, 1982). The anemones were allowed to expand in darkness, then removed from the *Thalassia testudinum* blades and transferred to plastic bags filled with 10% formalin in seawater (v/v). The basal disk diameters were measured; the coelenteron contents removed; and the number, maximum length, and type of each recognizable prey item (Newell and Newell, 1966) recorded at 50 × with a dissecting microscope and calibrated ocular micrometer.

Photosynthesis-irradiance relationships

Oxygen flux was recorded for anemones, within 2 h of collection, in a cylindrical clear acrylic chamber (75-ml volume) fitted with a Clark Beckman 1000 microcathode connected to a Linear chart recorder. Constant temperature (28°C) of the chamber seawater was maintained by a water jacket receiving water from a recirculating water bath. Even mixing of the water column, without disturbance to the anemone, was ensured by a pin-mounted magnetic stirrer. The chamber was positioned beneath a variable light source, consisting of a 250-W tungsten lamp projected through Corning 3405 and 3409 (50 mm^2) filters, with an 80B Kodak filter to convert incandescent light to a more "natural" spectrum experienced at depths of less than 5 m. The light source was calibrated with the Li-Cor quantum sensor (Model 192) and Li-Cor photometer (Model LI 185A) used in the behavioral studies. Two fans directed at the bulb and a heat filter prevented the light source from increasing the chamber temperature.

The electrode was calibrated between incubations with air-saturated seawater and oxygen-free seawater (with sodium sulphite). The oxygen concentration of seawater was reduced to between 50 and 60% air saturation by bubbling with gaseous nitrogen. Low-oxygen seawater was added to the chamber seawater during incubations to maintain a concentration of 75 to 100% air saturation, and chamber seawater was replaced during each reading. As a control for biological activity of the incubation medium and oxygen consumption by the cathode, oxygen flux was re-

corded for seawater alone in darkness for 30 min. No oxygen uptake was recorded for three such replicates.

Specimens of *B. globulifera* anemones were placed directly into the chamber, where they attached rapidly to the base. Because *B. antilliensis* required several hours for attachment, specimens were allowed to settle on pieces of plastic sheet, which were subsequently transferred to the base of the chamber. After a 5-min equilibration period, oxygen flux was recorded for 20 min at consecutive ascending irradiances 10, 30, 100, 200, 300, 400, and 500 μmol photons $\cdot m^{-2} \cdot s^{-1}$. In darkness, both species of anemone rapidly expanded. However, because *B. globulifera* anemones contracted much more rapidly under illumination than did *B. antilliensis* anemones, dark respiration rates were recorded at the beginning of incubations for *B. globulifera* and at the end of incubations, following a 20-min equilibration period, for *B. antilliensis*. Anemone biomass parameters were assessed at the termination of each incubation.

Oxygen flux measurements were standardized to sea anemone protein and to algal cell number for 10 specimens of *B. antilliensis* and 12 of *B. globulifera*. Hyperbolic tangent function curves (Chalker, 1981) were fitted to the net photosynthesis *versus* irradiance data with a least-squares regression analysis program. Mean P-I characteristics, photosynthetic capacity (P_{max}), photosynthetic efficiency (α), and I_k (the irradiance at which the initial slope of the curve (α) intercepts the horizontal asymptote) were derived for each species from the individual P-I curves. Saturation irradiance ($I_{0.95}$) was estimated from the irradiance at which photosynthesis was 95% of the maximum, where $I_{0.95} = 1.83 \times I_k$ (Chalker *et al.*, 1983).

CZAR index

The potential contribution of algal photosynthetically fixed carbon to animal respiratory requirements was estimated as $CZAR = (P_Z^N \times T)/R_A$ (Muscatine *et al.*, 1981), where P_Z^N is the total daily net carbon fixed by the algae, T is the fraction of P_Z^N translocated to the host, and R_A is the daily respiration of the animal in carbon equivalents. Respiration rates of the animal and algal components were assumed to be proportional to their measured and derived protein biomasses respectively (Muscatine *et al.*, 1983). Oxygen consumed in respiration was converted to carbon equivalents by using the respiratory quotient (RQ) multiplied by the molecular weight conversion factor of 0.375. The algal respiration rate was estimated as $r_Z = 1 - \beta(r_{Anemone}) \times 0.375\ RQ_{Anemone}$ and the animal respiration rate as $R_A = \beta(r_{Anemone})$, where $r_{Anemone}$ is the measured anemone rate of dark respiration and β is the protein biomass ratio. The anemone respiratory quotient calculated as $RQ_{Anemone} = [((1 - \beta)/RQ_Z) + \beta/RQ_A)]^{-1}$ was 0.8 for both *B. antilliensis* and *B. globulifera*. The algal and animal respiratory quotients (RQ_Z and RQ_A) were assumed to be 0.8 and 1.0, respectively (Muscatine *et al.*, 1981).

Total daily net carbon fixation by the algae (P_Z^N) was estimated as the gross photosynthetic capacity of the anemone (p_{max}^G) minus the derived algal respiration rate (r_Z), multiplied by the daily number of hours at saturation irradiance ($I_{0.95}$). For comparative purposes, the contribution made by symbiont photosynthesis at irradiances below saturation was assumed to be negligible (see Fig. 9). *In situ* irradiances were predicted from mean transmission of surface PAR to the study site depths, together with surface PAR recordings made at 30-min intervals on 22 February 1990 (with a maximum irradiance of 2100 μmol photons $\cdot m^{-2} \cdot s^{-1}$). The gross photosynthetic capacity of the anemone (p_{max}^G) was equal to the measured net photosynthetic capacity (p_{max}^N) plus the dark respiration rate of the anemone ($r_{Anemone}$), converted to carbon equivalents, assuming a photosynthetic quotient of 1.1 (Muscatine *et al.*, 1981).

The proportion of fixed carbon translocated from the symbionts to the host (T) was estimated by the growth rate method of Muscatine *et al.* (1983), using the equation $T = \mu_c - \mu/\mu_c \times 100\%$, where μ and μ_c are the algal and carbon specific growth rates, respectively. The algal population growth rate (μ) was derived from the mitotic index (Biomass parameters) using the equation of Wilkerson *et al.* (1983). The carbon-specific growth rate was calculated as $\mu_c = 1/C' \times \delta C/\delta t$, where C' is the standing stock of algal carbon (Sea anemone biomass parameters), and $\delta C/\delta t$ is the total net daily carbon fixed by the algae (P_Z^N). Translocation was not measured directly with ^{14}C, because the use of this radioactive isotope is known to underestimate carbon translocation *in vivo* (Muscatine *et al.*, 1983).

Statistical analysis

Data were analysed by the following parametric tests: Student's *t* test; two-factor analysis of variance (ANOVA); Scheffé's and Tukey-Kramer multiple range tests; and correlation analysis (Sokal and Rohlf, 1981). Nonparametric tests used were Wilcoxon's signed ranks; Mann-Whitney *U*; and χ^2 tests (Siegel and Castellan, 1988). Angular transformations (Sokal and Rohlf, 1981) were used on all percentage data prior to statistical analysis.

Results

Habitat

Bunodeopsis antilliensis (Figs. 1a, 2) was found on *Thalassia testudinum* blades in water shallower than 0.3 m in the West back reef and *B. globulifera* (Fig. 1b) at 3 m depth in the East back reef area of Discovery Bay, Jamaica.

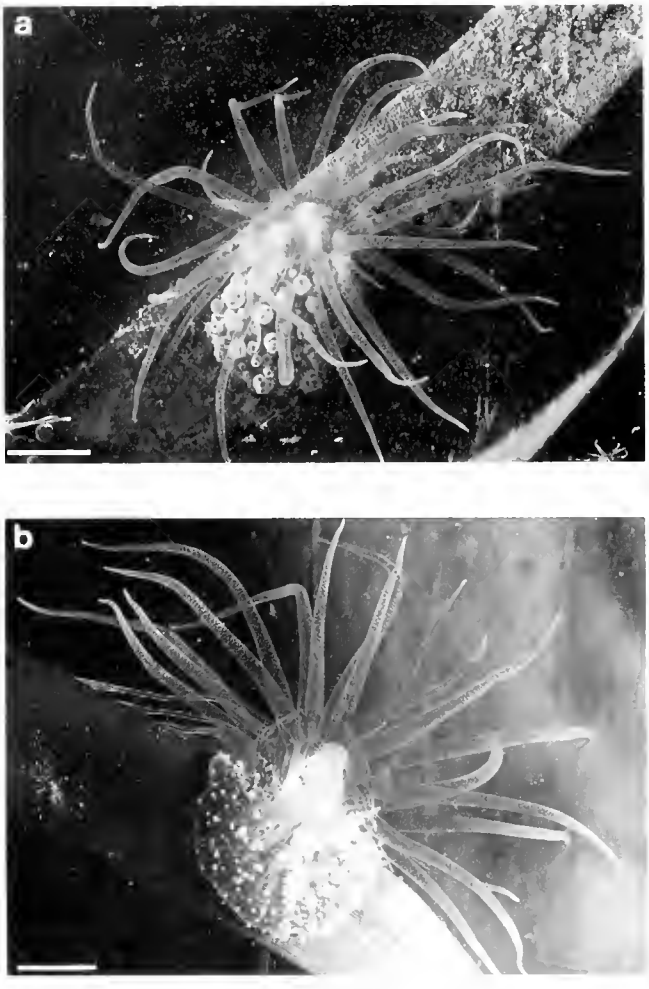

Figure 1. (a) *Bunodeopsis antilliensis* and (b) *B. globulifera* in expanded postures. Scale bar = 1 cm.

B. antilliensis anemones experienced higher ambient irradiances than *B. globulifera*, receiving 53 ± 2 and 26 ± 2% of surface irradiance (means ± SE; $N = 87$), respectively ($t_{(85)} = 11.23$; $0.01 < p > 0.05$).

Morphology and histology

Of the anemones collected, the larger specimens were *B. antilliensis* rather than *B. globulifera;* the basal disk diameters of the two species ranged from 5 to 34 mm and 4.4 to 15.2 mm, respectively. However, vesicle size (diameter) was not related to body size for either *B. antilliensis* ($r^2_{(10)} = 0.36$; $p > 0.05$) or *B. globulifera* ($r^2_{(10)} = 0.17$; $p > 0.05$). The vesicles of *B. antilliensis* (Fig. 2) were significantly larger than those of *B. globulifera*, with diameters (means ± SE) of 1.7 ± 0.2 and 0.7 ± 0.1 mm, respectively ($t_{(14)} = 4.17$; $0.01 < p < 0.05$). Assuming the vesicles to be spherical, this would represent mean volumes per vesicle of 2.6 mm^3 for *B. antilliensis* and 0.2 mm^3 for *B. globulifera*. Because the number of vesicles per anemone was directly related to body size for *B. antilliensis* ($r^2_{(10)} = 0.96$; $0.01 < p < 0.05$) but not for *B. globulifera* ($r^2_{(11)} = 0.05$; $p > 0.05$), the mean number of vesicles per anemone was not compared between species.

Light microscopy of paraffin sections demonstrated that the algal symbionts of *Bunodeopsis* were restricted to the endoderm, and were absent from the mesoglea and ectoderm. Transmission electron microscopy (Fig. 3) revealed that each algal cell was contained within a perisymbiont space, bounded by multiple membranes of host origin, typical of Cnidaria-dinoflagellate symbioses (Trench, 1971). The most obvious dinoflagellate ultrastructural features were the permanently condensed chromosomes in the nucleus (Dodge, 1973). Other distinguishing dinoflagellate characteristics included a single or multistalked pyrenoid surrounded by a starch sheath and groups of three thylakoids per lamella within the chloroplast. The algal symbionts of *B. antilliensis* and *B. globulifera* had a single or multilobed chloroplast and an accumulation body, which are characteristic of *Symbiodinium* (Blank, 1987). Invasive thylakoid membranes within the pyrenoid and a segmented starch sheath (Dodge, 1973) were not observed in the symbionts of *B. antilliensis* or *B. globulifera*. The symbionts of *B. antilliensis* and *B. globulifera* were not identified to species level.

Biomass parameters

The measured and derived algal and animal biomass parameters of *B. antilliensis* and *B. globulifera* are shown in Table 1. The two species of *Bunodeopsis* had similar densities of algal symbionts ($t_{(10)} = -0.7$; $p > 0.05$), which were of a similar size ($t_{(14)} = -1.29$; $p > 0.05$). The estimated standing stock of algal cell carbon and biomass ratios did not vary between species. However, the distri-

Figure 2. *Bunodeopsis antilliensis* in contracted posture, showing inflated vesicles (V). Scale bar = 1 cm.

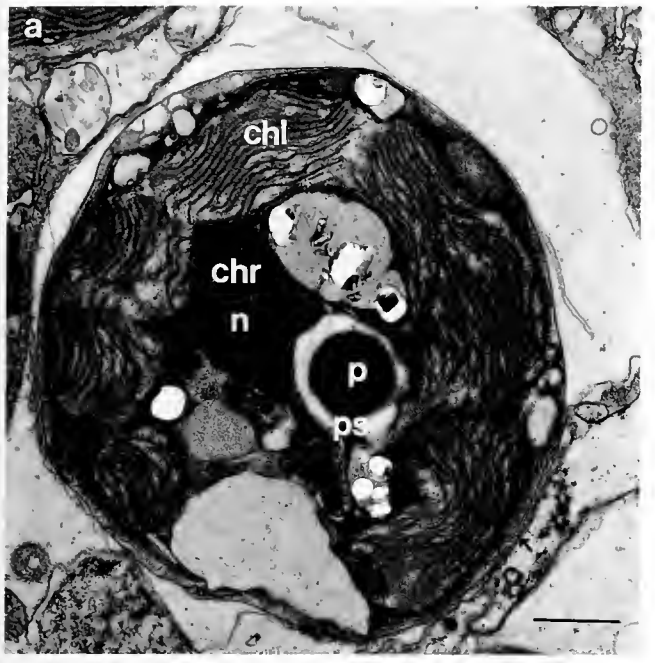

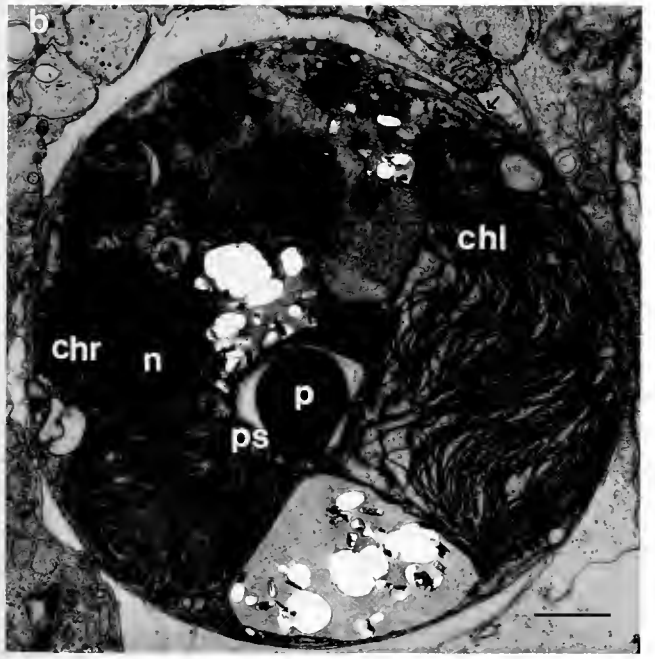

Figure 3. *Symbiodinium* in the vesicle endoderm of (a) *Bunodeopsis antilliensis* and (b) *B. globulifera* showing multiple membranes (↑); nucleus (n); chromosomes (chr); chloroplast (chl); pyrenoid (p); and pyrenoid stalk (ps). Scale bar = 1 μm.

bution of symbionts within the anemones was markedly different between the two species of *Bunodeopsis* (Fig. 4) (Two-factor ANOVA: $F_{(\text{species})(1,40)} = 1.37$, $p > 0.05$; $F_{(\text{body region})(3,40)} = 368.42$; $0.01 < p < 0.05$; $F_{(\text{interaction})(3,40)} = 103.10$; $0.01 < p < 0.05$). *B. globulifera* anemones had a higher proportion of symbionts in the tentacles (44%) than *B. antilliensis* (10%), which had most symbionts in the scapus and basal disk (85%) (Tukey-Kramer multiple comparisons test; $0.01 < p < 0.05$).

The diel cycles of symbiont cell division were phased in both *B. antilliensis* and *B. globulifera* (Fig. 5), with peak mitotic indices in the early morning. Symbionts from *B. globulifera* had a higher chlorophyll *a* content, 7.34 ± 0.77, than those from *B. antilliensis*, 4.51 ± 0.29 pg · cell^{-1} ($t_{(8)} = 3.45$; $0.01 < p < 0.05$). Chlorophyll c_2 content did not differ between the symbionts of *B. antilliensis* and *B. globulifera*, with 3.3 and 3.9 pg · cell^{-1}, respectively ($t_{(8)} = 1.19$; $p > 0.05$). The ratio of chlorophylls a:c_2 was higher for symbionts from *B. globulifera*, 1.88 ± 0.06, than from *B. antilliensis*, 1.40 ± 0.05 ($t_{(8)} = 7.46$; $0.01 < p < 0.05$).

Expansion and contraction behavior

In situ, almost all anemones of both species of *Bunodeopsis* were expanded at night, although marked differences in expansion and contraction behavior were observed during the day (Fig. 6). Under illumination, *B. antilliensis* anemones were contracted, whereas *B. globulifera* remained expanded, except at very high irradiances experienced at midday. The proportion of *B. globulifera* anemones in an expanded posture was found to be inversely related to irradiance (Fig. 7; $r^2_{(29)} = -0.69$; $0.01 < p < 0.05$). Under laboratory conditions of irradiance, untreated and cold-stripped anemones displayed patterns of expansion and contraction behavior similar to those observed *in situ* (Fig. 8). However, significantly more cold-stripped *B. globulifera* anemones than untreated anemones were contracted during the day (Scheffé's; $0.01 < p < 0.05$). In constant darkness, almost all anemones of both species were expanded, and the proportion of contracted *B. globulifera* was significantly higher for cold-stripped anemones than for the untreated group (Scheffé's; $0.01 < p < 0.05$). Cold-stripped anemones contained significantly fewer symbionts than untreated anemones, with densities (mean ± SE) of 0.03 ± 0.01 × 10^6 cells · mg protein^{-1} for *B. antilliensis* ($t_{(10)} = 13.19$; $0.01 < p < 0.05$), and 0.26 ± 0.05 × 10^6 cells · mg protein^{-1} for *B. globulifera* ($t_{(8)} = 6.51$; $0.01 < p < 0.05$). "Juvenile" anemones (with a basal disk diameter of less than 5 mm), which were formed by pedal laceration from "adults," were continually expanded, both under illumination and in darkness.

Zooplankton feeding

Prey items were found at various stages of digestion within the gastrovascular cavity, mesentery, and oral disk regions of *B. antilliensis* and *B. globulifera*. The compo-

Table I

Sea anemone biomass parameters of Bunodeopsis antillinesis *and* B. globulifera

Parameter	Method*	*B. globulifera*	*B. antilliensis*
Algal cell diameter (μm) (mean ± SE; N = 8)	M	7.95 ± 0.70	7.60 ± 0.34
Algal cell density ($\times 10^6 \cdot$ mg protein^{-1}) (mean ± SE; N = 6)	M	0.61 ± 0.04	0.65 ± 0.02
Algal carbon (pg · cell^{-1})	D	43.2	38.4
Standing stock of algal carbon (μg · mg protein^{-1})	D	26.4	25.0
Algal protein (pg · cell^{-1})	D	28.7	25.5
Protein biomass ratio (animal:total)	D	0.98	0.98
Peak mitotic index (%) (mean ± SE; N = 3)	M	5.0 ± 2.6	8.0 ± 1.9
Algal population growth rate (μ) (day^{-1})	D	0.05	0.08
Carbon specific growth rate (μ_c) (day^{-1})	D	1.90	2.56

* M = measured; D = derived.

sition of prey ingested by the two species was similar ($\chi^2_{(7)} = 9.14$; $p > 0.05$, for nighttime feeding), with Crustacea the most common prey type (Table II). Crustacea represented 90% and 84% of the total numbers of prey recorded for *B. antilliensis* and *B. globulifera*, respectively. Other prey types included polychaetes, mollusks, and urochordates. Although *B. antilliensis* anemones sampled were larger (mean basal disk diameter ± SE), 7.8 ± 0.29 mm, than *B. globulifera*, 6.2 ± 0.29 mm ($Z = 4.49$; $0.01 < p < 0.05$), no significant correlation was found between anemone size and number of prey caught for *B. antilliensis* ($r^2_{(70)} = 0.09$; $p > 0.05$) or *B. globulifera* ($r^2_{(70)} = 0.02$; $p > 0.05$). Similar total numbers of prey items were found in the 80 anemones of each species sampled during the 24-h period; 83 in *B. globulifera* and 88 in *B. antilliensis* (Wilcoxon's signed rank test for paired samples; $T_s = 16$; $p > 0.05$), which were also of a comparable size ($Z = 0.80$; $p > 0.05$). Both species ingested significantly more prey items at night than during the day (Mann-Whitney U test; $0.01 < p < 0.05$). At night, prey ingestion did not vary between species (Mann-Whitney U test $p > 0.05$); during the day, however, *B. globulifera* ingested significantly more prey than *B. antilliensis* (Mann-Whitney U test; $0.01 < p < 0.05$).

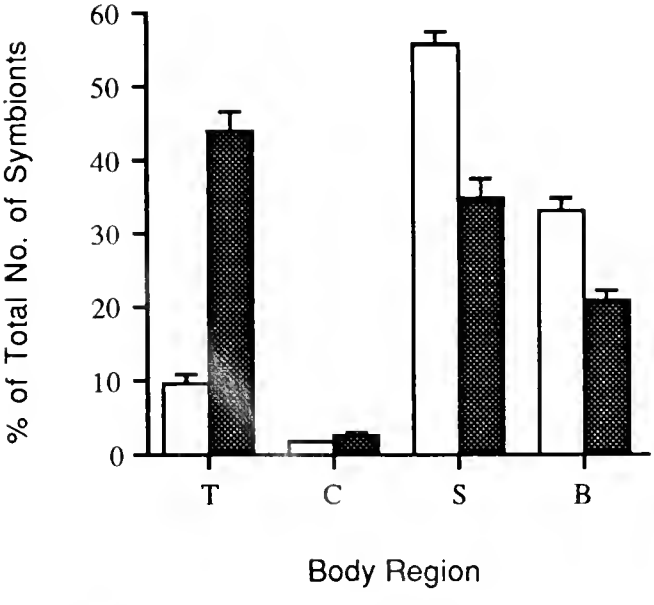

Figure 4. Distribution of symbionts within body regions; tentacles (T), capitulum (C), scapus (S) and basal disk (B) of *Bunodeopsis antillensis* (open bars) (N = 7) and *B. globulifera* (solid bars) (N = 5). Values are means ± SE.

Photosynthesis-irradiance relationships and CZAR

P-I curves for *B. antilliensis* and *B. globulifera* are shown in Figure 9. Both species of *Bunodeopsis* had sim-

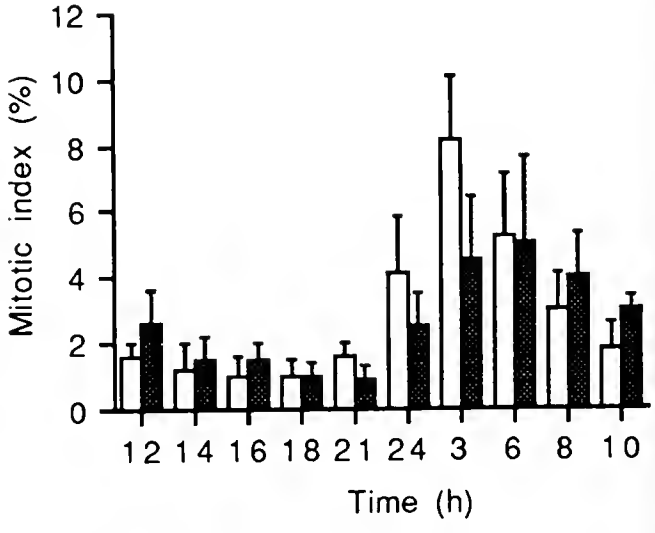

Figure 5. The diel cycle of symbiont cell division from *Bunodeopsis antilliensis* (open bars) and *B. globulifera* (solid bars). Values are means ± SE (N = 3).

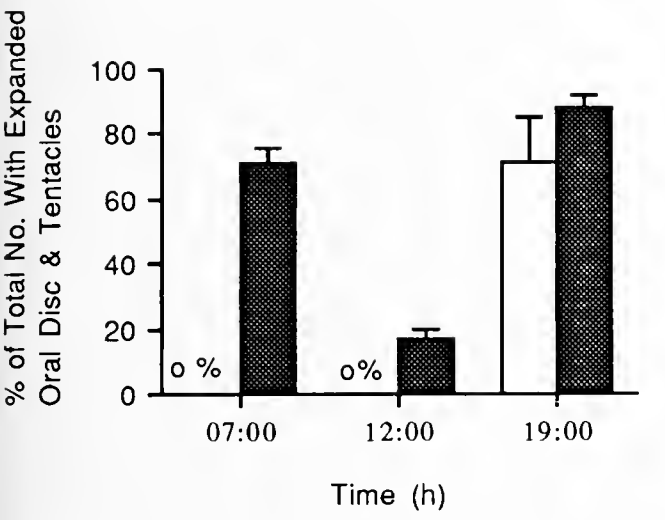

Figure 6. Oral disk and tentacle expansion and contraction in *Bunodeopsis antilliensis* (open bars) and *B. globulifera* (solid bars) *in situ*. Two-factor ANOVA: $F_{(species)(1,52)} = 42.83^*$; $F_{(time)(2,52)} = 51.43^*$; $F_{(interaction)(2,52)} = 10.46^*$ (*significant at $0.01 < p < 0.05$). 0% = No *B. antilliensis* anemones with expanded oral disk and tentacles.

ilar dark respiration rates ($r_{Anemone}$) and gross photosynthetic capacities (p^G_{max}) (Table III). The photosynthetic efficiencies (α; means ± SE) were 0.24 ± 0.02 for *B. globulifera* and 0.17 ± 0.03 $\mu gO_2 \cdot 10^6$ algae$^{-1} \cdot h^{-1}/\mu$mol photons $\cdot m^{-2} \cdot s^{-1}$ for *B. antilliensis*. However, the deeper living species *B. globulifera* attained photosynthetic capacity at a significantly lower saturation irradiance ($I_{0.95}$;

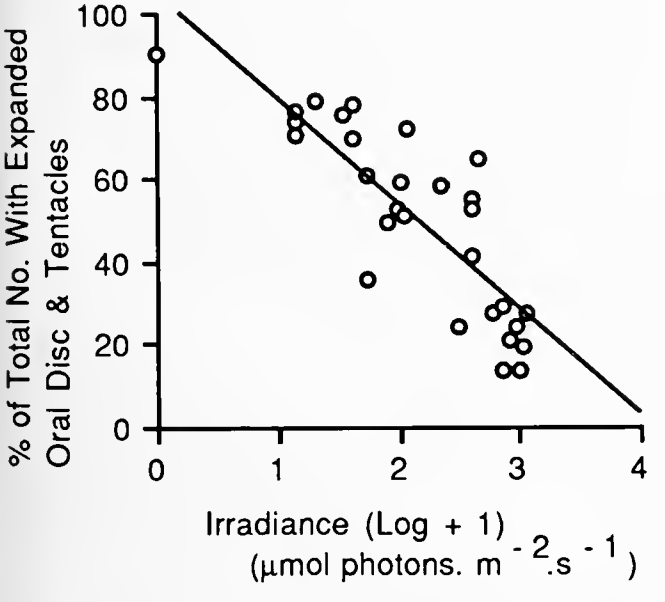

Figure 7. Variation of oral disk and tentacle expansion with irradiance in *Bunodeopsis globulifera*. Points were fitted by the method of least squares regression analysis.

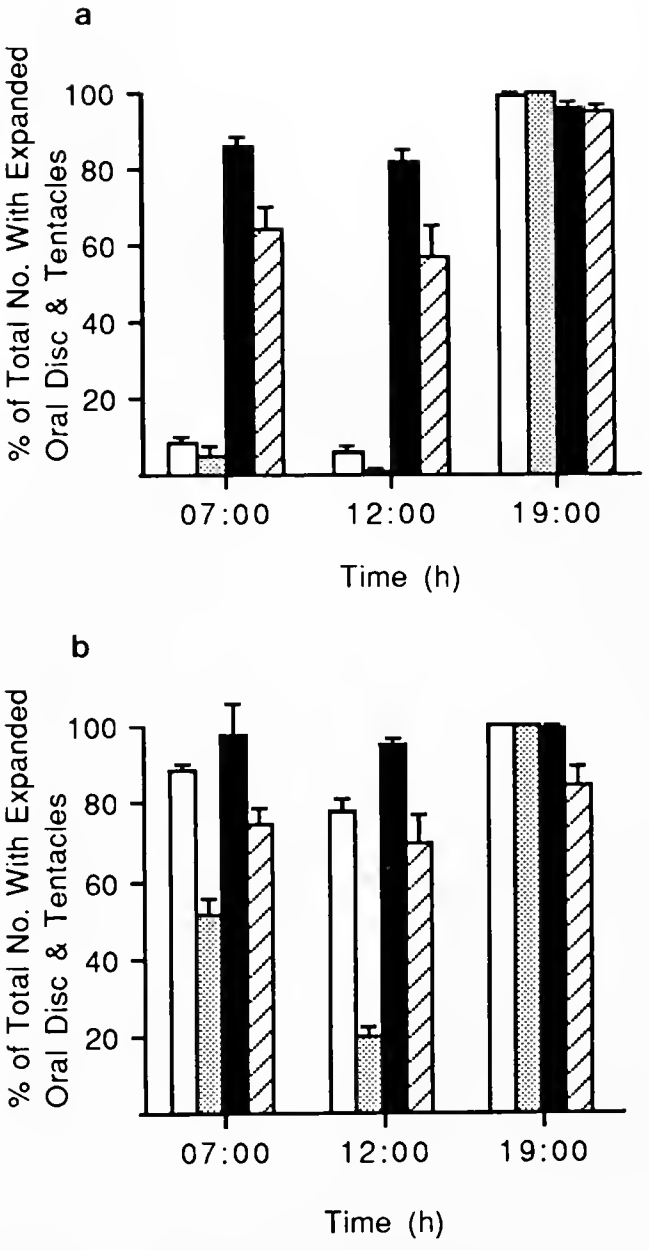

Figure 8. Oral disk and tentacle expansion and contraction in (a) *Bunodeopsis antilliensis* and (b) *B. globulifera* in aquaria under four treatment groups: untreated under ambient irradiance (open bars) and in constant darkness (solid bars); and cold-stripped under ambient irradiance (shaded bars) and in constant darkness (hatched bars). (a) Two-factor ANOVA; $F_{(treatment)(3,43)} = 139.24^*$; $F_{(time)(2,143)} = 425.25^*$; $F_{(interaction)(6,143)} = 50.31^*$. (b) Two-factor ANOVA; $F_{(treatment)(e,43)} = 89.41^*$; $F_{(time)(2,143)} = 117.67^*$; $F_{(interaction)(6,143)} = 27.38^*$ (*significant at $0.01 < p < 0.05$).

mean ± SE), 227 ± 18, than *B. antilliensis*, 436 ± 78 μmol photons $\cdot m^{-2} \cdot s^{-1}$, ($t_{(20)} = -2.85$; $0.01 < p < 0.05$). *B. globulifera* and *B. antilliensis* both experienced about 8.5 h of saturating irradiance as calculated from the diel cycle of PAR (Fig. 10), *in situ* measurements of transmission of surface irradiance to study site depth, and sat-

Table II

Total number of prey items identified in specimens of B. antilliensis *(N = 80) and* B. globulifera *(N = 80) during the day (0700 to 1800 h) and at night (2100 to 0600 h)*

	B. antilliensis		*B. globulifera*	
Prey Item	Day	Night	Day	Night
Crustacea				
Ostracoda	0	3	0	3
Copepoda	0	24	7	16
Decapoda	0	13	7	10
Brachyura	0	22	1	5
Isopoda	0	2	2	3
Amphipoda	2	13	6	10
Non-Crustacea				
Polychaeta	0	1	1	2
Other	0	8	0	10

uration irradiances ($I_{0.95}$). The total daily net carbon fixed (P_Z^N) by the algal symbionts of *B. antilliensis* was greater than for *B. globulifera*. However, the calculated amount of fixed carbon available for translocation to the host (T) did not vary between the two species, reflecting the similar-sized algal populations and peak mitotic indices (Table I). The overall potential contribution made by translocated symbiont carbon to the daily respiratory carbon requirements of the host animal (CZAR) was slightly greater in *B. antilliensis* (109%) than in *B. globulifera* (92%).

Discussion

This study discloses significant differences in both morphological and behavioral aspects of two tropical species of the symbiotic sea anemone *Bunodeopsis;* these differences appear to be related to the possession of intracellular algal symbionts. The algal symbionts found in both species of *Bunodeopsis* were closely similar to other algae of the genus *Symbiodinium* (Blank, 1987). The symbionts from the two host species did not differ in morphology, ultrastructure, or cell-cycle timing. However, further identification of these symbionts would require the use of molecular genetic techniques (Rowan and Powers, 1991). Comparisons of the results from these and similar studies must be interpreted with caution due to possible variation in the relationships between different host species and their symbionts.

The symbionts from *B. antilliensis* and *B. globulifera* were of a similar size (7 to 10 μm in diameter) to those from other tropical sea anemones (Muller-Parker, 1984, 1985; Steen and Muscatine, 1984; Smith, 1986; Cook *et al.*, 1988). The symbionts from both species of *Bunodeopsis* had a phased cell division cycle, with peak mitotic indices occuring during the early morning, characteristic of symbionts from other tropical sea anemones (Steen and Muscatine, 1984; Smith, 1986; Cook *et al.*, 1988). The peak mitotic indices of symbionts from *B. antilliensis* (8%) and *B. globulifera* (5%) were similar to those from fed *Aiptasia pallida* (7 to 8%) (Cook *et al.*, 1988), but much higher than those from *Zoanthus sociatus, Palythoa variabilis* (both 0.6%; Steen and Muscatine, 1984), and *A. pulchella* (0.3 to 1.1%; Muller-Parker, 1984, 1985, 1987; Wilkerson *et al.*, 1983; Steen, 1986). Consequently the population doubling times of symbionts from *B. antilliensis, B. globulifera,* and *A. pallida* (Cook *et al.*, 1988) were much shorter, 8 to 12 days, than those from *Z. sociatus, P. variabilis,* and *A. pulchella,* 28 to 137 days (Steen and Muscatine, 1984; Muller-Parker, 1984, 1985, 1987; Wilkerson *et al.*, 1983).

The density of algal symbionts in both *B. antilliensis* and *B. globulifera* was less than half that reported for

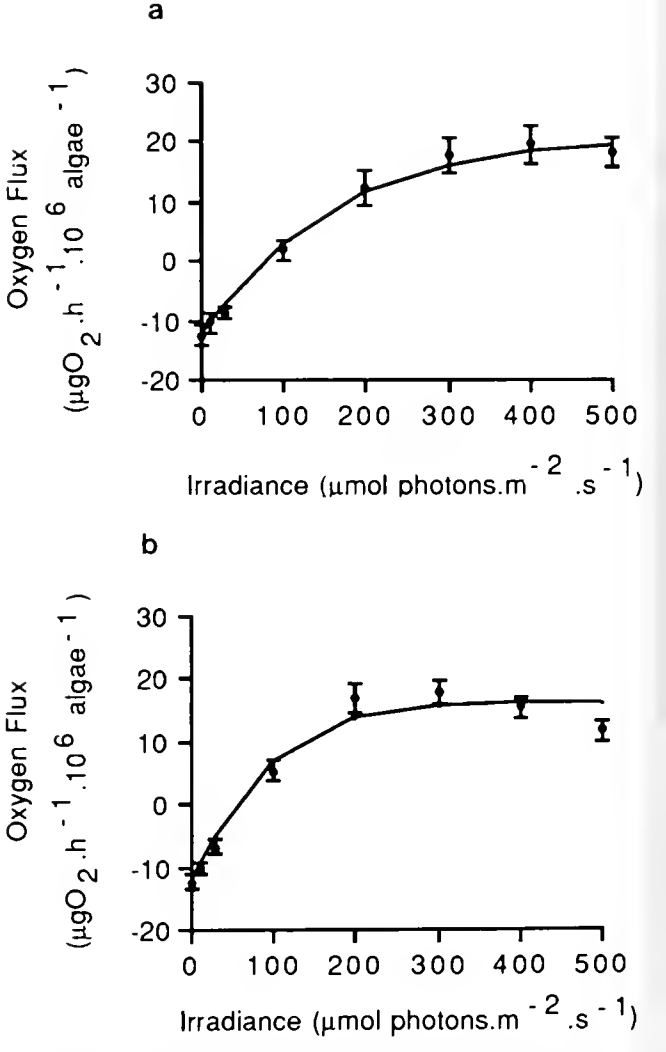

Figure 9. Net oxygen flux of the symbiotic association as a function of irradiance for (a) *Bunodeopsis antilliensis* ($N = 10$) and (b) *B. globulifera* ($N = 12$). Values are means ± SE.

Table III

P-I curve parameters (means ± SE) and CZAR of Bunodeopsis antilliensis *and* B. globulifera

Parameter		Method*	*B. globulifera* (N = 12)	*B. antilliensis* (N = 10)
Anemone respiration rate ($r_{Anemone}$)	($\mu gO_2 \cdot 10^6$ algae$^{-1} \cdot h^{-1}$)	M	−12.3 ± 1.1	−12.4 ± 1.6
Anemone respiration rate ($r_{Anemone}$)	($\mu gC \cdot$ mg protein$^{-1} \cdot h^{-1}$)	D	2.25	2.43
Animal respiration rate (R_A)	($\mu gC \cdot$ mg protein$^{-1} \cdot 24\ h^{-1}$)	D	52.9	57.2
Algal respiration rate (r_Z)	($\mu gC \cdot$ mg protein$^{-1} \cdot h^{-1}$)	D	0.045	0.049
Gross photosynthetic capacity (p^G_{Max})	($\mu gO_2 \cdot 10^6$ algae$^{-1} \cdot h^{-1}$)	D	28.6 ± 2.61	34.2 ± 4.67
Gross photosynthetic capacity (p^G_{Max})	($\mu gC \cdot$ mg protein$^{-1} \cdot h^{-1}$)	M	5.95	7.58
Net carbon fixed by algae (P^N_Z)	($\mu g \cdot$ mg protein$^{-1} \cdot 24\ h^{-1}$)	D	50.2	64.0
Carbon translocation (%)		D	97.4	96.9
CZAR (%)		D	92.4	108.5

* M = measured; D = derived.

several tropical species of *Aiptasia,* 1.6 to 3.5 × 10^6 cells · mg protein^{-1} (Steele, 1976; Svoboda and Porrmann, 1980; Muller-Parker, 1984, 1987; Clayton and Lasker, 1984; Cook *et al.,* 1988). *B. antilliensis* and *B. globulifera* displayed distinct morphological adaptations that seem to be related to the possession of symbionts. The most striking morphological features of these species are the vesicles, which are considerably larger in *B. antilliensis* than in *B. globulifera.* The relative importance of these auxiliary structures (Sebens and deReimer, 1977) for exposure of the symbionts to light was evident from the marked differences in the distribution of symbionts within the two host species. In *B. globulifera* the distribution of symbionts was relatively uniform, whereas in *B. antilliensis* the vesicle-containing scapus region had the highest proportion of symbionts, with a symbiont density approximately three times higher than in the tentacles. Based on areal densities, Sebens and deReimer (1977) found the symbiont density in the scapus region of *B. antilliensis* to be 12 times higher than that in the tentacles. Similar relationships between symbiont densities and auxiliary structures were found in the tropical corallimorphs *Lebrunia coralligens* and *L. danae,* with symbiont densities three or four times higher in the pseudotentacles than in the feeding tentacles (Sebens and deReimer, 1977), and in *Discosoma sanctithomae,* with symbiont densities four times higher in the diskal tentacles than in the oral disk margin (Elliott and Cook, 1989).

Linked to the differences in anemone morphology and distribution of symbionts are significantly different patterns of light-related expansion and contraction behavior. This behavior by the host can control exposure of the symbionts to light and consequently their photosynthetic capacity (Shick and Dykens, 1984). Under illumination, vesicle inflation by *B. antilliensis* and simultaneous vesicle inflation and tentacle expansion by *B. globulifera* were indicative of mechanisms to promote exposure of their symbiont populations to light. Vesicle inflation may also enhance the supply of carbon dioxide, because photosynthesis by symbiotic algae *in situ* may be carbon-dioxide-limited (Muscatine *et al.,* 1989). The role of algal symbionts in light-related behavioral responses is clearly seen in other tropical species that concentrate their symbionts in auxiliary structures (Gladfelter, 1975; Sebens and deReimer, 1977; Steele and Goreau, 1977; Lewis, 1984; Elliott and Cook, 1989; Shick *et al.,* 1991). Contraction by *B. globulifera* under high midday irradiances may result in shading of the symbionts in the tentacles, thereby decreasing symbiont photosynthesis and the potential for oxygen toxicity occuring in the host tissues (Shick and Dykens, 1984). In contrast, contraction of cold-stripped *B. globulifera* under low irradiances may be due to their reduced symbiont densities in comparison to untreated anemones. Continual expansion of small, or juvenile, *B. antilliensis* under illumination may reflect the relatively

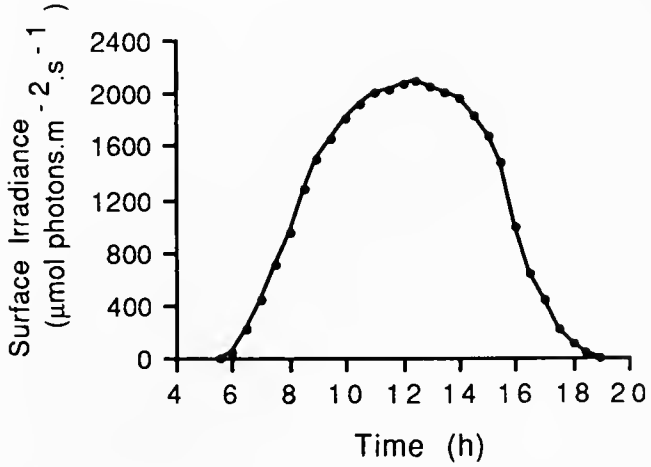

Figure 10. The diel cycle of irradiance at Discovery Bay (22 Feb.1990).

small energy saving resulting from contraction of a small compared to a large anemone (Robbins and Shick, 1980).

B. antilliensis and *B. globulifera* had expanded feeding tentacles at night, corresponding with the diel migration of zooplankton prey within Discovery Bay (Ohlhorst, 1982). Capture of more prey by *B. globulifera* than *B. antilliensis* during the day was presumably a direct consequence of their differences in light-related behavior. The present study of prey capture by *B. antilliensis* and *B. globulifera* is one of the few reported for tropical sea anemones (reviewed in Shick, 1991). These results emphasize the importance of nighttime sampling, with short intervals, because sea anemones may rapidly digest their prey (Sebens and Koehl, 1984; Zamer, 1986). Therefore, the apparent lack of prey found within the tropical corallimorph *Discosoma sanctithomae* (Elliott and Cook, 1989) and the coral *Porites porites* (Edmunds and Davies, 1989) may be artifacts due to the choice of sampling time and interval.

In association with differences in host habitat, morphology, and behavior, the algal symbionts exhibit responses to enhance photosynthesis and maximize cell division rates in low light environments (Prézelin, 1987). Variations in the photosynthetic pigment content and physiology between the symbionts from *B. antilliensis* and *B. globulifera* were indicative of responses to the different irradiance regimes of their respective host habitats. Characteristic of adaptation to lower habitat irradiances, symbionts from the deeper species *B. globulifera* had a higher chlorophyll *a* content than those from *B. antilliensis*. The chlorophyll *a* content of these symbionts was comparable to that of the symbionts from the tropical sea anemone *Aiptasia pallida*, 2 to 5 pg · cell^{-1} (Clayton and Lasker, 1984; Cook *et al.*, 1988; Lesser and Shick, 1989), but higher than for the symbionts from *A. pulchella*, 1.5 pg · cell^{-1} (Muller-Parker, 1984). The ratio of chlorophylls $a:c_2$ was lower for symbionts of *B. antilliensis* and *B. globulifera* than from *A. pulchella*, 2.2 to 3.7 (Muller-Parker, 1984, 1985, 1987). This was due to higher levels of chlorophyll c_2 in the symbionts from the two species of *Bunodeopsis* compared to those from *A. pulchella*, with 0.4 to 0.7 pg · cell^{-1} (Muller-Parker, 1984 and 1987).

The lower saturation irradiance and higher photosynthetic efficiency of symbionts from *B. globulifera* compared to those from *B. antilliensis* was also indicative of adaptation to lower light levels. These photosynthesis-irradiance responses compared well with those of symbionts from *A. pulchella* and *A. pallida* collected from habitats of differing irradiance regimes (Muller-Parker, 1984, 1985, 1987; Lesser and Shick, 1989). I_k values for symbionts from *B. antilliensis*, 238 μmol photons · m^{-2} · s^{-1}, were similar to those from *A. pulchella* collected from "sun" habitats during the summer, 288 μmol photons · m^{-2} · s^{-1} (Muller-Parker, 1987). Reflecting the differences in chlorophyll *a* content, the photosynthetic efficiencies (means ± SE; $N = 10$) of symbionts from *B. antilliensis* and *B. globulifera*, 0.24 ± 0.02 and 0.17 ± 0.03 μgO$_2$ · 10^6 cells · h^{-1}/μmol photons · m^{-2} · s^{-1}, were considerably higher than those from *A. pulchella* based on algal cell numbers (0.04 to 0.06 μg O$_2$ · 10^6 cells · h^{-1}/μmol photons · m^{-2} · s^{-1}) (Muller-Parker, 1984, 1987), but were similar when normalized to algal chlorophyll *a* content. Also, photosynthetic capacities of the symbionts from *B. antilliensis* and *B. globulifera* were almost twice that of *A. pulchella* based on algal cell number, of 10 μgO$_2$ · 10^6 cells · h^{-1} (Muller-Parker, 1984), but did not differ when normalized to algal chlorophyll *a* content.

The dark respiration rates for anemones of both species of *Bunodeopsis* compared well with those for *A. pulchella*, of 8.2 μgO$_2$ · mg protein · h^{-1} (Muller-Parker, 1984), and *A. pallida* (fed three times per week), of 10.7 μgO$_2$ · mg protein · h^{-1} (Clayton and Lasker, 1984). However, symbiont respiration rates based on algal biomass estimations were low for both *B. antilliensis* and *B. globulifera*. Because algal cell densities in both species of *Bunodeopsis* were low, the estimated biomass ratio of algal to total protein was also low. Higher algal biomasses have been estimated for *Z. sociatus* (17%; Steen and Muscatine, 1984), *A. pulchella* (18%; Muller-Parker, 1984), *Aulactinia stelloides* (15%; Smith, 1986), and *Anthopleura elegantissima* (14%; Dykens *et al.*, 1992).

In *B. antilliensis* and *B. globulifera*, the proportion of photosynthetically fixed carbon available for animal respiration was high, similar to that for the zoanthids *Z. sociatus* (95%) and *P. variabilis* (89%; Steen and Muscatine, 1984). High rates of translocation reflect low rates of carbon utilization by the algal symbionts for their own growth (Muscatine *et al.*, 1983). Calculated translocation rates of *B. antilliensis* and *B. globulifera* were high due to high carbon-specific growth rates and correspondingly low algal population growth rates. Despite low carbon-specific growth rates of the symbionts from *Z. sociatus* and *P. variabilis*, 0.2 · day^{-1}, compared to those for *B. antilliensis* and *B. globulifera*, algal population growth rates of *Z. sociatus* and *P. variabilis* were much lower, 0.02 and 0.01 · day^{-1}, respectively.

The values of CZAR estimated for *B. antilliensis* (109%) and *B. globulifera* (92%) suggest that both species are potentially autotrophic with respect to carbon available for animal respiration on days with 8.5 h of saturating irradiance. Although CZAR values may be high, essential nutrients such as nitrogen and phosphorus need to be acquired by host heterotrophy (Muller-Parker *et al.*, 1988). Both *B. antilliensis* and *B. globulifera* were found to feed extensively on zooplankton prey, providing an alternative nutrient source to the supply of carbon fixed photosynthetically by the symbionts. The sea anemone *Anemonia sulcata* was also found to be potentially autotrophic, with

CZAR estimated to be 116%, for freshly collected Mediterranean anemones experiencing 10 h of saturating irradiance daily (Stambler and Dubinsky, 1987). However, CZAR values for the tropical zoanthids *Z. sociatus* (48%) and for *P. variabilis* (13%) (Steen and Muscatine, 1984), were considerably lower than for *B. antilliensis* and *B. globulifera,* reflecting relatively low photosynthetic capacities of the symbionts and high rates of animal respiration in the zoanthids. CZAR calculated for the temperate anemone *Anthopleura elegantissima* was also low (assuming a translocation value of 90%), 17% for high shore and 40% for low shore anemones (Shick and Dykens, 1984; Zamer and Shick, 1987). Therefore, further investigations are required to assess the influence of host habitat and locality on the nutritional contribution made by the algal symbionts to their hosts.

In summary, despite morphological differences between *B. antilliensis* and *B. globulifera,* light-related behavior correlated with the distribution of symbionts within these two host species appears to maximize exposure of the symbiont populations to light. Although *B. antilliensis* and *B. globulifera* experience different irradiance regimes due to host habitat and posture, compensatory responses by the symbionts enhance light absorption and photosynthesis. *B. antilliensis* and *B. globulifera* display two distinct strategies, combining anemone morphology with symbiont distribution and photosynthetic physiology, that result in a similar contribution made by symbiont photosynthesis to animal respiration.

Acknowledgments

I wish to thank P. J. Day for supporting this research; R. D. Steele and I. M. Sandeman for enthusiastic discussions and for use of equipment; S. Douglas and J. Royes for invaluable field assistance; the staff and visitors to the Discovery Bay Marine Laboratory, especially W. H. Topley; J. Corrigan, M. Lomas and M. Amphlett for technical assistance; K. Sebens and M. Lesser for useful comments and suggestions on earlier ideas. This manuscript was greatly improved by comments from A. Douglas, B. Okamura and four anonymous reviewers.

Literature Cited

Blank, R. J. 1987. Cell architecture of the dinoflagellate *Symbiodinium* sp. inhabiting the Hawaiian stony coral *Montipora verrucosa. Mar. Biol.* **94:** 143–155.

Carlgren, O. 1924. On *Bolocerοides, Bunodeopsis* and their supposed allied genera. *Arkiv För Zoologi,* Band **17A**(1): 1–20.

Chalker, B. E. 1981. Simulating light saturation curves for photosynthesis and calcification by reef-building corals. *Mar. Biol.* **63:** 135–141.

Chalker, B. E., W. E. Dunlap, and J. K. Oliver. 1983. Bathymetric adaptations of reef-building corals at Davies Reef, Great Barrier Reef, Australia. II Light saturation curves for photosynthesis and respiration. *J. Exp. Mar. Biol. Ecol.* **73:** 37–56.

Clayton, W. S., and H. R. Lasker. 1984. Host feeding regime and zooxanthellal photosynthesis in the anemone *Aiptasia pallida* (Verrill). *Biol. Bull.* **167:** 590–600.

Cook, C. B., C. F. D'Elia, and G. Muller-Parker. 1988. Host feeding and nutrient sufficiency for zooxanthellae in the sea anemone *Aiptasia pallida. Mar. Biol.* **98:** 253–262.

Dodge, J. D. 1973. *The Fine Structure of Algal Cells.* Academic Press, London.

Duerden, J. E. 1897. *Bunodeopsis. Annals and Magazine of Natural History, London.* **6:** 1–15.

Dykens, J. A., J. M. Shick, C. Benoit, G. R. Buettner, and G. W. Winston. 1992. Oxygen radical production in the sea anemone *Anthopleura elegantissima* and its endosymbiotic algae. *J. Exp. Biol.* **168:** 219–241.

Edmunds, P. J., and P. S. Davies. 1989. An energy budget for *Porites porites* (Scleractinia) growing in a stressed environment. *Coral Reefs* **8:** 37–43.

Elliott, J., and C. B. Cook. 1989. Diel variation in prey capture behavior by the Corallimorpharian *Discosoma sanctithomae:* Mechanical and chemical activation of feeding. *Biol. Bull.* **176:** 218–228.

Fitt, W. K., R. L. Pardy, and M. M. Littler. 1982. Photosynthesis, respiration and contribution to community productivity of the symbiotic sea anemone *Anthopleura elegantissima. J. Exp. Mar. Biol. Ecol.* **61:** 213–232.

Fitt, W. K., and R. K. Trench. 1983. The relation of diel patterns of cell division to diel patterns of motility in the symbiotic dinoflagellate *Symbiodinium microadriaticum* Freudenthal in culture. *New Phytol.* **94:** 421–434.

Gladfelter, W. B. 1975. Sea anemone with zooxanthellae: simultaneous contraction and expansion in response to changing light intensity. *Science* **189:** 570–571.

Hyman, L. H. 1940. *The Invertebrates: Protozoa through Ctenophora.* McGraw-Hill Book Company Inc., New York.

Lesser, M. P., and J. M. Shick. 1989. Photoadaptation and defenses against oxygen toxicity in zooxanthellae from natural populations of symbiotic cnidarians. *J. Exp. Mar. Biol. Ecol.* **134:** 129–141.

Lewis, J. B. 1984. Photosynthetic production by the coral reef anemone, *Lebrunea coralligens* Wilson, and behavioral correlates of two nutritional strategies. *Biol. Bull.* **167:** 601–612.

Lowry, O. H., N. J. Rosenbrough, A. L. Farr, and R. J. Randall. 1951. Protein measurement with the Folin Phenol Reagent. *J. Biol. Chem.* **193:** 265–275.

Muller-Parker, G. 1984. Photosynthesis-irradiance responses and photosynthetic periodicity in the sea anemone *Aiptasia pulchella* and its zooxanthellae. *Mar. Biol.* **82:** 225–232.

Muller-Parker, G. 1985. Effect of feeding regime and irradiance on the photophysiology of the symbiotic sea anemone *Aiptasia pulchella. Mar. Biol.* **90:** 65–74.

Muller-Parker, G. 1987. Seasonal variation in light-shade adaptation of natural populations of the symbiotic sea anemone *Aiptasia pulchella* (Cargren, 1943) in Hawaii. *J. Exp. Mar. Biol. Ecol.* **112:** 165–183.

Muller-Parker, G., C. F. D'Elia, and C. B. Cook. 1988. Nutrient limitation of zooxanthellae: effects of host feeding history on nutrient uptake by isolated algae. Pp. 15–19 in *Proceedings of the 6th International Coral Reef Symposium, Townsville, Australia,* Vol. 3, J. H. Choat, ed.

Muscatine, L., and E. Cernichiari. 1969. Assimilation of photosynthetic products of zooxanthellae by a reef coral. *Biol. Bull.* **139:** 506–523.

Muscatine, L., P. G. Falkowski, and Z. Dubinsky. 1983. Carbon budgets in symbiotic associations. Pp. 649–658 in *Endocytobiology,* Vol. 2, E. A. Schenk and W. Schwemmler, eds. Walter de Gruyter, Berlin.

Muscatine, L., L. R. McCloskey, and R. W. Marian. 1981. Estimating the daily contribution of carbon from zooxanthellae to coral animal respiration. *Limnol. Oceanogr.* **26:** 601–611.

Muscatine, L., J. W. Porter, and I. R. Kaplan. 1989. Resource partitioning by reef corals as determined from stable isotope composition. *Mar Biol* **100:** 185–193.

Newell, R. C., and G. E. Newell. 1966. *Marine Plankton: A Practical Guide.* Hutchinson Educational Limited, London.

Ohlhorst, S. L. 1982. Diel migration patterns of demersal reef zooplankton. *J. Exp. Mar. Biol. Ecol* **60:** 1–5.

Parke, M., and I. Manton. 1967. The specific identity of the algal symbionts in *Convoluta roscoffensis. J. Mar. Biol. Assoc. U. K.* **47:** 445–464.

Prézelin, B. B. 1987. Photosynthetic physiology of dinoflagellates. Pp. 174–223 in *The Biology of Dinoflagellates,* Botanical Monographs, No. 12, F. J. R. Taylor, ed. Blackwell Scientific Publications, Oxford, UK.

Robbins, R. E., and J. M. Shick. 1980. Expansion-contraction behaviour in the sea anemone *Metridium senile*: environmental cues and energetic consequences. Pp. 101–116 in *Nutrition in the Lower Metazoa,* D. C. Smith and Y. Tiffon, eds. Pergamon Press, Oxford, UK.

Rowan, R., and D. A. Powers. 1991. A molecular genetic classification of zooxanthellae and the evolution of animal-algal symbioses. *Science* **251:** 1348–1350.

Sebens, K. P., and K. DeReimer. 1977. Diel cycles of expansion and contraction in coral reef anthozoans. *Mar Biol* **43:** 247–256.

Sebens, K. P., and M. A. R. Koehl. 1984. Predation on zooplankton by the benthic anthozoans *Alcyonium siderium* (Alcyonacea) and *Metridium senile* (Actiniaria) in the New England subtidal. *Mar Biol.* **81:** 255–271.

Shick, J. M. 1991. *A Functional Biology of Sea Anemones.* Chapman and Hall, London.

Shick, J. M., and J. A. Dykens. 1984. Photobiology of the symbiotic sea anemone *Anthopleura elegantissima*: Photosynthesis, respiration and behavior under intertidal conditions. *Biol. Bull.* **166:** 608–619.

Shick, J. M., M. P. Lesser, and W. R. Stochaj. 1991. Ultraviolet radiation and photooxidative stress in zooxanthellate Anthozoa: the sea anemone *Phyllodiscus semoni* and the octocoral *Clavularia* sp. *Symbiosis* **10:** 145–173.

Siegel, S., and N. J. Castellan. 1988. Non-parametric Statistics for the Behavioral Sciences. McGraw-Hill Book Co., New York.

Smith, G. J. 1986. Ontogenetic influences on carbon flux in *Aulactinia stellodes* polyps (Anthozoa: Actiniaria) and their endosymbiotic algae. *Mar Biol.* **92:** 361–369.

Sokal, R. R., and F. J. Rohlf. 1981. *Biometry.* W. H. Freeman and Company, New York.

Stambler, N., and Z. Dubinsky. 1987. Energy relationships between *Anemonia sulcata* and its endosymbiotic algae. *Symbiosis* 3: 233–248.

Steele, R. D. 1976. Light intensity as a factor in the regulation of the density of symbiotic zoxanthellae in *Aiptasia tagetes* (Coelenterata, Anthozoa). *J. Zool.* **179:** 387–405.

Steele, R. D., and N. I. Goreau. 1977. Breakdown of symbiotic zooxanthellae in the sea anemone *Phyllactis* (= *oulactis*) *floxculifera* (Actiniaria). *J. Zool.* **181:** 421–437.

Steen, R. G. 1986. Evidence for heterotrophy by zooxanthellae in symbiosis with *Aiptasia pulchella. Biol. Bull.* **170:** 267–268.

Steen, R. G., and L. Muscatine. 1984. Daily budgets of photosynthetically fixed carbon in symbiotic zoanthids. *Biol. Bull.* **167:** 477–487.

Steen, R. G., and L. Muscatine. 1987. Low temperature evokes rapid exocytosis of symbiotic algae by a sea anemone. *Biol. Bull.* **172:** 246–263.

Strathmann, R. R. 1967. Estimating the organic carbon content of phytoplankton from cell volume or plasma volume. *Limnol. Oceanogr.* **12:** 411–418.

Svoboda, A., and T. Porrmann. 1980. Oxygen production and uptake by symbiotic *Aiptasia diaphana* (Rapp). (Anthozoa, Coelenterata) adapted to different light intensities. Pp. 87–99 in *Nutrition in the Lower Metazoa,* D. C. Smith and Y. Tiffon, eds. Pergammon Press, Oxford, UK.

Taylor, D. L. 1969. The nutritional relationship of *Anemonia sulcata* (Pennant) and its dinoflagellate symbiont. *J. Cell Sci.* **4:** 751–762.

Trench, R. K. 1971. The physiology and biochemistry of zooxanthellae symbiotic with marine coelenterates (I–III). *Proc. R. Soc. Lond. Ser. B.* **177:** 225–264.

Trench, R. K., and R. J. Blank. 1987. *Symbiodinium microadriaticum* Freudenthal, *S. goreauii* sp. no., *S. kawagutii* sp. nov. and *S. pilosum* sp. nov.: Gymnodinoid dinoflagellate symbionts of marine invertebrates. *J. Phycol.* **23:** 469–481.

Tytler, E. M., and P. S. Davies. 1984. Photosynthetic production and respiratory energy expenditure in the anemone *Anemonia sulcata* (Pennant). *J. Exp. Mar. Biol. Ecol.* **81:** 73–86.

Verrill, A. E. 1900. Additions to the Anthozoa and the Hydrozoa of the Bermudas: Anthozoa. *Trans. Conn. Acad. Arts Sci.* **10:** 551–571.

Wilkerson, F. P., G. Muller-Parker, and L. Muscatine. 1983. Temporal patterns of cell division in natural populations of endosymbiotic algae. *Limnol. Oceanogr.* **28:** 1009–1014.

Zamer, W. E. 1986. Physiological energetics of the intertidal sea anemone *Anthopleura elegantissima* I Prey capture, absorption efficiency and growth. *Mar Biol.* **92:** 299–314.

Zamer, W. E., and J. M. Shick. 1987. Physiological energetics of the intertidal sea anemone *Anthopleura elegantissima.* II Energy balance. *Mar Biol.* **93:** 481–491.

Reference: *Biol. Bull.* **186**: 195–201. (April, 1994)

Neurophysiological Correlates of the Behavioral Response to Light in the Sea Anemone *Anthopleura elegantissima*

SARA J. SAWYER*, HAROLD B. DOWSE, AND J. MALCOLM SHICK**

Department of Zoology, University of Maine, 5751 Murray Hall, Orono, ME 04469-5751

Abstract. Neurophysiological responses to light in *Anthopleura elegantissima* do not involve the ectodermal slow system 1 (SS1). Activities in both the endodermal slow system 2 (SS2) and the through conducting nerve net (TCNN) change when the lighting changes, but the response is not consistent. Thus, photoreception in *A. elegantissima* probably occurs in the endoderm because SS2 and the TCNN are involved and SS1 is not. We hypothesize either that the photoreception occurs in sensory cells in a local nerve net, with the information then being transmitted to the muscles, or that the muscles themselves are light sensitive. In either case, the TCNN and SS2 become involved after the transduction, and as a consequence—rather than the cause—of muscular activation. The conducting systems of zooxanthellate specimens have a higher frequency of activity than those of apozooxanthellate individuals.

Introduction

Sea anemones have distinct behavioral responses to light (Fleure and Walton, 1907; Parker, 1918; Batham and Pantin, 1950a, 1954; North, 1956; North and Pantin, 1958; Zahl and McLaughlin, 1959). Pearse (1974a) noted that dark-adapted zooxanthellate specimens of *Anthopleura elegantissima* expand within five to ten minutes after exposure to light. Conversely, *Urticina felina* (=*Tealia crassicornis*), an azooxanthellate anemone, contracts within five minutes after exposure to intense light (Fleure and Walton, 1907).

Received 16 March 1993; accepted 25 January 1994.

* Present address: Department of Biology, University of California, Los Angeles, 405 Hilgard Ave., Los Angeles, CA 90024.

** To whom requests for reprints should be addressed.

Although sea anemones respond to light, no photoreceptor has been identified in these animals. Sensory cells have been described, but definite functions cannot readily be assigned to them (Batham *et al.*, 1960; Fautin and Mariscal, 1991; Shick, 1991). Batham and Pantin (1954) investigated the light response in *Metridium senile* and found that light acted on the parietal musculature in the endoderm. Because the action of light on the muscle was not abolished by magnesium chloride anesthesia (which inhibits myoneural transmission), they concluded that light was acting directly on the muscles in this anemone.

Cnidarians are morphologically the simplest animals to have a nervous system, and in actinarian anthozoans it comprises at least three different conducting systems, one with a conducting velocity 10–20 times faster than those of the other two. The through conducting nerve net (TCNN) has the fastest conducting velocity, up to 100 cm s^{-1}, whereas slow system 1 (SS1) conducts at 5–12 cm s^{-1}, and slow system 2 (SS2) at 3.0–5.3 cm s^{-1} (Josephson, 1966; Robson and Josephson, 1969; McFarlane, 1969, 1982; McFarlane *et al.*, 1988). The TCNN is found in the endoderm of the column and the ectoderm of the oral disc and tentacles. The SS1 is located in the ectoderm, whereas the SS2 is endodermal (McFarlane, 1982; McFarlane *et al.*, 1988).

Using extracellular recordings, Marks (1976) found that the burrowing anemone *Calamactis praelongus* responded to light with a local contraction of the column that was unaccompanied by TCNN activity. Light could also evoke pulses in the TCNN in this anemone, although Marks was not sure whether light acted on the TCNN directly or whether the TCNN was involved in the final processing of the light response. No slow-conducting systems were found in this anemone.

In the present investigation, extracellular recordings were used to evaluate the neurophysiological correlates of the response to a light:dark change in zooxanthellate and apozooxanthellate specimens of *Anthopleura elegantissima* and to provide the first such data on this species. Novel methods of data analysis were developed to allow integration of electrical activity over long time intervals.

Materials and Methods

Zooxanthellate and apozooxanthellate specimens of *A. elegantissima* were collected near Bodega Marine Laboratory, Bodega Bay, California, and shipped to Orono, Maine. Zooxanthellate anemones were maintained at a salinity of 30‰ in a 250-liter aquarium that received indirect natural illumination from a nearby window. This illumination was supplemented with light from a tungsten-halogen lamp (QF-500A) on a 10:14 hour light:dark cycle. Under these conditions, a minimum irradiance of 200 μmol photons m^{-2} s^{-1} was maintained when the lamp was on, as measured with a Li-Cor LI-185B quantum photometer fitted with a model LI-1905B cosine corrected sensor (photosynthetically active radiation, 400–700 nm). Apozooxanthellate anemones were maintained at 30‰ in a 40-liter aquarium in a darkened, temperature-controlled incubator. All water temperatures were 15 ± 2°C. Anemones were maintained in aquaria for no more than six months. All animals were fed previously frozen squid twice weekly and were starved for 48 hours before the experiments.

Electrophysiological recordings were made as follows. Two suction electrodes were placed on tentacles on opposite radii of an experimental anemone. The electrodes were made from 1-ml plastic syringes, each with a silver wire threaded through a hole in the barrel and out through the tip into a polyethylene tube. Metal Luer stubs were avoided because they introduce galvanic artifacts. Electrical stimuli were supplied by a Grass SD9 stimulator applied through a suction electrode attached to a tentacle approximately equidistant from the two recording electrodes. Signals from the recording electrodes were passed to a Grass P15 preamplifier and then to a DC amplifier. The recordings were displayed on a Tektronix 5103N storage oscilloscope and were stored on videotape (Sony Betamax) with a Nakamichi DHP-100 digital audio processor sampling at 44 kHz. For analysis, the data recorded on the videotape were reconverted to an analog signal and redigitized (84 Hz sampling rate) using a Zenith microcomputer with a Metrabyte DASH8 A/D converter driven by FORTRAN software. Illumination (200 μmol photons m^{-2} s^{-1}, measured at 400–700 nm) was provided by a Cole-Parmer low-noise illuminator with a fluorescent bulb. The anemones were maintained in plastic cups at 15 ± 1°C on a flow-through copper base plate cooled with a water circulator (Brinkman RC 6).

Individual preparations in which the through conducting nerve net (TCNN), slow system 1 (SS1), and slow system 2 (SS2) could not clearly be distinguished were not used. Recordings were taken while the animals were in the light (Before Dark, BD), in the dark (D), and then in the light again (After Dark, AD). Individuals in which a continuous recording could not be maintained were not used. All animals had at least a 20-min BD period, a 5-min D period, and a 5-min AD period. Overall, the recordings of five zooxanthellate (specimens S1–S5) and five apozooxanthellate (specimens A1–A5) anemones were analyzed. One of the zooxanthellate anemones (S2) received two dark periods. For this anemone, the intervals consisting of the before-dark, the first dark and the interdark periods are referred to as S2a, whereas the interdark, second dark and afterdark intervals are referred to as S2b.

The pattern of recorded events was analyzed as follows. Only TCNN and SS2 events that occurred on both electrodes simultaneously were scored. Because SS1 activity was very low, this criterion was relaxed, and events that occurred on only one electrode were included as well. These data were then grouped into sets of events per 15-s interval. The 15-s bin was chosen to decrease random variability and to enhance a pattern observed in the data scored per second. The distribution pattern of the data was determined with the Poisson probability distribution, the index of dispersion, the index of clumping, and Green's index (Ludwig and Reynolds, 1988). To determine the effect of light on the burst rate in the three recording periods (BD, D, AD) a Kruskal-Wallis nonparametric one-way ANOVA, Dunn's Multiple Comparison Test (Zar, 1984), and Spearman Rank Correlation (SAS) were performed for each anemone. The overall activity in the zooxanthellate versus apozooxanthellate anemones was compared with an ANOVA (SAS GLM procedure) and Duncan's Multiple Range Test.

Results

The electrical events in the TCNN, SS1, and SS2 of *A. elegantissima* following an electrical stimulus are shown in Figure 1. Bursts in these three conducting systems have similar appearances to those seen in other anthozoans (McFarlane, 1969, 1982; Shelton, 1982; McFarlane *et al.*, 1988).

Most experimental anemones showed some degree of contraction during the D treatment, which is the usual response to darkness in *A. elegantissima*. The burst rates measured during these experiments were tested to determine whether the activity in the different conducting systems was randomly distributed within the BD, D, and AD treatments. In treatments that were of short length, or where there was little activity, the distribution tended to be random. In all cases where the bursting was not

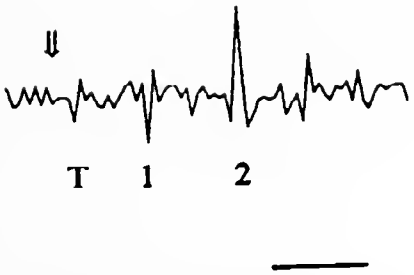

Figure 1. The appearance of activity in the three conducting systems of *Anthopleura elegantissima* after an electrical stimulus given at the arrow. The TCNN is marked by a T, SS1 by a 1, and SS2 by a 2. The scale is 200 ms.

randomly distributed, activity was clumped, as measured by Green's index. There was no apparent relationship between the distribution of the bursts in the conducting systems within the BD, D, and AD treatments and the effect of the light treatment on the burst rates.

The recordings were examined directly so we could determine which conducting system first becomes active after a change in the light treatment. In 6 of 11 cases, a signal from the TCNN was the event first seen when the light was turned off; in the remaining 5 cases an SS2 signal was first (there are 11 dark periods as anemone S2 had two dark periods). In seven cases, a TCNN signal was the first to appear at the beginning of the after-dark period, whereas four cases showed an SS2 pulse first. If an SS2 pulse was seen, it appeared within 2 s of the change in the light condition, but if a TCNN pulse was the first seen, it appeared between 2 and 60 s (and usually closer to 60 s) after the change in the light treatment. SS1 pulses were never seen directly after the light condition changed.

In eight specimens of *A. elegantissima,* a change in burst rate occurred in response to the dark treatment, but the exact effect varied among individuals (Figs. 2–4). Some animals showed an increased burst rate in the dark, whereas others showed a decreased rate. Still other animals had a burst rate in the dark that was different from the BD rate but not the AD rate, and some anemones showed the opposite pattern. Except in the case of anemone A3, to be discussed below, the length of the BD, D, and AD period did not seem to affect the rate changes (Table I). Still, although there is no single obvious trend in the time of occurrence, the rate change was clearly due in some manner to the change in illumination.

All five of the zooxanthellate (S1–S5) and three (A3–A5) of the apozooxanthellate specimens of *A. elegantissima* showed a statistically significant change in burst rate due to changes in illumination (Table II), although the system in which the change was seen varied among individuals. In seven anemones, a significant difference in burst rate within SS2 was attributable to the dark interval

Table I

Duration (min) of the Before Dark, Dark, and After Dark intervals

Anemone #	BD	D	AD	Total (min)
S1	25.00	5.00	5.00	30.00
S2a	31.00	6.00	10.00	47.00
S2b	10.00	5.00	15.26	67.26
S3	30.55	6.00	20.07	57.02
S4	30.31	7.00	9.43	47.14
S5	40.44	5.00	13.25	59.19
A1	31.10	6.00	18.56	57.06
A2	19.02	5.00	24.00	48.02
A3	24.48	20.00	10.00	54.48
A4	22.55	5.00	19.59	47.54
A5	34.00	5.00	20.00	59.03

(Fig. 2); in four of these anemones a significant difference in burst rate occurred within the TCNN as well (Fig. 3). In darkness, one anemone (A3) had a significant change in burst rate in the TCNN only (Fig. 3), and one anemone (S1) had a significant difference in burst rate within SS2, the TCNN, and SS1 (Figs. 2–4). The latter was the only anemone in which a significant change in burst rate due to the darkness was found in the SS1; this anemone had no SS1 bursts in the after-dark period, which may explain this finding. If the recording period in the AD interval had been longer, there would probably have been an SS1 burst, and then there would not have been a significant difference in frequency of activity in SS1. Two apozooxanthellate anemones (A1 and A2) showed no statistically significant changes in burst rates due to changes in illumination.

Anemone A3 showed a significant difference in burst rate only in the TCNN. The rate during the AD period

Table II

Results of the Kruskal-Wallis ANOVA comparing rates of activity in the BD, D, and AD intervals in each of the conducting systems

Anemone #	TCNN	SS2	SS1
S1	21.40†	22.83†	18.37†
S2	43.36†	42.69†	8.35
S3	10.19○	25.58†	2.98
S4	1.69	14.53•	4.76
S5	3.59	6.43*	2.39
A1	1.25	3.30	1.88
A2	0.91	3.70	0.98
A3	13.81•	0.03	4.12
A4	19.98†	10.73○	2.27
A5	1.09	7.72*	4.53

* $P < 0.05$.
○ $P < 0.01$.
• $P < 0.001$.
† $P < 0.0001$.

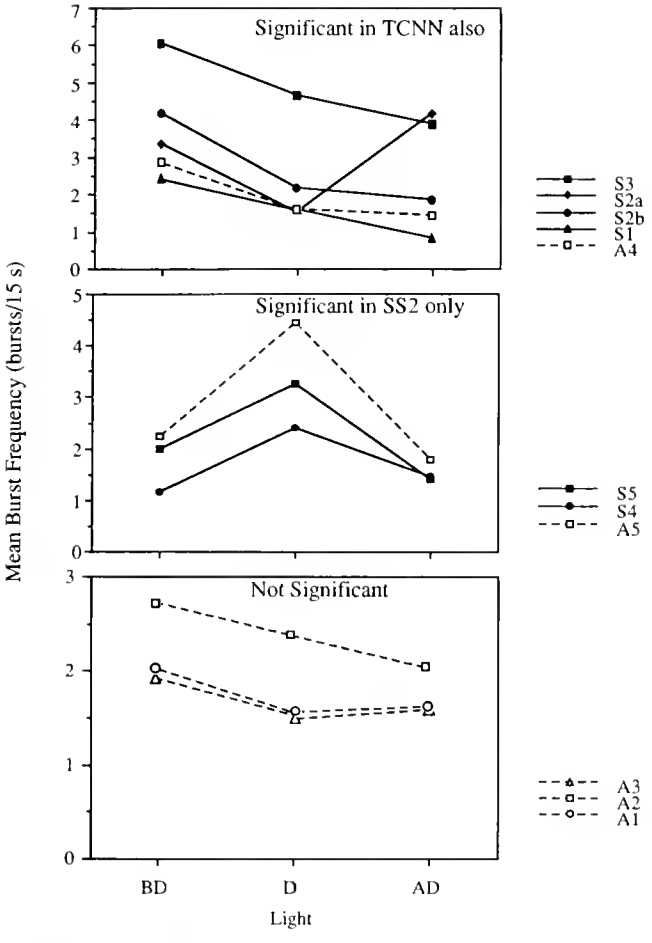

Figure 2. Averages of burst frequency in SS2 of 10 specimens of *Anthopleura elegantissima* during the BD, D, and AD intervals. Anemones are grouped by burst pattern. Those anemones in which there is a significant difference in activity in SS2 and in the TCNN are grouped together in the upper portion of the figure. Anemones in which there is a significant difference in activity only in SS2 are grouped together in the middle portion of the figure. Anemones in which there is no significant difference in activity in SS2 are grouped together in the bottom portion of the figure. Zooxanthellate (S) anemones are indicated by solid lines, and apozooxanthellate (A) anemones are indicated by dashed lines; numbers denote individual specimens. Standard errors are not shown, but range from 5 to 33% of the means.

was significantly lower than those in the BD and D intervals. This anemone had a 20-min dark period, the only dark period longer than 7 min (Table 1). This specimen was the only one to show significance in the TCNN alone. It is interesting that the only anemone having a long dark treatment was the only anemone not to show a significant change in SS2 burst rate resulting from the change in irradiance.

The frequency of activity in the TCNN, SS1, and SS2 is higher in zooxanthellate anemones than in apozooxanthellate individuals ($P < 0.0001$, Duncan's Multiple Range Test). This may be manifested in the greater responsiveness of the zooxanthellate anemones in behavioral studies (unpub. results), and also be related to the greater effect the dark treatment had on the burst rates, because all of the zooxanthellate anemones showed a significant effect of the treatment, whereas only three of the apozooxanthellate anemones did.

The burst rates in the three conducting systems were tested for correlation with each other. Seven anemones (S1, S2, S3, S5, A1, A3, and A4) had activity in the TCNN positively correlated with activity in SS2 ($P < 0.001$). Six anemones (S3, S5, A1, A3, A4, and A5) had activity in the TCNN positively correlated with activity in SS1 ($P < 0.03$), and four anemones (S2, S3, S5, and A1) had SS2 activity positively correlated with activity in SS1 ($P < 0.03$). Anemone A2 was the only one to show no correlation in activity among the conducting systems and no effect of the light treatments on burst rate. One anemone (A1) in which the light treatment did not have an effect

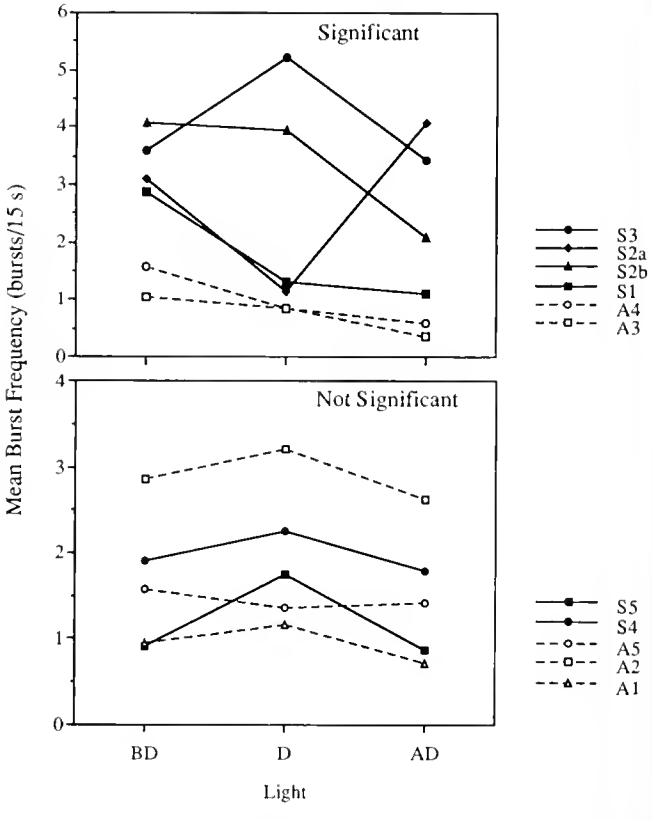

Figure 3. Averages of burst frequency in the TCNN of 10 specimens of *Anthopleura elegantissima* during the BD, D, and AD intervals. Anemones in which there is a significant difference in activity in the TCNN are grouped together in the top portion of the figure, whereas anemones in which there is not a significant difference in activity are grouped together in the bottom portion of the figure. Zooxanthellate (S) anemones are indicated by solid lines, and apozooxanthellate (A) anemones are indicated by dashed lines; numbers denote individual specimens. Standard errors are not shown, but range from less than 1 to 33% of the means.

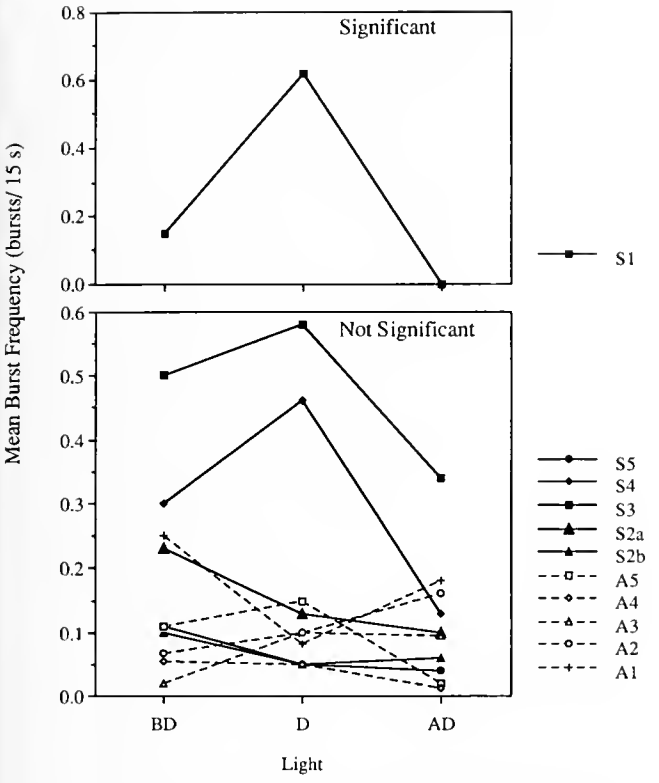

Figure 4. Averages of burst frequency in SS1 of 10 specimens of *Anthopleura elegantissima* during the BD, D, and AD intervals. The anemone in which there is a significant difference in activity in SS1 is shown in the top portion of the figure, whereas anemones in which there is not a significant difference in activity in SS1 are grouped together in the bottom portion of the figure. Zooxanthellate (S) anemones are indicated by solid lines, and apozooxanthellate (A) anemones are indicated by dashed lines; numbers denote individual specimens. Standard errors are not shown, but range from 2 to 100% of the means.

on burst rate did show correlation in activity among all three conducting systems. This anemone (A1) and the anemones S3 and S5 were the only individuals that showed correlation in activity among all the conducting systems.

Discussion

Because we never observed pulses in the ectodermal SS1 of *Anthopleura elegantissima* in response to a light-dark change, our results support the endodermal locus of the light response noted by Batham and Pantin (1950a, 1954) and by Marks (1976) in other species of anemones. McFarlane (1983) noted that SS1 is not spontaneously active in *C. parasitica*. This observation also pertains to *A. elegantissima*, where SS1 pulses were rare (Fig. 4). The number of recorded SS1 pulses may even have been artifactually high owing to the recording method, because some pulses recorded by only one electrode were classified as SS1. Because SS1 is not spontaneously active in *A. elegantissima* and is not activated by a change in irradiance, the ectoderm is probably not the site of photoreception in this sea anemone.

When the change in irradiance causes contraction in the anemones, the conducting systems could be involved in three ways: (1) the frequency of activity would increase in the TCNN and decrease in SS2, because SS2 is inhibitory to TCNN pacemaker activity (McFarlane, 1974a, b, 1983; McFarlane *et al.*, 1988; Pickens, 1988); (2) the frequency of activity in the TCNN could remain constant, while the burst rate in SS2 decreased; (3) SS2 activity could remain constant while TCNN activity increased. Any of these would produce a relative reduction of the inhibitory effects of the SS2.

In *A. elegantissima*, when the illumination changed, there was a change in activity in the TCNN and SS2 in some individuals (Figs. 2, 3). The frequency of activity in the TCNN did not increase when SS2 activity decreased (Figs. 2, 3), which would have been expected if the hypothesis were correct that in some way the light change reduces the inhibitory effects of SS2 on the TCNN. The conducting system responsible for initiating the light response cannot be specified because a change in light sometimes induced a pulse from the TCNN first and sometimes a pulse from SS2 first.

The large individual variation in the response of the conducting system to irradiance changes seems paradoxical. The change in irradiance obviously affected the anemones as they would often contract during the dark period and so pull off the suction electrodes. The recordings presented here may therefore be biased toward less responsive individuals because the data are from anemones that did not contract fully during the dark period.

The response to light itself is also difficult to explain. If a change in activity in the TCNN or SS2 is carrying the information regarding conditions of illumination, then the change in rate of activity should always be in the same direction. This was not the case, suggesting again that the data presented here are of necessity from anemones that did not fully contract, *i.e.*, those that may have perceived the change but failed to respond to it. This would argue that the TCNN and SS2 are not involved in the initial response to light.

In *C. parasitica*, SS2 activity can be triggered by endodermal sensory cells that detect stress between opposing muscle groups; as a muscle field contracts, SS2 activity is enhanced. This would act as a control over contraction (Batham *et al.*, 1960; McFarlane, 1974b). Spontaneous, or inherent, contractions are not always accompanied by activity in the TCNN in *C. parasitica*. These inherent contractions may result from activity in a local nerve net, and it is this local system that may integrate information from the sensory cells (McFarlane, 1974a, b).

Photoreception in *A. elegantissima* may occur in a sensory cell of a local neuronal network. This photoreceptive sensory cell could be directly connected to the muscles responsible for slow contraction. This local neuronal network might be similar to the one revealed by fluorescent antibodies to Antho-RFamide I and II in *C. parasitica* (Grimmelikhuijzen *et al.*, 1989) and by immunogold-labeling of the tentacular nerve plexus in *Anthopleura elegantissima* (Westfall and Grimmelikhuijzen, 1993). Thus light would affect the muscles of sea anemones without initially involving either the TCNN or SS2. Alternatively, the muscles themselves may be directly photosensitive. Batham and Pantin (1954) believed that the parietal muscles of *Metridium senile* were sensitive to light, although these authors were unable completely to separate the muscular response from possible sensory components. Marks (1976) determined that the parietal and circular muscles of *Calamactis praelongus* were locally sensitive to light. With strong stimuli, pacemakers of the nerve net were activated. This is similar to what is proposed for *A. elegantissima*. Light is perceived by sensory cells that are connected to muscles, or the light is perceived by the muscles themselves; if sufficient stimulus reaches the muscles, their tension changes, which subsequently alters the activity of the TCNN or SS2.

The effect of irradiance on the frequency of activity in the conducting systems of *A. elegantissima* may depend on the behavioral state of the anemone. Batham and Pantin (1950a, b) have noted that *Metridium senile* has distinct phases of spontaneous or inherent activity. The anemone's response to an external stimulus may depend on its behavioral phase. McFarlane (1973, 1983) has noted similar behavior in *C. parasitica*. No previous electrophysiological recordings investigating long-term behavioral patterns of *A. elegantissima* have been reported. As in *C. parasitica*, inherent activity in *A. elegantissima* is probably used to maintain body shape, and external stimuli are coded by changes in activity in the relevant conducting system. The direction and degree of change may depend on the prevailing behavioral phase of the anemone and on the strength of the stimulus.

The conducting systems in zooxanthellate specimens of *A. elegantissima* are much more active than those in apozooxanthellate conspecifics (Figs. 2, 3, 4) and also more active than those in azooxanthellate *C. parasitica* (*cf.* McFarlane, 1973). Greater activity in zooxanthellate *A. elegantissima* may reflect the extra sensory information that these animals are receiving from their algal endosymbionts. Electrophysiological responses to, *e.g.*, oxygen were not investigated, but these animals are sensitive to it (Pearse, 1974a, b; Fredericks, 1976; Shick and Brown, 1977). Certainly the internal P_{O_2} of zooxanthellate specimens of *A. elegantissima* can change quickly (Dykens and Shick, 1982). This added stimulation may be reflected in the higher activity levels in the conducting systems of the zooxanthellate specimens.

The electrophysiologically defined conducting systems (SS1, SS2, and TCNN) in sea anemones are responsible for coordinating a variety of behaviors, and each system has several different roles. SS2, for example, helps coordinate the rhythm of expansion and contraction, chemically induced shell climbing, feeding activity involving chemoreception, and tentacle movement (McFarlane and Lawn, 1972; McFarlane, 1974a, b, 1975, 1983; Boothby and McFarlane, 1986). These three conducting systems may be more global (McFarlane, 1984; McFarlane *et al.*, 1988) than the low-level, local systems that respond directly to every sensory input. Rather, these global conducting systems integrate and coordinate behavioral responses resulting from local perception of manifold sensory stimuli.

This investigation differs from other electrophysiological studies on sea anemones in the method of data collection and analysis. Storing the data on magnetic media allowed for a lengthy study of the electrical pulses in the three conducting systems. The statistical analysis of these data was an attempt to reveal the overall pattern of activity in response to a change in irradiance, rather than the minute-to-minute changes, which are highly variable. This is not the first attempt to examine and quantify long-term electrophysiological recordings of sea anemones (see McFarlane, 1973), but the method is more quantitative and may prove useful in future studies.

Acknowledgments

We thank Drs. P. A. V. Anderson, L. Kass, and D. McElroy for their help with the electrophysiology and the statistical analysis. This research was supported in part by NSF grant DCB-8509487 (Regulatory Biology Program) to J. M. Shick, and a grant from the Association of Graduate Students, University of Maine, to S. J. Sawyer.

Literature Cited

Batham, E. J., and C. F. A. Pantin. 1950a. Phases of activity in the sea-anemone, *Metridium senile* (L.), and their relation to external stimuli. *J. Exp. Biol.* **27:** 377–399.

Batham, E. J., and C. F. A. Pantin. 1950b. Inherent activity in the sea-anemone, *Metridium senile*. *J. Exp. Biol.* **27:** 290–301.

Batham, E. J., and C. F. A. Pantin. 1954. Slow contraction and its relation to spontaneous activity in the sea-anemone *Metridium senile* (L.). *J. Exp. Biol.* **31:** 84–103.

Batham, E. J., C. F. A. Pantin, and E. A. Robson. 1960. The nerve-net of the sea-anemone *Metridium senile*: the mesenteries and the column. *Q. J. Microsc. Sci.* **101:** 487–510.

Boothby, K. M., and I. D. McFarlane. 1986. Chemoreception in sea anemones: Betaine stimulates the pre-feeding response in *Urticina eques* and *U. felina*. *J. Exp. Biol.* **125:** 385–389.

Dykens, J. A., and J. M. Shick. 1982. Oxygen production by endosymbiotic algae controls superoxide dismutase in their animal host. *Nature* **297:** 579–580.

Fautin, D. G., and R. N. Mariscal. 1991. Cnidaria: Anthozoa. Pp. 267–358 in *Microscopic Anatomy of Invertebrates Vol. 2. Placozoa, Porifera, Cnidaria, and Ctenophora*, F. W. Harrison and J. A. Westfall, eds. Wiley-Liss, Inc., New York.

Fleure, H. J., and C. L. Walton. 1907. Notes on the habits of some sea anemones. *Zool. Anz.* **31:** 212–220.

Fredericks, C. A. 1976. Oxygen as a limiting factor in phototaxis and in intraclonal spacing of the sea anemone *Anthopleura elegantissima*. *Mar. Biol.* **38:** 25–28.

Grimmelikhuijzen, C. J. P., D. Graff, and I. D. McFarlane. 1989. Neurons and neuropeptides in coelenterates. *Arch. Histol. Cytol.* **52:** 265–278.

Josephson, R. K. 1966. Neuromuscular transmission in a sea anemone. *J. Exp. Biol.* **45:** 305–319.

Ludwig, J. A., and J. F. Reynolds. 1988. *Statistical Ecology: A Primer on Methods and Computing*. John Wiley & Sons, New York. 337 pp.

Marks, P. S. 1976. Nervous control of light responses in the sea anemone, *Calamactis praelongus*. *J. Exp. Biol.* **65:** 85–96.

McFarlane, I. D. 1969. Two slow conducting systems in the sea anemone *Calliactis parasitica*. *J. Exp. Biol.* **51:** 377–385.

McFarlane, I. D. 1973. Spontaneous electrical activity in the sea anemone *Calliactis parasitica*. *J. Exp. Biol.* **58:** 77–90.

McFarlane, I. D. 1974a. Excitatory and inhibitory control of inherent contractions in the sea anemone *Calliactis parasitica*. *J. Exp. Biol.* **60:** 397–422.

McFarlane, I. D. 1974b. Control of the pacemaker system of the nerve-net in the sea anemone *Calliactis parasitica*. *J. Exp. Biol.* **61:** 129–143.

McFarlane, I. D. 1975. Control of mouth opening and pharynx protrusion during feeding in the sea anemone *Calliactis parasitica*. *J. Exp. Biol.* **63:** 615–626.

McFarlane, I. D. 1982. *Calliactis parasitica*. Pp. 243–265 in *Electrical Conduction and Behaviour in 'Simple' Invertebrates*, G. A. B. Shelton, ed. Clarendon Press, Oxford.

McFarlane, I. D. 1983. Nerve net pacemakers and phases of behavior in the sea anemone *Calliactis parasitica*. *J. Exp. Biol.* **104:** 231–246.

McFarlane, I. D. 1984. Nerve nets and conducting systems in sea anemones: Two pathways excite tentacle contractions in *Calliactis parasitica*. *J. Exp. Biol.* **108:** 137–149.

McFarlane, I. D., D. Graff, and C. J. P. Grimmelikhuijzen. 1988. Evolution of conducting systems and neurotransmitters in the Anthozoa. Pp. 111–140 in *Evolution of the First Nervous Systems*, P. A. V. Anderson, ed. Plenum Press, New York.

McFarlane, I. D., and I. D. Lawn. 1972. Expansion and contraction of the oral disc in the sea anemone *Tealia felina*. *J. Exp. Biol.* **57:** 633–649.

North, W. J. 1956. Sensitivity to light in the sea anemone *Metridium senile* (L.). II. Studies of reaction time variability and the effects of changes in light intensity and temperature. *J. Gen. Physiol.* **10:** 715–733.

North, W. J., and C. F. A. Pantin. 1958. Sensitivity to light in the sea anemone *Metridium senile* (L.): adaptation and action spectra. *Proc. R. Soc. London, B* **148:** 385–396.

Parker, G. H. 1918. Actinian behavior. *J. Exp. Zool.* **22:** 193–229.

Pearse, V. B. 1974a. Modification of sea anemone behavior by symbiotic zooxanthellae: expansion and contraction. *Biol. Bull.* **147:** 641–651.

Pearse, V. B. 1974b. Modification of sea anemone behavior by symbiotic zooxanthellae: phototaxis. *Biol. Bull.* **147:** 630–640.

Pickens, P. E. 1988. Systems that control the burrowing behavior of a sea anemone. *J. Exp. Biol.* **135:** 133–164.

Robson, E. A., and R. K. Josephson. 1969. Neuromuscular properties of mesenteries from the sea-anemone *Metridium*. *J. Exp. Biol.* **50:** 151–168.

Shelton, G. A. B. 1982. Anthozoa. Pp. 203–242 in *Electrical Conduction and Behaviour in 'Simple' Invertebrates*, G. A. B. Shelton, ed. Clarendon Press, Oxford.

Shick, J. M. 1991. *A Functional Biology of Sea Anemones*. Chapman & Hall, London. 395 pp.

Shick, J. M., and W. I. Brown. 1977. Zooxanthellae-produced oxygen promotes sea anemone expansion and eliminates oxygen debt under environmental hypoxia. *J. Exp. Zool.* **201:** 149–155.

Westfall, J. A., and C. J. P. Grimmelikhuijzen. 1993. Antho-RFamide immunoreactivity in neuronal synaptic and nonsynaptic vesicles of sea anemones. *Biol. Bull.* **185:** 109–114.

Zahl, P. A., and J. A. McLaughlin. 1959. Studies in marine biology. IV. On the role of algal cells in the tissues of marine invertebrates. *J. Protozool.* **6:** 344–352.

Zar, J. H. 1984. *Biostatistical Analysis*. Prentice-Hall, Inc. New Jersey. 718 pp.

Reference: *Biol. Bull.* **186**: 202–212. (April, 1994)

Changes Occur in the Central Nervous System of the Nudibranch *Berghia verrucicornis* (Mollusca, Opisthobranchia) During Metamorphosis

DAVID J. CARROLL[1] AND STEPHEN C. KEMPF

Department of Zoology and Wildlife Science, 331 Funchess Hall, Auburn University, Auburn, Alabama 36830

Abstract. The structure of the larval and juvenile central nervous system (CNS) in *Berghia verrucicornis*, an aeolid nudibranch, was examined using 1-μm serial sections. The CNS consists of paired optic, cerebral, pleural (also known as sub- and supra-intestinal ganglia), pedal, and buccal ganglia, and a single visceral ganglion. A pleurovisceral loop is present. The organization of the CNS changes as the nudibranch undergoes metamorphosis. In general, there is a condensation of the CNS. The cerebral and pleural ganglia fuse to form the prominent cerebropleural ganglia. The single visceral ganglion fuses with the pleural portion of the left cerebropleural ganglion. The buccal ganglia enlarge and fully organize into a cortex of nerve cell bodies and medulla of nerve fibers. Rhinophoral ganglia develop anterior to each cerebropleural ganglion and a pair of nervous processes extend from each: one to the developing rhinophore and the other anteroventral toward the mouth and associated structures. These metamorphic changes are similar to those seen in other commonly studied opisthobranch species, suggesting that *Berghia verrucicornis* is an appropriate model for the developmental examination of structure and function in molluscan nervous systems.

Introduction

The use of opisthobranch mollusks for the investigation of neurobiological questions as diverse as the differentiation of neurons (Schacher *et al.*, 1979; McAllister *et al.*, 1983; Schacher, 1983; Bulloch, 1985), the connections between specific, individual neurons (Kandel *et al.*, 1967; Schacher, 1983), and the function of neurotransmitters during neurodevelopment (Goldberg and Kater, 1989) has contributed to our knowledge of the organization of neuronal systems. Opisthobranchs possess several unique features that make them useful as neural models. For instance, the relative simplicity of the nervous system and the accessibility of their neuron perikarya make opisthobranchs exceedingly convenient models for correlating animal behavior with nervous activity, as well as for delving into the cellular and molecular mechanisms driving the development and function of the nervous system (see Willows, 1971, 1973; Nagle *et al.*, 1989a, b; Baux *et al.*, 1990; Bedian *et al.*, 1991; Hickmott and Carew, 1991; Ziv *et al.*, 1991). Also, the fact that some aspects of the organogenesis of the molluscan central nervous system (CNS) resemble those of the vertebrate peripheral nervous system (PNS) may enable investigators to draw parallels between the ontogeny of the easily studied opisthobranch CNS and the more complex vertebrate PNS (Jacob, 1984; Bulloch, 1985; Cash and Carew, 1989).

In the past, to fully exploit opisthobranch mollusks as neurobiological models, it was necessary to devise protocols for maintaining the nudibranchs in the laboratory throughout their life cycle or to obtain the appropriate stage animal from the field as needed. A number of attempts at culturing these organisms in the laboratory have been successful (Kriegstein *et al.*, 1974; Bridges, 1975; Harris, 1975; Kempf and Willows, 1977; Switzer-Dunlap and Hadfield, 1977; Bickell [=Page] and Kempf, 1983; Paige, 1988); however, such culture work has been essentially limited to marine laboratories

Received 13 September 1992; accepted 24 January 1994.

[1] Present address: Department of Physiology, University of Connecticut Health Center, Farmington, Connecticut 06030.

Abbreviations: CNS = central nervous system; MFSA = Millipore-filtered (0.45 μm), seasoned, aquarium water; PNS = peripheral nervous system.

where fresh seawater and prey organisms are readily available.

Berghia verrucicornis is suitable for culture in inland laboratories because it has lecithotrophic larvae (the larvae derive energy from endogenous yolk reserves), it does not require a specific metamorphic inducer, and it feeds on the coelenterate *Aiptasia pallida,* a species amenable to laboratory culture (Hessinger and Hessinger, 1981). Thus, we are able to rear and maintain this nudibranch through successive generations at our inland laboratory by using artificial seawater and relatively simple techniques (Carroll and Kempf, 1990).

In this paper, as a prelude to the use of this species in neurodevelopmental studies, we describe the neuromorphology of two stages in the life history of *B. verrucicornis:* the veliger larval stage and the prefeeding juvenile stage. These stages occur approximately 12 and 14 days after oviposition at 22°C. The larval stage was chosen for examination because it represents the most developed stage in the CNS before metamorphosis. The prefeeding juvenile stage was selected to assess changes that occur in the gross neuromorphology of the CNS during and just after metamorphosis.

Materials and Methods

Animal culture

Animals were cultured according to the methods of Carroll and Kempf (1990). Briefly, adult nudibranch pairs were kept in bowls of Millipore-filtered (0.45 μm), seasoned aquarium water (MFSA) and fed the sea anemone *Aiptasia pallida* as needed. The culture bowl and MFSA were changed daily. Newly layed egg masses were removed to aerated egg mass cultures containing 300 ml of MFSA. Upon hatching from the egg mass, larvae were transferred to a metamorphosis culture dish containing several tiny *A. pallida.* Individual larvae began to metamorphose as soon as 1 day after hatching, and most of the larvae had reached the juvenile stage by 5 days after hatching. Juveniles began feeding soon after metamorphosis (3–5 days) and reached adulthood (indicated by the laying of their first egg mass) approximately 60 days after oviposition.

For culture or histological examination, veliger larvae were collected either by mechanically disrupting the egg mass at 11 days after oviposition or by concentrating larvae that had already hatched. One-day postmetamorphic individuals were gathered directly from the metamorphosis cultures. These two stages were then treated as described below.

Fixation and histological examination of pre- and postmetamorphic stages

Larvae and juveniles were relaxed in a 1:3 mixture of seawater and a saturated solution of chlorobutanol in MFSA. The specimens were fixed for 1 h in a primary fixative of 2.5% glutaraldehyde in 0.2 *M* Millonig's phosphate buffer and 0.14 *M* NaCl. Larval shells were decalcified by one of two methods: (1) before fixation, live larvae were treated with 2-[N-morpholino] ethanesulfonic acid (MES) in MBL artificial seawater according to the methods of Pennington and Hadfield (1989), or (2) after primary fixation, the larvae were placed into a 1:1 solution of 10% sodium-ethylenediaminotetraacetic acid (Na-EDTA) and primary fixative. Following primary fixation and decalcification, the specimens were rinsed in buffer and then secondarily fixed in a solution of 2% osmium tetroxide in 1.25% sodium carbonate buffer. After secondary fixation, specimens were washed in 1.25% sodium carbonate buffer and then dehydrated through an ethanol series to 100% propylene oxide before being infiltrated with a Poly/Bed 812-propylene oxide mixture and embedded in pure Poly/Bed 812 (Polysciences). The specimens were embedded in flat dishes by spreading them in a thin layer of plastic and curing overnight at 60°C. They were then cut out of the plastic mold and glued to metal studs for sectioning.

Serial sections of 1 μm were cut on a Reichart ultramicrotome, mounted on gelatin-coated glass slides, and stained with methylene blue-Azure II (Richardson *et al.,* 1960) or 1% Thionin in distilled water.

Ganglia and connective designations

Precise ganglia designations have proven extremely difficult in light of recent investigations by Page (1992a, b). Historically, the opisthobranch larval CNS has been described as a circumenteric ring consisting of the paired cerebral, pedal, and pleural ganglia linked by connectives around the esophagus (see Dorsett, 1986). A pair of buccal ganglia also exist in this region and are connected to the cerebral ganglia via the cerebrobuccal connectives. Extending from the pleural ganglia is a pleurovisceral loop that runs posterolateral, extending to the supraintestinal (right) and subintestinal (left) ganglia, and to the single visceral ganglion. In some opisthobranch larvae, the parietal ganglia are between the pleural and intestinal ganglia; in a few opisthobranchs, another ganglion, the osphradial, has been described as connected to the supraintestinal ganglion but outside of the pleurovisceral loop (Kriegstein, 1977; Page, 1992a). Metamorphosis entails an alteration in the CNS of opisthobranchs. In the anaspid *Aplysia californica,* the connectives lengthen and spread the ganglia further apart (Kriegstein, 1977). The opposite has been true for nudibranchs in which the cerebral and pleural ganglia fuse to form the large cerebropleural ganglia and the pleurovisceral loop shortens (Thompson, 1958, 1962; Tardy, 1970, 1974; Bonar and Hadfield, 1974; Kriegstein, 1977; Bonar, 1978). The above "blueprint"

of the opisthobranch CNS has arisen from histological studies on a variety of species.

Recently, Page (1992a, b) suggested a reinterpretation of the opisthobranch nervous system based upon an ultrastructural study of several stages in the life cycle of the nudibranch *Melibe leonina*. Ganglia were identified by comparing the placodal origin of their constituent neurons to those described for ganglia of developing prosobranchs. Using this approach, Page described a CNS that differs considerably from the generally accepted nudibranch plan. The cerebral ganglia of larval *M. leonina* are linked to the fused pleuropedal ganglia in the larval foot via two connectives: the cerebropedal and the cerebropleural. The visceral loop arises directly from the cerebral ganglia and consists of the supraintestinal ganglion (on the right, this may actually contain the parietal ganglion also), the osphradial ganglion (which lies outside the visceral loop but is connected to the supraintestinal ganglion), the subintestinal ganglion (on the left), and the single visceral ganglion. The novel notion in this interpretation is that the pleural ganglion lies outside of the visceral loop, and it fuses with the pedal ganglion in the larva. Metamorphosis in *M. leonina* also entails fusion of the constituent ganglia and incorporation of the visceral loop components into the cerebral ganglia. In this interpretation (Page, 1992a, b), the subintestinal and visceral ganglia fuse with the left cerebral ganglion and the supraintestinal ganglion fuses with the right cerebral ganglion, creating the left and right cerebroabdominal ganglia.

The data presented in the two Page studies (1992a, b) support her conclusions fully; however, the idea that ganglion designations based upon comparison to ectodermal ingression sites for developing prosobranch ganglia apply to all opisthobranchs is premature. Indeed, the fact that the pleural ganglion lies within the visceral loop of the CNS in some prosobranch adults lends some uncertainty to the global applicability of this scheme (Graham, 1985).

For the purposes of this study, we have chosen to remain with the classical designations for the components of the *B. verrucicornis* CNS for three reasons. First, the nomenclature used in the classical scheme is based upon studies of many opisthobranch species, and while it is true that the descriptions differ in some details, the basic layout provides ganglion identifications that will be familiar to most investigators. Second, the new interpretation by Page (1992a, b) introduces a novel concept (*i.e.*, the pleural ganglia are separate from the visceral loop) that, although supported by seemingly convincing evidence, has not yet become the accepted model for the opisthobranch CNS. Third, our primary purpose in this paper is to introduce *B. verrucicornis* as an appropriate model for future neurodevelopmental studies.

Measurements

Three measurements were made to determine whether the CNS of *B. verrucicornis* condensed during metamorphosis. These measurements were (1) the distance from the most anterior point of the organism to the most posterior aspect of the pleural ganglion divided by the total length of the same organism (Pd); (2) the length of the cerebropleural connective along the anterior-posterior axis; and (3) the distance from the most anterior aspect of the cerebral ganglion to the most posterior aspect of the pleural ganglion (AC-PP). The ganglia measured were those on the left side in both larvae and juveniles. A Student's *t*-test was used to determine any difference between the means at the 95% confidence level.

Results

Life history of Berghia verrucicornis

B. verrucicornis adults lay their egg masses as spirals containing several hundred embryos. The embryos develop and obtain the appearance of competence (*e.g.*, eyespots, retracted mantle, propodium) within the egg mass. Hatching occurs 11–12 days after oviposition, and the lecithotrophic larvae spend 1–5 days as swimming veligers. Larvae of *B. verrucicornis* are lecithotrophic and are competent to metamorphose as early as 1 day after they hatch. As the larvae approach metamorphosis, they generally settle to the bottom of the culture dish and attach to the substratum. Metamorphosis entails, in gross morphological terms, the loss of the larval shell and velum, as well as a reorganization of the general body plan (Fig. 1). Adulthood is attained approximately 60 days after oviposition. For a more complete description of the life history of this species, see Carroll and Kempf (1990).

Larval nervous system

At hatching, the larvae of *B. verrucicornis* possess all of the major ganglia commonly described (see *Ganglia and connective designations*, Materials and Methods) in competent nudibranch larvae (Thompson, 1958, 1962; Bickell [=Page] and Chia, 1979; Bickell [=Page] and Kempf, 1983; Kempf *et al.*, 1987; Page, 1992a, b). These ganglia are paired, with the exception of the single visceral ganglion, and have a cortex of nerve cell bodies and a medulla of nerve fibers (neuropil). The largest at hatching are the cerebral ganglia, located dorsal to the statocysts (Fig. 2a). Nerve fibers pass medially out of each cerebral ganglion to become part of the cerebral commissure that connects the left and right cerebral ganglia dorsal to the esophagus (Fig. 2b).

The cerebral ganglia are joined, via connectives, to at least three other pairs of ganglia: the optic, pedal, and pleural. Anterodorsal to the cerebral ganglia are the de-

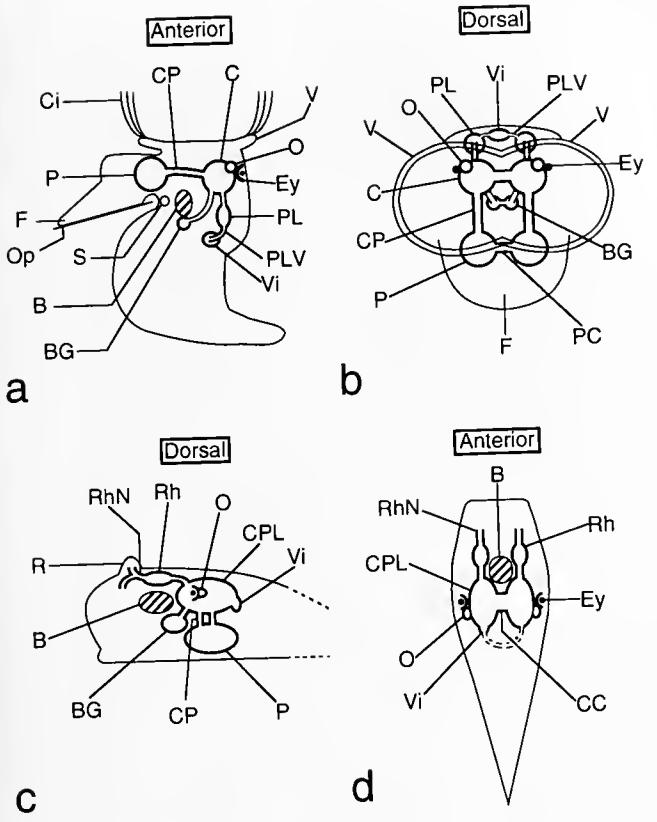

Figure 1. Schematic diagram of the veliger larva and prefeeding juvenile of *Berghia verrucicornis* showing the spatial relationship of the CNS to various larval and juvenile structures. (a) Sagittal view of the larva's left side. In the larva, the cerebral and pleural ganglia are discrete structures that are linked by the cerebropleural connective. The visceral ganglion lies near the midline of the larva and is connected to the left pleural ganglion by the pleurovisceral loop. The shell, which covers the ventral surface of the larva posterior to the foot and the entire dorsal surface, has been omitted in the drawing. The buccal ganglia lie posterior to the buccal mass. (b) Transverse view of the anterior end of the larva shown in (a). The buccal, cerebral, optic, pedal, and pleural ganglia are viewed through the velum. The visceral ganglion is depicted dorsal to the velum in this drawing. The portion of the pleurovisceral loop connecting the right pleural ganglion to the visceral ganglion is assumed to be present, but was not clearly discernible in 1-μm sections. (c) Sagittal view of the left side of a prefeeding juvenile. In the juvenile, the cerebral and pleural ganglia are fused to form the cerebropleural ganglia. As indicated, the visceral ganglion is tightly associated with the left cerebropleural ganglion at this stage and later will be completely incorporated into the left cerebropleural ganglion. The cerebropleural ganglia have now receded posterior to the buccal mass and new ganglia, the rhinophoral ganglia, have appeared between the cerebropleural ganglia and the anterior epidermis. Each buccal ganglion is now notably larger than it appeared in the larva. The dotted lines at the posterior end of the juvenile represent its body as it tapers towards the tail. (d) Frontal view from the dorsal surface of the juvenile. As noted above, the visceral ganglion has become tightly associated with the left cerebropleural ganglion. The pleurovisceral loop is assumed to extend to the right cerebropleural ganglion, but could not be traced along its entire length in 1-μm sections. B = buccal mass; BG = buccal ganglion; C = cerebral ganglion; CC = cerebral commissure; Ci = velar cilia; CP = cerebropedal connective; CPL = cerebropleural ganglion; Ey = eyespot; F = foot; O = optic ganglion; Op = operculum; P = pedal ganglion; PC = pedal commissure; PL = pleural ganglion; PLV = portion of the pleurovisceral loop; R = rhinophore; Rh = rhinophoral ganglion; RhN = rhinorphoral nerve; S = statocyst; V = velum; Vi = visceral ganglion.

veloping optic ganglia. Located lateral, and a little posterior, to each optic ganglion, are eyespots consisting of a pigmented retina and spherical lens. Ventral to the cerebral ganglia, the cerebropedal connectives pass anterior to the statocysts and join the pedal ganglia in the most dorsal portion of the larval foot (Fig. 2a). The pedal ganglia, consisting of a well-developed cortex and neuropil, are directly ventral to the statocysts and are connected to each other via the pedal commissure.

Immediately posterior to their respective left and right cerebral ganglia are the left and right pleural ganglia (Fig. 2c). Nerve fibers from the cerebral neuropils pass posterior through a short cerebropleural connective to their respective pleural ganglia. A connective between the pleural and pedal ganglia in the larva was not clearly discernible in our sections. Continuing posterior from the left and right pleural ganglia are connectives that run posteromedially to the single visceral ganglion (Fig. 2d) to complete the pleurovisceral loop. The visceral ganglion is located along the midline of the larva, immediately anterior to the visceral mass.

The fifth pair of ganglia in *B. verrucicornis* larvae are the buccal ganglia. These are located to the left and right of the developing buccal mass and medioventral to the pleural ganglia. Presumably, these ganglia are linked to the cerebral ganglia, although we have not positively identified these connectives in the larva. The buccal commissure connects the left and right buccal ganglia posterior to the buccal mass.

The postmetamorphic central nervous system

Changes in the postmetamorphic nervous system are most evident in the fusion of the ganglia and the corresponding condensation of the CNS (see below). The cerebral and pleural ganglia are fused into a single, large cerebropleural ganglion on both the left and right sides of the juvenile (Fig. 3a, b). The left and right cerebropleural ganglia are joined to their respective pedal ganglia via two connectives. Each connective appears to join a *distinct* neuropil in the cerebropleural ganglia; presumably these are the neuropils of the cerebral and pleural ganglia that are still undergoing the process of fusion. We consider the anterior connective on each side to be the cerebropedal connective and the posterior connective to be the pleuropedal connective. All the paired ganglia become more spherical than they are in the larval stage. The relative position of the optic ganglia, with respect to the eyespots and the cerebropleural ganglia, changes during metamorphosis. These ganglia are located anterolateral to the cerebral ganglia and immediately posterior to the eyespots in the postmetamorphic central nervous system.

New structures appear in the postmetamorphic nervous system. As mentioned above, the pleuropedal connectives

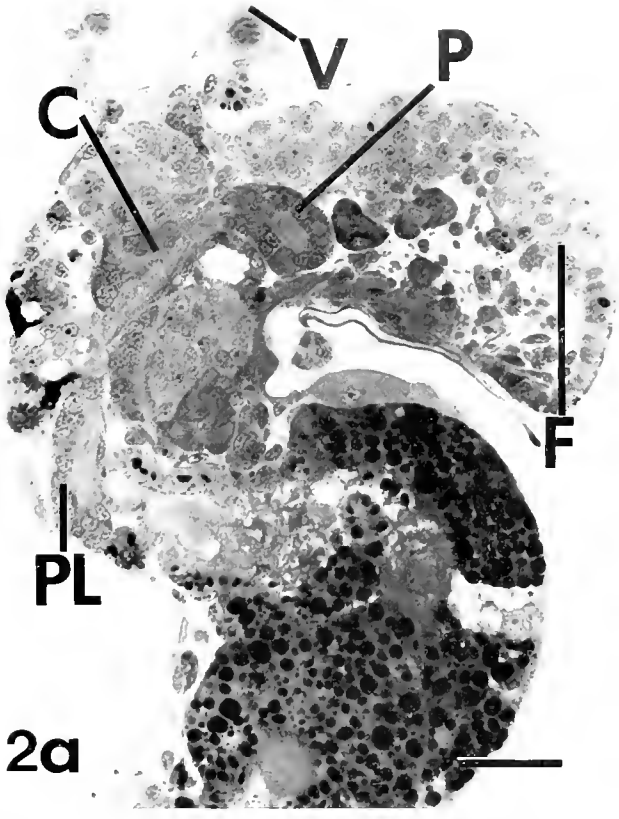
V
P
C
F
PL
2a

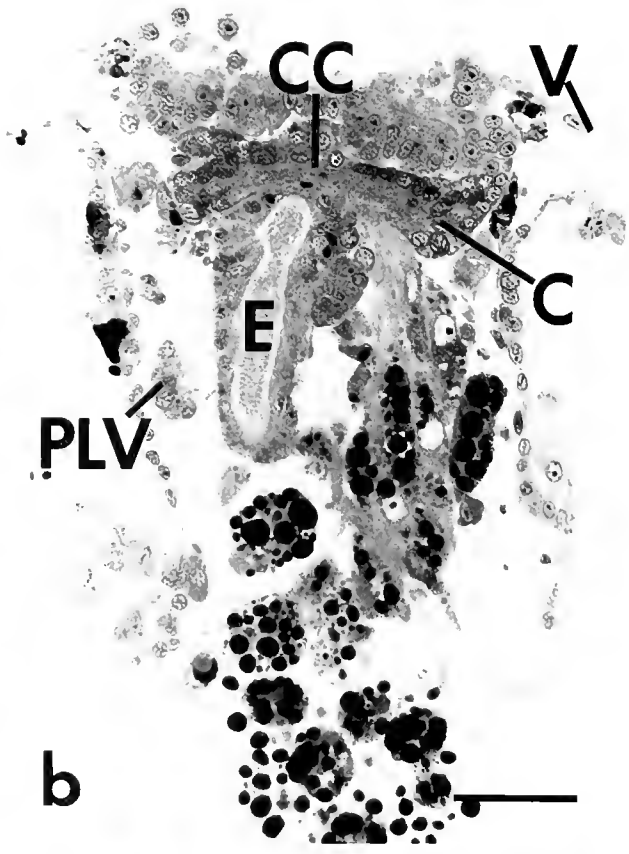
CC
V
C
E
PLV
b

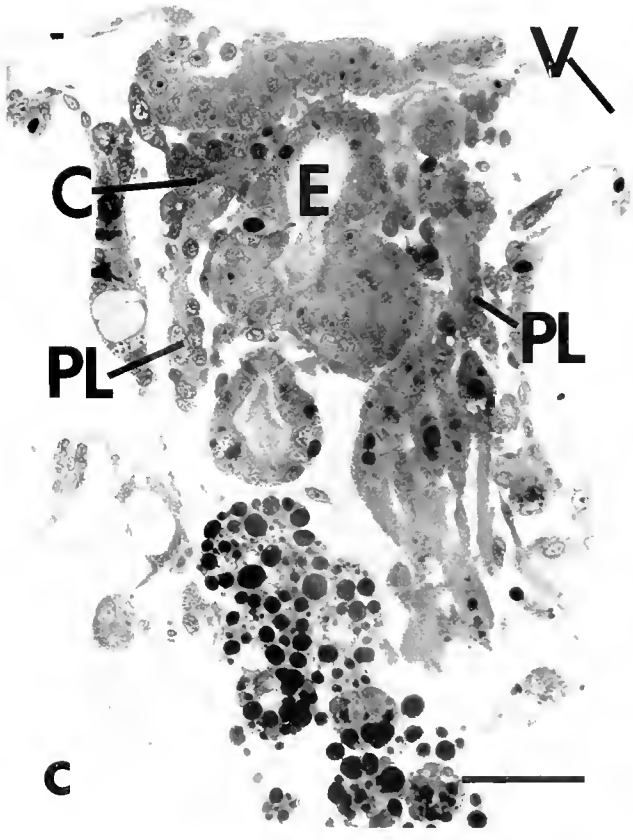
V
C
E
PL
PL
c

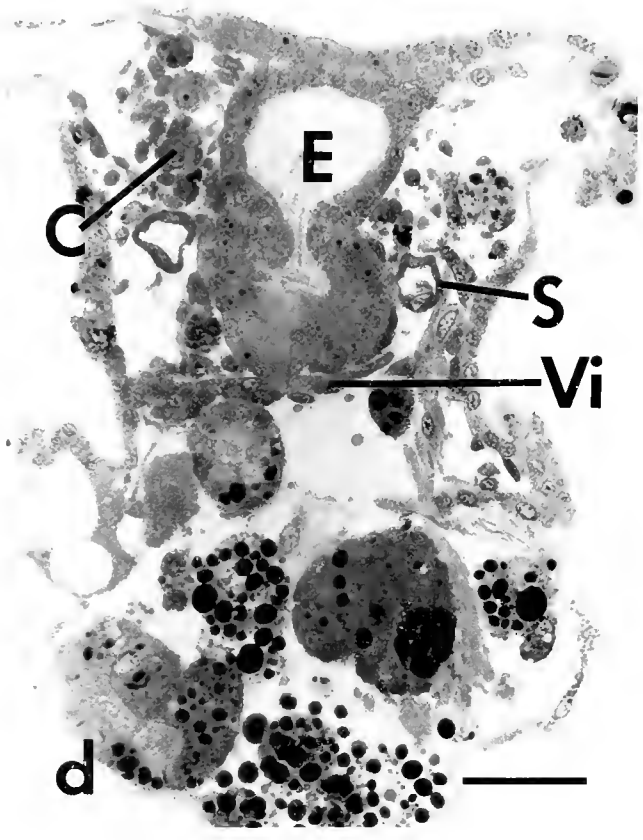
E
C
S
Vi
d

are now visible just anterior to the statocysts linking the pleural portion of the cerebropleural ganglia to the pedal ganglia. The cerebrobuccal connectives are now apparent, passing ventrally from each cerebropleural ganglion to its respective buccal ganglion. The buccal ganglia are located anteromedial to the statocysts, ventromedial to the cerebropleural ganglia, and dorsomedial to the pedal ganglia (Fig. 3e). Connectives join a new pair of ganglia, the rhinophoral ganglia, to their respective cerebropleural ganglia (3a, d). These rhinophoral ganglia are anterior to the cerebropleural ganglia, just beneath the dorsal epidermis (Fig. 3d) and are first seen in the newly metamorphosed juvenile. A nerve can be seen exiting each rhinophoral ganglion and extending into the developing rhinophores. Also arising from each rhinophoral ganglion is a nervous process that proceeds anteroventral, perhaps to the mouth, salivary glands, or oral tentacles. The visceral ganglion is now tightly associated with the left cerebropleural ganglion. The pleurovisceral loop can be followed from the visceral ganglion towards the right side of the juvenile; however, its connection to the right cerebropleural ganglion is not clearly evident. The pedal ganglia, located in the anterior region of the juvenile foot, have definite nervous processes passing into anterior and posterior portions of the foot.

Evidence for the condensation of the CNS during metamorphosis

Some of the morphological data presented above suggest that the CNS of *B. verrucicornis* condenses during metamorphosis. Evidence of condensation is seen in the fusion of the cerebral ganglia to their respective pleural ganglia in the 1-day postmetamorphic juvenile and the tight association between the visceral ganglion and the left cerebropleural ganglion in the juvenile (Fig. 4).

Three measurements were made to determine if the central nervous system had become more compact during metamorphosis (Table I). The first, Pd, determined the relative position of the cerebral and pleural ganglia in the larva and juvenile by dividing the distance from the most anterior aspect of the organism (larva and juvenile) to the posterior aspect of the pleural ganglion by the total length of the organism. (If the pleural ganglion was located in the most posterior portion of the organism, this value would be equal to 1. The more anterior the CNS is located, the smaller the number.) The relative position of these ganglia was the same in larva (0.51 ± 0.05, mean $\pm$ S.D., $n = 4$) and juvenile (0.45 ± 0.08). The second measurement recorded the length of the cerebropleural connective along the anterior-posterior axis. In this case, condensation of the CNS is evident even without measurement because the length of these connectives is reduced from 13.5 ± 5.1 μm in the larva to nothing in the juvenile by the fusion of the cerebral and pleural ganglia during metamorphosis. Finally, determination of the distance from the most anterior aspect of the cerebral ganglia to the most posterior aspect of the pleural ganglia (AC-PP) demonstrated that this distance was significantly greater in the larva (74.1 ± 13 μm) than in the juvenile (54.5 ± 5.0 μm).

Discussion

As discussed above, the nomenclature used to identify ganglia in opisthobranchs is in a state of flux, mainly due to the recent investigations of Page (1992a, b). In addition, other past studies are not in full agreement on ganglion identification and larval CNS structure (*e.g.*, Tardy, 1970, 1974). To assist in relating our interpretation of the structure of the larval and juvenile CNS in *Berghia verrucicornis* to that of past investigators' descriptions for other species of opisthobranchs, these various larval CNS morphologies are summarized in Figure 5.

In *B. verrucicornis*, the structures that constitute most of the juvenile and adult CNS are present when the larvae are released from the egg mass. These are the cerebral, optic, pedal, pleural, buccal, and visceral ganglia. The first five of these ganglia are paired, whereas the sixth, the visceral ganglion, is single (see below). The dendronotid *Tritonia diomedea*, which has a planktotrophic larval stage, exhibits a similar complement of ganglia as its larva approaches metamorphic competence; however, only the cerebral ganglia are present at hatching (Kempf *et al.*, 1987). The other ganglia develop during the larval life of this species. Another opisthobranch with a planktotrophic

Figure 2. Sections (1 μm) of a competent *Berghia verrucicornis* larva (the anterior end of the organism is toward the top of the page). (a). Sagittal section showing the relationship between the pedal, cerebral, and pleural ganglia. Notice the distance between the cerebral and pleural ganglia. These ganglia are distinct in the larval stage but fuse to form a single cerebropleural ganglion during metamorphosis. (b). Frontal section illustrating the cerebral commissure and its location adjacent to the anterior epidermis. (c). Frontal section depicting the connection between the right cerebral ganglion and the right pleural ganglion. (d). Frontal section showing the relationship of the visceral ganglion to the esophagus. This ganglion is part of the pleurovisceral loop. C = cerebral ganglion; CC = cerebral commissure; E = esophagus; F = larval foot; P = pedal ganglion; PL = pleural ganglion; PLV = portion of the pleurovisceral loop; S = statocyst; V = velum; Vi = visceral ganglion. Scale bar = 35 μm.

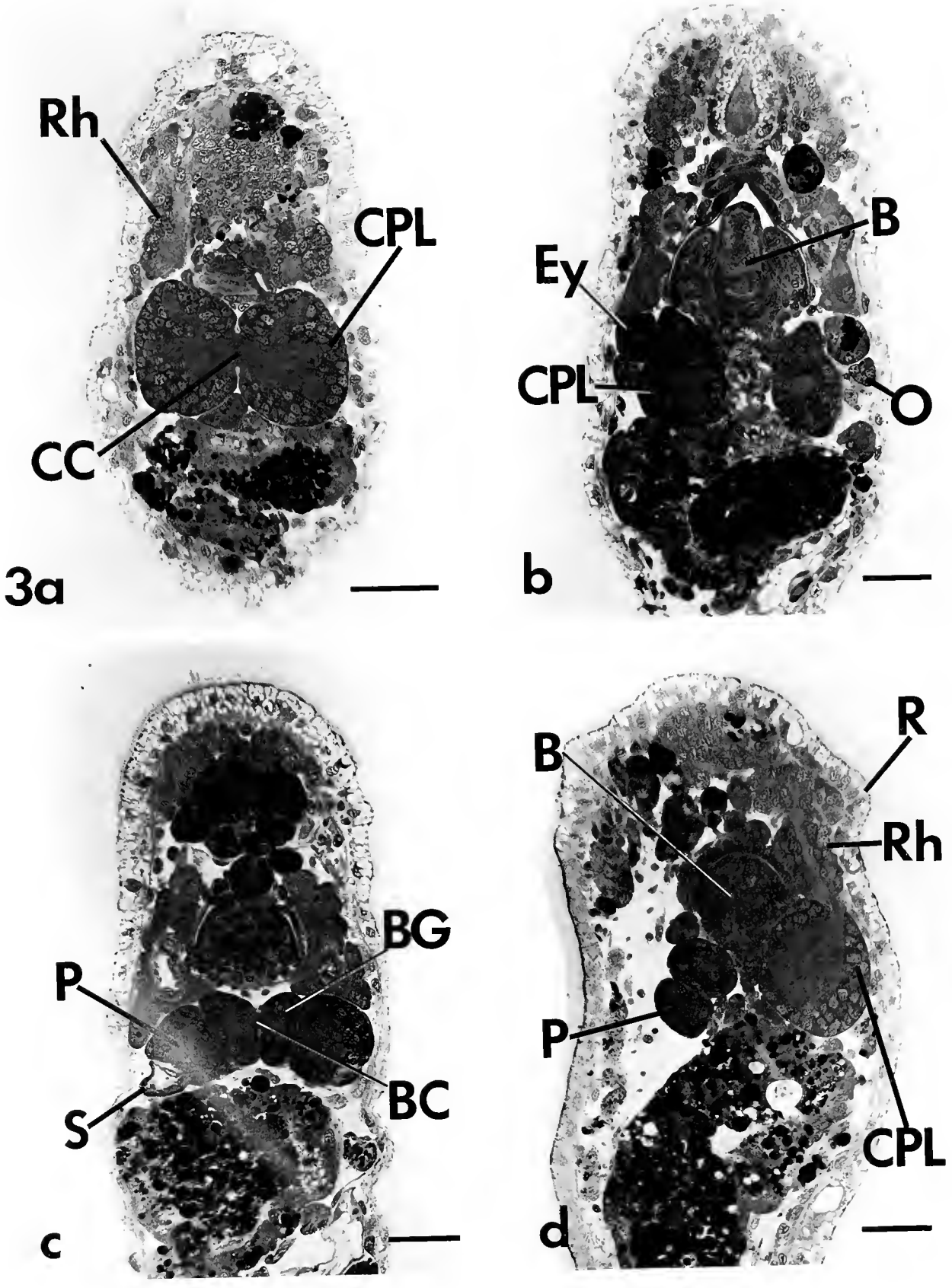
Rh
CPL
CC
3a
B
Ey
CPL
O
b
BG
P
BC
S
c
R
B
Rh
P
CPL
d

larva, the nudibranch *Melibe leonina*, has cerebral ganglia linked to primordia of the pedal ganglia via cerebropedal connectives at hatching (Page, 1992a, b). Also present at this stage is a complete pleurovisceral loop, though other ganglia commonly associated with this structure are absent at this early stage (Page, 1992a, b). As with *T. diomedea*, the other ganglia develop during the larval period. A similar scenario of CNS development is seen in the anaspid *Aplysia californica* (Kriegstein, 1977). The contrast in the timing of ganglion development between these species and *B. verrucicornis* reflects differences between the two developmental strategies (planktotrophic *vs.* lecithotrophic), rather than any real difference in the development of the central nervous system.

Some real differences are seen between the larval CNS in *A. californica* and *B. verrucicornis*. Kriegstein (1977) noted a pair of abdominal ganglia in *A. californica* that existed as part of a pleurovisceral loop and were located immediately anterior to the viscera. The right abdominal ganglion is described as a homolog of the supraintestinal ganglion, and the left as a combination of the subintestinal and visceral ganglia (Kriegstein, 1977). The visceral ganglion of *B. verrucicornis* may represent the fusion of one or more of these ganglia. Also present in *A. californica*, but not observed in *B. verrucicornis*, is the osphradial ganglion that is linked dorsally to the right abdominal ganglion by a short connective (Kriegstein, 1977).

The presence of a single visceral ganglion is not unique to *B. verrucicornis*. In the nudibranch *T. diomedea*, Kempf *et al.* (1987) note a single visceral ganglion that constitutes a part of the pleurovisceral loop. In *Acolidiella alderi*, Tardy (1970, 1974) recognizes a single abdominal ganglion that occurs in a well-developed pleurovisceral loop. The relative location of the abdominal ganglion in this species and its association with other ganglia suggest that it is homologous to the visceral ganglion in *B. verrucicornis*. Though Bickell (=Page) and Kempf (1983) did not report a visceral ganglion in competent larvae of *M. leonina*, more recent examination of this species' larva by Page has established its presence (1992a).

In this study we are treating the pleural ganglion as part of the visceral loop. The designation for this ganglion is the most difficult to justify, because a clear pleuropedal connective was not identified in the veliger larva; however, examination of the postmetamorphic CNS reveals a distinct connective between what we have designated the pleural (posterior) portion of the cerebropleural ganglia and their respective pedal ganglia. It is possible that all connections between major ganglia are not fully developed in larvae of *B. verrucicornis*, because we also failed to find definitive cerebrobuccal connectives in the competent veliger; however, these connectives were well developed in the one-day postmetamorphic juvenile. A similar situation may exist in the development of the *A. californica* CNS. Kriegstein (1977, p. 375) describes the pleuropedal connective as merging with the cerebropedal connective before passing into the pedal ganglion in the late larval stage of *A. californica*, but shows a distinct pleuropedal connective in the corresponding drawing (Kriegstein, 1977, Fig. 1a). In both cases, however, the pleural ganglia are included in the pleurovisceral loop.

An alternative explanation is that we do not resolve a pleuropedal connective in the larva because it is not present, and what we have designated the pleural ganglia are, as suggested by Page (1992a, b), the supra- and subintestinal ganglia. Furthermore, the appearance of another connective between the cerebral and pedal ganglia in the juvenile is actually the cerebropleural connective arising from the pleural ganglion, which has fused with the pedal ganglion. This interpretation is supported by the recent Page model for *M. leonina* (Page, 1992a, b); however, we are not convinced this is the case in *B. verrucicornis*. The connectives extending to the pedal ganglion on both the left and right sides appear to emerge from distinct neuropils in what we have designated the fused cerebropleural ganglion, while each pedal ganglion clearly possesses a single neuropil. This is suggestive of a fusion event between the former cerebral and pleural ganglia.

Tardy (1970, 1974) uses different terminology to describe the ganglia of the pleurovisceral loop in *Aeolidiella alderi;* some of these ganglia are clearly identical to those in *B. verrucicornis*. Contrary to many published descriptions (Kriegstein, 1977; Bickell [=Page] and Kempf, 1983; Kempf *et al.*, 1987; Page 1992a, b), Tardy (1970, 1974) considered the cerebral and pleural ganglia to be a single fused ganglion on the left and right sides of the competent

Figure 3. Sections (1 μm) of a 1-day postmetamorphic *Berghia verrucicornis* juvenile (the anterior end of the organism is towards the top of the page). (a) Frontal section showing the cerebral commissure. The cerebral commissure is located more posteriorly in the juvenile than in the larva, and the cerebral and pleural ganglia have fused to form the cerebropleural ganglia. (b). Frontal section through the cerebral and optic ganglia. The optic ganglia are positioned lateral to the cerebropleural ganglia and posterior to the eyespots. (c). Frontal section at the level of the statocysts. (d). Sagittal section displaying the newly formed right rhinophoral ganglion. The rhinophore, a sensory organ in the adult, is beginning to form anterodorsal to the rhinophoral ganglion. B = buccal mass; BC = buccal commissure; BG = buccal ganglion; CC = cerebral commissure; CPL = cerebropleural ganglion; Ey = eyespot; O = optic ganglion; P = pedal ganglion; R = rhinophore; Rh = rhinophoral ganglion; S = statocyst. Scale bar = 25 μm.

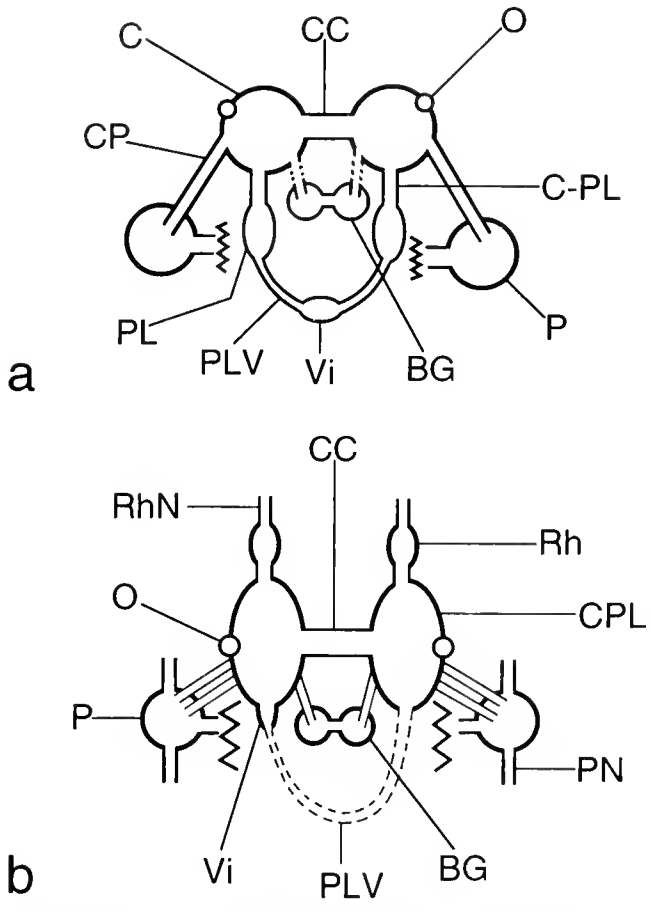

Figure 4. Diagram illustrating the organization of the (a) competent larval (11–12 days after oviposition) and (b) 1-day postmetamorphic (13–15 days after oviposition) CNS of *Berghia verrucicornis*. The anterior portion of the CNS is positioned toward the top of the page. In the 1-day postmetamorphic juvenile the cerebral and pleural ganglia are fused, and the visceral ganglion is being incorporated into the left cerebropleural ganglion. The dotted lines indicate portions of the cerebrobuccal connectives (a) and the pleurovisceral loop (b) that are assumed to be present, but could not be traced in 1-μm sections. The pedal commissure has been separated at the points indicated by the jagged lines. BG = right buccal ganglion; C = left cerebral ganglion; CC = cerebral commissure; CP = cerebropedal connective; CPL = right cerebropleural ganglion; C-PL = right cerebropleural connective; O = optic ganglion; P = pedal ganglion; PL = left pleural ganglion; PLV = portion of the pleurovisceral loop; PN = pedal nerve; Rh = rhinophoral ganglion; RhN = rhinophoral nerve; Vi = visceral ganglion.

veliger of *Aeolidiella alderi*. Just posterior to these putative cerebral ganglia, that author identified the left and right parietal ganglia. These ganglia were connected by a parietalvisceral loop that, moving from left to right, included infraintestinal, abdominal, and supraintestinal ganglia. The relative location of the pleural ganglia we have described in *B. verrucicornis* is the same as the parietal ganglia described by Tardy (1970, 1974) in larvae of *Aeolidiella alderi*. Presumably, in *B. verrucicornis*, the abdominal and the supra- and infraintestinal ganglion described by Tardy (1970, 1974) in *Aeolidiella alderi* are either fused with the visceral ganglion or with the pleural ganglia.

Other studies have reviewed the changes that occur in the opisthobranch central nervous system during metamorphosis (Marois and Carew, 1990). Many of these events are similar to what we observed in *B. verrucicornis*. In summary, (1) the central ganglia become more concentrated during metamorphosis (Thompson, 1958, 1962; Tardy, 1970, 1974; Bonar and Hadfield, 1974; Bonar, 1978; Page, 1992a, b). (2) The cerebral ganglia migrate from their position anterior to the buccal mass to lie above the buccal mass in the juvenile (Thompson, 1958, 1962; Tardy, 1970, 1974; Kriegstein, 1977). (3) The components of the pleurovisceral loop, namely the left pleuro-visceral connective and the visceral ganglion, are incorporated into the pleural portion of the left cerebropleural ganglion. (4) Similar to descriptions for *M. leonina*, new neural structures, the rhinophoral ganglia and associated connectives and nerves, are apparent in the newly metamorphosed juvenile of *B. verrucicornis* (Bickell [=Page] and Kempf, 1983; and Page, 1992a, b).

The short embryonic, larval, and juvenile life of *Berghia verrucicornis* and the ability to rear this nudibranch in the laboratory will make it a convenient model for neurodevelopmental studies. We are currently investigating the expression of specific neurotransmitters during development of *B. verrucicornis*, with the eventual aim of correlating neurotransmitter distribution and neuroanatomy with function.

Table I

Measurements of the larval and juvenile CNS

	Pd[a]	Cerebropleural connective (μm)[b]	AC-PP (μm)[b,c]
Larval I.D. #			
390#2	0.48	12.2	68.6
590#11	0.49	7.4	63.7
590#12	0.49	19.6	71.1
590#14	0.59	14.7	93.1
Juvenile I.D. #			
590#4	0.46	0	58.8
590#5	0.39	0	58.8
590#6	0.40	0	51.4
590#7	0.56	0	49.0

[a] Pd = the distance from the most anterior aspect of the organism to the most posterior aspect of the pleural ganglion divided by the total length of the same organism.

[b] There is a significant difference between the larva and juvenile for this measurement ($P < 0.05$).

[c] AC-PP = the distance from the most anterior aspect of the cerebral ganglion to the most posterior aspect of the ipsilateral pleural ganglion.

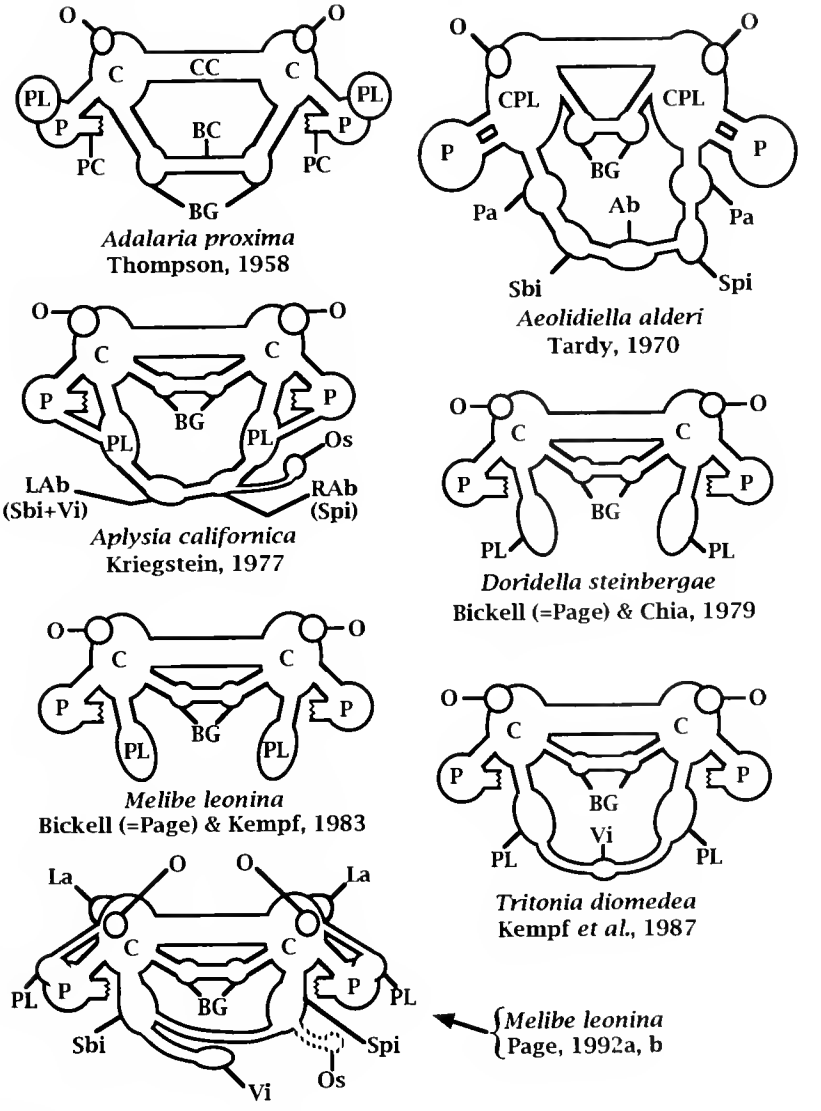

Figure 5. Schematic diagrams illustrating various published descriptions of the central nervous system of different species of competent opisthobranch veliger larvae. Ab = abdominal ganglion; BC = buccal commissure; BG = buccal ganglia; C = cerebral ganglion; CC = cerebral commissure; CPL = cerebropleural ganglion; La = labial ganglion; LAb = left abdominal ganglion; RAb = right abdominal ganglion; O = optic ganglion; Os = osphradial ganglion; P = pedal ganglion; Pa = parietal ganglion; PC = pedal commissure; PL = pleural ganglion; Sbi = subintestinal ganglion; Spi = supraintestinal ganglion; Vi = visceral ganglion.

Acknowledgments

The authors thank Drs. James Bradley and Christine Sundermann for the use of the microtome and photographic equipment, respectively. Barbara Estridge was very helpful, as always, on many matters, but most especially regarding use of the department's new Reichart ultramicrotome. Thanks also to Drs. James Bradley, Raymond Henry, and Curt Peterson for helpful critical comments on the text of this manuscript and to Dr. Yvonne Grimm-Jorgenson for hallway discussions. This research was supported by an Alabama Agricultural Experiment Station grant to S.C.K., AAES Journal No. 15-913124.

Literature Cited

Baux, G., P. Fossier, and L. Tauc. 1990. Histamine and FLRFamide regulate acetylcholine release at an identified synapse in *Aplysia* in opposite ways. *J. Physiol. London* **429:** 147–168.

Bedian, V., Y. Chen, and M. H. Roberts. 1991. Monoclonal antibodies recognize localized antigens in the eye and central nervous system of the marine snail *Bulla gouldiana*. *J. Histochem. Cytochem.* **39:** 311–319.

Bickell, L. R., and F. S. Chia. 1979. Organogenesis and histogenesis in the planktotrophic veliger of *Doridella steinbergae* (Opisthobranchia: Nudibranchia). *Mar. Biol.* **52:** 291–313.

Bickell, L. R., and S. C. Kempf. 1983. Larval and metamorphic morphogenesis in the nudibranch *Melibe leonina* (Mollusca: Opisthobranchia). *Biol. Bull.* **165:** 119–138.

Bonar, D. B. 1978. Morphogenesis at metamorphosis in opisthobranch molluscs. Pp. 177–196 in *Settlement and Metamorphosis of Marine Invertebrate Larvae*, F. S. Chia and M. E. Rice, eds. Elsevier, New York.

Bonar, D. B., and M. G. Hadfield. 1974. Metamorphosis of the marine gastropod *Phestilla sibogae* Bergh (Nudibranchia: Aeolidacea). I. Light and electron microscopic analysis of larval and metamorphic stages. *J. Exp. Mar. Biol. Ecol.* **16:** 227–255.

Bridges, C. B. 1975. Larval development of *Phyllaplysia taylori* Dall with a discussion of development in the Anaspidea. (Opisthobranchia: Anaspidea). *Ophelia* **14:** 161–184.

Bulloch, A. G. M. 1985. Development and plasticity of the molluscan nervous system. Pp. 335–408 in *The Mollusca*, Vol. 8, K. M. Wilbur and A. O. D. Willows, eds. Academic Press, Orlando, FL.

Carroll, D. J., and S. C. Kempf. 1990. Laboratory culture of the aeolid nudibranch *Berghia verrucicornis* (Mollusca: Opisthobranchia): some aspects of its development and life history. *Biol. Bull.* **179:** 243–253.

Cash, D., and T. J. Carew. 1989. A quantitative analysis of the development of the central nervous system in juvenile *Aplysia californica*. *J. Neurobiol.* **20**(1): 25–47.

Dorsett, D. A. 1986. Brains to cells: the neuroanatomy of selected gastropod species. Pp. 101–187 in *The Mollusca*, Vol. 9, A. O. D. Willows, ed. Academic Press, Orlando, FL.

Goldberg, J. I., and S. B. Kater. 1989. Expression and function of the neurotransmitter serotonin during development of the *Helisoma* nervous system. *Dev. Biol.* **131:** 483–495.

Graham, A. 1985. Evolution within the Gastropoda: Prosobranchia. Pp. 151–186 in *The Mollusca*, Vol. 10, E. R. Trueman and M. R. Clarke, eds. Academic Press, Orlando, FL.

Harris, L. G. 1975. Studies on the life history of two coral-eating nudibranchs of the genus *Phestilla*. *Biol. Bull.* **149:** 539–550.

Hessinger, D. A., and J. A. Hessinger. 1981. Methods for rearing sea anemones in the laboratory. Pp. 153–179 in *Laboratory Animal Management Marine Invertebrates*. Committee on Marine Invertebrates. National Academy Press, Washington, DC.

Hickmott, P. W., and T. J. Carew. 1991. An autoradiographic analysis of neurogenesis in juvenile *Aplysia californica*. *J. Neurobiol.* **22:** 313–326.

Jacob, M. H. 1984. Neurogenesis in *Aplysia californica* resembles nervous system formation in vertebrates. *J. Neurosci.* **4**(5): 1225–1239.

Kandel, E. R., W. T. Frazier, R. Waziri, and R. E. Coggeshall. 1967. Direct and common connections among identified neurons in *Aplysia*. *J. Neurophysiol.* **30:** 1352–1376.

Kempf, S. C., and A. O. D. Willows. 1977. Laboratory culture of the nudibranch *Tritonia diomedea* Bergh (Tritoniidae: Opisthobranchia) and some aspects of its behavioral development. *J. Exp. Mar. Biol. Ecol.* **30:** 261–276.

Kempf, S. C., B. Masinovsky, and A. O. D. Willows. 1987. A simple neuronal system characterized by a monoclonal antibody to SCP neuropeptides in embryos and larvae of *Tritonia diomedea* (Gastropoda: Nudibranchia). *J. Neurobiol.* **18:** 217–236.

Kriegstein, A. R., V. Castellucci, and E. R. Kandel. 1974. Metamorphosis of *Aplysia californica* in laboratory culture. *Proc. Natl. Acad. Sci. USA* **71:** 3654–3658.

Kriegstein, A. R. 1977. Development of the nervous system of *Aplysia californica*. *Proc. Natl. Acad. Sci. USA* **74**(1): 375–378.

Marois, R., and T. J. Carew. 1990. The gastropod nervous system in metamorphosis. *J. Neurobiol.* **21**(7): 1053–1071.

McAllister, L. B., R. H. Scheller, E. R. Kandel, and R. Axel. 1983. *In situ* hybridization to study the origin and fate of identified neurons. *Science* **222:** 800–808.

Nagle, G. T., S. D. Painter, and J. E. Blankenship. 1989a. The egg-laying hormone family: precursors, products and functions. *Biol. Bull.* **177:** 210–217.

Nagle, G. T., S. D. Painter, and J. E. Blankenship. 1989b. Post-translational processing in model neuroendocrine systems: precursors and products that coordinate reproductive activity in *Aplysia* and *Lymnaea*. *J. Neurosci. Res.* **23:** 359–370.

Page, L. 1992a. A new interpretation of the nudibranch central nervous system based on ultrastructural analysis of neurodevelopment in *Melibe leonina*. I. Cerebral and visceral loop ganglia. *Biol. Bull.* **182:** 348–365.

Page, L. 1992b. A new interpretation of the nudibranch central nervous system based on ultrastructural analysis of neurodevelopment in *Melibe leonina*. II. Pedal, pleural, and labial ganglia. *Biol. Bull.* **182:** 366–381.

Paige, J. A. 1988. Biology, metamorphosis and postlarval development of *Bursatella leachii plei* Rang (Gastropoda: Opisthobranchia) *Bull. Mar. Sci.* **42**(1): 65–75.

Pennington, J. I., and M. G. Hadfield. 1989. A simple, non-toxic method for the decalcification of living invertebrate larvae. *J. Exp. Mar. Biol. Ecol.* **130:** 1–7.

Richardson, K. C., L. Jarett, and F. H. Finke. 1960. Embedding in epoxy resins for ultrathin sectioning in electron microscopy. *Stain Technol.* **35:** 313–323.

Schacher, S., E. R. Kandel, and R. Woolley. 1979. Development of neurons in the abdominal ganglion of *Aplysia californica*. I. Axosomatic synaptic contacts. *Dev. Biol.* **71:** 163–175.

Schacher, S. 1983. Cellular interactions in the development of neurons in *Aplysia*. *Neuro. Res. Prog. Bull.* **20:** 870–911.

Switzer-Dunlap, M., and M. G. Hadfield. 1977. Observations on development, larval growth and metamorphosis of four species of Aplysiidae (Gastropoda: Opisthobranchia) in laboratory culture. *J. Exp. Mar. Biol. Ecol.* **29:** 245–261.

Tardy, J. 1970. Contribution a l'etude des metamorphoses chez les nudibranches. *Annls. Sci. Nat. Zool. Biol. Anim.* **12:** 229–370.

Tardy, J. 1974. Morphogenese du systeme nerveux chez les mollusques nudibranches. *Haliotis* **4:** 61–75.

Thompson, T. E. 1958. The natural history, embryology, larval biology and postlarval development of *Adalaria proxima* (Alder and Hancock) (Gastropoda: Opisthobranchia). *Phil. Trans. R. Soc. Lond. Ser. B* **242:** 1–58.

Thompson, T. E. 1962. Studies on the ontogeny of *Tritonia hombergi* Cuvier (Gastropoda: Opisthobranchia). *Phil. Trans. R. Soc. Lond. Ser. B* **242:** 171–218.

Willows, A. O. D. 1971. Giant brain cells in mollusks. *Sci. Am.* **224:** 69–76.

Willows, A. O. D. 1973. Gastropod nervous system as a model experimental system in neurobiological research. *Fed. Proc.* **32**(12): 2215–2223.

Ziv, I., C. Lustig, S. Markovich, and A. J. Susswein. 1991. Sequencing of behaviors in *Aplysia fasciata*—integration of feeding, reproduction and locomotion. *Behav. Neural. Biol.* **56:** 148–169.

Reference: *Biol. Bull.* **186:** 213–220. (April, 1994)

Energetics of the Ventilatory Piston Pump of the Lugworm, a Deposit-feeding Polychaete Living in a Burrow

ANDRÉ TOULMOND[1] AND PIERRE DEJOURS[2]

Observatoire Océanologique, Centre National de la Recherche Scientifique and Université Pierre-et-Marie-Curie, Roscoff, France

Abstract. The aim of this study was to tentatively estimate the energy cost of breathing in the lugworm, *Arenicola marina* (L.), a gallery-dwelling, piston-pump breather that moves water in a tail-to-head direction. Each tested lugworm was placed in a horizontal glass tube. The caudal end of the tube was connected to a well-aerated seawater reservoir at 20°C, and the cephalic end attached to a drop meter through a tube resistance. At the exit of the cephalic chamber the O_2 tension was recorded via an *in situ* O_2 electrode, and the hydrostatic pressure of the exhaled water was also recorded. Water flow rate, total O_2 uptake rate $\dot{M}_{O_2}^{TOT}$, O_2 extraction coefficient, and the mechanical power necessary to pump water through the resistive anterior exit of the apparatus ($\dot{W}_{MEC}$), were computed. The basal metabolic rate of each animal ($\dot{M}_{O_2}^{CONF}$) was separately estimated by the confinement method. $\dot{M}_{O_2}^{CONF}$ subtracted from $\dot{M}_{O_2}^{TOT}$ approximates $\dot{M}_{O_2}^{CB}$, the O_2 uptake rate necessary to activate the piston-pump breathing mechanism and to ensure the corresponding mechanical work rate, $\dot{W}_{MEC}$.

The results show that the energy cost of breathing, $\dot{M}_{O_2}^{CB}$, of the piston-pump-breathing *Arenicola* is very high, with mean values approximating 47% of the $\dot{M}_{O_2}^{TOT}$ value; that the mechanical power we measured, $\dot{W}_{MEC}$, is very low; and that the mechanical-to-metabolic efficiency, the ratio $\dot{W}_{MEC}/\dot{M}_{O_2}^{CB}$, does not exceed 1%. These observations are compared to those obtained in other piston-pump breathers, such as *Chaetopterus variopedatus* and *Urechis caupo*, and in ciliary filter feeders including polychaetes, bivalves, and ascidians.

Received 31 July 1993; accepted 27 January 1994.

[1] Address for correspondence: Dr. André Toulmond, Station Biologique, BP 74, 29682 Roscoff Cedex, France.

[2] Present address: Dr. Pierre Dejours, Centre d'Ecologie et Physiologie Energétiques, CNRS, 23 rue Becquerel, 67087 Strasbourg, France.

See the Appendix for a list of symbols used in the text.

Introduction

Most aquatic macrofauna burrowing in soft substrates maintain direct contact with the water covering the sediments via tube or gallery systems through which water is pumped. The animal thus meets its respiratory needs and, in the case of a filter feeder, eventually obtains the particulate matter on which it feeds (Newell, 1979). The lugworm, *Arenicola marina*, is a deposit feeder (Jacobsen, 1967). It lives in a permanent L-shaped gallery deeply dug in intertidal sands and communicating with the water column through a single posterior (caudal) opening. During high tide, the lugworm actively pumps water that flows over the animal's body and then percolates through the sand blocking the blind head-end of the burrow. In this piston-type pumping mechanism, the burrow is rhythmically sealed by tail-to-head peristaltic movements of the body wall which force the inspired seawater forward (Wells, 1966; Foster-Smith, 1978).

A positive displacement pump such as a piston pump is the only possible biological pump that can generate the high hydrostatic pressure needed to force water through a tube system with a high flow resistance. This pumping mechanism, however, can produce only moderate water flow rates, and it is considered to be energetically expensive (Walshe-Maetz, 1953; Mangum, 1976). Some indirect evidence suggests that this statement could be valid in the case of the lugworm: (1) despite the efficiency of its respiratory exchanger, which can extract up to 90% of the oxygen in normoxic water, the lugworm does not regulate its O_2 uptake rate below an O_2 partial pressure of 15 kPa in the inspired water; (2) hypoxia below 5.3 kPa is clearly

a signal to stop ventilating; (3) from data obtained in previous experiments under normoxic conditions, it can be calculated that the O_2 uptake necessary to cover the ventilatory work—that is, the energy cost of breathing, $\dot{M}_{O_2}^{CB}$—corresponds to about 40% of the total O_2 uptake (Toulmond, 1975, 1986; Toulmond and Tchernigovtzeff, 1984). The aim of this work is to obtain direct evidence concerning the characteristics and the energetics of the ventilatory piston pump of a deposit feeder, the lugworm, and to compare it with the piston pump of filter feeders such as *Chaetopterus variopedatus* (Brown, 1975; Riisgård, 1989) and *Urechis caupo* (Chapman, 1968; Pritchard and White, 1981).

Principles

The total O_2 uptake from the environment, $\dot{M}_{O_2}^{TOT}$, of a lugworm ventilating in its gallery during a certain period of time is the product of the water flow times the difference of O_2 concentration between inspired and expired water, itself resulting from the multiplication of the inspired-to-expired P_{O_2} difference by the O_2 solubility. $\dot{M}_{O_2}^{TOT}$ is the sum of three terms:

$$M_{O_2}^{TOT} = M_{O_2}^{CONF} + M_{O_2}^{CB} + \Delta M_{O_2}^{STO} \quad (1)$$

$M_{O_2}^{CONF}$ is the O_2 uptake of a lugworm doing no ventilatory work and is considered here as a measure of the basal metabolism of the animal. If the O_2 stores are kept constant, $M_{O_2}^{CONF}$ can be evaluated in a lugworm confined motion-free in a large closed flask, taking into account the flask volume and the initial and final ambient P_{O_2} values, the final P_{O_2} being above the critical point, P_C, the O_2 pressure below which the O_2 stores are used (Toulmond, 1975).

$M_{O_2}^{CB}$ is the O_2 uptake necessary to cover the ventilatory work, that is, the energy cost of breathing, CB.

$\Delta M_{O_2}^{STO}$ is the eventual change of O_2 stores. If the O_2 stores remain constant, $\Delta M_{O_2}^{STO}$ is null, and equation (1) is simplified to

$$M_{O_2}^{TOT} = M_{O_2}^{CONF} + M_{O_2}^{CB} \quad (2)$$

In this case, where the O_2 uptake from the environment is entirely used to cover the aerobic cellular metabolism, $M_{O_2}^{TOT}$ is the metabolic O_2 consumption, $M_{O_2}^{MET}$:

$$M_{O_2}^{MET} = M_{O_2}^{TOT} = M_{O_2}^{CONF} + M_{O_2}^{CB} \quad (2a)$$

If the O_2 stores change, $\Delta M_{O_2}^{STO}$ is different from zero. The term can be either negative (when the O_2 stores decrease) or positive (when the O_2 stores increase). Then equation (2a) becomes

$$M_{O_2}^{MET} = M_{O_2}^{TOT} \pm \Delta M_{O_2}^{STO} = M_{O_2}^{CONF} + M_{O_2}^{CB} \quad (3)$$

In practice, we measured the total O_2 uptake from the environment, $M_{O_2}^{TOT}$, of a lugworm ventilating in an artificial gallery through a given resistance, and the O_2 uptake of the same animal confined as described above, $M_{O_2}^{CONF}$. Owing to the special, periodical ventilation of the lugworm (see Discussion; Validity of the model), one has to distinguish two types of values for $M_{O_2}^{TOT}$.

The symbol $lgM_{O_2}^{TOT}$ corresponds to mean values obtained through "long duration" (91 to 178 min) measurement periods. In this first case, the O_2 stores can be considered as identical at the beginning and at the end of the measurement period, equation (2) applies, and the energy cost of breathing, $M_{O_2}^{CB}$, can be estimated.

The symbol $shM_{O_2}^{TOT}$ corresponds to values obtained through "short duration" (6 min) measurement runs. In this second case, the O_2 stores can be different at the beginning and at the end of a given measurement run, and equation (3) applies. Because the value of $\Delta M_{O_2}^{STO}$ is unknown, $M_{O_2}^{CB}$ cannot be estimated (see Discussion).

Materials and Methods

Experiments were carried out in Roscoff, Nord-Finistère, France, in August 1988 and in May–August 1989. Medium-sized lugworms, wet mass 15 to 20 g, were collected on the nearby Penpoull beach, brought back to the laboratory, and kept unfed overnight in local running seawater (temperature 14 to 16°C) to free the gut of sand.

Measurement of total O_2 uptake rate, $\dot{M}_{O_2}^{TOT}$, in an artificial gallery

The artificial gallery consisted of a straight glass tube 30 cm long, i.d. 1 cm, horizontally immersed in a 40-l holding tank (Fig. 1).

The rear (caudal) end of the tube was connected by glass tubing to an open, constant level, 1-l bottle containing seawater bubbled with air. To attenuate the transmission of vibrations, this tonometer was kept in a separate tank. Both tanks were supplied with decanted flowing natural seawater maintained at a thermostat setting of 20°C.

At the anterior (cephalic) end of the tube were serially fitted (1) a small acrylic chamber containing a Radiometer E5046 O_2 electrode, immediately followed by a T-connection to a P23BB Statham pressure gauge; (2) two different parallel lengths of tubing, provided with stopcocks, which gave two different resistance values, R1 or R2, at the exit; (3) a photocell drop counter.

The water level of the apparatus was continuously maintained the same at both ends of the system. Under these conditions, in accordance with Poiseuille's law, the lugworm ventilating from tail to head had to create a certain hydraulic pressure difference to overcome the terminal resistance of the system.

The three measured variables were the O_2 pressure in the expired water ($P_{E_{O_2}}$), the hydrostatic pressure difference before the exit resistance (ΔP_{HYD}), and the water flow (Vw).

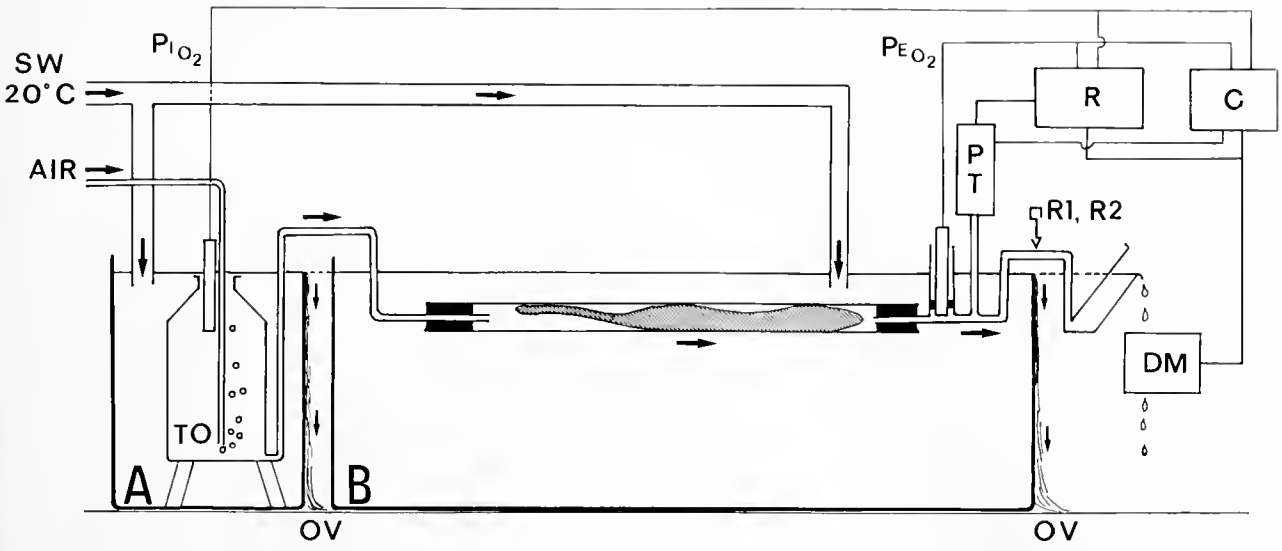

Figure 1. Apparatus. The glass tube containing the lugworm was placed in a thermostatted seawater bath. The rear (caudal) part of the tube was connected through very low-resistance glass tubing to a constant level tonometer (TO) equipped with an O_2 electrode measuring the O_2 partial pressure in the inspired water (PI_{O_2}). At the anterior (cephalic) end of the tube were serially fitted (1) a small acrylic chamber containing an O_2 electrode measuring the O_2 partial pressure in the expired water (PE_{O_2}), immediately followed by a T-connection to a pressure transducer (PT); (2) two different tubing lengths corresponding to two different exit resistances, R1 and R2; and (3) a photocell drop meter (DM). A and B: separated water baths; OV: overflow; R: potentiometric recorder; C: microcomputer; Arrows: direction of air or water circulation.

Twelve hours after collection, a lugworm (mean wet mass: 18.5 ± 1.7 g, $N = 10$) was placed unrestrained in the artificial gallery; measurements were started about 1 h later. Each experiment was carried out on a different animal and was divided into three periods lasting between 90 and 180 min each and corresponding to a different exit resistance. One day the sequence was R1, R2, R1 and the next day R2, R1, R2, to cancel the possible influence of fatigue. During each period, PE_{O_2}, ΔPHYD and $\dot{V}w$ were continuously recorded graphically by a potentiometric recorder. In parallel, when the lugworm ventilated in a regular and continuous way, PE_{O_2} and ΔPHYD were recorded on tape by a Hewlett-Packard HP85B microcomputer for separate runs each lasting 6 min. For each period, 12 to 15 runs were recorded.

During each run, the corresponding total volume of ventilated water, Vw, was collected and measured to the nearest 0.1 ml with a measuring cylinder. This value; the calibration coefficients for the O_2 electrode and the pressure gauge; the O_2 solubility coefficient at 20°C, $\alpha = 0.0000116$ μmol/(ml · Pa); and the O_2 pressure in the ingoing seawater, PI_{O_2}, were introduced into the computer, which calculated 6-min mean values of (1) the water flow rate, $\dot{V}w$; (2) the O_2 extraction coefficient, $Ew_{O_2} = (PI_{O_2} - PE_{O_2})/PI_{O_2}$; (3) the short duration total O_2 uptake rate, $sh\dot{M}_{O_2}^{TOT} = \dot{V}w\,(CI_{O_2} - CE_{O_2})$; (4) the specific ventilatory rate, $\dot{V}w/sh\dot{M}_{O_2}^{TOT}$; (5) the hydrostatic pressure difference, ΔPHYD; (6) the hydraulic resistance, $R = \Delta PHYD/\dot{V}w$; and (7) the mechanical power, $\dot{W}_{MEC} = \Delta PHYD \times \dot{V}w$, developed to push water from the cephalic end of the gallery to the final exit of the circuit. All values were expressed in SI units. For O_2 consumption, we took the value of 450 J/mmol O_2 as the SI unit for the oxy-energetic equivalent (see Dejours, 1981).

At the end of an experiment, the three periods were separately analyzed using the graphical record of PE_{O_2}, ΔPHYD, and the drop counter signal. The total duration of each period was measured, including the ventilatory arrests not lasting more than 20 min (beyond this duration, the O_2 stores are exhausted and the metabolism turns anaerobic), as well as the corresponding long duration mean total O_2 uptake, $lgM_{O_2}^{TOT}$, evaluated using the $sh\dot{M}_{O_2}^{TOT}$ previously calculated for each 6-min run. The O_2 uptake between two runs was obtained by interpolation.

Measurement of the basal metabolism rate, $\dot{M}_{O_2}^{CONF}$, by confinement

After the total O_2 uptake in the artificial gallery had been measured, the worm was transferred to a 575-ml opaque vessel wrapped in an aluminum sheet and filled with normoxic water. The vessel was thereafter closed hermetically and placed at 20°C. The confinement, which lasted about 90 min, was discontinued when P_{O_2} was around the critical O_2 pressure, roughly 15 kPa. Knowing

the volumes of the bottle and of the animal, the initial and final P_{O_2} of the water, and the confinement duration, we calculated the basal metabolic rate, $\dot{M}_{O_2}^{CONF}$.

Determination of the cost of breathing, $\dot{M}_{O_2}^{CB}$

Assuming that the O_2 stores were identical at the beginning and end of each long duration measurement period, the mean rate of energy cost of breathing was then calculated as $\dot{M}_{O_2}^{CB} = 1g\dot{M}_{O_2}^{TOT} - \dot{M}_{O_2}^{CONF}$.

Results

We conducted 22 experiments on 22 different lugworms. All animals responded similarly. The results reported here concern the last 10 experiments, the only ones to be completely analyzed. Results for *Arenicola* #21 were selected to illustrate this analysis because they were among the most representative of this very coherent set of experiments. Values are means ± 1 SD. Differences between means were evaluated using Student's *t* test with $P = 0.05$ as the fiducial limit of significance.

Figures 2 to 6 report results for *Arenicola* #21; a value of $\dot{M}_{O_2}^{CONF} = 3000\ \mu W$ was measured for this animal during an 89-min confinement period. Each point corresponds to one 6-min run. The ventilatory flow rate, $\dot{V}w$ (Fig. 2),

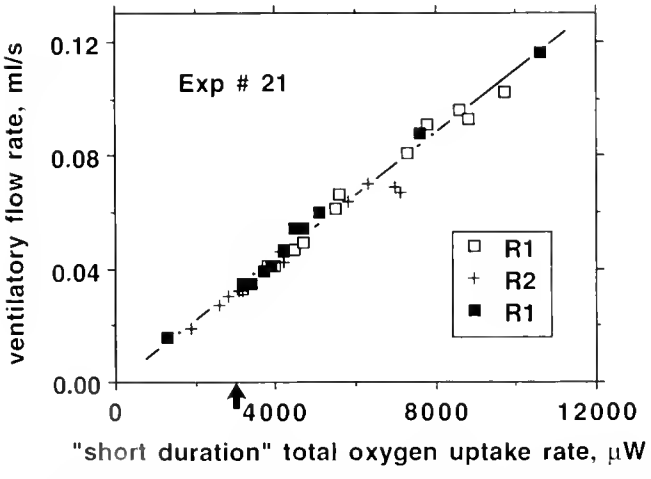

Figure 2. *Arenicola* #21 (wet mass: 17.2 g). Ventilatory flow rate, $\dot{V}w$, as a function of the "short duration" total O_2 uptake rate, $sh\dot{M}_{O_2}^{TOT}$ ($y = 0.000011\ x + 0.0009$; $r = 0.990$). Note that the slope of the regression line is the M_{O_2}-specific ventilation, namely 0.000011 ml/μJ (about 5 l/mmol O_2), a relatively low value for a water breather (Dejours, 1981), well in line with the high extraction coefficient in *Arenicola*. Open and closed squares correspond to breathing against a low resistance, R1, during the first and third period of the experiment; crosses concern breathing against the higher resistance R2 during the second period of the experiment (see text, Materials and Methods). The arrow on the abcissa corresponds to the value of the basal metabolism of lugworm #21, as measured by confinement. $\dot{M}_{O_2}^{CONF} = 3000\ \mu W$. Mean value of $\dot{M}_{O_2}^{CB} = 1150\ \mu W$. We took the value of 450 J for 1 mmol O_2 as the SI unit for the oxy-energetic equivalent (Dejours, 1981).

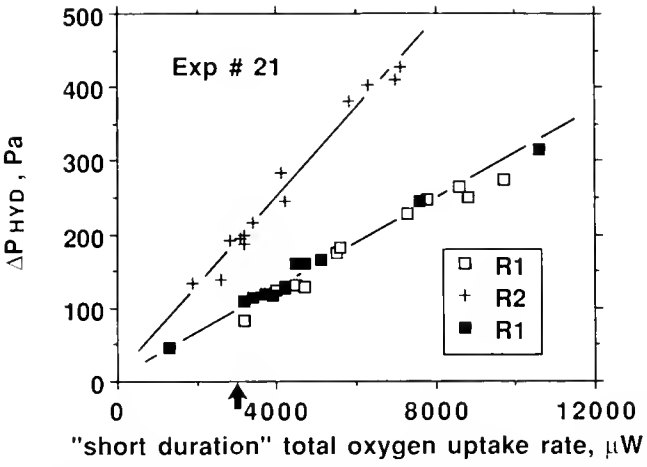

Figure 3. *Arenicola* #21. ΔPHYD, difference of hydrostatic pressure between the anterior chamber and atmosphere, as a function of the "short duration" total O_2 uptake rate, $sh\dot{M}_{O_2}^{TOT}$. R1 and R2 correspond to the low and high exit resistances opposed to exhaled water. Symbols as in Figure 2. Equation corresponding to R1: $y = 0.29\ x + 10.2$ ($r = 0.988$), and to R2: $y = 0.6\ x + 8.9$ ($r = 0.987$).

and the hydrostatic pressure difference, ΔPHYD (Fig. 3), were directly proportional to the short duration oxygen uptake rate, $sh\dot{M}_{O_2}^{TOT}$. These figures also show that there was no significant difference between the first and the subsequent periods, indicating that the animal did not tire. Figure 2 shows that the resistance (R1 or R2) apparently did not influence the ventilatory flow rate, whereas Figure 3 shows, as expected, that the hydrostatic pressure difference was higher in the experiments with greater expiratory load (R2 ~ 2R1).

Figure 4 describes the variations, as a function of $sh\dot{M}_{O_2}^{TOT}$, of the mechanical power, $\dot{W}_{MEC}$, developed to overcome the resistive respiratory loading, R1 or R2. Calculation of the corresponding log-log regressions shows that $\dot{W}_{MEC}$ varies as a quadratic function of $sh\dot{M}_{O_2}^{TOT}$, a necessary consequence of the linearity observed in Figures 2 and 3.

Finally, Figure 5 shows the variations of the difference of pressure between the anterior chamber and the ambient air, ΔPHYD, as a function of the ventilatory flow rate, $\dot{V}w$, through the exit resistances R1 and R2 whose mean values, respectively 2600 and 5900 Pa·s/ml, are given by the slope of the regression lines (see legend of Fig. 5). This figure also shows that, as needed by Poiseuille's equation, the ventilatory flow rate is directly and linearly proportional to ΔPHYD, and inversely proportional to the resistance of the setup. This fine tuning between the theory and the data can be considered as a positive argument for the validity of our measurement methods and the conditions in which the lugworm had to ventilate.

In some 6-min runs, we could estimate the pumping frequency of the piston pump's periodic activity by mea-

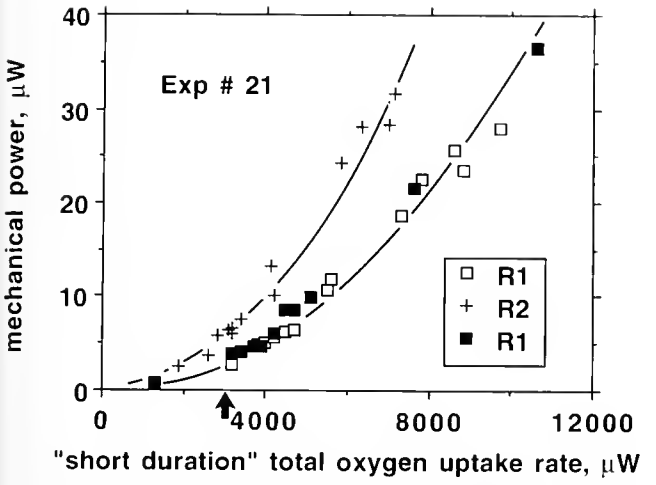

Figure 4. *Arenicola* #21. Mechanical power, $\dot{W}_{MEC}$, necessary to obtain the flow of water through either the low resistance R1 or the higher resistance R2, as a function of the total energy expenditure estimated as the "short duration" total O_2 uptake, $sh\dot{M}_{O_2}^{TOT}$. The drawn curves were fitted by eye. Symbols as in Figure 2. Equation corresponding to R1: $y = x^{1.91}/(7.9 \cdot 10^6)$ ($r = 0.991$) and to R2: $y = x^{1.99}/(6.3 \cdot 10^6)$ ($r = 0.991$) (see text).

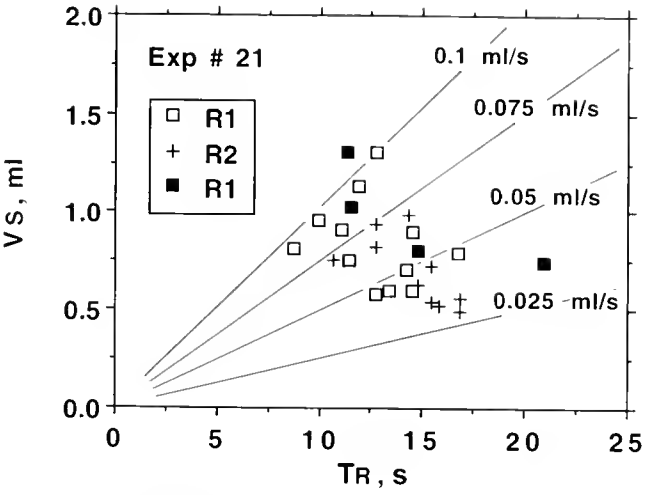

Figure 6. *Arenicola* #21. Water stroke volume, Vs, *versus* the duration of successive ventilatory cycles, TR, with the animal breathing through a low resistance, R1, or a high resistance, R2. The oblique lines correspond to various iso-ventilatory flow rates, in milliliters per second. Symbols as in Figure 2. Mean values for R1 ($N = 16$): Vs = 0.87 ± 0.23 ml; TR = 13.1 ± 2.9 s; $\dot{V}w$ = Vs/TR = 0.069 ± 0.026 ml/s. Mean values for R2 ($N = 10$): Vs = 0.70 ± 0.18 ml; TR = 14.5 ± 2.0 s; $\dot{V}w$ = Vs/TR = 0.049 ± 0.017 ml/s. Only the $\dot{V}w$ values are significantly different.

suring the duration of each respiratory period, TR, and calculating the stroke volume of the pump, Vs, according to the equation Vs = $\dot{V}w \times$ TR. Figure 6 shows that the breathing pattern was similar whether the animal was breathing against a low or high resistance. However, the ventilatory flow rate under high resistance was significantly lower than under low resistance, with a small, nonsignificant decrease of the stroke volume and a small, nonsignificant increase of the ventilatory period (see legend of Fig. 6 for statistics).

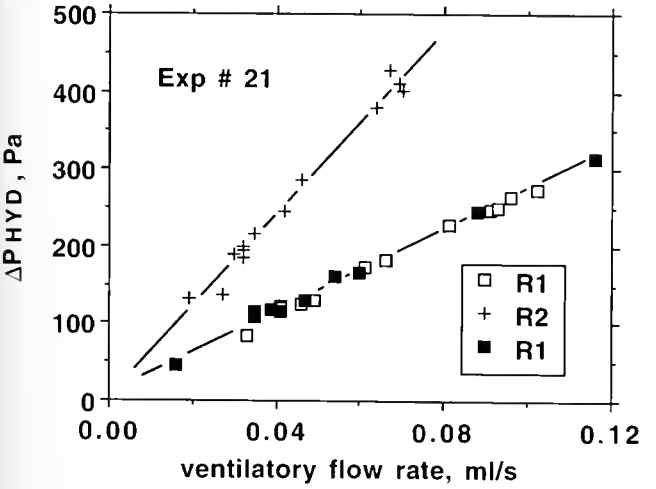

Figure 5. *Arenicola* #21. ΔPHYD, difference of pressure between the anterior chamber and atmosphere, as a function of $\dot{V}w$, the ventilatory flow rate through low and high resistances, R1 and R2. Values of ΔPHYD and $\dot{V}w$ from Figures 2 and 3. The slopes of the regression lines correspond to the mean values of R1 and R2, about 2600 and 5900 Pa · s/ml. Symbols as in Fig. 2. Equation corresponding to R1: $y = 2635\,x + 10$ ($r = 0.996$), and to R2: $y = 5917\,x + 5$ ($r = 0.991$).

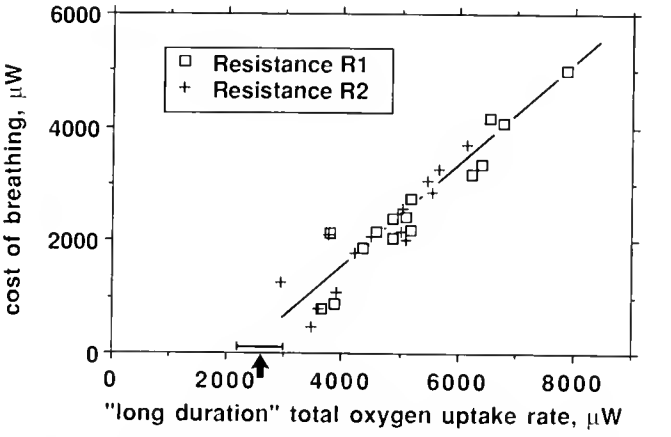

Figure 7. Energy cost of breathing, $\dot{M}_{O_2}^{CB}$, as a function of the "long duration" total O_2 uptake rate, $lg\dot{M}_{O_2}^{TOT}$, of *Arenicola* breathing through a resistance R1 (*ca* 2600 Pa · s/ml) or R2 (*ca* 5900 Pa · s/ml). Values for 10 experiments of three periods, each animal breathing successively through resistances R1, R2, R1 or R2, R1, R2. The arrow on the abcissa at 2600 ± 400 µW ($N = 10$) corresponds to the measure of the basal metabolism of the lugworm, *i.e.*, the mean O_2 uptake rate of an animal doing no ventilatory work, as measured by confinement, $\dot{M}_{O_2}^{CONF}$. The O_2 uptake rate above $\dot{M}_{O_2}^{CONF}$ is considered as the energy cost of breathing. The slope of the regression line ($y = 0.89\,x - 2024$; $N = 30$; $r = 0.838$) is not significantly different from the theoretical value of 1 (see equation 2).

Figure 7 summarizes for the 10 experiments the relationship between the energy cost of breathing, $\dot{M}_{O_2}^{CB}$, and the long duration total oxygen uptake rate, $lg\dot{M}_{O_2}^{TOT}$. Each value corresponds to one period of 126 ± 23 min (N = 30) and to either the R1 or R2 value of the resistance at the anterior exit. The $\dot{M}_{O_2}^{CB}/lg\dot{M}_{O_2}^{TOT}$ ratio varied between 0.14 and 0.64, with a mean value of 0.47. The regression line, corresponding to the mean variations of $\dot{M}_{O_2}^{CB}$ over $lg\dot{M}_{O_2}^{TOT}$, intersects the x-axis within the variation interval of the mean basal metabolism measured by the confinement method, $\dot{M}_{O_2}^{CONF}$ = 2600 ± 400 μW (N = 10). It is clear that there was no systematic difference between the R1 and R2 periods and that the energy cost of breathing increased linearly with the rise of $lg\dot{M}_{O_2}^{TOT}$.

Discussion

Validity of the model, hypotheses, and methods

Equation (2) is valid only in steady state conditions, that is, when the term $\Delta\dot{M}_{O_2}^{STO}$ is null. In the lugworm, the ventilation is periodic, with ventilatory bouts lasting 10 to 15 min, separated by pauses of a few minutes during which the O_2 stores can be partially depleted but then are quickly restored during the following ventilatory phase. Consequently, in the lugworm, equation (2) is valid only in the long term, in experiments that last a few hours and allow us to consider that any difference in the size of the O_2 stores at the beginning and at the end of an experiment is negligible relative to the overall O_2 uptake during the experiment. This is the case when we consider R1 and R2 periods lasting an average of 126 ± 23 min (Fig. 7).

Conversely, when we analyze separately each of the short 6-min runs in a given period (for example, *Arenicola* #21, Figs. 2 to 6), it is clear that equation (2) does not apply to all runs. This is demonstrated by Figs. 2 to 4, in which the lowest values of ventilatory flow rate, of ΔPHYD, and of mechanical power correspond to values of $sh\dot{M}_{O_2}^{TOT}$ that are lower or equal to $\dot{M}_{O_2}^{CONF}$, and consequently correspond to impossible negative or null values of this variable. Obviously, the term $\Delta\dot{M}_{O_2}^{STO}$ was not identical at the beginning and at the end of the corresponding runs: the lowest $sh\dot{M}_{O_2}^{TOT}$ values correspond to a depletion of the O_2 stores, whereas the highest $sh\dot{M}_{O_2}^{TOT}$ values correspond to their restoration. It is important to note that when the animal is in complete apnea, then $\dot{V}w = 0$, implying $sh\dot{M}_{O_2}^{TOT} = 0$, and the aerobic metabolism totally depends on the O_2 stores. In all cases, however, if our evaluations of $\dot{V}w$, ΔPHYD, and $sh\dot{M}_{O_2}^{TOT}$ are correct, then their analysis is pertinent, giving information on the ventilatory pump and its energetics.

Does $\dot{M}_{O_2}^{CONF}$ correctly estimate the basal O_2 uptake rate? A lugworm in a confinement vessel, deprived of normal contacts with its gallery walls, is never perfectly still. Actually, the tail-to-head peristaltic movements of the body wall are more or less preserved, but they do not produce a true external ventilatory current of seawater. Then the oxygen consumption corresponding to the mechanical work achieved during the confinement can be considered as negligible compared with that occurring in an animal ventilating through an exit resistance in its artificial gallery. However, it is quite certain that $\dot{M}_{O_2}^{CONF}$ slightly overestimates the basal metabolism, leading to the conclusion that $\dot{M}_{O_2}^{CB}$ is slightly underestimated.

Cost of breathing and energetics and respiratory strategy in the lugworm

It is clear from Figure 7 that the lugworm's energy cost of breathing, $\dot{M}_{O_2}^{CB}$, evaluated as $lg\dot{M}_{O_2}^{TOT}$ *minus* $\dot{M}_{O_2}^{CONF}$, varies considerably and is generally high, the $\dot{M}_{O_2}^{CB}$ *vs* $lg\dot{M}_{O_2}^{TOT}$ ratio varying between 0.14 and 0.64, with a mean value at 0.47. Our previous, more qualitative evaluations (Toulmond, 1975; Toulmond and Tchernigovtzeff, 1984; Toulmond, 1986) are directly confirmed, and it is demonstrated that the lugworm's ventilatory piston pump is energetically expensive.

$\dot{M}_{O_2}^{CB}$ has rarely been directly evaluated in invertebrates. The most recent studies on the energetics of invertebrate water pumps give the following values of the $\dot{M}_{O_2}^{CB}$ *vs* $\dot{M}_{O_2}^{TOT}$ ratio: 0.02 in the ascidian *Styela clava* (data from Riisgård, 1988); 0.03 in the polychaete *Sabella penicillus* (Riisgård and Ivarsson, 1990); 0.09 in the bivalve *Mytilus edulis* (data from Jørgensen *et al.*, 1988); 0.2 in *Chaetopterus variopedatus*, another polychaete (data from Riisgård, 1989); and 0.30 to 0.48 in *Urechis caupo* (Pritchard and White, 1981). The first three species have ciliary pumps. *Chaetopterus* and *Urechis*, like the lugworm, have a muscular piston pump and exhibit the highest $\dot{M}_{O_2}^{CB}$ *vs* $\dot{M}_{O_2}^{TOT}$ ratios. It is clear that a piston pump consumes a sizable amount of the total quantity of oxygen it obtains from the environment.

The flow rates we measured were never very high, between 0.02 and 0.12 ml/s in *Arenicola* #21 (Fig. 2). This compares well with data recalculated from values measured by previous authors in normoxic lugworms of various sizes: 0.02 to 0.12 ml/s (Van Dam, 1938); 0.03 to 0.07 ml/s (Krüger, 1964); 0.01 to 0.03 ml/s (Jacobsen, 1967); 0.01 to 0.02 ml/s (Foster-Smith, 1978). In *Arenicola* #21, the corresponding mean value of the specific ventilation, $\dot{V}w/sh\dot{M}_{O_2}^{TOT}$ = 5 l/mmol O_2, which is practically identical to that measured in normoxic lugworms (Toulmond and Tchernigovtzeff, 1984), is exceedingly low compared to values (in liters per millimole of O_2) reported for filter feeders: 7930 in *Sabella penicillus* (Riisgård and Ivarsson, 1990); 900 in the occasional suspension feeder *Nereis diversicolor* (Riisgård, 1991); and 560 to 1120 in *Chaetopterus variopedatus* (Riisgård, 1989). Jørgensen *et al.* (1986b) consider that filter feeders inhabiting coastal

waters typically process 340 l or more of water for each millimole of O_2 consumed. When considering the extremes of this set of specific ventilation values, it is easy to calculate that the O_2-extraction coefficient is about 80 to 1600 times lower in filter feeders (Ew_{O_2} between 0.0005 and 0.01) than it is in the normoxic lugworm ($Ew_{O_2} = 0.82 \pm 0.05$, $N = 37$, in *Arenicola* #21). The filter feeders, which process very large volumes of water to get enough food, are practically in equilibrium with the ambient medium as far as oxygen is concerned, and their oxygen needs are easily satisfied (Hazelhoff, 1939; Jørgensen, 1955), even when ambient hypoxia is severe (Massabuau *et al.*, 1991).

Foster-Smith (1978) postulated that the pumping mechanism of an animal must have been selected to work considerably below its maximum power most of the time. If the hypothesis is correct, then a relatively large change in the resistance of the system must have only small effects on the pumping rate. Our results effectively show that changing the resistance in our experimental setting makes little difference to pumping rate (Fig. 2) and to cost of breathing (Fig. 7). In the lugworm, the piston pump operates at rather high values of ΔPHYD, up to 430 Pa in *Arenicola* #21 (Fig. 3). This value agrees roughly with previous records in the literature (Foster-Smith, 1978; Toulmond *et al.*, 1984) and is well below the maximal possibilities of a lugworm. Actually, ΔPHYD values between 1000 and 1500 Pa were commonly observed in our experimental setting. Thus the hydrostatic pressure that can be developed by the piston pump of *Arenicola* is much higher than those that have been measured in filter feeders. Jørgensen *et al.* (1986a) give an upper limit of 50 Pa to the maximum pressure that can be developed by the bivalve ciliary pump. Even in those filter feeders that have a ventilatory piston pump, the maximal operating pressures are much lower than in the lugworm: about 80 Pa in *Chaetopterus* (Riisgård, 1989) and *Nereis diversicolor* (Riisgård, 1991); less than 100 Pa in *Urechis caupo* (Chapman, 1968). Obviously, in natural conditions, the lugworm needs a more powerful engine to overcome the resistance created by the sediment that blocks the blind head-end of its gallery. The mean values of our artificial resistances R1 and R2, calculated as the slopes of the regression lines in the ΔPHYD *vs* $\dot{V}w$ graph of Figure 5, were respectively about 2600 and 5900 Pa · s/ml. From the values of ΔPHYD and $\dot{V}w$ that can be found or calculated from data in the literature, the resistance $R = \Delta PHYD/\dot{V}w$ against which a given biological pump has to work to process water for filtration or respiratory purposes, or both, can be estimated. The values we found were (in Pa · s/ml) about 750 in *Urechis* (Chapman, 1968); 50 in *Chaetopterus* (Riisgård, 1989) and *Nereis* (Riisgård, 1991); 20 to 10 in *Mytilus* (Jørgensen *et al.*, 1986a); 10 in *Styela* (Riisgård, 1988); and 0.1 in *Sabella* (Riisgård and Ivarsson, 1990). These resistances are much lower than those we used in our experimental setting. Do such high resistances occur in natural conditions? There are no direct data. R1 and R2 were in fact chosen to avoid the worms' turning around head to tail in the glass tube; this behavior is common when the system resistance is too high and is also observed in *Chaetopterus* (Riisgård, 1989). The fact that our animals continued to pump against R1 and R2 means that these resistances must approximate those against which the lugworms have to work in natural conditions.

Figure 4 shows that the mechanical power developed by the piston pump of *Arenicola* #21 during normal ventilation, and calculated as $\dot{W}_{MEC} = \Delta PHYD \times \dot{V}w$, is very low compared to the energy cost of breathing, $\dot{M}_{O_2}^{CB}$. The efficiency of the pump, calculated as the ratio $\dot{W}_{MEC}/\dot{M}_{O_2}^{CB}$, is low or very low, depending on which run is considered, with a mean value of about 1% as in other tested animals. However, this efficiency is certainly underestimated, since $\dot{W}_{MEC}$ is only one part of the total mechanical power, $\dot{W}$, that is actually developed by the ventilating lugworm, and corresponds only to the work done on the water expelled from the experimental gallery. We know nothing about the work done inside the animal body: to each stroke volume of water ventilated in the headward direction must correspond an identical volume of coelomic fluid and blood moving backward inside the animal. We also do not know how much work is done by the body wall muscles forming and maintaining the peristaltic wave that acts as the piston of the pump. As far as we know, these two mechanical works have never been examined experimentally. We also did not take into account the mechanical work done to fill the posterior compartment of the apparatus, but this can be considered negligible owing to the very wide opening and very low resistance of the inlet tubing (Fig. 1). However, even if we consider that the sum of these three types of unmeasured mechanical work is approximately equivalent to the work necessary to expel water from the gallery, the pump efficiency is still only two times higher than previously estimated and remains very low, at about 2%.

Conclusion

To conclude, it is clear that in *Arenicola*, which ventilates its gallery with a piston pump, the cost of breathing is very high. However, it appears from the above discussion that we cannot precisely calculate the real mechanical efficiency of the process of breathing in the lugworm. This kind of difficulty has been met by Scheid (1987), in a comparison of the costs of breathing in mammals and fishes, and originates in the fact that, whatever animal is considered, breathing is a complex activity that cannot be completely isolated from some other functions such

as, in the case of the lugworm, the circulation of the blood and of the coelomic fluid.

Acknowledgments

We thank Ms. F. Kleinbauer, M.-M. Loth, and M. Schneider for their help in the preparation of the paper, Dr. S. Dejours for reviewing the manuscript, and Dr. J.-P. Truchot for helpful comments. We thank the anonymous referees for pertinent remarks that all improved the manuscript. This study was supported by the Centre National de la Recherche Scientifique (UPR 4601) and by the Institut Français de Recherche pour l'Exploitation de la Mer (URM 7).

Literature Cited

Brown, S. C. 1975. Biomechanics of water-pumping by *Chaetopterus variopedatus* Renier. Skeletomusculature and kinematics. *Biol. Bull.* **149:** 136–150.

Chapman, G. 1968. The hydraulic system of *Urechis caupo* Fisher & MacGinitie. *J. Exp. Biol.* **49:** 657–667.

Dejours, P. 1981. *Principles of Comparative Respiratory Physiology.* Elsevier/North-Holland, Amsterdam.

Foster-Smith, R. L. 1978. An analysis of water flow in tube-living animals. *J. Exp. Mar. Biol. Ecol.* **34:** 73–95.

Hazelhoff, E. H. 1939. Über die Ausnutzung des Sauerstoffs bei verschiedenen Wassertieren. *Z. Vgl. Physiol.* **26:** 306–327.

Jacobsen, V. H. 1967. The feeding of the lugworm, *Arenicola marina* (L.). Quantitative studies. *Ophelia* **4:** 91–109.

Jørgensen, C. B. 1955. Quantitative aspects of filter feeding in invertebrates. *Biol. Rev.* **30:** 391–454.

Jørgensen, C. B., P. Famme, H. S. Kristensen, P. S. Larsen, F. Mohlenberg, and H. U. Riisgård. 1986a. The bivalve pump. *Mar. Ecol. Prog. Ser.* **34:** 69–77.

Jørgensen, C. B., F. Mohlenberg, and O. Sten-Knudsen. 1986b. Nature of relation between ventilation and oxygen consumption in filter feeders. *Mar. Ecol. Prog. Ser.* **29:** 73–88.

Jørgensen, C. B., P. S. Larsen, F. Mohlenberg, and H. U. Riisgård. 1988. The mussel pump: properties and modelling. *Mar. Ecol. Prog. Ser.* **45:** 205–216.

Krüger, F. 1964. Messungen der Pumptätigkeit von *Arenicola marina* L. im Watt. *Helgol. Wiss. Meeresunters.* **Bd 1:** 70–91.

Mangum, C. P. 1976. Primitive respiratory adaptations. Pp. 191–278 in *Adaptations to Environment: Essays on the Physiology of Marine Animals,* R. C. Newell, ed. Butterworths, London.

Massabuau, J. C., B. Burtin, and M. Wheatly. 1991. How is O_2 consumption maintained independent of ambient oxygen in mussel *Anodonta cygnea*? *Respir. Physiol.* **83:** 103–114.

Newell, R. C. 1979. *Biology of Intertidal Animals* 3rd edition, Marine Ecological Surveys, Ltd, P.O.B. 6, Faversham, Kent, U.K.

Pritchard, A., and F. N. White. 1981. Metabolism and oxygen transport in the innkeeper *Urechis caupo*. *Physiol. Zool.* **54:** 44–54.

Riisgård, H. U. 1988. The ascidian pump: properties and energy cost. *Mar. Ecol. Prog. Ser.* **47:** 129–134.

Riisgård, H. U. 1989. Properties and energy cost of the muscular piston pump in the suspension feeding polychaete *Chaetopterus variopedatus*. *Mar. Ecol. Prog. Ser.* **56:** 157–168.

Riisgård, H. U. 1991. Suspension feeding in the polychaete *Nereis diversicolor*. *Mar. Ecol. Prog. Ser.* **70:** 29–37.

Riisgård, H. U., and N. M. Ivarsson. 1990. The crown-filament pump of the suspension-feeding polychaete *Sabella penicillus*: filtration, effects of temperature, and energy cost. *Mar. Ecol. Prog. Ser.* **62:** 249–257.

Scheid, P. 1987. Cost of breathing in water- and air-breathers. Pp. 83–92 in *Comparative Physiology: Life in Water and on Land. Fidia Res. Ser. Vol IX.* P. Dejours, L. Bolis, C. R. Taylor, and E. R. Weibel, eds. Liviana Press, Padova.

Toulmond, A. 1975. Blood oxygen transport and metabolism of the confined lugworm *Arenicola marina* (L.). *J. Exp. Biol.* **63:** 647–660.

Toulmond, A. 1986. Adaptations to extreme environmental hypoxia in water breathers. Pp. 123–136 in *Comparative Physiology of Environmental Adaptations, Vol. 2,* P. Dejours, ed. Karger, Basel.

Toulmond, A., and C. Tchernigovtzeff. 1984. Ventilation and respiratory gas exchanges of the lugworm *Arenicola marina* (L.) as functions of ambient P_{O_2} (20-700 Torr). *Respir. Physiol.* **57:** 349–363.

Toulmond, A., C. Tchernigovtzeff, P. Greber, and C. Jouin. 1984. Epidermal sensitivity to hypoxia in the lugworm. *Experientia* **40:** 541–543.

Van Dam, L. 1938. *On the Utilization of Oxygen and Regulation of Breathing in Some Aquatic Animals.* Volharding, Groningen.

Walshe-Maetz, B. M. 1953. Le métabolisme de *Chironomus plumosus* dans des conditions naturelles. *Physiol. Comp. Oecol.* **3:** 135–154.

Wells, G. P. 1966. The lugworm (*Arenicola*). A study in adaptation. *Neth. J. Sea Res.* **3:** 294–313.

Appendix

List of symbols

$M_{O_2}^{TOT}$, $\dot{M}_{O_2}^{TOT}$:	Total oxygen uptake, μJ, and total oxygen uptake rate, μW.
$sh\dot{M}_{O_2}^{TOT}$:	"Short duration" total oxygen uptake rate, μW.
$lg\dot{M}_{O_2}^{TOT}$:	"Long duration" total oxygen uptake rate, μW.
$M_{O_2}^{CONF}$, $\dot{M}_{O_2}^{CONF}$:	Basal metabolic oxygen uptake, μJ, and basal metabolic uptake rate, μW, obtained using the confinement method.
$M_{O_2}^{CB}$, $\dot{M}_{O_2}^{CB}$:	Energy cost of breathing, μJ, and rate of energy cost of breathing, μW.
$\Delta M_{O_2}^{STO}$, $\Delta \dot{M}_{O_2}^{STO}$:	Change in the oxygen stores, μJ, and rate of change in the oxygen stores, μW.
$\dot{W}_{MEC}$:	Mechanical power, μW.
PI_{O_2}, PE_{O_2}:	Oxygen partial pressure in inspired (I) and expired (E) water, kPa.
CI_{O_2}, CE_{O_2}:	Oxygen concentration in inspired (I) and expired (E) water, mmol/ml.
Vw, $\dot{V}$w:	Ventilatory flow, ml, and ventilatory flow rate, ml/s.
ΔP_{HYD}:	Hydrostatic pressure difference, Pa.
R1, R2:	Two different hydraulic resistances, Pa · s/ml.

Reference: *Biol. Bull.* **186:** 221–240. (April, 1994)

In Vivo Studies of Suspension-Feeding Processes in the Eastern Oyster, *Crassostrea virginica* (Gmelin)

J. EVAN WARD[1], ROGER I. E. NEWELL[2], RAYMOND J. THOMPSON[3], AND BRUCE A. MACDONALD[1]

[1]*Marine Research Group, Department of Biology, University of New Brunswick, Saint John, New Brunswick, E2L 4L5, Canada;* [2]*Horn Point Environmental Laboratory, Center for Environmental and Estuarine Studies, University of Maryland System, Cambridge, Maryland, 21613;* [3]*Marine Sciences Research Laboratory, Memorial University of Newfoundland, St. John's, Newfoundland, A1C 5S7, Canada*

Abstract. Suspension-feeding processes in the eastern oyster *Crassostrea virginica* (Gmelin, 1791) were examined, *in vivo*, with an endoscope linked to a video image-analysis system. We found that many of the previously published concepts of particle transport and processing in this species, obtained using surgically altered specimens or isolated organs, are incomplete or inaccurate. In particular, our observations demonstrate that (1) captured particles are transported along the gills by both mucociliary (marginal grooves) and hydrodynamic (basal tracts) processes; (2) the labial palps accept material from the gills both in mucus-bound particle strings (transported in marginal grooves), and suspended in particle slurries (transported in basal tracts); (3) the labial palps reduce the cohesive integrity of the mucous strings and disperse and sort the entrapped particles; (4) particles are ingested in the form of a slurry; and (5) ciliary activity on the labial palps is independent of that on the lips, allowing the oyster to filter particles from suspension and produce pseudofeces without ingesting any particulate matter. Because many ostreids have the same plicate gill structure, we believe that our conclusions are applicable to other oyster species. In addition, the present observations are consistent with other endoscopic examinations recently made on bivalves in different families. We conclude that accepted theories of particle handling in suspension-feeding bivalve mollusks must be modified to accommodate observations made with the endoscope.

Received 8 July 1993; accepted 3 January 1994.

Abbreviations: OIT—optical insertion tube of the endoscope.

Introduction

The eastern oyster *Crassostrea virginica* (Ostreidae, Bivalvia) is an ecologically important species, often forming dominant epibenthic populations on the Atlantic and Gulf Coasts of North America. These oyster populations can influence the surrounding environment through particle depletion, nutrient cycling, and biodeposition (Dame *et al.*, 1984; Jordan, 1987; Newell, 1988). In addition, *C. virginica* forms the basis of a commercially important fishery throughout its range. As a consequence of their ecological and economic value, eastern oysters have been studied extensively, and numerous reports about their ecology, physiology, and anatomy have been published (for reviews see Galtsoff, 1964; Eble *et al.*, 1994). Specifically, the capture of particles on the gills; transport of particulate matter to the labial palps, mouth, and stomach; and processing of food material in the alimentary system have been thoroughly described (*e.g.*, Menzel, 1955; Nelson, 1960; Galtsoff, 1964; Ribelin and Collier, 1977; Newell and Langdon, 1994; Langdon and Newell, 1994).

Unfortunately, methodological limitations have constrained the study of feeding processes in whole, intact oysters. Nelson (1923) and Menzel (1955) did describe some aspects of particle capture and transport in whole juvenile oysters; their light microscopical observations were made through the transparent shells of post-set specimens that had been allowed to metamorphose and grow attached to glass microscope slides. With these exceptions, however, most reports about particle capture and transport by the pallial organs have been based on observations of isolated structures, or examinations of structures in sur-

gically altered oysters (*e.g.*, Nelson, 1960; Galtsoff, 1964). Although such studies underlie our present understanding of suspension-feeding in most bivalve families, including the Ostreidae, problems inherent in the observational techniques may have led to erroneous or incomplete conclusions. For example, removal and isolation of the gills destroys the subtle hydrodynamic interactions that often exist between these structures and moving particles (Beninger *et al.*, 1992; Ward *et al.*, 1993), and perturbs the physiological and neurological mechanisms that control muscular and ciliary movement. Surgery can also alter the normal flow of water through the pallial cavity and may damage delicate feeding structures. Furthermore, surgery can stimulate excess mucus production and cause the feeding structures to function abnormally (Jorgensen, 1976).

In contrast, recently developed techniques in video endoscopy (Ward *et al.*, 1991) have allowed us to reevaluate suspension-feeding mechanisms in whole, intact bivalves (Beninger *et al.*, 1992; Ward *et al.*, 1993). There are many advantages of video endoscopy over previous techniques: (1) no surgical alteration of tissue is required; (2) the optical insertion tube (OIT) of the endoscope is small enough (1.7 mm diameter) to be inserted between demibranchs of the gill, between opposing labial palps, and even into the alimentary canal; and (3) video recording and image analysis facilitate observations and their documentation, and permit post-observational analysis of the biodynamics of particle processing.

In this study, we employed video endoscopy to examine, *in vivo*, the feeding structures and mechanisms in *C. virginica*. Particle kinematics were studied, from the point of capture on the gills, to post-ingestive processing in the stomach. Of particular interest were the modes of particle transport (*e.g.*, mucous-bound or suspended), and their implications for particle sorting and ingestion. We then used our results to address several fundamental questions about suspension feeding in intact oysters: (1) What are the mechanisms of particle sorting on the gills? (2) What is the mode of particle transport on the frontal surfaces and margins of the gills? (3) How are particles transferred from the gills to the labial palps? (4) what are the mechanisms of particle sorting and transport on the labial palps? (5) In what mode are particles ingested? (6) Are particles in the stomach tightly bound in mucus, or freely suspended? Finally, we compared our endoscopic observations of intact oysters with previous reports of feeding processes in order to better understand suspension-feeding mechanisms in the Ostreidae.

Materials and Methods

Ten *Crassostrea virginica* adults were maintained in an aerated 60-l aquarium at the Marine Sciences Research Laboratory, Memorial University of Newfoundland. Seawater in the container was replaced every other day, and was maintained at 15–21‰ and 15–20°C. Oysters were fed a daily maintenance ration of the cultured diatom *Chaetoceros muelleri* Lemmermann.

Specimens were prepared for endoscopy by carefully trimming a small section (about 3–6 cm in length × 0.5–1 cm in width) of the inhalant margin of the upper and lower valves. This was done without damaging the underlying mantle margins and produced a narrow opening in the shell. Trimming of the shell served three purposes. First, it allowed us to introduce the optical insertion tube (OIT) into the pallial cavity of an oyster, even when the specimen was closed and not feeding; second, it provided more freedom of movement for the OIT when the specimen was open and actively feeding; third, it prevented the shell edges from damaging the OIT when the specimen adducted its valves. Oysters prepared in this way were allowed to recover for at least one day before use; often shell repair began during the several weeks that these animals were held in the aquarium.

Several specimens were further manipulated so we could insert the OIT through the mouth and into the alimentary canal. Because *C. virginica* is monomyarian, the anterior portion of the body is not attached to the shell by muscles and could be carefully lifted through the narrow opening we had cut in the shell. The body was gently held in an extended position with several monofilament nylon lines attached to hooked retractors that were inserted into the outer portions of the visceral mass. This fully exposed the mouth and allowed us to insert the OIT. A similar procedure was used by investigators wishing to inject latex (Galtsoff, 1964) or food material (Newell and Langdon, 1986) directly into the oyster's alimentary system.

Endoscopy was performed according to methods described by Ward *et al.* (1991). Briefly, the endoscope (OIT = 1.7 mm in diameter) was connected to an optical zoom-adapter and attached to a monochrome, charge-coupled-device camera. The resolution of the video-endoscope was about 5 μm at a maximum magnification of about 150 ×. Video signals were recorded on an 8 mm VCR (Hi8). The recorded images were then digitized with a video digitizing board (RasterOps, Corp.) and enhanced for morphometric analysis with Adobe Photoshop software (Adobe Systems, Inc.).

Morphometric measurements made on the digitized images were calibrated by isolating the pallial organs (*e.g.*, gills, labial palps, lips) of several specimens, and measuring the width of various structures (*e.g.*, filaments, plicae, ciliated ridges) with a compound microscope and a calibrated ocular micrometer. Particle velocities could then be determined by counting the number of frames required

for a particle to traverse a known distance along a given organ; recording speed was 30 frames $\cdot s^{-1}$ (NTSC format). Velocities ($\mu m \cdot s^{-1}$) are presented as means $\pm$ 1 standard deviation.

During endoscopic examination, the oysters were held in an aerated, closed seawater system at the same temperature and salinity as the holding aquarium. The specimens were allowed to feed freely on natural seston supplemented with various particles, including silica (2–6 μm diameter), reflective red plastic particles (about 5 μm diameter, Radiant Color, Hercules Inc.), polystyrene microspheres (about 18 μm diameter, Polysciences Inc.), spray-dried *Tetraselmis* sp. (2–13 μm diameter, Celsys, Cell Systems Ltd.), and the diatom *C. muelleri* (about 6 μm diameter, cultured in f/2 medium; Guillard, 1975). Prior to use, *Tetraselmis* cells were pelleted twice in a centrifuge and resuspended in 1 liter of seawater; they were then resuspended by sonication at low power for 10 min. The polystyrene microspheres were cleaned with 30% H_2O_2 for 5 min and washed with 1 liter of filtered seawater or distilled water; they were then sonicated for 10 min. To increase particle concentration above the background level (10^4 particles $\cdot$ ml^{-1}), we delivered 2–5 ml of stock particle suspensions (10^5–10^6 particles $\cdot$ ml^{-1}), as needed, to the inhalant margin of oysters using a peristaltic pump or Pasteur pipet.

Whole cell extracts prepared from *C. muelleri* cultures were used to test the effects of chemical stimulation on feeding and particle selection. Diatom cells were pelleted in a centrifuge, frozen at −20°C, thawed, and sonicated for 30 min. The disrupted cells were then passed through a GF/A glass fiber filter, and the filtrate collected and stored at −20°C until used (Ward *et al.*, 1992). In some experiments, microspheres were treated with the algal extract. This was done by activating the spheres with 100 ml of 100% methyl alcohol and then treating them with 50 ml *C. muelleri* whole cell extract (Ward, 1989).

Results are based on the endoscopic examination of ten oysters, and are presented as a composite of these observations. In some instances, surgically altered specimens were observed with a dissecting microscope, recreating the conditions under which previous workers had obtained their results. Finally, to verify certain structural aspects of the anterior portion of the demibranchs, scanning electron microscopy (SEM) was performed on isolated gill segments according to standard procedures (Glauert, 1980; Bozzda and Russell, 1992).

The anatomy of ostreid gills is often described in terms that vary from one publication to another. This is because the gills of oysters arch around the adductor muscle to such a degree that, depending on their location, portions of the demibranchs can occupy a posteroventral, ventral, or anterior position. In this publication we use the terminology of Atkins (1937b) and Nelson (1960). The ciliated regions that lie along the attached edges of the gills are herein termed basal ciliated tracts. Synonyms for these tracts include the dorsal (Nelson, 1923; Menzel, 1955), proximal (Nelson, 1960), or axial (Yonge, 1926) tracts, grooves, or furrows. The ciliated grooves that lie along the free edges of the gills are herein termed marginal ciliated grooves. Synonyms for these grooves include the ventral (Nelson, 1923; Menzel, 1955), lower-marginal or free-marginal (Yonge, 1926), and terminal (Galtsoff, 1964; Bernard, 1974) grooves or furrows.

All anatomical drawings have the dorsal-ventral axis oriented so that ventral is at the top and dorsal is at the bottom of the sketch. Although this orientation does not adhere strictly to convention, it does match the perspective depicted in the endoscope micrographs. This circumstance arose because the OIT was always inserted through the inhalant margin of the shell, so that the free margins of the pallial structures were the first to come into view. Furthermore, this orientation more closely reflects the position of oysters in nature.

Results

For clarity, our observations of suspension feeding in *Crassostrea virginica* are grouped into two sections. In the first section we deal with the anatomy and function of the pallial organs and alimentary canal, with emphasis on our novel observations. In the second section we deal with the functional importance of these observations to suspension-feeding processes, and describe the capture and transport of particles by the feeding organs described in the first section. We do not recapitulate the detailed anatomy of these organs; rather, we present novel observations of organ movements and functions and describe particle transport from gills to stomach. Where appropriate, the results are placed in the context of previous descriptions of feeding in oysters.

A. Organ structure and function

1. Gills. The most conspicuous structures in the pallial cavity of the oyster are the deeply plicated, heterorhabdic gills, which have been described in detail previously (Fig. 1A) (Atkins, 1937c; Nelson, 1960; Galtsoff, 1964). With the endoscope we could clearly see the ordinary filaments and the interfilamentary spaces that lead to the ostia (Fig. 1B), as well as the metachronal waves produced by cilia.

Our observations of the gills by means of endoscopy, light microscopy, and SEM reveal that modifications of previously reported descriptions must be made. The marginal ciliated groove does not extend along the entire length of each demibranch. Instead, at the anterior portion adjacent to the palps, the groove becomes narrower and

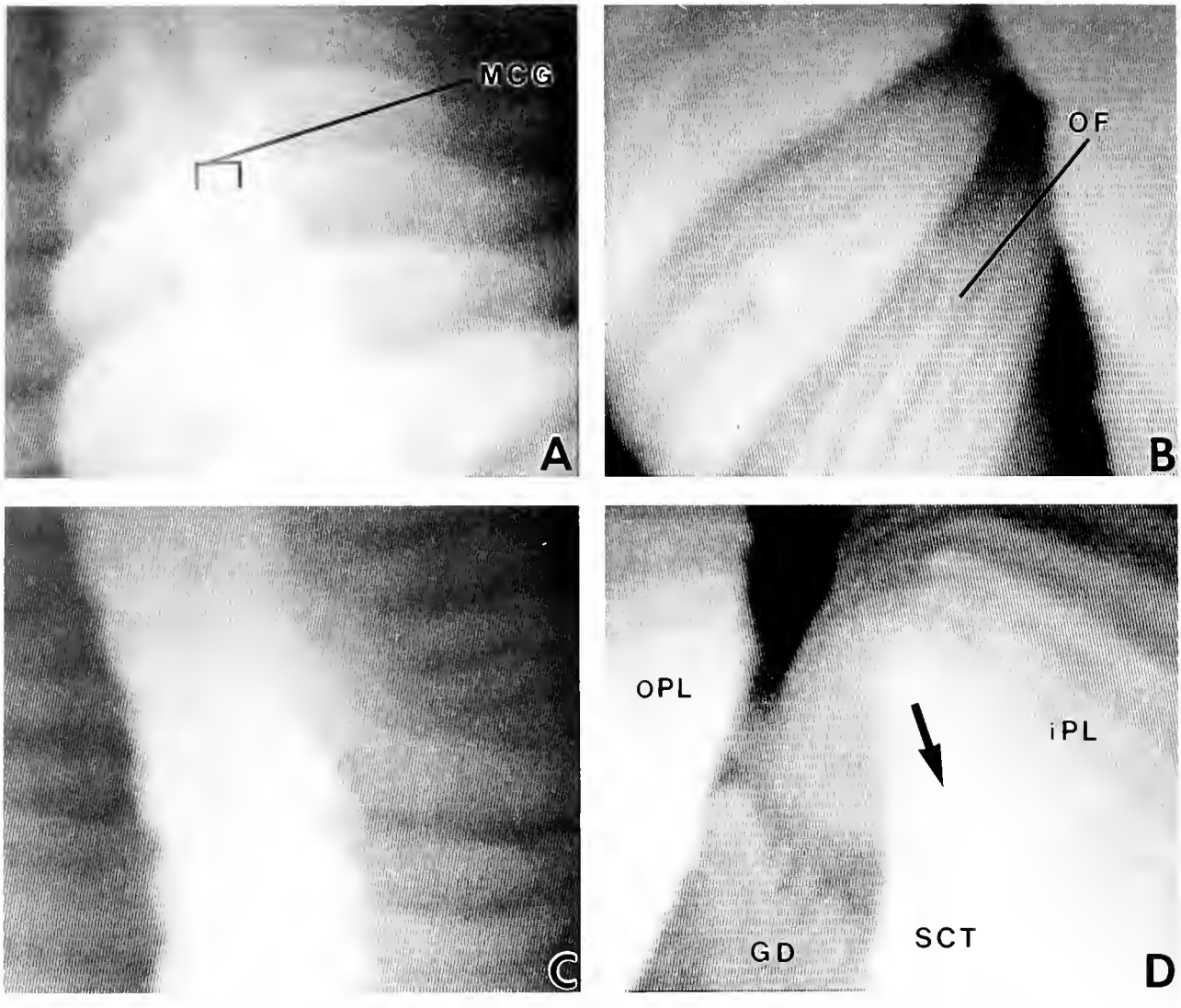

Figure 1. Video-endoscope micrographs showing, *in vivo*, several pallial structures of *Crassostrea virginica* (A) The margin of one gill demibranch is shown in normal feeding position. The deeply plicated structure of the demibranch can be seen. The ordinary filaments appear as lines running parallel to the axis of each plica (length of gill section = about 1.6 mm). (B) At higher magnification the ordinary filaments of the plicae are visible, as are the openings to the interfilamentary spaces that lead to the ostia, which appear as dark slits between the filaments (width of each filament = about 35 μm). (C) The margin of the gill demibranch displayed in A shown seconds later after contraction of the plicae. (D) A view of the anterior termination of one demibranch and the basal region of the surrounding labial palps. The ridged surfaces of opposing palp lamellae are visible. Note the smooth ciliated tract that lies at the posterior edge of each lamella and carries particles (*e.g.*, white dot) from the base of the palp towards the distal margin (arrow; width of each palp ridge = about 60 μm). (GD = gill demibranch, MCG = marginal ciliated groove, OF = ordinary filament, iPL = inner palp lamella, oPL = outer palp lamella, SCT = smooth ciliated tract).

shallower, resembling an indentation that runs along the midline of the margin (Fig. 2A, B). This indentation ends 2–3 plicae from the anterior termination of each demibranch (Fig. 3A). The transition from groove to indentation begins where the demibranch curves sharply towards its attached base on the visceral mass, about 7–10 plicae from the anterior termination of the demibranch (Figs. 2B; 3A). We call this anatomical location the "inflection point." It exists because the line of fusion of the ascending and descending lamellae is being distorted by the sharp decrease in height of each successive filament. The most anterior plica of each demibranch is composed

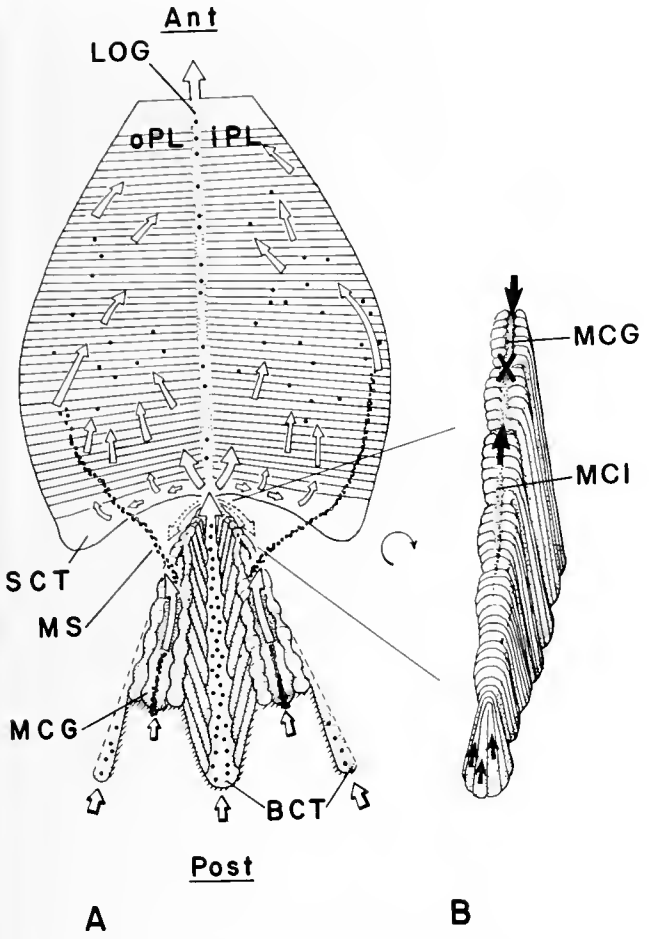

Figure 2. (A) Schematic diagram of the anterior portion of two demibranchs and their junction with one pair of labial palps of *Crassostrea virginica*. The palps are drawn folded back to reveal the direction of net particle movement (arrows) on the ciliated tracts and the ridged surfaces. Note that the cohesive integrity of mucous strings from the marginal ciliated grooves is reduced by the action of the palps so that the entrapped particles disperse. After sorting, particles are transported to the lips (smooth region at anterior edge of palp) and then mouth (not shown) for ingestion. (B) An enlargement of the anterior termination of one demibranch, which has been rotated 180° about its anterior-posterior axis. Note that the marginal groove becomes narrower and shallower 7–10 plicae from the termination. The transition from groove to indentation occurs at the inflection point of each demibranch (marked by X). Cilia in the groove and indentation beat in opposite directions (large arrows), and mucous balls form at the junction of these oppositely beating ciliary tracts (X). Excess particles from the basal gill-palp junction are transported to the marginal ciliated indentation (small arrows) via the ordinary filaments. (Ant = anterior, BCT = basal ciliated tract, LOG = lateral oral groove, MCG = marginal ciliated groove, MS = mucous string, iPL = inner palp lamella, oPL = outer palp lamella, Post = posterior, SCT = smooth ciliated tract).

entirely of ordinary filaments and wraps around the end of the demibranch, forming a rounded anterior termination (Fig. 2B). Along the entire anterior margin of each demibranch is a broad ciliated tract that covers the marginal indentation and transports material posteriorly towards the inflection point (Figs. 2B; 3B).

Our observations of gill movements within an intact oyster confirm previous reports made by Menzel (1955), Nelson (1960), and Galtsoff (1964). These findings include changes in the position of the demibranchs, and the occasional contraction and expansion of the plicae caused by the lateral movements of the ordinary filaments (Fig. 1A, C). Such movements of the gills probably force hemolymph into interfilamentary and interlamellar tissues (Elsey, 1935; Menzel, 1955; Galtsoff, 1964) and may facilitate the movement of water through the water tubes and into the epibranchial chamber.

2. Labial palps. The labial palps are positioned at the anterior termination of the gills. Endoscopic observations on the morphology of the palps confirm previous descriptions (Menzel, 1955; Nelson, 1960; Galtsoff, 1964), with only one modification. Along the entire free edge of each palp, nearest the gills, is a smooth, ciliated tract, two to three palp ridges wide. This tract, previously unreported, transports particles from the base of the palps to the apex (Figs. 1D; 2A).

The labial palps of oysters exhibited changes in muscular and ciliary activity that were positively correlated with increased particle capture and transport. When the particle concentration was low (10^4 particles $\cdot$ ml^{-1}), activity was also low. As concentration increased, more particles were transported anteriorly, and muscular and ciliary activity of the palps also increased.

During periods of active particle clearance, the palps constantly interacted with the gills. The apices of the palps would move along their adjacent demibranchs, from the ascending lamellae, across the marginal ciliated groove, to the descending lamellae, or *vice versa*. When this occurred, the inner and outer lamellae of one palp pair alternated between enclosing one and two demibranchs of a gill. The palps were often observed surrounding only one demibranch, but this condition did not interfere with the transfer of mucous strings from the gill to palp (see section B2). When actively removing material from the gills, the lamellae of each palp pair moved independently and alternated between being spread slightly apart and being closely appressed (Fig. 4A, B). When apart, some particles remained in close proximity to the ridged surfaces, while others occupied the space between the two opposing surfaces. The significance of this condition will be explained in section B2.

3. Lips and buccal region. The outer and inner lips of the oyster arise from the most anterior edge of the two outer and two inner palp lamellae, respectively (Fig. 5A; see also Galtsoff, 1964). Here, the ridged surfaces of the palps terminate and the smooth surfaces of the lips begin. The lateral walls of the lips possess broad tracts of cilia

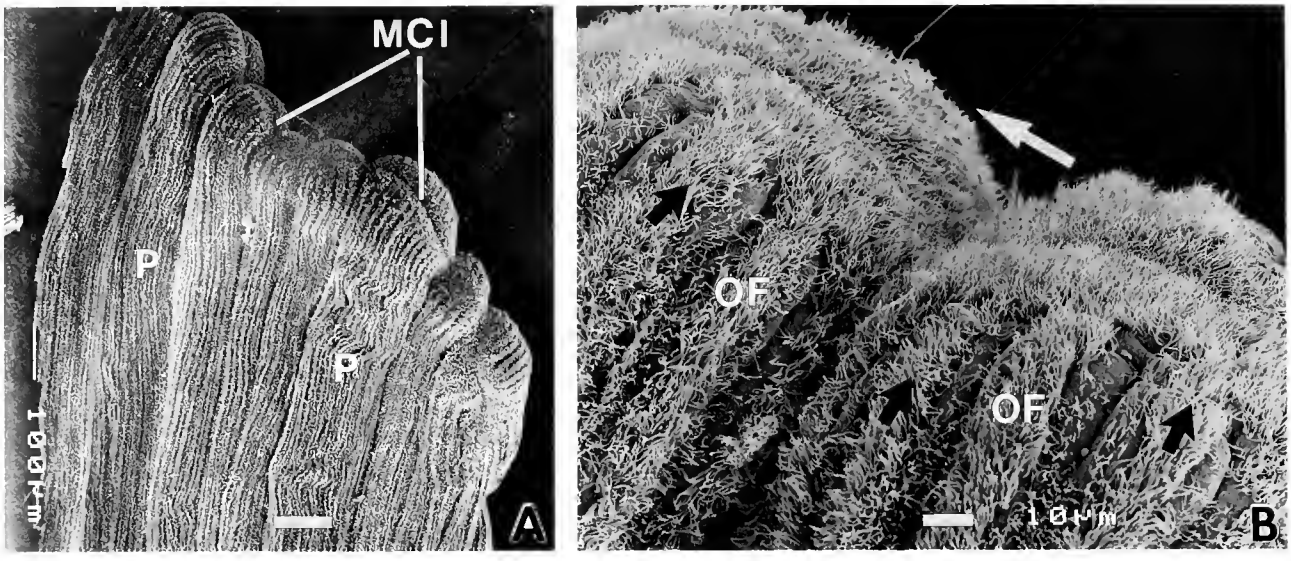

Figure 3. Scanning electron micrographs of the anterior termination of one gill demibranch of *Crassostrea virginica* (A) The distal edges of the seven most anterior plicae are shown, demonstrating that the marginal ciliated groove no longer exists and has formed an indentation that runs along the midline of the demibranch margin. Notice that the most anterior two plicae (far right side) lack this indentation. (B) Close up of the demibranch margin showing the ciliated tract that covers the indentation and directs particles posteriorly (white arrow). Notice the frontal cilia of the ordinary filaments that direct particles onto the marginal indentation (black arrows). Scale bars: A = 100 µm, B = 10 µm. (MCI = marginal ciliated indentation, OF = ordinary filament, P = plica).

that beat towards the mouth. A previously undescribed, highly ciliated tract runs along the entire free margin or ridge of the inner lip. When the inner lip is inserted into the outer lip, this ridge aligns with a ciliated tract on the outer lip (Figs. 4C, D; 5B). Prominent cilia on both the inner lip ridge and outer lip tract beat towards the mouth. A portion of the outer lip tract, just below the insertion of the inner lip, can be drawn in to form a gutter (Fig. 5B). The formation of this gutter usually coincided with active feeding.

The frequency of ciliary beating on the lips was not constant, nor was it associated solely with changes in particle capture and transport. On occasion, ciliary activity abruptly ceased and then, after a period of time, restarted. Furthermore, ciliary activity on the lips was independent of that on the palp ridges. Oysters that were feeding at background particle concentrations often had active gill and palp cilia but little or no ciliary activity on the lips. In one such specimen, several milliliters of *Chaetoceros muelleri* culture (10^6 cells · ml^{-1}) were introduced into the pallial cavity. Over a 5-min period, ciliary activity on the inner lip ridge and outer lip tract gradually increased until all cilia were actively beating.

In dissected oysters, cilia on the lips were either inactive or exhibited an irregular activity. In contrast, cilia on the gills and palps continued beating for many hours after dissection.

4. Esophagus and stomach. Our observations of the internal, gross morphology of the alimentary canal of an intact oyster confirm previous reports made by Owen (1955) and Galtsoff (1964). One modification of these reports, however, is that the stomach is not a chamber or cavity, but rather a compressed structure with walls that are tightly appressed. This is a consequence of the typhlosole protruding into the food-sorting caecum. The intestinal groove that carries rejected particles from the caecum is actually deep and concealed, hence preventing particles from reentering the main portion of the stomach (Purchon, 1977; Langdon and Newell, 1994). The conspicuous crystalline-style sac is lined with strong ridges that support tracts of actively beating cilia (Fig. 4E). The cilia rotated the style in a clockwise direction. To our knowledge, this study is the first to document crystalline style activity in an undissected bivalve.

B. Particle capture and transport

1. Gills. Particles entrained in the inhalant water current were first carried dorsally in the pallial cavity and then deflected laterally towards the frontal surfaces of the gill lamellae. Often, particles were drawn directly into the "troughs" between adjacent plicae, presumably by currents produced by the lateral cilia of the principal and transitional filaments that form each trough (Fig. 6; Nel-

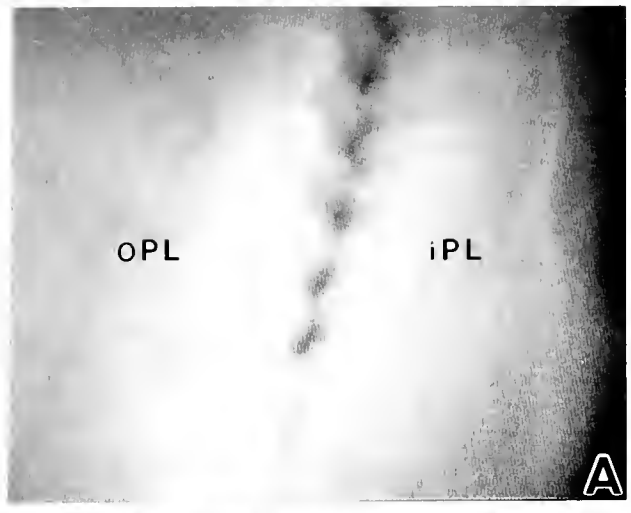

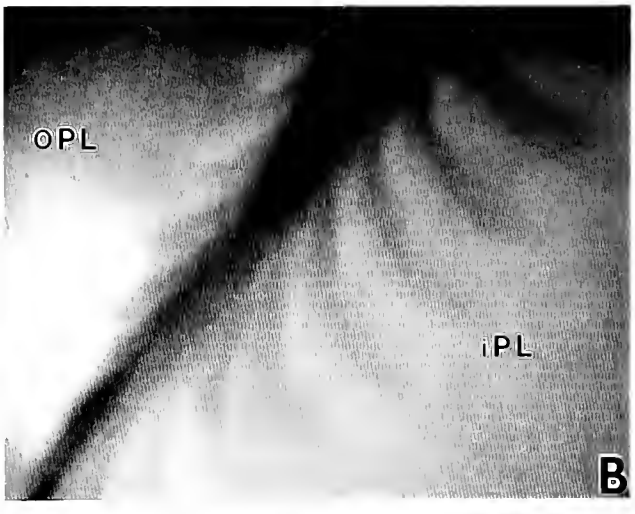

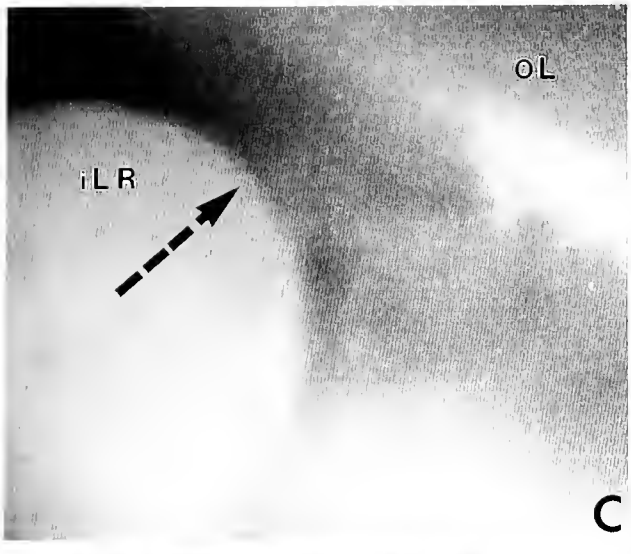

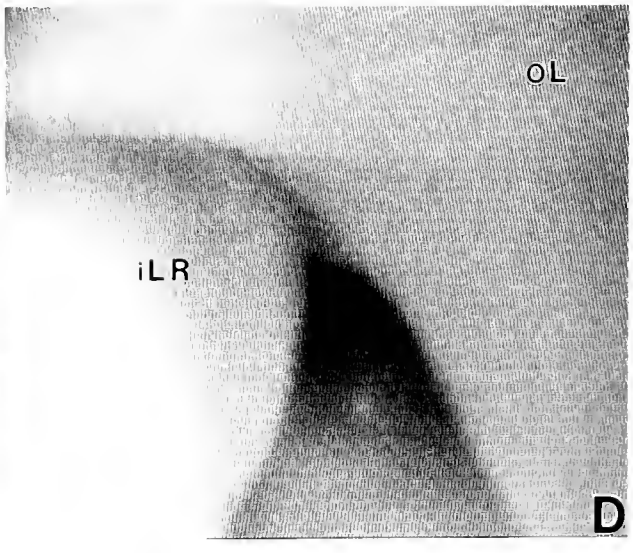

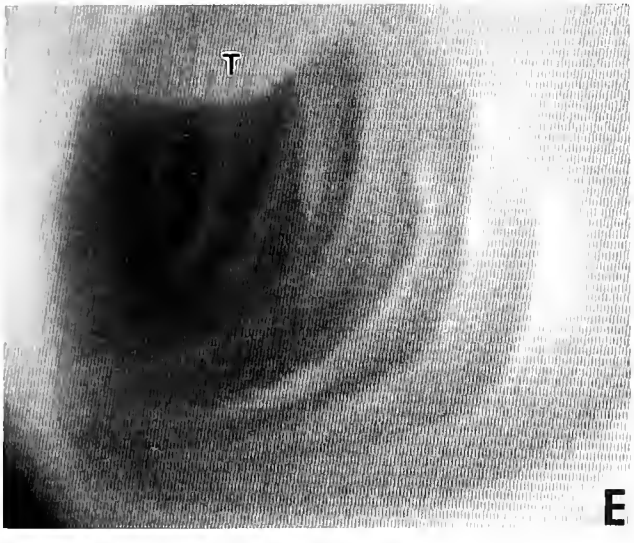

Figure 4. Video-endoscope micrographs showing, *in vivo*, several pallial and internal structures of *Crassostrea virginica*. (A) The distal margin of one pair of labial palps is shown with the lamellae closely appressed and (B) slightly apart. In B, note the ridged surfaces of the palps and the deep rejection tracts between each ridge (length of palp sections = about 600 μm). (C) In the buccal region, the highly ciliated inner lip ridge and outer lip are shown before and (D) after insertion of the inner lip into the outer (dashed arrow indicates inner lip movement; width of inner lip ridge = about 500 μm). (E) In the pyloric caecum of the stomach, the opening to the crystalline style sac is shown. Note the ciliated ridges that line the sac and rotate the crystalline style (not visible under our lighting conditions). Protrusion of one typhlosole can also be seen (diameter of sac = about 1.5 mm). (iLR = inner lip ridge, oL = outer lip, iPL = inner palp lamella, oPL = outer palp lamella, T = typhlosole).

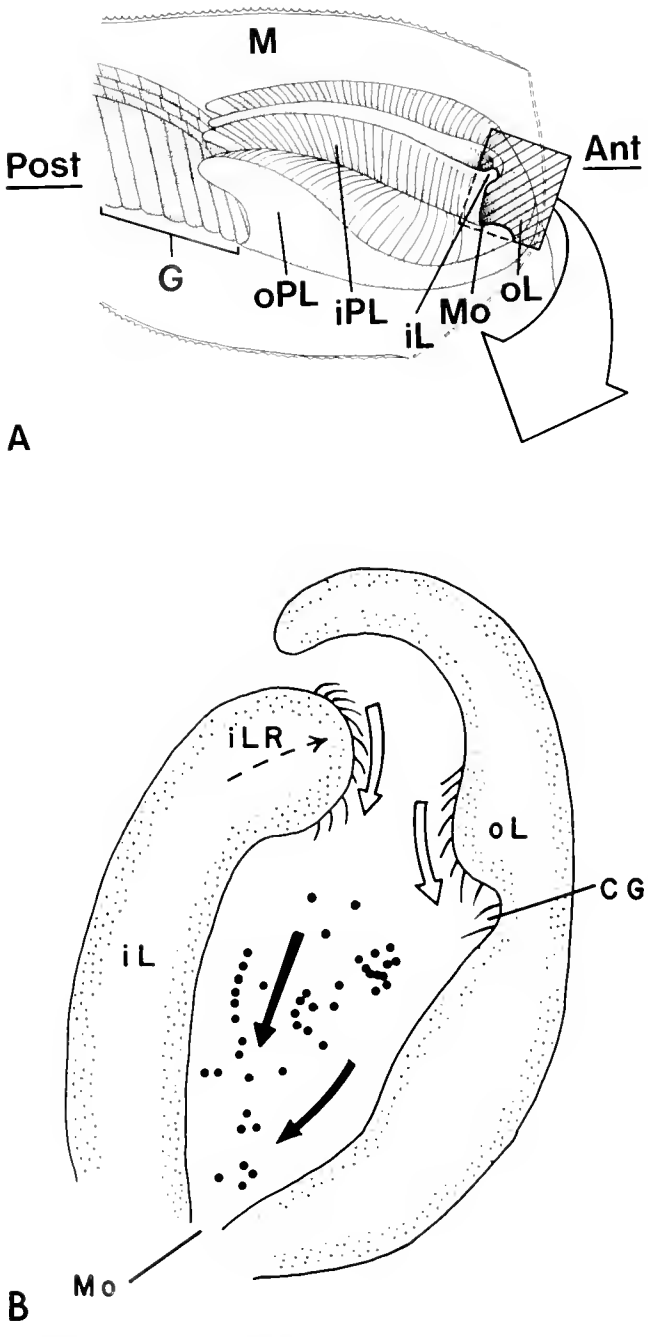

Figure 5. (A) Schematic diagram of the lips, labial palps, and anterior portion of the gills of *Crassostrea virginica* (redrawn after Galtsoff, 1964). The oral hood of the mantle is cut away to reveal the buccal region section shown in B. (B) An enlargement of the mid-longitudinal section of the buccal region. Prominent cilia on the inner lip ridge and outer lip tract beat orally (open arrows), and aid in the transport of particles into the mouth (solid arrows). Buccal region is shown before insertion of the inner lip ridge into the outer lip (dashed arrow indicates inner lip movement). Outer lip is shown with ciliated gutter formed which coincides with active feeding. (Ant = anterior, CG = ciliated gutter, G = gills, iL = inner lip, iLR = inner lip ridge, oL = outer lip, M = mantle, Mo = mouth, iPL = inner palp lamella, oPL = outer palp lamella, Post = posterior).

son, 1960; Galtsoff, 1964; Ribelin and Collier, 1977). Once in the plical troughs, particulate matter was directed basally, at a mean velocity of 740 ± 250 $\mu m \cdot s^{-1}$, towards the ciliated tracts that lie at the base of the gills (Table I; Fig. 6). Particles in the troughs appeared to be transported in suspension, but the high variation in particle velocity (Table I) suggests that some particles may have been carried directly on the frontal cilia of the surrounding transitional filaments.

Particles were also captured on the frontal surface of the ordinary filaments. The ordinary filaments form the sides and tops of the plicae, from the transitional filament on one side, to the transitional filament on the other, an area we term the plical "crest." Capture of particles by the ordinary filaments was not always instantaneous. Particles were often observed being deflected away from the frontal surface of one filament, only to accelerate towards the frontal surface of the same or an adjacent filament. These particles appeared to be "bouncing" from one ordinary filament to another on the crests of the plicae. Such particles usually moved perpendicularly to the long axis of the gill filaments and often moved into the plical troughs (Fig. 6).

Most particles captured on the ordinary filaments were directed—presumably by the coarse frontal cirri (Ribelin and Collier, 1977)—towards the marginal ciliated grooves that lie at the distal edges of the demibranchs. Occasionally, particles on the ordinary filaments were moved basally for a short distance—presumably by the fine frontal cilia (Ribelin and Collier, 1977)—before being transferred onto the tracts of the coarse frontal cirri and directed marginally (Fig. 6). On any ordinary filament, particles progressed uniformly at a mean velocity of 120 ± 30 $\mu m \cdot s^{-1}$ (Table I). Particles moved towards the marginal grooves in an orderly procession, with trailing particles never overtaking leading ones. The distance between a given particle and the underlying filament could not be estimated, because the separation was smaller than the resolution of the endoscope. But no particles were observed being transported in water currents, 20–25 μm above the filament surface, as proposed by Jørgensen (1975, 1981) for the mussel *Mytilus edulis*.

The manner in which large and small particles (18 μm and 5 μm diameter) were transported along the frontal surfaces of the ordinary filaments was similar. When oysters were provided only with small plastic particles, most of these were taken to the marginal ciliated grooves. When mixed with similar-sized *Chaetoceros muelleri* cells, more plastic particles were observed in the basal ciliated tracts. Polystyrene microspheres treated with diatom extract were transported to the basal tracts and marginal grooves in the same manner as untreated microspheres. We observed

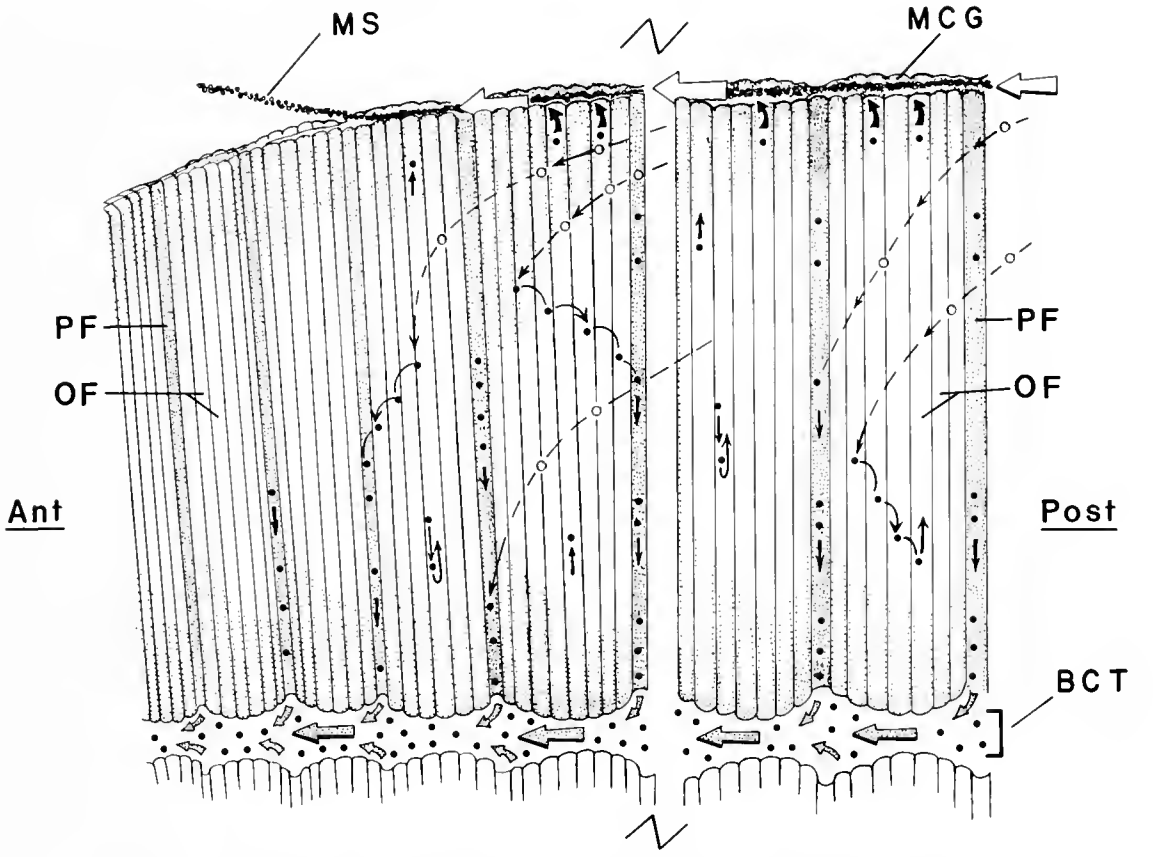

Figure 6. Schematic diagram of typical sections of one gill demibranch of *Crassostrea virginica* showing particle capture and transport on the lamella. Dashed lines indicate the path of particles before being captured by the gills (open circles), and solid lines indicate movement of particles after they contact the gill surface (solid circles). Note that after capture, some particles on the ordinary filaments reverse direction as they are passed from the fine frontal to the coarse frontal ciliated tracts. Other particles "bounce" from one ordinary filament to another and are usually deflected into the plical troughs. Note that a principal filament lies at the base of each plical trough. Particles in the basal tracts are transported anteriorly suspended in a slurry (stippled arrows), while those in the marginal grooves are transported anteriorly in a mucous string (open arrows). (Ant = anterior, BCT = basal ciliated tract, MCG = marginal ciliated groove, MS = mucous string, OF = ordinary filament, PF = principal filament, Post = posterior).

no obvious difference in the quantity of spheres that entered the tracts and grooves, regardless of treatment.

Particles that left the plical troughs and entered the basal ciliated tracts were immediately swept anteriorly in suspension (Figs. 6; 7A). No particles were observed entering these tracts from the ordinary filaments. Both individual particles and loose particle aggregations were observed being carried in cilia-generated currents within the basal tracts. When oysters were exposed to a higher particle concentration, individual particles became more numerous, aggregations became larger, and the material in the ciliated tracts took on the appearance of a slurry. Particles in this slurry moved anteriorly at a mean velocity of 820 $\pm$ 240 $\mu m \cdot s^{-1}$ (Table 1) and flowed around the base of each plica, conforming to the shape of the tract. Particles and clumps in the basal tracts frequently changed position relative to one another, and trailing particles often overtook leading ones. The movement of suspended material in the basal ciliated tracts contrasted with that in the marginal ciliated grooves (see below).

Particles that were transported to the distal edges of the ordinary filaments were carried into the marginal grooves by the coarse, terminal cirri. These cirri beat obliquely toward the palps (Atkins, 1937b), causing particles that were entering the grooves to move in an arc directed anteriorly (Fig. 6). In each marginal groove, particles were immediately incorporated into a continuous, cohesive mucous string (Figs. 6; 7B). Mucous strings were always observed inside the well-developed grooves, even when few particles were being captured and transported to the

Table I

Summary of direct observations of particle transport on the gills of the oyster, Crassostrea virginica

Location	Mode of particle transport	Mean velocity ± SD ($\mu m\ s^{-1}$)	Range ($\mu m\ s^{-1}$)	n
Frontal surface				
Plical trough	Hydrodynamic	740 ± 250	366–1225	11
Plical crest	Mucociliary	120 ± 30	70–163	10
Basal ciliated tract	Hydrodynamic	820 ± 240	462–1225	15
Marginal ciliated groove	Mucociliary	280 ± 30	245–318	10

Note that rate of transport in the plical troughs and basal ciliated tracts is about 3–5 times higher than that on the plical crests or in the marginal ciliated grooves (n = number of measurements made for each mean velocity determination).

grooves. Material in the marginal ciliated grooves moved anteriorly at a mean velocity of 280 ± 30 $\mu m \cdot s^{-1}$ (Table I). Once bound in mucus, particles maintained their relative positions, and trailing particles did not overtake leading ones. Thus, the movement of material in the marginal grooves was similar to that on the frontal surfaces of the ordinary filaments, although particles in the marginal grooves were clearly incorporated in a mucous matrix.

Mucous strings in the marginal ciliated grooves moved anteriorly towards the palps until they reached the termination of the grooves at the inflection points of the demibranchs. Here the material collected into masses that slowly revolved, forming balls of mucus-bound particles (Fig. 8A). These balls continued to grow until they were picked up by the labial palps (see section B2.), or were swept off the margins and onto the mantle by pallial water currents and then rejected as pseudofeces.

Particles that were carried on the ordinary filaments to the demibranch margins anterior to the inflection points, were transported posteriorly on the marginal ciliated indentations. These particles, which were moving in the opposite direction to those in the marginal grooves, were then incorporated into the mucous balls that formed at the inflection points (Figs. 2B; 8A).

2. Labial palps. Particulate matter that left the anterior termination of the basal ciliated tracts entered one of two small spaces between the gills and palps that we call the "basal gill-palp junction." These junctions are roughly triangular with the bases pointing towards, and accepting particles from, the basal tracts (Fig. 7C). In the eastern oyster, there are five basal tracts (two outer, two inner, one medial) and two lateral oral grooves of the palps (one left, one right; Nelson, 1960). Each gill-palp junction (left and right) received particles from at least one outer and one inner basal tract. Particulate matter in the medial tract was directed into either the left or right junction by the labial palps. The direction of flow of particles in the medial tract is controlled by adjustments in the positions of the posterior, proximal edges of the left and right inner palp lamellae.

Particulate matter in each basal gill-palp junction was in the form of a slurry, and individual particles left the junction in one of four directions: (1) into the lateral oral groove of the palps and directly towards the mouth, (2) onto the ridged surfaces of the palp lamellae, (3) onto the smooth, ciliated tract that lies along the posterior edge of each palp lamella and then distally, or (4) onto the marginal ciliated indentation at the anterior termination of each demibranch and then posteriorly (Figs. 2A, B; 7C). The mechanisms responsible for controlling the direction of particles from this junction could not be ascertained with our methods. But the process rapidly redirected particles and loose aggregations that continuously entered the gill-palp junctions at a mean velocity of 820 $\mu m \cdot s^{-1}$.

Under our experimental conditions, most particles entering the basal gill-palp junctions were directed into the lateral grooves or onto the ridged surfaces of the labial palps. Fewer particles were directed onto the smooth, ciliated tracts of the palps. Only at high ambient seston concentrations, which overloaded the gill-palp junctions, were particles directed onto the marginal indentations at the anterior terminations of the demibranchs.

Particles that were directed into the lateral oral grooves could subsequently be ejected onto the ridged sorting surfaces of the palps within the first few millimeters of the start of the grooves (Fig. 7D). Particulate matter that remained in the grooves beyond this location was never ejected, presumably being carried directly to the lips and mouth, and was not subjected to sorting by the palps. Distally moving particles on the smooth, ciliated tracts were usually redirected onto the ridged surfaces of the palp lamellae along the entire length of the tracts, but some particles were carried to the apices of the palps (Figs. 2A; 8A).

As described in section B1, particles in the marginal ciliated grooves of the demibranchs were carried anteriorly in mucous strings until they reached the inflection points where anteriorly directed ciliary action ceased. At these sites, the mucus-bound particle strings began rotating, forming balls as material continued to reach the same location (Fig. 8A). Occasionally, a mucous ball would continue to grow until it was swept off the margin of the demibranch by pallial water currents. More often, the apex of one palp lamella would contact the ball (Fig. 9A) and lift it onto the ridged palp surface. This action established the integrity of a particle string between the demibranch

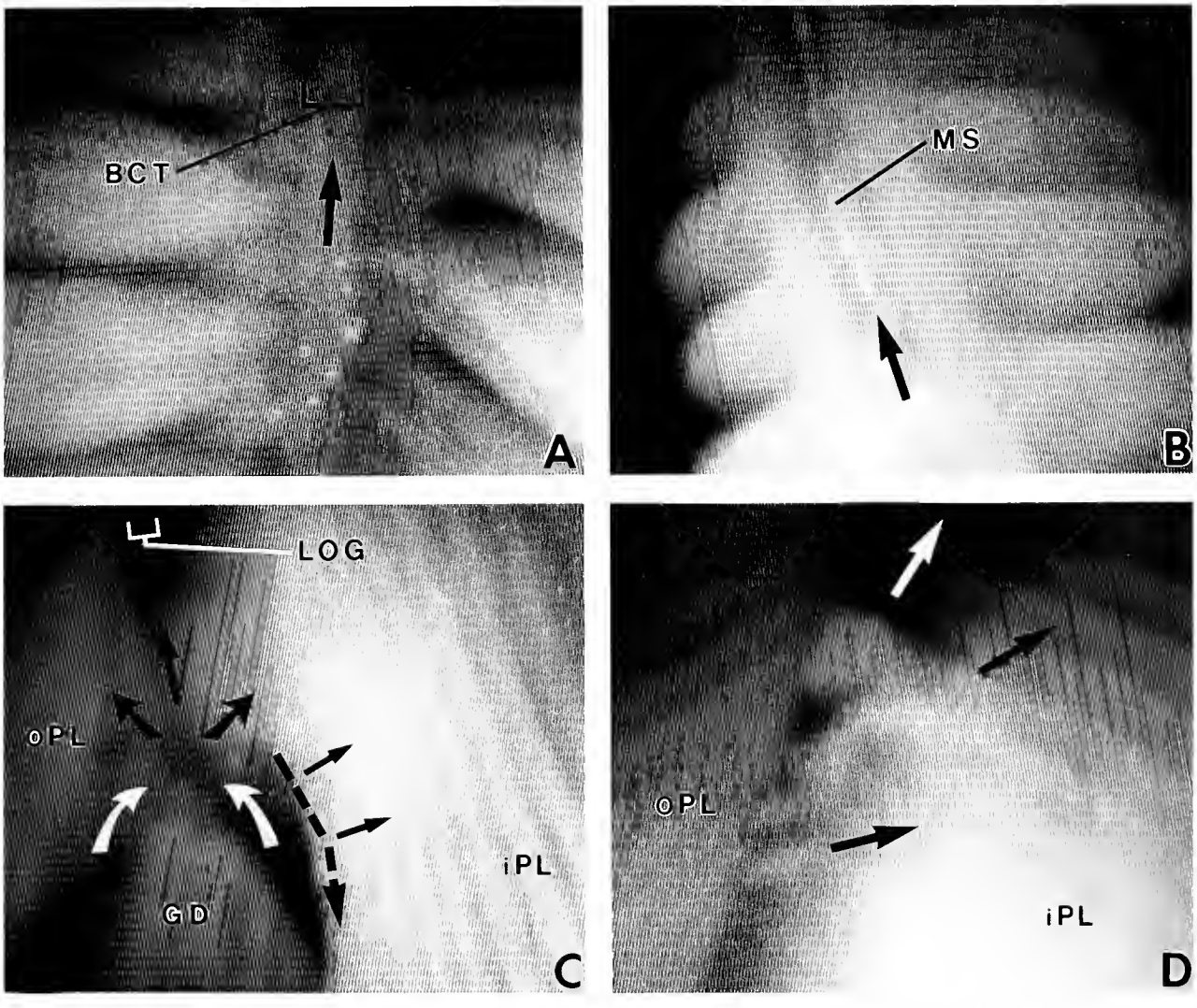

Figure 7. Video-endoscope micrographs showing, *in vivo*, the movement of particles on several pallial structures of *Crassostrea virginica*. Arrows indicate direction of net particle movement. (A) At the base of the gills, the plicae fuse to form the basal ciliated tracts. Particles (white spots) are transported anteriorly in each tract in suspension (length of gill section = about 1.0 mm). (B) At the margin of the gills, particles bound in a mucous string are transported anteriorly in each marginal ciliated groove (length of gill section = about 1.6 mm). (C) At the basal gill-palp junction, particles exit the basal tracts on either side of a gill demibranch (white arrows) and are directed, either anteriorly into the lateral oral groove, or onto the ridged surfaces of the palps (black arrows). Dashed arrow indicates movement of particles along the smooth ciliated tract of the inner palp lamella; these particles are then distributed across the ridged surface. Movement of particles onto the marginal ciliated indentation of the demibranch is not shown (width of each palp ridge = about 60 μm). (D) A particle aggregation being rejected from the lateral oral groove just anterior to the basal gill-palp junction shown in C. The aggregation is being disrupted by the action of the ridged surfaces of the two opposing palp lamellae. Arrows indicate direction of movement of smaller masses which are breaking from the original aggregation (width of each palp ridge = about 60 μm). See Figures 1–4 for descriptions of the form and function of pallial structures. (BCT = basal ciliated tract, GD = gill demibranch, LOG = lateral oral groove, MS = mucous string, iPL = inner palp lamella, oPL = outer palp lamella).

and palp, at a region that we call the "marginal gill-palp junction" (Figs. 8B; 9B). Unlike the basal junctions, the location of a marginal gill-palp junction is not fixed. Once the transport of a mucous string is established, the position at which the string leaves the marginal groove can move posteriorly. Mucous strings continually ran from the gills to the palps, even when few particles were carried in the strings. If a mucous string broke, the material in the mar-

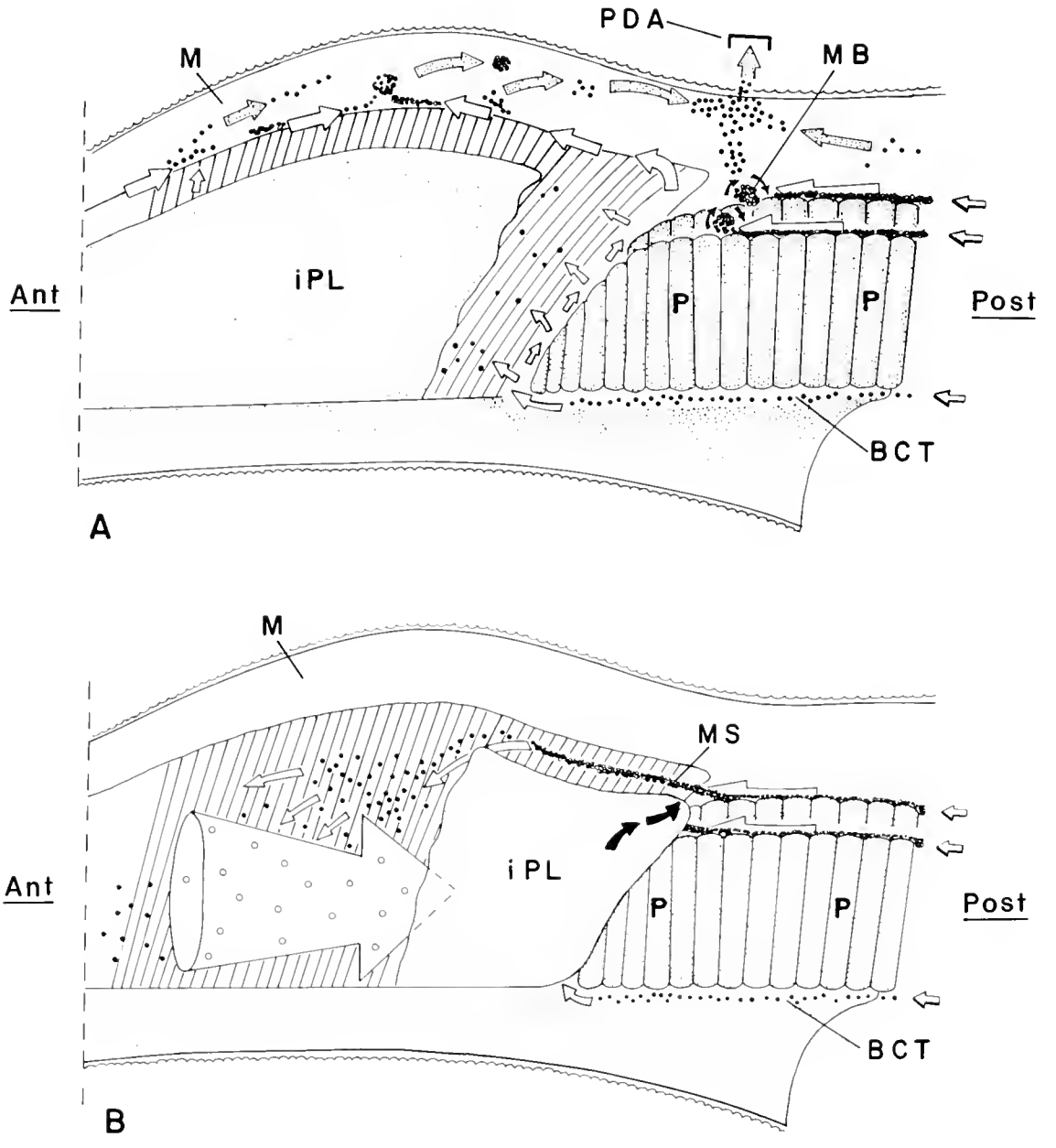

Figure 8. Schematic diagram of the gills and labial palps of *Crassostrea virginica*. The pallial structures are shown in a lateral view, and the inner palp lamella is drawn in cut-away to reveal the ridged surface of the opposing lamella. Arrows indicate direction of net particle movement. (A) The apices of the palps are retracted away from the demibranch margins and mucous balls form at the anterior termination of each marginal ciliated groove. Only particles from the basal tracts are transported onto the labial palps. Mucous balls and excess material from the distal margins of the palps can be transported onto mantle rejection tracts (stippled arrows), carried to the principal discharge area, and then expelled as pseudofeces. (B) The palp apices have contacted the demibranch margins, and particles are transported onto the palps in mucous strings. On the ridged surfaces, the cohesive integrity of the strings is reduced and the entrapped particles disperse (solid circles). When the two opposing palp lamellae spread slightly, some particles are directed posteriorly in an off-surface counter-current (open circles, large circular arrow). After sorting, particles are transported to the lips (smooth region at anterior edge of palp) and then the mouth (not shown) for ingestion. Mucous balls and strings can also be carried across the smooth surfaces of the palps and enter the space between opposing lamellae at the palp apices (solid arrows). (Ant = anterior, BCT = basal ciliated tract, MB = mucous ball, MS = mucous string, P = plica, iPL = inner palp lamella, PDA = principal discharge area, Post = posterior).

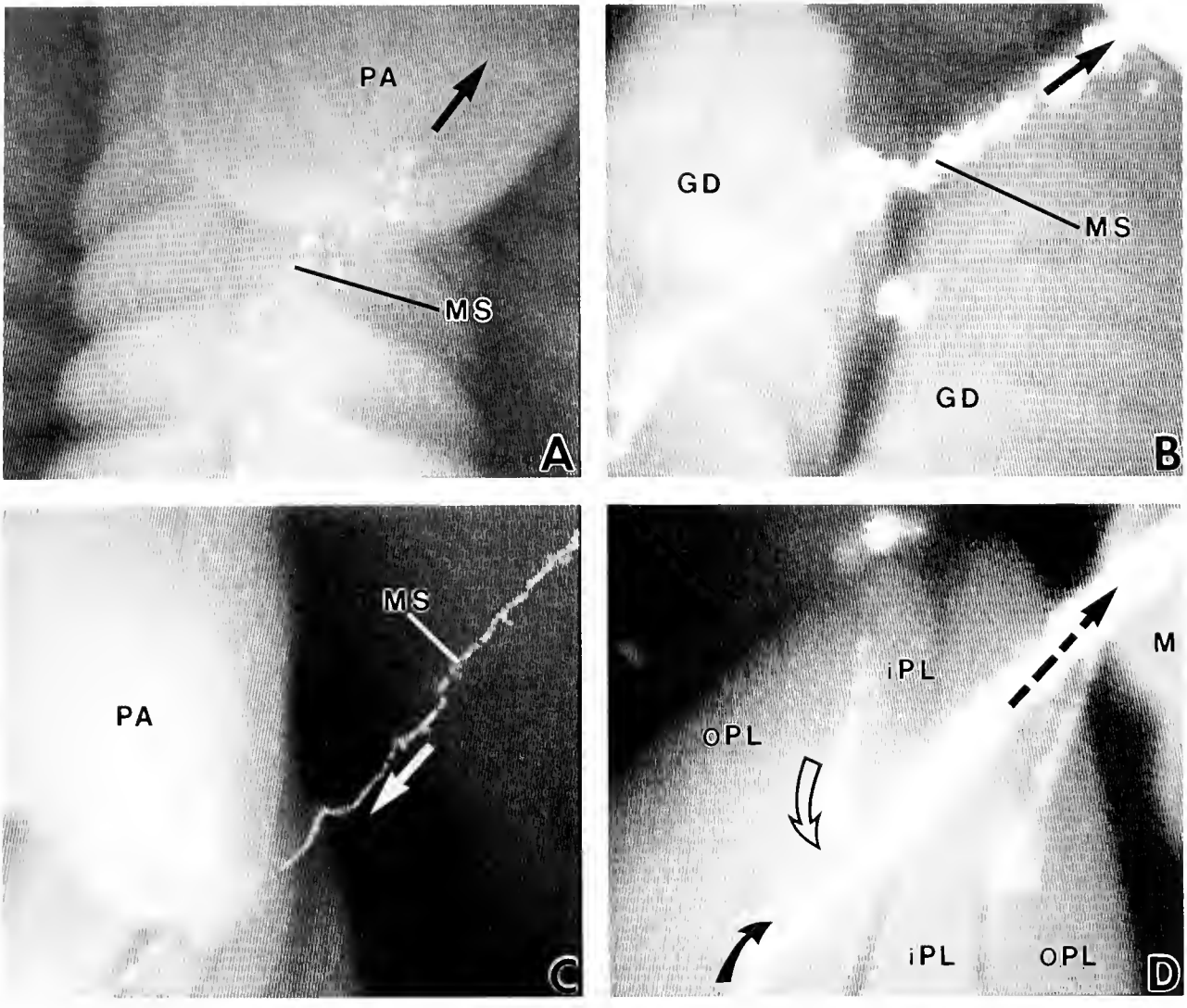

Figure 9. Video-endoscope micrographs showing, *in vivo*, the movement of mucus-bound particles on several pallial structures of *Crassostrea virginica*. Arrows indicate direction of net movement. (A) At the marginal gill-palp junction, the apex of one palp can be seen lifting material from the marginal groove and (B) establishing mucous string transport from demibranch to palp (width of each plica = about 250 μm). (C) At the marginal gill-palp junction, a mucous string is shown bridging the space between two adjacent demibranchs (width of each plica = about 250 μm). (D) Rejection of mucus-bound particles from the distal margins of the labial palps is shown. Material is transported both anteriorly (solid arrow) and posteriorly (open arrow) by cilia on the palp margins. At the junction of the two oppositely beating ciliated tracts, mucus-bound particle aggregations and strings form and are transported (dashed arrow) to mantle rejection tracts to be expelled as pseudofeces (length of palp section = about 4 mm). See Figures 1–4 for descriptions of the form and function of pallial structures. (GD = gill demibranch, M = mantle, MS = mucous string, PA = palp apex, iPL = inner palp lamella, oPL = outer palp lamella).

ginal groove began forming another mucous ball, and the process was repeated.

As described in section A2, the two lamellae of one pair of palps were often observed surrounding only one demibranch. This condition, however, did not prevent material from the unenclosed demibranch from reaching the ridged surfaces of the palps. The particle string from a marginal groove of an unenclosed demibranch could bridge the space between adjacent demibranchs, thereby joining the string moving from the groove of the enclosed demibranch (Fig. 9C). The bridge was established when a mucous ball on the unenclosed demibranch contacted the smooth ciliated surface of the closest palp lamella. The mucous ball, with attached string, was carried to the

apex of the palp, then transported around the free edge and onto the ridged surfaces of the two opposing palp lamellae (Fig. 8B).

Mucus-bound particle strings that were moving from the marginal grooves entered between opposing labial palp lamellae and were directed proximally by cilia on the ridged surfaces (Figs. 2A; 8B). Presumably, this material joined with that introduced from the basal ciliated tracts, which also was directed onto the ridged surfaces. Alternatively, strings could be transported anteriorly along the first two-thirds of the distal margins of the palps to a point close to the fusion of palps and lips (Fig. 8A; 9D). At this location, movement ceased because cilia on the remaining one-third of the margins were beating posteriorly. This arrangement is analogous to that on the margins of the gills. The mucus-bound material on the palp margins was then transferred to the mantle where it was rejected as pseudofeces through the "principal discharge" area (Galtsoff, 1964; Fig. 8A). Our observations on *C. virginica* are similar to those of Yonge (1926), who reported that tracts on the labial palp margins of *Ostrea edulis* beat in opposite directions.

The cohesive integrity of mucous strings from the marginal grooves, as well as any particle aggregations from the basal tracts, was disrupted as the material moved across the ciliated ridges of the labial palps (Figs. 2A; 7D; 8B). Particles were released from the mucous matrix, apparently by the mechanical action of the palps. Particles dispersed across the palps were initially in contact with the ridged surfaces and were transported, in general, towards the lips and mouth, presumably by mucociliary action. Other material, however, was in suspension in the space between each pair of opposing palp lamellae and was directed posteriorly towards the gill-palp junction in intermittent, pulse-like currents (Fig. 8B). These suspended particles appeared to be captured and directed back onto the ridged surfaces of the palps by the smooth ciliated tracts that lie at the free edges of the palp lamellae (Fig. 2A; 8A). Consequently, some of the material between opposing palp lamellae was in the form of a slurry. Occasionally, a portion of this slurry would escape from the space between the palps when the distal margins of the lamellae were not tightly appressed (*e.g.*, Fig. 4B). Material destined for rejection was transported to the distal margins of the palps, then onto the mantle, and rejected as pseudofeces (Fig. 8; 9D).

3. Lips and buccal region. Particles in the buccal region between the inner and outer lips were suspended in a slurry. This slurry, however, appeared more opaque than that between the palps, and the particle aggregations were more numerous. Probably the concentration of particulate matter in the buccal region is higher than that in the basal tracts or between the palps. When we exposed the oyster to a higher particle concentration, the slurry became so thick that the region became difficult to examine and the OIT became covered in mucus.

The slurry in the buccal region was moved towards the mouth by the combined action of the anteriorly beating cilia on the lateral edges of the lips (adjacent to the ridged surfaces of the palps), and the orally beating cilia on the inner lip ridge and outer lip tract (Fig. 5B). Thus, the insertion of the inner lip into the outer lip was very effective in preventing the slurry from escaping from the free margins of the lips. This was in contrast to the labial palp margins, which occasionally allowed particles to escape into the pallial cavity. Insertion of the inner lip into the outer lip also prevented material from entering the buccal region across the free margin of the inner lip, via the central gutter. Such movement of particles across the free margin of the inner lip was reported by Galtsoff (1964, p. 118) from observations of surgically altered oysters, but was never observed by us with the endoscope.

In dissected oysters, particles were not suspended in a slurry. Only a highly cohesive mucus-bound material was observed between the labial palps, lips, and in the buccal region.

4. Esophagus and stomach. Material entering the mouth, esophagus, and stomach of the oyster was in the form of a slurry. This ingested slurry was similar to that found in the buccal region, but appeared to be more opaque, containing numerous small and large particle aggregations. The slurry in the pyloric caecum was slowly swirled, probably by the rotating action of the style. Particle strings were never observed in the alimentary canal, nor were strings ever seen wound around the crystalline style.

Discussion

Many previous reports on the structure and function of the feeding organs in *Crassostrea virginica* were confirmed by our *in vivo*, endoscopic observations. But endoscopy also elucidated several important processes that were not found in literature accounts or were different from those previously reported. Many of these discrepancies could be due to artifacts that were produced when specimens were prepared for prior studies. For example, our endoscopic observations clearly show that particles in the basal tracts, between the labial palps, in the buccal region, as well as in the stomach are transported in the form of a slurry. Previous reports of continuous mucous strings or masses in these regions are incorrect (*e.g.*, Nelson, 1923, 1960; Bernard, 1974; Beninger *et al.*, 1991) and are probably a consequence of dissection which destroys the hydrodynamic properties of the slurry, causing it to collapse into what appears to be mucus-bound par-

ticle-strings, sheets and masses. Similarly, the ciliated tracts on the lips of the oyster have never been described before, probably because the lip-cilia are neurally controlled and cease to function normally after dissection.

Our endoscopic observations of particle capture and transport allow us to reevaluate the previously published concepts of suspension-feeding processes in *C. virginica*. We discuss below our combined observations of organ form and function, providing an integrated view of feeding dynamics in this species. We show, in particular, how our novel observations revise, refine and extend previous models of suspension-feeding mechanisms in *C. virginica*.

Particle capture by the gills

Our observations *in vivo* confirm the complexity of particle capture and are consistent with previous hypotheses concerning this process in bivalves with heterorhabdic gills (*e.g.*, Owen and McCrae, 1976; Owen, 1978; Beninger *et al.*, 1992). In *C. virginica*, particles are captured by the gills in either of two ways: they can be drawn directly into the plical troughs, or they can be captured on the plical crests (Fig. 6). Particles that enter the plical troughs directly are probably entrained by basally directed currents produced by the fine frontal cilia of the principal and transitional filaments. The mechanism of particle capture on the plical crests, however, seems to be more complex.

On the plical crests, particles are immediately captured by the frontal surfaces of ordinary filaments, or they are deflected away from those surfaces and "bounce" to adjacent filaments (Fig. 6). "Bouncing" or "jumping" of particles on the gill lamellae has been described previously in *C. virginica* (Galtsoff, 1964) and in several other bivalve species (Atkins, 1937a; Jørgensen, 1975, 1976; Beninger *et al.*, 1992). The cause of this "bouncing" is not known, but the phenomenon has been attributed to direct contact with cilia or cirri (Atkins, 1937a; Galtsoff, 1964) and to the influence of "local water currents produced by the activity of the metachronally beating band of lateral cilia" (Jørgensen, 1975, p. 216). Unfortunately, the resolution of the endoscope was not sufficient to elucidate the mechanism responsible for particle "bouncing." Jørgensen (1975, 1976) reported that "bouncing" occurred as particles passed between gill filaments and through the interfilamentary spaces, and suggested that particle "bouncing" is a characteristic of "leaky" gills, such as those treated with serotonin. Our observations, however, indicate that particle "bouncing" occurs on the frontal surfaces of filaments, not between filaments, in normal active gills. We suggest that such "bouncing" from one ordinary filament to another maintains particles in suspension above the plical crests and facilitates their deflection into the plical troughs.

After capture, particles are transferred from the laterofrontal cirri to the ciliated tracts on the frontal surface of the ordinary filaments. Ribelin and Collier (1977) suggested that captured particles must be transferred directly to the fine-frontal ciliated tracts, which beat basally, before being moved to the coarse frontal cirri which beat towards the gill margins. Our observations indicate that this sequence does not always occur. Although many particles were observed moving basally first and then reversing direction and moving marginally on the ordinary filaments, other entrained particles immediately moved toward the gill margins. This suggests that other mechanisms, in addition to the direct transfer of particles from the laterofrontal cirri to the fine frontal cilia, are involved in particle capture (*e.g.*, Jørgensen, 1990).

Particle transport by the gills

Previous research on bivalves has shown that the various ciliated tracts of the gill transport particles differently. For example, using isolated heterorhabdic gills of several bivalve species, Jørgensen (1976) noted that particles in the plical troughs move at a faster rate than particles on the plical crests. In juvenile *C. virginica*, Menzel (1955) observed that particles in the marginal grooves move slower than the more discrete particles in the basal tracts, and suggested that this was due to the greater amounts of viscous mucus in the former. Similarly, data from the ciliated surfaces of other organisms indicate that the transport rate of particles decreases as the viscosity of mucus increases (Winet and Blake, 1980; Winet *et al.*, 1982).

Our *in vivo* observations confirm the findings of Menzel (1955) and Jørgensen (1976), and we suggest that such variations in the speed of particle movement reflect functional differences (Table I). The gills of the oyster can be conceptualized as being composed of two distinct transport systems: (1) the plical crest–marginal groove system, and (2) the plical trough–basal tract system. These two systems can be distinguished based on the speed and uniformity at which they transport particles. Such differences reflect the distinctive transport mechanism of each system as explained below, and may be a consequence of anatomical structure (see Ward *et al.*, 1993).

Particles on the plical crests are transported in close association with the frontal surface of the ordinary filaments. These particles move uniformly at a mean velocity of 120 $\mu m \cdot s^{-1}$. In addition, particles on the same ordinary filament can pass in opposite directions as some are directed basally by the fine frontal cilia, while others are directed marginally by the coarse frontal cirri. This complex, bi-directional transport of particles is difficult to explain in hydrodynamic terms, but is characteristic of mucociliary transport. Once transferred to the marginal

groove, particles are bound in a cohesive mucous string. Particles within this string move uniformly and at a velocity ($\bar{X} = 280\ \mu m \cdot s^{-1}$) similar to that of particles on the frontal surface of the ordinary filaments (Table 1). We therefore conclude that mucociliary transport is responsible for moving particulate matter along both the plical crests and the marginal ciliated grooves (Fig. 6).

In contrast, particle movement in the plical troughs and basal ciliated tracts is less uniform than on the plical crest or in the marginal grooves, and particle velocity is 3–5 times greater (Table 1). Because the plical troughs lie deep within the plical folds, we had difficulty determining whether all particles in these troughs are transported in suspension. At the base of the gills, however, these particles exit the plical troughs as individuals or as small aggregations, and are immediately swept anteriorly, in suspension, by currents in the basal ciliated tracts (Fig. 6). We therefore conclude that hydrodynamic transport is primarily responsible for moving particles along both the plical troughs and the basal ciliated tracts. This conclusion is consistent with previous hypotheses of particle transport in these regions (Owen and McCrae, 1976; Jørgensen, 1976; Owen, 1978).

Particle selection on the gills

The role of the gills in particle selection has been debated in the literature for many years (*e.g.*, Nelson, 1923; Yonge, 1926; Atkins, 1937b; Menzel, 1955; Nelson, 1960; Newell and Langdon, 1994). In the oyster, the sorting of particles based on size and other criteria centers around the heterorhabdic nature of the gills and the two ciliated tracts that beat in opposite directions on the frontal surface of the ordinary filaments. According to the current dogma, small or more desirable particles enter the plical troughs and are carried by the principal filaments to the basal ciliated tracts. Larger and less desirable particles are more likely to be captured by the ordinary filaments, where further sorting occurs. On the ordinary filaments, the fine frontal cilia are thought to trap smaller, more nutritious particles and to transport them to the basal tracts, while less nutritious particles are transferred to the coarse frontal cirri and are then transported to the marginal grooves.

Our *in vivo* observations do not fully support this traditional concept. First, all particles delivered to the oysters, regardless of size or treatment, could enter the basal tracts and marginal grooves. Second, all particles on the ordinary filaments, regardless of size or treatment, were ultimately carried to the gill margin by the coarse frontal cirri. We never observed particles entering the basal tracts via the ordinary filaments, as suggested by Atkins (1937c) or by Ribelin and Collier (1977). If size influences selection on the gills, then the requisite size difference must be greater than that used in our study. Menzel (1955), however, also noticed that carmine particles were carried in both the basal tracts and marginal grooves of juvenile oysters, and he concluded that selection does not take place on the gills. Obviously, more detailed endoscopic studies need to be performed, and with a wider range of particle sizes and types, to elucidate the role of the gills in selection.

Particle transfer from gills to labial palps

The basal and marginal gill-palp junctions are more important in feeding than previously recognized. Indeed, the interactions between the gills and palps can control the quantity of material entering the buccal region in response to fluctuations in ambient particle concentrations. For example, during periods of low seston availability, individual particles and small particle aggregations enter the basal gill-palp junctions and are directed onto different regions of the palps for immediate ingestion or further processing and sorting. Various ciliated tracts of the palps, such as the smooth tract on the posterior edge, ensure that particles are evenly distributed across the ridged, sorting surfaces. At the marginal gill-palp junctions, the apices of the palps are usually in contact with the demibranchs and continually accept mucous strings from the marginal grooves. This material is pulled between the opposing palp lamellae for processing (Figs. 2A; 8B).

In contrast, during periods of high seston availability—when the gills are over-loaded or the ingestive capacity is exceeded—excess particles that enter the basal gill-palp junctions are directed onto the marginal ciliated indentations of the demibranchs and carried posteriorly. Posterior transport of this material ceases at the inflection point where the marginal ciliated groove and marginal ciliated indentation meet, and rotating mucous balls form. If the apices of the palps are retracted from the demibranch margins, the rotating mucous balls continue to grow. Eventually, these balls are swept off the margins and onto the mantle by pallial water currents, to be rejected as pseudofeces. Alternatively, mucous balls and strings can be lifted from the demibranchs by the palps and transported anteriorly, along the distal margins, directly to pseudofeces rejection tracts on the mantle. Menzel (1955) and Galtsoff (1964) observed such "food balls" or "masses" at the marginal gill-palp junctions, but concluded erroneously that these were produced by the palps. Furthermore, Galtsoff (1964) indicated that this material was transported posteriorly along the distal margins of the palps to the apices. Our observations clearly indicate that this report is incorrect. Material is transported anteriorly along most of the palp margins, from the apices to points posterior to the fusions with the lips (Fig. 8A).

Many previous reports have suggested that the marginal grooves of the oyster collect material destined for rejection, whereas the basal tracts accept material destined for ingestion (*e.g.*, Ribelin and Collier, 1977). Our observations show that this concept is not completely accurate and is highly dependent on particle concentration. For example, at low particle concentrations, mucous strings from the marginal grooves can be drawn into the labial palps, the entrapped particles dispersed and ingested. At high particle concentrations, when the basal gill-palp junctions become overloaded, particles from the basal tracts can be diverted posteriorly along the marginal indentation, incorporated into mucous balls, and rejected as pseudofeces.

Our findings (1) that the marginal groove effectively terminates at the inflection point of each gill demibranch, and (2) that the cilia of the demibranch beat posteriorly on the marginal indentation and anteriorly in the marginal groove, are particularly important. This anatomical arrangement serves to remove excess particles from the basal gill-palp junctions and prevents mucous strings from reaching the anterior termination of the gills and entering the basal junctions. The prevalence of this condition among the Bivalvia is not known. But Atkins (1937a), working with the protobranch bivalve *Nuculana minuta* Müller, reported that cilia lining the axial grooves of the primitive gills beat anteriorly up to the twelfth pair of leaflets from the anterior end. From that point on, the cilia beat posteriorly.

Particle transport and selection by the labial palps and lips

Material between the labial palps is composed of individual particles and small particle aggregations. As hypothesized by Newell and Jordan (1983), the palps reduce the cohesiveness of mucous strings and aggregations, and disperse the entrapped particles. Sorting and selection of individual particles by the palps is therefore possible. Our observations of the off-surface posterior movements of particles between the labial palps are similar to those of Galtsoff (1964), who described opposing currents along the lateral oral grooves of the palps. In undissected oysters, however, the countercurrent is clearly much stronger and extends from the lateral grooves to the distal margins of the palps. This countercurrent transports particles from the anterior portion of the palps to the smooth ciliated tracts at the posterior edge (Fig. 8B) and probably allows particles to be cycled over the active ridged surfaces several times before being ingested or rejected. Such a recirculative mechanism would increase the efficiency of particle sorting and selection.

Our observations on the motion of the labial palps of *C. virginica* differ slightly from those reported by Bernard (1974) for *C. gigas*. Using a hand-held cystoscope (endoscope), Bernard (1974) observed that each pair of labial palp lamellae of *C. gigas* was "always closely appressed." During the present study, however, we recorded many hours of video showing the opposing lamellae of the palps alternating between close approximation and slight separation (*e.g.*, Fig. 4A, B). As noted by Bernard (1974, p. 7), when the two lamellae are appressed the opposing surfaces can be thought of as "one entity, rather than two separate surfaces, [and] the result of ciliary activity is different." Our observations support this idea, and we suggest that the alternating positions have a functional significance. When the two lamellae are appressed, particles between the palps are in close proximity to both ridged surfaces, and sorting and anteriorward transport occurs. When the lamellae separate, particulate matter moves to occupy the semi-enclosed space between the opposing surfaces, and this suspended slurry is then transported posteriorly for resorting (Fig. 8B). The off-surface flow may be due to the lateral cilia of the gills, which generate the normal feeding currents of the oyster. When the palp lamellae separate slightly, water could be drawn from between the palps towards the gill, carrying the slurry posteriorly.

Food particles enter the buccal region in the form of a slurry. Insertion of the inner lip ridge into the outer lip forms a "hood" over the buccal region and prevents suspended particles from being dispersed. The cilia on the inner lip ridge and outer lip tract direct food orally and further reduce the possibility of particles escaping from the buccal region (Fig. 5B). These findings support the hypothesis of Gilmour (1964), who suggested that the lips of most monomyarians are modified to enclose the proximal oral grooves and to prevent food that is entering the mouth from being dislodged and lost.

Activation and deactivation of cilia on the palp ridges and lips of the oyster was observed many times, *in vivo*, during our study. Such spontaneous inhibition of pallial organ cilia has been reported previously (Menzel, 1955; Nelson, 1960; Galtsoff, 1964), but the behavioral and physiological factors that elicit variation in ciliary activity are not clear. On one occasion we found that ciliary activity on the inner lip ridge and outer lip tract was stimulated by the presence of the diatom *Chaetoceros muelleri*, suggesting that activity in this region is mediated by food material. The activity was perhaps a response to an increase in the number of particles in the pallial cavity or to metabolites produced by the diatoms, but further research is required to elucidate this behavior.

Regardless of the stimulus, the important point is that the cilia on the palp ridges and those on the lips are independently regulated. These findings suggest that the oyster is capable of discontinuous ingestion. Particles can

be removed from suspension and pseudofeces can be produced without ingestion taking place. Furthermore, ciliary activity on the palps continues after dissection, but that on the lips ceases to function normally. Jørgensen (1975) demonstrated that gill cilia of the mussel, *Mytilus edulis*, are under inhibitory nervous control. We suggest that cilia on the lips of *C. virginica* are also under direct neural control.

Particle ingestion

Material in the buccal region and alimentary canal is suspended in a slurry. No continuous mucous strings were ever observed in these regions, and no strings were observed wound around the crystalline style. Such a mechanism has been proposed by previous workers to explain the ingestion of mucus-bound material by bivalves, and was termed the "capstan (or windlass)" model (Orton, 1923; Morton, 1960; Purchon, 1977). Our *in vivo* observations, however, clearly indicate that this mechanism does not operate in *C. virginica*. Rather, a particle slurry is carried through the mouth and into the stomach, probably by the action of cilia that line the alimentary canal.

Our findings are consistent with the chemical nature of the alimentary canal and the mechanical properties of mucus. The pH of the esophagus and stomach of oysters ranges from 5.0 to 6.0 (Yonge, 1926; Galtsoff, 1964), and the isoelectric point and minimum viscosity of mucus falls within this range (Yonge, 1935). The slightly acidic conditions in the stomach, therefore, would keep the viscosity of the mucus-water slurry low and the accompanying particles suspended. In the stomach this slurry is swirled by the rotating style, as was suggested by Yonge (1926) and Nelson (1925). Rotation of material in the stomach probably enhances extracellular digestion and facilitates contact with the food sorting areas where particles are directed into the intestinal groove or into the ducts that lead to the digestive diverticula.

The role of mucus in feeding

We conclude that mucus plays an important role in the feeding process of oysters notwithstanding recent suggestions to the contrary (Jørgensen, 1990). Particle movement and velocity on the ordinary filaments are consistent with mucociliary transport. In the marginal grooves, material is clearly bound in a continuous mucous string, which is important in transporting food material across the marginal gill-palp junction to the labial palps, and in rejecting excess material as pseudofeces. The viscoelastic nature of the mucous string facilitates this process, enabling the string to bend around pallial organs and stretch across spaces between demibranchs while continuing to transport particles (*e.g.*, Fig. 9C).

In the basal tracts, particles are transported suspended in a slurry. But the free suspension of particles does not necessarily mean that mucus is absent. In the heterorhabdic gills of the scallop, *Placopecten magellanicus* (Gmelin), mucocytes that secrete a low viscosity mucus have been identified on the principal filaments and in the dorsal (basal) tracts (Beninger *et al.*, 1993). In addition, mucus has been chemically identified in the slurries that are transported in these tracts (Beninger *et al.*, 1992). In the scallop, therefore, transport along the dorsal (basal) tracts is by hydrodynamic action, but the medium is a mucous slurry. In the oyster, a similar slurry is present between the palps, in the buccal region, and in the stomach. The presence of mucus in these slurries can be inferred from the work of Beninger *et al.* (1991), who identified active mucocytes and mucus in the peribuccal, buccal, and esophageal regions of five species of bivalves, including *C. virginica*.

Our conclusion about the importance of mucus is supported by the rheological properties of this gel. As an amphoteric compound, the viscosity of mucus can change appreciably due to changes in the pH of the medium (Yonge, 1935). In addition, hydration, shear rate, and the type of mucopolysaccharides and concentration of glycoproteins produced by secretory cells can affect the viscosity of mucus (Litt *et al.*, 1977; Mitchell-Heggs, 1977; Silberberg, 1982; Beninger *et al.*, 1993). Changes in viscosity, in turn, can dramatically affect the rheology of mucus, the properties of which can range from Newtonian (hydrodynamic) to non-Newtonian (viscoelastic; *e.g.*, Winet and Blake, 1980). Thus, mucus is an ideal substance in which to transport particles. Variations in the viscosity and cohesiveness of mucus give the oyster maximum flexibility in rejecting, ingesting, and processing particulate matter.

Conclusions

Suspension-feeding in the eastern oyster *C. virginica* is accomplished by the coordination of both mucociliary and hydrodynamic processes. Particles removed from suspension are transported along the gills and to the labial palps in two different forms, mucous strings and slurries. The palps reduce the cohesiveness of mucous strings and particle aggregations, and disperse the entrapped particles. Particulate matter between opposing labial palp lamellae is not bound in cohesive mucus, so sorting and selection of individual particles is possible. Particles in the buccal region and alimentary canal are also suspended in a slurry. Particles can be routed in a variety of directions on the pallial organs and, together with independent control of ciliary activity on the labial palps and lips, allows the oyster maximum flexibility in particle processing, pseudofeces production, and ingestion.

Acknowledgments

We thank Debbie Kennedy for drawing the figures and Tracy Potter for SEM photographs. This work was funded by research grants from the Natural Science and Engineering Research Council of Canada (NSERC), the Canadian Centre for Fisheries Innovation (CCFI), and the University of Maryland Sea Grant College, USA. We appreciate their support.

Literature Cited

Atkins, D. 1937a. On the ciliary mechanisms and interrelationships of lamellibranchs. Part I: new observations on sorting mechanisms. *Q. J. Microsc. Sci.* **79:** 181–308.

Atkins, D. 1937b. On the ciliary mechanisms and interrelationships of lamellibranchs. Part II: sorting devices on the gills. *Q. J. Microsc. Sci.* **79:** 339–373.

Atkins, D. 1937c. On the ciliary mechanisms and interrelationships of lamellibranchs. Part III: types of lamellibranch gills and their food currents. *Q. J. Microsc. Sci.* **79:** 375–420.

Beninger, P. G., M. Le Pennec, and A. Donval. 1991. Mode of particle ingestion in five species of suspension-feeding bivalve molluscs. *Mar. Biol.* **108:** 255–261.

Beninger, P. G., S. St-Jean, Y. Poussart, and J. E. Ward. 1993. Gill function and mucocyte distribution in *Placopecten magellanicus* and *Mytilus edulis* (Mollusca: Bivalvia): the role of mucus in particle transport. *Mar. Ecol. Prog. Ser.* **98:** 275–282.

Beninger, P. G., J. E. Ward, B. A. MacDonald, and R. J. Thompson. 1992. Gill function and particle transport in *Placopecten magellanicus* (Mollusca: Bivalvia) as revealed using video endoscopy. *Mar. Biol.* **114:** 281–288.

Bernard, F. R. 1974. Particle sorting and labial palp function in the Pacific Oyster *Crassostrea gigas* (Thunberg, 1795). *Biol. Bull.* **146:** 1–10.

Bozzda, B. J., and L. D. Russell. 1992. *Electron Microscopy.* Jones and Bartlett Publ., Boston. 542 pp.

Dame, R. F., R. G. Zingmark, and E. Haskin. 1984. Oyster reefs as processors of estuarine materials. *J. Exp. Mar. Biol. Ecol.* **83:** 239–247.

Eble, A., V. S. Kennedy, and R. I. E. Newell, eds. 1994. *The Eastern Oyster, Crassostrea virginica.* Maryland Sea Grant Publication, Maryland. In press.

Elsey, C. R. 1935. On the structure and function of the mantle and gill of *Ostrea gigas* (Thunberg) and *Ostrea lurida* (Carpenter). *Trans. Roy. Soc. Canada* **Sect. 5:** 131–160.

Galtsoff, P. S. 1964. The American oyster, *Crassostrea virginica* (Gmelin). *U.S. Fish and Wildl. Serv., Fish. Bull.* **64:** 1–480.

Gilmour, T. H. J. 1964. The structure, ciliation and function of the lip-apparatus of *Lima* and *Pecten* (Lamellibranchia). *J. Mar. Biol. Assoc. U.K.* **44:** 485–498.

Glauert, A. M. 1980. Fixation, dehydration and embedding of biological specimens. North Holland Publ. Co., Amsterdam. 207 pp.

Guillard, R. R. 1975. Culture of phytoplankton for feeding marine invertebrates. Pp. 29–60 in *Culture of Marine Invertebrate Animals*, W. L. Smith and M. H. Chanley, eds. Plenum Publ., New York.

Jordan, S. J. 1987. Sedimentation and remineralization associated with biodeposition by the American oyster *Crassostrea virginica* (Gmelin). Ph.D. Dissertation, Univ. of Maryland.

Jorgensen, C. B. 1975. On gill function in the mussel *Mytilus edulis* L. *Ophelia* **13:** 187–232.

Jorgensen, C. B. 1976. Comparative studies on the function of gills in suspension feeding bivalves, with special reference to effects of serotonin. *Biol. Bull.* **151:** 331–343.

Jorgensen, C. B. 1981. A hydromechanical principle for particle retention in *Mytilus edulis* and other ciliary suspension feeders. *Mar. Biol.* **61:** 277–282.

Jorgensen, C. B. 1990. *Bivalve Filter-Feeding: Hydrodynamics, Bioenergetics, Physiology and Ecology.* Olsen and Olsen, Fredensborg. 140 pp.

Langdon, C. J., and R. I. E. Newell. 1994. Digestion and Nutrition. In press in *The Eastern Oyster, Crassostrea virginica, Chapter 6*, A. Eble, V. S. Kennedy and R. I. E. Newell, eds. Maryland Sea Grant Publication, Maryland.

Litt, M., D. P. Wolf, and M. A. Khan. 1977. Functional aspects of mucus rheology. Pp. 191–201 in *Mucus in Health and Disease: Advances in Experimental Medicine and Biology, Vol. 89*, M. Elstein and D. V. Parke, eds. Plenum Press, New York.

Menzel, R. W. 1955. Some phases of the biology of *Ostrea equestris* Say and a comparison with *Crassostrea virginica* (Gmelin). *Inst. Mar. Sci* **4:** 69–153.

Mitchell-Heggs, P. 1977. Physical properties of bronchial secretion. Pp. 203–215 in *Mucus in Health and Disease: Advances in Experimental Medicine and Biology, Vol. 89*, M. Elstein and D. V. Parke, eds. Plenum Press, New York.

Morton, J. E. 1960. The function of the gut in ciliary feeders. *Biol. Rev.* **35:** 92–140.

Nelson, T. C. 1923. The mechanism of feeding in the oyster. *Proc. Soc. Exp. Biol. Med* **21:** 166–168.

Nelson, T. C. 1925. Recent contributions to the knowledge of the crystalline style of lamellibranchs. *Biol. Bull.* **49:** 86–99.

Nelson, T. C. 1960. The feeding mechanism of the oyster. II. On the gills and palps of *Ostrea edulis, Crassostrea virginica* and *C. angulata*. *J. Morphol.* **107:** 163–203.

Newell, R. I. E. 1988. Ecological Changes in Chesapeake Bay: Are they the result of over harvesting the American oyster (*Crassostrea virginica*)? Pp. 536–546 in *Understanding the Estuary: Advances in Chesapeake Bay Research*, M. Lynch, ed. Chesapeake Research Consortium Publication 129, Virginia.

Newell, R. I. E., and J. Jordan. 1983. Preferential ingestion of organic material by the American oyster *Crassostrea virginica*. *Mar. Ecol. Prog. Ser.* **13:** 47–53.

Newell, R. I. E., and C. J. Langdon. 1986. Digestion and absorption of refractory carbon from *Spartina alterniflora* (Loisel) by the oyster, *Crassostrea virginica* (Gmelin). *Mar. Ecol. Prog. Ser.* **34:** 105–115.

Newell, R. I. E., and C. J. Langdon. 1994. The eastern oyster: mechanisms and physiology of larval and adult feeding. In press in *The Eastern Oyster, Crassostrea virginica, Chapter 5*, A. Eble, V. S. Kennedy and R. I. E. Newell, eds. Maryland Sea Grant Publication, Maryland.

Orton, J. H. 1923. An account of investigations into the cause or causes of the unusual mortality among oysters in English oyster beds during 1920 and 1921, Part I. *Rep. Fish. Invest., Series II* **6:** 1–199.

Owen, G. 1955. Observations on the stomach and digestive diverticula of the Lamellibranchia. I. The Anisomyaria and Eulamellibranchia. *Q. J. Microsc. Sci.* **96:** 517–537.

Owen, G. 1978. Classification and the bivalve gill. *Phil. Trans. R. Soc. Lond. B.* **284:** 377–385.

Owen, G., and J. M. McCrae. 1976. Further studies on the laterofrontal tracts of bivalves. *Proc. R. Soc. Lond. B.* **194:** 527–544.

Purchon, R. D. 1977. *The Biology of the Mollusca, 2nd edition* Pergamon Press, Oxford. 560 pp.

Ribelin, B. W., and A. Collier. 1977. Studies on the gill ciliation of the American oyster *Crassostrea virginica* (Gmelin). *J. Morph.* **151:** 439–450.

Silberberg, A. 1982. Rheology of mucus, mucociliary interactions, and ciliary activity. Pp. 25–28 in *Mechanism and Control of Ciliary Movement*, C. J. Brokaw and P. Verdugo, eds. Alan R. Liss, Inc, New York.

Ward, J. E. 1989. Marine microalgal metabolites: their influence on the feeding behavior of the blue mussel *Mytilus edulis* L. Ph.D. Dissertation, University of Delaware.

Ward, J. E., P. G. Beninger, B. A. MacDonald, and R. J. Thompson. 1991. Direct observations of feeding structures and mechanisms in bivalve molluscs using endoscopic examination and video image analysis. *Mar Biol* **111:** 287–291.

Ward, J. E., H. K. Cassell, and B. A. MacDonald. 1992. Chemoreception in the sea scallop *Placopecten magellanicus* (Gmelin). I. Stimulatory effects of phytoplankton metabolites on clearance and ingestion rates. *J Exp Mar Biol Ecol.* **163:** 235–250.

Ward, J. E., B. A. MacDonald, R. J. Thompson, and P. G. Beninger. 1993. Mechanisms of suspension feeding in bivalves: resolution of current controversies by means of endoscopy. *Limnol. Oceanogr* **38:** 265–272.

Winet, H., and J. R. Blake. 1980. On the mechanics of mucociliary flows. I. Observations of a channel model. *Biorheology* **17:** 135–150.

Winet, H., G. T. Yates, T. Y. Wu, and J. Head. 1982. On the mechanics of mucociliary flows. II. A fluorescent tracer method for obtaining flow velocity profiles in mucus. Pp. 29–34 in *Mechanism and Control of Ciliary Movement*, C. J. Brokaw and P. Verdugo, eds. Alan R. Liss, Inc., New York.

Yonge, C. M. 1926. Structure and physiology of the organs of feeding and digestion in *Ostrea edulis*. *J Mar. Biol Assoc U.K* **14:** 295–386.

Yonge, C. M. 1935. On some aspects of digestion in ciliary feeding animals. *J Mar Biol Assoc. U.K* **20:** 341–346.

Reference: *Biol. Bull.* **186:** 241–246. (April, 1994)

Regenerate Limb Bud Sufficient for Claw Reversal in Adult Snapping Shrimps

C. K. GOVIND AND A. T. READ

Life Sciences Division, Scarborough College, University of Toronto, 1265 Military Trail, Scarborough, Ontario, Canada M1C 1A4

Abstract. The paired, bilaterally asymmetric snapper and pincer claws in the adult snapping shrimp *Alpheus heterochelis* were simultaneously autotomized at the beginning of an intermolt, and the resulting growth of the limb buds was characterized into several stages. At the next molt the limb buds emerged as newly regenerated claws of the same morphotype as their predecessors. Next, the paired claws were autotomized sequentially, with the second autotomy timed to different stages of limb bud growth at the first autotomy site. When the snapper is autotomized and a limb bud varying from stages 1 to 5 is allowed to develop at this site before the pincer is removed, the paired claws regenerate in their previous configuration. Similarly, claw asymmetry is retained when the pincer claw is removed first and an early limb bud (stage 1–2) is allowed to form at this site before the snapper is autotomized. However, claw asymmetry is reversed if an advanced limb bud (stage 3–5) is allowed to form at the pincer site before the snapper claw is removed. Under these conditions a snapper regenerates at the pincer site and a pincer at the snapper site. Because the limb bud at this pincer site regenerates as a snapper rather than a pincer, claw transformation has occurred, with the stage 3–5 limb bud substituting for an intact pincer. Therefore, the minimal requirement for pincer-to-snapper transformation is a stage 3–5 limb bud. We postulate that the newly transforming snapper claw restricts regeneration at the contralateral old snapper site to a pincer, thereby ensuring that claw bilateral asymmetry is present, albeit reversed.

Introduction

The first pair of thoracic chelipeds, or claws, in adult snapping shrimps of the Alpheid family are much larger than the remaining thoracic limbs and are bilaterally asymmetric, consisting of a pincer and snapper claw. The snapper is a much hypertrophied structure almost half the size of the entire animal and is specialized into a powerful snapping tool; a hammer on the dactyl plunges into a matching socket on the pollex, resulting in a loud popping sound (hence the name snapping shrimps) and a jet stream of water (Hazlett and Winn, 1966). The snapping behavior is used in agonistic encounters and also in crushing the shells of bivalves (McLaughlin, 1982). The contralateral pincer claw is smaller and used primarily in burrowing and feeding (Read and Govind, 1991).

Claw laterality, or handedness, is random in snapping shrimps, and the snapper appears with equal probability on the right or left side of the animal. However, handedness may be switched in adult shrimps. This happens when the snapper claw is removed at the beginning of an intermolt and in its place a new limb bud regenerates which at the next molt unfolds into a pincer claw, while the contralateral intact pincer claw is transformed into a snapper claw (Przibram, 1901; Wilson, 1903). When only the pincer claw is removed, a new pincer regenerates in its place; when both claws are removed, the regenerates appear in the same morphotype as their predecessors.

The latter procedure of removing both claws within an intermolt was used in an original and imaginative manner by Darby (1934), who varied the time interval between the two autotomies in the tropical shrimp *Alpheus armillatus*. These shrimps live off the coast of Bahama in ocean temperatures of 28–30°C and have an intermolt period of 10.5 days, or 252 h. His findings may be summarized as follows. In the experiment in which the snapper claw is removed first and then the pincer claw, despite varying the time interval between the two autotomies from 20–120 h, the paired claws regenerated in their previous configuration. Autotomy of the pincer claw beyond 120 h

Received 14 September 1993; accepted 14 December 1993.

after autotomy of the snapper did not allow for a sufficiently advanced limb bud to form on the pincer site, and a claw failed to regenerate at this site at the next molt. Thus, sequential removal of first the snapper and then the pincer within a single intermolt was similar to simultaneous removal of both claws, as both procedures resulted in the regeneration of paired claws in their previous configuration (Wilson, 1903; Govind *et al.*, 1986).

In another series of experiments Darby (1934) removed first the pincer claw, soon after a molt, and then at varying time intervals the snapper. If the snapper claw was removed up to 29 h after pincer autotomy, the paired claws regenerated in their original configuration. Later removal of the snapper claw led increasingly to a reversal of claw asymmetry; *i.e.*, a pincer regenerated in place of the pristine snapper claw and a snapper regenerated in place of the pristine pincer claw. Thus, when the snapper claw was removed 33 h after pincer autotomy, reversal of asymmetry was seen in 50% of the animals; removal 40 h and 72 h after pincer autotomy produced reversal in 67% and 100% of the animals respectively. In these experiments in which the paired claws are autotomized sequentially, those with the shorter time interval between pincer and snapper autotomy are equivalent to removing both claws at the same time, because claw asymmetry is retained in the previous configuration, whereas those with the longer time intervals are equivalent to removing the snapper alone, because asymmetry is reversed. During these longer time intervals, what transpires that leads to reversal?

One of the events that transpires after a claw has been autotomized is the formation, at this site, of a limb bud that develops during the intermolt and emerges as a new claw at the next molt. Because reversal of claw asymmetry involves transformation of an existing pincer claw into a snapper, we considered the possibility that a limb bud may serve in place of an intact pincer as a suitable target for transformation. This would explain Darby's (1934) findings that claw asymmetry reverses at the longer time intervals between pincer and snapper autotomy, because a limb bud has had time to form at the pincer site. To test this hypothesis, we monitored the development of limb buds at the autotomy sites when both claws are removed simultaneously, producing a chart for limb bud growth. Using this growth chart, we repeated Darby's experiments but, rather than removing the second claw based on the time elapsed after removing the first claw, we removed the second claw at different stages of limb bud growth at the first autotomy site. We find that the presence of a sufficiently advanced limb bud at the pincer site when the snapper is autotomized leads to reversal of claw asymmetry, thereby explaining Darby's results. Additionally, our results demonstrate, for the first time, that the minimum requirement for pincer-to-snapper transformation is a limb bud.

Materials and Methods

Adult snapping shrimps of the species *Alpheus heterochelis* (Say) were collected from the tidal pools around Beaufort, North Carolina, and shipped to our laboratory in Scarborough, Ontario. The animals were held in 25-l glass aquaria equipped with a bottom gravel filter and partitioned into 12 compartments with fiberglass screens (Govind *et al.*, 1986). The aquaria were filled with artificial seawater that was kept at room temperature (22°C). A specially prepared diet—a blended mash of chicken livers and hearts, carrots and commercial cereal—was fed to the animals daily, and occasionally live food was provided in the form of *Tubifex* worms. The shrimps were sexed on arrival in the laboratory and their molt history during captivity was recorded.

Shrimps of both sexes were used, and only those with well-differentiated pincer and snapper claws were selected. These animals were allowed to molt twice before being used; this ensured that the claws were pristine, because earlier studies (Read and Govind, 1991) have shown that at least three intermolts are required for a newly regenerated limb to be fully differentiated. These claws are regarded as pristine in the present report (Fig. 1A). In our laboratory, the intermolt period was between 14 and 26 days (an average of 18.2 days) at 22°C.

Removal of a claw was accomplished by gently pinching the limb near the base of the merus, thereby inducing the animal to autotomize the claw at a preformed fracture plane. The following experiments were performed using this procedure.

(1) A day or two after a molt, the paired claws were removed within minutes of each other; this is regarded as

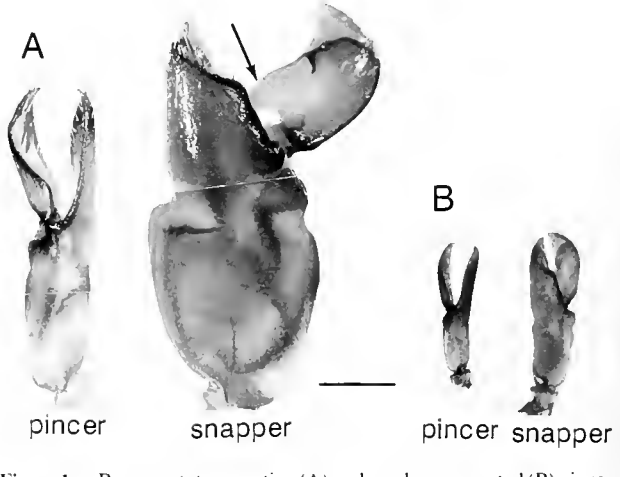

Figure 1. Representative pristine (A) and newly regenerated (B) pincer and snapper claws showing the hypertrophied snapper with the characteristic plunger on its dactyl (arrow). Pristine claws are asymmetric in size, whereas the newly regenerated ones are similar in size and substantially smaller. Scale 3 mm; magnification ×5.5.

simultaneous autotomy. The regenerating limb buds at both sites were monitored daily and sketches were made that were subsequently categorized into a series of developmental stages. The regenerating limb buds were also measured, in blind observations, under a dissecting microscope with a calibrated eyepiece. To reduce the chance of damaging the very delicate limb buds by repeated handling, measurements were made at 3–4 day intervals. Even so, 11 of the 27 animals suffered damage to the buds and were excluded from the study. To compensate for differences in animal size, limb bud measurements were expressed in terms of a regeneration (R) value where R = (limb bud length/carapace length) × 100 (Bliss, 1960).

(2) Within one or two days following a molt, the snapper claw was removed and the regenerating limb bud at this site was monitored daily. Next, the pincer claw was removed at varying stages of limb bud growth at the old snapper site. Of the 52 animals subjected to these sequential autotomies, 38 successfully regenerated paired claws at the next molt.

(3) The experimental protocol was similar to that in experiment 2, except that the pincer claw was removed first and at various stages of its limb bud growth the snapper claw was removed. Twenty-four of 36 animals successfully regenerated paired claws at the next molt.

Results

Stages of limb bud regeneration

Following autotomy of a claw, a new limb gradually regenerates at the base. The limb bud that forms is covered by a tough flexible cuticular coat that persists throughout the intermolt and is discarded only at the molt. Limb bud formation begins immediately as a small papilla (stage 1) that enlarges into an apical blastema (stage 2) (Fig. 2). The blastema elongates and acquires a club-like appearance distally. In the next stage (stage 3), a longitudinal furrow appears in the distal tip, marking the beginning of segmentation by dividing this region into the putative dactyl and propus segment. This is followed by the appearance of a series of transverse furrows along the length of the limb bud (stage 4). By stage 5, segmentation is complete and the limb has acquired typical pincer-like proportions. Further differentiation into a snapper-type claw is marked by the characteristic appearance of a plunger on the dactyl and a matching socket on the pollex (stage 6) and, in the case of a pincer-type claw, the appearance of a fringe of hair on the propus and dactyl of male shrimps. These six stages represent the major external landmarks in the regeneration of a claw and were used as markers in the present study.

Simultaneous snapper and pincer autotomy

Although earlier experiments (Darby, 1934; Govind *et al.*, 1986) had shown that simultaneous autotomy of both claws results in the regeneration of the paired claws in their previous configuration, these studies did not report on the growth of the limb buds. We repeated this experiment by autotomizing the paired claws within minutes of each other, one or two days after a shrimp had molted, and monitoring limb bud growth in the ensuing intermolt. Limb bud growth was qualitatively similar on the two sides and followed the criteria listed above. Moreover, the regenerate limb buds of the two sides were also similar in length throughout the intermolt (Fig. 3). At specific times during the intermolt, either the snapper or pincer bud would be slightly more advanced, but there was no consistent pattern and frequently both buds were equal in size. When these limb buds unfolded as claws at the next molt (Fig. 1B), they were much smaller than their predecessors (Fig. 1A) but otherwise similar in morphotype. In all 16 of the 27 animals that successfully regenerated paired claws, the previous asymmetric configuration was retained (Fig. 4A).

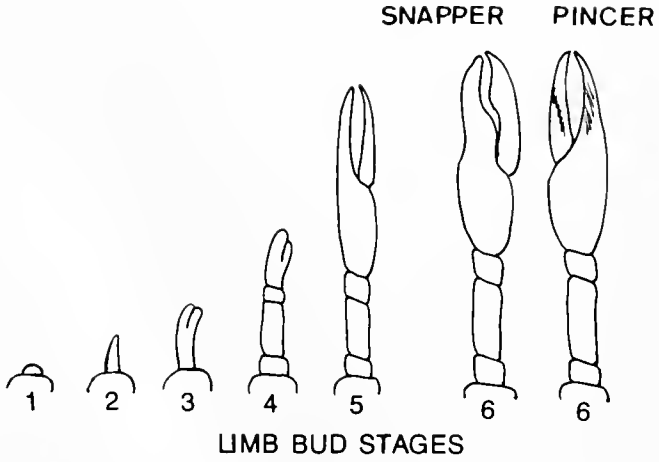

Figure 2. Stages in the regeneration of a limb bud at the site of an autotomized claw in adult snapping shrimps. The development of the limb bud, although a continuous process, has been categorized into six (1–6) separate stages based on external landmarks; at stage 6 the limb buds are differentiated into snapper and pincer types (see text for description of each stage).

Snapper autotomy followed by pincer autotomy

In this experiment, the snapper claw was autotomized one or two days after the shrimp had molted, and the pincer claw was then autotomized at different stages of limb bud regeneration on the snapper side. Thus, the pincer was removed at each stage of limb bud growth classified as stages 1 to 5. Of the 33 animals in which the pincer claw was autotomized at different limb bud stages, 24 animals successfully regenerated both claws. In all cases, the paired claws mimicked their previous configuration.

In a few additional trials, the pincer claw was also removed when the limb bud at the snapper site was at stage

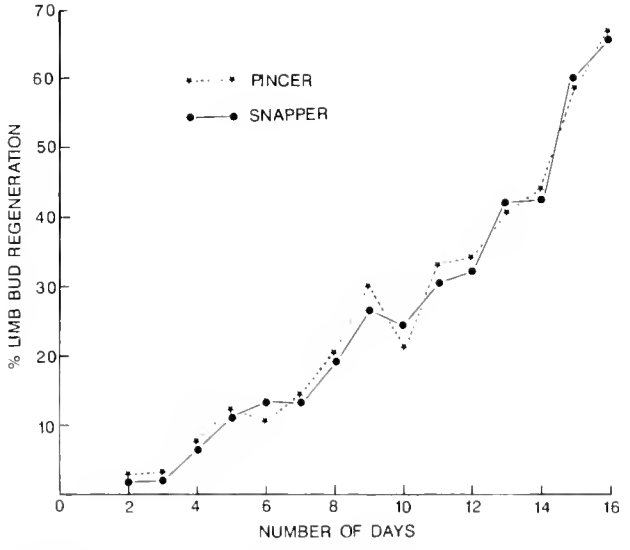

Figure 3. Percent regeneration of snapper and pincer limb buds in adult shrimps following simultaneous autotomy of both claws. Percent regeneration was obtained as follows: (limb bud length/carapace length) × 100. A total of 128 limb buds were measured from 16 animals; each data point represents an average of 4–5 measurements.

6 and already differentiated into a pincer claw. In these animals, a pincer appeared at the old snapper site, but a claw failed to form at the old pincer site because there was not enough time for limb regeneration.

Thus, allowing a limb bud to develop to an advanced stage at the snapper site before the pincer is removed leads to the regeneration of the paired claws in their previous configuration (Fig. 4B). In effect, this is similar to simultaneous autotomy of the paired claws, where the limb buds form at equivalent rates on the two sides and claw asymmetry is retained as described above.

Pincer autotomy followed by snapper autotomy

In this experiment, the snapper claw was autotomized at different stages of limb bud regeneration on the pincer side following autotomy of the pincer claw. At the next molt the morphotype of the newly regenerated paired claws was assessed in terms of retention or reversal of claw asymmetry. The results (Table I) show that with increasing time interval between removal of the paired claws, and hence increasing limb bud development, claw asymmetry was reversed. In other words, as the limb bud stage advances, the proportion of claw reversal increases until 100% reversal is reached at stage 3–5 limb buds.

Removal of the snapper claw when the limb bud is already sufficiently advanced to be discernible as a pincer type (stage 6) does not result in transformation; the limb bud at the pincer site unfolds as a pincer claw, whereas the snapper site lacks a newly regenerated limb or limb bud because of insufficient time for regeneration.

The results of this series of experiments may be summarized as follows (Fig. 4C): removal of the snapper claw when a limb bud of stage 1–2 is present at the pincer site results in retention of claw asymmetry at the next molt in 50% or more of the experimental animals, but removal of the snapper claw when a limb bud of stage 3–5 is present at the pincer site results in reversal of claw asymmetry in all of the experimental animals.

Discussion

When the paired claws were removed sequentially within an intermolt, they regenerated in their previous configuration if the snapper was autotomized first and a limb bud allowed to form at this site before the pincer was autotomized, providing there is enough time to regenerate a claw at the second site. This is the same as when the paired claws are autotomized simultaneously, the limb buds on the two sides regenerate at equivalent rates, and claw asymmetry is retained.

The paired claws also regenerate in their previous configuration when the pincer is removed first and an early limb bud (stage 1–2) is allowed to form before the snapper is removed in 50% or more of the animals. This is equivalent to removing both claws at the same time. However, paired claws regenerate in the reversed configuration in 100% of the animals when the pincer is removed and a more advanced limb bud (stage 3–5) is allowed to form at this site before the snapper is removed. This is equivalent to removing the snapper in the presence of an intact pincer, in which case the existing pincer claw transforms into a snapper at the next molt and a new pincer regenerates at the old snapper site. A stage 3–5 limb bud at the pincer site therefore acts like an intact, fully formed pincer claw in that they both transform into a snapper claw in response to removal of the contralateral snapper claw. In other words, a stage 3–5 limb bud is a suitable target for transformation.

Stage 3 limb buds are characterized by a longitudinal furrow marking the beginning of division of the two most distal segments, the dactyl and propus. The more proximal segments—carpus, merus, and basi-ischium—are delineated in stage 4 buds, and segmentation is complete with final delineation of the dactyl and propus in stage 5 limb buds. Although the most advanced stage 4 and 5 limb buds resemble an intact pincer limb in possessing all of the segments, stage 3 buds with just the beginning of segmentation least resemble an intact limb; yet a stage 3 bud may be signaled into developing as a snapper. It would appear that the transforming signal released with autotomy of the snapper claw can influence the differentiation of tissue, not only in intact pincer claws, but also in a developing limb bud at the pincer site. Thus, for example, the intact pincer claw has a closer muscle whose mixture

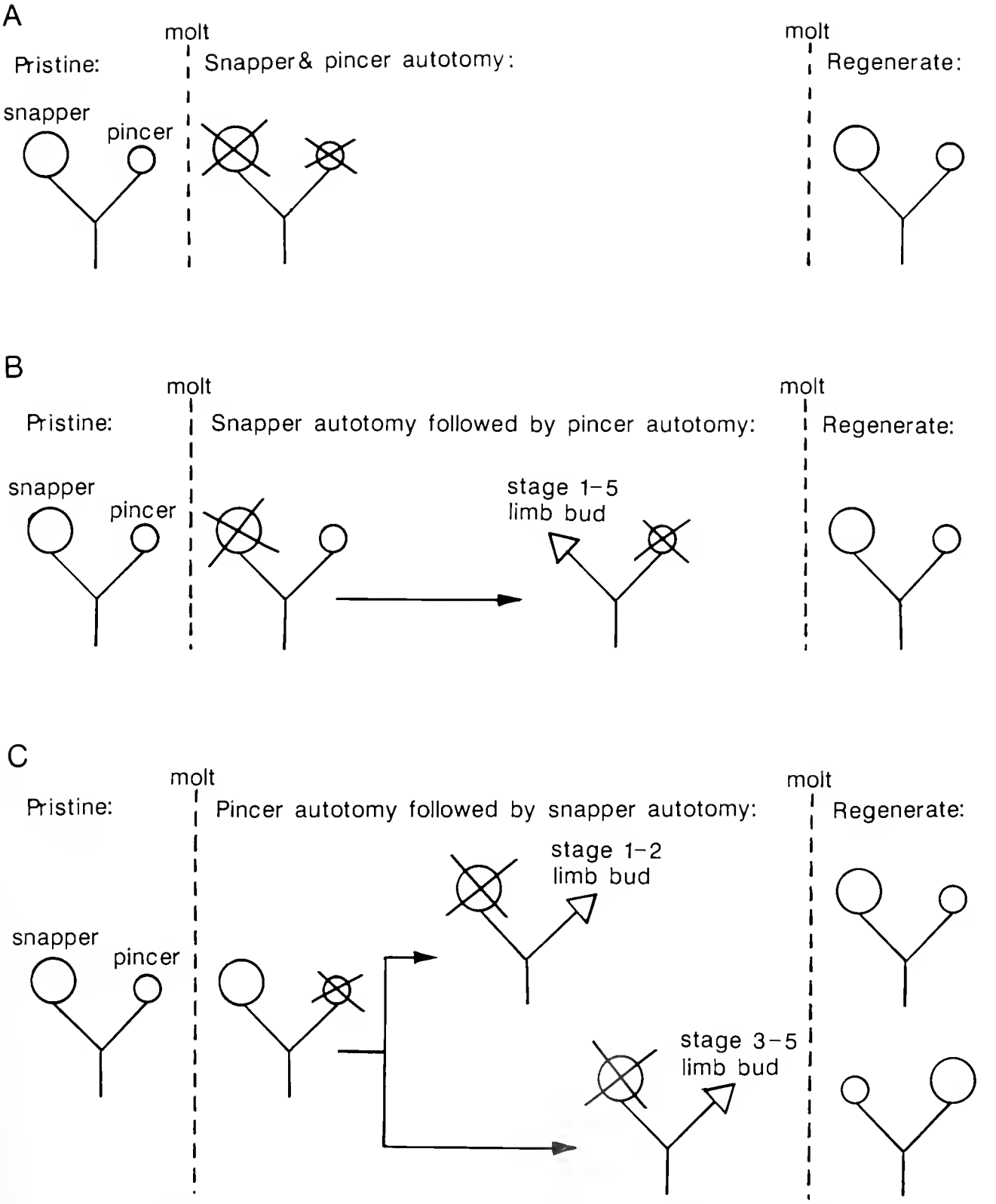

Figure 4. Pictorial representation of the configuration of the paired, asymmetric pincer and snapper claws of adult snapping shrimps in the following experiments. (A) Pincer and snapper claws autotomized simultaneously; regenerate claws appeared in the pristine configuration. (B) The snapper claw was autotomized and, at different limb bud stages at this site, the contralateral pincer claw was autotomized; the regenerate claws appeared in the pristine configuration. (C) The pincer claw was autotomized and, at different stages in the formation of a limb bud at this site, the snapper claw was autotomized; the regenerate claws appeared in the pristine configuration with stage 1–2 buds and in the reversed configuration with stage 3–5 limb buds.

Table I

Configuration of claw asymmetry, whether retained in the previous configuration or reversed, following autotomy of first the pincer claw and then the snapper claw during a single intermolt in adult snapping shrimps

Limb bud stage	Asymmetry retained		Asymmetry reversed	
	Number	%	Number	%
<1.0 (7/10)	6	86	1	14
1.0–1.5 (10/12)	5	50	5	50
2.0–2.5 (7/10)	3	42	4	58
3.0–4.0 (5/8)	0	0	5	100
>4.5 (9/12)	0	0	9	100

The pincer was removed first; then, at various stages of its limb bud development, the snapper was removed. Number in brackets shows the number successful over the number of trials.

of fast and slow fibers is transformed into purely slow fibers of a snapper type by selective death of the fast fibers (Mearow and Govind, 1986) and transformation of the slow fibers from pincer to snapper type (Mellon and Stephens, 1980). In contrast, in a stage 3 limb bud with just the beginning of segmentation, a fully formed closer muscle is unlikely to be present, yet its subsequent development is directed toward snapper muscle rather than pincer muscle.

Shrimps in which the snapper is autotomized after a stage 3–5 limb bud has formed on the pincer site regenerate a new pincer at the snapper site, resulting in reversal of claw asymmetry. The regeneration of a pincer claw at a snapper site requires explanation. Both Wilson (1903) and Darby (1934) considered the possibility that the pincer claw represents a progressive stage in the development of a snapper claw and that inhibition from the contralateral snapper claw can arrest its development. Hence, when the inhibition is removed with snapper autotomy, the pincer continues its development into a snapper, which at the same time restricts claw regeneration to a pincer type on the opposite side. In this way, bilateral asymmetry of the paired claws is ensured. This hypothesis, involving a cross-inhibitory mechanism, would explain why a pincer regenerates at the old snapper site during claw reversal in the present experiments—transformation of the limb bud into a snapper would restrict regeneration to a pincer claw on the opposite side. The hypothesis would also be tenable in cases where only the pincer claw is autotomized, because the intact snapper claw would restrict regeneration to a pincer claw at the autotomy site. However, the hypothesis is insufficient to explain the case in which paired claws are autotomized simultaneously and the regenerate claws appear in their previous configuration. With paired simultaneous autotomy, an additional mechanism would have to be invoked to allow the transforming signal to act at the old snapper site—either by preferentially channeling the signal to this site or by having receptors for the signal exclusively at this site.

Acknowledgments

We thank W. D. Kirby-Smith for generous supplies of snapping shrimps and Joanne Pearce for criticism of the manuscript. Financial support was provided by the Natural Sciences and Engineering Research Council of Canada.

Literature Cited

Bliss, D. E. 1960. Autotomy and regeneration. Pp. 561–589 in *The Physiology of Crustacea*, Vol. 1, T. H. Waterman, ed. Academic Press, New York.

Darby, H. H. 1934. The mechanism of asymmetry in the Alpheidae. *Carnegie Inst. Wash. Publ.* No. 435, 347–361.

Govind, C. K., K. M. Mearow, and A. Wong. 1986. Regeneration of fibre types in paired asymmetric closer muscles of the snapping shrimp, *Alpheus heterochelis*. *J. Exp. Biol.* **123:** 55–69.

Hazlett, B. A., and H. E. Winn. 1962. Sound production and associated behavior of Bermuda crustaceans *Panulirus, Gonodactylus, Alpheus*, and *Synalpheus*. *Crustaceana* **4:** 25–38.

McLaughlin, P. A. 1982. Comparative morphology of crustacean appendages. Pp. 197–256 in *The Biology of Crustacea*, Vol. 2, Embryology, Morphology and Genetics, D. E. Bliss, ed. Academic Press, New York.

Mearow, K. M., and C. K. Govind. 1986. Selective degeneration of fast muscle during claw transformation in snapping shrimps. *Dev. Biol.* **118:** 314–318.

Mellon, DeF. Jr., and P. I. Stephens. 1980. Modification in the arrangement of thick and thin filaments in transforming shrimp muscle. *J. Exp. Zool.* **213:** 173–179.

Przibram, H. 1901. Experimentell Studien über Regeneration. *Arch. Entwick. Mech.* **11:** 321–345.

Read, A. T., and C. K. Govind. 1991. Composition of external setae during regeneration and transformation of the bilaterally asymmetric claws of the snapping shrimp, *Alpheus heterochelis*. *J. Morphol.* **207:** 103–111.

Wilson, E. B. 1903. Notes on the reversal of asymmetry in the regeneration of chelae in *Alpheus heterochelis*. *Biol. Bull.* **4:** 197–210.

CONTENTS

Volume 186 Number 3

THE BIOLOGICAL BULLETIN

JUNE, 1994

Published by the Marine Biological Laboratory

THE
BIOLOGICAL BULLETIN

PUBLISHED BY
THE MARINE BIOLOGICAL LABORATORY

JUNE, 1994

Printed and Issued by
LANCASTER PRESS, Inc.
3575 HEMPLAND ROAD
LANCASTER, PA

THE BIOLOGICAL BULLETIN

THE BIOLOGICAL BULLETIN is published six times a year by the Marine Biological Laboratory, MBL Street, Woods Hole, Massachusetts 02543.

Subscriptions and similar matter should be addressed to Subscription Manager, THE BIOLOGICAL BULLETIN, Marine Biological Laboratory, Woods Hole, Massachusetts 02543. Single numbers, $37.50. Subscription per volume (three issues), $90.00 ($180.00 per year for six issues).

Communications relative to manuscripts should be sent to Michael J. Greenberg, Editor-in-Chief, or Pamela L. Clapp, Managing Editor, at the Marine Biological Laboratory, Woods Hole, Massachusetts 02543. Telephone: (508) 548-3705, ext. 428. FAX: 508-540-6902. E-mail: pclapp@hoh.mbl.edu.

POSTMASTER: Send address changes to THE BIOLOGICAL BULLETIN, Marine Biological Laboratory, Woods Hole, MA 02543.

Second-class postage paid at Woods Hole, MA, and additional mailing offices.
ISSN 0006-3185

INSTRUCTIONS TO AUTHORS

The Biological Bulletin accepts outstanding original research reports of general interest to biologists throughout the world. Papers are usually of intermediate length (10–40 manuscript pages). A limited number of solicited review papers may be accepted after formal review. A paper will usually appear within four months after its acceptance.

Very short, especially topical papers (less than 9 manuscript pages including tables, figures, and bibliography) will be published in a separate section entitled "Research Notes." A Research Note in *The Biological Bulletin* follows the format of similar notes in *Nature*. It should open with a summary paragraph of 150 to 200 words comprising the introduction and the conclusions. The rest of the text should continue on without subheadings, and there should be no more than 30 references. References should be referred to in the text by number, and listed in the Literature Cited section in the order that they appear in the text. Unlike references in *Nature*, references in the Research Notes section should conform in punctuation and arrangement to the style of recent issues of *The Biological Bulletin*. Materials and Methods should be incorporated into appropriate figure legends. See the article by Lohmann *et al.* (October 1990, Vol. **179**: 214–218) for sample style. A Research Note will usually appear within two months after its acceptance.

The Editorial Board requests that regular manuscripts conform to the requirements set below; those manuscripts that do not conform will be returned to authors for correction before review.

1. ***Manuscripts.*** Manuscripts, including figures, should be submitted in triplicate. (Xerox copies of photographs are not acceptable for review purposes.) The submission letter accompanying the manuscript should include a telephone number, a FAX number, and (if possible) an E-mail address for the corresponding author. The original manuscript must be typed in no smaller than 12 pitch or 10 point, using double spacing (*including* figure legends, footnotes, bibliography, etc.) on one side of 16- or 20-lb. bond paper, 8½ by 11 inches. Please, no right justification. Manuscripts should be proofread carefully and errors corrected legibly in black ink. Pages should be numbered consecutively. Margins on all sides should be at least 1 inch (2.5 cm). Manuscripts should conform to the *Council of Biology Editors Style Manual*, 5th Edition (Council of Biology Editors, 1983) and to American spelling. Unusual abbreviations should be kept to a minimum and should be spelled out on first reference as well as defined in a footnote on the title page. Manuscripts should be divided into the following components: Title page, Abstract (of no more than 200 words), Introduction, Materials and Methods, Results, Discussion, Acknowledgments, Literature Cited, Tables, and Figure Legends. In addition, authors should supply a list of words and phrases under which the article should be indexed.

2. ***Title page.*** The title page consists of a condensed title or running head of no more than 35 letters and spaces, the manuscript title, authors' names and appropriate addresses, and footnotes listing present addresses, acknowledgments or contribution numbers, and explanation of unusual abbreviations.

3. ***Figures.*** The dimensions of the printed page, 7 by 9 inches, should be kept in mind in preparing figures for publication. We recommend that figures be about 1½ times the linear dimensions of the final printing desired, and that the ratio of the largest to the smallest letter or number and of the thickest to the thinnest line not exceed 1:1.5. Explanatory matter generally should be included in legends, although axes should always be identified on the illustration itself. Figures should be prepared for reproduction as either line cuts or halftones. Figures to be reproduced as line cuts should be unmounted glossy photographic reproductions or drawn in black ink on white paper, good-quality tracing cloth or plastic, or blue-lined coordinate paper. Those to be reproduced as halftones should be mounted on board, with both designating numbers or letters and scale bars affixed directly to the figures. All figures should be numbered in consecutive order, with no distinction between text and plate figures. The author's name and an arrow indicating orientation should appear on the reverse side of all figures.

4. ***Tables, footnotes, figure legends, etc.*** Authors should follow the style in a recent issue of *The Biological Bulletin* in preparing table headings, figure legends, and the like. Because of the high cost of setting tabular material in type, authors are asked to limit such material as much as possible. Tables, with their headings and footnotes, should be typed on separate sheets, numbered with consecutive Roman numerals, and placed after

the Literature Cited. Figure legends should contain enough information to make the figure intelligible separate from the text. Legends should be typed double spaced, with consecutive Arabic numbers, on a separate sheet at the end of the paper. Footnotes should be limited to authors' current addresses, acknowledgments or contribution numbers, and explanation of unusual abbreviations. All such footnotes should appear on the title page. Footnotes are not normally permitted in the body of the text.

5. ***Literature cited.*** In the text, literature should be cited by the Harvard system, with papers by more than two authors cited as Jones *et al.*, 1980. Personal communications and material in preparation or in press should be cited in the text only, with author's initials and institutions, unless the material has been formally accepted and a volume number can be supplied. The list of references following the text should be headed Literature Cited, and must be typed double spaced on separate pages, conforming in punctuation and arrangement to the style of recent issues of *The Biological Bulletin*. Citations should include complete titles and inclusive pagination. Journal abbreviations should normally follow those of the U. S. A. Standards Institute (USASI), as adopted by BIOLOGICAL ABSTRACTS and CHEMICAL ABSTRACTS, with the minor differences set out below. The most generally useful list of biological journal titles is that published each year by BIOLOGICAL ABSTRACTS (BIOSIS List of Serials; the most recent issue). Foreign authors, and others who are accustomed to using THE WORLD LIST OF SCIENTIFIC PERIODICALS, may find a booklet published by the Biological Council of the U.K. (obtainable from the Institute of Biology, 41 Queen's Gate, London, S.W.7, England, U.K.) useful, since it sets out the WORLD LIST abbreviations for most biological journals with notes of the USASI abbreviations where these differ. CHEMICAL ABSTRACTS publishes quarterly supplements of additional abbreviations. The following points of reference style for THE BIOLOGICAL BULLETIN differ from USASI (or modified WORLD LIST) usage:

A. Journal abbreviations, and book titles, all underlined (for *italics*)

B. All components of abbreviations with initial capitals (not as European usage in WORLD LIST *e.g., J. Cell. Comp. Physiol.* NOT *J. cell. comp. Physiol.*)

C. *All* abbreviated components must be followed by a period, whole word components *must not* (*i.e., J Cancer Res.*)

D. Space between all components (*e.g., J. Cell. Comp. Physiol.*, not *J.Cell.Comp.Physiol.*)

E. Unusual words in journal titles should be spelled out in full, rather than employing new abbreviations invented by the author. For example, use *Rit Vísindafjélags Islendinga* without abbreviation.

F. All single word journal titles in full (*e.g., Veliger, Ecology, Brain*).

G. The order of abbreviated components should be the same as the word order of the complete title (*i.e., Proc.* and *Trans.* placed where they appear, not transposed as in some BIOLOGICAL ABSTRACTS listings).

H. A few well-known international journals in their preferred forms rather than WORLD LIST or USASI usage (*e.g., Nature, Science, Evolution* NOT *Nature, Lond., Science, N.Y.; Evolution, Lancaster, Pa.*)

6. ***Reprints, page proofs, and charges.*** Authors receive their first 100 reprints (without covers) free of charge. Additional reprints may be ordered at time of publication and normally will be delivered about two to three months after the issue date. Authors (or delegates for foreign authors) will receive page proofs of articles shortly before publication. They will be charged the current cost of printers' time for corrections to these (other than corrections of printers' or editors' errors). Other than these charges for authors' alterations, *The Biological Bulletin* does not have page charges.

CONTENTS

No 1, February 1994

No. 2, April 1994

No. 3, June 1994

Reference: *Biol. Bull.* **186:** 247–253. (June, 1994)

Hemocyte Aggregation in the Solitary Ascidian *Halocynthia roretzi:* Plasma Factors, Magnesium Ion, and Met-Lys-Bradykinin Induce the Aggregation

HIROKI TAKAHASHI, KAORU AZUMI, AND HIDEYOSHI YOKOSAWA*

Department of Biochemistry, Faculty of Pharmaceutical Sciences, Hokkaido University, Sapporo 060, Japan

Abstract. Hemocytes of the ascidian *Halocynthia roretzi* undergo aggregation in hemolymph that has been collected from the body through the tunic. To investigate the mechanisms involved, we first established two methods of measuring hemocyte aggregation. In one method, hemocyte aggregation was quantified by its reduction of light scattering intensity as measured with a fluorescence spectrophotometer. In the other method, the increase of transmittance accompanying aggregation was measured with an ELISA reader. We found that ascidian plasma, Mg^{2+}, and Met-Lys-bradykinin can induce the hemocytes of *H. roretzi* to aggregate. The aggregation induced by any of these three substances was inhibited by EDTA, *N*-ethylmaleimide, and cytochalasin B. Lipopolysaccharide had little inducing effect. We also demonstrated that, when *H. roretzi* plasma was treated with trypsin, low molecular weight aggregation-inducing substances were produced. These results suggest that metal ions and peptide-like substances present in the hemolymph play essential roles in the progression of hemocyte aggregation of *H. roretzi.*

Introduction

Coagulation of body fluid (hemolymph) in some species of invertebrates is analogous to blood clotting in vertebrates (Boolootian and Giese, 1959; Young *et al.,* 1972; Barwig, 1985; Levin, 1985; Iwanaga, 1993). Coagulation is thought to prevent the loss of hemolymph from a wound, and it may also immobilize microorganisms that invade the body. In animals such as mollusks (Bayne, 1981), however, hemolymph coagulation does not occur, although the hemocytes do aggregate.

Received 10 June 1993; accepted 6 April 1994.

* Author to whom reprint requests should be addressed.

We have been investigating the defense mechanisms of the solitary ascidian *Halocynthia roretzi,* in which hemocytes play an important role. The hemocytes contain two antimicrobial substances (Azumi *et al.,* 1990a, b) and a hemagglutinin that can agglutinate various bacteria (Azumi *et al.,* 1991a). The hemocytes also undergo several cellular defense reactions, such as phagocytosis (Fuke, 1979), a self and nonself recognition reaction (Fuke, 1980), and an enzyme release reaction (Azumi *et al.,* 1991b, 1993). Body fluid does not coagulate after the tunic of *H. roretzi* is injured, but the hemocytes do aggregate upon injury to the tunic or when hemolymph is collected through the tunic. This aggregation appears to be a cellular defense reaction that arrests bleeding. The mechanisms of hemocyte aggregation, however, have not yet been clarified.

Here we report two methods of measuring hemocyte aggregation of *H. roretzi* that have enabled us to characterize factors that are involved in the aggregation. We found that ascidian plasma, Mg^{2+}, and Met-Lys-bradykinin can induce the aggregation of ascidian hemocytes.

Materials and Methods

Hemolymph and hemocytes

Solitary ascidians, *H. roretzi,* were harvested in Mutsu Bay, Aomori Prefecture, Japan. The ascidians were chilled on ice for at least 30 min before collection of hemolymph to reduce the rate of aggregation, and the animals were kept on ice during the experiment. The tunic matrix was extensively washed with seawater, and a sample of hemolymph (1 ml) was collected from the space just beneath the epithelium at the tunic papilla through a 5-ml disposable plastic syringe with a 23-gauge needle. The total

hemolymph (50–100 ml) was also collected from individual animals: a cut was made in the tunic matrix, and the animals were allowed to bleed into 0.56 *M* NaCl containing 2.7 m*M* EDTA at pH 5.2 (EDTA solution). The EDTA and low pH prevented the hemocytes from aggregating. The volume of EDTA solution was equal to that of the original hemolymph. After centrifuging ($800 \times g$, 10 min) this twofold-diluted hemolymph, the resulting pellet (hemocytes) obtained from each animal was gently washed with 5 ml of Ca^{2+}-, Mg^{2+}-free Herbst's artificial seawater (Ca^{2+}-, Mg^{2+}-free HASW; 450 m*M* NaCl, 9.4 m*M* KCl, 32 m*M* Na_2SO_4, and 3.2 m*M* $NaHCO_3$, pH 7.6), and was then suspended individually in Ca^{2+}-, Mg^{2+}-free HASW. The hemocytes in the individual suspension were counted and adjusted to about 5×10^6 cells/ml.

Chemicals

Bovine pancreatic trypsin, cytochalasin B, kyotorphin, dynorphin (1-8), formyl-Met-Leu-Phe, Arg-Gly-Asp-Ser (RGDS peptide), and ADP were obtained from Sigma Chemical Co. (St. Louis, Missouri). Lipopolysaccharide (LPS) from *Escherichia coli* 026:B6 was purchased from Difco Laboratories (Detroit, Michigan). ACTH was from Bachem Feinchemikalien AG (Bubendorf, Switzerland). Peptide E and metorophinamide were from Peninsula Laboratories, Inc. (Belmont, California). Other biologically active peptides, such as Met-Lys-bradykinin, Met-enkephalin, and bradykinin potentiator C, were obtained from the Peptide Institute (Osaka, Japan).

Measurement of hemocyte aggregation

Method A: The hemolymph, or a suspension of hemocytes in Ca^{2+}-, Mg^{2+}-free HASW (1 ml, about 5×10^6 cells/ml), was added to a cuvette that contained a stirring bar and had been placed in a Hitachi 650-60 fluorescence spectrophotometer equipped with a holder controlled thermostatically at 15°C. The hemocyte suspension was stirred gently to promote aggregation, and the hemocyte aggregation that occurred spontaneously, or that was induced by addition of 100 μl of an inducer, was monitored by light scattering with excitation at 380 nm and emission at 400 nm.

Method B: 90 μl of a suspension of hemocytes in Ca^{2+}-, Mg^{2+}-free HASW (1×10^7 cells/ml) was added to each well of a 96-well plate and incubated at 4°C for 30 min to allow the hemocytes to attach to the bottom. The plate was placed on a Bio-Rad 2550 ELISA reader, and the absorbance at 405 nm [$(A405)_0$] was measured. After 10 μl of inducer was added to each well, the plate was shaken gently at 20°C for 10 min to promote aggregation and was then kept standing at 20°C. After 50 min, the absorbance at 405 nm [$(A405)_{60}$] was again measured. The degree of aggregation was defined as the difference in the transmittance (T) calculated from $A405$ before and after incubation at 20°C [$(T405)_{60} - (T405)_0$]. Percent aggregation in the presence of each inducer was calculated on the assumption that the degrees of aggregation observed in the presence and absence of 2 m*M* $MgCl_2$ were defined as 100% and 0%, respectively. Experiments were performed in triplicate, and the mean was calculated.

Plasma treatment

We used various preparations of plasma as inducers of aggregation: *Intact plasma* was prepared by centrifuging the hemolymph exuded from a cut made in the tunic and collected into a solution lacking EDTA. *Reacted plasma* was prepared by centrifuging the hemolymph after its hemocytes had been completely aggregated by incubation with agitation for 30 min at 20°C. *Acid-* or *alkali-treated plasma* was exposed to acid (pH 1) or alkali (pH 11) for one hour at 4°C and neutralized. *Heat-treated plasma* was heated to 90°C for 15 min. And *dialyzed plasma* was placed in dialysis tubing (10,000 molecular weight cut-off) and incubated overnight, at 4°C, against Ca^{2+}-, Mg^{2+}-free HASW.

Low molecular weight substances were produced from plasma by treatment with trypsin as follows: Intact plasma or dialyzed plasma was treated with 0.1 mg/ml trypsin at 20°C for 4 h. The reaction mixture was filtered through a Centricut membrane (10,000 molecular weight cut-off) by centrifugation ($2700 \times g$, 1 h); the filtrate contains the low molecular weight substances, but does not contain the trypsin (molecular weight, 23,000) and other high molecular weight substances present in the plasma. The inducing effect on hemocyte aggregation of the filtrate containing low molecular weight substances was tested.

Results

Aggregation of hemocytes in hemolymph

Whether the hemolymph of *H. roretzi* was collected by syringe and needle or through a cut made in the tunic, aggregation of the hemocytes was observed under the microscope. In the initial stage of aggregation, hemocytes containing many vacuoles with filament-like inclusions (hemocytes of type C named by Azumi *et al.*, 1993) make contact to form small homogeneous aggregates. At the same time, amoeba-like hemocytes (type A and B hemocytes) migrate toward and contact vacuolated cells containing several vacuoles of high density (type F hemocytes); this triggers and promotes the aggregation of the latter type F hemocytes themselves. Finally, several large heterogeneous aggregates including almost all types of hemocytes are formed. The aggregation reaction on a slide (*without shaking*) is complete within a 1-h incubation at

15°C; (the reaction takes place more rapidly *with shaking* and is then complete within about 10 min). The hemocytes seem to remain intact during an overnight incubation (the hemocytes lyse slightly during a much longer incubation).

The change in light scattering measured in a cuvette at 15°C (Fig. 1) occurs concomitantly with the aggregation observed microscopically; when we took up the hemocyte suspension at increasing time intervals and examined it microscopically, aggregate formation seemed to be roughly concurrent with the decrease of light scattering. The aggregation was strongly inhibited by the presence of 1 m*M* EDTA. Thus, the degree of aggregation can be quantified from the curve generated by this method (method A).

Ascidian specimens were placed on ice to reduce hemolymph circulation. When samples of hemolymph were collected with a syringe at increasing time intervals from the same location on the tunic (point A in Fig. 2), the rate of hemocyte aggregation measured at 15°C increased with time (upper panel of Fig. 2; the slopes at 58 min, 96 min, and 142 min became steeper in this order). Thus, hemocyte aggregation seems to be activated at the point on the tunic that was wounded by the syringe needle. Indeed, when hemocytes were collected from another point on the same animal (point B in Fig. 2) 234 min after the initial collection of hemocytes at point A, the rate of aggregation of hemocytes at point B was almost the same as that at point A at 0 min (lower panel of Fig. 2). But when the ascidian was put into seawater (15°C), allowing hemolymph circulation, the rate of aggregation of hemocytes at point B increased to that seen at point A at 142 min (data not shown). These results suggest that soluble factors inducing hemocyte aggregation are released from a tunic wound, or in the aggregation reaction, and circulate through the body cavity.

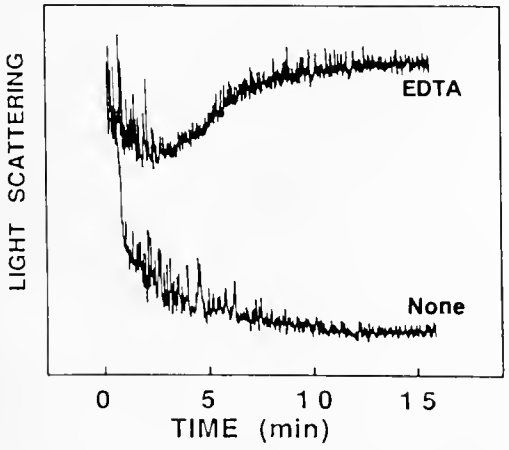

Figure 1. Effect of EDTA on aggregation of hemocytes in hemolymph of *Halocynthia roretzi*. The aggregation was measured at 15°C by method A. The concentration of EDTA used was 1 m*M*. The extent of light scattering is shown on the ordinate in arbitrary units.

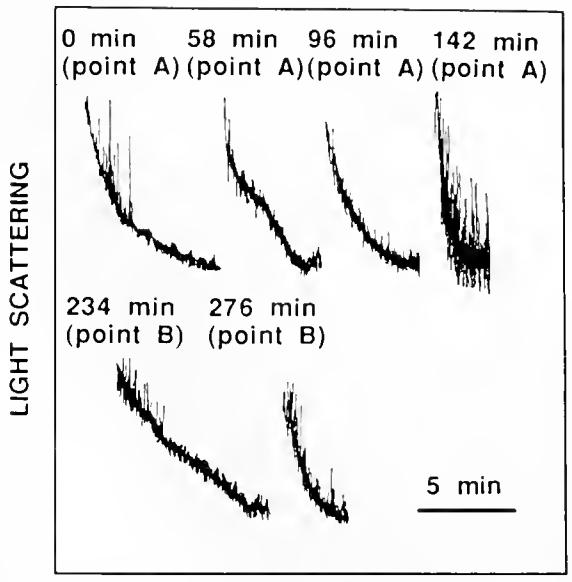

Figure 2. Activation of hemocyte aggregation in *Halocynthia roretzi*. Point A represents the same point on the tunic through which the hemolymph was repeatedly taken, and point B represents a different point on the tunic. The time between the initial collection of hemolymph (0 min) and subsequent collections is indicated above each record. The bar represents 5 min. The extent of light scattering is shown on the ordinate in arbitrary units.

Inducing effects of plasma and metal ions on aggregation of hemocytes

Isolated hemocytes of *H. roretzi* that had been collected from the hemolymph, washed, and resuspended in Ca^{2+}-, Mg^{2+}-free HASW exhibited a lower degree of aggregation than whole hemolymph. Moreover, hemocyte aggregation was stimulated by the addition of ascidian plasma (the final concentration was 10%), and the plasma-induced aggregation was dependent on temperature (Fig. 3). Thus, the plasma of *H. roretzi* seems to contain factors that can induce (or activate) the aggregation of hemocytes.

Because the aggregation, whether in hemolymph or in Ca^{2+}-, Mg^{2+}-free HASW supplemented with plasma, was inhibited by EDTA, a metal chelating agent, we next investigated the effects of metal ions on the aggregation. Magnesium ions ($MgCl_2$ or $MgSO_4$) induce the aggregation of hemocytes in a concentration-dependent manner (Fig. 4a). The aggregation reached a plateau at concentrations higher than 2 m*M* (aggregation was linear in the range of 0–2 m*M* Mg^{2+}). Of the other ions tested, 2 m*M* Mn^{2+}, Zn^{2+}, and Co^{2+} had inducing effects as strong as those of Mg^{2+}, whereas Ca^{2+} and Ni^{2+} had little effect (Fig. 4b). We usually measured the effects of Mg^{2+} on aggregation of hemocytes *with shaking* and detected its

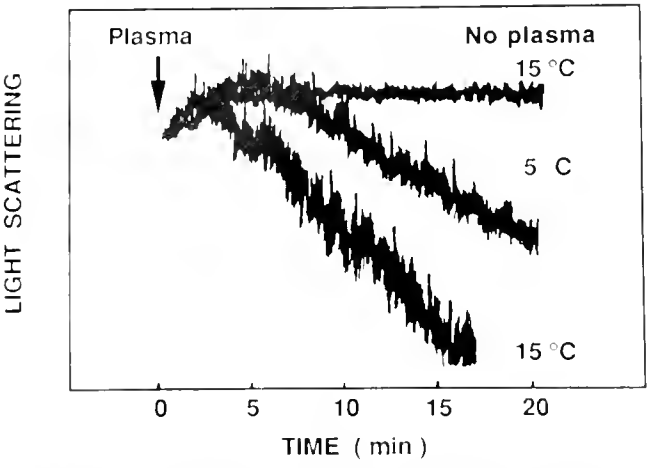

Figure 3. Aggregation of hemocytes of *Halocynthia roretzi* in the presence of 10% plasma at 5°C and at 15°C. In the absence of plasma, no aggregation occurred even at 15°C. The extent of light scattering is shown on the ordinate in arbitrary units.

inducing effects. *Without shaking*, however, Mg^{2+} had little inducing effect in contrast to the case of plasma; *i.e.*, the inducing effects of plasma were detectable irrespective of shaking.

Effects of various preparations of plasma on hemocyte aggregation

We developed method A to analyze the aggregation of *H. roretzi* hemocytes. This method is useful for tracing the progress of the reaction, but is too time-consuming for investigating the effects of various substances on aggregation. Therefore, we developed another quantitative method (B) in which an ELISA reader is used to measure the increased transmittance that should occur as hemocyte aggregates form. In fact, the transmission was increased at a rate consistent with the formation of aggregates detected microscopically. By this method, we confirmed that both plasma and Mg^{2+} induced the aggregation of *H. roretzi* hemocytes.

To characterize the plasma factor that can induce the aggregation of *H. roretzi* hemocytes, we used method B to examine the effects of various preparations of plasma (10%) on the aggregation. The plasma factor was stable under acidic and alkaline conditions and resistant to heat treatment; its molecular weight was less than 10,000 because dialyzed plasma had little inducing activity (Fig. 5a). In fact, the filtrate (containing low molecular weight substances) obtained from intact plasma by filtration through a Centricut filter (10,000 molecular weight cut-off) had inducing activity (control experiment in Fig. 5b), whereas that obtained from dialyzed plasma had little activity (second bar in Fig. 5b). The filtrate from trypsin-treated intact plasma had strong inducing activity (third bar in Fig. 5b). But the filtrate from trypsin-treated dialyzed plasma also had some inducing activity (fourth bar in Fig. 5b), suggesting that low molecular weight peptide-like inducing substances had been produced from plasma proteins by treatment with trypsin. Furthermore, the reacted plasma showed stronger effects than the intact

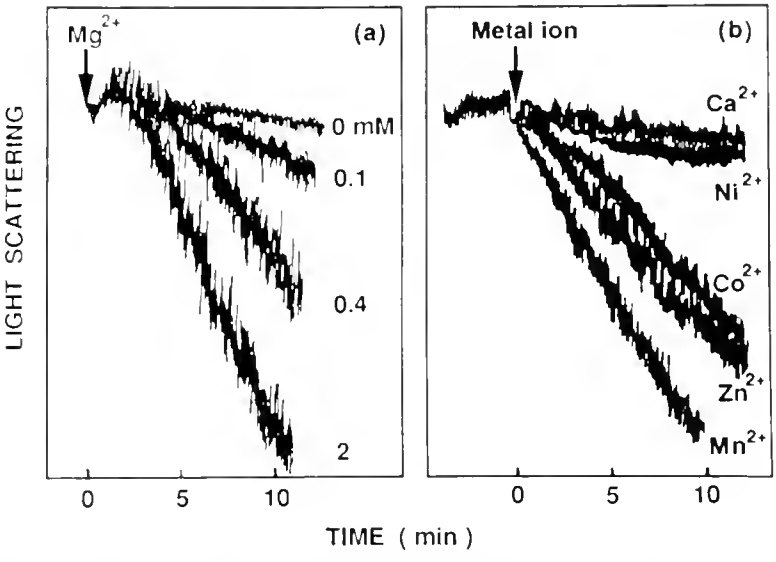

Figure 4. Aggregation of hemocytes of *Halocynthia roretzi* induced by metal ions. The respective metal ion was added to the hemocyte suspension in the Ca^{2+}-, Mg^{2+}-free HASW. (a) The extent of stimulation by Mg^{2+} was dependent on its concentration. (b) Mn^{2+}, Zn^{2+}, and Co^{2+} had an inducing effect, whereas Ca^{2+} and Ni^{2+} had little inducing effect. The concentration of metal ion used was 2 m*M*. The extent of light scattering is shown on the ordinate in arbitrary units.

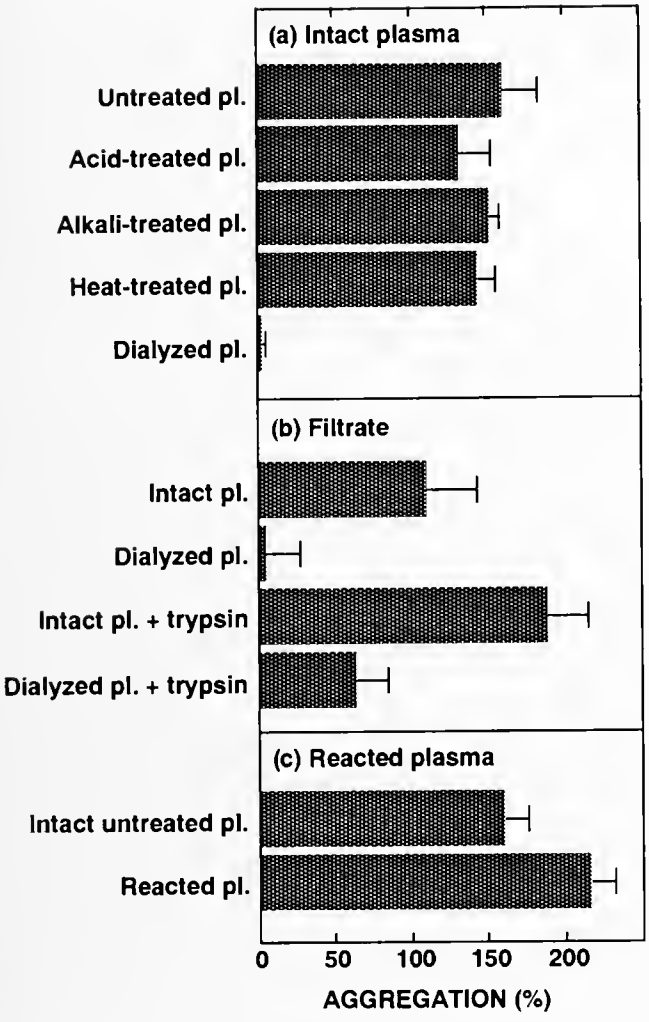

Figure 5. Effects of various preparations of plasma on the aggregation of hemocytes of *Halocynthia roretzi*. (a) Intact plasma was previously treated with acid, alkali, or heat (90°C), or was dialyzed, and effects of these preparations (10%) on the aggregation were measured by method B. (b) Intact plasma or dialyzed plasma was treated with or without trypsin (0.1 mg/ml) at 20°C for 4 h and filtered through a Centricut membrane (10,000 molecular weight cut-off). The effects of the resulting filtrates on the aggregation were measured by method B. (c) The effect of reacted plasma on the aggregation was measured by method B. Reacted plasma was collected from hemolymph in which the aggregation of hemocytes had been completed. The results shown are means of relative values of triplicate tests (±SD); the aggregation induced by 2 m*M* $MgCl_2$ was defined as 100%. Note that an approximately linear relationship exists between the extent of aggregation and the concentration of plasma factor tested in this experiment.

plasma (Fig. 5c), which suggests that one or more inducing substances are produced when the aggregation of hemocytes takes place in hemolymph.

Inducing effects of Met-Lys-bradykinin on hemocyte aggregation

Stefano *et al.* (1989a, b) have reported that Met-enkephalin triggers inflammatory responses from the hemocytes of the mollusk *Mytilus edulis* by inducing their morphological change, migration, and aggregation. To investigate whether neuropeptides, such as Met-enkephalin, would induce ascidian hemocytes to aggregate, we used method B to examine the effects of 26 biologically active peptides on the aggregation of *H. roretzi* hemocytes. Typical results are shown in Figure 6. Among peptides tested, Met-Lys-bradykinin induced the aggregation as strongly as Mg^{2+} (the maximum aggregation was observed at 2 μM). Despite the equivalence of these assay results, the aggregates formed in the presence of Met-Lys-bradykinin are larger in number and smaller in size than those in the presence of Mg^{2+}, and the inducing effect of Met-Lys-bradykinin was detectable even *without shaking*, suggesting that different intracellular mechanisms might underlie the two effects.

Bradykinin was a moderate stimulant. The peptides (1 μM) Lys-bradykinin, substance P, ACTH, and oxytocin also had moderate inducing activity similar to that of bradykinin. Supporting the possibility that the presence of endogenous bradykinin-like peptides may induce hemocyte aggregation, we obtained the interesting result that bradykinin potentiator C (1 μM), a kininase inhibitor, had a moderate inducing activity similar to that seen with bradykinin. This inhibitor may potentiate the activity of an endogenous peptide-like inducer by blocking inactivating proteases. On the other hand, Met-enkephalin, an inducer of hemocyte aggregation in *M. edulis*, had little effect on the aggregation of ascidian hemocytes. The following 19 peptides (1 μM) also had little inducing activity; Leu-enkephalin, α- and γ-endorphins, α- and β-neoendorphins, angiotensin I and II, mastoparan, LHRH, CGRP, somatostatin, neurotensin, physalaemin, sub-

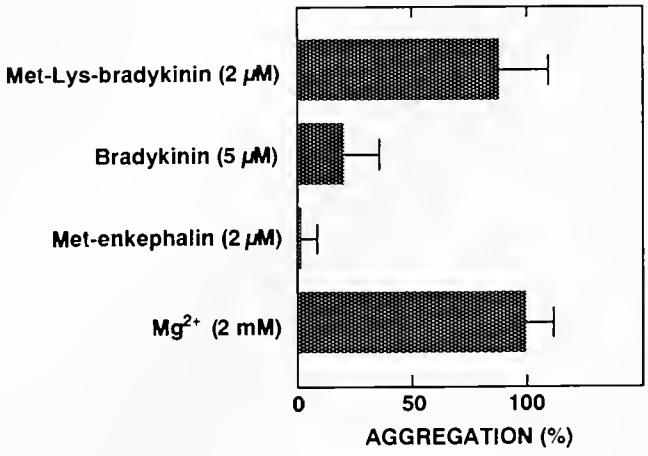

Figure 6. The effects of biologically active peptides on the aggregation of washed hemocytes of *Halocynthia roretzi*. The aggregation was measured by method B in Ca^{2+}-, Mg^{2+}-free HASW. Inducers used were Met-Lys-bradykinin (2 μM), bradykinin (5 μM), Met-enkephalin (2 μM), and Mg^{2+} (2 mM). The results shown are means of triplicate tests (±SD).

stance K, kyotorphin, dynorphin (1-8), peptide E, metorophinamide, and formyl-Met-Leu-Phe. In addition, ADP (1 m*M*), Arg-Gly-Asp-Ser (RGDS peptide) (0.001–1 m*M*), and LPS (1–100 μg/ml) also had little effects on the aggregation.

Inhibition of aggregation of hemocytes

Using method B, we examined the effects of several reagents on the hemocyte aggregation induced by 2 m*M* Mg^{2+}, 10% plasma, and 2.5 μ*M* Met-Lys-bradykinin. *N*-Ethylmaleimide (0.5 m*M*) completely inhibited the hemocyte aggregation induced by any of the inducers. EDTA (2 m*M*) and cytochalasin B (0.01 mg/ml) also strongly inhibited aggregation (about 80 and 60% inhibitions were observed with EDTA and cytochalasin B, respectively). Because the hemocyte aggregations induced by Met-Lys-bradykinin and Mg^{2+} are both inhibited by EDTA, we propose that the aggregation reaction consists of several stages, and that Met-Lys-bradykinin functions at a stage prior to an EDTA-sensitive event.

Discussion

We have been studying the roles of defense factors in the hemolymph of *H. roretzi* for about 10 years and have never observed clot formation, even at room temperature. In contrast, hemocyte aggregation has always been detectable. Moreover, when a part of the tunic is removed by cutting so that the muscle is exposed to seawater, the hemocytes seem to migrate to the area of injured tunic and to form aggregates. We therefore assumed that *H. roretzi* lacks the so-called coagulation system, which functions in maintaining hemostasis, and that instead the hemocyte aggregation system plays a role in stopping bleeding. Our previous qualitative observations also indicated that the aggregation of hemocytes is regulated by factors that are sensitive to temperature, EDTA, and pH. These factors must be characterized if the mechanisms of hemocyte aggregation in *H. roretzi* are to be clarified. In this study, we developed methods of measuring hemocyte aggregation and investigated several factors that may participate in the aggregation.

Of the two quantitative methods, one is based on the measurement, with a fluorescence spectrophotometer, of platelet aggregation in mammals. This method is useful for monitoring the kinetics of aggregation reaction, so we used it to demonstrate that aggregation is blocked in the presence of EDTA and that preformed hemocyte aggregates can be dissociated by the addition of EDTA. After dissociation by EDTA, however, the hemocytes never reaggregated, even upon addition of excess Mg^{2+}. Therefore, dissociation of hemocyte aggregates by EDTA is irreversible; the precise mechanism remains unclear. In contrast to our findings with *H. roretzi*, hemocyte aggregation in *Limulus polyphemus* was retarded by EDTA, but was reversible by the addition of metal ions (Kenney *et al.*, 1972). We have shown that ascidian plasma and metal ions, including Mg^{2+} but not Ca^{2+}, induced aggregation. In contrast, again, the aggregation of *L. polyphemus* hemocytes was induced more efficiently by Mg^{2+} ion than by Ca^{2+} ion (Kenney *et al.*, 1972), and aggregation of *Pomacea canaliculata* hemocytes was induced by Ca^{2+} ion, but not by Mg^{2+} ion (Shozawa and Suto, 1990). The differences in EDTA effects and in metal ion reactivity among the mollusk, the arthropod, and the ascidian remain unexplained, however.

Because the plasma factor is a heat-stable substance of low molecular weight, and because the plasma does contain metal ions, the inducing activity of the plasma could be due to metal ions. However, the result that low molecular weight peptide-like inducing substances are produced by trypsin treatment from dialyzed plasma lacking metal ions supports the idea that *H. roretzi* plasma contains inducing substances in addition to metal ions. Furthermore, the reacted plasma has a stronger effect on hemocyte aggregation than does the intact untreated plasma, which suggests that the hemocytes produce inducing substances during the aggregation reaction. Our preliminary finding, that the supernatant obtained from the hemocyte lysate by centrifugation has an inducing effect on hemocyte aggregation, is consistent with this assumption. The inducing substances found in reacted plasma and present in the lysate supernatant must be further defined. Circulating hemocytes do not aggregate, even though metal ions and plasma factors are present; but hemocyte aggregation in the hemolymph will occur at a restricted site on the tunic that has been damaged with a needle. This observation suggests that specific aggregation activation mechanisms, as yet unidentified, occur in *H. roretzi*.

Met-enkephalin has been reported to induce the aggregation of hemocytes of the mollusk *M. edulis*, and a Met-enkephalin-like substance has been demonstrated in hemolymph of this species (Stefano *et al.*, 1989a, b). These studies suggest that bioactive peptides such as Met-enkephalin may regulate hemocyte aggregation in the hemolymph of other animals. In the case of the ascidians, Met-Lys-bradykinin is the strongest inducer of hemocyte aggregation among the peptides tested, whereas Met-enkephalin has little effect. Bradykinin and Lys-bradykinin have weaker activity, thus the methionyl residue of Met-Lys-bradykinin may be necessary for the full expression of its inducing activity. These results suggest that a Met-Lys-bradykinin-like substance may be one of the candidates for a natural inducers. Our observations on the production of peptide-like inducing substances by trypsin treatment are consistent with this assumption. In addition, inducing effects of both plasma and Met-Lys-bradykinin

were detectable without shaking (under these conditions, inducing effects of Mg^{2+} were undetectable). The above observations, together with the fact that smaller aggregates are formed in the presence of Met-Lys-bradykinin than in the presence of Mg^{2+} and plasma (in the latter two cases aggregates of similar sizes are formed), lead us to propose that plasma contains factors other than Mg^{2+} and Met-Lys-bradykinin. In our current experiments, we are trying to isolate natural inducers from plasma of *H. roretzi*, and we have found a heat-stable, low molecular weight substance that can stimulate the aggregation of hemocytes. Gel filtration of this substance indicates an apparent molecular weight slightly larger than that of Mg^{2+}. Characterization of this factor is now in progress in our laboratory.

We have previously reported that the hemocytes of *H. roretzi* respond to LPS and release a protease (Azumi *et al.*, 1991b). In this study, we found that LPS has little inducing effect on *H. roretzi* hemocyte aggregation under the conditions used. Because LPS was included in the reaction mixture throughout the progression of the reaction, we conclude that substances produced by hemocytes in response to LPS treatment have little inducing activity, and that those substances are different from the inducing substances produced by hemocytes in the aggregation reaction. In the horseshoe crab, *L. polyphemus*, LPS triggers the exocytosis of components of the coagulation system from amebocytes and initiates the coagulation cascade system (Levin and Bang, 1964; Levin, 1985; Iwanaga, 1993). Even in the absence of LPS, the amebocytes of *L. polyphemus* aggregate immediately when the hemolymph is removed from the animal (Levin, 1985). As previously noted, there are also differences in EDTA action and metal ion reactivity between *L. polyphemus* and *H. roretzi*. However, as in *H. roretzi*, hemocyte aggregation is prevented by *N*-ethylmaleimide in *L. polyphemus* (Bryan *et al.*, 1964), indicating that the mechanisms of hemocyte aggregation in the two species may have some similarities.

Acknowledgments

We are grateful to Dr. T. Numakunai of the Asamushi Marine Biological Station, Tohoku University, for his cooperation in collecting ascidians. This work was supported in part by Grants-in-Aid for Scientific Research from the Ministry of Education, Science, and Culture of Japan, and by the Basic Research Core System of the Special Coordination Fund for Promoting Science and Technology in Japan.

Literature Cited

Azumi, K., H. Yokosawa, and S. Ishii. 1990a. Halocyamines: novel antimicrobial tetrapeptide-like substances isolated from the hemocytes of the solitary ascidian *Halocynthia roretzi*. *Biochemistry* **29:** 159–165.

Azumi, K., M. Yoshimizu, S. Suzuki, Y. Ezura, and H. Yokosawa. 1990b. Inhibitory effect of halocyamine, an antimicrobial substance from ascidian hemocytes, on the growth of fish viruses and marine bacteria. *Experientia* **46:** 1066–1068.

Azumi, K., S. Ozeki, H. Yokosawa, and S. Ishii. 1991a. A novel lipopolysaccharide-binding hemagglutinin isolated from hemocytes of the solitary ascidian, *Halocynthia roretzi*, it can agglutinate bacteria. *Dev. Comp. Immunol.* **15:** 9–16.

Azumi, K., H. Yokosawa, and S. Ishii. 1991b. Lipopolysaccharide induces release of a metallo-protease from hemocytes of the ascidian, *Halocynthia roretzi*. *Dev. Comp. Immunol.* **15:** 1–7.

Azumi, K., N. Satoh, and H. Yokosawa. 1993. Functional and structural characterization of hemocytes of the solitary ascidian, *Halocynthia roretzi*. *J. Exp. Zool.* **265:** 309–316.

Barwig, B. 1985. Isolation and characterization of plasma coagulogen (PC) of the cockroach *Leucophaea maderae* (Blattaria). *J. Comp. Physiol. B.* **155:** 135–143.

Bayne, C. J. 1981. Gastropod cells *in vitro*. Pp. 297–334 in *Advances in Cell Culture*, Vol. 1, K. Maramorosch, ed. Academic Press, New York.

Booloottian, R. A., and A. C. Giese. 1959. Clotting of echinoderm coelomic fluid. *J. Exp. Zool.* **140:** 207–229.

Bryan, F. T., C. W. Robinson, Jr., C. F. Gilbert, and R. D. Langdell. 1964. *N*-Ethylmaleimide inhibition of horseshoe crab hemocyte aggregation. *Science* **144:** 1147–1148.

Fuke, M. T. 1979. Studies on the coelomic cells of some Japanese ascidians. *Bull. Mar. Biol. St. Asamushi, Tohoku Univ.* **16:** 143–159.

Fuke, M. T. 1980. "Contact reactions" between xenogenic or allogenic coelomic cells of solitary ascidians. *Biol. Bull.* **158:** 304–315.

Iwanaga, S. 1993. The limulus clotting reaction. *Curr. Opin. Immunol.* **5:** 74–82.

Kenny, D. M., F. A. Belamarich, and D. Shepro. 1972. Aggregation of horseshoe crab (*Limulus polyphemus*) amebocytes and reversible inhibition of aggregation by EDTA. *Biol. Bull.* **143:** 548–567.

Levin, J. 1985. The role of amebocytes in the blood coagulation mechanism of the horseshoe crab *Limulus polyphemus*. Pp. 145–163 in *Blood Cells of Marine Invertebrates. Experimental Systems in Cell Biology and Comparative Physiology*, W. D. Cohen, ed. Alan R. Liss, New York.

Levin, J., and F. B. Bang. 1964. The role of endotoxin in the extracellular coagulation of *Limulus* blood. *Bull. Johns Hopkins Hosp.* **115:** 265–274.

Shozawa, A., and C. Suto. 1990. Hemocytes of *Pomacea canaliculata*. I. Reversible aggregation induced by Ca^{2+}. *Dev. Comp. Immunol.* **14:** 175–184.

Stefano, G. B., M. K. Leung, X. Zhao, and B. Scharrer. 1989a. Evidence for the involvement of opioid neuropeptides in the adherence and migration of immunocompetent invertebrate hemocytes. *Proc. Natl. Acad. Sci. U.S.A.* **86:** 626–630.

Stefano, G. B., P. Cadet, and B. Scharrer. 1989b. Stimulatory effects of opioid neuropeptides on locomotory activity and conformational changes in invertebrate and human immunocytes: evidence for a subtype of δ receptor. *Proc. Natl. Acad. Sci. U.S.A.* **86:** 6307–6311.

Young, N. S., J. Levin, and R. A. Prendergast. 1972. An invertebrate coagulation system activated by endotoxin: evidence for enzymatic mediation. *J. Clinic. Invest.* **51:** 1790–1797.

Reference: *Biol. Bull.* **186**: 254–262. (June, 1994)

Calcium Buffer Injections Inhibit Ooplasmic Segregation in Medaka Eggs

R. A. FLUCK[1,*], A. L. MILLER[2], V. C. ABRAHAM[1], AND L. F. JAFFE[2]

[1]*Biology Department, Franklin and Marshall College, Lancaster, Pennsylvania 17604-3003, and*
[2]*Marine Biological Laboratory, Woods Hole, Massachusetts 02543*

Abstract. Injection of the weak (K_D = 1.5 μM) calcium buffer 5,5′-dibromo-BAPTA into fertilized medaka eggs inhibited the formation of the blastodisc at the animal pole, the movement of oil droplets toward the vegetal pole, and cytokinesis. These inhibitory actions were dependent upon the concentration of the buffer but were independent of free [Ca^{2+}] in the injectate. Because this buffer has previously been shown to substantially suppress zones of elevated calcium at the animal and vegetal poles of the medaka egg, the results of the present study suggest that these zones are necessary for normal segregation of the ooplasm and its inclusions in the medaka egg.

Introduction

Nearly 20 years ago, cytosolic calcium gradients were postulated to organize developmental localization in eggs of plants and animals (Jaffe *et al.*, 1974; for reviews, see Jaffe and Nuccitelli, 1977; and Jaffe, 1986). Proof of this theory should have three parts (Gilkey *et al.*, 1978): (1) evidence of the existence of cytosolic calcium gradients in systems undergoing localization; (2) evidence that artificial induction of a cytosolic calcium gradient will cause localization; and (3) evidence that dispersion of a cytosolic calcium gradient will inhibit localization. Evidence for the existence of cytosolic calcium gradients in eggs was at first indirect, based on studies suggesting that, in developing fucoid eggs, rhizoids grow in the direction of high [Ca^{2+}] (Robinson and Jaffe, 1975; Nuccitelli, 1978). Since then such gradients have been directly demonstrated in a number of developing systems in which zones of elevated cytosolic [Ca^{2+}] have been identified: near the tip of the rhizoid of fucoid embryos (Berger and Brownlee, 1993), near the tip of growing pollen tubes (Miller *et al.*, 1992b), near the vegetal pole of fertilized *Xenopus laevis* eggs (Miller *et al.*, 1991), and near the animal and vegetal poles of fertilized medaka eggs (Fluck *et al.*, 1992b). In medaka eggs, these zones are present throughout the period of ooplasmic segregation (Fluck *et al.*, 1992b).

Regarding the second criterion—that artificial induction of a cytosolic calcium gradient will organize developmental localization—there is only indirect evidence. This evidence includes the occurrence of localization in fucoid eggs (Robinson and Cone, 1980) and ascidian eggs (Jeffery, 1982; Bates and Jeffery, 1988) exposed to a gradient of the calcium ionophore A23187. Other indirect evidence comes from the medaka egg, in which additional axes of ooplasmic segregation can be induced by "strong pricking" of the egg (Sakai, 1964), an action that might create a zone of elevated cytosolic [Ca^{2+}] at the wound.

The present study addresses the third criterion—that dispersion of a cytosolic calcium gradient will inhibit localization. We have pursued this question in the large (diameter = 1.2 mm) and remarkably clear medaka fish egg. In this egg, which consists of a thin (about 25 μm thick) peripheral layer of cytoplasm bounded by a plasma membrane and separated from a large yolk vacuole by a yolk membrane, ooplasmic segregation consists of the roughly simultaneous streaming of the bulk of the ooplasm and its inclusions toward the animal pole, the movement of oil droplets toward the vegetal pole, and the saltatory movement of some inclusions toward the vegetal pole (Sakai, 1965; Iwamatsu, 1973; Abraham *et al.*, 1993a). During and after ooplasmic segregation, zones of elevated cytosolic [Ca^{2+}] are present at both the animal and vegetal poles of the egg (Fluck *et al.*, 1992b).

Injection of the calcium buffer 5,5′ dibromo-BAPTA (referred to hereafter as dibromo-BAPTA) substantially dissipates these polar zones of elevated [Ca^{2+}] (Fluck *et*

Received 17 October 1993; accepted 10 March 1994.

* To whom correspondence should be addressed.

Abbreviations: BCECF, 2,7-bis-(2-carboxyethyl)-5-(and 6-)-carboxyfluorescein.

al., 1992b). The buffer also blocks the development of fucoid eggs (Speksnijder *et al.*, 1989); suppresses high calcium zones in, and inhibits the growth of, pollen tubes (Miller *et al.*, 1992b); inhibits cell cycle contraction waves (Miller *et al.*, 1992a) and cytokinesis (Miller *et al.*, 1993; Snow and Nuccitelli, 1993) in *X. laevis* embryos; and inhibits *X. laevis* nuclear membrane vesicle fusion *in vitro* (Sullivan *et al.*, 1993). This relatively weak calcium buffer (K_D = 1.5 μM; Pethig *et al.*, 1989) is believed to act as a shuttle buffer, one that binds Ca^{2+} at the high end of a $[Ca^{2+}]$ gradient and releases it at the low end of the gradient. In other words, the buffer facilitates the diffusion of Ca^{2+} within the cell. In the present study, we demonstrate that injection of dibromo-BAPTA into fertilized medaka eggs inhibits ooplasmic segregation. A preliminary account of these findings has been published (Fluck *et al.*, 1992a).

Materials and Methods

Biological material

Methods for removing gonads from breeding medaka (Yamamoto, 1967; Kirchen and West, 1976; Fluck, 1978; Abraham *et al.*, 1993a), preparing eggs for experimental use (Abraham *et al.*, 1993a), and fertilizing eggs *in vitro* (Yamamoto, 1967; Abraham *et al.*, 1993a) have been described previously. Gonads, gametes, and zygotes were placed in the same buffered saline solution used in other studies of the fertilized medaka egg (Fluck *et al.*, 1991, 1992b; Abraham *et al.*, 1993a): 111 mM NaCl; 5.37 mM KCl; 1.0 mM $CaCl_2$, 0.6 mM $MgSO_4$; 5 mM HEPES, pH 7.3.

Preparation of micropipettes

Glass micropipettes (0.8-mm diameter, Drummond Scientific Co., Broomall, Pennsylvania, Series I; or filamented, 1-mm diameter, Narashige U.S.A., Inc., Greenvale, New York, Series II and III) were made with a Narashige PN-3 microelectrode puller. The tips of the micropipettes were beveled at an angle of 20°C with a Narashige EG-4 microgrinder; this process was monitored with an audio system (Miller *et al.*, 1993). Tip diameter was approximately 5 μm at the widest part of the bevel.

Buffer solutions injected

Solutions of 50 mM (eggs in Series I–III) or 100 mM (some eggs in Series I) dibromo-BAPTA (Molecular Probes, Eugene, Oregon; tetrapotassium salt), $CaCl_2$, and 5 mM HEPES (Sigma Chemical Co., St. Louis, Missouri, titrated to pH 7.2 with KOH) were prepared in which $[Ca^{2+}]_{free}$ was set at 0.2 μM (Series I), 0.14 μM (Series II), or 0.3 μM (Series III). These values of $[Ca^{2+}]_{free}$ are within the range reported for the ooplasm of the fertilized medaka egg (Schantz, 1985).

Three types of controls were used. First, each batch of eggs included at least one egg into which we injected no fluids. A second type of control egg received 1.0–1.6 nl of 5 mM HEPES, pH 7.2, containing 50 or 100 mM K_2SO_4 or 125 mM KCl. A third type of control egg received 1.4 nl of a solution of 5,5′-dimethyl-BAPTA, a BAPTA-type buffer with a higher affinity for calcium (K_D = 0.15 μM; 50 mM 5,5′-dimethyl-BAPTA, tetrapotassium salt; 5 mM HEPES, pH 7.2; and sufficient $CaCl_2$ to set $[Ca^{2+}]_{free}$ at 0.2 μM).

Determining the amount of buffer to inject

According to facilitated diffusion theory, a final concentration of about 2 mM dibromo-BAPTA in the ooplasm should be sufficient to dissipate zones of elevated $[Ca^{2+}]$ in the micromolar range (Speksnijder *et al.*, 1989). Moreover, 2.7 mM dibromo-BAPTA has been shown to dissipate zones of elevated $[Ca^{2+}]$ at the poles of the fertilized medaka egg (Fluck *et al.*, 1992b). We thus microinjected enough 50 mM or 100 mM dibromo-BAPTA to achieve final buffer concentrations in the ooplasm of 0.5–7.0 mM. We estimated that the accessible ooplasmic volume was 27.6 nl (Fluck *et al.*, 1992b) and thus injected 0.26–1.96 nl of buffer. A number of investigators have shown that injectate volumes in this range have no detectable effect on the development of the medaka egg (Ridgway *et al.*, 1977; Gilkey, 1983; Yoshimoto *et al.*, 1985, 1986; Fluck *et al.*, 1991, 1992b); thus a purely mechanical effect of the injectate on development of the egg seems unlikely.

Microinjection

We used a low-pressure method (Hiramoto, 1962; Kiehart, 1982; Fluck *et al.*, 1991, 1992b) in Series I and a high-pressure method (Narashige IM-200 microinjection system, Fluck *et al.*, 1992b) in Series II and III. In both methods, we front-loaded the micropipettes. The pipettes were calibrated by injecting a small volume of the solution into vegetable oil and measuring the diameter of the spherical droplets.

Batches of two to six eggs were fertilized simultaneously in buffered saline solution, transferred to closely fitting holes drilled in a transparent plastic holder, and injected sequentially with fluid soon after fertilization (range, 5–30 min after fertilization; 12.5 ± 6.5 min, X ± SD, N = 104 eggs). Every batch included at least one control egg into which no fluid was injected.

The method for injecting fluid into the thin peripheral layer of ooplasm of the medaka egg has been described elsewhere (Ridgway *et al.*, 1977; Gilkey, 1983; Fluck *et al.*, 1991) and will only be summarized here. The micropipette, held in a micromanipulator, was advanced far enough to penetrate the chorion (shell) and plasma membrane but not the yolk membrane, which roughly con-

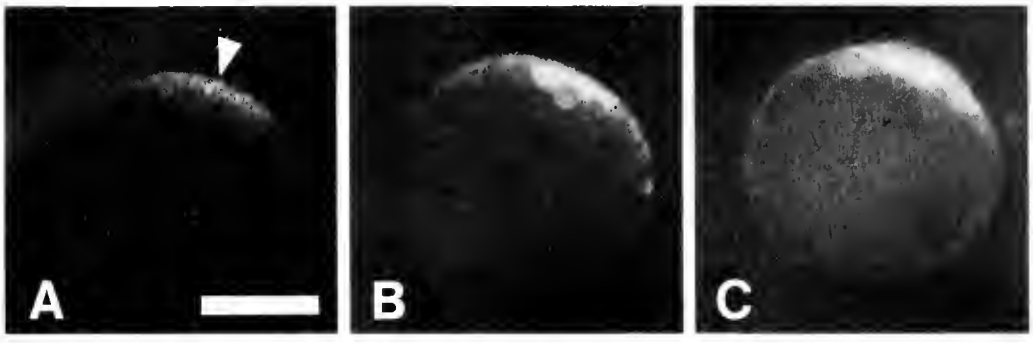

Figure 1. Diffusion of fluorescein around the medaka egg. The approximate position of the injection site is marked with an arrowhead. (A) By 5 min after injection of the dye, it had spread more than 50° arc in all directions around the egg. (B) By 18 min, it was present about 90° arc from the injection site. (C) At 74 min, it had spread to the antipode of the injection site. Scale bar, 250 μm.

formed to the shape of the micropipette. When fluid was injected into the ooplasm, it distended the yolk membrane near the tip of the micropipette, thus visually confirming that fluid had been injected into the ooplasm and not the yolk vacuole. As the pipette was slowly withdrawn, the yolk membrane returned to its normal position, causing the injectate to be spread quickly over a large area of the ooplasm. Fluid was injected either equatorially (within 30° arc of the equator) or near the vegetal pole (within 30° arc of the vegetal pole).

Dibromo-BAPTA was injected into the yolk vacuole of four eggs. Such eggs were penetrated with a micropipette in the usual manner, except that the tip of the pipette also penetrated the yolk membrane. The injectate thus did not distend the yolk membrane but did transiently change the optical properties of the yolk near the tip of the pipette, confirming that fluid had been injected.

We injected dibromo-BAPTA into eggs in three series of experiments: I (winter 1990, in which we successfully injected buffer into the ooplasm of 45 eggs from 12 females), II (winter 1992, 27 eggs from 4 females), and III (summer 1992, 20 eggs from 4 females). In addition, we injected solutions of K_2SO_4 or KCl into 15 eggs; injected dimethyl-BAPTA into 10 eggs from two females; injected dibromo-BAPTA into the yolk vacuole of 4 eggs; and monitored the development of 44 uninjected control eggs.

Observation of the effects of buffer injection

Ooplasmic movements in at least one egg in each batch were recorded by time-lapse video microscopy (Abraham *et al.*, 1993a), while other eggs were observed at regular intervals with a stereomicroscope. Room temperature was 18–19°C for Series I and II and 23–24°C for Series III; at these temperatures, the first cleavage begins, respectively, 130–140 min and 85–95 min after fertilization. In order to compare data from experiments at different temperatures, we have reported our results not only as "minutes after fertilization" but also as t_n, or normalized time, where $t_n = 1.0$ represents the time at which cytokinesis begins.

Injection of fluorescein into eggs

To estimate both the size of the area over which an injectate spreads immediately after injection and the time required for fluorescein to diffuse around the egg, we injected 1.5–2.0 nl of 50 μ*M* fluorescein (sodium salt, dissolved in 100 m*M* K_2SO_4, 5 m*M* HEPES, pH 7.2; Sigma Chemical Co.) into eggs. Using epi-illumination and a SIT camera (Dage/MTI, model 66DX), we examined these eggs within 5 min after injection and at regular intervals thereafter for up to 3 h.

Results

Movement of fluorescein around the egg

Within 5 min after injection, fluorescein was present in ooplasm within 50° arc (or 530 μm, assuming an egg diameter of 1190 μm) in all directions from the injection site (Fig. 1); this is equivalent to the molecule having spread initially into an area equal to 13% of the total surface of the egg and thus into a volume equal to 13% of the total volume of the ooplasm. The molecule spread as far as 90° arc in less than 15 min and reached the antipode of the injection site in about 75 min.

Immediate localized effects of dibromo-BAPTA

An immediate reaction of the eggs to injection of dibromo-BAPTA was an apparent expansion of the yolk membrane near the injection site, which caused the yolk vacuole to bulge into the ooplasm (Fig. 2A). This bulge usually subsided within 10 min in eggs receiving low concentrations of buffer (final cytosolic concentration < 4 m*M*). But in some of these eggs and in most eggs receiving higher concentrations of buffer, the bulge persisted and the yolk membrane over the bulge lysed (Table

I), releasing yolk into the ooplasm or, more often, into the perivitelline space. To determine whether [dibromo-BAPTA] and $[Ca^{2+}]_{free}$ significantly affected egg lysis, the probability of egg lysis was analyzed using a generalized additive model with $[Ca^{2+}]_{free}$ as a factor variable and a slightly nonlinear, nonparametric relationship, with 1.5 degrees of freedom (intermediate between a linear and a quadratic relationship) between final buffer concentration and the probability of lysis (function gam of the S-PLUS statistical package, S-PLUS Reference Manual, Version 3.0, Statistical Services, Inc., Seattle, Washington). An analysis of variance indicated that *P* values for the effect of $[Ca^{2+}]_{free}$ and [dibromo-BAPTA] on lysis were 0.012 and 3.4×10^{-7}, respectively.

Another immediate response to the injection of dibromo-BAPTA (final cytosolic concentration $\geq$ 1 m*M*), which made a convenient marker of the injection site, was the movement of nearby oil droplets away from the injection site and toward the top of the egg (Figs. 1B, C); the droplets appeared simply to float to the top of the egg. This movement began immediately upon injection of the buffer and was essentially over within 15 min. For comparison, the normal movement of oil droplets toward the vegetal pole during ooplasmic segregation continues for more than 140 min at 18–19°C and more than 95 min at 23–24°C (Sakai, 1965; Abraham *et al.*, 1993a). These immediate localized responses were not due to the mechanical effects of injection because we saw no such responses in control eggs receiving either KCl or K_2SO_4. Moreover, they were less prominent in eggs into which we injected dimethyl-BAPTA. Instead, these early responses were likely a response to the initially high concentration of dibromo-BAPTA near the injection site. Assuming that (1) injected buffer initially spread as far as injected fluorescein and (2) the accessible volume of the ooplasm is 27.6 nl (Fluck *et al.*, 1992b), we can estimate the initial concentration of buffer in the ooplasm soon after injection. For example, in eggs receiving enough 50 m*M* dibromo-BAPTA to achieve an estimated final concentration of 2.7 m*M* throughout the ooplasm, the initial concentration within 50° arc of the injection site would be about 21 m*M*.

Effects of dibromo-BAPTA on ooplasmic segregation

Dibromo-BAPTA inhibited ooplasmic segregation and the subsequent development of the embryos in a concentration-dependent manner (Table I and Fig. 2B–G), and these effects were independent of $[Ca^{2+}]_{free}$ in the injectate. Except for causing the early movement of oil droplets (described above) and a slight delay in the onset of cytokinesis (see below), low concentrations of dibromo-BAPTA (<2.0 m*M*) had no substantial effect on either the formation of the blastodisc or the movement of oil droplets toward the vegetal pole (Fig. 2H). However, buffer concentrations $\geq$ 2.6 m*M* inhibited the movement of oil droplets toward the vegetal pole and slowed the growth of the blastodisc (Table I; Fig. 2C, E–G). In addition, small aggregates of ooplasm often formed outside the blastodisc proper and on the side of the egg into which buffer had been injected (Fig. 2E, G). The specific effects of the buffer on oil droplet movement varied with the site of injection. Injection near the equator strongly inhibited oil droplet movement throughout the contralateral half of the embryo and caused the retention of oil droplets within the blastodisc at the animal pole (Fig. 2C, E, G). Injection near the vegetal pole resulted in the accumulation of oil droplets near the equator of the egg (Fig. 2F), the result of droplets in the vegetal hemisphere having floated to the top of the egg and those in the animal hemisphere having moved normally toward the equator.

Effects of dibromo-BAPTA on cytokinesis and embryonic axis formation

Dibromo-BAPTA delayed or blocked cytokinesis in a concentration-dependent manner. For example, when one group of eggs—from the same female and injected with differing amounts of buffer within a few minutes of each other—were examined 170 min after fertilization (18–19°C), the eggs had developed to the following stages: uninjected control, had completed first cleavage; 0.64 m*M* dibromo-BAPTA, was similar to control; 1.1 m*M* dibromo-BAPTA, was forming two unequal blastomeres; 2.0 m*M* dibromo-BAPTA, had not begun cytokinesis. The last egg in this group formed two incomplete furrows by 4.5 h after fertilization but did not go on to form an embryonic axis, whereas the two eggs that received lower amounts of buffer did form an embryonic axis. The inhibition of cytokinesis was more pronounced in eggs receiving buffer concentrations $\geq$ 2.6 m*M*. For example, of 24 eggs (Series I and II) receiving 2.6–3.6 m*M* dibromo-BAPTA, 9 did not divide and the other 12 divided from 40 min to more than 3 h after the controls did; whereas of eggs receiving >4 m*M* buffer, none underwent cytokinesis (Table I; Fig. 2E–G). Embryos receiving $\geq$2.6 m*M* dibromo-BAPTA did not form an embryonic axis.

Controls

Eggs injected with KCl (125 m*M*, 6 embryos) or K_2SO_4 (50 m*M*, 6 embryos; 100 m*M*, 3 embryos) near either the equator (12 embryos) or the vegetal pole (3 embryos) developed normally. There was neither an immediate response to the injectate nor an apparent effect on ooplasmic segregation, cell division, or formation of the embryonic axis. Moreover, injecting dibromo-BAPTA into the yolk vacuole had no apparent effect on the embryos.

In contrast to the pronounced effects of $\geq$2.6 m*M* dibromo-BAPTA on segregation, the effects of 2.6 m*M* dimethyl-BAPTA were slight or apparently absent. As

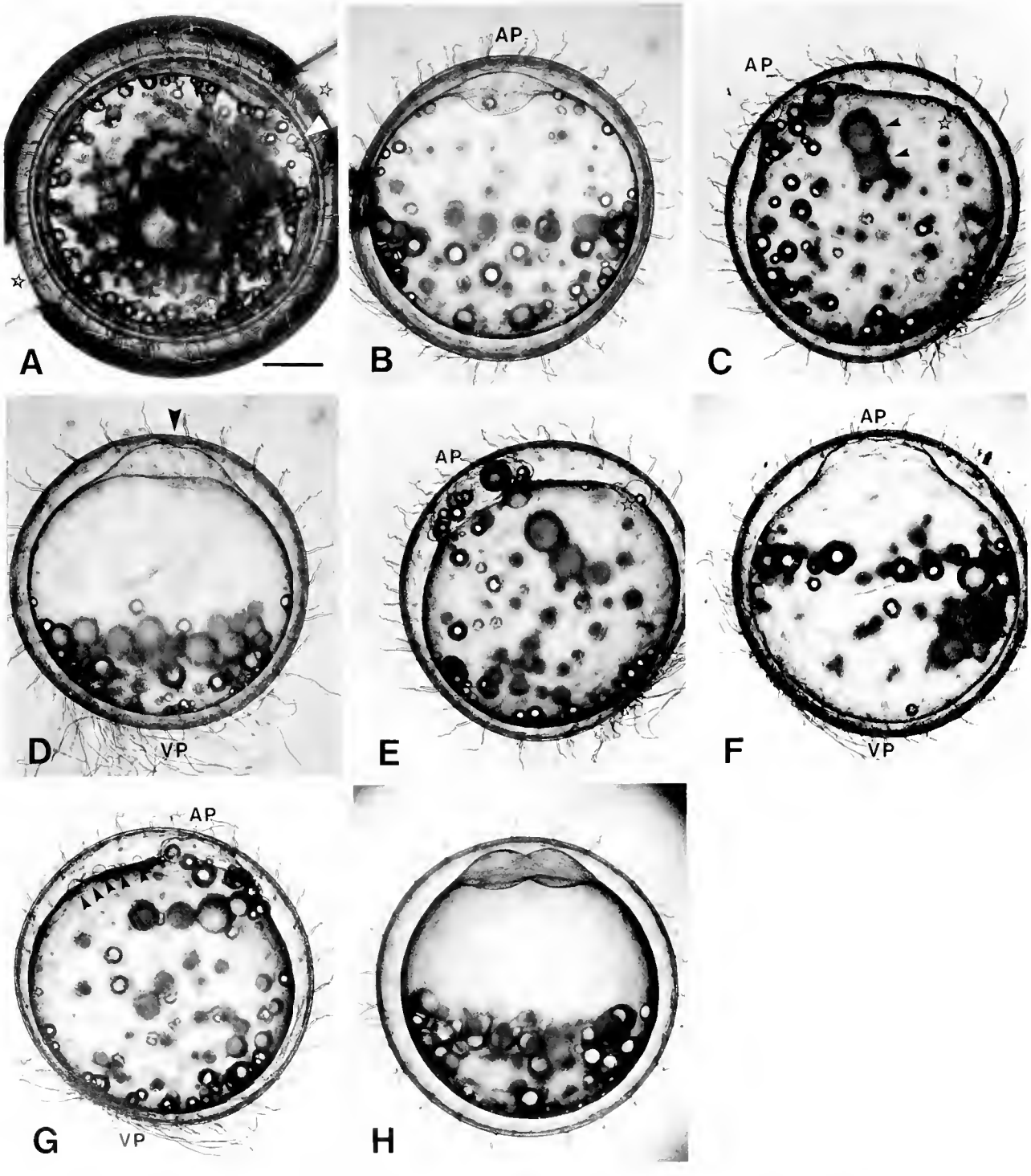

Figure 2. Effect of dibromo-BAPTA on segregation and cytokinesis in the medaka egg. Abbreviations: AP, animal pole; VP, vegetal pole. (A) Immediate local response to injection of 2.6 m*M* dibromo-BAPTA (free $[Ca^{2+}] \sim 0.2\ \mu M$). This photograph was taken 7 min after injecting enough dibromo-BAPTA to achieve a final concentration of 2.6 m*M* in the ooplasm. The egg is still in the injection chamber, the channels of which can be seen at the lower left and upper right (*). Note the bulge (white arrowhead) in the egg near the injection site. The dark mass near the center of the image is an accumulation of oil droplets on the top of the egg, that is, toward the viewer. The bulge eventually subsided, but after 177 min, when an uninjected control egg was at the four-cell stage, this egg had not yet divided. Scale bar, 250 μM. (B) Segregation in an

Table I

Inhibition of ooplasmic segregation and cytokinesis in the medaka egg by the injection of 5,5'-dibromo-BAPTA

[Free Ca^{2+}] μM[a]	[Dibromo-BAPTA] mM[b]	N	Number of embryos			
			Lysed[c]	Segregated normally	Cleaved normally	Formed embryonic axis
0.14	0.5–2.0	6	0	6	6[d]	6
0.14	2.6–3.6	11	1	0	0[e]	0
0.14	4.0–7.0	10	4	0	0	0
0.20	0.5–2.0	5	0	5	5[d]	4
0.20	2.6–3.6	21	7	0	0[e]	0
0.20	4.0–7.0	19	17	0	0	0
0.30	0.5–2.0	5	0	5	5[d]	5
0.30	2.6–3.6	12	6	0	0[e]	0
0.30	4.0–7.0	3	3	0	0	0

[a] Series I, 0.20 μM; Series II, 0.14 μM; Series III, 0.30 μM.
[b] Estimated final ooplasmic concentration. See text.
[c] The yolk membrane of these embryos lysed within 10 min after injection of the buffer.
[d] The cleavage appeared normal and occurred within 15 min after cleavage began in control eggs.
[e] If an egg did not divide within 40 min after cleavage began in control eggs, we classified it as "not dividing."

already noted, injection of this buffer produced a transient, small bulge at the injection site and caused a few oil droplets near the injection site to float to the top of the egg. However, ooplasmic segregation—both the formation of the blastodisc and the movement of oil droplets toward the vegetal pole—proceeded in a manner nearly indistinguishable from that in uninjected control eggs or eggs into which we injected KCl or K_2SO_4 (Fig. 2B, D). Of the 10 eggs receiving 2.6 mM dimethyl-BAPTA, all 10 cleaved, 7 of them dividing within 10 min (at 21°C) after the uninjected control eggs divided (Fig. 2D). Nine of these embryos went on

egg receiving 2.6 mM 5,5'-dimethyl-BAPTA, $t_n = 0.65$. The buffer was injected near the equator. The blastodisc that has begun to form at the animal pole is indistinguishable in its shape and size from the blastodisc in uninjected control eggs (Abraham *et al.*, 1993a) and eggs into which we injected KCl or K_2SO_4. All oil droplets but one have moved out of the blastodisc and toward the vegetal pole; the animal hemisphere is relatively devoid of oil droplets, which have moved toward the vegetal pole and formed a prominent ring just below the equator of the egg. (C) Effect of 2.7 mM dibromo-BAPTA (free $[Ca^{2+}] = 0.14$ μM) on oil droplet movement and formation of the blastodisc, $t_n = 0.62$. This egg is about the same age as the one shown in (B); dibromo-BAPTA was injected near the equator. Note the large number of oil droplets in the blastodisc at the animal pole of the egg, the large number of oil droplets in the animal hemisphere of the half of the egg opposite the injection site (which is marked by a star), and the absence of a ring of oil droplets near the equator of the egg. Oil droplets that were originally near the injection site have floated to the top of the egg and coalesced into two large oil droplets (arrowheads); this early effect of the buffer provided a convenient marker of the injection site. (D) Segregation and cytokinesis in an egg receiving 2.6 mM 5,5'-dimethyl-BAPTA, $t_n = 1.11$. This egg is nearly the same age as those shown in (E) and (F). Note the nascent cleavage furrow in the blastodisc (arrowhead) and the apparently normal accumulation of oil droplets near the vegetal pole. This egg was indistinguishable from uninjected control eggs except that it divided about 10 min (at 21°C) later than control eggs. (E) Inhibition of ooplasmic segregation and cytokinesis by 2.7 mM dibromo-BAPTA (free $[Ca^{2+}] = 0.14$ μM) on segregation, $t_n = 1.07$. This is the same egg shown in (C). Note the large number of oil droplets near the animal pole, the inhibition of the movement of oil droplets toward the vegetal pole, and the small accumulation of ooplasm near the injection site (*). (F) Inhibition of ooplasmic segregation and cytokinesis by 2.7 mM dibromo-BAPTA (free $[Ca^{2+}] = 0.30$ μM) on segregation, $t_n = 1.16$. Dibromo-BAPTA was injected near the vegetal pole of this egg. Note the small blastodisc at the animal pole and the ring of oil droplets near the equator. This egg did not cleave. (G) Accumulations of ooplasm outside the blastodisc, $t_n = 1.05$. Dibromo-BAPTA (2.7 mM, free $[Ca^{2+}] = 0.14$ μM, injected near the equator). Note the blebs of ooplasm (arrowheads) on the side of the egg on which the buffer was injected, the presence of oil droplets in the blastodisc, and the inhibition of the movement of oil droplets toward the vegetal pole. (H) Delay of cytokinesis caused by 1 mM dibromo-BAPTA (free $[Ca^{2+}] = 0.30$ μM), injected near the vegetal pole. The first cleavage has just begun in this egg, which was photographed at $t_n = 1.31$, a time when sibling control eggs had completed this cleavage. Note the normal appearance of the blastodisc and that all oil droplets have moved close to the vegetal pole.

to form an embryonic axis and appeared to develop normally.

Discussion

The final ooplasmic concentration of dibromo-BAPTA required to block ooplasmic segregation and cell division in the medaka embryo (*ca.* 2.6 m*M*) was comparable to that required to inhibit cell division in fucoid eggs (Speksnijder *et al.*, 1989), inhibit cell cycle contraction waves and cytokinesis in *X. laevis* eggs (Miller *et al.*, 1992a; Miller *et al.*, 1993; Snow and Nuccitelli, 1993), and dissipate cytosolic calcium gradients near the animal and vegetal poles of the medaka egg (Fluck *et al.*, 1992b). According to facilitated diffusion theory, the primary effect of such buffers is to dissipate cytosolic Ca^{2+} gradients by facilitating the diffusion of Ca^{2+} away from zones of elevated cytosolic $[Ca^{2+}]$. Thus, when high calcium regions begin to emerge within a cell, as they do at the animal and vegetal poles of the fertilized medaka egg, buffer molecules pick up Ca^{2+} there and diffuse to low calcium regions, where the bound Ca^{2+} is then released. The results of the present study suggest that these polar zones are necessary for the normal segregation of ooplasm and its inclusions in this egg. However, it is theoretically possible that the inhibition of segregation is caused by either an increase in $[Ca^{2+}]$ at sites away from the poles or the dissipation of the cytosolic calcium gradients.

Facilitated diffusion theory predicts that the Ca^{2+} buffer will be relatively ineffective as a shuttle buffer if its affinity for Ca^{2+} is too high. Such a buffer, for example 5,5′-dimethyl-BAPTA (K_D = 0.15 μM), will become saturated with Ca^{2+} at the high end of the Ca^{2+} gradient but will not release Ca^{2+} when it diffuses away from this region. The results of three studies, which have reported dimethyl-BAPTA to be from 2.7- to 18-fold less effective than dibromo-BAPTA (Speksnijder *et al.*, 1989; Snow and Nuccitelli, 1993; Sullivan *et al.*, 1993), are consistent with this prediction. The results of the present study, that dimethyl-BAPTA had far less effect on ooplasmic segregation and cytokinesis in the medaka than did dibromo-BAPTA, are consistent with these three previous studies and with this prediction of the theory.

Facilitated diffusion theory also predicts that the effect of a shuttle buffer should be independent of $[Ca^{2+}]$ in the injectate (Speksnijder *et al.*, 1989). In other words, the effect of the buffer is not to clamp cytosolic $[Ca^{2+}]$ at any particular value, but rather to facilitate calcium diffusion and thus dissipate calcium gradients in the cytoplasm. Our data are also consistent with this aspect of theory, at least as far as effects on ooplasmic segregation and cytokinesis are concerned. However, we did find that immediate localized responses to the injectate—herniation and subsequent lysis, the movement of oil droplets to the top of the egg—were a function of $[Ca^{2+}]$ in the injectate over the range 0.14–0.30 μM, with the probability of lysis increasing with $[Ca^{2+}]$. Our choice of $[Ca^{2+}]$ in the injectate was based primarily on a study of the medaka egg in which cytosolic $[Ca^{2+}]$ was measured with a calcium microelectrode (Schantz, 1985; see his Table 1). The occurrence of lysis in our study suggests that in the future we should set $[Ca^{2+}]$ in the injectate lower, perhaps to 50 nM or 100 nM, to reduce the probability of embryo lysis.

Two cytoskeletal systems—one involving microfilaments and another involving microtubules—are involved in ooplasmic segregation in the medaka egg. Formation of the blastodisc at the animal pole of the medaka and other teleost embryos is inhibited by cytochalasins (Katow, 1983; Ivanenkov *et al.*, 1987; Webb and Fluck, 1993) and DNase I (Ivanenkov *et al.*, 1987) and thus presumably involves the action of microfilaments, whereas the movement of oil droplets and the saltatory movement of other inclusions toward the animal and vegetal poles of the medaka egg are both inhibited by microtubule poisons—colchicine, colcemid, nocodazole—and thus presumably involve microtubules (Abraham *et al.*, 1993a; Webb and Fluck, 1993). Moreover, a microtubule-organizing center (MTOC) is present in the animal pole region of the medaka egg by t_n = 0.24, and the convergent array of microtubules near this center is disrupted by the injection of dibromo-BAPTA (Abraham *et al.*, 1993b). The assembly/disassembly and the function of both microfilaments and microtubules are controlled by a number of calcium-binding regulatory proteins (Weisenberg, 1972; Schliwa *et al.*, 1981; Keith *et al.*, 1983; Mooseker, 1985; Stossel *et al.*, 1985; Bray, 1992, pp. 147–148, 342). Facilitated diffusion theory predicts that calcium buffer concentrations similar to those found effective in the present study act by dissipating zones of cytosolic $[Ca^{2+}]_{free}$ in the micromolar range (Speksnijder *et al.*, 1989). An example of a protein that is responsive to changes in $[Ca^{2+}]_{free}$ in this range is calmodulin (Cheung, 1980), a protein that regulates the activity of proteins that interact with both microfilaments (Wolenski *et al.*, 1993) and microtubules (Ishikawa *et al.*, 1992).

Oil droplet movement in the animal hemisphere of the egg was more strongly inhibited when buffer was injected near the equator *versus* near the vegetal pole. One interpretation of these results is that structures/events in the animal pole region, for example the MTOC, are essential for oil droplet movement and that these are disrupted by dibromo-BAPTA. Given the circumference of the medaka egg (about 3700 μm), buffer injected near the equator would reach the animal pole of the egg sooner than buffer injected near the vegetal pole. To estimate the time required for dibromo-BAPTA to diffuse around the medaka egg, we used published values for the diffusion coefficients of molecules similar to dibromo-BAPTA (fura-2 in skeletal muscle, 3.6×10^{-7} cm^2 s^{-1}, Baylor and Hollingworth, 1988) and fluorescein (BCECF in fibroblasts, 2

$\times 10^{-6}$ cm^2 s^{-1}, Kao *et al.*, 1993). Assuming that the cytoplasm of the medaka egg is more similar to the cytoplasm of a fibroblast than to that of a skeletal muscle, we corrected the diffusion constant of fura-2 upward to 5.9 $\times 10^{-7}$ cm^2 s^{-1} (Kushmerick and Podolsky, 1969; Kao *et al.*, 1993) and then estimated the times required for molecules with these diffusion coefficients to diffuse around the egg (Einstein, 1956). The predicted values for BCECF were consistent with the rate of movement of fluorescein around the egg (Fig. 1), suggesting that our assumptions are valid. We estimate that the times required for dibromo-BAPTA to diffuse 90° and 180° arc from the injection site would thus be about 35 min and >3 h, respectively. In other words, buffer injected near the equator of an egg would reach the animal pole while segregation of the oil droplets was ongoing, but buffer injected near the vegetal pole would not.

The medaka egg appears to be a particularly good system in which to investigate the importance of cytosolic calcium gradients in ooplasmic segregation and the cytoplasmic localization of morphogenetic determinants in teleost embryos. If a fate map exists during early cleavage of the medaka embryo as it does in *Brachydanio rerio* embryo (Strehlow and Gilbert, 1993), this would suggest that particular cytoplasmic determinants might be found along particular meridians of the egg. If these determinants streamed into specific regions of the blastodisc during ooplasmic segregation, they would eventually segregate into particular blastomeres during cleavage. The geometry of the medaka egg makes it possible to pursue this problem by selectively interfering with segregation along particular meridians. Such interference could perhaps be achieved by the localized photolysis of caged calcium or caged calcium buffers that have been injected into the ooplasm (McCray and Trentham, 1989; Ashley *et al.*, 1991a, b).

The delay and inhibition of cytokinesis in eggs receiving dibromo-BAPTA, though suggestive and consistent with the results of other studies (Speksnijder *et al.*, 1989; Snow and Nuccitelli, 1993; Miller *et al.*, 1993), are difficult to interpret. Because the time of injection was not proximal enough to specific events accompanying cytokinesis—formation of the contractile band, formation of the furrow, zipping of the furrow, *etc.* (Fluck *et al.*, 1991)—the effect on cytokinesis could be indirect, caused by the inhibition of earlier events that are accompanied by a calcium pulse and which are themselves inhibited by BAPTA-type buffers. These events include nuclear envelope breakdown (Steinhardt and Alderton, 1988; Tombes *et al.*, 1992; Browne *et al.*, 1992) and the metaphase/anaphase transition (reviewed in Hepler, 1989). To determine whether dibromo-BAPTA specifically affects cytokinesis in the medaka egg, buffer injections must be timed much closer to cytokinesis. Such an approach has been successful in *X. laevis* (Snow and Nuccitelli, 1993; Miller *et al.*, 1993), and preliminary experiments (Abraham and Fluck, unpublished) suggest that it will be successful in the medaka as well.

Acknowledgments

Supported by NSF DCB-9017210 to RAF, NSF DCB-9103569 to LFJ, NSF BIR 9211855 to LFJ and ALM, and by grants from Franklin and Marshall College's Hackman Scholars Program and Harry W. and Mary B. Huffnagle Fund to VCA. We thank Albert Gough and Rick Moog for valuable discussions about diffusion, Tim Hesterberg for his help in statistical analysis, Jane McLaughlin for technical assistance, George Rosenstein for his aid in geometry, and Tamika Webb for helping to improve the text of the manuscript.

Literature Cited

Abraham, V. C., S. Gupta, and R. A. Fluck, 1993a. Ooplasmic segregation in the medaka (*Oryzias latipes*) egg. *Biol. Bull.* **184:** 115–124.

Abraham, V. C., A. L. Miller, L. F. Jaffe, and R. A. Fluck. 1993b. Cytoplasmic microtubule arrays in *Oryzias latipes* (medaka) eggs during ooplasmic segregation. *Biol. Bull.* **185:** 305–306.

Ashley, C. C., P. J. Griffiths, T. J. Lea, I. P. Mulligan, R. E. Palmer, and S. J. Simnett. 1991a. Use of fluorescent TnC derivatives and 'caged' compounds to study cellular phenomena. Pp. 177–203 in *Cellular Calcium: A Practical Approach,* J. G. McCormack and P. H. Cobbold, eds. IRL Press, Oxford.

Ashley, C. C., I. P. Mulligan, and T. J. Lea. 1991b. Ca^{2+} and activation mechanisms in skeletal muscle. *Quart. Rev. Biophys.* **24:** 1–73.

Bates, W. R., and W. R. Jeffery. 1988. Polarization of ooplasmic segregation and dorsal-ventral axis determination in ascidian embryos. *Dev. Biol.* **130:** 98–107.

Baylor, S. M., and S. Hollingworth. 1988. Fura-2 calcium transients in frog skeletal muscle fibres. *J. Physiol.* **403:** 151–192.

Berger, F., and C. Brownlee. 1993. Ratio confocal imaging of free cytoplasmic calcium gradients in polarising and polarised *Fucus* zygotes. *Zygote* **1:** 9–15.

Bray, D. 1992. *Cell Movements.* Garland Publishing, Inc., New York.

Browne, C. L., A. L. Miller, R. E. Palazzo, and L. F. Jaffe. 1992. On the calcium pulse during nuclear envelope breakdown (NEB) in sea urchin eggs. *Biol. Bull.* **183:** 370–371.

Cheung, W. Y. 1980. Calmodulin—an introduction. Pp. 1–12 in *Calmodulin and Cell Function,* Vol. 1, W. Y. Cheung, ed. Academic Press, Orlando.

Einstein, A. 1956. *Investigations on the Theory of the Brownian Movement.* Dover Publications, New York.

Fluck, R. A. 1978. Acetylcholine and acetylcholinesterase activity in early embryos of the medaka *Oryzias latipes,* a teleost. *Dev. Growth & Differ* **20:** 17–25.

Fluck, R. A., A. L. Miller, and L. F. Jaffe. 1991. Slow calcium waves accompany cytokinesis in medaka fish eggs. *J. Cell Biol.* **115:** 1259–1265.

Fluck, R. A., V. C. Abraham, A. L. Miller, and L. F. Jaffe. 1992a. Calcium buffer injections block ooplasmic segregation in *Oryzias latipes* (medaka) eggs. *Biol. Bull.* **183:** 371–372.

Fluck, R. A., A. L. Miller, and L. F. Jaffe. 1992b. High calcium zones at the poles of developing medaka eggs. *Biol. Bull.* **183:** 70–77.

Gilkey, J. C. 1983. Roles of calcium and pH in activation of eggs of the medaka fish, *Oryzias latipes. J. Cell Biol.* **97:** 669–678.

Gilkey, J. C., L. F. Jaffe, E. B. Ridgway, and G. T. Reynolds. 1978. A free calcium wave traverses the activating egg of the medaka, *Oryzias latipes. J. Cell Biol.* **76:** 448–466.

Hepler, P. K. 1989. Calcium transients during mitosis: observations in flux. *J. Cell Biol.* **109:** 2567–2573.

Hiramoto, Y. 1962. Microinjection of the live spermatozoa into sea urchin eggs. *Exp. Cell Res.* **27:** 416–424.

Ishikawa, R., O. Kagami, C. Hayashi, and K. Kohama. 1992. Characterization of smooth muscle caldesmon as a microtubule-associated protein. *Cell Motil. Cytoskel.* **23:** 244–251.

Ivanenkov, V. V., A. A. Minin, V. N. Meshcheryakov, and L. E. Martynova. 1987. The effect of local microfilament disorganization on ooplasmic segregation in the loach (*Misgurnus fossilis*) egg. *Cell Differ.* **22:** 19–28.

Iwamatsu, T. 1973. On the mechanism of ooplasmic segregation upon fertilization in *Oryzias latipes*. *Jap. J. Ichthyol.* **20:** 273–278.

Jaffe, L. F. 1986. Calcium and morphogenetic fields. Pp. 271–288 in *Calcium and the Cell*, D. Evered and J. Whelan, eds. John Wiley and Sons, Chichester, England.

Jaffe, L. F., and R. Nuccitelli. 1977. Electrical controls of development. *Ann. Rev. Biophys. Bioeng.* **6:** 445–476.

Jaffe, L. F., K. R. Robinson, and R. Nuccitelli. 1974. Local cation entry and self-electrophoresis as an intracellular localization mechanism. *Ann. N.Y. Acad. Sci.* **238:** 372–389.

Jeffery, W. R. 1982. Calcium ionophore polarizes ooplasmic segregation in ascidian eggs. *Science* **216:** 545–547.

Kao, H. P., J. R. Abney, and A. S. Verkman. 1993. Determinants of the translational mobility of a small solute in cell cytoplasm. *J. Cell Biol.* **120:** 175–184.

Katow, H. 1983. Obstruction of blastodisc formation by cytochalasin B in the zebrafish, *Brachydanio rerio*. *Dev. Growth & Differ.* **25:** 477–484.

Keith, C., M. DiPaola, F. R. Maxfield, and M. L. Shelanski. 1983. Microinjection of Ca^{++}-calmodulin causes a localized depolymerization of microtubules. *J. Cell Biol.* **97:** 1918–1924.

Kiehart, D. P. 1982. Microinjection of echinoderm eggs: apparatus and procedures. *Meth. Cell Biol.* **25:** 13–31.

Kirchen, R. V., and W. R. West. 1976. *The Japanese Medaka: Its Care and Development.* Carolina Biological Supply Company, Burlington, NC.

Kushmerick, M. J., and R. J. Podolsky. 1969. Ionic mobility in muscle cells. *Science* **166:** 1297–1298.

McCray, J. A., and D. R. Trentham. 1989. Properties and uses of photoreactive caged compounds. *Annu. Rev. Biophys. Biophys. Chem.* **18:** 239–270.

Miller, A. L., J. A. McLaughlin, and L. F. Jaffe. 1991. Imaging free calcium in *Xenopus* eggs during polar pattern formation and cytokinesis. *J. Cell Biol.* **115:** 280a.

Miller, A. L., R. A. Fluck, and L. F. Jaffe. 1992a. Cell cycle contraction waves in *Xenopus* are suppressed by injecting calcium buffers. *Biol. Bull.* **183:** 368–369.

Miller, D. D., D. A. Callaham, D. J. Gross, and P. K. Hepler. 1992b. Free Ca^{2+} gradient in growing pollen tubes of *Lilium*. *J. Cell Sci.* **101:** 7–12.

Miller, A. L., R. A. Fluck, J. A. McLaughlin, and L. F. Jaffe. 1993. Calcium buffer injections inhibit cytokinesis in *Xenopus* eggs. *J. Cell Sci.* **106:** 523–534.

Mooseker, M. S. 1985. Organization, chemistry, and assembly of the cytoskeletal apparatus of the intestinal brush border. *Annu. Rev. Cell Biol.* **1:** 209–241.

Nuccitelli, R. 1978. Ooplasmic segregation and secretion in the *Pelvetia* egg is accompanied by a membrane-generated electrical current. *Dev. Biol.* **62:** 13–33.

Pethig, R., M. Kuhn, R. Payne, E. Adler, T.-H. Chen, and L. F. Jaffe. 1989. On the dissociation constants of BAPTA-type calcium buffers. *Cell Calcium* **10:** 491–498.

Ridgway, E. B., J. C. Gilkey, and L. F. Jaffe. 1977. Free calcium increases explosively in activating medaka eggs. *Proc. Natl. Acad. Sci. USA* **74:** 623–627.

Robinson, K. R., and R. Cone. 1980. Polarization of fucoid eggs by a calcium ionophore. *Science* **207:** 77–78.

Robinson, K. R., and L. F. Jaffe. 1975. Polarizing fucoid eggs drive a calcium current through themselves. *Science* **187:** 70–72.

Sakai, Y. T. 1964. Studies on the ooplasmic segregation in the egg of the fish *Oryzias latipes*. I. Ooplasmic segregation in egg fragments. *Embryologia* **8:** 129–134.

Sakai, Y. T. 1965. Studies on the ooplasmic segregation in the egg of the fish *Oryzias latipes*. III. Analysis of the movement of oil droplets during the process of ooplasmic segregation. *Biol. Bull.* **129:** 189–198.

Schantz, A. R. 1985. Cytosolic free calcium-ion concentration in cleaving embryonic cells of *Oryzias latipes* measured with calcium-sensitive microelectrodes. *J. Cell Biol.* **100:** 947–954.

Schliwa, M., U. Euteneuer, J. C. Bulinski, and J. G. Izant. 1981. Calcium lability of cytoplasmic microtubules and its modulation by microtubule-associated proteins. *Proc. Natl. Acad. Sci. USA* **78:** 1037–1041.

Snow, P., and R. Nuccitelli. 1993. Calcium buffer injections delay cleavage in *Xenopus laevis* blastomeres. *J. Cell Biol.* **122:** 387–394.

Speksnijder, J. E., A. L. Miller, M. H. Weisenseel, T.-H. Chen, and L. F. Jaffe. 1989. Calcium buffer injections block fucoid egg development by facilitating calcium diffusion. *Proc. Natl. Acad. Sci. USA* **86:** 6607–6611.

Steinhardt, R. A., and J. Alderton. 1988. Intracellular free calcium rise triggers nuclear envelope breakdown in the sea urchin embryo. *Nature* **332:** 366–369.

Stossel, T. P., C. Chaponnier, R. M. Ezzell, J. H. Hartwig, P. A. Janmey, D. J. Kwiatkowski, S. E. Lind, D. B. Smith, F. S. Southwick, H. L. Yin, and K. S. Zaner. 1985. Nonmuscle actin-binding proteins. *Annu. Rev. Cell Biol.* **1:** 353–402.

Strehlow, D., and W. Gilbert. 1993. A fate map for the first cleavages of the zebrafish. *Nature* **361:** 451–453.

Sullivan, K. M. C., W. B. Busa, and K. L. Wilson. 1993. Calcium mobilization is required for nuclear vesicle fusion *in vitro*: implications for membrane traffic and IP_3 receptor function. *Cell* **73:** 1411–1422.

Tombes, R. M., C. Simerly, G. G. Borisy, and G. Schatten. 1992. Meiosis, egg activation, and nuclear envelope breakdown are differentially reliant on Ca^{2+}, whereas germinal vesicle breakdown is Ca^{2+} independent in the mouse oocyte. *J. Cell Biol.* **117:** 799–811.

Webb, T. A., and R. A. Fluck. 1993. Microfilament- and microtubule-based movements during ooplasmic segregation in the medaka fish egg (*Oryzias latipes*). *Mol. Biol. Cell* **4:** 274a.

Weisenberg, R. C. 1972. Microtubule formation *in vitro* in solutions containing low calcium concentrations. *Science* **177:** 1104–1105.

Wolenski, J. S., S. M. Hayden, P. Forscher, and M. S. Mooseker. 1993. Calcium-calmodulin and regulation of brush border myosin-I MgATPase and mechanochemistry. *J. Cell Biol.* **122:** 613–621.

Yamamoto, T. 1967. Medaka. Pp. 101–111 in *Methods in Developmental Biology*, F. M. Wilt and N. K. Wessells, eds. Thomas Y. Crowell Company, New York.

Yoshimoto, Y., T. Iwamatsu, and Y. Hiramoto. 1985. Cyclic changes in intracellular free calcium levels associated with cleavage cycles in echinoderm and medaka eggs. *Biomed. Res.* **6:** 387–394.

Yoshimoto, Y., T. Iwamatsu, K.-I. Hirano, and Y. Hiramoto. 1986. The wave pattern of free calcium release upon fertilization in medaka and sand dollar eggs. *Dev. Growth & Differ.* **28:** 583–596.

Reference: *Biol. Bull.* **186:** 263–270. (June, 1994)

The Endocrine Pathway Responsible for Oocyte Maturation in the Inarticulate Brachiopod *Glottidia*

GARY FREEMAN*

Turkey Point Marine Laboratory of Florida State University at Tallahassee and Center for Developmental Biology, Department of Zoology, University of Texas, Austin, Texas 78712

Abstract. An aqueous extract of lophophore from *Glottidia pyramidata* induces oocyte maturation and follicle cell retraction in pieces of ovary and spawning in intact animals. The extract does not act directly on large oocytes but indirectly, through some other cell type in the ovary. The activity of the extract is insensitive to boiling or protease treatment and passes through a filter with a molecular weight cutoff of 2000. Bromoadenosine 3′5′ cyclic monophosphate and dibutyryl 3′5′ cyclic monophosphate have the same oocyte-maturing and spawning-inducing properties as lophophore extract. The active component in lophophore extract presumably affects somatic cells in the ovary, stimulating a rise in cyclic monophosphate levels in these cells, which then secrete a factor that causes oocyte maturation.

Introduction

Living inarticulate brachiopods consist of three families: the Lingulacea, the Discinacea, and the Craniacea. The Lingulacea is the only group for which our knowledge of reproductive biology can be considered more than rudimentary. During the breeding season, in the two genera (*Lingula* and *Glottidia*) that make up this family, each female spawns more than once, with intervals of several days between spawnings. This has been directly observed in individuals followed daily for several months in the laboratory (Chuang, 1959) and inferred from studies on the ovaries of females in a cohort collected at different times during the breeding season (Paine, 1963). The periodic presence of young larvae in plankton tows, a few days after the large tidal fluctuations around full moon, suggests that spawning normally occurs at this time in animals in their natural habitat (Yatsu, 1902; Paine, 1963). Chuang (1959) has challenged this interpretation; however, his plankton tows were taken so far apart in time that his data do not meaningfully address this issue. Animals also appear to spawn in response to environmental stress during transfer to the laboratory (Chuang, 1959; Kumé, 1956; Paine, 1963).

All previous work with embryos and young larvae of inarticulate brachiopods has been done on naturally spawned eggs. It is possible to obtain fertilizable oocytes from articulate brachiopods outside their normal spawning season by removing the ovary and macerating it to free the oocytes (Reed, 1987). As the oocytes stand in seawater, the follicle cell layer around each oocyte is retracted, the oocyte germinal vesicle breaks down spontaneously, and the chromosomes condense on the meiotic apparatus in preparation for the first meiotic reduction division. When the ovary of the inarticulate brachiopod *Glottidia pyramidata* is treated in the same way, the follicle cell layer is shed; however, the germinal vesicle does not break down, and the oocyte will not develop following the addition of sperm. This paper presents a method for inducing oocyte maturation in *G. pyramidata* and outlines a possible endocrine pathway that leads to oocyte maturation and spawning.

Materials and Methods

Animals

Specimens of *G. pyramidata* were collected during minus tides at Alligator Harbor, Florida, by digging them out of their burrows. Animals and their sediment were transported to the laboratory where they were maintained in a tray with sediment about 4 cm deep, with seawater flowing over it. Most animals oriented themselves in the sediment with their anterior end perpendicular to the sed-

Received 5 October 1993; accepted 14 March 1994.

* Mailing address, University of Texas.

iment-seawater boundary and formed a three-hole slit typical of the entrance to their burrows. Animals fed and remained healthy under these conditions for at least a month. The valve lengths of the animals collected varied between 11 and 24 mm; all of these animals were sexually mature. Sexual maturity was assayed by noting the relative size of the gonad.

Tissue extracts

The effects of various tissue extracts on oocyte maturation were tested in a number of experiments. Aqueous extracts were made from a standard amount of adult *Glottidia* tissue. Because of their small size, more than one animal had to be used to obtain tissues for some experiments. After dissection, the tissue was blotted on a lint-free wipe, weighed, and broken up into small pieces with a watchmaker's forceps. One hundred microliters of distilled water was added to each 10 mg of tissue, and the tissue was homogenized with a tight-fitting pestle for 5 min in a 1.6-ml microcentrifuge tube. After homogenization, the tube was centrifuged or allowed to stand until the tissue debris had settled on the bottom; the supernatant was decanted and saved. In many experiments, all or part of the supernatant was boiled for 15 min prior to use. Tissue extracts were tested for biological activity by adding one part of a tissue extract to three parts of pasteurized seawater (PSW) and incubating pieces of gonad (*ca.* 1 mm^3) in this solution or in 1/2 serial dilutions of this solution in PSW. PSW was made by filtering seawater through a 0.45-μm Millipore filter and heating the seawater for 15 min above 80°C, but below boiling.

Culture procedures, ovary dissociation, and oocyte marking

All experiments were carried out at room temperature (21–24°C). Pieces of gonad were dissociated into single large oocytes and clusters of somatic cells by washing them three times and incubating them in calcium-free seawater for 90–120 min. (Calcium-free seawater consists of 425 m*M* NaCl, 9.4 m*M* KCl, 22.1 m*M* $MgCl_2$, 25.6 m*M* $MgSO_4$, 2.1 m*M* $NaHCO_3$ and 10 m*M* TES at pH 7.8–8.0.) At the end of this period, the gonad fragments were transferred to PSW and dissociated by pipetting the pieces up and down through a small-bore pipette. A 1% solution of the dye neutral red was prepared in distilled water. Five microliters of dye was added to 1 ml of PSW. Full-grown oocytes were incubated in this stain dilution for 5 min and washed in PSW. Stained oocytes can be distinguished from unstained oocytes for several hours because of their red coloration.

Preparation of motile sperm and fertilization

In some experiments, sperm were added to oocytes to see if the treatment would induce maturation and to eggs that had undergone maturation to see if they could be fertilized. A small piece of testis was dissected out, macerated in 1 ml of PSW, and diluted in about 100 ml of PSW. Most *Glottidia* sperm prepared in this way are nonmotile or move very slowly. Rapid sperm motility was induced by adding one drop of 1 *M* NH_4OH to the diluted sperm. One drop of the diluted sperm was added to oocytes or eggs in 1 ml of PSW.

Histology

Pieces of ovary were fixed in 1% osmium in PSW at 1–3°C for one hour, stored in 70% ethanol, dehydrated through an alcohol series, transferred to propylene oxide, and embedded in Epon equivalent. Sections were cut at 2 μM and stained with methylene blue and azure II. Pieces of ovary, isolated immature oocytes, and mature oocytes were fixed in 5% paraformaldehyde in PSW at 1–3°C for 10–30 min, transferred to PSW, and stained with the blue fluorescing DNA stain DAPI to visualize nuclei. A stock solution of DAPI was prepared by dissolving 1 mg of stain in 10 ml of distilled water and diluted 1/25 in PSW prior to the addition of fixed pieces of ovarian tissue or oocytes.

Results

Ovarian structure

The structure of the *Lingula* ovary has been described by Senn (1934) at the light microscope level and by Sawada (1973) at the electron microscope level of resolution. During the breeding season, the ovaries of a sexually mature *G. pyramidata* consist mostly, on a volume basis, of full-grown oocytes; however, intermingled with the full-grown oocytes are a number of previtellogenic oocytes and oocytes that are engaged in vitellogenesis but are not yet fully grown. Figure 1A shows a whole mount of a piece of fixed ovary viewed with transmitted light. The full-grown oocytes, each with its large germinal vesicle, are obvious. In Figure 1B the same piece of ovary is shown, using fluorescence to visualize DNA. The DNA stain is evident in the nuclei of follicle cells that surround each oocyte. The chromatin in germinal vesicles of large oocytes does not stain because it is too diffuse. Figure 2 presents a cross-section through a piece of ovary at low and high magnification, showing various details of ovarian structure. Each full-grown oocyte is surrounded by an extracellular envelope with oocyte microvilli extending into the envelope. The follicle cells cover this envelope. In addition to follicle cells, the interstices between oocytes may contain at least one other kind of somatic cell that may be similar to a cell type that Sawada refers to as a nutritive cell and that Senn refers to as a nurse cell. According to Sawada and Senn, this cell type is prominent during early stages of oogenesis prior to the reproductive season but

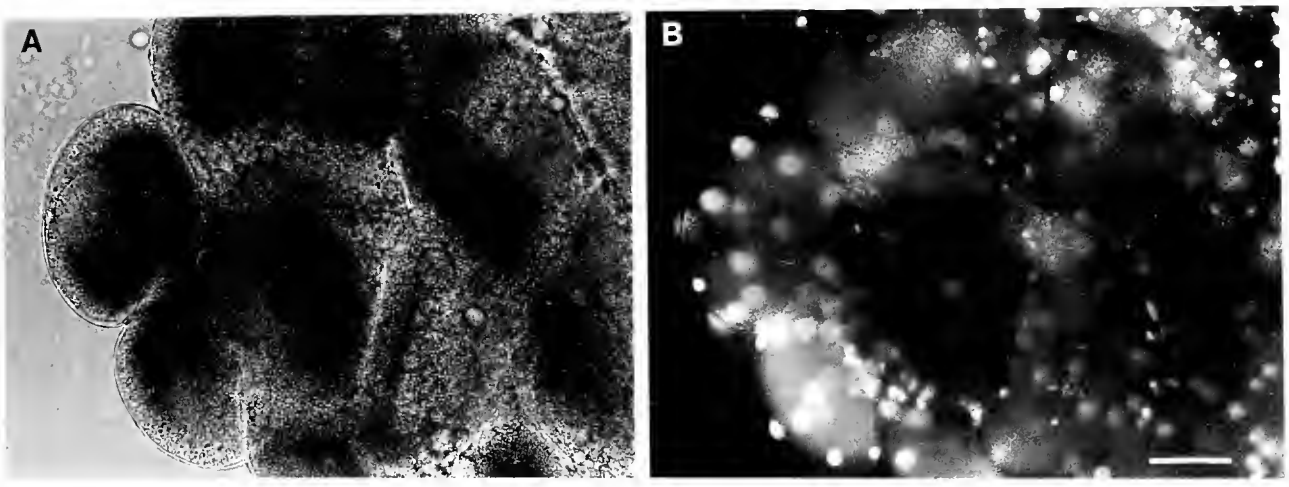

Figure 1. (A) Whole mount of ovarian lobe viewed with transmitted light showing full-grown oocytes. The translucent region in the oocyte on the extreme left indicates the position of its germinal vesicle. (B) View of the same ovarian lobe using fluorescence to visualize the nuclei of somatic cells in the ovary. Each oocyte is surrounded by a number of follicle cells. Because of the thickness of this preparation, not all somatic cell nuclei are in focus. For this reason, many of them give a diffuse fluorescence image. Both photographs are at the same magnification. Scale bar = 50 μm.

disappears in mature gonads; I have not seen this cell type. The full-grown oocytes form a polarized epithelium within the ovary. The germinal vesicle is located in the region of each oocyte that faces the coelomic space of the gonad, and the envelope that surrounds the oocytes is always thinnest on the opposite side of the oocyte facing the interior of the gonad (see *a* in Fig. 2B).

If one attempts to obtain oocytes by mechanically macerating the ovary, virtually all the oocytes are physically damaged: the envelope that surrounds the oocyte tears at the site where it is thinnest, and cytoplasm leaks out. Intact, undamaged oocytes can be obtained by washing and incubating pieces of ovary in several changes of calcium-free seawater (see Materials and Methods). Under these conditions, the follicular epithelium around the oocyte retracts, and the oocytes can be dissociated from the ovary. Oocytes obtained in this manner do not have follicle cells on their surface; this point was checked by staining fixed oocytes with DAPI. These follicle-cell-free oocytes still have an extracellular envelope with microvilli extending into the envelope. If these oocytes are cultured in PSW for up to 8 h, the germinal vesicle remains intact. When

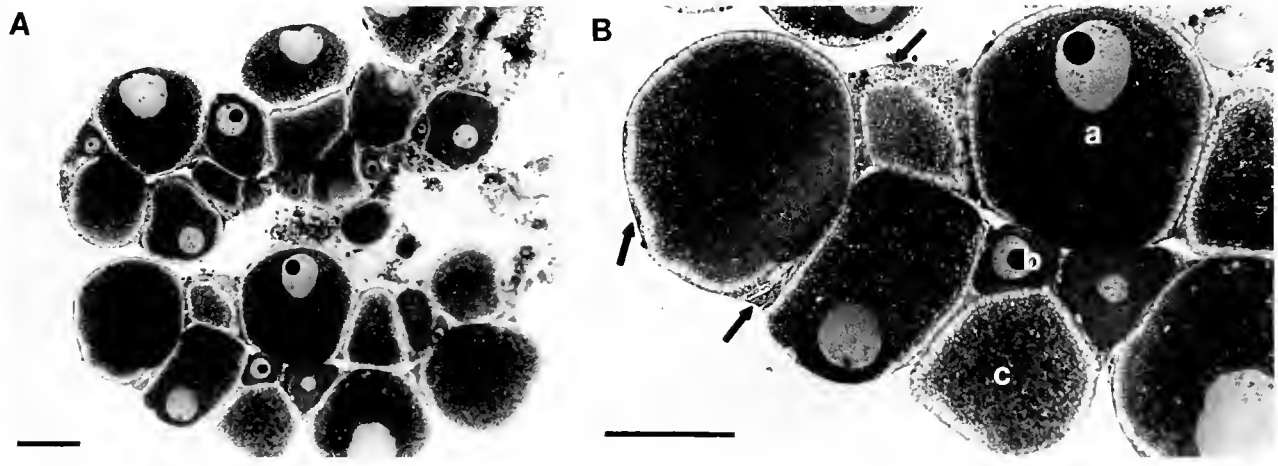

Figure 2. (A) Cross-section through two ovarian lobes at low magnification. The germinal vesicle of each oocyte has one nucleolus. (B) Cross-section through a region of a lobe at higher magnification. The envelope around each large oocyte and the follicle cells (arrows) covering the envelopes can be seen: (a) full grown oocyte, (b) previtellogenic oocyte, and (c) vitellogenic oocyte. Scale bars = 50 μm.

sperm are added to these oocytes, the germinal vesicle does not break down and development is not initiated. However, studies of fixed oocytes, stained with DAPI following exposure to sperm, indicate that sperm-egg fusion does occur in some cases.

The lophophore contains a factor that induces oocyte maturation

In a number of invertebrate and vertebrate animals, oocyte maturation in the ovary is controlled by hormones secreted by other organs (*e.g.*, Meijer, 1979a, b, for polychaetes and Shirai and Walker, 1988, for asteroids). Organ extracts from sexually mature *Glottidia* were tested for their capacity to induce oocyte maturation. Organ extracts were prepared from gut, liver, lophophore (including the mouth and the first part of esophagus), mantle, ovary, and testis (see Hyman, 1959, for a description of these organs). A piece of ovary was incubated in extract for up to 3 h and examined during this period for germinal vesicle breakdown of its oocytes. At the end of the incubation period, the piece of ovary was treated with calcium-free seawater to obtain free oocytes, and individual full-grown oocytes were examined for germinal vesicle breakdown by compressing them slightly under a coverslip and examining them with a compound microscope. At least three experiments were done for each organ, testing extracts of that organ from three animals. In the case of the gut, liver, lophophore, and mantle, extracts from both sexes were tested.

The only organ exhibiting oocyte-maturing activity was the lophophore. After 70–90 min of incubation in lophophore extract, the follicle cells around the oocyte retracted and the ovary dissociated into a pile of mature, full-grown oocytes and a residue composed of growing oocytes and follicle cells (Fig. 3). The germinal vesicles of these shed oocytes had broken down. DAPI staining of fixed oocytes showed that the chromosomes were condensed at metaphase and were located just under the cell surface in preparation for the first meiotic reduction division; there were no follicle cells around the oocytes. These matured oocytes were somewhat flattened, with a convex and concave side. When sperm are added to oocytes matured in this manner, the meiotic reduction divisions are completed and normal embryogenesis occurs.

In most experiments, an extract of 10 mg of lophophore in 100 μl of distilled water is still capable of inducing oocyte maturation when diluted 1/128 with PSW, but not when it is diluted to 1/256. Figure 4 summarizes the results of a number of experiments in which the last one-half dilution in a series that induced maturation is recorded. There was no sex-based difference in the concentration of oocyte-maturing activity in the lophophore.

The lophophore is a complex structure (Hyman, 1959; Storch and Welsch, 1976). There is a concentration of nerve cells, the subenteric ganglion, around the esophagus just below the mouth; nerve cell processes extend into the tentacular arms of the lophophore. To find out if a special region of the lophophore produces oocyte-maturing factor, the lophophore of a large animal was divided into two regions: the area around the mouth, which included the subenteric ganglion, and the two arms of the lophophore, which lack the subenteric ganglion. Extracts from both regions had the same oocyte-maturing activity (two experiments).

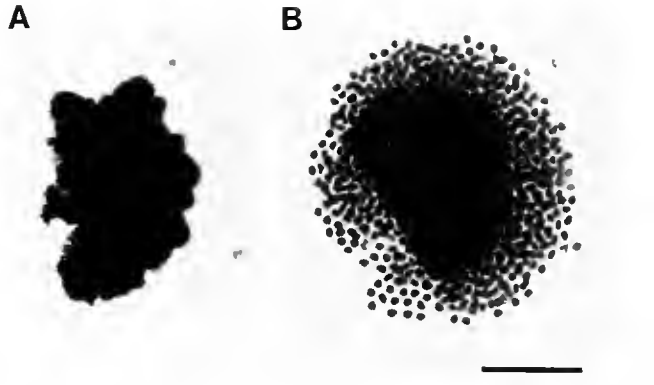

Figure 3. (A) A piece of ovary viewed with transmitted light just after being placed in a well with a 1/128 dilution of lophophore extract. (B) The same piece 95 min later showing its dissociation into a pile of large oocytes. Both photographs are at the same magnification. Scale bar = 1 mm.

Characterization of the lophophore extract

Three procedures were used to characterize the lophophore extract. In the first procedure, the extract was boiled to see if this treatment altered its activity. The results of a typical experiment are presented here. Lophophore extract was obtained from a male. Half of the supernatant was boiled for 15 min and the other half was stored on ice. A small amount of flocculent precipitate, presumably denatured protein, forms on boiling. Immediately after boiling, the boiled and unboiled extracts were serially diluted by 1/2 and the titer of the lowest dilution that would promote oocyte maturation was determined to be 1/128 for both boiled and unboiled extract. The remainder of the undiluted boiled and unboiled extract was frozen and retested for oocyte-maturing activity 24 h later. The lowest dilution of either extract that would induce maturation was 1/8, indicating that although lophophore extract is not heat labile, it loses activity in solution. Similar results were obtained using lophophore extract from either male or female animals in three separate experiments.

The second procedure examined the effect of protease treatment on the activity of lophophore extract. Extract

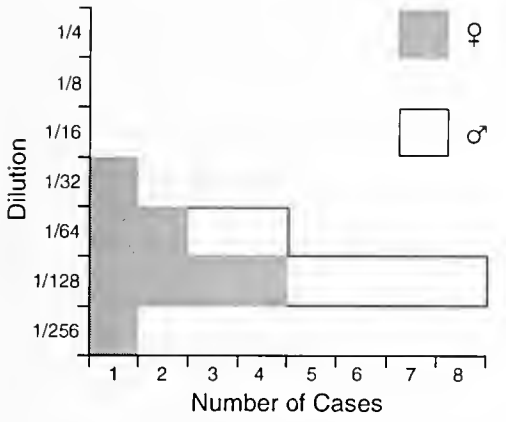

Figure 4. Histogram indicating the lowest 1/2 dilution of lophophore extract from a population of animals that induces oocyte maturation and follicle cell retraction in a piece of ovary. Each unit is one individual.

was boiled and diluted 1/32 with PSW. Then protease bound to agarose beads (Type VIII-A, 2–3 units per ml, Sigma) was slowly added to part of the diluted extract under a dissecting microscope until the solution could not accept any more. After 60 min of incubation at room temperature, the solution was centrifuged and the treated supernatant was collected. The last 1/2 dilution that would induce oocyte maturation in pieces of gonad was then compared for protease-treated and untreated extracts. In one experiment, this dilution was 1/128 for both extracts. In another experiment, it was 1/128 for the untreated extract and 1/64 for the protease-treated extract.

The third procedure characterized the lophophore extract by determining whether it would pass through a filter (Amicon) with a molecular weight cutoff of *ca.* 2000. Extract was boiled and diluted 1/32 with PSW prior to filtration. The lowest dilution of unfiltered solution that induced maturation in gonad pieces was 1/128, whereas the lowest dilution of filtered solution that induced maturation was 1/64. Because a large number of lophophores had to be dissected out and homogenized, this experiment was done only once.

These experiments indicate that the oocyte-maturing activity of the lophophore is due to a relatively small molecule and that it is probably not a peptide. The last part of the conclusion should be viewed with caution, however, because some small peptides can show marked resistance to boiling and protease activity.

The role of cAMP in inducing oocyte maturation

In many animals the levels of second messengers such as adenosine 3′5′ cyclic monophosphate (cAMP) changed markedly in oocytes or their follicle cells during oocyte maturation. In hydrozoans, an increase in cAMP levels in oocytes induces their maturation (Freeman and Ridgway, 1989). This compound was tested here to see if it would induce oocyte maturation in brachiopods. When animal cells are incubated in cAMP, they normally do not respond because this compound does not diffuse across the cell membrane, and there are no cAMP receptors on cell surfaces. For this reason, 8-bromoadenosine 3′5′ cyclic monophosphate (bromo cAMP) and dibutyryladenosine 3′5′ cyclic monophosphate (dibutyryl cAMP) were also tested; these cAMP derivatives can diffuse across cell membranes. In these experiments, summarized in Table I, a small piece of ovary was added to these compounds in PSW. The response of pieces of ovary to membrane-permeable cAMP derivatives was identical to their response to lophophore extract. Oocytes matured in this manner could be fertilized, and they developed into normal embryos. High concentrations of cAMP elicited only a marginal oocyte maturation response, but concentrations of bromo and dibutyryl cAMP that were 20–50 times lower were maximally effective in inducing maturation. The brominated derivative of 5′ adenosine monophosphate (bromo AMP), the breakdown product of cAMP, had no effect on oocyte maturation. These experiments show that cAMP derivatives induce oocyte maturation; however, they do not demonstrate that the oocyte-maturing activity in lophophore extract is a cAMP derivative.

Cyclic AMP derivatives and lophophore extract do not act directly on large oocytes to induce maturation

In a number of vertebrates and invertebrates, the neuroendocrine pathway that mediates oocyte maturation is made up of a number of components. For example, in asteroids, a factor from the radial nerve acts on the follicle cells that surround oocytes, causing them to secrete 1-methyl adenine, which then acts on the oocyte (Shirai and Walker, 1988). To find out if cAMP derivatives and

Table I

*The effect of different concentrations of cyclic AMP and cyclic AMP derivatives on oocyte maturation in pieces of gonad**

Compound	Conc m*M*	Maturation		
cAMP	100	±	±	−
	10	−	−	−
Bromo cAMP	5	+	+	+
	2	+	±	±
	1	±	−	−
Dibutyryl cAMP	5	+	+	+
	2	+	+	±
	1	±	±	±
Bromo AMP	20	−	−	−

* Each compound at each concentration was tested three times in experiments using pieces of ovary from different females. + = maturation, ± = marginal maturation, − = no maturation.

lophophore extract that cause maturation in pieces of isolated gonad will also cause isolated oocytes devoid of follicle cells to mature, pieces of gonad were incubated in calcium-free seawater (see Materials and Methods) to obtain isolated oocytes. These isolated oocytes were then treated with 5–10 m*M* of bromo or dibutyryl cAMP, or with 1/8 or 1/4 dilutions of lophophore extract in PSW; at the same time, pieces of ovary from the same animal were treated with the same concentrations of these agents. In every case oocyte maturation occurred in the intact piece of gonad, but in no case did it occur in oocytes devoid of follicle cells (117 from 7 animals). At the end of the experiment, the oocytes looked healthy and their germinal vesicles were intact.

The lack of maturation by isolated oocytes in the presence of cAMP derivatives or lophophore extract could reflect a subtle form of damage that the oocytes incurred during isolation. A reconstitution experiment was done to rule out this possibility. Isolated oocytes were stained lightly with neutral red so that they could be identified. These marked oocytes were placed either on or close to a piece of intact ovary that was then treated with 5–10 m*M* bromo cAMP, or with 1/4 or 1/64 dilutions of lophophore extract. This experiment was done three times. Of 46 stained oocytes, 28 underwent maturation as indicated by germinal vesicle breakdown; most of the 28 were in contact with the ovary. Maturation was first evident about 30 min after the ovary began to dissociate into oocytes. In control experiments, in which stained oocytes were placed on or close to a piece of ovary in the absence of bromo cAMP or lophophore extract, none of the 30 marked oocytes tested matured. These experiments suggest that cAMP derivatives or lophophore extract act in, or on, a somatic cell in the ovary, which then produces a factor that acts on large oocytes to mediate their maturation.

The oocyte-maturing activity in lophophore extract is part of an endocrine mechanism that mediates spawning

The oocyte-maturing activity in the lophophore could be a pharmacological fluke that has nothing to do with normal oocyte maturation. It could also be produced by a hormone that is released into the body cavity, where it functions as part of the normal endocrine pathway that mediates oocyte maturation and spawning.

During the night after animals are collected, they sometimes spawn (Paine, 1963). Spawning is obvious in females isolated individually in dishes without sediment, because one can see the eggs. The titer of oocyte-maturing activity in the lophophore of two females that spawned under these circumstances was tested the next morning by determining the lowest dilution by 1/2 in a series that induced oocyte maturation in pieces of ovary. In these experiments, the pieces of ovary used in the assay did not come from the females that had just spawned. The lowest dilutions that induced maturation were 1/8 and 1/16 for these two females. These results should be compared with the data on the lowest dilutions that normally induce maturation (Fig. 4). Two of the data points in Figure 4 come from females that were collected at the same time as the two females that spawned during the night. These two females did not spawn during the night. Lophophore extract from these females was prepared and tested at the same time the tests were done on the extracts from the two females that had spawned. The same set of ovarian fragments were used for all four tests. The lowest lophophore dilutions that induced maturation in these two cases were 1/64 and 1/128. This result indicates that just after a spawning there is much less oocyte-maturing activity in the lophophore. It suggests that the lophophore plays a role in normal spawning.

The breakdown of the germinal vesicle in oocytes and the dissociation of oocytes from a piece of isolated ovary do not constitute spawning. When spawning occurs in *Glottidia*, gametes are shed into the coelom, where they are expelled from the animal through its nephridiopores and pumped out of the shell. Spawning can be induced in these animals by injecting them with 25 μl of boiled lophophore extract diluted 1:3 with PSW or 25 μl of 20 m*M* dibutyryl cAMP in PSW. Large females with a valve length of 20 mm or more were used for these experiments. A 100-μl Hamilton syringe with a small-diameter hypodermic needle was used for the injections, which were made into the fluid-filled space that runs down the center of the pedicle. The pedicle, which is already partially contracted, contracts even more as a consequence of the injection, forcing the fluid in the center of the pedicle into the part of the animal covered by the valves. After the injection, each animal was placed in a separate dish with PSW and checked at intervals for eggs. Three of five animals injected with lophophore extract and two out of four animals injected with dibutyryl cAMP spawned. None of the five control animals injected with 25 μl of PSW spawned. Spawning began 2 to 3 h after the injection and lasted from 30 to 60 min. In each positive case, between 1000 and 5000 eggs were spawned. This experiment shows that lophophore extract and cAMP derivatives can elicit the entire maturation and spawning response in an intact animal.

Discussion

The fact that *Glottidia* spawns several times during its reproductive season and the observation that spawning is associated with the lunar cycle suggest that these animals may have an intrinsic mechanism for controlling the timing of spawning. The experiments reported here suggest

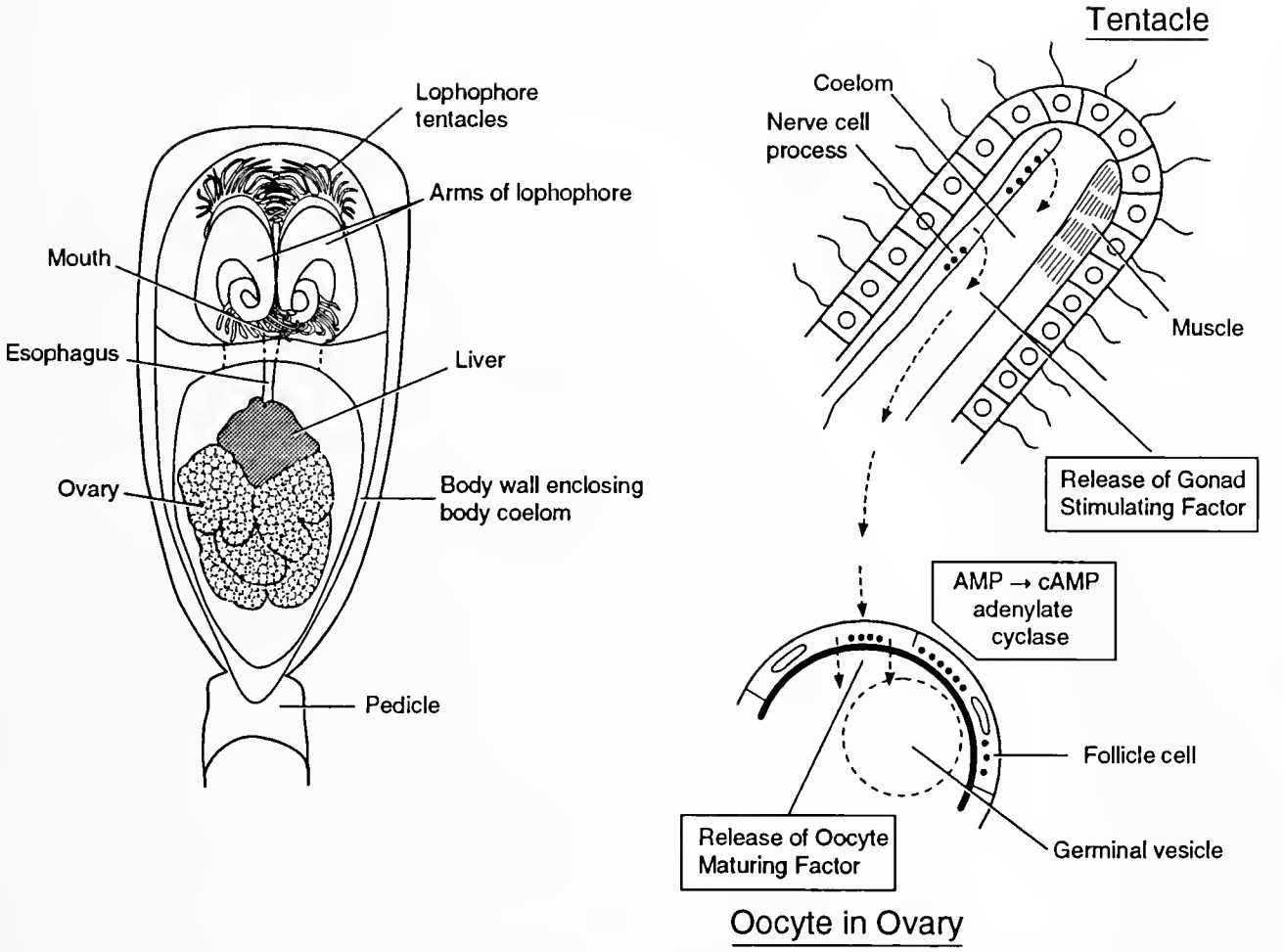

Figure 5. (Left) Diagram of the anterior region of *Glottidia* with one of its valves removed, showing the relative positions of the lophophore and ovary. They are in communication via the animal's coelomic space. (Upper right) Enlarged diagram of lophophore tentacle showing the release of gonad-stimulating factor. In this diagram, the factor is shown being released from a nerve cell process. (Lower right) Enlarged view of oocyte in ovary. The gonad-stimulating factor from the lophophore is shown stimulating cAMP synthesis in follicle cells. These cells then produce an oocyte-maturing factor that acts on oocytes, causing germinal vesicle breakdown.

that normal spawning is triggered when a cell type in the lophophore secretes a hormone with oocyte-maturing activity into the body cavity. Storch and Welsch (1976) describe the ultrastructure of the lophophore and tentacles of the related genus *Lingula,* and Hay-Schmidt (1992) describes the larval lophophore, with special reference to the nervous system, in *Lingula* and *Glottidia.* At present, it is not clear what cell types in the lophophore produce the oocyte-maturing activity. The lophophore is well innervated, and a neurosecretory product is certainly a possibility. In polychaetes and asteroids nerve cells produce hormones that play a role in oocyte maturation. The lophophore hormone then acts on a somatic cell in the ovary, presumably the follicle cell, perhaps increasing its cAMP levels. This leads to the release of another hormone that acts over a much smaller distance on large oocytes to trigger their maturation. Figure 5 outlines this hypothetical endocrine pathway. The oocyte-maturing hormone from the lophophore may also act on the follicle cells, causing them to retract, thereby facilitating oocyte shedding from the ovary. The presence of oocytes in the coelomic cavity may provide an impetus for spawning. Even though no experiments are reported here on spawning in males, the oocyte-maturing hormone is also found in the male lophophore, raising the possibility that this hormone also functions to cause sperm shedding into the coelom and spermiation.

At present, there is no operational way of distinguishing between the oocyte-maturing component of lophophore extract and the biologically active cAMP derivatives.

Cyclic AMP is not degraded by boiling (Sutherland, 1972) or by protease digestion, and its molecular weight is below 2000. Even though the possibility exists that the oocyte-maturing substance produced by the lophophore is identical to cAMP, our knowledge of the context in which cAMP functions in animal cells indicates that this is probably not the case. The oocyte-maturing activity of the lophophore clearly acts intercellularly, whereas cAMP functions intracellularly. The cellular slime mold *Dictyostelium* is the only example that I know of where cAMP functions in an extracellular context as a hormone (Gerisch, 1989). In this case, the cells that receive the signal have cAMP receptors on their surface membranes. Cyclic AMP cannot be the hormone in *Glottidia* because of the large quantities (100 m*M*) needed to give even a marginal oocyte-maturation response. If a cAMP derivative that could diffuse through a lipid bilayer were to function as a hormone, the cells in the lophophore that make the hormone would have a problem storing it. The only way to establish the identity of the lophophore hormone that acts on the gonad and the ovarian hormone that induces oocyte maturation is to purify these substances and carry out the appropriate chemical and structural studies on the molecules. The hypothetical role of lophophore hormone in raising cAMP levels in somatic cells in the ovary can be tested by measuring cAMP levels as a function of hormone treatment.

This study provides a way of obtaining fertilizable oocytes from inarticulate brachiopods at times other than natural spawning, thereby opening up the way for studies on embryogenesis and the early larvae of these animals.

Acknowledgments

I thank Dr. John Hitron, the Associate Director of the Turkey Point Marine Laboratory, and his staff for facilitating my work. I also thank Dr. Ross Ellington for giving me information on *G. pyramidata* collecting sites and telling me what to look for, and Dr. Shigeko Ooishi for translating the Sawada paper. I thank Judith Lundelius, David McCauley, and Hyla Sweet for critically reading this paper. This work was supported by NSF grant IBN-9307441.

Literature Cited

Chuang, S. H. 1959. The breeding season of the brachiopod *Lingula unguis*. *Biol. Bull.* **117:** 202–207.

Freeman, G., and E. B. Ridgway. 1988. The role of cAMP in oocyte maturation and the role of the germinal vesicle contents in mediating maturation and subsequent developmental events in hydrozoans. *Roux's Arch. Dev. Biol.* **197:** 197–211.

Gerisch, G. 1989. Cyclic AMP and other signals controlling cell development and differentiation in *Dictyostelium*. *Ann. Rev. Biochem.* **56:** 853–879.

Hay-Schmidt, A. 1992. Ultrastructure and immunocytochemistry of the nervous system of the larvae of *Lingula anatina* and *Glottidia* sp. (Brachiopoda). *Zoomorphology* **112:** 189–205.

Hyman, L. H. 1959. *The Invertebrates, Vol. 5. Smaller Coelomate Groups.* McGraw Hill, New York.

Kumé, M. 1956. The spawning of *Lingula*. *Nat. Sci. Rept. Ochanomizu Univ. Tokyo* **6:** 215–223.

Meijer, L. 1979a. Hormonal control of oocyte maturation in *Arenicola marina* (Annelida, Polychaeta) I. Morphological study of oocyte maturation. *Dev. Growth Differ.* **21:** 303–314.

Meijer, L. 1979b. Hormonal control of oocyte maturation in *Arenicola marina* (Annelida, Polychaeta) II. Maturation and fertilization. *Dev. Growth Differ.* **21:** 315–329.

Paine, R. T. 1963. Ecology of the brachiopod *Glottidia pyramidata*. *Ecol. Monogr.* **33:** 187–213.

Reed, C. G. 1987. Brachiopoda. Pp. 486–493 in *Reproduction and Development of Marine Invertebrates*, M. F. Strathman, ed. University of Washington Press, Seattle, Washington.

Sawada, N. 1973. Electron microscope studies on gametogenesis in *Lingula unguis*. *Zool. Mag.* **82:** 178–188 (In Japanese).

Senn, E. 1934. Die Geschlechtsverhaeltnisse der Brachiopoden, im besonderen die Spermato- und Oogenese der Gattung *Lingula*. *Acta Zool.* **15:** 1–154.

Shirai, H., and C. W. Walker. 1988. Chemical control of asexual and sexual reproduction in echinoderms. Pp. 453–476 in *Endocrinology of Selected Invertebrate Types*, H. Laufer and R. G. H. Dower, eds. Alan Liss Inc., New York.

Storch, V., and U. Welsch. 1976. Elektronenmikroskopische und enzymhistochemische Untersuchungen über Lophophor und Tentakeln von *Lingula unguis*. *Zool. Jb. Anat.* **96:** 224–237.

Sutherland, E. W. 1972. Studies on the mechanism of hormone action. *Science* **177:** 401–408.

Yatsu, N. 1902. On the development of *Lingula anatina*. *J. Coll. Imp. Univ. Tokyo* **17:** 1–112.

Reference: *Biol. Bull.* **186:** 271–284. (June, 1994)

Reproductive Cycling in Female *Fundulus heteroclitus*

SHYH-MIN HSIAO[1], MARK S. GREELEY JR.[1,*], AND ROBIN A. WALLACE[1,2]

[1]*The Whitney Laboratory, University of Florida, St. Augustine, Florida 32086, and* [2]*Department of Anatomy and Cell Biology, College of Medicine, University of Florida, Gainesville, Florida 32610*

Abstract. The ovaries of female *Fundulus heteroclitus* living in the northeastern Florida saltmarsh recrudesce in January and the fish initially spawn heavily during the subsequent full moons (a lunar pattern); they later spawn with less intensity during both the new and full moons (a semilunar pattern), and then regress in late September. In the laboratory, fish spawning against a vertical screen showed only semilunar periodicities, as observed for seven spawning groups under constant conditions (temperature 26 ± 1°C; photoperiod 14 h light to 10 h dark; excess food). Regardless of collection times (January, April, August, or September), these seven groups exhibited similar patterns of semilunar spawning for five to eight consecutive cycles whose periods (14.4 to 16.0 days) and phases (−1.7 to +8.4 days) were variable compared with concurrent full/new moon and spring tide cycles. These semilunar cycles, which occurred over the entire year in the laboratory, were thus free-running without entrainment and represent endogenous circasemilunar rhythms. In addition to annual and lunar/semilunar cycles, a tidal spawning cycle was also observed in the habitat. Fish apparently select the higher of the two semidiurnal tides for spawning, regardless of the daily light-dark cycle. This tidal cycle has not yet been tested in the laboratory.

Introduction

Most reproductively competent female fish exhibit annual cycles of ovarian development (Lam, 1983; Bye, 1984). The cycle begins with ovarian recrudescence, continues through a breeding period, and ends with ovarian regression. The recrudescence (which primarily involves vitellogenesis) is mostly under the influences of seasonal temperature and photoperiod. Later, during the breeding period, one or more clutches of ovarian follicles may develop progressively (Wallace and Selman, 1981a), often in synchrony with a combination of transient changes in temperature, illumination, spawning substrate availability, rainfall, moon phase, and tide, etc. (Lam, 1983; Bye, 1984; Stacey, 1984; Taylor, 1984). Ultimately, mature follicles ovulate and fish spawn at a specific time, a particular site, or both to maximize the immediate survival of eggs and hatchlings (Stacey, 1984; Taylor, 1984). Afterwards, a reproductive regression sets in to ensure that no hatchlings emerge and subsequently face a harsh environment inimical to their survival: follicles cease their growth and the ovary remains regressed until the next seasonal recrudescence. The seemingly direct responses of reproductive cycles to environmental influences do not necessarily exclude the involvement of endogenous organismal rhythms (Lam, 1983; Bye, 1984; Stacey, 1984). Such self-sustained rhythms schedule reproductive preparation, time receptivities for external cues, and, most important of all, can be entrained to follow repetitive environmental parallels (Elliot and Goldman, 1982).

Definitive studies of these reproductive cycles require a combination of both field observations and laboratory testing. However, the obvious complexity of reproductive physiology and its correlation to surmised environmental cues pose a difficulty for laboratory research. It is not surprising that most of the studies to date have been conducted in the field, but recent laboratory progress is encouraging. The endogenous nature of the annual cycle and the environmental cues that can phase-shift the cycle have been revealed in long-term laboratory observations (Bye, 1984; Bromage *et al.*, 1990), as exemplified by studies on rainbow trout, *Salmo gairdneri* (Scott and Sumpter, 1983; Duston and Bromage, 1991), stickleback, *Gasterosteus aculeatus* (Baggerman, 1980), and catfish, *Heteropneustes fossilis* (Sundararaj *et al.*, 1982). In these fish, ovarian development beyond recrudescence has been as-

Received 14 September 1993; accepted 30 March 1994.

* Present address: Environmental Sciences Division, Oak Ridge National Laboratory, P. O. Box 2008, Oak Ridge, Tennessee 37831-6038.

sumed to proceed spontaneously under the sole regulation of a circannual timer. However, the involvement of additional timers has never been excluded. For that matter, specific timers for follicle maturation and ovulation have been identified in other fish. For example, in the medaka, *Oryzias latipes*, a circadian timer apparently schedules the daily ovarian maturation for spawning at light onset (Iwamatsu, 1978; Ueda and Oishi, 1982; Weber and Spieler, 1987), and in the Gulf killifish, *Fundulus grandis*, a temperature-compensated circasemilunar timer is involved in ovarian maturation for spawning during spring tides (Hsiao and Meier, 1988, 1992). Although the circadian timer in medaka further regulates the timing of ovulation and spawning, in goldfish, *Carassius auratus*, the two processes, ovarian maturation and ovulation and spawning, are separately regulated. A gravid female goldfish with fully grown follicles does not spawn until warm temperature and a suitable spawning substrate become available; it then ovulates, under a circadian control, at midnight and spawns at first light (Stacey *et al.*, 1979).

Of all the fish employed in the above-mentioned studies, only *F. grandis* spawns with an important lunar/semilunar pattern related to semilunar tidal or moonlight cycles. Through the breeding season, this species and many other cyprinodonts exhibit lunar or semilunar spawning cycles that coincide with spring tides associated with synodic moonlight (29.6 days) on the Atlantic coast or with lunar declinational cycles (27.3 days) on the Gulf coast (Taylor, 1984). Depending on available habitat, they deposit their eggs during the daily high tides into empty mussel shells, marsh grass, or sand near or on the flooded surface of the marsh at or above the mean high waterline (Taylor, 1984). When the high tides recede, the eggs are left to incubate in a protected and humid environment until subsequent spring tides again flood the spawning site and the eggs hatch. One apparent advantage to such a reproductive strategy is that it ensures a predator-free and oxygen-rich location for developing embryos (Taylor and DiMichele, 1983). This strategy, however, demands an extraordinary organismal coordination with tidal/lunar environments.

Laboratory examination of semilunar/lunar reproductive activities in cyprinodonts has been initiated only recently (Taylor, 1986; Hsiao and Meier, 1986). Gradually, *Fundulus heteroclitus* has emerged as a promising laboratory model (Hsiao and Meier, 1989; Lin *et al.*, 1989; Taylor, 1991). Although this fish has been used in physiological, embryological, genetic, and environmental studies for decades (Huver, 1973; Atz, 1986), only in the past few years has it been shown to exhibit annual, lunar, semilunar, and tidal spawning cycles in the habitat (Day and Taylor, 1984; Taylor, 1984, 1986) and semilunar cycles in the laboratory (Hsiao and Meier, 1989; Taylor, 1991). Attention has recently been given to the interplay among internal hormonal rhythms, endogenous rhythmicity, and external entraining cues (Bradford and Taylor, 1987; Cochrane *et al.*, 1988; Hsiao and Meier, 1989; Taylor, 1991). Developmental aspects of the reproductive cycles, particularly the relationship between follicle growth and cyclic spawning, have also been examined (Taylor and DiMichele, 1980).

In the present investigation, the field and laboratory observations on reproductive cycling in female *F. heteroclitus* were extended at a northeast Florida site. Fish were sampled at intervals of about 2 days during a breeding season from January through October. Fish were also moved from their habitat into the laboratory several times during the year and their spawning patterns observed. Comparisons between field and laboratory data reveal mechanisms underlying the annual and semilunar reproductive cycles and indicate further research possibilities.

Materials and Methods

Field studies

Fish. Specimens of *F. heteroclitus* living in the saltmarsh along the Intracoastal Waterway near the Whitney Laboratory (St. Augustine, 29°40′ N latitude and 81°13′ W longitude) were collected with unbaited minnow traps. In 1984, samples containing five medium or large females [46 mm SL and larger, as classified by Kneib (1986)] were collected during daytime incoming tides at intervals varying from 1 to 4 days from early January through mid-September. Afterward, sampling was continued less frequently through mid-October. During spawning episodes in March and May 1985, females were also collected and examined at 3- to 4-h intervals over two consecutive spawning days to observe ovarian preparations for immediate spawning.

Adjusted tide tables (*Reed's Nautical Almanac & Coast Pilot*) were used to predict spring tides and semidiurnal high tides at the collection sites. In addition, tide measurements were taken by a mechanical recorder at the Whitney Laboratory dock on the Intracoastal Waterway to accurately predict daily high tides.

Fish were anesthetized with a solution of 3-aminobenzoic acid ethyl ester (MS-222; Sigma) within 1 h after capture. The fish were then weighed to the nearest 0.1 g and sacrificed by cervical incision. The single ovary (a fusion of two lobes) of each fish was removed, blotted dry, and weighed to the nearest milligram. A gonadal-somatic index (GSI = gonad weight × 100/total body weight) was then calculated.

Ovaries containing ovulated eggs were often difficult to handle without losing the eggs. To minimize error, we flushed ovaries before weighing: each ovary was opened laterally with sharp scissors and its eggs were shaken into a petri dish and counted as total eggs for a particular fish.

The final weight of each ovary was amended by the addition of egg weight estimated from the egg number and the average weight of a single egg [3.7 mg (Grecley *et al.*, 1991)].

Follicular development. Follicular development was indicated by stages and size distribution of follicles in each ovary. A small wedge-shaped sample of fresh ovary (minus ovulated eggs) was carefully cut with sharp scissors from the midportion of an ovarian lobe. Each sample was then placed individually in a petri dish containing a culture medium, FO solution (Wallace and Selman, 1978). Remaining ovarian tissue was reweighed to determine the proportion of the total ovary represented by the sample. Follicles in the sample were teased apart and those with diameters equal to or larger than 0.5 mm were measured to the nearest 0.1 mm (generally about 200 follicles per ovary piece). The apparent developmental stage of each follicle size-class was categorized according to morphological criteria (Selman and Wallace, 1986), and the presence and quantity of atretic follicles were noted (atretic follicles appeared somewhat opaque with irregular and flattened surfaces). Because follicle development is essentially uniform throughout the *F. heteroclitus* ovary (Taylor and DiMichele, 1980), measurements from each sample were proportionally converted to the total number of eggs or follicles per ovary. Finally, the data were standardized to a total egg or follicle number per gram of total body weight.

Data analysis. Due to the lack of a consistent daily or hourly continuity, the field data collected over months and over days were not analyzed through spectral time-series calculations. Instead, cycles were displayed graphically. In addition, the ovarian cycles were graphically compared with concurrent environmental cycles of high tide, moonlight, and daily photoperiod (Figs. 1–4).

Laboratory studies

Fish and spawning observations. Specimens of *F. heteroclitus* living in the saltmarsh surrounding the Intracoastal Waterway near the Whitney Laboratory were also collected for laboratory studies. Large fish—56 mm SL and larger, as classified by Kneib (1986)—were collected in January, April, August, and September 1991. Unbaited minnow traps were placed in the saltmarsh for as long as 24 h to obtain a large quantity of fish in one collection. In the laboratory, fish were kept in 550-l plain tanks or grouped in 550-l, 66-l, or 10-l partitioned spawning tanks. The concentrations were 188–300 fish per 550-l tank, 27 fish per 66-l tank, and 19 fish per 10-l tank. Each spawning tank was partitioned by a vertical black plastic screen with quarter-inch mesh to provide a narrow isolated compartment. Fish tend to spawn against the screen and eggs fall into the protected compartment. All tanks were aerated and filled with flowing seawater at 26.5 ± 1.5°C and 35 ppt salinity throughout the year. The lighting was fluorescent with a photoperiod of 14 h light to 10 h dark (LD 14:10). Twice daily, fish were fed to satiety with flakes (Wardley) that were left in the tank for at least 10 min after the initial vigorous feeding. The flakes were supplemented with cooked egg and crushed shrimp twice a month.

In each spawning tank, a fish group with a sex ratio of one male to three to eight females was maintained. The spawning was monitored by siphoning eggs out of the isolated compartment every 24 h. This technique was developed in studies of *F. grandis* and *F. heteroclitus* conducted in 38-l aquaria (Hsiao and Meier, 1986, 1989). To test whether our 550-l spawning tanks required extra spawning sites, we equipped the 550-l tank containing our first fish group A (250 females and 50 males) with an additional plastic screen folded as a cone and suspended in the middle of the tank. The cone was 30-cm long with a pointed top and an open bottom connected to a removable cup. Through daily removal of eggs from the cup, we monitored spawning at this extra site, which was found to be unnecessary (see Results); the remaining spawning tanks were equipped with vertical screens only.

Data analysis. Daily counts of eggs collected from the various fish groups were analyzed through SPECTRA time-series calculations (SAS Institute, Cary, North Carolina) to detect the presence of repeating cycles and their approximate periods. Nonlinear regression was used to fit sine curves to data series in which cycles had been identified. For each data series, ranges of sine curve amplitudes, phases, periods, and means were tested in extensive trials to produce the best fit for all or part of the series. Afterward, the fitted portion of a data series was divided into individual cycles at the lowest points of the matching sine curve with the original data bracketed in the cycles. A mean spawning date (±95% confidence limits) in each cycle was then calculated. This calculation often gave a peak spawning date slightly different from the date marked by the fitting sine curve. The mean spawning date was subtracted from the nearest new or full moon, thus providing the phase relation between the actual spawning peak and the concurrent moonlight cycle. Negative and positive phases respectively indicate that the spawning peak occurred before and after the new/full moon (Table I). The phases of successive cycles were analyzed by linear correlations to see if the variable spawning cycles of a data series have advanced or delayed sequentially in relation to the constant concurrent moonlight cycles (Table I). The phase relations were also graphed with parallel displays of daily egg counts for the various

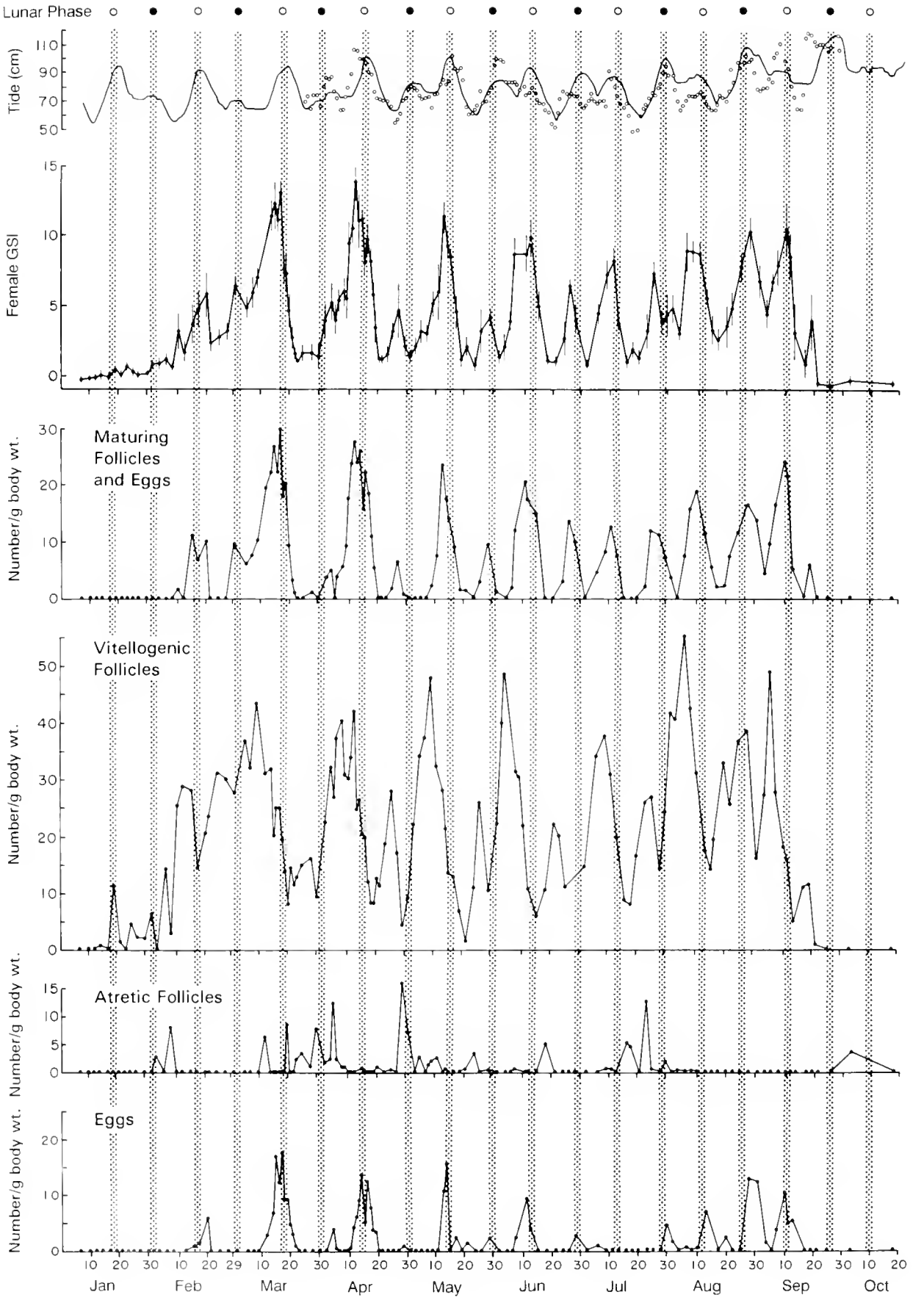
Lunar Phase
Tide (cm)
110
90
70
50
Female GSI
15
10
5
0
Maturing Follicles and Eggs
Number/g body wt.
30
20
10
0
Vitellogenic Follicles
50
40
30
20
10
0
Atretic Follicles
15
10
5
0
Eggs
20
10
0
10 20 30 10 20 29 10 20 30 10 20 30 10 20 30 10 20 30 10 20 30 10 20 30 10 20
Jan Feb Mar Apr May Jun Jul Aug Sep Oct

fish groups, concurrent cycles of moonlight, and predicted local tides (Figs. 5, 6).

Results

Field studies

Annual reproductive cycle. An annual reproductive cycle, containing lunar and semilunar spawning cycles, of females of *F. heteroclitus* inhabiting the northeastern Florida saltmarsh is illustrated by their variations in GSI and ovarian profile (Fig. 1). In January and early February, vitellogenic follicles gradually increased to the baseline of their cyclic appearance from February to September. In this later period, each cycle of vitellogenic follicles grew into a cycle of maturing follicles and ovulated eggs which, because of their relatively large size, contributed to high GSIs. The coexistence of high GSIs and maturing follicles plus eggs was transient, indicating a periodic discharge of ovarian products due to spawning. Thus, the first spawning episode in 1984 was identified to be during the spring tides associated with the full moon in mid-February. Subsequently, spawning episodes appeared successively at approximately lunar (29.6-day) or semilunar (14.8-day) intervals throughout the lengthy breeding season extending through September.

During the breeding season, in addition to exhibiting cyclic support for the spawning cycles, ovaries also revealed a discrete change in the size-frequency distribution of vitellogenic and maturing follicles (Fig. 2). At early successive full moon spring tides (*i.e.*, 15 February, 15 March, and 12 April), clutches of these follicles could not be easily distinguished from one another by size alone. As the season advanced, however, follicle clutches became more distinct. Later, during successive full moon spring tides (*i.e.*, 9 July, 10 August, and 11 September), clutches of follicles, particularly maturing follicles, rarely overlapped with smaller vitellogenic follicles. The size of the largest maturing follicles also tended to decrease during the breeding season. The formation of follicle clutches did not continue into the fall when the production of vitellogenic follicles suddenly ceased, resulting in a decrease in both maturing follicles and ovulated eggs and a subsequent increase in atretic follicles (Fig. 1). At this point, the breeding season ended.

Lunar and semilunar spawning cycles. After the first GSI peak at mid-February full moon, the next GSI peak occurred at the mid-March full moon and was followed by another GSI peak at the April full moon (Fig. 1). Between these early major GSI peaks were two minor GSI peaks associated with the new moon spring tides, but these minor peaks appeared to merge with the following full moon major peaks. Thus, there were three distinct large lunar spawning cycles during the early breeding season. It was not until late April that a well-defined new moon GSI peak appeared. Through time, size of the new moon GSI peaks increased while that of the full moon GSI peaks decreased until they were approximately equal after late June. Most GSI peaks began their decline right before or at new moon or full moon in coincidence with spring tides, indicating that spawning (discharge of ovarian products) strictly occurred at spring tides. The coincidence was lost in September; the last GSI peak, a minor one, occurred between the full and the following new moon. Overall, the breeding season was initially characterized by a lunar pattern of heavy spawning and later by a semilunar pattern of lighter spawning (Fig. 1). In addition, all lunar/semilunar spawning except the last cycle was consistently in synchrony with new/full moon cycles and the corresponding spring tides.

Throughout the study, the total number of maturing follicles and eggs (reflecting ovarian products that will soon be spawned) corresponded well with the GSI values (Fig. 1). To a lesser extent, this was also true for vitellogenic follicles, although their numbers tended to peak a few days earlier than those of maturing follicles plus eggs. Taken alone, however, the number of eggs in the ovary corresponded poorly with the cyclic fluctuation of GSI values and was not a good indication of spawning activity. This was probably because animals were collected only during the day, so females that spawned during the early morning hours were devoid of eggs when captured, unlike females that spawned in the late afternoon or early evening (see below).

Follicular growth cycles. A series of ovarian activities underlay each lunar or semilunar spawning cycle: vitellogenic follicles grew and accumulated and then passed on to form a peak of maturing follicles and ovulated eggs

Figure 1. Variations in gonadal-somatic index, (GSI, mean ± SD), the combined count of maturing follicles and eggs, vitellogenic follicles, atretic follicles, and ovulated eggs in *Fundulus heteroclitus* females collected from a northeastern Florida saltmarsh over the course of a breeding season. Each point represents a value derived from five fish. The predicted maximum height of daily high tide appears as a solid curve near the top of the figure, and the actual measurements of the maximum daily high tide are represented as small unfilled circles (discrepancies are due primarily to marsh structures and prevailing winds). Lunar phases are indicated at the top as new moons (large filled circles) and full moons (large unfilled circles). Vertical dotted bars mark the dates of new and full moons.

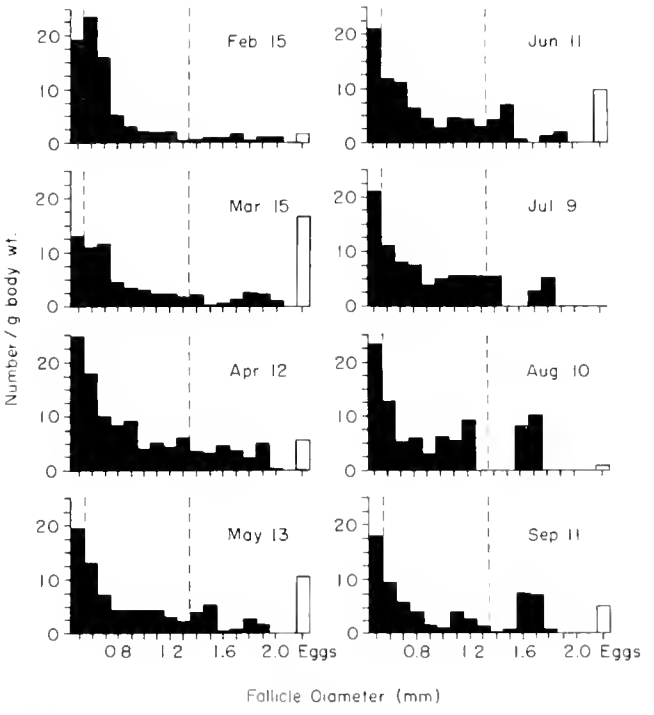

Figure 2. Subtle variations in the ovarian profiles (follicle size/frequency distributions) of *Fundulus heteroclitus* females collected during full moon spring tides in successive months of a breeding season. Each profile provides the mean number of various size follicles (filled bars) and ovulated eggs (unfilled bars) found for five fish on each sample date. In each histogram, the left dashed vertical line marks the transition from the cortical alveoli stage of development into vitellogenesis, and the right dashed vertical line marks the transition from vitellogenesis into maturation, as defined by Selman and Wallace (1986). Note the increased formation of distinct follicle clutches as the months progressed.

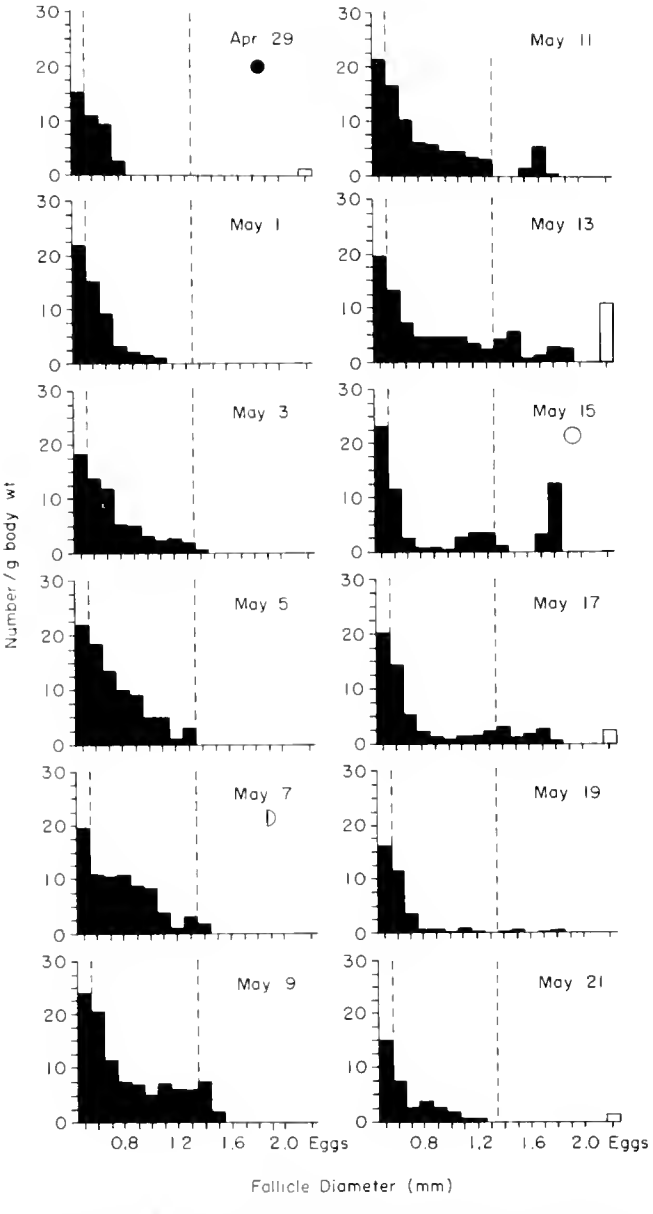

Figure 3. Variations in the ovarian profiles of *Fundulus heteroclitus* females collected during a 23-day interval encompassing a semilunar spawning period associated with the full moon (15 May). Each profile provides the mean number of various size follicles (filled bars) and ovulated eggs (unfilled bars) found for five fish on each sample date. In each histogram, the left dashed vertical line marks the transition from the cortical alveoli stage of development into vitellogenesis, and the right dashed vertical line marks the transition from vitellogenesis into maturation, as defined by Selman and Wallace (1986). Note the gradual accumulation of vitellogenic follicles, followed by recruitment of follicle clutches into maturation in preparation for spawning, and finally depletion of most larger follicles from the ovary. Lunar phases are indicated as new moon (filled circle), quarter moon (half unfilled circle), and full moon (unfilled circle).

(Fig. 1). Any failures in this process would result in atretic follicles, but these did not occur regularly during our observations (Fig. 1). Details of the vitellogenesis-maturation-ovulation transition during a lunar cycle were revealed by the ovarian profiles collected at 2-day intervals over a 23-day period (Fig. 3). After a minor new-moon spawn (29 April), the ovaries examined had few early vitellogenic follicles, no maturing follicles, and only a few ovulated eggs. During the next several days, however, mid- to late-vitellogenic follicles appeared and then accumulated in the ovary, and after the quarter moon on 7 May, a distinct clutch of maturing follicles also appeared. Afterward, vitellogenic follicles entered maturation, resulting in maturing follicles and ovulated eggs during days of spring tides (*i.e.*, 11, 13, 15 and 17 May) that occurred on and immediately preceded and followed the full moon (15 May). In these spawning days, follicles appeared to mature and ovulate in waves, one clutch after the other. At times (*e.g.*, 13 May), as one clutch began to mature, another was in late maturation, and the leading clutch had ovulated. This vigorous egg production exhausted the pool of vitellogenic follicles by the end of the spring tide series on 19 May. Two days later (21 May), mid-vitellogenic follicles appeared again, thus initiating another cycle

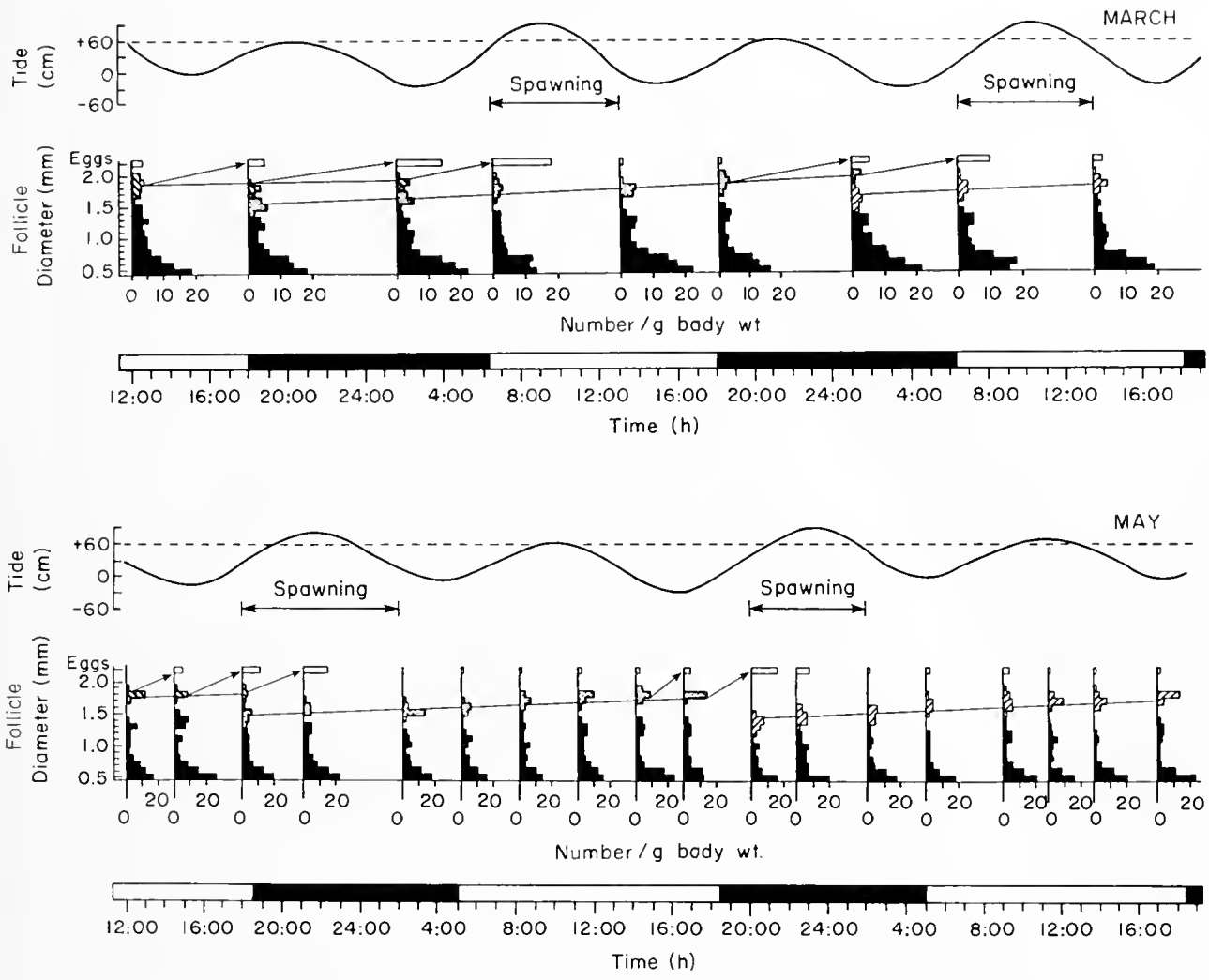

Figure 4. Ovarian profiles of *Fundulus heteroclitus* individuals collected over two-day periods of spring tides indicating preparations for selective tidal spawning. Samples were collected in either March or May (with time and photoperiod marked). Data for each time point represent the numerical averages for five (March) or six (May) females. Solid lines trace the successive development of three discernible follicle clutches during each two-day period. Arrows branching out from lines indicate the occurrence of ovulation. Semidiurnal tides at the time are presented as actual recorded tidal fluctuations from the mean water-line. Dashed lines through the tides reveal the approximate surface level of the upper saltmarsh.

of ovarian preparation for the next spawning episode. During this 23-day observation period, the numbers of late cortical alveolus-stage follicles (0.5-mm diameter) and early vitellogenic follicles (0.6- and 0.7-mm diameter) in each ovary remained relatively constant (Fig. 3). Apparently, the recruitment of follicle clutches in the ovary occurs instantly in early vitellogenesis, thus providing constant support for lunar/semilunar spawning by the repetitive and timely production of fully vitellogenic and maturational follicles.

Tidal ovulation and spawning. During days with spring tides, the ovary proceeds to its final preparation for spawning. The environmental correlates for the final steps are apparently not the semilunar moon phase or the semilunar tidal change, but the local semidiurnal tides. An apparent tidal spawning was observed immediately preceding the full moon of March and May 1985, with ovaries collected and examined at 3- to 4-h intervals over two consecutive spawning days in each month (Fig. 4). During the two days in March, a clutch of maturing follicles began to ovulate about 16-20 h before the spawning high tide. Ovulated eggs then accumulated and were spawned during the daytime high tide (note the disappearance of eggs from the ovary after the high tide). During the next 24 h, additional eggs were ovulated from another clutch of maturing follicles,

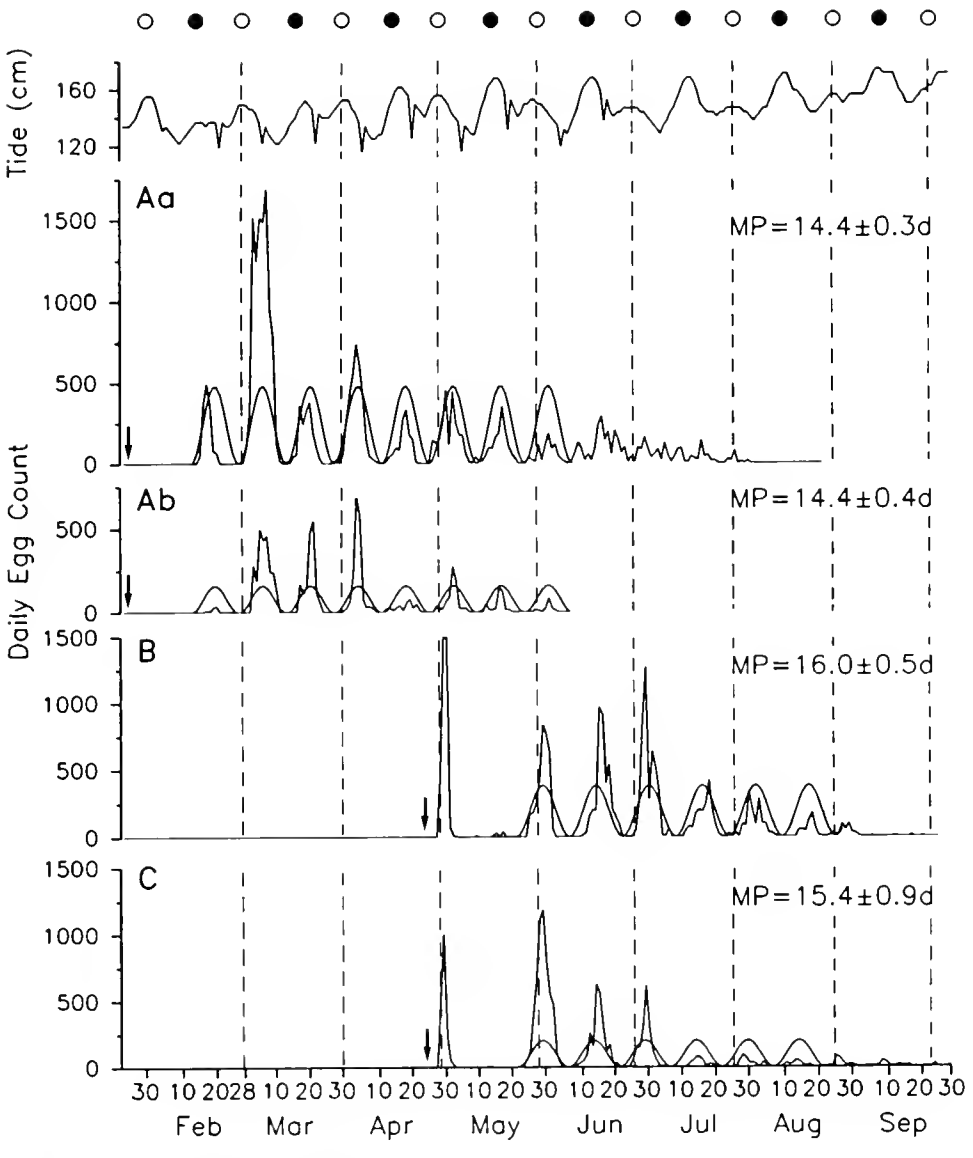

Figure 5. Cyclic variations in daily egg counts of fish groups A, B, and C. These groups were respectively obtained on 23 January, 24 April, and 26 April (marked by arrows). Spawning tanks holding each group were equipped with vertical screens as spawning substrates, with the exception of the tank for group A, which had a suspended screen cone as an extra substrate. Eggs collected from group A at the vertical and suspended screens are indicated as Aa and Ab, respectively. A part of each data series is significantly ($P < 0.01$) fitted by sine curves through nonlinear regressions with a calculated mean cycle period (MP) ± 95% confidence limits provided. Concurrent cycles of moonlight (full moon: unfilled circle; new moon: filled circle) and the predicted maximal daily high tide are indicated at the top of the figure for comparison. Vertical dotted lines mark the dates of full moons.

and spawning again occurred at the following daytime high tide. During the two days in May, a similar pattern was observed, but spawning occurred at the nighttime high tide. In both the March and May observations, two or three developing follicle clutches could be discerned over each two-day period. However, spawning occurred only at the higher of the two daily semi-diurnal tides, regardless of its daytime or nighttime appearance.

Laboratory studies

Semilunar spawning. Because the field data revealed a distinct annual reproductive cycle, fish collected from the

habitat at different seasons were expected to display various reproductive patterns—if any—in the laboratory. Surprisingly, regardless of their collection time, they all exhibited a similar reproductive progression containing five to eight semilunar spawning cycles (Figs. 5, 6).

In the winter, fish group A (250 females and 50 males in a 550-l spawning tank) was collected on 23 January and began spawning three weeks later. The spawning continued from February through July, with equivalent semilunar cycles observed at two egg collection sites, the vertical screen (Aa) and the suspended screen cone (Ab) (Fig. 5). The mean periods (14.4 ± 0.3 days for Aa and 14.4 ± 0.4 days for Ab) and phases (Fig. 5 and Table I) of eight consecutive cycles were similar for eggs collected at both sites and could be significantly correlated ($P < 0.01$) to sine curves. Accordingly, we concluded that a single egg collection site was sufficient to reveal the cyclic spawning of a captive group in the 550-l tank, and we used the vertical screen as the only collection site for eggs from fish collected subsequently. Although the semilunar cycles revealed by egg collections of Aa and Ab appeared similar to concurrent moonlight and tidal cycles, the dissociation between them was revealed by the differences in cycle periods and phases. The shorter mean cycle periods of Aa and Ab (as compared to a 14.8-day semilunar cycle) resulted in sequential reductions in their phases ($r = -0.77$, $P < 0.05$ in Aa; $r = -0.88$, $P < 0.01$ in Ab) relative to concurrent moonlight cycles: the mean spawning peaks in successive cycles occurred first at six days and drifted to two days after respective new/full moons (Table I).

In the spring, fish groups B (210 females and 25 males in a 550-l spawning tank) and C (163 females and 25 males also in a 550-l spawning tank) were collected four and two days, respectively, before the full moon on 28 April. On 28 and 29 April, both groups simultaneously spawned heavily in their separate tanks (Fig. 5). Afterward, there was a four-week pause before groups B and C spawned again, on another full moon (28 May). The semilunar spawning then lasted until August, and each group exhibited at least five consecutive cycles significantly matched by sine curves ($P < 0.01$). The mean periods were 16.0 ± 0.5 days for B and 15.4 ± 0.9 days for C. The longer periods of groups B and C (compared to 14.8 days) resulted in sequential phase delay ($r = 0.93$, $P < 0.01$ in B; $r = 0.90$, $P < 0.01$ in C) relative to concurrent moonlight cycles (Table I). The mean spawning peaks in successive cycles drifted from 1 to 8 days in B and 1 to 4 days in C after respective new/full moons (Table I).

In the summer, fish groups D and E (each containing 15 females and 4 males in a 10-l spawning tank) were collected on 20 August. They began spawning in the laboratory about three weeks later and continued spawning from September to December (Fig. 6). Although they were in small tanks, both groups also exhibited distinct semilunar cycles significantly ($P < 0.01$) fitted by sine curves for seven cycles. The mean periods were 14.4 ± 0.4 days for D and 14.5 ± 0.3 days for E (Table I). These relatively short periods (compared to 14.8 days) resulted in sequential phase advance ($r = -0.79$, $P < 0.05$ in D; $r = -0.86$, $P < 0.05$ in E) relative to concurrent moonlight cycles. The phases of successive cycles in D first went up from 3.7 days to 6.4 days and then dropped to −1.7 days and 1.1 days for the last two cycles. The phase progression in E indicated a smoother advance with a drift from four to about two days (Table I).

In the fall, a batch of fish was collected on 20 and 21 September and kept in a 550-l stocking tank without a vertical screen. A month later, on 26 October, the batch was divided into two groups, F and G (each containing 20 females and 7 males in a 66-l spawning tank). Thereafter, these groups spawned actively for three months from November through January, with distinct semilunar cycles significantly ($P < 0.01$) fitted by sine curves (Fig. 6). The mean cycle periods were 15.1 ± 0.7 days in F and 14.9

Table I

Mean period (MP) of semilunar spawning in laboratory fish groups A to G (±95% confidence limits) and phase shift against concurrent moonlight cycles

		Phase shift (days)[a]							
		Cycle:							
Group	MP	1	2	3	4	5	6	7	r[b]
Fish collected on 23 January, 1991									
Aa	14.4 ± 0.3	5.6	2.9	3.9	3.4	3.0	2.1	2.6	−0.77*
Ab	14.4 ± 0.4	6.2	4.0	4.4	3.6	3.8	1.7	2.5	−0.88**
Fish collected on 24 (B) and 26 (C) April 1991									
B	16.0 ± 0.5	1.0	4.1	3.8	5.5	5.4	8.4		+0.93**
C	15.4 ± 0.9	0.9	2.5	2.7	3.9	3.7	3.8		+0.90**
Fish collected on 20 August 1991									
D	14.4 ± 0.4	3.7	6.4	3.3	4.7	1.5	−1.7	1.1	−0.79*
E	14.5 ± 0.3	4.0	3.6	4.0	2.4	2.5	1.3	2.2	−0.86*
Fish collected on 20 and 21 September 1991									
F	15.1 ± 0.7	2.4	2.3	0.5	2.6	3.9			+0.60[ns]
G	14.9 ± 0.5	1.9	3.6	1.1	1.9	4.0			+0.36[ns]

[a] In each defined cycle fitted by sine curves (Figs. 5, 6), the date of the mean spawning peak (egg collection peak) was calculated and its phase relation to the concurrent moonlight cycle was determined. Negative and positive numbers respectively indicate the days that the peak occurred before and after the nearest new/full moon.

[b] * $P < 0.05$; ** $P < 0.01$; [ns]not significant.

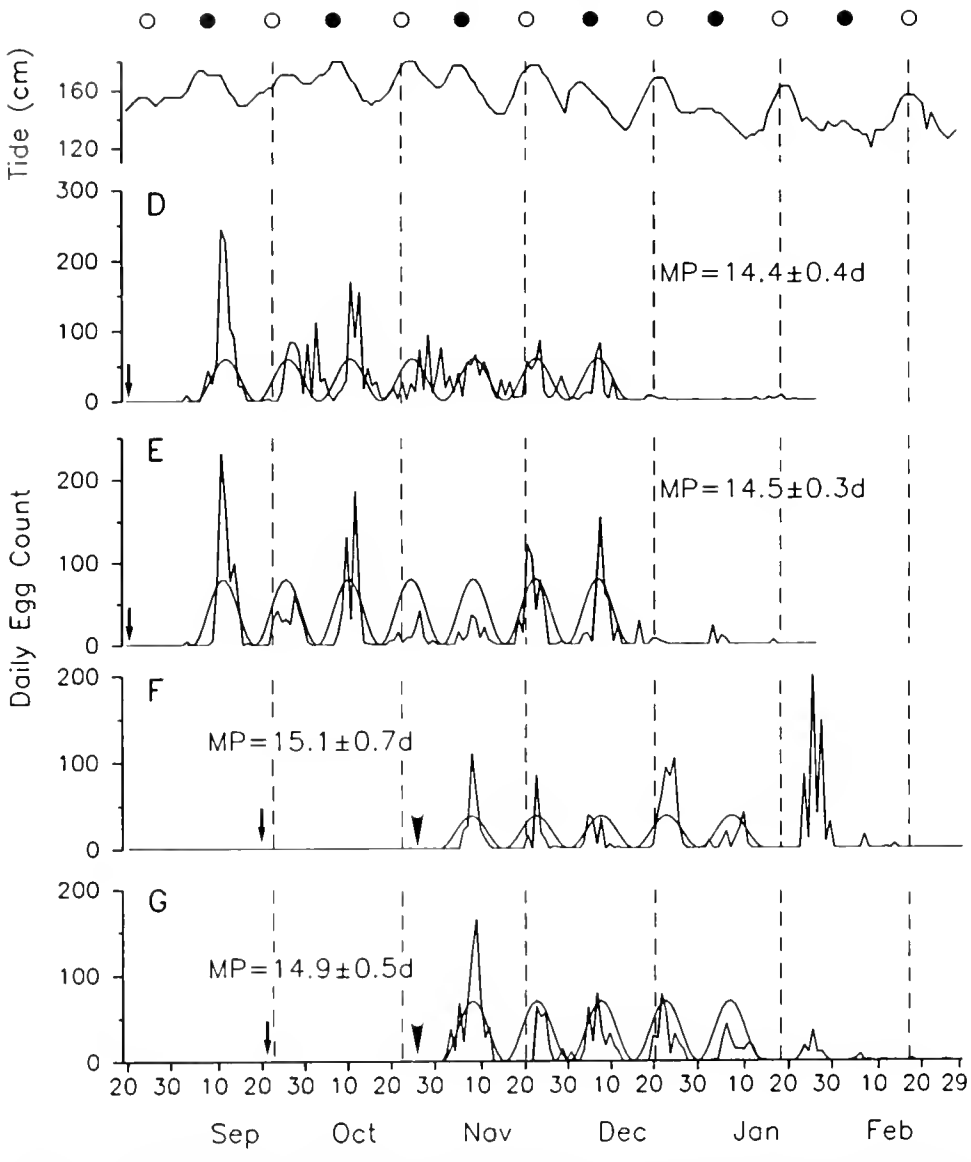

Figure 6. Cyclic variations in daily egg counts of spawning groups D, E, F, and G. Groups D and E and groups F and G were obtained from the habitat on 20 August and 20 and 21 September, respectively (marked by arrows). Groups F and G were initially held in a stocking tank for a month before being divided into two spawning groups on 26 October (arrowhead). A part of each data series is significantly ($P < 0.01$) matched by a sine curve through nonlinear regressions with a calculated mean cycle period (MP) ± 95% confidence limits provided. Concurrent cycles of moonlight (full moon: unfilled circle; new moon: filled circle) and the predicted maximal daily high tide are indicated at the top of the figure for comparison. Vertical dotted lines mark the dates of full moons.

± 0.5 days in G, with little difference from the 14.8-day moonlight cycle. Consequently, the spawning cycles stayed in phase and actually in synchrony with the concurrent moonlight cycle (Table I).

Overall, in addition to the indifference of laboratory spawning to season, the independence of semilunar spawning cycles from the concurrent moonlight cycle is apparent. Mean semilunar periods of the seven groups examined ranged from 14.4 to 16.0 days, and their cycle phases in relation to concurrent moonlight were not consistent. In contrast to the synchrony between lunar/semilunar GSI variations and moonlight cycles in wild fish (Fig. 1), there was no evidence that the laboratory spawning cycle was entrained or driven to follow a common cycle of moonlight or spring tide. Thus, the laboratory cycling was endogenously timed, free-running, and independent of environmental cues.

Furthermore, all seven laboratory groups, after about three to four months of spawning, appeared to enter a nonreproductive state, even though laboratory conditions (temperature, photoperiod, and feeding) remained the same. Although the spawning groups were monitored for one to two months after cyclic spawning ceased, the length and reversibility of the nonreproductive state were not further investigated.

Discussion

The extended field studies revealed the existence and interplay of annual, lunar/semilunar, and tidal reproductive activities. Parts of these activities persisted in the laboratory and are thus amenable to investigations of their underlying physiological mechanisms, particularly neurohormonal signaling along the hypothalamic-hypophyseal-ovarian axis. However, until the coexistence of annual, semilunar/lunar, and tidal reproductive activities can be more completely demonstrated in the laboratory, the interactive mechanisms among these cyclic activities cannot be well addressed.

Annual reproductive cycle

During our 10-month sampling period, females of *F. heteroclitus* inhabiting the northeastern Florida saltmarsh exhibited a distinct annual reproductive cycle. Their ovaries enlarged in late winter when the number of vitellogenic follicles gradually increased. During their breeding season in spring and summer, ovarian preparation for spawning occurred in cycles, with a peak of vitellogenic follicles preceding a peak of maturing follicles and ovulated eggs, leading to a spawning episode at spring tides (Fig. 1). From February to April, spawning peaks were large and took place at full moon spring tides, indicating a lunar pattern for the three cycles observed in 1984. From April to September, smaller spawning peaks occurred during both full and new moon spring tides, showing a semilunar pattern for the 10 cycles observed in 1984. Termination of the breeding season in late September was marked by a quick decline in vitellogenic and maturing follicles and a short period of irregular spawning. The fish then entered a reproductively quiescent phase. A similar annual cycle, including a breeding season during February through September with a transition from a lunar to a semilunar spawning pattern, has also been reported for *F. heteroclitus* in Georgia (Kneib, 1986). A less-detailed description of the annual cycle for *F. heteroclitus* on a north Carolina marsh reveals high GSIs from March through May and lower GSIs from June to August in reproductive females (Kneib and Stiven, 1978). The annual cycle for a Delaware population of *F. heteroclitus*, described in segments through several studies, has a restricted breeding season between April and August with a mixture of lunar and semilunar ovarian maturation cycles (Taylor *et al.*, 1979; Taylor and DiMichele, 1980; Day and Taylor, 1984; Taylor, 1986). The Massachusetts population living in the Woods Hole area has an even more restricted spawning season—from May through early summer—and the ovaries of these fish constantly contain maturational oocytes and eggs in May (Wallace and Selman, 1981b). It appears that this species, in general, spawns heavily when the temperature begins to rise and may extend its spawning opportunistically in the southern locations at summer high tides. Such an annual pattern was also observed in *Fundulus grandis* individuals living on the Alabama Gulf coast (Greeley and MacGregor, 1983; Greeley *et al.*, 1988). By exerting greater reproductive effort at the beginning of the season, a species may maximize its offspring's survival by ensuring a long growing season for most of the young (Greeley *et al.*, 1988).

Ovarian recrudescence in Florida *F. heteroclitus* began at a time [late January/early February (Fig. 1)] of short (LD $\approx$ 11:13) but increasing photoperiod, despite the lowest water temperatures of the year (13–15°C; pers. obs.). The increasing photoperiod and the cold temperature perhaps initiated the recrudescence. Possible environmental correlates of ovarian recrudescence have been explored in fish collected from a Delaware population in late October/December. Ovarian recrudescence of these fish was enhanced by their previous exposure to short days and low temperatures and occurred during long days (LD 13:11 or 15:9) at a warm temperature of 20°C over a period of 6 to 8 weeks (Day and Taylor, 1984). Long days and warm temperature were no longer necessary for recrudescence in females collected in March, and could not sustain reproductive activities of fish collected in late June beyond the normal breeding season. However, when females from the Florida habitat were collected in July and August and from October to February, they were maintained in reproductive condition beyond their breeding season under long photoperiod (LD 14:10) and warm temperature (25°C) without preconditioning (Lin *et al.*, 1989). These females retained high levels of gonadotropin activities in their pituitaries and carried gonadotropin-responsive follicles outside of the breeding season. An annual variation in seasonality in *F. heteroclitus* may dictate its variable ovarian responses to laboratory regimens of photoperiod and temperature (Day and Taylor, 1984; Taylor, 1986).

Nevertheless, the long breeding season in the field, punctuated by lunar and semilunar spawning cycles, collapsed at a time [late September (Fig. 1)] when temperature was still warm (28–30°C) and a uniform photoperiod (LD $\approx$ 12:12) had begun to decline. This collapse was probably not linked directly to a lack of pituitary gonadotropin content (as measured by a homologous

bioassay), which does not collapse in late September but only declines slowly later (Lin *et al.*, 1987). Instead, the steep decrease in vitellogenic and maturing follicles may have been due to a sudden termination of gonadotropin release, which may be linked to starvation. For example, previous studies on *F. heteroclitus* have shown the loss of follicular competence for maturation in starved females, an effect that can be reversed by either feeding or injection of gonadotropin [Wallace and Selman, 1978, 1980; see Holland and Dumont (1975) for similar effects of starvation and gonadotropin on vitellogenesis in *Xenopus laevis*]. The collapse of ovarian activities at the end of summer might, therefore, have been a result of seasonal food shortage (Kneib, 1986; Taylor, 1986; Lin *et al.*, 1989). The decline in size of the largest maturing follicles through the breeding season (Fig. 2) perhaps hinted at a decrease in resources for follicular growth. For *F. grandis*, fat storage (an indication of food availability) has also been linked to reproductive potential (MacGregor *et al.*, 1983). However, because semilunar spawning of *F. heteroclitus* kept in the laboratory and fed also collapsed after five to eight cycles (Figs. 5, 6), the correlation of starvation to the cessation of ovarian activities of wild fish in September is not conclusive. Alternatively, this cessation of reproductive activities can be explained as an expression of an endogenous seasonality progression.

Whether the seasonal transition in the annual cycle directly reflects environmental changes or expresses an underlying endogenous cycle, the transition was interrupted when the fish were collected and moved to the laboratory. During collection and early adaptation in the laboratory, fish usually stop eating and undergo some degree of ovarian regression (Wallace and Selman, 1978, 1980). Regardless of the season (January, April, August, or late September), laboratory fish nevertheless spawned within a few weeks of collection, and all exhibited only semilunar cycles instead of the lunar and semilunar cycles observed in wild fish (Fig. 1). The laboratory semilunar spawning then usually persisted for five to eight regular cycles and generally ended with a short irregular period leading to reproductive regression. The dissimilarity between wild and laboratory fish and the similarity among laboratory groups may suggest that the common stress fish experience during collection may have set their physiological state conducive for semilunar spawning.

Semilunar cycles

Throughout the breeding season, spawning activities of wild northeastern Florida *F. heteroclitus* were supported by successive development cycles of vitellogenic and maturing follicles (Figs. 1, 3). Cyclic ovarian activity thus appears restricted to gonadotropin-sensitive processes, *i.e.*, vitellogenesis and maturation (Wallace and Selman, 1981a). The recruitment of cortical alveolus-stage and early vitellogenic follicles into fully vitellogenic follicles began after each spawning period associated with full/new moon (Fig. 3). Vitellogenic follicles then grew to a diameter of 1.3–1.4 mm, entered maturation (when oocytes hydrate and become eggs), and eventually released their eggs for the next spawning period two weeks later. This organismal synchronization is indeed scheduled by an endogenously timed process as indicated by the laboratory results. The seven spawning groups observed in laboratory aquaria of different sizes exhibited free-running cycles with periods and phases that varied compared to constant concurrent tidal and moonlight cycles (Figs. 5, 6; Table I). The same result has been found for *F. grandis* (Hsiao and Meier, 1992). The possibility of subtle tidal/lunar factors that sustain corresponding activity cycles in laboratory animals (Brown, 1983) thus does not appear to be a serious consideration, either for *F. grandis* or *F. heteroclitus*.

An endogenous timer establishes an organizational basis for cyclic activities (see Introduction) and is generally temperature-compensated, as demonstrated for *F. grandis* (Hsiao and Meier, 1992), to protect its schedule from being destabilized by temperature fluctuations. Although temperature-compensation for the endogenous timer in *F. heteroclitus* has not been tested, its existence would be necessary under natural conditions. The Florida *F. heteroclitus* pace their spawning cycles in synchrony with constant new/full moons and spring tides throughout a temperature range from lows of 13–15°C in the late winter to highs of 28–30°C in the summer. The enhanced formation of distinct follicle clutches during the summer can be interpreted as demonstrating temperature-sensitive follicle growth (Wallace and Selman, 1978) confined by a temperature-compensated format for semilunar spawning. As temperature increases, each follicle clutch proceeds through maturation (and probably vitellogenesis) more rapidly and appears as a narrower and thus distinct band in its size-frequency chart (Fig. 2).

The environmental cues that entrain the endogenous lunar and semilunar cycles of the cyprinodonts are unknown. Because spring tides coincide with the new and full moons on the Atlantic coast, our field data do not have the resolution to discriminate between the involvement of tide and moonlight in spawning entrainment of *F. heteroclitus*. However, a recent laboratory study reveals an entrainment effect of moonlight on this fish (Taylor, 1991). The involvement of a semilunar high-tide cycle on the reproductive cycle of *F. grandis* living along the Gulf coast has also been shown. Spawning of this species follows the local tidal cycle instead of the moonlight cycle (Greeley and MacGregor, 1983; Hsiao and Meier, 1989). Along the Gulf, tidal changes reflect the declinational cycle of

the moon (27.3 days) rather than the synodic cycle of moonlight (29.6 days).

Tidal spawning cycles

Within the breeding season, in addition to lunar and semilunar spawning cycles, our frequent sampling over two-day periods during spring tides revealed a step-by-step ovarian preparation for tidal spawning. Counts of ovulated eggs in ovaries fluctuated dramatically with the daily ebb and flow of the tides. Follicles matured and ovulated in preparation for a spawning selectively directed at the higher tide of the two daily semidiurnal high tides, regardless of the daily light-dark rhythms (Fig. 4). This finding is unique compared to the tidal spawning described for *F. grandis* (Greeley and MacGregor, 1983) and *F. similis* (Greeley *et al.*, 1986), which was based on simple presence of eggs at nonspecific high tides. Specific selection of the higher daily tide obviously maximizes the use of high marsh surface as a spawning ground and minimizes egg loss by subsequent tidal flushing. If this highly specific temporal alignment could be studied in the laboratory, it would surely be a fertile research ground for studies of biological timing and its entrainment. Such a possibility was indirectly revealed in a case where locomotor activity of *F. grandis* was recorded for nine days (MacFarlane and Livingston, 1983). During this period, the differential between the activity rhythm and the light regimen of LD 12:12 produced a gradual delay of the daily peak of locomotor activity (which can be associated with spawning) from the offset to the onset of the light cycle. For directly detecting the daily change of spawning time in the laboratory, however, a monitor must be developed to count eggs at least once an hour.

Acknowledgments

This research, which is contribution No. 5 from the Center for Marine Gamefish Research, Whitney Laboratory, was supported by the Division of Sponsored Research, University of Florida, and by NSF grants DCB-8511260, DCB-8819005, and IBN-9306123 to R.A.W. We thank Lynn Milstead for excellent graphics support.

Literature Cited

Atz, J. W. 1986. *Fundulus heteroclitus* in the laboratory: a history. *Am. Zool.* **26:** 111–120.

Baggerman, B. 1980. Photoperiodic and endogenous control of the annual reproductive cycle in teleost fishes. Pp. 533–567 in *Environmental Physiology of Fishes*, M. A. Ali, ed. Plenum Press, New York, NY.

Bradford, C. S., and M. H. Taylor. 1987. Semilunar changes in estradiol and cortisol coincident with gonadal maturation and spawning in the killifish *Fundulus heteroclitus*. *Gen. Comp. Endocrinol.* **66:** 71–78.

Bromage, N., J. Duston, C. Randall, A. Brook, M. Thrush, M. Carrillo, and S. Zanuy. 1990. Photoperiodic control of teleost reproduction. Pp. 620–626 in *Progress in Comparative Endocrinology*, A. Epple, C. G. Scanes, and M. H. Stetson, eds. Wiley-Liss, New York.

Brown, F. A., Jr. 1983. The biological clock phenomenon: exogenous timing hypothesis. *J. Interdiscipl. Cycle Res.* **14:** 137–162.

Bye, V. 1984. The role of environmental factors in the timing of reproductive cycles. Pp. 187–205 in *Fish Reproduction: Strategies and Tactics*, G. W. Potts and R. J. Wootton, eds. Academic Press, London.

Cochrane, R. C., S. D. Zabludoff, K. T. Paynter, L. DiMichele, and R. E. Palmer. 1988. Serum hormone levels associated with spawning activity in the mummichog, *Fundulus heteroclitus*. *Gen. Comp. Endocrinol.* **70:** 345–354.

Day, J. R., and M. H. Taylor. 1984. Photoperiod and temperature interaction in the seasonal reproduction of female mummichogs. *Trans. Am. Fish. Soc.* **113:** 452–457.

Duston, J., and N. Bromage. 1991. Circannual rhythms of gonadal maturation in female rainbow trout (*Oncorhynchus mykiss*). *J. Biol. Rhythms* **6:** 49–53.

Elliot, J. A., and B. D. Goldman. 1982. Seasonal reproduction, photoperiodism and biological clocks. Pp. 377–423 in *Neuroendocrinology of Reproduction*, N. T. Adler, ed. Plenum Press, New York.

Greeley, M. S. Jr., and R. MacGregor III. 1983. Annual and semilunar reproductive cycles of the gulf killifish, *Fundulus grandis*, on the Alabama Gulf coast. *Copeia* **1983:** 711–718.

Greeley, M. S. Jr., K. R. Marion, and R. MacGregor III. 1986. Semilunar spawning cycles of *Fundulus similis* (Cyprinodontidae). *Environ. Biol. Fish.* **17:** 125–131.

Greeley, M. S. Jr., R. MacGregor III, and K. R. Marion. 1988. Changes in the ovary of the Gulf killifish, *Fundulus grandis* (Baird and Girard), during seasonal and semilunar spawning cycles. *J. Fish Biol.* **33:** 97–107.

Greeley, M. S. Jr., H. Hols, and R. A. Wallace. 1991. Changes in size, hydration and low molecular weight osmotic effectors during meiotic maturation of *Fundulus* oocytes *in vivo*. *Comp. Biochem. Physiol.* **100A:** 639–647.

Holland, C. A., and J. N. Dumont. 1975. Oogenesis in *Xenopus laevis* (Daudin) IV. Effects of gonadotropin, estrogen and starvation on endocytosis in developing oocytes. *Cell Tiss. Res.* **162:** 177–184.

Hsiao, S-M., and A. H. Meier. 1986. Spawning cycles of the Gulf killifish, *Fundulus grandis*, in closed circulation systems. *J. Exp. Zool.* **240:** 105–112.

Hsiao, S-M., and A. H. Meier. 1988. Semilunar ovarian activity of the Gulf killifish, *Fundulus grandis*, under controlled laboratory conditions. *Copeia* **1988:** 188–195.

Hsiao, S-M., and A. H. Meier. 1989. Comparison of semilunar cycles of spawning activity in *Fundulus grandis* and *F. heteroclitus* held under constant laboratory conditions. *J. Exp. Zool.* **252:** 213–218.

Hsiao, S-M., and A. H. Meier. 1992. Freerunning circasemilunar spawning rhythm of *Fundulus grandis* and its temperature compensation. *Fish Physiol. Biochem.* **10:** 259–265.

Huver, C. W. 1973. *A Bibliography of the Genus Fundulus*. G. K. Hall & Co., Boston. 138 pp.

Iwamatsu, T. 1978. Studies on oocyte maturation of the medaka, *Oryzias latipes*: relationship between the circadian cycle of oocyte maturation and activity of the pituitary gland. *J. Exp. Zool.* **206:** 355–364.

Kneib, R. T. 1986. Size-specific patterns in the reproductive cycle of the killifish, *Fundulus heteroclitus* (Pisces: Fundulidae) from Sapelo Island, Georgia. *Copeia* **1986:** 342–351.

Kneib, R. T., and A. E. Stiven. 1978. Growth, reproduction, and feeding of *Fundulus heteroclitus* (L.) on a north Carolina salt marsh. *J. Exp. Mar. Biol. Ecol.* **31:** 121–140.

Lam, T. J. 1983. Environmental influences on gonadal activity in fish. Pp. 65–116 in *Fish Physiology, Vol. 9B*, W. S. Hoar, D. J. Randall, and E. M. Donaldson, eds. Academic Press, New York.

Lin, Y-W. P., M. J. LaMarca, and R. A. Wallace. 1987. *Fundulus heteroclitus* gonadotropin(s) I. Homologous bioassay using oocyte maturation and steroid production by isolated ovarian follicles. *Gen Comp. Endocrinol.* **67:** 126–141.

Lin, Y-W. P., M. S. Greeley Jr., and R. A. Wallace. 1989. *Fundulus heteroclitus* gonadotropin(s) 2. Year-round husbandry of animals with active pituitaries and responsive follicles. *Fish Physiol. Biochem.* **6:** 139–148.

MacFarlane, R. B., and R. J. Livingston. 1983. Effects of acidified water on the locomotor behavior of the Gulf killifish, *Fundulus grandis*: a time series approach. *Arch. Environ. Contam. Toxicol.* **12:** 163–168.

MacGregor, R. III, M. S. Greeley Jr., W. C. Trimble, and W. M. Tatum. 1983. Seasonal variation of reproduction and fattening in Gulf killifish from brackish mariculture ponds. *Northeast Gulf Sci.* **6:** 23–32.

Scott, A. P., and J. P. Sumpter. 1983. A comparison of female reproductive cycles of autumn-spawning and winter-spawning strains on rainbow trout (*Salmo gairdneri* Richardson). *Gen. Comp. Endocrinol.* **52:** 79–85.

Selman, K., and R. A. Wallace. 1986. Gametogenesis in *Fundulus heteroclitus*. *Am. Zool.* **26:** 173–192.

Stacey, N. E. 1984. Control of the timing of ovulation by exogenous and endogenous factors. Pp. 207–222 in *Fish Reproduction, Strategies and Tactics*, G. W. Potts and R. J. Wootton, eds. Academic Press, London.

Stacey, N. E., A. F. Cook, and R. E. Peter. 1979. Spontaneous and gonadotropin-induced ovulation in the goldfish, *Carassius auratus*: effects of several external factors. *J. Fish. Biol.* **15:** 349–361.

Sundararaj, B., S. Vasal, and F. Halberg. 1982. Circannual rhythmic ovarian recrudescence in the catfish. *Adv. Biosci.* **42:** 319–337.

Taylor, M. H. 1984. Lunar synchronization of fish reproduction. *Trans. Am. Fish. Soc.* **113:** 484–493.

Taylor, M. H. 1986. Environmental and endocrine influences on reproduction of *Fundulus heteroclitus*. *Am. Zool.* **26:** 159–171.

Taylor, M. H. 1991. Entrainment of the semilunar reproductive cycle of *Fundulus heteroclitus*. Pp. 157–159 in *Proceedings of the Fourth International Symposium on the Reproductive Physiology of Fish*, A. P. Scott, J. P. Sumpter, D. E. Kime, and M. S. Rolfe, eds. FishSymp 91, Sheffield.

Taylor, M. H., and L. DiMichele. 1980. Ovarian changes during the lunar spawning cycle of *Fundulus heteroclitus*. *Copeia* **1980:** 118–125.

Taylor, M. H., and L. DiMichele. 1983. Spawning site utilization in a Delaware population of *Fundulus heteroclitus* (Pisces: Cyprinodontidae). *Copeia* **1983:** 719–725.

Taylor, M. H., G. J. Leach, L. DiMichele, W. M. Levitan, and W. F. Jacob. 1979. Lunar spawning cycle in the mummichog, *Fundulus heteroclitus* (Pisces: Cyprinodontidae). *Copeia* **1979:** 291–297.

Ueda, M., and T. Oishi. 1982. Circadian oviposition rhythm and locomotor activity in the medaka, *Oryzia latipes*. *J. Interdiscipl. Cycle Res.* **13:** 97–104.

Wallace, R. A., and K. Selman. 1978. Oogenesis in *Fundulus heteroclitus* I. Preliminary observations on oocyte maturation *in vivo* and *in vitro*. *Dev. Biol.* **62:** 354–369.

Wallace, R. A., and K. Selman. 1980. Oogenesis in *Fundulus heteroclitus* II. The transition from vitellogenesis into maturation. *Gen. Comp. Endocrinol.* **42:** 345–354.

Wallace, R. A., and K. Selman. 1981a. Cellular and dynamic aspects of oocyte growth in teleosts. *Am. Zool.* **21:** 325–343.

Wallace, R. A., and K. Selman. 1981b. The reproductive activity of *Fundulus heteroclitus* females from Woods Hole, Massachusetts, as compared with more southern locations. *Copeia* **1981:** 212–215.

Weber, D. N., and R. E. Spieler. 1987. Effects of the light-dark cycle and scheduled feeding on behavioral and reproductive rhythms of the cyprinodont fish, medaka, *Oryzia latipes*. *Experientia* **43:** 621–624.

Reference: *Biol. Bull.* **186:** 285–290. (June, 1994)

Endogenous Substrates for Energy Metabolism in Spermatozoa of the Sea Urchins *Arbacia lixula* and *Paracentrotus lividus*

MASATOSHI MITA[1]*, ATSUKO OGUCHI[2], SAKAE KIKUYAMA[2], IKUO YASUMASU[2], ROSARIA DE SANTIS[3], AND MASARU NAKAMURA[4]

[1]*Teikyo Junior College, Shibuya-ku, Tokyo 151, Japan,* [2]*Department of Biology, School of Education, Waseda University, Shinjuku-ku, Tokyo 169-50, Japan,* [3]*Department of Biology, Stazione Zoologica 'Anton Dohrn,' Villa Comunale, Napoli 80121, Italy, and* [4]*Department of Biology, Faculty of Medicine, Teikyo University, Hachioji, Tokyo 192-03, Japan*

Abstract. Energy metabolism was examined in the spermatozoa of the sea urchins *Arbacia lixula* and *Paracentrotus lividus,* which belong to the orders Arbacioida and Echinoida respectively. *P. lividus* spermatozoa contained various phospholipids and cholesterol, and their endogenous triglyceride (TG) content was quite low. After dilution of dry sperm in artificial seawater, the level of phosphatidylcholine (PC) decreased rapidly, but other phospholipids remained at constant levels. In contrast to those of *P. lividus,* the spermatozoa of *A. lixula* contained TG as well as phospholipids and cholesterol. Following incubation of *A. lixula* spermatozoa in artificial seawater, TG decreased, but there were no concomitant changes in the levels of phospholipids. Trace amounts of glycogen were present in both species. High lipase activity was demonstrated in *A. lixula* spermatozoa, but in *P. lividus* spermatozoa lipase activity was low and phospholipase A_2 activity was high. It is thus concluded that *A. lixula* spermatozoa obtain energy for swimming through oxidation of endogenous TG, whereas *P. lividus* spermatozoa use PC as a substrate for energy metabolism. This suggests that the system of energy metabolism in spermatozoa is different in the orders Arbacioida and Echinoida.

Introduction

Sea urchin spermatozoa start their flagellar movement immediately after being spawned into seawater. The flagellar movement results partly from reactions catalyzed by dynein ATPase (Gibbons and Gibbons, 1972; Christen *et al.,* 1982, 1983; Evans and Gibbons, 1986). Thus, energy metabolism to produce ATP is indispensable for swimming. Sea urchin spermatozoa could not use an exogenous substrate for energy metabolism because they swim in seawater, which contains hardly any nutrients. Previous studies in *Echinus esculentus* (Rothschild and Cleland, 1952) and *Hemicentrotus pulcherrimus* (Mohri, 1957a; Mita and Yasumasu, 1983) have shown that the endogenous phospholipid content of spermatozoa decreases following the initiation of flagellar movement. It has also been reported that *H. pulcherrimus* spermatozoa possess fatty acid oxidizing activity (Mohri, 1957b; Mita and Ueta, 1988, 1990). *H. pulcherrimus* spermatozoa generally contain various phospholipids and cholesterol (Ch), and their endogenous triglyceride (TG) and glycogen contents are extremely low (Mita and Yasumasu, 1983; Mita and Ueta, 1988, 1989). The decrease in the phospholipid content of *H. pulcherrimus* spermatozoa during swimming has recently been reported to be caused solely by a change in the level of phosphatidylcholine (PC) (Mita and Ueta, 1988). Similar findings for other sea urchins of the order Echinoida (Mita and Nakamura, 1993) indicate that PC is the main substrate for energy metabolism in these spermatozoa. The hydrolysis of PC in preference to other available phospholipids is related to the properties of phospholipase A_2 (Mita and Ueta, 1988, 1990; Mita and Nakamura, 1993).

In *Arbacia lixula* and *Paracentrotus lividus,* which belong to the orders Arbacioida and Echinoida respectively,

Received 6 August 1993; accepted 30 March 1994.

* Correspondence: Dr. M. Mita, Teikyo Junior College, 6-31-1, Honcho, Shibuya-ku, Tokyo 151, Japan.

the phospholipid content in the spermatozoa decreases following incubation in seawater (Mohri, 1964). On the other hand, the spermatozoa of *Glyptocidaris crenularis*, a member of the suborder Phymosomatoida of the order Arbacioida, contain TG as well as phospholipids and Ch, and use this endogenous TG to produce energy for swimming (Mita, 1991). This suggests that the spermatozoa of sea urchins in the order Arbacioida have an energy metabolic system different from that in the order Echinoida. Thus, it is still unclear whether the endogenous substrate used for energy metabolism by *A. lixula* spermatozoa is PC, TG, or a combination of the two. To clarify energy metabolism in sea urchin spermatozoa, the present study compared the energy production systems in spermatozoa of *A. lixula* and *P. lividus*.

Materials and Methods

Materials

Sea urchins, *A. lixula* and *P. lividus*, were collected in the Gulf of Napoli, Italy, and induced to spawn by intracoelomic injection of 0.5 *M* KCl. Semen was always freshly collected as "dry sperm" and kept undiluted on ice. The number of spermatozoa was calculated from the protein concentration, which was determined using a Micro BCA protein assay kit (Pierce, IL). The average protein content per 10^9 spermatozoa was 0.5 ± 0.1 mg in both species.

Incubation of spermatozoa

Dry sperm were diluted 100-fold in artificial seawater (ASW) consisting of 458 m*M* NaCl, 9.6 m*M* KCl, 10 m*M* $CaCl_2$, 49 m*M* $MgSO_4$, and 10 m*M* Tris-HCl at pH 8.2. After dilution and incubation for 1 h at 20°C, the sperm suspension was centrifuged at 3000 × *g* for 5 min at 0°C.

In a cell-free system, dry sperm were homogenized with 10 m*M* $CaCl_2$, 10 m*M* $MgCl_2$, 1 m*M* dithiothreitol, and 50 m*M* Tris-HCl at pH 7.5. The homogenate was incubated for 1 h at 20°C.

Assay of glycogen and glucose content

Before and after incubation of dry sperm in ASW, samples of spermatozoa were homogenized with 0.6 *M* perchloric acid. The glycogen content of the homogenate was determined by an enzymatic method (Keppler and Decker, 1984). The acidified homogenate was centrifuged at 10,000 × *g* for 10 min at 4°C, and the supernatant was used for the estimation of glucose after neutralization to pH 6.5–7.0 with KOH. Glucose was measured enzymatically according to the method of Kunst *et al.* (1984).

Analysis of lipids

The total lipid content of the spermatozoa was extracted by the method of Bligh and Dyer (1959) and analyzed by high-performance thin-layer chromatography (HPTLC), according to the method of Macala *et al.* (1983) with some modification, as previously described (Mita and Ueta, 1988, 1989). The amounts of PC, phosphatidylserine (PS), phosphatidylethanolamine (PE), cardiolipin (DPG), TG, Ch, and free fatty acid (FFA) in the sea urchin spermatozoa were determined densitometrically from the standard curves of the respective authentic lipids.

Estimation of lipase and phospholipase activity

Dry sperm were washed twice with 0.21 *M* mannitol, 0.07 *M* sucrose, and 10 m*M* Tris-HCl at pH 7.5 before being homogenized with 10 m*M* $CaCl_2$, 10 m*M* $MgCl_2$, 1 m*M* dithiothreitol, and 50 m*M* Tris-HCl at pH 7.5. The homogenate was incubated with 4.6 kBq [carboxyl-^{14}C]triolein (4.1 GBq/mmol), 2.3 kBq 1-palmitoyl-2-[1-^{14}C]arachidonyl-PC (1.9 GBq/mmol) or 2.3 kBq 1-palmitoyl-2-[1-^{14}C]arachidonyl-PE (1.9 GBq/mmol) for 1 h at 20°C in a total volume of 0.4 ml. The lipids were extracted according to Bligh and Dyer (1959). The radioactivity in the FFA fraction was separated by thin-layer chromatography (TLC) and measured by liquid scintillation spectrometry.

Oxygen consumption

Oxygen consumption in a sperm suspension was measured polarographically with an oxygen consumption recorder (Gilson 5/6H oxygraph, WI). Eighteen microliters of dry sperm (1–2 × 10^9 sperm) was incubated in 1.8 ml ASW in the closed vessel of the oximeter at 20°C. The concentration of saturated oxygen in ASW at 20°C was 234 nmol O_2/ml (Mita and Yasumasu, 1983). The diluted spermatozoa were left exposed to air until their oxygen consumption was determined. Total oxygen consumption was calculated from the respiratory rate and incubation period, as described previously (Mita and Yasumasu, 1983).

Reagents

The lipid standards were purchased from Sigma Chemical (St. Louis, MO). [Carboxyl-^{14}C]triolein, 1-palmitoyl-2-[1-^{14}C]arachidonyl-PC and 1-palmitoyl-2-[1-^{14}C]arachidonyl-PE were obtained from Du Pont–New England Nuclear (Wilmington, DE). All reagents and solvents were of analytical grade. HPTLC and TLC plates (silica gel 60) were obtained from E. Merck (Germany).

Statistical analysis

All data are expressed as means ± SEM for several experiments. Data were statistically analyzed by the Student's *t* test.

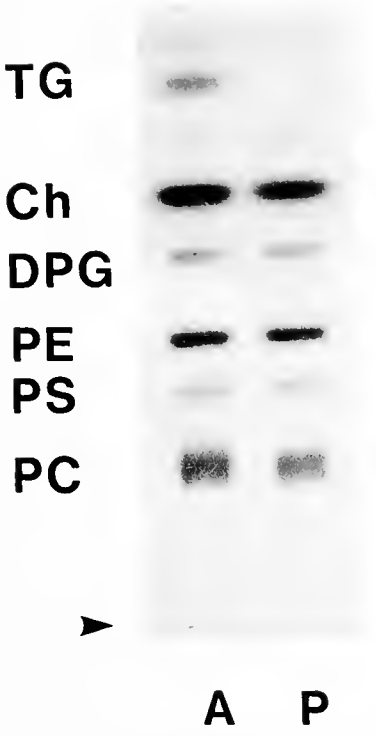

Figure 1. High-performance thin-layer chromatogram of sea urchin sperm lipids. Total lipids were extracted from dry sperm of *Arbacia lixula* (A) and *Paracentrotus lividus* (P) and 10 μg of each were applied to the HPTLC plate. Arrow shows origin.

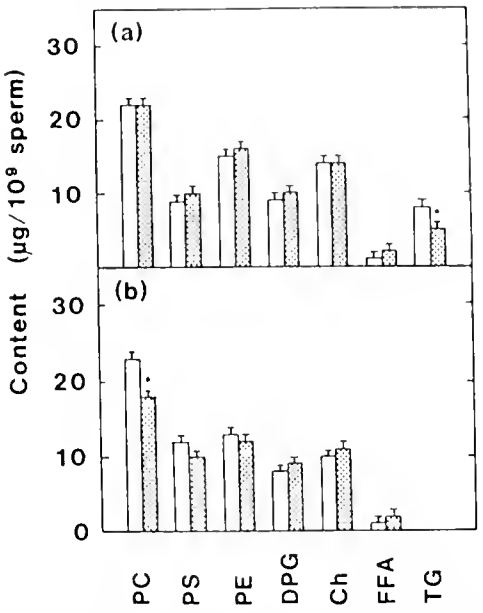

Figure 2. Changes in lipid levels after incubation of *Arbacia lixula* (a) and *Paracentrotus lividus* (b) spermatozoa. Before (clear) and after (dotted) dilution and incubation of dry sperm in seawater for 1 h at 20°C, lipids were extracted and analyzed by HPTLC. Each value is the mean of four separate experiments. Vertical bars show SEM. Data were analyzed statistically by Student's *t* test. **P* values are comparisons with dry sperm values ($P < 0.1$).

Results

Changes in lipid levels after incubation with seawater

The lipids in the spermatozoa of *P. lividus* comprised several kinds of phospholipid and Ch (Fig. 1). Among phospholipids, PC, PS, PE, and DPG were identified in the spermatozoa. Similar phospholipids and Ch were detected in *A. lixula* spermatozoa (Fig. 1). TG was also present at high concentrations in the *A. lixula* spermatozoa, whereas only a trace amount (<1 $\mu g/10^9$ sperm) was detectable in those of *P. lividus*.

When the dry sperm of *A. lixula* were diluted and incubated with ASW for 1 h at 20°C, the TG content decreased from 8 ± 1 $\mu g/10^9$ sperm to 5 ± 1 $\mu g/10^9$ sperm following the initiation of flagellar movement (Fig. 2a). The levels of phospholipids and Ch did not change significantly. In contrast, following incubation of *P. lividus* spermatozoa in ASW, PC decreased from 23 ± 1 $\mu g/10^9$ sperm to 18 ± 1 $\mu g/10^9$ sperm, with no concomitant change in the levels of other phospholipids (Fig. 2b).

Glycogen was present in the spermatozoa of both species, but at extremely low levels (Table I), and only a trace amount of glucose was present (Table I). There were no statistically significant changes during incubation.

Lipid metabolism in a cell-free system

When the homogenate obtained from the dry sperm of *A. lixula* was incubated for 1 h at 20°C, the TG content decreased and the FFA content increased (Table II). Essentially the same situation was found when intact spermatozoa were used (Fig. 2a). However, the levels of PC, PS, PE, DPG, and Ch showed no statistically significant change. On incubating the homogenate from the dry sperm of *P. lividus* for 1 h at 20°C, the PC content decreased (Table III), as it did in the intact spermatozoa (Fig. 2b). A slight decrease in PE content ($P < 0.05$) was

Table I

Change in the level of glycogen and glucose in Arbacia lixula *and* Paracentrotus lividus *spermatozoa*

	Glycogen ($\mu g/10^9$ sperm)		Glucose ($nmol/10^9$ sperm)	
Species	Dry	Incubation for 1 h	Dry	Incubation for 1 h
A. lixula	0.5 ± 0.1	0.4 ± 0.1	tr.	tr.
P. lividus	0.9 ± 0.1	0.8 ± 0.1	tr.	tr.

Dry sperm were diluted 100-fold in ASW and incubated for 1 h at 20°C. Each value is the mean ± SEM obtained from four separate experiments. tr., trace amount (less than 0.1 $nmol/10^9$ sperm).

Table II

Lipid metabolism in a cell-free system of Arbacia lixula *spermatozoa*

Lipids	Content (μg/mg protein)	
	Control	Incubation for 1 h
PC	39 ± 2	39 ± 2
PS	20 ± 1	21 ± 1
PE	28 ± 1	29 ± 2
DPG	16 ± 1	16 ± 1
Ch	24 ± 1	24 ± 1
FFA	3 ± 1	7 ± 1[b]
TG	11 ± 1	7 ± 1[a]

The homogenate of dry sperm with 10 m*M* $MgCl_2$, 10 m*M* $MgCl_2$, 1 m*M* dithiothreitol, and 50 m*M* Tris-HCl at pH 7.5 was incubated for 1 h at 20°C. Each value is the mean ± SEM obtained from three separate experiments. *P* values are comparisons with the control. [a]$P < 0.05$; [b]$P < 0.01$.

also observed during incubation. The FFA and lysophosphatidylcholine (Lyso PC) contents increased remarkably ($P < 0.001$). However, PS, DPG, and Ch levels did not change significantly. A trace amount of TG was present in *P. lividus* spermatozoa.

Phospholipase and lipase activities

When the homogenate of dry sperm from *A. lixula* was incubated with [carboxyl-^{14}C]triolein for 1 h at 20°C, the radioactivity was transferred from TG to FFA (Table IV). Lipase activity was found in *A. lixula* spermatozoa; however, incubation with 1-palmitoyl-2-[1-^{14}C]arachidonyl-PC or 1-palmitoyl-2-[1-^{14}C]arachidonyl-PE showed that only a little radioactivity was transferred to FFA by the action of phospholipase A_2. In the case of *P. lividus* spermatozoa, phospholipase A_2 activity was high, although lipase activity was extremely low (Table IV). The hydrolysis of PE was about one third that of PC. Phospholipase A_2 in *P. lividus* spermatozoa thus appears to have greater substrate specificity for PC.

Table III

Lipid metabolism in a cell-free system of Paracentrotus lividus *spermatozoa*

Lipids	Content (μg/mg protein)	
	Control	Incubation for 1 h
PC	43 ± 2	31 ± 2[a]
Lyso PC	tr.	6 ± 1[b]
PS	23 ± 2	21 ± 1
PE	30 ± 1	24 ± 2[a]
DPG	18 ± 1	20 ± 1
Ch	24 ± 1	23 ± 1
FFA	4 ± 1	25 ± 1[b]
TG	tr.	tr.

The homogenate of dry sperm with 10 m*M* $CaCl_2$, 10 m*M* $MgCl_2$, 1 m*M* dithiothreitol and 50 m*M* Tris-HCl at pH 7.5 was incubated for 1 h at 20°C. Each value is the mean ± SEM obtained from three separate experiments. tr., trace amount (less than 1 μg/10^9 sperm). *P* values are comparisons with the control. [a]$P < 0.05$; [b]$P < 0.001$.

Table IV

Activities of lipase and phospholipase A_2 in Arbacia lixula *and* Paracentrotus lividus *spermatozoa*

Substrate	Activity (nmol FFA released/h/mg protein)	
	A. lixula	*P. lividus*
PC	0.1 ± 0.1	7.9 ± 0.8
PE	tr.	2.4 ± 0.2
TG	1.4 ± 0.3	tr.

Each value is the mean ± SEM obtained from three separate experiments. tr., trace amount (less than 0.1 nmol FFA released/h/mg protein).

Oxygen consumption

Because oxygen is required for oxidation of the lipid, the amount of O_2 consumed by the spermatozoa of *A. lixula* and *P. lividus* was measured at various intervals after dilution in ASW (Fig. 3). The rate of O_2 consumption by the spermatozoa of both species decreased gradually during long-term incubation. In a 1-h incubation, 0.24 ± 0.03 μmol O_2 was consumed by 10^9 *A. lixula* spermatozoa

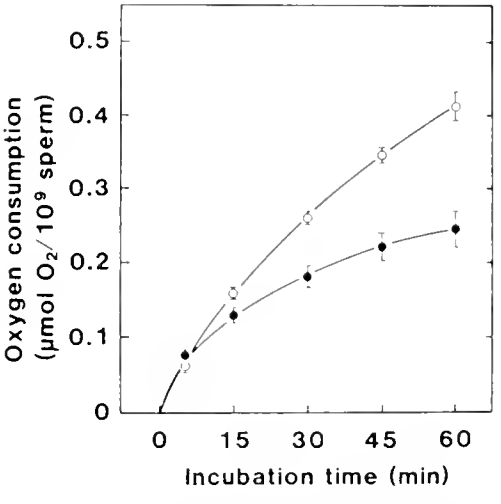

Figure 3. Oxygen consumption in *Arbacia lixula* (●) and *Paracentrotus lividus* (○) spermatozoa. Dry sperm were diluted 100-fold and incubated in seawater at 20°C. Each value is the mean of three separate experiments. Vertical bars show SEM.

and 0.41 ± 0.02 μmol O_2 was consumed by the same number of *P. lividus* spermatozoa.

Discussion

This study showed that the spermatozoa of *A. lixula*, which is a sea urchin of the order Arbacioida (suborder Arbacina), contained a high concentration of TG (Fig. 1). After incubation in ASW for 1 h at 20°C, the TG content of *A. lixula* spermatozoa decreased significantly, with no concomitant change in the levels of phospholipids (Fig. 2a). However, these findings are inconsistent with observations from a previous study (Mohri, 1964), which found that the phospholipid content of *A. lixula* spermatozoa decreased after incubation for 8 h at 20°C. The reason for this discrepancy is unclear, but it is possible that the decrease Mohri observed in phospholipid levels was due to contamination with dead spermatozoa during long-term incubation. Our data also showed lipase activity in *A. lixula* spermatozoa (Table IV). In the cell-free system, a considerable amount of TG was consumed during incubation at 20°C (Table II), indicating that TG is hydrolyzed by lipase. This accords with the results obtained from *G. crenularis* spermatozoa of the order Arbacioida (Mita, 1991). We also found trace amounts of glycogen and glucose in *A. lixula* spermatozoa (Table I). Thus, *A. lixula* spermatozoa may obtain energy through oxidation of fatty acids derived from endogenous TG.

In contrast, the spermatozoa of *P. lividus*, which belongs to the order Echinoida, contained only a trace amount of TG (Fig. 1) and showed low lipase activity (Table IV). The TG level is also low (<1 μg/10^9 sperm) in the spermatozoa of other sea urchins of the order Echinoida (Mita and Ueta, 1988, 1989; Mita and Nakamura, 1993). Thus, it seems unlikely that these spermatozoa use TG as a substrate for energy metabolism. After incubation of *P. lividus* spermatozoa in seawater, PC was shown to decrease significantly, whereas there were no significant changes in the levels of other phospholipids (Fig. 2b). These findings confirm previous reports that the spermatozoa of sea urchins of the order Echinoida use PC as a source of energy (Mita and Ueta, 1988; Mita and Nakamura, 1993). Although we found high concentrations of PC in *A. lixula* spermatozoa (Fig. 2a), there was no statistically significant change in the level of PC during incubation. It appears that this failure to utilize PC is due to the low activity of phospholipase A_2 in *A. lixula* spermatozoa (Table IV).

Our results showed that about 5 μg PC was consumed by 10^9 spermatozoa of *P. lividus* during incubation for 1 h at 20°C (Fig. 2b). Most of the fatty acid moieties in the PC of sea urchin spermatozoa consist of 20 carbons (Mita and Ueta, 1988, 1989; Mita and Nakamura, 1993). On this basis, we calculate that about 15 nmol of fatty acid per 10^9 spermatozoa is released from PC during incubation. The oxidation of 15 nmol fatty acid requires about 0.45 μmol O_2 per 10^9 spermatozoa, and this is consistent with the actual amount of O_2 (about 0.41 μmol) consumed during the 1-h incubation of 10^9 *P. lividus* spermatozoa at 20°C (Fig. 3). Similarly, about 4 μg TG was consumed by 10^9 spermatozoa of *A. lixula* during incubation for 1 h at 20°C (Fig. 2a). The amount of O_2 required to oxidize the fatty acid from this TG was calculated by basically the same procedure used to calculate PC consumption in *P. lividus* spermatozoa. The theoretical value is about 0.25 μmol O_2 in 10^9 spermatozoa, which correlates well with the actual consumption (Fig. 3).

In mammalian species, carbohydrate in the seminal plasma and female reproductive tract has been postulated to be responsible for the motility of spermatozoa (Peterson and Freund, 1976). Without seminal plasma, however, mammalian spermatozoa can maintain motility under aerobic conditions (Lardy and Phillips, 1941a). During incubation, the amount of endogenous phospholipid diminishes (Lardy and Phillips, 1941b). Thus, mammalian spermatozoa may also be capable of using endogenous lipids, particularly phospholipids, for energy metabolism.

It is interesting that the metabolic system responsible for energy production in the spermatozoa of sea urchins differs in the orders Arbacioida and Echinoida. On morphological grounds, it is generally considered that sea urchins of the order Echinoida have diverged further than those of the order Arbacioida (Mortensen, 1943; Durham and Melville, 1957; Shigei, 1974). Accordingly, replacement of TG by PC as the substrate may reflect differentiation or specialization of spermatozoa in the Echinoida. Presumably sea urchins of the order Echinoida, which have lost TG as a source of energy in their spermatozoa, are provided with a metabolic system that uses phospholipids, particularly PC.

Acknowledgments

This work was supported by the Japanese Society for Promotion of Science (JSPS) and the Italian National Research Council (CNR).

Literature Cited

Bligh, E. G., and W. J. Dyer. 1959. A rapid method of total lipid extraction and purification. *Can. J. Biochem.* **37**: 911–917.

Christen, R., R. W. Schackmann, and B. M. Shapiro. 1982. Elevation of intracellular pH activates sperm respiration and motility of sperm of the sea urchin *Strongylocentrotus purpuratus*. *J. Biol. Chem.* **257**: 14881–14890.

Christen, R., R. W. Schackmann, and B. M. Shapiro. 1983. Metabolism of sea urchin sperm. Interrelationships between intracellular pH, ATPase activity, and mitochondrial respiration. *J. Biol. Chem.* **258**: 5392–5399.

Durham, J. W., and R. V. Melville. 1957. A classification of echinoids. *J. Paleontol.* **31**: 242–272.

Evans, J. A., and I. R. Gibbons. 1986. Activation of dynein 1 adenosine triphosphatase by organic solvents and by Triton X-100. *J. Biol. Chem.* **261:** 14044–14048.

Gibbons, B. H., and I. R. Gibbons. 1972. Flagellar movement and adenosine triphosphatase activity in sea urchin sperm extracted with Triton X-100. *J. Cell Biol.* **54:** 75–97.

Keppler, D., and K. Decker. 1984. Glycogen. Pp. 11–18 in *Methods of Enzymatic Analysis*, H. U. Bergmeyer, ed. Vol. 6. VCH Publishers, Weinheim.

Kunst, A., B. Draeger, and J. Ziegenhorn. 1984. D-Glucose. Pp. 163–172 in *Methods of Enzymatic Analysis*, H. U. Bergmeyer, ed. Vol. 6. VCH Publishers, Weinheim.

Lardy, H. A., and P. H. Phillips. 1941a. The interrelation of oxidative and glycolytic processes as sources of energy for bull spermatozoa. *Am. J. Physiol.* **133:** 602–609.

Lardy, H. A., and P. H. Phillips. 1941b. Phospholipids as a source of energy for motility of bull spermatozoa. *Am. J. Physiol.* **134:** 542–548.

Macala, L. J., R. K. Yu, and S. Ando. 1983. Analysis of brain lipids by high performance thin-layer chromatography and densitometry. *J. Lipid Res.* **24:** 1243–1250.

Mita, M. 1991. Energy metabolism of spermatozoa of the sea urchin *Glyptocidaris crenularis*. *Mol. Reprod. Dev.* **28:** 280–285.

Mita, M., and M. Nakamura. 1993. Phosphatidylcholine is an endogenous substrate for energy metabolism in spermatozoa of sea urchins of the order Echinoidea. *Zool. Sci.* **10:** 73–83.

Mita, M., and N. Ueta. 1988. Energy metabolism of sea urchin spermatozoa, with phosphatidylcholine as the preferred substrate. *Biochim. Biophys. Acta* **959:** 361–369.

Mita, M., and N. Ueta. 1989. Fatty chain composition of phospholipids in sea urchin spermatozoa. *Comp. Biochem. Physiol.* **92B:** 319–322.

Mita, M., and N. Ueta. 1990. Phosphatidylcholine metabolism for energy production in sea urchin spermatozoa. *Biochim. Biophys. Acta* **1047:** 175–179.

Mita, M., and I. Yasumasu. 1983. Metabolism of lipid and carbohydrate in sea urchin spermatozoa. *Gamete Res.* **7:** 133–144.

Mohri, H. 1957a. Endogenous substrates of respiration in sea-urchin spermatozoa. *J. Fac. Sci. Univ. Tokyo IV* **8:** 51–63.

Mohri, H. 1957b. Fatty acid oxidation in sea-urchin spermatozoa. *Annat. Zool. Jap.* **30:** 181–186.

Mohri, H. 1964. Phospholipid utilization in sea-urchin spermatozoa. *Pubbl. Sta. Zool. Napoli* **34:** 53–58.

Mortensen, T. 1943. *A Monograph of the Echinoidae.* Vol. 6, Part 3, pp. 277–440. C. A. Reitzel, Copenhagen.

Peterson, R. N., and M. Freund. 1976. Metabolism of human spermatozoa. Pp. 176–186 in *Human Semen and Fertility Regulation in Men*, E. S. E. Hafez, ed. The C. V. Mosby Company, St. Louis.

Rothschild, Lord, and K. W. Cleland. 1952. The physiology of sea-urchin spermatozoa. The nature and location of the endogenous substrate. *J. Exp. Biol.* **29:** 66–71.

Shigei, M. 1974. Echinoids. Pp. 208–332 in *The Systematic Zoology*, T. Uchida, ed. Vol. 8b. Nakayama, Tokyo.

Reference: *Biol. Bull.* **186:** 291–299. (June, 1994)

Functional Consequences of Phenotypic Plasticity in Echinoid Larvae

MICHAEL W. HART[1] AND RICHARD R. STRATHMANN

Friday Harbor Laboratories, 620 University Road, Friday Harbor, Washington 98250, and Department of Zoology, NJ-15, University of Washington, Seattle, Washington 98195

Abstract. Phenotypic plasticity in feeding structures has been described for several larvae of marine invertebrates, including four species of echinoids. In these echinoids, larvae grown with scarce food grow a longer ciliated band than larvae grown with abundant food. Such phenotypic plasticity may be functionally significant if longer ciliated bands permit higher feeding rates when food is scarce. We replicate an earlier result showing that larvae of a sand dollar, *Dendraster excentricus*, grow longer ciliated bands in culture with scarce food. We show that these larvae can capture suspended food particles at the tips of longer arms, and that longer ciliated bands result in higher maximum clearance rates. The maximum clearance rate is enhanced by this phenotypic plasticity both early and late in larval life. However, longer ciliated bands did not completely compensate for reduced food supply: larvae grown with scarce food needed more time to complete larval development and metamorphosed into smaller juvenile sand dollars relative to larvae grown with abundant food.

Introduction

Phenotypic plasticity of form and development can affect the evolution of structures, behaviors, and life histories (Newman, 1988; Stearns, 1989; West-Eberhard, 1989). Mechanisms that produce plasticity should evolve when an advantageous alternative phenotype is reliably signaled, the demand for the alternative form is unpredictable, and the cost of expressing the alternative phenotype is high (Harvell, 1990). Demonstrating the functional significance of induced forms or behaviors requires knowledge of the natural history of species and their interactions with mates, food, predators, and the environment (*e.g.*, Dodson, 1989).

Marine invertebrate larvae exhibit a phenotypic plasticity modulated by the abundance of planktonic food (*e.g.*, Strathmann *et al.*, 1993). The echinopluteus larvae of sea urchins and sand dollars develop as two compartments that are partly independent physiological and developmental units. The larval feeding structure is a band of ciliated epithelial cells borne on long larval arms (Strathmann, 1971). The beat of these cilia is responsible for swimming and feeding by larvae (Strathmann, 1971). In contrast, the postlarval structures develop as a disc-shaped rudiment on the left side of the larval stomach (Okazaki, 1975). The two structures are functionally and developmentally independent of each other: the juvenile rudiment is not functional until very late in larval life, and the ciliated band is dismantled during metamorphosis (Okazaki, 1975). In at least four species of echinoids, larvae respond to low food levels in laboratory culture (Boidron-Metairon, 1988; Hart and Scheibling, 1988; Strathmann *et al.*, 1992) and in the plankton (Fenaux *et al.*, 1994) by altering the allocation of scarce materials to the growth of the ciliated band and the juvenile rudiment: when food is scarce, larvae grow longer arms and ciliated bands, and development of the rudiment is delayed.

Phenotypic plasticity of ciliated band growth may be a common adaptation among larvae of echinoids: it is shared by members of the Clypeasteroida and Echinoida, which diverged more than 200 million years ago (Wray, 1992). This type of plasticity of growth may have evolved more than once within the class, or it may be a shared ancestral feature of all extant echinoids. This plasticity has been assumed to be adaptive because it results in a larger feeding structure when food is scarce (Strathmann *et al.*, 1992). A measure of capacity for capturing food is

Received 15 October 1993; accepted 9 March 1994.

[1] Present address: Institute of Molecular Biology and Biochemistry, Simon Fraser University, Burnaby, BC, V5A 1S6, Canada.

the maximum clearance rate; clearance rate is the volume of water cleared of food per time. Ciliated band length is correlated with maximum clearance rate in comparisons among developmental stages of echinoid larvae (Strathmann, 1971; Hart, 1991). However, the effect of phenotypic plasticity of ciliated band growth on maximum clearance rates of plutei has not been measured.

We present an experimental test of the functional significance of phenotypic plasticity of ciliated band growth in echinoid larvae. (1) We show that larvae of the sand dollar *Dendraster excentricus* grow ciliated bands that are longer—in absolute length and in proportion to the size of the juvenile rudiment—when food is scarce (this effect of food on allometric growth of larvae was previously demonstrated for *Dendraster* by Boidron-Metairon, 1988). (2) The arms of plutei grow at the tips, and larvae with longer ciliated bands have grown longer arms by extending the arm tips. If particles cannot be caught near the arm tips, then variation in maximum clearance rates of larvae may be unrelated to or indirectly related to phenotypic plasticity of arm and band length. We show that larvae with longer arms and ciliated bands can capture particles at the tips of these longer arms. (3) Finally, we show that maximum clearance rates of larvae grown with scarce food are higher—in absolute units (early and late in development) and in relation to the growth of the juvenile rudiment (during most of the larval period)—than feeding rates for larvae grown with abundant food.

Materials and Methods

Adult sand dollars were collected at a site north of Puget Sound near Olga, Orcas Island, Washington State. Gametes were obtained for two experiments by injecting adults with 0.5 *M* KCl on 12 and 20 April 1993. Within an experiment, all embryos and larvae for the experiment were full siblings, obtained from eggs of a single female and sperm of a single male. In the first experiment, eggs were 128 μm in diameter (mean of 10 measurements, with all variation within ± 4 μm, the unit of measurement). In the second experiment, eggs were 130 μm in diameter (mean of 10 measurements, with variation not detectable within the 4-μm units of measurement).

When larvae were nearly ready to begin feeding (near the end of the second day), they were divided among replicate jars, with an estimated 300 larvae per jar. The first experiment had three replicate jars per treatment; the second experiment had two replicate jars per treatment. Each jar contained 1.5 l of seawater that had been filtered through a 0.45-μm membrane filter. The water was mechanically stirred by paddles pulled at 10 strokes min^{-1} (Strathmann, 1987). Jars were maintained at room temperature, which varied with the weather; but for the intervals of both experiments and for food treatments within experiments, the mean temperatures (17.7–17.9°C) were similar, and the range of temperatures (16.5–19°C) was the same.

Water was changed every 2 days by removing more than 1.3 l from the jars and replacing it with water that had been filtered the day before and held at room temperature. Antibiotics were added at each water change for a concentration of 30 μg penicillin ml^{-1} and 50 μg streptomycin sulfate ml^{-1}.

At every water change, cells of the alga *Rhodomonas* sp. were added to achieve a total concentration of 5.0 cells μl^{-1} for high food in both experiments, 0.3 cells μl^{-1} for low food in the first experiment, and 0.25 cells μl^{-1} for low food in the second experiment. Three replicate jars were used for each food treatment. After the last observations on clearance rates and larval dimensions in the first experiment, the remaining larvae were reared to maturity for a test of competence for metamorphosis (food concentrations in the jars were not measured precisely during this period, but were approximately 5.0 or 0.3 cells μl^{-1}). Experimental rearing for the first experiment was discontinued after testing for metamorphosis at 13 days of age (high food treatment) and 40 days (low food treatment). The second experiment was terminated when the animals were 9 days old.

The algal species and concentrations were selected on the basis of previous studies of echinoderm larvae. *Rhodomonas* has been determined to be a superior food for echinoplutei (Hinegardner, 1969; Leahy, 1986). With algae of similar size, echinoderm larvae reduced their clearance rates with more than 5.0 cells μl^{-1} (Strathmann, 1971), and grew at maximum rates at concentrations between 2 and 10 cells μl^{-1} (Lucas, 1982; Fenaux *et al.*, 1988); larvae of *D. excentricus* developed shorter arms and larger rudiments at 15 days of age when fed 6.0 cells μl^{-1} in contrast to 0.5 cells μl^{-1} (Boidron-Metairon, 1988).

We made videorecordings (30 frames s^{-1}) of single, free-swimming larvae as they captured 15-μm-diameter polystyrene spheres from suspension in 0.45-μm membrane-filtered seawater. For most larvae, the concentration of spheres was 3 μl^{-1}; for some very large larvae, we reduced the concentration of spheres to 1 or 2 μl^{-1}. Larvae were observed in a 63-ml chamber surrounded by a water-filled jacket that helped to buffer temperature changes during observation. Mean temperature $\pm$ 1 standard deviation (21.4 ± 0.7°C) and the range of temperatures (20–23°C) for these observations were several degrees higher than those for larval rearing.

From these videotapes, we chose intervals of continuous swimming and feeding by each larva, and from these intervals we counted particle captures. We converted the counts of particle captures to clearance rates by dividing the time rate of capture by the concentration of spheres

in suspension. Because these intervals do not include periods when feeding was slow or ceased, our method estimates maximum clearance rate for these larvae.

We measured the following morphological features of each larva after removing it from the observation chamber: posterior body length (from the posterior end to the postoral transverse ciliated band), stomach length (anterior to posterior), juvenile rudiment diameter, and ciliated band length (see Strathmann *et al.*, 1992). Body and stomach lengths were used as measures of the growth and development of larval parts that are not involved in particle capture. All of these features were measured from camera lucida drawings. Ciliated band length was measured by McEdward's (1985) method for three-dimensional reconstruction. Our criterion for rudiment formation was contact between the invaginating epidermal surface (the amnion) and the left coelom.

Differences among jars and between the two experiments but within treatments (only high or only low food) were tested by Model I analysis of covariance (ANCOVA). Measures of larval dimensions or clearance rates were dependent variables, larval age was the independent variable, and effects of jars and the two experiments were combined into a single covariate. These tests are therefore equivalent to comparisons of growth or increase in feeding rate during development among five different groups of larvae treated similarly (though reared in different containers or at different times). Because we assessed five simultaneous comparisons within each food treatment (four morphological variables and clearance rate), we discounted the usual alpha value for these tests by the sequential Bonferroni correction for multiple contrasts (Rice, 1989). There were no significant differences among jars or experiments (estimated as the interaction between larval age and the jar covariate) at either high or low concentrations of food. Plots of data for larval dimensions and clearance rates indicated no differences among jars or between experiments. Because effects of jars or experimental runs were not evident in statistical tests and inspection of plots, plutei from replicate jars and from the two experiments were lumped within treatments in the analysis of effects of high and low food.

Effects of food on larval dimensions and clearance rates were first tested with the interaction between food level and larval age included in a Model I ANCOVA. In these tests, if effects of the interaction were not significant ($P \geq 0.063$) and the F ratio for the interaction was less than twice the value of $F_{0.50}$ (Paull, 1950), we tested for effects of food level and age without including the interaction term in the ANCOVA model.

The relationships among rudiment diameter, stomach length, ciliated band length, and clearance rate were compared for the two food treatments in a Model II ANCOVA using the method of Hess (1993). Slopes were compared by a Student's t test (Clarke, 1980; McArdle, 1988). Elevations were not considered different if one elevation fell within the asymmetrical 95% confidence limits of the other.

Analyses of variance and covariance assume linear relationships between dependent and independent variables. In some cases, these bivariate relationships appeared nonlinear. We tested linearity in these plots by fitting quadratic regressions to each curve and estimating the value of the second-order coefficient in these regressions. For 18 simultaneous tests (Figs. 1, 2, 4, 5), we discounted the usual alpha value by the Bonferroni correction. We found four cases of significant nonlinear relationships: between ciliated band length or stomach length and larval age for larvae fed the smaller ration (Fig. 1A, B), and between maximum clearance rate and larval age for both groups of larvae (Fig. 4A). In the first two cases, we restricted our analysis of covariance to one portion of the data set (for larvae <10 days old) in which band length and stomach length increase linearly with age. In the other cases (Fig. 4A), we could not find an appropriate solution because both bivariate relationships were nonlinear but the curves differed in shape: that for larvae fed the larger ration was concave up (the second-order coefficient was significant and >0), and that for larvae fed the smaller ration was concave down (the second-order coefficient was significant and <0). We do not know of a single transformation that will render both relationships linear. We present the analysis of covariance of the untransformed data, acknowledging that this particular comparison violates an assumption of the test.

Metamorphosis of larvae from the first experiment was induced by exposure of larvae to materials associated with adult sand dollars. Sand from an aquarium with adult sand dollars was mixed with a small amount of water. Water and fine debris were then passed through a 70-μm-mesh sieve into bowls. Each bowl received larvae from a different jar, with initially an estimated 120 larvae per bowl. Larvae were exposed to water from adult sand at 13 days of age (high food treatment) or at 40 days (low food treatment). Remaining larvae and metamorphosed juveniles were counted the next day. We also measured the lengths of the tests of juveniles. We compared test diameters of juveniles in a nested analysis of variance, with jars nested within food treatments.

Results

Growth and development

The effects of algal food concentration on relative growth of the ciliated band of *Dendraster* larvae have been described previously by Boidron-Metairon (1988). Our measurements of larval growth and development in response to algal food are similar to hers. Though our mor-

phological results are not new, we present them in detail to show the basis for the observed differences in feeding capabilities of larvae.

Each of the four morphological measurements increased during larval development, and growth rate for each measurement varied significantly with food ration. Ciliated band length, stomach length, midline body length, and juvenile rudiment diameter increased more rapidly with larval age for larvae fed the larger food ration (Fig. 1). In the last case, the age of onset of rudiment formation was also delayed by several days for larvae fed the smaller ration. In each case, the statistical interaction between larval age and food ration was highly significant ($F_{1,d} > 51.90$, $P < 0.001$), where the denominator degrees of freedom (d) was 97 for larval dimensions (77 when only larvae <10 days old were considered; see Materials and Methods above) and 50 for rudiment diameters (the analysis of rudiment diameters included only those larvae in which rudiment formation had begun).

Growth of the ciliated band with respect to food ration was slightly more complex than growth of the other morphological measures. For older larvae (>7 days old), those fed the larger ration grew faster and therefore had longer ciliated bands, and there was a significant main effect of food ration on band length ($F_{1,43} = 18.268$, $P < 0.001$) (the interaction between food ration and larval age was not significant; $F_{1,42} = 3.616$, $P = 0.064$). However, for younger larvae (<7 days old), there was no significant interaction between food ration and larval age ($F_{1,52} = 3.071$, $P = 0.086$). The main effect of food ration on band length in the ANCOVA was not significant ($F_{1,53} = 1.864$, $P = 0.178$). This result suggests that larvae fed very small rations are initially capable of developing feeding structures as large as those of larvae fed larger rations.

A surprising difference is hidden in the apparent similarity of ciliated band lengths for larvae <7 days old from the two food treatments. If only the youngest larvae (3 days old) are considered, ciliated bands were significantly

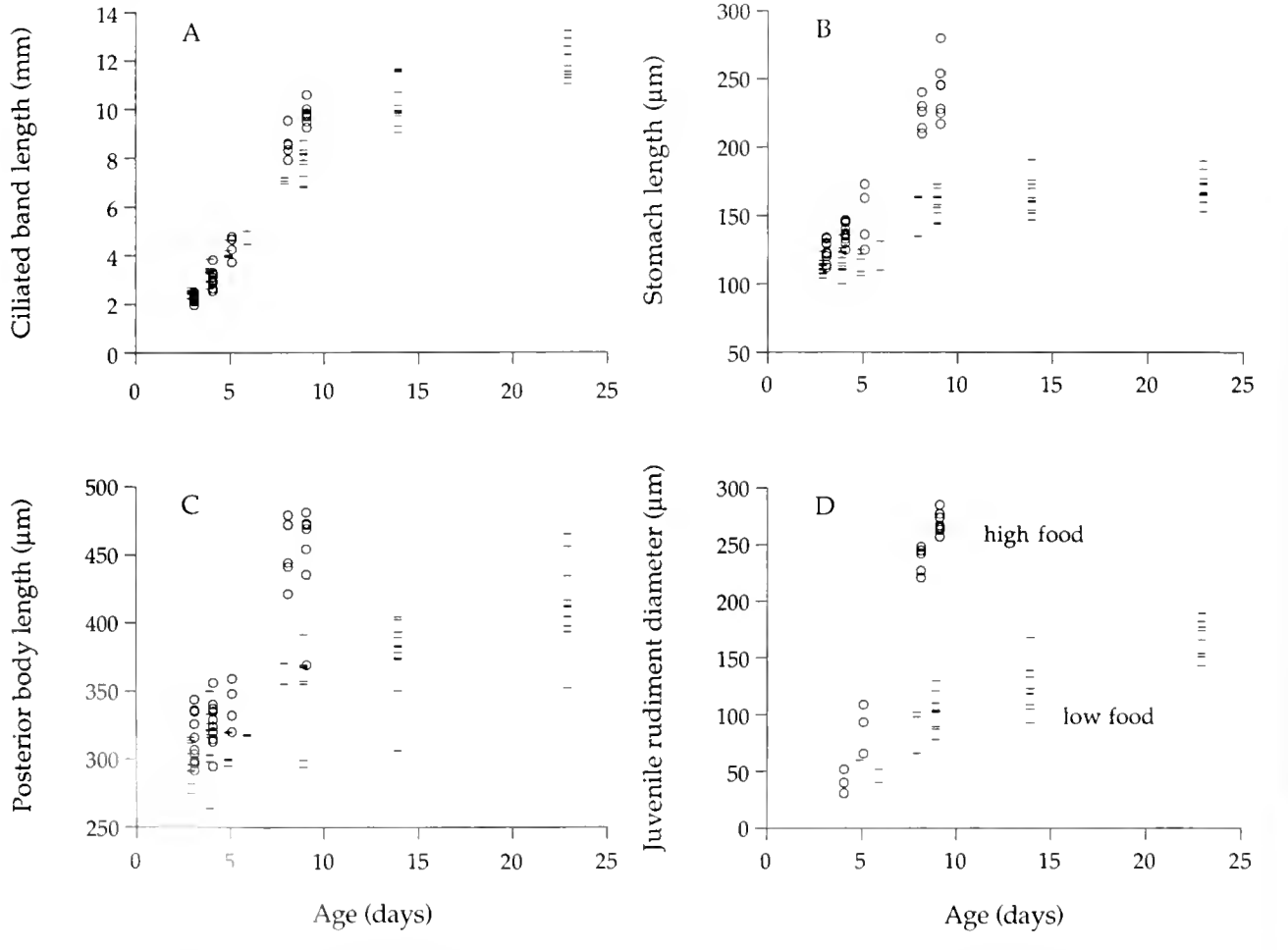

Figure 1. Growth of *Dendraster excentricus* larvae fed a small (250 or 300 cells ml^{-1}) or a large (5000 cells ml^{-1}) ration of *Rhodomonas* sp. Bars show larvae fed the small ration; circles show larvae fed the large ration. For clarity, values for different food rations on a single day are offset by ±0.2 days. A. Ciliated band length. B. Stomach length. C. Posterior body length. D. Juvenile rudiment diameter.

Table I

Ciliated band lengths and maximum clearance rates of 3-day-old Dendraster excentricus *larvae fed different concentrations of algal food (*Rhodomonas *sp)*

Food ration (cells ml^{-1})	Ciliated band length (mm)	Maximum clearance rate (μl min^{-1})
5000	2.28 ± 0.16	1.60 ± 0.29
300	2.46 ± 0.16	1.91 ± 0.29

Each entry is mean ± 1 standard deviation for 11 cases. Both comparisons (between food rations) are statistically significant ($P < 0.02$).

longer for those grown with scarce food than for those with abundant food (Table I) ($t = 2.946$, $P = 0.008$). This comparison gives the clearest example of altered allocation of materials to the feeding structure in response to food ration: the absolute length of ciliated band can be greater for larvae growing with scarce food. Because larvae fed the larger ration grew faster, this early difference in size was not apparent when all larvae 3–7 days old were considered.

In our experiments, many larvae fed the larger ration were capable of metamorphosis when 13 days old, and few of these larvae grew ciliated bands >10 mm (Fig. 1D). In contrast, larvae fed the smaller ration required much more time to reach metamorphic competence, and they continued to grow longer ciliated bands (up to 13.2 mm). Ciliated bands of all 23-day-old larvae from these cultures were longer than the longest bands measured for any larvae fed the larger ration.

Dendraster larvae also showed potential for allometric growth of the ciliated band relative to other parts of the posterior body in response to differences in food ration. Band length was greater relative to stomach length (for all larvae, Fig. 2A) or to rudiment diameter (for older larvae in which rudiment development had begun, Fig. 2B). There was a significant interaction between stomach or rudiment size and food ration (for both comparisons, $t > 4.81$, $P < 0.001$). In this sense, larvae fed the two different food rations follow different physiological rules for allocation of materials into growth of the feeding structure and the postlarval structures: if these allocation rules were fixed, then the two sets of data in Figure 2A or 2B should coincide. As a consequence of altering these allocation rules, larvae fed a smaller food ration develop a larger feeding structure relative to the growth of postlarval parts, and the feeding structure eventually grows larger in absolute size than the feeding structures of larvae fed a larger ration.

Particle capture at arm tips

Dendraster larvae fed either ration could capture polystyrene spheres at the arm tips. Figure 3, for example, shows a sphere captured at the tip of the right postoral arm of a 14-day-old larva feeding at 11.5 μl min^{-1}; this sphere made contact with the ciliated band twice more, at locations progressively nearer to the mouth, before it was ingested. The sequence of events (from initial capture to ingestion) took about 1.7 s (51 video frames), and the particle was transported about 700 μm from the tip to the base of the arm. This capture (and others like it) resembles particle captures described previously (Strathmann, 1971; Hart, 1991) and occurs by the localized reversal of the beat of cilia (Strathmann *et al.*, 1972; Hart, 1990).

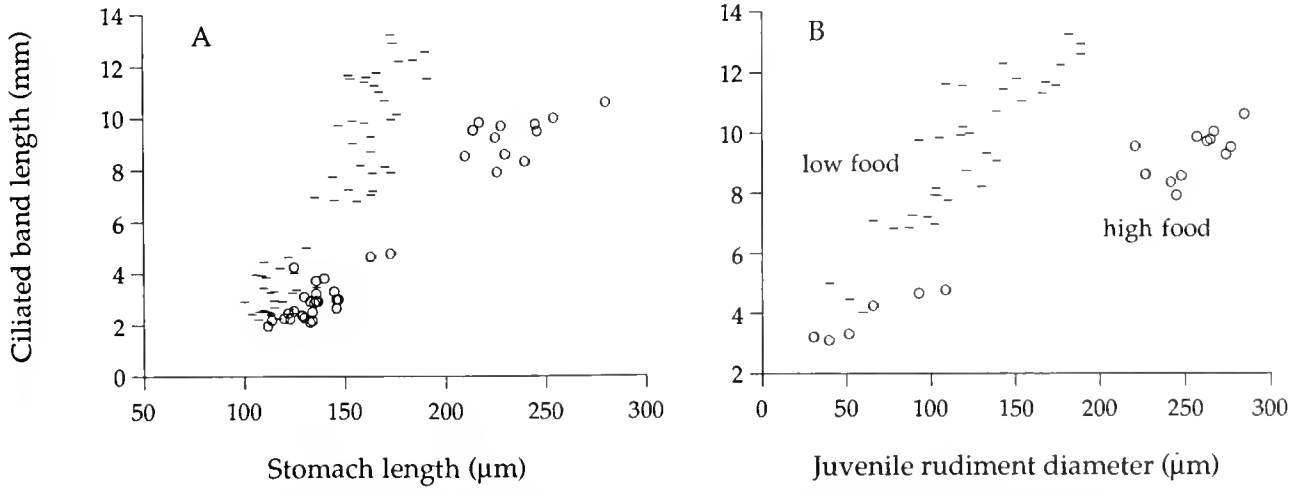

Figure 2. Ciliated band lengths relative to other measures of size of *Dendraster excentricus* larvae fed a small (250 or 300 cells ml^{-1}) or a large (5000 cells ml^{-1}) ration of *Rhodomonas* sp. Bars show larvae fed the small ration; circles show larvae fed the large ration. A. Ciliated band lengths relative to stomach length. B. Ciliated band lengths relative to juvenile rudiment diameter.

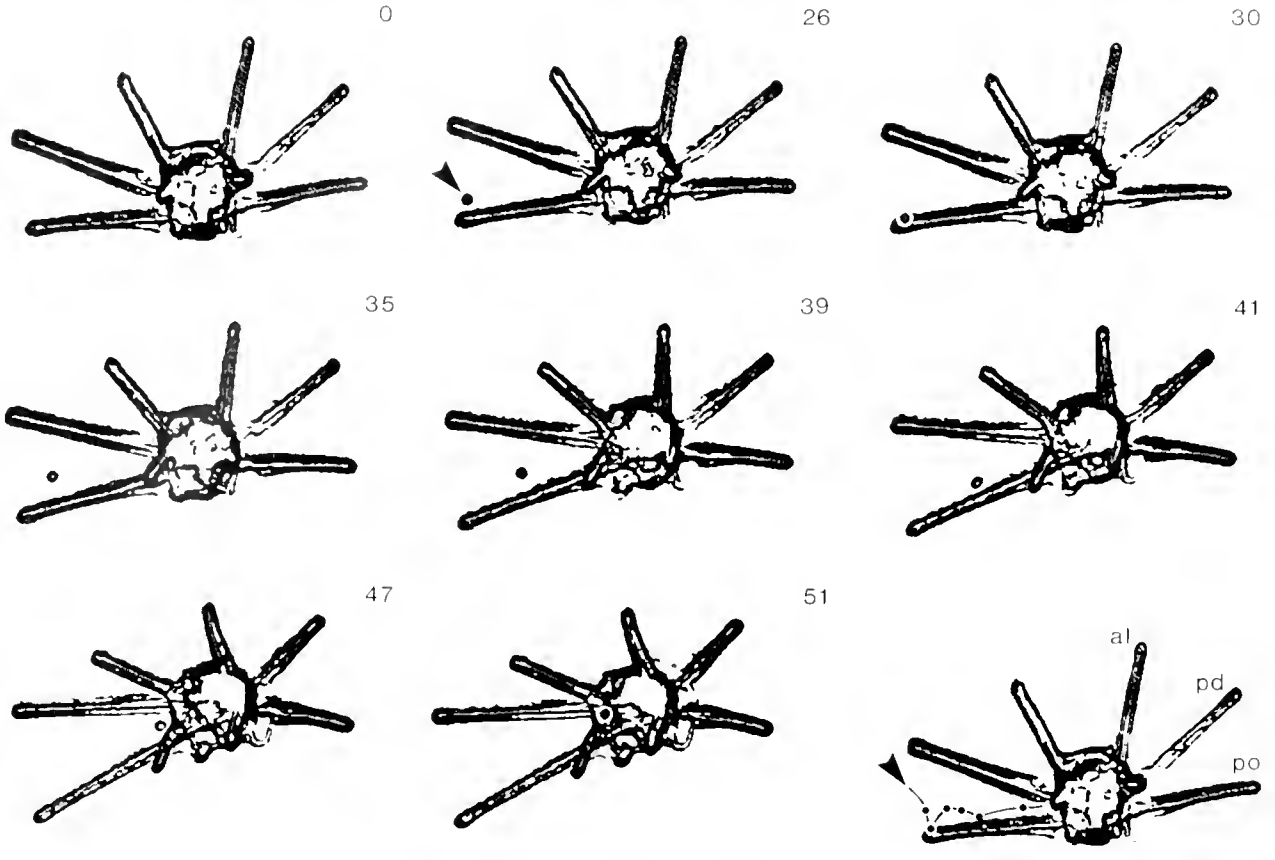

Figure 3. Capture of a polystyrene sphere by an 8-day-old *Dendraster excentricus* larva fed 250 cells ml^{-1} *Rhodomonas* sp. The larva is shown in anterior ventral view (swimming up toward the video camera). Video frame number (30 frames s^{-1}) is shown in the upper right of each panel. Each video frame was edited to enhance contrast and reduce background pixel values to near zero. An unintended result of this editing is an increase in the apparent size of the polystyrene sphere (by about 2×). The sphere (arrow) came into focus at frame 26, was captured with a localized change in direction of the ciliary current at the tip of the right postoral arm (30–35), moved toward the larval midline (39), was captured again midway along the length of the arm (41–47), and was ingested (51). Inset (lower right): interpolated path of the captured sphere begins at the arrow; dots show the location of the sphere in frames 26–47. For scale, the right postoral arm is about 700-μm long (actual scale is not known). Abbreviations: al, anterolateral arm; pd, posterodorsal arm; po, postoral arm.

Clearance rates

Maximum clearance rates of echinoderm larvae are highly correlated with ciliated band lengths (Strathmann, 1971; Hart, 1991). Developmental changes in feeding rates of *Dendraster* larvae were associated with changes in band length (Fig. 4A). For larvae >7 days old, there was a significant interaction between the effects of food ration and larval age on maximum clearance rate ($F_{1,42} = 9.497$, $P = 0.004$). Clearance rates increased more rapidly with age for larvae fed the larger ration, because these larvae rapidly grew ciliated bands at an early age. However, larvae fed the smaller ration eventually grew longer bands, and their clearance rates surpassed those of the largest larvae fed the larger ration. Mean maximum clearance rates of 23-day-old larvae (12.46 ± 1.63 μl min^{-1}, $n = 10$) fed the smaller ration were significantly greater than clearance rates of 9-day-old larvae fed the larger ration (10.28 ± 2.80 μl min^{-1}, $n = 7$) ($t = 2.687$, $P = 0.017$). For larvae <7 days old, there was no significant interaction between the effects of food ration and larval age on maximum clearance rate ($F_{1,52} = 0.315$, $P = 0.577$) and no significant main effect of food ration ($F_{1,53} = 3.603$, $P = 0.063$).

The functional significance of increased ciliated band length for larvae developing with scarce food is most evident from two comparisons: (1) maximum clearance rates of 3-day-old larvae with different band lengths, and (2) maximum clearance rates of larvae as a function of development of the postlarval structures. First, for 3-day-old larvae, clearance rates of larvae fed the smaller ration were significantly higher than those of larvae fed the larger

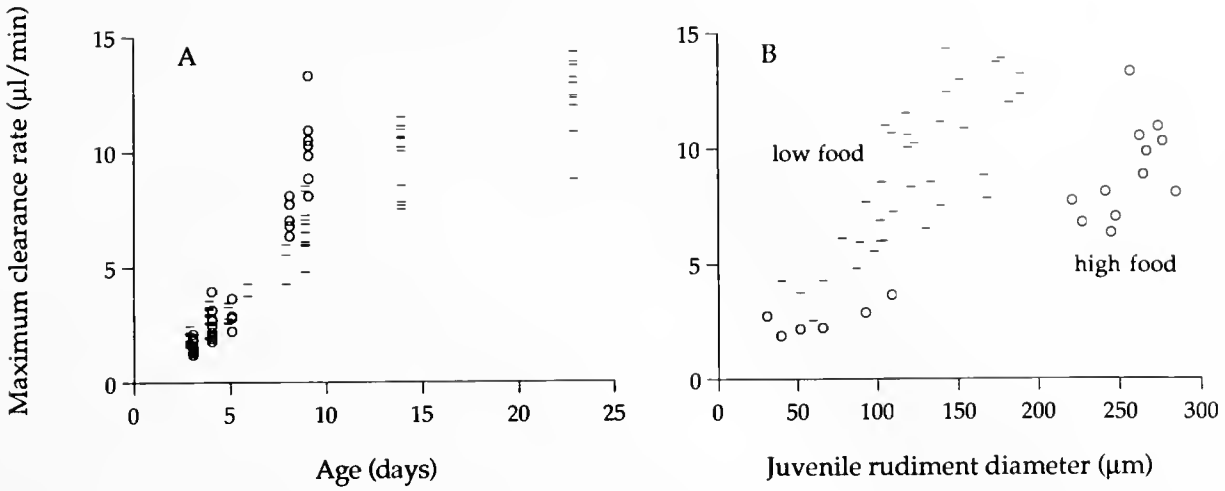

Figure 4. Maximum clearance rates of *Dendraster excentricus* larvae fed a small (250 or 300 cells ml^{-1}) or a large (5000 cells ml^{-1}) ration of *Rhodomonas* sp. Bars show larvae fed the small ration; circles show larvae fed the large ration. A. Clearance rates for larvae of different age. B. Clearance rates relative to juvenile rudiment diameter.

ration (Table I) ($t = 2.543$, $P = 0.019$). This difference demonstrates that the earliest manifestation of phenotypic plasticity in these larvae is accompanied by a measurable increase in feeding rate for larvae with scarce food. Second, at any stage of development of the juvenile rudiment, clearance rates of larvae fed the smaller ration were substantially higher than those of larvae fed the larger ration (Fig. 4B), and there was a significant interaction between the effects of food ration and rudiment diameter on feeding rate ($t = 4.927$, $P < 0.001$). A qualitatively similar result is obtained if stomach length or posterior body length is used as the index of growth and allocation to the development of postlarval structures. This difference demonstrates the functional consequences of altered rules for allocation of scarce materials within the larva later in development.

Growth with scarce food might have other effects on maximum clearance rate than an increase in ciliated band length, but we have no evidence of such additional effects. Maximum clearance rates increased with ciliated band length for larvae fed both rations (Fig. 5), and the relationship between feeding rate and band length was not significantly different between the two groups. There was no significant interaction between the effects of band length and food ration ($t = 0.208$, $P > 0.50$) and no significant main effect of food ration (the 95% confidence intervals around the estimated regression intercepts overlapped broadly, and the confidence intervals of each estimate included the estimated intercept of the other). This result suggests that maximum clearance rates per length of ciliated band are similar for larvae following different allocation rules for the growth of larval and postlarval parts. The only functional differences between larvae fed the two rations are that larvae fed the smaller ration allocate more material to the growth of the ciliated band, develop higher clearance rates at any stage of the development of postlarval structures, and eventually grow very long ciliated bands and develop very high feeding rates.

Survival and metamorphosis

The high survival rate in the cultures indicated that the observed differences in growth, allocation, and feeding rate were the result of developmental plasticity, not selective mortality of different genotypes at different concentrations of food. In the first experiment, survival—when adjusted for larvae removed for observation—was close to 100% at day 13 with both high and low concentrations of food. (Errors in the initial count resulted in a 5% apparent increase in larvae.) Survival remained high during continued observations of larvae in the three jars at the low concentration of food, with 78 to 81% survival over the next 23 days. In the second experiment, survival in the four jars was 88 to 98% on day 9, at the termination of the experiment.

Larvae from the first experiment were tested for competence for metamorphosis. More larvae proved competent at 13 to 14 days with abundant food than were competent at 40 to 41 days with scarce food, though the stimulus from the adult sand could also have differed (Table II). This result confirmed that the larvae on the smaller ration did develop more slowly toward competence for metamorphosis and did attain competence eventually. Larvae with abundant food formed larger juvenile tests than did larvae with scarce food (Table II). There were significant differences in test diameter among replicate

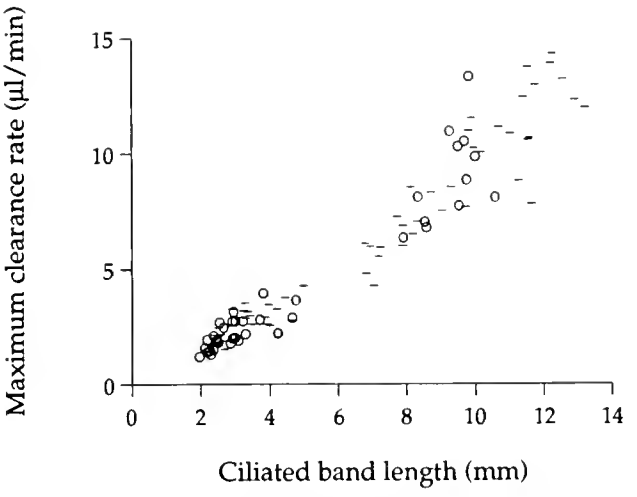

Figure 5. Maximum clearance rates relative to ciliated band length of *Dendraster excentricus* larvae fed a small (250 or 300 cells ml^{-1}) or a large (5000 cells ml^{-1}) ration of *Rhodomonas* sp. Bars show larvae fed the small ration; circles show larvae fed the large ration.

jars ($F_{3,95} = 6.051$, $P < 0.001$). In spite of this variation among jars, tests of individuals from the high food ration were significantly larger than those from the low food ration ($F_{1,3} = 15.943$, $P = 0.028$). The difference in test diameter appears to have resulted from differences in food for larvae rather than from different stages in the competent period, because percent metamorphosing was not related to mean test length.

Discussion

Our observations on form, particle captures, and clearance rates of *Dendraster* larvae demonstrate that phenotypic plasticity of arm growth and ciliated band length in plutei is functionally significant: it increases feeding rate when food is scarce. Plutei grow longer arms and ciliated bands, while the growth of the postlarval parts is delayed. The lengthened portions of the arms can capture particles, and thus clearance rates are increased absolutely and in relation to the development of postlarval parts.

We found phenotypic plasticity of larval growth at two stages of development. Early in development, larvae growing with scarce food were able to grow longer ciliated bands than were larvae of the same age with abundant food, after only one day of feeding. Late in development, larvae with scarce food also grew longer ciliated bands than did larvae with abundant food, but this difference did not appear until after larvae with abundant food had completed development and metamorphosis. This late difference in size must result from altered allocation of materials acquired during larval feeding. The contrast between results for early and late larval stages suggests that the scope for phenotypic plasticity early in development may depend on egg size, whereas the scope for plasticity later in development may depend on factors such as the efficiency of food digestion and assimilation.

Under the conditions of our experiment, increased growth of the ciliated band did not completely compensate for differences in amount of food: larvae feeding on the smaller ration took longer to complete larval development through metamorphosis and became smaller juveniles. Phenotypic plasticity of ciliated band length increased clearance rates of larvae feeding on the smaller ration, but we do not know whether this plasticity results in faster development than could occur with a fixed pattern of ciliated band growth when food is scarce. If so, then phenotypic plasticity of ciliated band growth might be adaptively (as well as functionally) significant. For example, such compensation might account for some of the observed insensitivity of larval growth to food abundance in the wild (see Olson and Olson, 1989).

The adaptive significance of this phenotypic plasticity in echinoplutei could be tested by comparing development times and postmetamorphic sizes for larvae following two different growth rules under the same conditions of scarce food: one rule favoring growth of the ciliated band (the bars in Fig. 2B), and another rule favoring growth of the juvenile rudiment (the circles in Fig. 2B). Unfortunately, larvae cannot yet be induced to follow the second allocation rule when they are grown with scarce food. We suggest, however, that this may be accomplished by manipulation of thyroid hormones (THs). Chino *et al.* (1994) recently described effects of TH supplements on development of the juvenile rudiment of three echinoid species. They show that late-stage plutei can be induced to form the juvenile rudiment in a dose-dependent response to exogenous TH in the absence of algal food, and they suggest that much of the TH found in larvae originates in algal food (larvae appear to synthesize little TH).

Table II

Metamorphosis of Dendraster excentricus *larvae fed high and low rations of food*

Food ration (cells ml^{-1})	Metamorphosed (%) $n = 120$	Test diameter (µm) $n = 20$
5000	68	341 ± 13
	58	336 ± 15
	22	352 ± 9
300	48	320 ± 11
	20	315 ± 15
	0	—

Larvae fed the high ration were 13 days old; larvae fed the low ration were 40 days old. Each entry is a result for one replicate jar. Test diameter (mean ± 1 standard deviation) does not include spines.

Acknowledgments

We were supported by NSF grant OCE9301655, the Natural Sciences and Engineering Research Council of Canada, and the Friday Harbor Laboratories. M. Strathmann helped with larval culture and L. Stockwell helped collect adult sand dollars. L. McEdward designed the equipment for measurement of ciliated band lengths.

Literature Cited

Boidron-Metairon, I. F. 1988. Morphological plasticity in laboratory-reared echinoplutei of *Dendraster excentricus* (Eschscholtz) and *Lytechinus variegatus* (Lamarck) in response to food conditions. *J. Exp. Mar. Biol. Ecol.* **119:** 31–41.

Chino, Y., M. Saito, K. Yamasu, T. Suyemitsu, and K. Ishihara. 1994. Formation of the adult rudiment of sea urchins is influenced by thyroid hormones. *Dev. Biol.* **161:** 1–11.

Clarke, M. R. B. 1980. The reduced major axis of a bivariate sample. *Biometrika* **67:** 441–446.

Dodson, S. 1989. Predator-induced reaction norms. *Bioscience* **39:** 447–452.

Fenaux, L., C. Cellario, and F. Rassoulzadegan. 1988. Sensitivity of different morphological stages of the larva of *Paracentrotus lividus* (Lamarck) to quantity and quality of food. Pp. 259–266 in *Echinoderm Biology*, R. D. Burke, P. V. Mladenov, P. Lambert, and R. L. Parsley, eds. Balkema, Rotterdam.

Fenaux, L., M. F. Strathmann, and R. R. Strathmann. 1994. Five tests of food-limited growth of larvae in coastal waters by comparisons of rates of development and form of echinoplutei. *Limnol. Oceanogr.*, **39:** 84–98.

Hart, M. W. 1990. Manipulating external Ca^{2+} inhibits particle capture by planktotrophic echinoderm larvae. *Can. J. Zool.* **68:** 2610–2615.

Hart, M. W. 1991. Particle capture and the method of suspension feeding by echinoderm larvae. *Biol. Bull.* **180:** 12–27.

Hart, M. W., and R. E. Scheibling. 1988. Comparing shapes of echinoplutei using principal components analysis, with an application to larvae of *Strongylocentrotus droebachiensis* Pp. 277–284 in *Echinoderm Biology*, R. D. Burke, P. V. Mladenov, P. Lambert, and R. L. Parsley, eds. A. A. Balkema, Rotterdam.

Harvell, C. D. 1990. The ecology and evolution of inducible defenses. *Quart. Rev. Biol.* **65:** 323–340.

Hess, H. C. 1993. The evolution of parental care in brooding spirorbid polychaetes: the effect of scaling constraints. *Am. Nat.* **141:** 577–596.

Hinegardner, R. T. 1969. Growth and development of the laboratory cultured sea urchin. *Biol. Bull.* **137:** 465–475.

Leahy, P. S. 1986. Laboratory culture of *Strongylocentrotus purpuratus* adults, embryos, and larvae. Pp. 1–13 in *Methods in Cell Biology*, Vol. 27, T. E. Schroeder, ed. Academic Press, New York.

Lucas, J. S. 1982. Quantitative studies of feeding and nutrition during larval development of the coral reef asteroid *Acanthaster planci* (L.). *J. Exp. Mar. Biol. Ecol.* **65:** 173–193.

McArdle, B. H. 1988. The structural relationship: regression in biology. *Can. J. Zool* **66:** 2329–2339.

McEdward, L. R. 1985. An apparatus for measuring and recording the depth dimension of microscopic organisms. *Trans. Am. Microsc. Soc.* **104:** 194–200.

Newman, R. A. 1988. Adaptive plasticity in development of *Scaphiopus couchii* tadpoles in desert ponds. *Evolution* **42:** 774–783.

Okazaki, K. 1975. Normal development to metamorphosis. Pp. 177–232 in *The Sea Urchin Embryo*, G. Czihak, ed. Springer, Berlin.

Olson, R. R., and M. H. Olson. 1989. Food limitation of planktotrophic marine invertebrate larvae: Does it control recruitment success? *Annu. Rev. Ecol. Syst.* **20:** 225–247.

Paull, A. E. 1950. On a preliminary test for pooling mean squares in the analysis of variance. *Ann. Math. Statist.* **21:** 539–556.

Rice, W. R. 1989. Analyzing tables of statistical tests. *Evolution* **43:** 223–225.

Stearns, S. C. 1989. The evolutionary significance of phenotypic plasticity. *Bioscience* **39:** 436–445.

Strathmann, M. F. 1987. *Reproduction and Development of Marine Invertebrates of the Northern Pacific Coast. Data and Methods for the Study of Eggs, Embryos, and Larvae.* University of Washington Press, Seattle. 670 pp.

Strathmann, R. R. 1971. The feeding behavior of planktotrophic echinoderm larvae: mechanisms, regulation, and rates of suspension feeding. *J. Exp. Mar Biol. Ecol.* **6:** 109–160.

Strathmann, R. R., T. L. Jahn, and J. R. C. Fonseca. 1972. Suspension feeding by marine invertebrate larvae: clearance of particles by ciliated bands of a rotifer, pluteus, and trochophore. *Biol. Bull.* **142:** 505–519.

Strathmann, R. R., L. Fenaux, and M. F. Strathmann. 1992. Heterochronic developmental plasticity in larval sea urchins and its implications for evolution of nonfeeding larvae. *Evolution* **46:** 972–986.

Strathmann, R. R., L. Fenaux, A. T. Sewell, and M. F. Strathmann. 1993. Abundance of food affects relative size of larval and postlarval structures of a molluscan veliger. *Biol. Bull.* **185:** 232–239.

West-Eberhard, M. J. 1989. Phenotypic plasticity and the origins of diversity. *Annu. Rev. Ecol. Syst.* **20:** 249–278.

Wray, G. A. 1992. The evolution of larval morphology during the post-Paleozoic radiation of echinoids. *Paleobiology* **18:** 258–287.

Reference: *Biol. Bull.* **186:** 300–308. (June, 1994)

Laboratory Studies on Molting and Growth of the Shore Crab, *Hemigrapsus sanguineus* de Haan, Parasitized by a Rhizocephalan Barnacle

TOHRU TAKAHASHI AND SHUHEI MATSUURA

Department of Fisheries, Faculty of Agriculture, Kyushu University, Hakozaki, Fukuoka 812, Japan

Abstract. Molting of shore crabs (*Hemigrapsus sanguineus*) parasitized by rhizocephalans (*Sacculina senta*) was observed in the laboratory, and the growth of the molted crabs was compared with that of unparasitized animals. Molting of the host was obstructed by the infestation, but was still possible. After the release of several broods of larvae, the externa (the external reproductive system of the parasite) detached from the host. Subsequent molting occurred within 40 days in about 80% of the animals, but in the remainder, it was delayed for at most 4 months. Soon after molting, a new externa protruded from the abdomen of every crab. Thus, the life-span of the externa and the molting of the host would seem to be closely connected. In the female, the molt frequency was reduced, but the molt increment of the parasitized crabs was not different from that in the unparasitized ones. In the male, however, both the molt frequency and the molt increment were reduced. Thus, the annual growth of parasitized males and females was about half that of unparasitized crabs.

Introduction

Rhizocephala (Crustacea, Cirripedia) are exclusively parasitic on crustaceans, mainly Decapoda. The first larva of a rhizocephalan hatches from the egg as a nauplius. Females of the subsequent larva (cypris) infect the host, and part of the parasite protrudes from the host's abdomen, acting as a saccular reproductive organ (externa). Male cypris larvae migrate through the mantle cavity of the externa into a receptacle where the male larva metamorphoses into a mass of sperm cells (Ichikawa and Yanagimachi, 1958, 1960; Yanagimachi, 1961a, b; Ritchie and Hoeg, 1981; Lützen, 1984; Hoeg, 1982, 1985a, b, 1987).

The internal part of the rhizocephalan parasite (the interna) branches and thus penetrates various parts of the body of the crustacean host, taking nourishment from its tissues. The effects on the host include difficulty in molting, changes in secondary sexual characteristics, and degeneration of the sexual organs (Reinhard, 1956; Hartnoll, 1967). In particular, sacculinized brachyuran crabs usually cease to molt after the parasite appears external to the host (Veillet, 1945; Reinhard, 1956; Hartnoll, 1967; Lützen, 1984).

Although such pervasive effects might be expected to decrease host survivorship or host reproduction, many local populations of *Hemigrapsus sanguineus* (Decapoda: Grapsidae) are, in fact, heavily infected by *Sacculina senta* (Cirripedia: Rhizocephala). In Amakusa and some other localities in Japan, the prevalence exceeds 70% and is positively correlated with size (Fig. 1, preliminary survey in April 1988). Sacculinized crabs are common among the large size classes, and many of the infected male crabs are feminized in their external form, having a wider abdomen and smaller chelipeds than unparasitized males.

The observed feminization of male crabs presents us with an apparent contradiction, for crustaceans cannot change their external form without molting. Indeed, Reinhard (1956) and Hartnoll (1967) mentioned that all the modifications of male hosts must appear before the externa erupts, since the presence of the externa prevents any further molting of the host.

Received 24 May 1993; accepted 25 February 1994.

Address for correspondence: Department of Fisheries, Faculty of Agriculture, Kyushu University, 6-10-1, Hakozaki, Higashi-ku, Fukuoka 812, Japan.

Abbreviations: U, unparasitized crabs; P, parasitized crabs displaying the externa(e) of *Sacculina*, and internally infected crabs; CW, carapace width.

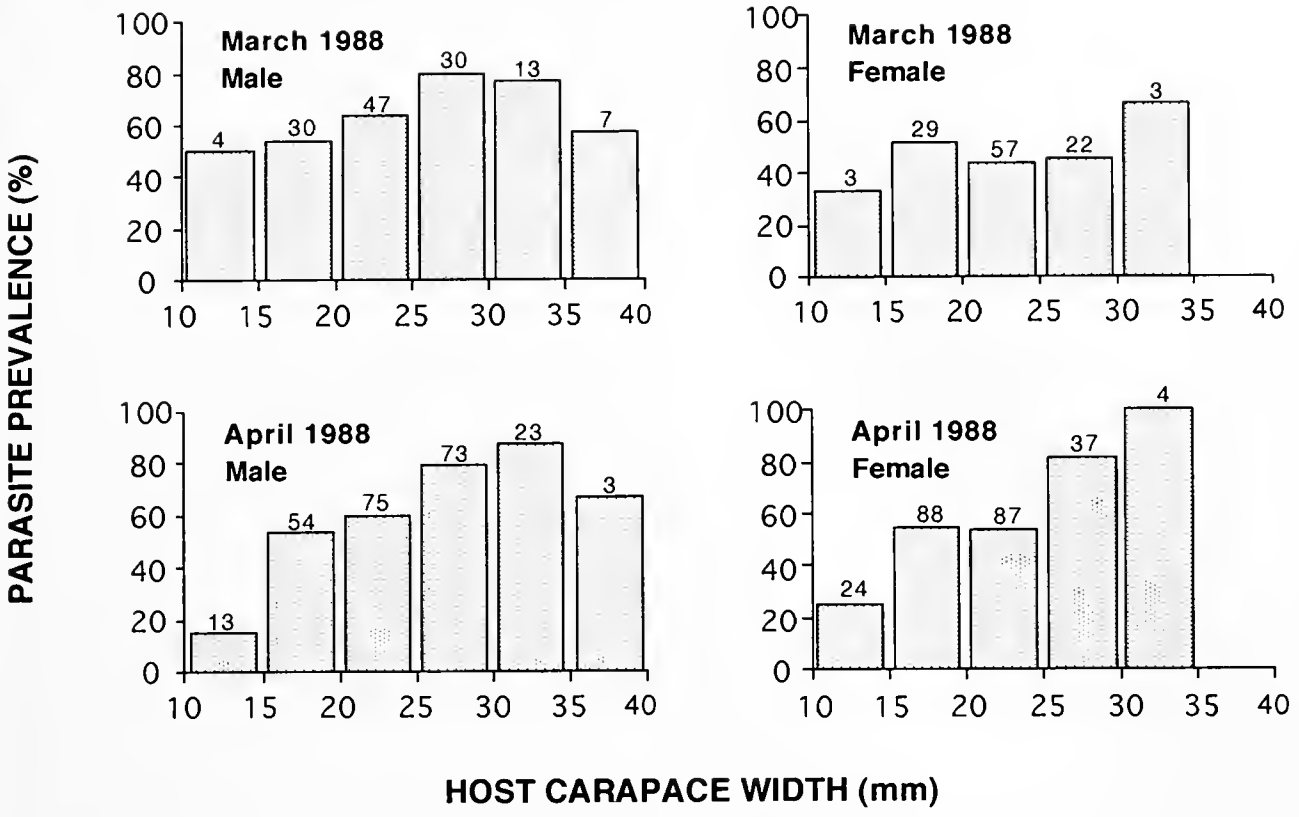

Figure 1. Size-specific prevalence (%) of *Hemigrapsus sanguineus* parasitized by *Sacculina senta*. Animals were adult males and females (>10 mm in carapace width) collected at Inuki Estuary, Amakusa, Japan, in April 1988. Numbers above each column represent the total number of animals collected in each size class.

O'Brien (1984) showed that the majid crab *Pugettia producta*, when parasitized by the sacculinid *Heterosaccus californicus*, undergoes a reduced number of molts preceding the allometric molt of puberty. The externa of the parasite emerges after this molt of puberty, which then becomes the terminal molt of *P. producta*. Such precocious maturity among parasitized crabs results in a negative relationship between size and prevalence; *i.e.*, the prevalence decreases with the host size. O'Brien and Van Wyk (1985) emphasized that this host-parasite relationship is characteristic of sacculinid infections.

However, the positive size-prevalence pattern of *Hemigrapsus sanguineus*, as shown in Figure 1, does not conform to that of *P. producta*. It indicates that host-sacculinid relationships do not share a single mechanism. The natural molt format of *H. sanguineus* is different from that of *P. producta:* the pubertal molt of *H. sanguineus* is not a terminal molt. Although many brachyurans do not stop molting after the molt of puberty, host-sacculinid relationships of such groups are little known, except that parasitized *Carcinus maenas* may resume molting if the externa of the *Sacculina carcini* is detached (Day, 1935; Veillet, 1945; Lützen, 1981).

This study demonstrates that parasitized shore crabs, *Hemigrapsus sanguineus*, do not stop molting or growing. We have investigated their molting processes and compared the growth of parasitized and unparasitized crabs. Finally, we infer the causal factor leading to the positive size-prevalence pattern of *H. sanguineus*.

Materials and Methods

Sacculinized crabs were collected from the pebbled intertidal zone of Inuki Coast (32°25′ N, 130°25′ E), Amakusa, Kyushu, Japan, where their prevalence had been found to be about 70% (Fig. 1). Unparasitized crabs were collected from Tomoe Cove (32°32′ N, 130°02′ E), Tomioka, Amakusa, where the prevalence of parasitized animals is below 1%.

From 1 February 1989 to 30 June 1990 (17 months), 40 adult crabs (>15 mm in carapace width) were kept in the laboratory (Aitsu Marine Biological Station, Kumamoto University). When one crab died, another specimen would be supplied, so that 64 crabs (36 sacculinized and 28 unparasitized) were reared during this study. As some of the sacculinized crabs carried multiple externae, a total

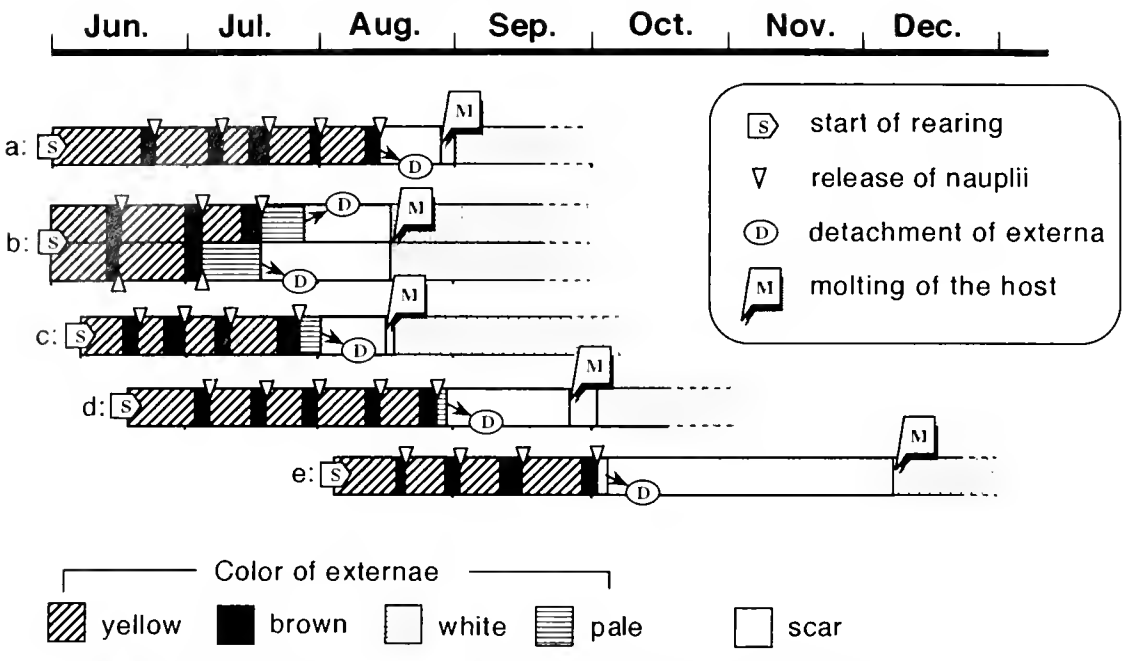

Figure 2. Examples of successive reproduction of the parasites and subsequent molting of the hosts. a–e: Six externae on five hosts changed their color along with the development of their incubated eggs. b: The host had two externae.

of 47 externae were attached on the 36 sacculinized crabs at the beginning of rearing. The crabs, kept individually in small plastic boxes with several holes (about 1.0 cm in diameter) in the bottom, were reared in running seawater that had been passed through a sand filter system to prevent any additional invasion by the cypris or nauplius larvae of *Sacculina*.

The mussel *Musculus senhousia* (Bivalvia, Mytilidae) and the green alga *Ulva pertusa* were kept in these plastic cases as nonpolluting living foods that could be eaten by the crabs at any time. In addition, at 1–3 day intervals, the crabs were fed artificial pellets that are ordinarily used for Kuruma prawn culture (Higashimaru Co., Ltd.). The quantity of food was controlled individually at each observation time, so there was always a little left over.

The color of the externae changed as the incubated eggs of the parasite developed, so the externae of the parasites were classified into four categories according to color (see Results). Before and after the molting of the host, the carapace width (CW) of the host was measured, with a hand caliper, to the nearest 0.05 mm.

Any increase in size at ecdysis was determined as the relative molt increment [100 (CW of postmolt − CW of premolt)/CW of premolt].

The various terms and abbreviations used in this paper are as follows:

Unparasitized crab (U): defined on the basis of its external appearance (no externa or scar, and not castrated); crabs with an internal infestation could not be completely excluded.

Sacculinized crab: parasitized crabs displaying one or more externae of *Sacculina senta*.

Parasitized crab (P): externally parasitized crabs ("sacculinized crabs") plus internally infected crabs that are not yet carrying externae or that have already lost their externae.

Results

Detachment of externae and subsequent molting of the host

The newly erupted externae are distinguishable because they are colorless, lack a mantle opening, and are less than 3 mm in diameter. They are virgin females; if a male cypris invades the receptacle, the externa begins to grow and change color. The color first gradually changes to yellow, then becomes brown when the externa contains embryos with eyes.

Thus, the color of externae can be classified into four categories: (1) white (virgin externa; maximum diameter is less than 3 mm); (2) yellow (normal type externa, with male cells in the receptacles); (3) brown (externa packed with mature embryos with eyes); and (4) pale (empty externa).

Some examples of the changes in the externae are shown in Figure 2. These externae dropped off the host after

several spawnings of nauplii. The other externae, which could not be drawn in Figure 2, showed similar succession patterns. The interval between two spawnings varied according to the temperature of the seawater. For instance, the interval was about 12 days in August when the average seawater temperature was 26.7°C; in November (18.3°C) it was 24 days. There was considerable individual variation.

While the eggs of a sacculinid were being incubated, its next brood was already being prepared. After the release of several broods of larvae, the externa detached, leaving a scar on the abdomen of the host. Only then was the host able to molt (Fig. 2).

Table I shows the number of days required for the host crab to molt after the externa had fallen off, and the number of days from the time of molting to the appearance of a new externa during the year from May 1989 to April 1990. The temporal distribution of the molt with respect to the detachment of the externae is shown in Table II. The unparasitized control crabs most frequently molted in July, whereas the parasitized animals had a broader molting period—from July to September. Although the parasites released larvae throughout the year, most of the detachment of externae occurred between June and October. Following detachment, most parasitized crabs molted within about 1 month. For instance, of the eight sacculinized crabs that lost their externae in June 1989, one specimen molted in June and the other seven molted before the end of July. In 21 of the 31 examples (67.7%), molting resumed within 30 days; in 25 examples (80.6%), it occurred within 40 days (Tables I and II).

The new externae sometimes appeared within 1–2 days after molting, when the carapace of the host was still soft; but others appeared later, after the host's new shell had become hard (Table I). One crab molted twice, and the new externa appeared after the second molting. Consequently, among 31 parasitized hosts, externae reappeared in all but one host, which failed in molting and died (Table I).

Table I

Time between the detachment of the externa and the next molt, and between that molt and the appearance of a new externa

Date of detachment of externa	Time to next molt (days)	Water temperature; from detachment to next molt (mean, range)	Time from molt to new externa (days)
31 May 1989	30	21.8, 20.9–22.5	7
2 June	18	21.6, 20.9–22.0	1
3 June	33	21.9, 20.9–22.5	3
5 June	32	21.9, 20.9–22.7	0
	8 +		
25 June	35*	22.4, 22.1–22.5	9**
		24.2, 22.1–25.9	
25 June	9	22.4, 22.1–22.5	17
25 June	8	22.4, 22.1–22.5	43
27 June	10	22.5, 22.1–22.7	0
30 June	23	23.6, 22.1–24.9	0
11 July	23	24.6, 23.8–25.7	1
16 July	16	25.1, 24.6–25.7	2
21 July	12	25.4, 24.9–25.7	3
22 July	29	26.4, 25.7–27.0	0
28 July	31	26.7, 26.5–27.0	0
10 August	9	26.8, 26.6–27.0	6
13 August	14	26.8, 26.5–26.7	4
21 August	51	24.9, 19.9–27.1	3
25 August	15	26.4, 25.7–27.1	2
27 August	112	21.6, 15.0–27.1	0
27 August	31	25.9, 24.6–27.1	***
31 August	28	25.7, 24.6–26.9	2
2 September	23	25.6, 24.6–25.9	0
3 September	6	25.8, 25.7–25.9	1
5 September	28	25.5, 24.6–26.2	1
12 September	13	25.5, 24.6–25.9	2
27 September	124	18.0, 9.8–24.9	2
2 October	117	18.0, 9.8–24.9	5
5 October	29	22.0, 19.9–24.6	3
6 October	72	19.4, 15.0–24.6	4
26 October	9	21.2, 20.8–21.5	0
9 January 1990	101	13.3, 9.8–16.2	13

* Molted twice (8 days to first molt and 43 days to second molt.
** Days from second molt.
*** Died (failed to molt).

Effects on growth of the host

The growth rate of crustaceans generally varies with the water temperature and is also affected by reproductive conditions. Because the temperature of the seawater is not stable and molting is seasonal, growth rates in different months could not be compared. Furthermore, because adult crabs (CW > 15 mm) molt only two or three times a year, only the relative growths of crabs that lived through a certain half or one-year period were compared (Table III). The half-year periods that were compared were between 1 April 1989 and 30 September 1989 (Section I), and between 1 October 1989 and 31 March 1990 (Section II). The one-year period was defined as extending from 15 April 1989 to 14 April 1990 because the number of crabs that lived a full year was greatest during that time.

In both sexes, the mean annual relative growth of parasitized crabs was about half that of unparasitized crabs. But the discrepancy between the growth of unparasitized and parasitized female crabs appears to have a different basis from that in males. Throughout Sections I and II, relative growths and relative molt increments of the parasitized males were clearly smaller than those of the unparasitized males. The molt frequency (number of molts) of the parasitized males was significantly smaller than that of the unparasitized males during the one-year period, though the difference was not significant during Section I or Section II. None of the parasitized female crabs molted during Section II. During Section I, all of the seven un-

Table II

Distribution of the detachment of externae and subsequent molts in each month (May 1989–April 1990)

Months when crabs lost externae	Number of crabs that lost externae	Month when parasitized crabs next molted [**number of crabs** (Days, or range, between loss of externa and molt)]											
		May	June	July	Aug	Sept	Oct	Nov	Dec	Jan	Feb	Mar	Apr
May	1		**1** (30)										
June	8		**1** (18)	**7** (8–35)									
July	5				**5** (12–31)								
Aug	7				**2** (9, 14)	**3** (15–31)	**1** (51)		**1** (112)				
Sep	5					**3** (6–23)	**1** (28)			**1** (124)			
Oct	4							**2** (9, 29)	**1** (72)	**1** (117)			
Nov	0												
Dec	0												
Jan	1												**1** (101)
Feb	0												
Mar	0												
Apr	0												
													Sample
Total molts per month	P	0	2	7	7	6	2	2	2	2	0	0	1	31
	U	1	1	10	2	0	4	3	3	1	1	0	2	28

P = parasitized; U = unparasitized controls.

parasitized females listed in Table I were ovigerous once, and their molt frequency, relative growth, and relative molt increments were not significantly different from those of the parasitized crabs ($P > 0.05$, Student's t test). Therefore, the difference between the annual growth of unparasitized and parasitized female hosts was mainly due to a difference in the molt frequency during Section II, whereas that of the males was due to a difference in both the molt frequency and the relative molt increment.

In Figure 3A, every relative molt increment of the male crabs is plotted against the premolt carapace width. The relative molt increments of the unparasitized control males tended to decrease with increasing crab size, and this fact should be noted when considering the male groups of this experiment: *i.e.*, the average premolt carapace width of the parasitized males used in this study [22.38 mm ± 3.55 (SD) ($n = 16$)] was significantly larger than that of the unparasitized males [19.10 mm ± 3.95 (SD) ($n = 14$)] ($P < 0.05$, t test). On the other hand, there was no significant difference between the average premolt carapace width of parasitized females [19.23 ± 2.50 (SD) ($n = 15$)] and that of unparasitized females [19.92 ± 2.85 (SD)] ($P = 0.49$, t test).

The regression line showing the correlation between the relative molt increment and carapace width for unparasitized control males was

$$Y = 31.95 - 0.88X,\ r = 0.61,$$

comparable to that reported for this species by Kurata (1962)

$$Y = 28.61 - 0.69X,\ r = 0.86,$$

(recalculated by us for animals larger than 15 mm) ($P > 0.05$, ANCOVA). To eliminate this size effect, the regression line for parasitized males

$$Y = 21.24 - 0.57X,\ r = 0.44$$

was compared with that for the unparasitized males used in this experiment and with that from Kurata (1962). The intercept of parasitized males was significantly smaller than that of the unparasitized males, both in this experiment and in that of Kurata (1962) ($P < 0.05$, ANCOVA). But the regression line calculated for parasitized males lacks any significant reliability ($P > 0.05$, F test). Then, translating the Y axis of Figure 3A into real postmolt carapace width, the regression lines of parasitized and unparasitized males were redrawn in Figure 3B (the so-called Hiatt's growth diagram; Hiatt, 1948). The regression lines that were recalculated are as follows:

$$\text{U: } Y = 3.51 + 0.97X\ (r = 0.95,\ P < 0.01,\ F \text{ test})$$

$$\text{P: } Y = 2.42 + 0.97X\ (r = 0.97,\ P < 0.01,\ F \text{ test}).$$

These two regression lines are parallel, but the intercept of parasitized males was significantly smaller than that of unparasitized males ($P < 0.05$, ANCOVA). Consequently,

Table III

Molt frequency, relative growth, and relative molt increments of crabs that lived through two half-year periods or that lived longer than one year

Period	Number of crabs	Number of molts in period (mean)	Relative growth (%)[a]: [means (SD)]	Relative molt increment (%)[b]: [means (SD)]
1 April 1989–30 September 1990 (Section I)	U ♂ 7	10 (1.43)	21.31 (9.45)	14.34 (4.04)
	P ♂ 5	4 (0.80)	5.95 (5.46)**	7.44 (4.99)**
	U ♀ 7	10 (1.43)	19.20 (8.74)	12.95 (3.53)
	P ♀ 4	6 (1.50)	19.84 (12.29)	12.59 (4.05)
1 October 1989–31 March 1990 (Section II)	U ♂ 8	6 (0.75)	12.16 (12.20)	15.79 (3.27)
	P ♂ 14	5 (0.36)	3.51 (5.55)*	9.84 (4.73)*
	U ♀ 9	7 (0.78)	8.84 (5.88)	11.37 (3.54)
	P ♀ 11	0*	0***	—
15 April 1989–14 April 1990 (One year)	U ♂ 7	12 (1.71)	26.69 (15.25)	14.73 (8.78)
	P ♂ 9	10 (1.11)*	10.26 (6.39)*	9.22 (4.72)*
	U ♀ 6	11 (1.83)	25.79 (7.32)	13.33 (4.89)
	P ♀ 5	4 (0.80)*	12.21 (13.13)*	14.85 (6.35)

Values are means ± SD; P = parasitized crabs; U = unparasitized.

[a] Relative growth (%) = 100 $(CW_e - CW_b)/CW_b$, where CW_e is carapace width at the end of the period, and CW_b is carapace width at the beginning.

[b] Relative molt increment (%) = 100 $(CW_{post} - CW_{pre})/CW_{pre}$, where *post* and *pre* refer to molt.

* Value for parasitized crabs is significantly smaller than that for unparasitized crabs. Mann Whitney U test was used for number of molts, and Student's t test was used for relative growth and relative molt increment: (***), $P < 0.001$; (**), $P < 0.01$; (*), $P < 0.05$.

the relative molt increments of parasitized males are smaller than those of unparasitized males.

The relative growths over 365 days are given in Table III. The average molt frequencies of male and female unparasitized crabs were 1.71 and 1.83 respectively, whereas those of parasitized crabs were 1.11 and 0.80 respectively. Therefore, after the loss of their externae, parasitized crabs had smaller relative growths than did unparasitized crabs, in both sexes.

Mortality of the host

The annual survival rates of unparasitized and parasitized crabs were 63.4% and 64.3% respectively—virtually indistinguishable values.

Discussion

Detachment of the externae, subsequent molting of the host, and regeneration of new externae

Parasitized *Hemigrapsus sanguineus* resume molting, and molt rather frequently, once the externa falls off. This resembles the response of a portunid host, *Carcinus maenas*, which molted after the externa of *Sacculina carcini* dropped off (Veillet, 1945; Lützen, 1981).

Heath (1971) and Lützen (1981) noted that a new externa of *S. carcini* appeared after the parasitized *C. maenas* molted. Lützen, however, concluded that regeneration of the externa did not play a significant part in the life cycle of the parasite. In the present study, new externae always appeared soon after molting in the infected crabs examined. Thus, the new externa had probably been prepared inside the host. Of 31 instances of molting, 21 appeared within 30 days of the molt, and 25 appeared within 40 days. Therefore, the life span of the externa and the molting of the host are closely related. This is schematically illustrated in Figure 4, a modification of Heath's model (Heath, 1971) with the resumption of molting replacing seasonality. Although detachment of the externa and molting of the host occurred frequently between June and October, the parasite reproduced continually throughout the year; thus the persistent reproduction of the parasite overshadowed the seasonality of the host.

Although the secondary eruption of externae is called *regeneration*, there is no direct evidence that a secondary externa sprouts from the same root as its antecedent. Indirect evidence suggests that regeneration may occur. For instance, Day (1935) found, in serial sections, a live main root trunk in a number of scarred or strongly feminized swimming crabs. But one cannot completely rule out the possibility that some of the new externa come from multiple infections.

Effects on host growth

The annual growth of both parasitized males and females was about half that of unparasitized crabs, but this

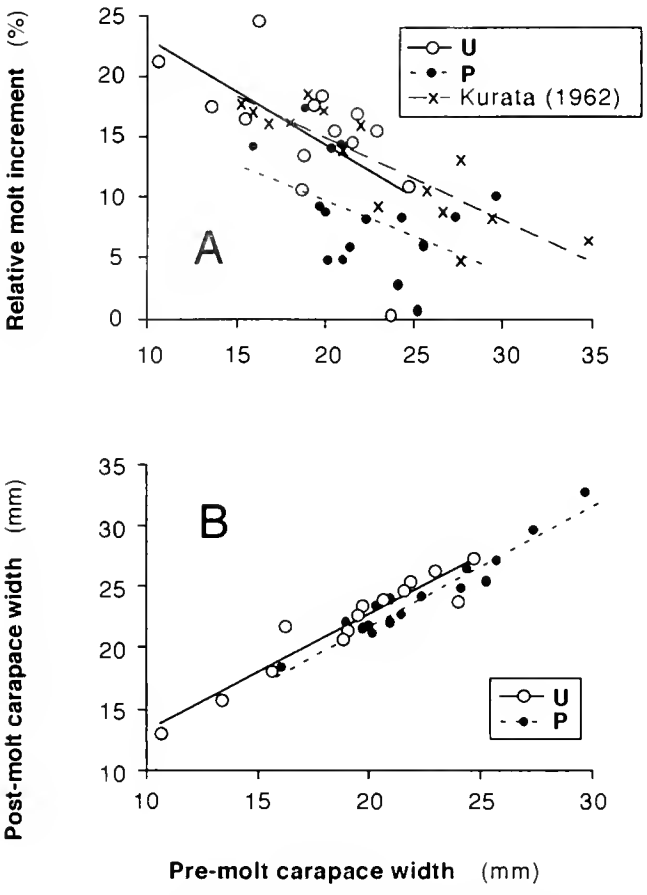

Figure 3. Premolt and postmolt relationships of parasitized and unparasitized male *Hemigrapsus sanguineus*. A: relationship between premolt carapace width and relative molt increment. B: Hiatt's growth diagram for male hosts.

discrepancy did not have the same basis in the two sexes. In the male, both the molt frequency and the molt increment of parasitized crabs were smaller than in the unparasitized crabs; but in the female, the discrepancy was mainly due to a difference in the molt frequency. During Section II (October–March) in particular, none of the parasitized females molted. During Section I, all seven unparasitized females recorded in Table III were ovigerous once, and this might have been a handicap to molting. The molting state of sacculinized crabs is similar to that of ovigerous females.

No study on the growth of sacculinized brachyuran hosts is comparable to the present study. But even if we examine the studies on the effects of rhizocephalans from a different family, the results are similar to those obtained in the present study. Hawkes *et al.* (1987) examined the growth of Alaskan blue king crabs, *Paralithodes platypus* (Decapoda, Anomura), parasitized by *Briarosaccus callosus*. There was no significant difference in the molt frequency between parasitized and unparasitized crabs, in either sex. The molt increment of parasitized males was significantly smaller than that of unparasitized males, and that of parasitized females was also smaller than that of unparasitized females, although not significantly.

Positive size-prevalence pattern

Inverse size-prevalence patterns are found in *Pugettia producta* parasitized by the sacculinid *Heterosaccus californicus* and in the mud crab *Rhithropanopeus harrisii* parasitized by *Loxothylacus panopei* (O'Brien, 1984; O'Brien and Van Wyk, 1985; O'Brien and Skinner, 1990). The authors of these reports describe the inverse size-prevalence pattern as typical of sacculinid-host associations. Contrary to these reports, we observed that the prevalence of *H. sanguineus* increased with the size of the host (Fig. 1). This pattern is rather similar to that of the peltogastrid rhizocephalan-host relationship (O'Brien and Van Wyk, 1985). These authors suggested that enhanced growth of parasitized hosts might be one factor determining the positive size-prevalence pattern, but such enhanced growth has not been documented in laboratory studies.

In the present study, *H. sanguineus* showed a positive size-prevalence pattern with suppressed host growth. The mechanisms that cause the size-prevalence pattern are not very clear, but we can suggest three reasonable factors.

1. *H. sanguineus* does not stop molting after the molt of puberty, whereas the molt of *P. producta* is a terminal molt.
2. Parasitized *H. sanguineus* can molt and grow even after the externae of the host have emerged.
3. The parasite does not have a lethal effect on the host.

Consequently, the parasite probably lives on after the detachment of the externa and then regenerates a new externa. Therefore, the high prevalence of parasitism among the large size classes may simply reflect the fact that the large host has been repeatedly exposed to infections, as suggested by Day (1935).

Acknowledgments

We thank Prof. K. Baba, Faculty of Education, Kumamoto University, for providing considerable encouragement and constructive criticism throughout this study, and Dr. T. Yamaguchi, Aitsu Marine Biological Station, Kumamoto University, for his advice and for the use of his laboratory facilities. We also thank Miss A. Ohkubo, Nakaminami Elementary School, Kumamoto Prefecture, who shared the labor involved in field and laboratory work.

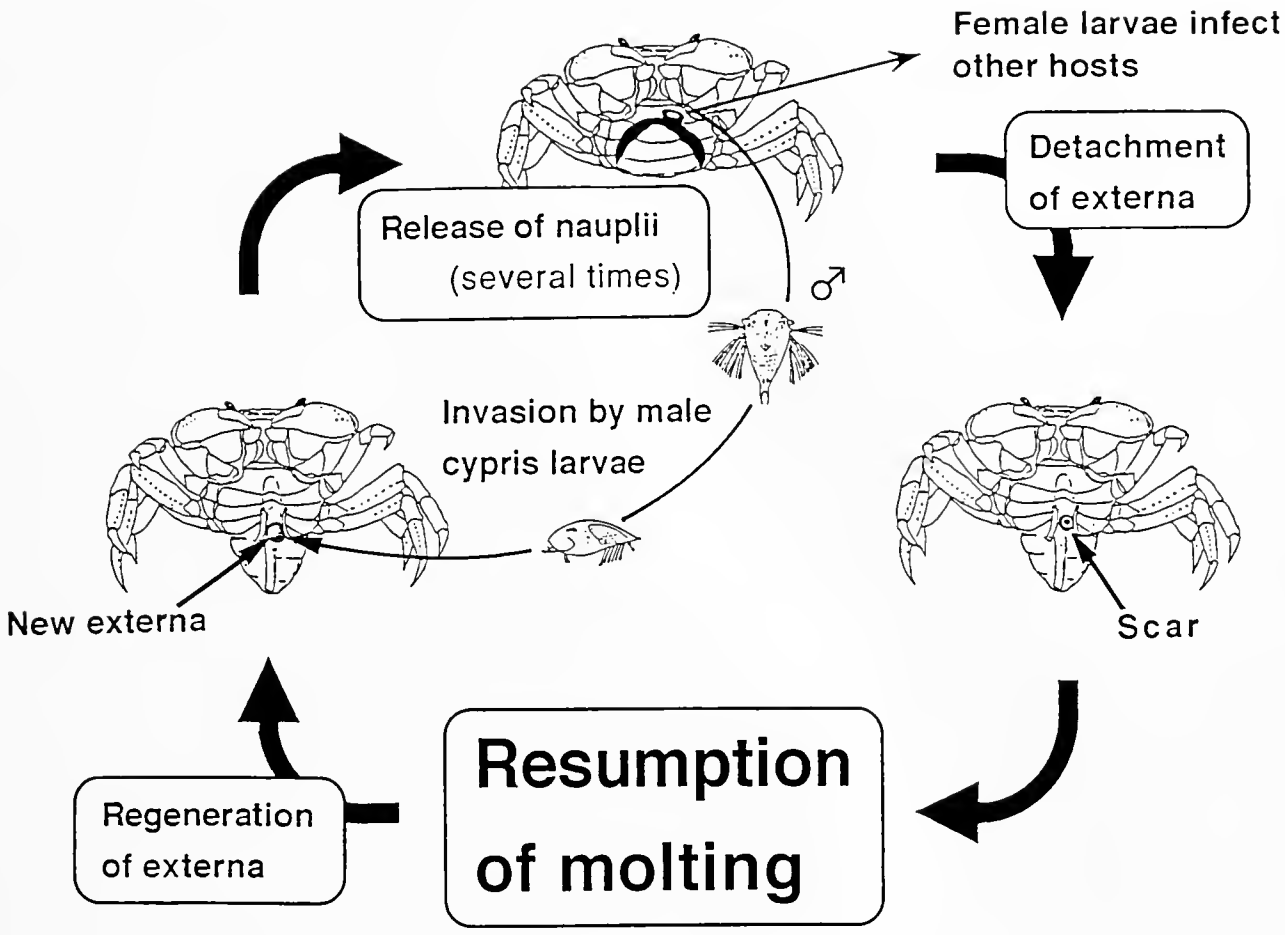

Figure 4. Relationship between the reproductive cycle of *Sacculina senta* and the molting of the host.

Literature Cited

Day, J. H. 1935. The life-history of *Sacculina*. *Q. J. Microsc. Sci.* **77:** 549–583.

Hartnoll, R. G. 1967. The effects of sacculinid parasites on two Jamaican crabs. *J. Linn. Soc. (Zool.)* **46:** 275–295.

Hawkes, C. R., T. R. Meyers, and T. C. Shirley. 1987. Growth of Alaskan blue king crabs, *Paralithodes platypus* (Brandt), parasitized by the rhizocephalan *Briarosaccus callosus* Boschma. *Crustaceana* **52:** 78–84.

Heath, J. R. 1971. Seasonal changes in a population of *Sacculina carcini* Thompson (Crustacea: Rhizocephala) in Scotland. *J. Exp. Mar. Biol. Ecol.* **6:** 15–22.

Hiatt, R. W. 1948. The biology of the lined shore crab, *Pachygrapsus crassipes* Randall. *Pac. Sci.* **2:** 135–213.

Høeg, J. T. 1982. The anatomy and development of the rhizocephalan barnacle *Clistosaccus paguri* Lillgeborg and relation to its host *Pagurus bernhardus* (L.). *J. Exp. Mar. Biol. Ecol.* **58:** 87–125.

Høeg, J. T. 1985a. Cypris settlement, kentrogon formation and host invasion in the parasitic barnacle *Lernaeodiscus porcellanae* (Müller) (Crustacea: Cirripedia: Rhizocephala). *Acta Zool., Stockh.* **66:** 1–45.

Høeg, J. T. 1985b. Male cypris settlement in *Clistosaccus paguri* Lillgeborg (Crustacea: Cirripedia: Rhizocephala). *J. Exp. Mar. Biol. Ecol.* **89:** 221–235.

Høeg, J. T. 1987. Male cypris metamorphosis and a new male larval form, the trichogon, in the parasitic barnacle *Sacculina carcina* (Crystacea: Rhizocephala). *Phil. Trans. R. Soc. London B.* **317:** 47–63.

Ichikawa, A., and R. Yanagimachi. 1958. Studies on the sexual organization of the Rhizocephala. I. The nature of the 'testis' of *Peltogasterella socialis* Kruger. *Annot. Zool. Japn.* **31:** 82–96.

Ichikawa, A., and R. Yanagimachi. 1960. Studies on the sexual organization of the Rhizocephala. II. The reproductive function of the larval (Cypris) males of *Peltogaster* and *Sacculina*. *Annot. Zool. Japn.* **33:** 42–56.

Kurata, H. 1962. Studies on the age and growth of Crustacea. *Bull. Hokkaido Reg. Fish. Res. Lab.* **24:** 1–115.

Lützen, J. 1981. Field studies on regeneration in *Sacculina carcini* Thompson (Crustacea: Rhizocephala) in the Isefjord, Denmark. *J. Exp. Mar. Biol. Ecol.* **53:** 241–249.

Lützen, J. 1984. Growth, reproduction and life span in *Sacculina carcini* Thompson (Cirripedia: Rhizocephala) in the Isefjord, Denmark. *Sarsia* **69:** 91–105.

O'Brien, J. 1984. Precocious maturity of the majid crab, *Pugettia producta*, parasitized by the rhizocephalan barnacle, *Heterosaccus californicus*. *Biol. Bull.* **166:** 384–395.

O'Brien, J., and D. M. Skinner. 1990. Overriding of the molt-inducing stimulus of multiple limb autotomy in the mud crab *Rhithropanopeus*

harrisii by parasitization with a rhizocephalan. *J. Crust. Biol.* **10:** 440–445.

O'Brien, J., and P. Van Wyk. 1985. Effects of crustacean parasitic castrators (epicaridean isopods and rhizocephalan barnacles) on growth of crustacean hosts. Pp. 191–218 in *Crustacean Issues Vol. 3*, A. M. Wenner, ed. A. A. Balkema, Rotterdam.

Reinhard, E. G. 1956. Parasitic castration of Crustacea. *Exp. Parasitol.* **5:** 79–107.

Ritchie, L. E., and J. T. Hoeg. 1981. The life history of *Lernaeodiscus porcellanae* (Cirripedia: Rhizocephala) and co-evolution with its porcellanid host. *J. Crust. Biol.* **1:** 334–347.

Veillet, A. 1945. Recherches sur le parasitisme des crabs et des Galathées par les Rhizocéphales et les Epicarides. *Ann. Inst. Océanogr.* **22:** 193–341.

Yanagimachi, R. 1961a. Studies on the sexual organization of the Rhizocephala. III. The mode of sex determination in *Peltogasterella*. *Biol. Bull.* **120:** 272–283.

Yanagimachi, R. 1961b. The life cycle of *Peltogasterella* (Cirripedia: Rhizocephala). *Crustaceana* **2:** 183–186.

Reference: *Biol. Bull.* **186:** 309–318. (June, 1994)

Excitatory Actions of FMRFamide-Related Peptides (FaRPs) on the Neurogenic *Limulus* Heart

JAMES R. GROOME[1,2†], MARK A. TOWNLEY[3], AND WINSOR H. WATSON III[3]

[1]*Marine Biological Laboratory, Woods Hole, Massachusetts, 02543,* [2]*Biology Department, Swarthmore College, Swarthmore, Pennsylvania 19081-1397, and* [3]*Zoology Department, University of New Hampshire, Durham, New Hampshire 03824*

Abstract. The actions of FMRFamide-related peptides (FaRPs) on the neurogenic heart of the horseshoe crab, *Limulus polyphemus,* were investigated. Excitatory chronotropic effects were produced by application of TNRNFLRFamide, SDRNFLRFamide, GYNRSFLRFamide, or pQDPFLRFamide to the intact heart preparation. Effects were dose-dependent with a threshold of 10^{-9} *M* or less. TNRNFLRFamide and SDRNFLRFamide increased the burst rate of the isolated *Limulus* cardiac ganglion.

Synthetic FaRPs produced inotropic excitation of the heartbeat as well. GYNRSFLRFamide, TNRNFLRFamide, SDRNFLRFamide, and pQDPFLRFamide increased heart contraction strength at a threshold dose of approximately 10^{-8} *M*. TNRNFLRFamide and SDRNFLRFamide enhanced electrically evoked contractions of the *Limulus* myocardium, elicited contracture in some preparations, and increased the excitability of cardiac muscle fibers.

The presence of cardioactive FaRPs in the *Limulus* central nervous system was suggested by reverse phase HPLC of acidified methanol extracts of *Limulus* nervous tissue. Four peaks of FaRP-like bioactivity were detected with the *Busycon* radula protractor muscle bioassay. These peaks also contained FaRP-like immunoreactivity. Two of these partially purified peaks produced excitatory chronotropic effects on the intact *Limulus* heart preparation similar to those produced by synthetic FaRPs.

Introduction

The FMRFamide-related peptides (FaRPs) are widely distributed in the Arthropoda (reviewed by Price and Greenberg, 1989; Greenberg and Price, 1992). The arthropod FaRPs occur as N-terminally extended variants of the tetrapeptides FMRFamide and FLRFamide. For example, TNRNFLRFamide and SDRNFLRFamide have been isolated from the lobster *Homarus* (Trimmer *et al.,* 1987), DRNFLRFamide and NRNFLRFamide from the crayfish *Procambarus* (Mercier *et al.,* 1991a), and GYNRSFLRFamide from the crab *Callinectes* (Krajniak, 1991). Pharmacological studies with a number of arthropod heart preparations have suggested a cardioregulatory role for N-terminally extended FaRPs (Kravitz *et al.,* 1987; Cuthbert and Evans, 1989; Krajniak, 1991; Mercier *et al.,* 1991b; Groome, 1993; Duve *et al.,* 1993). However, the cellular sites of action targeted by FaRPs on neurogenic arthropod hearts are unknown.

We have begun to examine the cellular and biochemical mechanisms underlying the effects of neuromodulators of the cardiac rhythm in the horseshoe crab, *Limulus polyphemus,* an organism suitable for detailed cellular studies (reviewed by Watson and Groome, 1989). Immunoreactivity to the neuropeptide FMRFamide has been detected in the central nervous system (CNS), cardiac ganglion, peripheral nerves and muscles of the horseshoe crab (Watson *et al.,* 1984; Gaus *et al.,* 1993; Groome, 1993). We decided to determine the actions of synthetic FaRPs on the neurogenic *Limulus* heart, as well as to characterize endogenous cardioactive FaRPs in *Limulus.* Our data indicate that several N-terminally extended FaRPs produce chronotropic and inotropic excitation of the *Limulus* heartbeat. These actions are a result of excitation of cardiac ganglion neurons, and enhancement of cardiac muscle fiber contractility and excitability. Partial purification of *Limulus* prosomal CNS extracts with HPLC reveals several peaks of FaRP-like bioactivity and immunoreactivity; two of these peaks also excite the *Limulus* heartbeat. Pre-

Received 23 August 1993; accepted 18 March 1994.

† Present address and author for correspondence: Biology Department, Utah State University, Logan, Utah 84322-5305.

liminary accounts of portions of this work have appeared in an earlier short report (Groome and Watson, 1991).

Materials and Methods

Preparations

Adult horseshoe crabs (*Limulus polyphemus*) were obtained from the Marine Resources Department at the Marine Biological Laboratory in Woods Hole, Massachusetts. They were maintained at 18 to 20°C in a flow-through seawater tank until used. Hearts were dissected as previously described (Watson *et al.*, 1984). The isolated, intact hearts were pinned in 10-ml resin-lined recording chambers and superfused from a 500-ml reservoir at 5 ml/min with filtered, natural seawater at room temperature (20–23°C) until the cardiac rhythm had stabilized. Contractions were monitored with a force transducer (Grass FT .03 C, Grass Instruments, Quincy, Massachusetts) and polygraph (Grass Model 7D). Test solutions were added at the same flow rate via a 20-ml reservoir, and preparations were washed for 30 min or more prior to the application of the next test solution.

Cardiac ganglia were dissected free from *Limulus* myocardia, pinned by their adhering connective tissue to the bottom of 5-ml recording chambers, and superfused at 5 ml/min. Neuronal activities were recorded extracellularly with a suction electrode; the signals were amplified and filtered with Grass P-15 preamplifiers and displayed with a polygraph. Myocardial rings (3 cm) were stretched over wire electrodes immersed in a 20-ml bath and stimulated with current pulses from a Grass S-88 stimulator. For each evoked contraction, two 50-ms pulses separated by an 80-ms delay were delivered; pulses were equal in intensity (2–5 V) and of opposite polarities. Stimulation parameters were adjusted to obtain contraction strengths of magnitude approximating those recorded from typical intact heart preparations. In other experiments, deganglionated myocardial rings were pinned to the bottom of 10-ml recording chambers. Spontaneous contractions were recorded, and test solutions were delivered as described above.

Peptides were obtained as follows: FMRFamide was obtained from Peninsula Laboratories (Belmont, California); pQDPFLRFamide and TNRNFLRFamide were obtained from Bachem (Torrence, California); SDRNFLRFamide was a gift from Dr. Eve Marder (Brandeis University, Waltham, Massachusetts); GYNRSFLRFamide, RNFLRFamide and FLRFamide were a gift from Dr. Michael J. Greenberg (Whitney Laboratory, St. Augustine, Florida).

Peptide extraction

The extraction procedure for FaRPs in *Limulus* nervous tissue followed the procedure of Trimmer *et al.* (1987). The protocerebra and circumesophageal ganglia (prosomal CNS) from 100 *Limulus* were dissected and placed in ice-cold methanol/acetic acid (99:1) containing 0.05% dithiothreitol; the tissues were then stored in groups of 10 at −20°C. Tissues were homogenized at 0°C, and centrifuged at 25,000 × *g* for 30 min at 4°C. The supernatant was removed, combined with the supernatant resulting from one repetition of this process with the centrifugation pellet, and dried on a rotary evaporator (Savant Instruments, Hicksville, New York). This material was resuspended in 0.1% trifluoroacetic acid (TFA, Pierce Chemical, Rockford, Illinois) and loaded onto Sep-Pak C_{18} cartridges pre-activated with 5 ml methanol and 5 ml 0.1% TFA. The cartridges were washed with 0.1% TFA and peptides were eluted with 60% methanol containing 0.1% TFA. This material was dried, resuspended in 0.1% TFA, and ultracentrifuged (Beckman TL-100, Beckman Instruments, Palo Alto, California) at 36,000 × *g* for 60 min at 4°C. The supernatants were dried and the material stored at −80°C until subjected to reverse phase HPLC.

High performance liquid chromatography (HPLC)

A Perkin-Elmer Series 410 BIO LC pump (Norwalk, Connecticut) and Rheodyne 7125 sample injector with 1-ml loop (Cotati, California) and a 7-μm spherical, 15 × 3.2 mm Polymeric RP guard column (Brownlee Labs, Santa Clara, California) were used in the first three HPLC runs. The extracts were reconstituted in 300 μl 0.1% TFA and filtered (Millex HV4, 0.45 μm, Millipore, Milford, Massachusetts); 250 μl was injected onto a C_8 or C_{18} reverse phase column. The mobile phase consisted of HPLC grade acetonitrile (Fisher Scientific, Fair Lawn, New Jersey), Milli-Q water (Millipore), and TFA. Flow rate was set at 1 ml/min and 1.5-ml fractions were collected. The $O.D._{204-285}$ of the eluate was monitored with a LKB 2140 Rapid Spectral detector. The fourth HPLC run was accomplished by K. Doble (Whitney Laboratory, University of Florida, St. Augustine, Florida) according to the protocol specified in Price *et al.* (1990). The HPLC columns and protocols employed sequentially were as follows:

Run 1: C_8 column (Aquapore RP-300, 7-μm spherical, 220 × 4.6 mm, Brownlee); 5 min isocratic 2% acetonitrile followed by a linear gradient to 60% acetonitrile over 55 min, with 0.1% TFA throughout.

Run 2: C_8 column (Aquapore RP-300); 5 min isocratic 5% acetonitrile followed by a linear gradient to 30% acetonitrile over 55 min, with 0.1% TFA throughout.

Run 3: C_{18} column (RP-18 Spheri-5, 220 × 4.6 mm, Brownlee) 5 min isocratic 10% acetonitrile and 0.1% TFA followed by a linear gradient to 37% acetonitrile over 55 min, with 0.1% TFA throughout.

Run 4: C_8 column (Aquapore RP-300, 7 μm spherical, 220 × 2.1 mm, Brownlee) with a linear gradient of 16–40% acetonitrile over 30 min, with 0.05% TFA throughout.

Bioassay

Fractions from HPLC runs were dried and resuspended in 1 ml Milli-Q water, and aliquots were analyzed for FaRP-like bioactivity with the *Busycon* radula protractor muscle (RPM, Nagle and Greenberg, 1982). Left-handed whelks (*Busycon contrarium*) were obtained from Gulf Specimens (Panacea, Florida) and maintained at room temperature in aerated natural seawater until used. The paired RPMs were tied at the odontophore and radula, suspended in a 1-ml vertical chamber, and superfused with aerated, filtered seawater. Peptides were added to the chamber with a syringe, and contractures were recorded with a force transducer and polygraph. FaRP-like bioactivities in individual fractions were calculated by comparing the contracture force elicited by samples to that produced by synthetic pQDPFLRFamide at a dose of 10^{-9} *M*, at regular intervals. This preparation was sensitive to picomolar quantities of FMRFamide, FLRFamide, RNFLRFamide, GYNRSFLRFamide, TNRNFLRFamide, SDRNFLRFamide, and pQDPFLRFamide. Active fractions were pooled and dried for further HPLC characterization, for analysis of effects on the *Limulus* heart (after HPLC runs 2 and 3), or for radioimmunoassay (after HPLC run 4).

Radioimmunoassay

We used two FaRP antisera, Q2 and S-253, in the radioimmunoassay; the protocol employed has been described in detail (Price *et al.*, 1990). The Q2 antisera was raised against pQDPFLRFamide and boosted with pDDPFLRFamide; it was used in this study at a final dilution of 1:625. The S-253 antiserum was raised against YGGFMRFamide and used at a dilution of 1:25,000.

Results

Chronotropic effects of FaRPs

Synthetic FaRPs were tested for their effects on the rate of contraction of the isolated *Limulus* heart. The peptides TNRNFLRFamide, SDRNFLRFamide, GYNRSFLRFamide, and pQDPFLRFamide consistently increased heart rate in a dose-dependent manner; the threshold dose for each of these peptides was approximately 10^{-9} *M* (Table I, Fig. 1). Chronotropic excitation gradually diminished after the peptide was washed off the preparation. The peptides RNFLRFamide, FLRFamide, and FMRFamide produced only slight increases in heart rate, at doses up to 10^{-5} *M*.

Table I

Effects of FaRPs on the intact heart preparation[a]

Peptide	Threshold[b] (n*M*)	EC_{50}[c] (n*M*)	Maximum[d] increase (%)	Relative[e] efficacy
A. Chronotropic effects				
SDRNFLRFa	0.3	3.4	58.7	1.00
TNRNFLRFa	0.3	2.9	57.0	0.97
GYNRSFLRFa	0.3	3.1	47.3	0.81
pQDPFLRFa	1.0	3.4	53.3	0.91
RNFLRFa	3.0	8.4	23.8	0.41
FMRFa	100	n.d.	5.9	0.10
FLRFa	300	n.d.	10.0	0.17
B. Inotropic effects				
SDRNFLRFa	3.0	40	32.7	1.00
TNRNFLRFa	3.0	30	33.9	1.04
GYNRSFLRFa	10	60	37.0	1.13
pQDPFLRFa	10	110	40.0	1.22
RNFLRFa	1000	n.d.	15.4	0.47
FLRFa	1000	n.d.	6.1	0.19
FMRFa	No response	n.d.	n.d.	n.d.

[a] Values calculated from dose-response data for each peptide (a = amide), over the range of 0.3 n*M* to 1.0 μ*M*. For the tetrapeptides and RNFLRFamide, doses up to 10 μ*M* were tested. A maximum of 6 trials, each with a different dose, were performed with each preparation, for a total *n* of 8 to 12 trials per dose. Where insufficient data were available, calculations were not determined (n.d.).

[b] Threshold defined as the dose at which the mean response exceeded the value of the standard deviation.

[c] EC_{50} calculated as the dose at which the mean response was half that of the maximum.

[d] Maximum increase taken from full or partial dose-response curves, using the mean response.

[e] Relative efficacies compare the maximum increase of each peptide to that for SDRNFLRFamide, for both chronotropic and inotropic effects.

The cellular basis for the chronotropic excitation elicited by application of synthetic FaRPs to the intact heart was investigated with the isolated cardiac ganglion preparation. At 10^{-8} *M*, TNRNFLRFamide and SDRNFLRFamide produced gradual and long-lasting increases in the burst rate of cardiac ganglion neurons (Fig. 2). This effect was associated with decreases in the interburst interval and the duration of individual bursts.

Inotropic effects of FaRPs

FaRPs with potent chronotropic effects increased the contraction amplitude of the *Limulus* heartbeat (Table I, Fig. 1). Dose-dependent inotropic excitation followed the administration of TNRNFLRFamide, SDRNFLRFamide, GYNRSFLRFamide, and pQDPFLRFamide. The peptides RNFLRFamide, FLRFamide, and FMRFamide had little inotropic effect at doses up to 10^{-5} *M*.

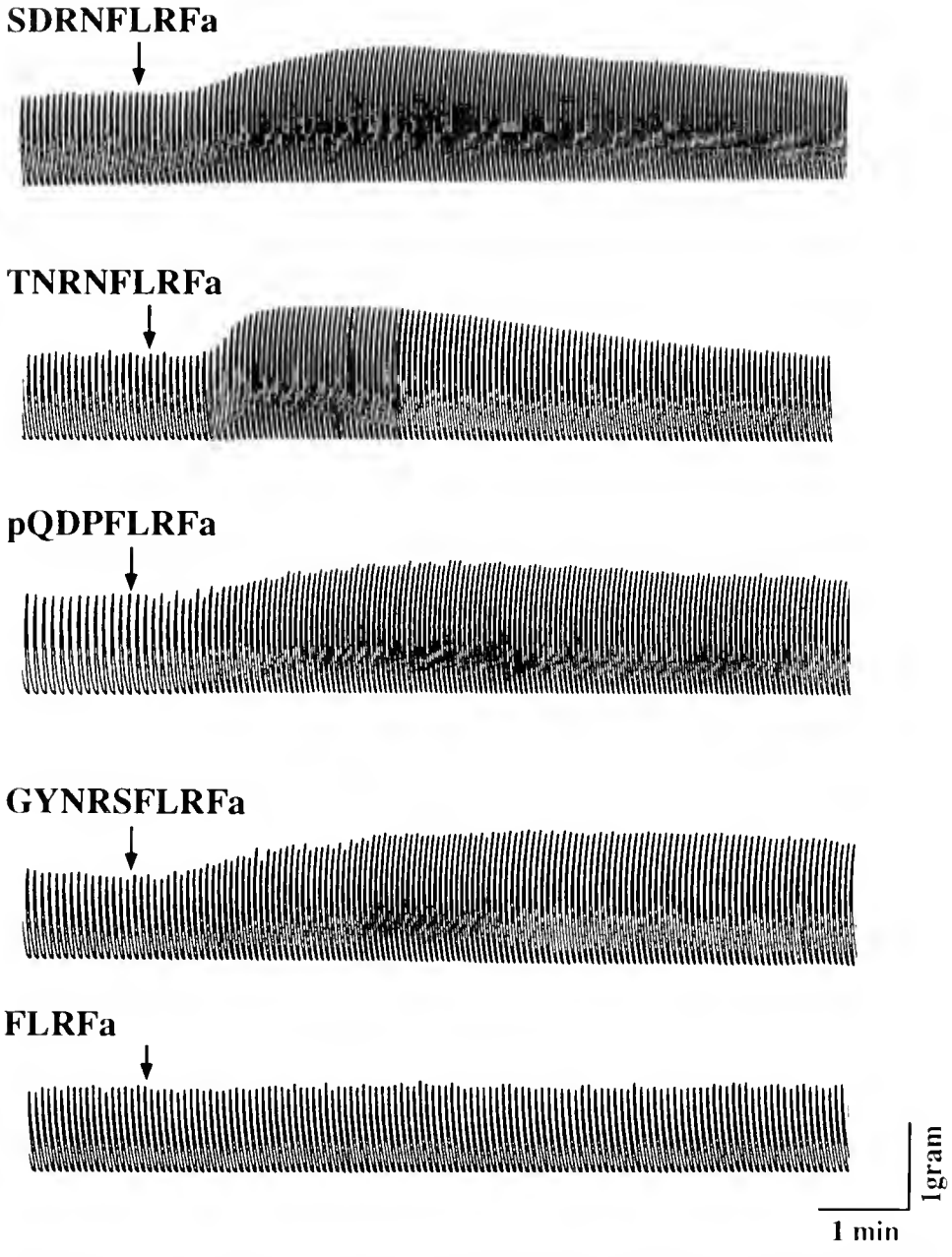

Figure 1. Effect of FaRPs (a = amide) on the intact *Limulus* heart preparation. At 10^{-7} *M*, N-terminally extended FaRPs produced chronotropic and inotropic excitation of the heartbeat, whereas FLRFamide, at 10^{-6} *M*, had little effect on this preparation.

To determine the effect of synthetic FaRPs on cardiac muscle contractility, deganglionated muscle rings were stimulated with current pulses at fixed intensities and rates. At 3×10^{-7} *M*, both TNRNFLRFamide and SDRNFLRFamide produced a gradual and long-lasting increase in the amplitude of evoked contractions (Fig. 3). At this dose, the inotropic effect was significantly greater than that observed with the same dose of TNRNFLRFamide, or SDRNFLRFamide, applied to the intact heart preparation. This difference may be attributable to negative inotropic effects associated with increased burst rate in the cardiac ganglia of intact heart preparations (Watson and Groome, 1989).

In a few experiments, these peptides increased the baseline tension as well as the amplitude of evoked contractions (Fig. 3A). Small oscillations in muscle tension between stimulating pulses also occurred occasionally during peptide administration. These observations sug-

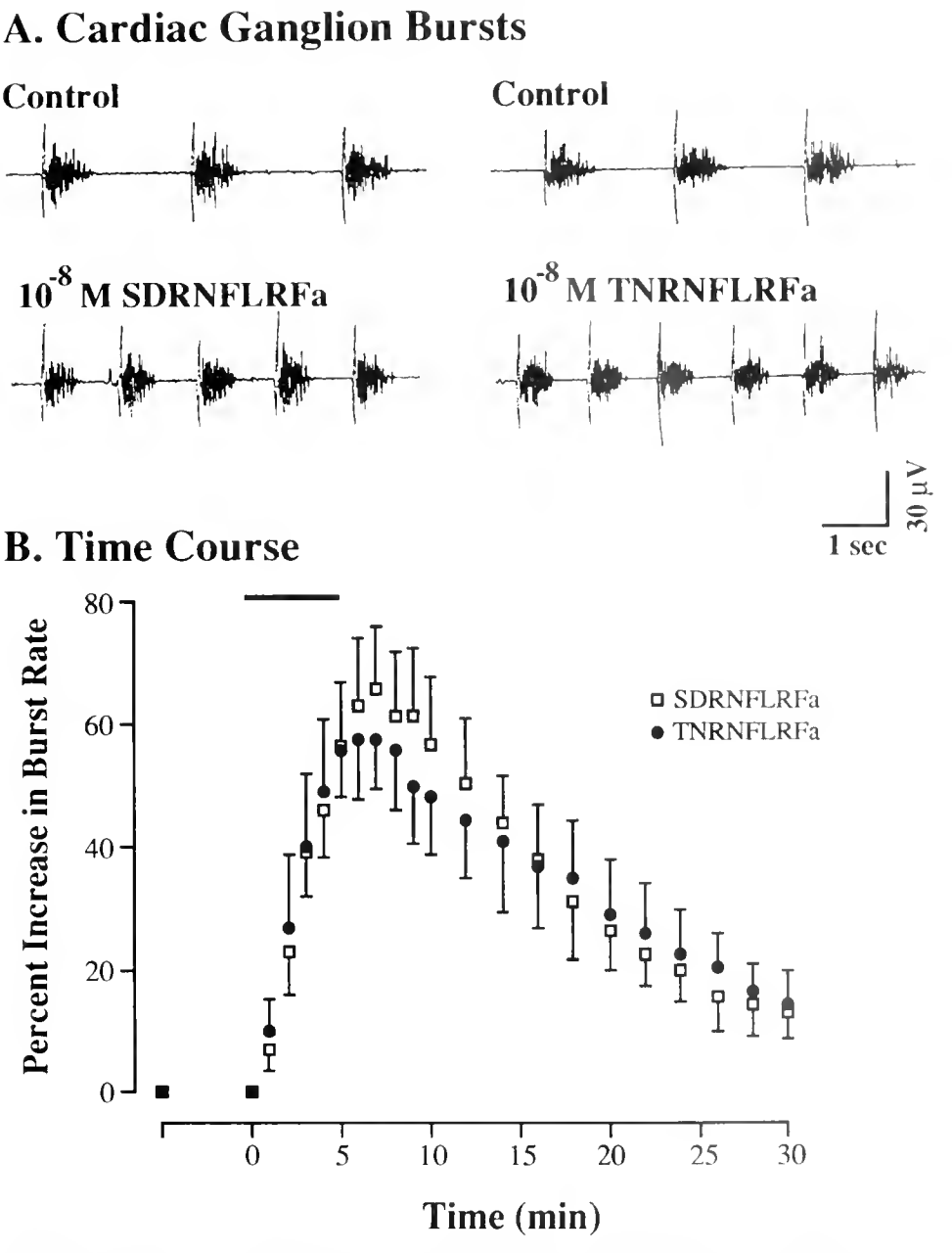

Figure 2. The chronotropic action of TNRNFLRFamide and SDRNFLRFamide (a = amide) on the *Limulus* heart is due to excitation of cardiac ganglion neurons. A. At 10^{-8} *M*, these peptides increased the rate of bursting in isolated ganglia, while decreasing the interburst interval and the duration of individual bursts. B. Time course of the effect of FaRPs on the isolated ganglion. The bar depicts the duration of peptide application.

gested that FaRPs alter the excitability of cardiac muscle fibers. To test this hypothesis, we applied FaRPs to deganglionated muscle rings. Both TNRNFLRFamide and SDRNFLRFamide, at 3×10^{-7} *M*, caused these preparations to beat irregularly in the absence of neural or electrical stimulation (Fig. 4). Peptide-induced contractions were abolished with the addition of 20 m*M* magnesium to the superfusion (data not shown).

Partial characterization of Limulus *FaRPs*

Acidified methanol extracts of the *Limulus* prosomal CNS were partially purified by reverse phase HPLC in three consecutive protocols; the purification was monitored with the *Busycon* RPM bioassay. With a linear gradient of 2 to 60% acetonitrile with the C_8 column, we detected two peaks of FaRP-like bioactivity. The sepa-

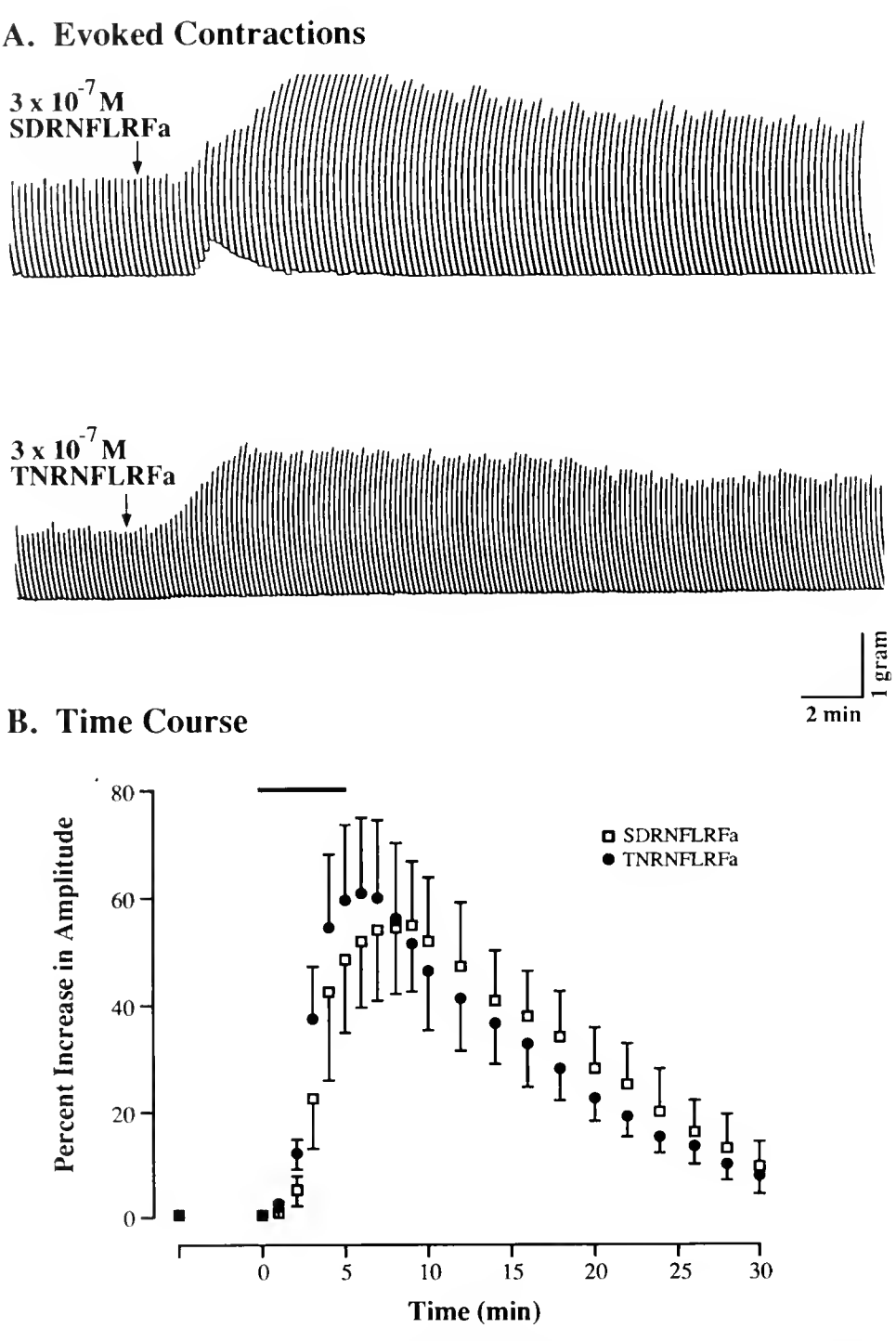

Figure 3. The peptides TNRNFLRFamide and SDRNFLRFamide (a = amide) increased the amplitude of electrically evoked contractions of the deganglionated *Limulus* myocardium. A. At 3×10^{-7} *M*, these peptides enhanced contraction amplitude, and occasionally increased baseline tension. B. Time course of the inotropic effect of FaRPs. The bar depicts the duration of peptide application.

rately pooled fractions from each peak were subjected to a linear gradient of 5 to 30% acetonitrile with the C_8 column, from which we detected three principal peaks of FaRP-like bioactivity. Aliquots from each of these bioactive peaks were tested on the *Limulus* heart, and marked cardioexcitation was elicited with application of the first and second peaks (data not shown). The separately pooled fractions from each of these three peaks were subjected

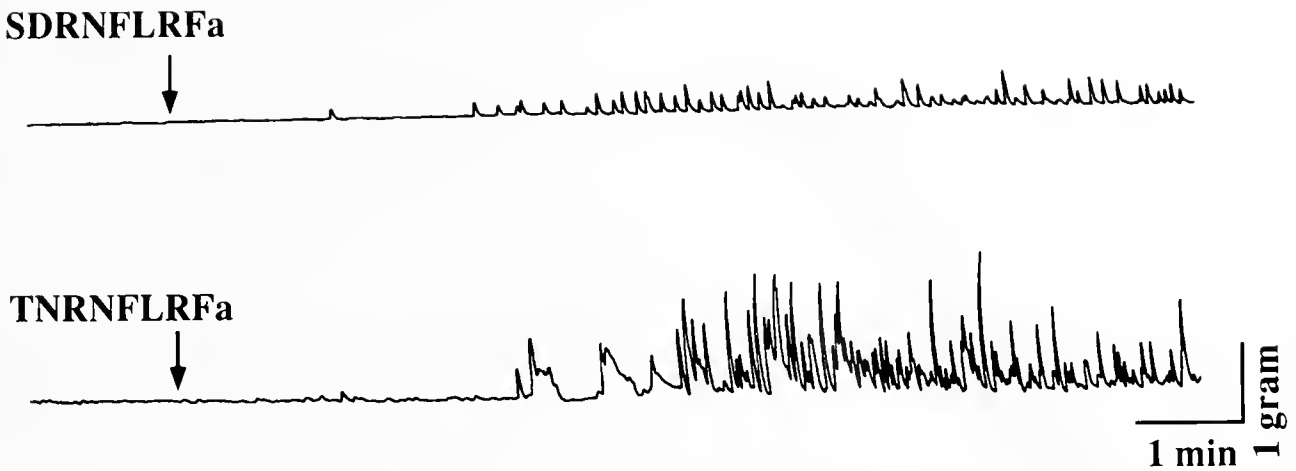

Figure 4. The peptides TNRNFLRFamide and SDRNFLRFamide (a = amide), each at 3×10^{-7} *M*, produced rhythmic contractions in unstimulated, deganglionated *Limulus* myocardia. This effect appeared after several minutes of superfusion of peptide and persisted for several minutes after the peptide was removed from the bath.

to 10 to 37% acetonitrile gradient with a C_{18} column, from which four peaks of FaRP-like bioactivity were detected (Fig. 5). The first three peaks had elution times near those for FMRFamide, TNRNFLRFamide, and pQDFLRFamide, while the fourth had an elution time later than that for any FaRP standard tested.

Aliquots from each of the peaks generated by the third HPLC run were subjected to a final characterization on another HPLC system, with analysis by radioimmunoassay with the S253 and Q2 antisera (Fig. 6). Immunoreactivity to one or both antisera was detected in each peak. Peak three from the third HPLC run displayed strong immunoreactivity to both antisera in fractions that had an elution time slightly longer than that of pQDPFLRFamide.

The four peaks of FaRP-like bioactivity from the third HPLC run were also tested on the *Limulus* heart preparation (Fig. 7). In each test, aliquots comprising 10 prosomal CNS equivalents, with respect to the original extraction, were used. Excitatory chronotropic effects were more consistently elicited than were increases in heart contraction amplitude, especially with peaks one and two. Peak one increased with heart rate by 42.2 ± 4.6% SEM ($n = 8$), and peak two produced even greater chronotropic excitation (61.4 ± 8.7% SEM increase, $n = 9$). Peak three increased heart rate by 15.8 ± 3.9% SEM ($n = 9$), and the effect of peak four was negligible (7.5 ± 2.7% SEM increase, $n = 9$). Inotropic effects were slight, ranging from an increase of 9.3 ± 3.3% SEM elicited by peak two, to the 13.0 ± 3.9% SEM increase elicited by peak one. Peaks three and four elicited increases in amplitude of 9.9 ± 3.0% SEM and 12.1 ± 4.5% SEM, respectively.

Discussion

This study shows that several FaRPs have pronounced excitatory actions on the neurogenic heart of the chelicerate arthropod *Limulus*. The crustacean peptides TNRNFLRFamide, SDRNFLRFamide, and GYNRSFLRFamide all increase the rate and strength of heart contractions at low doses, as does the molluscan peptide pQDPFLRFamide. Endogenous factors purified from the *Limulus* nervous system produce FaRP-like cardioexcitatory effects. These factors may play a cardioregulatory role in the horseshoe crab, and they may, in fact, be FaRPs.

Cellular actions of FaRPs on the neurogenic Limulus *heart*

Several N-terminally extended FaRPs increase both the rate and strength of *Limulus* heart contractions. In crustaceans, FaRPs have been detected in the pericardial organs and have excitatory effects on the heartbeat. These peptides are predominantly chronotropic in the blue crab *Callinectes* (Krajniak, 1991), whereas the peptide TNRNFLRFamide produces both chronotropic and inotropic excitation of the heartbeat in the lobster *Homarus* (Kravitz *et al.*, 1987). Similar cardioexcitatory effects of TNRNFLRFamide, SDRNFLRFamide, and native FaRPs are observed in the crayfish *Procambarus* (Mercier *et al.*, 1991a, b).

The cardioexcitatory effects of FaRPs on the *Limulus* heartbeat are mimicked by several biogenic amines (Augustine *et al.*, 1982). These amines elicit chronotropic excitation by increasing the firing frequency of pacemaker neurons and thus the burst rate of the *Limulus* cardiac ganglion (Augustine and Fetterer, 1985). The peptides

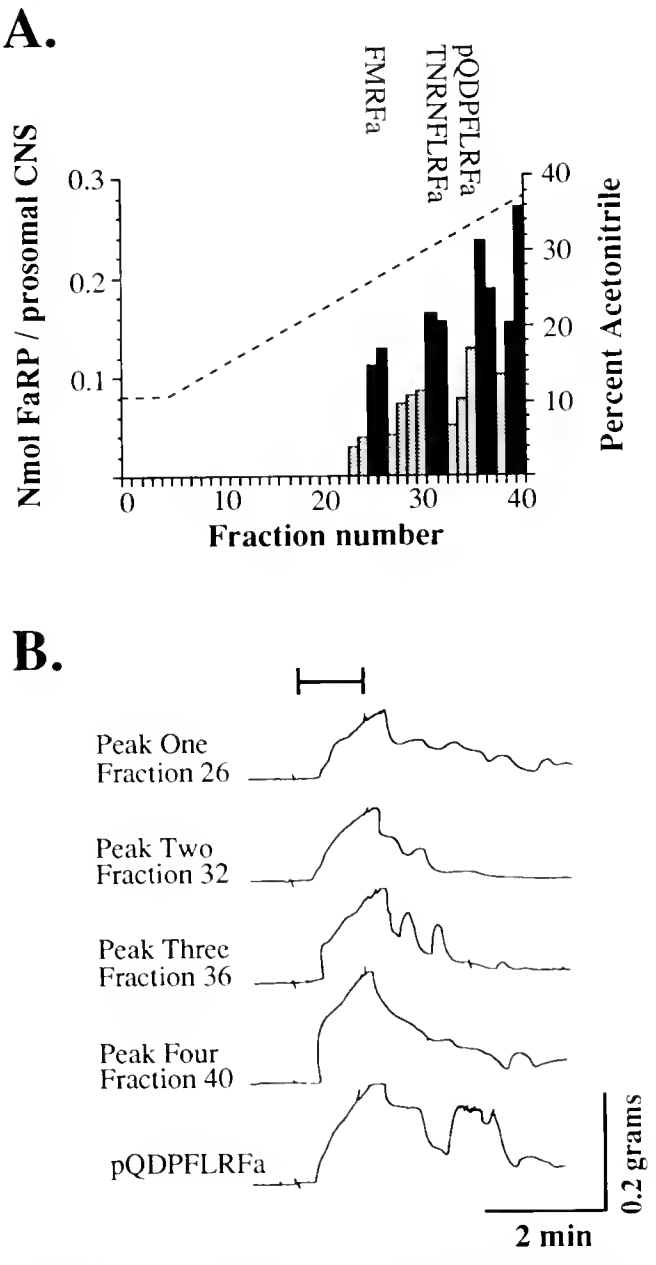

Figure 5. Reverse phase HPLC of acidified methanol extracts of the *Limulus* prosomal CNS as assayed for FaRP-like bioactivity with the RPM of *Busycon*. A. composite HPLC profile of the third HPLC run. The HPLC gradient used and the elution times of standard FaRPs (a = amide) are shown. Four bioactive peaks were detected (black), and these fractions were assayed further. B. Contractures of the *Busycon* RPM produced by peak fractions and by synthetic pQDPFLRFamide.

TNRNFLRFamide and SDRNFLRFamide also increase cardiac ganglion burst rate, probably by a similar cellular mechanism. The positive inotropic actions of FaRPs on the *Limulus* heart are, at least in part, due to an enhancement of cardiac muscle contractility. However, the effect of these FaRPs on transmitter release at the cardiac neuromuscular junction is not known. We have not failed to notice that the actions of TNRNFLRFamide and SDRNFLRFamide on the *Limulus* myocardium are similar to those produced by dopamine or proctolin (Watson and Groome, 1989). FaRPs might act *via* similar mechanisms, or might induce the release of these modulators from cardiac ganglion neurons.

Structure-activity relationship of synthetic FaRPs

The *Limulus* heart is responsive to several N-terminally extended FaRPs, whereas RNFLRFamide is less effective, and the tetrapeptides FLRFamide and FMRFamide are essentially inactive on this preparation. The relative po-

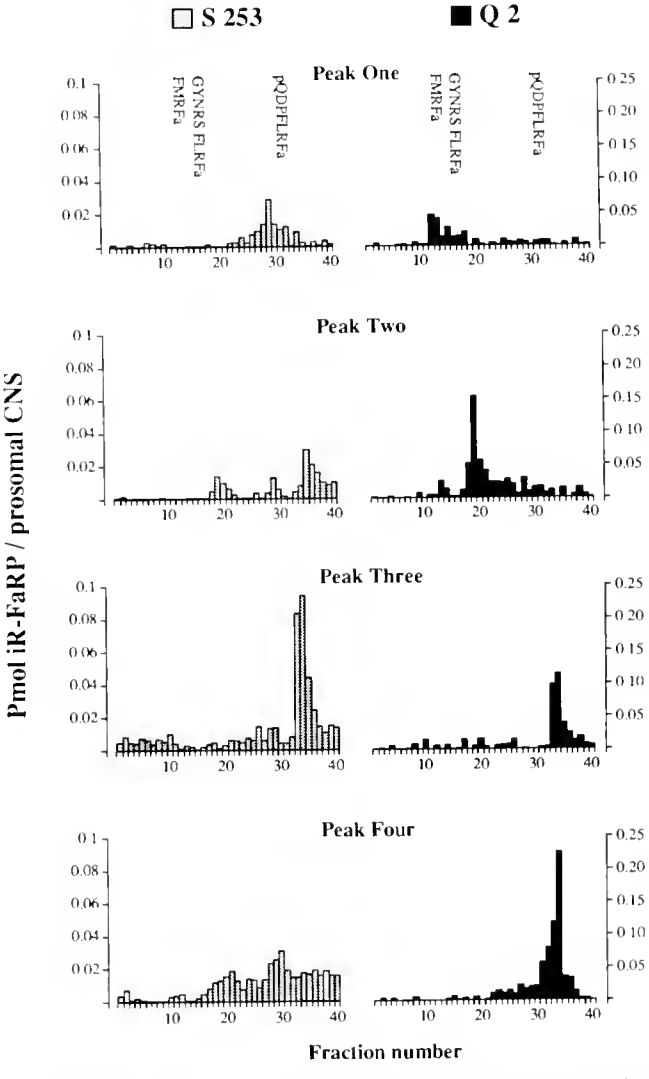

Figure 6. FaRP-like immunoreactivity in partially purified *Limulus* extracts. Each of the four bioactive peaks from the third HPLC run was subjected to further purification with a linear gradient of 16 to 40% acetonitrile. The profiles of immunoreactivity to the antisera S-253 and Q2 are shown, as are the elution times of synthetic FaRPs (a = amide).

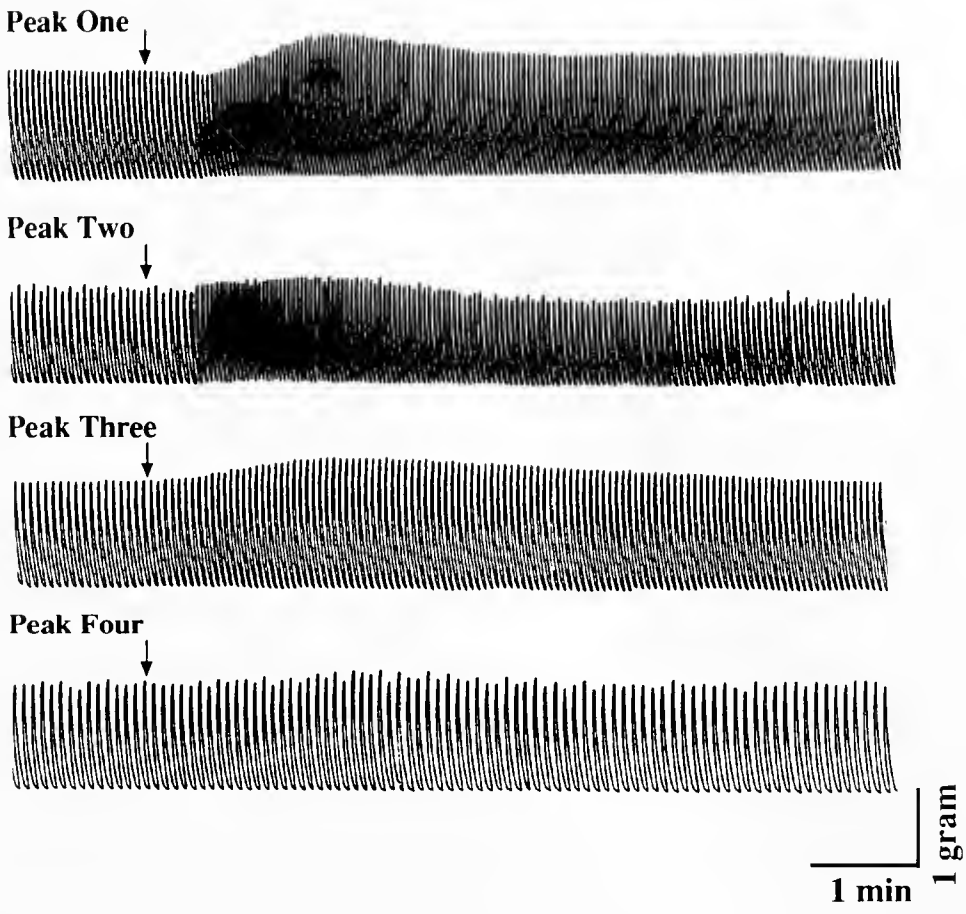

Figure 7. Cardioexcitatory effects of partially purified extracts of the *Limulus* prosomal CNS. Aliquots from each of the four peaks from the third HPLC run were tested on the intact heart preparation. Peaks one and two, which eluted near FMRFamide and TNRNFLRFamide respectively, promoted the greatest chronotropic excitation.

tencies of these peptides on heart rate and contractile force were quite similar, suggesting that *Limulus* cardiac ganglion neurons and cardiac muscle fibers possess similar, FaRP-like receptors. Because TNRNFLRFamide, SDRNFLRFamide, GYNRSFLRFamide, and pQDPFLRFamide all had excitatory effects, whereas RNFLRFamide was a weak agonist, we suggest that the FLRFamide sequence must be extended at the N terminus by at least three amino acids for full activation of FaRP receptors in the cardiac ganglion and in cardiac muscle. Similar N-terminal structural requirements for chronotropic excitation of the neurogenic heart of the blue crab *Callinectes* have been reported (Krajniak, 1991), and in both this species and *Limulus,* amino acid substitutions at the N-terminus are less restrictive than are extensions. Unlike *Limulus,* however, the *Callinectes* heart does not respond to low doses of pQDPFLRFamide (Krajniak and Greenberg, 1988). This heptapeptide, first isolated from the pulmonate mollusk *Helix* (Price *et al.,* 1985), is more potent than FMRFamide on the heart of that species, as we observed with the neurogenic heart of *Limulus.* These findings suggest that the structure-activity characteristics of the FaRP receptors in *Limulus,* crustaceans, and mollusks are similar.

Endogenous cardioactive FaRPs in Limulus

Reverse phase HPLC indicates that several factors with FaRP-like bioactivity and immunoreactivity are present in the *Limulus* nervous system. Peak one, which increases heart contraction rate, has an elution time near that of synthetic FMRFamide, which is inactive on the *Limulus* heart. The possibility of a FaRP in *Limulus*—which like FMRFamide is relatively hydrophilic but unlike FMRFamide has marked cardioexcitatory effects on the neurogenic heart—is an unexpected finding, and the sequences of peptides within this peak are of considerable interest. Initial mass spectrometry data suggest the pres-

ence of more than one peptide in peak one, as do the RIA data. Peak two also markedly increases heart contraction rate. This material eluted with a time near that of TNRNFLRFamide and SDRNFLRFamide, both of which have potent chronotropic effects. The third peak slightly increased heart rate and eluted with a time near that exhibited by another cardioactive FaRP, pQDPFLRFamide. These data raise the possibility that peaks two and three contain peptides similar to the synthetic FaRPs that have potent chronotropic effects on the *Limulus* heart. However, it will be necessary to sequence these peptides to obtain valid estimates of their relative abundances in the *Limulus* CNS and to establish their true physiological effects.

The sequences of five *Limulus* neuropeptides that react with antibodies to FMRFamide have been reported (Gaus *et al.*, 1993). Of these peptides, only one has a sequence (GGRSPSLRLRFamide) indicating that it is a FaRP. This peptide is not active on the *Limulus* heart. Of the remaining peptides, GHSLLHFamide has potent, *inhibitory* effects on the cardiac rhythm. Our findings suggest the presence of *Limulus* FaRPs distinct from these peptides.

In recent years the number of identified arthropod FaRPs has grown considerably. The structurally related cardioactive FaRPs in crustaceans all share the C-terminal sequence RXFLRFamide (see Krajniak, 1991). Our data suggest that the *Limulus* CNS may contain one or more peptides of similar structure. These peptides may have a cardioregulatory function similar to that of N-terminally extended FaRPs in crustaceans and mollusks.

Acknowledgments

The authors thank Karen Doble (Whitney Laboratory, St. Augustine, Florida) for HPLC and radioimmunoassay of *Limulus* extracts. We also thank Drs. Michael J. Greenberg (Whitney Laboratory) and Eve Marder (Brandeis University, Waltham, Massachusetts) for their generous contributions of peptides and advice, Dr. Ronald Calabrese (Emory University, Atlanta, Georgia) for advice on peptide purification strategies, and Lowell Ericsson (University of Washington, Seattle, Washington) for mass spectroscopy. Thanks are given to Dr. Kevin Krajniak (University of Charleston, South Carolina) for comments on an earlier draft of this manuscript. This work was supported by a Grass Foundation Fellowship to J.R.G., by a Swarthmore College grant to J.R.G., and by NIH grant HL 28440 to Dr. Michael J. Greenberg.

Literature Cited

Augustine, G. J., R. H. Fetterer, and W. H. Watson III. 1982. Amine modulation of the neurogenic *Limulus* heart. *J. Neurobiol.* **13:** 61–74.

Augustine, G. J., and R. H. Fetterer. 1985. Neurohormonal modulation of the *Limulus* heart: amine actions on cardiac ganglion neurones. *J. Exp. Biol.* **118:** 53–69.

Cuthbert, B. A., and P. D. Evans. 1989. A comparison of the effects of FMRFamide-like peptides on locust heart and skeletal muscle. *J. Exp. Biol.* **144:** 395–415.

Duve, H., A. J. Elia, I. Orchard, A. H. Johnsen, and A. Thorpe. 1993. The effects of calliFMRFamides and other FMRFamide-related neuropeptides on the activity of the heart of the blowfly *Calliphora vomitoria*. *J. Insect Physiol.* **39**(1): 31–40.

Gaus, G., K. E. Doble, D. A. Price, M. J. Greenberg, T. D. Lee, and B-A. Battelle. 1993. The sequences of five neuropeptides isolated from *Limulus* using antisera to FMRFamide. *Biol. Bull.* **184:** 322–329.

Greenberg, M. J., and D. A. Price. 1992. Relationships among the FMRFamide-like peptides. *Prog. Brain Res.* **92:** 25–37.

Groome, J. R. 1993. Distribution and partial characterization of FMRFamide-like peptides in the horseshoe crab, *Limulus polyphemus*. *Comp. Biochem. Physiol.* **104C**(1): 79–85.

Groome, J. R., and W. H. Watson III. 1991. Cardioregulatory peptides in *Limulus*: effects of F_1, F_2 and an endogenous FMRFamide-like peptide on the neurogenic heart. *Biol. Bull.* **181:** 353.

Krajniak, K. G. 1991. The identification and structure-activity relations of a cardioactive FMRFamide-related peptide from the blue crab *Callinectes sapidus*. *Peptides* **12:** 1295–1302.

Krajniak, K. G., and M. J. Greenberg. 1988. Structure-activity relations of FMRFamide-related peptides (FaRPs) on crustacean heart. *Soc. Neurosci. Abstr.* **14:** 533.

Kravitz, E. A., L. Kobierski, B. A. Trimmer, and M. F. Goy. 1987. Peptide F_1: a myoactive lobster peptide related to FMRFamide. *Soc. Neurosci. Abstr.* **13:** 1257.

Mercier, A. J., I. Orchard, M. Skerrett, and V. Tebrugge. 1991a. FMRFamide-related peptides from crayfish pericardial organs. *Soc. Neurosci. Abstr.* **17:** 200.

Mercier, A. J., I. Orchard, and V. Tebrugge. 1991b. FMRFamide-like immunoreactivity in the crayfish nervous system. *J. Exp. Biol.* **156:** 519–538.

Nagle, G. T., and M. J. Greenberg. 1982. A highly sensitive microbioassay for the molluscan neuropeptide FMRFamide. *Comp. Biochem. Physiol.* **71C:** 101–105.

Price, D. A., G. A. Cottrell, K. E. Doble, M. J. Greenberg, W. Jorenby, H. K. Lehman, and J. P. Riehm. 1985. A novel FMRFamide-related peptide in *Helix*. pQDPFLRFamide. *Biol. Bull.* **169:** 256–266.

Price, D. A., and M. J. Greenberg. 1989. The hunting of the FaRPs: the distribution of FMRFamide-related peptides. *Biol. Bull.* **177:** 198–205.

Price, D. A., W. Lesser, T. D. Lee, K. E. Doble, and M. J. Greenberg. 1990. Seven FMRFamide-related and two SCP-related cardioactive peptides from *Helix*. *J. Exp. Biol.* **154:** 421–437.

Trimmer, B. A., L. A. Kobierski, and E. A. Kravitz. 1987. Purification and characterization of FMRFamidelike immunoreactive substances from the lobster nervous system: isolation and sequence analysis of two closely related peptides. *J. Comp. Neurol.* **266:** 16–26.

Watson, W. H. III, J. R. Groome, B. M. Chronwall, J. Bishop, and T. L. O'Donohue. 1984. Presence and distribution of immunoreactive and bioactive FMRFamide-like peptides in the nervous system of the horseshoe crab, *Limulus polyphemus*. *Peptides* **5:** 585–592.

Watson, W. H. III, and J. R. Groome. 1989. Modulation of the *Limulus* heart. *Am. Zool.* **29:** 1287–1303.

Reference: *Biol. Bull.* **186:** 319–327. (June, 1994)

Cooling-Induced Activation of the Pericardial Organs of the Spiny Lobster, *Panulirus japonicus*

TAKETERU KURAMOTO AND MASAKI TANI

Shimoda Marine Research Center, University of Tsukuba 5-10-1, Shimoda, Shizuoka 415, Japan

Abstract. Ligamental nerves, extensions of the pericardial neurohemal organ of the spiny lobster, produce compound action potentials during cooling of the body, and become silent with warming. Heart-activators released from the pericardial organs into perfusate were collected from the antennule and leg stumps. The perfusate samples were bioassayed using the isolated heart and cardioarterial valves. The extent of heart activation was greatest in samples obtained during the first phase of cooling and was lowest during the initial phase of rewarming. The levels of cardioexcitor substances were clearly related to the firing behavior of the ligamental nerves. Moreover, one of the active factors produced responses identical to octopamine, a known pericardial organ amine. It is proposed that octopamine is released from the ligamental nerve terminals into the blood during cooling of the body.

Introduction

Alexandrowicz (1953) found neurohemal structures in the crustacean pericardium and called them pericardial organs. Since then, cardioactive substances of the organs have been examined using several decapod species (Welsh, 1961; Cooke and Sullivan, 1982). Dopamine and 5-hydroxytryptamine (serotonin) were identified first as pericardial amines (Florey and Florey, 1954; Cooke and Goldstone, 1970). Recently, proctolin, CCAP, and FMRFamide-related peptides were identified in the decapod pericardial organs (Sullivan, 1979; Kobierski *et al.*, 1987; Stangier *et al.*, 1987; Timmer *et al.*, 1987; Dircksen and Keller, 1988). The spiny lobster *Panulirus interruptus* has octopamine, serotonin, and proctolin but little dopamine in the pericardial organs (Sullivan *et al.*, 1977). These hormones are released by electrical stimulation of the organs (Cooke, 1964; Sullivan, 1978; Berlind and Cooke, 1970).

Serotonin activates the small cardiac neurons of decapods (Cooke and Hartline, 1975; Kuramoto and Ebara, 1988), whereas octopamine inhibits them (Benson, 1984) and directly enhances the cardiac muscle contraction (Kuramoto and Ebara, 1991). Thus it has been suggested that serotonin and octopamine exert antagonistic effects on the first and second systolic contraction (FSC and SSC) in *P. japonicus* (Kuramoto and Ebara, 1991). The pericardial peptides all may have excitatory actions on the heartbeat (Sullivan and Miller, 1984; Wilkens and McMahon, 1992; Yazawa and Kuwasawa, 1992). The flap muscles of cardioarterial valves regulate the cardiac outputs in crustaceans (Kuramoto and Ebara, 1984b; 1989; Kihara and Kuwasawa, 1984; Kihara *et al.*, 1985; Fujiwara-Tsukamoto *et al.*, 1992). The pericardial hormones modulate the flap muscle tension (Kuramoto and Ebara, 1984b, 1989; Kuramoto *et al.*, 1992). Much evidence suggests that the pericardial hormones exert their actions not only on the cardiovascular system but also on the respiratory, stomatogastric, and locomotor systems (Kravitz, 1988; Harris-Warrick *et al.*, 1989; Kuramoto, 1991; Rajashekhar and Wilkens, 1992). However, no one has yet shown that any natural stimuli result in activation of the pericardial organs. Here we report that the ligamental nerves, extensions of the pericardial organ of the spiny lobster, exhibit an increase in extracellularly recorded propagated electrical activity during a drop in temperature. If cardioactive factors increase in the blood as a result of the cooling-dependent neurosecretion, they can be detected rapidly and simply by our bioassay methods using the isolated heart and cardioarterial valves (Kuramoto and Ebara, 1984b, 1988, 1991).

In this report, we describe the firing properties of pericardial neurosecretory cells in response to cooling, and

Received 27 August 1993; accepted 25 March 1994.

Abbreviations: CCAP, crustacean cardioactive peptide; FSC, first systolic contraction; SSC, second systolic contraction.

demonstrate cooling-dependent increases of cardioactivators in body fluid. A preliminary account of this study has been reported (Kuramoto and Tani, 1991).

Materials and Methods

Japanese spiny lobsters (*Panulirus japonicus*, 200 g wt) were used for obtaining body fluid ($n = 10$) and for bioassay ($n = 10$). An antennule and a fifth leg of the animal were cut off. Body fluids emanating from the antennule and leg stumps were collected in glass bottles (15 ml) while the physiological saline maintained at room temperature (20 ± 1°C) was injected into the pericardium using a catheter. Because the antennal artery extends straight from the heart to the antennule, the cut antennule provides a direct sampling site for substances secreted into the heart from ligamental nerve terminals. In contrast, the pathway from the heart to the legs is less direct, so perfusate samples from the legs might contain substances released from many neurosecretory sites (Cooke and Sullivan, 1982). The duration sampled by each bottle was 2 or 3 min. To cool the body, the perfusion line was switched by a stopcock to the line for the cold saline (13–15°C). The dead time for flow of the perfusate through the tubing was about 10 s. The duration of cooling experienced by the lobster was 4 or 6 min, and each series of cooling and rewarming was repeated three or four times in each experiment.

Each sample of body fluids (perfusate) was injected by micropipette (1 ml) into the posterior right ostium of an isolated heart from another animal. The perfusate samples were also applied to the anterior and posterior valves (AV, PV) that had been isolated from the lobster heart. Contractions of the heart, AV, and PV were recorded with strain gauges. The recording methods and the characteristics of the heart and valves responding to the pericardial hormones have been reported (Kuramoto and Ebara, 1984a, b, 1988, 1989, 1991).

To record axonal impulses of the ligamental nerves, the pericardium was opened by removing the dorsal part of the thorax (Fig. 1a). To record impulses further from the proximal part of the third segmental nerves (root 3), the cephalic portion and the visceral organs in the thorax were removed ($n = 10$). Nerve impulses were recorded with glass suction electrodes. The pericardium and the thoracic ventral floor were perfused with the warm or cold saline using the perfusion lines described above. Fluid temperature either in the pericardial cavity or on the thoracic floor was monitored with an electronic thermometer using a platinum sensor. The electrical signals were displayed by either a pen recorder (dc—100 Hz) or a thermal dot-array recorder (NEC Sanei Omniace RT2108; dc—50 kHz).

Results

Electrical activity of the ligamental nerves for cooling

The dorsal nerves of the thoracic ganglia (root 3) enter the pericardium, and their branches extend along the three pairs of ligaments. Each of these nerves branches extensively on each ligament. The nerve terminals are distributed near the ostia (Fig. 1a). When the pericardial cavity was perfused with the cold saline, a train of impulses could be recorded from the proximal part of the ligamental nerve (Fig. 1b). The impulses stopped upon rewarming. Delay of the nerve responses from the start of pericardial cooling was about 20 s. The impulse frequency rose to over 5 Hz with the cooling. Large impulses recorded from a ligamental nerve were usually compound. The example shown in Figure 1c was composed of three kinds of impulses as judged by its waveform. Spontaneously generated impulses of the ligamental nerves were often observed at room temperature. However, they ceased with warming of 0.5–2°C (not shown in figure).

Cold stimulation also elicited a few kinds of impulses in the proximal part of root 3 with a delay shorter than 15 s. Figure 2 shows the typical firing pattern of the cool-sensitive neuron. With decreasing temperature (dT > 0.5°C), the cool-sensitive neurons either initiated impulses (Fig. 2a) or raised the frequency of spontaneous impulses (Fig. 2b). The magnitude of the increase in impulse frequency depended on the temperature decrease over a range of 0.5–5.5°C, and impulse frequency increased almost in inverse proportion to the cooling. For this example (Fig. 2b), the maximum rate of cooling was 4°C/min, indicating that the cool-sensitive neuron appeared to adapt slowly to the stimulation. However, the frequency did not always continue to increase with decreasing temperature. In Figure 2a, the response can be seen to plateau 1 min after the onset of stimulation. In contrast, the impulses elicited by cooling stopped quickly with either rewarming or slowing down of cooling rate. Spontaneous impulses of the cool-sensitive neurons also ceased with a small increase in temperature (0.5–2°C). These impulses that responded to cooling and rewarming were usually large in amplitude; most of the small-amplitude impulses were not so sensitive to the cold stimulation.

Bioassay of perfusate samples for cardioactive substances

When isolated hearts were treated with samples of the perfusate collected from cooled animals, the frequency and amplitude of the contractions increased tonically. In contrast, stimulation with perfusate samples collected before and after cooling produced only small, phasic changes in cardiac activity. These findings indicate that cardioac-

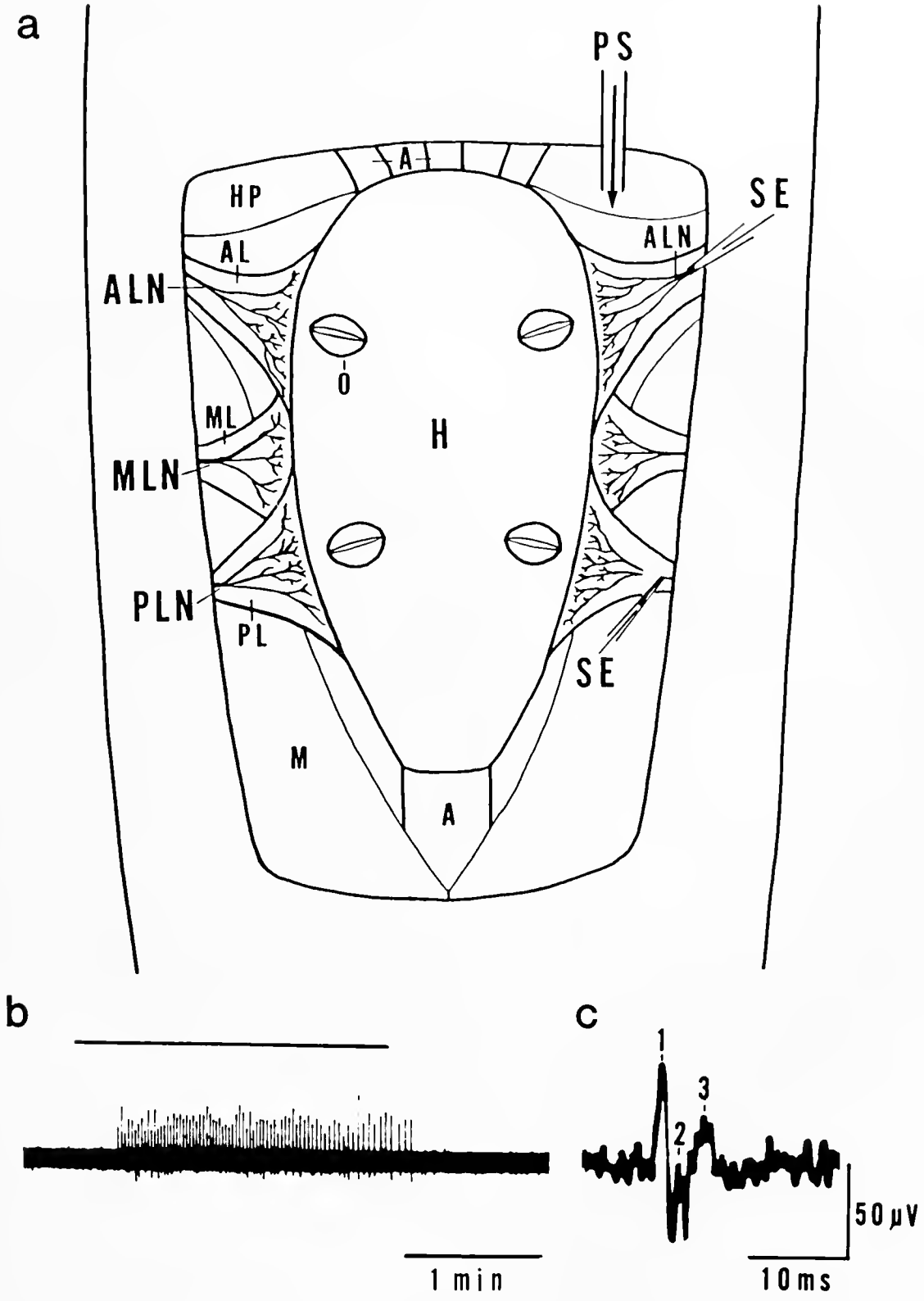

Figure 1. (a) The hepatopancreas (HP) and skeletal muscles (M) surround the heart (H), which is suspended by the anterior, median, and posterior ligaments (AL, ML, and PL). Three anterior and one posterior arteries (A) leave from the heart. Three pairs of ligamental nerves (ALN, MLN, and PLN) branch and terminate on the AL, ML, and PL, respectively, near ostia (O). The pericardial cavity was perfused with the physiological saline (PS) while impulse activity of the ligamental nerves was recorded with the suction electrode (SE). (b) An extracellular recording of electrical activity in an ALN in response to pericardial cooling ($dT = 3°C$). The duration of cooling is indicated by the bar. (c) The impulse waveform, shown by a fast speed, exhibiting three inflections (1–3).

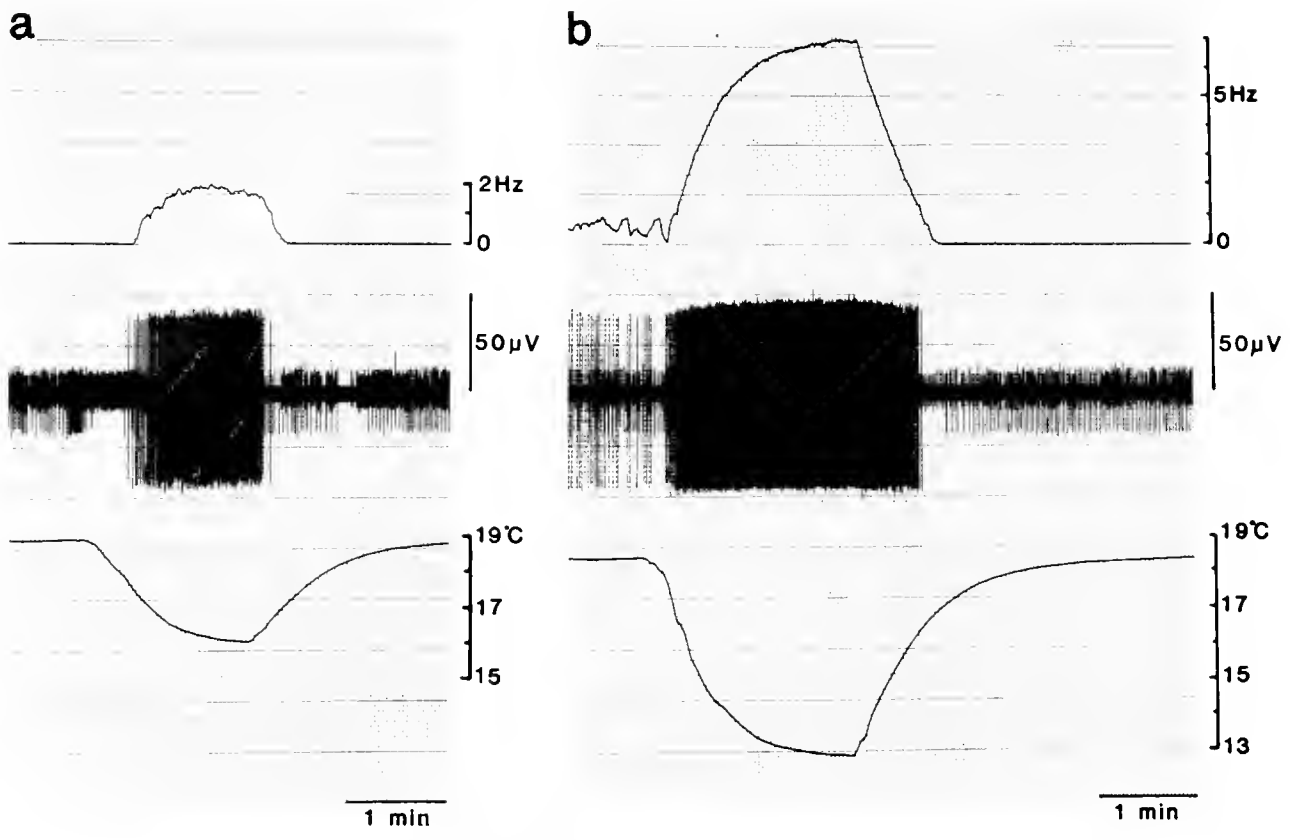

Figure 2. The electrical responses of cool-sensitive neurons in the proximal part of root 3 of the lobster thoracic ganglion. (a) A burst of large-amplitude impulses (middle record) triggered by cooling. The impulse frequency (upper trace) rose to 2 Hz when the temperature (lower trace) dropped from 19 to 16°C but declined during the latter portion of the period of cooling. The spontaneous impulses of small and medium amplitude were unaffected by the change in temperature. (b) Another recording from the same preparation as (a). The impulse frequency (upper trace) rose from 0.5 to 7 Hz in response to cooling (lower trace) from 18.5 to 13°C. Note that the increase in impulse frequency is closely related to the decrease in temperature, since the cooling rate (4°C/min) is higher than the rate at which spike adaptation occurs.

tivators are present in body fluids during periods of internal cooling.

Since the pericardial hormones octopamine and serotonin have differential effects on the FSC and the SSC, the cardiac responses to applied perfusate samples were scrutinized to identify selective differences in FSC or SSC activity. Figure 3 shows an example of the bioassays using a heart whose beat is deficient in the SSC (Kuramoto and Ebara, 1984a, 1988). The perfusate samples obtained before and after cooling had a slight action on the frequency of the SSC. In contrast, the perfusate samples collected during cooling enhanced the FSC over a 5-min period and increased the SSC for 2 min. These effects on the FSC and the SSC will be discussed later in connection with identification of cardioactivators contained in the sample.

The posterior cardioarterial valve (PV) contracted in response to samples of perfusates. The contractile activity was greatest during the first phase of cooling (C1) and lowest during the initial phase of rewarming (W1) (Fig. 4 a–d). The highest and lowest activities of these valves were comparable to those generated by 10^{-7}–10^{-6} M and 10^{-8} M or less octopamine, respectively (Fig. 4e, f).

The cardioactive factors in the perfusate were further examined using both the AV and PV. The largest responses were produced by body fluid sampled during the first phase of cooling (C1). Figure 5 shows an example of the positive results (10 from 16 trials). Active factors in the samples caused the AV to relax and the PV to contract. The relaxation could be observed clearly in the spontaneously contracting anterior cardioarterial valves. One component of the active fluid produced a rapid, short-term (a few minutes) relaxation of the AV, and another component did so slowly over long durations (5–6 min). The effect of octopamine on the AV is identical to the rapid relaxation of AV. Phentolamine (10^{-5} M), an an-

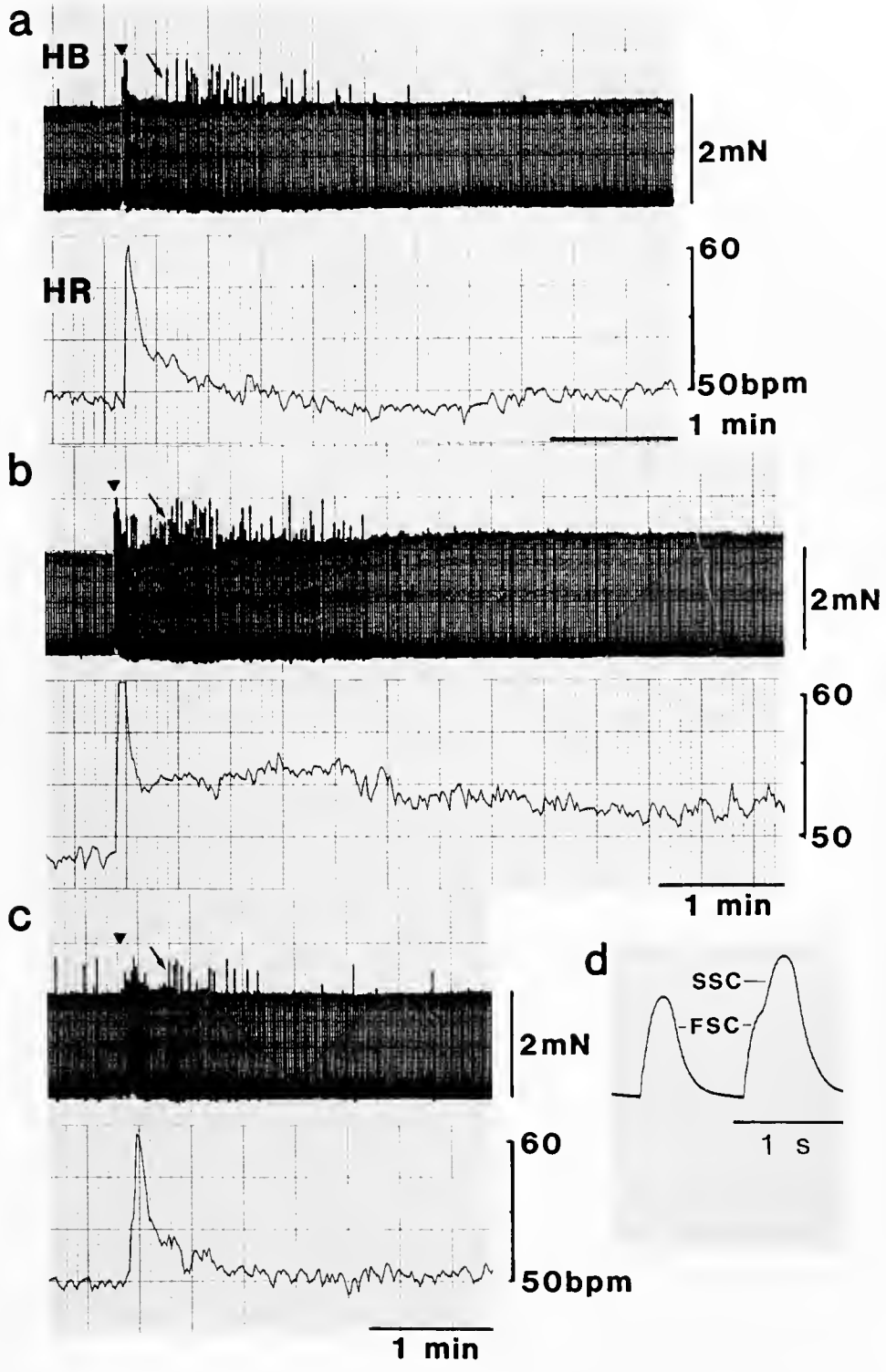

Figure 3. Bioassay for active factors in body fluid using the isolated lobster heart. The body fluid (BF) was collected from the antennule. The heart beat (HB) and rate (HR) were recorded while the perfusate sample (BF, 1 ml) was pulse-applied to the heart at the time indicated by an arrowhead. (a) Response to the BF before cooling. (b) The response to the BF during the first phase of cooling. (c) The response to the BF during the initial phase of rewarming. The rapid increase in beat amplitude (arrows in a–c) is due to the superimposition of SSC on the FSC as shown in (d). The long-lasting and remarkable increases in HR and FSC and the abundant SSC are observed in b.

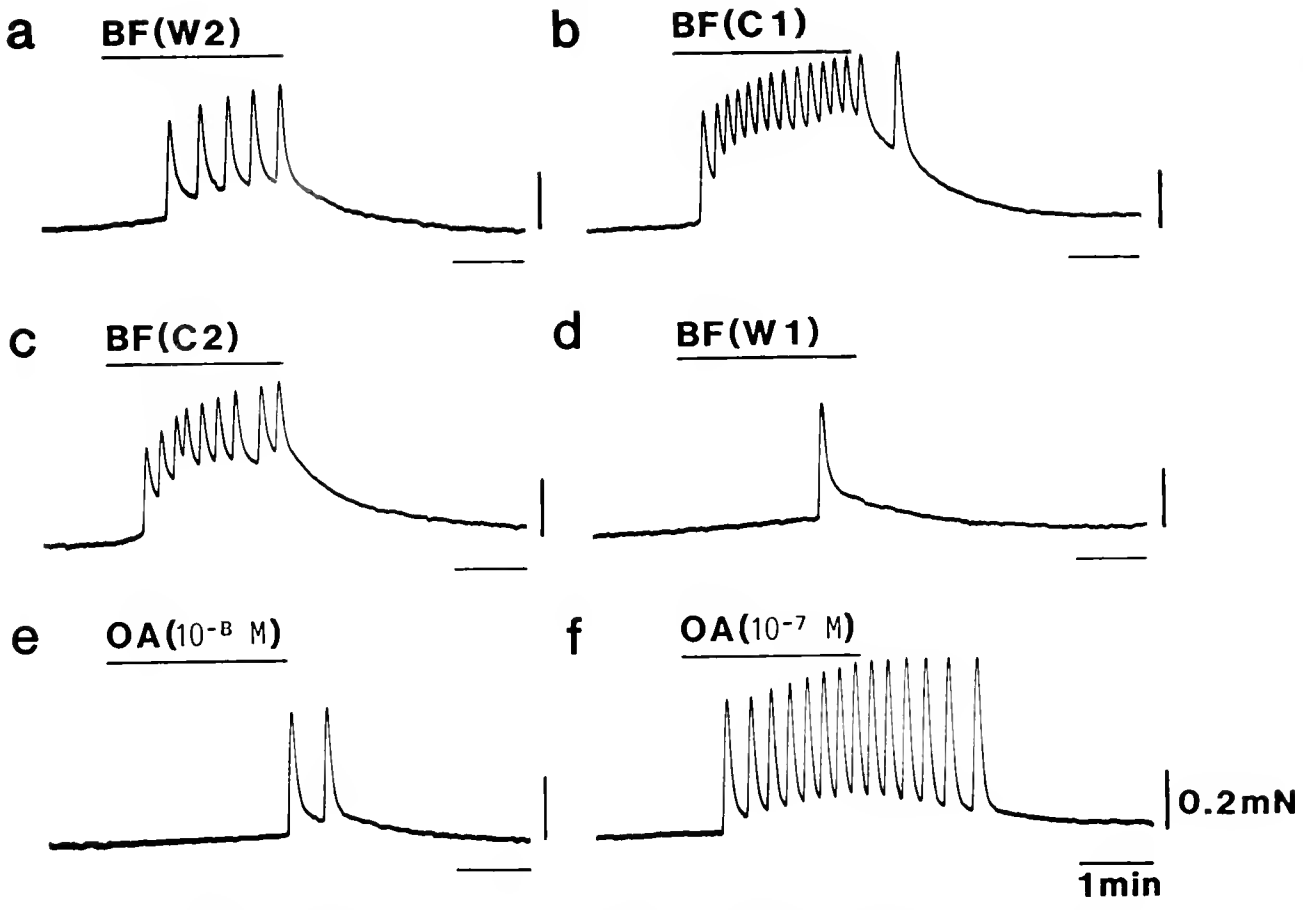

Figure 4. Bioassay of body fluid using the posterior cardioarterial valve of the lobster. The body fluid (BF) was collected from the leg. Each of the perfusate samples (BF, 2 ml) was applied to the valve (bars) while tension of the flap muscle was measured. (a) A typical response of the valve to the BF before cooling (W2). (b) The response to the BF during the first phase of cooling (C1). (c) The response to the BF during the late phase of cooling (C2). (d) The response to the BF during the initial phase of rewarming (W1). (e–f) Two examples of the valve response to octopamine (OA, 2 ml).

tagonist of octopamine, blocked the rapid relaxation of AV (not shown in figure). The relaxing activity of the samples obtained just after the onset of cooling was comparable to that of 10^{-7} *M* octopamine (Fig. 5b, c).

Discussion

The anatomical features of the ligamental nerve plexuses (Fig. 1a) are almost identical with those of *P. interruptus* (Sullivan *et al.*, 1977). Axons in the ligamental nerves come from the thoracic ganglia via root 3. The firing pattern of the ligamental nerves and root 3 in response to cooling was similar (Figs. 1b and 2a). Similar responses of the root 3 have also been observed in the ganglia isolated completely from the thorax of lobsters and shrimps (unpub. data).

The response of the ligamental nerve to cold stimulation occurred following a delay of 20 s. This is at least 5 s longer than the corresponding delay recorded in the proximal part of root 3 (<15 s). However, if the cold receptors were in the ganglia, 5 s might be sufficient to account for the time required for the cold saline perfusing the pericardium to arrive in the thoracic ganglia, and the time for neural conduction from the ganglia to the ligaments under the low temperature. Judging from the cardiac outflow, the latency of 5 s is reasonable (Spaargaren, 1974). The cooling-dependent firing was observed even in the isolated ganglia. Therefore, the impulse activity of the ligamental nerves might be driven by some of the cool-sensitive neurons in the thoracic ganglia.

The amine-containing neurons on thoracic nerve trunks of the lobster *Homarus americanus* extend their axons to the pericardial organs (Evans *et al.*, 1976a, b). However, these neurons fire with increasing temperature (Konishi and Kravitz, 1978). Therefore, they seem to be different from the neurosecretory cells that we found.

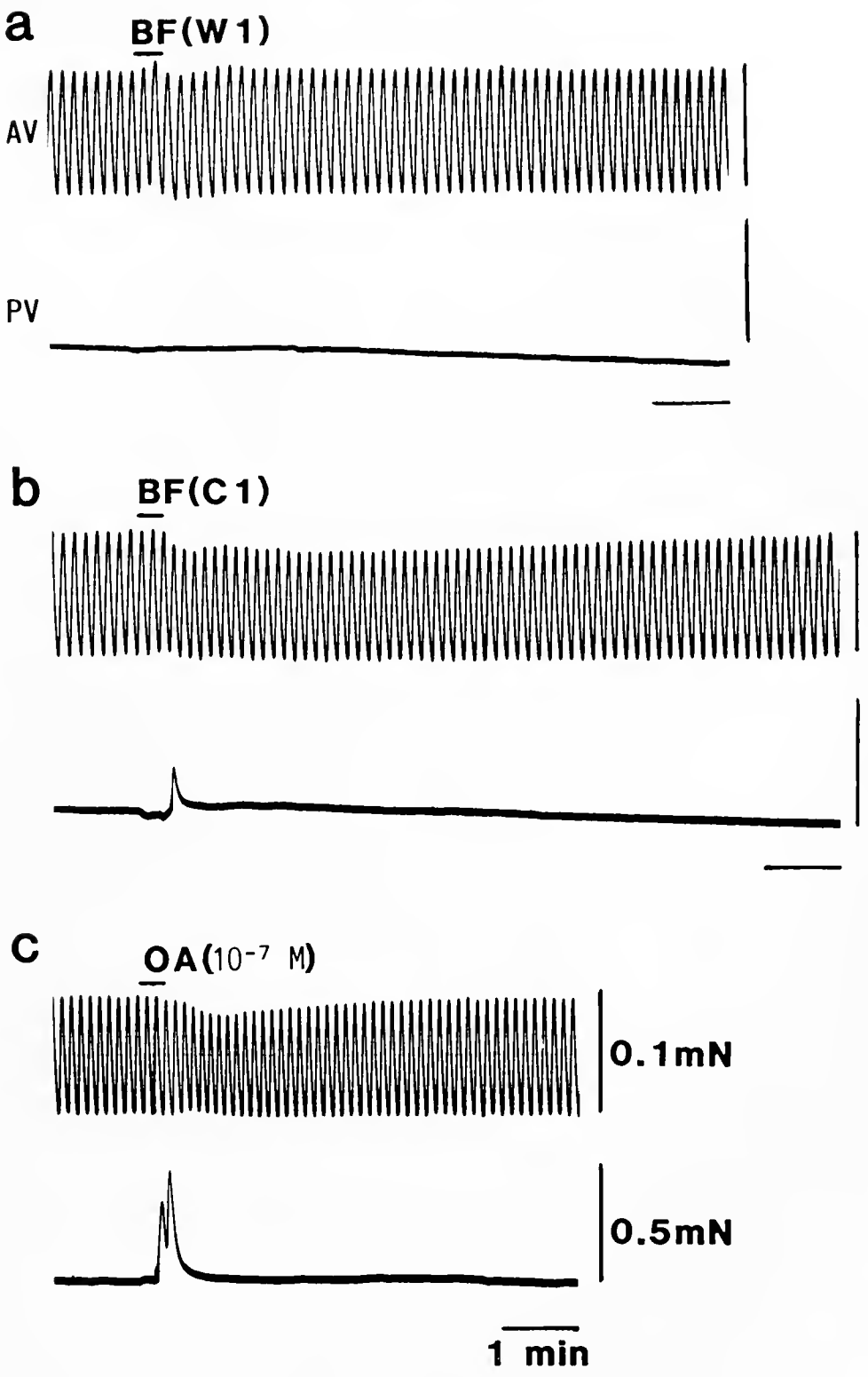

Figure 5. Bioassay of body fluid using the anterior and posterior cardioarterial valves (AV and PV). The body fluid was obtained from the antennule. Each of the perfusate samples (BF, 1 ml) was applied to the valves (bars) while alterations in their tension were recorded simultaneously. (a) Small responses of the AV and PV to the BF before cooling (W1). (b) Differential responses of the AV and PV to the BF during the first phase of cooling (C1). (c) The responses of AV and PV to octopamine (OA). The spontaneously contracting valve (AV) was useful to observe the relaxing effects.

The presence of cool-sensitive neurons in the thoracic and abdominal ganglia and the abdominal stretch receptors of the crayfish has been reported (Kerkut and Taylor, 1956, 1958; Winter, 1973). However, the transduction mechanisms and the physiological role of the neural activity have thus far been unclear. The present study suggests that this cool-sensitivity is probably related to the pericardial neurosecretion. That is, cardioactivators in blood increase with a drop of body temperature, as demonstrated by our bioassay methods (Figs. 3–5). The cardioactivators also may regulate the excitability of nerve and muscle cells.

Long-lasting augmentation of the FSC by octopamine and proctolin has been observed (Kuramoto and Ebara, 1991; unpub. data). Therefore, it seems likely that the tonic increase of FSC observed here (Fig. 3b) was caused by the actions of octopamine or some pericardial peptides present in the perfusate samples.

Serotonin elicits and enhances the SSC by its specific action on the small cardiac neurons (Kuramoto and Ebara, 1988). Therefore, the increase in beat amplitude resulting from the SSC (Fig. 3, arrows) is likely to have been produced by the action of serotonin in the samples.

The responses of the isolated cardioarterial valves provide further insight into the identity of the substances released during cold stimulation. The AV showed rapid and slow relaxations while the PV showed a slight contraction (Fig. 5b). This suggests that the perfusate may contain at least two active factors. Octopamine causes the AV to relax rapidly and the PV to contract, whereas serotonin relaxes both the AV and PV (Kuramoto and Ebara, 1984b). Therefore, the rapid and slow inhibitory factors may be octopamine and serotonin, respectively. Taken together with the sampling conditions, the body fluid sampled from the antennule during cooling probably contains a large amount of octopamine and an undetermined but lesser amount of serotonin. Confirmation of this hypothesis will require biochemical or electrochemical (HPLC) identification of the active factors. Nevertheless, we concluded that the lobster pericardial organs are activated by a decrease in body temperature and release their hormones, one of which is likely to be octopamine.

Acknowledgments

The authors thank Dr. Jerrel L. Wilkens for critical reading of an early draft of the manuscript and the technical staff of SMRC for assistance. Contribution No. 567 from Shimoda Marine Research Center.

Literature Cited

Alexandrowicz, J. S. 1953. Nervous organs in the pericardial cavity of the decapod Crustacea. *J. Mar. Biol. Assoc. U. K.* **31:** 563–580.

Benson, J. A. 1984. Octopamine alters rhythmic activity in the isolated cardiac ganglion of the crab, *Portunus sanginolentus*. *Neurosci. Lett.* **44:** 59–64.

Berlind, A., and I. M. Cooke. 1970. Release of a neurosecretory hormone as peptide by electrical stimulation of crab pericardial organs. *J. Exp. Biol.* **53:** 679–686.

Cooke, I. M. 1964. Electrical activity and release of neurosecretory material in crab pericardial organs. *Comp. Biochem. Physiol.* **13:** 353–366.

Cooke, I. M., and M. W. Goldstone. 1970. Fluorescence localization of monoamines in crab neurosecretory structures. *J. Exp. Biol.* **53:** 651–668.

Cooke, I. M., and D. K. Hartline. 1975. Neurohormonal alteration of integrative properties of the cardiac ganglion of lobster *Homarus americanus*. *J. Exp. Biol.* **63:** 33–52.

Cooke, I. M., and R. E. Sullivan. 1982. Hormones and neurosecretion. Pp. 205–391 in *The Biology of Crustacea*, Vol. 3, H. L. Atwood and D. C. Sandeman, eds. Academic Press, New York.

Dircksen, H., and R. Keller. 1988. Immunocytochemical localization of CCAP, a novel crustacean cardioactive peptide, in the nervous system of the shore crab, *Carcinus maenas* L. *Cell Tissue Res.* **254:** 347–360.

Evans, P. D., R. E. Kravitz, and B. R. Talamo. 1976a. Association of octopamine with specific neurones along lobster nerve trunks. *J. Physiol.* **262:** 51–70.

Evans, P. D., R. E. Kravitz, and B. R. Talamo. 1976b. Octopamine release at two points along lobster nerve trunks. *J. Physiol.* **262:** 71–89.

Florey, E., and Elisabeth Florey. 1954. Über die mögliche Bedeutung von Enteramin (5-oxytryptamine) als nervöser Aktionssubstanz bei Cephalo-poden und decapoden Crustaceen. *Z. Naturforsh.* **9b:** 58–68.

Fujiwara-Tsukamoto, Y., K. Kuwasawa, and J. Okada. 1992. Anatomy and physiology of neural regulation of haemolymph flow in the lateral arteries of the isopod crustacean, *Bathynomus doederleini*. Pp. 70–85 in *Comparative Physiology II*, R. B. Hill, K. Kuwasawa, B. R. McMahon, and T. Kuramoto, eds. Karger, Basel.

Harris-Warrick, B. M., R. E. Flamm, B. R. Johnson, and P. S. Katz. 1989. Modulation of neural circuits in Crustacea. *Am. Zool.* **29:** 1205–1320.

Kerkut, G. A., and B. J. R. Taylor. 1956. Effect of temperature on the spontaneous activity from the isolated ganglia of the slug, cockroach and crayfish. *Nature* **178:** 426.

Kerkut, G. A., and B. J. R. Taylor. 1958. The effect of temperature on the activity of poikilotherms. *Behaviour* **13:** 259–279.

Kihara, A., and K. Kuwasawa. 1984. A neuroanatomical and electrophysiological analysis of nervous regulation in the heart of an isopod crustacean, *Bathynomus doederleini*. *J. Comp. Physiol. A* **154:** 883–894.

Kihara, A., K. Kuwasawa, and T. Yazawa. 1985. Neural control of the cardio-arterial valves in an isopod crustacean, *Bathynomus doederleini*: excitatory and inhibitory junctional potentials. *J. Comp. Physiol. A* **157:** 529–536.

Kobierski, L. A., B. S. Beltz, B. A. Trimmer, and E. A. Kravitz. 1987. FMRFamidelike peptides of *Homarus americanus*: distribution, immuno-cytochemical mapping, and ultra structural localization in terminal varicosities. *J. Comp. Neurol.* **266:** 1–15.

Konishi, S., and E. R. Kravitz. 1978. The physiological properties of amine-containing neurones in the lobster nervous system. *J. Physiol.* **279:** 215–229.

Kravitz, E. R. 1988. Hormonal control of behavior: amines and the biasing of behavioral output in lobsters. *Science* **241:** 1775–1781.

Kuramoto, T. 1991. Effects of pericardial hormones on impulse activity of swimmeret motor neurons of *Procambarus clarkii*. *Comp. Biochem. Physiol.* **98A:** 185–190.

Kuramoto, T., and A. Ebara. 1984a. Effects of perfusion pressure on the isolated heart of the lobster, *Panulirus japonicus*. *J. Exp. Biol.* **109:** 121–140.

Kuramoto, T., and A. Ebara. 1984b. Neurohormonal modulation of the cardiac outflow through the cardioarterial valve in the lobster. *J. Exp. Biol.* **111:** 123–130.

Kuramoto, T., and A. Ebara. 1988. Effects of 5-hydroxytryptamine and filling pressure on the isolated heart of the lobster, *Panulirus japonicus*. *J. Comp. Physiol. B.* **158:** 403–412.

Kuramoto, T., and A. Ebara. 1989. Contraction of flap muscle in the cardioarterial valve of *Panulirus japonicus*. *Comp. Biochem. Physiol.* **93A:** 419–422.

Kuramoto, T., and A. Ebara. 1991. Effects of octopamine and filling pressure on the isolated heart of the lobster, *Panulirus japonicus*. *J. Comp. Physiol. B.* **161:** 339–347.

Kuramoto, T., Y. Hirose, and M. Tani. 1992. Neuromuscular transmission and hormonal modulation in the cardioarterial valve of the lobster, *Homarus americanus*. Pp. 62–69 in *Comparative Physiology Vol 11*, R. B. Hill, K. Kuwasawa, B. R. McMahon, and T. Kuramoto, eds. Karger, Basel.

Kuramoto, T., and M. Tani. 1991. Heart activation against dropping of body temperature in the spiny lobster, *Panulirus japonicus*. *Comp. Physiol. Biochem. Jpn.* **8:** 86 (abstract).

Rajashekhar, K. P., and J. L. Wilkens. 1992. Dopamine and nicotine, but not serotonin, modulate the crustacean ventilatory pattern generator. *J. Neurobiol.* **23:** 680–691.

Spaargaren, D. H. 1974. Measurements of relative rate of blood flow in the shore crab, *Carcinus maenas*, at different temperatures and salinities. *Neth. J. Sea Res.* **8:** 398–406.

Stangier, J., C. Hilbich, K. Beyreuther, and R. Keller. 1987. Unusual cardioactive peptide (CCAP) from pericardial organs of the shore crab *Carcinus maenas*. *Proc. Natl. Acad. Sci. USA* **84:** 575–579.

Sullivan, R. E. 1978. Stimulus-coupled ^{3}H-serotonin release from identified neurosecretory fibers in the spiny lobster, *Panulirus interruptus*. *Life Sci.* **22:** 1429–1438.

Sullivan, R. E. 1979. A proctolin-like peptide in crab pericardial organs. *J. Exp. Zool.* **210:** 543–552.

Sullivan, R. E., B. J. Friend, and D. L. Barker. 1977. Structure and function of spiny lobster ligamental nerve plexuses: evidence for synthesis, storage and secretion of biogenic amines. *J. Neurobiol.* **8:** 581–605.

Sullivan, R. E., and M. W. Miller. 1984. Dual effects of proctolin on the rhythmic burst activity of the cardiac ganglion. *J. Neurobiol.* **15:** 173–196.

Timmer, B. A., L. A. Kobierski, and E. A. Kravitz. 1987. Purification and characterization of FMRFamidelike immunoreactive substances from the lobster nervous system: isolation and sequence analysis of two closely related peptides. *J. Comp. Neurol.* **266:** 16–26.

Welsh, J. H. 1961. Neurohumors and neurosecretion. Pp. 281–311 in *The Physiology of Crustacea*, Vol. II, T. H. Waterman, ed. Academic Press, New York.

Wilkens, J. L., and B. R. McMahon. 1992. Intrinsic properties and extrinsic neurohormonal control of crab cardiac hemodynamics. *Experientia* **48:** 827–833.

Winter, C. 1973. The influence of temperature on membrane processes. Pp. 45–53 in *Effects of Temperature on Exothermic Organisms*, W. Wieser, ed. Springer, Berlin.

Yazawa, T., and K. Kuwasawa. 1992. Intrinsic and extrinsic neural and neurohumoral control of the decapod heart. *Experientia* **48:** 834–840.

Reference: *Biol. Bull.* **186:** 328–341. (June, 1994)

Biological Characteristics and Biomedical Applications of the Squid *Sepioteuthis lessoniana* Cultured Through Multiple Generations

PHILLIP G. LEE, PHILIP E. TURK, WON TACK YANG, AND ROGER T. HANLON

Marine Biomedical Institute, University of Texas Medical Branch, Galveston, Texas 77555-0863

Abstract. Providing squids—especially their giant axons—for biomedical research has now been achieved in 10 mariculture trials extending through multiple generations. The noteworthy biological characteristics of *Sepioteuthis lessoniana* are (1) this species is behaviorally and morphologically well suited to the laboratory environment; (2) the life cycle is completed in 4–6 months; (3) growth is rapid (12% and 5% wet body weight d^{-1} for 100 d and for the life span, respectively), with adult size ranging from 0.4–2.2 kg; (4) feeding rates are high (30% wet body weight d^{-1}), and a variety of live crustaceans and fishes are eaten; (5) crowding is tolerated (about 4 squids m^{-3}); (6) the incidence of disease and cannibalism is low; and (7) reproduction in captivity allows culture through three successive generations. Engineering factors contributed to culture success: (1) physical design (*i.e.*, size, shape, and painted pattern) of the culture tanks; (2) patterns of water flow in the culture tanks; (3) water filtration systems; and (4) spawning substrates. Initial production (a few hundred squids per year) suggests that large-scale culture will be able to supply the needs of the biomedical research community. The size (>400 μm in diameter) and characteristics of the giant axons of *Sepioteuthis* are appropriate for experimentation, and other studies indicate that the eye, oculomotor/equilibrium system, olfactory system, blood, and ink are equally suitable for research.

Introduction

The squid giant axon is a valuable preparation in biomedical research. Squids have been used as research models, not only for neuroscience, but for physiology (cardiac, circulatory, sensory and muscle), immunology, molecular biochemistry, nutritional biochemistry, oncology, aging, and ethology (Gilbert *et al.*, 1990). Squids also have commercial importance since they are eaten regularly in many regions of the world, especially the Orient and Southern Europe (Asian Development Bank/Infofish, 1991). To date no commercial culture projects have been initiated, but limited stocking programs have been investigated in Japan (Sato and Tsuzaki, 1984; Japan Sea Farming Fisheries Association, 1985; Nagata and Hirata, 1986).

Attempts to culture squids during the last 50 years have been unsuccessful due to the organism's small hatching size, unknown dietary habits, active behavior, and susceptibility to skin damage and disease resulting from captivity (Hanlon, 1990; Hanlon *et al.*, 1991). Only the loliginid species *Loligo opalescens* has ever been cultured from field-collected eggs to the first laboratory-spawned generation, demonstrating the potential for mass culture of squids (Yang *et al.*, 1983, 1986).

Compared to other loliginid squid species, *Sepioteuthis lessoniana* Lesson, 1830 (Figs. 1 and 2) appears to be the most adaptable to the laboratory environment (Hanlon *et al.*, 1991). It is a neritic species distributed throughout the Indo-West Pacific (Okutani, 1980; Dotsu *et al.*, 1981; Lu and Tait, 1983), and it is valuable to the Japanese fishery (Suzuki *et al.*, 1983). Laboratory studies of *S. lessoniana*, conducted by Choe and Oshima (1961), Choe (1966a,b), Inoha and Sezoko (1968), Saso (1979), Tsuchiya (1982) and Segawa (1987), have described the early life stages and life cycle and have verified growth rates estimated from fishery data (reviewed by Segawa, 1987). Several of these culture trials spanned much of the life cycle (200–300 d) and demonstrated high growth rates (260 mm mantle length, ML, in 306 d; Tsuchiya, 1982).

Received 19 May 1993; accepted 1 March 1994.

Abbreviations: ML, dorsal mantle length; BW, wet body weight; IGR, instantaneous growth rate; G_p, parental generation; G_1, first laboratory generation; G_2, second laboratory generation; G_3, third laboratory generation; scuba, self-contained underwater breathing apparatus.

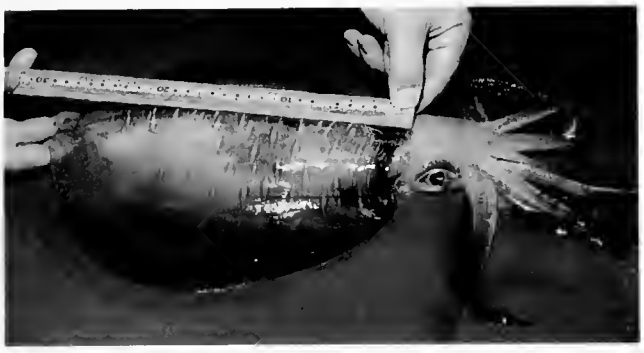

Figure 1. Adult *Sepioteuthis lessoniana* 280 mm ML and 2.21 kg BW after 194 days of culture. Note the extensive fin that is characteristic of the genus.

LaRoe (1971) reared the smaller Caribbean species *S. sepioidea* to 77 g in 146 d. The consistency of successful egg incubation and hatchling culture and the large size attained in the laboratory suggested that *S. lessoniana* might possess developmental, physiological, and behavioral characteristics suited to laboratory culture.

We have cultured this species continuously since September 1987 and have made 10 culture trials. *S. lessoniana* is unique among the larger loliginid species for its tolerance to handling and confinement, and it thus has great potential both as a non-mammalian model for biomedical research and as a commercial mariculture species. Our principal objectives were to evaluate and quantify the suitability of the species for culture in terms of growth, behavior, reproduction, and environmental tolerances. This report describes in detail 2 of the 10 culture trials, as they represent the major features of this species in captivity. In addition, *S. lessoniana* was evaluated concurrently for use as a giant axon preparation and for other biomedical research studies. Trial One was the first successful attempt to culture squids through multiple generations: the parental generation (G_p) originated from eggs collected in the field and was followed by first (G_1), second (G_2), and third (G_3) laboratory generations spawned in laboratory culture tanks. Trial Two was a subsequent production experiment in which larger numbers of parental generation (G_p) squids were cultured from field-collected eggs.

Materials and Methods

Egg transport

Sepioteuthis lessoniana egg strands for Trial One (G_p) were collected by a scuba diver (R. T. Hanlon) from rock and seagrass substrates and, prior to shipping, were held in flow-through aquaria at Kominato Laboratory, Tokyo University of Fisheries, Chiba Prefecture, Japan. The egg strands were shipped in 2-mil-thick plastic bags secured in polystyrene boxes, measuring 71 cm L × 39 cm W × 26 cm H, with 3.5-cm-thick walls. Fresh filtered seawater and gaseous O_2 were added to the bags in equal volumes (7 l total volume). Frozen chemical ice packs wrapped in newspaper were added to each box for a ratio of 150 g ice l^{-1} of seawater. The number of egg strands per bag, the volume of shipping water per egg strand, and the developmental stages (Segawa, 1987) of the embryos were varied among the bags so that changes in water quality (pH and NH_4-N) could be evaluated through a range of packing densities. When the eggs arrived in Texas, they were acclimated to the temperature, salinity, and water conditions of the hatchery tanks; *i.e.*, culture water was added to the shipping bags at a rate that limited temperature change to 0.5°C h^{-1}. Eggs for Trial Two (G_p) were collected, with the aid of scuba, from submerged trees in Tokushima Prefecture, Japan; the eggs were handled similarly to Trial One.

Laboratory-spawned eggs (G_1, G_2, and G_3) were removed from the production tanks and placed in hatchery tanks. Artificial substrates mimicking sea grass (plastic aquarium grass) or reef structures (carbonate rock and polyvinylchloride pipe) were provided for spawning. Frequently, artificial egg strands (silicone strands; Yang *et al.*, 1986) were tied to these substrates to further induce egg laying. The temperature and salinity of the production and hatchery tanks were matched prior to transfer, and the eggs were kept submerged at all times.

Tank characteristics, egg care, and hatching

Squid eggs, whether laboratory-spawned or field-collected, were incubated in 1.8-m circular hatchery tanks (described in Yang *et al.*, 1989; Turk and Lee, 1991) con-

Figure 2. Young *Sepioteuthis lessoniana* (*ca.* 60 days) showing a response to disturbance that can be shown even by hatchlings. Note the elaborate body patterning and posture.

taining natural seawater collected in the Gulf of Mexico at least 80 km offshore from Galveston, Texas. These tanks were equipped with a screened central core where the water was removed by siphon to the filter tank. The 1.8-m circular filter bed included an undergravel biofilter and protein skimmer. Filtered water was drawn from beneath the biofilter and pumped back to the culture tank through a particle filter (35-μm pore diameter), an activated carbon filter, and two 30-W ultraviolet (UV) sterilizers; the filtered water was discharged at the water surface through 2.5-cm spray bars. The flow pattern was circular (2.5 cm s^{-1}, measured halfway between the core and the tank wall).

The eggs were incubated 10 to 15 cm from the surface in groups of five to seven strands placed in plastic baskets or hung by threads from the spray bars. The eggs were examined daily; spent strands (completely hatched) and those with undeveloped embryos or with arrested development were removed. Care was taken to avoid disturbing the embryos, either by sudden mechanical perturbations or light intensity changes, or by extended exposure to light greater than 10–20 lx. Some egg strands in each trial (10–100%) were exposed to an iodine bath (100 ppm for 10 min at 48–96 h intervals) to kill bacteria, protozoans, and microinvertebrates that occurred on and in the egg strand tunic.

Hatchling and production culture

Upon hatching, the squids were reared in hatchery tanks for 4–6 weeks until they were >3–4 cm dorsal mantle length (ML). The incident lighting was increased with an overhead 400-W metal halide light (10–100 lx), but the center of the tank (about 45% of the area) was darker due to the addition of a small circular opaque cover. Water current was also variable due to the plastic egg baskets that hung in the tank. The hatchlings were therefore given a choice of light levels and current patterns. Dead squids and the remains of food organisms were removed by siphoning twice a day.

Juvenile squids were moved from the hatchery tanks to either a production raceway (6.1 m L × 2.4 m W × 0.9 m H, 15,000 l artificial seawater) or a large circular production tank (6.5 m circular by 1.75 m deep, 50,000 l artificial seawater). The filtration systems for the production tanks were similar to those used in the hatchery tanks (Yang *et al.*, 1989; Turk and Lee, 1991). During transfer, squids were caught in plastic beakers (>2 l) or in soft nylon nets, transferred immediately to 30-l ice chests, and transported quickly to the production tanks where the ice chests were submerged and the squids released. The squids were frequently, but not always, anaesthetized with 0.5–1.0% $MgCl_2$ solution to reduce stress during transport (Messenger *et al.*, 1985).

Water quality

Water quality (temperature, salinity, dissolved oxygen, pH, ammonia, nitrite, and nitrate) was monitored separately in each culture tank. Trace elements (Wimex brand) were added biweekly to replace those removed by water filtration and the squids. The pH and salinity were measured three times weekly. Ammonia-nitrogen levels (NH_4-N) were determined using the methods of Solorzano (Strickland and Parsons, 1972); nitrite (NO_2-N) was determined by the Shinn method (as applied to seawater by Bendschneider and Robinson in Strickland and Parsons, 1972); and nitrate (NO_3-N) was determined with prepackaged reagents (Hach Nitro Ver). Ammonia and nitrite were measured weekly, and nitrate was measured monthly or as needed.

Foods and feeding

Food organisms were added to the hatchery tanks soon after the squids hatched, usually within 48 h. Estuarine-collected (Galveston Bay, TX) and hatchery-reared crustaceans and fishes were the primary food organisms during the first 60 d. Larger shrimps and fishes were included as the squids grew. All food organisms were quarantined in filtered seawater for 24 h and were then rinsed with hatchery tank water before being fed to the squids. Food was added frequently, 6–8 times d^{-1} at first (0–60 d), and less frequently (3–5 times d^{-1}) thereafter. Food remains and feces were siphoned out of the tanks daily (1–2 times d^{-1}). During a specific period (days 38–94) of the G_p generation in Trial One, feeding rate was quantified by weighing the food offered to the squids at each feeding and by weighing the amount of uneaten food siphoned from the tank daily. Feeding rates were determined from estimates of squid biomass and the amount of food ingested daily (food offered minus uneaten remains).

Survival and growth

Squid mortalities were counted daily, and a representative sample of freshly dead squids (10–100%) was weighed to the nearest milligram wet body weight (BW) and measured to the nearest millimeter ML. Necropsies were performed when unexplained mortalities occurred. Once the number of squids that died during a trial and the number of squids transferred to a production tank were known, the number of hatchlings with which the experiment began could then be calculated, and survival rates could be estimated. Population growth rates are expressed as instantaneous growth rates (IGR; % BW d^{-1}) over a specific period of the life cycle. The IGR of cephalopods is typically calculated using an exponential function (Forsythe and Van Heukelem, 1987) and the formula is $BW(g) = ae^{b(t_2-t_1)}$, where a is the y-intercept, e the natural logarithm, and b equals the IGR for the time period t_2–t_1.

Daily biomass was estimated from the number of squids surviving each day, and from the recorded live BW of the squid on that day or from the estimated BW per squid for that day based on the IGR.

Behavior

Squid behavior was monitored mainly by observation through the glass windows installed in every hatchery and production tank; video and still photography were used occasionally. Observations were more frequent during initial hatching (1–4 times h^{-1}) and at the onset of reproductive activity (1–2 times h^{-1}) than during the intermediate period of growth and maturation (6–10 times d^{-1}).

Results

Egg transport

Trial One G_p eggs arrived from Japan on 2 September 1987. Ninety-five strands of stage 19–20 (Segawa, 1987) eggs were shipped in four bags at densities of 7.1, 6.7, 4.2, and 3.8 strands per liter of seawater. Transit time, from the beginning of packing to the beginning of unpacking, was 31 h. The temperature on arrival was 21.5°C in all four bags, while the pH and ammonia ranged from 7.50 and 1.55 ppm, respectively, in the most densely packed bag, to 7.70 and 0.91 ppm, respectively, in the least densely packed bag. Although the pH was lower and the ammonia concentrations higher than desired (8.0 and 0.1 ppm, respectively), no correlations between packing density, water quality, or hatching rate were established. Egg transport conditions for Trial Two (24 July 1990) were similar to those of Trial One (initial packing temperature, 20°C).

Egg development and hatching

Field-collected eggs. All field-collected eggs (G_p) were selected at the time of collection by visual inspection of the ova so that the fertility rate of the eggs approached 100% (Table I). At an average of five fertile ova per strand, there were approximately 475 ova shipped for Trial One. Forty-nine percent (235/475) of the ova hatched normally. Trial Two was started with 355 egg strands having an average of 4.1 fertile ova per strand for a total of 1456 embryos. The hatching rate of 37% (542/1466) was lower than that in Trial One. The hatching rates of the G_p eggs were significantly higher ($P < 0.01$) than for the subsequent laboratory-spawned eggs (G_1, G_2, G_3).

Egg strands from both trials were treated with iodine dips (100 ppm); these dips reduced bacterial counts on the surface of the egg tunic by 100-fold, from 10^5 to $<10^3$ colonies cm^{-2}. More concentrated dips (300 ppm) killed all surface bacteria, <10 colonies cm^{-2}. The iodine dips were uniformly effective against all bacteria, since 41 bacterial isolates were exposed to the iodine treatment (100 ppm) and no resistant forms were identified. The egg tunics appeared to deteriorate less when treated than when left untreated, but neither hatching rate nor hatchling survival were correlated with the iodine treatment ($P > 0.01$).

Spawning in the laboratory. At the beginning of the spawning period (148 days post hatching), the Trial One parental generation (G_p) comprised nine females. These females averaged 246 mm ML (range = 215–350 mm ML) and 953 g BW (range = 630–1866 g BW). We cannot be sure that every one of these nine females participated in egg laying, but 1857 G_1 egg strands were laid, an average of 206 egg strands or 1030 total embryos per female (at 5 ova per strand).

In the two subsequent generations (that produced G_2 and G_3 eggs), the spawning period started on days 182 and 230, respectively. The fecundity was 61 egg strands (553 egg strands/9 females) or 305 embryos for each of nine G_1 females, and 659 egg strands (1979 egg strands/3 females) or 3294 embryos for each of three G_2 females. The G_1 and G_2 females that participated in egg laying averaged 260 mm ML (range = 167–312 mm ML) and 1073 g BW (range = 288–1518 g BW) and 214 mm ML (range = 185–230 mm ML) and 682 g BW (range = 578–787 g BW), respectively.

Egg fertility ranged from 49.8% to 73.8% (Table I), and laboratory-spawned egg masses were often flawed mor-

Table I

Egg fertility, hatching rate, and hatchling survival (upon transfer from hatchery to production tanks) for laboratory-cultured Sepioteuthis lessoniana *in Trial One*

Parental generation	Hatchling generation	Strands laid (#)	Percent fertile (%)	Fertile embryos (#)	Hatching rate (%)	Survival in hatching tank (%)
Field collected	G_P	95	≈100.0	≈475	49.0	13
G_P	G_1	1857	73.8	6,850	5.9	40
G_1	G_2	553	73.8	2,040	0.8	29
G_2	G_3	1979	49.8	4,185	1.5	NA[1]

[1] The G_3 hatchlings were reared for only 2 weeks before the trial was terminated.

phologically; thus the hatching rates (0.8–5.6%) were significantly lower than those of the field-collected G_p eggs (49%). Some egg strands did not remain attached to the substrate; others were not sealed at one or both ends, causing the ova to slip out of the tunic sheath; still others were misshapen and contained no ova. All egg strands that appeared normal were incubated for more than 96 h in the production tanks, completing the most critical period of organogenesis. The egg strands were then treated with iodine and transferred to hatchery tanks containing fresh seawater of a temperature and salinity matched closely to that of the production tanks.

Survival and growth

Hatchlings averaged 5.3 mm ML (range 3.5–6.4 mm ML) and 8.2 mg BW (range 4.3–12.0 mg BW) during the three successive generations in Trial One (Fig. 3). The G_1 and G_2 hatchlings survived better in the hatchery tanks than the G_p hatchlings (Table 1; Fig. 4). Most mortalities were the result of premature hatching and starvation, but in a significant number the cause could not be determined. When the juveniles were transferred to the production tanks, survival rates improved to >70% (Fig. 4). During this 150–300 day production phase, the principal causes of death were tank system design (*i.e.*, jumping from tank, inking, and being sucked into the plumbing), 7–18%; cannibalism, 11–17%; starvation associated with cataracts, 2–11%; senescence or unidentified causes, 34–55%; and harvest for scientific experimentation, 22–32%. Cannibalism usually occurred after a squid was already moribund, so most mortalities attributed to cannibalism had another cause initially. More squids could have been used for experiments, but they were kept for broodstock, and eventually died after a period of senescence.

Trial Two consisted of 42 culture days in two hatchery tanks and 333 culture days in three production tanks (two raceways and the large circular production tank). On the night of day 206, the adult squids in the large circular production tank (55,000 l) suddenly became excited and began to ink, so that by morning the entire tank was black with ink. The whole episode was captured on videotape because an increase in irritability of the squids had been noticed and a camera had been installed to monitor the tank at night. Squid densities were the highest yet cultured in our tanks, 5.6 squids m^{-3}, and the nitrates were the highest recorded—94.4 ppm. Therefore, nitrate was believed to be acting as an irritant, initiating the inking behavior that eventually caused the death of all but one squid. In subsequent trials, additional protein skimmers and carbon filtration were added to all production tanks, and nitrate levels have been controlled (<50 ppm) by water exchanges. Deaths due to nitrate-induced inking have thus been avoided.

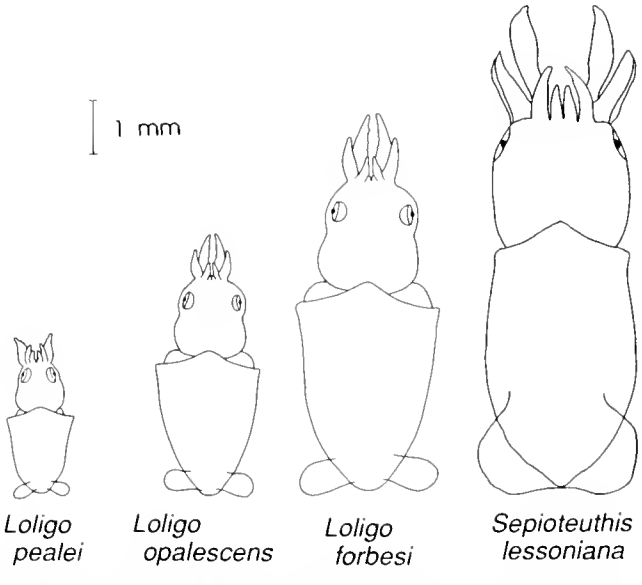

Figure 3. Sizes of various loliginid squids at hatching. Note the large body size and fin of *Sepioteuthis lessoniana*

The instantaneous growth rate (IGR) for the entire life cycle declined with each generation in Trial One (5.3, 4.9, 3.9% BW d^{-1}, respectively), as did the maximum adult size, 2.21, 1.92, and 1.49 kg BW and 360, 328, and 301 mm ML, respectively (Fig. 4). The IGR for the first 100 days of the life cycle was 8.2, 12.0, and 8.5% BW d^{-1}, respectively. One obvious effect of laboratory culture was lengthening of the life cycle. The G_2 generation's life span was 100 d longer than those of the previous two generations. Trial Two produced an IGR of 3.9% BW d^{-1} over the entire life cycle, with a maximum of 8.6% during the first 40 d in the hatchery tank. The maximum adult size was 0.838 kg.

Water quality

High standards for water quality were the goal for all trials, and the control of nitrogen waste products improved with each generation. Ammonia levels were held below the recommended 0.10 NH_4-N ppm except during egg transport and in the G_p generation when both hatchery and production tanks were repeatedly above this level. Although the ammonia concentration in shipping bags (1.5 ppm) was more than an order of magnitude greater than our goal of 0.1 ppm, the hatching rate of the field-collected eggs was significantly better ($P < 0.01$; 49 and 37% in Trials One and Two) than for the laboratory-spawned eggs (G_1, 5.6%; G_2, 0.8%; G_3, 1.5%). The high levels of ammonia present in the Trial One G_p generation were due to the acclimation of the filter bed bacteria to a new temperature regime (21–26°C compared to earlier trials at 11–18°C). In addition, the biomass of squids in

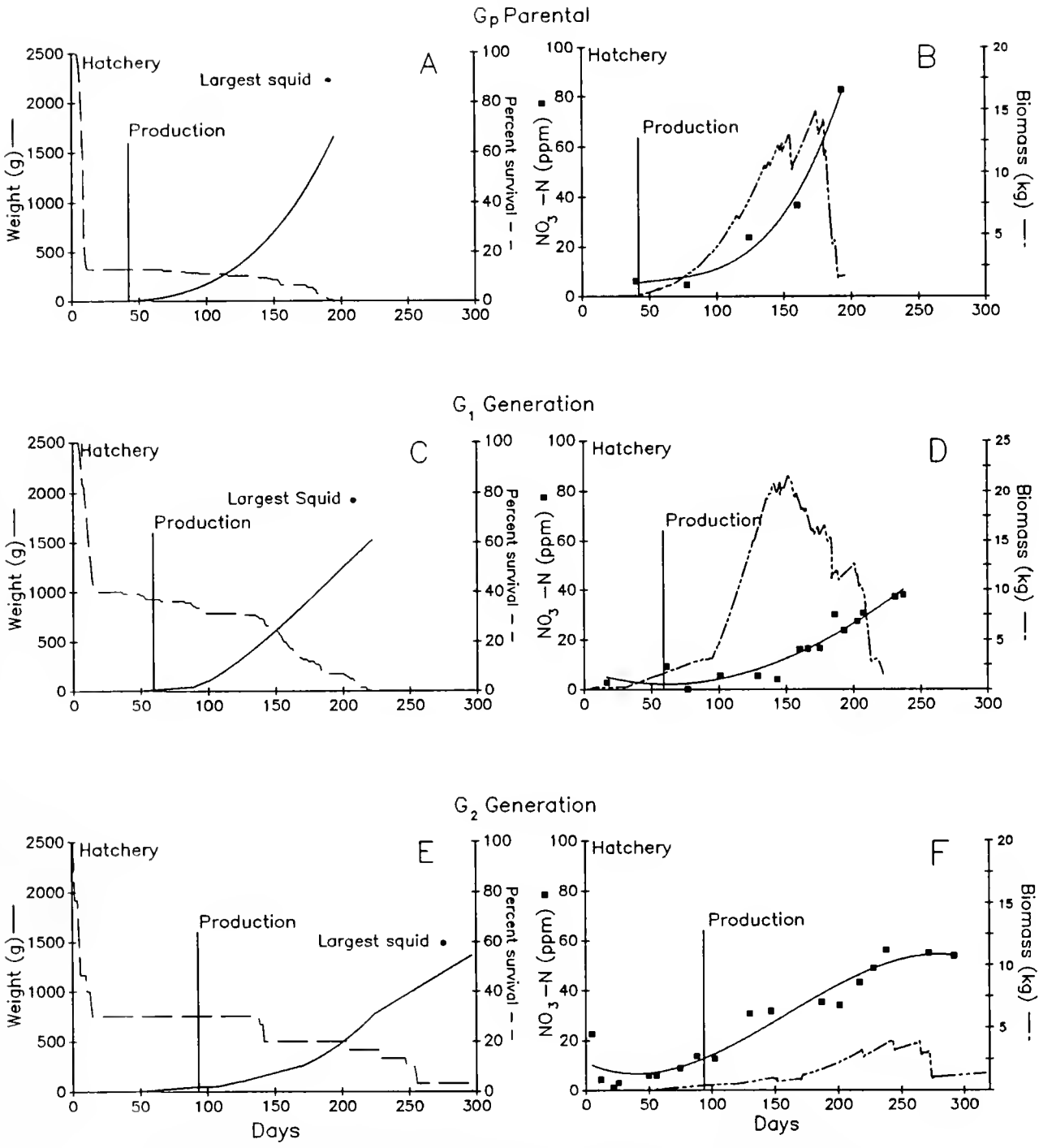

Figure 4. Survival and growth (4A, 4C, 4E) of squids, and water quality and biomass (4B, 4D, and 4F) in Trial One (three consecutive generations). See text.

the production tanks was 10–50 times higher than in previous trials (1–5 kg m^{-3} *versus* 0.10 kg m^{-3}). The increased biomass became a problem also in the production tanks near the end of the G_1 and G_2 generations, but no mortalities could be associated with these increased levels. Nitrite levels (recommended <0.10 ppm) were held below 0.02 NO_2-N ppm in the hatchery tanks and below 0.05 ppm in the production tanks. Nitrate levels NO_3-N were never a problem in the hatchery tanks because of the short duration of the culture period and the low biomass, but the levels in the production tanks eventually exceeded our goal of <50 ppm in the G_p (84 ppm) and G_2 (62 ppm) generations (Fig. 4). Note the similarities in the respective slopes of the biomass and nitrate curves

during the G_p and G_2 generations, confirming the direct effects of squid biomass on nitrate accumulation.

The pH was maintained at 8.0 ± 0.09 in Trial One, and the lowest levels were 7.70, 7.75, and 7.80 for the G_p, G_1 and G_2 generations, respectively. When the pH began to drop, sodium bicarbonate was added to readjust the pH to 8.0; usually several additions over 72 h were required to reestablish a pH of 8.0. The salinity of all tanks in all generations was held above 32 ppt, with the mean being 33.2 ± 0.8. Temperature was steady in all generations, with a mean of 23.2 ± 0.6°C.

Similar patterns of fluctuation in pH (8.1 ± 0.16) and metabolite levels (NH_4-N, 0.02 ± 0.03 ppm; NO_2-N, 0.02 ± 0.03 ppm) were observed in Trial Two, except that nitrate levels increased to 94.4 ppm in the large circular production system immediately before the inking episode described above. Temperature and salinity were held within narrow limits, 23.2 ± 0.9°C and 34.2 ± 1.0 ppt.

Foods and feeding behavior

Live food was added to the hatchery tanks within 48 h of a major hatch (>100 hatchlings) and 6–10 times per day thereafter. Field-collected mysid shrimp (*Mysidopsis almyra*), hatchery-reared penaeid (*Penaeus vannamei*) and palaemonid (*Palaemonetes* sp.) shrimp larvae and hatchery-reared guppies (*Poecilia reticulata*) were the primary food organisms during the first 60 d of each trial (Fig. 5). Field-collected penaeid shrimps (*Penaeus setiferus* and *Penaeus aztecus*), palaemonid shrimp, and several estuarine fish species were included when available in the appropriate size (<1 cm).

Feeding rates varied from 26 to 33% BW d^{-1} during this 60-d hatchery period. Within the first day of hatching, squids would follow mysids or palaemonid shrimp larvae to the bottom and would even prey successfully upon shrimps and fishes equaling their own size. Within a few weeks, squids could be seen grasping three fishes at once. Food preferences were not clear—squids tried to capture a variety of the prey that were offered (Fig. 5). As with *Loligo*, there seemed to be some squids that were more successful in capturing prey organisms, and the number of unsuccessful attacks decreased gradually during the first few weeks.

After transfer to the production tanks, the squids (>5 g BW) were fed progressively larger shrimp and fishes 3–6 times per day (Fig. 5). The predominant species were the penaeid shrimps (*P. setiferus* and *P. aztecus*) and estuarine fishes (*Cyprinodon variegatus, Poecilia latipinnea*, and *Mugil cephalus*). Other fishes (both field-collected and laboratory-cultured) were added as available. Feeding rates during the entire production phase (days 60–300) varied from 20 to 35% BW d^{-1}, with a mean of 27.8% BW d^{-1}. We noticed that squids several months old would not actively pursue schooling fishes (mullet, *M. cephalus*, and

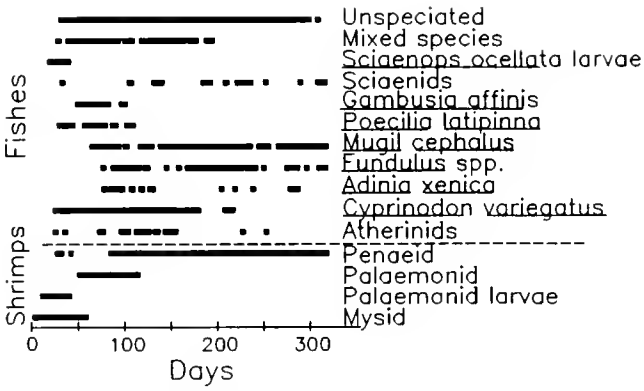

Figure 5. Food timeliness throughout the culture in Trial One. See text.

molly, *P. latipinnea*), except when an individual fish would leave the school. By two months of age, squids had been conditioned to the opening of the tank top, and their response to food was enhanced. The squids showed no preference for either species of shrimp or for any species of fish that was offered during a 56-d period (days 38–94) of the Trial One parental generation (G_p) in which feeding rate was quantified for individual food species.

Effects of light on behavior

Squids were reared in constant low light for most of the life cycle. Young squids generally avoided both the brightest and darkest parts of the tank. Thus, a round piece of black plastic placed over the center of the circular hatchery tank created a shaded central area in contrast to the more brightly lit walls. Squids spent more time in the middle of the tank, resulting in less wall contact and thus less fin damage. However, for the G_1 generation of Trial One, lighting was used to manipulate the behavior of both the squids and their food organisms during the hatchery phase of culture. Four incandescent lamps were placed around the perimeter of the circular hatchery tank, and the light was cycled 15 min on/30 min off throughout the day; this on/off cycle caused the mysid shrimp to move up and down in the water column, enhancing feeding opportunities by the squids. Typical light levels in the hatchery tanks were 85 lx in the bright areas and 5 lx in the shaded portions; in the production tanks the levels were between 10 and 20 lx.

Schooling behavior

The large, robust hatchlings (5 mm ML) were strong swimmers from the outset, and schooling was evident within 2 weeks in every trial. These schools comprised up to 40 individuals, and formed most often when human disturbance in and around the tank was strong. Squids schooled tightly when first transferred into the production

tanks, but within a day or two they acclimated to the tank and dispersed.

Body patterning

A noteworthy feature of the *S. lessoniana* hatchlings was the well-developed ability to produce complex body patterns from the moment of hatching. Figure 2 illustrates one such complex pattern that includes a postural component (Upward V curl of the arms) as well as various chromatic components, most notably the transverse mantle bars. Comparable patterning in other loliginid squid species does not occur before 4 months of age. A complete list of body patterning components does not appear in this publication, but the repertoire of *S. lessoniana* is moderately less diverse than that of *S. sepioidea* in the Caribbean (Moynihan and Rodaniche, 1982) and far more diverse than those of the other species of *Loligo* that we have cultured.

Reproductive behavior

Reproductive behavior occurred throughout the last quarter of the life cycle. Spawning was sometimes accompanied by sudden profuse inking (which in this case was not due to high levels of nitrate). Males became aggressive and engaged in agonistic contests that involved mainly posturing and body pattern displays, but the details have never been documented well. Invariably, when the ink was filtered out of the water within several hours, eggs were found to have been laid in the tank. Mating occurred by two methods: the "head-head" position (seen only twice) and the "male-parallel" position in which the male grasped the female from slightly underneath and inserted the hectocotylus into the mantle cavity of the female (illustrated by Segawa, 1987; Segawa *et al.,* 1993). This latter approach was variable because the male also grasped the female from above, and in one odd observation a male approached a female from underneath by swimming upside down, but no copulation actually occurred. Only temporary mating pairs were seen. On occasion, males were seen to accompany females as they laid eggs; this "mate guarding" has been observed in nature, too (Segawa *et al.,* 1993).

Females required specific substrates on which to lay egg strands: (1) tall, thin artificial plants similar to the Japanese seaweed *Sargassum ringgoldianum* (Segawa, 1987), or (2) arches constructed of polyvinyl chloride pipe, with artificial plants and rocks attached to them. These arches were highly successful—squids laid nearly all their egg strands on these structures.

Giant axons

The giant axon of *S. lessoniana* is very similar in gross morphology to that of other loliginid squids (Fig. 6). The diameters of fresh preparations of giant third-order axons (Fig. 7) were measured under a dissecting microscope after fine dissection and before use in membrane biophysics and axon injury experiments. The measurements were made distal ($\approx$1 cm) to the cell body. In addition to the axon measurements made in the two trials described herein, Figure 7 includes the axon diameters from squids grown in six other culture trials (N = 137). The average diameter of the axons from adult *S. lessoniana* (>400 g) was 434 $\pm$ 68 μm.

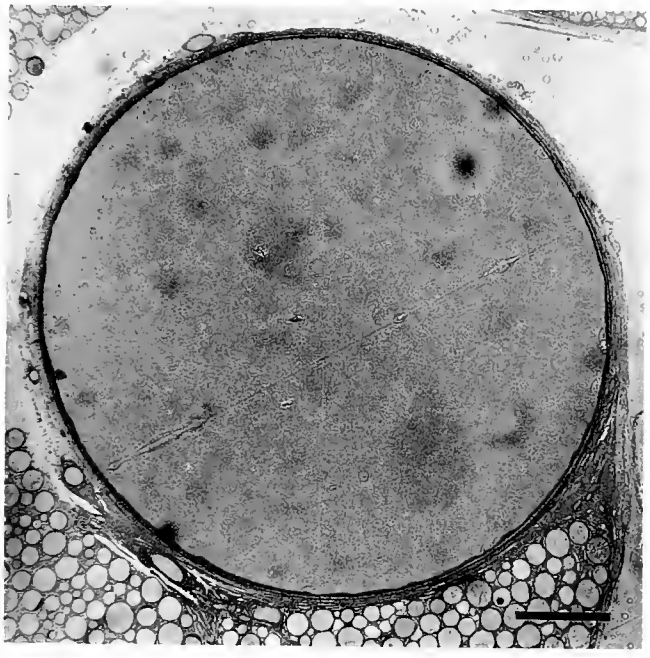

Figure 6. Giant axon of *Sepioteuthis lessoniana* (560 μm diameter). The dissected axon ($\approx$1 cm distal of cell body) was fixed with a glutaraldehyde and osmium solution, sectioned, and photographed by light microscopy. Bar = 100 μm.

General features of the axon include a large diameter (>400 μm), enabling internal perfusion, internal dialysis, axonal-wire voltage clamp techniques, and video light microscopy of structural changes induced by injury; one giant axon per stellate ganglion (two total per squid); a useful length of giant axon preparation ($\approx$5 cm); a mantle thickness and opacity greater than for other *Loligo,* necessitating improved contrast for quick dissection; cellular injury responses similar to those of *Loligo pealei;* channel types identical to those in *L. pealei,* as verified by similar pharmacological effects of ion channel blockers (tetrodotoxin and 4-amino-pyridine); and electrical impedance similar to those for *L. pealei* (Krause *et al.,* 1992; Krause, 1993). Finally, *S. lessoniana* have been anesthetized repeatedly with $MgCl_2$ during transport from one culture system to another with no mortality. The ability to anesthetize a squid raises new possibilities for both surgical procedures and long-term investigations of chronic injury to the nervous system.

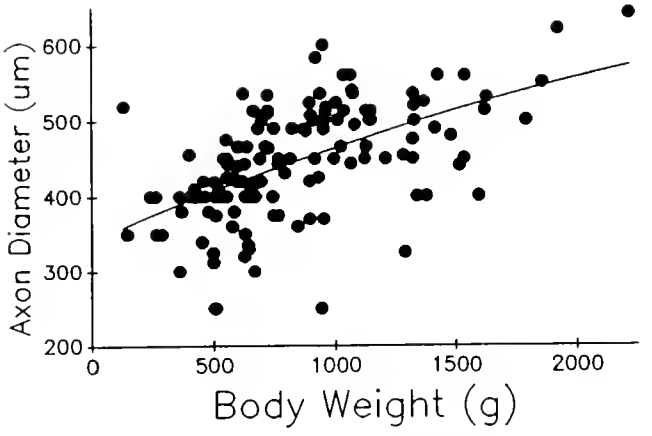

Figure 7. Axon diameters of laboratory-cultured *Sepioteuthis lessoniana* ($N = 137$). Note the large variation relative to body weight.

Discussion

We have successfully cultured *Sepioteuthis lessoniana* through multiple laboratory generations (G_0, G_1, and G_2), and this is the first time that any squid has been cultured through more than one generation (Hanlon *et al.*, 1991). The squid *Loligo opalescens* had been cultured through one generation twice in our facilities, but the G_1 generation was reared for only 10 days (Yang *et al.*, 1986). Other investigators have reared squids through most of one life cycle (Choe, 1966a; LaRoe, 1971; Yang *et al.*, 1980, 1983; Hanlon *et al.*, 1987, 1989; Segawa, 1987) or successfully spawned field-collected adults in the laboratory (Ikeda, 1933; Larcombe and Russell, 1971), but none have cultured squids from egg to egg. Most of the early failures were due to the selection of a species with physiological and behavioral characteristics not amenable to culture, to inadequate tank system design (both engineering and behavioral), to lack of appropriate foods, or to poor water quality.

The large hatchling size (5 mm ML) and high growth rate (>12% BW d^{-1} in the first 100 d) are important biological characteristics for the laboratory culture of *S. lessoniana* because less time is spent in the hatchling and juvenile stages. The fact that *S. lessoniana* is a warm-water squid largely explains its higher growth rate when compared to that of other laboratory-reared squids, which were generally cold-water species (Yang *et al.*, 1980, 1986; Turk *et al.*, 1986; Hanlon *et al.*, 1987, 1989). The behavior of *S. lessoniana* in laboratory tanks was also pivotal to their successful growth and reproduction in captivity. These laboratory-cultured *S. lessoniana* fill a significant gap in the temporal availability of squids for biomedical research.

Behavioral attributes

The outstanding feature of *S. lessoniana* is behavioral adaptability to the confines of the laboratory tanks. In addition to advances in culture technology, the proper selection of a species with behavior amenable to laboratory culture was a key element responsible for the success of this culture program. In nature, *S. lessoniana* occurs inshore, near temperate rock reefs or coral reefs, and this may partially explain its adaptability to tanks (Segawa, 1987; Jackson, 1990). Throughout all life stages, *S. lessoniana* often hovers near vertical structures, and this behavioral attribute—which helps it adapt to the confines of the laboratory—is different from other loliginid squids.

The large fins of *S. lessoniana*—in both hatchlings and adults—allow it to maneuver in and around objects better than other squids. This improved control results in less contact with tank walls, reducing skin damage that has frequently been described for other squids (Summers, 1974; Leibowitz *et al.*, 1977; Hulet *et al.*, 1979). We found, as did LaRoe (1971), that *Sepioteuthis* appears to orient above dark substrates such as it might encounter in nature (*e.g.*, seagrass beds); thus, our production tanks had dark bottoms to calm the squids and keep them away from the walls. Furthermore, possibly as part of the adaptation of this genus to reef structures, the skin appears to be thicker and stronger (although this deserves future examination), resulting in less skin damage when the squids strike the walls or bottom of the tank. As a result, *Sepioteuthis* seems less prone to chronic mantle infections than *Loligo*. The gladius of many *S. lessoniana* adults is broken internally 2–3 cm from the tail due to wall collisions during agonistic contests and courtship behavior. These breaks heal and form scar tissue, but do not become infected secondarily as in *Loligo* (*cf.* Hanlon and Forsythe, 1990). All of these features contribute to the ease with which this species can be caught, handled, and even shipped to potential users at remote locations.

The hatchlings (5 mm ML; Fig. 3) are unique among squids because of their relatively large size and advanced development. Hatchling squids are robust, and the fins are already large and strong, enabling them to capture a wide array of foods. The larger fins and overall size enable them to school within 2 weeks, much earlier than *Loligo* spp. that must grow for 20–60 days before they are large enough to swim independently of currents (Yang *et al.*, 1986; Hanlon *et al.*, 1989). All loliginids studied thus far began schooling when they attained sizes of 4–10 mm ML; *S. lessoniana* is 5 mm ML at hatching.

Lighting affects squid behavior. Hatchling squids stayed near the interface of light and dark areas, and thus light could be manipulated to keep them away from the walls, avoiding skin damage. By maintaining constant low light, we prevented the strong reaction of squids (jetting and hitting the tank walls) to sudden changes in light intensity described by LaRoe (1971) for *S. sepioidea;* yet sexual maturation was not inhibited, as had been reported in some species under constant bright light (Mangold, 1987). Maturation and successful reproduction in all of our cul-

ture trials were not inhibited, but seemed to be accelerated (*i.e.*, 6-month cycle compared with 11- to 13-month cycle in nature; Segawa, 1987).

Mating behavior of *S. lessoniana* was described by Segawa (1987) and Segawa *et al.* (1993), who observed males positioning themselves underneath females (the "male-parallel" position) for 3–4 s while they transferred spermatophores. Our laboratory observations differ somewhat. We observed the "head-head" position, which is common in many loliginid squids (*cf.* Hurley, 1978; Arnold, 1984), and we also have the curious observation of the male approaching the female by swimming upside down while below the female. Segawa (1987) and Segawa *et al.* (1993) noted: "The male remained above the spawning substratum and escorted the female." Our observations corroborate this temporary mate-guarding behavior of males, a tactic that has been observed in other squids (*e.g., Loligo pealei;* Griswold and Prezioso, 1981) and that is common in polygynous animal species. This behavior ensures that fertilized eggs are laid before other males mate with the females (Smith, 1984).

The life cycle was accelerated in the laboratory, and this may have caused the time-limited episodes of reproduction and death. Confining squids at high densities may exaggerate this aspect of their life cycle in comparison to the natural spawning activity of this genus (Tsuchiya, 1981; Segawa, 1987; Segawa *et al.*, 1993).

Culture methods and comparisons

The culture of *S. lessoniana* required significant improvements in five areas of husbandry: (1) design of behaviorally acceptable culture tanks (*i.e.*, size, shape, color, and water flow), (2) water quality management to accommodate high metabolic rate and ink removal, (3) feeding regimen, (4) spawning methodology, and (5) egg handling methodology. The first three of these were particularly important to early hatchling survival and growth, whereas the latter two led to higher fecundity and reduced egg tunic deterioration. These improvements were gradually implemented, beginning with the G_p generation, so that the accrued benefits are evident in Trial One, but especially evident in Trial Two in which high numbers of hatchlings were cultured. The greatest density and biomass of squids were attained in Trial Two, using the large 6.5-m circular production tank. To compare the above improvements with current and previous reports of squid culture, each improvement will be discussed sequentially.

The shape, size, color, and water flow pattern of the culture tanks. These were important factors determining early hatchling survival. Hatchlings tended to swim gently near objects at the edge of shadowed areas and occasionally swam the circumference of the circular hatchery tank. Although tanks of similar volume (1500 l) had been used to rear *Sepioteuthis* spp. (1900 l, LaRoe, 1971; 1200 l, Segawa, 1987), they were rectangular so that hatchlings were concentrated in the corners. For this reason, a circular hatchery tank that is between 1.5 and 2.5 m in diameter and that includes some vertical and horizontal structure (usually the baskets that held unhatched eggs) is recommended. Water depth should be between 75 and 125 cm so that the squids can choose their position. The color and reflectance of the tank walls were important factors in the feeding of hatchlings in earlier squid rearing trials (*e.g.,* LaRoe, 1971; Yang *et al.*, 1983, 1989). Uniformly dark walls are recommended because they reflect less incident light and highlight translucent food organisms. In production tanks, however, a high-contrast speckled wall pattern was used so that the juvenile squids could detect the wall easily, and they very rarely bumped into the walls in these tanks.

Water quality. Water quality was maintained at the highest standards: <0.10 ppm NH_4-N, <0.05 ppm NO_2-N, <50 ppm NO_3-N, and >8.0 pH. The only exceptions to these standards were during egg transport when pH was low (7.5) and ammonia high (1.5 ppm), and near the end of the production cycle when nitrates exceeded 50 ppm. The production of dissolved and suspended organic matter from partially eaten food and squid inking were the major challenges to the maintenance of water quality. Improvements in filtration and water quality have been identified as the reason for improved survival of squids maintained in recirculating seawater tanks (Matsumoto and Shimada, 1980; Yang *et al.*, 1989; Hanlon *et al.*, 1989; Hanlon, 1990). The most effective components of the filtration system were the protein skimmers (or foam fractionators) and activated carbon that removed the black melanin pigment of the ink, as well as other dissolved organic matter; mortality due to heavy inking has been avoided. Declining pH then became the most important water quality parameter, but buffering was provided by the large, submerged oyster shell biofilters and, when necessary, a dose of sodium bicarbonate (Yang *et al.*, 1989). The ever increasing nitrate concentrations were corrected by water exchanges, so that levels were usually less than 50 ppm (G_1 and G_2).

Feeding regimen. Individuals of *S. lessoniana* consumed 20–30% of their body weight in live food organisms each day, placing extraordinary pressure on the available food resources. This high feeding rate equaled estimates from field work (LaRoe, 1971; Segawa, 1990), but was about 2–3 times that for other loliginid squids that have been reared in captivity (*L. opalescens, L. pealei* and *L. forbesi;* Yang *et al.*, 1986; Hanlon *et al.*, 1987, 1989). Food was occasionally limiting in Trial Two. Food is particularly important during the juvenile stage (<100 g) when the squids are growing rapidly (IGR > 10% BW d^{-1}). Food supplies were identified by both LaRoe (1971) and Segawa (1987) as the major factor limiting mass culture.

Table II

Recent biomedical uses for squids

Research topics	Species[1]	References
Membrane biophysics	Sl, Ss, Lp	Fishman, 1993; DiPolo and Beague, 1989; DiPolo *et al.*, 1989; Caputo *et al.*, 1988
Ion channel	Sl, Ss, Lb, Lo, Lp	Gilly *et al.*, in press; DiPolo and Beague, 1993; Correa *et al.*, 1993; Chow, 1991; Fishman and Tewari, 1990; Perozo *et al.*, 1989
Neuron development and injury	Sl, Lb, Lo, Lp, So	Krause *et al.*, in press; Krause *et al.*, 1992; Gilly *et al.*, 1991; Fishman *et al.*, 1990; Tewari and Fishman, 1990; Stein *et al.*, 1989
Cell biology	Sl, Lb, Lp, Ii, So	Lee *et al.*, 1994; Portner *et al.*, 1991; Heming *et al.*, 1990; Mangum, 1990
Muscle biomechanics	Sl, Lb, Lp, Ii, So	Johnsen and Kier, 1993; Kier and Schachat, 1992; Kier, 1991
Chemical reception	Sl, Lb, Lo	Lee, 1994; Gilly and Lucero, 1992; Lucero *et al.*, 1992
Vision and oculomotor physiology	Sl, Lb, Lp, So	Sivak *et al.*, in press; Kito *et al.*, 1992; Langmack and Saibil, 1991; Budelmann, 1990; Fong *et al.*, 1988
Behavior and pharmacology	Lb, Lo	Gilly *et al.*, 1991; Cooper *et al.*, 1990; Hanlon *et al.*, 1990
Melanin synthesis	So	Chedekal *et al.*, 1992; Zeise *et al.*, 1992
Developmental biology	Sl, Lp	Arnold, 1990; Segawa, 1987

[1] Sl, *Sepioteuthis lessoniana*; Ss, *Sepioteuthis sepioidea*; Lb, *Lolliguncula brevis*; Lo, *Loligo opalescens*; Lp, *Loligo pealei*; Ii, *Illex illecebrosus*; So, *Sepia officinalis*

The development of methods for capturing, transporting, and acclimating large quantities of field-collected food organisms, *i.e.*, mysids, shrimp, and fishes, played a major role in this culture program. In addition to field-collected crustaceans and fishes, laboratory-cultured crustaceans and fishes were fed (<15% of total diet). Moreover, *S. lessoniana* has recently been reared for 50% of its life cycle on dead fish, with no effect on growth or digestive physiology (DiMarco *et al.*, 1993), and the sepioid squid *Sepia officinalis* has been reared for several months on prepared diets (Castro *et al.*, 1993). Research continues to focus on the formulation of economical diets to meet the nutritional requirements of cephalopods (Lee, 1994).

Spawning and egg handling. Eggs shipped overseas should be packed at lower densities to improve water quality during shipment. The recorded values of 7.5 pH and 1.55 ppm ammonia were potential problems (we recommend >8.0 pH and <0.10 ppm ammonia), so that the extra cost of shipping due to added water (<3 egg strands per liter of seawater) would be a good investment. Although hatching rate of the air-shipped, field-collected eggs was significantly greater ($P < 0.01$) than that of the laboratory-spawned eggs (37–49% *versus* <6%), the hatchling survival rate was lower (13% *versus* 29–40%). The lower hatchling survival rate cannot be specifically attributed to poor water quality during transport, but it could have been a contributing factor.

The use of artificial reefs and artificial sea grass in the tanks as spawning substrate proved to be excellent methods for triggering spawning and for collecting the eggs. The daily culling of infertile eggs and repeated exposure to iodine appeared to improve hatching of some egg strands, and these dips significantly lowered the number of bacteria on the surface of the tunics. But many protozoans and microinvertebrate epibionts were found to survive the iodine dips or to recolonize the tunics, so that the deterioration of the tunics could be a result of these organisms and not the bacteria. The hatching rates—especially in subsequent laboratory generations—were low and thus require improvement.

Certain bacteria with antifungal properties are reported to benefit crustacean egg tunics (Gil-Turnes *et al.*, 1989; Gil-Turnes and Fenical, 1992). Moreover, in cephalopod females, the accessory nidamental glands that provide the jelly for egg tunics contain normally growing bacteria (Bloodgood, 1977; Biggs and Epel, 1991). These bacteria have been isolated from the tunics and may serve a similar role to those identified in Crustacea. Iodine dips have not been required for subsequent laboratory-spawned eggs because the incidence of tunic deterioration has decreased, but dips have been continued for wild-collected G_p eggs. Iodine is recommended only when tunic deterioration becomes an overwhelming problem for hatching.

Biomedical uses

The practical result of these improved technologies and the identification of a suitable squid species is that—for the first time—large loliginid squids are available by laboratory culture. This temporal and numerical increase in availability should have a positive effect on several biomedical research fields, particularly axon biophysics, that have been restrained by the limited and seasonal availability of squids (Table II).

The diameter of the axons in this species is highly variable (434 ± 68 μm) and could not be correlated to sex, length, or wet weight (Fig. 7); even some small adults (<350 g BW) had large axons (>350 μm). This confirms quantitatively what many giant axon researchers have reported concerning the weak relationship between squid

size and axon diameter. Neurophysiologists who have used both the cultured squid *S. lessoniana* and the Woods Hole squid *Loligo pealei* confirm the biophysical similarities of the axon preparations (Krause, 1993; Krause *et al.*, in press; Dr. John Russell, Medical College of Pennsylvania, pers. comm.). Thus, supplemental cultured squid stocks could fulfill research needs when squids are not available at Woods Hole.

Prospects for selective breeding. The large variation in axon diameter for differently sized squids (Fig. 7) raises the consideration of selective breeding to produce larger giant axons in smaller squids. The cost savings would be substantial, and recent research indicates that loliginid squids have ample genetic variability to make selective breeding possible. The pelagic squids (*i.e.*, Ommastrephidae) possess low levels of genetic variability (Romero and Amaratunga, 1981; Carvalho *et al.*, 1992) compared to neritic squids (*i.e.*, Myopsida; Carvalho and Loney, 1989; Brierley *et al.*, 1993; Suzuki *et al.*, 1993). Since *S. lessoniana* falls into the latter category, it may be possible to select for specific traits like axon size. No genetic investigations have been conducted with *S. lessoniana*, but this is a topic of current research in our laboratory.

In summary, squid culture is now a reality, and *S. lessoniana* is the species of choice. Laboratory culture is labor-intensive, but *S. lessoniana* has a rapid growth rate that minimizes the life span. The environmental requirements have been described, and *S. lessoniana* has reproduced repeatedly in laboratory tanks. The primary obstacles to large-scale culture are the supply of food and the low hatching rate associated with frequent egg tunic deterioration. Finally, *S. lessoniana* has suitable axons, and its tolerance to anaesthesia and handling raises the possibility that research areas requiring surgical procedures followed by long-term maintenance can be developed successfully.

Acknowledgments

We acknowledge the hospitality and assistance of our Japanese collaborator, Dr. Susumu Segawa, and thank the personnel at Izu Oceanic Park (H. Masuda, Director), the personnel at Tokushima-Ken Fisheries Experimental Station, and John W. Forsythe, all of whom assisted with the collection and transportation of squid egg strands. Many present and past MBI staff members contributed to the success of this project: Dr. William S. Fisher, John W. Forsythe, F. Paul DiMarco, Joanne Hollyfield, William Browning, Vivian Kahla, Lea Bradford-O'Connor, Bobby Day, Mike Harrelson, John Dobias, Douglas Brining, and Ronald Smith. The authors were assisted by Laura Koppe and Kay Kantowski in preparing this manuscript.

We thank Kay Cooper for Figure 6, and John W. Forsythe for Figures 1 and 2. We are grateful for continued support on NIH grants DHHS RR01024 and DHHS RR04226 and the Marine Medicine General Budget Account of the Marine Biomedical Institute.

Literature Cited

Arnold, J. M. 1984. Cephalopods. Pp. 419–454 in *The Mollusca, Vol. 7: Reproduction.* A. S. Tompa, N. H. Verdonk, and J. A. M. van den Diggelaar, eds. Academic Press, New York.

Arnold, J. M. 1990. Evolution and intelligence of the cephalopods. Pp. 3–9 in *Squid as Experimental Animals.* D. L. Gilbert, W. J. Adelman, Jr., and J. M. Arnold, eds. Plenum Press, New York.

Asian Development Bank/Infofish. 1991. *Cephalopods.* AOB/Infofish Global Industry Update, Infofish, Kuala Lumpur, Malaysia. 127 pp.

Biggs, J., and D. Epel. 1991. The egg-capsule sheath of *Loligo opalescens:* structure and association with bacteria. *J. Exp. Zool.* **259:** 263–267.

Bloodgood, R. A. 1977. The squid accessory nidamental gland: ultrastructure and association with bacteria. *Tissue & Cell* **9:** 197–208.

Brierley, A. S., J. P. Thorpe, M. R. Clarke, and H. R. Martins. 1993. A preliminary biochemical genetic investigation of the population structure of *Loligo forbesi* Steenstrup, 1856 from the British Isles and the Azores. Pp. 61–70 in *Recent Advances in Cephalopod Fisheries Biology.* T. Okutani, R. K. O'Dor, and T. Kubodera, eds. Tokai University Press, Tokyo.

Budelmann, B. U. 1990. The statocysts of squid. Pp. 421–439 in *Squid as Experimental Animals.* D. L. Gilbert, W. J. Adelman, Jr., and J. M. Arnold, eds. Plenum Press, New York.

Caputo, C., F. Bezanilla, and R. DiPolo. 1988. Currents related to the sodium-calcium exchange in squid giant axon. *Biochim. Biophys. Acta* **986:** 250–256.

Carvalho, G. R., and K. H. Loney. 1989. Biochemical genetic studies on the Patagonian squid, *Loligo gahi* d'Orbigny. 1. Electrophoretic survey of genetic variability. *J. Exp. Mar. Biol. Ecol.* **126:** 231–241.

Carvalho, G. R., A. Thompson, and A. L. Stoner. 1992. Genetic diversity and population differentiation of the shortfin squid *Illex argentinus* in the south-west Atlantic. *J. Exp. Mar. Biol. Ecol.* **158:** 105–121.

Castro, B. G., F. P. DiMarco, R. H. DeRusha, and P. G. Lee. 1993. The effects of surimi and pelleted diets on the laboratory survival, growth, and feeding rate of the cuttlefish *Sepia officinalis. J. Exp. Mar. Biol. Ecol.* **170:** 241–252.

Chedekel, M. R., A. B. Ahene, and L. Zeise. 1992. Melanin standard method: empirical formula 2. *Pigm. Cell Res.* **5:** 240–246.

Choe, S. 1966a. On the eggs, rearing, habits of the fry, and growth of some Cephalopoda. *Bull. Mar. Sci.* **16:** 330–348.

Choe, S. 1966b. On the growth, feeding rates and the efficiency of food conversion for cuttlefishes and squids. *Korean J. Zool.* **9:** 72–80.

Choe, S., and Y. Oshima. 1961. On the embryonal development and growth of the squid *Sepioteuthis lessoniana* Lesson. *Venus* **21:** 462–476.

Chow, R. 1991. Cadium block of squid calcium currents. *J. Gen. Physiol.* **98:** 751–770.

Cooper, K. M., R. T. Hanlon, and B. U. Budelmann. 1990. Physiological color change in squid iridophores. II. Ultrastructural mechanisms in *Lolliguncula brevis. Cell Tissue Res.* **259:** 15–24.

Correa, A. M., C. Caputo, R. Morales, and F. Bezanilla. 1993. Characterization of ionic channels in tropical squid giant axons. *Biophys. J.* **64**(2): A92.

DiMarco, F. P., P. E. Turk, J. M. Scimeca, Jr., W. J. Browning, and P. G. Lee. 1993. Laboratory survival, growth, and digestive gland histology of squids reared on living and non-living fish diets. *Lab. Anim. Sci.* **43:** 226–231.

DiPolo, R., and L. Beague. 1989. Asymmetrical properties of the Na-Ca exchanger in voltage clamped, internally dialyzed squid axons under symmetrical ionic conditions. *Acta Physiol. Scand. Suppl.* **1989:** P14.

DiPolo, R., and L. Beague. 1993. Effects of some metal-ATP complexes on Na^+-Ca^{2+} exchange in internally dialysed squid axons. *J Physiol.* **462:** 71–86.

DiPolo, R., L. Beauge, and H. Rojas. 1989. In dialyzed squid axons Ca^{2+i} activates Ca^{2+o}-Na^{+i} and Na^{+o}-Na^{+i} exchanges in the absence of Ca chelating agents. *Biochim. Biophys. Acta* **978:** 328–332.

Dotsu, K., Y. Shima, and Y. Natsukari. 1981. Ecology and fisheries of the oval squid, *Sepioteuthis lessoniana* Lesson in Goto Islands, Nagasaki Prefecture. Pp. 457–465 in *The Life of Goto Islands.* Biological Society of Nagasaki Prefecture.

Fishman, H. 1993. Assessment of conduction properties and thermal noise in cell membranes by admittance spectroscopy. *Bioelectromagnetics* **Suppl. 1:** 87–100.

Fishman, H. M., and K. P. Tewari. 1990. Single Ca^{2+} channels in patches of axosomes from transected squid axon. *Biophys. J* **57:** 523a.

Fishman, H. M., K. P. Tewari, and P. G. Stein. 1990. Injury-induced vesiculation and membrane redistribution in squid giant axon. *Biochim. Biophys. Acta* **1023:** 421–435.

Fong, S.-L., P. G. Lee, K. Ozaki, R. Hara, T. Hara, and C. D. B. Bridges. 1988. IRBP-like proteins in the eyes of six cephalopod species—immunochemical relationship to vertebrate interstitial retino-binding protein (IRBP) and cephalopod retinal-binding protein. *Vision Res.* **28:** 563–573.

Forsythe, J. W., and W. F. Van Heukelem. 1987. Growth. Pp. 135–156 in *Cephalopod Life Cycles,* Vol. II. P. R. Boyle, ed. Academic Press, London.

Gilbert, D. L., W. J. Adelman, Jr., and J. M. Arnold, eds. 1990. *Squid as Experimental Animals.* Plenum Press, New York. 516 pp.

Gilly, W. F., and M. T. Lucero. 1992. Behavioral responses to chemical stimulation of the olfactory organ in the squid. *J Exp Biol.* **162:** 231–249.

Gilly, W. F., B. Hopkins, and G. O. Mackie. 1991. Development of giant axons and neural control of escape responses in squid embryos and hatchlings. *Biol. Bull.* **180:** 209–220.

Gilly, W. F., M. T. Lucero, M. Perri, and J. Rosenthal. In press. Control of the spatial distribution of sodium channels in the squid giant axon and its cell bodies. In *Cephalopod Neurobiology: International Symposium.* J. Abbott, R. Williamson, and L. Maddock, eds. Oxford University Press, UK.

Gil-Turnes, M. S., and W. Fenical. 1992. Embryos of *Homarus americanus* are protected by epibiotic bacteria. *Biol Bull* **182:** 105–108.

Gil-Turnes, M. S., M. E. Hay, and W. Fenical. 1989. Symbiotic marine bacteria chemically defend crustacean embryos from a pathogenic fungus. *Science* **246:** 116–118.

Griswold, C. A., and J. Prezioso. 1981. *In situ* observations on reproductive behavior of the long-finned squid, *Loligo pealei. Fish. Bull.* **78:** 945–947.

Hanlon, R. T. 1990. Maintenance, rearing and culture of teuthoid and sepioid squids. Pp. 35–62 in *Squid as Experimental Animals* D. L. Gilbert, W. J. Adelman, Jr., and J. M. Arnold, eds. Plenum Press, New York.

Hanlon, R. T., and J. W. Forsythe. 1990. 1: Diseases of Mollusca: Cephalopoda. 1.1. Diseases caused by microorganisms; 1.3. Structural abnormalities and neoplasia. Pp. 23–46 and 203–204 in *Diseases of Marine Animals, Vol. III: Cephalopoda to Urochordata.* O. Kinne, ed. Biologische Anstalt Helgoland, Hamburg.

Hanlon, R. T., P. E. Turk, P. G. Lee, and W. T. Yang. 1987. Laboratory rearing of the squid *Loligo pealei* to the juvenile stage: growth comparisons with fishery data. *Fish. Bull.* **85:** 163–167.

Hanlon, R. T., W. T. Yang, P. E. Turk, P. G. Lee, and R. F. Hixon. 1989. Laboratory culture and estimated life span of the Eastern Atlantic squid, *Loligo forbesi* Steenstrup, 1856 (Mollusca: Cephalopoda). *Aquacult. Fish. Manage.* **20:** 15–34.

Hanlon, R. T., K. M. Cooper, B. U. Budelmann, and T. D. Pappas. 1990. Physiological color change in squid iridophores. I. Behavior, morphology and pharmacology in *Lolliguncula brevis. Cell Tissue. Res.* **259:** 3–14.

Hanlon, R. T., P. E. Turk, and P. G. Lee. 1991. Squid and cuttlefish mariculture: an updated perspective. *J Ceph. Biol.* **2:** 31–40.

Heming, T. A., C. G. Vanoye, S. E. S. Brown, and A. Bidani. 1990. Cytoplasmic pH recovery in acid-loaded haemocytes of squid, *Sepioteuthis lessoniana. J Exp. Biol.* **148:** 385–394.

Hulet, W. H., M. R. Villoch, R. F. Hixon, and R. T. Hanlon. 1979. Fin damage in captured and reared squids. *Lab. Anim. Sci.* **29:** 528–533.

Hurley, A. C. 1978. School structure of the squid *Loligo opalescens. Fish. Bull.* **76:** 433–442.

Ikeda, H. 1933. Sex correlated markings in *Sepioteuthis lessoniana* Ferussac. *Venus* **3:** 324–329. (In Japanese with English summary.)

Inoha, M., and M. Sezoko. 1968. The experiment on the culture of Aori-ika (white squid) *Sepioteuthis lessoniana. Ryukyu (Okinawa) Fish. Res. Lab.* **1967 Progress Report:** 139–145.

Jackson, G. D. 1990. Age and growth of the tropical near-shore loliginid squid *Sepioteuthis lessoniana* determined from statolith growth-ring analysis. *Fish. Bull. US* **88:** 113–118.

Japan Sea Farming Fisheries Association (JSFFA). 1985. *Farming Fisheries Seed Production, Procurement and Releasing Statistics for 1983* JSFFA Publication, Tokyo. 298 pp. (In Japanese.)

Johnsen, S., and W. M. Kier. 1993. Intramuscular crossed connective tissue fibres: skeletal support in the lateral fins of squid and cuttlefish. *J Zool* **231:** 311–338.

Kier, W. M. 1991. Squid cross-striated muscle: the evolution of a specialized muscle fiber type. *Bull. Mar. Sci.* **49:** 389–403.

Kier, W. M., and F. H. Schachat. 1992. Biochemical comparison of fast- and slow-contracting squid muscle. *J Exp. Biol.* **168:** 41–56.

Kito, Y., J. C. Partridge, M. Seidou, K. Narita, T. Hamanaka, M. Michinomae, N. Sekiya, and K. Yoshihara. 1992. The absorbance spectrum and photosensitivity of a new synthetic "visual pigment" based on 4-hydroxyretinal. *Vision Res.* **32:** 3–10.

Krause, T. L. 1993. *Rapid Membrane Repair in Two Transected Giant Axons.* Ph.D. Dissertation, University of Texas, Austin, TX. 193 pp.

Krause, T. L., H. M. Fishman, M. L. Ballinger, and G. D. Bittner. 1992. Seal formation in two transected giant axons suggests two models of sealing. *Soc. Neurosci.* **18:** 407–411.

Krause, T. L., H. M. Fishman, and G. D. Bittner. In press. Extent and mechanisms of sealing in transected giant axons of squid and earthworms. *J. Neurosci.*

Langmack, K., and H. Saibil. 1991. Signal transduction in photoreceptors. *Biochem. Soc. Trans.* **19:** 858–860.

Larcombe, M. F., and B. C. Russell. 1971. Egg laying behaviour of the broad squid *Sepioteuthis bilineata (lessoniana). N. Z. J Mar. Freshwater Res.* **5:** 3–11.

LaRoe, E. T. 1971. The culture and maintenance of the loliginid squids *Sepioteuthis sepioidea* and *Doryteuthis plei. Mar. Biol.* **9:** 9–25.

Lee, P. G. 1994. Cephalopod nutrition; fueling the system. *Mar. Behav Physiol* **25:** 35–51.

Lee, P. G., W. L. Lee-Jane, J. J. Salazar, and V. Holoubek. 1994. The absence of formation of benzo[α]pyrene/DNA adducts in cuttlefish (*Sepia officinalis,* Mollusca: Cephalopoda). *Environ. Mol. Mutagen.* **23:** 70–73.

Leibowitz, L., T. R. Meyers, R. Elston, and P. Chaney. 1977. Necrotic exfoliative dermatitis of captured squid (*Loligo pealei*). *J. Invertebr. Pathol.* **30:** 369–376.

Lu, C. C., and R. W. Tait. 1983. Taxonomic studies on *Sepioteuthis* Blainville (Cephalopoda: Loliginidae) from the Australian region. *Proc. R Soc. Victoria* **95:** 181–204.

Lucero, M. T., F. T. Horrigan, and W. F. Gilly. 1992. Electrical responses to chemical stimulation of squid olfactory receptor cells. *J. Exp. Biol* **162:** 231–249.

Mangold, K. 1987. Reproduction. Pp. 157–200 in *Cephalopod Life Cycles, Vol. II. Comparative Reviews.* P. R. Boyle, ed. Academic Press, New York.

Mangum, C. P. 1990. Gas transport in the blood. Pp. 443–468 in *Squid as Experimental Animals.* D. L. Gilbert, W. J. Adelman, Jr., and J. M. Arnold, eds. Plenum Press, New York.

Matsumoto, G., and J. Shimada. 1980. Further improvement upon maintenance of adult squid (*Doryteuthis bleekeri*) in a small circular and closed-system aquarium tank. *Biol. Bull.* **159:** 319–324.

Messenger, J. B., M. Nixon, and K. P. Ryan. 1985. Magnesium chloride as an anaesthesic for cephalopods. *Comp. Biochem. Physiol.* **82C:** 203–205.

Moynihan, M., and A. F. Rodaniche. 1982. *The Behavior and Natural History of the Caribbean Reef Squid* Sepioteuthis sepioidea. *With a Consideration of Social, Signal and Defensive Patterns for Difficult and Dangerous Environments. Advances in Ethology* **25.** Verlag Paul Parey, Berlin.

Nagata, W. D., and H. Hirata. 1986. Mariculture in Japan: past, present, and future prospectives. *Mini Review Data File Fish. Res.* **4:** 1–38.

Okutani, T. 1980. Biology of Cephalopoda—6. Systematics and life history of the Loliginidae. *Aquabiology* **1980:** 20–25.

Perozo, E., F. Bezanilla, and R. DiPolo. 1989. Modulation of K channels in dialyzed squid axons. ATP-mediated phosphorylation. *J. Gen. Physiol.* **93:** 1195–1218.

Portner, H. O., D. M. Webber, R. G. Boutilier, and R. K. O'Dor. 1991. Acid-base regulation in exercising squid (*Illex illecebrosus, Loligo pealei*). *Am. J. Physiol.* **261:** R239–R246.

Romero, M. C. L., and T. Amaratunga. 1981. Preliminary results of biochemical-genetic population structure study of the squid, *Illex illecebrosus.* Third Annual Meeting Northwest Atlantic Fisheries Organization, *NAFO SCR Doc. 81:IX:103.* Ser. No. N405.

Saso, N. 1979. On the culture of aori-ika, *Sepioteuthis lessoniana.* Pp. 85–86 in *25th All Japan Fisheries Workers Activity Results Reporting Convention Materials.* All Japan Federation of Fisheries Cooperation Association. (In Japanese.)

Sato, H., and T. Tsuzaki. 1984. Seed production of *Sepioteuthis lessoniana* Lesson. *Saibai* (*Sea Farming*) **29:** 20–23. (In Japanese.)

Segawa, S. 1987. Life history of the oval squid, *Sepioteuthis lessoniana,* in Kominato and adjacent waters central Honshu, Japan. *J. Tokyo Univ. Fish.* **74:** 67–105.

Segawa, S. 1990. Food consumption, food conversion and growth rates of the oval squid *Sepioteuthis lessoniana* by laboratory experiments. *Nippon Suisan Gakkasihi* **56:** 217–222.

Segawa, S., T. Izuka, T. Tamashiro, and T. Okutani. 1993. A note on mating and egg deposition by *Sepioteuthis lessoniana* in Ishigaki Island, Okinawa, Southwestern Japan. *Venus* **52:** 101–108.

Sivak, J. G., J. A. West, and M. C. Campbell. In press. Growth and optical development of the ocular lens of the squid (*Sepioteuthis lessoniana*). *Vision Res.*

Smith, R. L. 1984. *Sperm Competition and the Evolution of Animal Mating Systems.* Academic Press, Orlando, FL.

Stein, P. G., H. M. Fishman, and K. P. Tewari. 1989. Axoballs: spontaneous formation of large vesicles after injury of squid axons. *Biophys. J.* **55:** 588a.

Strickland, J. D. H., and T. R. Parsons. 1972. A practical handbook of seawater analysis. *Fish. Res. Board Can. Bull.* **167:** 1–310.

Summers, W. C. 1974. Studies on the maintenance of adult squid (*Loligo pealii*). II. Empirical extensions. *Biol. Bull.* **146:** 291–301.

Suzuki, S., A. Kuwahara, and K. Washio. 1983. Study on the fishing conditions and an ecological aspect of squids, *Loligo edulis budo* and *Sepioteuthis lessoniana* in the coastal waters off Kyoto Prefecture. *Bull. Soc. Fish. Oceanogr. Res.* **42:** 21–27.

Suzuki, H., M. Ichikawa, and G. Matsumoto. 1993. Genetic approach for elucidation of squid family. Pp. 531–536 in *Recent Advances in Cephalopod Fisheries Biology.* T. Okutani, R. K. O'Dor, and T. Kubodera, eds. Tokai University Press, Tokyo.

Tewari, K. P., and H. M. Fishman. 1990. Rapid production of axosomes: a novel ion channel preparation from squid giant axon. *Biophys. J.* **57:** 319a.

Tsuchiya, M. 1981. On the spawning of the squid, *Sepioteuthis lessoniana* Lesson at Amitori Bay, Iriomote Island, Okinawa. *Bull. Inst. Oceanic Res. Dev., Tokai Univ. Notes* **3:** 53–75.

Tsuchiya, M. 1982. On the culture of the squid, *Sepioteuthis lessoniana* Lesson (Loliginidae), from hatching to the whole life in Iriomote Island, Okinawa. *Bull. Inst. Oceanic Res. Dev., Tokai Univ. Notes* **4:** 49–70. (In Japanese with English summary.)

Turk, P. E., and P. G. Lee. 1991. Design and economic analyses of airlift *versus* electrical pump driven recirculating aquaculture systems. Pp. 271–283 in *Engineering Aspects of Intensive Aquaculture.* Proceedings from the Aquaculture Symposium at Cornell University, Northeast Regional Aquacultural Engineering Service, Ithaca, NY. *NRAES* **49:** 271–283.

Turk, P. E., R. T. Hanlon, L. A. Bradford, and W. T. Yang. 1986. Aspects of feeding, growth and survival of the European squid *Loligo vulgaris* Lamarck, 1799, reared through the early growth stages. *Vie Milieu* **36:** 9–13.

Yang, W. T., R. T. Hanlon, M. E. Krejci, R. F. Hixon, and W. H. Hulet. 1980. Culture of California market squid from hatching—first rearing of *Loligo* to subadult stage. *Aquabiology* **2**(6): 412–418. (In Japanese with English summary.)

Yang, W. T., R. T. Hanlon, M. E. Krejci, R. F. Hixon, and W. H. Hulet. 1983. Laboratory rearing of *Loligo opalescens,* the market squid of California. *Aquaculture* **31:** 77–88.

Yang, W. T., R. F. Hixon, P. E. Turk, M. E. Krejci, W. H. Hulet, and R. T. Hanlon. 1986. Growth, behavior, and sexual maturation of the market squid, *Loligo opalescens,* cultured through the life cycle. *Fish. Bull.* **84:** 771–798.

Yang, W. T., R. T. Hanlon, P. G. Lee, and P. E. Turk. 1989. Design and function of closed seawater systems for culturing loliginid squids. *Aquacult. Eng.* **8:** 47–65.

Zeise, L., R. B. Addison, and M. R. Chedekel. 1992. Bioanalytical studies of eumelanins. 1. Characterization of melanin the particle. XIVth International Pigment Cell Conference Proceedings, *Pigm. Cell Res. Suppl.* **2:** 48–53.

Reference: *Biol. Bull.* **186**: 342–348. (June, 1994)

High Ammonia and Low pH in the Urine of the Ghost Crab, *Ocypode quadrata*

M. C. DE VRIES[1]*, D. L. WOLCOTT*, AND C. W. HOLLIDAY**

**Department of Marine, Earth and Atmospheric Sciences, North Carolina State University, Raleigh, North Carolina 27695-8208, and **Department of Biology, Lafayette College, Easton, Pennsylvania 18042*

Abstract. Nitrogen excreted into the urine (<1 m*M*) has generally been considered a negligible component of total nitrogen output of crustaceans. But concentrations of ammonia >100 m*M* were found in the urine of laboratory-held *Ocypode quadrata*, suggesting that this notion might not be applicable to all crustaceans. To address this issue, hemolymph and urine were removed from freshly captured *O. quadrata* and analyzed for nitrogenous catabolites and major ions. Hemolymph composition was similar to that of other crustaceans, but the urine was acidic ($\bar{X}$ pH = 5.50) and contained ammonia, often at >100 m*M*. Other nitrogenous catabolites in the urine (urea, amino acids, and uric acid) were much less concentrated: totaling <12 m*M* on average. The ionic composition of the urine was similar to that of other crustaceans, with the exception that Na was much less concentrated than Cl^-. Total osmolality of hemolymph and urine was similar. The Na^+/K^+ ATPase activity was greater in the antennal glands than in the posterior gills of *O. quadrata*, suggesting that this enzyme is important for ammonia concentration and Na resorption. This pattern of enzyme activity was not present in two terrestrial brachyurans whose urine contains little ammonia. The evolutionary significance of high ammonia concentrations in the urine of ghost crabs is unclear.

Introduction

Previous research has demonstrated that the gills and digestive tract are the major organs of nitrogen excretion in decapod crustaceans (Horne, 1968; Gifford, 1968; Cameron and Batterton, 1978; Harris and Andrews, 1985; Graszynski and Bigalke, 1987; Greenaway and Morris, 1989; Greenaway and Nakamura, 1991; Wolcott, 1991). The renal organ of decapods is important for water balance (review, Mantel and Farmer, 1983) and acid-base balance (Wheatly, 1985), and has been thought to be unimportant in nitrogen excretion. Urine contained nitrogen concentrations generally totaling less than 1 m*M* in the species studied (Horne, 1968; Mangum *et al.*, 1976; Cameron and Batterton, 1978; Harris and Andrews, 1985; Greenaway and Morris, 1989; Greenaway and Nakamura, 1991; Wolcott, 1991), and was neutral or of slightly alkaline pH (Cameron and Batterton, 1978; Truchot, 1979; Wolcott, 1991).

Aquatic decapods primarily excrete ammonia at the gills. Most terrestrial crabs also employ the gills for nitrogen excretion; however, in this case the fluid bathing the gills is not water from the environment, but urine. Urine is passed from the nephropores to the branchial chambers, where salts are resorbed, typically in association with ammonia excretion (Greenaway and Nakamura, 1991; Wolcott and Wolcott, 1984, 1985, 1991; Wolcott, 1991). The nitrogen content and acid-base status of urine before and after reprocessing by the gills have been measured only in herbivorous (low nitrogen input) species. The relatively small volume of urine passed to the branchial chambers can apparently accommodate the amounts of ammonia excreted by herbivores (Greenaway and Nakamura, 1991; Wolcott, 1991). Terrestrial crabs that are carnivorous must eliminate greater amounts of nitrogen, but because the amount of fluid into which ammonia can be excreted is limited, the risk of ammonia toxicity is increased.

The terrestrial brachyuran *Ocypode quadrata*, which inhabits exposed beaches on the Atlantic coast of the Americas, is primarily carnivorous (Wolcott, 1978) and

Received 3 May 1993; accepted 10 March 1994.

[1] Present address: Duke University Marine Laboratory, Beaufort, NC 28516.

reprocesses urine (Wolcott and Wolcott, 1985). Our preliminary data from laboratory-held *Ocypode quadrata* showed high concentrations (>100 m*M*) of ammonia in acidic (pH < 6) urine, a pattern atypical of crustaceans but typical of vertebrates. Deamination of dietary protein in the liver of vertebrates decreases urinary pH and increases urinary ammonia output (Minnich, 1972; Scott, 1972; Pitts, 1974; Long and Skadhauge, 1983; Halperin *et al.*, 1985; Dantzler, 1989). Moreover, carnivorous and omnivorous mammals have more acidic urine than herbivores (Long and Giebisch, 1979). Comparable data are scant for invertebrates.

We therefore characterized the ionic and nitrogenous composition of urine and hemolymph from *O. quadrata* freshly captured from the field. Results suggested possible mechanisms of ammonia concentration in the renal organ. Consequently, we also measured the activities of the Na^+/K^+ ATPases in the antennal glands and other ion-transporting tissues of *O. quadrata*, and compared them to the activities in two species of herbivorous terrestrial crabs, *Cardisoma guanhumi* and *Gecarcinus lateralis*, for which previous research had demonstrated low urinary nitrogen concentrations (Wolcott, 1991). Na^+/K^+ ATPases are important in excretion of NH_4^+ across gills of aquatic crabs and fishes (Towle *et al.*, 1976; review, Evans and Cameron, 1986; Towle and Hølleland, 1987), and may play a role in ammonia transport by other organs.

Materials and Methods

Collection of animals and samples

Ghost crabs, *Ocypode quadrata* (Fabricius), were captured after dusk on Bogue Bank, North Carolina, and immediately brought back to the laboratory where the urine was collected. Animals were restrained by being strapped to a board; the nephropore cover was deflected, and the tip of a fire-drawn pipette was inserted just inside the nephropore. Urine flow usually began immediately upon nephropore deflection; when this did not occur, gentle suction was applied by mouth tube. To minimize air exposure of the sample and possible pH change, the pH was immediately measured with a Microelectrodes, Inc., Model 710 electrode. pH measurements (of blood samples) obtained using a completely anaerobic procedure for sample withdrawal agreed to within 1% of values from the minimal air exposure method described above. The remaining urine was frozen for later analyses.

The crabs were kept overnight in plastic containers with a small amount of moist sand from their habitat. The following morning, a fire-drawn pipette was inserted into the arthrodial membrane of a leg and hemolymph was withdrawn. According to previous research on *O. quadrata*, the hemolymph ion concentrations for an individual can increase or decrease by as much as 15% over an 8-h period (Hall, 1982; Wolcott and Wolcott, 1985), although the average change is considerably less. For this reason, we considered the 8 h elapsed time between urine and hemolymph collection to be unimportant for urine to hemolymph comparisons.

Chloride concentration, osmolality, and pH were measured immediately on whole blood. After a clot had formed in the remaining sample, it was disrupted and the sample was centrifuged (10 min at 10,000 rpm, 4°C); the serum was drawn off and frozen for later analyses. Urine and serum for atomic absorption spectrophotometry were frozen in sealed hematocrit tubes.

Analytical methods

Osmolality was measured with a Wescor osmometer (Model 5100B). Cl^- concentrations were measured on 2-μl samples with a Buchler-Cotlove direct readout automatic titrator. For blood we first placed the sample into 0.5 ml of deionized water to free any Cl^- that might be trapped within the clot. Ammonia was measured by the Berthelot method (Sigma Technical Bulletin No. 640). Urea was hydrolyzed by urease (Sigma Chemical Co.), and the urea concentration estimated by difference in ammonia between hydrolyzed and unhydrolyzed samples of urine and hemolymph. Amino acids were measured in urine (only) as ninhydrin positive substances (method of Lee and Takahashi, 1966) after precipitation of the proteins with trichloroacetic acid. Uric acid was measured by the difference in absorbance (292 nm) of samples hydrolyzed and unhydrolyzed by uricase (Sigma Kit No. 292). Total nitrogen was measured on urine (only) by Nesslerization (Fisher Scientific) after micro-Kjeldahl digestion and distillation. Concentrations of Na, Mg, K, and Ca were measured by atomic absorption spectrophotometry (AAS; Perkin Elmer Model 2400). AAS measures the concentrations of both the ionized and elemental forms of these species, but most of these elements exist as ions in blood and urine.

The amount of water absorbed or secreted into the primary urine during modification was not estimated with marker studies. Thus urine/hemolymph ratios may not reflect simple reabsorption or secretion of a molecule. Rather, they may be considered estimates of relative absorption or secretion.

To be certain that the high ammonia concentrations we measured with the Berthelot assay were not due to an interfering substance in the urine of *O. quadrata*, we used suppressed ion chromatography (CS3 columns) to analyze urine from laboratory-held crabs for ammonium. The eluant was 0.5 m*M* DL-2,3-diamino-propionic acid monohydrochloride in 12 m*M* HCl, and the regenerant was 0.05 *M* tetrabutylammonium hydroxide. The retention time of ammonium was 3.38 min with a precision of 3.5%

from six standard runs. These laboratory-held animals had urinary ammonia concentrations similar to those of the freshly captured animals (measured by the Berthelot assay).

For the purposes of this paper, ammonia refers to a combination of ionized (NH_4^+) and unionized (NH_3) forms of this molecule.

Na^+/K^+ ATPase assays

Cardisoma guanhumi were collected at Fort Pierce, Florida, and maintained in the laboratory in individual habitats that included a pool of dilute (<50%) seawater at the bottom of an artificial burrow. *Gecarcinus lateralis* were collected at Spittal Pond, Bermuda, and maintained in the laboratory in individual plastic mouse cages (8.5-l) containing a petri dish of dilute seawater. Water was renewed twice weekly, and crabs were fed leaf litter and lettuce *ad libitum*. Holding conditions for the herbivorous species support long-term survival (>4 years) and multiple successful moltings. *C. guanhumi* and *G. lateralis* had been in the laboratory for about 10 months, overwintering on a seasonally varying light-dark cycle, before sacrifice for enzyme assays.

Ocypode quadrata used for enzyme assays were collected as described previously for this species. *O. quadrata* were maintained in plastic mouse cages (8.5-l) containing acid-washed sand dampened (10% water by weight) with dilute seawater. This species was fed dried squid 2–3 times per week for at least 10 days before sacrifice. All species were given access to dilute medium to stimulate reclamation of ions by the gills through the induction of gill Na^+/K^+ ATPases, thus precluding the underestimation of enzyme activity.

Detailed procedures for measuring specific enzyme activity of Na^+/K^+ ATPases appear in Holliday (1985), but are briefly as follows. Animals were killed by disrupting the ventral nerve cord. Three tissues—antennal gland, the basal portion of gill 7, and claw muscle—were removed from each crab, rinsed, and homogenized by hand in cold homogenizing medium. The basal portions of posterior gills were selected for assay because they have been implicated in sodium transport in several species of osmoregulating crabs (reviewed by Towle, 1984). Claw muscle was included as a 'reference.' Though ions are transported within it, muscle is unimportant for the overall ion balance of the organism.

Enzyme activity was measured as the phosphate liberated from ATP by each homogenate in two reaction media, one containing optimum concentrations of all ions and the other lacking potassium and containing ouabain. After 15 min at 30°C, the reaction was stopped and phosphate measured colorimetrically. Enzyme activity was calculated as the difference in phosphate liberated by each homogenate into the media, and is expressed as μmoles PO_4 liberated $\cdot$ mg^{-1} protein $\cdot$ h^{-1}. Protein concentrations in the homogenates were measured colorimetrically with the Bio-Rad protein assay (Bio-Rad Laboratories, Richmond, CA); bovine serum albumin was the standard.

Statistical analyses

Differences between mean concentrations of each variable measured in the hemolymph and urine were tested by paired *t* tests. Exceptions were pH and ammonia, which deviated from normality and so did not fit the assumptions of parametric statistics. A Wilcoxon test was used to test for differences between these variables. For simplicity, nonparametric Spearman correlations were used for all associations between variables tested. Measurements are expressed as means ±95% confidence intervals unless otherwise stated. For specific activity of Na^+/K^+ ATPases, differences among the means for each tissue were tested by one-way ANOVA followed by multiple comparison (Bonferroni) tests within each species.

Results

The pH of urine from freshly caught *Ocypode quadrata* was significantly lower and more variable ($\bar{X}$ = 5.50; range = 4.68–7.56) than that of hemolymph ($\bar{X}$ = 7.58; range = 7.42–7.68; Wilcoxon $Z = 4.78$, $P < 0.0001$). In addition to being more acidic, urine contained >100 times more ammonia than hemolymph (Table I). Ion chromatography confirmed that the high urine ammonia concentrations observed with the Berthelot assay were due to ammonia, rather than to a potentially interfering substance such as an amine. Ion chromatography yielded concentrations 23.7% higher on average than the Berthelot assay (n = 4). Urea concentrations in urine and hemolymph were similar and were low compared with urine ammonia (Table I). When concentrations of ammonia-, urea-, and amino-nitrogen are summed, they account for an average of 88% of the total Kjeldahl-nitrogen measured, when comparing individuals for which all of the nitrogenous variables were measured. Thus in Table I, we are accounting for a majority of the nitrogenous catabolites in the urine. Of the accountable nitrogen in the urine, ammonia-N = 90.9%, urea-N = 5.8%, amino-N = 3.3%, and uric acid-N = 0.1%.

Na and Cl^- are the major ionic constituents of both urine and hemolymph of *O. quadrata* (Table II). For all inorganic elements measured, and for total osmolality, there was a significant difference in concentration between the urine and the hemolymph (Table II). For total osmolality and Cl^-, this difference is fairly small but consistent. The concentrations of these elements in the urine appear to be strongly regulated. Mg and K appear to be

Table I

Nitrogenous components of urine and hemolymph from freshly captured Ocypode quadrata

	Nitrogen concentration (m*M*)				
Fluid	Ammonia-N	Urea-N	Amino-N	Uric Acid-N	Kjeldahl-N
Urine	116.31 ± 34.85 (n = 18)	7.43 ± 2.40 (n = 18)	4.16 ± 2.03 (n = 18)	0.12 ± 0.08 (n = 14)	179.6 ± 73.1 (n = 8)
Hemolymph	0.86 ± 0.39 (n = 17)	6.52 ± 1.02 (n = 18)	—	Undetectable (n = 10)	—
U/H	135.24	1.14	—	—	—
P	0.0001*	0.551			

P value is for Wilcoxon Test (ammonia) and paired t test (urea).

preferentially secreted and Na and Ca resorbed, probably as ions (Table II).

When comparing concentrations in the urine and hemolymph of each variable measured, a significant correlation was found only for total osmolality (r = 0.557, P = 0.038). This suggests that for all variables except total osmolality, the processes that regulate the concentration of the substance in the urine are not dependent simply upon the concentration of that substance in the hemolymph.

Urine ammonia concentrations were correlated with several variables measured, including urine pH, Cl^-, Na, and Mg (r = −0.707, P = 0.001; r = 0.628, P = 0.005; r = −0.682, P = 0.005; r = 0.635, P = 0.015, respectively). The two negative correlations (ammonia *vs.* pH and ammonia *vs.* Na) are suggestive of ion exchange processes that might result in high urinary ammonia.

For all species, Na^+/K^+ ATPase activity of claw muscle was low and significantly different from that of antennal gland (Table III). Specific enzyme activity of antennal gland was significantly lower than or not different from that of gill 7 for the two species (*C. guanhumi* and *G. lateralis*) with low urine ammonia. ATPase activity of antennal gland from *O. quadrata* was significantly greater than activity of gill 7.

Discussion

Urine removed from the bladders of freshly captured *Ocypode quadrata* is acidic and the ammonia concentration is up to 134 times greater than that of the hemolymph. This urine to hemolymph ratio for ammonia is two orders of magnitude higher in *O. quadrata* than in previously studied crustaceans (1.0–3.8) (Green *et al.*, 1959; Cameron and Batterton, 1978; Harris and Andrews, 1985), though the hemolymph ammonia falls within published values (Gifford, 1968; Horne, 1968; Mangum *et al.*, 1976; Cameron and Batterton, 1978; Henry and Cameron, 1981; Wood and Boutilier, 1985; Greenaway and Morris, 1989; Greenaway, 1991). Other nitrogenous catabolites (urea, free amino acids, and uric acid) were present in low levels in the hemolymph and urine of ghost crabs, as in other decapods (Horne, 1968; Gifford, 1968; Henry and Cameron, 1981; Greenaway and Nakamura, 1991; Wolcott, 1991).

This extremely high concentration of urine ammonia has implications for the overall nitrogen balance of the

Table II

Ionic and elemental constituents of urine and hemolymph from freshly captured Ocypode quadrata

	Concentration (m*M*)*					
Fluid	Cl^-	Mg	Na	K	Ca	Osmolality
Urine (n = 13–18)	415 ± 13	43.8 ± 14.1	254.6 ± 50.5	19.5 ± 3.4	9.3 ± 1.2	788.2 ± 29.0
Hemolymph (n = 16–17)	378 ± 10	12.2 ± 1.6	413.1 ± 39.0	7.7 ± 1.1	13.8 ± 1.8	841.3 ± 17.1
U/H	1.09	3.59	0.62	2.53	0.72	0.94
P	0.0006	0.0024	0.0002	0.0005	0.001	0.0031

* mOsm/kg for osmolality.

P value is for paired t test.

Whole blood was analyzed for Cl^- and osmolality.

Table III

Specific enzyme activities of Na^+/K^+ATPase (μmol $PO_4 \cdot mg^{-1}$ protein $\cdot h^{-1}$) from various tissues of brachyurans on dilute media

Taxon	Tissue		
	Antennal gland	Gill 7	Claw muscle
Cardisoma guanhumi			
($n = 6$)	3.93 ± 0.48	13.25 ± 0.51	1.84 ± 0.58
$F = 897.4$			
$P < 0.0001$	A	B	C
Gecarcinus lateralis			
($n = 6$)	8.83 ± 3.56	4.80 ± 3.34	2.16 ± 0.73
$F = 10.59$			
$P < 0.0016$	A	A/B	B
Ocypode quadrata			
($n = 14$)	29.60 ± 5.2	17.01 ± 3.21	1.25 ± 0.49
$F = 75.2$ $P < 0.0001$	A	B	C

Activity values are means ± 95% confidence intervals. Results of analysis of variance and groupings by Bonferroni tests (experimentwise $\alpha = 0.05$) appear below each species. Means with different letter designations are significantly different from one another (within each species).

organism. The rate of release of urine after reprocessing by the gills of *O. quadrata* (about 2% body weight/day; De Vries and Wolcott, 1993) can serve as a conservative estimate of the rate of urine production. This estimate falls within the range of urine production rates observed for other terrestrial crabs (Harris, 1977; Kormanik and Harris, 1981; Greenaway *et al.*, 1990). Use of this value and the data from Table I yields an output of ammonia of 2500 μmol $N \cdot kg^{-1} \cdot day^{-1}$ via urine, which is 1–2 orders of magnitude greater than the urinary nitrogen output rate of every crab studied, whether aquatic or terrestrial (Binns, 1969; Cameron and Batterton, 1978; Harris and Andrews, 1985; Greenaway and Nakamura, 1991). In addition, this estimate approximates the combined rates for all nitrogen output routes in *Geograpsus grayi* (also a carnivore), the species with the highest nitrogen output rate yet measured for terrestrial crabs (Wood and Boutilier, 1985; Wolcott and Wolcott, 1987; Greenaway and Morris, 1989; Greenaway and Nakamura, 1991; Wolcott, 1991). Other routes of nitrogen excretion in *O. quadrata* were insignificant (De Vries and Wolcott, 1993; Wolcott and DeVries, unpub. data). Urine production rates (before reprocessing by the gills) must be measured and a rigorous nitrogen budget must be constructed under controlled conditions in the laboratory if we are to better our understanding of this phenomenon.

The urine of *O. quadrata* is isosmotic with the hemolymph, but not isoionic. In this study, Mg and K appeared to be secreted, and Ca and especially Na resorbed. Gifford (1962) found similar patterns of secretion and reabsorption of the major cations during urine formation by freshly collected *Ocypode albicans* (= *quadrata*), though the magnitude of the modification for each ion measured was less. The renal organs of other terrestrial and semiterrestrial decapods also appear capable of modifying the inorganic content of the urine to some degree. The urine and hemolymph of those species have concentrations of the major ions (except Na) that are similar to the concentrations found in *O. quadrata* (review, Mantel and Farmer, 1983; present study).

The sodium in the urine of *O. quadrata* is about 150 m*M* lower than both the Na in the hemolymph and the Cl^-. Low urinary Na concentrations have been previously described for *O. quadrata* (Gifford, 1962) and *U. pugilator* (Green *et al.*, 1959), though this pattern is the exception among crustaceans (review, Mantel and Farmer, 1983). Nevertheless, for *O. quadrata*, like other crustaceans, the gills are the major organ of salt balance (review, Mantel and Farmer, 1983). Gills of *O. quadrata* can resorb 90% of the salt in the urine during reprocessing (Wolcott and Wolcott, 1985).

Low concentrations of Na and high concentrations of ammonia in the urine could result from action of Na^+/K^+ ATPases, with substitution of NH_4^+ for K^+. This ionic substitution has been demonstrated at physiological pH in isolated gill membrane vesicles (Towle and Holleland, 1987). Moreover, specific activity of Na^+/K^+ ATPases in the antennal gland is higher than that in the posterior gills of *O. quadrata*. Terrestrial crabs with little urinary nitrogen do not show this increased activity, suggesting that the enzyme is important for the transport of ammonia by the renal organ of *O. quadrata*. Similar ratios (gill: antennal gland) and absolute values of Na^+/K^+ ATPase activities were found in *Cardisoma carnifex* and *Gecarcinus lalandii*, congeners of the low urinary nitrogen species that we assayed (Towle, 1981).

The low urine pH and the negative correlation between urine pH and urine ammonia suggest acid-trapping as another possible mechanism of ammonia concentration within the urine. This mechanism entails the diffusion of NH_3 dissolved in the hemolymph, down its partial pressure gradient, and into the acidic urine; there it would immediately be ionized to NH_4^+, which would maintain the gradient. Action of Na^+/H^+ antiporters may contribute to the lowering of urine pH by the renal organ, as well as to the reduction of Na concentration. Na^+/H^+ antiporters have been found in gills of crabs (Towle, 1985), but have not been studied in their renal organs. Other mechanisms of ammonia transport across membranes are also possible (reviews in Kormanik and Cameron, 1981; Evans and Cameron, 1986; Regnault, 1987).

Although *O. quadrata* was initially selected for study because of its high-nitrogen diet, the vertebrate-like pattern of low pH and high ammonia in the urine appears to have a taxonomic component within the Decapoda as well.

Every species within the family Ocypodidae that has been studied has a high-ammonia urine of acidic or neutral pH, despite gross differences in dietary nitrogen inputs. The ocypodid *Uca pugilator* is probably omnivorous (Miller, 1961; Robertson and Newell, 1982) and produces high-ammonia urine ($\bar{X}$ = 75 m*M* [Green *et al.*, 1959]; $\bar{X}$ = 92 m*M* [Wolcott and De Vries, unpub. data]) of neutral pH ($\bar{X}$ = 7.1, [Wolcott and De Vries, unpub. data]). *Ucides cordatus*, another ocypodid, also produces high-ammonia, acidic urine ($\bar{X}$ ammonia = 80 m*M*; $\bar{X}$ pH = 6.0 [Wolcott and De Vries, unpub. data]), although this species is primarily herbivorous (Garcia and Bonnelly de Calventi, 1983). One might speculate that ancestral Ocypodidae were carnivorous, and that the mechanisms for forming a high-ammonia, acidic urine were retained when herbivory evolved in some members of the family.

Like urinary composition, the primary mode of nitrogen excretion may prove to vary along taxonomic lines. Of the species studied, gecarcinids (three species) release waste nitrogen into the branchial fluid primarily as ammonia (Greenaway and Nakamura, 1991; Wolcott, 1991); a grapsid releases primarily NH_3 gas at the gills (Greenaway and Nakamura, 1991); a coenobitid releases uric acid into the feces (Greenaway and Morris, 1989); and ocypodids (three species) excrete ammonia directly into the urine (Green *et al.*, 1959; De Vries and Wolcott, 1993; present study). This plasticity in chemistry and mode of nitrogen excretion among terrestrial crabs may be related to the proposed independent colonization of the land by various families and genera (Little, 1983; Hartnoll, 1988). For the Ocypodidae at least, the previously held notion that the crustacean renal organ is unimportant for nitrogen excretion must be reconsidered. Whether the special urinary characteristics of this group serve functions in addition to the elimination of nitrogen is open for investigation.

Acknowledgments

We wish to thank J. Willey for doing the ion chromatography, T. D'Arconte and T. Wolcott for technical assistance, T. Boynton for assistance collecting animals, and R. Forward and the Duke University Marine Laboratory for providing facilities. This work was supported by the Department of Marine, Earth and Atmospheric Sciences, North Carolina State University, and NSF grant DCB 8905019.

Literature Cited

Binns, R. 1969. The physiology of the antennal gland of *Carcinus maenas* (L.) 5. Some nitrogenous constituents in the blood and urine. *J. Exp. Biol.* **51:** 41–45.

Cameron, J. N., and C. V. Batterton. 1978. Antennal gland function in the freshwater blue crab, *Callinectes sapidus:* water, electrolyte, acid-base and ammonia excretion. *J. Comp. Physiol.* **123:** 143–148.

Dantzler, W. H. 1989. *Comparative Physiology of the Vertebrate Kidney.* Springer-Verlag, Berlin.

De Vries, M. C., and D. L. Wolcott. 1993. Gaseous ammonia evolution is coupled to reprocessing of urine at the gills of ghost crabs. *J. Exp. Zool.* **267:** 97–103.

Garcia, M., and I. Bonnelly de Calventi. 1983. *El cangrejo de manglar en la Republica Dominicana.* Empreso Editorial Gaviota (Gaviota Press), Santo Domingo, Rep. Dom.

Evans, D. H., and J. N. Cameron. 1986. Gill ammonia transport. *J. Exp. Zool.* **239:** 17–23.

Gifford, C. A. 1962. Some aspects of osmotic and ionic regulation in the blue crab, *Callinectes sapidus,* and the ghost crab *Ocypode albicans. Publ. Inst. Mar. Sci., Univ. Texas* **8:** 97–125.

Gifford, C. A. 1968. Accumulation of uric acid in the crab *Cardisoma guanhumi. Am. Zool.* **8:** 521–528.

Graszynski, K., and T. Bigalke. 1987. Osmoregulation and ion transport in the extremely euryhaline fiddler crabs *Uca pugilator* and *Uca tangeri* (Ocypodidae). *Zool. Beitraege* **30:** 339–358.

Green, J. W., M. Harsch, L. Barr, and C. L. Prosser. 1959. Regulation of water and salt by the fiddler crabs, *Uca pugnax* and *Uca pugilator. Biol. Bull.* **116:** 76–84.

Greenaway, P. 1991. Nitrogenous excretion in aquatic and terrestrial crustaceans. *Mem. Queensland Mus.* **31:** 215–227.

Greenaway, P., and S. Morris. 1989. Adaptations to a terrestrial existence by the robber crab, *Birgus latro* L. III. Nitrogenous excretion. *J. Exp. Biol.* **143:** 333–346.

Greenaway, P., and T. Nakamura. 1991. Nitrogenous excretion in two terrestrial crabs *Gecarcoidea natalis* and *Geograpsus grayi. Physiol. Zool.* **64:** 767–786.

Greenaway, P., H. H. Taylor, and S. Morris. 1990. Adaptations to a terrestrial existence by the robber crab *Birgus latro.* VI. The role of the excretory system in fluid balance. *J. Exp. Biol.* **152:** 505–519.

Hall, L. A. 1982. Osmotic and ionic regulation in overwintering ghost crabs. *Ocypode quadrata,* Masters thesis, North Carolina State University, 47 pp.

Halperin, M. L., M. B. Goldstein, B. J. Stinebaugh, and R. L. Jungas. 1985. Biochemistry and physiology of ammonium excretion. Pp. 1471–1490 in *The Kidney: Physiology and Pathophysiology,* Vol. 2, D. W. Seldin and G. Giebisch, eds. Raven, New York.

Harris, R. R. 1977. Urine production rate and water balance in the terrestrial crabs *Gecarcinus lateralis* and *Cardisoma guanhumi. J Exp. Biol.* **68:** 57–67.

Harris, R. R., and M. B. Andrews. 1985. Total NPS pool and ammonia net efflux rate changes in *Carcinus maenas* during acclimation to low environmental salinity. *Comp. Biochem. Physiol.* **82A:** 301–308.

Hartnoll, R. G. 1988. Evolution, systematics, and geographical distribution. Pp. 6–54 in *Biology of the Land Crabs,* W. W. Burggren and B. R. McMahon, eds. Cambridge University Press, Cambridge.

Henry, R. P., and J. N. Cameron. 1981. A survey of hemolymph and tissue compounds in terrestrial decapods of Palau. *J. Exp. Zool.* **218:** 83–88.

Holliday, C. W. 1985. Salinity-induced changes in gill Na, K-ATPase activity in the mud fiddler crab, *Uca pugnax. J. Exp. Zool.* **233:** 199–208.

Horne, F. R. 1968. Nitrogen excretion in crustacea-I. The herbivorous land crab *Cardisoma guanhumi* Latreille. *Comp. Biochem Physiol.* **26:** 687–695.

Kormanik, G. A., and J. N. Cameron. 1981. Ammonia excretion in the seawater blue crab (*Callinectes sapidus*) occurs by diffusion and not Na^+/NH_4^+ exchange. *J. Comp. Physiol.* **141:** 457–462.

Kormanik, G. A., and R. R. Harris. 1981. Salt and water balance and antennal gland function in three Pacific species of terrestrial crab (*Gecarcoidea lalandii, Cardisoma carnifex, Birgus latro*). I. Urine

production and salt exchanges in hydrated crabs. *J. Exp. Zool.* **218:** 97–105.

Lee, Y. P., and T. Takahashi. 1966. An improved colorimetric determination of amino acids with use of ninhydrin. *Anal. Biochem.* **14:** 71–77.

Little, C. 1983. *The Colonization of Land* Cambridge University Press, New York.

Long, S., and G. Giebisch. 1979. Comparative physiology of renal tubular transport mechanisms. *Yale J. Biol. Med.* **52:** 525–544.

Long, S., and E. Skadhauge. 1983. Renal acid excretion in the domestic fowl. *J. Exp. Biol.* **104:** 51–58.

Mangum, C. P., S. U. Silverthorn, J. L. Harris, D. W. Towle, and A. R. Krall. 1976. The relationship between blood pH, ammonia excretion and adaptation to low salinity in the blue crab *Callinectes sapidus*. *J. Exp. Zool.* **195:** 129–136.

Mantel, L. H., and L. L. Farmer. 1983. Osmotic and ionic regulation. Pp. 53–161 in *The Biology of Crustacea*, Vol. 5, D. E. Bliss, ed. Academic Press, New York.

Miller, D. C. 1961. The feeding mechanism of fiddler crabs, with ecological considerations of feeding adaptations. *Zoologica* **46:** 89–100.

Minnich, J. E. 1972. Excretion of salts by reptiles. *Comp. Biochem. Physiol.* **41A:** 535–549.

Pitts, R. F. 1974. *Physiology of the Kidney and Body Fluids* Year Book Medical Publishers, Chicago.

Regnault, M. 1987. Nitrogen excretion in marine and freshwater Crustacea. *Biol. Rev.* **62:** 1–24.

Robertson, J. R., and S. Y. Newell. 1982. Experimental studies of particle ingestion by the sand fiddler crab *Uca pugilator* (Bosc). *J. Exp. Mar. Biol. Ecol.* **59:** 1–21.

Scott, D. 1972. Excretion of phosphorus and acid in the urine of sheep and calves fed either roughage or concentrate diets. *Q. J. Exp. Physiol.* **57:** 379–392.

Towle, D. W. 1981. Transport-related ATPases as probes of tissue function in three terrestrial crabs of Palau. *J. Exp. Zool.* **218:** 89–95.

Towle, D. W. 1985. Amiloride-sensitive Na^+/H^+ exchange in membrane vesicles from crab (*Callinectes sapidus*) gill (Abstract). *Am. Zool.* **25:** 31.

Towle, D. W., and T. Holleland. 1987. Ammonium ion substitutes for K^+ in ATP-dependent Na^+ transport by basolateral membrane vesicles. *Am. J. Physiol.* **252:** 479–489.

Towle, D. W., G. E. Palmer, and J. L. Harris III. 1976. Role of gill $Na^+ + K^+$-dependent ATPase in acclimation of blue crabs (*Callinectes sapidus*) to low salinity. *J. Exp. Zool.* **196:** 315–322.

Truchot, J. P. 1979. Mechanisms of the compensation of blood respiratory acid-base disturbances in the Shore Crab, *Carcinus maenas* (L.). *J. Exp. Zool.* **210:** 407–416.

Wheatly, M. G. 1985. The role of the antennal gland in ion and acid-base regulation during hyposaline exposure of the Dungeness crab *Cancer magister* (Dana). *J. Comp. Physiol. B* **155:** 445–454.

Wolcott, D. L. 1991. Nitrogen excretion is enhanced during urine recycling in two species of terrestrial crab. *J. Exp. Zool.* **259:** 181–187.

Wolcott, D. L., and T. G. Wolcott. 1987. Nitrogen limitation in the herbivorous land crab *Cardisoma guanhumi*. *Physiol. Zool.* **60:** 262–268.

Wolcott, T. G. 1978. Ecological role of ghost crabs, *Ocypode quadrata* (Fabricius) on an open beach: scavengers or predators? *J. Exp. Mar. Biol. Ecol.* **31:** 67–82.

Wolcott, T. G., and D. L. Wolcott. 1984. Salt conservation by extrarenal resorption in *Cardisoma guanhumi*. *Am. Zool.* **25:** 78A.

Wolcott, T. G., and D. L. Wolcott. 1985. Extrarenal modification of urine for ion conservation in ghost crabs, *Ocypode quadrata* (Fabricius). *J. Exp. Mar. Biol. Ecol.* **91:** 93–107.

Wolcott, T. G., and D. L. Wolcott. 1991. Ion conservation by reprocessing of urine in the land crab *Gecarcinus lateralis* (Freminville). *Physiol. Zool.* **64:** 344–361.

Wood, C. M., and R. G. Boutilier. 1985. Osmoregulation, ionic exchange, hemolymph chemistry, and nitrogenous waste excretion in the land crab *Cardisoma carnifex*: a field and laboratory study. *Biol. Bull.* **169:** 267–290.

Reference: *Biol. Bull.* **186:** 349–355. (June, 1994)

The Adhesive Protein cDNA of *Mytilus galloprovincialis* Encodes Decapeptide Repeats but No Hexapeptide Motif

KOJI INOUE AND SATOSHI ODO

Kamaishi Institute, Marine Biotechnology Institute, Heita, Kamaishi, Iwate 026, Japan

Abstract. A mussel is attached to hard surfaces by its byssus, which consists of a bundle of threads, each with a fibrous collagenous core coated with adhesive proteins. We constructed a cDNA library from RNA isolated from the foot of the mussel *Mytilus galloprovincialis* sampled in Japan. The library was probed with a nucleotide sequence corresponding to a part of the decapeptide repeat motif in the major adhesive protein of the closely related species *M. edulis,* and a clone including the whole coding region of the same adhesive protein of *M. galloprovincialis* was isolated. The sequences of the signal and nonrepetitive regions of the protein of *M. galloprovincialis* were homologous to those of *M. edulis,* despite several substitutions and a deletion of 18 amino acids. The repetitive region included a tetradecapeptide sequence and 62 repeats of the same decapeptide motif as in *M. edulis,* but hexapeptide sequences present in *M. edulis* were absent in the protein of *M. galloprovincialis.* In the decapeptide motif, two tyrosine residues, two lysine residues, and one of the two proline residues were highly conserved, but other residues were frequently substituted. In some residues in the decapeptide motif, specific codon usages were observed, suggesting that the nucleotide sequence itself has a function.

Introduction

Mussels in the genus *Mytilus* are distributed globally in temperate marine intertidal zones. They attach themselves to solid intertidal surfaces by means of the byssus. The byssus is a bundle of threads each consisting mainly of a fibrous collagenous core coated by adhesive proteins. The protein components of the byssus have been extensively studied in *M. edulis* (Waite, 1987, 1992, for reviews). A major adhesive protein is a 130 kDa protein containing a high proportion of 3,4-dihydroxyphenylalanine (DOPA) residues (Waite and Tanzer, 1981; Waite, 1983). The protein is reported to be largely composed of tandem repeats of the decapeptide Ala-Lys-Pro-Ser-Tyr-Hyp-Hyp-Thr-DOPA-Lys, where Hyp is 3- or 4-hydroxyproline (Waite *et al.,* 1985). Other mussel species have similar proteins, each with a unique repeat motif (Waite, 1986; Waite *et al.,* 1989; Rzepecki *et al.,* 1991). Partial sequences of cDNA and genomic DNA encoding the adhesive protein were reported in *M. edulis* (Strausberg *et al.,* 1989; Filpula *et al.,* 1990). The complete amino acid sequence of the adhesive protein from *M. edulis* has been deduced from its cDNA (Laursen, 1992). These studies showed that this adhesive protein contains more than 80 tandem repeats, of which more than 70 are decapeptides and others are hexapeptides.

In this study, we isolated a cDNA clone containing the whole coding region of the adhesive protein from another major species of mussel, *M. galloprovincialis,* which is closely related to *M. edulis* (Gosling, 1984; Gardner, 1992; Geller *et al.,* 1993). We have found that the cDNA encodes a polypeptide containing 62 repeats of the decapeptide found in *M. edulis,* as well as a tetradecapeptide, but no hexapeptide repeat.

Received 10 January 1994; accepted 28 March 1994.

Materials and Methods

Isolation of mRNA

Mussels (*M. galloprovincialis*) about 4 cm in shell length were sampled at Miyako Bay, Iwate prefecture, Japan. The foot was isolated from 12 mussels and the total RNA

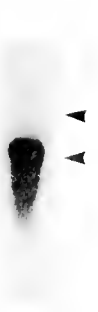

Figure 1. Northern blot analysis of RNA extracted from the foot of *Mytilis galloprovincialis*. One microgram of RNA was electrophoresed on a 1% agarose gel, transferred onto a nylon membrane, and hybridized with the oligonucleotide probe corresponding to a part of the decapeptide sequence. Allowheads indicate the position of 18S and 28S rRNA.

was extracted using the Total RNA Separator Kit (Clontech Laboratories, Palo Alto, CA). Poly(A)$^+$RNA was isolated using the mRNA separator (Clontech Laboratories, Palo Alto, CA).

Northern blot hybridization

Poly(A)$^+$RNA was electrophoresed on a 1% agarose gel, transferred onto a nylon membrane, and hybridized with a [^{32}P]ATP-labeled oligonucleotide probe,

ATA(T,A)GTTGGAGGATAA(C,G)TTGGCTT,

that corresponds to a part of the antisense sequence of the decapeptide repeats of *M. edulis* (Strausberg *et al.*, 1989).

Screening of the cDNA library

cDNA was synthesized using the cDNA Synthesis Kit Plus (Amersham). A cDNA library was constructed using the cDNA cloning system lambda gt10 (Amersham). The library was screened using the same probe used for the northern blotting. Ten positive clones were picked up and the size of inserts was determined by excising with *Eco*RI. The longest insert was subcloned into a plasmid vector, BluescriptIISK+ (Stratagene). Restriction analysis of the BluescriptIISK+ subclone was performed using *Apa*I, *Bam*HI, *Eco*RI, *Hinc*II, *Hind*III, *Kpn*I, *Not* I, *Pvu*II, *Pst*I, *Sac*I, *Sal*I, *Sca*I, *Sma*I, *Spe*I, *Xba*I and *Xho*I.

Sequencing

To determine the whole sequences of both strands of the insert, the plasmid containing the insert was digested with *Apa*I/*Hin*dIII or *Sac*I/*Xba*I, and deletion derivatives were produced using the Kilo-Deletion Sequence Kit (Takara, Kyoto, Japan). The original subclone, 28 *Apa*I/*Hin*dIII-generated clones, and 17 *Sac*I/*Xba*I-generated clones were sequenced using a 373A DNA sequencer (Applied Biosystems Inc.).

Results

Northern blot hybridization

To examine the efficiency of the probe and to obtain information about the length of the target, northern blot hybridization was carried out. As shown in Figure 1, an intense signal was detected at a position slightly higher than 18S rRNA. This result indicates that the probe is applicable to the screening of the adhesive protein of *M. galloprovincialis*. It also indicates that the target mRNA is expressed in the foot and its length is more than 2.4 kb.

Outline of the structure of the adhesive protein cDNA

About 5×10^4 clones were screened, and more than 50 positive plaques were detected. Of 10 randomly selected clones, 2 were found to have inserts of about 2.5 kb. The longer clone was chosen for further analysis because the shorter one lacked the first several nucleotides (data not shown). Because no restriction site for 16 different enzymes could be found on the insert, deletion derivatives were generated for nucleotide sequence determination. The determined sequence was 2/520 bp, as shown in Figure 2. The coding region determines 751 amino acids, which consist of three distinct parts: the signal peptide of 24 residues, a nonrepetitive region of 76 residues, and a long repetitive region. The amino acid sequence of the signal peptide was similar to that of the *M. edulis* adhesive protein: 22 of 24 residues were conserved between the two species. The amino acid sequence of the nonrepetitive region was also conserved, but several substitutions and a deletion of 18 amino acids were observed (Fig. 3). The repetitive region included 62 repeats of the same decapeptide motif found in *M. edulis*. Although the hexapeptide motif characteristic of *M. edulis* was not observed in the repeats, an irregular tetradecapeptide was seen between the 55th and 56th repeats (Fig. 2, Table I). The sequence of the 3'-untranslated region was also conserved between *M. galloprovincialis* and *M. edulis*, although the termi-

Figure 2. Nucleotide and deduced amino acid sequences of the adhesive protein of *Mytilis galloprovincialis*. Underlined sequence indicates the signal peptide. Also underlined is the polyadenylation signal. Numbers under the amino acid sequence indicate numbers of decapeptide repeats. The asterisks represent the termination codon.

```
      10        20        30        40        50        60        70        80        90        100       110       120
CTGCATCATGGAGGGAATCAAATTAAATCTGTGCCTCTTGTGTATATTTACCTGTGACATCTTGGGTTTTTCAAATGGTAACATATACAACGCTCATGGTTCAGCTTATGCAGGTGCAAG
      M  E  G  I  K  L  N  L  C  L  L  C  I  F  T  C  D  I  L  G  F  S  N  G  N  I  Y  N  A  H  G  S  A  Y  A  G  A  S

      130       140       150       160       170       180       190       200       210       220       230       240
TGCTGGGGCTTACAAGACACTGCCTAATGCATATCCATACGGAACAAAGCATGGACCAGTATACAAACCTGTGAAGACAAGTTATCATCCTACGAATAGTTATCCGCCAACATATGGATC
 A  G  A  Y  K  T  L  P  N  A  Y  P  Y  G  T  K  H  G  P  V  Y  K  P  V  K  T  S  Y  H  P  T  N  S  Y  P  P  T  Y  G  S

      250       260       270       280       290       300       310       320       330       340       350       360
AAAGACAAACTATCTGCCACTTGCAAAGAAGCTGTCATCTTACAAACCTATTAAGACAACATATAATGCAAAGACAAATTATCCACCAGTTTATAAACCTAAGATGACTTATCCTCCAAC
 K  T  N  Y  L  P  L  A  K  K  L  S  S  Y  K  P  I  K  T  T  Y  N  A  K  T  N  Y  P  P  V  Y  K  P  K  M  T  Y  P  P  T
                                                                  1                                   2

      370       380       390       400       410       420       430       440       450       460       470       480
TTATAAACCTAAGCCCAGTTATCCTCCAACATATAAACCAAAGCCAAGTTATCCAGCAACTTATAAATCCAAGTCAAGTTATCCCTCTTCATACAAACCTAAGAAAACTTATCCTCCAAC
 Y  K  P  K  P  S  Y  P  P  T  Y  K  P  K  P  S  Y  P  A  T  Y  K  S  K  S  S  Y  P  S  S  Y  K  P  K  K  T  Y  P  P  T
      3                                   4                                   5                                   6

      490       500       510       520       530       540       550       560       570       580       590       600
ATATAAACCTAAACTAACCTATCCTCCAACATATAAACCAAAACCAAGTTATCCTCCAACATATAAACCAAAGCCAAGTTATCCAGCAACTTATAAATCCAAGTCAAGTTATCCCCCTTC
 Y  K  P  K  L  T  Y  P  P  T  Y  K  P  K  P  S  Y  P  P  T  Y  K  P  K  P  S  Y  P  A  T  Y  K  S  K  S  S  Y  P  P  S
      7                                   8                                   9                                   10

      610       620       630       640       650       660       670       680       690       700       710       720
ATATAAAACTAAGAAAACTTATCCCTCTTCATATAAACCTAAGAAAACTTATCCTTCAACGTATAAACCAAAAGTGAGTTATCCCCCAACATACAAATCAAAAAAGTCTTATCCTCCAAT
 Y  K  T  K  K  T  Y  P  S  S  Y  K  P  K  K  T  Y  P  S  T  Y  K  P  K  V  S  Y  P  P  T  Y  K  S  K  K  S  Y  P  P  I
      11                                  12                                  13                                  14

      730       740       750       760       770       780       790       800       810       820       830       840
ATATAAGACAAAGGCAAGTTATCCATCATCATATAAACCTAAAAAAACGTATCCTTCAACTTATAAACCCAAGATAAGTTATCCACCAACGTATAAAGCAAAGCCCAGTTATCCAACATC
 Y  K  T  K  A  S  Y  P  S  S  Y  K  P  K  K  T  Y  P  S  T  Y  K  P  K  I  S  Y  P  P  T  Y  K  A  K  P  S  Y  P  T  S
      15                                  16                                  17                                  18

      850       860       870       880       890       900       910       920       930       940       950       960
TTATAGAGCAAAACCAAGCTATCCTTCAACTTATAAGGCAAAACCAAGTTATCCTCCAACTTATAAAGCAAAACCAAGTTATCCTCCAACTTATAAAGCAAAGCCAACTTATCCTTCAAC
 Y  R  A  K  P  S  Y  P  S  T  Y  K  A  K  P  S  Y  P  P  T  Y  K  A  K  P  S  Y  P  P  T  Y  K  A  K  P  T  Y  P  S  T
      19                                  20                                  21                                  22

      970       980       990       1000      1010      1020      1030      1040      1050      1060      1070      1080
GTATAAAGCAAAACCAAGCTATCCTCCAACTTATAAAGCAAAACCAAGCTATCCTCCAACGTATAAAGCAAAACCGAGTTATCCACCATCATATAAACCTAAAACAACTTATCCTCCAAG
 Y  K  A  K  P  S  Y  P  P  T  Y  K  A  K  P  S  Y  P  P  T  Y  K  A  K  P  S  Y  P  P  S  Y  K  P  K  T  T  Y  P  P  S
      23                                  24                                  25                                  26

      1090      1100      1110      1120      1130      1140      1150      1160      1170      1180      1190      1200
TTATAAACCTAAGATAAGTTATCCTCCAACTTATAAGGCAAAACCAAGTTATCCTCCAATTTATAAAGCAAAACCAAGTTATCCTCCAACTTATAAAGCAAAACCAAGTTATCTTCCAAC
 Y  K  P  K  I  S  Y  P  P  T  Y  K  A  K  P  S  Y  P  P  I  Y  K  A  K  P  S  Y  P  P  T  Y  K  A  K  P  S  Y  L  P  T
      27                                  28                                  29                                  30

      1210      1220      1230      1240      1250      1260      1270      1280      1290      1300      1310      1320
TTATAAAGCAAAACCAAGTTATCCCCCAACGTATAAAGCAAAACCGAGATATCCTACAACTTATAAAGCAAAACCAAGTTATCCTCCAACTTATAAAGCAAAACCAAGTTATCCTCCAAC
 Y  K  A  K  P  S  Y  P  P  T  Y  K  A  K  P  R  Y  P  T  T  Y  K  A  K  P  S  Y  P  P  T  Y  K  A  K  P  S  Y  P  P  T
      31                                  32                                  33                                  34

      1330      1340      1350      1360      1370      1380      1390      1400      1410      1420      1430      1440
GTATAAAGCAAAACTAAGTTATCCTCCAACGTATAAAGCAAAACCGAGTTATCCTCCAACTTATAAAGCAAAACCAAGTTATCCTCCAACTTATAAAGCAAAACCAAGTTATCCTCCAAC
 Y  K  A  K  L  S  Y  P  P  T  Y  K  A  K  P  S  Y  P  P  T  Y  K  A  K  P  S  Y  P  P  T  Y  K  A  K  P  S  Y  P  P  T
      35                                  36                                  37                                  38

      1450      1460      1470      1480      1490      1500      1510      1520      1530      1540      1550      1560
TTATAAAACAAAGCCAAGTTATCCTCGAACGTATAAAGCAAAACCAAGTTATTCTTCAACTTATAAAGCAAAACCAAGTTATCCTCCAACTTATAAAGCAAAACCAAGTTATCCTCCAAC
 Y  K  T  K  P  S  Y  P  R  T  Y  K  A  K  P  S  Y  S  S  T  Y  K  A  K  P  S  Y  P  P  T  Y  K  A  K  P  S  Y  P  P  T
      39                                  40                                  41                                  42

      1570      1580      1590      1600      1610      1620      1630      1640      1650      1660      1670      1680
GTATAAAGCAAAGCCAAGTTATCCTCCAACTTATAAAGCAAAACCAAGTTATCCTCCAACATATAAAGCAAAACCAAGTTATCCCCCAACTTATAAAGCAAAACCAAGTTATCCTCAAAC
 Y  K  A  K  P  S  Y  P  P  T  Y  K  A  K  P  S  Y  P  P  T  Y  K  A  K  P  S  Y  P  P  T  Y  K  A  K  P  S  Y  P  Q  T
      43                                  44                                  45                                  46

      1690      1700      1710      1720      1730      1740      1750      1760      1770      1780      1790      1800
TTATAAAGCAAAATCAAGTTATCCTCCAACTTATAAAGCAAAGCCAAGTTATCCTCCAACTTATAAAGCAAAACCAAGTTATCCTCCAACTTATAAAGCAAAGCCAAGTTATCCTCCAAC
 Y  K  A  K  S  S  Y  P  P  T  Y  K  A  K  P  S  Y  P  P  T  Y  K  A  K  P  S  Y  P  P  T  Y  K  A  K  P  S  Y  P  P  T
      47                                  48                                  49                                  50

      1810      1820      1830      1840      1850      1860      1870      1880      1890      1900      1910      1920
TTATAAAGCAAAACCAAGTTATCCTCCAACTTATAAAGCAAAGCCAAGTTATCCTCCAACTTATAAAGCAAAACCAAGTTATCCTCCAACTTATAAAGCAAAACCAAGTTATCCTCCAAC
 Y  K  A  K  P  S  Y  P  P  T  Y  K  A  K  P  S  Y  P  P  T  Y  K  A  K  P  S  Y  P  P  T  Y  K  A  K  P  S  Y  P  P  T
      51                                  52                                  53                                  54

      1930      1940      1950      1960      1970      1980      1990      2000      2010      2020      2030      2040
TTATAAAGCAAAACCAAGTTATCCTCCAACTTATAAAGCAAAGCCAAGTTATCCAGCAACTTATCCTTCAACGTATAAAGCAAAGCCAAGTTATCCTCCAACTTATAAAGCAAAACCAAG
 Y  K  A  K  P  S  Y  P  P  T  Y  K  A  K  P  S  Y  P  A  T  Y  P  S  T  Y  K  A  K  P  S  Y  P  P  T  Y  K  A  K  P  S
      55                                  tetradecapeptide                    56                                  57

      2050      2060      2070      2080      2090      2100      2110      2120      2130      2140      2150      2160
TTATCCTCCAACATATAAACCAAAGCCAAGTTATCCACCAACATATAAATCCAAGTCAAGTTATCCCTCTTCATACAAACCTAAGAAAACTTATCCCCCCACATATAAACCTAAACTAAC
 Y  P  P  T  Y  K  P  K  P  S  Y  P  P  T  Y  K  S  K  S  S  Y  P  S  S  Y  K  P  K  K  T  Y  P  P  T  Y  K  P  K  L  T
                58                                  59                                  60                                  61

      2170      2180      2190      2200      2210      2220      2230      2240      2250      2260      2270      2280
CTATCCCCCAATATATAAACCAAAGCCAAGTTATCCTCCAACATACAAATCTAGTTACCCTCCTAGATATAAAAAAAAAGATCAGCTATCCATCACAATATTAAGTGAAGACAAGTTATCC
 Y  P  P  I  Y  K  P  K  P  S  Y  P  P  T  Y  K  S  S  Y  P  P  R  Y  K  K  K  I  S  Y  P  S  Q  Y  *
                62

      2290      2300      2310      2320      2330      2340      2350      2360      2370      2380      2390      2400
CCAAGCATATGAACCAACAAACAGCTATTAATCTCAATATTAAAAGTATTAATTAAAATATTCATATTACTGTACTACACATTTTAACGTTTGTGTTGATGAGGAACAGATGAACATTTG

      2410      2420      2430      2440      2450      2460      2470      2480      2490      2500      2510      2520
AAAGTAATACATAATCGGGGTTAATGATTTGTTATATTCAATCTTTATGTTTGTGATTGGTTATGTTCTTGAAATATTGTTTAAAATAAATGTTTATTTTTTAAAAAAAAAAAAAAAAAA
```

```
                Signal                          Non-repetitive
Mg      1   MEGIKLNLCLLCIFTCDILGFSNG NIYNAHGSAYAGASAGAYKTLPNAYPYGTKHGPVYK
            *************** * ****** ****** * ********** **********  ****
Me      1   MEGIKLNLCLLCIFTFDVLGFSNG NIYNAHVSSYAGASAGAYKKLPNAYPYGTKPEPVYK

Mg     61   PVKTSY-------------------HPTNSYPPTYGSKTNYLPLAKKLSSYKPIKTTYN
            ******                    ** ********************************
Me     61   PVKTSYSAPYKPPTYQPLKKKVDYRPTKSYPPTYGSKTNYLPLAKKLSSYKPIKTTYN

            Repetitive
Mg    101   AKTNYPPVYKPKMTYPPTYKPKPSYPPTYKPKPSYPATYKSKSSYPSSYKPKKTYPPTYK
            ********************************** **     *** *  **  ** *  *******
Me    119   AKTNYPPVYKPKMTYPPTYKPKPSYPPTYKSKP----TYKPKITYPPTYKAKPSYPPTYK
            1          2          3          4          5          6
```

Figure 3. Comparison of the peptide sequences of the signal region, the nonrepetitive region, and the first part of the repetitive region of adhesive protein from *Mytilis galloprovincialis* with those of *M. edulis* described by Laursen (1992). Asterisks indicate the homology between the corresponding sequences. Me and Mg represent sequences of *M. edulis* and *M. galloprovincialis*, respectively.

nator codons were in different positions and several base substitutions were observed (Fig. 4).

Variation of amino acids in the decapeptide motif

As observed in *M. edulis*, some amino acids in the decapeptide motif were sometimes substituted. Substitutions were frequent in the first 17 and last 5 repeats, but they were less common in the middle of the repetitive region. The variation of amino acids in the first three repeats was identical with that of *M. edulis* (Fig. 3) (Filpula *et al.*, 1990; Laursen, 1992), whereas the fourth repeat differed between the two species; *i.e.*, it was a decapeptide in *M. galloprovincialis* but a hexapeptide in *M. edulis*. Figure 5 lists the frequency of substitutions of each amino acid in the decapeptide motif in the whole repetitive region. The most conserved residues were the two tyrosine residues and the lysine at position 2, which were perfectly conserved. The lysine at position 10 and the proline at position 6 were also highly conserved. Other residues suffered considerable variation. The first alanine, the fourth serine, and the eighth threonine were often replaced with proline, threonine, and serine, respectively.

Table 1

Number of decapeptide, hexapeptide, and tetradecapeptide motifs in adhesive proteins of Mytilus galloprovincialis *and* M. edulis

Motif	*M. galloprovincialis*	*M. edulis*[1]	*M. edulis*[2]
Decapeptide	62	71	72
Hexapeptide	0	13	14
Tetradecapeptide	1	0	0

[1] According to Laursen (1992).
[2] According to Filpula *et al.* (1990).

Codon usage in the decapeptide motif

Among the conserved residues, two tyrosine residues and the lysine at position 10 showed highly specific codon usage. All the tyrosine at position 5 and most of the tyrosine at position 9 were coded by TAT (Fig. 5). Most of the lysine residues at position 10 were coded by AAA, but the AAG codon was not as rare at the position of the second lysine (Fig. 5). In other residues, specific codon usage was also observed. For example, the third and sixth proline residues were preferentially coded by CCA and the seventh proline by CCT. In addition, the fourth serine and the eighth threonine were preferentially coded by AGT and ACT, respectively. The first alanine, which was the most substituted residue in the decapeptide motif, was coded only by GCA. Thus, codon usage pattern was highly specific in several residues in the decapeptide motif.

Discussion

The locations of two tyrosine and two lysine and one of the three proline residues in the decapeptide motif were well conserved in the adhesive protein of *M. galloprovincialis*. These residues are also well conserved in the decapeptide repeats of *M. edulis* (Filpula *et al.*, 1990; Laursen, 1992). Tyrosine and lysine residues are also found in the repeat motifs of other mussels (Rzepecki *et al.*, 1991; Laursen, 1992; Waite, 1992) following the paradigm x-Y* -x-x-x-Y*-K, where Y* denotes tyrosine or DOPA. The presence and location of these residues are thought to be critical for the function of adhesive proteins of mussels.

```
Mg 2234 AAAAAGATCAGCTATCCATCACAATATTAAGTGAAGACAAGTTATCCCCAAGCATATGAA
        ********************  **** ***  *************** ******* **
Me      AAAAAGATCAGCTATCCATCATCATATAAAGCTAAGACAAGTTATCCCCCAGCATATAAA

Mg 2294 CCAACAAACAGCTATTAATCTCAATATTAAAAGTATTAATTAAAATATTCATATTACTGT
        ********** ***************************** ********** ********
Me      CCAACAAACAGATATTAATCTCAATATTAAAAGTATTAACTAAAATATTCACATTACTGT

Mg 2354 ACTACACATTTTAACGTTTGTGTTGATGAGGAACAGATGAACATTTGAAAGTAATACATA
        ********************* ****************************************
Me      ACTACACATTTTAACGTTTGTATTGATGAGGAACAGATGAACATTTGAAAGTAATACATA

Mg 2414 ATCGGGGTTAATGATTTGTTATATTCAATCTT--TATGTTTGTGATTGGTTATGTTCTTG
        ********************************  ************ ************
Me      ATCGGGGTTAATGATTTGTTATATTCAATCTTAATATGTTTGTGATTTGTTATGTTCTTG

Mg 2474 AAATATTGTTTAAAATAAATGTTTATTTTTT(Poly A)
        ** ******** ******* ******* ***
Me      AAGTATTGTTTCAAATAAAAGTTTATTCTTTTCTGGT(Poly A)
```

Figure 4. Comparison of the nucleotide sequence from the last part of the repetitive region to the poly(A) tail of *Mytilis galloprovincialis* with the same region of *M. edulis* reported by Strausberg *et al.* (1989). Asterisks indicate the homology between the corresponding sequences. The underlined sequence indicates the stop codon. Me and Mg represent sequences of *M. edulis* and *M. galloprovincialis*, respectively.

1		2		3		4		5	
A(38)	GCA(38)	K(62)	AAA(37)	P(42)	CCA(37)	S(50)	AGT(46)	Y(62)	TAT(62)
P(17)	CCT(10)		AAG(25)		CCG(3)		AGC(3)		
	CCA(6)				CCC(2)		TCT(1)		
	CCC(1)			K(6)	AAA(5)	T(10)	ACT(7)		
S(4)	TCC(3)				AAG(1)		ACC(2)		
	TCT(1)			S(4)	TCA(4)		ACG(1)		
T(3)	ACA(2)			L(3)	CTA(3)	N(1)	AAT(1)		
	ACT(1)			T(2)	ACA(2)	R(1)	AGA(1)		
				I(2)	ATA(2)				
				V(1)	GTG(1)				
				A(1)	GCA(1)				
				M(1)	ATG(1)				

6		7		8		9		10	
P(60)	CCT(43)	P(47)	CCA(45)	T(50)	ACT(31)	Y(62)	TAT(59)	K(61)	AAA(58)
	CCA(8)		CCC(1)		ACA(10)		TAC(3)		AAG(3)
	CCC(9)		CCT(1)		ACG(9)			R(1)	AGA(1)
L(1)	CTT(1)	S(9)	TCA(6)	S(8)	TCA(6)				
S(1)	TCT(1)		TCT(3)		TCT(1)				
		T(2)	ACA(2)		AGT(1)				
		A(2)	GCA(2)	I(3)	ATA(2)				
		R(1)	CGA(1)		ATT(1)				
		Q(1)	CAA(1)	V(1)	GTT(1)				

Figure 5. Frequencies of amino acid substitutions and codon usages in the decapeptide motif of the adhesive protein of *Mytilis galloprovincialis*. Numbers in parentheses indicate the frequencies of each of the amino acids and codons, respectively.

In the previous and present studies, three motifs—decapeptide, hexapeptide, and tetradecapeptide—were observed. We noticed that these motifs can be divided into two submotifs, (Y)KAKPSY (submotif A) and (Y)PPTY (submotif B), according to the position of the tyrosine residues. The hexapeptide, decapeptide, and tetradecapeptide motifs corresponded to A, A + B, and A + B + B, respectively, though minor variations were observed in the positions of Ala, Pro, Ser, and Thr residues. The decapeptide motif is obviously the basic motif of the adhesive protein. The hexapeptide motif is apparently also a functional unit, or at least it does not prevent the function, because it is not rare in the repetitive region of *M. edulis*. The tetradecapeptide may also be a functional unit because it is composed of the same submotifs.

In the nucleotide sequence of the repetitive region, specific codon usage was observed. It is interesting that the codon usage in one of the two lysine residues was highly specific but the other was not. In addition, the alanine residues were often replaced with proline or other amino acids, but all the alanine residues at this position were coded only by GCA. The third proline was also frequently substituted by various amino acids, but the CCA codon was preferentially used for proline, and the codons whose third bases are A were preferentially used for other amino acids. The same tendencies were observed in the gene for the adhesive protein of *M. edulis* (Filpila *et al.*, 1990). These conserved nucleotides suggest that the specific nucleotide sequences have some functional significance (*e.g.*, in the transcriptional regulation as reported in fibroin mRNA (Mita *et al.*, 1988) or in the replication of genome); but information is insufficient for discussion at present.

M. galloprovincialis is thought to have originated in the Mediterranean Sea and to have been accidentally introduced into Japan (Wilkins *et al.*, 1983). Because it has many morphological and genetical characteristics in common with *M. edulis*, these two species have been thought to be closely related (Seed, 1992, for a review) or even to be subspecies of *M. edulis* (Gosling, 1984; Gardner, 1992; for reviews). Even with the use of mitochondrial ribosomal DNA sequences (Geller *et al.*, 1993), it is difficult to distinguish between these two species. They appear to maintain genetic differentiation, however, even though hybridization is possible between them (McDonald *et al.*, 1991). Two different sequences of the adhesive protein from two different strains have been reported; one is derived from the cDNA sequence described by Laursen (1992), and the other is from the partial genomic sequence by Filpula *et al.* (1990). The latter lacks the N-terminal sequence, but the former sequence from the 53th residue to the end of the nonrepetitive region was identical with the corresponding sequence of the latter at the amino acid level. The signal region and the nonrepetitive region of *M. galloprovincialis* had amino acid sequences similar to but not identical with those of *M. edulis*. It has been reported that two *M. edulis* sequences in the repetitive region were identical in the first nine and last five repeats and only the distribution pattern of hexapeptides in the middle of the repetitive region was different. The hexapeptides that exist in the repetitive region of *M. edulis* were not found in the sequence of *M. galloprovincialis;* a tetradecapeptide was found instead. We determined partial sequences of other cDNA clones of *M. galloprovincialis*, but also failed to find any hexapeptides (data not shown). However, more information is required before we can discuss the correlation of sequence differences with diversity among populations and species. We are now using polymerase chain reaction to look for interspecific and intrapopulation variation in adhesive protein sequences. The sequence of the adhesive protein may offer a key to understanding not only the function of this protein but also the genetic diversity among different populations and species of mussels.

Acknowledgments

The authors express their sincere thanks to Drs. J. Herbert Waite and Shigeaki Harayama for critical reading of the manuscript, and to Dr. Nobuhiko Takamatsu for helpful advice. We also thank Drs. Shigetoh Miyachi and Wataru Miki for support in this study. This work was part of the Industrial Science and Technology Frontier Program supported by the New Energy and Industrial Technology Development Organization.

Literature Cited

Filpula, D. R., S-M. Lee, R. P. Link, S. L. Strausberg, and R. L. Strausberg. 1990. Structural and functional repetition in a marine mussel adhesive protein. *Biotechnol. Prog.* **6:** 171–177.

Gardner, J. P. A. 1992. *Mytilus galloprovincialis* (Lmk) (Bivalvia, Mollusca): the taxonomic status of the Mediterranean mussel. *Ophelia* **35:** 219–243.

Geller, J. B., J. T. Carlton, and D. A. Powers. 1993. Interspecific and intrapopulation variation in mitochondrial ribosomal DNA sequences of *Mytilus* spp. (Bivalvia: Mollusca). *Mol. Mar. Biol. Biotechnol.* **2:** 44–50.

Gosling, E. M. 1984. The systematic status of *Mytilus galloprovincialis* in western Europe: a review. *Malacologia* **25:** 551–568.

Laursen, R. A. 1992. Reflections on the structure of mussel adhesive proteins. Pp. 55–74 in *Structure, Cellular Synthesis and Assembly of Biopolymers. Results and Problems in Cell Differentiation*, Vol. 19, S. T. Case, ed. Springer-Verlag, Berlin.

McDonald, J. H., R. Seed, and R. K. Koehn. 1991. Allozymes and morphometric characters of three species of *Mytilus* in the Northern and Southern Hemispheres. *Mar. Biol.* **111:** 323–333.

Mita, K., S. Ichimura, and M. Zama. 1988. Specific codon usage pattern and its implications on the secondary structure of silk fibroin mRNA. *J. Mol. Biol.* **203:** 917–925.

Rzepecki, L. M., S.-S. Chin, J. H. Waite, and M. F. Lavin. 1991. Molecular diversity of marine glues: polyphenolic proteins from five mussel species. *Mol. Marine Biol. Biotechnol.* **1:** 78–88.

Seed, R. 1992. Systematics, evolution and distribution of mussels belonging to the genus *Mytilus*: an overview. *Am. Malac. Bull.* **9:** 123–137.

Strausberg, R. L., D. M. Anderson, D. Filpula, M. Finkelman, R. Link, R. McCandliss, S. A. Orndorff, S. L. Strausberg, and T. Wei. 1989. Development of a microbial system for production of mussel adhesive protein. Pp. 453–464 in *Adhesives from Renewable Resources.* ACS Symposium Series 385, R. W. Hemingway and A. H. Conner, eds. American Chemical Society, Washington, DC.

Waite, J. H. 1983. Evidence for a repeating Dopa and hydroxyproline containing decapeptide in the adhesive protein of *Mytilus edulis*. *J. Biol. Chem.* **258:** 2911–2915.

Waite, J. H. 1986. Mussel glue from *Mytilus californianus* Conrad: a comparative study. *J. Comp. Physiol. B* **156:** 491–496.

Waite, J. H. 1987. Nature's underwater adhesive specialist. *Int. J. Adhesion Adhesives* **7:** 9–14.

Waite, J. H. 1992. The formation of mussel byssus: anatomy of a natural manufacturing process. Pp. 55–74 in *Structure, Cellular Synthesis and Assembly of Biopolymers. Results and Problems in Cell Differentiation,* Vol. 19. S. T. Case, ed. Springer-Verlag, Berlin.

Waite, J. H., and M. L. Tanzer. 1981. Polyphenolic substances of *Mytilus edulis*. *Science* **212:** 1038–1040.

Waite, J. H., T. J. Housley, and M. L. Tanzer. 1985. Peptide repeats in a mussel glue protein: theme and variations. *Biochemistry* **24:** 5010–5014.

Waite, J. H., D. C. Hansen, and K. T. Little. 1989. The glue protein of ribbed mussels (*Geukensia demissa*): a natural adhesive with some features of collagen. *J. Comp. Physiol. B* **159:** 517–525.

Wilkins, N. P., K. Fujino, and E. M. Gosling. 1983. The Mediterranean mussel *Mytilus galloprovincialis* Lmk. in Japan. *Biol. J. Linn. Soc.* **20:** 365–374.

INDEX

N

O

P

Q

R

S

T

U

V

W

Y

Z

CONTENTS